WOODHEAD PUBLISHING IN MATERIALS

Bioceramics and their clinical applications

Edited by Tadashi Kokubo

JMM JAPAN MEDICAL MATERIALS

CRC

WP

Bioceramics and their clinical applications

Related titles:

Dental biomaterials: Imaging, testing and modelling
(ISBN 978-1-84569-296-4)
Dental biomaterials: Imaging, testing and modelling focuses on the techniques required to undertake research in dental biomaterials. The text forms an instructive and practical review of the scientific methods applied to dental biomaterials, with appropriate case studies. The book includes chapters discussing the practicalities of working on dental biomaterials, such as reviewing the mechanisms of cutting tooth tissue and methods for characterising dental hand piece performance. Optical and electron imaging techniques for biomaterial interfaces are reviewed and specific materials, applications and experimental techniques are discussed. There are also chapters reviewing the development and application of computer models to this complex area.

Biomaterials, artificial organs and tissue engineering
(ISBN 978-1-85573-737-2)
Biomaterials are materials and devices that are used to repair, replace or augment the living tissues and organs of the human body. The purpose of this wide-ranging introductory textbook is to provide an understanding of the needs, uses and limitations of materials used in the human body and to explain the biomechanical principles and biological factors involved in achieving the long-term stability of replacement parts in the body. This book examines the industrial, governmental and ethical factors involved in the use of artificial materials in humans and discusses the principles and applications of engineering of tissues to replace body parts. This approach necessarily incorporates a wide range of reference material because of the complex multidisciplinary nature of the biomedical materials, biomechanics, artificial organs and tissue engineering fields. An accompanying CD-ROM provides supplementary information and illustrations to support the book.

Biomedical polymers
(ISBN 978-1-84569-070-0)
This book reviews the structure, processing and properties of biomedical polymers. It discusses the various groups of biopolymers including natural polymers, synthetic biodegradable and non-biodegradable polymers. Chapters also review the application of biomedical polymers in such areas as scaffolds for tissue engineering, drug delivery systems and cell encapsulation. The book also considers the use of polymers in replacement heart valves and arteries, in joint replacement and in biosensor applications.

Details of these and other Woodhead Publishing materials books, as well as materials books from Maney Publishing, can be obtained by:

- visiting our web site at www.woodheadpublishing.com
- contacting Customer Services (e-mail: sales@woodhead-publishing.com; fax: +44 (0) 1223 893694; tel.: +44 (0) 1223 891358 ext.130; address: Woodhead Publishing Ltd, Abington Hall, Abington, Cambridge CB21 6AH, England)

If you would like to receive information on forthcoming titles, please send your address details to: Francis Dodds (address, tel. and fax as above; e-mail: francisd@woodhead-publishing.com). Please confirm which subject areas you are interested in.

Maney currently publishes 16 peer-reviewed materials science and engineering journals. For further information visit www.maney.co.uk/journals

Bioceramics and their clinical applications

Edited by
Tadashi Kokubo

Woodhead Publishing and Maney Publishing
on behalf of
The Institute of Materials, Minerals & Mining

WPNL2204

CRC Press
Boca Raton Boston New York Washington, DC

WOODHEAD PUBLISHING LIMITED
Cambridge England

WPNL2204

Woodhead Publishing Limited and Maney Publishing Limited on behalf of
The Institute of Materials, Minerals & Mining

Woodhead Publishing Limited, Abington Hall, Abington
Cambridge CB21 6AH, England
www.woodheadpublishing.com

Published in North America by CRC Press LLC, 6000 Broken Sound Parkway, NW,
Suite 300, Boca Raton, FL 33487, USA

First published 2008, Woodhead Publishing Limited and CRC Press LLC

British Library Cataloguing in Publication Data
A catalogue record for this book is available from the British Library.

Library of Congress Cataloging in Publication Data
A catalog record for this book is available from the Library of Congress.

Woodhead Publishing ISBN 978-1-84569-204-9 (book)
Woodhead Publishing ISBN 978-1-84569-422-7 (e-book)
CRC Press ISBN 978-1-4200-7207-5
CRC Press order number: WP7207

The publishers' policy is to use permanent paper from mills that operate a sustainable forestry policy, and which has been manufactured from pulp which is processed using acid-free and elementary chlorine-free practices. Furthermore, the publishers ensure that the text paper and cover board used have met acceptable environmental accreditation standards.

Project managed by Macfarlane Production Services, Dunstable, Bedfordshire, England (e-mail: macfarl@aol.com)

Typeset by SNP Best-set Typesetter Ltd., Hong Kong
Printed by TJ International Limited, Padstow, Cornwall, England

WPNL2204

Contents

Contributor contact details

(* = main author)

Editor

Professor Tadashi Kokubo
Department of Biomedical Sciences
College of Life and Health Sciences
Chubu University
1200 Matsumoto-cho
Kasugai
Aichi 487-8501
Japan
E-mail: kokubo@isc.chubu.ac.jp

Chapter 1

Professor John Currey
Department of Biology
University of York
York YO10 5YW
UK
E-mail: jdc1@york.ac.uk

Chapter 2

Professor Yumi Tanaka and Professor Kimihiro Yamashita*
Institute of Biomaterials and Bioengineering
Tokyo Medical and Dental University
2-3-10 Kanda-Surugadai
Chiyoda-ku
Tokyo 101-0062
Japan
E-mail: yama-k.bcr@tmd.ac.jp

Chapter 3

Dr Satoshi Hayakawa*, Dr Kanji Tsuru and Professor Akiyoshi Osaka
Biomaterials Laboratory
Graduate School of Natural Science and Technology
Okayama University
3-1-1 Tsushima
Okayama 700-8530
Japan
E-mail: satoshi@cc.okayama-u.ac.jp

Chapter 4

Professor Michael V. Swain* and
Dr Li-Hong He
Biomaterials Research Unit
Faculty of Dentistry
University of Sydney
Sydney Dental Hospital
Surry Hills
NSW 2010
Australia
E-mail: mswain@mail.usyd.edu.au

Chapter 5

Professor Ian C. Clarke*
LLU Orthopedic Research Center
Department of Orthopedics
Loma Linda University Medical
Center
14606 Loma Linda Drive
Loma Linda, CA 92354
USA
E-mail: ianclarke4@msn.com

Allen Gustafson
Gustafson Orthopedics
Redlands Blvd
Loma Linda, CA 92354
USA

Chapter 6

Dr Christine Knabe
Department of Experimental
Dentistry
Charité University Medical Center
Berlin
Campus Benjamin Franklin
4-6 Assmannshauser Str.
D-14197 Berlin
Germany
E-mail: christine.knabe@charite.de

and

Visiting Associate Professor
Thomas Jefferson University
Department of Orthopaedic
Surgery
501 Curtis Building
1015 Walnut Street
Philadelphia, PA 19107-5099
USA

Professor Paul Ducheyne*
Center for Bioactive Materials and
Tissue Engineering
School of Engineering & Applied
Science
University of Pennsylvania
Skirkanich Hall
210 S. 33rd Street
Philadelphia, PA 19104-6391
USA
E-mail: ducheyne@seas.upenn.edu

Chapter 7

Dr Hiroaki Takadama* and
Professor Tadashi Kokubo
Department of Biomedical
Sciences
College of Life and Health
Sciences
Chubu University
1200 Matsumoto-cho
Kasugai
Aichi 487-8501
Japan
E-mail: takadama@isc.chubu.ac.jp
kokubo@isc.chubu.ac.jp

Chapter 8

Professor Takashi Nakamura and Dr Mitsuru Takemoto*
Department of Orthopaedic Surgery
Graduate School of Medicine
Kyoto University
Shogoin
Kawahara-cho 54
Sakyo-ku
Kyoto 606-8507
Japan
E-mail: m.take@kuhp.kyoto-u.ac.jp
ntaka@kuhp.kyoto-u.ac.jp

Chapter 9

Professor J.D. de Bruijn* and K Shankar
School of Engineering and Materials Science & IRC in Biomedical Materials
Queen Mary University of London
Mile End Road
London E1 4NS
UK

Professor J.D. de Bruijn and Dr H. Yuan
Progentix BV
Prof. Bronkhorstlaan 10-d
3723 MB Bilthoven
The Netherlands
E-mail: j.d.debruijn@qmul.ac.uk

Dr H. Yuan and Dr P. Habibovic
Department of Tissue Regeneration
University of Twente
The Netherlands

Chapter 10

Professor Besim Ben-Nissan*, Andy H. Choi and Rebecca Cordingley
Department of Chemistry, Materials and Forensic Science
University of Technology
PO Box 123
Broadway
NSW 2007
Australia
E-mail: b.ben-nissan@uts.edu.au

Chapter 11

Professor Jérôme Chevalier* and Dr Laurent Gremillard
Université de Lyon, Mateis, INSA-Lyon
UMR CNRS 5510
20 Avenue Albert Einstein
69621 Villeurbanne
France
E-mail: jerome.chevalier@insa-lyon.fr
laurent.gremillard@insa-lyon.fr

Chapter 12

Dr Julian R. Jones
Department of Materials and Institute of Biomedical Engineering
Imperial College London
South Kensington Campus
London SW7 2AZ
UK
E-mail: julian.r.jones@imperial.ac.uk

Chapter 13

Professor Tadashi Kokubo
Department of Biomedical Sciences
College of Life and Health Sciences
Chubu University
1200 Matsumoto-cho
Kasugai
Aichi 487-8501
Japan
E-mail: kokubo@isc.chubu.ac.jp

Chapter 14

Professor John L. Ricci* and Michael J. Weiner
New York University College of Dentistry
345 East 24th Street
New York, NY 10010
USA
E-mail: john.ricci@nyu.edu

Sachin Mamidwar and Harold Alexander
Orthogen Corporation
Springfield, NJ 07081
USA

Chapter 15

Christian Rey*, Christèle Combes and Christophe Drouet
CIRIMAT
ENSIACET
118 route de Narbonne
31077 Toulouse Cedex 4
France
E-mail: christian.rey@ensiacet.fr
Christele.Combes@ensiacet.fr
Christophe.Drouet@ensiacet.fr

Sayda Somrani
IPEIT
2 rue Jawhar El Nahrou
Monfleury
1089 Tunis
Tunisia
E-mail: sayda.somrani@ipeit.rnu.tn

Chapter 16

Professor Racquel Zapanta LeGeros* and Professor John P. LeGeros
Department of Biomaterials and Biomimetics
New York University College of Dentistry
345 East 24th Street
New York, NY 10010
USA
E-mail: rzl1@nyu.edu
jpl4@nyu.edu

Chapter 17

Professor Guy Daculsi*
INSERM
U 791
Nantes University
Laboratory for osteo-articular and dental tissue engineering
1 place Alexis Ricordeau
44042 Nantes
France

and

INSERM Clinical Investigation Center
CHU of Bordeaux
Bordeaux
France
E-mail: Guy.Daculsi@univ-nantes.fr

Professor Racquel Zapanta LeGeros
Associate Chair and Professor
Department of Biomaterials and Biomimetics
L. Linkow Professor in Implant Dentistry
New York University College of Dentistry
345 East 24th Street
New York, NY 10010
USA
E-mail: rzl1@nyu.edu

Chapter 18

Dr Eng San Thian* and Dr Serena M. Best
Department of Materials Science and Metallurgy
University of Cambridge
Pembroke Street
Cambridge CB2 3QZ
UK
E-mail: E.S.Thian.02@cantab.net

Chapter 19

Professor Kunio Ishikawa
Department of Biomaterials
Faculty of Dental Science
Kyushu University
3-1-1, Maidashi
Higashi
Fukuoka 812-8582
Japan
E-mail: ishikawa@dent.kyushu-u.ac.jp

Chapter 20

Dr Sander C.G. Leeuwenburgh*, Dr Joop G.C. Wolke and Professor John A. Jansen
Department of Periodontology and Biomaterials
Radboud University Nijmegen Medical Center
Philips van Leydenlaan 25
PO Box 9101
6500 HB Nijmegen
The Netherlands
E-mail: s.leeuwenburgh@dent.umcn.nl
j.wolke@dent.umcn.nl
j.jansen@dent.umcn.nl

Professor Klaas de Groot
Institute for Biomedical Technology
University of Twente
PO Box 217
7500 AE Enschede
The Netherlands
E-mail: k.degroot@tnw.utwente.nl

Chapter 21

Professor Tadashi Kokubo*,
Dr Hiroaki Takadama and
Dr Tomiharu Matsushita
Department of Biomedical
Sciences
College of Life and Health
Sciences
Chubu University
1200 Matsumoto-cho
Kasugai
Aichi 487-8501
Japan
E-mail: kokubo@isc.chubu.ac.jp
takadama@isc.chubu.ac.jp
matsushi@isc.chubu.ac.jp

Chapter 22

Professor Chikara Ohtsuki
Department of Crystalline
Materials Science
Graduate School of
Engineering
Nagoya University
Furo-cho Chikusa-Ku
Nagoya 464-8603
Japan
E-mail: ohtsuki@apchem.nagoya-
u.ac.jp

Chapter 23

Professor Van P. Thompson* and
Professor E. Dianne Rekow
New York University
New York, NY 10010
USA
E-mail: van.thompson@nyu.edu

Chapter 24

Professor W. Höland* and
Dr. V. Rheinberger
Ivoclar Vivadent AG
Benderer Str. 2
Li-9494
Schaan
Liechtenstein
E-mail: wolfram.hoeland@
ivoclarvivadent.com

Chapter 25

Heimo O. Ylänen
Åbo Akademi University
Turku
Finland

and

Biomaterials Centre
University of Turku
Itäinen Pitkäkatu 4 B
FI-20520
Turku
Finland
E-mail: heimo.ylanen@utu.fi

Chapter 26

Professor Takao Yamamuro
Kyoto University
Kyoto
Japan

and

Research Institute for Production
Development
15 Morimoto-cho
Shimogamo
Sakyo-ku
Kyoto 606-0805
Japan
E-mail: mozume-takaoyama@
sweet.odn.ne.jp

Chapter 27

Dr H. Oonishi,* Dr H. Oonishi, Jr and Dr S.C. Kim
H. Oonishi Memorial Joint Replacement Research Institute
Tominga Hospital
4-48, 1-chome minato-machi, Naniwa-ku
Osaka 556-0017
Japan
E-mail: oons-h@ga2.so-net.ne.jp

L.L. Hench and J. Wilson
Bioglass Research Center
University of Florida
USA

Dr E. Tsuji
Osaka Prefectural Industrial Engineering Research Institute
Osaka
Japan

Dr H. Fujita
Kyoto Katsura Hospital
Kyoto
Japan

Dr H. Oohashi
Department of Orthopaedic Surgery
Osaka Nakatsu Saiseikai Hospital
Osaka
Japan

K. Oomamiuda
Olympus Terumo Biomaterials Corp.
Shizuoka
Japan

Chapter 28

Laurent Sedel
Orthopaedic Department
University of Paris 7
Paris
France

and

Hôpital Lariboisière (APHP)
2 rue Ambroise Paré
75010 Paris
France
E-mail: laurent.sedel@lrb.aphp.fr

Chapter 29

Dr H. Oonishi,* Dr S.C. Kim and Dr H. Oonishi, Jr.
H. Oonishi memorial Joint Replacement Research Institute
Tominaga Hospital
4-48, 1-chome minato-machi
Naniwa-ku
Osaka 556-0017
Japan
E-mail: oons-h@ga2.so-net.ne.jp

S. Masuda, M. Kyomoto and M. Ueno
Japan Medical Materials Corporation
Osaka
Japan

Chapter 30

Hajime Ohgushi
Research Institute for Cell
Engineering (RICE)
National Institute of Advanced
Industrial Science and
Technology (AIST)
3-11-46 Nakouji
Amagasaki City
Hyogo 661-0974
Japan
E-mail: hajime-ohgushi@aist.go.jp

Preface

This book presents a comprehensive review of the present art of bioceramics, from basic science to clinical applications. Systematic research into ceramics for biomedical applications started in the early 1970s. Over the past 40 years, the variety of ceramics tried in biomedical applications has greatly expanded. In the early stages, ceramics developed for engineering applications were applied to biomedical uses. Ceramics specific to biomedical applications were then designed and synthesized. New processes for the fabrication of ceramics were also developed and the composition and structure of ceramics are now highly and precisely controlled. Methods for the analysis of the structure of ceramics have also greatly progressed. In early studies, the responses of living tissues to ceramics were evaluated by observation by optical microscopy. However, biological analysis is now performed at the molecular level, in combination with physical techniques. Long-term clinical data are now available. These findings give important suggestions for designing new kinds of ceramics for biomedical applications.

All of these developments are reviewed in this book by the world's most prominent researchers in each area of bioceramics. The book starts with discussion of the properties of bone, then proceed to the general properties of bioceramics, the characteristics of each bioceramic, and their clinical applications. Each chapter covers basic concepts through to the most up-to-date findings, thus providing both the beginner and the experienced person with an overview of bioceramics. People who want to know more detail can proceed to the original data via the plentiful references cited at the end of each chapter. This book should become a standard systematic textbook in both the fields of materials sciences and medical sciences.

A book of this type was published in 1993 by L.L. Hench and J. Wilson, entitled *An Introduction to Bioceramics* (World Scientific). It was a good standard textbook in this field; however, more than 14 years have passed since its publication and a new book has been keenly awaited. I believe that the present book can meet this application. However, here I must express a concern. There are two types of bioceramic that were included in the book

by Hench, but are not included in the present book. They are pyrolytic carbon, used in heart valves, and yttrium aluminosilicate glass, used in radiotherapy. These ceramics still play an important role clinically but, unfortunately, neither has been included in this book because of limits to the size of the volume.

Here, I would like to call your attention to the great contribution made by the pioneers in this field. Prof. W. Bonfield, Prof. P. Boutin, Prof. D.E. Day, Prof. K. de Groot, Prof. U.M. Gross, Prof. G. Heimke, Prof. L.L. Hench, Prof. F. Hulbert, Prof. A.K. Karlsson, Prof. S. Niwa, Prof. Yamauro and Prof. A. Yli-Urpo are some of these pioneers. Without their contribution, we could not have achieved the present state of the development of bioceramics.

I hope that this book will be a landmark on which future development of bioceramics will be based. However, I would like to remember that our goal is not only the development of bioceramics, but also making a contribution to the welfare of human beings, in particular those with disease, through the development of bioceramics.

Finally, I would like to acknowledge the continuous encouragement of my wife Reiko, two daughters Sayaka and Mai and son Jin.

Tadashi Kokubo
Kasugai, Aichi

Part I

Fundamentals of bioceramics

1

The structure and mechanical properties of bone

J CURREY, University of York, UK

1.1 Introduction

Bone is an extremely hierarchical composite. This is one of the things that makes it extremely difficult to analyse properly. This chapter attempts to make some sense of bone's mechanical properties in the context of its structure. This structure has been fashioned by millions of generations of natural selection. Any advantageous change that can be produced incrementally, and whose advantage appears immediately, will almost certainly have been incorporated into the structure of bone. There is one thing that has happened over the last century or so that is quite new, and that is the existence of a large proportion of people who live so long after they have reproduced that natural selection is no longer interested in them. The orthopaedic trials of old age, such as osteoporosis and osteoarthritis, essentially do not exist as far as natural selection is concerned. This is a problem for workers who design drugs and procedures for old people. They are always working against the grain, as it were. I shall say virtually nothing about disease in this chapter, but it should always be kept in mind.

1.2 Structure

Bone is a composite of mineral, collagen, non-collagenous proteins, other organics and water. It is one of a set of vertebrate mineralised tissues that uses some version of calcium phosphate as their mineral. First there are the tissues that have as their principal organic component type I collagen. These are bone itself, dentine and enameloid. Enameloid is a structure covering the teeth of many fish, and seems (usually!) to be a very highly mineralised collagen-based tissue (Sasagawa *et al.*, 2006), rather like the petrodentine of the lungfish *Lepidosiren* (Currey and Abeysekera, 2003). Next there is calcified cartilage. This occurs in two main places. One is a temporary calcification of type II collagen-based cartilage. This occurs in the metaphyses

of growing long bones, and is soon eroded and replaced by bone. The other, which is much more interesting from the mechanical point of view, is in the permanent skeletal structures of well-mineralised type II collagen-based cartilage structures found almost entirely in the chondrichthyean fishes, the sharks, rays and so on (Summers, 2000). All these different types of mineralised collagens are an embarrassment to people who like neat classifications, but biology is like that (Donoghue *et al.*, 2006). Lastly there is enamel. This is very highly mineralised, and its distinguishing feature is that the organic component, such as it is, is not collagen at all.

Bone's organic material is about 90% by mass collagen type I. The other organics are various non-collagenous proteins and glycoproteins. The function of these other organics is the subject of intense research. Some of them have 'biological' functions; for instance, bone sialoprotein and bone morphogenetic protein have roles in the initiation and control of mineralisation and it has been suggested that a glycoprotein is necessary for the determination of apatite nucleation sites.

The bone mineral is the version of calcium phosphate called hydroxyapatite, whose unit cell contains $Ca_{10}(PO_4)_6(OH)_2$. The crystals are impure. In particular about 4–6% of carbonate replaces the phosphate, making the mineral more truly a carbonate apatite (dahllite). The shape of the crystal is to some extent in dispute, and partially this is because it is different in different tissues. It is certainly true that in one direction the crystals are small, of the order of 5 nm. They are about 40 nm wide, but sometimes they are hardly wider than 5 nm. What is less clear is the size of the crystals in their long direction (which is the *c*-axis of the crystal). They can be at least 50 nm long, and it is quite possible that they can join, or grow, until they are several hundreds of nanometres long (Ziv and Weiner, 1994). This small size in one direction may have, as we shall see, profound mechanical implications. One of the reasons that the habit and size of mineral crystal in bone are still not determined fully is that the crystals come in very small lumps, so small in fact that, as has frequently been pointed out (e.g. Boskey, 2001), much of the unit cell is actually sitting on the surface of the crystal. As a result preparation for examination is in danger of altering the size and chemical composition of the crystals. A discussion of biological apatites is given in Chapter 16.

One of the key problems of bone structure is how the mineral relates topographically to the collagen. This is, surprisingly, still a matter of considerable dispute. Some mineral crystals lie within the fibrils, somewhat disrupting them as they grow, and some lie between the crystals. The crystals lying within the fibrils are oriented with their long (*c*) axes along the same axis as that of the collagen fibril. Those lying between the fibrils are not constrained in this way. It seems that the mineral lying within the fibrils first nucleates in the 'Hodge-Petruska' gaps, particularly the 'e' band. It then

coalesces and extends along the long axis of the collagen fibrils, disrupting them to some extent (Landis *et al.*, 1993, 1996).

Some people, for instance Weiner *et al.* (1999), Jäger and Fratzl (2000) and Gao *et al.* (2003), think that most of the crystals are within the fibrils. Others, for instance Pidaparti *et al.* (1996) (using best fit to acoustic measurements) and Fritsch and Hellmich (2007), think they mostly lie outside the collagen, or rather that the mineral and collagen form interpenetrating phases. Sasaki *et al.* (2002) suppose that about three-quarters of the mineral lies outside the collagen, and Hellmich and Ulm (2002) suppose that almost 100% of the mineral lies outside the collagen. It is not possible to reconcile these ideas, and no doubt the matter will be resolved soon. Certainly, the methods that involve direct visualisation of bone would suggest that much of the mineral is within the fibrils. However, when it comes to modelling bone's stiffness and fracture, it is important that we know the truth!

Bone is a classic hierarchical structure, with different relationships between structures becoming important at different levels. These levels can be briefly characterised as:

- mineral + collagen;
- fibrils;
- fibres;
- lamellar vs. woven bone;
- fibrolamellar vs. Haversian bone;
- compact vs. cancellous bone;
- whole bones.

These levels are partially shown in Table 1.1, along with some other structures (such as osteocyte lacunae).

I should mention (parenthetically, as a zoologist) that human bone is rather unusual among the whole set of bone materials that exist. First, most species of vertebrates do not have any bone cells lying within the hard tissue at all. Most species of vertebrates are bony fish, and the great majority of these have acellular bone. Coming to more familiar animals, such as birds and mammals, humans are unusual in having such extensive Haversian (secondary) remodelling of the tissue. This is partially because humans live on average a long time, so there is time for remodelling to occur, but also it seems to be a function of our rather large size, and also other innate characteristics. One often sees in the literature statements to the effect that the 'The secondary osteone (Haversian system) is the primary unit of bone.' This is not true at all of mouse-sized birds and mammals, which have no remodelling, and not even true of mammals in general. Even in humans, because of bone's hierarchical construction, it is not true, because there is no level at which it is correct to talk about the 'primary unit'.

Table 1.1 Table showing the main morphological features of bone

Woven bone	Parallel-fibred bone	Lamellar bone
Fibrils 0.1–0.3 μm wide, arranged in a felt	Intermediate	Fibrils 2–3 μm wide in sheets (lamellae) 2–10 μm thick (Fig. 1.1)
Bone cells (osteocytes)		
Roughly isodiametric ca 20 μm in diameter		Oblate spheroids 5:1 greatest to least axes. Major axis about 20 μm long
Connected to each other and, indirectly, to blood channels by cell processes in tubes (canaliculi) 0.2–0.3 μm wide. About 50–100 canaliculi per cell		
Four types of bone microscopically		
Lamellar	Woven	Fibrolamellar	Secondary osteones
In large lumps in reptiles In circumferential lamellae in mammals and birds	In large lumps in young animals and in fracture calluses	Alternating sheets of lamellar and woven bone, with 2-dimensional sheets of blood vessels. About 200 μm between repeats	(Haversian systems) Cylinders of lamellar bone. Solid save central tube for blood vessels. About 200 μm in diameter
Primary and secondary (Figs 1.1 and 1.2)	*Primary*	*Primary* (Fig. 1.2)	*Secondary* (Fig. 1.3)
Two types of bone macroscopically			
Compact bone		Cancellous (trabecular) bone	
Solid, only porosity for canaliculi, osteocyte lacunae, blood channels and erosion cavities		Porosity visible to the naked eye. Rods and plates of lamellar bone. Multiply connected, never forming closed cells (Fig. 1.4)	

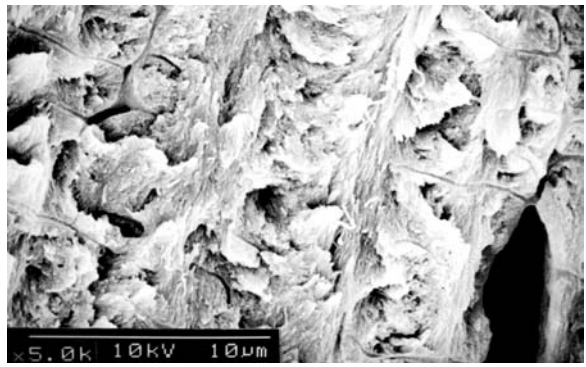

1.1 Scanning electron micrograph of fracture surface of lamellar bone. The lamellae are in rotating sheets that repeat their orientation about every 8μm. The large cavity (lacuna) would contain an osteocyte in life. Note the thin half-tubes running WNW to ESE. These are fractured 'canaliculi', the tubes that allow the osteocytes to communicate with each other. There are about 50–100 canaliculi per lacuna. The fact that the fracture surface has run long several of them suggests that they are brittle, possibly by having hypermineralised sheaths, like dentinal tubules.

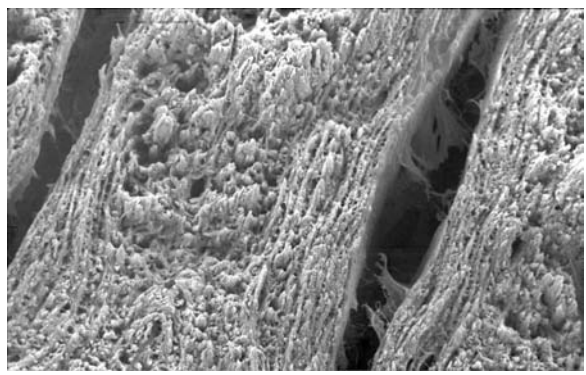

1.2 Scanning electron micrograph of fracture surface of fibrolamellar bone. The fracture surface is normal to the long axis of the whole bone. The repeat distance is about 200μm. The large cavities are spaces for blood vessel networks. Each blood vessel network is flanked by lamellar bone, which in turn has more randomly arranged woven bone between it and the next lamellar bone.

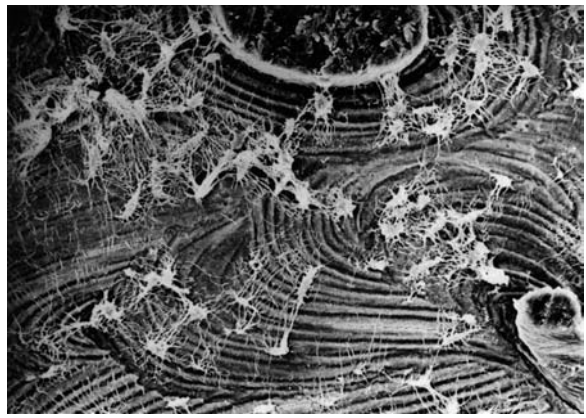

1.3 Scanning electron micrograph of Haversian (secondarily remodelled) bone. The bone was infiltrated with resin before being polished and the bone etched away a little. The resin was not etched, allowing one to see the osteocyte lacunae and their connecting canaliculi. Note how different layers of the lamellar bone etch differentially. Width of field of view about 200μm. (Courtesy Dr Peter Atkinson)

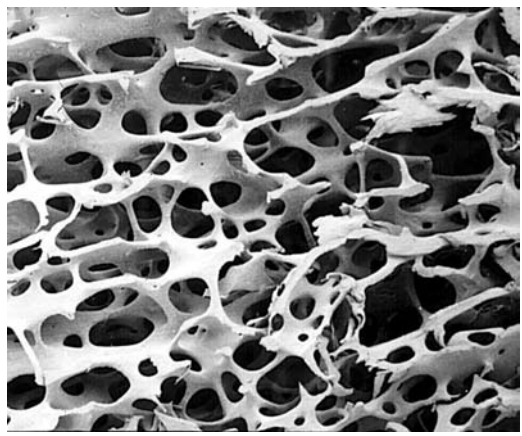

1.4 Cancellous bone. Both the bone and the spaces (filled in life with marrow fat) are interconnected.

1.3 Mechanical properties

Because the mechanical properties of bone are so important, and because this matter is not dealt with elsewhere, I discuss here a couple of mechanical concepts, particularly as they relate to relatively stiff materials.

1.3.1 Stress and strain

One must distinguish 'stress' and 'strain' since they are totally different concepts. *Stress* is the intensity of force. If one pushes or pulls on a structure with a known force, this in itself gives no idea as to the intensity of the force, which must be obtained by dividing by the cross-sectional area. This is true for simple pushes and pulls of uniform-shaped structures; if the structure is being twisted or bent, or has a complex shape, then determining stress in it becomes more complicated.

Strain is a proportional change in length. If a rod is pulled so that its length is increased by 1% then it is said to have undergone a strain of +0.01. If it is shortened by 1% then the strain is –0.01. (There is a tendency in the literature these days to use the word 'microstrain'. This is strain multiplied by a million, so the strains of + and –0.01 would be + and –10000. Personally I dislike this usage, because it leaves redundant zeros at the end of the number.) Again, when the structures are of complicated shape, or loaded in ways other than pure pulling or pushing, then the strain situation becomes very complicated. For instance there are 'shear' strains that refer to changes in shape rather than changes in length. Nevertheless if one remembers that stress is an intensity of force, and strain is a proportional change in length one will not go far wrong. Strains, being proportions, are pure numbers, while stresses are measured in newtons per square metre, or pascals (Pa). This is a very small stress, and usually is multiplied by a million to give megapascals (MPa) or one thousand million to give gigapascals (GPa). These values do *not* have redundant zeros at the end.

1.3.2 Mechanical properties of compact bone

Figure 1.5 shows a load–deformation curve for a specimen of hydrated bone loaded in tension. First there is a rising part, nearly straight, in which load is proportional to deformation. At the 'yield' point the situation changes, and the curve becomes much flatter. There is a large increase in deformation with little increase in load. Then the specimen breaks. This load–deformation curve can be normalised – turned into a stress–strain curve – by dividing the force by the cross-sectional area of the specimen, and the

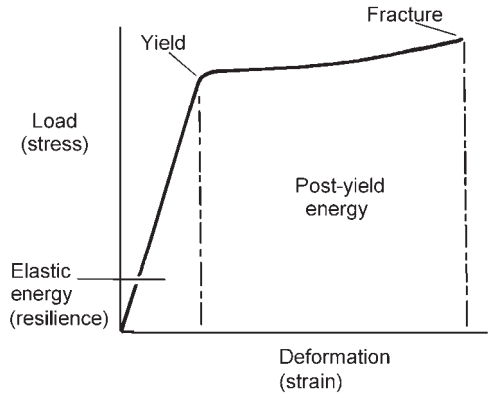

1.5 Load–deformation curve of a specimen of compact bone loaded in tension.

deformation by the original length of the specimen. This normalisation allows one to talk in general about bone behaviour without being very concerned with the specimen size (although, in fact, larger specimens, and bones, are probably rather weaker, after normalisation for size has taken place (Taylor and Kuiper, 2001), though some disagree, saying the effect is in the opposite direction (Danova *et al.*, 2003)). The slope of the rising, straight part of the curve is stress divided by strain, and is the 'Young's modulus of elasticity', that is the stiffness of the bone material. In compact bone it has, very roughly, a value of 15 GPa. The place where the slope changes direction abruptly is called the 'yield' point or region. At the yield point the stress is very roughly 120 MPa, and the strain is very roughly 0.008. After this point irrecoverable damage is being done to the specimen. However, the work under the stress–strain curve after the yield point is useful *in extremis* because work must be done on the specimen to bring it to the final stress or strain, and so the specimen, or rather the bone from which the specimen comes, may be able to withstand a blow although it may be damaged in the process. The total area under the stress–strain curve is a rough measure of the 'toughness' of the material. The area under the part before the yield point is called the 'resilience' of the material, and is the energy that can be absorbed without the specimen being damaged.

So, from a tensile test of compact bone one can obtain a number of important properties of the bone material:

- Young's modulus of elasticity, the stiffness;
- resilience;
- yield stress and strain;

- fracture stress (the strength of the bone) and strain;
- work absorbed by the bone before fracture.

Note that one often talks of the stiffness and strength of a *whole bone*, without regard to the actual modulus of elasticity or fracture strength. Stiffness of a whole bone depends, of course, on how big the bone is. A big bone will require a larger load to produce the same proportional deformation, and so it is stiffer than a small bone. One must therefore keep the distinction between stiffness and strength of a whole bone, and of the bone material, clear. Usually the context makes it clear what is being talked about. Toughness, as given, say, by the area under the stress–strain curve of a smooth specimen, is useful for many purposes, but engineers are usually interested in the effects of cracks in a specimen. Toughness of a material is probably best described as the ability to make the increase in length of potentially dangerous cracks difficult. The opposite of toughness is brittleness. Different bone materials, as we shall see, have different 'notch sensitivities'. This is how much the energy absorbed is reduced by the presence of a crack or notch. A tough material has less notch sensitivity than a brittle one. The whole science of fracture mechanics has grown up to quantify and predict such brittle vs. tough behaviour. Various measures are used, with varying success, that attempt to remove the effect of specimen shape and produce a value of toughness that tells one about the behaviour of the material, rather than the specimen. I shall barely discuss them here. Finally, there is fatigue. A bone may eventually fail when it is loaded many times to a stress that it can bear perfectly well if loaded to it only a few times. This behaviour is of great importance clinically because active people load their bones many times each day and, if the loads imposed produce strains anywhere near the yield strain, a fatigue crack may initiate and start to travel. Fatigue fractures are important in people who load their bones extremely or unwontedly, such as athletes and military recruits.

Table 1.2 gives some representative values of the mechanical properties of compact bone loaded along the length of the bone. The first, modal, value given is that of 'ordinary' bone, such as one might find in the long bone of a bovine or human. After it there may be values showing the range of values found when more 'unusual' bones are considered. This is a very rough and ready table, but gives some guidance as to properties and their potential range.

1.3.3 The importance of mineral content for the mechanical properties of compact bone

Bone at some level can be considered to be little more than tendon stiffened by mineral, and it is of course not surprising that mineral content has a

Table 1.2 Some values of mechanical properties of bone

Property	Modal value[a]	Upper limit[b]	Lower limit[c]	Comments
Young's modulus of elasticity (*E*)	15 GPa	45 GPa *densirostris* rostrum	6 GPa Deer antler	Probably same in tension, compression and bending
Tensile yield Stress	120 MPa		10 MPa Ear bones, *densirostris*	Higher in compression
Tensile strength	150 MPa	300 MPa Some deer antler	15 MPa Ear bones, *densirostris*	
Ultimate tensile strain	0.03	0.12 Deer antler	0.002 Ear bones	
Compressive strength	250 MPa			
Bending strength	250 MPa		30 MPa Ear bone	
Fatigue life at 0–100 MPa tension	1000		200 Antler	Cycles for a 10% reduction in modulus

This is for orientation purposes only, and original work should be consulted for definitive values.
[a] This is the value near which most 'ordinary' bone would lie.
[b] 'Upper limit' Approximately the largest value for the property that has been recorded.
[c] 'Lower limit' approximately the lowest value for the property that has been reported.
All values (except fatigue) are for quasi-static tests, that is at low strain rates.

strong effect on Young's modulus. Less obvious, perhaps, is the deleterious effect that mineral has on bone's toughness properties.

For dry bone, mineral ≈ (total mass – organics). Usually we do not know the proportion of other organics present apart from collagen. The collagen is by far the major component.

Figure 1.6 is a ternary diagram showing the relative amounts, by mass, of mineral, collagen and water in various wet vertebrate bony tissues. The points fall more or less in a line between least highly mineralised bones and most highly mineralised; water is reduced somewhat more rapidly than collagen. The variation is considerable. For instance deer antler is about 35% collagen, 45% mineral and 20% water; whereas whale ear

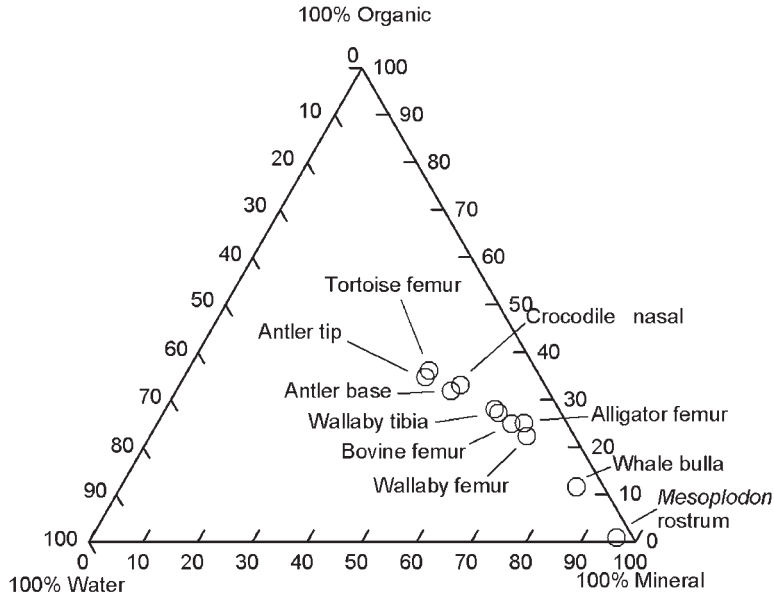

1.6 Ternary diagram of the composition of wet compact bone from a number of sources.

bone is about 85% mineral (de Buffrénil *et al.*, 2004) and, even more extreme, the rostrum of the toothed whale *Mesoplodon densirostris* is almost entirely mineral, though ear bone and rostrum are still bone, having some collagen (Rogers and Zioupos, 1999; Zioupos *et al.*, 1997; Zylberberg *et al.*, 1998).

Figures 1.7 and 1.8 (Currey, 2004), referring to *dry* weights, show Young's modulus (stiffness) and work of fracture (a good measure of toughness) as a function of mineral content. Work of fracture is the work done in fracturing a specimen that has been notched in a way so that the crack travels slowly, and not catastrophically. It more truly represents the work done in creating the new surfaces than the work under a load–deformation curve (Tattersall and Tappin, 1966). As mineral increases so stiffness increases disproportionately, but work of fracture decreases even more sharply. The mineral content has a profound effect on pre- and post-yield mechanical properties. Of course, it has been known for many years that it is very difficult to produce materials with both high toughness and high stiffness (Kelly and Macmillan, 1987) and this is seen very starkly in bone. An interesting feature of the amount of mineral in mineralised tissues is that there seems to be a gap in the mineral between pure organic collagen-based

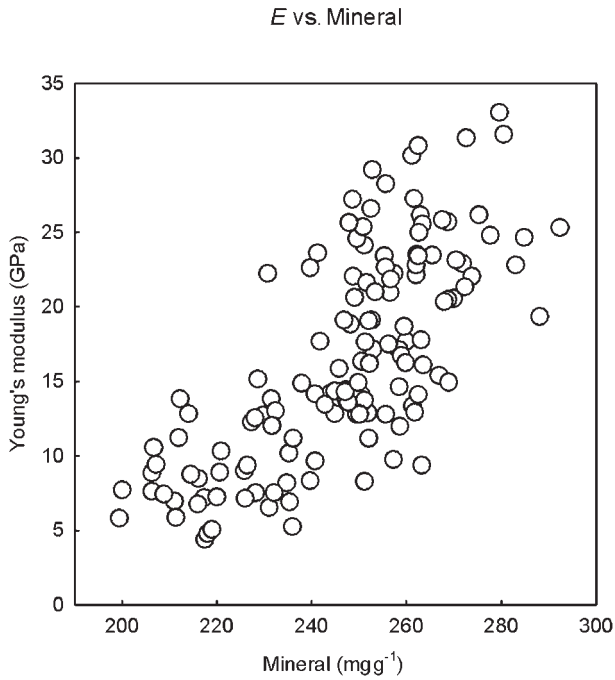

1.7 Young's modulus of wet specimens as a function of mineral content of dry bone. The specimens are taken from a variety of sources. The relationship is messy, though clear. Porosity has a negative effect on Young's modulus, and using both mineral and porosity as explanatory variables produces a tighter cloud of points (not shown).

materials (such as cartilage and tendon) and collagen-based mineralised tissues such as bone. Figure 1.9 (Currey *et al.*, 2004) shows the impact energy absorption and notch sensitivity (the reduction in impact energy induced by the presence of a notch) of various mammalian mineralised bony tissues. It can be seen that as the mineral decreases the impact energy absorption increases, and the notch sensitivity decreases. Indeed, antler bone cannot be shown on this diagram, because it was virtually impossible to break wet laboratory specimens in impact. Since antler bone, the least mineralised of all known mammalian mineralised tissues, seems to be notch-insensitive in impact, no adaptive purpose would be served by having mineralised tissues of a lower mineralisation than antler. It would not be any better in impact, yet would have a lower stiffness. This may explain the cut-off in mineralisation seen in mammals.

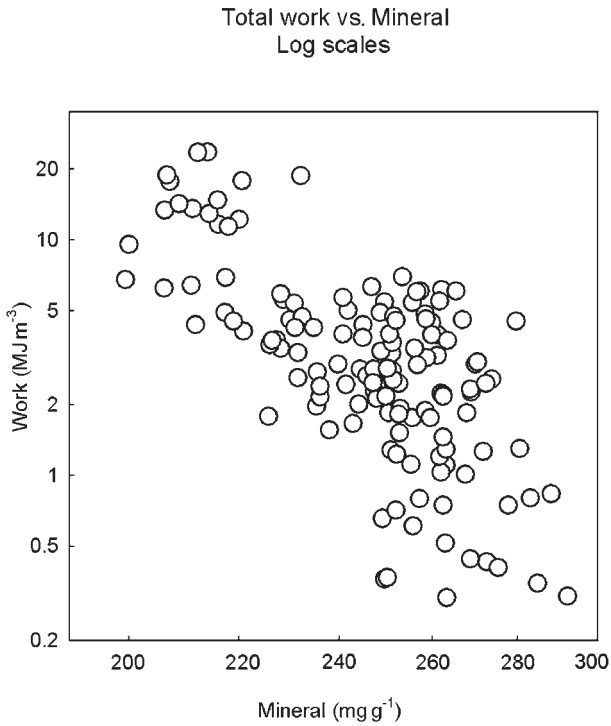

1.8 Total work under the tensile-stress–strain curve of compact bone as a function of mineral content. The specimens are the same specimens as shown in Fig. 1.7. Note log scales on the abscissa and, particularly, the ordinate. There is a marked decline of work as the mineral content increases. (Porosity has virtually no effect on work.)

1.3.4 The mode of interaction of mineral and the water and organic components of bone

There are many ways in which collagen and the hydroxyapatite-like mineral *could* interact. Walsh and Guzelsu wrote that the combined electrostatic interactions between cationic and anionic sites would be powerful, and that even direct bond formation between the two types of material could occur. Various other methods of bonding have been proposed (Walsh and Guzelsu 1994). Wilson *et al.* (2006) argue, with some experimental evidence, that water plays an important role, both in stabilising the imperfect lattice of the hydroxyapatite, and also in possibly coupling the mineral and the bone. Suffice it to say that tight bonding between the collagen and apatite is possible, and most workers in deriving models for the behaviour of bone assume a perfect bond between the two types of material.

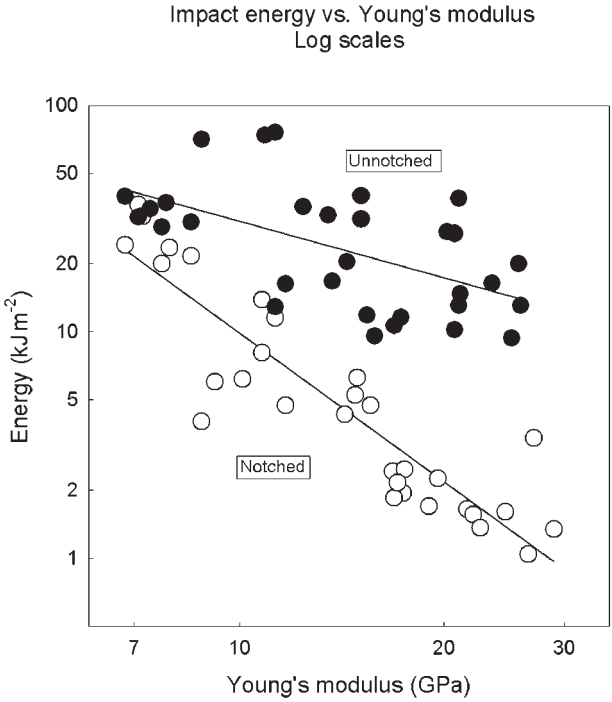

1.9 Impact energy absorption of compact bone specimens from a variety of sources. Filled circles: un-notched specimens. Open circles: notched specimens. The distance between the two lines is a measure of the notch sensitivity of the bone. Antler would be slightly off to the left of the diagram, about where the two regression lines would meet, but values are not shown, because many antler specimens would not break in impact, whether un-notched or notched. The straight solid slanting lines are the regression lines.

1.3.5 Role of mineral in stiffness

Because mineral is so much stiffer than collagen and water, it is not surprising that the modulus of elasticity increases with mineralisation. Unfortunately, despite many attempts, there seem to be no good analytical accounts of why the stiffness increases at the rate it does. The very early attempt of Katz (1971) showed that the stiffness of bone lay between that predicted by the so-called Reuss and Voigt models, but these bounds were so far apart that this was not very helpful. Somewhat more recent attempts by, for example, Sasaki *et al.* (1991) and Wagner and Weiner (1992) can predict the stiffness in one direction, but fail to predict properly the mechanical anisotropy of bone – the extent to which its stiffness is different when it is loaded in

different directions. Probably the reasons for the lack of analytical solutions are (1) that the direction of long axis of the mineral crystals varies markedly throughout the bone, over a few micrometres, and (2) that we are really ignorant of the aspect ratio of the mineral crystals – the ratio of the greatest to the least dimension. These two variables are very important in any equation relating mineral volume fraction to Young's modulus of elasticity (Jäger and Fratzl, 2000). Fritsch and Hellmich (2007), on the other hand, claim that most mineral is outside of the collagen and oriented in every direction, and can therefore be modelled as isotropic spherical objects in a mechanically anisotropic collagen matrix. They propose a micromechanical model of bone in which the anisotropy is predicted well, and in which there are different anisotropies at different length scales. It is difficult to know what to make of such a (to me) counterintuitive treatment of mineral, but much of their modelling does seem to predict values close to those produced by ultrasonic testing.

What has been shown is that when bone is strained, the strain in the mineral is less than the overall strain of the specimen. This is to be expected, of course, but it is good to see the common-sense expectation borne out experimentally. The ratio of whole-tissue strain to collagen fibril strain to mineral particle strain in wet bone was found by Gupta *et al.* (2006) to be about 12:5:2. Similar results, albeit on relatively dry specimens, were found by Fujisaki and Tadano (2007).

1.3.6 Role of mineral in yield and fracture – what yields, what fractures?

The effects of changes of mineralisation on fracture properties are even more obscure than their effect on stiffness. What happens when bone yields (if it yields, rather than breaking completely brittly) is that microfractures develop. These are a myriad of initially tiny fractures, or at least linear 'disturbances' of the bone (Burr *et al.*, 1985; Zioupos, 2001). They can be very short, say 5 μm long (Fig. 1.10; Reilly, 2000), though many workers concentrate on larger, more obvious cracks, say 100 μm long. The critical point about them is that these cracks initiate, and therefore increase, the compliance of the specimen, but do not increase in length if the load is increased. The work done on extending the specimen is used up in multiplying the number of microfractures, and thereby increasing the compliance of the specimen. Eventually some fuse, become really long and dangerous, and the specimen breaks in two. In bone of greater mineralisation the process of initiation of microfractures is inhibited, and the bone becomes progressively more brittle. One can explain this by suggesting that as the mineralisation increases there is a tendency for the mineral crystals to join up to form larger lumps, which are weaker than small lumps. Gao *et al.* (2003),

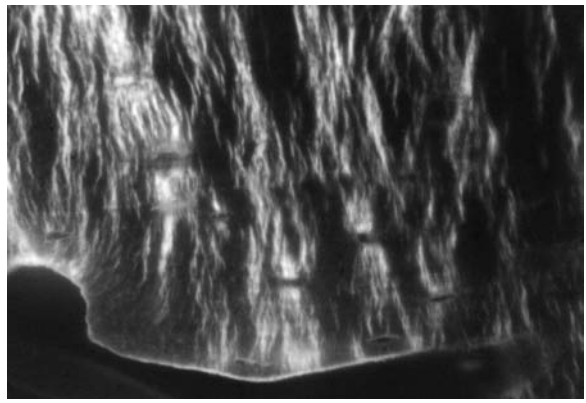

1.10 Confocal microscope picture of compact bone loaded in tension (horizontally in this picture). The dark horizontally elongated spots are the osteocyte lacunae. The dark band at the bottom is a blood vessel. Microdamage, mainly originating at the osteocyte lacunae, runs roughly normal to the direction of load. The damage (which is not of patent cracks, because the specimen still has considerable stiffness, and does not fall apart) has lengths as small as 5μm. (Courtesy Dr Gwen Reilly)

quantifying and deepening an earlier suggestion by myself (Currey, 1984), point out that very small sizes of the mineral crystals are too small to allow them to develop fatal 'Griffith' flaws, and therefore they will be very strong, and that any lack of cohesion will either be in the organic material, or at the organic–mineral interface. Gao *et al.* also point out that there is an optimum aspect ratio of the mineral crystals, and this relates to the organic content. Mother of pearl, in mollusc shell, has about 3% organic material and a rather low aspect ratio, about 10, while bone has a high organic content, and a much higher aspect ratio, possibly as high as 30–40 in well-developed bone. These values for bone and for mother of pearl will tend to make the mineral and the organic material fracture at the same stress, the optimum situation. Ballarini *et al.* (2005) on the other hand consider that the small size of the crystals is not important, that small crystals break, and that the strength of bone depends on other features that prevent catastrophic failure.

There have been a number of attempts from the examination of fracture surfaces to determine whether bone breaks in the mineral, the organic material, or at the interface between them. This work usually involves examination by high-resolution scanning electron microscopy or by scanning probe nanomicroscopy. I must admit I find the pictures much less convincing than do the authors, and in my opinion the matter is as yet unresolved.

Tai *et al.* (2006) using a completely different approach, suggest that in compression the granular crystals interact by friction, and because this mechanism is not available in tension, this difference accounts for bone's lower strength in tension. I do not find this very convincing, but I mention it because it is so different from the approach of most people.

1.3.7 Mechanical importance of remodelling

The bone of many vertebrates (though not most bony fishes, which make up the majority of vertebrate species) undergoes considerable modelling and remodelling. Conventionally, 'modelling' refers to the changing of the external form of the bone, either by the addition or removal of bone from external surfaces. The function of modelling is fairly clear: it adapts the bone's shape to the loads falling on it. Roughly, bone is added where strains are higher, and removed where the strains are lower. How this is brought about is extremely clinically important, still unclear and anyhow beyond the scope of this chapter. Conventionally, internal 'remodelling' refers to the production of new bone within the body of old bone by the formation, within cavities carved out by osteoclasts, of cylindrical secondary osteones, or Haversian systems as they are often called. Internal remodelling has many functions attributed to it – taking out microcracks, improving the grain of the bone, preventing bone from becoming too highly mineralised – and so on (Currey, 2002, pp. 368–377) and there is no consensus yet as to the cause or causes, although taking out microcracks is certainly one function.

For our purposes it is sufficient to note that newly laid down bone is less highly mineralised than older bone. The process of mineralisation in bone is rapid at first but then slows, approaching its final state asymptotically. This is because as the bone becomes mineralised the rate of diffusion of ions through the tissue of the bone inevitably declines. As a result secondary osteones are more highly mineralised near their core, where the blood channel is, and are less highly mineralised at the periphery. There is then a sudden upwards jump in mineralisation as one passes into the 'interstitial lamellae' which are pre-existing and therefore necessarily older than the secondary osteone. This variation in mineralisation is reflected in the elastic properties as shown by nanoindentation (Rho *et al.*, 1999). Whether these mechanical heterogeneities will make the bone stronger or weaker is unclear. Probably, by introducing strain concentrations, they will make the initiation of cracks easier. However, the perimeter of the secondary osteone, where there is a 'cement sheath' of different properties from the rest of the bone, seems to be a line of weakness, which breaks up as the crack approaches, and will make it difficult for cracks to spread into, and therefore through, the secondary osteone (Yeni and Norman, 2000).

1.3.8 Cancellous bone

Cancellous bone is bone with obvious holes in it; these are visible to the naked eye (Fig. 1.4). The bone does not form closed cells, so the bone, and the marrow, are always interconnected with themselves. The bone material making the cancellous bone is similar in its general constitution and histology to lamellar bone. It seems, nevertheless, to have a somewhat lower mineral content and therefore lower Young's modulus and strength than ordinary bone (Guo and Goldstein, 1997; Bayraktar *et al.*, 2004). Some fairly recent estimates, for instance by Bini *et al.* (2002) and suggesting values for Young's moduli as low as 1.9 GPa, cannot be right because in my laboratory we have found values for Young's modulus for *whole blocks* of cancellous bone, holes and all, of 6 GPa, implying that the material modulus must be considerably higher (Hodgskinson and Currey, 1992). However, the difference in the mechanical properties between compact bone and cancellous bone is determined much more by the amount of bone per unit volume, rather than the precise material properties of the cancellous bone itself. It is a general rule that Young's modulus and compressive strength of the cancellous structure (not the bony material) are proportional roughly to (apparent density)^2, where apparent density is the volume of bone per unit of tissue overall (Rice *et al.*, 1988). Since cancellous bone usually has an apparent density of about 10–20%, this implies that, compared with compact bone, it has a stiffness and strength of about 1–4%. Any difference in material properties is likely to have a trivial effect compared with these differences in apparent density (Day *et al.*, 2004). The anisotropy of the arrangement of the bony struts is also important. If the struts are oriented mainly in one direction, the bone will be stiffer and stronger in that direction than in directions at large angles to it.

Like compact bone cancellous bone undergoes modelling/remodelling, though because the trabeculae and sheets are rather thin, it is not often that complete secondary osteones are formed. Instead one often finds hemi-osteones, where a gutter is scooped out of the bone by osteoclasts, and then filled in with new bone. This all means that the difference between modelling and remodelling is not as clear-cut as it is in compact bone.

1.3.9 Whole bones, interaction of compact and cancellous bone

The properties of a whole bone, which in the end is what is important for the animal, are produced by the marriage of the *material properties* of the bone and its *architecture*; that is, how the material is arranged, the thickness of the walls of the bone, its second moment of area and so on. Bones are

of such complex shapes that virtually no successful attempts have been made to characterise the mechanical behaviour of whole bones. Nowadays one can get quite detailed data on the architecture of whole bones by the use of micro-CT. Translating this into the behaviour of the whole bone requires the use of computer-solved finite element models. These too are becoming rapidly more powerful, being able to take into account anisotropy and non-linear effects. Unfortunately they must also be fed with values for Young's modulus in order to perform, and usually this is what is lacking. Young's modulus, even of compact bone, varies considerably along the length of a single bone (Kim and Walsh, 1992). The usually severely anisotropic Young's modulus of cancellous bone structure also varies considerably over quite small distances, and is therefore very difficult to incorporate into a finite element model.

Another problem with using finite element models to predict the behaviour of whole bones is that the mechanical behaviour of the junction between the cancellous and compact bone is very poorly understood. In places where the change from compact to cancellous bone is abrupt, such as in sandwich bones like the iliac crests, this may not be too much of a problem. However, in other places, such as in the transition from cancellous bone with a thin cortex of compact bone to simple compact bone, such as occurs in the femoral shaft, the problem is very considerable. The bone becomes more and more cancellous (or less and less compact) with distance, and one cannot tell the finite element program what the modulus is, one has to impose a *material* Young's modulus, and tell the program to work out the overall *structural* modulus itself! Clearly, the possibility of the model not imitating life closely are considerable.

1.4 Some clinical matters

Differences in the amount of mineralisation, and in the shape and size of the mineral crystals may have clinical importance, and I mention three examples here.

1.4.1 Osteogenesis imperfecta

Osteogenesis imperfecta (OI) is a case study in how difficult it is to separate the effects of collagen changes from mineral changes in their effect on mechanical properties. Osteogenesis imperfecta (brittle bone disease) is a heritable type I collagen disorder which results in weak bones, though whether they are actually more *brittle* is less clear. The mouse osteogenesis imperfecta model (oim) which seems to have similar phenotype to severe OI in humans is frequently studied. In these mice, post-yield deformation is reduced, and the fracture surface is smoother, as is characteristic of brittle

fracture (Jepsen *et al.*, 1996). However, care is needed, because the effect may be partially indirect. The collagen is obviously seriously deranged, this itself leads to a derangement of mineral size and shape; the mineral crystals are more variable in size and orientation (Grabner *et al.*, 2001). Furthermore, the ratio of woven to lamellar bone increases (Jepsen *et al.*, 1996), and the mineral/organic ratio increases, leading to a greater microhardness (Grabner *et al.*, 2001). An increase in the mineral/organic ratio in normal bones reduces the post-yield strain, and therefore in itself will make the bone more brittle.

1.4.2 Hypermineralisation

Hypermineralisation is a frequent feature of older people's bones. Small volumes, a few hundreds of micrometres across, become extremely highly mineralised (Vajda and Bloebaum, 1999). This is dangerous for two reasons. One is that when the bone is loaded, the large difference in modulus will produce stress concentrations in the vicinity of the hypermineralised volume, and in the volume itself. Since the hypermineralised tissue is likely to be brittle, it may well crack under loads under which ordinary tissue would not. The other dangerous feature is that any cracks that do form in the hypermineralised volume are likely to spread as far as the edges because, unlike ordinary bone, which has some toughness, it will be brittle. So, not only may there be one or more cracks or so in the volume, but the length of any crack is likely to be *much* longer than the ordinary microcracks that form in bone, and may well exceed the Griffith criterion for danger. As mentioned above, the mineral in ordinary bone is in very small lumps, and therefore may be resistant to fracture.

1.4.3 Bisphosphonates

The considerable use of bisphosphonate drugs in the treatment of osteoporosis has led to worries about the increased danger of brittle fracture in the skeleton. Bisphosphonates interfere with osteoclasts, and prevent the erosion of cavities, and so of bone turnover. There are two problems here. One is that the bone is ageing unnaturally, because it is not replaced. This may lead to some degree of hypermineralisation, with concomitant reduced toughness. The other problem is that any microcracks that form will not be removed by remodelling. It must be said that it is far from clear as to whether these effects actually occur to an extent that is dangerous (e.g. Mashiba *et al.*, 2005; Zoehrer *et al.*, 2006). (Bisphosphonates certainly have a dramatic effect in reducing fractures, at least in the early years of their use. That is, of course, why they are used.) One gets the feeling that people who study this phenomenon are

surprised that the good effect of bisphosphonates in preventing bone loss is not matched by its bad effect in allowing the accumulation of microdamage.

1.5 Future trends

Increased computer speeds and refinements of many techniques mean that in ten years' time our ability to examine bone in detail will be greatly in advance of our present ability. Finite element modelling will be able to cope with anisotropy and non-linearity much more than now and micro-computer tomography (CT) will allow very refined imaging of cancellous bone. Nano-microscopy, Fourier transform infrared (FTIR), Raman spectroscopy and other spectroscopic methods will all be refined to give us a much better idea of, for instance, the separate mechanical behaviour of the organic and mineral parts of bone. Of course, there is, for many of these techniques, the danger that the power of the method will outrun our ability to interpret the results sensibly. This happened in the early days of finite element modelling and, indeed, sometimes still happens today! Another area in which we can expect great advances (and lots of dubious papers) is in the relationship between genetics and mechanical properties. Exploring this relationship has hardly begun, but will soon become very important. In such multidisciplinary efforts, the participants – biologists, geneticists, engineers, physicists and clinicians – should make a real and painful effort to *understand* what the others are saying (painful because of the intellectual difficulty involved, and also because of the necessity of altering one's mind set) so that unwarranted assumptions are challenged.

1.6 Sources of further information and advice

A comprehensive book on bone's mechanical properties, though it has little to say on fracture mechanics, is edited by Cowin (2001). My own more idiosyncratic book on bone (Currey, 2002) may be of interest. There have, of course, been advances since, but the literature is extremely diffuse. This can be seen by glancing at the literature list in my short list of references; the 49 non-book references come from 26 different journals, several of them not listed below. Journals that particularly often have articles on bone mechanical properties are: *Journal of Biomechanics, Journal of Biomechanical Engineering, Bone, Journal of Bone and Mineral Research, Journal of Orthopaedic Research, Biomaterials, Journal of Experimental Biology, Journal of Biomedical Materials Research* and *Calcified Tissue International,* but there are many many others that have occasional articles. No journal has a large proportion of all 'bone mechanical' articles

published. Many journals such as *Engineering Fracture Mechanics* and *Journal of Materials Science,* which at first sight seem nothing to do with bone, often have articles that would be interesting to people who are concerned with bone mechanics. Articles on the structure of bone are to be found in many of those journals listed above, and also in *Anatomical Record, Journal of Anatomy, Journal of Structural Biology,* and many others.

Many years ago, in 1980, Julian Vincent and I organised a Conference on 'Mechanical Properties of Biological Materials'. We wrote later that what struck us was that biologists, as well as their frequent, acknowledged, lack of mathematics and physics, seemed intent on re-inventing the mechanical wheel. On the other hand, the materials scientists, the other group present, were 'vincibly ignorant' of the extraordinary rich diversity of biology. Admittedly bone is a less broad field than biology, but this is still to a large extent the case. It is almost impossible these days to do good research without involving people from several disciplines including, may I say, someone who is statistically inclined!

1.7 References

Ballarini R, Kayacan R, Ulm F-J, Belytschko T and Heuer A H (2005), 'Biological structures mitigate catastrophic fracture through various strategies', *Int J Fracture*, **135**, 187–197.

Bayrakter H H, Morgan E F, Niebur G L, Grayson E, Morris G E, Wong E K and Keaveny T M (2004), 'Comparison of the elastic and yield properties of human femoral trabecular and cortical bone tissue', *J Biomech*, **37**, 27–35.

Bini F, Marinozzi A, Marinozzi F and Patanè F (2002), 'Microtensile measurements of single trabeculae stiffness in human femur', *J Biomech*, **35**, 1515–1519.

Boskey A L (2001), 'Bone mineralization', in Cowin S C, *Bone Mechanics Handbook*, Boca Raton, CRC Press, 5-1–5-33.

de Buffrénil V, Dabin W and Zylberberg L (2004), 'Histology and growth of the cetacean petro-tympanic bone complex', *J Zool Lond*, **262**, 371–381.

Burr D B, Martin R B, Schaffler M B and Radin E L (1985), 'Bone remodelling in response to *in vivo* fatigue microdamage', *J Biomech*, **18**, 189–200.

Cowin S C (2001), *Bone Mechanics Handbook*, Boca Raton, CRC Press.

Currey J (1984), *The Mechanical Adaptations of Bones*, Princeton, NJ, Princeton University Press, 56–58.

Currey J D (2002), *Bones: Structure and Mechanics*, Princeton, NJ, Princeton University Press.

Currey J D (2004), 'Incompatible mechanical properties in compact bone', *J Theoret Biol*, **231**, 569–580

Currey J D and Abeysekera R M (2003), 'The microhardness and fracture surface of the petrodentine of *Lepidosiren* (Dipnoi), and of other mineralised tissues', *Arch Oral Biol*, **48**, 439–447.

Currey J D, Brear K and Zioupos P (2004), 'Notch sensitivity of mammalian mineralized tissues in impact' *Proc Roy Soc London*, **271B**, 517–522.

Danova N A, Colopy S A, Radtke C L, Kalscheur V L, Markel M D, Vanderby R Jr, McCabe R P, Escarcega A J and Muir P (2003), 'Degradation of bone structural properties by accumulation and coalescence of microcracks', *Bone*, **33**, 197–205

Day J S, Ding M, Bednarz P, van der Linden J C, Mashiba T, Hirano T, Johnston C C, Burr D B, Hvid I, Sumner D R and Weinans H (2004), 'Bisphosphonate treatment affects trabecular bone apparent modulus through micro-architecture rather than matrix properties', *J Orth Res*, **22**, 465–471.

Donoghue P C J, Sansom I J and Downs J P (2006), 'Early evolution of vertebrate skeletal tissues and cellular interactions, and the canalization of skeletal development', *J Exp Zool*, **306B**, 278–294.

Fritsch A and Hellmich C (2007), ' "Universal" microstructural patterns in cortical and trabecular extracellular and extravascular bone materials: micromechanics-based prediction of anisotropic elasticity', *J Theoret Biol*, **244**, 597–620.

Fujisaki K and Tadano S (2007), 'Relationship between bone tissue strain and lattice strain of HAp crystals in bovine cortical bone under tensile loading', *J Biomech*, **40**, 1832–1838.

Gao H, Baohua Ji, Jäger I L, Arzt E and Fratzl P (2003), 'Materials become insensitive to flaws at nanoscale: lessons from nature', *PNAS*, **100**, 5597–5600.

Grabner B, Landis W J, Roschger P, Rinnerthaler S, Peterlik H, Klaushofer K and Fratzl P (2001), 'Age- and genotype-dependence of bone material properties in the osteogenesis imperfecta murine model (oim)', *Bone*, **29**, 453–457.

Guo X E and Goldstein S A (1997), 'Is trabecular bone tissue different from cortical bone tissue?', *Forma*, **12**, 185–196.

Gupta H S, Seto J, Wagermaier W, Zaslansky P, Boeseke P and Fratzl P (2006), 'Cooperative deformation of mineral and collagen in bone at the nanoscale', *PNAS*, **103**, 17741–17746.

Hellmich C H and Ulm F J (2002), 'Are mineralized tissues open crystal foams reinforced by crosslinked collagen? – some energy arguments', *J Biomech*, **35**, 1199–1212.

Hodgskinson R and Currey J D (1992), 'Young's modulus, density and material properties in cancellous bone over a large density range', *J Mat Sci Mat Med*, **3**, 377–381.

Jäger I and Fratzl P (2000), 'Mineralized collagen fibrils: a mechanical model with a staggered arrangement of mineral particles', *Biophys J*, **79**, 1737–1746.

Jepsen K J, Goldstein S A, Kuhn J L, Schaffler M B and Bonadio J (1996), 'Type-I collagen mutation compromises the post-yield behavior of Mov13 long bone', *J Orth Res*, **14**, 493–499.

Katz J L (1971), 'Hard tissue as a composite material – I: bounds on the elastic behavior', *J Biomech*, **4**, 455–473.

Kelly A and Macmillan N H (1987), *Strong Solids*, New York, Oxford University Press.

Kim H D and Walsh W R (1992), 'Mechanical and ultrasonic characterization of cortical bone', *Biomimetics*, **1**, 293–310.

Landis W J, Song M J, Leith A, McEwen L and McEwen B F (1993), 'Mineral and organic matrix interaction in normally calcifying tendon visualized in 3 dimensions by high-voltage electron microscopic tomography and graphic image-reconstruction', *J Struct Biol*, **110**, 39–54.

Landis W J, Hodgens K J, Arena J, Song M J and McEwen B F (1996), 'Structural relations between collagen and mineral in bone as determined by high voltage electron microscopic tomography', *Micros Res Tech*, **33**, 192–202.

Mashiba T, Mori S, Burr D B, Komatsubara S, Cao Y P, Manabe T and Norimatsi H (2005), 'The effects of suppressed bone remodeling by bisphosphonates on microdamage accumulation and degree of mineralization in the cortical bone of dog rib', *J Bone Min Metab*, **23**, 36–42 Suppl. S.

Pidaparti R M V, Chandran A, Takano Y and Turner C H (1996), 'Bone mineral lies mainly outside collagen fibrils: predictions of a composite model for osteonal bone', *J Biomech*, **29**, 909–916.

Reilly G C (2000), 'Observations of microdamage around osteocyte lacunae in bone', *J Biomech*, **33**, 1131–1134.

Rho J Y, Zioupos P, Currey J D and Pharr G M (1999), 'Variations in the individual thick lamellar properties within osteons by nanoindentation', *Bone*, **25**, 295–300.

Rice J C, Cowin S C and Bowman J A (1988), 'On the dependence of elasticity and strength of cancellous bone on apparent density', *J Biomech*, **21**, 155–168.

Rogers K D and Zioupos P (1999), 'The bone tissue of the rostrum of a *Mesoplodon densirostris* whale: a mammalian biomineral demonstrating extreme texture', *J Mat Sci Lett*, **18**, 651–654.

Sasagawa I, Ishiyama M and Akai J (2006), 'Cellular influence in the formation of enameloid during odontogenesis in bony fishes', *Mat Sci Engng C*, **26**, 630–634.

Sasaki N, Ikawa T and Fukuda A (1991), 'Orientation of mineral in bovine bone and the anisotropic mechanical properties of plexiform bone', *J Biomech*, **24**, 57–61.

Sasaki N, Tagami A, Goto T, Taniguchi M, Nakata M and Hikichi K (2002), 'Atomic force microscopic studies on the structure of bovine femoral cortical bone at the collagen fibril-mineral level', *J Mat Sci Mat Med*, **13**, 333–337.

Summers A P (2000), Stiffening the stingray skeleton – an investigation of durophagy in myliobatid stingrays (Chondrichthyes, Batoidea, Myliobatidae)', *J Morph*, **243**, 113–126.

Tai K, Ulm F-J and Ortiz C (2006), 'Nanogranular origins of the strength of bone', *Nano Lett*, **6**, 2520–2525.

Tattersall H G and Tappin G (1966), 'The work of fracture and its measurement in metals, ceramics and other materials', *J Mat Sci*, **1**, 296–301.

Taylor D and Kuiper J H (2001), 'The prediction of stress fractures using a "stressed volume" concept', *J Orthop Res*, **19**, 919–926.

Vajda E G and Bloebaum R D (1999), 'Age-related hypermineralization in the female proximal human femur', *Anat Rec*, **255**, 202–211.

Wagner H D and Weiner S (1992), 'On the relationship between the microstructure of bone and its mechanical stiffness', *J Biomech*, **25**, 1311–1320.

Walsh W R and Guzelsu N (1994), 'Compressive properties of cortical bone: mineral-organic interfacial bonding', *Biomaterials*, **15**, 137–145.

Weiner S, Traub W and Wagner H D (1999), 'Lamellar bone: structure-function relations', *J Struct Biol*, **126**, 241–255.

Wilson E E, Awonusi A, Morris M D, Kohn D H, Tecklenburg M M J and Beck L W (2006), 'Three structural roles for water in bone observed by solid-state NMR', *Biophys J*, **90**, 3722–3731.

Yeni Y N and Norman T L (2000), 'Calculation of porosity and osteonal cement line effects on the effective fracture toughness of cortical bone in longitudinal crack growth', *J Biomed Mater Res*, **51**, 504–509.

Zioupos P (2001), 'Accumulation of *in-vivo* fatigue microdamage and its relation to biomechanical properties in ageing human cortical bone', *J Micros*, **201**, 270–278.

Zioupos P, Currey J D, Casinos A and de Buffrénil V (1997), 'Mechanical properties of the rostrum of the whale *Mesoplodon densirostris*, a remarkably dense bony tissue', *J Zool Lond*, **241**, 725–737.

Ziv V and Weiner S (1994), 'Bone crystal sizes – a comparison of transmission electron-microscopic and X-ray-diffraction line-width broadening techniques', *Conn Tiss Res*, **30**, 165–175.

Zoehrer R, Roschger P, Paschalis E P, Hofstätter J G, Durchschlag E, Fratzl P, Phipps R and Klaushofer K (2006), 'Effects of 3- and 5-year treatment with risedronate on bone mineralization density distribution in triple biopsies of the iliac crest in postmenopausal women', *J Bone Min Res*, **21**, 1106–1112.

Zylberberg L, Traub W, de Buffrénil V, Allizard F, Arad T and Weiner S (1998), 'Rostrum of a toothed whale: ultrastructural study of a very dense bone', *Bone*, **23**, 241–247.

2

Fabrication processes for bioceramics

Y TANAKA and K YAMASHITA, Tokyo Medical and Dental University, Japan

2.1 Introduction

The term 'bioceramics' refers to biocompatible ceramic materials, applicable for biomedical or clinical uses. Bioceramics can be produced in crystalline and amorphous forms, and they are generally classified from their chemical compositions into two groups; calcium phosphates (CP) and others, including yttria (Y_2O_3)-stabilized tetragonal zirconia (ZrO_2) (Y-TZP), alumina (Al_2O_3) and some silicate and phosphate families of glasses and crystallized glasses (glass-ceramics). Table 2.1 summarizes the bioceramic products in terms of compositions and shapes. The most clinically used ceramics of the CP group are hydroxyapatite ($Ca_5(PO_4)_3OH$, HA) and β-tricalcium phosphate ($Ca_3(PO_4)_2$, β-TCP), for they are analogous to the inorganic constituents of hard tissues of vertebrates. Use of Y-TZP and alumina is attributable to their excellent mechanical strength and toughness. The glasses and crystallized glasses in the SiO_2–P_2O_5–CaO–Na_2O system are classified as bioactive glasses and bioactive glass-ceramics. They have also been recognized as bioactive and resolvable ceramics; in particular so-called A-W glass-ceramics have been synthesized using a scientific design of strength and biocompatibility.

Clinical applications require various shapes of bioceramics from thin films and nano-sized powders to porous or dense bodies. Bone substitutes use massive porous HA, β-TCP and their mixture: defective bones which are not always exposed to high stress can be replaced by porous HA or β-TCP. Commercial porous products of HA with a porosity of 70–80% are already distributed to clinics and hospitals. Highly dense ceramics of Y-TZP and alumina are applied to hip joint balls and cups, while thin films of HA are coated on hard metals for artificial teeth and hip joints. In order to satisfy these demands, an appropriate fabrication method and process must be chosen for each clinical device. For fine fabrication of tough Y-TZP cups and balls, fine-grained ceramics of Y-TZP must be sintered with pure and fine powders under a controlled sintering program. In general, tough and

Table 2.1 Compositions and shapes of the various bioceramics

Category	Materials and compositions	Shapes
Calcium phosphate (CP) group	**Hydroxyapatite** (HAp (or HA)) $Ca_5(PO_4)_3OH$	**Sintered body** (dense and porous) **Powder** **Coating** **Composite** **Fiber**
	β-Tricalcium phosphate (β-TCP) $Ca_3(PO_4)_2$	**Sintered body** (dense and porous) **Powder**
	Others	
	Dicalcium phosphate anhydrate (monetite, DCP or DCPA) $CaHPO_4$	**Powder**
	Dicalcium phosphate dihydrate (brushite, DCP2 or DCPD) $CaHPO_4 2H_2O$	**Powder**
	Calcium pyrophosphate (CPP) $Ca_2P_2O_7$	**Powder**
	α-Tricalcium phosphate (α-TCP) $Ca_3(PO_4)2$	**Powder**
	Tetracalcium phosphate (TeCP) $Ca_4(PO_4)_2O$	**Powder**
	Octacalcium phosphate (OCP) $Ca_8H_2(PO_4)_6 5H_2O$	**Powder**
	Amorphous calcium phosphate (ACP) $Ca_3(PO_4)_2 nH_2O$	**Powder**
Others	**Yttria-stabilized tetragonal zirconia** (Y-TZP) Y_2O_3-ZrO_2	**Sintered body** (dense)
	Aluminum oxide (alumina) Al_2O_3	**Sintered body** (dense)
	Titanium oxide (titania) TiO_2	**Sintered body** (dense)
	Silicon nitride Si_3N_4	**Sintered body** (dense)
	Silicon carbide SiC	**Sintered body** (dense)
	Carbon C	**Fiber**
	Bioactive glasses system	
	SiO_2-P_2O_5-Na_2O-CaO	**Bulk**
	SiO_2-P_2O_5-Na_2O-K_2O-CaO-MgO	**Bulk**
	SiO_2-P_2O_5-CaO-Al_2O_3	**Bulk**
	Bioactive glass-ceramics system	
	SiO_2-P_2O_5-CaO-MgO (A-W)	**Bulk**
	SiO_2-P_2O_5-Na_2O-K_2O-CaO-MgO (Ceravital)	**Fiber**

strong ceramics consist of fine-grained microstructure, whose average grain diameter is less than 1 μm. It is important to eliminate impurities from bioceramics; even minor impurities bring harm to a body, or provoke critical defect in the mechanical properties of bioceramics during long implantation *in vivo*.

To undertake advantageous sintering, it is essential to control chemical and ceramic powder processing. The preparation of pure, fine powders enables the microstructure of bioceramics to be controlled. In this chapter, the general principles and methods of conventional fabrications will first be overviewed, then prevailing techniques are briefly introduced with some examples from commercial products. Lastly, recent advances in potential methods will be summarized.

2.2 Conventional processing of ceramics

Crystalline bioceramic products are generally prepared through sintering moulded powders at high temperatures. As introduced above, tough and strong ceramic products must consist of pure, fine and homogeneous microstructures. To attain this, pure powders with small average size and high surface area must be used as the starting sources. The sintering procedure is carried out according to a controlled temperature program of furnaces in adjusted ambience of air with necessary additional gasses. Bioactive glasses are conventionally prepared by melting the starting powders with adjusted compositions and pouring them into a mould, then annealing to release induced stresses at a designated temperature in a furnace for a sufficient time. Bioactive glass-ceramics are obtained by crystallizing bioactive glasses at appropriate high temperatures. First, starting powders must be prepared.

2.2.1 Powder processing

Powders are synthesized according to dry and wet chemical routes: dry chemical process uses the high-temperature chemical reactions among solid-state sources. High-temperature treatment is necessary for enhancement of diffusion process of ions. A desired bioceramic product (AB) is generally made from the sources A and B via a solid-state reaction expressed as $A(s) + B(s) \rightarrow AB(s)$. An example for HA is shown in eq. [2.1], where A and B are $Ca_2P_2O_7$ (pyrocalcium phosphate) and $CaCO_3$ powder. As HA includes hydroxide ions, the reaction must be done under controlled water vapour supply.

$$3Ca_2P_2O_7 + 4CaCO_3 + H_2O(g) \rightarrow Ca_{10}(PO_4)_6(OH)_2 + 4CO_2(g) \qquad 2.1$$

On the other hand, thermal decomposition of compounds (A → B + C) can be used for preparation of powders; $CaHPO_4 \cdot 2H_2O$ or $CaHPO_4$ is thermally decomposed to various pyrocalcium phosphates from amorphous to α-, β- and γ-forms. Which polymorph is formed depends on the heating temperature, as eq. [2.2].

$$2(CaHPO_4 \cdot 2H_2O) \rightarrow Ca_2P_2O_7 + 5H_2O(g) \qquad 2.2$$

The powders thus prepared are generally coarse owing to agglomeration of particles during a solid-state reaction at high temperature. Inhomogeneity of products is also a problem in dry routes, because source elements must diffuse through the initially formed layers at powder interfaces to continue further chemical reactions. Ball-milling is effective for crushing and grinding reacted powders; thereafter high-temperature treatment is repeatedly required for the ball-milled powders.

Wet-chemical methods use solutions as starting sources. The wet chemical process is widely used to synthesize crystalline bioceramics, because high compositional homogeneity can be easily achieved at low temperature. The advantage arises from the use of a liquid state precursor, in which the source elements are thoroughly mixed at the atomic level.

The phenomenon of crystalline precipitation mainly consists of two steps; the first is crystal nucleation from an unstable supersaturated solution and the second is a crystal growth developed both by the transport and the kinetics of the crystal sources from the environment into the crystal nuclei. Each step of the crystal nucleation and the growth can be controlled by various factors such as starting solutes, solvents, additives, density (supersaturation degree) of solution, pH, temperature, pressure and stirring condition, and so on. The morphology control of the crystal is determined by the combination of those factors. For example, in the preparation of mono-dispersed spherical crystals, a rapid crystal nucleation and a subsequent slow crystal growth are essential. When there is a time-lag in the nucleation step and the growth rate is fast, the early generated nuclei grow large while the later ones are just forming. The agglomeration of the nuclei is also a negative factor for the preparation of the mono-dispersed crystal. The use of dispersants prevents nuclei agglomeration. If the precipitates have a wide size distribution, Ostwald ripening is applied to reduce the distribution of the crystal. Ostwald ripening is one of the coarsening phenomena based on the difference of the solubility among the crystals of various sizes. When the crystals are precipitated from the supersaturated solution, the larger ones grow and the smaller ones dissolve with time to reduce the interfacial free energy. This effect usually appears just before reaching the equilibrium state. Here, the total volume of the crystals is kept during the ripening while crystal numbers decrease with time.

For several bioceramics, the wet-chemical process is regarded as the best synthesis method; commercialized HA powders are generally obtained from mixed solutions of calcium and phosphate salts via the precipitation method, the hydrothermal method, the spray or gel pyrolysis method, etc. Here, $Ca(NO_3)_2$, $Ca(OH)_2$ or $CaCl_2$ and $(NH_4)_2HPO_4$ or H_3PO_4 are preferably used as calcium and phosphorus sources, respectively. For instance, aqueous solutions of calcium and phosphorus are homogeneously mixed and solidified in aqueous solutions to form HA precursors [2.3]. The obtained HA precursors then undergo Ostwald ripening to be changed to HA crystallites.

$$10Ca^{2+} + 6(PO_4)^{3-} + 2OH^- \rightarrow Ca_{10}(PO_4)_6(OH)_2 \qquad 2.3$$

In this process, the pH of solutions must be kept over 10 to precipitate HA particles. To perform this, CO_2 must be purged from the ambient gas in reaction vessels.

Alternatively in the case of Y-TZP, co-preparation, hydrolysis and sol–gel methods are generally applied. Among them, the co-preparation method from a mixed solution of YCl_3 and $ZrOCl_2$ is advantageous to achieve homogeneous doping at lower cost. The method simultaneously precipitates two or more compounds with different solubilities.

The hydrothermal method is also a popular technique. It is a kind of wet-chemical process promoted under high-pressured water above 100 °C. Although the condition under the pressure of several tens of MPa below 300 °C is commonly selected for this method, conditions up to 400 MPa and 800 °C are permitted by using high-pressure apparatus. The hydrothermal method is particularly effective in the crystallization of poorly soluble compounds: it enables the synthesis of HA whiskers and small-sized single crystals which are hardly obtained both via dry-chemical and wet-chemical processes under ordinary pressure and temperature. $CaHPO_4$ (monetite), $CaHPO_4{\cdot}2H_2O$ (brushite) and ACP (amorphous calcium phosphate) are used as a starting compound for the synthesis of HA whiskers. Organic acid with an ability to mask a particular crystal plane of HA is added into the reaction system with the aim of the control of the growth direction. Citric acid, oxalic acid and ethylenediamine tetraacetic acid (EDTA) are the representative additives for this purpose.

Drying is the necessary treatment in the wet-chemical process. The process sometimes determines the secondary particle structure of the crystalline powders, because the agglomeration of crystalline easily occurs with the desolvation. Drying is mainly divided into heating and non-heating processes. In addition to the usual convective, conductive and radiation drying by external heat sources, internal heat drying induced by electromagnetic wave is also classified into the heating process. Widely used hot-gas drying, hot-plate drying, infrared drying, spray-drying and microwave

drying are examples of heating processes. On the other hand, reduced-pressure drying, freeze-drying, centrifugal drying, drying by desiccating agent, ultrasonic drying and critical point drying are classified as non-heating processes. For the representative ones in the bioceramics processing, the brief descriptions are given below.

The spray-drying technique is suitable to the large-scale and low-cost production of fine powders with superior granule characteristic for molding. The technique is carried out by atomizing solutions with precipitated powders through a nozzle at a controlled rate into a heated chamber with a vessel to capture dried powders (Fig. 2.1). Here, solvent immediately evaporates when the solution is sprayed into a chamber with supplying powders of the particle size below the sprayed droplets. The use of cyclone is indispensable for this technique for effective drying. Alternatively, there is a method called spray-pyrolysis in which drying and the pyrolysis reaction are carried out at the same time.

Freeze-drying proceeds through the freezing process of wet precipitated powders and the following evacuation of air under freezing. The solidified solvent is then changed directly into vapor by supplying latent heat of sublimation and removed from the drying object (Fig. 2.2). This technique provides fine powders with large surface areas (Fig. 2.3). The dried powders are subjected to a forming process to produce the shapes desired before sintering.

In most drying processes, a wet body goes through a condition that the surface is partially soaked by the solvent and is partially exposed to the ambient gas-phase. Under this condition, the drying object is subject to the interface tension between the solvent and the ambient gas. The fine structure is easily damaged in the usual drying method. In contrast,

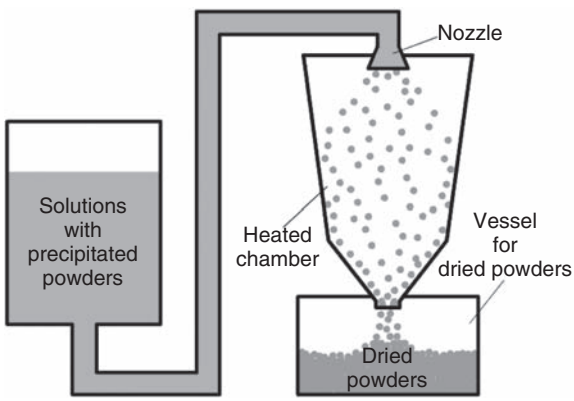

2.1 Schematic view of the spray-drying apparatus.

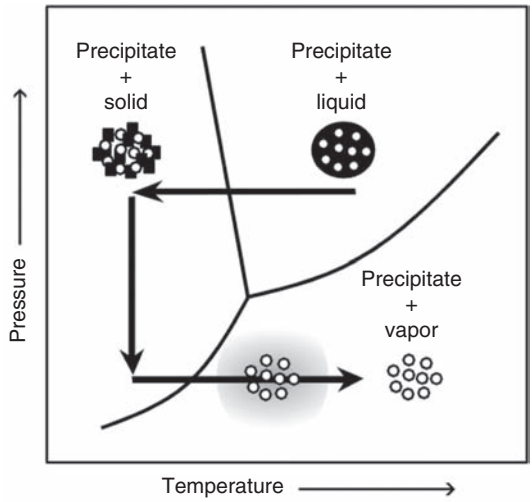

2.2 Principle of the freeze-drying technique.

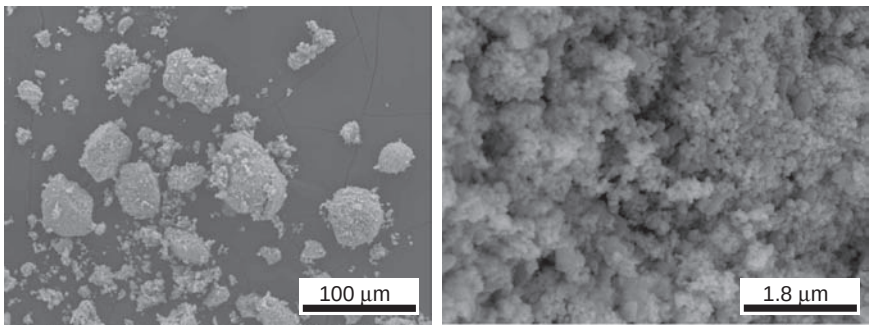

2.3 SEM photographs of HA powders obtained via freeze-drying.

supercritical drying can avoid the influence of the interface tension, because the solvent is removed via the supercritical state. In this method, the original solvent is firstly exchanged by liquid carbon dioxide and the liquid carbon dioxide is then removed after changed into supercritical state achieved under relatively mild conditions (the critical point of carbon dioxide is at 31.06 °C under a pressure of 7.28 MPa).

2.2.2 Forming of green body

Forming is one of the important processes in making bioceramic products. Forming is carried out through various techniques using either dried powders with additives or wet powders with viscous fluid. Deflocculants

(glues) are usually inorganic chemicals of sodium carbonates and sodium silicates, and organic polymers of polyacryl acid. Organic additives of polyvinyl alcohol (PVA), methyl cellulose and paraffin are used for forming, strengthening and making green bodies plastic (Table 2.2). The simple forming of green bodies is uniaxial compaction of powders mixed with appropriate organic binders and deflocculants of a few wt% in a desirably shaped mold. To avoid locally remained stress or increase green density (up to 60% of theoretical values), cold isostatic pressing (CIP) is sometimes employed, which enables uniform pressing in a soft rubber mold. The method is done according to Archimedes principle using Ar gas or water as the medium of equiaxial pressure.

A slurry of wet powders (slip) with or without organic binders can be shaped by directly pouring into plaster molds. The slip casting technique provides forming of various shapes and large bodies (Fig. 2.4). As plaster molds absorb the water from slip, slip is dried in molds. Although green bodies are naturally separated from molds because of shrinkage during drying, some additives of silicone or olive oil are used to support the separation. Because dried green bodies are subjected to sintering after removal

Table 2.2 Various techniques of the green body formation with organic additives and solvents

Methods	Additives	Solvent
Uniaxial compaction	Water-soluble resin (polyvinyl alcohol), gum arabic, etc. 3.0~5.0 wt%	Water 0~1.0 wt%
Cold isostatic pressing	Water-soluble resin (polyvinyl alcohol), gum arabic, etc. 2.0~5.0 wt%	Water 0~1.0 wt%
Slip casting	Methylcellulose, sodium alginate, etc. 0.5~3.0 wt%	Water 30.0~60.0 wt%
Pressure mold forming	Water-soluble resin (polyvinyl alcohol), paraffin, etc. 8.0~15.0 wt%	Water 15.0~30.0 wt%
Injection mold forming	Thermoplastic resin, paraffin, etc. 10.0~25.0 wt% Plasticizer (phthalate ester, etc.) 0.5~5.0 wt%	
Doctor blade method	Acrylic ester, polyvinyl butyral, etc. 8.0~15.0 wt% Plasticizer (phthalate ester, etc.) 3.0~8.0 wt%	Water, alcohol, ketone, etc. ~50.0 wt%

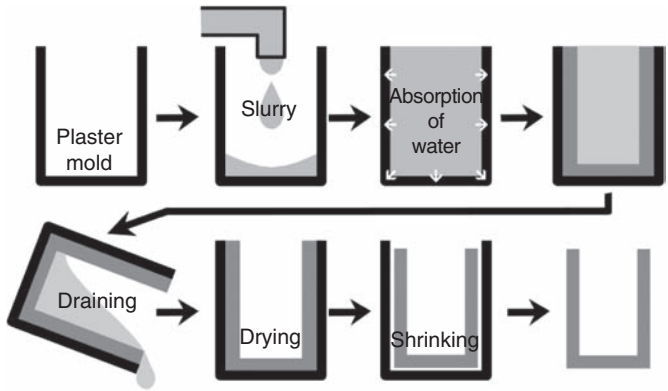

2.4 Slip casting procedure.

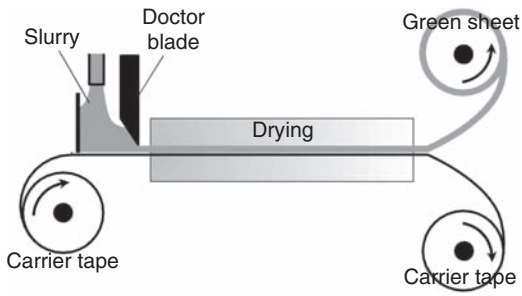

2.5 Schematic view of the doctor blade method.

from plaster molds, green bodies must have sufficient stiffness for handling.

In case of pressure mold forming, slurries are poured into a vacuum chamber and well stirred with screw shaped blades. The mixed slurries are pushed out with pressure through a nozzle to a desired shape such as pipes, honeycomb cakes and thick films.

In addition to the above techniques, both doctor blade and colander methods are well known as representative techniques to form ceramic green sheets from slurries. Figure 2.5 is a schematic view of the doctor blade method. The slurries, mixed with additives (binders, plasticizers and dispersants), are cast on the carrier tape with uniform thickness, dried and peeled from carrier tape in the continuous production system. In this method, the thickness of green sheets can be exactly defined by controlling the passing speed of carrier tape and by adjusting the gap between the carrier tape and the knife-edge of the doctor blade. The colander method

is also a continuous production technique of green sheets in which the slurries are flattened by a pair of rotating rolls. To control the thickness of the green sheets, the gap between rolls and the rotating speed are adjusted. The obtained green sheets by these methods are usually punched into objective shape by dies and sintered into ceramics.

Although electrophoretic deposition (EPD) is a well-developed coating technology, it is primarily a method of forming green bodies. The principle and technique are rather convenient; ceramic powders suspended in a solvent are driven in a dc field to metal substrates as electrodes (Fig. 2.6). When powders are suspended in a solvent, surfaces of powders are charged. The sign of surface charges depends on the characteristics of both powders and solvents. After arrival at substrate surfaces, powders are discharged and deposited on substrates. The electrophoresis phenomenon is described by the Helmholtz equation (eq. [2.4]):

$$u = \frac{\varepsilon \zeta E}{4\pi\eta} \qquad 2.4$$

where u is the velocity of powder ($m\,s^{-1}$), ε the dielectric constant of solvent ($F\,m^{-1}$), ζ the ζ potential (V), E the applied electric field ($V\,m^{-1}$), η the viscosity ($N\,s\,m^{-2}$). The value of u is actually the relative velocity between powders and solvent and is important in determining the initial deposition rate. Larger sized powders show greater viscosity resistance and slower deposition as a result. Consequently, the choice of an appropriate solvent is important for given powders to adjust the parameters of ε, ζ and η. It

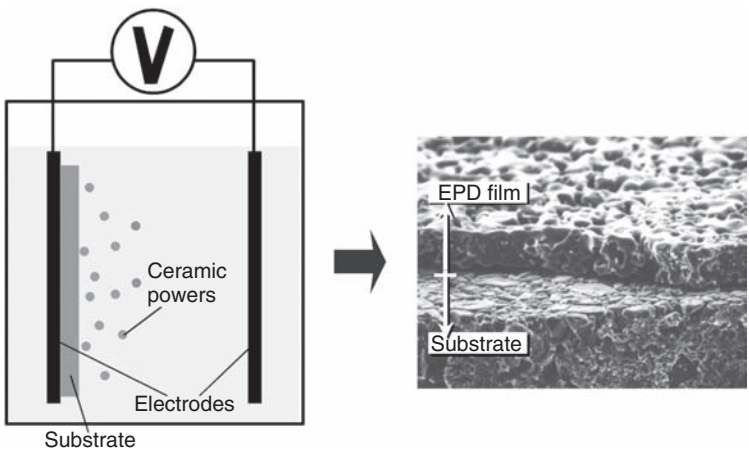

2.6 Schematic view of the electrophoretic deposition method and SEM photograph of HA film on insulating substrate obtained by the electrophoretic deposition.

must be remembered that that water electrolysis occurs and produces bubbles on electrode substrates. Because of a lack of chemical bonding between powders and substrates, deposited bodies are generally sintered at high temperatures after drying.

2.2.3 Sintering

The microstructure of ceramics consists of grains, grain boundaries, pores and impurity phases if any (Fig. 2.7). The mechanical properties of bioceramics strongly depend upon the microstructure; densely sintered bodies with fine grains are tougher and stronger than porous ones with larger grains. Cracks originating at the edges around surfaces run down through large grains until breakdown, while grain boundaries restrict the propagation of cracks. Impurities must be eliminated for deterioration of mechanical properties as well as for biomedical safety. Fine-grained and densely sintered Y-TZP and alumina with less than 1% porosity are employed for biomedical devices exposed to high stresses such as cups for hip joints. For bone substitutes replacing damaged natural bones, on the other hand, porous HA, TCP and their mixture (HA/TCP) bodies with large pores more than 200 μm in diameter are preferable because of complete biointegration. Thus the microstructure of bioceramics plays important roles in biomedical applications, and the characteristics of microstructures are determined by the sintering.

Sintering is the hardening process of green bodies at a high temperature, but much lower than the melting point of a material. When solids are heated to high temperatures, constituent ions or atoms are driven to move to compensate for the surface energy differences among their convex and concave surfaces. Bottlenecks are formed and grow among powders at the initial stage (Fig. 2.8). As a result, strong chemical bonds are formed among powders, and loosely compacted green bodies are hardened to ceramic materials. Lattice defects (unoccupied lattice sites) are required for forming pathways for ions and atoms to move through the lattice structures. As ionic

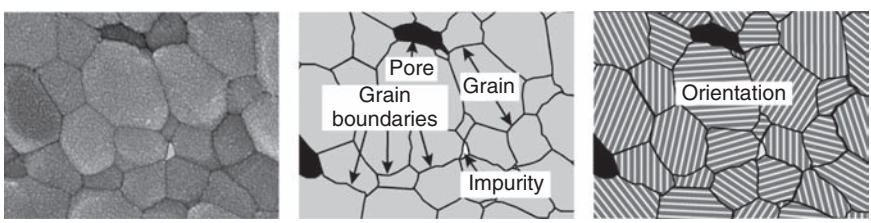

2.7 Microstructure of a sintered body.

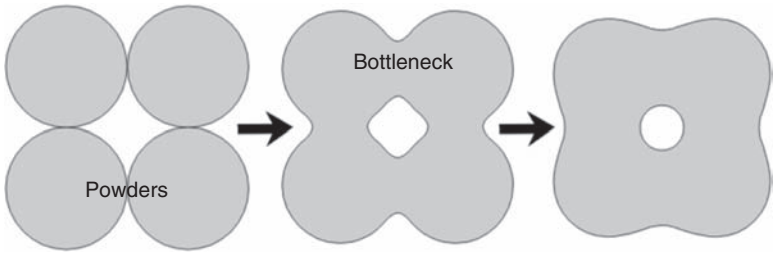

2.8 Bottleneck formation between particles under the sintering.

transport occurs exponentially in accordance with temperature (eq. [2.5]), sintering is done at a high temperature.

$$D = A\exp\left(-\frac{E_a}{RT}\right) \qquad 2.5$$

where D is the diffusion coefficient of ions, and A, R and E_a are the pre-exponential term, gas constant and an activation energy for diffusion at temperature T, respectively. Sintering temperature also depends on the composition and crystalline phase of bioceramics; Y-TZP and HA ceramics are conventionally sintered at 1400 and 1200 °C, respectively. The sintered ceramics are therefore polycrystalline materials consisting of numerous enlarged and coagulated grains of random orientation (Fig. 2.7). Metal oxides ceramics are usually sintered in air; however, as sintering is carried out at high temperatures, the ambience of sintering should be chosen carefully for HA and silicon nitride because of phase decomposition due to dehydration or oxidation through interactions with ambient gases.

Densification also proceeds with sintering, because gases filling gaps among powders move towards the outside of powders and green bodies shrink owing to decrease of distances among powders. The gaps left after densification are referred to as open and closed pores; the former are located near surfaces and the latter are surrounded with grains and grain boundaries inside a ceramic material. The final stage of sintering is both the development of grain boundaries, which are the interfaces among grains, and grain growth. An average grain size increases with aggregation of grains in order to decrease the interfacial energy. The driving force (ΔG) due to the interfacial energy difference is expressed as follows:

$$\Delta G = \gamma(1/r_1 + 1/r_2) \qquad 2.6$$

where γ is the interfacial energy, and $1/r_1$ and $1/r_2$ are the reciprocals of the radii of curved surfaces. The equation indicates that concave and convex grain boundaries transform to flat surfaces with sintering. As grain size (d) increases in proportion to the root of sintering time (t) with grain growth

(eq. [2.7]), sintering for shorter time is desired to obtain fine-grained ceramic bodies:

$$\Delta d \propto \sqrt{t} \qquad 2.7$$

In order to promote sintering for densification, some additives of oxides are used as sintering aids for silicon nitrides (Si_3N_4), where added Al_2O_3 is reacted and melted to accelerate ionic transport for neck growth and densification. Hot pressing sintering is employed as an advanced technique, which is carried out under uniaxial pressure. Hot pressing has the advantage of enhanced densification at a lower temperature, giving inhibition of grain growth. A more advanced method is the sintering with hot isostatic pressing (HIP) which uses inert gases of Ar or He, or hexagonal boron nitride (BN) as the transmitting medium for pressure. Although HIP requires a large-scale instrument and is costly, it is effective for sintering of complex-shaped, homogeneous and large-scale components.

As mentioned above, porous sintered bodies of CP with large pore sizes (>100 μm) are preferable for bone substitutes and scaffolds for cell migration and bone conduction. Pores interconnect through networks. The popular method to fabricate such porous bodies is to remove porogens previously mixed with green body. The porogens conventionally used are combustible or solvent-soluble ones such as carbon, cellulose, starch, polyvinyl alcohol, polyvinyl butyral, polystyrene, polyurethane and polymethyl methacrylate in the form of fine particles, beads, fibers, sponge and gel. The porogens are burned to create large pores during sintering. Porous HA is conveniently obtained by following procedure: pH-regulated HA slurries are impregnated into cellulose sponge and then sintered at 1200–1280 °C. This method usually gives the porosity of 70–85%.

A unique method called the 'foam–gel' technique is also applied to the fabrication of porous bodies. First, slurries of HA both with the cross-linking agent and foaming agent of polyethyleneimine and polyoxyethylene lauryl ether are well stirred into foam, then and gelatinized by the addition of water-soluble cross-linking agent such as poly-functional epoxy compound after being poured into a mold. The obtained foamy gel is removed from the mold and dried, followed by sintering at 1200 °C. This method gives an HA body with a porosity up to 75% (Fig. 2.9). There is another newly developed processing method, named the 'freeze-casting' technique. This method provides three-dimensionally interconnecting pores into ceramics during sublimation of the frozen vehicle. Briefly, HA slurry mixed with a vehicle such as camphene is poured into a mold and solidified at a temperature below the freezing point of the vehicle. The frozen vehicle is then sublimated and the obtained porous green body is sintered at 1250 °C into HA porous ceramics.

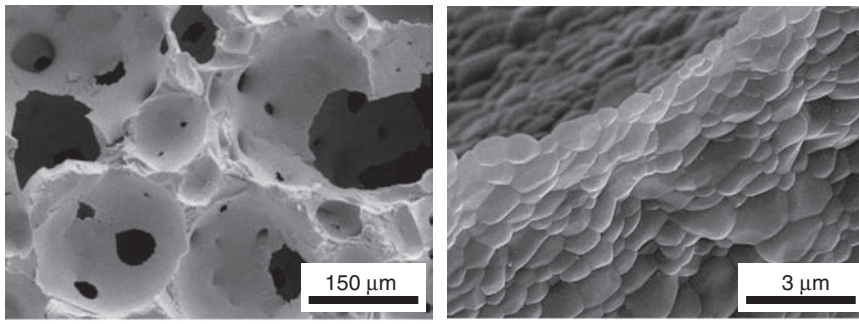

2.9 SEM photographs of porous HA obtained by the foam–gel technique.

2.2.4 Machining

To produce the accurate shaping necessary for the fine design of bioceramics, machine finishing is essential. However, cutting tools developed for metals are usually useless for bioceramics because of their fragility. Convenient finishing techniques are grinding and polishing. Grinding and polishing use whetstones with polishing fluid and cloth, glass or metal. Whetstones are usually diamond, alumina, silicon carbide (SiC), boron nitride (B_4C) and silica (SiO_2). Mica-containing glass-ceramic is the machinable material in the K_2O–MgO–Al_2O_5–B_2O–SiO_2–F system. The microstructure of the glass-ceramic is controlled for improvement of machinability. Because of the cleavage fracture, the controlled microstructure of crystallized glass hinders the extension of fracture generated during machining.

2.3 Conventional and chemical processing of glasses and glass-ceramics

2.3.1 Conventional processing

The chemical compositions of conventional bioactive glasses include silicate (SiO_2), phosphate (P_2O_5), alkaline (Na_2O, K_2O) and/or alkaline earth oxides (CaO, MgO). The most prevailing bioactive glass, 45S5 made by Hench, has the composition of SiO_2 (46.1 wt%), P_2O_5 (2.6 wt%), Na_2O (24.4 wt%) and CaO (26.9 wt%). Glasses are conventionally made by rapid cooling of melted resources such as metal oxides, carbonates and fluorides. To form a shape, melts are poured into a desirably fabricated mold.

Even with the same chemical compositions, the amorphous structures of glasses are different from crystalline ceramics in random arrangement of ions and ionic groups (Fig. 2.10). The tetrahedral units of silicate and phosphate form networks as skeleton structures for strengthening galsses, and

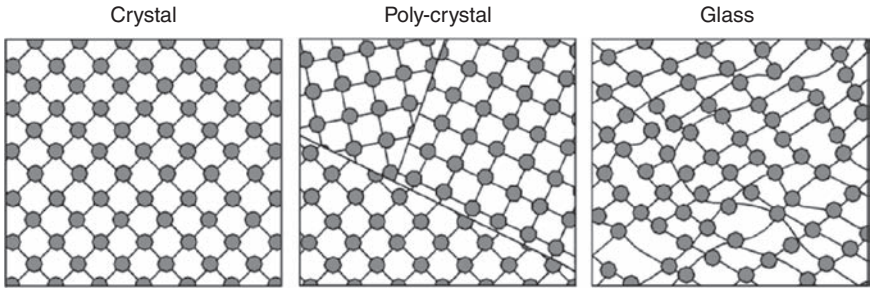

2.10 Schematics of the microstructure of crystal, poly-crystal and glass.

alkaline and alkaline earth ions locate among these tetrahedra to break the networks (eq. [2.8]); the bridging oxygens with silicon atoms (Si–O–Si) are separated with sodium ions, giving non-bridging oxygen (Na–O–Si)

$$\equiv Si–O–Si\equiv + Na_2O \rightarrow \equiv Si–O–Na + Na–O–Si\equiv \qquad 2.8$$

These alkali and alkaline earth ions are named as modifiers, and the addition of modifiers not only decreases the melting point but also changes the viscosity of melts, and the density, refractive index, glass transition temperature (see below) and hardness of glasses. In addition to glass making, alkaline and alkaline earth ions are indispensable for bioactivity.

Glass forming is solidification from liquid, and the characteristic profile is understood using volume expansion change with temperature (Fig. 2.11). Because glass structure is thermodynamically metastable, melts must be cooled with a fast cooling rate so as not to be crystallized at around the melting point (T_m). As can be seen from the figure, glass structure is primarily different from that of the liquid. As the glass structure is not in an equilibrium state, ionic or atomic rearrangements are restricted during cooling. Consequently, glasses involve inner stresses. To relax the remaining stresses, glasses must be annealed at an appropriate temperature. The important property concerning annealing of glasses is the glass transition temperature (T_g), where a supercooled melt shrinks with a discontinuous expansion coefficient for glass (Fig. 2.11). T_g is defined by the cross-point between the temperature dependences of supercooled melt and glass in volume changes. Roughly speaking, T_g is two-thirds T_m. The value of T_g changes with cooling rate; a faster cooling rate gives a higher T_g. This means that the density of glass is theoretically dependent upon the cooling rate; however, in practice this has little meaning. As a glass structure is relaxed to the equilibrium state for a shorter time at higher temperatures than T_g, annealing of glass is in practice carried out for a longer time at a substantially lower temperature than T_g.

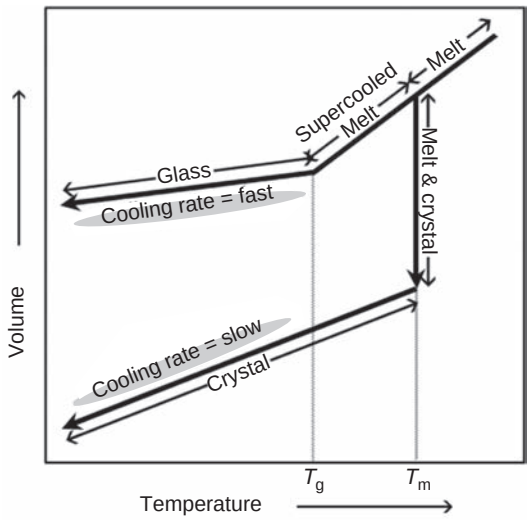

2.11 Volume changes with the melt–glass transition and the melt–crystal transition depending on temperature.

When annealed in an equilibrium state at a temperature between T_m and T_g, glass is transformed to the crystalline phase. The temperature is called crystallization temperature (T_c). Crystallization initially takes place both on the surface and the interior of glasses. The crystallized glasses are referred to as glass-ceramics, and then glass-ceramics are made through annealing glasses above T_c. The crystallization process of glasses is generally characterized with X-ray diffraction (XRD), optical and electron microscopies, and differential thermal analyses (DTA).

The advantage of glass-ceramics lies in the highly dense and fine-grained microstructure with 1 μm in average grain diameter. Kokubo made clinically applicable bioactive glass-ceramics with the chemical composition of SiO_2 (34.2 wt%), P_2O_5 (16.3 wt%), CaO (44.9 wt%) and MgO (4.6 wt%). These glass-ceramics comprise HA grains crystallized in a mechanically strong wollastonite ($CaSiO_3$) matrix. They are referred to as A-W glass-ceramics. The mechanical properties of A-W glass-ceramics are reportedly 200 MPa and 2.0 MPa $m^{1/2}$ for bending strength and fracture toughness (K_{IC}), respectively. Ceravital is also the bioactive glass-ceramic with the chemical composition of SiO_2 (46.2 wt%), P_2O_5 (11.7 wt%), CaO (34.0 wt%) and MgO (2.9 wt%), with alkali oxides Na_2O (4.8 wt%) and K_2O (0.4 wt%).

2.3.2 Sol–gel processing

In addition to the conventional processing of glasses, the sol–gel method is also a popular technique. The term ‘sol’ denotes the stable colloidal

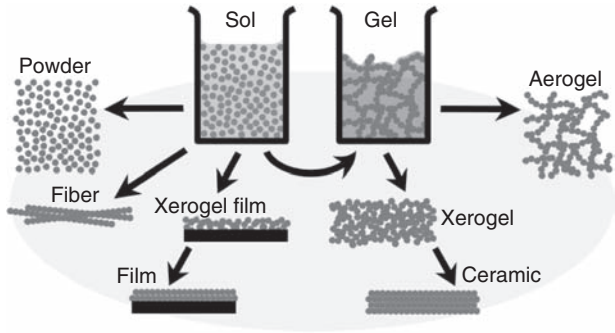

2.12 Various products prepared by sol–gel processing.

solution, consisting of colloids with enough fluidity. The term 'gel' is the self-supportable hardened body obtained from sol, in which the solvent is retained by the framework consisted of polymerized colloids.

The sol–gel method is a kind of wet-chemical process (see Section 2.2.1) and is an important technique. Various morphologies including porous body, thin film and fiber can be easily obtained under relatively mild conditions by controlling the sol–gel transition of precursor solution (Fig. 2.12). This method can also be used for processing of ceramics in addition to glasses.

Although many different compounds such as chloride and nitrate salts are used as the precursors for the sol–gel method, the typical ones are metal alkoxide ($M(OR)_n$, R: alkyl group, M: metal). The first step of sol–gel transition using alkoxide is hydrolysis from $M(OR)_n$ into $M(OR)_{n-m}(OH)_m$.

$$M(OR)_n + m/2H_2O \rightarrow M(OR)_{n-m}(OH)_m + mRO \qquad 2.9$$

The reaction between alkoxide and water is promoted in solvent with a high affinity for both of water and alkoxide. The generated $M(OR)_{n-m}(OH)_m$ undergoes condensation polymerization to M–O–M with time and forms a sol. The sol obtained is then changed into a gel with the increase of the M–O–M network. The schema of sol–gel transition using $Si(OC_2H_5)_4$ (tetraethoxysilane; TEOS) is described in Fig. 2.13. On the other hand, $C_6H_5PCl_2$ is preferably used for HA instead of alkoxide, because high volatility of P-containing alkoxide is inadequate for the sol–gel technique. $C_6H_5PCl_2$ is firstly hydrolyzed with pure water mixed with acetone and then oxidized by air after the addition of appropriate amount of $Ca(NO_3)_2{\cdot}4H_2O$. The obtained mixture changes to a sol below 50 °C and to a polymer by further heating. The polymer of HA precursor is generally used for dip coating of HA on substrates.

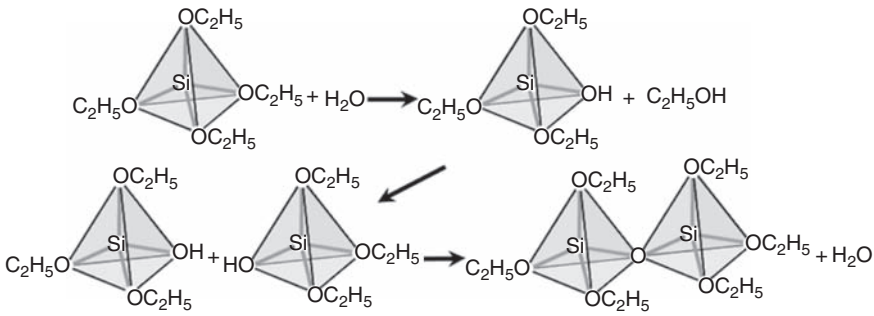

2.13 Schema of the sol–gel transition using TEOS.

2.4 Coatings

Bioceramics also have the brittleness that is inherent to ceramic materials. To overcome the shortage, coatings of bioceramic layers on strong metals or flexible polymers are employed. The prevailing coatings are made of HA: artificial tooth and hip joints are composed of HA layers coated on Ti components. Some reports on the other CP (β-TCP, $CaHPO_4$), Y-TZP and TiO_2 have recently appeared. Adhesion strength of coating layers with Ti metals is first taken into consideration for clinical applications because of long-term use *in vivo*. Second, composition of coated layers must be adequately adjusted, because ceramic coatings sometimes encounter compositional deviation from desired composition during coating.

HA coating techniques have been developed using conventional industrial technologies of ceramic thin and thick films coatings via gas → solid (film), solid → gas → solid (film), or liquid or liquid/solid (slurry) → solid (film) (Fig. 2.14). The routes of gas → solid (film) and solid → gas → solid (film) are well-developed industrial technologies of chemical vapor deposition (CVD) and physical vapor deposition (PVD), respectively. The route liquid or liquid/solid (slurry) → solid (film) uses the similar process to those of bulk bioceramics. This section introduces potential coating methods under development as well as practical ones.

2.4.1 Plasma spraying

Considering such conditions, the optimum technique for HA coatings of clinical devices is plasma-spraying of HA layers (Fig. 2.15a). The method utilizes a set-up to spray HA powders through arch plasma to metal substrates (Fig. 2.15b). Source powders, of several to a few tens μm in diameter, are fed into the plasma where the temperature of the center rises to ca. 10000–30000 °C, then sprayed with a speed of ca. 300–500 $m\,s^{-1}$ to the

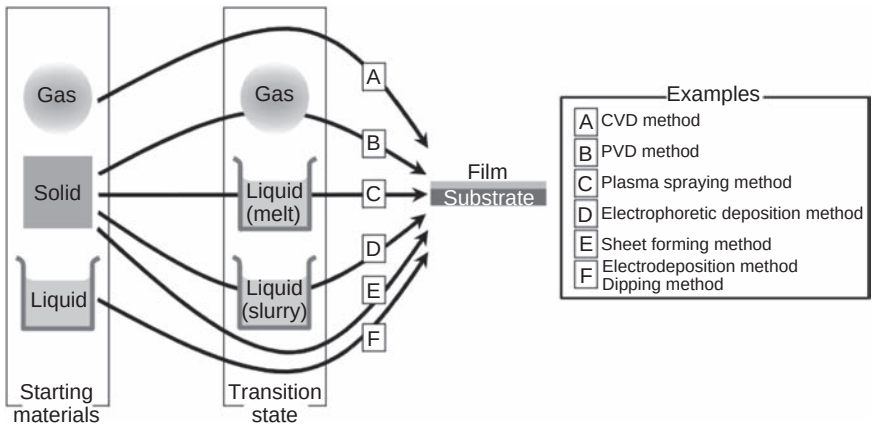

2.14 Various routes of the film formation.

surface of substrates. The deposited HA layers in lamellar structure are partially melted and decomposed to other calcium phosphates such as ACP, TCP and $Ca_4(PO_4)_2O$ (tetra-calcium phosphate: TeCP) (eq. [2.10]).

$$HA \rightarrow TCP/ACP/\ TeCP/CaO \qquad 2.10$$

An experimental result, however, shows that the partially melted HA powders do not lead to the complete dehydration of lattice OH because of a small thermal conductivity of HA. In order to recover the decomposed HA structure or dehydrated water, post-hydrothermal treatment is effective. The chemical reaction is the converse of that in eq. [2.10].

$$TCP/ACP/\ TeCP/CaO + H_2O\ (l/g) \rightarrow HA \qquad 2.11$$

The coating route is therefore solid → solid (film). Because of weak chemical bonding of HA layers to substrates, the sufficient adhesion strength has not yet been attained. To improve the adhesion strength, Ti powders are pre-coated by plasma spraying before HA coatings. The HA coatings thus plasma sprayed have been already applied to numerous artificial screwed tooth and stems of hip joints, because powders can be sprayed on both large and small areas of complex convex and concave surfaces.

2.4.2 Electrodeposition

Electrodeposition is the electric technique using a convenient set-up which deposits HA layers on a substrate as the cathode through chemical reactions driven by dc current (Fig. 2.16). HA layers with a thickness of 2–3 μm can be coated on the cathode metal with a dc voltage of a few

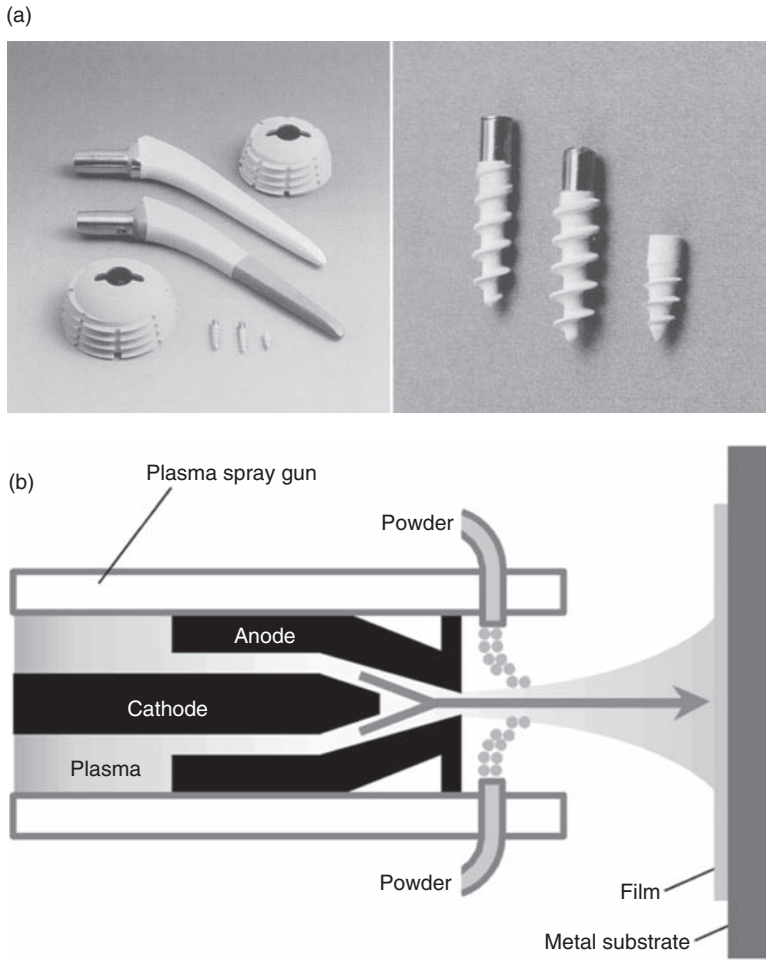

2.15 (a) Photographs of the clinical used plasma sprayed HA films on Ti substrate (femoral components and dental implants; Eurocoating, Spa., Italy) and (b) schematic view of the plasma spray apparatus.

volts for 0.5 h to an aqueous solution. Because an aqueous solution containing Ca^{2+} and PO_4^{3-} ions and ionic groups is used as a starting medium, the solution must be initially adjusted to be acidic (pH < ca. 5). Taking the solubility of HA, an aqueous solution of $Ca(H_2PO_4)_2{\cdot}H_2O$ (MCP) with some additives such as $NaNO_3$ and NaF is usually used as the starting solution. The deposition for coating takes place due to the nominal chemical reactions of $CaHPO_4 \rightarrow CaHPO_4{\cdot}2H_2O \rightarrow HA$. The possible rate-determining reactions are the reduction/oxidation on the cathode shown as follows:

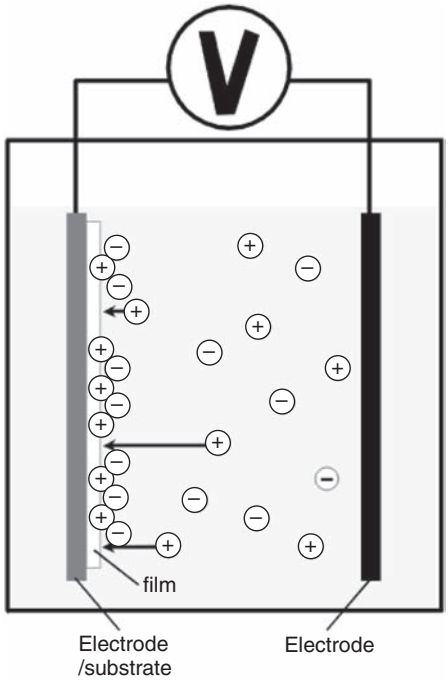

2.16 Schematic view of the electrodeposition method.

$$Ca^{2+} + HPO_4^{2-} \rightarrow CaHPO_4\ (s)$$

$$Ca^{2+} + H_2PO_4^{-} + 2H_2O \rightarrow CaHPO_4{\cdot}2H_2O\ (s)$$

$$Ca^{2+} + HPO_4^{2-} + OH^{-} \rightarrow HA\ (s) + H_2O + H^{+}$$

It has been experimentally noticed that the coated HA is usually nonstoichiometric HA. The deposition characteristics strongly depend both on temperature and composition of solution. Recent reports demonstrate the effectiveness of simulated body fluid (SBF) instead of MCP solution; HA layers are deposited under the application of 2 V for 1 h to Ti substrate at room temperature followed by annealing at 200–1000 °C. Adhesion strength needs to be improved in this technique.

2.4.3 Biomimetic and sputtering methods

The biomimetic method is applied to coat HA not only on ceramics but also on metals and polymers. Kokubo prepared an SBF with the similar inorganic composition with body fluid. Because SBF involves supersaturated calcium and phosphate ions, CP precursors nucleate and apatitic crystals grow on solid surfaces (Fig. 2.17). The apatitic solids grown are identified as bone-like carbonate-containing HA. On the basis of the prin-

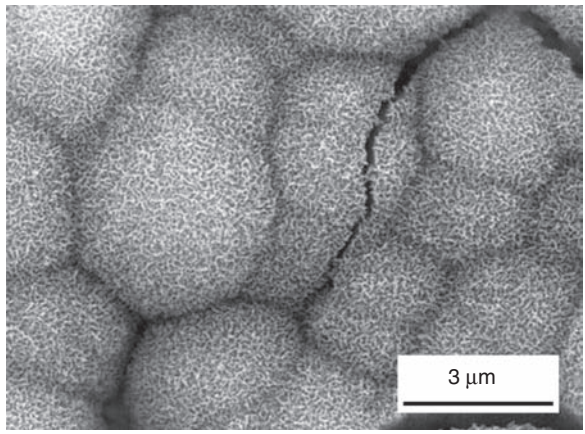

2.17 SEM photograph of the surface of HA layer on alkali-treated YSZ substrate deposited in SBF.

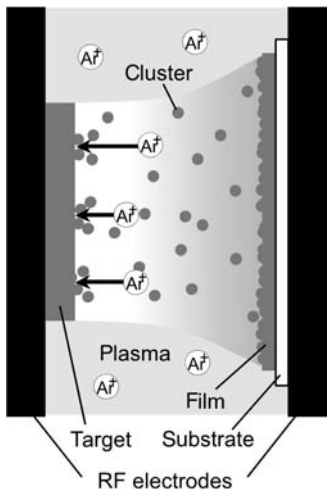

2.18 Schematic view of the sputtering apparatus.

ciple, bone-like apatite coating is proposed. Kokubo proposed the pretreatment of substrates with alkaline solution to form nucleation sites on substrate surfaces.

Sputtering is also an advanced coating technology for biomedical purposes. When a target made of source powders or plate is exposed to bombardment of gaseous plasma such as Ar^+, component atomic or ionic clusters are sputtered from the surface with the aid of the kinetic energy to the ambience. The sputterred clusters are acceleratingly transported in a dc field to the substrate at the opposite side (Fig. 2.18). The adhesion strength

between the deposited layer and a substrate is generally strong; however, the deposition rate is rather slow. The recent technique utilizes ion beam for bombardment to enhance sputtering efficiency. It should be considered that incorporation of water is necessary to form an HA layer and for deviation of the Ca/P ratio from the stoichiometric value.

2.5 Recent advances

In addition to the above conventional ceramics processing techniques, various new techniques have been developed. Some important ones are briefly introduced below.

2.5.1 CAD/CAM technique

CAD/CAM (computer-aided design/computer-aided manufacturing) attracts increasing attention and has already been applied in dentistry to dental restorations with ceramics. CAD/CAM enables the build up of tailor-made ceramics with complicated structures. In this method, sintered porous ceramics of α-Al_2O_3 for dental restorations are automatically cut into objective shapes according to the digital data stored in the computer. In general, original data for the shapes are collected by 3-D scanning of target specimens. CAD/CAM-fabricated ceramics are also obtained through the process: firstly, the green body is sliced as x-sectional pieces along the digital data. Second, the objective shapes are built up by combining the sliced pieces, then sintered.

2.5.2 Gel casting method

The gel casting method is also rather new. In this method, slurries mixed with organic monomers and polymeric initiator are firstly poured into a mold and the monomers are polymerized by controlling external conditions. The slurries used in this method are basically the same as those used in the slip casting process (see Section 2.2.2), but different from conventional slip casting. Gel casting enables all particles in slurries to be fixed almost at the same time in the mold. This has the advantage of obtaining homogeneous green bodies.

2.5.3 Microwave sintering

When green bodies are irradiated with microwaves, internal water absorbs microwaves and the molecular vibration of water is increasingly accompa-

nied by the frictional heat generation. Sintering of green bodies using internal heat generated by microwaves is called microwave sintering. Compared with conductive or radiation heating, microwave heating is superior to usual sintering both in heating time and heat efficiency. Short-term sintering is advantageous in the preparation of homogeneous and dense sintered body with fine-grained microstructure. Moreover, local heating can be performed with this method.

2.6 Summary

The use of cell technology and tissue engineering requires excellent biomaterials to retain and cultivate cells and tissues both *in vitro* and *in vivo*. Polymers and metals have indeed been developed for biomedical applications, but bioceramics have been implanted for a longer time and proved to be safe for humans. Considering this, bioceramics are expected to be further developed for such newly proposed aims of regenerative medicine. In addition to sintered bodies and conventional glasses, thin films and powders of bioceramics are under development because of their convenience in clinical handling. Composites of bioceramics with polymers are also recent advances in fabrication technology of bioceramics.

It is lastly stressed that very few materials have been developed since the discovery of the above conventional bioceramics such as calcium phosphates, stabilized zirconia, alumina and bioactive glasses. It is necessary to create new bioceramics for a lasting development in the future.

2.7 Bibliography

Fischman G, Clare A, Hench L L (ed) (1995), *Bioceramics: Materials and Applications*, Ohio, The American Ceramic Society.

Hench L L, Ulrich D R (ed) (1984), *Ultrastructure Processing of Ceramics, Glasses, and Composites*, New York, Wiley Interscience Inc.

Kanazawa T (1989), *Inorganic Phosphate Materials*, Tokyo, Kodansha.

Kingery W D, Bowen H K, Uhlmann D R (1960), *Introduction to Ceramics*, New York, Wiley-Interscience Inc.

Omatete O O, Janney M A, Strehlow R A (1991), 'Gelcasting – a new ceramic forming process', *Am Ceram Soc Bull*, **70** (10), 1641–1649.

Onoda G Y, Hench L L (ed) (1978), *Ceramic Processing before Sintering*, New York, John Wiley & Sons Inc.

Pinsky H M, Champleboux G, Sarment P D (2007), 'Periapical surgery using CAD/CAM guidance: preclinical results', *J Endod*, **33** (2), 148–151.

Rudolph H, Luthardt G R, Walter H M (2007), 'Computer-aided analysis of the influence of digitizing and surfacing on the accuracy in dental CAD/CAM technology', *Comput Biol Med*, **37** (5), 579–587.

Vijayan S, Varma H (2002), 'Microwave sintering of nanosized hydroxyapatite powder compacts', *Mater Lett*, **56** (5), 827–831.

Vossen J L, Kerned W (1978), *Thin Film Processes*, New York, Academic Press Inc.

Wang X, Fan H, Xiao Y, Zhang X (2006), 'Fabrication and characterization of porous hydroxyapatite/β-tricalcium phosphate ceramics by microwave sintering', *Mater Lett*, **60** (4), 455–458.

Yanagida H, Koumoto K, Miyayama M, Yamada H (1996), *The Chemistry of Ceramics*, Tokyo, Maruzen.

Zhang F Z, Takeaki K, Fuji M, Takahashi M (2006), 'Gelcasting fabrication of porous ceramics using a continuous process', *J Eur Ceram Soc*, **26** (1), 667–671.

3

The microstructure of bioceramics and its analysis

S HAYAKAWA, K TSURU and A OSAKA,
Okayama University, Japan

3.1 Introduction

Bioceramics are produced in a variety of forms and phases and provide many different functions in repair of the human body. In many biomedical applications bioceramics are used in the form of bulk or porous materials with a specific shape such as implant, prostheses, or prosthetic devices. In addition, bioceramics are used in powder form to fill defect spaces while the natural repair processes restore function and are used as a coating on a substrate, or a second phase in a composite material to achieve the enhanced mechanical and biological activities such as osteoinduction or osseointegration.

Bioceramics are prepared by many different preparation methods and thus result in different phases such as single crystal, polycrystalline, glass, glass-ceramics, or composites. The characterization of the microstructure of bioceramics should be observed from many viewpoints such as chemical composition (stoichiometry or purity), homogeneity, phase distribution, morphology, grain size/grain shape, grain boundaries, crystallite size, crystallinity, pores, cracks and surface, etc.

3.2 Effects of processing ceramics on their microstructures

Common powder preparation methods for bioceramics include solid-state reaction or decomposition, liquid reaction such as precipitation or co-precipitation, spray pyrolysis, freeze-drying, sol–gel route, etc. Characteristics such as morphology, stoichiometry, and level of crystallinity vary from one processing method to another. The disadvantages of these processing methods are limited homogeneity, agglomeration of particles, and low purity (non-stoichiometry), which are dependent on the processing condition.

Hydroxyapatite (HA) shows excellent biocompatibility not only with hard tissue but also with soft tissue and promotes osseointegration when

directly implanted into a bony defect. Therefore, HA has been used in orthopedic surgery in both powder and bulk forms. However, its inferior mechanical properties prevent its use in load-bearing situations.

A stoichiometric and well-crystallized HA powder can be produced by solid-state reactions where the raw calcium compounds such as $CaHPO_4$, $Ca(OH)_2$ or $Ca_3(PO_4)_2$ with appropriate ratio are well mixed, compressed, and sintered above 950 °C. (LeGeros and LeGeros, 1993). This method requires a high temperature and a long heat-treatment time. From the viewpoint of dissolution and reprecipitation in the body, stoichiometric HA ceramic can be considered as a bioactive and nonbiodegradable bioceramic.

On the other hand, wet-chemical processes such as precipitation, hydrolysis, and sol–gel method often lead to the formation of non-stoichiometric HA powders, contamination with such ions as carbonate, hydrogen phosphate, potassium, sodium, nitrate, and chloride, and thus to the formation of calcium-deficient hydroxyapatites. These uncontrollable variables may cause significant changes in crystallographic characteristics and chemical properties. The dissolution of HA is governed by various factors such as the grain size, morphology, surface area, chemical composition, crystal structure, crystallinity, and micro-porosity of the materials.

Substitution of ions in the apatite affects properties such as crystallite size and morphology, lattice dimensions, and solubility. Fluoride substitution (F for OH) causes an increase in crystallite size and decrease in solubility. Carbonate substitution causes a reduction in crystallite size and an increase in solubility. Magnesium (Mg for Ca) is incorporated to a very limited extent and has similar effects to CO_3. Mg and CO_3 cause synergistic effects on the crystallite size and dissolution properties of the apatite (LeGeros, 2001). Dense HA having porosity less than 5% by volume can be produced by compressing or compacting the apatite powder into a mold at a pressure of 60–80 MPa and by subsequent sintering in air atmosphere at desired temperatures ranging from 950–1300 °C. The microporosity of dense HA is dependent on the temperature and duration of sintering (LeGeros and LeGeros, 1993; Shi D., 2006).

Alumina (Al_2O_3) ceramics have been used in ball-heads in artificial hip joint prostheses and dental implants because of their excellent biocompatibility, thin capsule formation, low coefficients of friction, and low wear rates (Hench, 1991; Hulbert, 1993). Except for dental implants where single crystal sapphire is sometimes used, fine-grained polycrystalline α-Al_2O_3 is commonly used. It is produced by pressing and sintering at temperatures ranging from 1600 to 1800 °C. The strength, fatigue resistance, and fracture toughness of polycrystalline α-Al_2O_3 ceramics are dependent on the grain size and percentage of doping additives (e.g. MgO), i.e. purity. An increase in average grain size decreases the mechanical properties and exposure to

simulated physiological media causes a significant effect on the strength and fatigue behavior of Al_2O_3 ceramics due to subcritical crack growth (Ritter *et al.*, 1979; Hench and Ethridge, 1982). Subcritical crack growth in an aqueous environment has to be minimized when a high strength of reliable components must be guaranteed for a long period of use. Water is known to promote subcritical crack growth in both single crystalline Al_2O_3 (sapphire) (Wiederhorn., 1969) and in polycrystalline alumina ceramics (Evans, 1992). Water promotes subcritical crack growth preferentially (i) in the local regions of lattice disorder along grain boundaries, and/or (ii) in microstructural regions with segregated impurities in grain boundaries (Krell *et al.*, 2003). The relevance of small grain size and narrow grain size distribution to achieve good mechanical properties in alumina ceramic is quite clear in the biomaterials field (Heimke, 1983). Remarkable progress in terms of further improvements in the wear resistance (Krell, 1996) and strength (Krell and Blank 1996) has been achieved during the past ten years by the development of microstructures with grain sizes <1 μm. Nano-phase alumina, titania, and HA have been described by Webster *et al.* (2000a,b, 2001). They are distinguished by their small grain size (less than 100 nm) and are supposed to selectively enhance adhesion and function of osteoblasts and at the same time to decrease the adhesion of fibroblasts. It is suggested that the adsorption of greater quantities of vitronectin on nano-phase than on conventional alumina ceramics may partially explain this phenomenon.

Porous HA and Al_2O_3 ceramics can be fabricated by using a suitable foaming agent. Porous materials are mechanically weaker than the relevant bulk forms dependent on the porosity. As the porosity increases, the strength of the porous materials decreases rapidly. Since much surface area is also exposed to surrounding media, the effects of the environmental conditions on decreasing the strength become more important than for dense, nonporous materials (Hench and Ethridge, 1982).

Glass and glass-ceramics are very attractive materials for biomedical application because:

- they are easy to shape (molding);
- their chemical composition is very flexible (though dependent on the glass-forming region of the relevant system);
- glass shows isotropic properties.

Glass can be produced by the conventional melt-quenching technique. Glass-ceramics are derived from a glass (mother glass), produced by using the conventional melt-quenching followed by a crystallization due to thermal treatment. When surface nucleation and crystal growth take place in the mother glass, inferior mechanical properties sometimes result. In this case, the mother glass is first pulverized, and the green compacts of the mother glass powder is heated at an appropriate heating schedule, in which

sintering and crystallization take place at the same time. Pulverization and heating are sometimes iterated to secure the mechanical properties of the products.

Special glass and glass-ceramics that can provide a direct chemical bond between the implant and surrounding hard tissues (bioactive) were developed by Hench (Hench *et al.*, 1972; Hench, 1991; Hench and Wilson 1993). The base composition in most bioactive glasses and glass-ceramics are SiO_2, Na_2O, CaO, and P_2O_5 (Cao and Hench, 1996). The surface reactivity of bioactive glass or glass-ceramics can be controlled by the chemical composition. The formation of a hydroxycarbonate apatite (HCA) layer at the interface between the bioactive glass and hard tissue is believed to be the prerequisite condition for achieving stable bone tissue bonding. The apatite formation mechanism was reported by Hench (1991) and Kokubo *et al.* (2001). Kokubo *et al.* suggested that dissolved silica species with silanol groups play an important role in the formation of HCA. Fluoride additions can promote the formation of the HCA layer while reducing the rate of network dissolution of the bioactive glass (Hench, 1991). On the other hand, Al_2O_3 can inhibit bone bonding, as can other multivalent cations such as Ta_2O_5, TiO_2, Sb_2O_3, and ZrO_2 (Gross and Strunz, 1985; Gross *et al.* 1988). Osaka and coworkers (Imayoshi *et al.*, 1997; Osaka *et al.*, 1998) examined the *in vitro* apatite formation on a series of pseudo binary silicate glasses of composition $xM_mO_n{\cdot}(50 - x/2) \cdot (CaO \cdot SiO_2)$ ($x < 10$ mol%; M = V, Cr, Mn, Co, Zn, W, Ta) with thin-film X-ray diffraction, infrared spectroscopy, and scanning electron micrograph after they were soaked in a simulated body fluid (Kokubo solution, SBF; Kokubo *et al.*, 1992). The Zn-glass and Ta-glasses were little corrosive, while Co-glass was corrosive. Co, Zn, and Ta ions remained in the resulting silica gel layer, preventing apatite formation. The Cr and Mn ions were released into the SBF as well as remaining in the silica gel layer where adsorbed calcium phosphates remained amorphous. The Cr-glass was similar to the Zn-glass regarding *in vitro* bioactivity. Addition of WO_3 shortened the induction time of apatite formation. The V-glass had a longer induction time than the mother glass but causes no effect on the growth of apatite nuclei.

One of the disadvantages of the bioactive glasses is their poor mechanical properties. The main reason for development of bioactive glass-ceramics is to produce implant materials with superior mechanical properties. The glass-ceramics can be considered as glass-crystal composites containing various kinds of crystalline phases with controlled sizes and contents (Kokubo, 1993).

Most clinically acceptable bone substitutes are totally resorbable prostheses and autogenous cancellous bone. The implant is remodeled by osteoclast activity and is eventually replaced by osteoid. Calcium phosphate implants show excellent resorption characteristics. Tricalcium phosphate

(TCP, $Ca_3(PO_4)_2$) has been developed as a bioactive and biodegradable bone substitute (Metsger *et al.*, 1982; Wiltfang *et al.*, 2002). Although the calcium phosphate implants are replaced by normal bone tissue, the load-bearing capacity is significantly weakened during the remodeling process because the rate of biodegradation of TCP is too fast. In order to reduce the rate of biodegradation, biphasic calcium phosphate (BCP) (composite ceramic that consists of mixtures of both the HA and β-TCP phases) ceramics have been used as a bone graft material over the past decade (Daculsi, 1998). The solubility of BCP will be closer to β-TCP or HA depending on the β-TCP/HA weight ratios in the composite ceramics. The solubility of these composite ceramics can be modified by varying their composition (impurities or substituents). Characteristics such as crystallinity, particle size, morphology, specific surface area, and defects play an important role in the degree of solubility. It is also dependent on the physical form of the ceramics when introduced in the human body: powder or bulk, dense or porous.

3.3 Imaging techniques for ceramics

3.3.1 X-ray diffraction

Coherent scattering of X-rays from crystalline materials leads to diffraction and diffraction patterns provide information about the structure and chemical composition of crystalline materials. The X-ray diffraction (XRD) technique is described in detail in several texts (Cullity, 1978; Stout and Jensen, 1989; Jenkins and Snyder, 1996). The sample must be crystalline to identify the phase. X-ray powder diffraction is used in the identification of crystalline phases in solid samples, evaluating the lattice parameter and other information such as crystallite size and lattice distortion, quantitative determination of phases in multiphase samples, and finding the orientation in single crystals or preferred orientation in the polycrystalline samples.

Compositional analysis is based on the fact that an X-ray diffraction pattern is unique for each crystalline material. Thus, chemical identification is completed when an exact match can be found between the pattern of the unknown material and an authentic sample. The identification of the phase from XRD patterns usually requires some standard patterns such as JCPDS (powder diffraction file of organic and inorganic phases), NBS crystal data, and Cambridge File of Organic Single Crystal Structural Data. These XRD patterns are available in software for X-ray powder diffraction. For the physical mixture, the powder diffraction pattern is the sum of the patterns of the individual materials. Therefore, the diffraction pattern can be used to identify the crystalline phases in a mixture. The concentrations of the crystalline phases can be determined by methods based on comparing the

intensities of the diffraction peaks with standard patterns. If the crystal structure of the phases is known, the concentration of each phase can be determined by Rietveld analysis (Rietveld, 1969; Young, 1993). In the Rietveld method, a theoretical diffraction pattern is computed, and the difference between the theoretical and observed patterns is minimized. The effects of factors such as preferred orientation, texturing, and particle size broadening must be minimized.

The narrower the XRD peaks, the greater is the length of continuity of atomic planes and the larger is the crystallite size (Elliott, 2002). As the grain or crystallite size becomes smaller, XRD analysis senses the decrease in length-scale of atomic planar continuity, which could be observed as a broadening of the diffraction peaks. HA is represented as $Ca_{10}(PO_4)_6(OH)_2$ and is characterized by a Ca/P ratio of 1.67. Stoichiometric HA is monoclinic with space group $P2_1/b$, exhibiting lattice parameters, $a = 0.94\ 15$ nm, $b = 2a$, $c = 0.688\ 15$ nm, $\gamma = 120°$ (Elliott, 1994). Earlier studies showed that it also could exhibit the hexagonal structure with space group $P6_3/m$. Typical XRD patterns from HA and hydroxyl-carbonated apatite (HCA) prepared by the wet-chemical process are shown in Fig. 3.1. It shows that carbonate substitution causes the broadening of the diffraction peaks, indicating a reduction in crystallite size. In addition to the crystallite size, the widths of XRD peaks contain some information about the strain within the crystallite (Baig *et al.*, 1999), which arises from regions of distorted unit-cell patterns that are continuous with regions of regularity/perfection. If the clusters of atoms, and thus the individual unit cells, are identical to each other (in terms of chemistry, size, shape, charge, and location) and perfectly aligned, then the crystallite will be unstrained. The widths of its XRD peaks will be the

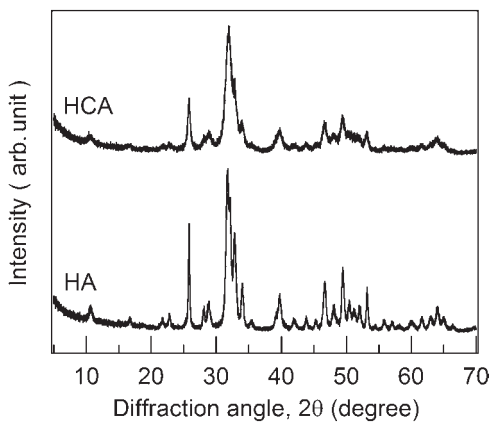

3.1 Powder X-ray diffraction patterns of hydroxyapatite particles (HA) and hydroxy-carbonated apatite (HCA).

same throughout the diffraction patterns, and their width will indicate the crystallite size. In contrast, a crystallite that is strained undergoes a decrease in its long-range order; this decrease is probably different in different directions. Therefore, the widths of its peaks in the X-ray diffraction patterns will not be uniform (Elliott, 2002; Wopenka and Pasteris, 2005).

3.3.2 Analysis of chemical composition of ceramics

Although phase characterization and identification of bulk materials are possible, surface analysis still remains a challenge. Since the composition near the surface is not always the same as the bulk, information given by bulk analysis methods may lead to misinterpretation of structure/function relationships. The main question in the biomaterials research regards the relationship between surface properties (chemical composition and differences between bulk and surface, morphology, etc.) and the biological response (Vogler, 1996). Qualitative or quantitative information about the chemical composition of the surface of materials can be derived from electron, ion, and photon emissions from the outermost layers of the surface. The most widely applicable techniques for characterizing the surface chemistry of glass and ceramics are Auger electron spectroscopy (AES), X-ray photoelectron spectroscopy (XPS), and secondary ion mass spectroscopy (SIMS). However, these surface analytical techniques require the use of ultra-high vacuum environment. The analysis conditions are limited and do not correspond to those found normal in the environment.

Auger electron spectroscopy (AES)

Auger electron spectroscopy (AES) can provide information on the chemical composition, which is based on a two-step process as shown schematically in Fig. 3.2. When an electron is emitted from inner atomic orbital through collision with incident electrons or X-rays, the resulting vacant site is soon filled by another electron from an outer orbital. The energy released in the transition may appear as an X-ray photon or may be transferred to another electron in an outer orbital, which is ejected from the atom with a kinetic energy E_k given by:

$$E_k = E_1 - E_2 - E_3^* \tag{3.1}$$

where E_1 and E_2 are the binding energies of the atom in the singly ionized state and E_3^* is the binding energy for the doubly ionized state (Rahaman Mohamed, 2007). The ejected electron (Auger electron) moves through the solid and soon loses its energy through inelastic collisions with bound electrons. However, if the Auger electron is emitted sufficiently close to the surface, it may escape from the surface and can be detected by an electron

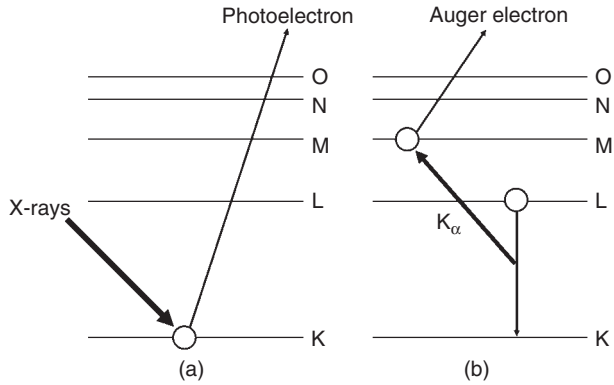

3.2 Interaction of incident X-rays with a solid, producing the atomic excitation with the emission of a photoelectron (a), followed by de-excitation with the emission of an Auger electron (b).

spectrometer. The number of electrons is plotted as a function of the kinetic energy of electrons. Since each type of atom has its own characteristic electron energy levels, the peaks in the observed Auger spectrum can be used to determine the elemental composition by comparison with standard Auger spectra for the elements. Thus, AES is largely used for elemental analysis. For ceramics materials, which are mostly insulating, electrostatic charging of the surface may occur and this leads to large shifts in the energies of the Auger electrons, making reliable analysis of the spectra difficult (Rahaman Mohamed, 2007).

It is possible to make depth scans by combination with surface etching, where the etching is carried out by an Argon ion beam sputtering. Such depth profiling mode is important because the composition of the surface is usually different from that of the bulk. The interface composition could be analyzed in depth by using AES, which is a useful tool to provide insight into the processes occurring at the surface of the materials. By using AES, Clark *et al.* (1976) and Kim *et al.* (1989) investigated the reaction stages that occur on the bioglass side of the interface between bioglass and tissue, and the early stage of calcium phosphate layer formation on the surface of the bioglass, respectively.

X-ray photoelectron spectroscopy (XPS)

X-ray photoelectron spectroscopy (XPS) is one of the most important methods for detecting the chemical composition and evaluating the chemical bonding states (or oxidation state) as well as the electronic structure of the surface (outermost 5–10 nm of ceramic materials). The sample is irradiated by a source of low-energy X-rays that leads to the emission of electrons

from the lower energy atomic orbitals by the photoelectric effect as shown in Fig. 3.2. The kinetic energy of the emitted photoelectrons, E_k, is given by:

$$E_k = h\nu - E_b - W \qquad 3.2$$

where $h\nu$ is the energy of the incident X-ray photon, E_b is the binding energy of the photoelectron, and W is the work function of the spectrometer (Rahaman Mohamed, 2007). By measuring the E_k, in a spectrometer (hemispherical analyzers and multichannel detectors) with a known W, the binding energy can be determined from Eq. (3.2). The data are commonly plotted as the number of emitted electrons (counts) vs. the binding energy. The binding energy of an electron is characteristic of the atom and orbital from which the electron was emitted. We are generally concerned with the core electrons with XPS. For qualitative analysis, a low-resolution, wide-scan spectrum covering a wide energy range (typically binding energy values of 0 to 1254 eV(Mg K_α) or 1487 eV (Al K_α)) serves as the basis for determining the elemental composition of the surface. The position of each peak in the spectrum is compared with standard spectra to determine the element present. Typical survey XPS spectra from commercial β-TCP and HA are shown in Fig. 3.3. It shows that Ca, P, O, and C contamination are present. Most of the carbon was so-called adventitious carbon due to adsorption of impurity hydrocarbons and actually used for binding energy calibration by setting its binding energy to 284.6 eV to correct for the sample charging (Wagner *et al.*, 1979).

For quantitative analysis, the principal peak for each element is selected and its intensity (peak area after removal of the background on the basis

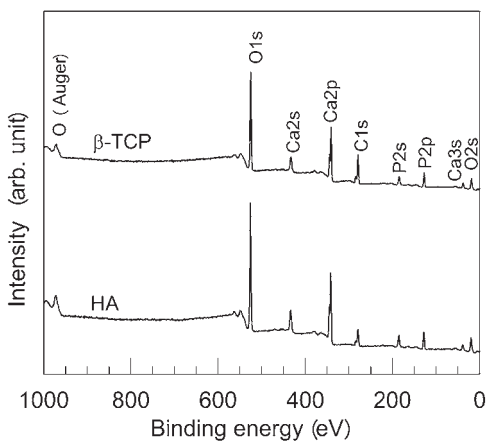

3.3 Survey XPS spectra from commercial β-TCP and HA.

of Shirley baseline subtraction; Shirley, 1972) is measured (Liu *et al.*, 2000).

The fractional atomic concentration of an element A is given by:

$$C_A = (I_A/S_A)/(\sum I_j/S_j) \quad 3.3$$

where I_j is the measured peak intensity of the element j and S_j is the atomic sensitivity factor for that peak (Rahaman Mohamed, 2007). The atomic sensitivity factors, which can be calculated theoretically or derived empirically, are usually provided in the reference manuals supplied by the manufacturer of the instrument. The accuracy of the quantitative analysis (less than 10%) is similar to that for AES (Rahaman Mohamed, 2007). Information about the chemical bonding and oxidation state of the surface atoms can be determined from the chemical shifts in the peak positions in the XPS spectrum. For ceramics, which are mostly insulating, electrostatic charging of the surface may occur and this leads to peak shape distortion from differential charge up on the surface of the non-conductive material, making reliable analysis of the spectra difficult. However, the surface charging can be neutralized by setting an Ni mesh screen 1 mm above the sample surface and flooding with low-energy electrons (5~7 eV) (Matsumoto *et al.*, 1995; Hayakawa *et al.*, 1998).

XPS is also a useful tool to provide insight into the chemical or biomimetic processes occurring at the surface of the biomaterials. An example of an application is the study of the process of apatite formation on bioactive Ti–6Al–4V alloy in SBF by Takadama *et al.* (2001). They reported that the bioactive alloy forms Ti–OH groups on its surface by exchanging Na^+ ions from the surface sodium titanate layer with H_3O^+ ions in the fluid. The Ti–OH groups on the alloy thereafter induce the apatite formation indirectly, by forming a calcium titanate and an amorphous calcium phosphate. The calcium titanate is postulated to gain a positive charge with increasing soaking time to interact with the negatively charged phosphate ions in the SBF, consequently forming an amorphous calcium phosphate, which later stabilizes into crystalline apatite.

3.3.3 Electron microscopy

Transmission electron microscopy (TEM)

Transmission electron microscopy (TEM) is dedicated to micro-structural analysis of solid materials down to the sub-nanometer scale. The photons are replaced by high-energy electrons (>100 kV) and the glass lenses by electromagnetic lenses. The electron beam passes an electron-transparent sample and an enlarged image is formed using a set of lenses. TEM provides

the possibility of taking high-resolution pictures and collecting diffraction patterns on small crystals or grains. The image contrast is obtained by the interaction of the electron beam with the sample: a part of the electrons will be diffracted. By means of an aperture, one or more diffracted beams are selected for the formation of the image. One can distinguish between different materials as well as image individual crystals and crystal defects. Also, it is possible to obtain the chemical composition by combination with energy-dispersive X-ray analysis (EDX), which is a semi-quantitative technique.

Some examples of applications are as follows. Daculsi *et al.* (1991) reported the presence of hexagonal parallelepiped lattice defects in addition to other defect structures in crystals of ceramic HA sintered at 950 °C but not in those prepared at 1250 °C. Microcrystals observed on the surface of ceramic HA after implantation in bony sites were identified as apatite by selective electron diffraction with TEM (Tracy and Doremus, 1984). Xin *et al.* (2006) reported that the *in situ* phase transformation of octacalcium phosphate (OCP) to HA was observed by TEM, in which the transformation was induced by electron beam irradiation. The transformation process and crystal structure changes were examined via bright-field images, electron diffraction, high-resolution transmission electron microscopy (HRTEM) and the fast Fourier transformation pattern of HRTEM images. Takadama *et al.* (2000) investigated the mechanism of apatite nucleation induced by Si–OH groups, where collodion films supported by titanium grids were faced to the CaO, SiO_2-based glass taking a distance of 0.5 mm in SBF at 36.5 °C and they were observed under TEM-EDX after soaking in SBF for various periods. Silicate ions dissolved from the glass were attached on the surface of the collodion film within 6 h, and combined with calcium ions in SBF to form an amorphous calcium silicate within 12 h. These calcium ions combined with the phosphate ions in SBF to form an amorphous calcium phosphate within 2 days. This amorphous calcium phosphate transformed into a crystalline apatite within 4 days.

Energy-filtering TEM (EF-TEM)

The elemental mapping approach can be the best way to analyze nanometer-scale features in materials such as fine particles and interfaces/boundaries, since two-dimensional fluctuations in composition around the nanometer-scale features, which may be missed by line-scan analyses, can be revealed in images of elemental distributions. Such elemental distributions can be obtained by a transmission electron microscope equipped with an energy filter (Botton and Phaneuf, 1999; Wittig *et al.*, 2001; Omura *et al.*, 2002) (EF-TEM), or a scanning transmission electron microscope with an X-ray energy dispersive spectrometer (STEM-XEDS) and/or an

electron energy loss spectrometer (STEM-EELS). The spatial resolution of the fixed beam EF-TEM technique can reach sub-nanometer ranges. Sample preparation methods such as the focused ion beam (FIB) technique are also essential to the successes of energy filtering methods in solving materials science problems.

Scanning electron microscopy (SEM)

Scanning electron microscopy (SEM) is a most useful characterization technique for micro-structural analysis of solid materials down to the sub-micrometer scale. SEM can be used to image the surfaces of ceramic materials or fracture surfaces of porous materials. It is possible to obtain the chemical composition by combination with EDX. Ohtsuki *et al.* (1991, 1992) prepared various kinds of glasses with different compositions in the ternary system $CaO–SiO_2–P_2O_5$ by a conventional melt-quenching technique and then soaked these glasses in SBF at 36 °C for various periods in order to investigate what kinds of material form the bone-like apatite layer on their surfaces in the living body. Apatite formation on their surfaces was examined by thin film (TF)-XRD analysis and SEM observation.

3.3.4 Fourier transform infrared (FT-IR) spectroscopy

Fourier-transformed infrared (FT-IR) spectroscopy is a useful characterization technique for molecular analysis of bulk samples and surface or near-surface species, as well as Raman scattering spectroscopy (or Raman spectroscopy). The molecular analysis means the recognition and the quantitative analysis of structural units in unknown compounds. The species are identified by their characteristic vibrational frequencies. For a vibrational mode to be IR active, the vibration must alter the dipole moment of the molecule: in contrast, a mode of vibration is Raman active when it changes polarizability of the relevant molecule or material. In either IR or Raman spectroscopy, when the photon energy equals the energy difference between ground and excited state (change in vibrational energy), the photons of specific wavenumbers between 10^2 and $10^4\,cm^{-1}$ induce a transition from a vibrational ground level of the molecule to an excited state. This transition can be detected as absorption of photons with energy equal to the energy difference of the involved vibrational levels because the molecule in the excited level returns very fast to the ground state by thermal relaxation. Since both provide similar information, this section describes about the IR spectroscopy.

Several IR absorption bands are caused by fundamental vibrations which can be classified into four types:

1 Stretching vibrations (one or more of the bond lengths change).
2 Planar bending vibrations (one or more bond angles change, while the bond lengths remain constant).
3 Out-of-plane bending vibrations (one atom oscillates through a plane defined by at least three neighboring molecules).
4 Torsion vibrations (a dihedral angle (the angle between two planes, which have one bond in common) is changed).

The bending vibrations are sometimes split into rocking, twisting, and wagging bands. The vibrations can also be classified by symmetry, where symmetrical vibrations retain the symmetry of the group and asymmetrical vibrations disturb one or more of the symmetry elements of the molecule (Fadini and Schnopel, 1989). The IR activity and degeneracy of a molecular vibration depend on the molecular symmetry. When the molecule is present in a crystal, the symmetry of the surrounding of the molecule in the unit cell (site symmetry) determines the selective rules. Therefore, the basic structure of the species and phase composition of compounds can be determined by the spectral locations of their IR absorption bands. The plot of a compound's IR transmission or absorbance vs. wavenumber is its 'fingerprint', which identifies the material when compared to reference spectra.

Typical FT-IR absorption spectra from HA and HCA prepared by the wet chemical process are shown in Fig. 3.4. Since the phosphate ion is a tetrahedral molecule (PO_4), it has four normal modes of vibration (ν_1, ν_2, ν_3, and ν_4); only ν_3 and ν_4 are IR-active on the basis of the molecular symmetry. The HA sample produced the characteristic phosphate (ν_3, ν_4) and

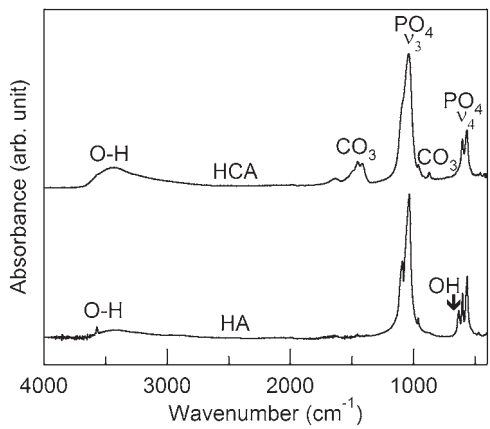

3.4 FT-IR absorption spectra of hydroxyapatite (HA) and hydroxycarbonated apatite(HCA).

hydroxide bands (LeGeros, 2001). In addition to these phosphate and hydroxide bands, the HCA sample produced bands corresponding to carbonate groups ranging from 1600 to 1400 cm^{-1} for the ν_3 bands (asymmetric stretching vibration), around 880 cm^{-1} for the ν_2 bands (bending out-of-plane vibration), and at 755 cm^{-1} for the ν_4 band (bending in-plane vibration). (Rey *et al.*, 1991). The intensity of the band corresponding to the librational mode of hydroxyl groups at approximately 630 cm^{-1} reduced remarkably as a result of carbonate substitution; the same effect was observed for the band at approximately 3572 cm^{-1}, corresponding to the hydroxyl stretching mode.

One of the major problems in FT-IR spectroscopy is that water is a very strong IR absorber. Water vapor has very strong, sharp IR absorption bands around 1700 and 3700 cm^{-1} that are hard to correct. Therefore, the amount of water vapor in the atmosphere within the spectrometer is often reduced by purging with dry nitrogen gas or by putting the optical part of the FT-IR spectrometer in vacuum.

FT-IR spectroscopy has been used extensively in the study of the mineral phase in both synthetic apatites and homogenized calcified tissues from animals and humans. With micro-FT-IR spectroscopy one can analyze the chemical composition of materials without altering morphology (Carr, 2001; Petra *et al.*, 2005). This powerful technique permits the study of spatially inhomogeneous systems such as bone, providing information from all tissue components (both organic and inorganic). The use of synchrotron IR beam for micro-spectroscopy offers the great advantage of 100–1000 times greater brightness, compared with the IR beam of a thermal (globar) source. The long wavelengths of IR radiation limit the spatial resolution that can be achieved, and spatial resolution is of paramount importance for the study of inhomogeneous biological tissues, such as bone. The use of a synchrotron IR source permits the micro-spectroscopic study of very small surface areas of biological samples, with acceptable signal-to-noise ratio (S/N), at apertures even smaller than the wavelength of light used (Carr, 2001).

Infrared reflection spectroscopy (IRRS) is one of the techniques for examining the surface structure of a material to a depth of approximately 0.5 μm (Sanders and Hench, 1973). It is a nondestructive technique developed for the study of reactions between aqueous solutions and the surfaces of glasses and ceramics. The information obtained is averaged over the entire sampling depth and one can obtain qualitative and semiquantitative data regarding the condition of the surface. Hench summarized the sequence of the reaction stages which occur on the surface of the bioactive glass when a bond with bone tissue is formed (Hench, 1991).

3.3.5 Solid-state nuclear magnetic resonance (NMR) spectroscopy

Solid-state nuclear magnetic resonance (NMR) spectroscopy is a powerful technique for providing information about the structure of materials and the dynamics of processes occurring within those materials. For example, solid-state NMR can monitor the structural change in the phase transition and formation and growth of crystalline phase from colloids, glasses, or gels. For detecting the NMR spectrum, a nucleus must possess a nuclear spin. Nuclei with odd mass number have half-integer spins (e.g. ^{1}H, ^{11}B, ^{13}C, ^{19}F, ^{23}Na, ^{27}Al, ^{29}Si, ^{31}P) are of most interest for solid-state NMR. The angular momentum of a spinning nucleus is a function of its spin quantum number I which can have either integer or half-integer values. When such a nucleus is placed in a strong magnetic field, the energy levels between the various spin states are split owing to the Zeeman interaction. The differences between the various energy levels are small and the transitions are only possible between adjacent energy levels, with the absorption or emission of a photon in the radio-frequency (RF) range. The frequency of the RF radiation is measured in an NMR experiment. The nuclei in different structural environments in solids may experience slightly different magnetic fields because they are shielded by the surrounding electrons and consequently absorb photons of slightly different frequencies. The resonance frequencies (1/2 to –1/2) are usually reported as chemical shifts (δ) relative to an external standard compound (Mackenzie and Smith, 2002).

The NMR spectra of solids shows line broadening due to various interactions between the dipole moments of the nuclei, between the quadrupole moments of quadrupolar nuclei and the electric field gradient (EFG) at the nucleus, and by anisotropy of the electronic shielding at different sites in the structure. This broadening does not arise in the liquid state because the atomic motion is faster than the interaction frequency, allowing all nuclei in a particular atomic environment to experience the same average magnetic field and producing a long spin–spin relaxation time (T_2), hence producing an extremely narrow NMR line. The NMR interactions giving rise to line broadening in solids can be cancelled out or reduced by spinning the sample very rapidly at an angle of 54.7° to the axis of the applied external magnetic field. The angle is called the magic angle. Magic angle spinning (MAS) removes the dipole–dipole and chemical shift anisotropy (CSA) interactions, as well as the first-order quadrupolar interactions (Andrew, 1981).

Figure 3.5 shows the ^{31}P MAS-NMR spectra of calcium pyrophosphate (β-$Ca_2P_2O_7$) observed with different spinning speeds. It is noted that the NMR lines equispaced on each side of the central resonance (spinning side

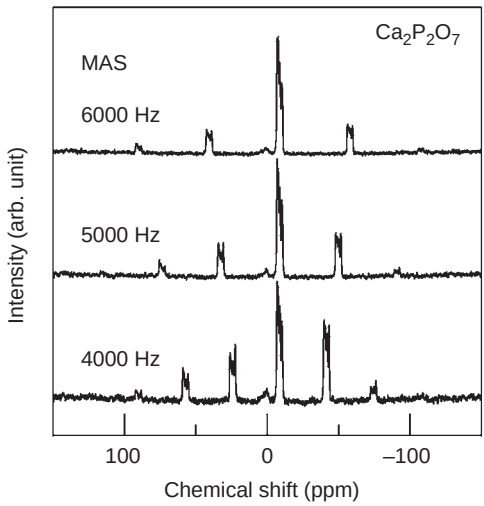

3.5 ^{31}P MAS-NMR spectra of pyrophosphate (β-$Ca_2P_2O_7$) observed with different spinning speeds.

bands) are caused by modulation of the interaction by the physical act of spinning the sample. The NMR spectra have intensities that depend on the relative magnitudes of the spinning speed and the magnitude of the interaction being averaged. Since they are harmonics of the spinning speed, they can be distinguished from true peaks because their position changes with the spinning speed, moving away from the central peak at higher speeds. The central peak position indicates the isotropic chemical shift (δ_{iso}), the average chemical shift which is experienced by the nucleus.

Some examples of applications are structural analysis of bioglass and bioceramics; Bioglass® materials use the Na_2O–CaO–P_2O_5–SiO_2 system and are currently used to replace hard tissue (Hench, 1991). Their structure has been studied by ^{23}Na, ^{29}Si, and ^{31}P NMR (Lockyer *et al.*, 1995) and was shown to consist of Q^2 ($Si(OSi)_2(O^-)_2$) and Q^3 ($Si(OSi)_3O^-$) glass networks, the former associated preferentially with Ca^{2+} and the latter with Na^+. Hayakawa *et al.* (1999) measured ^{29}Si and ^{31}P MAS-NMR spectra for $20Na_2O \cdot 80SiO_2$ glass particles before and after being soaked in an SBF (Kokubo solution, pH = 7.4; Kokubo *et al.*, 1992) for various periods up to 14 days. Not only the structure of bulk glass and glass surface but also the chemical states of calcium phosphates adsorbed on the glass surface were examined. As shown in Fig. 3.6, the bulk glass before soaking in the SBF showed two ^{29}Si MAS-NMR resonances at –100 and –110 ppm, attributable to Q^3, $Si(OSi)_3ONa$, and Q^4, $Si(OSi)_4$, units, respectively. A new, –105 ppm peak, due to $Q^3(OH)$, $Si(OSi)_3OH$, units appeared after soaking in the SBF and grew with the soaking period. Thus in the SBF the glass network was

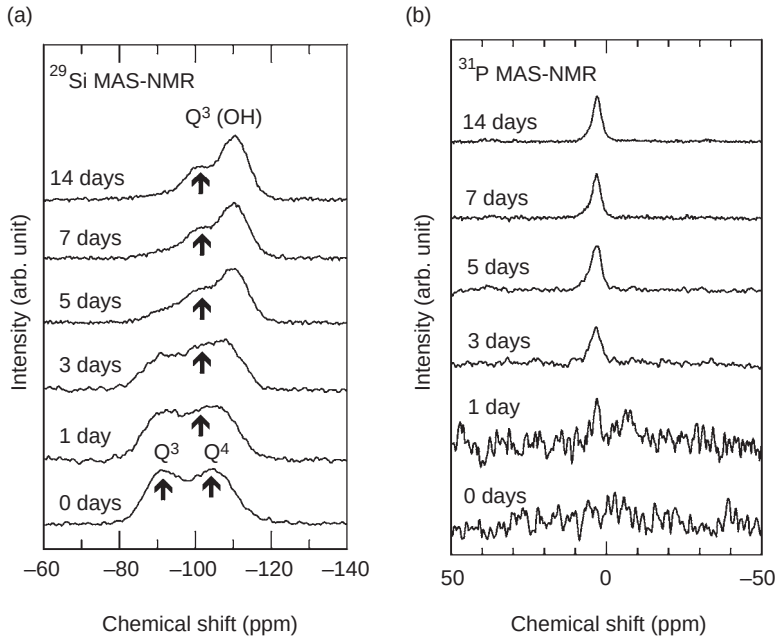

3.6 ^{29}Si and ^{31}P MAS-NMR spectra for $20Na_2O \cdot 80SiO_2$ glass particles before and after being soaked in a simulated body fluid (SBF: Kokubo solution, pH = 7.4; Kokubo, 1992) for various periods up to 14 days.

degraded and hydrolyzed, that is, the dissolution of the Na^+ ions from the glass network and the formation of Si–O^- groups took place. After soaking for 1 day a ^{31}P MAS-NMR resonance of orthophosphate (PO_4^{3-}) ions deposited on the glass surface appeared at ca. 3.0 ppm and grew with the soaking period. It was concluded that the hydrated silica gel layer composed of $Si(OSi)_3O^-$ units provided the negatively charged sites which induced or promoted the precipitation of calcium phosphates leading to apatite nucleation and crystallization.

Sfihi and Rey (2002) and Cazalbou *et al.*(2005) suggested that HA crystal was covered with an amorphous hydrated surface layer by two-dimensional ^{1}H–^{31}P heteronuclear correlation (HETCOR) NMR spectroscopy (Santos *et al.*, 1994) and confirmed that the obtained HA samples exhibited a metastable hydrated surface layer involving HPO_4^{2-} ions and water molecules. Jäger *et al.* (2006) studied the structure of *nanocrystalline HA* based on the quantification of the ^{31}P and ^{1}H NMR spectra using experimental information (e.g. line shapes) from two-dimensional NMR experiments. They proposed that these nanocrystals consist of a crystalline HA core covered by a disordered surface layer. The Ca/P ratio of the surface layer, 1.52 was

estimated from the NMR data that compares well with the value of 1.51 from chemical analysis. The surface of nanocrystalline HA has nothing in common with the bulk composition.

Among functional monomers used in contemporary dental adhesives, 10-methacryloyloxydecyl dihydrogen phosphate (MDP) was found to chemically interact most intensively and stably with HA (Yoshida *et al.*, 2004). This effect was thought to be at the basis of the superior bonding effectiveness of MDP-based self-etch adhesives to enamel/dentin. In order to fully elucidate the chemical interaction and reactivity of MDP with HA, Fukegawa *et al.* (2006) used ^{31}P cross-polarization(CP)-MAS NMR spectroscopy and powder X-ray diffraction. The intense chemical interaction of MDP with HA can be ascribed to superficial dissolution of HA induced by the MDP adsorption and subsequent deposition of MDP-calcium salt with lower solubility than $CaHPO_4 \cdot 2H_2O$.

3.3.6 Other surface or macropore imaging techniques

Scanning tunneling microscopy (Binnig *et al.*, 1982; Latyshev *et al.*, 1989; Rohrer H., 1994), atomic force microscopy AFM; (Binnig *et al.*, 1986) and related techniques also provide information about the surface topography of bioceramics (Webster *et al.*, 2000a). Farina *et al.* (1999) used AFM in order to study the outermost layer of the tooth surfaces in terms of particle arrangement, packing, and size distribution. It was found that AFM gives high-contrast, high-resolution images and is an important tool as a source of complementary and/or new structural information. Kamiya *et al.* (2004) reported on AFM analysis of the formation of carbonate-containing hydroxyapatite on a calcite surface due to the reaction with phosphoric acid or phosphate in the initial stage, where the cleaved calcite was immersed in phosphoric acid or diammonium hydrogenphosphate under various conditions. The calcite dissolved upon immersion in phosphoric acid and many pits, oriented in a particular direction, were observed on the calcite surface. When the calcite was soaked in diammonium hydrogenphosphate, reaction products; carbonate-containing hydroxyapatite, also aligned in a particular direction, were observed on the calcite surface. Onuma (2006) has studied the growth and phase transition mechanisms of HA and its interaction with a growth factor protein in a simulated physiological environment by using AFM and real-time phase shift interferometry. He performed *in situ* observations of growth in simulated human body fluid solutions seeded with millimeter-sized HA single crystals produced by hydrothermal synthesis, and measured the normal growth rate. The growth units of HA crystals are supposed to be clusters rather than simple ions and that growth proceeds through the accumulation of these clusters.

Biomaterials research has been advancing in recent years, particularly in the field of tissue engineering. A typical tissue engineering device comprises cells and scaffolds. Cells and cellular product provide the biological function while synthetic materials give the structural support. Biomaterials have been used as a supporting scaffold for the growth of cellular components. The scaffold will provide the physicochemical signals to control cellular interactions, give the structural support, and also provide sites for cell attachment, migration, and tissue ingrowth. In the development of bone substitutes, high porosity and interconnected pores are required for the following considerations (Shi, 2006):

- Porous materials have large surface area, resulting in a high tendency to bioresorb, which induces high bioactivity.
- Interconnected pores permit tissue ingrowth and thus anchor the prosthesis with the surrounding bone tissue, preventing the loosening of implants.

The interconnected porosity acts as an organization of vascular canals which can ensure the blood and nutrition supply for the bone. The dimension of the interconnected system must be at least 100 μm in diameter in order to provide a blood supply to the host tissue (Hulbert *et al.*, 1987). Therefore, for macroporous tissue scaffold, it is important to characterize the three-dimensional pore network. Mercury porosimetry can be used to obtain size distribution of the channels between pores, but is a destructive technique. X-ray micro-computer tomography (μCT) is an excellent technique for obtaining three-dimensional images of scaffold pore networks. The μCT instrument can have resolutions of up to 2 μm in three dimensions and 1 μm resolution by using a synchrotron X-ray source (Toda *et al.*, 2006). Recently, methods of quantifying the porous networks have been developed using three-dimensional image analysis techniques, so that pore and interconnect size distribution can be obtained nondestructively (Weiss *et al.*, 2003; Atwood *et al.*, 2004; Vanis *et al.*, 2006).

3.4 Summary

Recently, *nanocrystalline HA* (nano HA) has been found to be more interesting than micrometer-sized HA from a biological and medical viewpoint because of its similarity to minerals in natural bone. Compared with conventional micrometer-scale HA, nano HA offers the possibility to enhance the rate of bone-bonding formation and to have excellent mechanical properties due to its high surface area to volume ratio, superior chemical homogeneity and microstructural uniformity (Catledge *et al.*, 2002). The rate of HA bonding to bone was demonstrated to be dependent not on the composition but on the release of calcium and phosphate ions from HA,

determining the development of implant–bone interfacial strength (van Blitterswijk *et al.*, 1986). Sufficient dissolution of calcium and phosphate species is necessary to form bone-like apatite and bone bonding. The dissolution law of nano HA has been proven to be very different from that of conventional HA, and the dissolution of nano HA is dominated by its particle size (Hench, 1991). The particle-size effect is explained by the fact that small-sized particles of HA may be degradable and stimulate bone ingrowth as they dissolve in the physiological environment (Uota *et al.*, 2005). Osteoblastic cell behaviors on nano HA play a crucial role in osteogenesis and subsequent osseointegration. A knowledge of the correlation of cellular reactions and structures of nano HA would be of importance for the understanding of the interaction at the nano HA–bone interface on the cellular level. In addition, since the adsorption of cellular and plasma proteins on bioceramics plays important roles in the host response processes, the study of this phenomenon is also important for understanding the molecular basis of biocompatibility and for designing novel biomaterials with required properties or advanced functions. However, few studies have been carried out to assess the direct or indirect effects of nano-phase bioceramics on the protein adsorption and aggregation with conformational change at the nano-interface involving the surface of the nano-phase bioceramics and proteins. One should clarify the microstructure of such nano-phase bioceramics from many viewpoints such as chemical composition (stoichiometry or purity), homogeneity, phase distribution, morphology, grain size/grain shape, grain boundaries, crystallite size, crystallinity, pores, cracks and surface, and their chemical interaction with various cells and cellular proteins with chemical binding functional groups.

Many imaging techniques have been developed for characterizing the chemical composition, microstructure, and the surface of bioceramics. However, one should pay attention to the limit of various analytical techniques in terms of difference in resolution and sensitivity on the basis of their principles. For example, owing to the lack of the long-range ordering, the determination of the structure of glass or glass-ceramics materials is possible exclusively using spectroscopic methods, which are sensitive to short-range ordering. It is commonly assumed that the structure of amorphous materials is closely related to the structure of the relevant crystalline materials. Therefore, the interpretation of the spectra of amorphous materials is based on the spectroscopic studies of the corresponding crystalline materials.

3.5 References

Andrew E. R., (1981), 'Magic angle spinning,' *Int. Rev. Phys. Chemi.*, **1**, pp. 195–224.

Atwood R. C., Jones, J. R., Lee P. D., Hench L. L., (2004), 'Analysis of pore interconnectivity in bioactive glass foams using X-ray microtomography,' *Scripta Mater*., **51**[11], pp. 1029–1033.

Baig A. A., Fox J. L., Young R. A., Wang Z., Hsu J., Higuchi W. I., Chhettry A., Zhuang H., Otsuka M., (1999), 'Relationships among carbonated apatite solubility, crystallite size, and microstrain parameters,' *Calcif. Tissue Int*., **64**[5], pp. 437–449.

Binnig G., Rohrer H., Gerber C., Weibel E., (1982), 'Surface studies by scanning tunneling microscopy', *Phys. Rev. Lett*., **49**[1], pp. 57–61.

Binnig G., Quate C. F., Gerber C., (1986), 'Atomic force microscope,' *Phys. Rev. Lett*., **56**[9], pp. 930–933.

van Blitterswijk C. A., Grote J. J., Kuijpers W., Daems W. Th., de Groot K., (1986), 'Macropore tissue ingrowth: a quantitative and qualitative study on hydroxyapatite ceramic,' *Biomaterials*, **7**[2], pp. 137–143.

Botton G. A., Phaneuf M. W., (1999), 'Imaging, spectroscopy and spectroscopic imaging with an energy filtered field emission TEM,' *Micron*, **30**, pp. 109–119.

Cao W., Hench L. L., (1996), 'Bioactive Materials,' *Ceramic Int*., **22**, pp. 493–507.

Carr L. G., (2001) 'Resolution limits for infrared micro-spectroscopy explored with synchrotron radiation,' *Rev. Sci. Instrum*. **72**, p. 1.

Catledge S. A., Fries M. D., Vohra Y. K., Lacefield W. R., Lemons J. E., Woodard S., Venugopalan R., (2002), 'Nanostructured ceramics for biomedical implants,' *J. Nanosci. Nanotechnol*. **2**[3, 4], pp. 293–312.

Cazalbou S., Eichert D., Ranz X., Drouet C., Combes C., Harmand M. F., Rey C., (2005), 'Ion exchanges in apatites for biomedical application,' *J. Mater. Sci.; Mater Med*., **16**, pp. 405–409.

Clark A. E., Pantano C. G., Hench L. L., (1976), 'Auger spectroscopic analysis of bioglass corrosion films,' *J. Am. Ceram. Soc*., **59**[1–2], pp. 37–39.

Cullity B. D., (1978), '*Elements of X-ray Dffraction*,' 2nd ed, Addison-Wesley, Reading, MA.

Daculsi G., (1998), 'Biphasic calcium phosphate concept applied to artificial bone, implant coating and injectable bone substitute,' *Biomaterials*, **19**[16], pp. 1473–1478.

Daculsi G., LeGeros R. Z., LeGeros J. P., Mitre D., (1991), 'Lattice defects in calcium phosphate ceramics; high resolution TEM ultrastructural study,' *J. Appl. Biomat*. **2**, pp. 147–152.

Elliott J C., (1994), *Structure and Chemistry of the Apatites and other Calcium Orthophosphates*, Elsevier, Amsterdam.

Elliott J. C., (2002), 'Calcium phosphate biominerals,' in: Kohn M. J., Rakovan J., Hughes J. M. (Eds.), *Phosphates: Geochemical, Geobiological and Material Importance, Reviews in Mineralogy and Geochemistry*, vol. **48**, Mineralogical Society of America, Washington, DC, pp. 427–454.

Evans A. G., (1992), 'A method for evaluating the time-dependent failure characteristics of brittle materials – and its application to polycrystalline alumina,' *J. Mater. Sci*., **7**, pp. 1137–1146.

Fadini A., Schnopel F. M., (1989) '*Vibrational Spectroscopy: Methods & Applications*,' Wiley, New York.

Farina M., Schemmel A., Weissmüller G., Cruz R., Kachar B., Bisch P. M., (1999), 'Atomic force microscopy study of tooth surfaces,' *J. Struct. Biol*., **125**[1], pp. 39–49.

Fukegawa D., Hayakawa S., Yoshida Y., Suzuki K., Osaka A., Van Meerbeek B., (2006), 'Chemical interaction of phosphoric acid ester with hydroxyapatite,' *J. Dent. Res*., **85**[10], pp. 941–944.

Gross U., Strunz V., (1985), 'Interface of various glasses and glass-ceramics in a bony implatation bed,' *J. Biomed. Mater. Res*., **19**, pp. 251–271.

Gross U., Kinne R., Schmit H. J., Strunz V., (1988), 'The response of bone to surface active glass and glass-ceramics,' *CRC Critical Rev. Biocompatibility*, **4**, pp. 155–179.

Hayakawa S., Nakao A., Ohtsuki C., Osaka A., Matsumoto S., Miura Y., (1998), 'An X-ray photoelectron spectroscopic study of the chemical states of fluorine atoms in calcium silicate glasses,' *J. Mater Res*., **13**[3], pp. 739–743.

Hayakawa S., Tsuru K., Ohtsuki C., Osaka A., (1999), 'Mechanism of apatite formation on a sodium silicate glass in a simulated body fluid,' *J. Am. Ceram. Soc*., **82**[8], pp. 2155–2160.

Heimke G., (1983), 'Bioinert ceramics,' In: Vincenzini P., (Ed.) *Ceramics in Surgery*, Elsevier, Amsterdam, NL, pp. 33–41.

Hench L.L., (1991), 'Bioceramics: from concept to clinic,' *J. Am. Ceram. Soc*., **74**[7], pp. 1487–1510.

Hench L. L., Ethridge E. C., (1982), *Biomaterials An Interfacial Approach*, in Biophysics and Bioengineering Series Vol. **4**, Academic Press, Inc., New York.

Hench L. L., Wilson J., (1993), 'An introduction to bioceramics', in *Advanced Series in Ceramics*, vol. **1**, World Scientific, London, pp. 41–73.

Hench L. L., Splinter R. J., Allen W. C., Greenlee, Jr, T. K., (1972), 'Bonding mechanisms at the interface of ceramic prothetic materials,' *J. Biomed. Mater. Res*., **2**, pp. 117–141.

Hulbert S., (1993) 'The use of alumina and zirconia in surgical implants,' in Hench L. L., Wilson J., Eds., *Advanced Series in Ceramics* – Vol. 1. *An Introduction to Bioceramics*, World Scientific Publishing, Singapore, pp. 25–40.

Hulbert S. F., Bokros J. C., Hench L. L., Wilson J., Heimke G., (1987), 'Ceramics in clinical applications: past, present and future,' *High Tech. Ceram*., pp. 189–213.

Imayoshi N., Ohtsuki C., Hayakawa S., Osaka A., (1997), 'Effect of multivalent cations in calcium silicates on bioactivity,' in Ed. Sedel L. and Rey C., *Bioceramics*, Vol. **10**, Pergamon, Paris, France. pp. 41–44.

Jäger C., Welzel T., Meyer-Zaika W., Epple M., (2006), 'A solid-state NMR investigation of the structure of nanocrystalline hydroxyapatite,' *Magn. Reson. Chem*., **44**, pp. 573–580.

Jenkins R., Snyder R. L., (1996), '*Introduction to X-ray Powder Diffractometry*,' John Wiley & Sons, New York.

Kamiya M., Hatta J., Shimada E., Ikuma Y., Yoshimura M., Monma H., (2004), 'AFM analysis of initial stage of reaction between calcite and phosphate,' *Mater. Sci. Eng. B*, **111**[2–3], pp. 226–231.

Kim C. Y., Clark A. E., Hench L. L., (1989), 'Early stages of calcium-phosphate layer formation in bioglasses,' *J. Non-Cryst. Solids*, **113**[2–3], pp. 195–202.

Kokubo T., (1993), 'A/W glass-ceramic: processing and properties,' in Hench L. L., Wilson J., (Eds.) *Advanced Series in Ceramics* Vol. **1**, *An Introduction to Bioceramics*, World Scientific Publishing, Singapore, pp. 75–88.

Kokubo T., Kushitani H., Ohtsuki C., Sakka S., Yamamuro T., (1992), 'Chemical reaction of bioactive glass and glass-ceramics with a simulated body fluid,' *J. Mat. Sci.: Mat. Med.*, **3**, pp. 79–83.

Kokubo T., Kim H.-M., Kawashita M., Nakamura T., (2001) 'Process of calcification on artificial materials,' *Z. Kardiol*, **90**, Suppl. 3, III/86-III/91.

Krell A., (1996), 'Improved hardness and hierarchic influences on wear in submicron sintered alumina,' *Mater. Sci. Eng. A*, **209**, pp. 156–163.

Krell A., Blank P., (1996), 'The influence of shaping method on the grain size dependence of strength in dense submicrometre alumina,' *J. Eur. Ceram. Soc.*, **16**, pp. 1189–1200.

Krell A., Pippel E., Woltersdorf J., Burger W., (2003), 'Subcritical crack growth in Al_2O_3 with submicron grain size,' *J. Eur. Ceram. Soc.*, **23**, pp. 81–89.

Latyshev A. V., Assev A. L., Krasillnikov A. B., Stenin S. I., (1989), 'Transformations on clean Si(111) stepped surface during sublimation,' *Surf. Sci.*, **213**[1, 2], pp. 157–169.

LeGeros R. Z., (2001) 'Formation and transformation of calcium phosphates: relevance to vascular calcification,' *Z. Kardiol.* **90**, Suppl 3, III/116 III/124.

LeGeros R. Z., LeGeros J. P., (1993), 'Dense hydroxyapatite,' in Hench L. L., Wilson J., (Eds) *Advanced Series in Ceramic*s Vol. 1, *An Introduction to Bioceramics*, World Scientific Publishing, Singapore, pp. 139–180.

Liu H. B., Campbell C. T., Graham D. J., Ratner B. D., (2000), 'Surface characterization of hydroxyapatite and related calcium phosphates by XPS and TOF-SIMS,' *Anal. Chem.* **72**, pp. 2886–2894.

Lockyer M. W. G., Holland D., Dupree R., (1995), 'NMR investigation of the structure of some bioactive and related glasses,' *J. Non-Cryst. Solids*, **188**[3], pp. 207–219.

Mackenzie K. J. D., Smith M. E., (2002), Pergamon Materials Science Series, Cahn R.W., (Ed). '*Multinuclear Solid-State NMR of Inorganic Materials*,' Pergamon Press, Oxford.

Matsumoto S., Miura Y., Nanba T., Osaka A., (1995), *Proceedings of XVII International Congress on Glass*, Beijing **3**, pp. 72–77.

Metsger D. S., Driskell T. D., Paulsrud J. R., (1982), 'Tricalcium phosphate ceramic – a reasonable bone implant: review and current status,' *J. Am. Dent. Assoc.*, **105**[6], pp. 1035–1038.

Ohtsuki C., Kokubo T., Takatsuka K, Yamamuro T., (1991), 'Compositional dependence of bioactivity of glasses in the system $CaO–SiO_2–P_2O_5$: its *in vitro* evaluation,' *Nippon Seramikkusu Kyokai Gakujyutu Ronbunshi* (in English), **99**[1], pp. 1–6.

Ohtsuki C., Kokubo T., Yamamuro T., (1992), 'Mechanism of apatite formation on $CaO–SiO_2–P_2O_5$ glasses in a simulated body fluid,' *J. Non-Cryst Solids*, **143**, pp. 84–92.

Omura T., Watanabe M., Tomokiyo Y., (2002), 'Quantitative evaluation of zero-loss and core-loss images by using EF-TEM,' *J. Electron Microsc.* **51** (Suppl.), S87–S96.

Onuma K., (2006), 'Recent research on pseudobiological hydroxyapatite crystal growth and phase transition mechanisms,' *Prog. Crystal Growth Characterization Mater*., **52**[3], pp. 223–245.

Osaka A., Hayakawa S., Ohtsuki C., (1998), 'Effect of cations on surface reactions and apatite nucleation on silicate glasses in a body environment, in LeGeros R. Z. and LeGeros J. P., (Eds.) *Bioceramics*, Vol. **11**, World Scientific, Singapore, pp. 489–492.

Petra M., Anastassopoulou J., Theologis T., Theophanides T., (2005) 'Synchrotron micro-FT-IR spectroscopic evaluation of normal paediatric human bone,' *J. Molec. Struct*., **733**, pp. 101–110.

Rahaman Mohamed N., (2007), *Ceramic Processing*, CRC Press, Taylor & Francis Group, Boca Raton, London, pp. 130–133.

Rey C., Renugo Palakrishnan V., Collins B., Glimcher M. J., (1991) 'Fourier transform infrared spectroscopy study of the carbonate ions in bone mineral during aging,' *Calcif. Tissue Int*., **49**, pp. 251–258.

Rietveld J. M., (1969), 'A profile refinement method for nuclear and magnetic structures,' *J. Appl. Cryst*., **2**, pp. 65–71.

Ritter J. E., Greenlee D. C., Palmaer R. A., Hench L. L., (1979), 'Use of fracture mechanics theory in lifetime predictions for alumina and bioglass-coated alumina,' *J. Biomed. Mater. Res*., **13**, pp. 251–263.

Rohrer H., (1994), 'Scanning tunneling microscopy: a surface science tool and beyond,' *Surf. Sci*., 299, pp. 956–964.

Sanders D. M., Hench L. L., (1973), 'Mechanism of glass corrosion,' *J. Am. Ceram. Soc*., **56**, pp. 373–377.

Santos R. A., Wind R. A., Bronnimann C. E., (1994) '^{1}H CRAMPS and ^{1}H-^{31}P HetCor experiments on bone, bone mineral, and model calcium phosphate phases,' *J. Magn. Reson. B*, **105**, pp. 183–187.

Sfihi H., Rey C., (2002), '1-D and 2-D double resonance heteronuclear magnetic resonance study of the local structure of type B carbonate fluoroapatite,' in Fraissard J. and Lapina B. (Eds.), *Magnetic Resonance in Colloid and Interface Science*, Nato ASI series II, Vol 76, Kluwer Academic Publisher, New York. pp. 409–422.

Shi D., (2006), '*Introduction to Biomaterials*', Tsinghua University Press, World Scientific Publishing Co. Pte. Ltd., Beijing.

Shirley D. A., (1972), 'High-resolution X-ray photoemission spectrum of the valence bands of gold,' *Phys. Rev., B* **5**[12], pp. 4709–4714.

Stout G. H., Jensen L. H., (1989), *X-ray Structure Determination*, John Wiley & Sons, New York.

Takadama H., Kim H.-M., Miyaji F., Kokubo T., Nakamura T., (2000) 'Mechanism of apatite formation induced by silanol groups – TEM observation,' *J. Ceram. Soc. Japan*, **108**, pp. 118–121.

Takadama H., Kim H-M., Kokubo T., Nakamura T., (2001), 'XPS study of the process of apatite formation on bioactive Ti-6Al-4V alloy in simulated body fluid,' *Sci. Technol. Adv. Mater*., **2**, pp. 389–396.

Toda H., Ohgaki T., Uesugi K., Kobayashi M., Kuroda N., Kobayashi T., Niinomi M., Akahori T., Makii K., Aruga Y., (2006), 'Quantitative assessment of microstructure and its effects on compression behavior of aluminum foams via high-resolution synchrotron X-ray tomography,' *Metall. Mater. Trans, A*, **37A** [4], pp. 1211–1219.

Tracy B. M. Doremus R. H., (1984), 'Direct electron microscopy studies of the bone–hydroxyapatite interface,' *J. Biomed. Mater. Res*., **18**, pp. 719–726.

Uota M., Arakawa H., Kitamura N., Yoshimura T., Tanaka J., Kijima T., (2005), 'Synthesis of high surface area hydroxapatite nanoparticles by mixed surfactant-mediated approach,' *Langmuir*, **21**[10], pp. 4724–4728.

Vanis S., Rheinbach O., Klawonn A., Prymak O., Epple, M., (2006), 'Numerical computation of the porosity of bone substitution materials from synchrotron microcomputer tomographic data,' *Mat.-wiss. u. Werkstofftech*. **37**[6], pp. 469–473.

Vogler A., (1996), 'On the biomedical relevance of surface spectroscopy,' *J. Electron Spectrosc. Relat. Phenom.*, **81**, pp. 237–247.

Wagner C. D., Riggs W. M., Davis L. E., Moulder J. F., Muilenberg G. E. (editors) (1979), '*Handbook of X-ray Photoelectron Spectroscopy, a Reference Book of Standard Data for Use in X-Ray Photoelectron Spectroscopy*,' Perkin-Elmer Corp., Physical Electronics Div., Norwalk, CT.

Webster T. J., Ergun C., Doremus R. H., Siegel R. W., Bizios R., (2000a), 'Enhanced functions of osteoblasts on nanophase ceramics,' *Biomaterials*, **21**, pp. 1803–1810.

Webster T. J., Ergun C., Doremus R. H., Siegel R. W., Bizios R., (2000b), 'Specific proteins mediate enhanced osteoblast adhesion on nanophase ceramics,' *J. Biomed. Mater. Res*., **51**[3], pp. 475–483.

Webster T. J., Ergun C., Shadler L. S., Siegel R. W., Bizios R., (2001), 'Mechanism of enhanced osteoblast adhesion on nanophase alumina involve vitronectin,' *Tissue Eng*., **7**, pp. 291–301.

Weiss P., Obadia L., Magne D., Bourges X., Rau C., Weitkamp T., Khairoun I., Bouler J. M., Chappard D., Gauthier O., Daculsi G., (2003), 'Synchrotron X-ray microtomography (on a micron scale) provides three-dimensional imaging representation of bone ingrowth in calcium phosphate biomaterials,' *Biomaterials*, **24**[25], pp. 4591–4601.

Wiederhorn S. M., (1969), *Fracture of Ceramics*, National Bureau of Standards Special Publication **303**, pp. 217–241.

Wiltfang J., Merten H. A., Schlegel K. A., Schultze-Mosgau S., Kloss F. R., Rupprecht S., Kessler P., (2002), 'Degradation characteristics of α and β tri-calcium-phosphate (TCP) in minipigs,' *J. Biomed. Mater. Res*. (*Appl. Biomater*.) **63**, pp. 115–121.

Wittig J. E., Al-Sharab J. F., Bentley J., Evans N. D., Nolan T. P., Sinclair R., (2001), 'Quantitative EFTEM of Cr grain boundary segregation in CoCrTa,' *Microsc. Microanal*. **7** (Suppl. 2), pp. 298–299.

Wopenka B., Pasteris J. D., (2005), 'A mineralogical perspective on the apatite in bone,' *Mater. Sci. Eng. C*, **25**, pp. 131–143.

Xin R., Leng Y., Wang N., (2006), '*In situ* TEM examinations of octacalcium phosphate to hydroxyapatite transformation,' *J. Cryst. Growth*, **289**[1], pp. 339–344.

Yoshida Y., Nagakane K., Fukuda R., Nakayama Y., Okazaki M., Shintani H., Inoue S., Tagawa Y., Suzuki K., De Munck J., Van Meerbeek B., (2004), 'Comparative study on adhesive performance of functional monomers,' *J. Dent. Res*., **83**, pp. 454–458.

Young, R. A., (1993), *The Rietveld Method*, Oxford University Press, New York.

4

Mechanical properties of bioceramics

M V SWAIN and L-H HE, University of Sydney, Australia

4.1 Introduction of basic definitions

4.1.1 Stress/strain

The stress–strain relationship is the basic parameter to describe and evaluate a material. The quantitative treatments of deformation usually employ the concept of *stress*, which is the pressure at any point in a body submitted to a load and expressed as:

$$\sigma = \frac{F}{A} \tag{4.1}$$

where F is the force on the supporting area A. Because force, F, has direction, the stress, σ, should be defined by not only in terms of its magnitude but also direction. From this point of view, stress can be divided into three types: tensile stress, compressive stress and shear stress. Material will experience deformation under certain stress. *Strain* quantifies the deformation of a body to stress and is defined as the ratio between the total deformation in one direction of a specimen and the length of the specimen in the same direction. Setting original length and increment of length as L and ΔL, separately, the strain, ε, can be expressed as:

$$\varepsilon = \frac{\Delta L}{L} \tag{4.2}$$

This equation does not consider the change of reference axes and is known as the nominal or engineering strain. More correctly, the true strain should be used,

$$\varepsilon = \int_{L_0}^{L_1} \frac{dL}{L} = \ln \frac{\Delta L}{L} \tag{4.3}$$

This equation takes into account the change in the reference length L from its initial value L_0 to its value L_1 at each step of deformation.

Table 4.1 List of mechanical properties of some advanced bioceramics (Hench, 1998; Marshall *et al.*, 2001; Guazzato *et al.*, 2004; Yin *et al.*, 2006)

Bioceramics	Flexural strength (MPa)	Weibull modulus (m)	Elastic modulus (GPa)	Hardness (GPa)	Poisson's ratio	Fracture toughness ($MPa\,m^{1/2}$)
Cortical bone	50–150	–	7–30	–	–	2–12
Human tooth enamel	8–35	–	9–90	3.2–4.4	–	0.52–1.3
Human tooth dentin	31–104	–	11–20	0.25–0.8	–	2.8–3.1
Sintered hydroxyapatite	115–120	–	80–110	500 (HV)	–	1.0
Pressable ceramic (IPSEmpress I)	106 (17)	9.0	65 (1.5)	6.5 (0.4)	–	1.2 (0.14)
Pressable ceramic (IPSEmpress II)	303 (49)	8.0	90 (3.7)	5.5 (0.2)	–	3.0 (0.65)
Full sintered zirconia ceramic (Vita Zirkon)	840 (140)	7.5	220 (7.5)	12 (0.2)	0.33	7.4 (0.62)
Glass ceramic (MGC-fine)	–	–	70.5	4.15 (0.07)	–	1.04 (0.04)
Glass-infiltrated zirconia ceramic (Vita In-Ceram Zirconia)	476 (50)	10.5	240 (9)	11 (0.9)	0.26	4.9 (0.36)
Glass-infiltrated alumina ceramic (Vita In-Ceram Alumina)	440 (50)	9.5	265 (10)	11 (1.1)	0.25	3.6 (0.26)
Feldspathic porcelain (Vita D)	95 (20)	5.0	64	–	0.21	0.9
Feldspathic porcelain (Vita Alpha)	95 (15)	5.0	60	–	0.22	0.9
Alumina bioceramic ($Al_2O_3 > 99.8\%$)	595	–	400	2300 (HV)	–	5–6

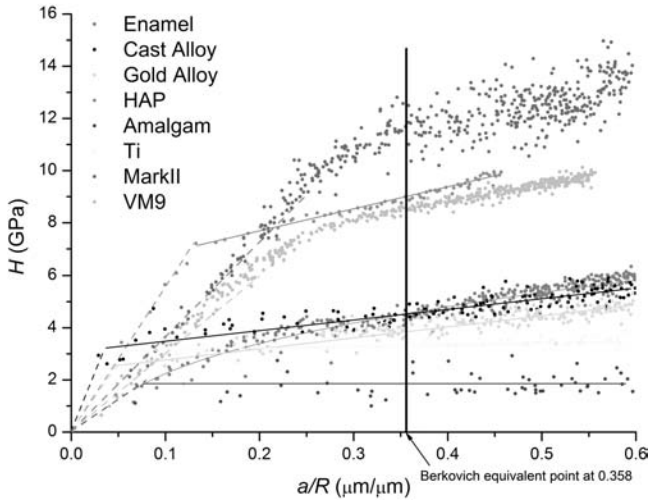

4.1 Indentation *H–a/R* (stress-strain) curve of human mature enamel compared with different dental ceramics and alloys.

When a given force (described by stress, σ) is applied to a material, the associated deformation can be specified by the resulting strain, ε. Therefore, the stress–strain curve has long been considered one of the most important parameters to evaluate material. With the curve, the deformation, which is strain, of any stress value can be predicted.

In the materials science field, stress–strain curves of most materials have been determined using uniaxial tensile/compressive tests. The yield stress, elastic modulus and fracture force can all be read from the curve. But, because of the brittleness of bioceramics, it is hard to determine the stress–strain curve of ceramics using a similar method. Recently, with the development of the nanoindentation technique and associated theoretical contact mechanics, indentation stress–strain curves may be drawn with spherical indenters (Beghini *et al.*, 2006; Herbert *et al.*, 2001). Although there are still some difference between the uniaxial stress–strain curve and indentation stress–strain curve, the indentation stress–strain curve can still reflect both elastic and plastic responses of materials. Figure 4.1 illustrates the indentation stress–strain curves of different dental ceramics and compares them with those of enamel and metallic alloys. This kind of comparison provides a new way to rank and select the biomaterials.

4.1.2 Elastic modulus

From Hooke's law, we know that, within the elastic range, the strain has a linear relationship with stress. And the term *Hookean behavior* is used to

describe the usual case in which a given strain component varies linearly with stress in components (Guy, 1972). From this point of view, *elastic modulus* is known as the ratio of stress to strain below the proportional limit. It represents the magnitude of the interatomic stiffness of a material within the elastic range when tensile or compressive forces are applied. It is also an indication of the amount of reversible deformation that will occur in a structure when a load is applied. From the definition of stress and strain, elastic modulus can be derived as follows:

$$E = \frac{\sigma}{\varepsilon} = \frac{F/A}{\Delta L/L} = \frac{FL}{\Delta LA} \tag{4.4}$$

Elastic modulus is a basic parameter to describe the material. Not only researchers but also clinical practitioners are interested in this value, because it may assist with the selection of restorative biomaterials with more similar deformable properties to those of the material it is replacing.

For force-bearing structures, a high elastic modulus is often required to limit the deflection on loading and still returns to its original shape after being stressed. It has been reported that increasing the elastic modulus of a supporting core structure of a dental restorative material might be a way of improving the fracture resistance of all-ceramic dental crown/bridge structures (Lee and Wilson, 2000).

Several methods have been developed to measure the elastic modulus of materials. Most common are bending tests, nanoindentation measurement and nondestructive methods.

Bending tests

The elastic modulus of ceramics is usually determined by bending tests, because deflection is more easily measured than very small tensile or compressive elongations. For three-point bending, elastic modulus can be calculated by:

$$E = \frac{Fl^3}{4bh^3y} \tag{4.5}$$

where F is loading force and y is deflection of the sample; l is the distance between the supports, b and h are width and height of the cross-section, respectively.

For four-point bending, elastic modulus is equal to:

$$E = \frac{3Fl_0^2l_1}{4bh^3y} \tag{4.6}$$

where F is loading force and y is deflection of the sample; l_0 is the distance between the inner load points, l_1 is the distance between the inner and outer

supports and b and h are width and height of the cross-section, respectively.

Nanoindentation tests

Based on Snedden's theoretical work (Snedden, 1965), Oliver and Pharr developed a method of measuring elastic modulus of a material with a nanoindentation machine (Oliver and Pharr, 1992). The Berkovich indenter, a three-sided pyramid-shaped diamond indenter, is usually used to do the measurement. The effective elastic modulus, E^*, can be calculated by fitting the unloading indentation force–displacement curve (see Fig. 4.2):

$$E^* = \frac{1}{\beta}\frac{\mathrm{d}P}{\mathrm{d}h}\frac{1}{2}\frac{\sqrt{\pi}}{\sqrt{A}} \qquad 4.7$$

in which $\mathrm{d}P/\mathrm{d}h$ is the stiffness at the beginning of unloading, A is the contact area and β is a correction factor (1.034 for Berkovich indenter). The unloading stiffness, $\mathrm{d}P/\mathrm{d}h$, can be calculated from the derivative of the initial unloading curve.

The effective elastic modulus is determined by the elastic modulus and Poisson's ratio (which is the ratio of transverse contraction strain to longitudinal extension strain in the direction of stretching force) of sample and indenter based upon the following relationship:

$$\frac{1}{E^*} = \frac{(1-\nu^2)}{E} + \frac{(1-\nu'^2)}{E'} \qquad 4.8$$

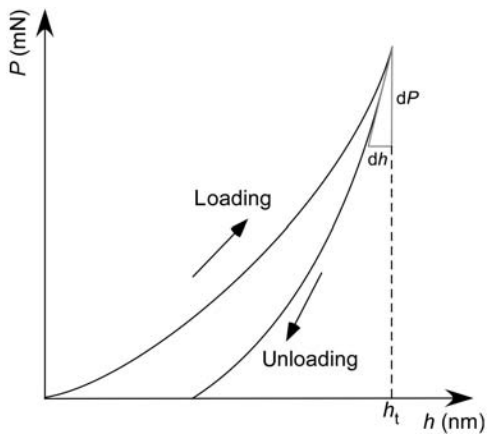

4.2 Schematic diagram of indentation force–displacement curve. (h_t is total penetration depth).

Here, E, E' and ν, ν' are elastic modulus and Poisson's ratio of the sample and indenter, respectively. Knowledge of the elastic modulus and Poisson's ratio of diamond, which are ~1000 GPa and 0.007, means that the elastic modulus of the sample can be calculated.

This method is of high precision and is convenient; it can be used to measure micro-scale samples. Sometimes, because of the size limit of bioceramic materials, especially those porous scaffold materials, it is difficult to measure the real elastic modulus of the material without the influence of pores inside. Under this condition, the nanoindentation technique has an advantage.

Nondestructive methods

Nondestructive methods on elastic modulus measurement are also named dynamic methods (ASTM, 1990), which include: frequency of oscillation of the rod method, ultrasonic pulse transit-time method, resonant ultrasound spectroscopy, free oscillation torsion pendulum and impulse excitation of vibration. Although usually specific equipment is required, these nondestructive methods have become widely popular for elastic modulus measurement because of their simplicity and repeatability and because they are nondestructive.

Knowledge of the elastic modulus is clinically relevant, because it may assist with the selection of a restorative material with similar deformable properties to those of the material it is replacing, e.g. bone or enamel. Bioceramics with comparable elastic properties to those of nature tissues can decrease the stress concentration at the bonded material–tissue interface, as for instance with occlusal loads on restored teeth and marginal bonding.

4.1.3 Hardness

Hardness may be the most widely used parameter for evaluating and comparing materials. The *hardness* of a material usually is considered as a measure of the resistance to permanent indentation (Boyer, 1987). The principal purpose of the hardness test is to determine the suitability of a material, or the particular treatment to which the material has been subjected. The ease with which the hardness test can be applied has made it the most common method of inspection for most materials.

The general procedure for hardness assessment can be summarized as: a standardized force or weight is applied to an indenter pressing into the surface of a material to create a symmetrical shaped indentation (residual impression). The dimensions of the indentation (area, depth or width) are measured at a microscopic level, and entered in a specific hardness formula

according to the type of tests. Therefore, the hardness value is different for different test methods. The most common used hardness test methods include: Brinell hardness test, Knoop hardness test, Vickers hardness test and nanoindentation hardness test.

Because of the size limit of bioceramic samples, micro- and nano-hardness tests may be the best choices. Diamond Knoop and Vickers indenters are usually chosen in microhardness tests, while the Berkovich indenter is the most common one for nano-hardness tests. In Knoop and Vickers microhardness testing, the hardness value is determined by measuring the size of the unrecovered indentation with a microscope and using established formulas. Vickers hardness is calculated as:

$$\mathrm{HV} = \frac{1.8544P}{d^2}, \tag{4.9}$$

where P is load (kg) and d is mean diagonal of the indentation (mm). Knoop hardness has the equation of,

$$\mathrm{HK} = \frac{P}{0.07028l^2}, \tag{4.10}$$

where P is load (kg) and l is the measured length of the long diagonal (mm).

For nano-hardness testing, the hardness value is based on the definition of hardness, which is,

$$H = \frac{P}{A}. \tag{4.11}$$

Here, load P is controlled by the machine and contact area A is calculated from penetration depth with a geometrical relationship. For a Berkovich indenter, the contact area has the relationship with contact depth is $A = 24.5h_\mathrm{p}^2$ although the tip needs to be calibrated for very shallow impression depths. Oliver and Pharr (1992) also proved the relationship between h_p and h_t as:

$$h_\mathrm{p} = h_\mathrm{t} - \varepsilon\frac{P}{\mathrm{d}P/\mathrm{d}h}. \tag{4.12}$$

For Berkovich indenter, ε = 0.75. Therefore, from the force-displacement curve (Fig. 4.2), the hardness of the material can also be calculated using equations 4.11 and 4.12.

4.1.4 Fracture strength

Strength can be defined as the maximum tensile stresses that a material can endure before fracture occurs. It might also be defined as force per unit

area required to initiate and propagate a crack to the fracture point. Strength is an important mechanical property to evaluate the performance of brittle materials such as bioceramics. The inability of ceramics to reduce the tensile stresses at the tip of the cracks by deformation in an inelastic manner explains why they are much weaker in tension rather than in compression and also why bioceramics normally fail in areas of tensile stresses. Therefore, tensile strength is considered more significant than compressive strength in the brittle material field.

Several methods have been introduced to measure the tensile strength of materials. They include bending flexural tests and biaxial flexural strength tests. For the three-point bending flexural test, by following ASTM C 1161, flexural strength, σ_F, can be calculated with:

$$\sigma_F = \frac{3Pl}{2bd^2}, \tag{4.13}$$

where P is breaking load (N), l is test span (m), b and d are width and thickness of the specimen respectively. The corners of the specimens need to be trimmed to minimize the failure probability from corner cracks because of such cracks are more deleterious to strength than surface cracks.

The calculation of biaxial flexural strength, σ_F, can be found in ASTM F 394-78:

$$\begin{aligned} \sigma_F &= -0.2387P(X - Y)/d^2, \\ X &= (1 + \nu)\ln(B/C)^2 + [(1 - \nu)/2](B/C)^2, \\ Y &= (1 + \nu)[1 + \ln(A/C)^2] + (1 - \nu)(A/C)^2, \end{aligned} \tag{4.14}$$

where P is breaking load (N), d is specimen thickness, ν is Poisson's ratio, A is the radius of support circle, B is the radius of the tip of piston and C is the radius of specimen disk. The recommended crosshead speed for these flexural strength tests is 0.5 mm/min. This speed may influence the results because of the sub-critical crack propagation, which will be discussed later in this chapter.

To describe the scatter of strength because of the nature of the flaws in the sample, Weibull (1951) suggested an empirical distribution function. The influence of specimen volume was incorporated into strength appraisal where the concept of *failure probability*, F, is used to describe the variability in strength of brittle materials. With this function, the failure probability of a specimen at any applied stress can be predicted. Too high failure probability should be avoided by changing the design or improving the material selected.

The empirical method to describe the strength distribution of brittle material is named the *Weibull approach*. This approach is based on a 'weakest link' idea, in which the strength of the body depends on the strength of the weakest unit inside. The Weibull approach assumes a simple power-law stress function and has three-parameter distribution and two-parameter distribution forms.

The three-parameter distribution of failure probability, F, under tensile stress, σ, has the expression:

$$F = 1 - \exp\left[-\int_V \left(\frac{\sigma - \sigma_{\min}}{\sigma_0}\right)^m \mathrm{d}V\right], \tag{4.15}$$

where σ_0 is the characteristic strength, m is the *Weibull modulus* and $\sigma_{\min}$ is the minimum strength. The characteristic strength, σ_0, can be interpreted as the uniaxial strength of a body with unit volume at a failure probability of 0.632. The Weibull modulus characterizes the distribution or variability of strength. Lower m means greater scatter of the strength, while higher m suggests better reliability and safety.

More frequently, two-parameter distribution is used by assuming $\sigma_{\min} = 0$. Thus, Eq. (4.15) can be simplified as:

$$\ln\ln\left(\frac{1}{1-F}\right) = m\ln\sigma_{\max} - m\ln\sigma_0^*, \tag{4.16}$$

in which $\sigma_{\max}$ is the maximum applied stress and $\sigma_0^* = \sigma_0(L_F V)^{1/m}$. L_F is named the loading factor, which reflects the stress distribution in the body. Similar to σ_0, σ_0^* represents the specific characteristic strength of a body at $F = 0.632$ for particular V and L_F. Based on this equation, the Weibull modulus of the material can be read from the slope of regression line of $\ln\ln(1/(1 - F))$ versus $\ln\sigma_{\max}$.

For brittle bioceramics, flaws, which influence the scatter of strength and reliability of the material, are usually introduced during the fabrication processes. Different techniques may produce different numbers of flaws and thus influence the reliability of the structure. A comparative research (Tinschert *et al.*, 2000) on dental ceramics verified this assumption, in which the results indicated that industrially prepared ceramics are more structurally reliable than dental laboratory-prepared ceramics for dental applications. This may be because materials produced in a dental laboratory experience more critical processes such as thermal sintering cycles and water and binder phases removal while heating and all of these processes may introduce more flaws into the structure. In conclusion, from the point of view of fracture strength, bioceramics, long-term functioning materials in critical environments, need not only high strength, but, more importantly, high reliability (high Weibull modulus).

4.1.5 Fracture toughness

Since crack propagation and subsequent fracture is known to be the major problem that leads to ultimate structural failure, it is important to know the threshold condition of crack propagation. Therefore, fracture mechanics concepts have been applied to characterise the criteria of crack propagation of brittle materials such as bioceramics. The strength of a brittle material, σ_a, is related to the critical stress intensity factor, K_c, at a crack tip can be calculated with the following equation:

$$K = Y\sigma_a\sqrt{c}, \tag{4.17}$$

in which c is the radius of a crack and Y is a geometrical factor. Irwin (1958) analyzed the crack propagation procedure from a critical stress point of view and concluded the criteria of crack propagation, which is stress field intensity, K, of crack tip should be bigger than a certain value K_c. K_c is critical stress intensity level at which a given flaw starts growing.

In mode I (uniaxial tension) crack model, this threshold value is also named as the fracture toughness, K_{Ic}, which indicates the ability of a material to resist crack propagation and its consequent catastrophic failure. The definition of fracture toughness in ASTM E-24 is: the resistance to crack propagation under plain strain conditions, which means strain value of crack tip should be kept constant while crack start propagating.

Fracture toughness is one of the most important mechanical properties that delineate the fracture behavior of a specific material. It has gained wide acceptance as a technique suitable for the assessment of a ceramic material's ability to resist crack propagation. In the biomaterials field, fracture toughness values may help us to evaluate the serviceability, long-term clinical success and performance of the brittle materials. It has been proven that materials with high fracture toughness demonstrate improved clinical performance and reliability than low fracture toughness one (Fischer and Marx, 2002).

Various methods and techniques have been used for the determination of the fracture toughness of brittle materials. These methods can be divided into two main groups. One comprises traditional notched and pre-cracked sample tests, e.g. compact tension, double cantilever beam, single-edge notched beam, single-edge pre-cracked beam and chevron notch. Another includes indentation tests such as indentation fracture and indentation strength. The detailed schedules and calculation of each method can be found in relative test handbooks or fracture mechanism textbooks (Anderson, 1995; ASTM, 1999).

4.1.6 Fatigue

The failure of a material due to repeated stressing is known as *fatigue* (Guy, 1972). It is an important concept in the design and operation of most structures and has long been used in metal material and structure design fields. Because of the brittleness of ceramics, fatigue of ceramic, especially bioceramics, is still a new and difficult field to explore.

Most bioceramics experience cyclic loads during their serving life. Therefore, anti-fatigue ability should be taken into serious consideration of the material development and structure design. Using a finite element analysis, Brockenbrough and Suresh (1987) showed that when the cyclic stress leads to permanent strains, the resulting residual stresses that arise in the matrix material in the vicinity of a stress concentration are distinctly different from those induced under monotonic loading conditions. This effect of permanent strains causes a mode of failure that is unique to cyclic loading conditions.

Under cyclic loading, microcracks may initiate at grain boundaries and interphase regions, and along the interfaces between the matrix and the reinforcement. Several processes may contribute to the irreversible deformation and fatigue of brittle materials relating to such microcracks, which are (Suresh, 1998):

- frictional sliding of the mating surfaces of the microcracks;
- progressive wear and breakage of the bridging ligaments connecting the mating surfaces of cracks;
- wedging of debris particles into the mating surfaces of cracks;
- releasing of residual stresses at grain boundaries and interfaces;
- stress-induced shear or dilatational transformations such as mechanical twins or martensitic lamellae.

In the metal area, the fatigue properties of material can be described by crack propagation curve, da/dN-ΔK curve. Paris and coworkers (Paris and Erdogan, 1963; Paris *et al.*, 1961) showed that in this curve, the fatigue crack growth increment da/dN has an empirical power law relationship with the stress intensity factor range ΔK as follows:

$$\frac{da}{dN} = C \cdot \Delta K^n, \tag{4.18}$$

where C and n are scaling constants, which are influenced by the material microstructure, environment and load ratio, R. A study of dental feldspathic porcelain with an indentation technique generated the results of 4 and 2×10^{-6} for n and C, respectively (White, 1993). This study indicated that the relationship for metals could also be used in the ceramic area to describe the fatigue property of bioceramics.

Another practical method to evaluate the influence of fatigue on bioceramics is the cyclic contact-loading test. Usually, a Hertzian or ball-induced contact mode was chosen in these tests. The investigation conducted by Jung *et al.* (2000) on four different kinds of dental ceramics showed that after 10^6 contact cycles with loads from 200 to 3000 N, strength of all samples degraded. Moreover, after a very large number of contact cycles, all materials showed an abrupt transition in damage mode which is not observed in a comparative static loading test. These results indicate that cyclic loading may add additional damage to a bioceramic material and its structure. Under functional loading conditions, this fatigue property of bioceramics should be included into our considerations of material selection and structure design.

4.2 Reinforcement of bioceramics and its significance

The *in vivo* conditions of bioceramic structures are critical. High localised stresses on certain points of the structure and the surrounding erosion environment all ask for high mechanical properties of bioceramics. At this stage, the hardness and fracture strength of most bioceramics can meet the need to serve as substitute structures such as dental crown/bridge and artificial joints. The major problem is how to improve the fracture toughness of the material to resist crack propagation under cyclic loads so that the life and reliability of bioceramic medical structures can be guaranteed. The basic mechanisms of ceramic reinforcement (Evans, 1984; Green, 1998), such as crack deflection, bridging and phase transformation will be introduced briefly in this section.

4.2.1 Toughening due to crack deflection

As the crack extends, the crack path will change when the tip of the crack meets a second phase in the material such as reinforcement particles. In addition there are often residual stresses associated with such particles as they have a different coefficient of thermal expansion and different elastic moduli values from the matrix. Considerably more energy will be used for the crack tip to pass through the particle. Therefore, a crack tip will change its direction to avoid these particles; more energy is required to change the crack direction (Fig. 4.3).

4.2.2 Toughing due to the bridging of the second phase reinforcement particles

The reinforcement particles behind the crack tip can also act as ‘bridges’ between two surfaces of a crack. As these particles are embedded into both

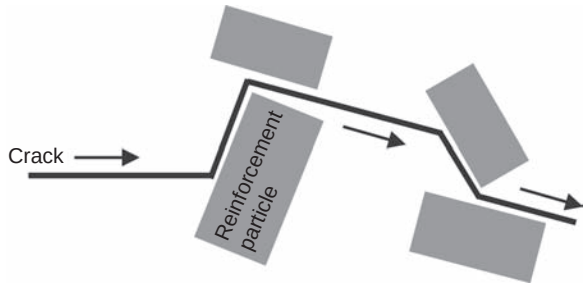

4.3 Schematic diagram of crack deflection due to reinforcement particles.

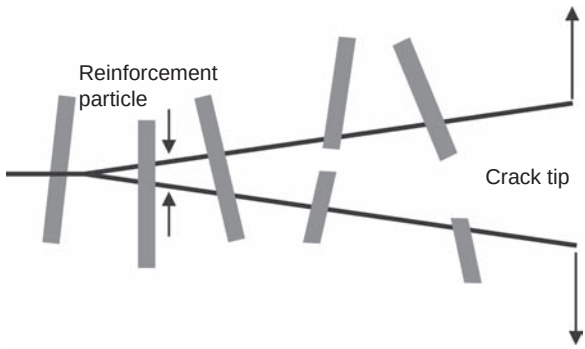

4.4 Schematic diagram of bridging behind the crack tip.

surfaces of the crack, which reduces the stress intensity at the crack tip and further extension of the crack requires addition external loading to break or extract these 'bridging' particles first (Fig. 4.4).

4.2.3 Toughening due to stress-induced phase transformation of material

The incorporation or manufacture of a material from a metastable phase material provides for stress-induced transformation about the crack tip of such a material to impart toughening. Volume dilation associated with such a localized phase transformation can decrease the effective tensile stresses at the tip of crack by adding localized compressive stresses (Fig. 4.5).

The above-mentioned mechanisms build a stress shielded area in the crack processing zone and reduce the stresses of crack tip dramatically. These kinds of toughening effect can be summarized as *R*-curve behavior of the material. *R-curve behavior* can be depicted as the energy dissipation rate during fracture can increase as the crack extends (Green, 1998). It has

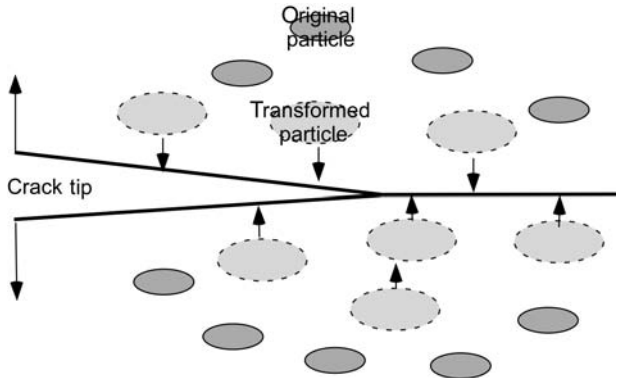

4.5 Schematic diagram of stress-induced phase transformation at the tip of crack.

positive influence on the strength, scatter-in-strength and long-term strength behavior of the material. Therefore, for bioceramics, *R*-curve behavior is a desirable mechanical effect to resist crack propagation and structural failure. Tests with indentation flexure strength method on different dental ceramics showed that most toughened ceramic materials exhibited a rising *R*-curve with crack extension and this behavior was more pronounced for the high strength materials (Fischer *et al.*, 2002).

Zirconia-based ceramics, which have been used in the medical field for several years as core material of dental all-ceramic crown/bridge, artificial joints and other medical devices (Piconi and Maccauro, 1999), are a good example of these transformation toughening mechanisms. The remarkable mechanical properties of zirconia are mainly due to the tetragonal to monoclinic (t–m) phase transformation. The t–m transformation, which can be induced by external stresses, such as the stresses at the tip of cracks, results in a 4% increase of volume that causes localized compressive stresses to develop about the crack tip. It is this clamping constraint about the crack tip that must be overcome in order for the crack to propagate, explaining the increased fracture toughness of zirconia compared with other ceramics. Transformation toughening can occur when the zirconia particles are in the metastable tetragonal form, and on the verge of transformation. The metastability of the transformation is dependent on the composition, size, shape of the zirconia particles, the type and amount of the stabilizing oxides, the interaction of zirconia with other phases and the processing. Furthermore, transformation toughening is not the only mechanism acting in zirconia-based ceramics. Micro-crack toughening, contact shielding and crack deflection can also contribute, to a different degree, to the toughening of the ceramic (Guazzato *et al.*, 2004).

4.3 The effects of flaws and environment on mechanical properties

No material block or structure is perfect. Brittle solids contain a population of small microscopic flaws named *Griffith flaws*. The presence of these flaws can cause marked reductions in fracture strength. Defects such as cracks, pores and grain boundary defects, are usually generated during the processing procedures such as cutting, pressing or sintering. These defects serve as potential sites for the nucleation of a dominant crack. The functioning environments of most bioceramic structures are also critical. These structures experience chemical erosion, thermal or mechanical cycles, contact forces and wear. All of these factors will introduce Griffith flaws and lower the mechanical properties and life of the structure.

The essential problem that influences the mechanical properties of bioceramic is the presence of defects or cracks. As brittle material, bioceramics are easily affected by flaws and the influences of such cracks on mechanical properties are controlled by two aspects, which are crack initiation and crack propagation.

4.3.1 Basic description of fracture mechanisms

To clarify stress concentration and fracture of bioceramics, we should start the discussion from the concept of the theoretical cleavage strength and fracture criterion. In atomic scale, from the consideration of the interatomic potential, the stress is expected to increase initially as a function of the interplanar spacing d. At a certain point, the stress will reach a maximum value, after which, with the increasing of interplanar spacing d, stress decreases. This maximum stress is termed the *theoretical cleavage stress*, σ_{th} (Green, 1998). the theoretical cleavage strength is found to be a material property and can be expressed as:

$$\sigma_{th} = \sqrt{\frac{E\gamma}{d_0}}, \tag{4.19}$$

where E is elastic modulus, γ is the surface energy and d_0 is the equilibrium interplanar spacing (under zero stress).

Stress concentration can be described as stress at the tip of defect or crack that is much bigger than the applied stress. We consider the crack in an infinite plate subject to uniaxial tension (Fig. 4.6) as an elliptical hole and the elastic solution can be expressed as (Green, 1998):

$$\sigma_{tip} = \sigma(1 + 2\sqrt{c/\rho}) \approx 2\sigma\sqrt{c/\rho}, \tag{4.20}$$

in which σ is uniaxial tensile stress, c is half the length of the defect and ρ is the radius of curvature at the ends of the major axis of the defect.

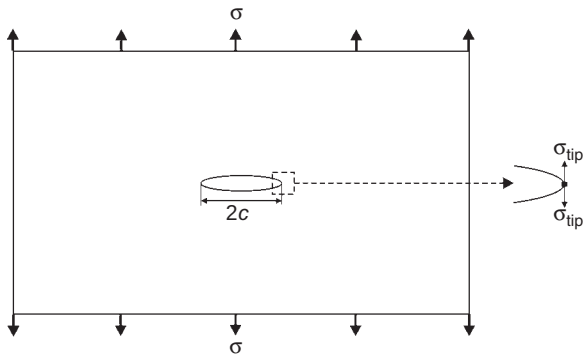

4.6 An internal defect in a large plate under the action of a uniaxial tensile stress.

From this equation, if ρ approaches atomic dimensions, the stress concentrated at the tip of crack, σ_{tip}, would become very large. This phenomenon is termed the *stress concentration* of defects.

The simplest method to evaluate fracture should be to equate the highest tensile stress associated with a crack, σ_{tip}, to the theoretical cleavage stress, σ_{th}. Fracture stress, σ_f, can be predicted by combining Eqs. (4.19) and (4.20). But for atomically sharp cracks this method may not be appropriate, because the stresses at the crack tip would be so high that the stress field is not expected to be linear elastic. Moreover, at these dimensions, treating the material as a continuum has limitations. Thus, a new approach is needed to resolve the problem.

Fortunately, in a pioneering work, Griffith (1920) postulated that materials already contain (pre-existing) cracks and it is the stress concentration associated with these cracks that gives strengths less than the theoretical cleavage stress. By considering the condition of a cracked body in an isolated system under the action of applied tractions with the energy method, Griffith deduced the famous equation of the critical stress for crack extension (the fracture stress σ_f):

$$\sigma_f = \sqrt{\frac{2E\gamma}{\pi c}}. \qquad 4.21$$

This equation is commonly termed the *Griffith equation* in which E is elastic modulus, γ is the surface energy and c is initial crack size. In this work, Griffith approved both theoretically and experimentally that fracture stress is inversely proportional to $\sqrt{c}$.

All the above theoretical analysis indicates that the strength of a bioceramic and its structure may be influenced by cracks in it. Therefore, to understand the mechanical evaluation of bioceramic structures, it is

necessary to learn the performance of cracks first, including the initialization and propagation.

4.3.2 Crack initialization due to flaws and environment

Different flaws and factors, such as pores and grain boundary defects, thermal cycles, impact force, and wear, will cause cracks.

Pores

The mechanical model described in Fig. 4.6 and Eq. (4.20) can also be used to explain the effects of pores and grain boundary defects. In short, pores and grain boundary defects will lead to stress concentration thereby making cracks easier to initiate and propagate.

Pores inside the material are usually generated during the laboratory manufacturing procedure. Considering dental porcelain-fused-to-metal (PFM) techniques as a good example, the technician mixes the ceramic powder with water to form a paste to facilitate the crown/bridge build-up. During firing and ceramic powder sintering processes, water will evaporate, making it virtually impossible to avoid the generation of pores. Research showed that porosity of dental porcelains was sensitive to the powder/liquid ratio (Zhang *et al.*, 2004), which means different technician-based procedures will lead to a range of the resultant mechanical properties for same material. Recently, more high-strength all-ceramic materials have been introduced into the dental field, not only because of their high strength, but also because they are all prefabricated, which means there are fewer pores and other defects. Some other bioceramic materials, especially those that act as scaffolds for tissue engineering, in contrast, need different size of pores to provide space for cells and other tissues. These pores will definitely decrease the strength of the material. Research has indicated that different size and shape of pores influenced the mechanical strength of the material (Liu, 1996). Therefore, it is still a challenge to optimize such porous bioceramic structures to meet the needs of both mechanical and biological requirements.

Thermal cycles

Bioceramic structures usually function at body temperature environment and the thermal cycle may be negligible under this condition. But they may experience critical thermal cycles during manufacture processes. Take dental porcelain fused to metal with a slight difference on thermal and elastic properties as an example. During crown/bridge construction, the materials need to be heated to a temperature of nearly 900 °C, which is much higher

than the glass transition point of the porcelain. If the heating or cooling speed cannot be well controlled, such thermal cycles may introduce defects into the structure because of the presence of the thermal residual stresses.

Cyclic/impact contact forces

The contact between the bioceramics appliances and opposing structures can be normalised as the standard Hertzian contact, which is the ball-on-flat contact (Fig. 4.7). This situation is very common in dental and orthopedic loading situations involving bioceramics. This kind of Hertzian contact has been well documented (Lawn, 1998).

The average contact pressure P_0 is:

$$P_0 = \left(\frac{3E}{4k}\right)^{2/3} \frac{1}{\pi} \left(\frac{P}{r^2}\right)^{1/3}. \quad 4.22$$

The maximum tensile stress in the specimen occurs at the contact circle:

$$\sigma_m = \frac{1}{2}(1-2\nu)P_0. \quad 4.23$$

The maximum shear stress is located along the contact axis at a depth ≈0.5a below the surface:

$$\tau_m = 0.48P_0 \quad 4.24$$

Under impact conditions, the initial contact motion is much bigger than static contact because initial contact energy includes not only static load

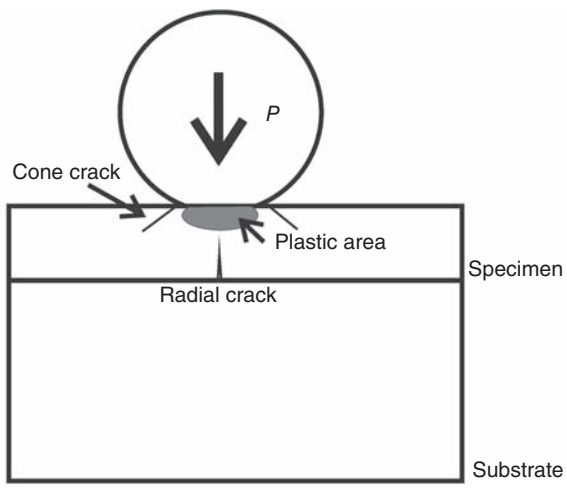

4.7 Typical Hertzian contact model.

but also kinetic energy. The maximum tensile and shear stresses may be bigger than the equivalent static contact condition. If the tensile stresses about the contact area along with the presence of a defect result in the localized stress intensity factor exceeding the K_{Ic} of a material, a crack will initiate. The extent of crack propagation is limited as the diminishing stress field with distance from the contact area results in a crack arrest rather than unstable propagation through the indented structure.

Under cyclic contact loading, while the cone cracks and radial cracks may propagate under the cyclic force, the damage of the material in the plastic zone may accumulate and lead to the deterioration of the strength property of the specimen. This has been demonstrated by cyclic contact research on ceramics (Kim *et al.*, 1999), in which two models of damage are observed. One is the conventional tensile-driven cone cracking ('brittle' mode) and the other is shear-driven microdamage accumulation ('quasi-plastic' mode). Strength losses are caused by the cone cracks and subsequent more deleterious reductions are caused by the radial cracks. Another investigation of a coarse-grained alumina (Fett *et al.*, 2005) showed that delayed failure in bar cyclic contact fatigue loading tests is caused by a reduction of the friction between the crack surfaces due to cyclic loading and by a related increase of the effective stress intensity factor until the fracture toughness of the material is reached. Meanwhile, the processes about the irreversible fatigue damage mentioned above may also play roles in such cyclic contact damage.

Wear

Some bioceramic structures such as denture and artificial joints have sliding contact with opposing structures. Under this condition, surface wear is an unavoidable problem for these structures. Wear will produce cracks and surface fracture by different mechanisms, e.g. abrasive wear, fatigue wear and corrosive wear (Mair *et al.*, 1996). These cracks may propagate at a latter time under functional stresses. From this point of view, wear is an important factor to reduce the mechanical properties of structures.

Terheci has mentioned that surface fatigue during wear maybe an important reason for the surface destruction of ceramic materials (Terheci, 1998). Surface fatigue wear plays an important role in the wear of the orthopedic and dental bioceramics and other dental and natural materials they are in contact with. Mashal also indicated that the main mechanism involved in the wear of ceramic is the detachment of a particle from a surface, which is usually associated with crack propagation and fracture (Mashal, 1995). The main process of dental material surface contact damage, especially the wear of brittle and/or compound material, is surface fatigue

generation and accumulation of residual stress, crack initiation and propagation followed by particle detachment.

Contact mechanics analysis in Fig. 4.8 shows the stress distribution near sliding contact area. With the repeated change of sliding direction, the cyclic changing tangential/compressive stresses within the contact area are the main reasons for the surface fatigue, residual stress and crack propagation. Figure 4.9 illustrates the subsurface damage in a 3-D manner.

Wear properties of bioceramics in the form of various appliances have been well investigated (Bolton, 2002; Mair *et al.*, 1996; Teoh, 2000; Teoh

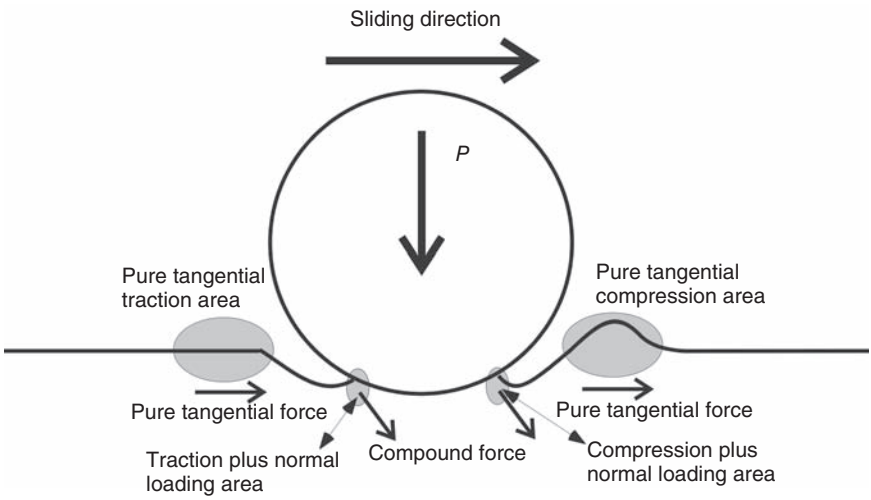

4.8 Two-dimensional schematic illustrating stress field distribution during local sliding contact.

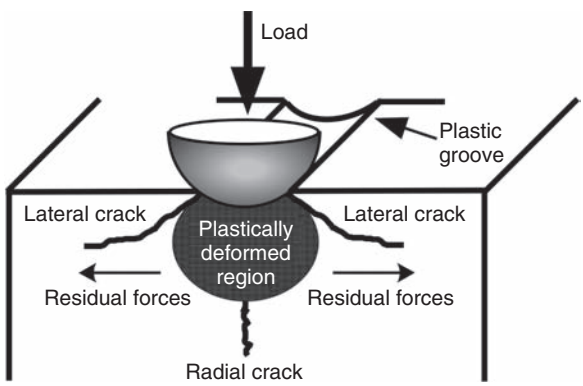

4.9 Three-dimensional schematic representation of the formation of cracks by sliding contact with sphere particles.

et al., 1998; Willmann, 2001). For those structures where contact occurs directly with another part made of similar materials, such as artificial joints, a reduction of the wear rate, surface destruction and wear debris of the whole contact system is anticipated. For structures in contact with natural tissues, such as teeth, we would like the material to have similar or even slightly greater wear rate than the natural tissue to protect the opposite tissue from excessive wear and destruction.

4.3.3 Crack propagation due to flaws and environment

The crack propagation of bioceramics *in vivo* is mainly due to subcritical crack propagation by chemical erosion and stress. It is not always the case that failure only occurs when $K_I \geq K_{Ic}$. Crack propagation that occurs at a K_I which is lower than K_{Ic} is usually called *subcritical crack propagation*. Several mechanisms may lead to subcritical crack propagation, but the focus of research has concentrated on stress-induced corrosion. This behavior has been extensively studied in silicate glasses but it can also occur in many polycrystalline ceramics (Green, 1998). The stress corrosion on ceramic can be explained by Fig. 4.10. It is well known that the silicon dioxide framework is sensitive to water molecules. As shown in Fig. 4.10, an H_2O molecule upon entering the crack tip region reacts and finally breaks the bonds of silicon dioxide at the crack tip. Other environmental species may also react at the crack tip and cause the bond breakage in a similar form.

Because of this kind of stress erosion reaction, cracks at the surface of ceramic structures may propagate at a lower critical stress intensity factor in an aqueous environment. Therefore, the response of ceramic to stress corrosion becomes an important question to determine whether crack propagation of ceramic will occur in an erosive environment. Figure 4.11 is a typical response of crack propagation of ceramic under an aqueous erosive environment. There are three distinct regions of crack velocity, v, as a function of stress intensity factor K. Initially, when the stress intensity factor reaches a threshold value, K_I^0, subcritical crack propagation becomes

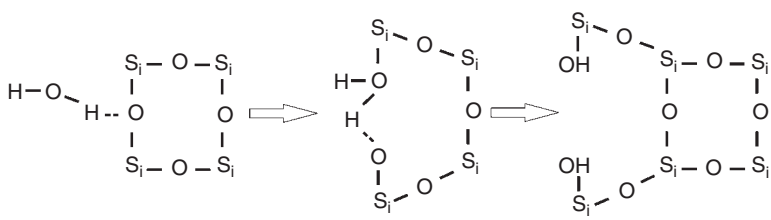

4.10 Schematic of H_2O reacting with SiO_2 at the crack tip and leading to crack propagation.

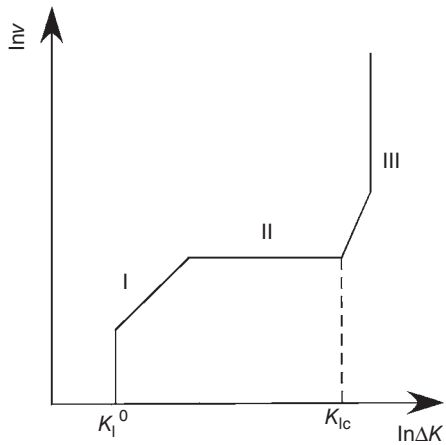

4.11 Schematic trend of crack velocity, *v*, during subcritical crack growth as a function of stress intensity factor, *K*.

activated. After that, crack velocity, v, increases rapidly with the growing K value (region I). This region is usually related to the stress-assisted chemical reaction-driven crack growth. At higher stress intensity levels the crack velocity enters a plateau region (region II), in which the stress intensity factor has little influence on the velocity. This is because the transportation speed of chemical erosive species limits the propagation of the crack tip. Eventually the crack tip stress intensity levels reach the fracture toughness K_{Ic} of the material (region III), resulting in catastrophic crack propagation.

With the knowledge of subcritical crack propagation, consideration of the structural reliability and service longevity in service are possible. Regarding regions II and III as high-speed crack propagation mechanisms the lifetime of the material is mainly dependent upon crack propagation of region I. Therefore, most researches were concentrated on the region I behaviors of material. Evans (1972) summarized the v–K relationship of region I in an empirical equation:

$$v = AK_I^n, \tag{4.25}$$

in which A and n are constants and named as *subcritical crack growth parameters*. Large numbers of experiments have shown that this equation can satisfactorily describe the region I behavior of ceramic material. n is also known as the *subcritical crack growth index* which depends only on material and environment. This parameter reflects the influence of environment on material. A smaller n value indicates the environment (erosive species) is very sensitive for the material and subcritical crack may grow quickly.

Because of the importance of subcritical crack growth in the life prediction of a structure, several methods have developed to study this behavior of material. In general, all methods can be divided into two categories: direct measurement methods and indirect measurement methods; each has its advantages as well as disadvantages. Direct methods need pre-cracked samples and can observe the details of crack propagation while indirect methods usually use intact samples and can simulate nature crack propagation and destroy better. Double torsion (DT) and double cantilever beam (DCB) samples are mostly used in direct measurements and with some fracture mechanical analysis, the *v–k* relationship can be determined.

By considering the basic equation of stress intensity factor (Eq. 4.17) and subcritical crack propagation equation (Eq. 4.25), for any stress cycle $\sigma(t)$, the fracture strength σ_F has a relationship with stress rate $d\sigma/dt$ as:

$$\ln \sigma_F = \frac{1}{n+1}\left\{\ln[B(n+1)S_I^{n-2}] + \ln\left(\frac{d\sigma}{dt}\right)\right\}. \quad 4.26$$

S_I is the initial inert strength, n is subcritical crack growth index and $B = \frac{2K^2_{IC}}{(n-2)Y^2 v_0}$. By changing the stress rate, subcritical crack growth index, n, can be obtained from the slope $[1/(n+1)]$ of $\ln\sigma_F - \ln d\sigma/dt$ curve. This method is also termed as the *dynamic fatigue* method. With the n value, the failure time, t_f, of the material under certain stress σ_A can be predicted as:

$$t_f = \frac{BS_I^{n-2}}{\sigma_A{}^n}. \quad 4.27$$

This is the base of life prediction of bioceramic structures. Similar methods have been summarised and used in bioceramic evaluations (Barinov *et al.*, 1998; Lohbauer *et al.*, 2002; Qiao *et al.*, 2002; Ritter, 1995).

4.4 Lifetime prediction and proof test

Lifetime prediction of different structures has long been a goal for materials engineers. Several methods have been developed to predict the life of engineering structures and been very successful in metal structure area. Numerous cyclic stress–life (S-N) curves of different metallic materials have been drawn and been used in life prediction. The basic life prediction processes are listed in Fig. 4.12.

In brittle material area, because of the complexity of cyclic damage mechanisms and fast catastrophic crack propagation when $K_I \geq K_{Ic}$, life prediction becomes difficult and unpredictable. Few S-N curves are available

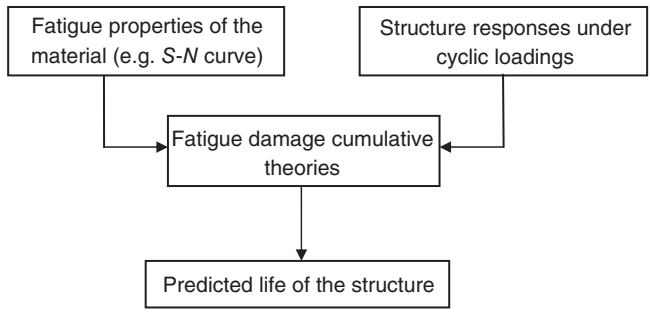

4.12 Schematic flowchart of structure life prediction analysis procedures.

at this stage, because of the large scatter of test data. Moreover, most damage cumulative theories developed from metallic materials are not suitable in a brittle material field. Therefore, life prediction of brittle structures is mainly based on the knowledge of subcritical crack growth mentioned above. Several efforts have been developed in this area (Fischer *et al.*, 2003; Lohbauer *et al.*, 2002; Seidelmann *et al.*, 1982). The general method to evaluate the lifetime of bioceramic structures is to measure the subcritical crack growth parameters (dynamic fatigue parameters) and calculate the lifetime with the help of finite element technique. The CARES/Life (Ceramic Analysis and Reliability Evaluation of Structure Life Prediction) software (NASA Lewis Research Center, Cleveland, OH, USA) is such a software package to predict the reliability and life of structures made from advanced ceramics and other brittle materials such as glass, graphite and inter-metallics. The CARES/Life software links with several commercially available finite element analysis packages, including ANSYS® and ABAQUS®. It accounts for the phenomenon of subcritical crack growth (SCG) by utilising the power law relationship (Eq. 4.25), as well as other algorithms, and can predict the failure of structure by simulating thermomechanical and/or proof test loading such as the Weibull modulus.

Medical appliance systems must be safe and, show excellent reliability and good biocompatibility during its long-term *in vivo* service. But, because of the unavoidable nature of flaws and cracks, some new bioceramic medical appliances may fail shortly after the implantation. Therefore, the proof test was designed to reveal those structures with microscopic defects and reduce the failure probability of the implanted appliances. By definition, a *proof test* refers to a predetermined and specific test designed to verify the suitability of certain structures for the intended purpose. The common procedure of proof test is to subject every product to a proof load σ_P, which is larger than the maximum physiological load σ_{max} *in vivo*. The ratio of the

proof load to the maximum load is defined as the *safety factor*. Those parts that survive the proof test without any fracture or crack initiation/propagation may be regarded as suitable and have significantly reduced failure probability under physiological loads. Several proof test methods have been developed to test different medical appliances. Now, before entering the market, most medical appliances, such as artificial joint systems and heart pumps, need to pass proof tests to meet the requirement of the US Food and Drug Administration (FDA).

In short, the proof test rejects defective products in the production line before being implanted into human body, and reduce the clinical failure of artificial parts.

4.5 Summary

Because of the excellent biocompatibility, matching shade, good anti-corrosion ability, bioceramics are ever more widely being used in the biomedical field. Most of these bioceramic appliances need to bear forces during their lives. Therefore, the mechanical properties became the most important factors to rank and select proper material. With the rapid development of modern material science and technology, more and more high-strength, high-toughness bioceramics have been developed and introduced into biomedical usage. The ever-more critical evaluation of existing and new bioceramic appliances will greatly increase the security and confidence of the medical usage of these materials.

In conclusion, in a mechanical point of view, a bioceramic and its appliances need to meet the following standards:

- similar elastic modulus, hardness and stress–strain relationship as the natural tissue;
- high fracture toughness and subcritical crack growth index;
- good wear resistance and minimal fatigue crack growth susceptibility;
- all bioceramic appliances should undergo proper designed proof test to guarantee their quality.

4.6 References

ASTM (1990) *Dynamic Elastic Modulus Measurements in Materials*, Philadelphia, ASTM.

Anderson, T. L. (1995) *Fracture Mechanics: Fundamentals and Applications*, Boca Raton, CRC Press.

Barinov, S. M., Ivanov, N. V., Orlov, S. V. & Shevchenko, V. J. (1998) Dynamic fatigue of alumina ceramics in water-containing environment. *Ceramics International* **24**, 421–425.

Beghini, M., Bertini, L. & Fontanari, V. (2006) Evaluation of the stress–strain curve of metallic materials by spherical indentation. *International Journal of Solids and Structures*, **43**, 2441–2459.

Bolton, J. D. (2002) Problems with wear in artificial orthopaedic joint replacements: a review. *Key Engineering Materials*, **230–232**, 447–454.

Boyer, H. E. (1987) *Hardness Testing*, Metals Park, OH, ASM International.

Brockenbrough, J. R. & Suresh, S. (1987) Constitutive behaviors of a microcracking brittle solid in cyclic compression. *Journal of the Mechanics and Physics of Solids*, **35**, 721–742.

Evans, A. G. (1972) Method for evaluation the time-dependent failure characteristics of brittle materials and its application to polycrystalline alumina. *Journal of Materials Science*, **7**, 1137.

Evans, A. G. (1984) *Fracture in Ceramic Materials: Toughening Mechanisms, Machining Damage, Shock*, Park Ridge, Noyes Publications.

Fett, T., Kraft, O. & Munz, D. (2005) Fatigue failure of coarse-grained alumina under contact loading. *Materialwissenschaft und werkstofftechnik*, **36**, 163–170.

Fischer, H. & Marx, R. (2002) Fracture toughness of dental ceramics: comparison of bending and indentation method. *Dental Materials*, **18**, 12–19.

Fischer, H., Rentzsch, W. & Marx, R. (2002) R-Curve behavior of dental ceramic materials. *Journal of Dental Research*, **81**, 547–551.

Fischer, H., Weber, M. & Marx, R. (2003) Lifetime prediction of all-ceramic bridges by computational methods. *Journal of Dental Research*, **82**, 238–242.

Green, D. J. (1998) *An Introduction to the Mechanical Properties of Ceramics*, Cambridge, Cambridge University Press.

Griffith, A. A. (1920) The phenomenon of rupture and flow in solids. *Philosophical Transactions of the Royal Society of London*, **A221**, 163–198.

Guazzato, M., Albakry, M., Ringer, S. P. & Swain, M. V. (2004) Strength, fracture toughness and microstructure of a selection of all-ceramic materials. *Dental Materials*, **20**, 441–456.

Guy, A. G. (1972) *Introduction to Materials Science*, New York, McGraw-Hill Book Company.

Hench, L. L. (1998) Bioceramics. *Journal of the American Ceramic Society*, **81**, 1705–1727.

Herbert, E. G., Pharr, G. M., Oliver, W. C., Lucas, B. N. & Hay, J. L. (2001) On the measurement of stress–strain curve by spherical indentation. *Thin Solid Films*, **398–399**, 331–335.

Irwin, G. R. (1958) Fracture. In Fluegge, S. (Ed.) *Handbuck der Physik*, Berlin, Springer-Verleg.

Jung, Y. G., Peterson, I. M., Kim, D. K. & Lawn, B. R. (2000) Lifetime-limiting strength degradation from contact fatigue in dental ceramics. *Journal of Dental Research*, **79**, 722–731.

Kim, D. K., Jung, Y. G., Peterson, I. M. & Lawn, B. R. (1999) Cyclic fatigue of intrinsically brittle ceramics in contact with spheres. *Acta Materialia*, **47**, 4711–4725.

Lawn, B. R. (1998) Indentation of ceramics with spheres: a century after Hertz. *Journal of the American Ceramic Society*, **81**, 1977–1994.

Lee, S. K. & Wilson, P. R. (2000) Fracture strength of all-ceramic crowns with varying core elastic moduli. *Australian Dental Journal*, **45**, 103–107.

Liu, D. M. (1996) Control of pore geometry on influencing the mechanical property of porous hydroxyapatite bioceramic. *Journal of Materials Science Letters*, **15**, 419–421.

Lohbauer, U., Petschelt, A. & Greil, P. (2002) Lifetime prediction of CAD/CAM dental ceramics. *Journal of Biomedical Materials Research*, **63**, 780–785.

Mair, L. H., Stolarski, T. A., Vowles, R. W. & Lloyd, C. H. (1996) Wear: mechanisms, manifestations and measurement. Report of a workshop. *Journal of Dentistry*, **24**, 141–148.

Marshall, G. W. Jr., Balooch, M., Gallagher, R. R., Gansky, S. A. & Marshall, S. J. (2001) Mechanical properties of the dentinoenamel junction: AFM studies of nanohardness, elastic modulus, and fracture. *Journal of Biomedical Materials Research*, **54**, 87–95.

Mashal, Y. A.-H. (1995) The role of fracture mechanics parameters in glass/ceramic wear. *Engineering Fracture Mechanics*, **52**, 43–47.

Materials, A. S. F. T. A. (1999) *Standard Test Methods for Determination of Fracture Toughness of Advanced Ceramics at Ambient Temperature*, Philadelphia, ASTM.

Oliver, W. C. & Pharr, G. M. (1992) An improved technique for determining hardness and elastic modulus using load and displacement sensing indentation experiments. *Journal of Material Research*, **7**, 1564–1583.

Paris, P. C. & Erdogan, F. (1963) A critical analysis of crack propagation laws. *Journal of Basic Engineering*, **85**, 528–534.

Paris, P. C., Gomez, M. P. & Anderson, W. P. (1961) A rational analytic trend of fatigue. *The Trend in Engineering*, **13**, 9–14.

Piconi, C. & Maccauro, G. (1999) Zirconia as a ceramic biomaterial. *Biomaterials*, **20**, 1–25.

Qiao, G. J., Wang, H. J. & Jin, Z. H. (2002) Comparison between fatigue behavior of some ceramics: a new concept of intrinsic stress-corrosion exponent $n(0)$ *International Journal of Fatigue*, **24**, 499–508.

Ritter, J. E. (1995) Critique of test methods for lifetime predictions. *Dental Materials*, **11**, 147–151.

Seidelmann, U., Richter, H. & Soltész, U. (1982) Failure of ceramic hip endoprostheses by slow crack growth – lifetime prediction. *Journal of Biomedical Materials Research*, **16**, 705–713.

Snedden, I. N. (1965) The reguation between load and penetration in the axisymmetric Bossinesq problem for a punch of arbitrary profile. *International Journal of Engineering Science*, **3**, 47–57.

Suresh, S. (1998) *Fatigue of Materials*, Cambridge, Cambridge University Press.

Teoh, S. H. (2000) Fatigue of biomaterials: a review. *International Journal of Fatigue*, **22**, 825–837.

Teoh, S. H., Thampuran, R. & Seah, W. K. H. (1998) Coefficient of friction under dry and lubricated conditions of a fracture and wear resistant P/M titanium–graphite composite for biomedical applications. *Wear*, **214**, 237–244.

Terheci, M. (1998) Wear by surface fatigue on a new foundation. Part II. Particle detachment mechanisms and quantitative aspects. *Wear*, **218**, 191–202.

Tinschert, J., Zwez, D., Marx, R. & Anusavice, K. J. (2000) Structural reliability of alumina-, feldspar-, leucite-, mica- and zirconia-based ceramics. *Journal of Dentistry*, **28**, 529–535.

Weibull, W. (1951) A statistical distribution function of wide application. *Journal of Applied Mechanics*, **9**, 293–297.

White, S. N. (1993) Mechanical fatigue of a feldspathic dental porcelain. *Dental Materials*, **9**, 260–264.

Willmann, G. (2001) Improving bearing surfaces of artificial joints. *Advanced Engineering Materials*, **3**, 135–141.

Yin, L., Song, X. F., Song, Y. L., Huang, T. & Li, J. (2006) An overview of *in vitro* abrasive finishing & CAD/CAM of bioceramics in restorative dentistry. *International Journal of Machine Tools & Manufacture*, **46**, 1013–1026.

Zhang, Y. L., Griggs, J. A. & Benhan, A. W. (2004) Influence of powder/liquid mixing ratio on porosity and translucency of dental porcelains. *Journal of Prosthetic Dentistry*, **91**, 128–135.

5

The design of ceramics for joint replacement

I C CLARKE, Loma Linda University Medical Center, USA and
A GUSTAFSON, Gustafson Orthopedics, USA

5.1 Introduction

The history of total hip replacements (THR) began after World War II with various metal-on-metal (MOM) bearing concepts (Clarke and Campbell, 1989; Amstutz *et al.*, 1992). Over the decade 1955–1965, various MOM bearings were developed using large ball diameters (32, 35 and 41.5 mm) by European surgeons, including McKee, Muller and Ring. However, in 1963, the small metal ball concept was introduced (Charnley *et al.*, 1969: 7/8 inch; 22.25 mm) using a cemented polyethylene cup (MPE). This MPE concept received widespread acceptance and use of MOM bearings quickly dwindled out by the early 1970s (reappearing around 1985). It later became apparent that cemented polyethylene cups could fail for a variety of reasons. including sepsis, inadequate implant positioning, inferior fixation and poor-quality bone stock. However beyond 6–8 years' follow-up, osteolysis became a major cause of revision, being a destructive process created by the body's reaction to accumulating wear debris (Clarke and Campbell, 1989; Amstutz *et al.*, 1992).

By 1970, a European surgeon, Pierre Boutin, had anticipated the 'polyethylene disease' and began clinical studies with ceramic-on-ceramic (COC) bearings (Boutin, 1972). Later the German surgeons Griss, Mittelmeier and Salzer accelerated the development of COC-bearing concepts (Amstutz *et al.*, 1992; Clarke and Willmann, 1994), which also made ceramic–polyethylene (CPE) combinations possible. Thus the decade from 1963 to 1973 saw three competing bearing concepts emerge, plastic, metal and ceramic (MPE or CPE, MOM, COC). However, from 1970 onwards, the MPE and CPE bearings have dominated the American marketplace.

With today's patient populations living longer and being much more active, the goal is to determine what combination of materials and THR design features will best minimize risk of osteolysis for >20 years of quite active use. Thus over the past few years both MOM and COC designs have seen a resurgence in the USA. Food and Drug Administration (FDA)

Table 5.1 History of alumina ceramic used in THR bearings

Date	Ceramic THR developments for alumina-based THR
1970	Introduction of alumina-on-alumina bearings (P. Boutin MD)
1973–74	Introduction of modular ceramic balls (P. Griss MD, H. Mittelmeier MD)
1977	Introduction of HIPped alumina bearings
1977	Clinical series of ceramic THR begins in Paris (L. Sedel MD)
1981–90	USA clinicals with COC (H. Mittelmeier MD: Autophor™, Xenophor™)
1989	FDA approval for MPE (28/32 mm alumina; Y-TZP zirconia)
2003	FDA approval for COC (Biolox-forte™ 28, 32 mm)
2003	FDA approval for Biolox-delta™ (28, 32 mm) on UHMWPE liners

Table 5.2 Historical limitations of ceramic THR designs

Feature	Details
Safety	32 mm alumina balls much less fracture risk than 28 mm diameter
Safety	Thick and bulky monoblock cups (strength and coverage requirements)
Function	Poor range of motion (skirted balls)
Function	Limited neck-length adjustments in ceramic balls (strength requirement)
Fixation	Incompatible with flexible bone–cement (alumina ceramic most rigid)
Fixation	Osseous integration not feasible (alumina ceramic quite inert)
Fixation	Coatings (bone ingrowth) contraindicated due to stress-riser effects
Fixation	Cup fixation limited (a few large pegs, screw-in, etc.)

approvals to market COC designs have accumulated since the first introduction in January 2003 (Table 5.1), However there were also features of historical ceramic designs (Clarke, 1992) that brought certain limitations into the clinical arena (Table 5.2). Thus, we shall examine the role of design and material strategies in contemporary ceramic hip replacements.

5.2 Developmental period of alumina bearings

Ceramic THR systems evolved in the 1970s, the most well known being those developed by Drs Boutin, Mittelmeier and Furlong. These could use

alumina ball diameters varying from 28 to 35 mm in diameter. There was no comparable ceramic development period in the USA. To gain access to the American market, an orthopedic corporation had to provide the FDA with sufficient pre-clinical and clinical data to get permission to market. The only company to attempt this over the decade 1981–1991 was Richards Surgical Inc. (now Smith and Nephew, Memphis, TN) using the experience of Professor H. Mittelmeier from Hamburg, Germany (Table 5.1).

With the press-fit Autophor™, clinical reports from the USA noted a major problem with painfully loose stems, amounting from 15 to 80% incidence (Miller, 1986; Mahoney, 1990; Ivory, 1994; Shih, 1994; Huo, 1996). Short-term revision rates varied from 2% (Miller, 1986) to more than 30% (Mahoney, 1990). Nevertheless, this unique ceramic experience did pave the way in 1989 for the FDA's down-classification for ceramic balls to be used with polyethylene cups (CPE), i.e. 28 and 32 mm femoral heads in either alumina or zirconia ceramic (Tables 5.1 and 5.3).

Sedel's orthopedic group (University of Paris) has provided a series of COC clinical studies over a 30-year period (Sedel *et al.*, 1990, 1994, 2000, 2004). From 1970 to 1977 the ceramic femoral heads were either screwed or epoxied onto the femoral stems (Hamadouche *et al.*, 2002). A series of 118 consecutive cemented and non-cemented THRs were reviewed from a 1979 series (90% of cases with known outcome). For the cup revisions, 19 of 23 were due to dislocation of the ceramic cup out of the bone–cement sheath typically at 10–12 years' follow-up (Hamadouche *et al.*, 2002). There were no ceramic fractures. Wear measured in retrievals averaged 0.025 mm/year and osteolysis was rare. In consequence revisions were performed into healthy bone stock.

Further clinical studies from the Paris group (1990 to 1992 era) provided results for a mesh-backed cup in young patients (<55 years of age). The non-cemented cup and cemented-stem survival rates at 9 years were 98% and 100%, respectively (Bizot *et al.*, 2004). However 38% of the mesh-cups

Table 5.3 Regulatory overview of all-alumina THR used in the USA

Date	Ceramic studies under FDA guidelines
1981	Ceramic THR studies begin in USA (Autophor™ and non-modular cups)
1990	End of Autophor™ use in USA
1997	Beginning of FDA-monitored COC clinical studies (modular cups)
1998	Clinical studies (Osteonics, $N = 500$ cases; Wright Medical, $N = 300$ cases)
2003	1st FDA approvals for alumina balls and liners (Biolox-Forte™: 28, 32 mm)

had a partial radiolucent zone that may have reflected a lack of adequate bone ingrowth. Owing to ultra-low wear rates experienced with such COC bearings, osteolytic complications were exceedingly rare. This encouraging experience set the stage for future development of the modular ceramic cups in 1989.

In 1997, orthopaedic companies began the 1st FDA-monitored, multi-center clinical studies (Table 5.3) of alumina-on-alumina THR (Garino, 2000; D'Antonio *et al.*, 2002, 2005). The ceramic implants were all Biolox-forte™ type (Ceramtec Inc., Germany). In 2000, Ceramtec introduced a new composite ceramic as Biolox-delta™ in Europe (Willmann, 1999, 2000). This zirconia-toughened alumina ceramic provided almost double the strength and fatigue resistance of Biolox-forte™. Thus from the point of view of a composite ceramic, the alumina phase provided the ideal bearing surface while the zirconia phase contributed to strength and toughness. By the end of 2006, FDA approval has generally been for the 28 and 32 mm Biolox-delta balls combined with polyethylene cups in various devices, although one company also has a 36 mm delta/polyethylene approval.

5.2.1 Clinical wear experience of alumina bearings

Experience with ultra-high molecular weight polyethylene (UHMWPE) cups has shown that migration of the femoral head represents wear and can be detected on standard X-rays with the passage of sufficient time. On the other hand, COC bearings have demonstrated ultra-low wear over a 36-year period. Thus with ceramic cups, the wear has been so low as to be radiographically unmeasurable (Hamadouche *et al.*, 2002). Unlike metal-on-metal bearings, the alumina ceramic is inert and so nothing can be gained from surrogate wear studies of blood, serum or urine. Also the presence of any osteolysis on radiographs was a rare event with COC bearings (Nevelos *et al.*, 1999; Hamadouche *et al.*, 2002). Thus our knowledge on ceramic wear has to come from implant retrieval and wear debris studies.

The average ceramic wear was reported to be of the order 5–25 μm/year (Hamadouche *et al.*, 2002; Mittelmeier and Heisel, 1992). However much higher wear rates have also been reported. One of the more complete retrieval studies examined 11 Ceraver and 11 Mittlemeier bearings (Nevelos *et al.*, 1999, 2001a). Six of the 22 cases revealed ceramic ball and cup wear in same or higher range compared with UHMWPE cups, i.e. 0.05 to 0.6 mm/year per component bearing (Fig. 5.1). It has been hypothesized that such wear problems likely reflected poorer quality alumina along with design, range-of-motion and fixation problems unique to monoblock cups. In particular, problem patients with vertically migrating cups should be revised within 3 months (Hamadouche *et al.*, 2002). Anecdotal experience with some patients walking for many months on such tilted cups has shown

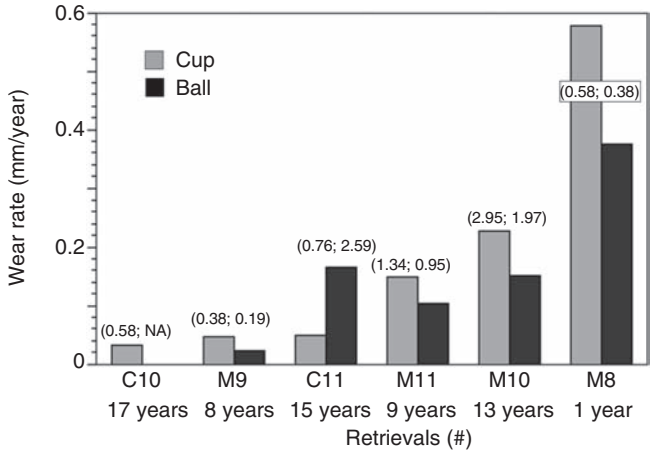

5.1 Comparison of the six highest wear rates in retrieved ceramic couples from complex revision cases (drawn from Nevelos *et al.*, 2001a). Implants labeled Ceraver (C) and Mittelmeier (M) total hip replacements. Wear in four cups was 1.4 to 2 times higher than in their mating balls. The maximum wear is indicated in millimeters (cup; ball pairings). Key (Nevelos *et al.*, 1999): M8: 18-year-old female CDH, cup at 55° with four dislocations and cup loosened within 1 year (average wear = 262 mm^3/year). M9: 41-year-old bilateral CDH, cup 75° vertical and migrated 3–4 mm into poor bone (average wear = 9 mm^3/year). M10: 37-year-old patient with 70° vertical cup whose stripe wear developed into 'severe' wear category. M11: In take-down arthrodesis in 46-year-old patient, problems developed at 7 years with both implants loosened but patient refused operation for further 2 years (average wear = 120 mm^3/year).

considerable wear and even the risk of cup fracture (Sedel, 2000; Keggi, 2006). For example, a patient 31 years old with a loose ceramic cup (tilting from 60° to 70° vertical) produced a combined wear rate of 0.96 mm in one year (Fig. 5.1: M8). A 15-year follow-up also with a loose cup (migrating and tilting 53° to 66° vertical) produced 2.59 mm of linear wear on the femoral head (Fig. 5.1: C11). Thus in such cases with loose, migrating and vertically tilting cups, the volumetric wear could range from 10 to 260 mm^3/year (Nevelos *et al.*, 2001a). Hopefully such severe cases of rim wear will be non-existent with contemporary, modular cups.

The main wear area on COC bearings is generally so finely polished that it is virtually invisible to the naked eye and requires microscopic analysis (Shishido *et al.*, 2003; Manaka *et al.*, 2004; Walter *et al.*, 2003). Scanning electron microscopy (SEM) analysis of stripe wear showed rougher surfaces due to grain pullout that contrasted with the wear of non-stripe areas that showed mild relief polishing of individual grains and some pitting. The 'stripe' wear is visible as a dull, lunar area on the femoral head and a cir-

cumferential area adjacent to the bevel on the cup rim (Griss, 1984; Dorlot, 1992; Shishido *et al.*, 2003; Nevelos *et al.*, 2001a; Walter *et al.*, 2003). Even as little as 1 μm wear can dull the highly polished ceramic surfaces (Walter *et al.*, 2003). Stripe wear has been attributed to various factors, including negative clearance between ball and cup, vertically inclined cups, or cups migrating and tilting after loosening. It has also been suggested that stripe wear was likely to be a natural consequence of using rigid cups, i.e. a stress concentration effect of the rigid cup rim wearing on the femoral ball during normal hip function (Clarke *et al.*, 2005a). In our COC implant retrievals at Loma Linda University Medical Center (LLUMC), three examples with 16 to 22 years' follow-up showed broad superior wear scars (main wear zones) and varied wear stripes more peripherally. For comparison between clinical and simulator wear maps, the alumina wear progression was ranked into five grades by SEM observations of surface burnishing and pitting (Shishido *et al.*, 2003). The ceramic surface in the main wear zone was fairly intact (grade # 4) whereas the peripheral wear zones showed extensive surface disruption (grade # 5).

In contemporary ceramic designs, macroscopic evidence of stripe wear has been quantified on specific sites of the femoral head and the beveled rim of the ceramic liner (Table 5.4). Cup and liner wear averaged 0.3 and 0.4 mm^3/year, respectively, and maximum measured THR wear (ball + cup) was 3.5 mm^3/year (Walter *et al.*, 2003). The width of the femoral stripes averaged three times that of the liners. The stripes were retroverted on average 20° and sited at 47° latitude, indicating that they were formed in the 90°-flexed position. The explanation offered was that the stripes formed during repetitively loaded, flexion activities such as stair climbing or rising from a chair. This contrasted with two stems that had subsided; their femoral stripes were still retroverted but less inclined at 5° and situated nearer the equator at 8° latitude. These appeared to have been formed during normal walking.

Table 5.4 Summary of retrieval study of contemporary ceramic THR (Walter *et al.*, 2003)

Parameters	Clinical details
Retrievals	11 balls, 8 liners
Alumina	Biolox-forte™ (Ceramtec Inc, Germany)
Vendor	Stryker Inc., Mawah, NJ
Follow-up	2.5 year maximum
Stripe orientation	Posteriorly inclined, 20° average tilt (stable THR)
Latitudinal site	47° above the equator (stable THR)
Stripe wear average	Cups = 0.3 mm^3/year; balls = 0.4 mm^3/year
High stripe wear	Maximum THR wear = 3.5 mm^3/year

Thus it has become obvious that stripes dominated the ceramic wear process and therefore created the most ceramic debris. This would appear to be one of the consequences of using rigid acetabular cups. Loosening and tilting of monoblock acetabular designs was probably a common pathway to greatly accelerated ceramic wear in both ceramic balls and cups. However even in complex clinical cases with such high wear, signs of osteolysis were amazingly absent. Thus the ceramic debris may be the least reactive of the biomaterials used for THR.

5.2.2 Laboratory wear experience of alumina bearings

Boutin (1972) first described the run-in wear phase of COC bearings with linear wear as low as 10 μm during the first million cycles in the wear machine; thereafter COC wear became undetectable. This biphasic nature of ceramic wear (run-in; steady-state phases) greatly complicates inter-laboratory comparison (Table 5.5). Run-in wear will appear to vary greatly depending on which test duration the first wear measurement is taken (Fig. 5.2: points A and D). In the first example, the peak run-in wear is over by 0.25 Mc (million cycles) duration (OC) but steady-state wear has not initiated until 1 Mc duration (DE). Thus the transition point (Y) is a virtual concept at the intersection of the two linear-regression trends. In the second example, there is a well-defined transition point (A) at 0.5 Mc duration but a wear measurement taken at 1 Mc would miss this. Thus a well-defined run-in wear phase would necessitate wear measurements at 0.2 Mc intervals to beyond 1 Mc duration. Note that wear measurements from retrieval studies are quite different in that they can only assess the 'overall' average (OB), which will be different from both run-in and steady-state wear values. Short-term retrieval studies will tend to reflect more the run-in wear phase and long-term studies will tend to reflect more of the steady-state wear phase. Thus it may be advantageous for simulator studies to provide 'overall' wear rates (Stewart *et al.*, 2001, 2003).

Table 5.5 Summary of simulator wear trends for alumina–alumina bearings under standard (STD) simulator test modes (Clarke *et al.*, 2003a)

Simulator wear assessments	Wear (mm^3/Mc)
'Run-in' range	0.02–1.1
'Run-in' average	0.5
'Steady-state' range	0.02–0.05
'Steady-state' average	<0.05
'Overall' average	0.1

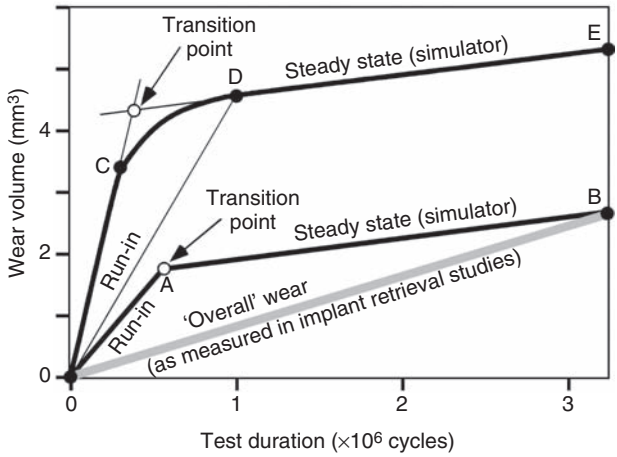

5.2 Representation of 'overall' wear (OB) as measured in implant retrieval studies to run-in (OA) and steady-state (AB) wear phases as measured in laboratory studies. Some wear trends will tend to show a gradual transition between run-in (OC) and steady-state (DE) wear phases.

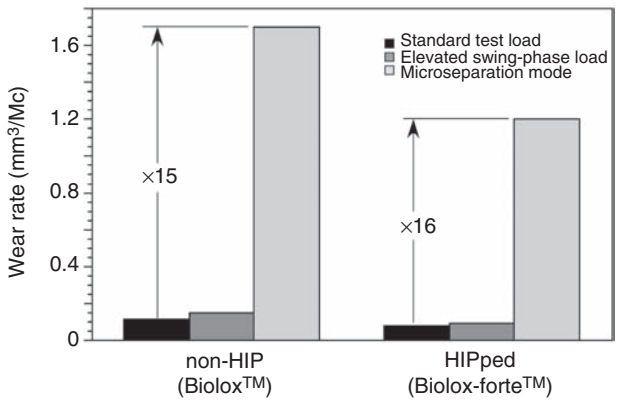

5.3 Comparison of alumina–alumina wear (HIPped and non-HIP types) under standard simulator test mode, then with elevated swing-phase load and also the most severe test mode of microseparation (Nevelos *et al.*, 2001a,b).

The Leeds Group UK performed a variety of studies on alumina–alumina bearings in both HIPped and non-HIPped ceramics (HIP = hot isostatic pressing). Alumina wear in simulator tests with standard and elevated swing-phase loads was generally around 0.1 mm^3/Mc (Fig. 5.3 and Table 5.6). They also introduced 'mild' and 'severe' micro-separation during simulator

Table 5.6 Wear for alumina THR (Biolox-forte) studied under 'mild' and 'severe' microseparation (MSX) test modes compared with standard (STD) simulator mode (Stewart *et al.*, 2001)

Test mode	Run-in (mm^3/Mc)	Steady state (mm^3/Mc)	'Overall' (mm^3/Mc)	'Overall' ratio
Standard	0.11	0.05	0.07	reference
Mild MSX	0.55	0.1	0.2	×3.0
Severe MSX	4	1.3	1.84	×28
Ratio (MSX/STD)	×36	×26	×28	

swing-phase and successfully demonstrated the peripheral stripe wear as seen on COC retrievals. Compared with the standard simulator model, the mild and severe test modes increased COC wear ×3 to 28-fold, respectively (Table 5.6). Thus the microseparation test mode raised the simulator wear rates into the mid-range of that reported in contemporary COC retrieval studies (Table 5.4). Also the non-HIPped THR (Biolox) produced 50% more wear than HIPped type (Biolox-forte).

We followed the example of the Leeds Group and modified our hip simulators to run microseparation wear studies. We diametrically matched a set of 36 mm femoral heads and cups (Biolox-forte™) over a narrow tolerance range. All THR demonstrated stripe wear phenomenon within 100 000 cycles, corresponding to the superior cup rim impinging on the ball during relocation at the end of the swing phase (Green *et al.*, 2005b, 2007). Typically two narrow stripe regions were initiated on the femoral heads corresponding to the two load impacts in the Paul load profile: one at 45–60° and one at 75–90° (measured from pole of ball). These scars elongated over the course of the study to form broad stripes. The cups showed a narrow stripe beginning with approximately 20–40° arc along the rim. Due to grain excavation, the stripes always showed a more severe grade of wear than the central wear zone. Our overall wear of 1.5 mm^3/Mc for 36 mm Biolox-forte THR was therefore slightly lower than the prior study with 28 mm diameter COC (Table 5.6) but quite comparable overall given the many differences represented by our simulator machines and test parameters.

Frictional torque studies in the laboratory have also shown an advantage for COC bearings. With the current trends to large diameter bearings in THR, COC bearings have shown the same or lower friction than the historical metal–polyethylene bearings whereas the nature of MOM bearings created a greatly increased frictional moment (Fig. 5.4).

5.2.3 Risks of alumina bearings

The downside with alumina ceramic has been some uncertain risk of brittle fracture, rim chipping and squeaking phenomena (Table 5.7). The alumina

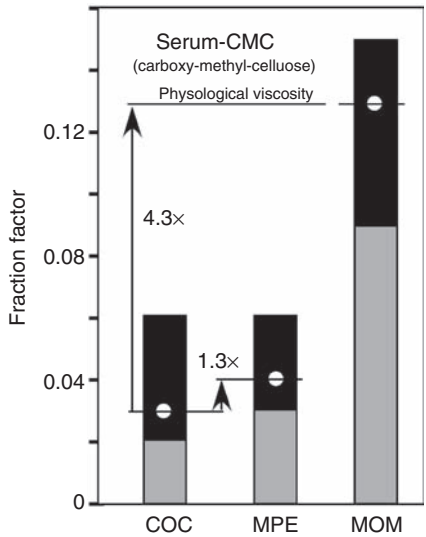

5.4 Friction studies for all-ceramic (COC) compared with metal-polyethylene (MPE) and all-metal (MOM) bearings run under serum lubrication with variable viscosity (Scholes and Unsworth, 2006).

Table 5.7 Summary of limitations in ceramic THR designs

ID #	Feature	Observations	Details
1	Brittle	Fractures	Incidence decreased over 3 decades to 1/10 000
2	Rim chips	Impingement risk	Not seen as major problem (<3%)
3	Ball diameter	Limited by cup design	32 mm preferred; new trend to 36 mm
4	Ball design	Neck-lengths	Adjustments limited (safety requirements)
5	Cup design	Rim enhancements	Not risked (safety requirements)
6	Stripe wear	Relatively common	Higher wear (not seen as problem in 36 years)
7	Squeaking	Transient or permanent	Controversial in 2008

implant technology has been improved continuously over the past three decades with substantially refined grain size, density and reduced inclusion levels. For example, the bending-strength of the original Biolox™ was improved by 40% over three decades. Related developments have been improved manufacturing processes, including the use of laser-markings

instead of the earlier engraving method that could have represented a stress-riser in ceramic. In 1995–1997, the HIP process was introduced by some manufacturers, the most well-known type being marketed as Biolox-forte™. Another significant improvement was the introduction of the 'proof' test. The goal of the proof test was to eliminate the weakest balls in each lot by temporarily loading them to a stress state above the physiological requirements. Prior to this introduction, only 2–3% of each lot was studied in a destructive 'burst' test. With the proof test, 100% of alumina implants could be stressed before leaving the factory. The majority of contemporary alumina implants now come from CeramTec in Germany, Ceraver in France, Kyocera in Japan, Metoxit in Switzerland and Morgan Matroc in the UK.

Surveying ceramic series in recent major journals and congress, there were 11 studies representing over 35 000 cases in total followed for 3–25 years and reported fracture cases numbered only 24 (Tateiwa *et al.*, 2008). A unique survey of hip complications in the 1990 era showed a fracture risk of approximately 1.4 per 1000 ceramic balls used in the USA. One company's database holding more than 2.5 million records described the overall fracture risk as 1 per 10 000 cases (Willmann and von Chamier, 1998). Beginning in 1998, contemporary ceramic liners in the FDA's database numbered >2400, with zero fractures reported by the FDA (July 2003). There was noted a 2–3% incidence of rim chipping during surgery with some cup designs (Garino, 2000; D'Antonio *et al.*, 2002, 2005).

Squeaking and clicking of ceramic hip joints has also been raised as an issue (Table 5.7). In one of our cases we noted that squeaking and clicking could be one consequence of the femoral neck impinging on the rim of the ceramic cup and creating both femoral and acetabular notches with accompanying metallosis (Eickmann *et al.*, 2003). This was essentially similar to a previous finding with all-metal bearings (Iida *et al.*, 1992). Thus bearing diameters and optimal functional positioning of implants may be important issues (Walter *et al.*, 2003). Whether such squeaking is transient or permanent may also have an influence on revision decisions (Table 5.8).

5.2.4 Conclusions on alumina experience

In monoblock ceramic hip designs from the 1970s, up to 3 mm of linear wear could be detected in a few poorly functioning cases. Corresponding volumetric wear rates ranged from 10 to 260 mm^3/year. The common explanations were that cups were too close to the vertical, cup loosening, migration and more vertical tilting with the patients continuing to function like this for some time. However, even in such poorly functioning cases, after 10–15 years, there appeared to be minimal risk of a debris-mediated osteolysis.

Table 5.8 Possible mechanisms of squeaking and clicking sounds in rigid bearings

ID #	Feature	Clinical	Details
1	Mismatched ceramic types	Morlock *et al.* (2001)	Case report
2	Mismatched ball : cup diameters		
3	Neck/cup-rim impingement	Eickmann *et al.* (2003)	Case report
4	Vertical cup malalignment	Walter 2003	Clinical study
5	Stripe wear	Walter 2003	Clinical study
6	Microseparation		
7	Cracked ceramic component		
8	Lubricant starvation		
9	3rd body abrasive wear		

The modern metal-backed cup with a taper-locked ceramic liner was introduced in 1989 and contemporary ceramic designs use hemispherical, metal-backed cups with a taper-locked liner. Wear in contemporary alumina THR was very low, as represented by linear wear rates of 5–50 μm/year. Volumetric wear was only measurable in the 50% of retrieved implants that featured stripe wear and averaged <1 mm^3/year with a maximum of 3.5 mm^3/year. Contemporary THR trends are to use ball diameters of 32 and 36 mm and possibly even larger. Such large COC bearings confer the advantage of much lower frictional torques than MOM bearings (Fig. 5.4).

In the laboratory, the alumina bearings showed an initial high-wear phase during run-in that normally decreased four- to eight-fold within 1 million cycles and going into the steady-state wear phase. In standard test mode, the overall wear of alumina THR was generally around 0.1 mm^3/year. Under the most severe test mode of microseparation this could be elevated some 15-fold by the stripe wear. Microseparation wear-rates of 1.2 and 1.5 mm^3/Mc overall for 28 mm and 36 mm diameters respectively, were mid-range to retrieval studies of contemporary THR designs that featured stripe wear. Thus, there was good agreement between laboratory and clinical wear predictions. Nevertheless, the 'severe' microseparation test modes in two laboratories produced acceptably low wear rates. Ceramic retrievals over 20 years have also shown only a mild progression of such stripe wear zones.

Fracture risk in the USA in the mid-1990s was reported as 14 per 10 000 (0.14%) cases and from a major ceramic manufacturer as 1 per 10 000 cases (0.01%). The trend to increased diameters of ceramic balls (32, 36 mm and larger) will make a positive contribution to safety on the femoral side but will do nothing for the ceramic liner insert.

Thus in overview, alumina ceramic has shown excellent potential over a 36-year history (Table 5.9) that helps offset the limitations of a brittle material (Tables 5.6 and 5.7).

Table 5.9 Benefits of alumina ceramic implants documented over 36 years

ID #	Feature	Observations	Details
1	Corrosion	Totally inert	No fluids penetrate; no ceramic dissolution
2	Metastability	Totally stable	No phase transformation possible
3	Tribology	Non-sensitive bearing	Tolerates adverse lubrication modes
4	Tribology	Very hard surface	Extremely resistant to 3rd body abrasion
5	Tribology	Laboratory wear	COC considered highest wear resistance
6	Clinicals	Coherent history	Many studies over 36 years
7	Clinicals	Osteolysis	Exceedingly rare
8	Biology	Cell cultures	Alumina = most benign form of debris
9	Biology	Animal studies	Alumina = most benign form of debris
10	Biology	Retrieval studies	Alumina = most benign form of debris
11	Biology	Non-allergenic	No adverse reports
12	Biology	Non-carcinogenic	No adverse reports

5.3 Introduction to zirconia THR

Zirconia ceramic became widely used for orthopedic joint replacements from 1985 onwards (Cales, 1995; Chevalier *et al.*, 1999). Not much has been published on the magnesia-stabilized zirconia (Mg-Zr). The yttria-stabilized tetragonal zirconia polycrystalline ceramic (Y-TZP) was marketed as an extremely strong and fatigue-resistant bioceramic. The 28 mm and 32 mm zirconia–polyethylene (ZrPE) hip systems were approved by the FDA in 1989. However the clinical reports for Y-TZP THRs revealed many anomalies over a 15-year history (Clarke *et al.*, 2003a).

Korean Zr/PE studies reported good clinical results with 7 years' follow-up (Kim *et al.*, 2001) as did the UK's clinical experience beyond a decade (Wroblewski *et al.*, 2004; Stewart *et al.*, 2005). The first significant insight came from a Japanese clinical team who noted surface transformations with substantial cratering on two retrieved zirconia balls (Haraguchi, 2001). Finally, in 1999 an unfortunate manufacturing change by one vendor (St Gobain Desmarquest, France) brought zirconia sales to a sudden halt (Clarke *et al.*, 2003a). A change in their sintering processes resulted in a

large number of fractured Prozyr™ balls, initiating a worldwide recall in 1999 that was concluded by 2001. This was unfortunate because other types, such as magnesia-stabilized zirconia, were available for THR and total knee replacement (TKR) designs. Nevertheless, this short-lived Prozyr™ fracture problem helped re-define the critical role of manufacturing in the 'metastability' of a Y-TZP zirconia ceramic.

The contemporary zirconia bearings used in USA have an oxygen-diffused, zirconia ceramic surface some 5 μm thick (Good *et al.*, 2003). This has been used on a metal zirconium balls and on the femoral condylar implants of total knee replacements (Oxinium™: Smith and Nephew Inc, Memphis Inc.). Zirconia used for monoblock femoral condyles has been implanted in Europe and Japan but has not seen approval by the FDA.

5.3.1 Y-TZP zirconia is a 'metastable' ceramic

Y-TZP ceramic has the ability to transform from the tetragonal phase, which is its high-energy state, into the monoclinic phase as its lowest energy state. This tetragonal to monoclinic transformation will occur under certain environmental conditions, and produces a net 4% volume expansion in the monoclinic crystal. Thus when a fracture crack tries to propagate through a matrix composed of 100% tetragonal grains, this sudden loss of matrix constraint allows for the spontaneous expansion of tetragonal into monoclinic grains and the resulting compressive-stresses will further inhibit any crack growth. This tetragonal to monoclinic transformation is the basis for the superior strength of zirconia and is termed the 'transformation toughening' effect (Garvie *et al.*, 1975).

5.3.2 Y-TZP zirconia transforming to monoclinic phase *in vivo*

So what level of zirconia's monoclinic phase is to be found on the articular surface of zirconia balls? Studies of new Prozyr™ balls (St Gobain Desmarquest, France) processed in either batch or tunnel furnaces showed surface monoclinic averaging 4% (5.7% max) on articular surfaces (Masonis *et al.*, 2004; Stewart *et al.*, 2005). The most detailed study came from a clinical series begun in 1988 with Prozyr™ balls (Hernigou and Bahrami, 2003). The ominous finding comparing 12 years' follow-up with that at 5 years was that the wear with 28 mm Zr/PE had quadrupled and was also five-fold higher than with their 32 mm Al/PE controls. The three French retrievals revealed that non-HIPped Prozyr femoral heads could transform with 20–30% monoclinic between 4–11 years' use in the patient (Hernigou and Bahrami, 2003; Chevalier, 2006). These data appeared

identical to the retrieval report on Japanese HIPped zirconia (Haraguchi *et al.*, 2001).

Our Peterson Tribology Research Center retrieval lab has collected more than 100 zirconia femoral heads with some showing a visual 'misting' on articulating surfaces (Walter *et al.*, 2005). These revealed extensive areas of cratering along with considerable transformation from tetragonal to monoclinic phase. This appeared to peak in the main wear region (polar) and at equatorial regions corresponding to edge effects by the polyethylene cup. Unlike alumina surfaces where the wear process appeared as a mild relief polishing of grains, the zirconia surface appeared to crumble and form extensive craters. We compared Prozyr retrievals at 8 and 9 years' follow-up from Sydney and LLUORC, respectively (Green, 2003a,b; Walter *et al.*, 2005). Monoclinic transformation was detected up to 85%, the highest ever recorded for zirconia implants. The articulating surface roughness had also increased dramatically (Ra = 100–250 nm) due to extensive cratering in the areas of habitual polyethylene contact.

5.3.3 Laboratory wear studies with Y-TZP zirconia and polyethylene cups

It was interesting that the simulator studies consistently predicted a major wear advantage for Zr/PE bearings (Table 5.10). There was no identification of zirconia transformation or surface cratering at the end of the typical, 5 million cycles laboratory test (McKellop *et al.*, 1992; Saikko, 1994; Derbyshire, 1994). Obviously the laboratory test conditions can be very different from the clinical situation. Simulator run-time (5 million cycles) amounts only to

Table 5.10 Comparison of main differences between retrieval studies of zirconia/polyethylene performance and results from simulator studies

ID #	Retrieval studies Zr/PE	Simulator studies Zr/PE at 5 Mc
1	'Misting' on zirconia bearing surfaces	No misting observed
2	>20% monoclinic within 3 years	No transformation
3	Surface roughness increased >200 nm	No roughness changes
4	Surface cratering within 3–5 years	No cratering described
5	Zr/PE wear typically increased > 5 years	Zr/PE wear < (Co/PE, Al/PE)

Al/PE = alumina/polyethylene, Co/PE = cobalt–chrome/polyethylene, Zr/PE = zirconia/polyethylene.

about 2 months' test duration. The simulator study may also be discontinuous, spread over 3–4 months' duration due to different down-time requirements. At first glance it would appear intuitively likely that the simulator's 24-hour cycling at elevated temperatures (close to 100 °C) could have accelerated the surface transformation of zirconia balls. However, the metastability of the zirconia balls was clearly not challenged by any simulator study (Brown and Clarke, 2006). The fact that zirconia balls could transform *in vivo* to 20–80% monoclinic within a 3–10-year time-frame indicates how little we know of the tribological–hydrothermal events occurring under the polyethylene cup. Thus simulator wear studies were not capable of predicting the clinical performance of a metastable ceramic.

5.3.4 Conclusions on Y-TZP zirconia experience

The 20-year clinical history of zirconia–polyethylene hip joints has revealed a troubling fact. Use of a 'metastable' ceramic femoral head resulted in retrievals with monoclinic transformations as high as 80% within 10 years of follow-up. This was contrary to expert predictions that even non-HIPped zirconia would show less than 5% monoclinic after such exposure. The severity of the fracture experience with 'TH' Prozyr balls in 1998–2001 served to dramatize how critical the manufacturing process was for such metastable zirconia. In contrast, the standard simulator wear studies did not challenge the metastable nature of zirconia femoral heads over test durations consisting of 5 million load cycles. In overview, the simulator studies of Zr/PE combinations missed the mark, predicting superior wear performance compared to controls. As noted by Walter *et al.* (2005), patients with Zr/PE hip-joint replacements may have to be monitored for adverse changes.

5.4 Introduction to alumina matrix composite (AMC) ceramics

While HIPped alumina has performed well over 36 years, it is also clear that a stronger ceramic would be eminently desirable. Various zirconia–alumina composites have been evaluated as implant materials over the last decade (Toni *et al.*, 1999; Kaddick and Pfaff, 2000, 2002). One composite ceramic containing 17% by volume of zirconia has been trade marked Biolox® *delta* (CeramTec Medical Products: Willmann, 2000). This alumina matrix composite (AMC) has been in clinical use in Europe from year 2000. In the USA, the FDA approved the AMC femoral heads for use with polyethylene inserts (510 K process, June 2000). It is estimated that more than 35 000 AMC femoral heads have been implanted since 2000 (Heros, 2006, personal communication).

5.4.1 Mechanical properties of alumina matrix composite ceramic

The strengthening and toughening technologies of such an alumina matrix composite can be viewed as three contributory mechanisms (Table 5.11). The properties of the alumina were enhanced by combining the toughening effects of zirconia with additional platelet-like anisotropic crystals. Such constituents activated the synergetic effects of strength and toughness of the composite (Table 5.12). The hardness was improved by alloying the material with chromium oxide, which created a solid solution with the alumina matrix. The distribution of chromium inside the alumina atomic lattice activated a colorizing effect similar to that of natural ruby. In particular, compared with the gold standard alumina used worldwide since 1977, the AMC fracture toughness was increased 150% while the ball burst strength improved 160% (Table 5.12). In addition the hardness of the AMC material was just slightly lower than that of the control alumina.

5.4.2 Laboratory wear with alumina matrix composite THR

Detailed wear studies have been published for AMC ceramics used in COC combinations. Less is known about the AMC/PE combinations. The wear

Table 5.11 Three methods of improving alumina ceramic using alumina–matrix composite technology (Willmann, 2000)

ID #	AMC ceramic feature	Technology of AMC ceramics
1	Transformation toughening	Produced by addition of small zirconia particles homogeneously dispersed in the alumina matrix
2	Platelet reinforcement	Produced by *in situ* formation of elongated oxide crystals
3	Matrix hardening	Produced by creation of solid solution with chromium oxide

Table 5.12 Comparison of characteristic mechanical values – alumina matrix composite (AMC) vs. alumina (Al) (Willmann, 2000)

Property	Units	Al	AMC	Change
4 point bending strength	MPa	580	1250	+210%
Fracture toughness	$MPa.m^{0.5}$	4.0	5.7	+150%
Ball 'burst' strength 28 L	kN	52	83	+160%
Hardness HV_1	GPa	20	17	–15%

Table 5.13 Simulator wear study in 'severe' microseparation test mode for alumina matrix composite balls (AMC: 28 mm) run on alumina (Al) and AMC cups (Stewart *et al.,* 2003)

THR	Run-in (mm^3/Mc)	Steady state (mm^3/Mc)	Overall (mm^3/Mc)
AMC/AMC	0.32	0.12	0.16
AMC/Al	0.99	0.51	0.61
Ratio	×3	×4	×4

properties of zirconia-toughened composites have been studied by both ring-on-flat wear machine and by hip simulator (Kaddick and Pfaff, 2000, 2002). With AMC ball and cup combinations run in standard test mode, the overall wear to 10 Mc duration was quite low, averaging 0.03 mm^3/Mc. Therefore the AMC wear rates appeared similar to alumina controls in standard test mode (Table 5.5). Insley *et al.* (2002) reported on two types of AMC under microseparation test mode. The N-AMC type had composition 25% zirconia and remainder alumina, whereas C-AMC type had 24% zirconia and 1% mixed oxides. The latter showed approximately a 2.5-fold wear reduction under microseparation mode compared with alumina controls. In this group's subsequent report, the wear of AMC/alumina and AMC/AMC combinations were compared under their 'severe' microseparation mode. The AMC/AMC combination averaged three- to four-fold less wear than the AMC/alumina combination (Table 5.13). Compared with the prior study of alumina THR (Table 5.6), the AMC/AMC reduced run-in, steady-state and overall wear rates were reduced by 11 to 13-fold (Table 5.13).

At LLUORC we studied the four alumina and AMC combinations (ball/cup: AMC/AMC, AMC/Al, Al/AMC and Al/Al) simultaneously in a 12-station hip simulator. This was the first simulator study of the four ceramic combinations using Biolox-forte and Biolox-delta and the first report on wear in large-diameter, ceramic bearings. It is also the first report of zirconia transformation during hip simulation. With 10 wear measurements taken from start-up to 1 million cycles, we have also documented for the first time the run-in wear phase for ceramics under a severe stripe-formation mode (Green *et al.*, 2007). All implants had evidence of stripe wear by 0.1 Mc duration in this microseparation study. On the femoral heads this appeared as a broad scar at sites +75 to +90° from the pole and a narrower scar at sites +45 to +60°. Over the study to 5.0 Mc duration, these two stripes coalesced forming a large stripe spanning a 45–90° arc relative to the pole. Overall the alumina had the largest stripe areas and AMC the least. Similarly, all ceramic liners showed stripe wear juxtaposed to the cup bevel. At 0.1 Mc, the stripes were narrow and subtended a circumferential arc of +10° to +90°.

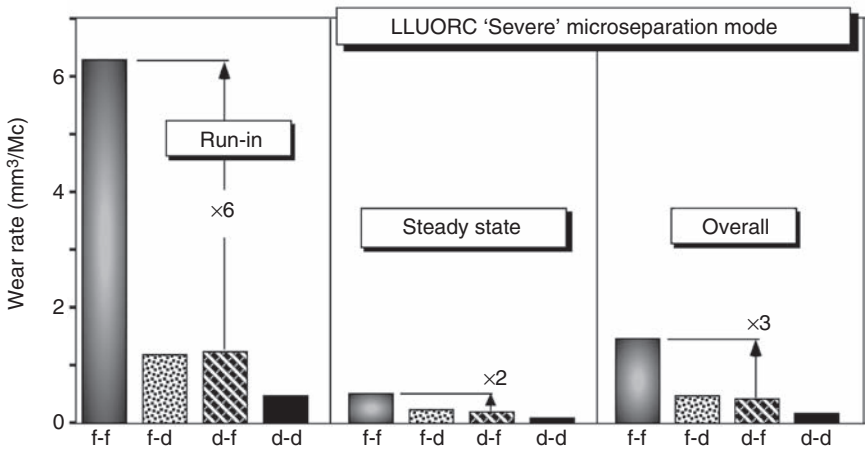

5.5 Summary of LLUORC simulator wear data for alumina and AMC wear study to 5 Mc duration. Run-in was over 0–1 Mc and steady-state 1–5 Mc duration (Green *et al.*, 2007). Key f-f, Biolox-forte ball and forte cup; f-d, Biolox-forte ball and delta cup; d-f, Biolox-delta ball and forte cup; d-d, Biolox-delta ball and delta cup.

These progressed gradually along the bevel circumference to a maximum arc of 180° for alumina cups and also had expanded radially towards the central wear zone.

The largest difference in wear rates was during the run-in phase with delta hybrids averaging a 6-fold decrease and the AMC/AMC combination averaging a 12-fold reduction compared with alumina controls (Fig. 5.5). However in the steady-state phase, the latter had a 4-fold reduction. Overall at 5 Mc duration, the delta hybrids saw a reduction of 3-fold and AMC/AMC a reduction of 6-fold compared with alumina controls.

The AMC matrix is predominantly composed of the large alumina grains (1 μm size) interspersed with smaller tetragonal zirconia grains (sub-micrometer size). The AMC ceramic implant comes with a combination of tetragonal and already transformed monoclinic grains (12–14%) on the alumina-dominated articulating surface (Fig. 5.6). The hydrothermal, pressure–temperature phenomenon between ceramic ball and cup will transform the additional tetragonal phase in the zirconia surface to monoclinic followed by grain erosion due to wear. In our study we measured up to 30% monoclinic phase by the end of 5 Mc duration. Continuing wear will release combinations of alumina, tetragonal and monoclinic grains. However the dominant and much harder alumina matrix will control the wear process.

Thus Biolox-delta used in COC-bearing combinations were more resistant to stripe wear than Biolox-forte. Therefore the AMC implants repre-

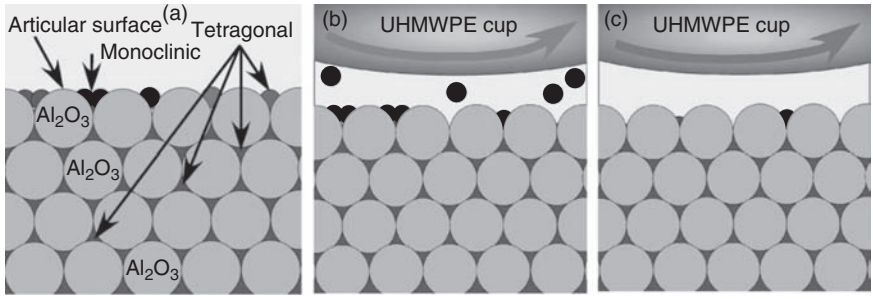

5.6 Cross-section of AMC ceramic ball showing steps in wear of articulating surface. (a) The ceramic matrix is predominantly composed of the large MGA grains (light gray; 1μm size) interspersed with smaller tetragonal zirconia grains (dark gray; sub-micrometer size). (b) Hydrothermal effects created by pressure-temperature frictional phenomena between ceramic ball and cup transforms approximately 30% of remaining tetragonal grains to monoclinic phase (black) in surface layers with some erosion due to wear process. (c) Continuing wear process will release combinations of alumina, tetragonal and monoclinic grains. However the dominant and harder matrix of micrometer size alumina grains will control the wear process.

sented an optimized combination of high-strength composite core, a hard alumina articular surface and maximum wear resistance to stripe wear.

5.4.3 Conclusions on alumina matrix composites

The introduction of AMC ceramic for femoral heads and acetabular inserts provides implants with almost double the strength and fatigue resistance of the alumina used as the gold standard for past 36 years. Two independent laboratory studies running under 'severe' wear test mode have concluded that AMC combinations will reduce stripe wear by three- to six-fold. Clinical follow-ups are still too short to determine the efficacy of this new ceramic and no retrieval studies have been reported. Therefore it is not yet possible to verify the role of any monoclinic transformation in the distributed zirconia phase of AMC bearings used *in vivo* against ceramic or polyethylene cup inserts.

5.5 Summary

Alumina has been the mainstay of the ceramic THR for over 38 years. Any concerns regarding alumina wear debris and osteolysis have been discounted over the past 17 years of clinical experience with metal-backed ceramic liners. However the small incidence of fractures with alumina

implants continues to be a discussion point. Contemporary alumina is reputed to have a fracture rate <0.01%. In FDA-monitored studies, over 2700 cases were enrolled and five manufacturers were involved with 28 mm and 32 mm metal-backed ceramic cups. With follow-ups now extending over 8 years, there have been zero fractures reported in this group. The trend to 32 mm and 36 mm femoral heads will add increased safety to such designs.

The Y-TZP zirconia femoral heads (28, 32 mm) had been approved for sale in the USA by 1989. While there are no definitive long-term studies of Zr/PE bearings, there are enough disquieting clinical and retrieval studies to discourage use of this combination. Use of this 'metastable' zirconia femoral-head resulted in retrievals with monoclinic transformations as high as 80% within 10 years of follow-up. This was contrary to expert predictions that zirconia implants would show less than 5% monoclinic after such exposure. The severity of the fracture experience with Prozyr balls in 1998–2001 also served to dramatize how critical the manufacturing process was for such metastable ceramics.

Femoral heads of the new AMC are approved for use with polyethylene cups. With double the strength and fatigue resistance of alumina, the AMC implants should abate fracture concerns. Two independent laboratory studies under severe microseparation test mode agreed that AMC bearings further reduced the already low wear seen with alumina bearings. AMC surfaces have 12–14% surface content of monoclinic phase and this increased to around 30% in simulator studies run to 5 million cycles' duration. Clinical follow-ups in Asia and Europe are still too short to assess the efficacy of this new ceramic and no retrieval studies have been reported. There has not yet been opportunity to verify the role of any monoclinic transformation in the distributed zirconia phase of retrieved AMC bearing on polyethylene or ceramic cup inserts.

5.6 Conclusions

Ceramic-on-ceramic appears to be the optimal THR bearing being totally inert, having ultra-low wear and the alumina debris being the least reactive in the body. Its wear and biological performance over 37 years *in vivo* have been admirable. However alumina ceramic has the disadvantage of being a brittle material. Thus fracture has been a persistent although fortunately a rare occurrence with alumina implants. So by today's standards, contemporary ceramic designs have been limited by the necessary thickness of the ceramic liner with its metal backing and concomitantly smaller diameters of femoral heads.

The newly developed alumina matrix composite (AMC) doubles the factor of safety over alumina and has performed extremely well in 'severe'

simulator test modes with COC combinations. This material is quite unlike the yttria-stabilized zirconia (Y-TZP) that had been abandoned by 2000. AMC behaves much more like the alumina 'gold standard'. The substantial improvement in mechanical properties and the excellent wear behavior even under 'severe' microseparation wear makes the AMC material a promising new addition. Femoral heads of AMC have now become available in some THR designs for use with metal-backed UHMWPE cups. However the all-ceramic AMC bearing is not yet approved for marketing as we progress through 2008.

5.7 Acknowledgements

Our grateful thanks to many scientists and surgeons for ceramic collaborations and discussions, including H.C. Amstutz MD, B. Ben-Nissan PhD, J. D'Antonio MD, C. Delauney MD, A. Essner MS, J. Fisher PhD, K. Keggi MD, H.A. McKellop PhD, H. Oonishi MD, G. Pezzotti PhD, C. Piconi MD, D. Schroeder MS, L. Sedel MD, W.K. Walter MD, W.L. Walter MD, A. Wang PhD and in particular to the late G. Willmann PhD. We also acknowledge industry's financial support for laboratory wear studies of ceramic THR, including Amedica, Biomet, CeramTec, Joint Medical Products Corporation, Smith and Nephew and Stryker. We gratefully acknowledge also the support of the Peterson Foundation and the Orthopedic Department of Loma Linda University.

5.8 References and further reading

Amstutz HC, Campbell P, Kossovsky N, Clarke IC (1992). Mechanism and clinical significance of wear debris-induced osteolysis. *Clin Orthop*, **276**: 7–18.

Amstutz HC, Clarke IC (1991). Chapter 1: Evolution of hip arthroplasty. In *Hip Arthroplasty*, Vol. 1–14. Edited by Amstutz, H. C., New York, Churchill.

Bizot P, Hannouche D, Nizard R, Witvoet J, Sedel L (2004). Hybrid alumina total hip arthroplasty using a press-fit metal-backed socket in patients younger than 55 years. A six- to 11-year evaluation. *J Bone Joint Surg Br*, **86**(2): 190–194.

Bizot P, Banallec L, Sedel L, Nizard R (2000). Alumina-on-alumina total hip prostheses in patients 40 years of age or younger. *Clin Orthop*, **379**: 68–76.

Boutin P (1972). [Total arthroplasty of the hip by fritted aluminum prosthesis. Experimental study and 1st clinical applications]. *Rev Chir Orthop Reparatrice Appar Mot*, **58**(3): 229–246.

Brown S, Clarke IC (2006). Triggering the phase transformation of zirconia balls *in vivo* and *in vitro*. In *Trans Soc Biomat*, April 26–29, Pittsburgh, p. 103.

Cales B (1995). Y-TZP zirconia ceramic hip joint heads. Key-issues for a high reliability. In: *Euro Cer Soc 4th Conf*. Riccione, Italy, p. 45–52.

Cales B, Stefani WY, Lilley E (1994). Long-term *in vivo* and *in vitro* aging of a zirconia ceramic used in orthopaedy. *J Biomed Mater Res*, **28**: 619–624.

Charnley J, Kamangar A, Longfield MD (1969). The optimum size of prosthetic heads in relation to the wear of plastic sockets in total replacement of the hip. *Med Biol Eng*, **7**(1): 31–39.

Chevalier J (2006). What future for zirconia as a biomaterial? *Biomaterials* **27**: 535–543.

Chevalier J, Cales B, Drouin JM (1999). Low-temperature aging of Y-TZP ceramics. *J Amer Ceram Soc*, **82**(8): 2150–2154.

Clarke IC (1992). Role of ceramic implants. Design and clinical success with total hip prosthetic ceramic-to-ceramic bearings. *Clin Orthop*, **282**: 19–30.

Clarke IC (2006). Metastable nature of zirconia femoral heads from a 20-year perspective of clinical and simulator wear studies. In *Seminars in Arthroplasty*, Cadmus Pub.

Clarke I, Campbell P (1989). Interface failure dynamics: osteoclastic and macrophagic bone loss. In *Progress in Bioengineering*, Vol. 104–115. Edited by Kenedi, R. M., and Paul, J. P., Strathclyde University.

Clarke IC, Willmann G (1994). Structural ceramics in orthopedics. In *Bone Implant Interface*, Vol. 203–252, Edited by Cameron, H. U., St. Louis, Mosby.

Clarke IC, Williams P, Shishido T, Good V, Oonishi H, Gustafson A (2002). Hip simulator validations of alumina THR wear rates for run-in and steady-state wear phases. In *Proc. 7th Int. Biolox Symposium*, pp. 20–26. Edited by Willmann, G.

Clarke IC, Manaka M, Green DD, Williams P, Pezzotti G, Kim YH, Ries M, Sugano N, Sedel L, Delauney C and others (2003a). Current status of zirconia used in total hip implants. *J Bone Joint Surg Am* **85-A** Suppl 4: 73–84.

Clarke IC, Manaka M, Shishido T, Oonishi H, Gustafson GA, Boehler M (2003b). Tribological and material properties for all-alumina THR – convergence with clinical retrieval data. In *Bioceramics in Joint Arthroplasty*, pp. 1–17, Edited by Zippel H. and Dietrich M., Steinkopff Verlag, Darmstadt.

Clarke IC, Donaldson T, Bowsher JG, Nasser S, Takahashi T (2005a). Current concepts of metal-on-metal hip resurfacing. *Orthop Clin North Am*, **36**(2): 143–162, viii.

Clarke IC, Green DD, Tateiwa T, Williams P, Donaldson T (2005b). Stripe wear simulation of the stripe-scar phenomenon compared in alumina–alumina and alumina–composite hip implants. *Tribol Trans* Oct. 24–27, 2004.

D'Antonio J, Capello W, Manley M, Bierbaum B (2002). New experience with alumina-on-alumina ceramic bearings for total hip arthroplasty. *J Arthroplasty*, **17**(4): 390–397.

D'Antonio J, Capello W, Manley M, Naughton M, Sutton K (2005). Alumina ceramic bearings for total hip arthroplasty: five-year results of a prospective randomized study. *Clin Orthop Relat Res*, **436**: 164–171.

Derbyshire B, Fisher J, Dowson D, Hardaker C, Brummitt K (1994). Comparative study of the wear of UHMWPE with zirconia ceramic and stainless steel femora heads in artificial hip joints. *Med Eng Phys*, **16**: 229–236.

Dorlot JM (1992). Long-term effects of alumina components in total hip prostheses. *Clin Orthop*, **282**: 47–52.

Eickmann T, Clarke I, Gustafson A (2003). Squeaking in a ceramic on ceramic total hip. *In 8th Biolox Symposium*, pp. 187–192. Edited by Dietrich M., Berlin, Germany, Steinkopff Verlag, Darmstadt, 2003.

Furlong RJ, Osborn JF (1991). Fixation of hip prostheses by hydroxyapatite ceramic coatings. *J Bone Joint Surg Br*, **73**(5): 741–745.

Garino JP (2000). Modern ceramic-on-ceramic total hip systems in the United States: early results. *Clin Orthop*, **379**: 41–47.

Garvie RC, Hannink RH, Pascoe RT (1975). Ceramic steel? *Nature*, **258**: 703–704.

Good V, Ries M, Barrack RL, Widding K, Hunter G, Heuer D (2003). Reduced wear with oxidized zirconium femoral heads. *J Bone Joint Surg Am*, **85-A** Suppl 4: 105–110.

Green D *et al.* (2003a). Zirconia ceramic femoral heads in the USA – retrieved zirconia heads – 2 to 10 years out. In *49th Annual Meeting of the Orthopaedic Research Society*, Orthopaedic Research Society.

Green D *et al.* (2003b). 2 and 10 year retrievals of zirconia femoral heads-XRD, SEM and Raman spectroscopy studies. In *105th Annual Meeting of The American Ceramic Society*, American Ceramic Society, Nashville, Tennesse.

Green DD, Donaldson TK, Williams PA, Pezzotti G, Clarke IC (2005a). Ceramic-on-ceramic under micro separation test configuration for THR – a study of like-on-like and hybrid combinations. *18th Ann Symp Int Soc Tech Arthroplasty*, September 29–October 2, Kyoto, Japan.

Green DD, Williams P, Donaldson T, Clarke IC (2005b). *Biolox-Forte vs. Biolox-Delta Under Micro Separation Test Mode in the USA*. Orthopaedic Research Society, Washington, DC.

Green DD, Donaldson T, Williams P, Pezzotti G, Clarke I (2007). Long term strip wear rates of 3rd and 4th generation ceramic-on-ceramic under microseparation. In: *Proc 53rd Ann Meet Ortho Res Soc*. San Diego, California, p. 1776.

Griss P (1984). Four- to eight-year postoperative results of the partially uncemented Lindenhof-type ceramic hip endoprosthesis. In *The Cementless Fixation of Hip Endoprostheses*, Vol. 220–224. Edited by Morscher E, Springer-Verlag.

Hamadouche M, Boutin P, Daussange J, Bolander ME, Sedel L (2002). Alumina-on-alumina total hip arthroplasty: a minimum 18.5-year follow-up study. *J Bone Joint Surg Am*, **84-A**(1): 69–77.

Haraguchi K, Sugano N, Nishi T, Miki H, Oka K, Yoshikawa H (2001). Phase transformation of a zirconia ceramic head after total hip arthroplasty. *J Bone Joint Surg Br*, **83**: 996–1000.

Hernigou P, Bahrami T (2003). Zirconia and alumina ceramics in comparison with stainless-steel heads: polyethylene wear after a minimum ten-year follow-up. *J Bone Joint Surg Br*, **85-B**: p. 504–509.

Heros RJ, Willmann G (1998). Ceramic in total hip arthroplasty: history, mechanical properties, clinical results, and current manufacturing state of the art. In *Seminars in Arthroplasty*, Vol. 9, Elsevier pp. 114–122.

Huo MH, Martin RP, Zatorski LE, Keggi KJ (1996). Total hip replacements using the ceramic Mittelmeier prosthesis. *Clin Orthop*, **332**: 143–150.

Iida H, Kaneda E, Takada H, Uchida K, Kawanabe K, Nakamura T (1999). Metallosis due to impingement between the socket and the femoral neck in a metal-on-metal bearing total hip prosthesis. A case report. *J Bone Joint Surg Am*, **81**(3): 400–403.

Insley GM, Turner I, Fisher J, Streicher RM (2002). *In vitro* testing and validation of zirconia toughened alumina (TZA). In: Proc 7th Int Biolox Symposium. Edited by Willmann, G, Darmstadt, H Steinkopff Verlag.

Ivory JP, Kershaw CJ, Choudhry R, Parmar H, Stoyle TF (1994). Autophor cementless total hip arthroplasty for osteoarthrosis secondary to congenital hip dysplasia. *J Arthroplasty*, **9**(4): 427–433.

Jacobs JJ, Skipor AK, Campbell PA, Hallab NJ, Urban RM, Amstutz HC (2004). Can metal levels be used to monitor metal-on-metal hip arthroplasties? *J Arthroplasty*, **19**(8 Suppl 3): 59–65.

Kaddick C, Pfaff HG (2000). Wear study in the alumina–zirconia system. In *Bioceramics in Hip Joint Replacement* (Proceedings 5th International CeramTec Symposium), Vol. 146–150. Edited by Zweymuller, K., New York, Georg Thieme Verlag.

Kaddick C, Pfaff HG (2002). Results of hip simulator testing with various wear couples. In *Proc. 7th Int. Biolox Symposium*, pp. 16–20. Edited by Willmann, G.

Keggi K (2006). My 30 years expericence in total hip arthroplasty. In *8th Annual Workshop for 'Current Concepts in Hip, Knee and Spine'*, Mammoth Lakes, CA, Sept 8th.

Kim YH, Kim JS, Cho SH (2001). A comparison of polyethylene wear in hips with cobalt-chrome or zirconia heads. A prospective, randomised study. *J Bone Joint Surg Br*, **83**(5): 742–750.

Mahoney OM, Dimon JH, 3rd (1990). Unsatisfactory results with a ceramic total hip prosthesis. *J Bone Joint Surg Am*, **72**(5): 663–671.

Manaka M, Clarke IC, Yamamoto K, Shishido T, Gustafson A, Imakiire A (2004). Stripe wear rates in alumina THR – comparison of microseparation simulator study with retrieved implants. *J Biomed Mater Res*, **69B**(2): 149–157.

Masonis JL, Bourne RB, Ries MD, McCalden RW, Salehi A, Kelman DC (2004). Zirconia femoral head fractures: a clinical and retrieval analysis. *J Arthroplasty*, **19**: 898–905.

McKellop H, Lu B, Benya P (1992). Friction, lubrication and wear of cobalt, chromium, alumina and zirconia hip prostheses compared on a joint simulator. *38th Annual Meeting of the Orthopaedic Research Society*, Washington, DC.

Miller EH, Heidt RS, Welch MC, Harding WG, Heidt RS, Jr., Lawhon SM (1986). Self-bearing, uncemented, ceramic total hip replacement arthroplasty. *Instr Course Lect*, **35**: 188–202.

Mittelmeier H, Heisel J (1992). Sixteen-years' experience with ceramic hip prostheses. *Clin Orthop*, **282**: 64–72.

Morlock M, Nassut R, Janssen R, *et al.* (2001). Mismatched wear couple zirconium oxide and aluminum oxide in total hip arthroplasty. *J. Arthrop.* **16**: 1071–1074.

Nevelos JE, Ingham E, Doyle C, Fisher J, Nevelos AB (1999). Analysis of retrieved alumina ceramic components from Mittelmeier total hip prostheses. *Biomaterials*, **20**(19): 1833–1840.

Nevelos J, Ingham E, Doyle C, Streicher R, Nevelos A, Fisher J (2000). Micro-separation in vitro produces clinically relevant wear of ceramic-ceramic total hip replacements. *Bioceramics*. Zurich-Uetikon: Trans Tech Publications Ltd, pp. 529–532.

Nevelos JE, Prudhommeaux F, Hamadouche M, Doyle C, Ingham E, Meunier A, Nevelos AB, Sedel L, Fisher J (2001a). Comparative analysis of two different types of alumina-alumina hip prosthesis retrieved for aseptic loosening. *J Bone Joint Surg Br*, **83**(4): 598–603.

Nevelos JE, Prudhommeaux F, Hamadouche M, Doyle C, Ingham E, Meunier A, Nevelos AB, Sedel L, Fisher J (2001b). Comparative analysis of two different types of alumina–alumina hip prosthesis retrieved for aseptic loosening. *J Bone Joint Surg Br*, **83**(4): 598–603.

Nizard RS, Sedel L, Christel P, Meunier A, Soudry M, Witvoet J (1992). Ten-year survivorship of cemented ceramic–ceramic total hip prosthesis. *Clin Orthop*, **282**: 53–63.

Prudhommeaux F, Hamadouche M, Nevelos J, Doyle C, Meunier A, Sedel L (2000). Wear of alumina-on-alumina total hip arthroplasties at a mean 11-year followup. *Clin Orthop*, **379**: 113–122.

Saikko V (1994). Wear of polyethylene acetabular cups against zirconia femoral heads studied with a hip joint simulator. *Wear*, **176**: 207–212.

Schmalzreid TP, Clarke IC, McKellop H (1998). Bearing surfaces. In *The Adult Hip*, pp. 247–265. Edited by Callaghan J. J., Rosenberg A. and Rubash H., Philadelphia, Lippincott-Raven Publishers.

Scholes SC, Unsworth A (2006). The effects of proteins on the friction and lubrication of artificial joints. *Proc Imech E*, **220**(H): 687–693.

Sedel L (2000). Evolution of alumina-on-alumina implants: a review. *Clin Orthop Relat Res*, **379**: 48–54.

Sedel L, Kerboull L, Christel P, Meunier A, Witvoet J (1990). Alumina-on-alumina hip replacement. Results and survivorship in young patients. *J Bone Joint Surg Br*, **72**(4): 658–663.

Sedel L, Nizard RS, Kerboull L, Witvoet J (1994). Alumina–alumina hip replacement in patients younger than 50 years old. *Clin Orthop*, **298**: 175–183.

Sedel L, Nizard R, Bizot P (2000). Osteolysis and ceramic bearing surfaces. *J Bone Joint Surg Am*, **82-A**(10): 1519; author reply 1520–1521.

Sedel L, Hamadouche M, Bizot P, Nizard R (2004). Long term data concerning the use of alumina on alumina bearings in total hip replacements. In *Bioceramics-15*, Vol. 15, pp. 769–772. Edited by Ben-Nissan B. Sher D. and Walsh W. Enfield, New Hampshire, Trans Tech Publications.

Shih CH, Wu CC, Lee ZL, Yang WE (1994). Localized femoral osteolysis in cementless ceramic total hip arthroplasty. *Orthop Rev*, **23**(4): 325–328.

Shishido T, Clarke IC, Williams P, Boehler M, Asano T, Shoji H, Masaoka T, Yamamoto K, Imakiire A (2003). Clinical and simulator wear study of alumina ceramic THR to 17 years and beyond. *J Biomed Mater Res*, **67B**(1): 638–647.

Skyrme AD, Richards S, John A, Chia M, Walter WK, Walter WL, Zicat B (2005). Polyethylene wear rates with zirconia and cobalt chrome heads in the ABG Hip. *Hip International*, **15**: 63–70.

Stewart T, Tipper JL, Streicher R, Ingham E, Fisher J (2001). Long-term wear of HIPed alumina on alumina bearings for THR under microseparation conditions. *J Mater Sci: Mater Med*, **12**: 1053–1056.

Stewart TD, Tipper JL, Insley G, Streicher RM, Ingham E, Fisher J (2003). Long-term wear of ceramic matrix composite materials for hip prostheses under severe swing phase microseparation. *J Biomed Mater Res B Appl Biomater*, **66**(2): 567–573.

Stewart T, Flemming N, Wroblewski BM, Fisher J (2005). *The Stability and Durability of Zirconia Femoral Heads*. Orthopaedic Research Society, Washington DC.

Tateiwa T, Clarke IC, Williams P, Garino J, Manaka M, Shishido K, Yamamoto M, Imakiire A (2008). Ceramic THR in USA – safety and risk issues revisited. *Amer J Orthopaedics*, available on-line (www.amjorthopedics.com).

Toni A, Affatato S (1999). New wear couples for THR – simulator testing. In *Reliability and Long-term Results of Ceramics in Orthopaedics*, Vol. 2191–2197. Edited by Sedel L. and Willmann G., Stuttgart, George Thieme Verlag.

Walter WL, Insley G, Walter WK, Tuke M (2003). The mechanics of stripe wear formation in a modern ceramic on ceramic bearing. In *70th Annual Meeting AAOS*, p. 278, New Orleans, Louisiana.

Walter WL, Skyrme, AD, Richards S, Chai M, Green D, Walter WK, Zicat B (2005). Polyethylene wear rates with zirconia and cobalt chrome heads. In *51st ORS*, p. 1194, Washington, DC.

Willmann, G (1999). A new material concept for bioceramics in orthopedics. In *Reliability and Long-term Results of Ceramics in Orthopedics*, pp. 62–63. Edited by Sedel L. and Willmann G., Stuttgart, Georg Thieme Verlag.

Willmann, G (2000). New generation ceramics. In *Bioceramics in Hip Joint Replacement*, pp. 127–135. Edited by Willmann G. and Zweymuller K., Stuttgart, Georg Thieme Verlag.

Willmann G, von Chamier, W (1998). The improvements of the material properties of Biolox offer benefits for THR. In *Bioceramics in Orthopaedics – New Applications*, pp. 19–24.

Wroblewski M *et al.* (2004). Wear of ultra-high-molecular-weight polyethylene cup articulating with 22.225 mm zirconia diameter head in cemented total hip arthroplasty. *J Orthop Sci*, **9**(3): 253–255.

6

Cellular response to bioactive ceramics

C KNABE, Charité Medical University, Germany and
Thomas Jefferson University, USA and
P DUCHEYNE, University of Pennsylvania, USA

6.1 Introduction – clinical significance

The ability to bond to bone tissue is a unique property of bioactive ceramics. This has led to their wide clinical use in both orthopedics as well as dentistry. Bioactive ceramics are used as bone substitute materials for bone grafting and as coatings for titanium and its alloy. These coatings have been found to accelerate initial stabilization of implants by enhancing bony ingrowth and stimulating osseous apposition to the implant surface, promoting a rapid fixation of the devices to the skeleton.[1–7] Most commonly long-term stable calcium-phosphates which exhibit a low biodegradability such as hydroxapatite are used for producing bioactive calcium phosphate coatings.[1–7] Since Chapter 20 is specifically dedicated to calcium phosphate coatings, this topic will only be touched upon shortly in the present chapter.

The current gold standard for bone reconstruction in orthopedics and cranio-maxillofacial repair is the use of autogenous bone grafts.[8–10] Of the more than 1 million fractures that are treated with osteosynthetic materials each year in the USA, approximately 80% of these require adjuvant grafting.[10] Resorption of the alveolar ridge after tooth extraction frequently mandates site development by augmentation before dental implants can be placed.[11–13] Although autogenous bone grafts are currently the standard of care, bone substitute materials are extensively studied in order to avoid harvesting autogenous bone. In fact, there are several disadvantages associated with using autogenous grafts: the additional surgical site, donor site morbidity exceeding that at the treatment site, often insufficient volume of harvested bone, and, in dentistry, the need for general anesthesia to harvest extraoral bone.[14–16] Among alternative graft choices, synthetic bone substitute materials benefit from several advantages over freeze-dried human allografts or bovine deproteinized bone xenografts. They excel in terms of safety profile, as there is no risk of disease transmission or immunological challenges.[17] As a result, there has been increasing demand and an ongoing

search for synthetic, biodegradable bone substitute materials that degrade rapidly, but still stimulate osteogenesis at the same time, thereby resulting in bone repair and regeneration with fully functional bone tissue.[16]

Owing to their ability to stimulate bone formation bioactive calcium phosphate ceramics and bioactive glasses are excellent candidate grafting materials for bone augmentation.[4,18–21] Among the bioactive ceramics most commonly investigated for use in bone regeneration are β-tricalcium phosphate (β-TCP)[18–20,22–26], hydroxyapatite (HA)[4,20,27,28] and bioactive glass.[4,21,29,30] All of these materials are biocompatible[18–20] and osteoconductive.[18–30] However, they differ considerably in the rate of resorption. HA resorbs very slowly compared with β-TCP[20,22–27] and bioactive glass.[4,21,29,30]

Recent improvements in tricalcium phosphate (TCP) ceramics include products with a high phase purity (>99%) and homogeneous solubility characteristics, so as to prevent premature separation of microparticles from the structural compound.[31] In the past, these types of microparticle have been shown to elicit inflammatory tissue reponses.[31] Furthermore, the use of TCP particles with increased porosity has been proposed in order to increase the biodegradability.[31–33] These particles exhibit a material structure with micro-, meso- and macropores, which is designed to enhance the degradation process. This structure allows for a reduced bulk density. The microporosity allows circulation of biological fluids, increases the specific surface area and thus accelerates the degradation process. The interconnectivity of the pores creates a capillary force that actively draws cells and nutrients in the center of the particles. The macroporosity is created to encourage the ingrowth of bone by permitting penetration of cells and vascularization.[31]

Particularly in non-load-bearing applications a biomaterial used as a bone substitute should be a temporary material serving as a scaffold for bone remodeling. The material must degrade in a controlled fashion into non-toxic products that the body can metabolize or excrete via normal physiological mechanisms.[20] Moreover, this substance should be resorbable and should undergo complete remodeling and substitution by newly formed functional bone tissue.[9,16,20,23] Thus, ideally bioactive calcium phosphate ceramics for use in bone augmentation should exhibit good bone bonding behavior by stimulating enhanced bone formation at the interface in combination with a high degradation rate, thereby meeting a balance between rapid bone formation and rapid biodegradation.

In modern dentistry, the use of oral implants has become a common treatment to replace missing or lost teeth.[11] Furthermore, resorption of the alveolar ridge after tooth extraction frequently mandates site development by augmentation before implants can be placed.[11–13] Among the various techniques to reconstruct or enlarge a deficient alveolar ridge, the concept of guided bone regeneration (GBR) has become a predictable and well-

documented surgical approach[8] for localized lateral ridge augmentation. Furthermore, augmentation of the maxillary sinus floor with autogenous bone grafts has become a well-established pre-implantology procedure for alveolar ridge augmentation of the posterior maxilla.[34] Recently, the use of tricalcium phosphate and bioactive glass 45S5 particles as alloplastic bone graft materials for alveolar ridge augmentation and sinus floor elevation procedures has received increasing attention in implant dentistry.[22–26,29,30,32,33,35–37] This is due to an overall effort to develop augmentation procedures that involve reduced surgical effort, thereby increasing patient comfort in addition to decreasing treatment cost, while yielding the same clinical success rates as conventional procedures that utilize autogenous bone grafts. As a result, in recent years an increasing number of clinical studies have been published which provide valuable data regarding the biodegradability as well as the bone regenerative capacity of these materials in a clinical setting (Fig. 6.1), since these data were derived from histological studies of human biopsies.[22–26,29,30,32,33,35–37]

Even with β-TCP, biodegradation has been reported to be incomplete 9.5 months after grafting in the human mandible.[22] Histologic examination of

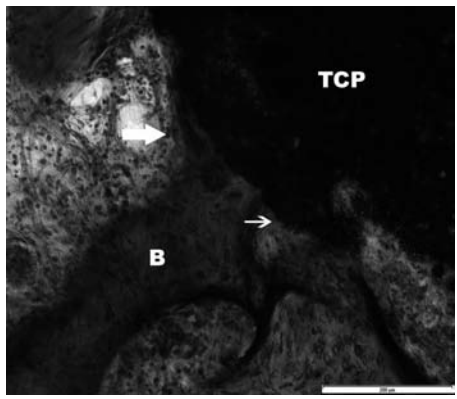

6.1 Resin-embedded human biopsy stained immunohistochemically for osteocalcin after deacrylation. The biopsy was sampled 6 months after augmentation of the sinus floor with with β-tricalcium phosphate (TCP) particles. Intense staining of cells and unmineralized fibrous matrix (of the osteogenic mesenchym) lining the newly formed bony trabeculae (B) that are in contact with the TCP particle (TCP) is present (block arrow). In addition, intensive staining of the yet unmineralized matrix in contact with the TCP particle is visible (arrow). These findings demonstrate the good bone bonding properties of TCP. Furthermore, 6 months after implantation bone formation and matrix mineralization are still actively progressing in the tissue surrounding the TCP particles. Undecalcified sawed section counterstained with hematoxylin. Bar = 200 μm.

these biopsies revealed that 34% of the biopsy consisted of mineralized bone tissue and 29% of remaining β-TCP.[22] Biopsies sampled at 8 months after sinus floor augmentation consisted of 20% mineralized bone and 44% remaining β-TCP.[22] Biopsies sampled at 12 months after sinus floor augmentation in the apical area close to the Schneiderian membrane consisted of 26.7% mineralized bone and 42.4% remaining β-TCP when TCP particles with a standard porosity of 35% were used (Fig. 6.1). When TCP particles with an increased porosity (65%) were used, these biopsies displayed 35.5% mineralized bone and only 24.7% remaining β-TCP.[32,33]

With respect to bioactive glass 45S5 (BG) particles (composition (weight%): 45% SiO_2, 24.5% NaO_2, 24.5% CaO and 6% P_2O_5) of a narrow size range, Tadjoedin *et al*.[30] reported that after grafting in the human sinus floor the transformed BG particles appeared to resorb within 1–2 years. When using mixtures of 80, 90 and 100% BG particles and 20, 10 and 0% autogenous bone, histomorphometric analysis of biopsies harvested at 4, 6 and 15 months showed the grafts to consist of 27% of mineralized bone tissue at 4 months, of 36% of bone at 6 months and of 42% of bone at 15 months. The volume of the biologically transformed BG particles in the biopsies decreased from 29% at 4 months to 15% at 6 months and 8% at 15 months.[30] Given the clinical findings with current bone substitute materials,[22–26,29-33] there continues to be interest in bone substitute materials which degrade more rapidly, but still stimulate osteogenesis at the same time [9,16]

As a result considerable efforts have been undertaken to produce rapidly resorbable bone substitute materials, which exhibit good bone bonding behavior by stimulating enhanced bone formation at the interface in combination with a high degradation rate. This has led to the synthesis of a new series of bioactive, rapidly resorbable glassy crystalline calcium–alkali–orthophosphate materials.[38–44] These are glassy crystalline calcium–alkali–orthophosphates, which exhibit stable crystalline $Ca_2KNa(PO_4)_2$ phases.[38–44] These materials have a higher solubility than TCP and therefore they are designed to exhibit a higher degree of biodegradability than TCP.[38–40] On this basis, they are considered as excellent alloplastic materials for alveolar ridge augmentation.[38–44]

To fill bone defects, calcium phosphates are mainly applied as granules. Bone substitutes with improved surgical handling properties include moldable calcium phosphate cements in paste form that can be either introduced into a bony defect with a spatula or injected with a syringe; they subsequently set *in situ*,[42,45–50] which makes them an intriguing group of materials for bone reconstruction. Over the past decade various bioactive calcium phosphate cements have been developed.[45–50] In most cases hydroxyapatite is formed during setting, which limits their biodegradability.[45,49] More recent developments include cements, which form calcium-deficient hydroxyapatite (CDHA)[42,46,47] or TCP[48] during setting and cements which form calcium–

alkali–phosphates during setting.[50] These cements are designed for higher biodegradability.[50]

As outlined above bioactive calcium phosphate ceramics and glasses are known to stimulate bone tissue formation.[51–53] Over the past decade, efforts have focused on understanding the underlying mechanisms. In these studies, attention was directed towards the atomic and molecular phenomena occurring at the material surface and their effects on the reaction and signaling pathways of cells and tissues. This implied that studies were conducted to elucidate any of the cellular activities leading up to tissue formation, including cell attachment, differentiation and extracellular-matrix formation.[51]

Given the great clinical need, obtaining this understanding is of critical importance, since once these mechanisms are identified and studied, it should be possible to alter biomaterial molecular components and surface characteristics in ways that promote optimal cell adhesion, proliferation and differentiation, leading to more expeditious and enhanced bone formation in combination with a desirable biodegradability, and thus to create bioactive ceramics which are optimally tailored towards their clinical application.

6.2 Mechanisms of bioactivity

6.2.1 Surface transformation and protein adsorption events of bioactive ceramics

The nature of the biomaterial and its surface characteristics play important roles in determining bone adaptation to the implant material. Surface reactivity is one of the common characteristics of bone bioactive ceramics. It contributes to their bone bonding ability and their enhancing effect on bone tissue formation. During implantation, reactions occur at the material–tissue interface that lead to time-dependent changes in the surface characteristics of the implant material and the tissues at the interface.[51] With bioactive ceramics, solution-mediated surface reactions take place after immersion in biological fluids. These reactions include dissolution, reprecipitation and ion-exchange phenomena in combination with protein adsorption events occurring at the bioactive ceramic surface (Fig. 6.2).[51,55–62] A key element of bone bioactive behavior is the development of a carbonated apatite surface after immersion in biological fluids.[51,55,59,60] In previous review papers we summarized these events that were reported to occur at the bioactive ceramic–tissue interface.[51,54] The following list does not imply a ranking in terms of time sequence or importance: (1) dissolution from the ceramic;[54,55,57,59,60,63–65] (2) precipitation from solution onto the ceramic;[54,55,57,59,60,63,64,66] (3) ion exchange and structural rearrangement at the ceramic–tissue interface;[54,55,57,59,60,63] (4) interdiffusion from the surface

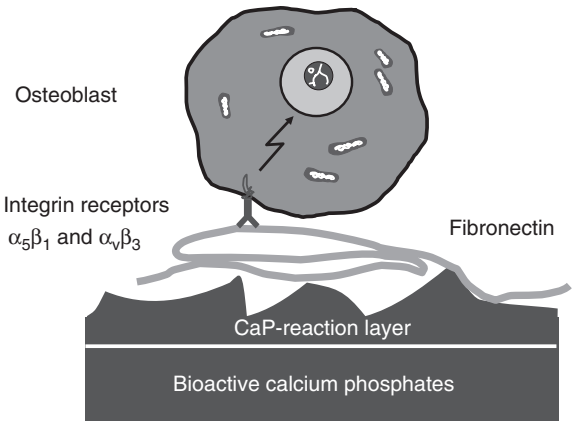

6.2 Schematic diagram illustrating the events that take place at the interface between the bioactive ceramics and the surrounding biological milieu and thereby establish bioactive behavior. Contact with biological fluids leads to dissolution and reprecipitation phenomena and results in the formation of a calcium phosphate surface reaction layer and serum protein adsorption. The nature of this surface reaction layer, which in its turn influences the structure of the adsorbed protein modulates the structure of the adsorbed serum protein. Thereby specific adhesive motifs within the molecule are exposed to osteoblasts and osteoprogenitor cells that are migrating to the implant surface, which then has an effect on subsequent cell adhesion via integrin receptors and activation of intracellular signaling pathways. Activation of these intracellular signaling mechanisms modulates cellular differentiation, bone matrix formation and mineralization, resulting in bone bonding and a stimulatory effect on bone tissue formation.

boundary layer into the ceramic;[67] (5) solution-mediated effects on cellular activity;[68,69] (6) deposition of either the mineral phase (a), or the organic phase (b), without integration into the ceramic surface;[64,70–73] (7) deposition with integration into the ceramic;[64,71] (8) chemotaxis to the ceramic surface;[74] (9) cell attachment and proliferation;[68,73,75] (10) cell differentiation;[74] and (11) extracellular matrix formation.[72,73,75]

The observation of what transpires at the interface, however, does not represent a mechanistic explanation for the effect that bioceramics have on bone tissue formation. We can focus on mechanisms by relying on an increasing body of evidence that suggests that bone bonding and bone tissue ingrowth enhancement are the result of multiple, parallel and sequential reactions at the material–tissue interface. These interactions are related either to physicochemical phenomena that occur in the presence or absence of cells, or to reactions affected by cellular activity. An important aspect of the overall reaction sequence between these materials and tissues is that,

in the absence of a biologically equivalent, calcium-deficient, carbonate-containing hydroxyapatite (c-Ap) surface upon implantation, dissolution, precipitation and ion exchange reactions lead to a biologically equivalent apatitic surface on the implanted material (Fig. 6.2). This reaction does not proceed by itself, but is accompanied by parallel reactions, such as adsorption and incorporation of biological molecules and attachment of surrounding cells. Furthermore, cells that have adhered to the ever-reacting material surface interact with the material and produce some of the surface changes. In the inverse direction, i.e. from material to environment, there is both a solution-mediated as well as surface-controlled effect on cellular activity, organic matrix deposition and mineralization. The gradual change of the ceramic surface to become a biologically equivalent HA with small crystal dimensions is a rate-determining step in the cascade of events underlying bioactive behavior. All phenomena, collectively, lead to the gradual incorporation of the bioactive implant into developing bone tissue. Moreover, for mechanisms to be uniquely identified, it is important to establish the extent of each of these reactions and the sequence in which they occur.

Formation of a biologically equivalent apatitic surface, a common characteristic of bioactive materials, can be reproduced *in vitro* by immersion experiments using a simulated physiologic solution that mimics the typical ion concentrations in body fluids. These *in vitro* physicochemical analyses are useful to explain the observations on *ex vivo* specimens.[65,76] Such experiments have shown that the materials with high solubility also readily induce the precipitation of a biologically equivalent apatite on their surface. Using this *in vitro* immersion methodology, considerable evidence has been obtained that reveals the mechanisms of surface reactions.[59,60,64,76] The reactions include dissolution, precipitation and ion exchange accompanied by absorption and incorporation of biological molecules.[61,62,66,68,77] Furthermore it has been demonstrated that this surface reaction layer does not form as a result of inorganic reactions first, followed by biologically driven events next, but that serum proteins do have a major effect on the properties of the surface reaction layer.

To explore the effect of proteins on the formation of surface reaction layers on bioactive glass, we analyzed the atomic and molecular changes in bioactive glass 45S5 surface during immersion in protein-free buffer solution and protein-containing culture medium using various complementary techniques including atomic force microscopy (AFM), Rutherford backscattering spectroscopy (RBS) and Fourier transform infrared spectroscopy (FTIR).[62] When immersed in serum-free solutions, AFM showed that the surface of bioactive glass reacted non-uniformly. After 5 min immersion, the glass surface showed a rough texture due to the formation of particles on the surface. With increasing immersion time, the particles increased in size and number. Unlike the reaction on the substrates immersed in serum-free

solution, a uniform layer of globules, presumably proteins, covered the substrates immersed in serum-containing solutions. As the immersion time increased, the density of globules increased and the layer thickened. RBS of the outermost surface layers revealed that substrates formed Si-rich surface layers in the first hour of immersion in the absence or presence of serum proteins. In addition, the RBS spectra showed that the formation of the calcium phosphate layer was different in serum-containing solutions relative to the serum-free solutions. FTIR analysis revealed that, in the serum-free solution, crystalline hydroxyapatite was formed by transformation from the initially formed amorphous calcium phosphate. In contrast, immersion in serum-containing solutions only produced an amorphous calcium phosphate.

Given the repeated observation of the absence of crystalline hydroxyapatite when proteins co-adsorb, it is unlikely that, *in vivo*, adsorption of biological molecules will take place subsequent to the transformation of an amorphous calcium phosphate-rich layer to carbonated apatite, as was previously suggested.[78] The present data suggest that serum proteins adsorb in tandem with the occurrence of solution-mediated reactions leading to formation of a silica-gel. Amorphous calcium phosphate phases accumulate in this Si-rich matrix.

In solutions more closely approaching the physiological state, the maturation of amorphous calcium phosphate to crystalline hydroxyapatite does not take place readily. The proteinaceous layer which adsorbs onto the glass interferes with the solid to liquid interaction of the amorphous calcium phosphate layer. Whereas amorphous calcium phosphate can form exclusively as the result of physicochemical phenomena in the solid glass phase, it is suggested here that adsorbed serum proteins impede the nucleation and growth reactions by which it would transform to carbonated apatite. The physicochemical reactions in the glass are not blocked however, as Ca and P diffusion leads to a continuously thickening of the Ca–P-rich zone under the adsorbed protein layer. In this context, it an important aspect that the surface composition and structure of the surface reaction layer in their turn influence serum protein adsorption. There is support for the view that the enhanced cellular and tissue responses to bioactive ceramics are related to enhanced fibronectin adsorption at their surfaces.[61,77] Also it is noteworthy that surface chemistry of the biomaterial surface, i.e. the surface reaction layer in the case of bioactive ceramics, modulates the structure and activity of adsorbed fibronectin (Fig. 6.2).[79] Hence, the adsorption of the protein layer is also critical in terms of providing attachment sites for bone cells such as osteoblasts and their progenitors (Fig. 6.2). The cell adhesion and intracellular signalling events are the subject of Section 6.2.3.

In addition, the solution-mediated effects require adequate consideration. This involves first analyzing the release of soluble ions from these

bioactive substrata and second investigating their effect on the cellular response,[51,68,80–83] which will be dealt with in more detail in the next section.

6.2.2 The effect of bioactive ceramics on the expression of the osteoblastic phenotype *in vitro*

Calcium phosphate ceramics[5–7,20,25,26,31–33] and glass ceramics[21,28–30] are known to bond to bone. Differences among these materials are reflected in the rate of bone formation on their surfaces.[25,26,31–35] Bioactive calcium phosphate ceramics stimulate bone formation.[7,28,31,33,34] This requires the ability to differentiate osteoprogenitor cells into osteoblasts at their surfaces. Therefore, in order to evaluate the stimulatory potential of bioactive ceramics on osteogenesis it is logical to examine the effect of these materials on osteoblastic differentiation. Thus, over the last decade various assays have been developed and used, which permit studying the effect of bioceramics on the expression of osteogenic markers *in vitro*.[7,42,43,51,68,69,73,84,85]

Osteoblast differentiation is defined by three principal biological periods: cellular proliferation, cellular maturation and matrix mineralization.[86–88] Differentiating osteoblasts are known to synthesize type I collagen, alkaline phosphatase (ALP), and other non-collagenous extracellular bone matrix proteins such as osteonectin, osteocalcin, osteopontin and bone sialoprotein.[86–89] These bone-matrix proteins have proven to be particularly useful osteogenic markers to characterize the different stages of osteoblast differentiation.[86] Type I collagen is expressed during the initial period of proliferation and extracellular-matrix synthesis, whereas ALP is expressed during the post-proliferative period of extracellular-matrix maturation, and the expression of osteopontin, osteonectin, osteocalcin and bone sialoprotein occurs later during the third period of extracellular-matrix mineralization.[86–89] Osteopontin peaks twice during proliferation and then later but prior to BSP and osteocalcin.[86,89] Osteonectin is found in preosteoblasts, osteoblasts, osteocytes and newly formed osteoid in matrix.[90] This protein has the ability to bind to collagen and promote hydroxyapatite formation *in vitro*.[90] Bone sialoprotein is characterized by its ability to mediate initial formation of hydoxyapatite crystals[91] and is transiently expressed very early[86,88,91] and then upregulated again in differentiated osteoblasts actively involved in mineralization.[86,88,91] Consequently, since there is no specific single marker for osteoblasts, the cellular expression of a range of non-collagenous and collagenous proteins as well as alkaline phosphatase has to be assayed, when examining cellular differentiation.

When studying the effect of bioactive ceramics for bone regeneration on cellular behavior it is important to examine cell proliferation and differentiation, first because these materials should posses the ability to

differentiate osteoprogenitor cells into osteoblasts and second because proliferation and differentiation of osteoblasts are affected by the chemistry of substrata.[92,93] As a result, numerous authors studied the response of osteoblasts or bone marrow stromal cells to various bioactive ceramics in terms of messenger RNA and translated proteins that form an array of osteogenic parameters as a measure of phenotypic differentiation. It has been reported that various bioactive calcium phosphates significantly affected cellular growth and the temporally dependent expression of an array of bone-related genes and proteins. Moreover, various investigators were able to show that bioactive glasses and glass ceramics,[51,68,69,73,80,83–85,94,95] hydroxyapatite,[7,96] various calcium phosphates[7,95] and calcium–alkali–orthophosphate ceramics[42,43,95,97] stimulated osteoblast differentiation *in vitro*.

El-Ghannam *et al.* studied the cellular response to bioactive glass (BG) 45S5 disks that were preconditioned by a two-step procedure which resulted in the transformation of the BG surface to a crystalline, carbonated calcium phosphate apatite onto which serum proteins were adsorbed in a second step.[68,84] The authors demonstrated greater differentiation for osteoblasts, which were cultured on the preconditioned BG45S5 compared with when identical cells were grown on the native glass[84] or hydroxyapatite surfaces.[68] These findings were corroborated by a more recent study,[85] in which enhanced alkaline phosphatase activity of rat bone marrow stromal cells was demonstrated when these cells were cultured on preconditioned BG 45S5 disks compared with when identical cells were grown on tissue culture plastic controls.

In recent years, several studies were performed which examined the effect of rapidly resorbable calcium–alkali–orthophosphate bone substitute materials on the expression of osteogenic markers characteristic of the osteoblastic phenotype and compared this behavior with that of the currently clinically used materials β-tricalcium phosphate (TCP) and bioactive glass 45S5. These studies showed that several calcium–alkali–orthophosphate materials supported osteoblast differentiation to a greater extent than TCP.[42,43,95,96] More recently, it was demonstrated that the glassy-crystaline calium–alkali–orthophosphate material GB9, which contains the crystalline phase $Ca_2KNa(PO_4)_2$ and a small armorphous portion containing silica phosphate, had a significantly greater stimulatory effect on osteoblastic proliferation and differentiation when compared with β-TCP,[42,43] preconditioned bioactive glass 45S5[43] and other calcium–alkali–orthophosphate materials of varying composition.[42,43] Figure 6.3 shows that osteoblastic cells grown for 14 days on GB9 expressed significantly higher levels of the osteogenic markers type I collagen, alkaline phosphatase, osteopontin, ostoenectin and bone sialoprotein compared with when identical cells were grown on β-TCP and BG45S5. Furthermore, BG45S6 induced significantly greater expression of the majority of these osteogenic markers when compared to

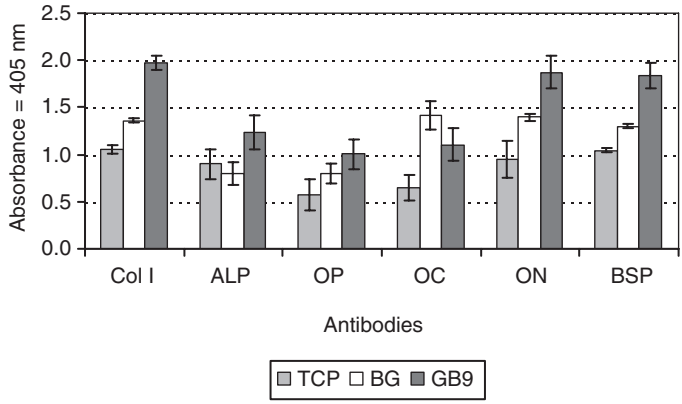

6.3 The temporal expression of osteogenic proteins by osteoblasts cultured on different calcium phosphate materials for 14 days. Intracellular protein expression by human osteoblasts is at 14 days of culture on tricalcium phosphate (TCP), bioactive glass 45S5 (BG) and GB9. Results are normalized to the internal control β-actin protein for each substratum. All values are mean ± standard deviation of eight measurements. Col I, Type I collagen; ALP, alkaline phosphatase; OP, osteopontin; OC, osteocalcin; ON, osteonectin; and BSP, bone sialoprotein.

β-TCP. Figure 6.4 shows the expression profile of bone sialoprotein by human osteoblasts, which were cultured over 21 days on TCP, BG and GB9. Bone sialoprotein is an osteogenic marker, which is characteristic of the later stages of osteoblast differentiation, i.e. of the terminally differentiated osteoblast, which is actively involved in extracellular matrix mineralization. At 3 and 14 days, cells cultured on GB9 expressed significantly higher levels of BSP than cells grown on BG45S5. In addition, at 7, 14 and 21 days, BSP expression was greater for cells grown on GB9 and BG45S5 compared with cells cultured on TCP (Fig. 6.3).

In this context, it also is of considerable interest to explore the effect of soluble ions released from these bioactive substrata on the cellular response.[68,69] Several investigators used experimental set-ups and *in vitro* models, which allowed for dissociating between solution-mediated and surface-mediated effects on the cellular response. This is in contrast to the *in vivo* setting, in which it is not possible to dissociate these two effects. Thus, when addressing this issue, utilizing adequate *in vitro* models offers a significant advantage over *in vivo* experiments.[51,68,69,81,82] Xynos *et al.*[83] reported that bioactive glass 45S5 stimulated osteoblast proliferation and differentiation when culturing primary human osteoblasts on the bioactive-glass ceramic substrate. Previously, Ducheyne and coworkers.[51,80] and El-Ghannam *et al.*[68] had shown this effect with a rodent cell line and shown it

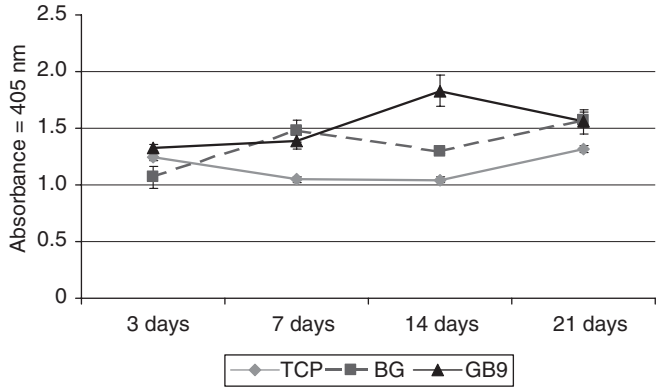

6.4 The expression of bone sialoproteins by osteoblasts cultured on different bioceramics for 3 weeks depicted as a function of time. Results are normalized to the internal control β-actin protein for each time point and each substratum. All values are mean ± standard deviation of eight measurements. TCP, tricalcium phosphate; BG bioactive glass.

to be associated with cell membrane receptor activation. In order to determine whether this stimulation of osteogenesis by bioactive glasses occurs through direct contact between substrate and cells or through ions released during their biodegradation, Xynos *et al*. studied the relationship between this stimulation and ionic products of bioactive glass dissolution.[81,82] They observed that these ionic products increased osteoblast proliferation.[81] They suggested that this effect was mediated by insulin-like growth factor II whose expression was upregulated.[81] Furthermore, they demonstrated enhanced gene expression of various growth factors and extracellular matrix regulators including cell surface receptors, signal transduction factors and transcription factors.[82]

Radin *et al.*[85] conducted a study, in which rat bone marrow stromal cells were cultured in the presence of but not in contact with BG45S5 disks (Fig. 6.5). These cells showed enhanced osteoblast differentiation compared with cells that were cultured in the presence of tissue culture plastic controls (Fig. 6.5), However, even greater osteoblast differentiation was noted when cells were cultured in physical contact with the BG45S5 disks. They also examined the release of BG dissolution products into the cell culture medium and concluded that both surface- and solution-mediated effects play a role in the osteogenic effect of BG. These data emphasize the synergistic nature of the solution-mediated and the surface-mediated effects of bioactive glass (BG) 45S5 on osteoblast function. Yao *et al*.[69] took these experiments a step further and showed that cells which were cultured on porous BG45S5 substrata released signaling factors into the cell culture

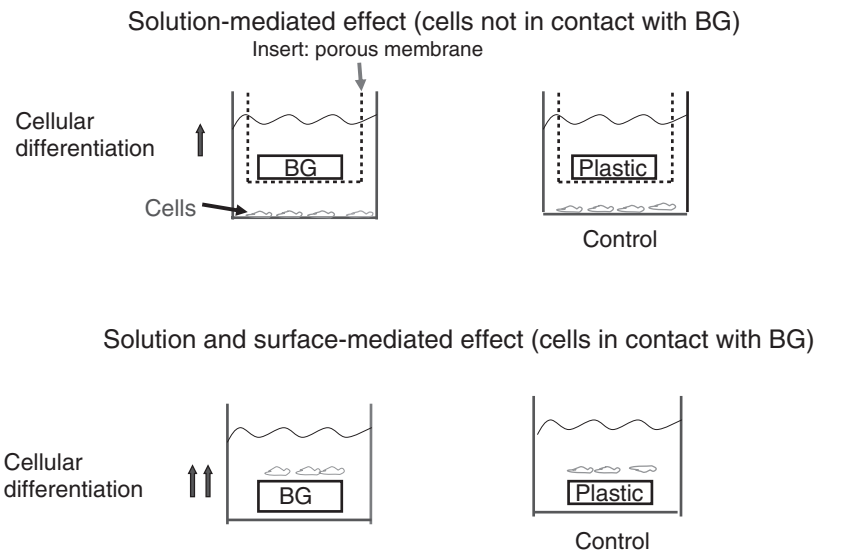

6.5 Schematic diagram demonstrating the experimental set-up of cell culture studies elucidating solution-mediated versus surface-mediated effects of bioactive glass (BG) 45S5 on osteoblast function: rat bone marrow stromal cells which are cultured in the presence but not in contact with BG45S5 disks showed enhanced osteoblast differentiation compared with cells that were cultured in the presence of tissue culture plastic controls. However, even greater osteoblast differentiation was noted when cells were cultured in physical contact with the BG45S5 disks. Hence, both surface- and solution-mediated effects play a role in the osteogenic effect of BG.

medium which caused enhanced cellular differentiation of osteoblasts, which were cultured in the presence of these cell seeded scaffolds but physically separated at the bottom of the cell culture dish. This enhancement of cellular differentiation was greater than that found when cells were solely cultured in the presence of the BG45S5 scaffold.[69]

6.2.3 Intracellular signaling events regulating the stimulatory effect of bioactive ceramics on cell function

To decipher the complexity of the reactions at the bioactive ceramic–bone interface, it is logical first to analyze the surface transformation and protein adsorption events and then to study the osteoblast responses to these bioactive surfaces (Fig. 6.2). Although numerous studies have investigated cellular responses to bioactive ceramics, little is known about the intracellular events that take place in osteoblasts at these bioceramic surfaces. As

outlined above, numerous authors were able to show that bioactive glasses and glass ceramics, hydroxyapatite, various calcium phosphates and calcium–alkali–orthophosphate ceramics were able to stimulate osteoblast differentiation *in vitro*.[7,51,68,69,73,80,83–85,94–98] However, the intracellular signaling events that follow osteoblast attachment to these bioactive ceramics, leading to differences in osteoblast activity, are not known. Because cell signaling affects cell proliferation and differentiation, it is important to understand the cell signaling pathways induced by osteoblast–implant material interactions.[99]

The cellular interactions between osteoblasts and the biomaterial surface are thought to be mediated primarily by membrane-associated adhesion receptors belonging to the integrin superfamily.[99–102] Integrins are transmembrane heterodimers composed of an α- and a β-subunit and are connected to the cytoskeleton.[103,104] Bone cells express the following integrin receptors $\alpha_1\beta_1$, $\alpha_2\beta_1$, $\alpha_3\beta_1$, $\alpha_5\beta_1$, $\alpha_v\beta_3$ and $\alpha_v\beta_5$.[105–107] The interaction of osteoblasts with implant surfaces is mediated largely by the β1 subfamily.[99–101] It is also noteworthy that surface chemistry of the biomaterial surface modulates the structure and activity of adsorbed fibronectin.[79,108] Integrins $\alpha_5\beta_1$ and $\alpha_v\beta_3$ bind to and compete for the central cell binding domain of the fibronectin molecule.[109] The differences in fibronectin conformation alter integrin binding and thus can result in selective binding of the $\alpha_5\beta_1$ integrin or $\alpha_v\beta_3$ integrin or binding of both $\alpha_5\beta_1$ and $\alpha_v\beta_3$ integrin.[79] Recent findings suggest that selective binding of the $\alpha_5\beta_1$ integrin leads to upregulation of osteoblastic differentiation and matrix mineralization.[110] In addition to their role as adhesion receptors, integrins are also involved in transducing signals from the extracellular matrix to the interior of the cell.[111,112] resulting in the activation of signaling molecules and regulation of gene expression, thus modulating cellular migration, proliferation, differentiation and apoptosis (Figs 6.2 and 6.6).[104,112–114]

Interaction between osteoblasts and bone matrix components via integrins leads to a rearrangement of cytoskeletal components and activation of specific signaling proteins localized at focal adhesions and focal adhesion kinase (FAK) (Fig. 6.6).[99] Activation of FAK is considered to play a critical role in control of adhesion-dependent cell survival and proliferation.[114,115] Recent studies have demonstrated that osteoblast adhesion to titanium alloy and fibronectin resulted in activation of FAK and mitogen-activated protein (MAP) kinase signal transduction pathways.[99] FAK associates with several signaling proteins, e.g. the src-family of protein-tyrosine kinases: Src-homology collagen (Shc) and growth factor receptor-bound protein 2 (Grb2) (Fig. 6.6). One downstream signaling protein in the integrin-generated signaling pathway is the adaptor protein Shc. Mitogen-activated protein kinase (MAPK) p44 (extracellular signal-regulated kinase 1 – Erk1) and p42 MAPK (extracellular signal-regulated kinase 2 – Erk2) are impor-

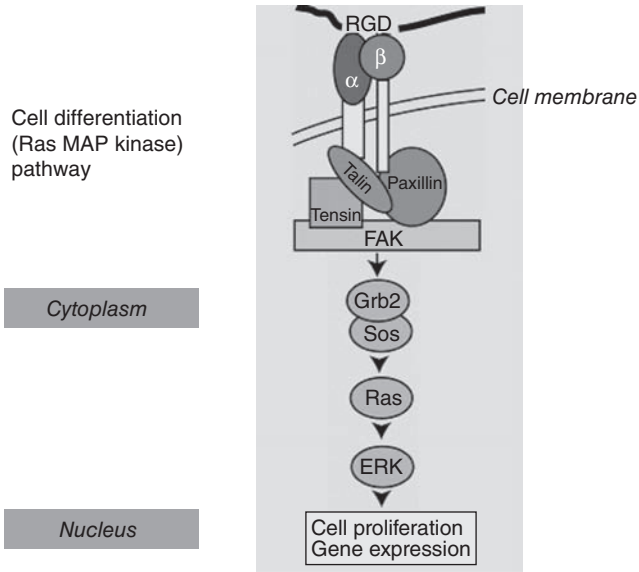

6.6 Integrin signaling pathway. Binding of the integrin receptor activates focal adhesion kinase (FAK) along with other focal adhesion proteins. FAK activates the cell differentiation (ERK or Ras/MAPkinase) pathway in addition to cell survival pathways.

tant mediators of cellular responses to intracellular signaling proteins. FAK interaction with Shc creates a Grb2-binding site thus linking FAK to the Ras/MAPK (mitogen-activated protein kinase) pathway (Fig. 6.6).[116] The Shc-Grb2 complex induces Ras activation via Grb2-associated son of sevenless (SOS), a cytoplasmic GTP (guanosine triphosphate) exchange protein.[117] Ras then stimulates the Erk1/Erk2 MAP kinase cascade, which plays an important role in cellular differentiation and growth (Fig. 6.6). Activated MAP kinases (Erk1/2) translocate to the nucleus and are able to phosphorylate and activate transcription factors including c-fos and c-jun, members of the activator protein-1 (AP-1) transcription factor complex, which control gene expression (Fig. 6.6).[99,102] The AP-1 complex initiates early transcription events, which lead to cell proliferation and/or can affect differentiation. Furthermore, AP-1 has an important role in osteoblast differentiation and bone development. AP-1 sites are known to be present in the promoters of many bone-specific genes such as type I collagen, alkaline phosphatase, osteocalcin and osteopontin.[99,102] In addition, possible interaction with the p38 pathway is of interest.[118,119] Ivaska and coworkers[120] reported a novel signaling mechanism in human osteosarcoma cells (SaOS-2) mediated by $\alpha_2\beta_1$ integrin involving isoform-specific activation of the p38 signaling protein. Recent data suggest a possible interaction between the Ras/MAPK pathway and the p38 pathway.[119]

Furthermore, the effect on apoptosis is of importance. Activation of the PI3K/Akt (phosphatidylinositol-3-kinase/protein kinase B) survival pathway results in depression of apoptosis.[121] Consequently, activation of this pathway would be expected by bioactive ceramics, which stimulate osteogenesis.

The effect of bioactive bone substitute materials on these signaling pathways controlling osteoblast function and differentiation is at present not well understood. Elucidation of these reactions has been hampered by the inadequacy of the experimental techniques that could be used. Excellent techniques to study integrin-mediated adhesion and the intracellular pathways that are triggered, were established only recently.[99–100,118,121–125] In addition, advanced surface analytical methods have been combined with molecular biological techniques only over the past decade. Doing so, however, greatly helped in achieving a better understanding of the surface transformations of bioactive, resorbable ceramics and the protein adsorption events associated with immersion in biological fluids.[51,55–58,61,62] Current research efforts combine these two powerful analytical methodologies (advanced surface analytical methods and molecular biological assays). The understanding resulting from combining these methods to examine integrin-mediated cell adhesion and intracellular signaling mechanisms with methods to analyze protein adsorption events and surface and solution-mediated reactions has greatly advanced our ability to unravel the complex reactions at the bioactive ceramic–bone interface.

6.2.4 Correlation of *in vitro* and *in vivo* events: the effect of bioactive ceramics on the osteoblastic phenotype *in vivo*

Correlating *in vitro* data with *in vivo* phenomena adds to our understanding of the bone–bioactive ceramic interface considering the hypothesis that enhanced osteoblastic cell differentiation *in vitro* leads to more and more expeditious and more copious bone formation at the bone–biomaterial interface *in vivo*. In order to test this hypothesis, correlation of the *in vitro* and *in vivo* data is, of course, needed. This includes (1) correlating quantitative expression of the osteogenic markers *in vitro* with the amount of bone formed after bioceramics implantation and (2) quantifying the expression of these markers in histological sections obtained from *in vivo* experiments in comparison with the expression of the various markers *in vitro*.

To this end, a study was performed in which the effect of the same selection of bioactive ceramics on the expression of osteogenic markers was studied *in vitro* as well as *in vivo*.[44] This required the development of an adequate hard tissue histology technique.[126] Histological evaluation of the

bone–biomaterial interface requires undecalcified polymethylmethacrylate (PMMA) sections.[127,128] While various assays have been developed which permit studying the effect of biomaterials on the expression of osteogenic markers *in vitro*,[42,43,68,69,84] there have been considerable difficulties in visualizing the expression of these markers in undecalcified implant material containing sections of bone obtained from *in vivo* studies. Methylmethacrylate (MMA), the resin of choice for undecalcified bone histology, can only be used for bone enzyme and immunohistochemistry, if the exothermic polymerization procedure is avoided. In fact, enzyme activity and tissue antigenicity are both destroyed by the thermal energy. Paraffin, the standard embedding medium for bone enzyme and immunohistochemistry, can be used only for demineralized tissue, which, of course, cannot be applied to specimens which contain ceramic or metal implant materials. Only recently have low-temperature embedding resins with improved tissue antigenicity preservation and respective embedding techniques become available that permit bone enzyme and immunohistochemical analysis on resin-embedded hard tissue sections.[126,129,130] In addition a new technique that facilitates immunohistochemical analysis of osteogenic markers on undecalcified sawed sections of bone which contain ceramic implant materials was developed.[32,33,126] This rendered it possible to study the effect of ceramic bone substitute materials on osteoblast differentiation and tissue maturation on *ex vivo* specimens by visualizing active osteoblasts in their different stages of differentiation at the bone–biomaterials interface. This was in addition to visualizing the expression of various osteogenic markers in the mineralized and unmineralized extracellular matrix components.[32,33,126]

Utilizing this novel hard tissue technology rendered it possible to study the effect of identical bioactive ceramics on the expression of osteogenic markers *in vitro* and *in vivo* and to test the above-stated hypothesis.[44] In this study calcium–alkali–orthophosphate ceramic bone substitute materials were implanted in the sheep mandible and compared with currently clinically used synthetic bone substitute materials (β-TCP, Bioactive glass 45S5). These materials were selected because previous *in vitro* studies demonstrated that they stimulated greater differentiation of osteoblasts compared to cells grown on tricalcium phosphate ceramic.[42,95] The various calcium phosphate materials (particle size 300–355 μm) were implanted in the sheep mandible for 1, 4, 12 and 24 weeks to regenerate critical size membrane-protected defects as described by von Arx *et al.*[9] Autogenous bone chips and empty hole defects, which were filled with collagen sponges, served as controls.[44] This study included examining the above-mentioned calcium–alkali–orthophosphate material GB9 (Section 6.2.2.). As outlined above, *in vitro* GB9 displayed a significantly greater stimulatory effect on osteoblast proliferation and differentiation compared to TCP, BG45S5 and other calcium alkali orthophosphates.[43] These findings correlated with

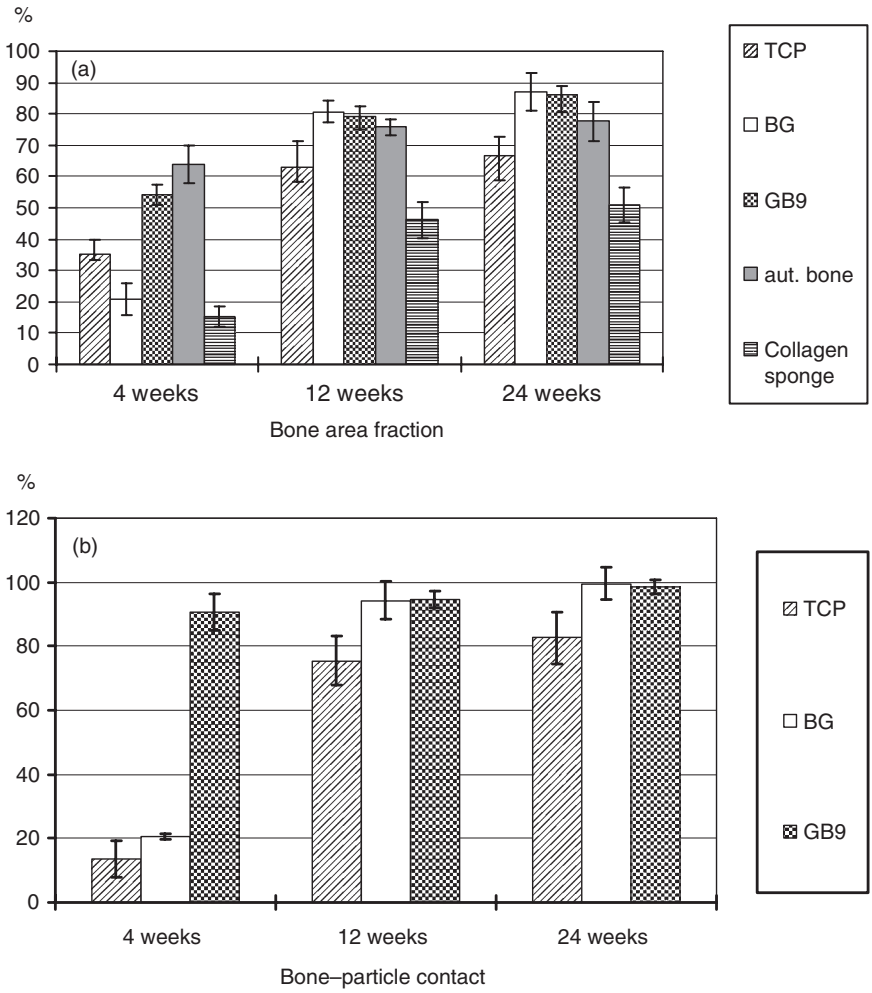

6.7 Histomorphometric results of mandibular defects augmented with various calcium phosphates after 1, 4, 12 and 24 weeks of implantation: (a) bone area fraction in the augmented defect area; (b) bone-particle contact after 1, 4, 12 and 24 weeks of implantation; (c) particle area fraction; and (d) particle size. All values are mean ± standard deviation of five measurements. TCP, tricalcium phosphate; BG, bioactive glass; aut. bone, autogenous bone chips; collagen, empty hole defects filled with a collagen sponge.

enhanced bone formation and bone–particle contact (i.e. bone bonding behavior) *in vivo* (Figs 6.7a,b and 6.8), which was accompanied by enhanced expression of type I collagen (Fig. 6.8), osteopontin, osteocalcin (Fig. 6.9), osteonectin and bone sialoprotein *in vivo*.[44] This was associated with a sig-

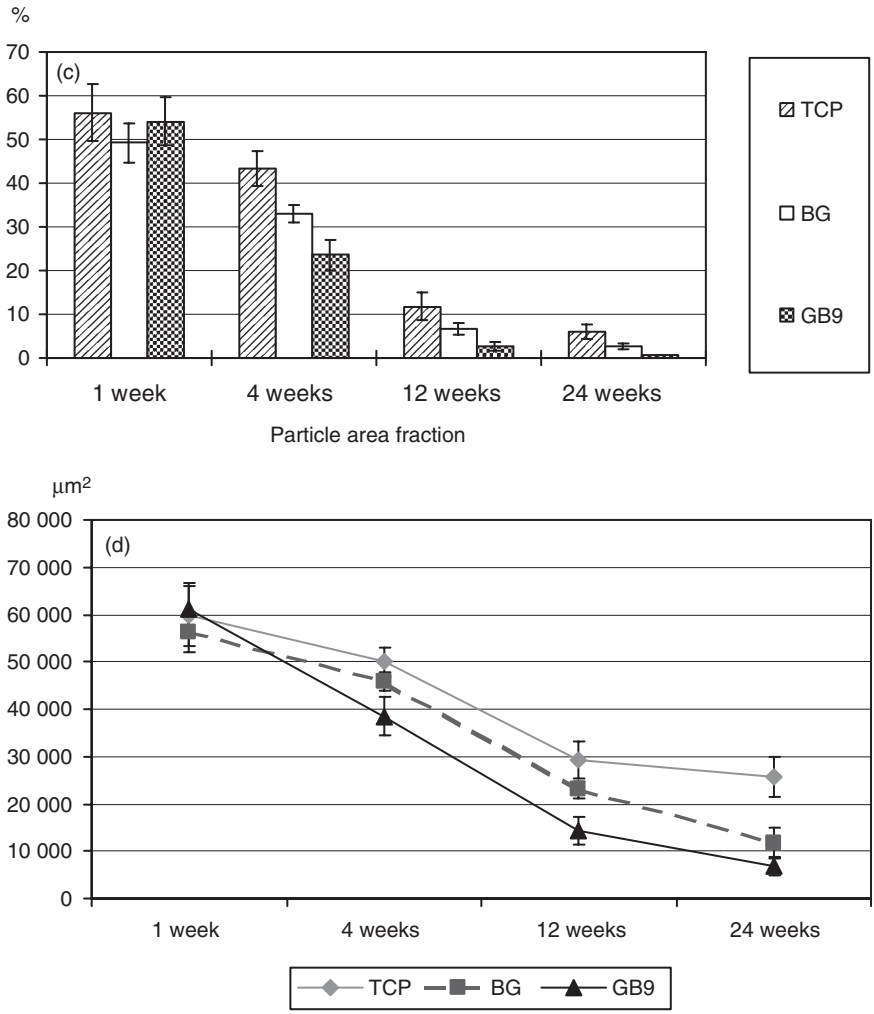

6.7 Continued

nificantly greater decrease in particle area fraction and particle size over time, i.e. a significantly greater biodegradation (Fig. 6.7c,d).[44]

Furthermore, it is noteworthy that with GB9 already after 4 weeks a significantly greater bone–particle contact was noted compared with all other calcium phosphates (Figs 6.7b and 6.8). By 12 weeks, defects, which were augmented using GB9, displayed greater bone formation than defects, which were augmented with autogenous bone chips.[44] These findings are clinically very significant, since autogenous bone is considered to be the gold standard.

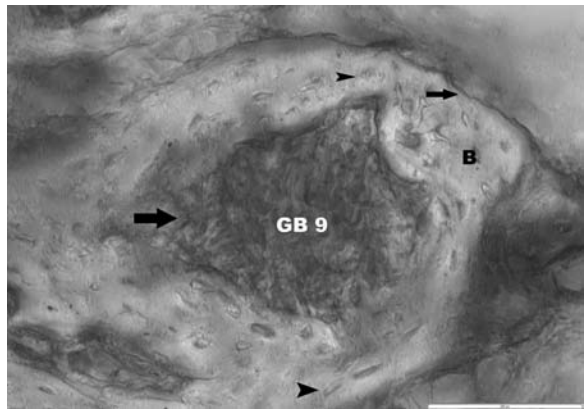

6.8 Histomicrograph of GB9 particle 4 weeks after implantation in the sheep mandible. Immunodetection of type I collagen in deacrylated sawed section of mandibular defect. After 4 weeks, the particle (GB9) is already almost fully covered by newly formed bone tissue. Immunodetection of type I collagen in deacrylated section of mandibular defect 4 weeks after augmentation with GB9. Strong staining of the newly formed bone matrix (B) in contact with the particle is present (block arrow). In addition moderate cellular staining of osteocytes is visible (arrow heads). Furthermore, strong staining of the osteoid and bone matrix lining the periphery of the newly formed bone is evident (small arrow). This is indicative that bone formation and matrix mineralization are actively progressing both at the surface of the degrading particle as well as in the periphery of the newly formed bone. These findings demonstrate the excellent bone bonding and bone regenerative capacities of the calcium–alkali–orthophosphate material GB9, which is capable of stimulating bone formation at its surface as early as 4 weeks after implantation. Undecalcified sawed section counterstained with hematoxylin. Bar = 200 μm.

BG45S5 displayed good bone regenerative capacities and bone bonding behavior (Figs 6.7a,b, 6.10 and 6.11), but the biodegradability was lower than GB9 (Fig. 6.7c,d).[44]

Correlating *in vivo* results with the data from the *in vitro* studies which elucidate the mechanisms by which bioactive ceramics materials induce enhanced osteoblastic differentiation is of great value, since taken together these studies facilitate characterizing the tissue response at the bone–biomaterial interface *in vitro* and *in vivo* at a molecular level and, thus, can contribute significantly to obtaining a fundamental understanding of the processes involved in tissue integration of bioactive implant materials.

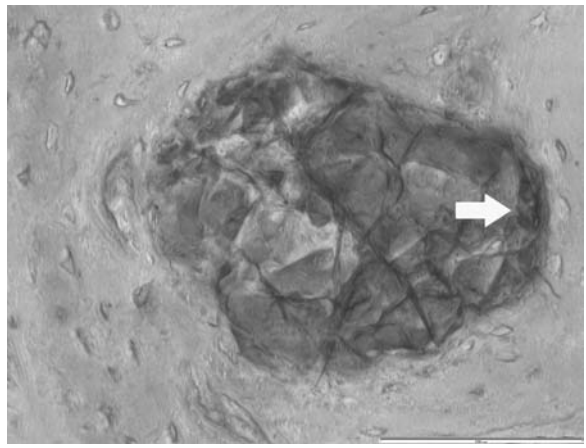

6.9 Immunodetection of osteocalcin in deacrylated section of mandibular defect 12 weeks after augmentation with GB9. Histomicrograph of residual GB9 particle and surrounding bone tissue. Areas with strong osteocalcin staining of cells and mineralized bone matrix in contact with the particle are present (arrow). This is indicative that after 12 weeks' bone formation and matrix mineralization are still actively progressing at the surface of the degrading particle. Undecalcified sawed section counterstained with hematoxylin. Bar = 100 μm.

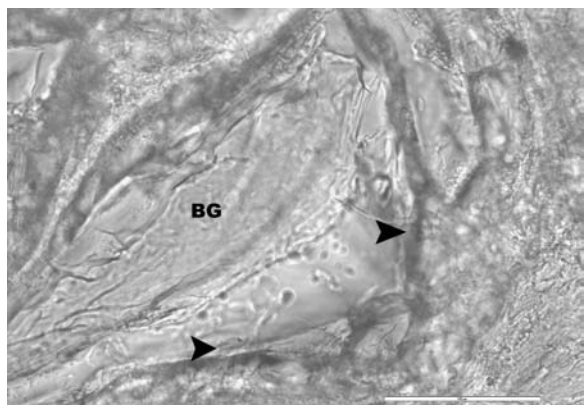

6.10 Immunodetection of alkaline phosphatase in deacrylated section of mandibular defect 1 week after augmentation with Bioglass (BG) 45S5. Histomicrograph of Bioglass 45S5 particle and surrounding tissue. Strong staining of cells and the yet unmineralized matrix in contact with the particle is visible (arrowheads). This is indicative that already after 1 week of implantation BG stimulates bone formation at its surface. These findings underscore the excellent bioactivity and the stimulatory effect of BG 45S5 on bone tissue formation. Undecalcified sawed section counterstained with hematoxylin. Bar = 100 μm.

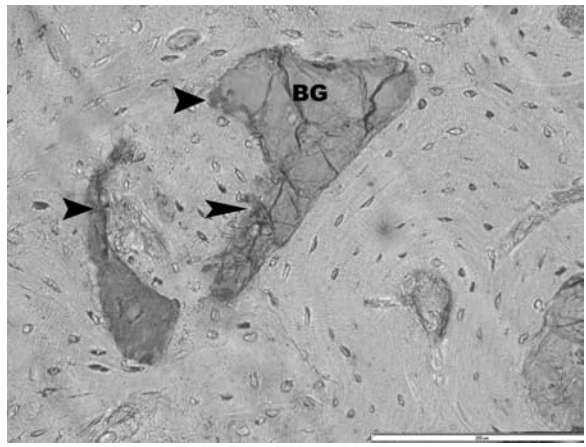

6.11 Immunodetection of bone sialoprotein in deacrylated section of mandibular defect 24 weeks after augmentation with Bioglass 45S5. Histomicrograph of residual excavated Bioglass 45S5 particle (BG) and surrounding bone tissue. Areas with strong osteocalcin staining of cells and mineralized bone matrix in contact with the particle are present (arrowheads). This is indicative that bone formation and matrix mineralization are still actively progressing at the surface of the degrading particle. Undecalcified sawed section counterstained with hematoxylin. Bar = 200 μm.

6.3 Mechanisms of biodegradation of bioceramics

Biodegradation of bioactive ceramics used for bone regeneration can occur either by physicochemical dissolution or by cellular, i.e. osteoclastic activity, or by a combination of both. For tricalcium phosphate[29,37] and bioactive glass 45S5[25] histological findings from animal studies and human biopsies showed that these materials degrade mainly by physicochemical dissolution and that the role played by osteoclasts was only minor. These results are in agreement with own findings when examining human biopsies[32,33] and specimens from the sheep study outline above.[44] In these studies, undecalcified histologic sections were stained for tartrate-resistant acid phosphatase (TRAP) activity to identify cells with osteoclastic activity in the vicinity of the various calcium phosphate bone substitute materials. In these sections stained for TRAP activity no multinucleate TRAP-positive osteoclasts were found in fibrous mesenchyme infiltrating the degrading TCP, BG45S5 and calcium–alkali–orthophosphate particles or in the mineralized bone tissue in contact with the various calcium phosphate particles, while in the positive controls (experimental fracture healing sites) numerous multinucleate TRAP positive cells were present. These findings are in agreement

with observations by Müller-Mai *et al.*[131] who also noted that degradation of calcium–alkali–orthophosphate materials occurred mainly by physicochemical dissolution rather than by osteoclastic activity.[131] With regard to hydroxyapatite-based calcium phosphate materials, however, it has been reported that biodegradation occurs mainly by osteoclastic activity.[74] It has been speculated that these differences in degradation behavior between hydroxyapatite and TCP or BG45S5 are related to the pH, which increases during the dissolution process.[31] Dissolution of TCP, BG45S5 and calcium–alkali–orthophosphates leads to a more alkaline milieu at the material surface, whereas dissolution of hydroxyapatite is associated with a lower pH.[74] This certainly is an interesting issue requiring further investigation.

6.4 Summary

Bioactive calcium phosphate ceramics and glasses are known to bond directly to bone and to enhance bone tissue formation. This has led to their constantly increasing clinical use. Numerous studies have contributed to enhancing our understanding regarding the stimulatory effect of bioactive ceramics on bone tissue formation. Significant progress has been made in revealing solution-mediated surface reactions that take place close to the surface of bioactive ceramics. Advanced surface analysis methods have been combined with molecular techniques in order to facilitate a better understanding of the surface transformations of bioactive, resorbable ceramics and the protein adsorption events that are associated with immersion in biological fluids. A considerable body of knowledge has been generated regarding the effect of various bioactive ceramics on osteoblast differentiation *in vitro*. Very recent studies provided insight into the effect of bioactive ceramics on bone cell differentiation and tissue maturation *in vivo*, thereby allowing for correlation of *in vitro* and *in vivo* events. Moreover, techniques became available to study integrin-mediated cell adhesion and the subsequently activated intracellular signalling pathways that regulate cell function including cellular differentiation and cell survival. As a result, current research efforts often combine two powerful analytical methodologies (advanced surface analysis methods and techniques to examine integrin-mediated cell adhesion and signaling mechanisms) to elucidate the mechanisms by which bioactive ceramics induce enhanced osteoblastic differentiation. Once reaction pathways are clearly identified, the means have become available to alter biomaterial molecular components and surface characteristics in ways that promote optimal cell adhesion, proliferation and differentiation. Thus new bioactive materials can be created whose surface chemistry preferentially boosts the osteogenic cascade thereby leading to more and more expeditious and copious bone formation.

6.5 Acknowledgements

Support over the years from various agencies is gratefully acknowledged. Part of the work was supported by the German Research Foundation DFG (KN 377/2-1, KN377/3-1, KN377/5-1), by the Osteology Foundation, by the NIH (AR-40194, DE-10639, DE-13051, DE1380), NSF (BCS-9202314, BCS-9309053), NASA (NAG9-817, NAG8-1483) and VA (1189-RA).

Furthermore, the authors wish to thank numerous colleagues who contributed to the work presented in this chapter: Prof. Dr I. Shapiro, PD Dr M. Stiller, Dr G. Berger, Dr S. Radin, Dr G. Gildenhaar, Dr A. Houshmand, Dr Ch. Koch, Dr H. Renz, Dr A. El-Ghannam, Ms A. Kopp, Ms I. Borchert, Mrs K. Schulze-Dirksen, Ms E. Rieger-Rüdiger, Mrs I. Schwarz.

6.6 References

1. Ducheyne P, Hench LL, Kagan A, Martens M, Mulier JC, Burssens A, 'The effect of hydroxyapatite impregnation on bonding of porous coated implants', *J Biomed Mat Res*, 1980 **14**, 225–37.
2. de Groot K, Wolke JG, Jansen JA, 'Calcium phosphate coatings for medical implants', *Proc Inst Mech Eng*, 1998 **212**, 137–47. Review.
3. Geesink RG, 'Osteoconductive coatings for total joint arthroplasty', *Clin Orthop*, 2002 **395**, 53–65. Review.
4. Ducheyne P, 'Bioactive calcium phosphate ceramics and glasses', in Sedel L and Cabanela M, *Hip Surgery*: *New Materials and Developments*, London, Martin Dunitz, 1998, 75–82.
5. Denissen HW, Klein CP, Visch LL, van den Hooff A, 'Behavior of calcium phosphate coatings with different chemistries in bone', *Int J Prosthodont*, 1996 **9**, 142–8.
6. Ducheyne P, Beight J, Cuckler J, Evans B, Radin S, 'Effect of calcium phosphate coating characteristics on early post-operative bone tissue ingrowth', *Biomaterials*, 1990 **11**, 531–40.
7. Knabe C, Berger G, Gildenhaar R, Klar F, Zreiqat H, 'The modulation of osteogenesis *in vitro* by calcium titanium phosphate coatings', *Biomaterials*, 2004 **25**, 4911–19.
8. Buser D, Dula K, Hess D, Hirt HP, Belser UC, 'Localized ridge augmentation with autografts and barrier membranes', *Periodontology 2000*, 1999 **19**, 151–63. Review.
9. von Arx T, Cochran DL, Hermann JS, Schenk RK, Buser D, 'Lateral ridge augmentation using different bone fillers and barrier membrane application. A histologic and histomorphometric pilot study in the canine mandible', *Clin Oral Implants Res*, 2001 **12**, 260–69.
10. Praemer A, Furner S, Rice DP, *Musculoskeletal Conditions in the United States*, Park Ridge, American Academy of Orthopaedic Surgeons, 1999.
11. Belser UC, Mericske-Stern R, Bernard JP, Taylor TD, 'Prosthetic management of the partially dentate patient with fixed implant restorations', *Clin Oral Implants Res*, 2000 **11** (Suppl 1), 126–45. Review.

12. Ganz SD, Valen M, 'Predictable synthetic bone grafting procedures for implant reconstruction: part two', *J Oral Implantol*, 2002 **28**, 178–83.
13. Winkler S, 'Implant site development and alveolar bone resorption patterns', *J Oral Implantol*, 2002 **28**, 226–29.
14. Kalk WW, Raghoebar GM, Jansma J, Boering G, 'Morbidity from iliac crest bone harvesting', *J Oral Maxillofac Surg*, 1996 **54**, 1424–9.
15. Kaptein ML, Hoogstraten J, de Putter C, de Lange GL, Blijdorp PA, 'Dental implants in the atrophic maxilla: measurements of patients' satisfaction and treatment experience', *Clin Oral Implants Res*, 1998 **9**, 321–6.
16. Wheeler SL, 'Sinus augmentation for dental implants: the use of alloplastic materials', *J Oral Maxillofac Surg*, 1997 **55**, 1287–93. Review.
17. Ouhayoun JP, 'Risques de transmission à l'homme de pathologies virale par de substituts oseux d'origine humaine ou animale', in *Rapport sur l'état des recherches concernant les risques associés à l'utilisation à des fins thérapeutiques de produits d'origine humaine ou de produits et procédés de substitution*, Paris, Edition INSERM, 224–30, 1995.
18. Metsger DS, Driskell TD, Paulsrud JR, 'Tricalcium phosphate ceramic – a resorbable bone implant: review and current status', *J Am Dent Assoc*, 1982 **105**, 1035–8. Review.
19. Hollinger JO, Brekke J, Gruskin E, Lee D, 'Role of bone substitutes', *Clin Orthop*, 1996 **324**, 55–65. Review.
20. Yaszemski MJ, Payne RG, Hayes WC, Langer R, Mikos AC, 'Evolution of bone transplantation: molecular, cellular and tissue strategies to engineer human bone', *Biomaterials*, 1996 **17**, 175–85.
21. Hench LL, 'Bioceramics', *J Am Ceram Soc*, 1998 **81**, 1705–28. Review.
22. Zerbo IR, Bronckers AL, de Lange GL, van Beek GJ, Burger EH, 'Histology of human alveolar bone regeneration with a porous tricalcium phosphate. A report of two cases', *Clin Oral Implants Res*, 2001 **12**, 379–84.
23. Wiltfang J, Merten HA, Schlegel KA, Schultze-Mosgau S, Kloss FR, Rupprecht S, Kessler P, 'Degradation characteristics of alpha and beta tri-calcium-phosphate (TCP) in minipigs', *J Biomed Mater Res*, 2002 **63**, 115–21.
24. Zerbo IR, Zijderveld SA, de Boer A, Bronckers AL, de Lange G, ten Bruggenkate CM, Burger EH, 'Histomorphometry of human sinus floor augmentation using a porous β-tricalcium phosphate: a prospective study', *Clin Oral Implants Res*, 2004 **15**, 724–32.
25. Zerbo IR, Bronckers AL, de Lange G, Burger EH, 'Localisation of osteogenic and osteoclastic cells in porous β-tricalcium phosphate particles used for human maxillary sinus floor elevation', *Biomaterials*, 2005 **26**, 1445–51.
26. Szabo G, Huys L, Coulthard P, Maiorana C, Garagiola U, Barabas J, Nemeth Z, Hrabak K, Suba Z, 'A prospective multicenter randomized clinical trial of autogenous bone versus β-tricalcium phosphate graft alone for bilateral sinus elevation: histologic histomorphometric evaluation', *Int J Oral Maxillofac Implants*, 2005 **20**, 371–81.
27. Eggli PS, Muller W, Schenk RK, 'Porous hydroxyapatite and tricalcium phosphate cylinders with two different pore size ranges implanted in the cancellous bone of rabbits', *Clin Orthop Rel Res*, 1988 **232**, 127–38.
28. Ducheyne P, de Groot K, '*In vivo* surface activity of a hydroxyapatite alveolar bone substitute – a note', *J Biomed Mat Res*, 1991 **15**, 441–5.

29. Tadjoedin ES, de Lange GL, Holzmann PJ, Kulper L, Burger EH, 'Histological observations on biopsies harvested following sinus floor elevation using a bioactive glass material of narrow size range', *Clin Oral Implants Res*, 2000 **11**, 334–44.
30. Tadjoedin ES, de Lange GL, Lyaruu DM, Kuiper L, Burger EH, 'High concentrations of bioactive glass material (BioGran) vs. autogenous bone for sinus floor elevation', *Clin Oral Implants Res*, 2002 **13**, 428–36.
31. Peters F, Reif D, 'Functional materials for bone regeneration from β-tricalcium phosphate', *Materialwissenschaft und Werkstofftechnik*, 2004 **35**, 203–7.
32. Knabe C, Koch Ch, Rack A, Stiller M, 'Histological and immunohistochemical study of biopsies sampled after sinus floor augmentation using tricalcium phosphate particles with varying porosity', *Transactions 31st Annual Meeting of the Society for Biomaterials USA*, Pittsburgh, Pennsylvania, USA, Society for Biomaterials USA, 2006, 371.
33. Knabe C, Koch Ch, Rack A, Stiller M, 'Effect of β-tricalcium phosphate particles with varying porosity on osteogenesis after sinus floor augmentation in humans', *Biomaterials*, 2008, in press.
34. Timmenga NM, Raghoebar GM, van Weissenbruch R, Vissink A, 'Maxillary sinus floor elevation surgery. A clinical, radiographic and endoscopic evaluation', *Clin Oral Implants Res*, 2003 **14**, 322–328.
35. Artzi Z, Kozlovsky A, Nemcovsky CE, Weinreb M, 'The amount of newly formed bone in sinus grafting procedures depends on tissue depth as well as the type and residual amount of the grafted material,' *J Clin Periodontol*, 2005 **32**, 193–9.
36. Zijderveld SA, Zerbo IR, van den Bergh JP, Schulten EA, ten Bruggenkate CM, 'Maxillary sinus floor augmentation using a beta-tricalcium phosphate (Cerasorb) alone compared to autogenous bone grafts', *Int J Oral Maxillofac Implants*, 2005 **20**, 432–40.
37. Suba Z, Takacs D, Matusovits D, Barabas J, Fazekas A, Szabo G, 'Maxillary sinus floor grafting with β-tricalcium phosphate in humans: density and microarchitecture of the newly formed bone', *Clin Oral Implants Res*, 2006 **17**, 102–8.
38. Berger G, Gildenhaar R, Ploska U, 'Rapid resorbable, glassy crystalline materials on the basis of calcium alkali orthophosphates', *Biomaterials*, 1995 **16**, 1241–8.
39. Berger G, Gildenhaar R, Ploska U, 'Rapid resorbable materials based on a new phase: $Ca_2KNa(PO_4)_2$', in Wilson J, Hench LL and Greenspan DC, *Bioceramics 8*, Oxford, Butterworth-Heinemann, 1995, 453–6.
40. Schneider M, Gildenhaar R, Berger G, 'Investigations of phase relations in the system $CaO–Na_2O–K_2O–P_2O_5$ Part I: Characterization of the compound $Ca_2KNa(PO_4)_2$', *Cryst Res Technol*, 1994 **29**, 671–5.
41. Knabe C, Gildenhaar R, Berger G, Ostapowicz W, Fitzner R, Radlanski RJ, Gross U, '*In vitro* investigation of novel calcium phosphates using osteogenic cultures', *J Mater Sci Mater Med*, 1998 **9**, 337–45.
42. Knabe C, Berger G, Gildenhaar R, Meyer J, Howlett CR, Markovic B, Zreiqat H, 'The effect of rapidly resorbable calcium phosphates and a calcium phos-

phate bone cement on the expression of bone-related genes and proteins *in vitro*', *J Biomed Mater Res*, 2004 **69A**, 145–54.
43. Knabe C, Houshmand A, Berger G, Ducheyne P, Gildenhaar R, Stiller M, 'Effect of rapidly resorbable bone substitute materials on the temporal expression of the osteoblastic phenotype *in vitro*', *J Biomed Mater Res A*, 2007, Epub ahead of print.
44. Knabe C, Berger G, Gildenhaar R, Koch Ch, Jonscher S, Rack A, Seligmann H, Stiller M, 'Effect of rapidly resorbable calcium–alkali–orthophosphate bone substitute materials on osteogenesis and osteoblastic phenotype expression *in vivo*,' *Transactions 32nd Annual Meeting of the Society for Biomaterials USA*, Chicago, Illinois, USA, 2007, 262.
45. Schmitz JP, Hollinger JO, Milam SB, 'Reconstruction of bone using calcium phosphate bone cements: a critical review', *J Oral Maxillofac Surg*, 1999 **57**, 1122–6.
46. Khairoun I, Boltong MG, Driessens FCM, Planell JA, 'Effect of calcium carbonate on the compliance of an apatitic bone cement', *Biomaterials*, 1997 **18**, 1535–9.
47. Ooms EM, Wolke JG, van der Waerden JP, Jansen JA, 'Trabecular bone response to injectable calcium phosphate (Ca-P) cement', *J Biomed Mater Res*, 2002 **61**, 9–18.
48. Cuisinier FJG, Wieber A, Tenenbaum H, van Landuyt P, Lemaitre J, 'Injectable calcium phosphate hydraulic cement (CPHC) used as periodontal tissues regeneration. A study in a dog model', *J Appl Biomater Biomech*, 2003 **1**, 186–93.
49. Wolff KD, Swaid S, Nolte D, Bockmann RA, Holzle F, Muller-Mai C, 'Degradable injectable bone cement in maxillofacial surgery: indications and clinical experience in 27 patients', *J Craniomaxillofac Surg*, 2004 **32**, 71–9.
50. Gildenhaar R, Berger G, Knabe C, Lehmann E, 'Development of alkali containing calcium phosphate cements', *Key Eng Mater*, 2008, **361–3**, 331–4.
51. Ducheyne P, Qiu Q, 'Bioactive ceramics: the effect of surface reactivity on bone formation and bone cell function', *Biomaterials*, 1999 **20**, 2287–303. Review.
52. Hench LL, 'Bioactive glasses, ceramics, and composites', *Bone–Implant Interface*, 1994 **9**, 181–90. Review.
53. Ohgushi H, Okumura M, Tamai S, Shors EC, Caplan AI, 'Marrow cell induced osteogenesis in porous hydroxyapatite and tricalcium phosphate: a comparative histomorphometric study of ectopic bone formation', *J Biomed Mater Res*, 1990 **24**, 1563–70.
54. Ducheyne P, Bianco P, Radin S, Schepers E, 'Bioactive materials: mechanisms and bioengineering considerations', in Ducheyne P, Kokubo T, and van Blitterswijk CA, *Bone-bioactive Biomaterials*, Leiderdorp, Netherlands, Reed Healthcare Communications, 1993, 1–12.
55. Radin SR, Ducheyne P, 'The effect of calcium phosphate ceramic composition and structure on *in vitro* behavior. II. Precipitation', *J Biomed Mat Res*, 1993 **27**, 35–45.
56. Radin S, Ducheyne P, 'Effect of serum proteins on solution-induced surface transformations of bioactive ceramics', *J Biomed Mater Res*, 1996 **30**, 273–9.

57. Radin S, Ducheyne P, Rothman B, Conti A, 'The effect of *in vitro* modeling conditions on the surface reactions on bioactive glass', *J Biomed Mat Res*, 1997 **37**, 363–75.
58. Radin S, Ducheyne P, Berthold P, Decker S, 'Effect of serum proteins and osteoblasts on the surface transformation of a calcium phosphate coating: a physicochemical and ultrastructural study', *J Biomed Mat Res*, 1997 **39**, 234–43.
59. Kokubo T, Kushitani H, Ohtsuki C, Sakka S, Yamamuro T, 'Chemical-reaction of bioactive glass and glass-ceramics with a simulated body-fluid', *J Mater Sci Mater Med Sci*, 1992 **3**, 79–83.
60. Kokubo T, 'Bioactivity of glasses and glass ceramics', in Ducheyne P, Kokubo T and van Blitterswijk CA, *Bone-bioactive Biomaterials*, Leiderdorp, Netherlands, Reed Healthcare Communications, 1993, 31–46.
61. El-Ghannam A, Ducheyne P, Shapiro IM, 'Effect of serum protein adsorption on osteoblast adhesion to bioactive glass and hydroxyapatite', *J Orthop Res*, 1999 **17**, 340–5.
62. Kaufmann EA, Ducheyne P, Radin S, Bonnell DA, Composto R, 'Initial events at the bioactive glass surface in contact with protein containing solutions,' *J Biomed Mat Res*, 2000 **52**, 825–30.
63. Hench L, Splinter R, Greenlee T, Allen W, 'Bonding mechanisms at the interface of ceramic prosthetic materials', *J Biomed Eng*, 1971 **2**, 117–41.
64. LeGeros RZ, Daculsi G, Orly I, Gregoire M, Heughebaert M, Gineste M, Kijkowska R, 'Formation of carbonate apatite on calcium phosphate materials: dissolution/precipitation processes', in Ducheyne P, Kokubo T, and van Blitterswijk CA, *Bone-bonding Biomaterials*, Leiderdorp, Netherlands, Reed Healthcare Communications, 1993, 201–12.
65. Ducheyne P, Radin S, King L, 'The effect of calcium-phosphate ceramic composition and structure on *in vitro* behavior; I. Dissolution', *J Biomed Mat Res*, 1993 **27**, 25–34.
66. Neo M, Nakaruma T, Yamamuro T, Ohtsuki C, Kokubo T, 'Transmission microscopic study of apatite formation on bioactive ceramics *in vivo*', in Ducheyne P, Kokubo T, and van Blitterswijk CA, *Bone-bonding Biomaterials*, Leiderdorp, Netherlands, Reed Healthcare Communications, 1993, 111–20.
67. Ducheyne P, Kim CS, Pollack SR, 'The effect of phase differences on the time-dependent variation of the zeta potential of hydroxyapatite', *J Biomed Mat Res*, 1992 **26**, 147–68.
68. El-Ghannam AE, Ducheyne P, Shapiro I, 'Porous bioactive glass and hydroxyapatite stimulate bone cell function *in vitro* along different time lines', *J Biomed Mater Res*, 1997 **36**, 167–80.
69. Yao J, Radin S, Leboy PS, Ducheyne P, 'Solution mediated effect of bioactive glass in poly (lactic-co-glycolic acid)-bioactive glass composites on osteogenesis of marrow stromal cells', *J Biomed Mater Res A*, 2005 **75**, 794–801.
70. de Bruijn JD, Bovell YP, van Blitterswijk CA, 'Structural arrangements at the interface between plasma sprayed calcium phosphates and bone', *Biomaterials*, 1994 **15**, 543–50.
71. Daculsi G, LeGeros RZ, Nery E, Lynch K, Kerebel B, 'Transformation of biphasic calcium phosphate ceramics *in vivo*: ultrastructural and physicochemical characterization', *J Biomed Mat Res*, 1989 **23**, 883–94.

72. de Bruijn JD, Davies JE, Klein CPAT, de Groot K, van Blitterswijk CA, 'Biological responses to calcium phosphate ceramics', in Ducheyne P, Kokubo T, and van Blitterswijk CA, *Bone-bonding Biomaterials*, Leiderdorp, Netherlands, Reed Healthcare Communications, 1993, 57–72.
73. El-Ghannam A, Ducheyne P, Shapiro IM, 'Bioactive material template for *in vitro* synthesis of bone', *J Biomed Mat Res*, 1995 **29**, 359–70.
74. Schepers E, Declercq M, Ducheyne P, Kempeneers R, 'Bioactive glass particulate material as a filler for bone lesions', *J Oral Rehab*, 1991 **18**, 439–52.
75. Matsuda T, Davies JE, 'The *in vitro* response of osteoblasts to bioactive glass', *Biomaterials*, 1987 **8**, 275–84.
76. Radin SR, Ducheyne P, 'The effect of calcium phosphate ceramic composition and structure on *in vitro* behavior. II. Precipitation', *J Biomed Mat Res*, 1993 **27**, 35–45.
77. Davies JE, 'Mechanisms of endosseous integration', *Int J Prosthodont*, 1998 **11**, 391–401. Review.
78. Hench LL, 'Bioceramics: from concept to clinic', *J Am Cer Soc*, 1991 **74**(7), 1487–510.
79. Keselowsky BG, Collard DM, Garcia AJ, 'Surface chemistry modulates fibronectin conformation and directs integrin binding and specificity to control cell adhesion', *J Biomed Mater Res A*, 2003 **66**, 247–59.
80. Ducheyne P, El-Ghannam A, Shapiro I, 'Effect of bioactive glass templates on osteoblast proliferation and *in vitro* synthesis of bone like tissue', *J Cell Biochem*, 1994 **56**, 162–7.
81. Xynos ID, Edgar AJ, Buttery LD, Hench LL, Polak JM, 'Ionic products of bioactive glass dissolution increase proliferation of human osteoblasts and induce insulin-like growth factor II mRNA expression and protein synthesis', *Biochem Biophys Res Commun*, 2000 **276**, 461–5.
82. Xynos ID, Edgar AJ, Buttery LD, Hench LL, Polak JM, 'Gene-expression profiling of human osteoblasts following treatment with the ionic products of Bioglass 45S5 dissolution', *J Biomed Mater Res*, 2001 **55**, 151–7.
83. Xynos ID, Hukkanen MV, Batten JJ, Buttery LD, Hench LL, Polak JM, 'Bioglass 45S5 stimulates osteoblast turnover and enhances bone formation *in vitro*: implications and applications for bone tissue engineering', *Calcif Tissue Int*, 2000 **67**, 321–9.
84. El-Ghannam A, Ducheyne P, Shapiro IM, 'Formation of surface reaction products on bioactive glass and their effects on the expression of the osteoblastic phenotype and the deposition of mineralized extracellular matrix', *Biomaterials*, 1997 **18**, 295–303.
85. Radin S, Reilly G, Bhargave G, Leboy PS, Ducheyne P, 'Osteogenic effects of bioactive glass on bone marrow stromal cells', *J Biomed Mat Res*, 2005 **73A**, 21–9.
86. Sodek J, Cheifitz S, 'Molecular regulation of osteogenesis', in Davies JE, *Bone Engineering*, Toronto, Canada, em squared Inc, 2000, 31–43.
87. Aubin JE, 'Advances in the osteoblast lineage', *Biochem Cell Biol*, 1998 **76**, 899–910. Review.
88. Aubin JE, 'Osteogenic cell differentiation', in Davies JE, *Bone Engineering*, Toronto, Canada, em squared Inc, 2000, 19–30.

89. Fisher LW, Termine JD, 'Noncollagenous proteins influencing the local mechanisms of calcification', *Clin Orthop*, 1985 **200**, 362–85.
90. Termine JD, Kleinman HK, Whitson SW, Conn KM, McGarvey ML, Martin GR, 'Osteonectin, a bone-specific protein linking mineral to collagen', *Cell*, 1981 **26**, 99–105.
91. Oldberg A, Franzen A, Heinegard D, 'The primary structure of a cell-binding bone sialoprotein', *J Biol Chem*, 1988 **263**, 19430–2.
92. Schwartz Z, Boyan BD, 'Underlying mechanisms at the bone–biomaterial interface', *J Cell Biochem*, 1994 **56**, 340–7. Review.
93. Howlett CR, Chen N, Zhang X, Akin FA, Haynes D, Hanley L, Revell P, Evans P, Zhou H, Zreiqat H, 'The effect of biomaterial chemistries on the osteoblastic molecular phenotype and osteogenesis: *in vitro* and *in vivo* studies', in Davies JE, *Bone Engineering*, Toronto, Canada, em squared Inc, 2000, 240–55.
94. Salih V, Franks K, James M, Hastings GW, Knowles JC, 'Development of soluble glasses for biomedical use. Part 2: The biological response of human osteoblast cell lines to phosphate-based soluble glasses', *J Mater Sci Mater Med Sci*, 2000 **11**, 615–20.
95. Knabe C, Stiller M, Berger G, Reif D, Gildenhaar R, Howlett CR, Zreiqat H, 'The effect of bioactive glass ceramics on the expression of bone-related genes and proteins *in vitro*', *Clin Oral Implants Res*, 2005 **16**, 119–27.
96. Knabe C, Howlett CR, Klar F, Zreiqat H, 'The effect of different titanium and hydroxyapatite-coated dental implant surfaces on phenotypic expression of human bone-derived cells' *J Biomed Mater Res*, 2004 **71A**, 98–107.
97. Knabe C, Berger G, Gildenhaar R, Howlett CR, Markovic B, Zreiqat H, 'The functional expression of human bone-derived cells grown on rapidly resorbable calcium phosphate ceramics', *Biomaterials*, 2004 **25**, 335–44.
98. Wang C, Duan Y, Markovic B, James B, Howlett CR, Zhang X, Zreiqat H, 'Phenotypic expression of bone-related genes in osteoblasts grown on calcium phosphate ceramics with different phase compositions', *Biomaterials*, 2004 **25**, 2507–14.
99. Krause A, Cowles EA, Gronowicz G, 'Integrin-mediated signaling in osteoblasts on titanium implant materials', *J Biomed Mater Res*, 2000 **52**, 738–47.
100. Gronowicz G, McCarthy MB, 'Response of human osteoblasts to implant materials: integrin-mediated adhesion', *J Orthop Res*, 1996 **14**, 878–87.
101. Rezania A, Healy KE, 'Integrin subunits responsible for adhesion of human osteoblast-like cells to biomimetic peptide surfaces', *J Orthop Res*, 1999 **17**, 615–23.
102. Cowles EA, Brailey LL, Gronowicz GA, 'Integrin-mediated signaling regulates AP-1 transcription factors and proliferation in osteoblasts', *J Biomed Mater Res*, 2000 **52**, 725–37.
103. Hynes RO, 'Integrins: a family of cell surface receptors', *Cell*, 1987 **48**, 549–54.
104. Hynes RO, 'Integrins: versatility, modulation, and signaling in cell adhesion', *Cell*, 1992 **69**, 11–25. Review.
105. Gronthos S, Stewart K, Graves SE, Hay S, Simmons PJ, 'Integrin expression and function of human osteoblast-like cells', *J Bone Miner Res*, 1997 **12**, 1189–97.

106. Hughes DE, Salter DM, Dedhar S, Simpson R, 'Integrin expression in human bone', *J Bone Miner Res*, 1993 **8**, 527–33.
107. Saito T, Albelda SM, Brighton CT, 'Identification of integrin receptors on cultured human bone cells', *J Orthop Res*, 1994 **12**, 384–94.
108. Garcia AJ, Ducheyne P, Boettiger D, 'Effect of surface reaction stage on fibronectin-mediated adhesion of osteoblast-like cells to bioactive glass', *J Biomed Mater Res*, 1998 **40**, 48–56.
109. Danen EH, Aota S, van Kraats AA, Yamada KM, Ruiter DJ, van Muijen GN, 'Requirement for the synergy site for cell adhesion to fibronectin depends on the activation state of integrin alpha 5 beta', *J Biol Chem*, 1995 **270**(37), 21612–18.
110. Keselowsky BG, Collard DM, Garcia AJ, 'Integrin binding specificity regulates biomaterial surface chemistry effects on cell differentiation', *Proc Natl Acad Sci USA*, 2005 **102**(17), 5953–7.
111. Juliano RL, Haskill S, 'Signal transduction from the extracellular matrix', *J Cell Biol,* 1993 **120**, 577–85.
112. Rosales C, O'Brien V, Kronberg L, Julinao RL, 'Signal transduction by cell adhesion receptors', *Biochem Biophys Acta*, 1995 **1242**, 77–98.
113. Bates RC, Lincz LF, Burns GF, 'Involvement of integrins in cell survival', *Cancer Metastasis Rev*, 1995 **14**, 191–203. Review.
114. Yamada KM, Miyamoto S, 'Integrin transmembrane signaling and cytoskeletal control', *Curr Opin Cell Biol*, 1995 **7**, 681–9. Review.
115. Richardson A, Parsons JT, 'Signal transduction through integrins: a central role for focal adhesion kinase?', *Bioessays*, 1995 **17**, 229–36.
116. Dedhar S, 'Integrin-mediated signal transduction in oncogenesis: an overview', *Cancer Metastasis Rev*, 1995 **14**, 165–72.
117. Harmer SL, DeFranco AL, 'Shc contains two Grb2 binding sites needed for efficient formation of complexes with SOS in B lymphocytes', *Mol Cell Biol*, 1997 **17**, 4087–95.
118. Noth U, Tuli R, Seghatoleslami R, Howard M, Shah A, Hall DJ. 'Activation of p38 and Smads mediates BMP-2 effects on human trabecular bone-derived osteoblasts', *Exp Cell Res*, 2003 **291**(1), 201–11.
119. Nohe A, Keating E, Knaus P, Petersen NO, 'Signal transduction of bone morphogenetic protein receptors', *Cell Signal*, 2004 **16**, 291–9.
120. Ivaska J, Reunanen H, Westermarck J, Koivisto L, Kahari VM, Heino J, 'Integrin alpha2beta1 mediates isoform-specific activation of p38 and upregulation of collagen gene transcription by a mechanism involving the alpha2 cytoplasmic tail', *J Cell Biol*, 1999 **147**, 401–16.
121. Adams CS, Shapiro IM, 'Mechanisms by which extracellular matrix components induce osteoblast apoptosis', *Connect Tissue Res*, 2003 **44** (Suppl 1), 230–39. Review.
122. Grigoriou V, Shapiro IM, Cavalcanti-Adam EA, Composto RJ, Ducheyne P, Adams CS, 'Osteoblast apoptosis and survival is regulated by integrin-mediated surface attachment', *J Biol Chem*, 2005 **280**, 1733–9.
123. Risbud MV, Fertala J, Vresilovic EJ, Albert TJ, Shapiro IM, 'Nucleus pulposus cells upregulate PI3K/Akt and MEK/ERK signaling pathways under hypoxic conditions and resist apoptosis induced by serum withdrawal', *Spine*, 2005 **30**, 882–9.

124. Razzouk S, Shapiro IM, 'Detection of apoptotic gene expression in human osteoblast-like cells by cDNA microarrays', *J Bone Miner Metab*, 2003 **21**(5), 261–7.
125. Szymczyk KH, Shapiro IM, Adams CS, 'Ionizing radiation sensitizes bone cells to apoptosis', *Bone*, 2004 **34**, 148–56.
126. Knabe C, Kraska B, Koch Ch, Gross U, Zreiqat H, Stiller M, 'A method for immunohistochemical detection of osteogenic markers in undecalcified bone sections', *Biotech Histochem*, 2006 **81**, 313–19.
127. Gross UM, Strunz V, 'Surface staining of sawed sections of undecalcified bone containing alloplastic implants', *Stain Technol*, 1977 **52**, 217–19.
128. Donath K, Breuner G, 'A method for the study of undecalcified bones and teeth with attached soft tissues: The Saege-Schliff (sawing and grinding) technique', *J Oral Pathol*, 1982 **11**, 318–26.
129. Roeser K, Johansson CB, Donath K, Albrektsson T, 'A new approach to demonstrate cellular activity in bone formation adjacent to implants', *J Biomed Mater Res*, 2000 **51**, 280–91.
130. Johansson CB, Röser K, Bolind P, Donath K, Albrektsson T, 'Bone-tissue formation and integration of titanium implants: an evaluation with newly developed enzyme and immunohistochemical techniques', *Clin Implant Dent Relat Res*, 1999 **1**, 33–40.
131. Müller-Mai C, Berger G, Voigt C, Bakki B, Gross U, 'The bony reaction to rapidly degradable glass-ceramics based on the new phase $Ca_2KNa(PO_4)_2$', in Sedel L and Rey C, *Bioceramics 10*, Oxford, Butterworth-Heinemann, 1997, 53–6.

7

In vitro evaluation of bone bioactivity

H TAKADAMA and T KOKUBO, Chubu University, Japan

7.1 Introduction

Artificial materials implanted into bone defects are generally encapsulated by fibrous tissue, which isolates them from surrounding bone, and consequently they do not bond to living bone. This is a normal protective reaction of the living body against foreign materials. However, because of this reaction, artificial materials usually cannot be used as bone substitutes.

Hench *et al.* (1972) first showed that some glasses in the Na_2O–CaO–SiO_2–P_2O_5 system, called Bioglass®, spontaneously bond to living bone without the formation of fibrous tissue on their surfaces. Since then, various kinds of synthetic materials, such as sintered hydroxyapatite, sintered beta-tricalcium phosphate, biphasic ceramics of hydroxyapatite and tricalcium phosphate and glass-ceramic A-W, have also been found to bond to living bone. These materials are now called bioactive materials and are clinically used as important bone substitutes. However, even these bioactive materials cannot replace all autografts. Bioactive materials with higher bone-bonding ability and different mechanical properties need to be developed.

How can we find bioactive materials? Most of the bioactive materials hitherto developed form an apatite layer on their surfaces in the living body and then bond to bone through this apatite layer. This *in vivo* apatite formation can be reproduced on the surfaces of materials in simulated body fluid (SBF) with ion concentrations nearly equal to those of human blood plasma. Based on these findings, it is considered useful to examine apatite formation on a material in SBF as a preliminary to animal experiments to find bone-bonding materials as it allows the number of animal experiments required for finding bone-bonding materials to be reduced. Currently, SBF is used by many researchers for *in vitro* evaluation of the bone bioactivity of materials and SBF has been standardized as a solution for *in vitro* evaluation of apatite-forming ability of implant materials by the International Organization for Standardization.

In this chapter, the ion concentrations of SBF, the correlation of the bone-bonding ability of materials with apatite formation on their surfaces in SBF, and some applications of *in vitro* evaluation of bone-bonding ability and the mechanisms of apatite formation are described.

7.2 Ion concentrations of SBF

Hench *et al.* (1972) first showed that bone-bonding glasses in the Na_2O–CaO–SiO_2–P_2O_5 and Na_2O–SiO_2 systems form a calcium phosphate layer on their surfaces in the living body and bond to the living bone through this calcium phosphate layer. They found that the calcium phosphate layer on their glasses can be formed *in vitro* in a solution buffered at pH 7.4 by Tris(hydroxymethyl)amine and hydrochloric acid (Tris buffer solution).

Later, it was found by Kitsugi *et al.* (1987) that glass-ceramic A-W, containing crystalline apatite and wollastonite in a glassy matrix, also forms a calcium phosphate layer on its surface in the living body and bonds to bone through this calcium phosphate layer. This was identified by X-ray diffraction as crystalline apatite (Kokubo *et al.,* 1990a). Kokubo *et al.* (1990b, c) showed that this *in vivo* apatite formation can be reproduced in an organic substance-free, acellular SBF with ion concentrations nearly equal to those of human blood plasma. However, this initial SBF proposed by Kokubo *et al.* lacked the sulphate ions that are included in human blood plasma (Neuman and Neuman, 1958). Subsequently, the ion concentrations of SBF were corrected and published in a paper in 1991 by Kokubo, as shown in Table 7.1 (Kokubo, 1991). Hereafter, this corrected SBF was used widely as 'SBF' by various researchers.

It should be noted, however, that the corrected SBF is richer in chloride ions and poorer in hydrogencarbonate ions than human blood plasma, as

Table 7.1 Ion concentrations of SBFs and human blood plasma

	Ion concentration/m*M*							
	Na^+	K^+	Mg^{2+}	Ca^{2+}	Cl^-	HCO_3^-	HPO_4^{2-}	SO_4^{2-}
Human blood plasma	142.0	5.0	1.5	2.5	103.0	27.0	1.0	0.5
Initial SBF	142.0	5.0	1.5	2.5	148.8	4.2	1.0	0
Corrected SBF	142.0	5.0	1.5	2.5	147.8	4.2	1.0	0.5
Revised SBF	142.0	5.0	1.5	2.5	103.0	27.0	1.0	0.5
Newly improved SBF	142.0	5.0	1.5	2.5	103.0	4.2	1.0	0.5

seen in Table 7.1. Oyane *et al.* (2003a, b) proposed a revised SBF, in which both the concentrations of chloride and hydrogencarbonate ions were set to the level of human blood plasma. However, calcium carbonate tended to precipitate during testing or preservation of this revised SBF, because it is supersaturated with respect to not only hydroxyapatite, but also to calcium carbonate. Later, Takadama *et al.* (2004) proposed a newly improved SBF, in which only the concentration of chloride ions was set to the level of human blood plasma, but the hydrogencarbonate ion concentrations were not changed from the corrected SBF. This improved SBF was compared with the corrected SBF in its stability as well as in reproducibility of apatite formation on synthetic materials by 10 research institutes. It was found that there was no difference between them. As a result, the corrected 'SBF' was submitted to the International Organization for Standardization as the solution for *in vitro* evaluation of apatite-forming ability of implants and approved as ISO 23317 June 2007. A protocol for preparing SBF and methods for examining apatite formation are given in Section 7.7 (Kokubo and Takadama, 2006).

7.3 Correlation of *in vivo* bone-bonding ability and *in vitro* apatite-forming ability in SBF

Following glass-ceramics, crystalline ceramics, inorganic–organic composites and metals have been confirmed to bond to living bone by animal experiments.

Glasses:

- Bioglass-type Na_2O–CaO–SiO_2–P_2O_5 glasses (Ogino *et al.*, 1980; Kokubo *et al.*, 1990b)
- Na_2O–CaO–B_2O_3–Al_2O_3–SiO_2–P_2O_5 glasses (Anderson and Karlsson, 1991)
- CaO–SiO_2 glasses (Ebisawa *et al.*, 1990; Ohura *et al.*, 1991)

Glass-ceramics

- Ceravital type apatite-containing glass-ceramics in the Na_2O–K_2O–MgO–CaO–SiO_2–P_2O_5 system (Ohtsuki *et al.*, 1991a)
- Apatite- and wollastonite-containing glass-ceramic A-W in the MgO–CaO–SiO_2–P_2O_5 system (Kitsugi *et al.*, 1987; Kokubo *et al.*, 1990b)
- Bioverite-type apatite- and fluorophlogopite-containing glass-ceramics in the Na_2O–MgO–CaO–Al_2O_3–SiO_2–P_2O_5–F system (Höland *et al.*, 1985)

Crystalline ceramics

- Sintered hydroxyapatite (Kokubo *et al.*, 1988; Neo *et al.*, 1992; Kim *et al.*, 2004)

- Sintered beta tricalcium phosphate (Kotani *et al.*, 1991; Ohtsuki *et al.*, 1991b; Neo *et al.*, 1993)
- Hydroxyapatite and beta tricalcium phosphate biphasic ceramics (LeGeros *et al.*, 2003)
- Calcium sulphate (Chan *et al.*, 2004)
- Calcite (Ohtsuki *et al.*, 1989; Fujita *et al.*, 1991)

Inorganic–organic composites

- Polyethylene containing glass-ceramic A-W particles (Juhasz *et al.*, 2003, 2004)

Metals

- Ti metal and its alloy subjected to NaOH and heat treatments (Kim *et al.*, 1996; Nishiguchi *et al.*, 2003)
- Ti metal subjected to H_2O_2 and heat treatments (Wang *et al.*, 2001)
- Ta metal subjected to NaOH and heat treatments (Kato *et al.*, 2000; Miyazaki *et al.*, 2000)

Most of the bone-bonding materials described above were reported to bond to living bone through a layer of apatite or calcium phosphate in the references given after the materials described above: only beta-tricalcium phosphate and calcite bond to living bone without a detectable apatite or calcium phosphate layer at their interfaces. Pictures of the interface of Bioglass® (Virolainen *et al.*, 1997) and sintered hydroxyapatite (Neo *et al.*, 1992) with neighbouring bone are shown in Figs 7.1 and 7.2. Those for glass-ceramics A-W and NaOH- and heat-treated Ti metal are given in Chapters

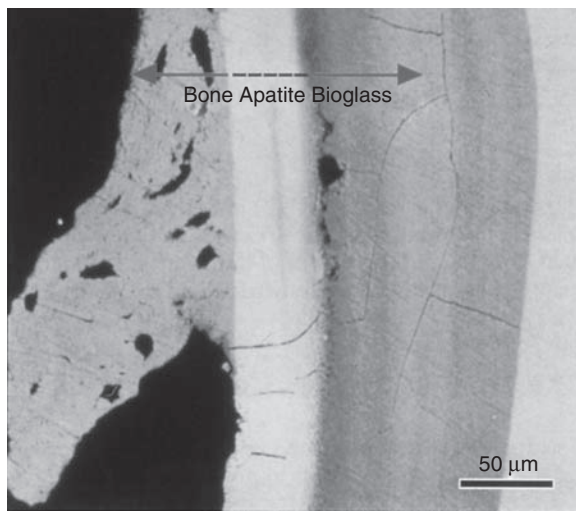

7.1 SEM picture of apatite layer formed at interface between Bioglass® glass and tibial bone of rat (Virolainen *et al.,* 1997).

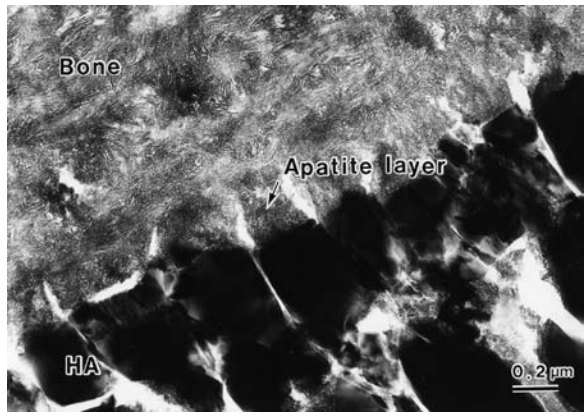

7.2 TEM picture of apatite layer formed at interface between sintered hydroxyapatite (HA) and tibial bone of rat, 10 weeks after implantation (Neo *et al.*, 1992).

13 and 21 addressing bioactive glass-ceramics and titania-based bioactive materials, respectively. The thickness of the apatite or calcium phosphate layer at the interface varies largely with the type of material and animals used.

All the bone-bonding materials except beta calcium phosphate (Kotani *et al.*, 1991) and calcite (Fujita *et al.*, 1991) were also reported to form a layer of apatite or calcium phosphate on their surfaces in SBF in the references given after the materials described above. Pictures of the apatite layers formed on a $CaO–SiO_2$ glass (Ebisawa *et al.*, 1990) and sintered hydroxyapatite (Kokubo *et al.*, 1988) in SBF are shown in Figs 7.3 and 7.4.

Some glasses in the $Na_2O–CaO–SiO_2$ system also bond to living bone through an apatite layer formed on their surfaces in the living body. The rates of bone formation around the glass particles decreases with increasing SiO_2 content of the glasses from 50 to 70 mole% with a constant molar ratio of Na_2O to CaO of 1 (Fujibayashi *et al.*, 2003). The times required for the glasses to be fully covered with apatite in SBF increases with increasing SiO_2 content (Kim *et al.*, 1995), with good correlation, as shown in Fig. 7.5.

It can be said from these findings that the apatite-forming ability of a material in SBF can be an index of bone-bonding ability of the material.

7.4 What types of material form apatite?

Human body fluid is supersaturated with respect to apatite, even under normal conditions (Neuman and Neuman, 1958). Despite this, apatite does

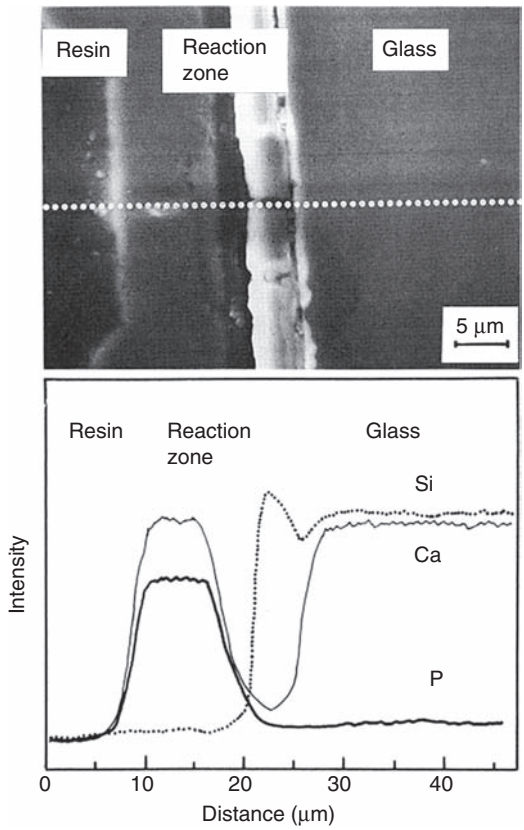

7.3 SEM picture of apatite layer formed on a $CaO–SiO_2$ glass after soaking in SBF for 20 days (Ebisawa *et al.,* 1990).

not precipitate everywhere in the body, except at sites of bone tissue, as the energy barrier for its apatite nucleation is very high. This means that once apatite nuclei are formed on a material in the living body, they can grow spontaneously by consuming calcium and phosphate ions from the surrounding body fluid. Various types of simple metal oxide gels were prepared by sol–gel methods and soaked in SBF. As a result, it was found that gels of SiO_2 (Li *et al.*, 1992), TiO_2 (Li *et al.*, 1994), ZrO_2 (Uchida *et al.*, 2001), Ta_2O_5 (Miyazaki *et al.*, 2001a) and Nb_2O_5 (Miyazaki *et al.*, 2001b) form apatite on their surfaces, as shown in Fig. 7.6, but Al_2O_3 did not (Li *et al.*, 1994). This indicates that functional groups such as Si-OH, Ti-OH, Zr-OH, Nb-OH and Ta-OH on these gels are effective for apatite nucleation. Tanahashi and Matsuda (1997) examined the apatite-forming ability in SBF of self-assembled monolayers with various functional groups and showed that functional groups such as COOH and PO_4H_2 are also effective for

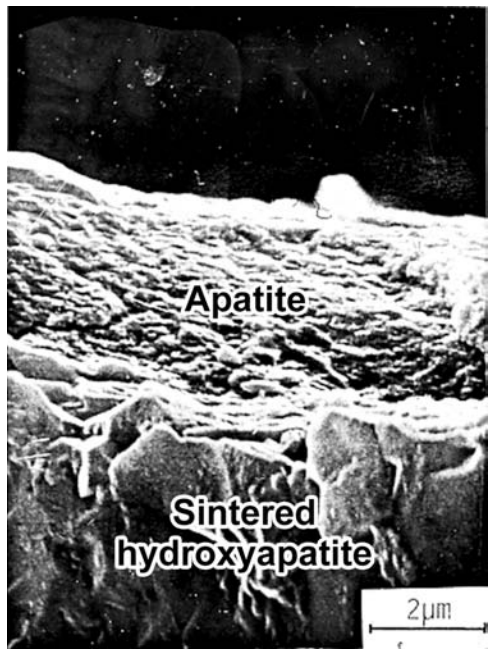

7.4 SEM picture of apatite layer formed on hydroxyapatite sintered at 1200 °C after soaking in SBF for 60 days (Kokubo *et al.*, 1988).

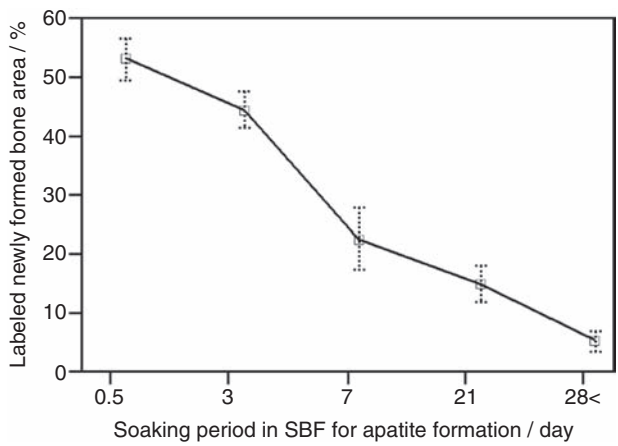

7.5 Percentage of bone formation on a cross-section of a defect of rabbit femur filled with glass particles 6 weeks after implantation against the time required for the glasses to form apatite on their surfaces in SBF (Fujibayashi *et al.*, 2003).

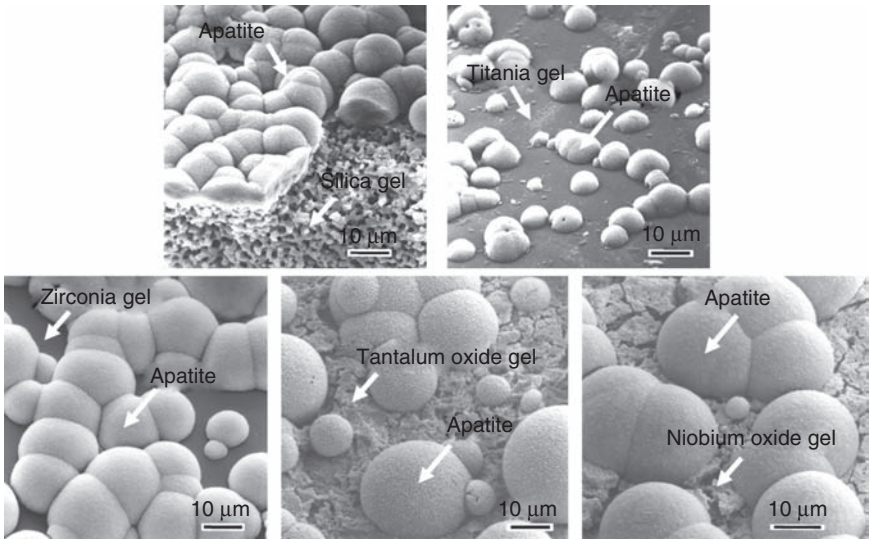

7.6 Apatite formation induced on various metal oxide gels in SBF (Li *et al.*, 1992, 1994; Miyazaki *et al.*, 2001a, 2001b; Uchida *et al.*, 2001).

apatite nucleation. The catalytic effects of these functional groups have been attributed to their negative charges. These fundamental findings are useful for designing new kinds of bone-bonding material. Bioactive titanium metal and alloys, which are described in Chapter 21 on titania-based materials, have been developed on the basis of this kind of fundamental findings.

7.5 Mechanisms of apatite formation

The mechanisms of apatite formation in SBF on materials having Si-OH and Ti-OH groups on their surfaces have been studied in detail. Apatite formation on a Na_2O–SiO_2 glass having Si-OH groups is described in papers by Takadama *et al.* (2001, 2002). Apatite formation on titanium metal having Ti-OH groups is described in Chapter 21. The mechanism of apatite formation on sintered hydroxyapatite in SBF, which was revealed by TEM observations and zeta potential measurements, is schematically shown in Fig. 7.7 (Kim *et al.*, 2004, 2005).

1 The sintered hydroxyapatite is initially negatively charged on its surface and combines with positively charged Ca^{2+} ions in the surrounding fluid, as shown in Fig. 7.8.
2 Ca-rich amorphous calcium phosphate is formed on the sintered hydroxyapatite. As the Ca^{2+} ions accumulate, the sintered hydroxy-

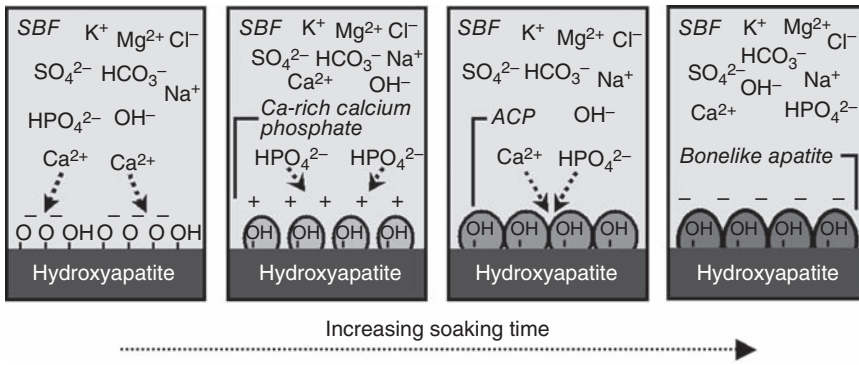

7.7 Schematic representation of mechanism of apatite formation on the sintered hydroxyapatite in SBF (Kim *et al.*, 2004).

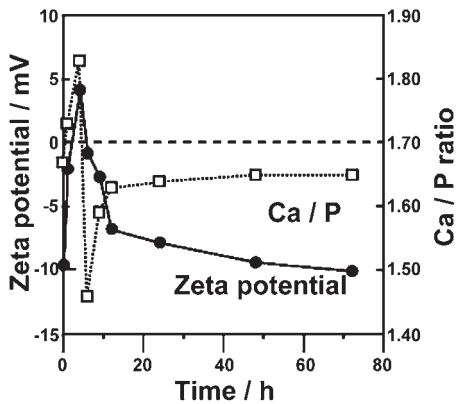

7.8 Variation of zeta potential and Ca/P ratio on the surface of sintered hydroxyapatite as a function of soaking time in SBF (Kim *et al.*, 2004).

apatite becomes positively charged on its surface and reacts with negatively charged phosphate ions.

3 Ca-poor amorphous calcium phosphate is formed.

4 This amorphous calcium phosphate is eventually transformed into more stable crystalline bone-like apatite.

This mechanism is also essentially the same in SBF containing proteins (Kokubo *et al.*, 2003).

7.6 Summary

Most bone-bonding materials bond to living bone through an apatite layer that is formed on their surfaces in the living body. This apatite formation

can be reproduced *in vitro* in an acellular SBF with ion concentrations nearly equal to those of human blood plasma. It is thus quite useful to examine apatite-forming ability on a material's surfaces in SBF to predict the bone-bonding ability of a material as a preliminarily to animal experiments.

7.7 Appendix: protocol for preparing SBF

7.7.1 Preparation of SBF

Reagents for SBF

The following powdered reagent grade chemicals have to be stored in a desiccator. Ion-exchanged distilled water is used for the preparation of SBF.

- Sodium chloride (NaCl: concentration 99.5%)
- Sodium hydrogencarbonate ($NaHCO_3$: concentration 99.5%)
- Potassium chloride (KCl: concentration 99.5%)
- Di-potassium hydrogen phosphate trihydrate ($K_2HPO_4{\cdot}3H_2O$: concentration 99.0%)
- Magnesium chloride hexahydrate ($MgCl_2{\cdot}6H_2O$: concentration 98.0%)
- Calcium chloride ($CaCl_2$: concentration 95.0%)
- Sodium sulphate (Na_2SO_4: concentration 99.0%)
- Tris-hydroxymethyl aminomethane: (Tris: $(HOCH_2)_3CNH_2$: concentration 99.0%)
- 1 M hydrochloric acid
- pH standard solutions (pH 4, 7 and 9)

Preparation of SBF

As SBF is supersaturated with respect to apatite, an inappropriate preparation method can lead to the precipitation of apatite in the solution. Always make sure that during preparation the solution remains colourless and transparent and that there is no deposit on the surface of the bottle. If any precipitation occurs, stop preparing the SBF, abandon the solution and restart, washing the apparatus and preparing SBF again.

In order to prepare 1000 ml of SBF, first put 700 ml of ion-exchanged distilled water with a stirring bar into a 1000 ml plastic beaker. Set it in a water bath on a magnetic stirrer and cover with a watch glass or plastic wrap. Heat the water in the beaker to 36.5 ± 1.5 °C with stirring.

Dissolve the reagents one by one into the solution at 36.5 ± 1.5 °C in the order given in Table A.1, taking care of the warnings in the following list:

Table A.1 Order, amounts, weighting containers, purities and formula weights of reagents for preparing 1000 ml of SBF

Order	Reagent	Amount/g	Container	Purity	Formula weight
1	NaCl	8.035	Weighing paper	99.5%	58.4430
2	$NaHCO_3$	0.355	Weighing paper	99.5%	84.0068
3	KCl	0.225	Weighing bottle	99.5%	74.5515
4	$K_2HPO_4{\cdot}3H_2O$	0.231	Weighing bottle	99.0%	228.2220
5	$MgCl_2{\cdot}6H_2O$	0.311	Weighing bottle	98.0%	203.3034
6	1.0*M*-HCl	39*	Graduated cylinder	–	–
7	$CaCl_2$	0.292	Weighing bottle	95.0%	110.9848
8	Na_2SO_4	0.072	Weighing bottle	99.0%	142.0428
9	Tris	6.118	Weighing paper	99.0%	121.1356
10	1.0*M*-HCl	0 to 5*	Syringe	–	–

* ml.

- In the preparation of SBF, glass containers should be avoided. A plastic container with a smooth surface and no scratches is recommended, because apatite nucleation can be induced at the surface of a glass container or the edge of scratches. If the container has scratches, replace it with a new one.
- Never dissolve several reagents simultaneously. Dissolve a reagent only after the preceding one (if any) is completely dissolved.
- As the reagent $CaCl_2$, which has great effect on the precipitation of apatite, usually takes a granular form and takes considerable time to dissolve one granule at a time, completely dissolve one before initiation of dissolution of the next.
- Measure the volume of 1 M HCl in a cylinder after washing it with 1 M HCl.
- Measure hygroscopic reagents such as KCl, $K_2HPO_4{\cdot}3H_2O$, $MgCl_2{\cdot}6H_2O$, $CaCl_2$ and Na_2SO_4 in as short a period as possible.

Insert the electrode of the pH meter into the solution. Just before dissolving the Tris, the pH of the solution should be 2.0 ± 1.0.

Set the temperature of the solution at 36.5 ± 0.5 °C, and take care that it does not rise above 38 °C. If the volume of the solution is less than 900 ml, add ion-exchanged distilled water up to 900 ml.

With the solution temperature between 35 and 38 °C, preferably 36.5 ± 0.5 °C, dissolve the Tris into the solution little by little, taking careful note of the pH change. After adding a small amount of Tris, stop and wait until the reagent already introduced is dissolved completely and the pH has become constant; then add more Tris. Note that it is important not to add

a large amount of Tris into the solution at any one time because the radical increase in local pH of the solution can lead to the precipitation of apatite. If the solution temperature is not within 36.5 ± 0.5 °C, add Tris to raise the pH to 7.30 ± 0.05, and then stop adding it and wait for the solution temperature to reach 36.5 ± 0.5 °C. With the solution at 36.5 ± 0.5 °C, add more Tris to raise the pH to under 7.45. The pH should not pass over 7.45 at 36.5 ± 0.5 °C, taking account of the pH decrease with increasing solution temperature (the pH falls about 0.05/°C at 36.5 ± 1.5 °C).

Make sure that the temperature of the solution is maintained at 36.5 ± 0.5 °C. When the pH has risen to 7.45 ± 0.01, stop dissolving Tris, then dropwise add 1 M HCl by syringe to lower the pH to 7.42 ± 0.01, taking care that the pH does not fall below 7.40. After the pH has fallen to 7.42 ± 0.01, dissolve the remaining Tris little by little until the pH has risen to ≤7.45. If any Tris remains, add the 1 M HCl and Tris alternately into the solution. Repeat this process until the whole amount of Tris is dissolved, but keeping the pH within the range of 7.42–7.45. After dissolving the whole amount of Tris, adjust the temperature of the solution to 36.5 ± 0.2 °C. Adjust the pH of the solution by dropwise adding 1 M HCl to give a pH of 7.42 ± 0.01 at 36.5 ± 0.2 °C, and then finally adjust it to 7.40 exactly at 36.5 °C, on the condition that the rate of solution temperature increase or decrease is less than 0.1 °C/min.

Remove the pH meter electrode from the solution, rinse it with ion-exchanged distilled water and add the washings into the solution.

Pour the pH-adjusted solution from the beaker into a 1000 ml volumetric flask. Rinse the surface of the beaker with ion-exchanged distilled water several times and add the washings into the flask, fixing the stirring bar with a magnet so as to prevent it from falling into the volumetric flask.

Add ion-exchanged distilled water up to the marked line (it is not necessary to adjust exactly, because the volume becomes smaller after cooling), put a lid on the flask and close it with plastic film.

After mixing the solution in the flask, keep it in water to cool it to 20 °C.

After the solution temperature has fallen to 20 °C, add distilled water up to the marked line.

Confirmation of the ion concentrations of SBF

Prepared SBF should have the ion concentrations shown in Table 7.1. In order to confirm the ion concentrations of the SBF, chemical analysis of the SBF is recommended, because SBF is a metastable solution supersaturated with respect to apatite. Note that it is also recommended that the apatite-forming ability of standard glasses should be examined in the prepared SBF. The chemical compositions of the standard glasses are shown in Table A.2.

Table A.2 The compositions of the standard glasses in the SiO_2–Na_2O–CaO system

Standard glass	Composition/mol%		
	SiO_2	Na_2O	CaO
Glass A	50	25	25
Glass B	55	22.5	22.5
Glass C	60	20	20

When standard glasses A, B and C are soaked in SBF, an apatite layer should be detected by thin-film X-ray diffraction and/or scanning electron microscopy after soaking for 12, 24 and 120 h, respectively.

Preservation of SBF

Prepared SBF should be preserved in a plastic bottle with a tightly applied lid and kept at 5–10 °C in a refrigerator. The SBF should be used within 30 days after preparation.

7.7.2 Procedure for the apatite-forming ability test

For dense materials, measure the specimen dimensions and calculate the surface area with an accuracy of 2 mm^2 for a thin plate. Calculate the volume of SBF that is used for testing using equation (7.1):

$$V_s = S_a / 10, \tag{7.1}$$

where V_s is the volume of SBF (ml) and S_a is the apparent surface area of the specimen (mm^2). For porous materials, the volume of SBF should be greater than the calculated V_s.

Put the calculated volume of SBF into a plastic bottle or beaker. After heating the SBF to 36.5 °C, a specimen should be placed in the SBF as shown in Fig. A.1. The entire specimen should be submerged in the SBF. Note that in rare cases, apatite may homogeneously precipitate in the SBF and can thus be deposited on the surface of a specimen. Therefore, it is recommended that the specimens be placed in the SBF as shown in Fig. A.1(a) or (b). In cases of placement as shown in Fig. A.1(b), apatite formation should be examined on the lower surface of the specimen.

After soaking in the SBF at 36.5 °C for periods up to 4 weeks, remove the specimen from the SBF and gently wash it with pure water. The specimen should be dried in a desiccator without heating. Bone-bonding materials usually form apatite on their surfaces within 4 weeks. Specimens, once taken out of SBF and dried, should not be soaked again.

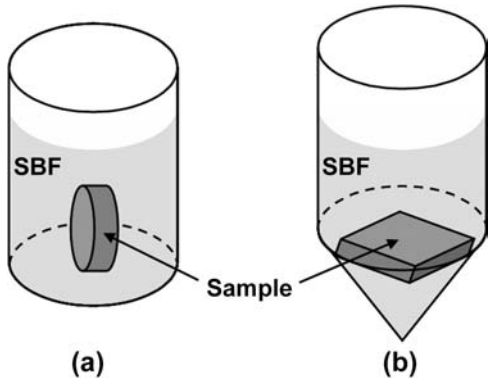

A.1 Arrangements of specimen in the SBF.

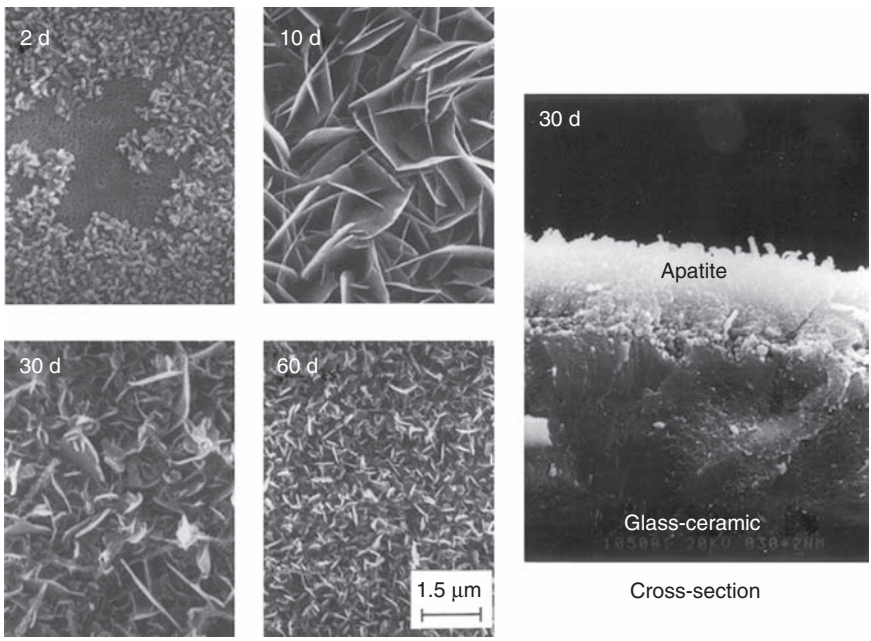

A.2 SEM pictures of surfaces and a cross-section of glass-ceramics A-W soaked in SBF for various periods (Kokubo *et al.*, 1990b).

7.7.3 Method for examining apatite formation

Apatite formation on materials in SBF is easily examined by scanning electron microscope (SEM) observation and thin-film X-ray diffraction (TF-XRD) of the specimens soaked in SBF for various periods.

In SEM observation, the dried specimen should be thinly metal-coated to induce electroconductivity. The SEM photos should be taken at both high

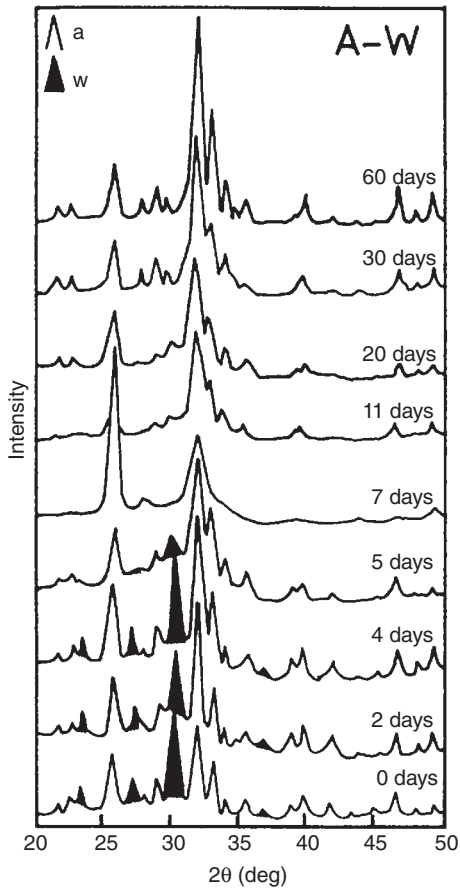

A.3 TF-XRD patterns of surfaces of glass-ceramics A-W soaked in SBF for various periods: (a) apatite, (w) wollastonite (Kokubo *et al.*, 1990b).

(around ×10 000) and low (around ×1000) magnifications. Apatite formation can be observed under SEM as a function of soaking time in SBF, as shown for glass-ceramics A-W in Fig. A.2.

TF–XRD measurement should be performed in the range of 3–50° in 2 theta (θ) using CuKa (λ = 0.154 05 nm) radiation as the source at a rate of 2°/min and with a 1° glancing angle against the incident beam on the specimen surface. Apatite formation can be detected by TF–XRD as a function of soaking time in SBF, as shown for glass-ceramic A-W in Fig. A.3.

7.8 References

Anderson Ö H, Karlsson K H (1991), 'On the bioactivity of silicate glass', *J Non-Cryst Solids*, **129**, 145–151.

Chan H, Mijares D, Ricci J L (2004), '*In vitro* dissolution of calcium sulfate: evidence of bioactivity', *Transactions of the Seventh World Biomaterials Congress*, Australian Society for Biomaterials Inc., Victoria, Australia. p. 627.

Ebisawa Y, Kokubo T, Ohura K, Yamamuro T (1990), 'Bioactivity of $CaO{\cdot}SiO_2$-based glasses: *in vitro* evaluation', *J Mater Sci Mater Med*, **1**, 239–244.

Fujibayashi S, Neo M, Kim HM, Kokubo T, Nakamura T (2003), 'Comparative study between *in vivo* bone ingrowth and *in vitro* apatite formation on Na_2O-CaO-SiO_2 glasses', *Biomaterials*, **24**, 1349–1356.

Fujita Y, Yamamuro T, Nakamura T, Kotani S, Ohtsuki C, Kokubo T (1991), 'The bonding behavior of calcite to bone', *J Biomed Mater Res*, **25**, 991–1003.

Hench L L, Splinter R J, Allen W C, Greenlee T K (1972), 'Bonding mechanisms at the interface of ceramic prosthetic materials', *J Biomed Mater Res*, **2**, 117–141.

Höland W, Vogel W, Naumann K, Gummel J (1985), 'Interface reaction between machinable bioactive glass-ceramics and bone', *J Biomed Mater Res*, **19**, 303–312.

Juhasz J A, Best S M, Bonfield W, Kawashita M, Miyata N, Kokubo T, Nakamura T (2003), 'Apatite-forming ability of glass-ceramic apatite–wollastonite–polyethylene composites: effect of filler content', *J Mater Sci Mater Med*, **14**, 489–495.

Judasz J A, Ishii S, Best S M, Kawashita M, Neo M, Kokubo T, Nakamura T, Bonfield W (2004), 'Bone-bonding ability of glass-ceramic apatite–wollastonite–polyethylene composites', *Transactions of the Seventh World Biomaterials Congress*, Australian Society for Biomaterials Inc., Victoria, Australia. p. 665.

Kato H, Nakamura T, Nishiguchi S, Matsusue Y, Kobayashi M, Miyazaki T, Kim H-M, Kokubo T (2000), 'Bonding of alkali- and heat-treated tantalum implants to bone', *J Biomed Mater Res*, **53**, 28–35.

Kim H-M, Miyaji F, Kokubo T, Ohtsuki C, Nakamura T (1995), 'Bioactivity of Na_2O-CaO-SiO_2 glasses', *J Am Ceram Soc*, **78**, 2405–2411.

Kim H-M, Miyaji F, Kokubo T, Nakamura T (1996), 'Preparation of bioactive Ti and its alloys via simple chemical surface treatment', *J Biomed Mater Res*, **32**, 409–417.

Kim H-M, Himeno T, Kawashita M, Kokubo T, Nakamura T (2004), 'The mechanism of biomineralization of bone-like apatite on synthetic hydroxyapatite: an *in vitro* assessment' *J R Soc Interface*, **1**, 17–22.

Kim H-M, Himeno T, Kokubo T, Nakamura T (2005), 'Process and kinetics of bonelike apatite formation on sintered hydroxyapatite in a simulated body fluid', *Biomaterials*, **26**, 4366–4373.

Kitsugi T, Nakamura T, Yamamuro T, Kokubo T, Shibuya T, Takagi M (1987), 'SEM-EPMA observation of three types of apatite containing glass ceramics implanted in bone: the variance of a Ca, P-rich layer', *J Biomed Mater Res*, **21**, 1255–1271.

Kokubo T (1991), 'Bioactive glass ceramics: properties and applications', *Biomaterials*, **12**, 155–163.

Kokubo T, Takadama H (2006), 'How useful is SBF in predicting *in vivo* bone bioactivity?', *Biomaterials*, **27**, 2907–2915.

Kokubo T, Kushiyani M, Ebisawa Y, Kitsugi T, Kotani S, Oura K, Yamamuro T (1988), 'Apatite formation on bioactive ceramics in body environment' in: Oonishi H, Aoki H, Sawai K, *Bioceramics*, Tokyo: Ishiyaku EuroAmerica, 157–162.

Kokubo T, Ohtsuki C, Kotani S, Kitsugi T, Yamamuto T (1990a), 'Surface structure of bioactive glass-ceramic A-W implanted into sheep and human vertebra' in G Heimke, *Bioceramics. Vol. 2*, Cologne: German Ceramic Society, 105–112.

Kokubo T, Ito S, Huang Z T, Hayashi T, Sakka S, Kitsugi T, Yamamuro T (1990b), 'Ca, P-rich layer formed on high-strength bioactive glass-ceramic A-W', *J Biomed Mater Res*, **24**, 331–343.

Kokubo T, Kushitani H, Sakka S, Kitsugi T, Yamamuro T (1990c), 'Solutions able to reproduce *in vivo* surface-structure changes in bioactive glass-ceramic A-W', *J Biomed Mater Res*, **24**, 721–734.

Kokubo T, Himeno T, Kim H-M, Kawashita M, Nakamura T (2003), 'Process of bonelike apatite formation on sintered hydroxyapatite in serum-containing protein', *Bioceramics*, *Vol. 16*, Switzerland: Tran Tech Pub, 139–142.

Kotani S, Fujita Y, Kitsugi T, Nakamura T, Yamamuro T, Ohtsuki C, Kokubo T (1991), 'Bone bonding mechanism of beta-tricalcium phosphate', *J Biomed Mater Res*, **25**, 1303–1315.

LeGeros R Z, Lin S, Rohanizadeh R, Mijares D, LeGeros J P (2003), 'Biphasic calcium phosphate bioceramics: preparation, properties and applications', *J Mater Sci Mater Med*, **14**, 201–209.

Li P, Ohtsuki C, Kokubo T, Nakanishi K, Soga N, Nakamura T, Yamamuro T (1992), 'Apatite formation induced on silica gel in a simulated body fluid', *J Am Ceram Soc*, **75**, 2094–2097.

Li P, Ohtsuki C, Kokubo T, Nakanishi K, Soga N, de Groot K (1994), 'The role of hydrated silica, titania, and alumina in inducing apatite on implants', *J Biomed Mater Res*, **28**, 7–15.

Miyazaki T, Kim HM, Miyaji F, Kokubo T, Kato H, Nakamura T (2000), 'Bioactive tantalum metal prepared by NaOH treatment', *J Biomed Mater Res*, **50**, 35–42.

Miyazaki T, Kim H-M, Kokubo T, Kato H, Nakamura T (2001a), 'Induction and acceleration of bonelike apatite formation on tantalum oxide gel in simulated body fluid', *J Sol-Gel Sci Technol*, **21**, 83–88.

Miyazaki T, Kim H-M, Kokubo T, Ohtsuki C, Kato H, Nakamura T (2001b), 'Apatite-forming ability of niobium oxide gels in a simulated body fluid', *J Ceram Soc Japan*, **109**, 929–933.

Neo M, Kotani S, Nakamura T, Yamamuro T, Ohtsuki C, Kokubo T, Bando Y (1992), 'A comparative study of ultrastructures of the interfaces between four kinds of surface-active ceramic and bone', *J Biomed Mater Res*, **26**, 1419–1432.

Neo M, Nakamura T, Ohtsuki C, Kokubo T, Yamamuro T (1993), 'Apatite formation on three kinds of bioactive material at an early stage *in vivo*: a comparative study by transmission electron microscopy', *J Biomed Mater Res*, **27**, 999–1006.

Neuman W, Neuman M (1958), *The Chemical Dynamics of Bone Mineral*, Chicago, IL: University of Chicago, p. 34.

Nishiguchi S, Fujibayashi S, Kim H-M, Kokubo T, Nakamura T (2003), 'Biology of alkali- and heat-treated titanium implants', *J Biomed Mater Res A*, **67**, 26–35.

Ogino M, Ohuchi F, Hench L L (1980), 'Compositional dependence of the formation of calcium phosphate films on bioglass', *J Biomed Mater Res*, **14**, 55–64.

Ohtsuki C, Aoki Y, Kokubo T, Fujita Y, Kotani S, Yamamuro T (1989), 'Bioactivity of limestone and abalone shell', *Transactions of the 11th Annual Meeting of Japanese Society for Biomaterials*, 27–28 October 1989, Kyoto, Japan. p. 12.

Ohtsuki C, Kushitani H, Kokubo T, Kotani S, Yamamuro T (1991a), 'Apatite formation on the surface of Ceravital-type glass-ceramic in the body', *J Biomed Mater Res*, **25**, 1363–1370.

Ohtsuki C, Kokubo T, Neo M, Kotani S, Yamamuro T, Nakamura T, Bando Y (1991b) 'Bone-bonding mechanism of sintered β-3CaO-P_2O_5', *Phos Res Bull*, **1**, 191–196.

Ohura K, Nakamura T, Yamamuro T, Kokubo T, Ebisawa Y, Kotoura Y, Oka M (1991), 'Bone-bonding ability of P_2O_5-free CaO–SiO_2 glasses', *J Biomed Mater Res*, **25**, 357–365.

Oyane A, Onuma K, Ito A, Kim HM, Kokubo T, Nakamura T (2003a), 'Formation and growth of clusters in conventional and new kinds of simulated body fluids', *J Biomed Mater Res*, **64A**, 339–348.

Oyane A, Kim HM, Furuya T, Kokubo T, Miyazaki T, Nakamura T (2003b). 'Preparation and assessment of revised simulated body fluids', *J Biomed Mater Res*, **65A**, 188–195.

Takadama H, Kim H-M, Kokubo T, Nakamura T (2001), 'Mechanism of biomineralization of apatite on a sodium silicate glass: TEM-EDX study *in vitro*', *Chem Mater*, **13**, 1108–1113.

Takadama H, Kim H-M, Kokubo T, Nakamura T (2002), 'X-ray photoelectron spectroscopy study on the process of apatite formation on a sodium silicate glass in simulated body fluid', *J Am Ceram Soc*, **85**, 1933–1936.

Takadama H, Hashimoto M, Mizuno M, Kokubo T (2004), 'Round-robin test of SBF for *in vitro* measurement of apatite-forming ability of synthetic materials', *Phos Res Bull*, **17**, 119–125.

Tanahashi M, Matsuda T (1997), 'Surface functional group dependence on apatite formation on self-assembled monolayers in a simulated body fluid', *J Biomed Mater Res*, **34**, 305–315.

Uchida M, Kim H-M, Kokubo T, Nakamura T (2001), 'Bonelike apatite formation induced on zirconia gel in simulated body fluid and its modified solutions', *J Am Ceram Soc*, **84**, 2041–2044.

Virolainen P, Heikkila J, Yli-Urpo A, Vuorio E, Aro HT (1997), 'Histomorphometric and molecular biologic comparison of bioactive glass granules and autogenous bone grafts in augmentation of bone defect healing', *J Biomed Mater Res*, **35**, 9–17.

Wang XX, Hayakawa S, Tsuru K, Osaka A (2001), 'A comparative study of *in vitro* apatite deposition on heat-, H_2O_2-, and NaOH-treated titanium surfaces', *J Biomed Mater Res*, **54**, 172–178.

8

Osteoconduction and its evaluation

T NAKAMURA and M TAKEMOTO, Kyoto University, Japan

8.1 Introduction

Originally, osteoconduction referred to the bone graft healing process that provided scaffolding for the ingrowth of vessels and osteoprogenitor cells for the purpose of graft incorporation by the host (known as creeping substitution) (Goldberg and Stevenson, 1987; Davies and Hosseini, 1999). The protein matrix and mineral phase of a bone graft (i.e., autograft and allograft) provide this quality. In the field of biomaterials, Wilson-Hench suggested a definition of osteoconduction as a process where bone is directed to conform to a material's surface (Wilson-Hench, 1987). Today, osteoconduction is generally interpreted to mean the apparent growth of bone tissue 'along' an implant's surface (Jarcho, 1981; Davies and Hosseini, 1999). Many materials can be used as osteoconductive materials, and more are being developed. These include processed human bone ('allograft bone'), purified collagen, Bioglass, several calcium phosphate ceramics, and glass ceramic A-W. Titanium-based metals are nearly bioinert materials that possess limited osteoconductivity, and therefore we recently developed specific chemical and thermal treatments whereby the osteoconductivity of titanium metal is effectively enhanced due to the formation of a bioactive titania surface layer (Kokubo *et al.*, 1996; Kim *et al.*, 1999; Nishiguchi *et al.*, 1999, 2001a,b, 2003; Fujibayashi *et al.*, 2001; Uchida *et al.*, 2002; Takemoto *et al.*, 2005). Osteoconduction is now recognized as being essential for stable long-term orthopedic and dental implants.

Osteoinduction, as opposed to osteoconduction, is a biological process that induces local mesenchymal cells to differentiate into bone-producing cells. Urist (1965) and Urist and Strates (1971) introduced this concept after initial studies on the osteoinductive properties of demineralized bone matrix (DBM) and bone morphogenetic protein (BMP). Autogenous bone is thought to provide both of these functions. When some osteoconductive biomaterials have a specific porous structure, they are known to become osteoinductive in soft tissues without the addition of osteogenic cells or

BMPs (Yamasaki and Sakai, 1992; Ripamonti *et al.*, 1993; Yang *et al.*, 1996; Yuan *et al.*, 2001; Fujibayashi *et al.*, 2004). The osteoinductivity of biomaterials is discussed in the following chapter.

8.2 The mechanism of osteoconduction

In observations of bone ingrowths into porous or tube-shaped implants, bone appears to 'grow', or spread, into deeper pores. However, bone matrix has no inherent capacity to grow or to spread (Davies and Hosseini, 1999). What is invading the porous implant or spreading the implant surface is a population of migratory capillaries, fibrovascular tissues and osteogenic cells, which is followed by the later development of new bone formation. In this process, no intermediate fibrocartilaginous stage occurs. Similar to primary fracture healing with stable osteosynthesis, the clinical success of fixation by osteoconduction depends on a stable implant–bone interface.

Osteogenic cells, which generally work much better when they have a matrix or scaffold to attach to, may originate either in pre-existing pre-osteoblasts or osteoblasts that are activated by trauma, or in cells recruited from primitive mesenchymal cells by osteoinduction (Frost, 1989a,b). Therefore, the anatomical location and the condition of the implant bed, as well its biomaterial properties, have a strong influence on the process of osteoconduction. In particular, in the absence of a proper blood supply from the surrounding tissue, bone growth, including bone conduction, does not occur (Albrektsson and Johansson, 2001).

In addition to the surrounding tissue conditions, there are three important features of the osteoconductivity of the biomaterials: the surface chemistry, the surface topography and the architectural geometry (i.e. the porous structure). Regarding the surface chemistry, bioactive materials (see Chapter 7), such as calcium phosphate ceramics, possess a high osteoconductivity compared to the nearly bioinert materials (e.g. titanium metal) having limited osteoconductivity. The second important parameter to consider is the organization of the surface topography. *In vitro*, many authors have demonstrated the phenomenon of contact guidance of osteoblasts (Anselme, 2000). On smooth surfaces, bone cells are randomly oriented. In 5 μm grooves, they are aligned parallel to the direction of the grooves, while they are not in 0.5 μm grooves (Chesmel *et al.*, 1995). *In vivo*, the use of a roughened surface also provides an enhanced bone-implant apposition and implant fixation strength (Goldberg *et al.*, 1995; Wennerberg *et al.*, 1997; Buser *et al.*, 1999; Hacking *et al.*, 2003; Takemoto *et al.*, 2006). The third important feature of osteoconductivity is a porous implant structure, whose size, extent and interconnectivity allow for bony ingrowths and the invasion of blood vessels. Several investigators have studied bone ingrowths into porous materials with different pore sizes (Hulbert *et al.*, 1970; Bobyn *et al.*,

1980; Cook *et al.*, 1985), and the consensus seems to be that the optimum pore size for bone ingrowths is 100–400 μm. As computer technology advances, high-resolution X-ray microcomputer tomography (micro-CT) has recently become available, and this technique provides a practical solution to the analysis of porous structures (Atwood *et al.*, 2004; Moore *et al.*, 2004; Ho and Hutmacher, 2006; Otsuki *et al.*, 2006). It has been suggested that narrow pore throats in the interconnectivity have an adverse effect on tissue differentiation in the pores (Otsuki *et al.*, 2006).

8.3 Monitoring osteoconduction

Osteoconductive ability is not absolute, and should be compared using a comparative study in which the variables comprising of the substrate material, porous structure, surface topography and surface chemistry are highly controlled (Bauer and Muschler, 2000). For example, when matched by size, shape and surface texture, hydroxyapatite is more osteoconductive than titanium (Hacking *et al.*, 2002), and titanium is more osteoconductive than a similar segment of CoCr alloy or stainless steel.

Considering that osteoconduction refers to the apparent growth of bone 'along' an implant's surface, we should perform quantitative assessment of osteoconductivity by measuring the bone ingrowth and apposition. The fraction of bone area in a porous area available for bone ingrowth is calculated (the bone area ingrowth) to assess bone ingrowth, and to assess bone apposition, the fraction of bone in contact with the outer perimeter of the implant is also calculated (the bone–implant contact). These calculations are preferably carried out using bone histomorphometric methods utilizing an optical microscope (Fig. 8.1a and c). For accurate analysis, it is important to prepare thin histological sections. However, in general, preparing thin sections containing metallic or ceramic implants is difficult using conventional grinding techniques. Thicker sections show a shadow effect that makes it difficult to state whether or not true direct bone contact has been achieved, and to evaluate bone area ingrowth accurately (Albrektsson and Johansson, 2001). Incident-light fluorescence microscopy provides for a more accurate image (Fig. 8.1b and d), and backscattered electron imaging in a scanning electron microscope (BSE-SEM) is the most preferable methods to evaluate bone–implant contact and osteoconduction (Fig. 8.1e) (Boyde and Wolfe, 1999).

8.4 Approaches to encourage osteoconduction

Bioactive materials, including Bioglass, hydroxyapatite (HA), other calcium phosphate-based biomaterials and glass-ceramic A-W, can bond to living bone directly (Hench and Wilson, 1993), and they generally possess high

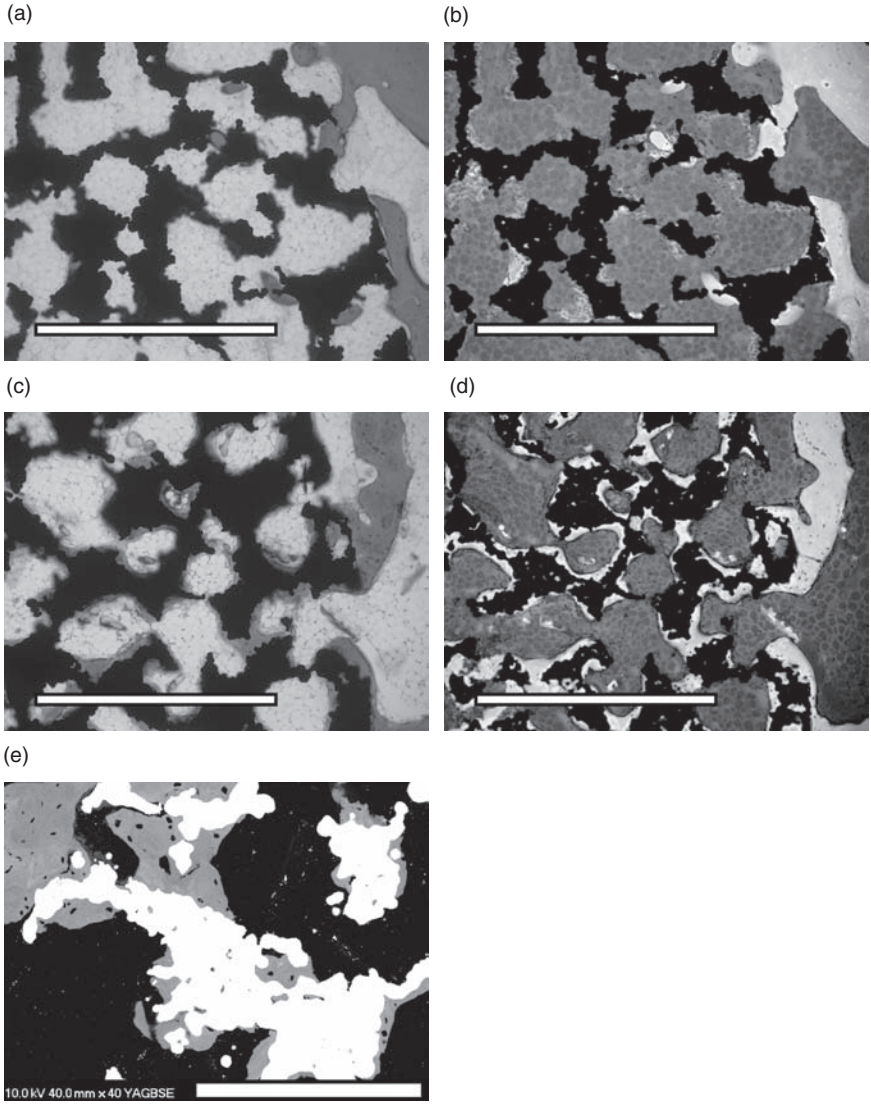

8.1 Histological observation of bone ingrowth using various methods. Optical microscope photographs (a and c), incident-light fluorescence microscopic photographs (b and d), and a BSE-SEM photograph (e) of histological slides of porous titanium implanted into rabbit femoral condyle for a period of 6 weeks. Here (a, b) = untreated porous titanium; (c, d, e) = chemically and thermally treated porous titanium. The scale bar = 1000 μm. The stain used in a–d was Stevenel's blue and van Gieson's picrofuchsin. The apparent growth of bone 'along' the implant surface (osteoconduction) can be seen in the chemically and thermally treated porous titanium (c, d, e), while it is less evident in the untreated porous titanium (a, b). A comparison of the optical microscopy (a, c), incident-light fluorescence microscopy (b, d), and BSE-SEM microscopy (e) is more accurate in evaluating bone-implant contact.

osteoconductivity. However, except for glass-ceramic A-W, their mechanical properties are not adequate for load-bearing conditions. Therefore, most orthopedic load-bearing devices (such as total hips, total knees and spinal fusion cages) and dental implants are made of more mechanically strong bioinert materials, such as stainless steel, titanium alloys, alumina ceramics and zirconia ceramics. Because true bonding between these materials and bone is rarely achieved, many approaches have been reported to encourage bioactivity and osteoconductivity in these materials.

One approach to increase osteoconduction is to coat the implant surface with various calcium phosphates (chemical alteration), and plasma-sprayed calcium phosphate coatings are one of the most extensively examined methods, the efficiency of which has been confirmed by many reports (Geesink *et al.*, 1988; Jasty *et al.*, 1992). Plasma-sprayed hydroxyapatite coatings for total joint arthroplasty have been in clinical use since the mid-1980s (Geesink, 2002). Geesink *et al.* reported a clinical survival rate of 97% in a series with a minimum of 11 years' follow-up for the femoral component of a total hip arthroplasty in a young active patient population (average age = 53 years) (Geesink, 2002).

There are some concerns with plasma-sprayed hydroxyapatite coatings. One is the relatively poor bonding between the substrate and the plasma-sprayed coating. The high residual stress resulting from the mismatch in the thermal expansion coefficients of the HA coating ($13.3 \times 10^{-6} K^{-1}$) and the titanium substrate ($8.4–8.8 \times 10^{-6} K^{-1}$) is thought to be responsible for the low bonding strength between the two materials (Liu *et al.*, 2004). Another concern is the resorption and degradability of HA coatings in biological environments. These may lead to disintegration of the coating, resulting in the loss of both the coating–substrate bonding strength and the implant fixation. During plasma spraying, the molten HA particles deposited on the metal substrate are quenched at a high cooling rate, leading to the formation of amorphous calcium phosphate compounds and a reduction in the crystallinity of the coating. The amorphous and metastable compounds are more soluble than the crystalline HA is, and this accelerates fixation of the implant onto the bone and promotes bone remodeling and attachment (Nagano *et al.*, 1996). However, from the perspective of long-term performance of the implant, a high degree of crystallinity in the plasma-sprayed HA coating is deemed desirable.

Being a line-of sight process, plasma-sprayed calcium phosphate coatings have difficulty in coating the inside of three-dimensional structures, such as cages, porous materials and other complex shapes. Another suitable coating is the so-called biomimetic coating, in which a bone-like apatite layer is produced by immersion of a metal substrate into a simulated body fluid (SBF) (Abe *et al.*, 1990). This technique allows for the homogeneous deposition of a calcium phosphate layer within a porous implant, and thus, treated

implants show excellent osteoconductivity (Barrere *et al.*, 2003; Habibovic *et al.*, 2005; Takemoto *et al.*, 2006), although the relatively poor bonding between the coating and substrate is still an issue of concern.

Another approach to encourage osteoconduction is based on surface topography alterations. Bioactive materials are osteoconductive, even with smooth surfaces. However, bioinert materials combined with a micro-rough surface, also exhibit the phenomenon of bone apposition, which is similar to osteoconduction (Hacking *et al.*, 2002). This phenomenon can be explained by a cell–material interaction, where the material's surface topography is known to be important for cell orientation and migration (Anselme, 2000). The osteoblastic phenotype and the degree of bone contact have been shown to be responsive to topography, with polished surfaces producing lower levels of material–bone contact, and bone formation is preferentially observed at the base of grooves and crevices (Gray *et al.*, 1996). Thus, bioactive materials with an enhanced osteoblast response due to surface topographic alteration are expected to form a new approach for improved tissue repair and implant lifespan (Dalby *et al.*, 2002). Many methods have been reported that produce micro-rough surfaces, such as blasting (Goldberg *et al.*, 1995; Wennerberg *et al.*, 1997), chemical etching (Hacking *et al.*, 2003; Takemoto *et al.*, 2006) and both techniques (Buser *et al.*, 1999). These methods create irregular surface features of the order of several micrometers to submicrometer scale. Such treated implants with a micro-rough surface have been shown experimentally and clinically to be rigidly fixed by bone apposition or ingrowths, which are widely used in dental applications (Cochran *et al.*, 2002).

Recently, we have developed a chemical and thermal treatment that converts the surface of titanium and titanium-alloy implants into bioactive surfaces (Kokubo *et al.*, 1996; Kim *et al.*, 1999; Nishiguchi *et al.*, 1999, 2001a,b, 2003; Fujibayashi *et al.*, 2001; Uchida *et al.*, 2002; Takemoto *et al.*, 2005). In this method, a titanium surface is converted into titania with a microporous surface, and this can form a bone-like apatite layer on the implant surface *in vivo* and *in vitro* when soaked in a simulated body fluid (Abe *et al.*, 1990; Kokubo *et al.*, 1990), similar to Bioglass, hydroxyapatite and glass-ceramic A-W (see Chapters 7 and 21). Through this bioactive surface, chemically and thermally treated titanium possesses a bone-bonding ability, which has been confirmed by detachment tests (Nishiguchi *et al.*, 1999, 2001a; Fujibayashi *et al.*, 2001). The osteoconductivity of porous titanium implants is greatly enhanced using this chemical and thermal treatment (Nishiguchi *et al.*, 2001b; Takemoto *et al.*, 2005) (Fig. 8.1). Chemically and thermally treated titanium total hip prosthesis implants are now under clinical trials in our institute.

With the development of surface engineering, many other basic studies into methods for enhancing the osteoconductivity of biomaterials have

been reported, including alternate soaking process (Taguchi *et al.*, 1998), anodic oxidation for titanium (Liang *et al.*, 2003; Yang *et al.*, 2004) and others. The use of proper surface treatments will expand the application range of osteoconductive materials to satisfy clinical needs.

8.5 Evaluation of the bonding strength using pushout test and tensile test

The direct apposition of bone onto an implant's surface is the desired clinical outcome for peri-implant healing, because it provides the necessary mechanical stability and anchorage of the orthopedic implants and dental endosseous implants to allow load-bearing functions. *In vivo*, bone–implant bonding is achieved by either bioactivity (chemical bonding) or mechanical interlocking by a micro-rough surface, which is strictly related to osteoconduction. Since a major purpose in implant-related research in orthopedic and dental surgery is to achieve a proper fixation of the implant into the surrounding bone, a mechanical test that actually measures the implant fixation is desired (Dhert and Jansen, 1999). Various test methods are now available for the mechanical evaluation of retrieved implants. Pushout and detachment tests are simple tests that can easily be performed using low-cost instrumentation. Pushout tests measure the force required to move an implant in the surrounding bone, and allow for the calculation of the so-called pushout strength. In detachment tests, where a load is applied in the direction perpendicular to the tissue biomaterial interface, the direct bonding strength between the bone and the biomaterial can be measured. In both tests, the strength depends on three factors. One is the adhesive strength between the bone and the implant, which is related to the bioactivity and mechanical interlocking. The second is the mechanical strength of the treated surface, and the third is the mechanical strength of the substrate material. After testing, we can determine which factor (surface bioactivity, mechanical strength of the treated surface, or the mechanical strength of the substrate) should be improved on by observation of the test sample.

8.5.1 Pushout test method (Nishiguchi's method: Nishiguchi *et al.,* 2001a,b)

Cylindrical implants (diameter = 6 mm, length = 13 mm) were prepared for experiments, and the implant materials were evaluated *in vivo* using the hemi-transcortical cylindrical model in dogs. Adult female beagle dogs weighing 10–12 kg were used. The animals were anesthetized using an intramuscular administration of ketamine hydrochloride (50 mg/kg) followed by diazepam (5 mg) and atropine sulfate (0.5 mg). Just before the operation, an

additional dose of 30 mg/kg ketamine hydrochloride was injected intramuscularly. The operations were performed in the usual sterilized manner. The dogs were placed in the right decubitus position, and a lateral skin incision was made on the left thigh, exposing the middiaphyseal region of the left femur. Using a drill bit, a 6.1 mm diameter hemi-transcortical cylindrical hole was made, and just before insertion of the implants, the hole was irrigated with saline containing ipasemycin sulfate to remove any shards of bone. The implant was then inserted through the unilateral cortex, and seated into place as tightly as possible using finger pressure. Each implant was inserted with its center located 1.4 cm away from the next implant. Seven implants were inserted into each femur (Fig. 8.2a). The fascia and the subcutaneous layers were then closed with silk sutures, and the skin was closed with skin staples. The surgical procedures were performed bilaterally. At a given post-implantation time, the dogs were killed with an overdose of intravenous pentobarbital sodium and both femora were retrieved.

The implants were numbered from 1 (proximal) to 7 (distal) (Fig. 8.2a). Each extracted femur was cut into pieces, perpendicular to its axis, with each piece containing one implant. The bones containing Implants 2–6 were then split longitudinally (Fig. 8.2b). The bones containing Implants 1 and 7 were prepared for histological examination. In the pushout tests, each implant-containing bone sample was mounted on a special metal platform with a central circular opening, which supported the bone to within 1 mm

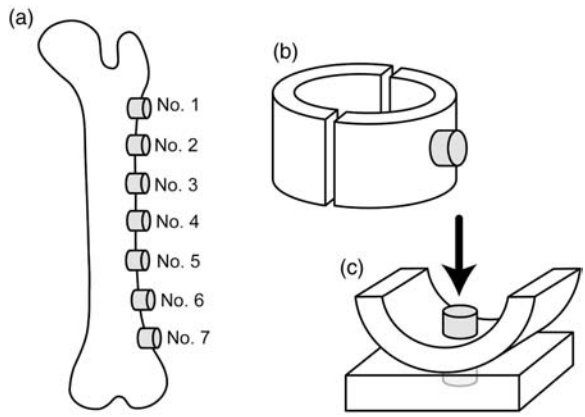

8.2 Implantation method and sample preparation for pushout tests. (a) Evenly spaced implants were implanted into each femur through the lateral cortex only. (b) The extracted femora were cut into pieces, orientated perpendicular to the axis, with each piece containing one implant. (c) The pushout test. The support jig was arranged so that the pushing load was applied perpendicular to the end of each implant.

of the bone–implant interface. This jig was designed to keep the pushing load parallel to the long axis of the implant (Fig. 8.2c). The pushing load was applied to the end of the implant using a Shimadzu Model AG-10 TB universal testing machine (Shimazdu, Kyoto, Japan) employing a crosshead speed of 0.5 mm/min until the peak load was obtained. The thickness of the cortical bone in contact with the implant was measured at two sites for each pushout sample. The average thickness was calculated and used to determine the contact area according to the following formula: interface area = 3.14 × implant diameter (6 mm) × average cortical thickness. The shear strength at the interface was calculated by dividing the load at failure by the interfacial area.

8.5.2 Practical recommendations for pushout testing

Pushout testing can be effective in demonstrating differences in the interfacial bonding strength of various types of bone implant. However, no standard method is available, and we should not consider that tests performed by various investigators in different experiments are comparable. Therefore, it has to be recommended that researchers use a strictly designed protocol for their mechanical tests, and mention as much detail as possible (Dhert and Jansen, 1999). Moreover, to obtain the best possible impression about an implant fixation, it is recommended to combine mechanical tests with histomorphometrical measurements.

8.5.3 Detachment test method (Nakamura's detaching test: Nakamura *et al.,* 1985; Nakamura and Nishiguchi, 1999)

The biomaterial to be tested was shaped into a $15 \times 10 \times 2\,mm^3$ rectangular plate. The implants were sterilized using a conventional ethylene oxide gas process and implanted into the metaphyses of the tibiae of mature male Japanese white rabbits weighing 2.8–3.2 kg. The rabbits were anesthetized with intravenous injections of pentobarbital sodium (0.5 ml/kg), an intramuscular injection of ketamine hydrochloride (10 mg/kg) and local administration of a solution of 0.5% lidocaine. After shaving, disinfection and draping, a straight 3 cm skin incision was made over the medial side of the knee, and the fascia and periosteum were incised and retracted to expose the tibial cortex. Using a dental burr, a $16 \times 2\,mm^2$ hole was made from the medial to the lateral cortex running parallel to the longitudinal axis of the tibial metaphysis. After irrigation of the hole with saline, the ceramic plates were implanted in a frontal direction, perforating the tibia and protruding from the medial to the lateral cortex (Fig. 8.3a). The fascia and skin were

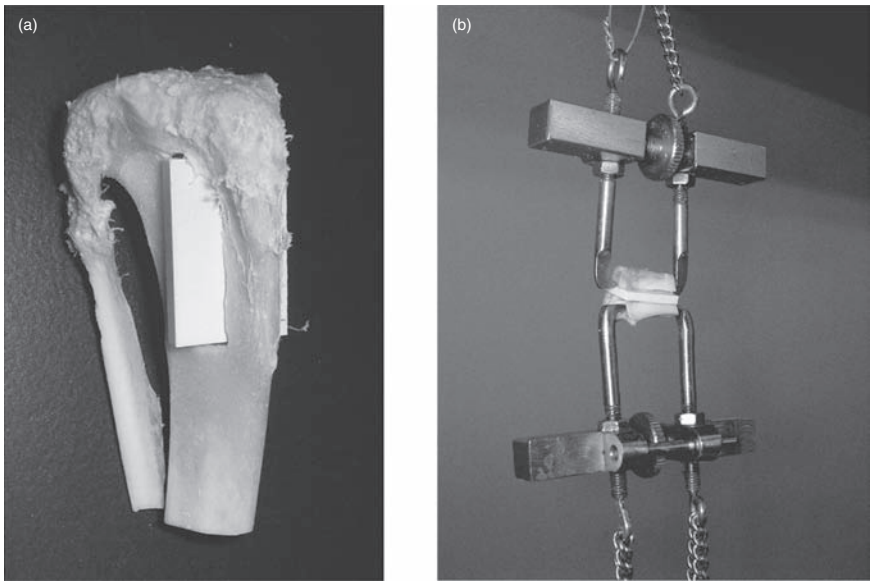

8.3 Photographs of rabbit tibiae in the detaching test. (a) Implanted rabbit tibia. (b) Application of a tensile load by holding the anterior and posterior cortices until detachment occurred. Care was taken so that traction was applied perpendicular to the surface of the implant by adjusting the apparatus.

closed in layers. The surgical procedures were performed bilaterally. At a given post-implantation time, the rabbits were killed with an overdose of intravenous pentobarbital sodium.

After death, segments of the proximal tibial metaphyses containing the implanted plates were retrieved and prepared for the detaching tests. The bone tissue surrounding the plates was removed on both sides and at the ends using a dental burr. Traction was applied through hooks holding the bone segments using a crosshead speed of 35 mm/min using an Instron-type autograph (Model 1011, Aikoh Engineering Co., Ltd, Nagoya, Japan) (Fig. 8.2b). Care was taken so that the strain is applied perpendicular to the surface of the implant, by carefully adjusting the apparatus. The detaching failure load was measured when the plate was detached from the bone. If the plate was detached before the test, then the failure load was defined as zero newtons.

8.5.4 Detachment strength of various biomaterials

As the detaching test is simple, and the results are consistent, clear and easy to compare, this test is considered particularly useful as an initial procedure

for evaluating bone–implant bonding. We can compare bone-bonding strengths with previously reported data on bioactive coatings on titanium alloy and bulk biomaterials. Since 1985, when Nakamura *et al.* developed this test method, several different researchers at Kyoto University have carried out this test to evaluate the bone-bonding strength of different biomaterials, such as bioactive ceramics (Nakamura *et al.*, 1985; Kitsugi *et al.*, 1996), nearly bioinert ceramics (Nakamura *et al.*, 1985), titanium alloy (Takatsuka *et al.*, 1995), titanium alloy coated with bioactive materials (Takatsuka *et al.*, 1995) and chemically and thermally treated titanium metal (Nishiguchi *et al.*, 1999; Fujibayashi *et al.*, 2001). The results are summarized in Table 8.1.

8.6 Summary

Today, osteoconduction is generally accepted to mean the apparent growth of bone tissue 'along' an implant's surface. Many materials are available as osteoconductive materials, and more are being developed. In osteoconduction, a population of migratory capillaries, fibrovascular tissues and osteogenic cells invade the porous implant or spread over the implant surface, which is followed by the later development of new bone formation. In this process, osteogenic cells generally work much better when they have a matrix or scaffold to attach to. The anatomical location and the condition of the implant bed, as well as the biomaterial properties, have a strong influence of the process of osteoconduction.

With regards to the material properties, there are three important features of the osteoconductivity of the biomaterials: the surface chemistry, the surface topography and the architectural geometry (porous structure), which should be compared using a comparative study in which the variables of these properties are highly controlled. In such studies, bone area ingrowth and bone–implant contact are calculated using bone histomorphometric methods.

Many approaches have been reported to encourage bioactivity and osteoconductivity of bioinert materials, such as titanium. In the chemical alteration approach, plasma-sprayed calcium phosphate coatings or biomimetic coatings are performed. In the surface topography alteration approach, many methods have been reported that produce a micro-rough surface, including blasting, chemical etching and both techniques. Chemical and thermal treatments that convert the surface of titanium and titanium–alloy implants into bioactive surfaces have recently become available, where the surface of the titanium metal is converted into titania with microporous surface.

In vivo, bone–implant bonding is achieved by either bioactivity (chemical bonding) or mechanical interlocking through a micro-rough surface, which

Table 8.1 Detaching strength of various biomaterials

	4 weeks	8 weeks	10 weeks	16 weeks	25 weeks
AW glass-ceramic (AW-GC) (Nakamura *et al.*, 1985)		7.43 kgf			8.15 kgf
Dense hydroxyapatite (Nakamura *et al.*, 1985)		6.28 kgf			7.90 kgf
45S5 Bioglass (Nakamura *et al.*, 1985)		2.75 kgf			
Alumina (Nakamura *et al.*, 1985)		0.13 kgf			
ß-Tricalcium phosfate (Kitsugi *et al.*, 1996)			31.65 N		47.04 N
Ti6Al4V (Takatsuka *et al.*, 1995)	0.0014 kgf	0.0029 kgf		0.334 kgf	2.852 kgf
Bioglass-coated Ti6Al4V (Takatsuka *et al.*, 1995)		1.04 kgf		2.72 kgf	
AW-coated Ti6Al4V (Takatsuka *et al.*, 1995)		2.03 kgf		2.39 kgf	
TCP-coated Ti6Al4V (Takatsuka *et al.*, 1995)		3.91 kgf		4.23 kgf	
Pure titanium (Nishiguchi *et al.*, 1999)	0 N	0.02 kgf		0.33 kgf	0.237 N
(Fujibayashi *et al.*, 2001)		0 N		0.388 N	
Alkali- and heat-treated Ti (Nishiguchi *et al.*, 1999)	0.688 N	2.71 kgf		4.13 kgf	53.875 N
(Fujibayashi *et al.*, 2001)		14.438 N		29.60 N	
Sodium-free alkali and heat-treated Ti (Fujibayashi *et al.*, 2001)	12.713 N	20.488 N		18.562 N	13.550 N

is strictly related to osteoconduction. In pushout and detachment tests, the strength of direct bonding between bone and the biomaterial can be measured, where the strength depends on the surface bioactivity, the mechanical strength of the treated surface and the mechanical strength of the material substrate.

8.7 References

Abe Y, Kokubo T & Yamamuro T (1990), 'Apatite coating on ceramics, metals and polymers utilizing a biological process', *J Mater Sci Mater Med*, **1**, 239–244.

Albrektsson T & Johansson C (2001), 'Osteoinduction, osteoconduction and osseointegration', *Eur Spine J*, **10** Suppl 2, S96–101.

Anselme K (2000), 'Osteoblast adhesion on biomaterials', *Biomaterials*, **21**, 667–681.

Atwood R C, Jones J R, Lee P D & Hench L L (2004), 'Analysis of pore interconnectivity in bioactive glass foams using X-ray microtomography', *Scripta Mater*, **51**, 1029–1033.

Barrere F, van der Valk C M, Meijer G, Dalmeijer R A, de Groot K & Layrolle P (2003), 'Osteointegration of biomimetic apatite coating applied onto dense and porous metal implants in femurs of goats', *J Biomed Mater Res*, **67B**, 655–665.

Bauer T W & Muschler G F (2000), 'Bone graft materials. An overview of the basic science', *Clin Orthop*, 10–27.

Bobyn J D, Pilliar R M, Cameron H U & Weatherly G C (1980), 'The optimum pore size for the fixation of porous-surfaced metal implants by the ingrowth of bone', *Clin Orthop Relat Res*, 263–270.

Boyde A & Wolfe L A (1999), 'Spatial and temporal patterns of bone growth around endosseous implants: a critical study of microscopic methods', in Davies J E, *Bone Engineering*, Toronto, em squared incorporated, 321–331.

Buser D, Nydegger T, Oxland T, Cochran D L, Schenk R K, Hirt H P, Snetivy D & Nolte L P (1999), 'Interface shear strength of titanium implants with a sandblasted and acid-etched surface: a biomechanical study in the maxilla of miniature pigs', *J Biomed Mater Res*, **45**, 75–83.

Chesmel K D, Clark C C, Brighton C T & Black J (1995), 'Cellular responses to chemical and morphologic aspects of biomaterial surfaces. II. The biosynthetic and migratory response of bone cell populations', *J Biomed Mater Res*, **29**, 1101–1110.

Cochran D L, Buser D, ten Bruggenkate C M, Weingart D, Taylor T M, Bernard J P, Peters F & Simpson J P (2002), 'The use of reduced healing times on ITI implants with a sandblasted and acid-etched (SLA) surface: early results from clinical trials on ITI SLA implants', *Clin Oral Implants Res*, **13**, 144–153.

Cook S D, Walsh K A & Haddad R J, Jr. (1985), 'Interface mechanics and bone growth into porous Co-Cr-Mo alloy implants', *Clin Orthop Relat Res*, 271–280.

Dalby M J, Di Silvio L, Gurav N, Annaz B, Kayser M V & Bonfield W (2002), 'Optimizing HAPEX topography influences osteoblast response', *Tissue Eng*, **8**, 453–467.

Davies J E & Hosseini M M (1999), 'Histodynamics of endosseous wound healing', in Davies J E, *Bone Engineering*, Toronto, em squared incorporated, 1–14.

Dhert W J A & Jansen J A (1999), 'The validity of a single pushout test', in An Y H & Draughn R A, *Mechanical Testing of Bone and the Bone–Implant Interface*, Boca Raton, CRC Press LLC, 477–488.

Frost H M (1989a), 'The biology of fracture healing. An overview for clinicians. Part I', *Clin Orthop Relat Res*, 283–293.

Frost H M (1989b), 'The biology of fracture healing. An overview for clinicians. Part II', *Clin Orthop Relat Res*, 294–309.

Fujibayashi S, Nakamura T, Nishiguchi S, Tamura J, Uchida M, Kim H M & Kokubo T (2001), 'Bioactive titanium: effect of sodium removal on the bone-bonding ability of bioactive titanium prepared by alkali and heat treatment', *J Biomed Mater Res*, **56**, 562–570.

Fujibayashi S, Neo M, Kim H M, Kokubo T & Nakamura T (2004), 'Osteoinduction of porous bioactive titanium metal', *Biomaterials*, **25**, 443–450.

Geesink R G (2002), 'Osteoconductive coatings for total joint arthroplasty', *Clin Orthop Relat Res*, 53–65.

Geesink R G, de Groot K & Klein C P (1988), 'Bonding of bone to apatite-coated implants', *J Bone Joint Surg Br*, **70**, 17–22.

Goldberg V M & Stevenson S (1987), 'Natural history of autografts and allografts', *Clin Orthop Relat Res*, 7–16.

Goldberg V M, Stevenson S, Feighan J & Davy D (1995), 'Biology of grit-blasted titanium alloy implants', *Clin Orthop Relat Res*, 122–129.

Gray C, Boyde A & Jones S J (1996), 'Topographically induced bone formation *in vitro*: implications for bone implants and bone grafts', *Bone*, **18**, 115–123.

Habibovic P, Li J, Van Der Valk C M, Meijer G, Layrolle P, Van Blitterswijk C A & De Groot K (2005), 'Biological performance of uncoated and octacalcium phosphate-coated Ti6Al4V', *Biomaterials*, **26**, 23–36.

Hacking S A, Tanzer M, Harvey E J, Krygier J J & Bobyn J D (2002), 'Relative contributions of chemistry and topography to the osseointegration of hydroxyapatite coatings', *Clin Orthop Relat Res*, 24–38.

Hacking S A, Harvey E J, Tanzer M, Krygier J J & Bobyn J D (2003), 'Acid-etched microtexture for enhancement of bone growth into porous-coated implants', *J Bone Joint Surg Br*, **85**, 1182–1189.

Hench L L & Wilson J (1993), *Introduction to Bioceramics*, World Scientific, Singapore.

Ho S T & Hutmacher D W (2006), 'A comparison of micro CT with other techniques used in the characterization of scaffolds', *Biomaterials*, **27**, 1362–1376.

Hulbert S F, Young F A, Mathews R S, Klawitter J J, Talbert C D & Stelling F H (1970), 'Potential of ceramic materials as permanently implantable skeletal prostheses', *J Biomed Mater Res*, **4**, 433–456.

Jarcho M (1981), 'Calcium phosphate ceramics as hard tissue prosthetics', *Clin Orthop*, 259–278.

Jasty M, Rubash H E, Paiement G D, Bragdon C R, Parr J & Harris W H (1992), 'Porous-coated uncemented components in experimental total hip arthroplasty in dogs. Effect of plasma-sprayed calcium phosphate coatings on bone ingrowth', *Clin Orthop*, 300–309.

Kim H M, Miyaji F, Kokubo T, Nishiguchi S & Nakamura T (1999), 'Graded surface structure of bioactive titanium prepared by chemical treatment', *J Biomed Mater Res*, **45**, 100–107.

Kitsugi T, Nakamura T, Oka M, Senaha Y, Goto T & Shibuya T (1996), 'Bone-bonding behavior of plasma-sprayed coatings of BioglassR, AW-glass ceramic, and tricalcium phosphate on titanium alloy', *J Biomed Mater Res*, **30**, 261–269.

Kokubo T, Kushitani H, Sakka S, Kitsugi T & Yamamuro T (1990), 'Solutions able to reproduce *in vivo* surface-structure changes in bioactive glass-ceramic A-W', *J Biomed Mater Res*, **24**, 721–734.

Kokubo T, Miyaji F, Kim H M & Nakamura T (1996), 'Spontaneous formation of bonelike apatite layer on chemically treated titanium metals', *J Am Ceram Soc*, **79**, 1127–1129.

Liang B, Fujibayashi S, Neo M, Tamura J, Kim H M, Uchida M, Kokubo T & Nakamura T (2003), 'Histological and mechanical investigation of the bone-bonding ability of anodically oxidized titanium in rabbits', *Biomaterials*, **24**, 4959–4966.

Liu X, Chu P K & Ding C (2004), 'Surface modification of titanium, titanium alloys, and related materials for biomedical applications', *Mater Sci Eng R: Reports*, **47**, 49–121.

Moore M J, Jabbari E, Ritman E L, Lu L, Currier B L, Windebank A J & Yaszemski M J (2004), 'Quantitative analysis of interconnectivity of porous biodegradable scaffolds with micro-computed tomography', *J Biomed Mater Res A*, **71**, 258–267.

Nagano M, Nakamura T, Kokubo T, Tanahashi M & Ogawa M (1996), 'Differences of bone bonding ability and degradation behaviour *in vivo* between amorphous calcium phosphate and highly crystalline hydroxyapatite coating', *Biomaterials*, **17**, 1771–1777.

Nakamura T & Nishiguchi S (1999), 'Tensile testing of bone–implant interface', in An Y H & Draughn R A, *Mechanical Testing of Bone and the Bone–Implant Interface*, Boca Raton, CRC Press LLC, 489–497.

Nakamura T, Yamamuro T, Higashi S, Kokubo T & Itoo S (1985), 'A new glass-ceramic for bone replacement: evaluation of its bonding to bone tissue', *J Biomed Mater Res*, **19**, 685–698.

Nishiguchi S, Nakamura T, Kobayashi M, Kim H M, Miyaji F & Kokubo T (1999), 'The effect of heat treatment on bone-bonding ability of alkali-treated titanium', *Biomaterials*, **20**, 491–500.

Nishiguchi S, Fujibayashi S, Kim H M, Kokubo T & Nakamura T (2003), 'Biology of alkali- and heat-treated titanium implants', *J Biomed Mater Res*, **67A**, 26–35.

Nishiguchi S, Kato H, Fujita H, Oka M, Kim H M, Kokubo T & Nakamura T (2001a), 'Titanium metals form direct bonding to bone after alkali and heat treatments', *Biomaterials*, **22**, 2525–2533.

Nishiguchi S, Kato H, Neo M, Oka M, Kim H M, Kokubo T & Nakamura T (2001b), 'Alkali- and heat-treated porous titanium for orthopedic implants', *J Biomed Mater Res*, **54**, 198–208.

Otsuki B, Takemoto M, Fujibayashi S, Neo M, Kokubo T & Nakamura T (2006), 'Pore throat size and connectivity determine bone and tissue ingrowth into porous implants: three-dimensional micro-CT based structural analyses of porous bioactive titanium implants', *Biomaterials*, **27**, 5892–5900.

Ripamonti U, Van den Heever B & Van Wyk J (1993), 'Expression of the osteogenic phenotype in porous hydroxyapatite implanted extraskeletally in baboons', *Matrix*, **13**, 491–502.

Taguchi T, Kishida A & Akashi M (1998), 'Hydroxyapatite formation on/in poly(vinyl alcohol) hydrogel matrices using a novel alternate soaking process', *Chem Lett*, 711–712.

Takatsuka K, Yamamuro T, Nakamura T & Kokubo T (1995), 'Bone-bonding behavior of titanium alloy evaluated mechanically with detaching failure load', *J Biomed Mater Res*, **29**, 157–163.

Takemoto M, Fujibayashi S, Neo M, Suzuki J, Kokubo T & Nakamura T (2005), 'Mechanical properties and osteoconductivity of porous bioactive titanium', *Biomaterials*, **26**, 6014–6023.

Takemoto M, Fujibayashi S, Neo M, Suzuki J, Kokubo T & Nakamura T (2006), 'Bone-bonding ability of a hydroxyapatite coated zirconia–alumina nanocomposite with a microporous surface', *J Biomed Mater Res A*, **78**, 693–701.

Uchida M, Kim H M, Kokubo T, Fujibayashi S & Nakamura T (2002), 'Effect of water treatment on the apatite-forming ability of NaOH-treated titanium metal', *J Biomed Mater Res*, **63**, 522–530.

Urist M R (1965), 'Bone: formation by autoinduction', *Science*, **150**, 893–899.

Urist M R & Strates B S (1971), 'Bone morphogenetic protein', *J Dent Res*, **50**, 1392–1406.

Wennerberg A, Ektessabi A, Albrektsson T, Johansson C & Andersson B (1997), 'A 1-year follow-up of implants of differing surface roughness placed in rabbit bone', *Int J Oral Maxillofac Implants*, **12**, 486–494.

Wilson-Hench J (1987), *Osteoinduction*, Amsterdam, Elsevier.

Yamasaki H & Sakai H (1992), 'Osteogenic response to porous hydroxyapatite ceramics under the skin of dogs', *Biomaterials*, **13**, 308–312.

Yang B, Uchida M, Kim H M, Zhang X & Kokubo T (2004), 'Preparation of bioactive titanium metal via anodic oxidation treatment', *Biomaterials*, **25**, 1003–1010.

Yang Z, Yuan H, Tong W, Zou P, Chen W & Zhang X (1996), 'Osteogenesis in extraskeletally implanted porous calcium phosphate ceramics: variability among different kinds of animals', *Biomaterials*, **17**, 2131–2137.

Yuan H P, Yang Z J, de Bruijn J D, de Groot K & Zhang X D (2001), 'Material-dependent bone induction by calcium phosphate ceramics: a 2.5-year study in dog', *Biomaterials*, **22**, 2617–2623.

9

Osteoinduction and its evaluation

J D DE BRUIJN, Progentix BV, The Netherlands and Queen Mary University of London, UK; K SHANKAR, Queen Mary University of London, UK; H YUAN, Progentix BV and University of Twente, The Netherlands and P HABIBOVIC, University of Twente, The Netherlands

9.1 Introduction

Recently, there has been a vast interest in material-induced bone formation, or material-directed osteoinduction. This is not only because osteoinduction is becoming a generally accepted phenomenon that can occur with a specific group of biomaterials, but also because of its potential clinical applicability. At this point of research and development, it is possible to induce significant amounts of bone by these so-called instructive materials without the necessity of adding cells and/or growth factors such as bone morphogenetic proteins (BMPs).

Herein, we will focus on the phenomenon of osteoinduction in relation to how it was originally demonstrated by Urist for demineralised bone matrix and BMPs and in relation to the current data that have been generated using purely inorganic, synthetic materials. We will review several possible routes to demonstrate osteoinduction *in vitro* and *in vivo* and will finally focus on two mechanisms that may play a role in material-induced bone formation.

9.2 Osteoinduction

9.2.1 The phenomenon

Bone and cartilage formation has been found in extraskeletal tissues after implantation of devitalised tissue and tissue extracts as early as the beginning of the 20th century (Huggins, 1931; Levander, 1934; Bertelsen, 1944; Urist and McLean, 1952; Urist *et al.*, 1979). At that time, however, consistent results have rarely been obtained and little was known about elements involved in this process.

In 1958 Bridges and Pritchard performed a screening study in rabbits in order to examine the fate of a variety of devitalised tissues and other substances introduced in the rabbit soft tissue and to study the histological

changes occurring after procedures that consistently resulted in bone or cartilage formation (Bridges and Pritchard, 1958). The results of this study showed that tissues containing hypertrophic cartilage consistently induced bone if devitalised with alcohol, acetone, hydrochloric acid or heating to 55 °C, while skeletal and cardiac muscle and tissues containing smooth muscle, which were devitalised with alcohol and acetone, consistently induced cartilage followed by bone. It was concluded that induction was due to liberation of chemical substances, possibly of protein nature, from the implants, and that these substances may be identical in hypertrophic cartilage and muscle.

In 1965 Urist set a landmark in the research into osteoinduction by publishing a report in which osteoinduction by hydrochloric acid-decalcified diaphyseal bone was consistently shown in muscles of rabbits, rats, mice and guinea pigs (Urist, 1965). Urist illustrated that bone formation in extraskeletal implants of decalcified bone matrix occurs in the interior of cavities, and that new osteoblasts are not derived from elements of the donor tissue, but from proliferating pluripotent, ingrowing cells of the host.

Another highly valuable report in osteoinduction was published by Friedenstein in 1968 in which bone induction by transitional epithelium was described (Friedenstein, 1968). The author defined osteoinduction as 'the induction of undifferentiated inducible osteoprogenitor cells (IOPCs) that are not yet committed to the osteogenic lineage to form osteoprogenitor cells'. This induction only takes place in the presence of inducing substances, such as transitional epithelium or demineralised bone.

Later work by Urist and coworkers led to the conclusion that a discrete protein within the demineralised bone matrix (DBM) was the sole inducer of bone formation. This finding was published in 1971 and this protein was named bone morphogenetic protein (BMP) (Urist and Strates, 1971). BMP was shown to be involved in the bone formation cascade of chemotaxis, mitosis, differentiation, callus formation and finally bone formation. Different groups showed that BMPs have the ability to induce *de novo* endochondral bone formation when implanted in ectopic sites of different experimental animals. Proof that BMP could be extracted from DBM and still retain its ability to form bone came in 1977 (Urist *et al.*, 1977).

9.2.2 Osteoinduction by bone morphogenetic proteins

To date over 20 BMPs are known (Kawabata *et al.*, 1998). Besides BMP-1, which is a metalloprotease (Kessler *et al.*, 1996), BMPs belong to the transforming growth factor beta (TGF-β) superfamily (Wozney and Rosen, 1998; Schmitt *et al.*, 1999). When DBM (or BMPs) are implanted ectopically in rodents, a cascade of events, similar to embryonic bone formation and fracture healing, is initiated. First, the chemotaxis of undifferentiated mesen-

chymal cells occurs, followed by cell proliferation. Then, these cells differentiate into chondroblasts and chondrocytes, followed by the formation of cartilaginous extracellular matrix including type II collagen and proteoglycans. The chondrocytes mature and become hypertrophic, and cartilage starts to mineralise. Following the period of chondrogenesis, blood vessels appear at the implantation site. Bone-forming cells are consequently observed, and while calcified cartilage is removed by osteoclasts, bone matrix is produced. Once bone has been formed, haemopoietic bone marrow appears within the bone. Finally, bone undergoes remodelling (Wozney, 1994). Figure 9.1 illustrates a sequence of events during osteoinduction by BMPs.

Although it is generally thought that BMP-induced bone formation is endochondral (Reddi, 1981), recent reports have shown that, depending on the carrier on which BMPs are implanted in the body, osteoinduction by BMPs can be either endochondral or intramembranous. For example, fibrous collagen membrane (Sasano *et al.*, 1993), hydroxyapatite (Kuboki *et al.*, 1995) and biomimetic CaP coatings (Liu *et al.*, 2005) in combination with BMP have shown intramembranous bone induction. In contrast, BMPs on fibrous glass membrane and insoluble bone matrix showed that ectopic bone was formed following the process of endochondral ossification (Sasano

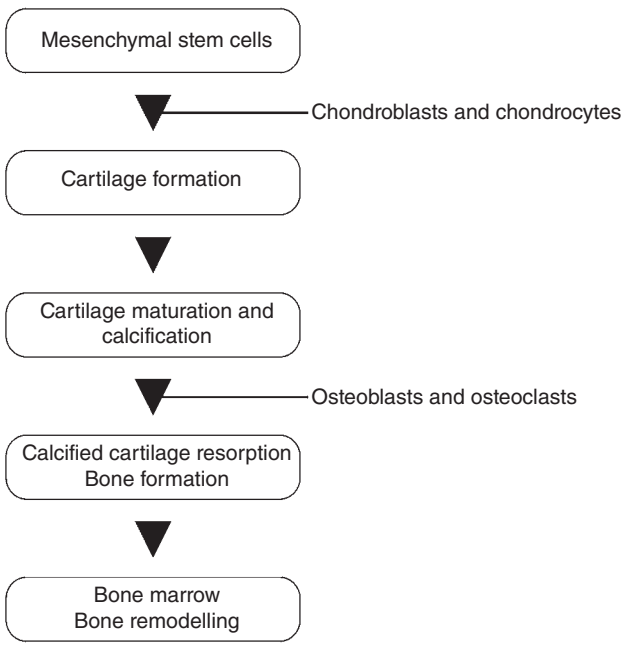

9.1 Sequence of events in endochondral bone formation.

et al., 1993; Kuboki *et al.*, 1995). The exact reason for the observed difference between different carriers is not completely understood. It has been proposed that differences in vascularisation as well as differences in local oxygen concentrations might be of importance in the process of differentiation of the undifferentiated cells into either chondroblasts or directly into osteoblasts (Caplan, 1990). For both optimal vascularisation and oxygen levels, the ultrastructure of the carrier has been proposed to be relevant (Ripamonti *et al.*, 1992).

Osteoinductive capacity of BMPs has mostly been tested in rodents, either subcutaneously or intramuscularly. In comparative studies, more bone was induced intramuscularly than subcutaneously or intra-fatty, suggesting again the importance of vascularisation in ectopic bone formation, as it is generally accepted that the level of vascularisation is higher in the muscle than in other soft tissues investigated (Yoshida *et al.*, 1998; Okubo *et al.*, 2000). Only a few reports describe osteoinduction by BMPs in higher animals, namely in monkeys and baboons (Hosny and Sharawy, 1985; Ripamonti, 1991a; Aspenberg *et al.*, 1992; Miyamoto *et al.*, 1993). Besides the observations of the differences in response to BMPs between different species (Miyamoto *et al.*, 1993), there are reports showing differences in response to ectopically implanted BMPs, between individuals of the same species, probably due to genetic differences (Marusic *et al.*, 1999).

9.2.3 Osteoinduction by synthetic biomaterials

Soon after Urist's description of osteoinduction by DBM and the suggestion that BMPs are responsible for the process of osteoinduction, Winter and Simpson (1969) described an observation of bone induction by a sponge made of poly-hydroxyethyl methacrylate (poly-HEMA), that was at that time used for, e.g., breast augmentations, in soft tissue of pigs. The authors observed that the implanted sponge became calcified prior to bone formation. Calcification of the used sponge was also observed after subcutaneous implantation in rats. The observed phenomenon of bone induction by the polymeric sponge could not be explained by Urist's theory, as the sponge neither contained nor produced BMPs. Interestingly, in earlier reports it was observed that bone was induced by tendons and arteries only if they were first calcified *in vivo*, as reviewed by de Groot (1973). Although the exact underlying phenomenon was not known, these observations suggested that calcification, and hence calcium phosphates, might play an important role in the process of osteoinduction. In the past decade a number of groups have reported osteoinduction by synthetic biomaterials ranging from calcium phosphate ceramics to metallic implants, as reviewed in Section 9.3.1.

The exact mechanism of osteoinduction by biomaterials is still largely unknown. It is furthermore unknown whether the mechanisms of osteoinduction by BMPs and osteoinduction by biomaterials are the same. In some reports by Ripamonti and coworkers it is hypothesized that endogenous BMPs are collected in the biomaterial post-implantation and that they consequently induce bone formation ectopically (Ripamonti *et al.*, 1999; Ripamonti, 2000). The authors, however, failed to give conclusive evidence for their hypothesis. In a pilot study by Yuan and coworkers it was suggested that BMPs do play a role in osteoinduction by biomaterials, although this role does not seem to be essential (Yuan, 2001). The limited number of animals used in this pilot study limited the reliability of its results.

The three apparent differences in osteoinduction by BMPs and biomaterials are that (1) bone induced by biomaterials is always intramembranous (Ripamonti, 1991b; Yuan *et al.*, 2002) while BMP-induced bone can be formed via both the endochondral (Reddi, 1981) and intramembranous (Kuboki *et al.*, 1995; de Bruijn *et al.*, 2000) pathway; (2) in small animals such as rodents bone is very rarely induced by biomaterials (Ohgushi *et al.*, 1989; Goshima *et al.*, 1991; Ohgushi *et al.*, 1993; Klein *et al.*, 1994; Yang *et al.*, 1996), but easily by BMPs (Reddi, 1992, 1994; Wozney, 1992) and (3) while bone is mostly observed within the internal porosity of biomaterials and not at the periphery, bone formation by BMPs is regularly seen on the outside of the carrier and even in the soft tissue distant from the carrier surface (Yuan *et al.*, 2001d; Liu *et al.*, 2005).

9.3 Ceramics to promote osteoinduction

9.3.1 Overview of osteoinductive biomaterials

In the last decade, a large number of publications illustrated osteoinduction by diverse calcium phosphate biomaterials, such as synthetic hydroxyapatite ceramic in dogs (Yamasaki, 1990; Zhang, 1991; Yamasaki and Sakai, 1992; Klein *et al.*, 1994; Ripamonti, 1996), coral derived hydroxyapatite ceramic in dogs, monkeys and baboons (Ripamonti, 1991b; Vargervik, 1992; Pollick *et al.*, 1995; Ripamonti, 1996), α- and β-tricalcium phosphate, biphasic calcium phosphate, α- and β-pyrophosphate in dogs, sheep and goats (Vargervik, 1992; Yuan *et al.*, 1997, 1998, 1999; Yuan 2001a, 2002; Gosain *et al.*, 2002; Le Nihouannen *et al.*, 2005; Habibovic *et al.*, 2005b, 2006a,c). In addition, calcium phosphate cements (Yuan *et al.*, 2000; Gosain *et al.*, 2002) and coatings (de Bruijn *et al.*, 2000; Barrere *et al.*, 2003; Habibovic *et al.*, 2004, 2005a) were shown to be osteoinductive when implanted ectopically in sheep, dogs and goats. Besides calcium phosphate containing biomaterials, osteoinduction was also observed in alumina ceramic (Yuan *et al.*,

2001c), titanium (Fujibayashi *et al.*, 2004; Takemoto *et al.*, 2005) and glass-ceramics (Yuan *et al.*, 2001b) in dogs. The last group of materials was shown to be able to precipitate a calcium phosphate layer on their surface in a calcium- and phosphate-rich environment, and their *in vivo* ectopic bone formation was preceded by the process of calcification.

9.3.2 Material characteristics important for osteoinduction

From the literature, the following is known about the relevance of different material characteristics in the process of osteoinduction.

Macrostructure (pre- and post-implantation)

Bone induction by calcium phosphate ceramics was never observed on flat ceramic surfaces. All osteoinductive ceramics had either a porous macrostructure (Yamasaki, 1990; Ripamonti, 1991b; Yamasaki and Sakai, 1992; Vargervik, 1992; Toth *et al.*, 1993; Klein *et al.*, 1994; Yuan *et al.*, 1997, 1998, 2001a; Gosain *et al.*, 2002; Habibovic *et al.*, 2005b, 2006a) or a macrostructure that contained well-defined concavities (Ripamonti *et al.*, 1999). Bone formation was never observed on the peripheries of porous implants, and was always found inside the pores or concavities, aligning the surface. Recently, it has been reported that the pre-existence of macropores in a biomaterial is not essential for osteoinduction to occur (de Bruijn *et al.*, 2006). Abundant bone induction around an implanted agglomerate of irregular microparticles measuring 212–300 μm in diameter was seen after 12-week intramuscular implantation in dogs (Fig. 9.2).

Bone induction in calcium phosphate cements was observed only in the pores and surface crevices formed due to degradation of cements (Yuan *et al.*, 2000; Gosain *et al.*, 2002) and never on the flat cement surfaces. Biomimetic octacalcium phosphate coating induced bone only when applied

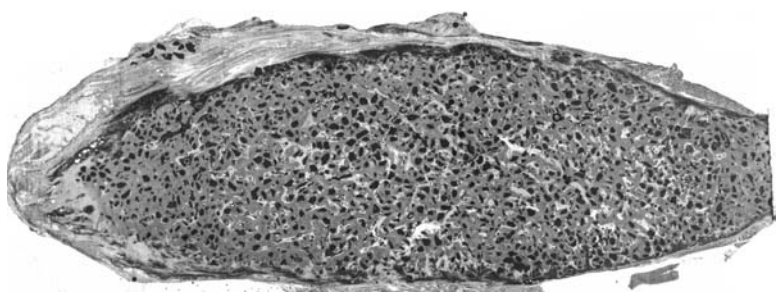

9.2 Osteoinduction after intramuscular implantation of 1 cc microporous tricalcium phosphate granulate containing irregular particles measuring 212–300 μm in diameter.

on porous scaffolds, and the bone formation was observed inside the pores, and not on the implant periphery (de Bruijn *et al.*, 2000; Barrere *et al.*, 2003). Similarly, bone formation was observed inside the octacalcium phosphate-coated hollow titanium cylinders, contrary to the dense coated titanium cylinders (Barrere *et al.*, 2003).

Glass-ceramic (Yuan *et al.*, 2001b), alumina-ceramic (Yuan *et al.*, 2001c), polymeric sponge (Winter and Simpson, 1969) and titanium (Fujibayashi *et al.*, 2004; Takemoto *et al.*, 2005), all with a porous macrostructure, were reported to be osteoinductive. Titanium implants that induced ectopic bone formation possesses a complex macrostructure, due to the production technique used. The same porous metal, produced in the form of fibrous mesh, i.e. with a more simple porous structure, was not osteoinductive (Fujibayashi *et al.*, 2004).

Microstructure

Recent publications have shown that microporosity is an essential element in osteoinduction by biomaterials. When microporosity of biphasic calcium phosphate ceramic was increased by lowering the temperature at which the ceramic was sintered, or by other differences in production methods, the relative amount of induced bone was significantly increased (Figs 9.3 and 9.4) (Habibovic *et al.*, 2005b, 2006a,c). However, it has been shown that there is a limit up to which osteoinductive potential of a ceramic can be increased by increasing its porosity, as a mechanically stable surface of the

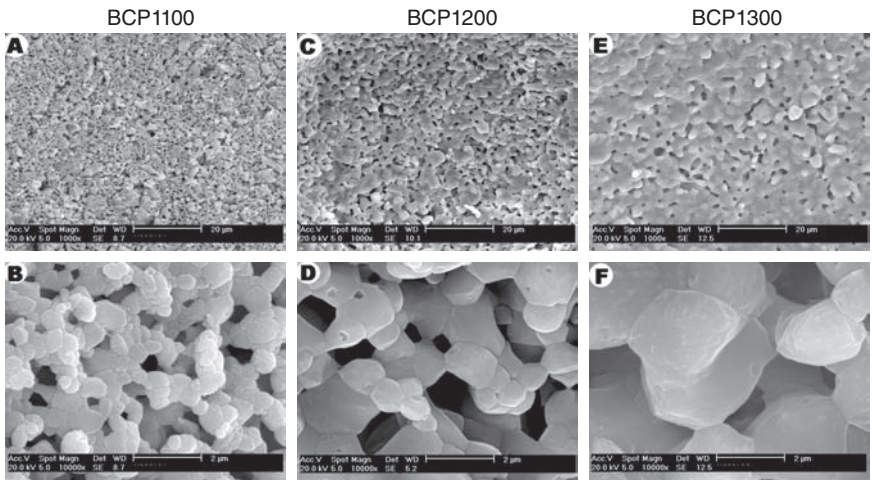

9.3 Biphasic calcium phosphate scaffolds sintered at different temperatures (1100, 1200 or 1300 °C) result in various surface micro-structures. BCP100 has the smallest grain size and the highest microporosity.

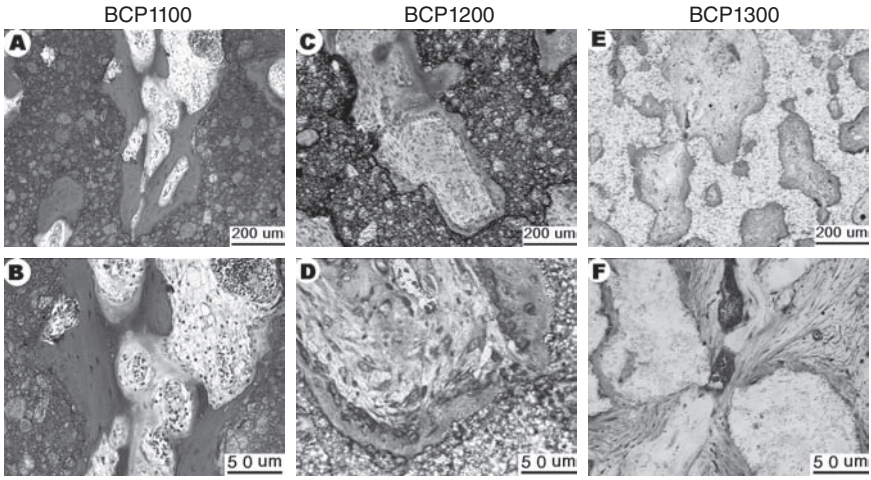

9.4 Osteoinduction in materials from Fig. 9.3 after 12 weeks intramuscular implantation in dogs.

material is needed in order to facilitate new bone formation (Habibovic *et al.*, 2006a).

Pores and surface crevices of osteoinductive calcium phosphate cements have a rough microstructure caused by both chemical dissolution and osteoclastic resorption of the material (Yuan *et al.*, 2000; Gosain *et al.*, 2002). Also octacalcium phosphate coating that is inductive when applied on the surface of porous implants has a rough microstructure due to large crystals that grow perpendicularly to the surface during the biomimetic coating formation process (de Bruijn *et al.*, 2000; Barrere *et al.*, 2003; Habibovic *et al.*, 2004, 2005a).

Glass-ceramic, alumina-ceramic and titanium (Yuan *et al.*, 2001b,c; Fujibayashi *et al.*, 2004) possess a rough surface due to the production techniques used. Only chemically/thermally treated titanium implants induce bone (Fujibayashi *et al.*, 2004; Takemoto *et al.*, 2005). The result of such a treatment was the formation of micropores on the metal surface, which were absent on the untreated implants.

Chemical composition (presence of calcium phosphate)

Most synthetic biomaterials so far shown to be osteoinductive contain calcium phosphates, which suggests the importance of calcium and phosphate ions in the process of osteoinduction by biomaterials. When a biphasic calcium phosphate ceramic, consisting of hydroxyapatite and β-tricalcium phosphate, was compared with a pure hydroxyapatite ceramic with similar macro- and microstructure, more bone was found in the former, more

soluble, ceramic. This suggests that more soluble calcium phosphate phases are more osteoinductive in comparison with less soluble ones (Habibovic *et al.*, 2005b). However, implantation of highly soluble carbonated apatite ceramic did not result in bone induction, again suggesting that a relatively stable surface is needed for facilitation of ectopic bone formation (Habibovic *et al.*, 2006a). Poly-HEMA sponge, alumina ceramic and titanium did not contain calcium phosphates initially. Nevertheless, all these materials have been shown to calcify *in vitro* when immersed in SBF (Fujibayashi *et al.*, 2004). A similar process of calcification, which is possibly a precursor of bone formation, is expected to take place *in vivo* (Winter and Simpson, 1969; Yuan *et al.*, 2001c; Fujibayashi *et al.*, 2004).

In summary, it can be concluded that the macrostructure, via pre-existing macroporosity or the presence of inter-particle space, microstructure (e.g. microporosity or an enhanced surface micro-roughness or microtexture) and chemical composition all play an important role in material-directed osteoinduction.

9.4 Evaluation of osteoinduction

9.4.1 *In vitro*

With regard to the suspected osteoinductive nature of DBM, several *in vitro* studies have been performed as indicated below. The majority of these studies, however, were unable to confirm the osteoinductive behaviour of these materials in the chosen *in vitro* system. For example, Adkisson *et al.* (2000) developed a 'rapid quantitative bioassay of osteoinduction' by using SaOS-2 osteosarcomas and studies cell proliferation rates under influence of DBM. However, correlation between cell proliferation and osteoinduction was not strong. Osteogenic factors, like BMP, are not commonly associated with mitogenic response. Zhang *et al.* (1997) and Wolfinbarger and Zhang (1993) used human periosteal cells and human dermal fibroblasts to relate cellular ALP activity to DBM osteoinductivity. In these studies, the authors failed to show a clear correlation between *in vitro* assays and *in vivo* bone formation. Carnes *et al.* (1999) used an immature osteoprogenitor cell line, 2T9, to investigate the effect of DBM on the cell differentiation. They failed to show any effect on differentiation and concluded that there are no soluble factors being released from DBM into the culture medium. Han *et al.* (2003) assayed ALP activity of the C2C12 cells in a culture in the presence of DBM, and succeeded correlating it with the *in vivo* bone formation. The last study mimics the *in vivo* situation more than other described studies, although the expression of ALP is not the most sensitive marker for the osteogenic differentiation. In summary, as DBM is currently in clinical use with generally satisfactory results, this could mean two things: either

the materials are not osteoinductive or the *in vitro* tests are insufficient to show the osteoinductive nature of the materials.

Investigating osteoinduction by synthetic biomaterials *in vitro* is even more complicated than assays to test osteoinduction by DBM and BMPs, as existing assays do not take into account a possible interaction between the material and cell culture medium that may occur in addition to the interaction between the biomaterials and the cells. We have performed some initial studies looking at protein production and gene expression, but most results were either inconclusive or in contrast with the *in vivo* findings. An overview of the preliminary results and limitations of the existing *in vitro* assays for biomaterials research has recently been reviewed in detail (Habibovic *et al.*, 2006b).

9.4.2 *In vivo*

To date, the best method to determine the osteoinductivity of materials is ectopic *in vivo* implantation. Ectopic bone formation gives the true indication of osteoinductivity of a material and the material that gives ectopic bone formation can be called an osteoinductive material. The most often used ectopic sites to demonstrate osteoinduction of materials are subcutis (under skin) and muscle (thigh muscle, back muscle and rectus abdominis).

Different animal species have been used to evaluate osteoinduction of materials and it has been shown that the capacity of a material to induce bone formation ectopically varies with animal species. Material-induced bone formation has so far been seen in baboons (Ripamonti, 1991a, 1996), monkeys (Vargervik, 1992), dogs (Yamasaki and Sakai, 1992; Klein *et al.*, 1994, Yang *et al.*, 1996; Yuan *et al.*, 1999, 1998, 2001a, 2006a; de Bruijn *et al.*, 2000), pigs (Winter and Simpson, 1969; Yang *et al.*, 1996), sheep (Gosain *et al.*, 2002; Le Nihouannen *et al.*, 2005), goats (Yuan *et al.*, 2002; Habibovic *et al.*, 2004, 2005b, 2006a,c), rabbits (Kurashina *et al.*, 2002; Yuan *et al.*, 2006b) and mice (Yuan *et al.*, 2006b). By implanting a same material in different animal species, Ripamonti and coworkers demonstrated that baboons have a higher capacity to give material-induced bone formation than dogs, while only very limited amount of bone was observed after ectopic implantation in rabbits (Ripamonti, 1996). Yuan *et al.* (2006b) compared two calcium phosphate ceramics in dogs, rabbits, rats and mice, and demonstrated that by improving the osteoinductive potential of osteoinductive materials, material-induced bone formation can occur in rabbits and mice. Higher incidence of bone formation and more bone was seen in dogs than in rabbits, while only a limited amount of bone was found in a few mice used in the experiment. Material-induced bone formation has so far not been reported in rats unless osteogenic cells and/or additional growth factor-

containing matrix are used. In addition, evidence for material-induced osteoinduction has even been reported in humans (Green *et al.*, 1995).

The ability to give material-induced bone formation in ectopic sites varies with materials. Yuan *et al.* (2006a) compared osteoinductive potential of two types of calcium phosphate ceramics in muscle of dogs for different time periods ranging from one week to one year. It was found that, although both calcium phosphate ceramics induced bone formation intramuscularly, in one of them bone formation took place earlier than in the other one, suggesting that the former ceramic had a higher osteoinductive potential than the latter one. Such a chronological study provides an experimental way to evaluate osteoinductive potentials of osteoinductive materials, as the time point at which bone formation takes place is an indicator of osteoinductive potential of a material.

The potential clinical importance of osteoinductive biomaterials has been demonstrated by a few studies in which the same materials were implanted both ectopically and orthotopically. By comparing two calcium phosphate ceramics with different osteoinductive potentials in muscle and femoral cortex of dogs, Yuan *et al.* (2006a) showed that the ceramic with a higher osteoinductive potential gave faster bone formation and earlier repair of the orthotopic defect. Using a critical-sized bone defect in goat iliac wing, Habibovic *et al.* (2006c) demonstrated that an osteoinductive calcium phosphate ceramic was able to repair such a defect in 12 weeks, while the similar, but non-osteoinductive calcium phosphate ceramic failed to do so.

Because of the lack of proper *in vitro* models to evaluate osteoinductive potentials of materials, most studies on material-induced bone formation were conducted *in vivo*. The data so far obtained from *in vivo* studies changed the general idea that materials themselves can only be osteoconductive but not osteoinductive. However, how and why the osteoinductive materials are able to trigger cells inside an ectopic implantation site to differentiate into the osteogenic lineage and form bone are still largely unknown. One of the reasons that the exact mechanism of osteoinduction is not yet completely unravelled is the above described difficulty to obtain material-induced ectopic bone formation in general experimental animals such as rabbits, rats and mice.

9.5 Mechanism of material-induced bone formation

Taking the above-described material properties that are of influence on osteoinductivity of biomaterials into account, two hypotheses have been put forward regarding the occurrence of osteoinduction by inorganic synthetic materials. The first emphasises a material-related role, while the second involves a more biological role for this phenomenon. Both hypotheses are briefly described below and could act synchronously.

9.5.1 Material-directed hypothesis for osteoinduction

Based on the influence of different material characteristics on ectopic bone formation, the following material-related hypothesis can be given regarding the mechanism that underlies the phenomenon of osteoinduction by biomaterials. The presence of a macroporous structure after implantation, or well-defined three-dimensional concavities, has been shown to be a prerequisite for osteoinduction by biomaterials (Ripamonti *et al.*, 1999; Barrere *et al.*, 2003; Fujibayashi *et al.*, 2004). Such a well-interconnected macroporous structure is of importance for an adequate supply of the body fluids with nutrients throughout the implant. Accompanied with this supply, the release of calcium and phosphate ions, believed to be the origin of the bioactivity of calcium phosphate biomaterials (Geesink *et al.*, 1988; Kay and Cook, 1993; Hanawa *et al.*, 1997; Ripamonti *et al.*, 1999), takes place, followed by the precipitation of a biological carbonated apatite layer (Le Huec *et al.*, 1998). The precipitation of this apatite layer occurs when the concentration of calcium and phosphate ions has reached the super-saturation level in the material vicinity. This might explain the experimental fact that the bone induction always takes place in the supersaturated pores in the centre of implant and not at the, less saturated, outer surface of the implant (Kruyt *et al.*, 2004). The formed bone-like biological carbonated apatite layer could be a physicochemical trigger for (local) stem cells to differentiate into the osteogenic lineage, similar to being in an orthotopic environment, or could include growth factors that induce this process. The involvement of BMPs has already been proposed by Ripamonti *et al.* (1999) and Yuan *et al.* (2001d). The resulting pathway for hypothesis is summarised in Fig. 9.5.

It is relevant to note that our previous research has shown that bone induction only occasionally occurs in smaller animals (mice, rats), while the same material would reproducibly give rise to bone induction in larger animals (goats and dogs). Besides the difference in implant size, which has been reported to be of importance in bone induction (Habibovic *et al.*, 2006a), there is also a difference in implant location (subcutaneous for small animals and intramuscular for larger animals). We recently reported that the subcutis is a less inductive implantation site than muscle (Habibovic *et al.*, 2006a). Finally, we observed large differences in the osteoinductive potential of a given material between individual animals (Habibovic *et al.*, 2005b, 2006a,c), which has also been reported for BMP-induced bone formation (Miyamoto *et al.*, 1993; Geesink *et al.*, 1999; Marusic *et al.*, 1999). It is therefore conceivable that BMPs do play a role in osteoinduction by biomaterials, but as long as conclusive evidence has not been provided, other possibilities should be left open.

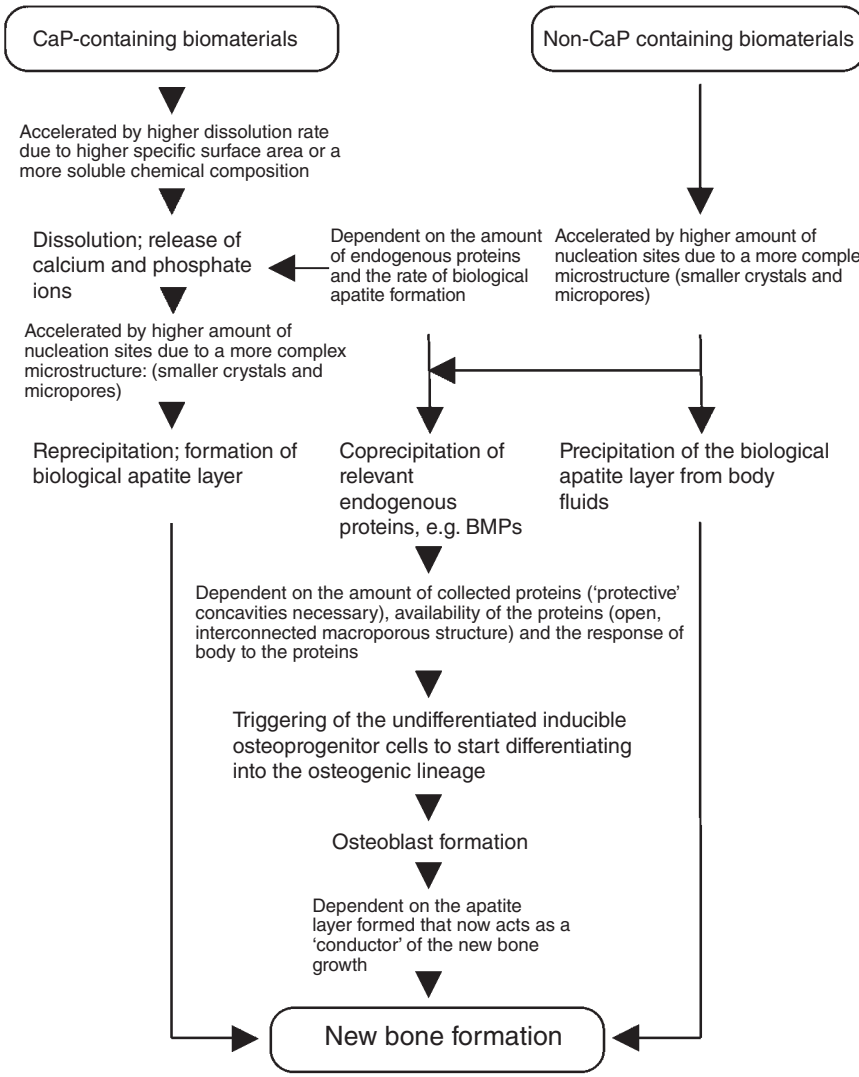

9.5 Flowchart showing the proposed involvement of material-related processes (dissolution/(re)precipitation and endogenous protein incorporation) in material-directed osteoinduction.

9.5.2 Biology-directed hypothesis for osteoinduction

Concurrent with the above-described material-directed hypothesis of osteoinduction by biomaterials, another biological factor could also be involved. This relates to the inflammatory reaction that occurs after the implantation of biomaterials (Le Nihouannen *et al.*, 2005). Caplan and Boyan (1994)

hypothesised that the initial inflammatory response after implantation of a biomaterial brings in and provides factors that attract mesenchymal stem cells. One such factor could be prostaglandin E2 (PGE2) which is produced by macrophages that are present around biomaterials during the inflammatory phase (Thomsen and Gretzer, 2001; Refai *et al.*, 2004). Micro-rough surfaces, unique for osteoinductive materials, have been reported to stimulate PGE2 production by macrophages (Thomsen and Gretzer, 2001). We have recently shown (unpublished) that macrophages indeed produce higher quantities of PGE2 in response to micro-rough hydroxyapatite as compared with smooth surfaces (Fig. 9.6), while PGE2 was also shown to be chemotactic for human mesenchymal stem cells (Fig. 9.7) and stimulates

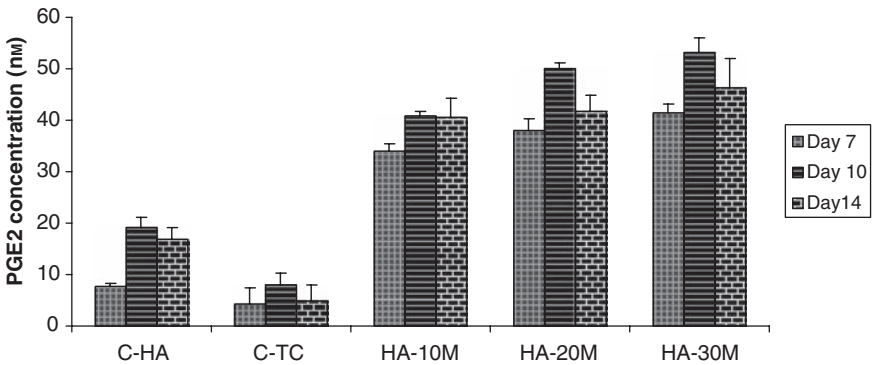

9.6 PGE2 production by macrophages in response to smooth HA (HA-C), tissue culture plastic (C-TC) and (micro-rough) hydroxyapatite surfaces that have been etched in maleic acid for 10, 20 or 30 minutes (HA-10M, HA-20M and HA-30M).

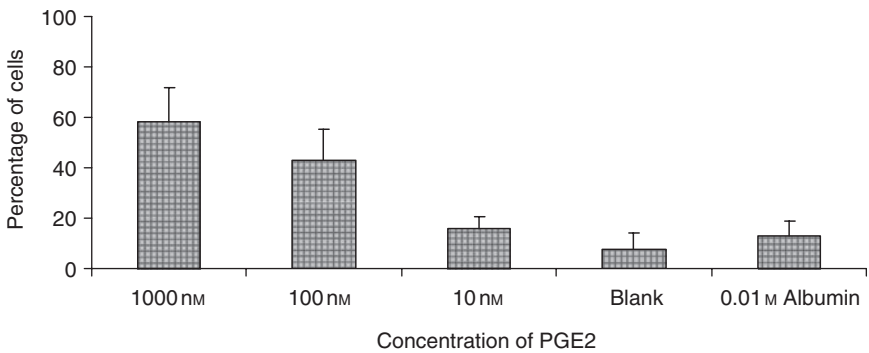

9.7 Chemotactic migratory response of mesenchymal stem cells (MSCs) to PGE2 using the Transwell chamber model. The graph depicts the number of MSCs that have migrated through the micro-pores of a filter when challenged with various concentrations of PGE2, while there is no effect when using BSA.

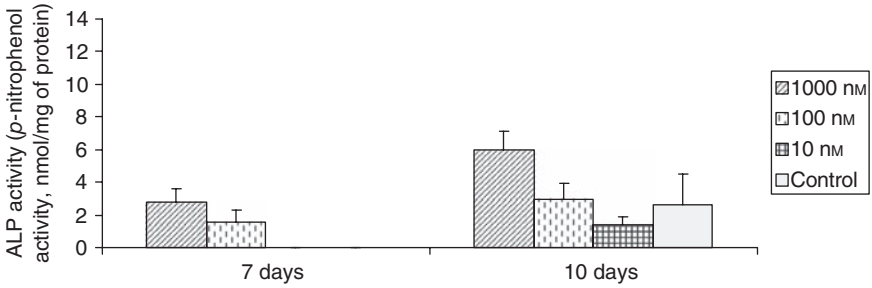

9.8 Effect of PGE2 concentration on osteogenic differentiation of mesenchymal stem cells at 7 and 10 days. Osteogenic differentiation was evaluated by measuring alkaline phosphatase activity per protein content.

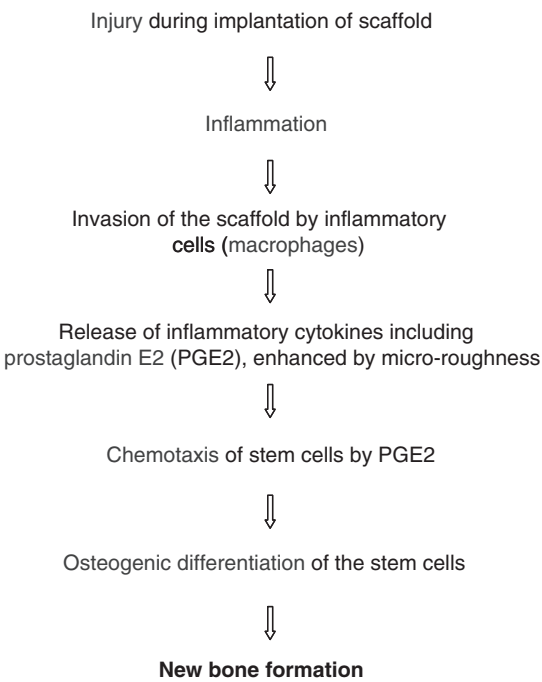

9.9 Flowchart showing the proposed involvement of inflammation in material-directed osteoinduction.

their osteogenic differentiation (Fig. 9.8). The possible role of inflammation in material-directed osteoinduction is summarised in Fig. 9.9.

9.6 Summary and future trends

In summary, it can be concluded that material-induced bone formation has been shown in many studies. It is not a phenomenon that happens only

occasionally in ectopic sites, but has a clear clinical significance in that these materials can stimulate bone regeneration comparable to autologous bone grafts and BMPs. The presence of specific material compositions and surface microstructures plays an important, yet not fully understood, role. The authors consider that this new and exciting group of bone-inducing materials has a promising future for the repair and regeneration of bone with the ultimate goal to replace autograft, allograft/DBM and BMPs.

9.7 References

Adkisson, H. D., Strauss-Schoenberger, J., Gillis, M., Wilkins, R., Jackson, M. & Hruska, K. A. (2000) Rapid quantitative bioassay of osteoinduction. *J Orthop Res*, **18**, 503–11.

Aspenberg, P., Wang, E. & Thorngren, K. G. (1992) Bone morphogenetic protein induces bone in the squirrel monkey, but bone matrix does not. *Acta Orthop Scand*, **63**, 619–22.

Barrere, F., van der Valk, C. M., Dalmeijer, R. A., Meijer, G., van Blitterswijk, C. A., de Groot, K. & Layrolle, P. (2003) Osteogenecity of octacalcium phosphate coatings applied on porous metal implants. *J Biomed Mater Res*, **66A**, 779–88.

Bertelsen, A. (1944) Experimental investigations into post-foetal osteogenesis. *Acta Orthop Scand*, **15**, 139–81.

Bridges, J. B. & Pritchard, J. J. (1958) Bone and cartilage induction in the rabbit. *J Anat*, **92**, 28–38.

de Bruijn, J. D. & Yuan, H. (2006) Osteoinductive calcium phosphate, European patent EP1829564.

de Bruijn, J. D., Yuan, H., Dekker, R., Layrolle, P., de Groot, K. & van Blitterswijk, C. A. (2000) Osteoinductive biomimetic calcium-phosphate coatings and their potential use as tissue-engineering scaffolds. In Davies, J. E. (Ed.) *Bone Engineering.* Toronto, Canada, em squared.

Caplan, A. I. (1990) Cartilage begets bone versus endochondral myelopoiesis. *Clin Orthop Relat Res*, **261**, 257–67.

Caplan, A. I. & Boyan, B. D. (1994) Endochondral bone formation: The lineage cascade, In Hall, B. (Ed.) *Mechanisms of bone development and growth*, Boca Raton, CRC Press, p. 6–57.

Carnes, D. L., Jr., de la Fontaine, J., Cochran, D. L., Mellonig, J. T., Keogh, B., Harris, S. E., Ghosh-Choudhury, N., Dean, D. D., Boyan, B. D. & Schwartz, Z. (1999) Evaluation of 2 novel approaches for assessing the ability of demineralized freeze-dried bone allograft to induce new bone formation. *J Periodontol*, **70**, 353–63.

Friedenstein, A. Y. (1968) Induction of bone tissue by transitional epithelium. *Clin Orthop Relat Res*, **59**, 21–37.

Fujibayashi, S., Neo, M., Kim, H. M., Kokubo, T. & Nakamura, T. (2004) Osteoinduction of porous bioactive titanium metal. *Biomaterials*, **25**, 443–50.

Geesink, R. G., de Groot, K. & Klein, C. P. (1988) Bonding of bone to apatite-coated implants. *J Bone Joint Surg Br*, **70**, 17–22.

Geesink, R. G., Hoefnagels, N. H. & Bulstra, S. K. (1999) Osteogenic activity of OP-1 bone morphogenetic protein (BMP-7) in a human fibular defect. *J Bone Joint Surg Br*, **81**, 710–18.

Gosain, A. K., Song, L., Riordan, P., Amarante, M. T., Nagy, P. G., Wilson, C. R., Toth, J. M. & Ricci, J. L. (2002) A 1-year study of osteoinduction in hydroxyapatite-derived biomaterials in an adult sheep model: part I. *Plast Reconstr Surg*, **109**, 619–30.

Goshima, J., Goldberg, V. M. & Caplan, A. I. (1991) The osteogenic potential of culture-expanded rat marrow mesenchymal cells assayed *in vivo* in calcium phosphate ceramic blocks. *Clin Orthop Relat Res*, **262**, 298–311.

Green, J. P., Wojno, T. H., Wilson, M. W. & Grossniklaus, H. A. (1995) Bone formation in hydroxyapatite orbital implants. *Am J Ophthalmol*, **120**(5), 681–681.

de Groot, K. (1973) Some considerations about bone-induction. *Calc Tiss Res*, **13**, 335–7.

Habibovic, P., van der Valk, C. M., van Blitterswijk, C. A., de Groot, K. & Meijer, G. (2004) Influence of octacalcium phosphate coating on osteoinductive properties of biomaterials. *J Mater Sci Mater Med*, **15**, 373–80.

Habibovic, P., Li, J., van der Valk, C. M., Meijer, G., Layrolle, P., van Blitterswijk, C. A. & de Groot, K. (2005a) Biological performance of uncoated and octacalcium phosphate-coated Ti_6Al_4V. *Biomaterials*, **26**, 23–36.

Habibovic, P., Yuan, H., van der Valk, C. M., Meijer, G., van Blitterswijk, C. A. & de Groot, K. (2005b) 3D microenvironment as essential element for osteoinduction by biomaterials. *Biomaterials*, **26**, 3565–75.

Habibovic, P., Sees, T. M., van den Doel, M. A., van Blitterswijk, C. A. & de Groot, K. (2006a) Osteoinduction by biomaterials – physicochemical and structural influences. *J Biomed Mater Res A*, **77**, 747–62.

Habibovic, P., Woodfield, T., de Groot, K. & van Blitterswijk, C. (2006b) Predictive value of *in vitro* and *in vivo* assays in bone and cartilage repair – what do they really tell us about the clinical performance? *Adv Exp Med Biol*, **585**, 327–60.

Habibovic, P., Yuan, H., van den Doel, M., Sees, T. M., van Blitterswijk, C. A. & de Groot, K. (2006c) Relevance of osteoinductive biomaterials in critical-sized orthotopic defect. *J Orthop Res*, **24**, 867–76.

Han, B., Tang, B. & Nimni, M. E. (2003) Quantitative and sensitive *in vitro* assay for osteoinductive activity of demineralized bone matrix. *J Orthop Res*, **21**, 648–54.

Hanawa, T., Kamiura, Y., Yamamoto, S., Kohgo, T., Amemiya, A., Ukai, H., Murakami, K. & Asaoka, K. (1997) Early bone formation around calcium-ion-implanted titanium inserted into rat tibia. *J Biomed Mater Res*, **36**, 131–6.

Hosny, M. & Sharawy, M. (1985) Osteoinduction in rhesus monkeys using demineralized bone powder allografts. *J Oral Maxillofac Surg*, **43**, 837–44.

Huggins, C. (1931) The formation of bone under the influence of epithelium of the urinary tract. *Arch Surg*, **22**, 377–408.

Kawabata, M., Imamura, T. & Miyazono, K. (1998) Signal transduction by bone morphogenetic proteins. *Cytokine Growth Factor Rev*, **9**, 49–61.

Kay, J. F. & Cook, S. D. (1993) Biological profile of calcium phosphate coatings. In Geesink, R. G. & Manley, M. T. (Eds.) *Hydroxyapatite Coatings in Orthopaedic Surgery.* New York, USA, Raven Press.

Kessler, E., Takahara, K., Biniaminov, L., Brusel, M. & Greenspan, D. S. (1996) Bone morphogenetic protein-1: the type I procollagen C-proteinase. *Science*, **271**, 360–62.

Klein, C., de Groot, K., Chen, W., Li, Y. & Zhang, X. (1994) Osseous substance formation induced in porous calcium phosphate ceramics in soft tissues. *Biomaterials*, **15**, 31–4.

Kruyt, M. C., de Bruijn, J. D., Yuan, H., van Blitterswijk, C. A., Verbout, A. J., Oner, F. C. & Dhert, W. J. (2004) Optimization of bone tissue engineering in goats: a peroperative seeding method using cryopreserved cells and localized bone formation in calcium phosphate scaffolds. *Transplantation*, **77**, 359–65.

Kuboki, Y., Saito, T., Murata, M., Takita, H., Mizuno, M., Inoue, M., Nagai, N. & Poole, A. R. (1995) Two distinctive BMP-carriers induce zonal chondrogenesis and membranous ossification, respectively; geometrical factors of matrices for cell-differentiation. *Connect Tissue Res*, **32**, 219–26.

Kurashina, K., Kurita, H., Wu, Q., Ohtsuka, A. & Kobayashi, H. (2002) Ectopic osteogenesis with biphasic ceramics of hydroxyapatite and tricalcium phosphate in rabbits. *Biomaterials*, **23**, 407–12.

Le Huec, J. C., Clement, D., Brouillaud, B., Barthe, N., Dupuy, B., Foliguet, B. & Basse-Cathalinat, B. (1998) Evolution of the local calcium content around irradiated beta-tricalcium phosphate ceramic implants: *in vivo* study in the rabbit. *Biomaterials*, **19**, 733–8.

Le Nihouannen, D., Daculsi, G., Saffarzadeh, A., Gauthier, O., Delplace, S., Pilet, P. & Layrolle, P. (2005) Ectopic bone formation by microporous calcium phosphate ceramic particles in sheep muscles. *Bone*, **36**, 1086–93.

Levander, G. (1934) On the formation of new bone in bone transplantation. *Acta Chir Scand*, **74**, 425–426.

Liu, Y., de Groot, K. & Hunziker, E. B. (2005) BMP-2 liberated from biomimetic implant coatings induces and sustains direct ossification in an ectopic rat model. *Bone*, **36**, 745–57.

Marusic, A., Katavic, V., Grcevic, D. & Lukic, I. K. (1999) Genetic variability of new bone induction in mice. *Bone*, **25**, 25–32.

Miyamoto, S., Takaoka, K. & Ono, K. (1993) Bone induction in monkeys by bone morphogenetic protein. A trans-filter technique. *J Bone Joint Surg Br*, **75**, 107–10.

Ohgushi, H., Goldberg, V. M. & Caplan, A. I. (1989) Heterotopic osteogenesis in porous ceramics induced by marrow cells. *J Orthop Res*, **7**, 568–78.

Ohgushi, H., Dohi, Y., Tamai, S. & Tabata, S. (1993) Osteogenic differentiation of marrow stromal stem cells in porous hydroxyapatite ceramics. *J Biomed Mater Res*, **27**, 1401–7.

Okubo, Y., Bessho, K., Fujimura, K., Konishi, Y., Kusumoto, K., Ogawa, Y. & Iizuka, T. (2000) Osteoinduction by recombinant human bone morphogenetic protein-2 at intramuscular, intermuscular, subcutaneous and intrafatty sites. *Int J Oral Maxillofac Surg*, **29**, 62–6.

Pollick, S., Shors, E. C., Holmes, R. E. & Kraut, R. A. (1995) Bone formation and implant degradation of coralline porous ceramics placed in bone and ectopic sites. *J Oral Maxillofac Surg*, **53**, 915–22.

Reddi, A. H. (1981) Cell biology and biochemistry of endochondral bone development. *Coll Relat Res*, **1**, 209–26.

Reddi, A. H. (1992) Regulation of cartilage and bone differentiation by bone morphogenetic proteins. *Curr Opin Cell Biol*, **4**, 850–55.

Reddi, A. H. (1994) Bone and cartilage differentiation. *Curr Opin Genet Dev*, **4**, 737–44.

Refai, A. K., Textor, M., Brunette, D. M. & Waterfield, J. D. (2004) Effect of titanium surface topography on macrophage activation and secretion of proinflammatory cytokines and chemokines. *J Biomed Mater Res A*, **70**(2), 194–205.

Ripamonti, U. (1991a) The induction of bone in osteogenic composites of bone matrix and porous hydroxyapatite replicas: an experimental study on the baboon (*Papio ursinus*). *J Oral Maxillofac Surg*, **49**, 817–30.

Ripamonti, U. (1991b) The morphogenesis of bone in replicas of porous hydroxyapatite obtained from conversion of calcium carbonate exoskeletons of coral. *J Bone Joint Surg Am*, **73**, 692–703.

Ripamonti, U. (1996) Osteoinduction in porous hydroxyapatite implanted in heterotopic sites of different animal models. *Biomaterials*, **17**, 31–5.

Ripamonti, U. (2000) Smart biomaterials with intrinsic osteoinductivity: geometric control of bone differentiation. In Davies, J. M. (Ed.) *Bone Engineering.* Toronto, Canada, em squared.

Ripamonti, U., Ma, S. & Reddi, A. H. (1992) The critical role of geometry of porous hydroxyapatite delivery system in induction of bone by osteogenin, a bone morphogenetic protein. *Matrix*, **12**, 202–12.

Ripamonti, U., Crooks, J. & Kirkbride, A. N. (1999) Sintered porous hydroxyapatites with intrinsic osteoinductive activity: geometric induction of bone formation. *South African J Sci*, **95**, 335–43.

Sasano, Y., Ohtani, E., Narita, K., Kagayama, M., Murata, M., Saito, T., Shigenobu, K., Takita, H., Mizuno, M. & Kuboki, Y. (1993) BMPs induce direct bone formation in ectopic sites independent of the endochondral ossification *in vivo*. *Anat Rec*, **236**, 373–80.

Schmitt, J. M., Hwang, K., Winn, S. R. & Hollinger, J. O. (1999) Bone morphogenetic proteins: an update on basic biology and clinical relevance. *J Orthop Res*, **17**, 269–78.

Takemoto, M., Fujibayashi, S., Matsushita, T., Suzuki, J., Kokubo, T. & Nakamura, T. (2005) Osteoinductive ability of porous titanium implants following three types of surface treatment. *51st Annual Meeting of the Orthopaedic Research Society.* Washington, DC.

Thomsen, P. & Gretzer, C. (2001) Macrophage interactions with modified material surfaces, *Curr Opin in Solid State and Mater Sci*, **5**, 163–76.

Toth, J. M., Lynch, K. L. & Hackbarth, D. A. (1993) Ceramic-induced osteogenesis following subcutaneous implantation of calcium phosphates. *Bioceramics*, **6**, 9–13.

Urist, M. R. (1965) Bone: formation by autoinduction. *Science*, **150**, 893–9.

Urist, M. R. & McLean, F. C. (1952) Osteogenetic potency and new-bone formation by induction in transplants to the anterior chamber of the eye. *J Bone Joint Surg Am*, **34-A**, 443–76.

Urist, M. R. & Strates, B. S. (1971) Bone morphogenetic protein. *J Dent Res*, **50**, 1392–406.

Urist, M. R., Granstein, R., Nogami, H., Svenson, L. & Murphy, R. (1977) Transmembrane bone morphogenesis across multiple-walled diffusion chambers.

New evidence for a diffusible bone morphogenetic property. *Arch Surg*, **112**, 612–19.
Urist, M. R., Grant, T. T., Lindholm, T. S., Mirra, J. M., Hirano, H. & Finerman, G. A. (1979) Induction of new-bone formation in the host bed by human bone-tumor transplants in athymic nude mice. *J Bone Joint Surg Am*, **61**, 1207–16.
Vargervik, K. (1992) Critical sites for new bone formation. In Habal, M. B. & Reddi, A. H. (Eds.) *Bone Grafts and Bone Substitutes.* Philadelphia, USA, W B Saunders.
Winter, G. D. & Simpson, B. J. (1969) Heterotopic bone formed in a synthetic sponge in the skin of young pigs. *Nature*, **223**, 88–90.
Wolfinbarger, L., Jr. & Zheng, Y. (1993) An *in vitro* bioassay to assess biological activity in demineralized bone. *In Vitro Cell Dev Biol Anim*, **29A**, 914–16.
Wozney, J. M. (1992) The bone morphogenetic protein family and osteogenesis. *Mol Reprod Dev*, **32**, 160–67.
Wozney, J. M. (1994) Molecular biology of the bone morphogenetic proteins. In Urist, M. R., O'Connor, B. T. & Burwell, R. G. (Eds.) *Bone Grafts, Derivatives and Substitutes.* Oxford, UK, Butterworth-Heineman Ltd.
Wozney, J. M. & Rosen, V. (1998) Bone morphogenetic protein and bone morphogenetic protein gene family in bone formation and repair. *Clin Orthop Relat Res*, **346**, 26–37.
Yamasaki, H. (1990) Heterotopic bone formation around porous hydroxyapatite ceramics in the subcutis of dogs. *Japan J Oral Biol*, **32**, 190–92.
Yamasaki, H. & Sakai, H. (1992) Osteogenic response to porous hydroxyapatite ceramics under the skin of dogs. *Biomaterials*, **13**, 308–12.
Yang, Z., Yuan, H., Tong, W., Zou, P., Chen, W. & Zhang, X. (1996) Osteogenesis in extraskeletally implanted porous calcium phosphate ceramics: variability among different kinds of animals. *Biomaterials*, **17**, 2131–7.
Yoshida, K., Bessho, K., Fujimura, K., Kusumoto, K., Ogawa, Y., Tani, Y. & Iizuka, T. (1998) Osteoinduction capability of recombinant human bone morphogenetic protein-2 in intramuscular and subcutaneous sites: an experimental study. *J Craniomaxillofac Surg*, **26**, 112–15.
Yuan, H. (2001) *Osteoinduction of calcium phosphates. Thesis, Biomaterials Research Group, University of Leiden*, Leiden, The Netherlands.
Yuan, H., Yang, Z., Zou, P., Li, Y. & Zhang, Z. (1997) An investigation of the osteoinduction of synthetic porous phase-pure hydroxyapatite ceramic. *Biomed Eng Appl Bas Com*, **9**, 274–8.
Yuan, H., Yang, Z., Li, Y., Zhang, Z., de Bruijn, J. D. & de Groot, K. (1998) Osteoinduction by calcium phosphate biomaterials. *J Mater Sci Mater Med*, **9**, 723–6.
Yuan, H., Kurashina, K., de Bruijn, J. D., Li, Y., de Groot, K. & Zhang, X. (1999) A preliminary study on osteoinduction of two kinds of calcium phosphate ceramics. *Biomaterials*, **20**, 1799–806.
Yuan, H., Li, Y., de Bruijn, J. D., de Groot, K. & Zhang, X. (2000) Tissue responses of calcium phosphate cement: a study in dogs. *Biomaterials*, **21**, 1283–90.
Yuan, H., de Bruijn, J. D., Li, Y., Feng, Z., Yang, K., de Groot, K. & Zhang, X. (2001a) Bone formation induced by calcium phosphate ceramics in soft tissue of dogs: a comparative study between alpha-TCP and beta-TCP. *J Mater Sci Mater Med*, **12**, 7–13.

Yuan, H., de Bruijn, J. D., Zhang, X., van Blitterswijk, C. A. & de Groot, K. (2001b) Bone induction by porous glass ceramic made from Bioglass (45S5). *J Biomed Mater Res*, **58**, 270–76.

Yuan, H., de Bruijn, J. D., Zhang, X., van Blitterswijk, C. A. & de Groot, K. (2001c) Osteoinduction by porous alumina ceramic. *European Conference on Biomaterials.* 16th ed. London, UK.

Yuan, H., de Bruijn, J. D., Zhang, X., van Blitterswijk, C. A. & de Groot, K. (2001d) Use of an osteoinductive biomaterial as a bone morphogenetic protein carrier. *J Mater Sci Mater Med*, **12**, 761–6.

Yuan, H., van den Doel, M., Li, S. H., van Blitterswijk, C. A., de Groot, K. & de Bruijn, J. D. (2002) A comparison of the osteoinductive potential of two calcium phosphate ceramics implanted intramuscularly in goats. *J Mater Sci Mater Med*, **13**, 1271–5.

Yuan, H., van Blitterswijk, C. A., de Groot, K. & de Bruijn, J. D. (2006a) A comparison of bone formation in biphasic calcium phosphate (BCP) and hydroxyapatite (HA) implanted in muscle and bone of dogs at different time periods. *J Biomed Mater Res A*, **78**, 139–47.

Yuan, H., van Blitterswijk, C. A., de Groot, K. & de Bruijn, J. D. (2006b) Cross-species comparison of ectopic bone formation in biphasic calcium phosphate (BCP) and hydroxyapatite (HA) scaffolds. *Tissue Eng*, **12**, 1607–15.

Zhang, M., Powers, R. M., Jr. & Wolfinbarger, L., Jr. (1997) A quantitative assessment of osteoinductivity of human demineralized bone matrix. *J Periodontol*, **68**, 1076–84.

Zhang, X. (1991) A study of porous block HA ceramics and its osteogenesis. In Ravaglioli, A. & Krajewski, A. (Eds.) *Bioceramics and the Human Body*. Amsterdam, The Netherlands, Elsevier Science.

Part II

Types of bioceramics

10

Alumina ceramics

B BEN-NISSAN, A H CHOI and R CORDINGLEY,
University of Technology, Australia

10.1 Introduction

Aluminium oxide (Al_2O_3), more commonly known as alumina, is the most widely used oxide ceramic material. As a raw material, Al_2O_3 powder is produced in large quantities from the mineral bauxite, by the Bayer process. Its applications are widespread in engineering and biomedical applications. Some common examples include spark plugs, tap washers, pump seals, electronic substrates, grinding media, abrasion-resistant tiles, cutting tools, bioceramics, orthopaedic and dental applications, body armour, laboratory ware and wear parts for the textile and paper industries.

Degenerative joint disease is recognised as an increasing problem for society, a direct result of an ageing population. During 2000, joint replacement procedures numbered more than 1.6 million, most performed as a result of arthritis. When a person has joint pain and joint immobility, the main concern is the relief of that pain and the return to a healthy and functional lifestyle. The degeneration of joints often makes surgical repair or replacement necessary.

The word arthritis literally means joint inflammation. There are several forms of arthritis, most of which affect the joints of the body. Osteoarthritis is the most common form, and the hip is one of the common joints affected by this. Osteoarthritis is the degeneration of the articular surface of the joint. It is a degenerative process, which directly results in the wearing out of the articulating cartilage on the joint's surface. Over time, the joint surfaces slowly deteriorate until the underlying bone is exposed. Exposed bone results in a painful joint when it moves and bears weight. As a result, hip pain and stiffness increase and the bones articulate without the load-distributing effect of the cartilage. Other hip problems that produce similar symptoms include rheumatoid arthritis and avascular necrosis (injury and loss of blood supply to the bones).

Osteoarthritis is the primary diagnosis leading to joint replacement. People over the age of 65 make up the primary target for joint replacement,

and growth of the world's elderly population will outpace that for the overall population (200–400% over the next 30 years in developing countries alone). The market for joint replacement products is expected to grow at a steady rate of 5–10% annually over the next few decades. The strongest growth in this market has been in bone growth stimulators, biologics and spinal implants and instruments. Table 10.1 outlines the orthopaedic product sales by segment.

High-purity alumina is normally classified as that with a purity of 99.99% and has been developed as an alternative to surgical metal alloys for orthopaedic and dental applications such as total hip replacement. Due to its high hardness, low friction and excellent wear and corrosion resistance, alumina is suitable for use as articulating surfaces in orthopaedic applications. To achieve the long-term stability of alumina in orthopaedic applications, the material must be free of porosity, and its microstructure must be fine and homogeneous. Medical-grade alumina has a very low concentration of sintering additives, very small grain size, and a narrow grain-size distribution. Such a microstructure is capable of inhibiting static fatigue and slow crack growth while the ceramic is under load. Recently, alumina matrix composites were selected as the best new family

Table 10.1 Worldwide orthopaedic product sales in 2003: by market segment (US$ billions)

Product segment	2001	2003
Reconstructive devices[a]	4.9	6.9
Fracture fixation[b]	1.4	1.9
Spinal implants/instrumentation[c]	1.5	2.9
Arthroscopy/soft tissue repair[d]	1.2	3.2
Orthobiologics[e]	1.0	N/A
Other products[f]	3.0	4.1
Total market	13.1	19

Source: The Worldwide Orthopaedic Market.
[a] Hip, knee, shoulder, elbow, wrist, ankle and digit implants.
[b] Internal (plates, screws, nails, pins, wires) fixation and external fixation products.
[c] Internal fixation devices and disectomy and vertebroplasty products.
[d] Scopes, cameras, instruments, soft-tissue implants and repair kits.
[e] Bone-graft substitutes, allograft, autogenous bone and soft-tissue replacement products and viscoelastics.
[f] Power equipment, casting materials, soft goods, bracing systems, bone-growth stimulators, maxillofacial fixation products, diagnostics, cement and cement mixing/delivery systems, infection control equipment, pulsed lavage/irrigation systems, continuous passive motion machines, etc.

of ceramics to provide the foundation for an expanded use of ceramics in orthopaedics.

This chapter provides an insight into the physical properties and microstructure of alumina ceramics and their mechanical and tribological properties, new generation and currently used medical grade alumina bioceramics, current status of major implant production companies and the current research, development, and applications of alumina ceramics and its composites in the biomedical field.

10.2 Physical properties of alumina

There are four basic classes of materials used in clinical practice for biomedical implants and devices. They can be classified as: bioceramics, bio-metals (metals that can be used as biomaterials), bio-polymers and composites. These classes of materials have combinations of properties determined by the composition and the production methods utilised, while each set of properties has its own benefits and limitations. Recently, a new range of composites were introduced, and these can be termed as inorganic–organic composites, some utilising natural materials and appropriately named as hybrids. In terms of hardness of the materials, ceramics are the hardest of solids, and are then followed by metals. Some of the mechanical properties of ceramic and metallic biomaterials, as well as the natural materials, are presented in Table 10.2.

Many applications of ceramics are based upon unique physical, mechanical and thermal properties. Density, biocompatibility, strength and wear resistance are the main important issues for their biomedical applications. Density is an important physical property (see Fig. 10.1). Open porosity is an important density parameter and is often a crucial measurement. The porosity of a substance reveals the volume of pores present in the material. It can have a strong effect on the properties of a ceramic material. Open porosity can reduce the strength and allow permeability to gases or liquids. Therefore, it is often important to determine the nature of the porosity in addition to determining the density.

Additives or impurities determine the colour of alumina, in addition to the sintering atmosphere, and by the interaction with ionising radiation. Alumina is generally white but can sometimes be pink (88% alumina) or brown (96% alumina). When chromium oxide (Cr_2O_3) is added, it reacts with Al_2O_3 to form a solid solution. The amount of chromium oxide added will determine whether the colour of alumina changes to pink or ruby. When medical-grade alumina is sintered in air together with the addition of magnesia, it will appear as ivory. Alumina turns white when it is sintered in reducing atmosphere or if it contains traces of silica (Willmann, 2003).

Table 10.2 Mechanical properties of biomaterials (modified from Lutton and Ben-Nissan, 1997)

	Density (g/cm^3)	Young's modulus (GPa)	Fracture toughness ($MPom^{1/2}$)	Compressive strength (MPa)	Tensile strength (MPa)
Ceramics					
Alumina	3.98	420	3–5.4	4400	282–551
Zirconia (TZP)	5.74–6.08	210	6.4–10.9	1990	800–1500
Silicon nitride (HPSN)	3.3	304	3.7–5.5	3700	700–1000
Hydroxyapatite (3% porosity)	–	7–13	3.05–3.15	350–450	38–48
Metals					
Titanium (Ti–6Al–4V)	4.43	114	44–66	450–1850	900–1172
Cr-Co-Mo	8.3	210	120–160	480–600	400–1030
Stainless steel (316L)	8.0	193	20–95	–	515–620
Human tissue					
Cortical bone	1.7–2.0	3.8–11.7	2–12	88–164	82–114
Cancellous bone	–	0.2–0.5	–	23	10–20
Cartilage	–	0.002–0.01	–	–	5–25
Other					
Bone cement (PMMA)	–	2.24–3.25	1.19	80	48–72
UHMWHD polyethylene	0.94	0.69	–	20	38–48

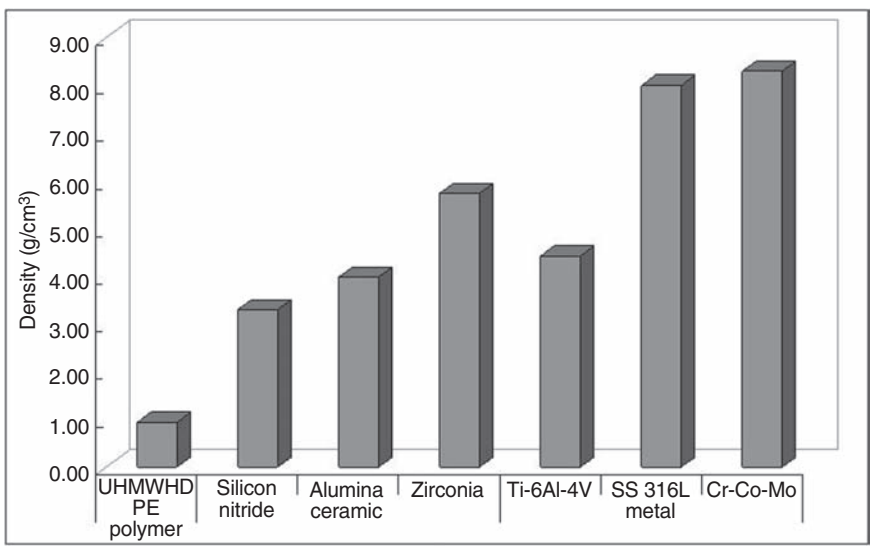

10.1 The densities of various biomaterials.

10.3 Mechanical properties of alumina

When a metallic material yields under load, such as in a mechanical testing, line defects or dislocations move through its structure. Metals are intrinsically soft and ductile due to their appropriate slip systems, which allow for yielding. Metals can be shaped easily by machining or by casting from molten state without any major difficulties. However, most ceramics are intrinsically hard, due to their ionic, covalent and/or mixed bonding, which presents an enormous lattice resistance to the motion of dislocations, hence they cannot be shaped by melting and casting. This hardness and strength of ceramics can be exploited in areas where wear resistance is required, specifically in articulating joints in orthopaedic applications.

In general, the high toughness of metals are be derived from its crack-tip plasticity. The fracture energy is absorbed in the plastic zone, generating a tortuous path that makes the propagation of the crack much more difficult. Although some plasticity can also occur at the tip of a crack in a ceramic material, nevertheless the energy absorption is relatively small, which results in a low fracture toughness value. Most ceramics, including alumina, have values of fracture toughness (K_{IC}) roughly one-fiftieth of those of ductile materials (see Fig. 10.2).

Because of their strong bonding, alumina ceramics have very high melting or, more appropriately, dissociation temperatures, hence the production of alumina ceramics can only be achieved with high-temperature sintering. During the sintering process, powders are heated usually to two-thirds of their melting temperature. As shown earlier, during this densification particles bond together to form necks between the particles, which subsequently reduce the surface area and cause the powder to consolidate.

10.4 Bioinert ceramics in articulation

Ceramics are considered hard and brittle materials with relatively poor tensile properties. However, they have excellent compressive strength, high resistance to wear and favourably low frictional properties in articulation. The low frictional properties are enhanced by the fact that ceramics are hydrophilic with good wettability (see Fig. 10.3) and can be highly polished, which provides a superior load-bearing surface with itself or against polymeric materials in a physiological environment. Bioceramics used singularly or with additional natural, organic or polymeric materials are among the most widely accepted of all biomaterials for hard and soft tissue applications.

Interest in ceramics for biomedical applications has increased over the past 30 years. The ceramics that are used in implantation and clinical

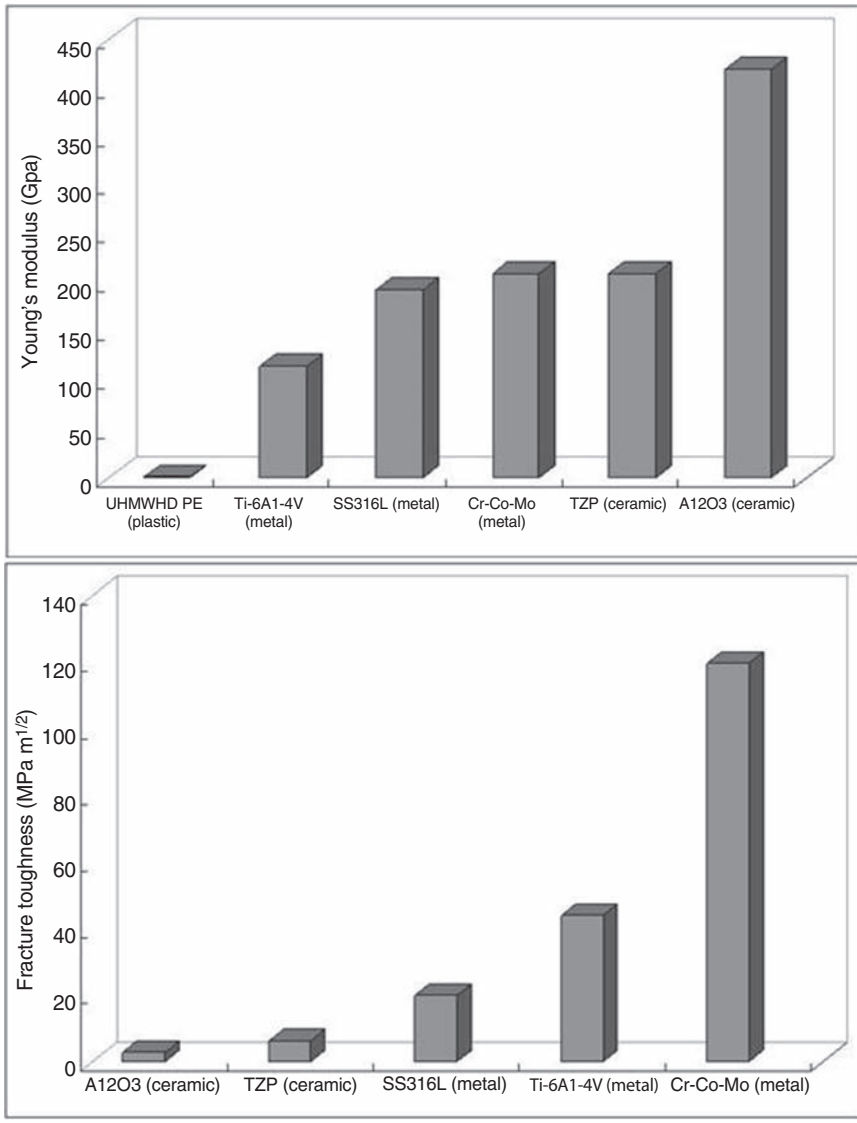

10.2 The plot of comparative Young's modulus and fracture toughness values of a number of current metallic and ceramic biomaterials.

purposes include aluminium oxide (alumina), bioglass®, glass-ceramics, calcium phosphates (hydroxyapatite and β-tricalcium phosphate) and crystalline or glassy forms of carbon and its compounds, and until recently, partially stabilised zirconia (PSZ) (both yttria (Y-TZP) and magnesia sta-

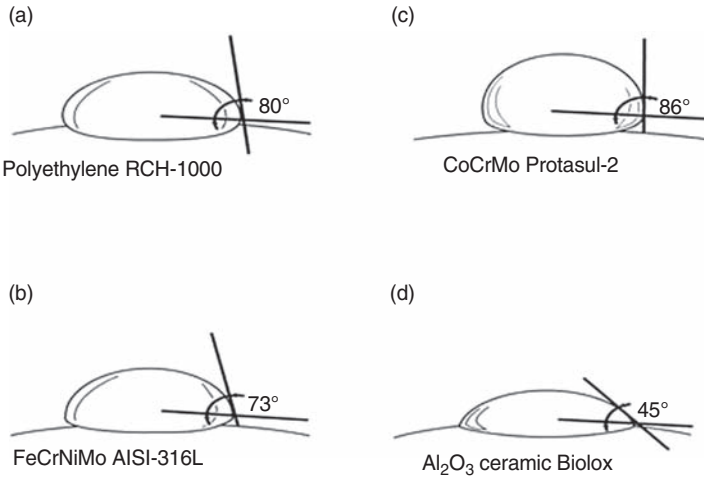

10.3 Hydrophilic/hydrophobic behaviour shown by wetting angles of different orthopaedic biomaterials: (a) polyethylene (RCH-1000), (b) FeCrNiMo, AISI-316L stainless steel, (c) CoCrMo alloy (Protasul-2), (d) alumina ceramic (Biolox).

bilised (Mg-PSZ)). It is worth mentioning that the use of the PSZ zirconia femoral head had virtually ceased due to a high rate of fracture. The first indication of a problem occurred near the end of 2000. Currently, zirconia is being used as an additive to improve the strength of alumina. Some new-generation alumina containing PSZ is also entering the dental implant area (Kim *et al.*, 2003).

Historically, Sir John Charnley introduced the metal-on-plastic total hip replacement (THR) in 1962. Most total joint prostheses consist of an articulation of a metal alloy on ultra-high molecular weight polyethylene (UHMWPE). This latter material did not have the strength for weight-bearing joint replacements, or for inter-medullary nails or bone plates. Both cobalt chrome alloy and stainless steel are used for the bearing surface of joints and can be used for the entire femoral component of hips and knees, and also for other joints such as the shoulder and the ankle.

Metal-on-metal articulation in a total joint prosthesis has a high coefficient of friction resulting in poor wear, unless it has a very high surface finish, which decreases the wearing of the articulating surface. In the early 1970s a metal alloy stem was employed with an alumina femoral head on a UHMWPE acetabular cup. This design has reportedly reduced wear during the past 30 years, with rates as much as 10–20 times lower than the wear rates of metal-on-metal alone.

UHMWPE and recently developed highly cross-linked polyethylene (HCPE) are at present the preferred materials for use in conjunction with a metal or ceramic prosthesis. Creep in PE remains a problem. Wear of the polyethylene component of these prostheses does occur, and these wear particles can sometimes cause a severe tissue reaction and eventual loosening of the implant. UHMWPE is being improved in both strength and wear characteristics. It is essential that the bearing surface in contact with the polyethylene be very highly polished. The quality of the finish on the bearing surface is critical to the wear characteristics of the UHMWPE. HCPE has proven to be a better material for articulating surfaces.

Alumina, and until recently, zirconia ceramics and their composites, are currently used in THR as the femoral head and liners generating reductions in wear particles from ultra-high molecular weight polyethylene used in various other combinations (Oonishi *et al.*, 1992).

10.5 Medical-grade alumina

The main aim for the prerequisites of medical grade bioceramics was to identify materials that are bioinert to a human body for a period of more than 10 years. According to Willmann (1997), the bioceramic must offer a high resistance against corrosion in a human body environment. This can be achieved only by using a high-purity oxide ceramic based on purified raw materials that are free of impurities such as silicates and alkaline oxides.

In terms of mechanical properties, the bioceramic should not deform when loaded in physiological situations. The safety of the ceramic components is correlated to its mechanical strength. So the objective has to be to improve the mechanical strength and all properties that are correlated to strength. As explained above, this can be achieved by using technologies such as hot isostatic pressing (HIP) subsequent to the process of sintering. A very important prerequisite is an excellent surface finish; this is of significance for the articulating surfaces of the femoral head and cup insert. An excellent surface finish can easily be achieved if the ceramic material is homogeneous, has no porosity and its microstructure consists of small fine grains. In alumina ceramic this can be achieved by using magnesium oxide (MgO) as a sintering aid. Again, HIP can be used to improve the density and the microstructure of the bioceramic. For medical-grade alumina, the phase is corundum (α-Al_2O_3). It is known to be a very stable phase.

The German Standards' Institute (DIN) published the first recognised requirements for alumina in orthopaedics in 1979 as DIN 58835. This standard was adopted two years later by the International Standards Organization

Table 10.3 Standards for high-purity alumina for orthopaedic implant use

	ISO 6474 (1981)	ISO 6474 (1994)	ASTM F603 (2000)
Bulk density (g/cm^3)	>3.90	>3.94	>3.94
Grain size (μm)	<7.0	<4.5	<4.5
Flexural strength (MPa)	NA	>250	>400

(ISO) as ISO 6474 (1981) and two years later still by the American Society for Testing and Materials (ASTM) as ASTM F603 (2000).

The ISO standard was revised in 1994, and this revision resulted in the requirements for bulk density, grain size and biaxial flexural strength being made tougher (see Table 10.3). These standards also list a number of additional requirements that must be satisfied including purity, allowed constituents, compression strength, wear resistance and fatigue strength. The ISO standard 6474 also includes a screening test, which describes a ring-on-disk test for the wear couple alumina–alumina. Once a material passes this examination, the time-consuming simulator testing will be performed. To be considered as medical-grade, the alumina has to pass this test *in vitro*.

These standards are necessary to ensure the production of a high-quality material for biomedical applications. The chemical, physical and mechanical requirements serve as criteria for a high-purity, consistent product that can be implanted in the human body. These requirements provide specifications for biocompatible grades of alumina for use in physiological environments.

10.6 Current alumina bioceramics

High-purity alumina bioceramics have been developed as an alternative to surgical metal alloys for total hip prosthesis and tooth implants. Their high hardness, low friction coefficient and the excellent corrosion resistance of alumina offer a very low wear rate at the articulating surfaces in orthopaedic applications. Alumina has the ability to be polished to a high surface finish.

Other applications for alumina in orthopaedic and maxillofacial applications include porous coatings for femoral stems, alumina spacers employed specifically in revision surgery (Huckstep and Sherry, 1996), knee prostheses (see Fig. 10.4), and in the past as polycrystalline and single crystal forms in dental applications as tooth implants (Hench, 1988; Oonishi *et al.*, 1992, 2003; Sedel, 2000).

10.4 Photograph of bi-surface knee femoral component made of alumina ceramics from Kyocera (Ueno *et al.,* 2003).

Medical-grade alumina has a very low concentration of sintering additives, normally less than 0.5 wt%. The microstructure of medical-grade alumina consists of a narrow grain-size distribution with very small grain size of less than 7 μm. Such a microstructure is capable of inhibiting static fatigue and slow crack growth while the ceramic is under load.

The average grain size of current medical-grade alumina is 1.4 μm, and surface finish is usually controlled to a roughness of less than 0.02 μm. However, unless its surface is modified or used directly in articulating areas, alumina has a fundamental limitation as an implant material for other applications in that, like other 'inert' biomaterials, a non-adherent fibrous membrane may develop at the interface. In certain circumstances interfacial failure can occur, leading to loosening, as was observed in some earlier dental implant designs.

The mechanical behaviour of alumina ceramics in simulated physiological environments has led to long-term survival predictions when subjected to sub-critical stresses. The stress magnitude of medical-grade alumina was estimated to be 112 MPa for a 50-year period with a 99.9% survival probability (Ben-Nissan, 1993).

As the past 30 years have shown, alumina can be reliably employed in a ceramic hip joint ball, considering the magnitude of the tensile stresses that

the implant will encounter. In a recent work by Oonishi *et al.* (2003), the authors have reported that in THA a decrease in wear by 25–30% was noted when comparing alumina/UHMWPE to that of metal/UHMWPE in hip simulator tests and clinical results. Wear on THA when using alumina/alumina was observed to be near zero in a similar hip simulator test (Sedel, 1999).

In knee simulator tests, UHMWPE wear against alumina decreased to one-tenth of that against metal. Oonishi *et al.* (2003) and Sedel (1999) have further reported that, clinically, no revisions were carried out due to the PE wear problems during the past 23 years.

In retrieved cases, the UHMWPE surface against alumina was very smooth; however, in a comparative study on the UHMWPE surface against metal, many fibrils and scratches were found, showing extremely good performance of alumina ceramics against UHMWPE (Cordingley *et al.*, 2003).

Alumina-on-alumina bearings in total hip replacements have been successfully used since the early 1970s. Since their initiation by Boutin *et al.* (1988), more than 2.5 million femoral heads and nearly 100 000 liners have been implanted worldwide. Alumina-on-alumina implants have been FDA-monitored since 1987. It can be conditionally stated that 'Alumina processes excellent tribologic properties and extra low debris generation could, in theory, provide an answer to osteolysis' (Willmann, 1997).

In the 1990s, Professor Willmann rightly suggested that the success rate of the alumina rests on the larger than 28 mm head size femoral heads. Several *in vitro* and *in vivo* studies using larger than 28 mm femoral heads demonstrated the advantage of using alumina-on-alumina pairing in young patients, and patients with high-demand body functions (Willmann, 2000).

A clinical study was conducted by Antonio *et al.* (2005) to compare the results of hips with ceramic-on-ceramic bearing implants with hips with metal-on-polyethylene bearing implants to determine whether the two bearings were at least equivalent in their performance. Results of their study suggest that alumina ceramics perform as well as the metal-on-polyethylene in clinical scores, but the patients with ceramic bearings had fewer revisions and less osteolysis. They have also concluded that this new alumina ceramic bearing provides a safe option for younger and more active patients.

The lubricant used in laboratory evaluations of total hip-joint simulation tests has been shown to significantly influence the wear results. The articulation of femoral heads in total hip replacements using hip simulators with alpha-calf serum as a lubricant was conducted by Clarke (2003). Alumina/alumina and zirconia/alumina couples were investigated. During the zirconia/alumina wear evaluation, where zirconia was employed as the head and alumina as the liner, the head showed little weight loss and the alumina

liner indicated a typical run-in phase followed by steady-state weight loss. The study has also revealed promise for hard/hard THR systems, whereby wear rates were three times less in order of magnitude when compared with PE cups. It is worth mentioning that this study has employed alpha-calf serum at a 50% concentration, whereby most other studies published were carried out using either water or saline solution, which can be quite detrimental to some of the other ceramic implants.

The purpose of a retrospective study conducted by Hamadouche *et al.* (2002) was to report the results, after a minimum of 18.5 years of follow-up, in a consecutive series of total hip arthroplasties performed with an alumina-on-alumina combination. The mean acetabular wear rate was less than 0.025 mm per year. They concluded that with the alumina-on-alumina total hip arthroplasty, minimal wear rates and limited osteolysis can be expected up to 20 years after the operation, provided that sound acetabular component fixation is obtained.

10.7 Current manufacturers of alumina bioceramics

High-purity alumina bioceramics are currently commercially available from various producers. A brief overview and history of some of the manufacturers of alumina bioceramics are presented in the following section. The physical and mechanical properties of their alumina products are listed in Table 10.4.

Morgan Advanced Ceramics (MAC) (Worcestershire, UK) began manufacturing orthopaedic devices in 1985 and quickly became a recognised supplier of ceramic femoral heads for hip replacements. MAC Bioceramics has the longest clinical history for alumina ceramic materials, HIP Vitox® alumina since 1985.

Dynamic-Ceramic Limited is a specialist advanced ceramic manufacturing, trading and consultancy company. Located in the UK, Dynamic-Ceramic has been producing advanced ceramic solutions since 1987 to customers

Table 10.4 The physical properties of alumina bioceramics from various manufacturers

	Morgan Advanced Ceramics	Dynamic Ceramics	CeramTec	Ceramaret	Kyocera
Purity (%)	99.9	99.9	99.9	99.9	99.9
Density (g/cm^3)	3.978	3.92	4	3.95	13.95
Particle Size (μm)	1.2	N/A	N/A	1–5	N/A

worldwide. Dynamic-Ceramic produces a range of alumina called Dynallox® alumina for biomedical applications.

CeramTec combines over 100 years of experience stemming from a number of innovative companies which have always been among the leaders in the field of high-performance ceramics. CeramTec is active in the biomedical field, electronics, electrical engineering, hermetic systems, piezo-technology, medical technology, mechanical systems, chemicals, textiles, industrial equipment, machining or metal cutting, and many other segments.

Ceramaret designs and produces components from advanced ceramics, such as alumina and synthetic sapphire and ruby. The company has several decades of experience in the design, manufacturing and processing of advanced ceramics and other hard materials.

The Kyocera Corporation was founded in 1959 as a producer of fine ceramics. By combining these engineered materials with metals and plastics, and integrating them with other technologies, Kyocera Corporation has become a leading supplier of engineered ceramics, semiconductor packages, electronic components, solar energy systems, medical and dental implants, telecommunications equipment and document solutions equipment.

10.8 New-generation alumina bioceramics

The introduction of the use of ceramics in the field of orthopaedic implants in the early 1970s has brought about the widespread recognition that the proper application of ceramics can resolve many challenges existing in orthopaedic surgery. Of these, the greatest contribution has been made in the wear reduction area in total joint replacement, as it is now universally accepted that the use of an alumina ceramic substantially reduces wear and the often-resultant osteolysis.

10.8.1 Biolox

Two different materials are used by CeramTec in the manufacture of its products. The first one, Biolox® Forte, is a pure alumina material, which has been the backbone of CeramTec's product and readily available for many years. The second one is the Biolox® Delta, which is an alumina matrix composite material. It has been specifically engineered with substantially improved mechanical properties so that new applications, such as spine and knee components, as well as larger and thinner versions of existing components, such as the femoral heads and inserts, can be developed and reliably used clinically. In this respect, both these materials are complementary. They are not alternatives, nor are they replacements for each other. Both of these materials can be used either articulating against polyethylene, or

Table 10.5 The physical and mechanical properties of Biolox® Delta and Forte (CeramTec)

Property	Biolox® Delta	Biolox® Forte
Density (g/cm^3)	>4.36	3.9
Young's modulus (GPa)	350	380
Flexural strength (MPa)	1203 ± 101	466 ± 106
Fracture toughness (MPom$^{1/2}$)	4.1	2.75
Hardness (HV)	1840 ± 60	1878 ± 60
Grain size (μm)	0.6	3

to each other. Table 10.5 lists the physical and mechanical properties of the Biolox® products.

In terms of strength magnitudes, Biolox® Delta has higher strength than Biolox® Forte, as far as application is concerned. However, it is worth mentioning that it is the loads applied to the components that determine service life, no matter what the strength of the material may be. The magnitude of these loads and the resulting stresses depend to a large extent on the product geometry, the design of the entire implant system, the surgical technique used and the post-operative behaviour of the patient. From a tribological point of view, the ability to be wetted well by a liquid is mandatory for low wear rate. The smaller the wetting angle, the better the lubrication. When the wetting angles were compared between metal, polyethylene and Biolox® ceramics, it was discovered that Biolox® ceramics provides better lubrication. Polar liquids such as synovial liquid are extremely well wetted by Biolox® Forte components. This is achieved by the formation of a microfilm of lubrication on the articulation surface generated by the van der Waals forces between water and the alumina crystal structure.

The alumina-on-alumina system offers the option of very low wear rates. The wear rate of modern ceramic wear couples with hip simulators is extremely low. Walter *et al.* (2004) studied 16 bearings retrieved from a series of 1588 cementless hip arthroplasties with third-generation Biolox® Forte alumina ceramic-on-ceramic bearings to characterize the mechanism of stripe wear formation. None of these bearings was retrieved for bearing failure. The average wear volume was 0.4 mm^3 per year in the heads and 0.3 mm^3 per year in the liners. Mapping of wear stripes on the heads and liners showed that the majority do not occur with normal walking; instead they probably occur with edge loading when the hip is flexed, such as with rising from a chair or with climbing a high step.

A retrieval analysis of two ceramic couples was conducted by Willmann *et al.* (2003). Two hemispheric press-fit cups with a Biolox® Forte ceramic

inlay were retrieved and analysed after 24 months of *in vivo* function. They observed neither chipping off, nor rim contact of the ceramic inserts due to impingement or subluxation. They also noticed that the surface roughness finish of the articulating surfaces had changed, and there were also no scratches and no signs of third body wear. The wear rate was below detection limit.

Biolox® Forte

Biolox® Forte possesses strong bonding between aluminium and oxygen ions, which is accountable for the extremely good corrosion resistance. That is the main reason why components made of this material provide excellent biocompatibility in the human body. Biolox® Forte is bioinert and is highly resistant to all chemical reactions as a result of its high purity and the strong chemical bonding of its crystalline structure.

Biolox® Forte components have a Vickers hardness of approximately 2000. With the exception of diamond, this constitutes the hardest material known. Since it is approximately three times harder than metal, a Biolox® Forte component would remain undamaged if it were scratched during implantation. However, in contrast, if the surface of a metallic component were scratched, both a depression and a protrusion would form, in other words, a groove. This causes a serious problem, as an increase in wear in articulation between metallic implants with polyethylene components.

The wear resistance of Biolox® Forte components can be derived from factors such as the loads encountered *in vivo* are not able to deform the components and the improved surface finish. It also possesses other excellent mechanical properties such as extremely high elastic modulus and high compressive strengths. This leads to Biolox® Forte having excellent dimensional stability.

Biolox® Delta

A high-performance ceramic biocomposite material intended for special medical applications requiring the highest performance, which was not previously possible using ceramics, has been manufactured by CeramTec, and is called Biolox® Delta. In these applications it was reported that it can provide improved versatility and reliability.

Alumina and partially stabilized zirconia (Y-PSZ) are accepted and standardised ceramic materials for clinical applications. These ceramics have a long clinical history in total hip replacement. Although effective, both materials have specific potential disadvantages. For example, alumina exhibits excellent hardness and wear properties; however, it is a brittle material with

a risk of fracture. This hard but brittle combination of material properties means that certain design restrictions apply. PSZ partially stabilized zirconia has only 50% of alumina's hardness but transformation toughening improves its fracture resistance. Therefore, its overall toughness and bending strength are substantially higher than those of alumina. Therefore, an ideal material would be a material that combines the best properties of zirconia and alumina. This leads to the new generation of ceramics, known as zirconia-toughened alumina (ZTA).

Biolox® Delta is an alumina matrix composite composed of approximately 75% alumina and approximately 25% yttria-stabilised tetragonal polycrystalline zirconia (Y-TZP). It combines the excellent material properties of alumina ceramics in terms of chemical and hydrothermal stability with extremely low wear, superior mechanical strength and improved fracture toughness. The zirconia and other additives provide the improved mechanical properties. The increase in strength and toughness in ZTA is attributable to the stress-induced transformation-toughening mechanism which is introduced with the addition of optimized amounts of fine zirconia particles dispersed throughout the alumina body. In principle it is based on the transformation-toughening theory in that, as a crack grows through the ceramic, the crystal structure of the zirconia particles in the region of the crack will change from the metastable tetragonal phase to the stable monoclinic phase.

The change is expected to increase the volume of the particles by about 3–4% and produces compressive stresses in the alumina matrix. These stresses in turn close the crack and act as an energy barrier to further crack growth. The addition of zirconia to the alumina matrix was introduced to increase fracture toughness and strength. However, long-term clinical studies are needed to prove its effectiveness as a new-generation high-performance material.

The microstructure of Biolox® Delta is shown in Fig. 10.5. The dark grains of the alumina matrix are generally less than 0.8 μm in size. Within this matrix are scattered many smaller light-coloured grains of zirconia and fewer elongated oxides of chromium and strontium. The improved properties of Biolox® Delta are reported to be achieved as a result of the high density of the material and the very small grain size of the alumina matrix. The first toughening mechanism involves the introduction of nano-sized, Y-TZP in a stable alumina matrix. The Y-TZP grains are spatially separated from one another in order to reduce the likelihood of structural transformation as well as preventing the initiation and propagation of cracks.

In addition to normal transformation-toughening, a second toughening mechanism is expected to be operational with the addition of an oxide additive, which forms platelet-like crystals. These platelets are reported to

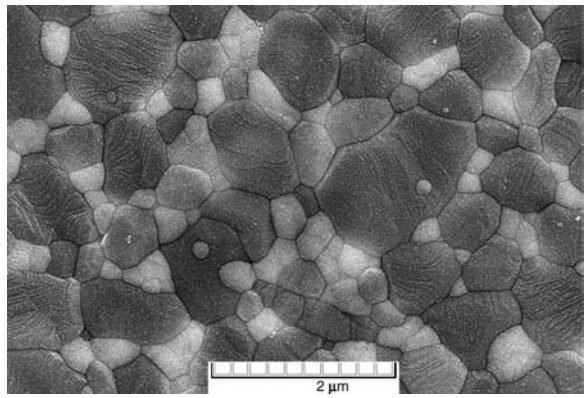

10.5 SEM image of Biolox® Delta showing alumina matrix grains, zirconia grains (white) and mixed oxide platelets.

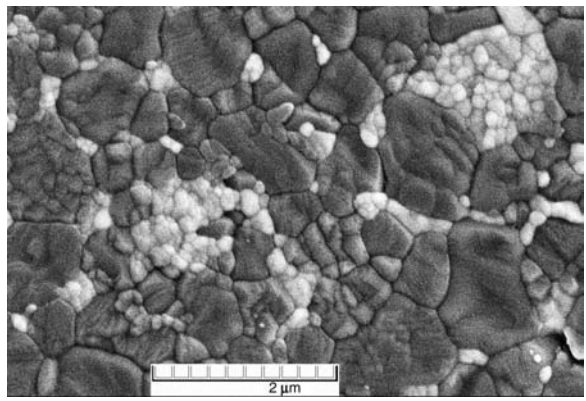

10.6 Microstructure of the NZTA showing large agglomerates of zirconia grains in white throughout the alumina matrix.

dissipate energy by deflecting cracks, thereby increasing strength and toughness (Pfaff and Rack, 2000).

10.8.2 Other zirconia-toughened alumina

In 2002, Insley *et al.* (2002) developed a new batch-processed ZTA ceramic. The new ZTA ceramic (NZTA) is composed of 75% alumina and 25% zirconia, with no presence of mixed oxides. Figure 10.6 shows the microstructure of the NZTA, which consists of large agglomerates of zirconia grains in white throughout the alumina matrix.

In terms of mechanical properties, the NZTA has a significantly lower flexural strength than compared with the commercially available Biolox®

Table 10.6 Physical and mechanical properties between Biolox® Delta and NZTA

		Biolox® Delta	NZTA
Flexural strength (MPa)		1203 ± 101	800 ± 131
Grain size (μm)	Al	0.872 ± 0.26	1105 ± 0.45
	Zr	0.355 ± 0.09	0.265 ± 0.05

Delta. Insley *et al.* stated that the main reason for this difference can be explained by considering the microstructure of their ceramic. Biolox® Delta has a much finer grain size, which results in its superior strength property (see Table 10.6). Apart from the grain size, the dispersion of the zirconia grains in the alumina matrix is also different. Once again, long-term clinical studies are required to prove its effectiveness as a new-generation high-performance orthopaedic biomaterial.

10.9 Summary

An improved understanding of currently used bioceramics in human implants and in bone replacement materials could contribute significantly to the design of new-generation prostheses and post-operative patient management strategies. Overall, the benefits of advanced ceramic materials in biomedical applications have been universally appreciated, specifically, in terms of their strength, biocompatibility and wear resistance. Improvement in the manufacturing process, such as the use of hot isostatic pressing, can result in the higher densities and small grain structures required by the bioceramics. These manufacturing processes permit the achievement of a near theoretical density with the addition of appropriate sintering aids and very fine grain structure, which result in optimisation of strength and avoiding the propagation of cracks and fracture. The tribological properties of alumina ceramic against itself are outstanding, with a linear wear rate 4000 times lower than that of metal-on-polyethylene. The excellent frictional characteristics are due in part to high wettability because of the hydrophilic surface. This is achieved by the formation of a microfilm of lubrication on the articulation surface generated by the van der Waals forces between water and the alumina crystal structure. These properties, demonstrated both *in vitro* and from the analysis of retrieved implants, are responsible for the limited amount of wear particles produced and the subsequent moderate biological reaction to ceramic wear debris. The clinical and radiological long-term results with alumina-on-alumina are expected to show exceptionally long-term survival in patients with high physical demands.

10.10 References and further reading

Antonio J D, Capello W, Manley M, Naughton M and Sutton K (2005), 'Alumina ceramic bearings for total hip arthroplasty', *Clin Ortho Relat Res*, **436**, 164–171.

ASTM Standard F603–00 (2000), 'Standard specification for high-purity dense aluminum oxide for medical application'.

Ben-Nissan B (1993), 'Review: reliability and finite element analysis in ceramic engineering design', *Mater Forum*, **17**, 105–125.

Boutin P, Christel P, Dorlot J M, Meunier A, de Roquancourt A, Blanquaert D, Herman S, Sedel L and Witvoet J (1988), 'The use of dense alumina–alumina ceramic combination in total hip replacement', *J Biomed Mater Res*, **22**, 1203–1232.

Clarke I C (2003), 'Clinical and tribological perspective of wear in alumina–alumina THR', in Ben-Nissan B, Sher D and Walsh W, *Bioceramics 15*, Switzerland, Trans. Tech. Publications, 755–764.

Cordingley R, Kohan L, Ben-Nissan B and Pezzotti G (2003), 'Alumina and zirconia bioceramics in orthopaedic applications', *J Aust Ceram Soc*, **39**, 20–28.

Green D D, Pezzotti G, Sakakura S, Ries D M and Clarke I C (2003), 'Zirconia ceramic femoral heads in the USA', in *49th Annual Meeting of the Orthopaedic Research Society*, New Orleans, Louisiana, 1392.

Hamadouche M, Boutin P, Daussange J, Bolander M E and Sedel L (2002), 'Total hip arthroplasty, a minimum 18.5-year follow-up study', *J Bone Joint Surg Am*, **84**, 69–77.

Hench L L (1988), 'Bioactive ceramics', in Ducheyne P and Lemons J E, *Bioceramics: Materials Characteristics vs.* in vivo *Behavior*, New York, Ann. of the New York Academy of Science, Vol. 523, 54–71.

Huckstep R L and Sherry E (1996), 'Replacement of the proximal humerus in primary bone tumours', *Aus New Zeal J Surg*, **66**, 97–100.

Hulbert F, Bokros J C, Hench L L, Wilson J and Heimke G (1997), 'Ceramics in clinical applications, past, present and future', In Vincenzini P, *Ceramics in Clinical Applications*, Amsterdam, Elsevier Sci. Publications, 3–27.

Insley G M, Turner I, Fisher J and Streicher R M (2002), '*In-vitro* testing and validation of zirconia toughened alumina', in the *Proceedings of the 7th Biolox® Symposium*, Stuttgart, Germany, 26–31.

ISO 6474 (1981), 'Implants for surgery – ceramic materials based on high purity alumina'.

ISO 6474 (1994), 'Implants for surgery – ceramic materials based on high purity alumina revision 2'.

Kim D J, Lee D Y and Han J S (2003), 'Low temperature stability of zirconia/alumina hip joint heads', in Ben-Nissan B, Sher D and Walsh W, *Bioceramics 15*, Switzerland, Trans. Tech. Publications, 831–834.

Lutton P P and Ben-Nissan B (1997), 'Biomaterials in the marketplace: focus on orthopaedic and dental applications', *Mater Tech*, **12**, 121–126.

Oonishi H, Takayaka Y, Clarke I C and Jung H (1992), 'Comparative wear studies of 28-mm ceramic and stainless steel total hip joints over a two to seven year period', *J Long-Term Effects Med Implants*, **2**, 37–47.

Oonishi H, Clarke I C, Good V, Amino H, Ueno M, Masuda S, Oomamiuda K, Ishimaru H, Yamamoto M and Tsuji E (2003), 'Needs of bioceramics to longevity

of total joint arthroplasty', in Ben-Nissan B, Sher D and Walsh W, *Bioceramics 15*, Switzerland, Trans. Tech. Publications, 735–754.

Pfaff H G and Rack R (2000), 'A new material concept for bioceramics in orthopaedics', in the *Proceedings of the 5th Biolox® Symposium*, Stuttgart, Germany, 136–140.

Sedel L (1999), 'Tribology and clinical experience of alumina–alumina articulations', in *Proceeding of the 66th Annual Meeting of the American Academy of Orthopaedic Surgeons*, Anaheim, CA, 120.

Sedel L (2000), 'Evolution of alumina-on-alumina implants: a review', *Clin Orthop Relat Res,* **379**, 48–54.

Ueno M, Ikeuchi K, Nakamura T and Akagi M (2003), 'Comparison of the wear properties of polyethylene plate in total knee prostheses (TKP) using different femoral component materials', in Ben-Nissan B, Sher D and Walsh W, *Bioceramics 15*, Switzerland, Trans. Tech. Publications, 801–804.

Walter W L, Insley G M, Walter W K and Tuke M A (2004), 'Edge loading in third generation alumina ceramic-on-ceramic bearings', *J Arthoplasty*, **19**, 402–413.

Willman G (1997), 'Biolox® forte heads and cup inserts for THR – what a surgeon should know', in *Bioceramics in Orthopaedics – New Application,* Enke, Stuttgart.

Willmann G (2000), 'Experience on zirconia ceramic femoral head', in *Zirconia Femoral Heads for Total Hip Prostheses*, 6th World Biomaterial Congress Workshops, Hawaii, USA.

Willman G (2003), 'The color of bioceramics', in Ben-Nissan B, Sher D and Walsh W, *Bioceramics 15*, Switzerland, Trans. Tech. Publications, 785–788.

Willmann G, Schikora N and Pitto R P (2003), 'Retrieval of ceramic wear couples in total hip arthroplasty', in Ben-Nissan B, Sher D and Walsh W, *Bioceramics 15*, Switzerland, Trans. Tech. Publications, 813–816.

11

Zirconia ceramics

J CHEVALIER and L GREMILLARD, INSA-Lyon, France

11.1 Introduction

The concept of stress-induced phase transformation in zirconia ceramics represents one of the most remarkable innovations in the ceramic field. Indeed, it was shown in the 1970s (Garvie *et al.*, 1975) that zirconia exhibits a transformation toughening mechanism acting to resist crack propagation. The stress-induced phase transformation involves the transformation of metastable tetragonal crystallites to the monoclinic phase at or around the crack tip, which, accompanied by a volumetric expansion, superimposes compressive stresses to the existing stress field. Yttria-stabilized zirconia ceramics (Y-TZP) belong to this family of toughened materials. They can exhibit a strength of more than 1000 MPa with a toughness of about 6–10 MPa $m^{1/2}$. Y-TZP were therefore introduced in orthopaedics to overcome the problem of alumina brittleness and especially its sensitivity to delayed failure. The use of zirconia has opened the way towards new implant designs that were not possible with alumina (i.e. 22 mm femoral heads). After more than 20 years of use in orthopaedics, however, the clinical results associated with the use of zirconia are confusing and controversial. Indeed, phase transformation, beneficial when localised and confined around a propagating crack, may also occur at the surface of the implants in the presence of body fluids, leading to progressive roughening and micro-cracking. This progressive degradation of zirconia from the surface is often referred to as ageing. If clinical results reported before 2000 were satisfactory, with an especially low failure rate, failures of implants in 2001 and current retrieval analysis have shown that ageing occurs *in vivo* and constitutes the main issue for the lifetime of zirconia implants. There is therefore a trend today in orthopaedics to develop alternative materials to the standard Y-TZP, as it is the case with alumina–zirconia composites. At the same time, Y-TZP ceramics are increasingly used for dental applications, since they offer the opportunity to develop devices that are not available with other ceramic materials. No problem with ageing has been reported so far for Y-TZP for

dental applications, which may also benefit from 20 years of research and optimisation from orthopaedics.

As mechanical properties and durability of zirconia are directly related to its crystallography, the first section will provide information on crystallography of zirconia and the main characteristics of the tetragonal to monoclinic transformation. The second section will present the process of zirconia orthopaedic (i.e. femoral heads for total hip replacement, THR) and dental (i.e. dental restoration) devices. Then, both the positive (transformation toughening) and negative aspects (ageing) of the tetragonal to monoclinic transformation will be documented. Finally, the future of zirconia and zirconia-based ceramics will be discussed.

11.2 Crystallography and phase transformation in zirconia

Mechanical properties and durability of zirconia ceramics are directly linked to their crystallography. It is indeed the evolution from one metastable polymorph (tetragonal phase) to the stable one (monoclinic phase) that explains both the phase transformation toughening mechanism responsible for the high mechanical properties of zirconia and its sensitivity to low-temperature degradation (ageing).

Pure zirconia at atmospheric pressure exhibits three polymorphs: monoclinic, tetragonal and cubic phases, from low to high temperature. The monoclinic phase is stable at low temperature (below 1170 °C for pure zirconia). It can be described in the $P2_1/c$ space group. In this structure, the Zr atoms have a sevenfold coordination with the O sublattice. The tetragonal phase exists between 1170 and 2360 °C. The structure is a distorted calcium fluorite type ($P4_2/nmc$), and Zr atoms possess an 8-fold coordination. The cubic phase is stable at high temperature, from around 2360 °C to the melting point (2680 °C). It is a calcium fluorite type structure (face centred cubic, Fm3m). However, the O atoms are displaced from the (0.25,0.25,0.25) position toward a higher z, which may be due to the tendency of the Zr atoms to form a 7-fold coordination (Green *et al.*, 1989).

Neither the tetragonal nor the cubic phase of pure zirconia exist at low temperature as bulk materials. However they can both be stabilised at room temperature by the additions of oxides. The mechanism of stabilisation is still under discussion. Some authors point out an easier ordering of the anions when the cation lattice is disordered, which would allow the zirconia lattice to achieve a more stable state and thus remain cubic or tetragonal after cooling. Others suggest that the change in the electronic charge balance allow the cubic or tetragonal structure to survive (Green *et al.*, 1989). The roles of the oxygen vacancies and of the internal stresses due to the differences in ionic radii are also evoked. Table 11.1 shows the crystallographic

Table 11.1 Crystallographic structure of the three phases of zirconia at room temperature

	Cubic (Mg-PSZ)	Tetragonal (3Y-TZP)	Monoclinic
Space group	Fm3m (225)	$P4_2/nmc$ (137)	$P2_1/c$ (14)
***a* (Å)**	5.073	3.6055	5.144
***b* (Å)**			5.133
***c* (Å)**		5.1797	5.347
β (deg)			98.88
Zr site and positions	4*a*	2*a*	4*e* $x = 0.2734$ $y = 0.0395$ $z = 0.2083$
O site and positions	32*f*, $x = 0.2834$ $y = 0.2834$ $z = 0.2834$ Atoms are slightly displaced from the 8*c* position (0.25,0.25,0.25)	4*d*, $z = 0.185$	4*e* $x = 0.0700$ $y = 0.3317$ $z = 0.3447$ 4*e* $x = 0.4496$ $y = 0.7569$ $z = 0.4792$

features of the three phases of zirconia at room temperature (cubic phase being stabilised by magnesia, and tetragonal phase by yttria).

Zirconia can be stabilised under two different forms:

- For stabilisers with a very low solubility at high temperatures (where cation migration is possible), precipitated systems are formed. These systems are called PSZ (for partially stabilised zirconia), and may be obtained with the addition of magnesia or calcia. Magnesia partially stabilised zirconia (Mg-PSZ) was the first zirconia introduced in orthopaedics. However, the strength and fracture toughness values of Mg-PSZ are modest.
- If the solubility of the stabiliser is high, a solid solution can be formed at high temperature and retained at low temperature. Zirconia is then called TZP, for tetragonal zirconia polycrystal. TZPs are obtained with the addition of ceria (Ce-TZP) or yttria (Y-TZP). Today, only 3Y-TZP (stabilised with 3 mol% Y_2O_3) is used in clinical application.

In 3Y-TZP, the tetragonal phase is retained at room temperature (although some cubic phase can appear for long sintering times or high sintering temperatures). This phase is metastable and can evolve toward the monoclinic phase. The tetragonal to monoclinic phase transformation in 3Y-TZP is martensitic in nature. As a consequence, crystallographic correspondences exist between the parent (tetragonal) and the product (monoclinic) phase, and can be described by habit planes and directions (shape strain) as summarised in Table 11.2 (Deville *et al.*, 2004a). The tetragonal

Table 11.2 Crystallographic features of the tetragonal–monoclinic martensitic transformation in zirconia (Deville *et al.*, 2004a)

Lattice correspondence	Lattice invariant shear[a]	Magnitude of $\vec{g}$	Habit plane normal[b]	Shape strain[b]	Shape strain amplitude	Shear component	Volume change
ABC 1	$(011)[0\bar{1}1]$	0.0344	$\begin{bmatrix}-0.9537\\0.0055\\0.3005\end{bmatrix}$	$\begin{bmatrix}-0.0026\\0.0028\\0.1640\end{bmatrix}$	0.1640	0.1556	0.0518
ABC 2	$(011)[0\bar{1}1]$	0.0344	$\begin{bmatrix}0.0915\\-0.0171\\-0.9956\end{bmatrix}$	$\begin{bmatrix}0.1597\\-0.0007\\-0.0373\end{bmatrix}$	0.1640	0.1556	0.0518
BCA 1	$(110)[1\bar{1}0]$	0.0344	$\begin{bmatrix}0.0034\\0.3935\\-0.9193\end{bmatrix}$	$\begin{bmatrix}0.0030\\0.1751\\0.0186\end{bmatrix}$	0.1761	0.1683	0.0518
BCA 2	$(110)[1\bar{1}0]$	0.0344	$\begin{bmatrix}-0.0168\\-0.9996\\-0.0241\end{bmatrix}$	$\begin{bmatrix}-0.0040\\-0.0558\\0.1670\end{bmatrix}$	0.1761	0.1683	0.0518
CAB 1	$(101)[10\bar{1}]$	0.0027	$\begin{bmatrix}0.3006\\-0.9537\\-0.0001\end{bmatrix}$	$\begin{bmatrix}0.1640\\-0.0026\\-0.0002\end{bmatrix}$	0.1640	0.1556	0.0518
CAB 2	$(101)[10\bar{1}]$	0.0027	$\begin{bmatrix}-0.9958\\0.0915\\0.0003\end{bmatrix}$	$\begin{bmatrix}-0.0373\\0.1597\\-0.0001\end{bmatrix}$	0.1640	0.1556	0.0518

Input parameters: t-phase: $a_t = 5.128$ Å, $c_t = 5.224$ Å; m-phase: $a_m = 5.203$ Å, $b_m = 5.217$ Å, $c_m = 5.388$ Å, $\beta_m = 98.91°$.
[a] Expression in the lattice axis system of the tetragonal parent phase.
[b] Expression in the orthonormal axis system bounded to the tetragonal lattice axis system.

to monoclinic (t–m) transformation is accompanied by shear strain (amplitude of ≈ 0.16) and volume expansion (around 0.05).

Lange (1982) described the thermodynamics of t–m transformation in zirconia considering the simple ideal case of a spherical tetragonal particle in a matrix. The change of total free energy (ΔG_{t-m}) due to the transformation is given by equation 11.1:

$$\Delta G_{t-m} = \Delta G_c + \Delta U_{SE} + \Delta U_S \qquad 11.1$$

where ΔG_c (<0 at low temperature) is the change in chemical free energy (dependent on temperature and composition), ΔU_{SE} (>0) is the change in strain energy associated with the transformation of particles (dependent on the surrounding matrix, the size and shape of the particle and the presence of stresses) and ΔU_S (>0) the change in energy associated with surface phenomena (creation of new interfaces and micro-cracking).

By decreasing $|\Delta G_c|$ and increasing ΔU_{SE}, the addition of Y_2O_3 decreases the driving force of t–m transformation, hence its temperature (ZrO_2–Y_2O_3 diagram in Fig. 11.1, Scott, 1975; Fabrichnaya and Aldinger, 2004), making

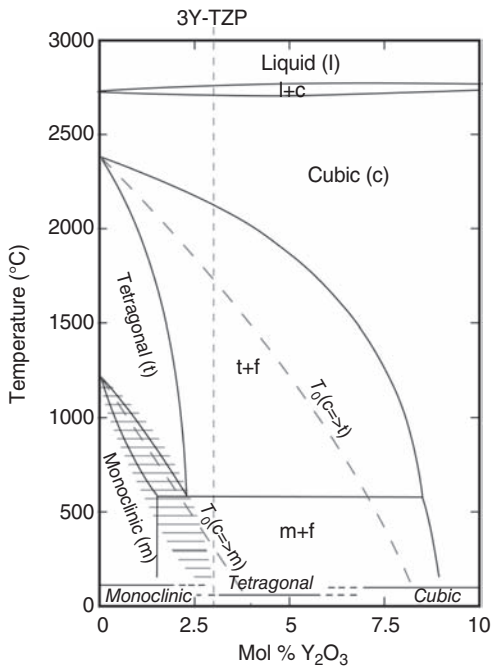

11.1 ZrO_2–Y_2O_3 phase diagram (after Scott, 1975). Metastable phases retained at room temperature are indicated just above the horizontal axis. The dashed lines indicate the temperatures T_0 for the non-equilibrium monoclinic–tetragonal and cubic–tetragonal transition regions (after Fabrichnaya and Aldinger, 2004).

possible the retention of metastable tetragonal phase in dense bodies at room temperatures. ΔU_{SE} is directly related to the surrounding matrix modulus: high matrix modulus will increase ΔU_{SE}, stabilising the tetragonal phase. It is also directly influenced by applied or internal stresses: tensile stresses will act to reduce ΔU_{SE}, destabilising the t phase.

It is thus obvious that t–m transformation will not be identical in bulk and on the surface, since ΔU_{SE} and ΔU_S are not the same. In particular, on the surface for some configurations all the volume change due to the transformation can be accommodated by a surface uplift (Chevalier *et al.*, 2007). This accommodation is not possible in the bulk. Thus, whereas a critical size for t–m transformation in bulk may exist (Garvie and Swain, 1985), it may not exist or may be very small on the surface (Deville *et al.*, 2004b) where all the elastic energy released during the t–m transformation of a particle can be relaxed through a volume change.

11.3 Processing of zirconia ceramics: from powder to implants

The processing of zirconia implants is here described for the two major applications: femoral heads for THR, and dental restorations. The final properties of zirconia implants are directly related to the processing steps: forming, sintering, microstructure development and machining in particular. These steps can be found in different orders for different implants and/or producers, but in all cases, it must be kept in mind that a defect introduced in a processing step will not be eliminated in the next steps, and will subsist in the final product.

3Y-TZP is generally available to implant manufacturers in the form of spray-dried powder. The first step consists in forming the pieces. Femoral heads (Fig. 11.2) are generally isostatically pressed in rubber moulds, directly in the shape of spheres. They are then sintered, at temperatures varying from 1350 to 1500 °C. In order to reach a sufficient density (>99% of the theoretical density of zirconia), it is necessary to use high sintering temperature, and thus 'coarse' grain (>0.5 μm) materials are obtained, with the risk of accelerated ageing (Matsui *et al.*, 2003; Chevalier *et al.*, 2004; Chevalier, 2006). So the best option seems to sinter at lower temperature (between 1350 and 1400 °C). Then the grains retain a small size (~0.3 μm), but the density is only around 97%. Thus, a hot isostatic pressing (HIP) follows (around 1400 °C and up to 2000 bar). This treatment allows the conservation of fine grains and an increase of the density to 99.5%. Most of the time, HIP is conducted in argon. This results in the introduction of oxygen vacancies in zirconia and gives it a dark colour. Therefore, zirconia femoral heads undergo a third thermal treatment, called whitening: the heads are heated in air to around 1200 °C to cure the oxygen vacancies. At this stage, the final

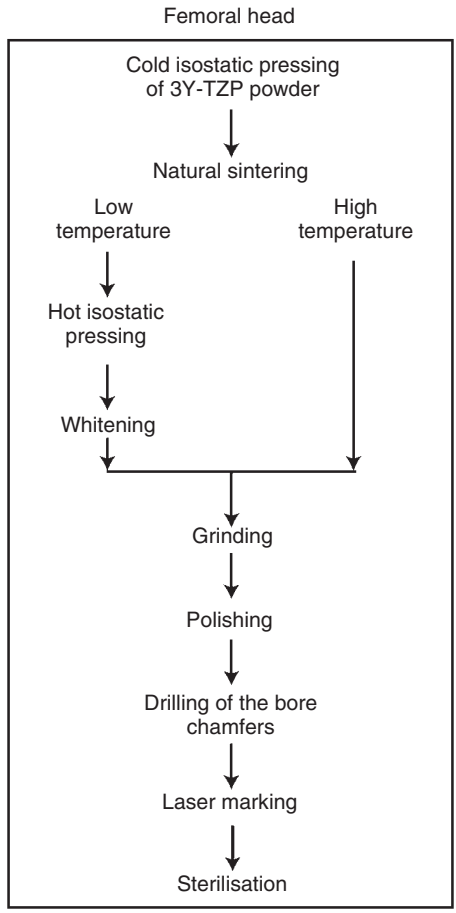

11.2 Synopsis of the process of zirconia femoral heads.

material (white) is obtained. All the remaining operations are machining and polishing. After thermal treatments, the pieces are almost spherical. They are ground (in batches) between two parallel rotating plates, with finer and finer diamond particles. Perfect spheres are obtained, and a final polishing can be done in a tumbler with very fine diamond particles, so as to obtain roughness lower than 5 nm and sphericity lower than 1 µm. Tumbling is a very important step, since ageing is very sensitive to surface stresses (Deville *et al.*, 2006). The last processing steps are the machining of the conic bore and of the chamfer. Then a laser marking is realised, either on the chamfer on at the bottom of the bore. At this step, the work of the ceramic manufacturer is finished. Sterilisation (with gamma or ultraviolet rays) and packaging is made by the distributor of the prostheses.

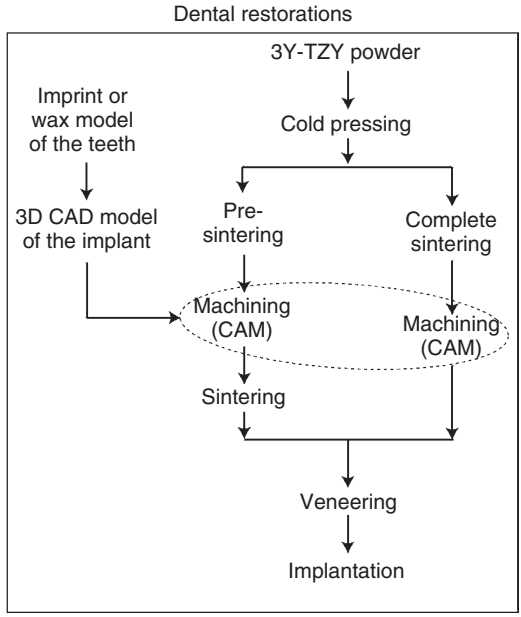

11.3 Synopsis of the process of zirconia dental restorations (i.e. bridges or crowns).

The processing of dental implants is slightly different. We will develop here only the process of ceramic dental restoration (Fig. 11.3). Dental restorations (bridges, crowns) are realised on demand, to fit the shape of the original teeth of the patient. This is possible thanks to the progress in CAD-CAM (computer-aided design/manufacturing) technology. Basically, a wax model of the patient's teeth is realized and 3D measurements on the model are entered in a computer. These data are then used to control the precise machining necessary to obtain pieces with the right shape. The machining can be done either on pre-sintered (Filser *et al.*, 2001; Suttor *et al.*, 2001; Papanagiotou *et al.*, 2006) or on fully dense zirconia blocks (Besimo *et al.*, 2001). Once again to date the only zirconia used is 3Y-TZP. The machining of pre-sintered (with around 50–55% of the final density) zirconia blocks is much easier. But the shrinkage during sintering imposes to machine pieces that are approximately 20% larger than the final dimensions, thus the final dimensions (after sintering) are not completely known. Machining of fully dense blocks is technically more difficult, wears the machining hardware at much higher rate, and may introduce microcracks in the material (Luthardt *et al.*, 2004). However, it offers higher precision and simpler thermal treatments since only one-step sintering is sufficient. An important point about dental restoration is the physical aspect: it must fit the physical

aspect of natural teeth in colour and translucency. Depending on the thermal treatment and purity of the starting zirconia powder, zirconia may be translucent, and very small additions of certain oxides may change its hue without affecting either its sintering ability or its mechanical properties. When the desired translucency and colour cannot be achieved with zirconia alone, veneering is conducted with a low-fusing glass (for example, fluoro-apatite glass ceramic). The glass coating must have a coefficient of thermal expansion close to that of zirconia ($\sim 9 \times 10^{-6}$) to avoid cracking of the coating.

11.4 Mechanical properties of zirconia: taking benefit from phase transformation toughening

The metastable nature of tetragonal grains was the basis for the development of zirconia as a 'tough' ceramic in the 1970s and 1980s. Garvie *et al.* (1975) showed that the mechanical strength of zirconia is improved by the tetragonal to monoclinic transformation at the vicinity of an advancing crack. The large stresses appearing around a crack lead to the t–m transformation. The stress field associated with the volume expansion due to the transformation opposes the tensile applied stress field at the crack tip. This is illustrated in a schematic drawing in Fig. 11.4.

Giving a comprehensive review of toughening mechanisms is beyond the scope of the present chapter. The interested reader may refer to the

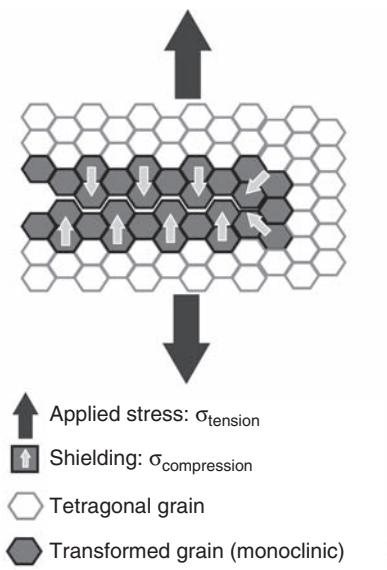

11.4 Stress-induced tetragonal–monoclinic transformation at the crack tip in zirconia, leading to crack shielding.

excellent book *Transformation Toughening of Ceramics* (Green *et al.*, 1989) for details. However, some insight in the transformation toughening mechanics is useful to understand the mechanical behaviour of zirconia. McMeeking and Evans (1982) developed modelling of phase transformation toughening at the beginning of the 1980s. The stress-induced transformation leads to a shielding – K_{Ish} – of the applied stress intensity factor K_I. This means that the real stress intensity factor at the crack tip – K_{Itip} – is lower than that applied by the external forces, according to:

$$K_{Itip} = K_I - K_{Ish} \tag{11.2}$$

The shielding stress intensity factor was evaluated as:

$$K_{Ish} = \frac{0.214 E V_f e^T h^{1/2}}{(1-\nu)} \tag{11.3}$$

where E is the Young modulus, V_f the volume fraction of transformable particles, e^T the volume dilatation associated to the transformation, ν the Poisson ratio, and h the transformation zone width, which is a function of the applied stress intensity factor:

$$h = \left[\frac{3^{1/2}(1+\nu)^2}{12\pi}\right]\left[\frac{K_1}{\sigma_m^c}\right]^2 \tag{11.4}$$

where σ_m^c is the critical local stress leading to phase transformation and K_I the applied stress intensity factor.

A combination of Eqns. 11.3 and 11.4 gives:

$$K_{Ish} = C_{sh} K_I \tag{11.5}$$

with

$$C_{sh} = \frac{0.214 E V_f e^T (1+\nu)}{(1-\nu)\sigma_m^c}\left(\frac{\sqrt{3}}{12\pi}\right) \tag{11.6}$$

Equation 11.5 shows that the higher the applied stress intensity factor, the higher is the shielding stress intensity factor due to the phase transformation. This is confirmed by experimental results (Chevalier *et al.*, 1999a).

Reporting Eqn. 11.5 in Eqn. 11.2 the stress intensity factor at the crack tip can be expressed as follows:

$$K_{Itip} = (1 - C_{sh}) K_I \tag{11.7}$$

This relation means that only a proportion of the applied stress intensity factor is used for crack propagation. This has a major effect on toughness and slow crack growth resistance. The toughening ability of a given zirconia is directly dependent on the critical local stress leading to phase transformation, σ_m^c. In other words, the microstructure will play a major role in transformation toughening, since σ_m^c will depend on the grain size, the

amount of phase stabiliser, etc. The variation of the toughness versus grain size in biomedical grade 3Y-TZP ceramics ranges from 6 to 7.5 MPa $m^{1/2}$ for grain size in the interval 0.3–1.2 μm (above this value, 3Y-TZP are no longer stable), to be compared with 3–4 MPa $m^{1/2}$ for typical alumina ceramics.

3Y-TZP ceramics were introduced in orthopaedics to overcome the problem of alumina brittleness and especially its sensitivity to delayed failure. K_{IC} has provided the basis of the first theories of fracture. However, it is now well recognised that failure of ceramics can occur even when stressed under K_{IC} (or σ_R). Indeed, K_{IC} (and σ_R) only represents a critical level for fast crack growth. Ceramic materials are susceptible to slow crack propagation at K_I values under K_{IC}. This slow crack growth is notable for its extreme sensitivity to the applied load and it tends also to depend on concentration of environmental species (i.e. water), temperature and other extraneous variables. That means that under appropriate conditions, cracks keep on growing for some time until they cause fracture without warning. Since it is not possible to completely avoid imperfections and micro-cracks during the production of sintered bioceramic materials, under these 'appropriate' conditions, cracks will grow in a slow manner before catastrophic failure. All aspects of slow crack growth in ceramics are covered in Lawn (1993).

As a general trend, slow crack growth is described on the basis of V (crack velocity) versus K_I (stress intensity factor) diagram. Slow crack growth in bioceramics is attributed to stress-assisted corrosion at the crack tip, or any pre-existing defect in the ceramic. It is indeed the combined effect of high stresses at the crack tip and the presence of water or body fluid molecules (reducing surface energy at the crack tip) that induce crack propagation in a slow manner. Recently, the presence of a threshold in the stress intensity factor, under which no crack propagation occurs, has been the subject of important research in the ceramic field (Wan *et al.*, 1990). The threshold corresponds to crack equilibrium with a null crack velocity, therefore below which propagation does not occur. For ceramic implants, the threshold determines a safety range of use.

Above the threshold K_{I0}, three stages are generally observed in oxide ceramics. Region I, for low applied stress intensity factors, depends strongly on applied stress, temperature and chemical concentration. In this region, the environmental species react with the ceramic bonds in the crack front-tip. This region is reaction-rate controlled. Region II is insensitive to applied stress, suggestive of a transport process in which the active environmental species are increasingly unable to keep pace with the crack front-tip as K_I increases. Thus this region depends on the diffusion of the corrosive species from the environment to the crack tip. Region III is associated with fast fracture, thus with K_{IC}. Figure 11.5 represents the V–K_I curves of biomedical grade alumina and 3Y-TZP zirconia ceramics. Both toughness, K_{IC}, and

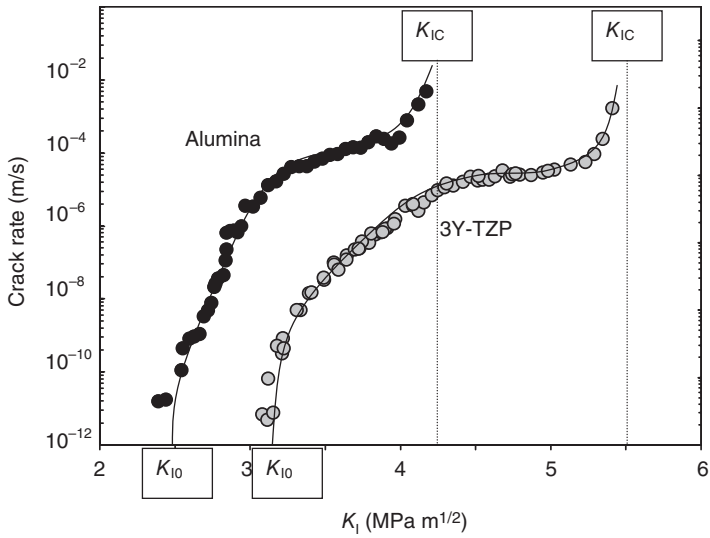

11.5 Crack propagation behaviour of alumina and 3Y-TZP zirconia.

threshold, K_{I0}, of zirconia are superior to alumina. The difference in crack resistance is, however, larger for large stress intensity factors, a property that could be anticipated from eqn. 11.5: the larger the applied K_I the larger the reinforcement. The higher crack resistance of zirconia, compared with alumina, associated with an especially low grain size (typically 0.5 μm versus 2 μm for alumina) leads to a dramatic increase of the strength: up to 2 GPa for zirconia, as compared with 'only' 800 MPa for the best alumina.

Another important aspect is the surface t–m transformation associated with surface grinding. This transformation induced by grinding generates a thin surface layer with a compressive state. The thickness of the surface layer depends on the severity of the surface treatment. It can reach a few tens of micrometres for surfaces machined under 'severe' conditions, with compressive stresses of hundreds of MPa. Thus, even samples machined under severe conditions exhibit high strength, associated with large apparent toughness (20 MPa m$^{1/2}$) and low sensitivity to slow crack growth. This represents a major advantage over alumina where machining flaws are often responsible for failure.

All these advantages are traduced in final components: there is experimental evidence that the ultimate compressive load of zirconia femoral heads is 2–2.5 times higher than that of alumina ball heads of the same design, i.e. for the same diameter and neck length (Piconi and Maccauro, 1999).

11.5 Ageing of zirconia: a negative consequence of phase transformation

Ageing of zirconia is the negative consequence of the transformation ability of the tetragonal phase, described in Section 11.2. Indeed, in the presence of water molecules (or body fluids), the surface of zirconia pieces can transform progressively to the monoclinic phase. The reader may refer to Chevalier *et al.* (2007) to get a comprehensive treatment of ageing in zirconia. Ageing is faster around 250 °C, but occurs even at room temperature (i.e. *in vivo*). Although ageing of zirconia has been known for decades (Kobayashi *et al.*, 1980), the first stages of the transformation are still discussed. However, the role of water molecules is clear (Yoshimura *et al.*, 1987). Several experimental results show that water radicals penetrate the zirconia lattice during exposure to a humid atmosphere. In Y-TZP, the diffusion of water radicals is facilitated by the presence of numerous vacancies due to the trivalent character of yttrium. Recent work by Schubert and Frey (2005) show that the penetration of water radicals leads to a lattice contraction, which results in the formation of tensile stresses in the surface grains that destabilise the tetragonal phase by reducing ΔU_{SE} in eqn. 11.1. Martensitic transformation of grains (or part of grains) at the surface can then proceed (nucleation stage). This nucleation of the transformation leads to a cascade of events occurring neighbour to neighbour: the transformation of one grain leads to a volume increase, stressing the neighbouring grains and to micro-cracking. This offers a path for the water to penetrate the specimen. The transformation occurs therefore by a nucleation and growth process (Chevalier *et al.*, 1999b), well described by the Mehl–Avrami–Johnson laws. The degradation process of zirconia by ageing is schematized in Fig. 11.6. The t–m transformation provokes micro-cracking around the transformed zones that allow an easier access of the water to the bulk and thus a progressive extension of the t–m transformation to the bulk.

The consequences of the ageing process on the long-term performance of zirconia implants can be twofold: ageing is indeed associated with roughening and micro-cracking. Roughening occurs as the transformation at the surface is associated with volume expansion. The transformation is thus associated with surface uplifts. This will inevitably impact the wear performance of hip joint heads, as roughening will increase the wear rate of the antagonist part of the prosthesis, whereas the coupled effect of surface microcracking and wear will generate pull-out of zirconia grains. The biological interaction of small particles with the immune system cells then becomes critical. It is currently believed that particles generated at the contact surfaces enter the peri-prosthetic tissues, where they trigger macrophage reactions. Macrophages then release pro-inflammatory cytokines that stimulate bone resorption, leading to osteolysis, eventual loosening of

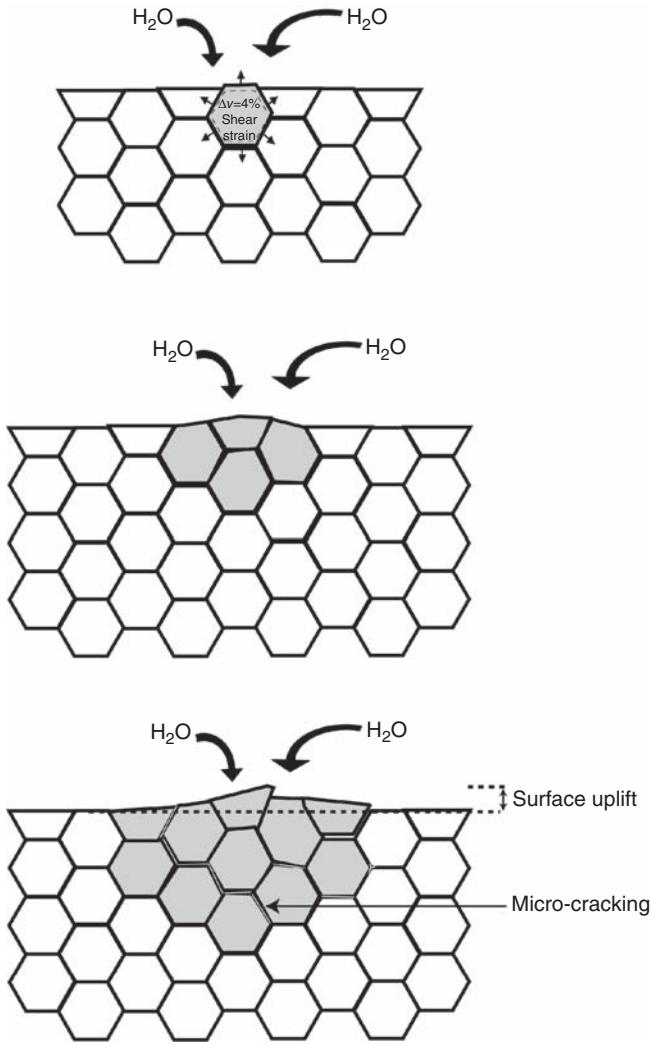

11.6 Schematic representation of ageing at the surface of zirconia. Transformation initiates first on isolated grains at the surface, due to water diffusion in the lattice and then propagates to the neighbours by a near-to-near mechanism. Ageing consequences are roughening and micro-cracking at the surface.

the prosthesis, and a need for replacement. Moreover, micro-cracking around the transformed zone generates defects. Defects generated in stressed regions of the implant may grow with the transformed zone until they reach a threshold size for slow crack propagation to proceed; the fracture of the implant is then unavoidable.

The microstructure plays a key role on ageing, through four principal features: density, grain size, homogeneity and surface state. A high density is probably the most important parameter to limit ageing. Indeed, low density – especially the presence of open porosity – offers water molecules an easy access to the bulk of the material, resulting in ageing not only on the surface of the zirconia piece, but on all the internal surfaces (pore and crack surfaces). Then the material rapidly loses its cohesion and the decrease in mechanical properties can be dramatic.

Many authors have pointed out the important influence of grain size on ageing. Although a critical grain size – below which no transformation is possible – may not exist (see Section 11.2), the beneficial effect of reducing the grain size on the ageing kinetics is widely recognised (Lawson, 1995). However, decreasing the grain size also leads to a decrease in toughness and slow crack propagation threshold, mostly because of less efficient phase transformation toughening. A grain size–density–ageing relationship was evidenced (Muñoz-Saldaña *et al.*, 2003), but still needs to be refined.

3Y-TZP sintered at usual temperatures typically contains up to 15% cubic phase. For long sintering times or high sintering temperatures, bimodal microstructures can appear, the cubic grains being larger than the tetragonal ones and the yttrium having been pumped out of the tetragonal phase (Matsui *et al.*, 2003). The tetragonal grains that are next to the cubic phase are thus depleted in yttrium and act as preferential nucleation sites for ageing (Chevalier *et al.*, 2004).

Both surface tensile micro-stresses (Deville *et al.*, 2006) and tensile stresses on a large scale (Li *et al.*, 2001) trigger the t–m transformation, since they decrease ΔU_{SE} (eqn. 11.1). The only way to limit surface stresses during elaboration is to carefully control machining: rough polishing induces compression stresses that delay ageing, but the surface state is not suitable for wear applications (i.e. femoral heads); fine polishing leads to an acceptable roughness, but removes the compressive stresses and allows the apparition of tensile stresses along the residual scratches. Thus a fine polishing without any scratches is needed. Such a surface state is attainable with 1 μm diamond abrasive.

All the considerations concerning density, grain size and homogeneity of the microstructure also apply to dental implants. However, control of the surface as careful as for the femoral heads is not possible in the case of dental implants, for which to our knowledge there is no polishing step with so small an abrasive. Ageing may not have a significant incidence on the mechanical properties of a Y-TZP dental implant. But it could affect its functional properties in at least three ways. The surface uplifts related to ageing could affect the aesthetic of the implant after a few years. More important, if significant ageing takes place on the part of a post that ensures the link with bone, the progressive micro-cracking of the zirconia surface

may lead to a progressive loosening of the implant. Finally, sand-blasting can sometimes be used to induce compressive stresses on the surface of the implant and thus increase its strength (Oblak *et al.*, 2004); however, this process induces also a microcracking of the surface, and sand-blasted 3Y-TZP specimens exhibit a strong decrease in strength after ageing (Oblak *et al.*, 2004), which makes this treatment irrelevant, and maybe dangerous, for zirconia dental implants. In summary, the consequences of ageing on dental implants are not yet fully known, and must be studied carefully.

11.6 Current biomedical applications of zirconia: from orthopaedic to dental applications

Nowadays, a major issue in orthopaedics, especially for THR, is the generation of wear debris by the implant (Campbell *et al.*, 2004). The standard artificial joints consist of a polymer cup made of ultra-high molecular weight polyethylene (UHMWPE), placed in the acetabulum via a metal-back component, and a metal (stainless steel or cobalt chromium alloy) ball affixed to a metal stem introduced in the femur. Any use of the joint, such as walking, results in cyclic articulation of the polymer cup against the metal ball. During the reciprocating motion of normal joint use, UHMWPE fibrils are then released, mostly by adhesive wear, to form submicrometre-sized wear debris. This results in billions of tiny polymer particles being shed into the surrounding synovial fluid and tissues. The biological interaction with small particles in the body then becomes critical and may lead to osteolysis and implant loosening. The use of bioceramic materials, in comparison with metals, reduces the wear rate of the polyethylene components and produces negligible amounts of metal ion release. Owing to the low roughness exhibited by ceramic heads (typically lower than few nanometres) and their good wettability, abrasion is reduced significantly if ceramic femoral heads are used with acetabular cups made of polyethylene and almost completely avoided when using ceramic femoral heads together with ceramic cup inserts. Approximately 20% of the prosthetic femoral heads manufactured in the world are made of ceramic, with a strongly growing market (i.e. more than 25% growth for the alumina–alumina coupling between 2002 and 2004). Up to the year 2000, approximately 40% of ceramic heads were zirconia and the remaining alumina. If the clinical follow-up with alumina ceramics is very good, it must be kept in mind that their use has been restricted to a limited number of designs of hip components, for which the mechanical loading is less demanding. As an example, 22 mm heads are not currently manufactured using alumina ceramics, for reliability reasons. Alumina is not used for total knee replacement (TKR), where ceramics could also improve the wear properties.

Alumina–alumina coupling also exhibits a significant increase of failure ratios. This is related to its modest mechanical properties. Yttria-stabilised zirconia therefore became a popular alternative to alumina in the 1990s because of substantially higher fracture toughness and strength. The use of zirconia opened the way towards new implant designs that were not possible with alumina, more brittle. An example is the use of zirconia for 22 mm heads, and the development of zirconia knees by some companies. The development of zirconia femoral heads for THR was carried out mainly in Japan by Kyocera (now Japan Medical Materials Co., Osaka, Japan) and in France by Saint Gobain Advanced Ceramics Desmarquest (Evreux, France) which became the global market leader selling zirconia femoral heads under the trade name Prozyr®. From 1985 to 2000, the French company sold more than 350 000 hip joint heads worldwide. Within this period, only 28 brittle fractures were reported (Cales, 2000), representing a fracture rate lower than 0.01% (1 per 10 000 units). Moreover, most of the failures were associated to abnormal use of the hip joint heads (revision replacement surgery without change of the metallic femoral stem, traumatism, etc.) and were reported in the early period of fabrication (before 1993). With the systematic use of proof tests on all implants in the mid-1990s, the fracture rate even fell to 0.002% (1 per 50 000 units). Zirconia was therefore considered as the second generation of ceramic hip joint heads, providing low wear rates and high safety.

In January 1998, to face the increasing commercial demand of zirconia hip joint heads (100 000 units per year), Saint Gobain Desmarquest introduced a tunnel furnace in place of the usual batch furnace (kiln). A tunnel furnace provides a continuous sintering operation and leads to a reduction of processing time for larger series. Without going into details as to the two technologies, the main differences lie in the sintering cycle (Masonis *et al.*, 2004) and atmosphere, giving rise to a difference in microstructure after sintering. All the other processing steps were kept identical. New hip joint heads were called 'TH-balls', whereas the first generations of heads sintered in kiln were called 'BH-balls'. By the end of 2000, two major orthopaedic companies (Depuy France and Smith & Nephew) reported an unusual brittle fracture rate for zirconia TH-balls. Only seven batches (a batch representing roughly 600 heads) were affected by the high failure rate (http://www.prozyr.com/PAGES_UK/Biomedical/figures.htm). They were all processed during the first phase of industrialisation of TH-balls, and the fractures occurred only months after implantation. Some 356 fractures were reported in the seven batches, corresponding to a mean failure ratio of 8% (up to 36% for batch TH-93038). This was a dramatic difference from the overall fracture rates reported in the prior 15 years. The French Medical Agency immediately suspended sales of the TH-balls (http://agmed.sante.gouv.fr/htm/alertes/filalert/dm010811.htm), and the FDA issued a notice (http://www.fda.gov/cdrh/recalls/zirconiahip.html).

The failure origin is now associated with an accelerated ageing in the TH-batches. Even if limited in time and number, and clearly identified to be process controlled, these events have had a catastrophic impact for the use of zirconia. In 2001, Saint Gobain Desmarquest decided to stop Prozyr® activity and the global market sale decreased by more than 90% between 2001 and 2002 with no evidence of a clear renewal. Moreover, some clinical reports show that zirconia can exhibit a progressive ageing degradation even under 'normal' situation, which limits the long-term stability of zirconia orthopaedic implants (Clarke *et al.*, 2003; Chevalier *et al.*, 2007). Alternative alumina–zirconia composites are today preferred in orthopaedics. At the same time, the dental community discovered, at the beginning of the 21st century, the aesthetic and mechanical benefits of using zirconia. For these dental applications, the zirconia market has increased by more than 12% per year. Because of its excellent mechanical properties zirconia is used for dental crowns as well as for multiple-unit bridge frameworks. In combination with layering ceramics, it gives highly aesthetic dental restorations with a lifelike appearance (cf. Chapter 24). Apart from the design of conventional bridge frameworks, inlay-retained bridges can be fabricated with 3Y-TZP. So far, no evidence of low-temperature degradation has been reported for zirconia-based dental implants. However, as 3Y-TZP for dental application is strictly identical to the 'orthopaedic' grade zirconia, the issue of LTD must be kept in mind.

11.7 On the future of zirconia

Among biomaterials, biomedical grade zirconia has led to large controversy among scientists, industrialists and clinicians. Biomedical grade zirconia was introduced 20 years ago in orthopaedics to solve the problem of alumina brittleness and the consequent potential failure of implants. Today, more than 600 000 zirconia femoral heads have been implanted worldwide, mainly in the US and in Europe. Moreover, zirconia is now presented as the next generation material for dental restoration. On the one hand, biomedical grade zirconia exhibits the best mechanical properties of oxide ceramics: this is the consequence of phase transformation toughening, which increases its crack propagation resistance. On the other hand, due to this ability to transform, zirconia is prone to ageing in the presence of water. The tendency of zirconia to ageing, shown both *in vitro* and *in vivo* (for orthopaedic implants), and the negative consequences on the implants integrity may have a detrimental impact on its clinical use.

The bad experience of Prozyr® zirconia femoral heads in 2001 and recent clinical results highlight the insufficiency of current ISO and ASTM standards to ensure complete safety of zirconia products. No reference to ageing is made after 20 years' experience in the orthopaedic community, and much

more for other fields, even though this is the major drawback of this material. ISO and ASTM standards concerning zirconia are currently under revision and should consider this aspect. This is a key for the future for both orthopaedic and dental applications. For example, it is today still possible to process 3Y-TZP with a real grain size approaching 1 μm (the ISO standard referring to a linear intersection distance of 0.6 μm), while a number of studies clearly show dramatic decrease of ageing resistance for a real grain sizes above 0.6 μm (i.e. linear intersect distance of 0.4 μm). Ageing being thermally activated, accelerated tests can be performed at temperatures higher than 37 °C, in the framework of the classical time–temperature equivalence principle. The standard, now forbidden, steam sterilization procedure at 134 °C was proven to induce some degree of ageing. It is therefore a good basis to propose an accelerated test in ISO or ASTM standards. It was for example calculated that 1 hour of autoclave treatment at 134 °C had theoretically the same effect as 2–4 years *in vivo* (Chevalier *et al.*, 1999b). Steam sterilization for 5 hours should avoid heavy and long experiments to assess the ageing sensitivity of a given zirconia prior to commercialisation. X-ray diffraction (XRD) analysis was traditionally used to follow quantitatively the transformation. More sensitive methods were proposed in recent works. In particular, optical interferometer (Chevalier *et al.*, 1999b) and atomic force microscopy (Deville *et al.*, 2005), generally used for roughness measurements, are powerful tools to quantify the first stages of ageing, since it is traduced by topographic changes. Associated with standard scanning electron microscopy and XRD analysis, they should be conducted also for the scientific analysis of explanted materials.

The differences observed both under *in vitro* and *in vivo* situations have shown that some zirconia products behave well. It is difficult to talk about 'ageing-free' zirconia since the transformation occurring upon ageing consists of a 'natural' return back to the monoclinic equilibrium state. However, the transformation kinetics can be much affected by microstructural issues. Some solutions were proposed in the literature, but were hardly followed by industrial changes. Among them, the addition of small amounts of silica (Gremillard *et al.*, 2002) or the use of yttria-coated instead of co-precipitated powders (Piconi *et al.*, 1998) seem to have a clear benefit to the ageing resistance, while preserving good toughness and strength. These solutions were proposed in the Y-TZP system. It has to be said that the issue of ageing of zirconia medical devices stands to the use of yttria as a dopant. Yttrium, as a trivalent ion, creates oxygen vacancies that help hydroxyl group diffusion in the lattice. Ceria-doped zirconia ceramics were almost never considered although they exhibit superior toughness (up to 20 MPa $m^{1/2}$) and reduced ageing sensitivity (due to the tetravalent character of cerium ion). There is thus still a door open for zirconia ceramics with

improved properties. Another option promoted by scientists and companies is the development of alumina–zirconia composites. This may be the way to benefit from zirconia transformation toughening without the major drawback associated with its transformation under steam or body fluid condition. In the recent literature concerning alumina–zirconia composites for biomedical applications, different compositions have been tested, from the zirconia-rich to the alumina-rich side (Affatato *et al.*, 1999; De Aza *et al.*, 2002). Major ceramic companies are developing such materials. A composite material processed with 80% tetragonal zirconia polycrystals (ZrO_2-TZP) and 20% alumina (Al_2O_3) is reported to have outstanding mechanical and tribological properties. The alumina-toughened zirconia (ATZ) BioHip®, developed by Metoxit AG (Thayngen, Switzerland), has a bending strength of up to 2000 MPa, indicating that it can withstand loads that are four times greater than conventional Al_2O_3 implants. This product is still not in the market. At the same time, Ceramtec AG (Plochingen, Germany) recently developed Biolox® Delta, which consists of approx. 75% aluminum oxide, the basis for hardness and wear resistance, and approx. 25% zirconium oxide, for improved mechanical properties. A strength higher than 1150 MPa is reported, associated with a toughness of 8.5 MPa $m^{1/2}$. This product is now in the market.

The addition of alumina to zirconia clearly hinders ageing, or at least reduces drastically its kinetic. It is shown that strength of Biolox® Delta for example does not decrease even when repeatedly steam sterilised. However, 'no decrease in strength' does not mean necessary 'no ageing', since other manifestations of ageing are grain pull out and roughening. Few studies have been devoted to ageing in alumina–zirconia systems, but they show that, even if limited and possibly reduced to zero, some degree of degradation can be observed, depending on microstructural features. As an example, ageing may be significant in a 3Y-TZP–alumina composite, above 16 vol.% zirconia (Pecharroman *et al.*, 2003). This critical content is related to the percolation threshold above which a continuous path of zirconia grains allows transformation to proceed. Any extrapolation to other laboratory scale or industrial composites could be hazardous, but it shows again how ageing must be checked carefully prior to clinical development of a given alumina–zirconia composite. Anyway, the presence of zirconia aggregates, especially if the zirconia is stabilized with yttria, should be avoided (Gutknecht *et al.*, 2007).

In the absence of any clinical report of ageing in dental applications, 3Y-TZP still has a strong potential as a biomaterial, due to its excellent mechanical properties. Because scientists and companies are now aware of ageing and owing to the improvement in the monitoring of the degradation, one should expect that no critical issues appear in this field in the future.

11.8 Sources of further information

This short chapter aims to highlight some important aspects of zirconia ceramics. More in-depth understanding of transformation toughening is possible from the book *Transformation Toughening of Ceramics*, from Green *et al.* (1989) and from the recent review paper from Kelly and Rose (2002). During the pioneering years of the research work on zirconia, a series of international conferences was devoted to the science and technology of zirconia. Two books were published following these conferences. The reader may refer to *Advances in Ceramics*, Vol. 3 – Science and *Technology of Zirconia* and to *Advances in Ceramics*, Vol. 12 – *Science and Technology of Zirconia II* published by the American Ceramic Society. The authors of the current chapter have recently published a review on ageing and its negative impact on orthopaedic implants (Chevalier *et al.*, 2007). Clinical data and retrieval analysis may also be obtained from Clarke *et al.* (2003).

A non-exhaustive list of zirconia implants producers is given below:

- Morgan Advanced Ceramics: http://www.morganbioceramics.com/about.htm
- Kinamed, Ceramic knee system, in collaboration with Kyocera, http://www.kinamed.com/gemKneeSystem.html
- Metoxit: http://www.metoxit.com
- HTI Technologies: http://www.htitechnologies.com/implant/

11.9 References

Affatato S, Testoni M, Cacciari G, Toni A (1999), 'Mixed oxides prosthetic ceramic ball heads. Part 2: effect of the ZrO_2 fraction on the wear of ceramic on ceramic joints', *Biomaterials*, **20**, 1925–29.

Besimo CE, Spielmann HP, Rohner HP (2001), 'Computer assisted generation of all-ceramic crowns and fixed partial dentures', *Int. J. Comput. Dent.*, **4**, 243–62.

Cales B (2000), 'Zirconia as a sliding material: histologic, laboratory, and clinical data', *Clin. Orthop. Relat. Res.*, **379**, 94–112.

Campbell P, Shen F-W, McKellop H (2004), 'Biologic and tribologic considerations of alternative bearing surfaces', *Clin. Orthop.*, **418**, 98–111.

Chevalier J (2006), 'What future for zirconia as a biomaterial', *Biomaterials*, **27**, 535–43.

Chevalier J, Olagnon C, Fantozzi G (1999a), 'Subcritical crack propagation in 3Y-TZP ceramics, static and cyclic fatigue', *J. Am. Ceram Soc.*, **82**, 3129–38.

Chevalier J, Cales B, Drouin JM (1999b), 'Low-temperature ageing of Y-TZP ceramics', *J. Am. Ceram. Soc.*, **82**, 2150–54.

Chevalier J, Deville S, Munch E, Jullian R, Lair F (2004), 'Critical effect of cubic phase on ageing in 3 mol% yttria-stabilized zirconia ceramics for hip replacement prosthesis', *Biomaterials*, **25**, 5539–45.

Chevalier J, Gremillard L, Deville S (2007), 'Low temperature degradation of zirconia and its implication on biomedical implants', *Ann. Rev. Mater. Sci.*, **37**, 1–32.

Clarke IC, Manaka M, Green DD, Williams P, Pezzotti G, *et al.* (2003), 'Current status of zirconia used in total hip implants', *J. Bone Joint Surg. Ser. A*, **85**, 73–84.

De Aza AH, Chevalier J, Fantozzi G, Schehl M, Torrecillas R (2002), 'Crack growth resistance of alumina, zirconia and zirconia toughened alumina ceramics for joint prostheses', *Biomaterials*, **23**, 937–45.

Deville S, Guenin G, Chevalier J (2004a), 'Martensitic transformation in zirconia Part I. Nanometer scale prediction and measurement of transformation induced relief', *Acta Mater.*, **52**, 5697–707.

Deville S, Guenin G, Chevalier J (2004b), 'Martensitic transformation in zirconia Part II. Martensite growth', *Acta Mater.*, **52**, 5709–21.

Deville S, Gremillard L, Chevalier J, Fantozzi G (2005), 'A critical comparison of methods for the determination of the ageing sensitivity in biomedical grade yttria-stabilized zirconia', *J. Biomed. Mater. Res. B*, **72**, 239–45.

Deville S, Chevalier J, Gremillard L (2006), 'Influence of surface finish and residual stresses on the ageing sensitivity of biomedical grade zirconia', *Biomaterials*, **27**, 2186–92.

Fabrichnaya O, Aldinger F (2004), 'Assessment of thermodynamic parameters in the system ZrO_2–Y_2O_3–Al_2O_3', *Zeitschrift für Metallkunde/Mater. Res. Adv. Techn.*, **95**, 27–39.

Filser F, Kocher P, Weibel F, Luthy H, Scharer P, Gauckler LJ (2001), 'Reliability and strength of all-ceramic dental restorations fabricated by direct ceramic machining (DCM)', *Int. J. Comput. Dent.*, **4**, 89–106.

Garvie RC, Swain MV (1985), 'Thermodynamics of the tetragonal to monoclinic phase transformation in constrained zirconia microcrystals – Part I In the absence of an applied stress field', *J. Mater. Sci.*, **20**, 1193–200.

Garvie RC, Hanninck RH, Pascoe RT (1975), 'Ceramic steel?', *Nature*, **258**, 703–4.

Green DJ, Hanninck RHJ, Swain MV (1989), *Transformation Toughening of Ceramics*, CRC Press, Boca Raton, Florida (US).

Gremillard L, Chevalier J, Fantozzi G, Epicier T (2002), 'Improving the durability of a biomedical grade zirconia ceramic by the addition of silica', *J. Am. Ceram. Soc.*, **85**, 401–5.

Gutknecht D, Chevalier J, Garnier V, Fantozzi G (2007), 'Key role of processing to avoid low temperature ageing in alumina zirconia composites for orthopaedic application', *J. Europ. Ceramic Soc.*, **27**, 1547–52.

Kelly P, Rose L (2002), 'The martensitic transformation in ceramics – its role in transformation toughening', *Prog. Mater. Sci.*, **47**, 463–557.

Kobayashi K, Kuwajima H, Masaki T (1980), Phase change and mechanical properties of ZrO_2–Y_2O_3 solid electrolyte after ageing, *Solid State Ionics*, **3/4**, 489–93.

Lange FF (1982), 'Transformation toughening. 1. Size effects associated with the thermodynamics of constrained transformations', *J. Mater. Sci.*, **17**, 225–34.

Lawn B (1993), *Fracture of Brittle Solids*, 2nd edn., Cambridge University Press, Cambridge, UK.

Lawson S (1995), 'Environmental degradation of zirconia ceramics', *J. Europ. Ceramic Soc.*, **15**, 485–502.

Li J, Zheng Q, Hashida T (2001), 'Degradation of yttria-stabilized zirconia at 370K under a low applied stress', *Mat. Sci. Eng. A.*, **297**, 26–30.

Luthardt RG, Holzhuter MS, Rudolph H, Herold V, Walter GA (2004), 'CAD/CAM-machining effects on Y-TZP ceramics', *Dent. Mater.*, **20**, 655–62.

Masonis JL, Bourne RB, Ries MD, McGalden RW, Salehi A, Kelman DC (2004), 'Zirconia femoral head fractures: a clinical and retrieval analysis', *J. Arthroplast.*, **19**, 898–905.

Matsui K, Horikoshi H, Ohmichi N, Ohgai M, Yoshida H, Ikuhara Y (2003), 'Cubic-formation and grain-growth mechanisms in tetragonal zirconia polycrystal', *J. Am. Ceramic Soc.*, **86**, 1401–8.

McMeeking R, Evans A (1982), 'Mechanics of transformation toughening in brittle materials', *J. Am. Ceramic. Soc.*, **65**, 242–6.

Muñoz-Saldaña J, Balmori-Ramirez H, Jaramillo-Vigueras D, Iga T, Schneider GA (2003), 'Mechanical properties and low-temperature ageing of tetragonal zirconia polycrystals processed by hot isostatic pressing', *J. Mater. Res.*, **18**, 2415–26.

Oblak C, Jevnikar P, Kosmac T, Funduk N, Marion L (2004), 'Fracture resistance and reliability of new zirconia posts', *J. Prosthet. Dent.*, **91**, 342–8.

Papanagiotou HP, Morgano SM, Giordano RA, Pober R (2006), '*In vitro* evaluation of low-temperature ageing effects and finishing procedures on the flexural strength and structural stability of Y-TZP dental ceramics', *J. Prosthet. Dent.*, **96**, 154–64.

Pecharroman C, Bartolome J, Requena J, Moya JS, Deville S, Chevalier J, Fantozzi G, Torrecillas R (2003), 'Percolative mechanism of ageing in zirconia containing ceramics for medical applications', *Adv. Mater.*, **15**, 507–11.

Piconi C, Maccauro G (1999), 'Zirconia as a ceramic biomaterial', *Biomaterials*, **20**, 1–25.

Piconi C, Burger W, Richter H, Cittadini A, Maccauro G, Covacci V, Bruzzese N, Ricci G, Marmo E (1998), 'Y-TZP for artificial joint replacements', *Biomaterials*, **19**, 1489–94.

Schubert H, Frey F (2005), 'Stability of Y-TZP during hydrothermal treatment: neutron experiments and stability considerations', *J. Europ. Ceramic Soc.*, **25**, 1597–602.

Scott HG (1975), 'Phase relationships in the zirconia–yttria system', *J. Mater. Sci.*, **10**, 1527–35.

Suttor D, Bunke K, Hoescheler S, Hauptmann H, Hertlein G (2001), 'LAVA – the system for all-ceramic ZrO_2 crowns and bridge frameworks', *Int. J. Comput. Dent.*, **4**, 195–206.

Wan K, Lathabais S, Lawn B (1990), 'Crack velocity functions and thresholds in brittle solids', *J. Europ. Ceramic Soc.*, **6**, 259–68.

Yoshimura M, Noma T, Kawabata K, Somiya S (1987), 'Role of H_2O on the degradation process of Y-TZP', *J. Mater. Sci. L.*, **6**, 465–7.

12
Bioactive glass

J R JONES, Imperial College London, UK

12.1 Introduction – the discovery of Bioglass®

Bioactive glasses are amorphous silicate-based materials which are compatible with the human body, bond to bone and can stimulate new bone growth while dissolving over time. They therefore have the potential to restore diseased or damaged bone to its original state and function (bone regeneration).

The first bioactive glass was discovered by Larry Hench and colleagues in 1969, at the University of Florida, and was the first material seen to form an interfacial bond with host tissue after implantation (Hench *et al.*, 1971). The glass composition of the first bioactive glass was 46.1% SiO_2, 24.4% NaO, 26.9% CaO and 2.6% P_2O_5, in mol%, termed 45S5 Bioglass®, which is now a trademarked name. Hench chose this composition as it provided a large amount of CaO with some P_2O_5 in a Na_2O–SiO_2 matrix. The composition is very close to a ternary eutectic, making it easy to melt. The first implants were in rat femora. After 6 weeks they were removed with great difficulty. A quantitative evaluation of interfacial shear strength in rat and monkey models showed that the strength of the interfacial bond between Bioglass® and cortical bone was equal to or greater than the strength of the host bone (Piotrowski *et al.*, 1975; Hench *et al.*, 1977; Weinstein *et al.*, 1980).

Hench's discovery launched the field of bioactive ceramics and Bioglass® particulate has been in clinical use since 1985 (US Biomaterials Corp., Alachua, Florida). Later studies have found that other compositions and glass types are bioactive, some even bonding to soft tissue. The interest in bioactive glasses now focuses on their ability to stimulate new bone growth and its potential to be used in the development of constructs that can stimulate the body's own regenerative mechanisms to restore damaged bone to its original state and function. This chapter will describe the properties of different bioactive glasses and review the cutting edge progress towards using them in regenerative medicine.

12.2 The bone-bonding mechanism

The bonding of bioactive glasses to bone has been attributed to the formation of a carbonated hydroxyapatite (HCA) layer on the glass surface on contact with body fluid. The HCA is similar to bone mineral and therefore forms a bond. *In vitro* studies showed that the Bioglass® formed an apatite layer in test solutions without calcium or phosphate ions. Transmission electron micrographs of the interface between the glasses implanted *in vivo* and the host bone also contained evidence of interfacial HCA crystals (Hench *et al.*, 1971). The HCA crystals were bonded to layers of collagen fibrils produced at the interface by osteoblasts. The chemical bonding of the HA layer to collagen created the strongly bonded interface (Hench *et al.*, 1971; Hench and Paschall, 1973).

Formation of the HCA layer occurs as a result of a rapid sequence of chemical reactions on the surface of the implant when exposed to body fluid (Pantano *et al.*, 1974; Greenspan and Hench, 1976; Hench, 1998b, 1991). There are five proposed reaction stages that lead to the rapid release of soluble ionic species and the formation of a high surface area hydrated silica and polycrystalline hydroxy carbonate apatite (HCA) bi-layer on the glass surface:

- Stage 1: Rapid exchange of Na^+ and Ca^{2+} with H^+ or H_3O^+ from solution, causing hydrolysis of the silica groups, which creates silanols (Si-OH), e.g.

  $$\text{Si-O-Na}^+ + \text{H}^+ + \text{OH}^- \rightarrow \text{Si-OH}^+ + \text{Na}^+_{(aq)} + \text{OH}^-$$

  Ion exchange is diffusion controlled with a $t^{1/2}$ dependence. The pH of the solution increases as a result of H^+ ions in the solution being replaced by cations.
- Stage 2: Stage 1 increases the hydroxyl concentration of the solution, which leads to attack of the silica glass network. Soluble silica is lost in the form of $Si(OH)_4$ to the solution, resulting from the breaking of Si-O-Si bonds and the continued formation of Si-OH (silanols) at the glass solution interface:

  $$\text{Si-O-Si} + \text{H}_2\text{O} \rightarrow \text{Si-OH} + \text{OH-Si}$$

  This stage is an interface-controlled reaction with a $t^{1.0}$ dependence.
- Stages 3–5: Condensation and repolymerisation of the Si-OH groups is then thought to occur, leaving a silica-rich layer on the surface, depleted in alkalis and alkali-earth cations (stage 3). Ca^{2+} and PO_4^{3-} groups then migrate to the surface through the silica-rich and from the surrounding fluid, forming a $CaO–P_2O_5$-rich film on top of the silica-rich layer (stage 4). The $CaO–P_2O_5$ film crystallises as it incorporates OH^- and CO_3^{2-} anions from solution to form a mixed hydroxycarbonate apatite (HCA) layer.

This mechanism was based on soda-lime–silica glass corrosion mechanisms (Doremus *et al.*, 1983) and should complete within hours. In glass corrosion terms, the formation of a silica-rich layer and a protective layer on top of that would be a type IV corrosion surface. The kinetics of these two stages implied that stage 1 was the rate-determining step for bone bonding. However, recent work suggests that this may not be necessarily true.

The biological mechanisms of bonding that follow HCA layer formation are thought to involve the adsorption and desorption of growth factors, followed by the attachment and synchronised proliferation and differentiation of osteoprogenitor cells (Hench and Polak, 2002). Osteoblasts (bone growing cells) lay down extracellular matrix (collagen-based matrix), which will mineralise to create a nanocomposite of mineral and collagen on the surface of the bioactive glass implant while the dissolution of the glass continues over time (Ducheyne and Qiu, 1999).

Bioactive glasses have been found to bond more rapidly to bone than synthetic hydroxyapatite (sHA), and to be osteoinductive, i.e. they stimulate new bone growth on the implant away from the bone/implant interface. sHA is classified as osteoconductive, i.e. it encourages bone to grow along the implant from the bone/implant interface (Oonishi *et al.*, 1999). The suggested mechanisms for osteoinduction and osteogenesis due to bioactive glass will be discussed later.

12.3 Making Bioglass®

The original Bioglass® was produced by melt-processing, which involves melting high-purity oxides (SiO_2, Na_2CO_3, $CaCO_3$ and P_2O_5) in a crucible in a furnace at 1370 °C (Hench *et al.*, 1971). Platinum crucibles must be used to ensure there is no contamination of the glass. Bioglass® particulate is made by pouring the melt into water to quench, creating a frit. The frit is then dried and ground to the desired particle size range. Bioglass® can also be poured into pre-heated (350 °C) moulds (e.g. graphite) to produce rods or as-cast components. Although calcium and phosphate components were in the glass composition because of their presence in bone, soda was added merely to reduce the melting point of the system so that it could be melted in a conventional furnace.

12.4 Bioactive glass compositions

The compositional range for bonding of bone to bioactive glasses and glass-ceramics is illustrated in Fig. 12.1. Glasses with the highest level of bioactivity lie in the middle (region E) of the Na_2O–CaO–SiO_2 diagram (assuming a constant 6 wt% of P_2O_5) (Hench, 1998b). The boundaries are kinetic boundaries not phase equilibrium boundaries. Compositions that exhibit

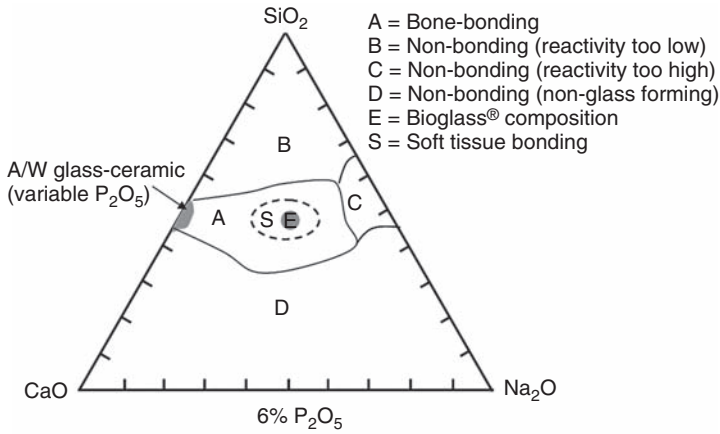

12.1 Compositional diagram for bone-bonding. Note regions A, B, C, D. Region S is a region of Class A bioactivity where bioactive glasses bond to both bone and soft tissues and are gene activating.

slower rates of bonding lie between 52 to 60% by weight of SiO_2 in the glass. Compositions with greater than 60% SiO_2 (region B) do not bond and are bio-inert. Increasing the surface area of the glass by making a particulate or a nanoporous sol–gel-derived glass extends the bone-bonding compositions to higher percentages of SiO_2 in the glass (see later). Adding multivalent cations, such as Al^{3+}, Ti^{4+} or Ta^{5+} to the glass shrinks the bone bonding boundary (Greenspan and Hench, 1976; Gross and Strunz, 1980, 1985). The scientific basis for the compositional boundaries is associated with the rate of the surface reactions of the glasses. However, it is the role of the multivalent ions in the glass network that dictates how the rate of these surface reactions.

Andersson *et al.* (1990) modified the 45S5 compositional range and implanted 16 different compositions of the SiO_2–Na_2O–CaO–P_2O_5–Al_2O_3–B_2O_3 system into rabbit tibia. The glasses were divided into five groups according to their *in vivo* behaviour. Bone bonding occurred *in vivo* for glasses that can form an HCA layer formation on a silica-rich surface layer when tested in Tris buffer solution *in vitro*. They observed that the silica layer must be sufficiently hydrated, i.e. contain OH groups to promote HCA deposition. The results suggested that alumina inhibits bone bonding by retarding the formation rate of a silica-rich layer, by stabilising the silica structure enough to prevent calcium phosphate build-up within the layer. Compositions within boundaries similar to those in Fig. 12.1 bonded to bone; glasses outside the bioactive boundary did not bond. Up to about 1.5 wt% Al_2O_3 can be included in the glass without destroying the bioactivity.

12.5 Soft tissue interactions

Until 1981 it was assumed that only calcified tissues would form a bond to bioactive materials. Wilson *et al.* (1981) were the first to show that soft connective tissues could also form a bond to 45S5 Bioglass® if the interface was immobile. They later found that only glass compositions with rapid reaction rates form a soft tissue bond (Wilson and Noletti, 1990). These glasses are restricted to the compositions in the region S in Fig. 12.1. When the glass composition exceeds 52% by weight of SiO_2 the glass will bond to bone but not to soft tissues. This finding provided the basis for clinical use of Bioglass® in ossicular replacement and also for implants to maintain the alveolar ridge of endentulous patients.

12.6 Mechanisms of bioactivity

Fig. 12.1 shows that the bioactivity of glasses depends on their composition. Oonishi *et al.* (1999, 2000) and Wheeler *et al.* (2000) indicated large differences in rates of *in vivo* bone regeneration and extent of bone repair for different glasses, resulting in two classes of bioactivity. Class A bioactive glasses stimualte *both* osteoconduction and osteoinduction (Hench, 1998a,b; Wilson and Low, 1992). Class B bioactivity occurs when only osteoconduction is present; i.e. bone migration along an interface (Hench 1998a,b). The reasons for different degrees of bioactivity have long been linked to the glass composition and the stability of the glass network in relation to the bioactivity mechanism listed in Section 12.2, i.e. as the rate of corrosion (dissolution) of a glass increases, the rate of formation of the HCA layer will increase, allowing bone bonding to occur more rapidly. However this would only explain an improved osteoconductivity of Bioglass® over a less bioactive composition, not the cause of osteoinduction. Therefore the mechanism for osteoinduction is more complicated. It is vital to understand the biological response to the bioactive glasses, i.e. what signals do the osteogenic cells such as osteoblasts receive from the material? As Bioglass® degrades it releases silica, calcium, sodium and phosphate species into solution. It is thought that the combination of some of these ions triggers the cells to produce new bone, especially critical concentrations of soluble silicon and calcium ions (Hench and Polak, 2002).

All cells continually interact with their environment through receptors that detect cytokines, chemokines, mechanical stress, gases and physiologically important ions. Cell surface receptors such as integrins interact with the extracellular matrix causing cascades of cell signalling molecules that (via transcription factors) activate or deactivate gene expression. The genes are transcribed to mRNA and translated to proteins. These proteins deter-

mine the cell response to the initial stimuli, i.e. proliferation (cell multiplication), differentiation, matrix formation or cell death.

Molecular biology studies have shown that seven families of genes involved in osteogenesis have been stimulated by bioactive glass dissolution products (Hench, 2000; Xynos 2000a,b, 2001; Hench *et al.*, 2003, Bielby *et al.*, 2004, 2005; Jell and Stevens, 2006), including IGF-II with IGF binding proteins and proteases that cleave IGF-II from their binding proteins (Xynos *et al.*, 2000a).

It is thought that bioactive glasses determine gene expression by the rate and type of dissolution ions released, which interact with the integrins. The intracellular signalling pathways, however, remain uncertain (Jell and Stevens, 2006).

It is important to ascertain which ions cause osteoinduction via gene expression, and at what concentrations. The effect has been seen to be concentration dependent (Xynos *et al.*, 2001), with approximately 17–20 ppm of soluble Si and 88–100 ppm of soluble Ca ions required. Sodium ions are not thought to be beneficial to cells, and phosphate content of the glass is not thought to affect gene expression, although it may be needed in the body fluid for the extracellular matrix to mineralise and form HCA. Recent studies have shown that phosphate is not required to be released from the glass for extracellular matrix production and bone cells can mineralise, as long as it is present in the solution (Jones *et al.*, 2007b). This has been supported by work by Reffitt *et al.* (2003), who showed enhanced differentiation of osteoblastic cell lines when exposed to soluble silica (orthosilicic acid) and that the collagen extracellular matrix production increased in all cells treated with orthosilicic acid. In fact, dietary silica supplements have long been associated with increased bone mineral density (Jugdaohsingh *et al.*, 2004), prevention of osteopenia (Rico *et al.*, 2000) and Si-doped hydroxyapatite materials have recently showed enhanced bone bonding compared with conventional synthetic HA (Porter *et al.*, 2003, 2004).

12.7 Sol–gel-derived bioactive glasses

For a melt-derived glass to bond to bone, the silica content has to be 60 mol% or lower. However, HCA layer formation and bone bonding can be achieved for glasses with up to 90 mol% silica if the glass is sol–gel-derived (Li *et al.*, 1991). The first sol–gel-derived bioactive glasses were developed in the early 1990s by Li *et al.* (Hench and West, 1990; Hench and Vasconcelos 1990; Li *et al.*, 1991; Pereira *et al.*, 1994, 1995; Pereira and Hench, 1996). A series of compositions were studied. The 58S (60 mol% SiO_2, 36 mol% CaO and 4 mol% P_2O_5) composition, which was a close resemblance to the melt-derived compositions developed previously, was

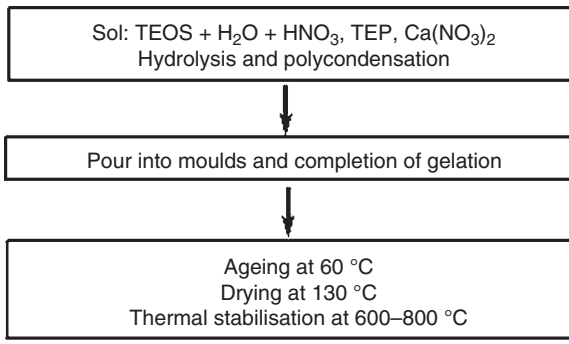

12.2 A flow diagram of the process for sol–gel bioactive glass synthesis.

found to form the HCA surface layer more rapidly than any melt-derived glass (Sepulveda *et al.*, 2002b).

The sol–gel process is shown schematically in Fig. 12.2 and involves the hydrolysis of alkoxide precursors to create a sol, which is a colloidal-like solution. In the case of silicate-based bioactive glasses, the precursor would be a silicon alkoxide such as tetraethyl orthosilicate (TEOS) or similar. As TEOS is insoluble in water, the hydrolysis reaction requires a catalyst, usually acidic. If other components apart from silica are required in the glass composition they are added to the sol either as other alkoxides or as salts. In the case of 58S, phosphate is incorporated by adding triethyl phosphate (TEP) and calcium nitrate tetrahydrate. The sol can be considered as a solution of silica species that can undergo polycondensation. The polycondensation reaction forms the basis of the silica network (Hench and West, 1990). The viscosity of the sol increases as Si–O–Si bonds form, eventually (usually within 3 days) creating a gel with water and ethanol by-products of the condensation reaction. The gel is then aged at 60 °C for 3 days and then dried at 60 °C for 24 h, 90 °C for 24 h and 130 °C for 48 h to remove the water and alcohol, using carefully controlled low heating rates. The final step is to heat the dried gel to at least 600 °C in order to remove organic by-products and especially nitrates from the calcium nitrate, which burn off at approximately 560 °C (Saravanapavan and Hench, 2003a).

12.7.1 Nanoporosity

Sol–gel derived glasses have a specific surface area two orders of magnitude higher than melt-derived glasses (Pereira *et al.*, 1995; Sepulveda *et al.*, 2001). This is because gel-glasses contain a nanoporous network that is inherent to the sol–gel process, whereas melt-derived glasses are fully dense. The nanopores are usually in the range of 1–30 nm diameter. According to

IUPAC standands, pores below 2 nm should be termed micropores and those with diameters between 2 and 50 nm should be termed mesopores (Branton *et al.*, 1994). However, not all authors follow this convention. In this chapter, pores of less than 100 nm in diameter will be generally referred to as nanopores.

The nanopores are created during the polycondensation reaction. The aqueous by-products of the reaction become trapped within the silica network, preventing a fully dense silica-based network forming. These aqueous droplets must then be evaporated during drying. This is the reason the drying process must be carefully controlled. As the nanopores are connected by pore throats narrower than the pore diameter (Saravanapavan and Hench, 2003b), the water and alcohol molecules follow a tortuous path from the centre of the gel to the surface. If drying conditions are too rapid or the evaporation path too tortuous, the gel will crack as capillary pressures will be too great. This is the reason why large monoliths (greater than 10 mm thickness) are difficult to produce without cracking. The nanopore size is affected by the processing method (Assink and Kay, 1988; Arcos, 2002), the pH of the catalyst (Brinker and Scherer, 1990) and the nominal composition (Balas *et al.*, 2001; Arcos *et al.*, 2002; Salinas *et al.*, 2002). Compositional affects are due to changes in network connectivity when a network modifier, such as calcium, is added; the pore diameter increases due to the network becoming less connected.

12.7.2 Enhanced bioactivity

Sol–gel-derived bioactive glasses are generally more bioactive than melt-derived glasses of similar compositions. Also, melt-derived glasses with silica contents greater than 60 mol% are considered not bioactive, whereas the limit for a sol–gel-derived bioactive glass is 80 mol%. The enhanced bioactivity is due to the nanoporosity and enhanced surface area (Sepulveda *et al.*, 2002b). In fact, sol–gel glasses can be considered as mostly surface as the nanopores are thought to be completely interconnected. The enhanced surface area causes increased rates of dissolution, accelerating stages 1 and 2 of the bioactivity mechanism. Because of this, sol–gel-derived glasses can be considered truly bioresorbable. However, enhanced dissolution is not the only story for enhanced bioactivity. Bioactive gel-glasses have been simplified by reducing the compositions to a two-component (CaO and SiO_2) system, which formed an HCA layer as rapidly as the 58S composition (Saravanapavan *et al.*, 2003). This was the first indication that phosphorus was not required for bioactivity.

One reason for this is that one part of the bioactivity mechanism is the formation of Si–OH groups, which are thought to play a role in HCA layer nucleation. Apatite layers can be nucleated on various materials that have

a high concentration of surface OH groups when they are placed in solutions that contain high concentrations of calcium and phosphate ions (Li *et al.*, 1994). This has even been demonstrated on polymers (Miyazaki *et al.*, 2003). Sol–gel-derived glasses inherently contain a substantial number of OH groups in the glass network. This is because even in glasses produced with only silica in the nominal composition, OH groups become network modifiers and break up the network. Hence, several sol–gel-derived silicas have nanoporosity, often microporosity, and also dissolve in solution.

A further advantage of sol–gel-derived glasses is that their surfaces can be modified by a variety of surface chemistry methods, e.g. with amine groups, that can make the surface hydrophobic and attractive to specific proteins (Lenza *et al.*, 2002). Specially designed proteins can also therefore be attached to the material surface prior to implantation to obtain novel bioactivity by delivering the proteins to the desired wound or defect site (Lenza *et al.*, 2003).

12.7.3 Scaffolds

Scaffolds are templates for three-dimensional (3D) tissue growth. Cells can be grown on scaffolds in a bioreactor outside the body, which can then be implanted (tissue engineering) (Ohgushi and Caplan, 1999). Alternatively, scaffolds are implanted directly into the body (*in situ* tissue regeneration). In both cases, the materials must adapt to the physiological environment and should dissolve over time, leaving a regenerated tissue (Hench and Polak, 2002).

The properties of bioactive glasses, such as bone bonding, osteoinduction and controlled resorbabilty, make them very appealing materials as scaffolds for bone regeneration as long as they can be processed into forms that can act as 3D templates for bone growth, i.e. mimicking the structure of porous bone. A scaffold should have a pore network that is interconnected in 3D, with interconnections large enough to allow cell migration, fluid flow (nutrient delivery and waste removal) and bone to grow in 3D (Jones *et al.*, 2006b). The minimum interconnect size for bone with a blood supply to grow in is thought to be 100 μm (Hulbert *et al.*, 1972).

Unfortunately, the Bioglass® composition is generally unsuitable for the production of porous scaffolds. This is because a sintering process is employed in all known methods for the processing of glass powder into porous structures. Sintering requires glasses to be heated above their glass transition temperature in order to initiate localised flow and the Bioglass® composition crystallises immediately above its glass transition. Once Bioglass® crystallises, it loses its bioactivity.

However, by foaming sol–gel-derived bioactive glasses, porous scaffolds have been developed that may fulfil the criteria for an ideal scaffold (Sepulveda *et al.*, 2002a). The process is shown in Fig. 12.3 and involves the

rapid gelation of the sol. The sol is foamed by vigorous agitation with the aid of a surfactant, as the viscosity rapidly increases. On gelation, the spherical bubbles become permanent in the gel and as drainage occurs in the foam struts, the gel shrinks and the bubbles merge, interconnects open up at the point of contact between neighbouring bubbles, creating a highly connected network similar to trabecular bone (Fig. 12.4). A hierarchical pore structure

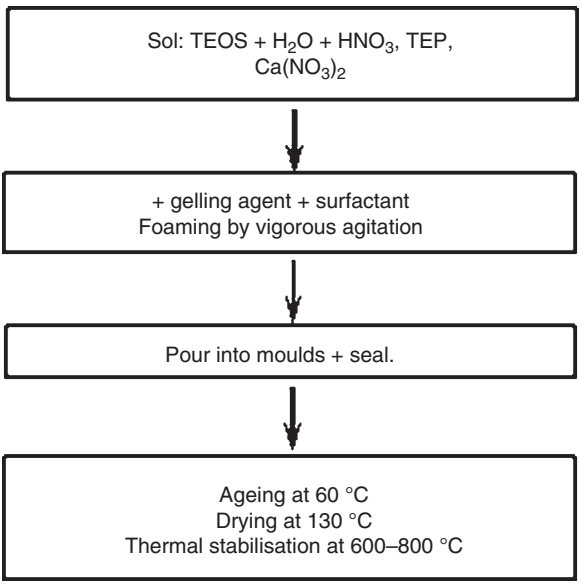

12.3 A flow diagram of the sol–gel foaming process.

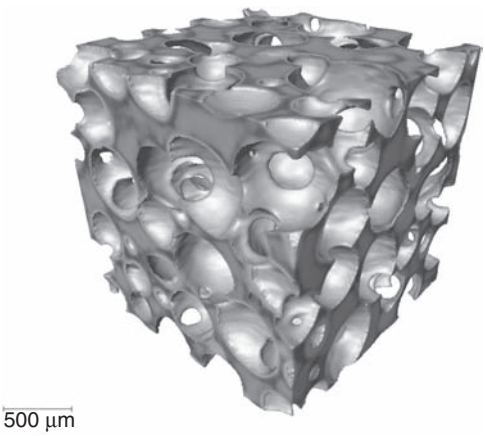

12.4 X-ray microtomography (μCT) image of a typical bioactive glass scaffold produced by the sol–gel foaming process. Image: Gowsihan Poologasundarampillai.

is created because the nanoporosity inherent to the sol–gel process is maintained and can be controlled (Jones *et al.*, 2007a). Compressive strengths of 2.4 MPa while maintaining modal interconnect diameters above 100 μm have been achieved by tailoring the nanoporosity by controlling the final sintering temperature of the process (Jones *et al.*, 2006a). The strength values are similar to those of clinically used porous hydroxyapatite (ISO, 2000) and are continually rising as the process is improved.

Cell response studies on the scaffolds have found that primary human osteoblasts lay down mineralised immature bone tissue, without additional signalling species. This occurred in scaffolds of both the 58S composition (Gough *et al.*, 2004) and the 70S30C composition (Jones *et al.*, 2007b), which showed that phosphate is not required in the glass composition for bone matrix production and mineralisation to occur.

12.7.4 Quantification of 3D pore networks and their properties

Whatever material is used as a scaffold, it is vital to be able to characterise the pore networks of scaffolds in 3D to ensure the scaffold has the potential to allow 3D bone growth. Traditionally scanning electron microscopy (SEM) and mercury intrusion porosimetry have been used. However, these characterisation techniques have several disadvantages. SEM micrographs can be misleading as they are images of porous surfaces so the real 3D shape and connectivity of the pores cannot be imaged or quantified. Percentage porosity is commonly used as a characterisation parameter, however it is meaningless for scaffold design as scaffolds must have large, connected pores but two materials can have the same percentage porosity as an ideal scaffold but have many very small pores (Jones *et al.*, 2006b).

For *in vivo* tests or clinical trials it is imperative to know the exact structure of the pore network before and after implantation, therefore a non-destructive technique is required for imaging and quantification of the scaffold. 3D images X-ray microcomputer tomography (μCT) can be used to non-destructively image scaffolds prior to implantation and after an implant has been removed. Figure 12.4 shows a μCT image of a typical bioactive glass scaffold produced by the sol–gel foaming process and shows that the pore network of the scaffold is very highly interconnected and mimics the pore structure of trabecular bone.

Many authors have used μCT images to display the pore networks of their scaffolds, but little has been done to quantify the images. Now, novel 3D image analysis methods have been developed to quantify the structure. Three algorithms were applied to μCT images in order to quantify the pore networks of bioactive glass scaffolds. A dilation algorithm is applied to obtain distance maps of the pores. A 3D watershed algorithm is applied to

the distance map to divide the image into individual pores and a top-down algorithm identifies the interconnections. The effect of processing conditions on the pore network as a whole or on an individual pore and its interconnects can be followed (Jones *et al.*, 2007a). The μCT data can also be input into finite element models to predict mechanical properties and permeability as a function of specific pore networks.

12.8 Clinical products

Despite all these developments, clinical products that use bioactive glasses remain surprisingly few, especially when compared with the less bioactive synthetic hydroxyapatite. This may be due to regulatory issues in that too much bioactivity cannot be claimed under the current FDA regulations; there are regulatory procedures for a medical device and for osteogenic drugs, but not for something that is implanted and dissolves over time releasing osteogenic agents. To date, all Bioglass® devices placed into use in the United States have been cleared via the 510[k] process. Thus, the Bioglass® devices have been able to demonstrate equivalence in safety and efficacy to devices that were already in commerce prior to 1976 (Warren *et al.*, 1989).

The first Bioglass® device was cleared for marketing in the United States in 1985 and was used to treat conductive hearing loss by replacing the bones of the middle ear. The device was called the 'Bioglass® Ossicular Reconstruction Prosthesis' (MEP®) and was a solid, cast Bioglass® structure that acted to conduct sound from the tympanic membrane to the cochlea. The advantage of the MEP® over other devices in use at the time was its ability to bond with soft tissue (tympanic membrane) as well as bone tissue. A modification of the MEP design was made to improve handling in the surgery and it is used clinically with the trademark name of the Douek Med.

The second Bioglass® device to be placed into the market was the 1988 Endosseous Ridge Maintenance Implant (ERMI®), which was cleared via the 510[k] process. The device was designed to support labial and lingual plates in natural tooth roots and to provide a more stable ridge for denture construction following tooth extraction. The devices were simple cones of 45S5 Bioglass® that were placed into fresh tooth extraction sites. They bonded to the bone tissue and proved to be extremely stable. A 5 year study quantified the substantial improvements in clinical success over Class B bioactive HA tooth root implants (Stanley *et al.*, 1997).

The first particulate material cleared for sale in the United States was PerioGlas®, which was cleared via the 510[k] process in December, 1993 and produced by USBiomaterials, Alachua, Florida. In 1995, PerioGlas® obtained a CE Mark and marketing of the product began in Europe. The

initial indication for the product was to restore bone loss resulting from periodontal disease in infrabony defects (Karatzas *et al.*, 1999). During a 10 year clinical history, PerioGlas® has demonstrated excellent clinical results with virtually no adverse reactions to the product and is sold in over 35 countries.

Bioactive glass particles have also been shown to undergo continual dissolution after the formation of the HCA layer in mandible sites, to such an extent that a hollow shell of HCA remained, in which new bone formed (Radin *et al.*, 2000). This lead to the product Biogran®, which is Bioglass® granules, marketed by Orthovita Corp.

Building on the successes of PerioGlas® in the market, a Bioglass® particulate for orthopaedic bone grafting was introduced into the European market in 1999, under the trade name NovaBone®. The product was cleared for general orthopaedic bone grafting in non-load-bearing sites in February 2000. To date, NovaBone® is being sold in the United States and Europe, as well as in China and a number of other countries.

Bioglass® particulate is also used for the treatment of dentinal hypersensitivity. The Bioglass® material used in this application is a very fine particulate that is incorporated into toothpaste, or used with an aqueous vehicle and applied to the tooth surface around exposed root dentin. When Bioglass® particles are put in contact with dentin, they adhere to the surface, rapidly form a hydroxycarbonate apatite layer and occlude exposed tubules, thereby relieving pain. Studies have shown that the Bioglass® particulate performs better than current therapies in relatively low concentrations (Gillam *et al.*, 2002). Early in 2004, FDA cleared two products for sale through the 510[k] process, and product sales began in mid-2004 by Novamin Corp., Alachua, Florida.

The most important modification of bioactive glasses was the development of A/W (apatite/wollastonite) bioactive glass-ceramic by Yamamuro, Kokubo and colleagues at Kyoto University, Japan. Composition modification and higher processing temperatures lead to a very fine-grained glass-ceramic composed of very small apatite (A) and wollastonite ($W = CaSiO_3$) crystals bonded by a bioactive glass interface (Nakamura *et al.*, 1985). Mechanical strength, toughness and stability of AW glass-ceramics (AW-GC) in physiological environments are excellent and bone bonded to A/W-GC implants with high interfacial bond strengths (Yoshii *et al.*, 1988). The AW-GC material was approved for orthopaedic applications in Japan with particular success in vertebral replacement and spinal repair (Neo *et al.*, 1992).

Products involving sol–gel-derived bioactive glasses have started to appear. Novabone Corp. recently modified their product by introducing sol–gel-derived glass particles of the 58S composition. The aim is that the 58S particles will dissolve more rapidly than the Bioglass® particles, creating

spaces that will encourage bone ingrowth between the Bioglass® particles. The new Novabone® product was FDA approved in 2005 and was the first product containing sol–gel-derived bioactive glasses to be FDA approved, which paves the way for bringing the scaffolds to the clinic.

Novathera Ltd, Cambridge, UK, have developed a wound-healing gel that incorporates particles of the 70S30C gel-glass composition, which is modified by 2 mol% of silver ions, termed Theraglass®. Low concentrations of silver ions have been found to be bactericidal without killing useful cells (Bellantone *et al.*, 2002).

2.9 Summary

Since the invention of Bioglass®, the first bioactive ceramic, bioactive glasses have been found to bond to bone, to dissolve over time, releasing ions that stimulate bone cells at the genetic level, causing osteoinduction. It is this biological mechanism that must be fully understood if bioactive glasses and other bioactive materials are to be fully optimised. Different compositions and sol–gel-derived glasses have also been found to be bioactive. Bioglass® medical and dental products are sold in 35 countries; however, the role of bioactive glasses in regenerative medicine will be fulfilled by 3D scaffold development. Bioactive glasses will play an important role in bone regeneration, but it will not be the original Bioglass® composition.

12.10 References

Arcos, D., Greenspan, D. C., Vallet-Regi, M. (2002) Influence of the stabilization temperature on textural and structural features and ion release in SiO_2-CaO-P_2O_5 sol–gel glasses. *Chem. Mater.,* **14,** 1515–1522.

Andersson, G., Liu, K. H., Karlsson, L., Niemi, J., Miettinen, J., Juhanoja, J. (1990) *In vivo* behavior of glasses in the SiO_2-Na_2O-CaO-P_2O_5-Al_2O_3-B_2O_3 system, *Mater Sci. Mater. Med.* **1** (4): 219–227.

Assink, R. A., Kay, B. D. (1988) Sol–gel kinetics 1. Functional-group kinetics. *J. Non-Cryst. Solids,* **99,** 359–370.

Balas, F., Arcos, D., Perez-Pariente, J., Vallet-Regi, M. (2001) Textural properties of SiO_2-CaO-P_2O_5 glasses prepared by the sol–gel method. *J. Mater. Res.,* **16,** 1345–1348.

Bellantone, M., Williams, H. D., Hench, L. L. (2002) Broad-spectrum bactericidal activity of Ag_2O-doped bioactive glass. *Antimicrob. Agents Chemother.,* **46,** 1940–1945.

Bielby, R. C., Christodoulou, I. S., Pryce, R. S., Radford, W. J. P., Hench, L. L., Polak, J. M. (2004) Time- and concentration-dependent effects of dissolution products of 58S sol–gel bioactive glass on proliferation and differentiation of murine and human osteoblasts. *Tissue Eng.,* **10,** 1018–1026.

Bielby, R. C., Pryce, R. S., Hench, L. L., Polak, J. M. (2005) Enhanced derivation of osteogenic cells from murine embryonic stem cells after treatment with

ionic dissolution products of 58S bioactive sol–gel glass. *Tissue Eng.,* **11,** 479–488.

Branton, P. J., Hall, P. G., Sing, K. S. W., Reichert, H., Schuth, F., Unger, K. K. (1994) Physisorption of argon, nitrogen and oxygen by Mcm-41, a model mesoporous adsorbent. *J. Chem. Soc. F. Trans.,* **90,** 2965–2967.

Brinker, J., Scherer, G. W. (1990) *Sol–Gel Science: The Physics and Chemistry of Sol–Gel Processing,* Boston, Academic Press.

Doremus, R. H., Mehrotra, Y., Lanford, W. A., Burman, C. (1983) Reaction of water with glass – influence of a transformed surface-layer. *J. Mat. Sci.,* **18,** 612–622.

Ducheyne, P., Qiu, Q. (1999) Bioactive ceramics: the effect of surface reactivity on bone formation and bone cell function. *Biomaterials,* **20,** 2287–2303.

Gillam, D. G., Tang, J. Y., Mordan, N. J., Newman, H. N. (2002) The effects of a novel Bioglass® dentifrice on dentine sensitivity: a scanning electron microscopy investigation. *J. Oral Rehab.,* **29,** 305–313.

Gough, J. E., Jones, J. R., Hench, L. L. (2004) Nodule formation and mineralisation of human primary osteoblasts cultured on a porous bioactive glass scaffold. *Biomaterials,* **25,** 2039–2046.

Greenspan, D. C., Hench, L. L. (1976) Chemical and mechanical-behavior of bioglass-coated alumina. *J. Biomed. Mater. Res.,* **10,** 503–509.

Gross, U. M., Strunz, V. (1980) The anchoring of glass-ceramics of different solubility in the femur of the rat. *J. Biomed. Mater. Res.,* **14,** 607–618.

Gross, U., Strunz, V. (1985) The interface of various glasses and glass-ceramics with a bony implantation bed. *J. Biomed. Mater. Res.,* **19,** 251–271.

Hench, L. L. (1991) Bioceramics – from concept to clinic. *J. Am. Ceram. Soc.,* **74,** 1487–1510.

Hench, L. L. (1998a) Bioactive materials: the potential for tissue regeneration. *J. Biomed. Mater. Res.,* **41,** 511–518.

Hench, L. L. (1998b) Bioceramics. *J. Am. Ceram. Soc.,* **81,** 1705–1728.

Hench, L. L. (2003) Glass and genes: the 2001 W. E. S. Turner Memorial Lecture. *Glass Technol.,* **44,** 1–10.

Hench, L. L., Paschall, H. A. (1973) Direct chemical bonding of bioactive glass-ceramic materials and bone. *J. Biomed. Mats. Res. Symp.,* **4,** 25–42.

Hench, L. L., Polak, J. M. (2002) Third-generation biomedical materials. *Science,* **295,** 1014–1017.

Hench, L. L., Vasconcelos, W. (1990) Gel-silica science. *Annu. Rev. Mater. Sci.,* **20,** 269–298.

Hench, L. L., West, J. K. (1990) The Sol–gel process. *Chem. Rev.,* **90,** 33–72.

Hench, L. L., Splinter, R. J., Allen, W. C., Greenlee, T. K. (1971) Bonding mechanisms at the interface of ceramic prosthetic materials. *J. Biomed. Mater. Res.,* **2,** 117–141.

Hench, L. L., Pantano, C. G., Buscemi, P. J., Greenspan, D. C. (1977) Analysis of Bioglass fixation of hip prostheses. *J. Biomed. Mater. Res.,* **11,** 267–282.

Hench, L. L., Polak, J. M., Xynos, I. D., Buttery, L. D. K. (2000) Bioactive materials to control cell cycle. *Mat. Res. Innov.,* **3,** 313–323.

Hulbert, S. F., Morrison, S. J., Klawitte, J. J. (1972) Tissue reaction to 3 ceramics of porous and non-porous structures. *J. Biomed. Mater. Res.,* **6,** 347–374.

ISO 13779–1:2000 (2000) *Implants for surgery – Hydroxyapatite – Part 1: Ceramic hydroxyapatite*.

Jell, G., Stevens, M. M. (2006) Gene activation by bioactive glasses. *J. Mater. Sci. Mater. Med.,* **17,** 997–1002.

Jones, J. R., Ehrenfried, L. M., Hench, L. L. (2006a) Optimising bioactive glass scaffolds for bone tissue engineering. *Biomaterials,* **27,** 964–973.

Jones, J. R., Lee, P. D., Hench, L. L. (2006b) Hierarchical porous materials for tissue engineering. *Phil. Trans. Roy. Soc. A,* **364,** 263–281.

Jones, J. R., Poologasundarampillai, G., Atwood, C. R., Bernard, D., Lee, P. D. (2007a) Non-destructive quantitative 3D analysis for the optimisation of tissue scaffolds. *Biomaterials,* **28** (7): 1404–1413.

Jones, J. R., Tsigkou, O., Coates, E. E., Stevens, M. M., Polak, J. M., Hench, L. L. (2007b) Extracellular matrix formation and mineralization of on a phosphate-free porous bioactive glass scaffold using primary human osteoblast (HOB) cells. *Biomaterials,* **28,** 1653–1663.

Jugdaohsingh, R., Tucker, K. L., Qiao, N., Cupples, L. A., Kiel, D. P., Powell, J. J. (2004) Dietary silicon intake is positively associated with bone mineral density in men and premenopausal women of the Framingham Offspring cohort. *J. Bone. Min. Res.,* **19,** 297–307.

Karatzas, S., Zavras, A., Greenspan, D., Amar, S. (1999) Histologic observations of periodontal wound healing after treatment with PerioGlas in nonhuman primates. *Int. J. Periodontics Restor. Dent.,* **19,** 489–499.

Lenza, R. F. S., Vasconcelos, W. L., Jones, J. R., Hench, L. L. (2002) Surface-modified 3D scaffolds for tissue engineering. *J. Mater. Sci. Mater. Med.,* **13,** 837–842.

Lenza, R. F. S., Jones, J. R., Vasconcelos, W. L., Hench, L. L. (2003) In vitro release kinetics of proteins from bioactive foams. *J. Biomed. Mater. Res. A,* **67A,** 121–129.

Li, P. J., Ohtsuki, C., Kokubo, T., Nakanishi, K., Soga, N., Degroot, K. (1994) The role of hydrated silica, titania, and alumina in inducing apatite on implants. *J. Biomed. Mater. Res.,* **28,** 7–15.

Li, R., Clark, A. E., Hench, L. L. (1991) An investigation of bioactive glass powders by sol–gel processing. *J. Appl. Biomater.,* **2,** 231–239.

Miyazaki, T., Ohtsuki, C., Akioka, Y., Tanihara, M., Nakao, J., Sakaguchi, Y., Konagaya, S. (2003) Apatite deposition on polyamide films containing carboxyl group in a biomimetic solution. *J. Mater. Sci. Mater. Med.,* **14,** 569–574.

Nakamura, T., Yamamuro, T., Higashi, S., Kokubo, T., Itoo, S. (1985) A new glass-ceramic for bone-replacement – evaluation of its bonding to bone tissue. *J. Biomed. Mater. Res.,* **19,** 685–698.

Neo, M., Kotani, S., Nakamura, T., Yamamuro, T., Ohtsuki, C., Kokubo, T., Bando, Y. (1992) A comparative-study of ultrastructures of the interfaces between 4 kinds of surface-active ceramic and bone. *J. Biomed. Mater. Res.,* **26,** 1419–1432.

Ohgushi, H., Caplan, A. I. (1999) Stem cell technology and bioceramics: from cell to gene engineering. *J. Biomed. Mater. Res.,* **48,** 913–927.

Oonishi, H., Hench, L. L., Wilson, J., Sugihara, F., Tsuji, E., Kushitani, S., Iwaki, H. (1999) Comparative bone growth behavior in granules of bioceramic materials of various sizes. *J. Biomed. Mater. Res.,* **44,** 31–43.

Oonishi, H., Hench, L. L., Wilson, J., Sugihara, F., Tsuji, E., Matsuura, M., Kin, S., Yamamoto, T., Mizokawa, S. (2000) Quantitative comparison of bone growth behavior in granules of Bioglass®, A-W glass-ceramic, and hydroxyapatite. *J. Biomed. Mater. Res.,* **51,** 37–46.

Pantano, C. G., Clark, A. E., Hench, L. L. (1974) Multilayer corrosion films on Bioglass® surfaces. *J. Am. Ceram. Soc.,* **57,** 412–413.

Pereira, M. M., Hench, L. L. (1996) Mechanisms of hydroxyapatite formation on porous gel-silica substrates. *J. Sol–gel Sci. Technol.,* **7,** 59–68.

Pereira, M. M., Clark, A. E., Hench, L. L. (1994) Calcium-phosphate formation on sol–gel-derived bioactive glasses *in-vitro*. *J. Biomed. Mater. Res.,* **28,** 693–698.

Pereira, M. M., Clark, A. E., Hench, L. L. (1995) Effect of texture on the rate of hydroxyapatite formation on gel-silica surface. *J. Am. Ceram. Soc.,* **78,** 2463–2468.

Piotrowski, G., Hench, L. L., Allen, W. C., Miller, G. J. (1975) Mechanical studies of bone Bioglass interfacial bond. *J. Biomed. Mater. Res.,* **9,** 47–61.

Porter, A. E., Patel, N., Skepper, J. N., Best, S. M., Bonfield, W. (2003) Comparison of *in vivo* dissolution processes in hydroxyapatite and silicon-substituted hydroxyapatite bioceramics. *Biomaterials,* **24,** 4609–4620.

Porter, A. E., Patel, N., Skepper, J. N., Best, S. M., Bonfield, W. (2004) Effect of sintered silicate-substituted hydroxyapatite on remodelling processes at the bone–implant interface. *Biomaterials,* **25,** 3303–3314.

Radin, S., Ducheyne, P., Falaize, S., Hammond, A. (2000) *In vitro* transformation of bioactive glass granules into Ca-P shells. *J. Biomed. Mater. Res.,* **49,** 264–272.

Reffitt, D. M., Ogston, N., Jugdaohsingh, R., Cheung, H. F. J., Evans, B. A. J., Thompson, R. P. H., Powell, J. J., Hampson, G. N. (2003) Orthosilicic acid stimulates collagen type 1 synthesis and osteoblastic differentiation in human osteoblast-like cells *in vitro*. *Bone,* **32,** 127–135.

Rico, H., Gallego-Lago, J. L., Hernandez, E. R., Villa, L. F., Sanchez-Atrio, A., Seco, C., Gervas, J. J. (2000) Effect of silicon supplement on osteopenia induced by ovariectomy in rats. *Calc. Tiss. Int.,* **66,** 53–55.

Salinas, A. J., Martin, A. I., Vallet-Regi, M. (2002) Bioactivity of three $CaO–P_2O_5–SiO_2$ sol–gel glasses. *J. Biomed. Mater. Res.,* **61,** 524–532.

Saravanapavan, P., Hench, L. L. (2003a) Mesoporous calcium silicate glasses. I. Synthesis. *J. Non-Cryst. Solids,* **318,** 1–13.

Saravanapavan, P., Hench, L. L. (2003b) Mesoporous calcium silicate glasses. II. Textural characterisation. *J. Non-Cryst. Solids,* **318,** 14–26.

Saravanapavan, P., Jones, J. R., Pryce, R. S., Hench, L. L. (2003) Bioactivity of gel-glass powders in the $CaO–SiO_2$ system: a comparison with ternary ($CaO–P_2O_5–SiO_2$) and quaternary glasses ($SiO_2–CaO–P_2O_5–Na_2O$). *J. Biomed. Mater. Res. A,* **66A,** 110–119.

Sepulveda, P., Jones, J. R., Hench, L. L. (2001) Characterization of melt-derived 45S5 and sol–gel-derived 58S bioactive glasses. *J. Biomed. Mater. Res.,* **58,** 734–740.

Sepulveda, P., Jones, J. R., Hench, L. L. (2002a) Bioactive sol–gel foams for tissue repair. *J. Biomed. Mater. Res.,* **59,** 340–348.

Sepulveda, P., Jones, J. R., Hench, L. L. (2002b) *In vitro* dissolution of melt-derived 45S5 and sol–gel-derived 58S bioactive glasses. *J. Biomed. Mater. Res.,* **61,** 301–311.

Stanley, H. R., Hall, M. B., Clark, A. E., King, C. J., Hench, L. L., Berte, J. J. (1997) Using 45S5 bioglass cones as endosseous ridge maintenance implants to prevent alveolar ridge resorption: a 5-year evaluation. *Int. J. Oral Max. Impl.,* **12,** 95–105.

Warren, L. D., Clark, A. E., Hench, L. L. (1989) An investigation of Bioglass powders – quality assurance test procedure and test criteria. *J. Biomed. Mater. Res.,* **23B,** 201–209.

Weinstein, A. M., Klawitter, J. J., Cook, S. D. (1980) Implant–bone interface characteristics of Bioglass dental implants. *J. Biomed. Mater. Res.,* **14,** 23–29.

Wheeler, D. L., Eschbach, E. J., Hoellrich, R. G., Montfort, M. J., Chamberland, D. L. (2000) Assessment of resorbable bioactive material for grafting of critical-size cancellous defects. *J. Orthop. Res.,* **18,** 140–148.

Wilson, J., Low, S. B. (1992) Bioactive ceramics for periodontal treatment – comparative-studies in the patus monkey. *J. Appl. Biomater.,* **3,** 123–129.

Wilson, J., Noletti, D. (1990) Bonding of Soft Tissues to Bioglass®. In Yamamuro, T., Hench, L. L., Wilson, J. (Eds.) *Handbook of Bioactive Ceramics.* Boca Raton, Fl, CRC Press.

Wilson, J., Pigott, G. H., Schoen, F. J., Hench, L. L. (1981) Toxicology and biocompatibility of Bioglasses. *J. Biomed. Mater. Res.,* **15,** 805–817.

Xynos, I. D., Edgar, A. J., Buttery, L. D. K., Hench, L. L., Polak, J. M. (2000a) Ionic products of bioactive glass dissolution increase proliferation of human osteoblasts and induce insulin-like growth factor II mRNA expression and protein synthesis. *Biochem. Biophys. Res. Commun.,* **276,** 461–465.

Xynos, I. D., Hukkanen, M. V. J., Batten, J. J., Buttery, L. D., Hench, L. L., Polak, J. M. (2000b) Bioglass® 45S5 stimulates osteoblast turnover and enhances bone formation *in vitro*: Implications and applications for bone tissue engineering. *Calc. Tiss. Int.,* **67,** 321–329.

Xynos, I. D., Edgar, A. J., Buttery, L. D. K., Hench, L. L., Polak, J. M. (2001) Gene-expression profiling of human osteoblasts following treatment with the ionic products of Bioglass® 45S5 dissolution. *J. Biomed. Mater. Res.,* **55,** 151–157.

Yoshii, S., Kakutani, Y., Yamamuro, T., Nakamura, T., Kitsugi, T., Oka, M., Kokubo, T., Takagi, M. (1988) Strength of bonding between A–W glass-ceramic and the surface of bone cortex. *J. Biomed. Mater. Res.,* **22B,** 327–338.

13

Bioactive glass-ceramics

T KOKUBO, Chubu University, Japan

13.1 Introduction

Synthetic materials implanted into bone defects are generally encapsulated by a fibrous tissue to isolate them from the surrounding bone, and they cannot be used as bone substitutes. However, Hench *et al.* (1972) showed that some Na_2O–CaO–SiO_2–P_2O_5 glasses bond to living bone without forming fibrous tissue around them. These are known as Bioglass®, and are expected to be useful as bone substitutes in various applications. However, their mechanical strength is not as high as that of human cortical bone. To improve their mechanical strength, various types of glass precipitating different crystalline phases have been prepared, known as glass-ceramics. Ceravital®, which precipitates apatite in Na_2O–K_2O–MgO–CaO–SiO_2–P_2O_5 glass (Brömer *et al.*, 1973), glass-ceramic A-W, which precipitates apatite and wollastonite in MgO–CaO–SiO_2–P_2O_5 glass, Bioverit®, which precipitates apatite and phlogopite in Na_2O–MgO–CaO–Al_2O_3–SiO_2–P_2O_5–F glass (Höland *et al.*, 1985), Ilmaplant®, which precipitates apatite and wollastonite in Na_2O–K_2O–MgO–CaO–SiO_2–P_2O_5–CaF_2 glass (Berger *et al.*, 1989), and glass-ceramics that precipitate canasite in Na_2O–K_2O–CaO–CaF_2–P_2O_5–SiO_2 glass (Miller *et al.*, 2002) are examples.

Among these, glass-ceramic A-W has been the most widely used clinically. The fabrication process, mechanical properties, biological properties, bone-bonding mechanism and apatite-forming mechanism of glass-ceramic A-W are described in this chapter. Clinical applications of this glass-ceramic are described in Chapter 26.

13.2 Fabrication process

Bone is a composite consisting of an assembly of nanometre-size apatite particles reinforced by collagen fibres. In view of this fact, it is expected that a composite of apatite with a fibrous phase may exhibit a high mechanical strength as well as bioactivity.

Beta-wollastonite, which has a chemical composition of $CaO \cdot SiO_2$, and has the silicate chain structure shown in Fig. 13.1, occurs in a fine fibrous form in nature. However, it is difficult to produce a dense and homogeneous composite of hydroxyapatite and β-wollastonite using an ordinary sintering process of a powder mixture, because the fibrous phase is not easily dispersed uniformly in an apatite powder. However, certain types of glass can give a composite in which one or more types of crystalline particles are homogeneously dispersed in a glassy matrix when it is subjected to an appropriate heat treatment.

The $3CaO \cdot P_2O_5$–$CaO \cdot SiO_2$ pseudobinary system has a eutectic point at the 36 wt% ($3CaO \cdot P_2O_5$)–64 wt% ($CaO \cdot SiO_2$) composition at a temperature of 1420 °C (Fig. 13.2). A partial replacement of $CaO \cdot SiO_2$ with

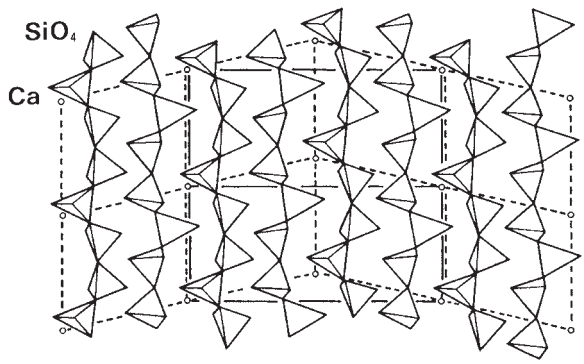

13.1 Structure of β-wollastonite.

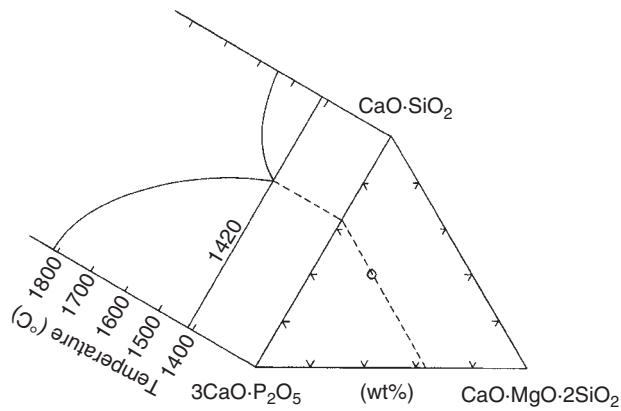

13.2 Pseudo-ternary system of $CaO \cdot SiO_2$–$CaO \cdot MgO \cdot 2SiO_2$–$3CaO \cdot P_2O_5$. A small open circle in the triangle denotes the base composition of glass-ceramic A-W.

$CaO \cdot MgO \cdot 2SiO_2$ decreases the liquidus temperature. In view of this, we chose a composition of 36 wt% ($3CaO \cdot P_2O_5$), 40 wt% ($CaO \cdot SiO_2$), 24 wt% ($CaO \cdot MgO \cdot 2SiO_2$), i.e. 4.6 (MgO), 44.9 (CaO), 34.2 (SiO_2), 16.3 (P_2O_5) in wt% was selected as a base composition of the parent glass in our study (Kokubo *et al*., 1982).

A batch mixture was prepared using reagent grade MgO, $CaCO_3$, SiO_2 and $CaHPO_5 \cdot 2H_2O$. These were placed in a Pt–10% Rh crucible, melted at 1450 °C for 2 h in a SiC furnace, poured onto a stainless steel plate, and then pressed into a plate about 2 mm thick. This glass plate was then placed on a platinum plate and heated to 1050 °C at a heating rate of 5 °C/min in a SiC furnace.

Fine-grained apatite and fibrous β-wollastonite were precipitated in the glass using this heat treatment. However, large cracks were formed in the interior of the crystallised product (Fig. 13.3), because the fibrous wollastonite precipitated perpendicular to the outer surface of the glass (Kokubo *et al*., 1986).

To suppress the preferred orientation of the wollastonite, the glass plate was crushed into a powder with a particle size below 44 μm, and uniaxially and subsequently isostatically pressed into a disc, and then subjected to the same heat treatment described above. As a result, fine-grained apatite and wollastonite homogeneously precipitated in the glass. However, the crystallised product contained 3.5% porosity, because the glass powder compact began to crystallise before full sintering had occurred. The addition of CaF_2 to the composition described above in 0.5–100 wt% ratios provided a fully densified crystallised product, because it decreased the softening tempera-

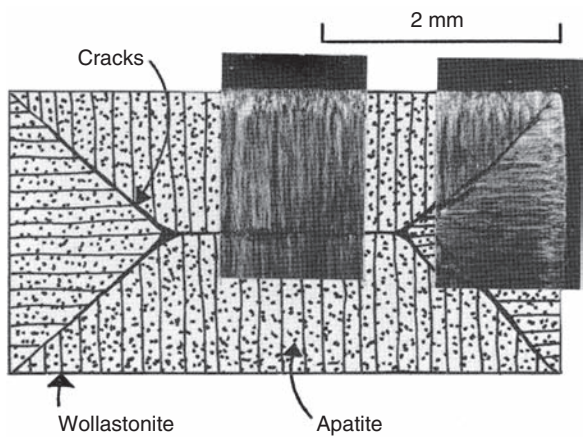

13.3 Cross-section of crystallised product of a glass plate with the base composition of glass-ceramic A-W (Kokubo *et al.*, 1986).

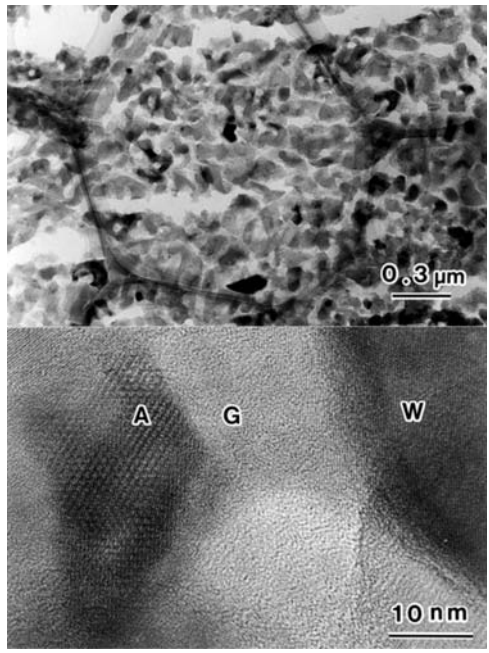

13.4 Transmission electron micrograph of glass-ceramic A-W. A: apatite, W: wollastonite, G: glassy phase (Ohtsuki *et al.*, 1995).

ture of the glass powder, whereas it increased the crystallisation temperature of the wollastonite.

Figure 13.4 shows a transmission electron micrograph of the crystallised product. The nanometre-sized apatite and wollastonite were homogeneously dispersed in the glassy matrix (Ohtsuki *et al.*, 1995). This crystallised product is known as glass-ceramic A-W after the names of the crystalline phases it contains. The apatite was speculated to be oxyfluoroapatite from the composition of the glass. The apatite, β-wollastonite and glassy phase content were calculated to be 38, 34 and 28 wt%, respectively, from the intensities of the X-ray diffraction peaks (Kokubo, 1991a). The density of glass-ceramic A-W is 3.078 g/cm^3. Glass-ceramic A-W can be machined into various shapes for bone substitutes, as shown in the chapter 26 that discusses bioactive glass-ceramics.

13.3 Mechanical properties

The bending strength and fracture toughness of glass-ceramic A-W is shown in Fig. 13.5, which compares the values of the parent glass G, glass-ceramic A, precipitating only apatite, sintered hydroxyapatite and human cortical

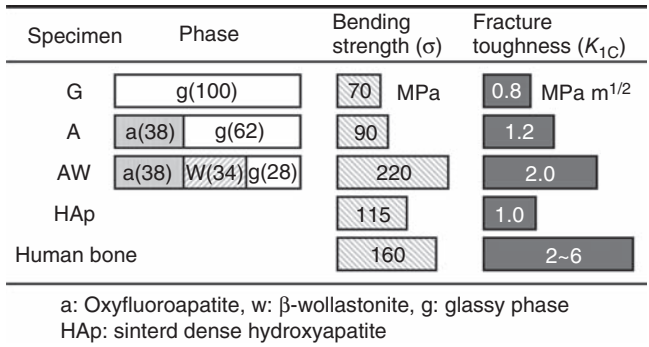

13.5 Phase, bending strength and fracture toughness of glass G, glass-ceramic A, glass-ceramic A-W, sintered hydroxyapatite (HAp) and human cortical bone.

bone (Kokubo *et al*., 1985). The bending strength of 220 MPa of glass-ceramic A-W is higher than that of human cortical bone. Comparing the bending strength of glass-ceramic A-W with that of glass G and glass-ceramic A, it is evident that the high bending strength of glass-ceramic A-W is conferred by the precipitation of the wollastonite in addition to the apatite.

Glass-ceramic A-W shows a fracture toughness of 2.0 MPa $m^{1/2}$, whereas glass G and glass-ceramic A show fracture toughnesses of 0.8 and 1.2 MPa $m^{1/2}$, respectively. This means that the high bending strength of glass-ceramic A-W is attributed to its high fracture toughness. Glass-ceramic A-W has a fracture surface energy of 15.9 J/m^2, whereas glass G and glass-ceramic A have fracture surface energies of 3.3 and 6.4 J/m^2, respectively. Therefore, the high fracture toughness of glass-ceramic A-W is attributed to the high fracture surface energy. Glass G and glass-ceramic A show fairly smooth fracture surfaces, whereas glass-ceramic A-W shows a much rougher fracture surface (Fig. 13.6). Other mechanical properties of glass-ceramic A-W are listed in Table 13.1.

To evaluate the usefulness of this glass-ceramic as a bone substitute under load-bearing conditions, its fatigue properties were measured in a simulated body fluid (SBF) with ion concentrations nearly equal to those of the human blood plasma at 36.5 °C. Figure 13.7 shows the dependence of the bending strength of glass-ceramic A-W in an SBF on the stressing rate, compared with glass G, glass-ceramic A and sintered hydroxyapatite (Kokubo *et al*., 1987a). It can be seen from the data in Fig. 13.7 that the dependence of the bending strength on the stressing rate, which is an indication of the fatigue properties, of glass-ceramic A-W is lower than that of glass G and glass-ceramic A. Glass-ceramic A-W is speculated to be able to withstand more than 10 years' use in the living body, even under

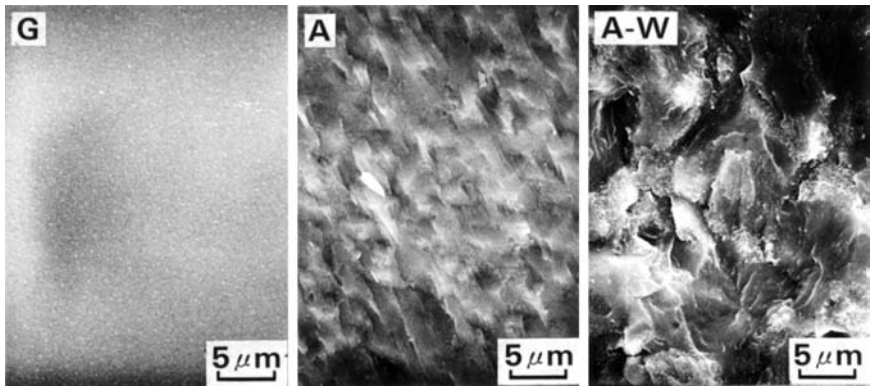

13.6 SEM pictures of fracture surfaces of glass G, glass-ceramic A and glass-ceramic A-W (Kokubo *et al.*, 1985).

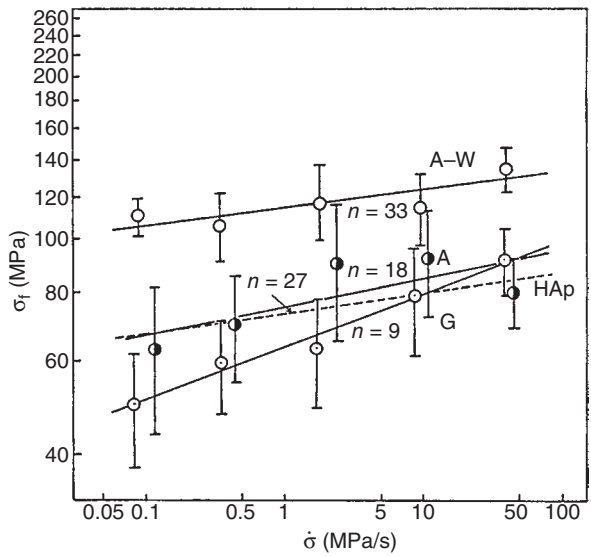

13.7 Dependence of bending strength of upon stressing rate (σ) of glass-ceramic A-W in SBF, in comparison with those of glass G, glass-ceramic A and sintered hydroxyapatite (HAp) (Kokubo *et al.*, 1987a).

Table 13.1 Some mechanical properties of glass-ceramic A-W

Bending strength	220 MPa
Compressive strength	1080 MPa
Young's modulus	118 GPa
Vickers hardness	680 HV
Fracture toughness	2.0 MPa $m^{1/2}$

continuous loading of a bending stress of 65 MPa. The stability of the mechanical strength of glass-ceramic A-W has also been evaluated using animal experiments (Kitsugi *et al*., 1987a).

13.4 Biological properties

The response of living tissue to glass-ceramic A-W was examined by implanting rectangular samples $10 \times 15 \times 2\,mm^3$ in size into the tibial metaphyses of a rabbit (Nakamura *et al*., 1985). Figure 13.8 shows a contact microradiograph of a cross-section of an interface between glass-ceramic A-W and bone 25 weeks after implantation. The glass-ceramic A-W directly contacted with the bone without intervention of any fibrous tissue. When a tensile stress was applied perpendicularly to the interface, the fracture occurred not at the interface, but in the bone (Fig. 13.9). It can be seen from these figures that the glass-ceramic A-W was tightly bonded to living bone.

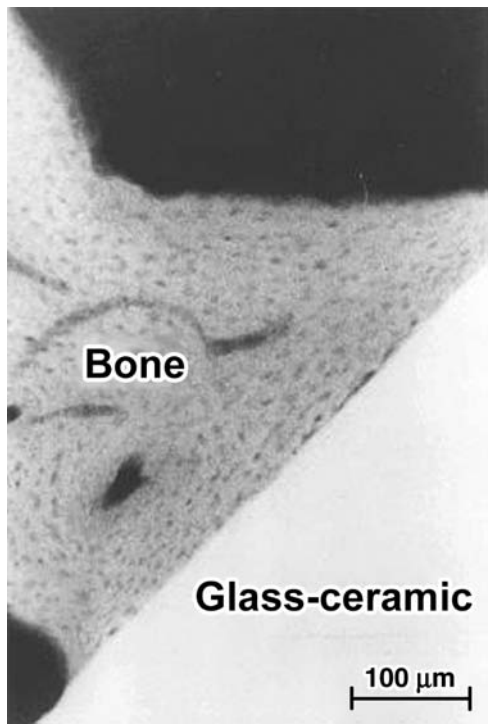

13.8 Contact microradiograph of an interface of glass-ceramic A-W and rabbit tibia.

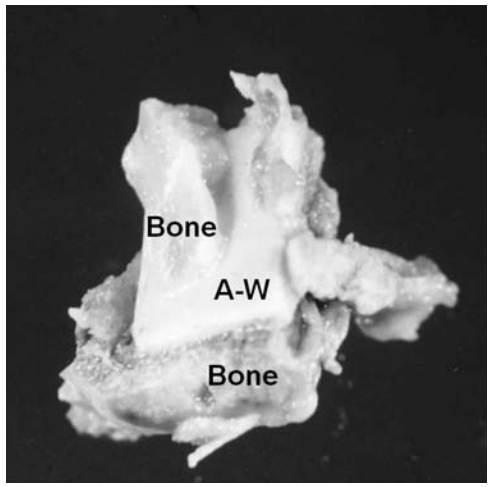

13.9 Fracture surface of bone connected to glass-ceramic A-W (Nakamura *et al.*, 1985).

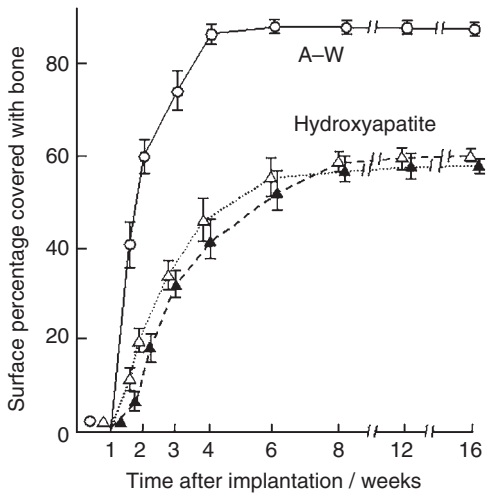

13.10 Surface percentage of granules of glass-ceramic A-W and sintered hydroxyapatite covered with newly grown bone in rabbit tibia as a function of time after implantation.

When granular particles of glass-ceramic A-W, 200–325 μm in size, were implanted into a hole drilled at a rat's tibia, they were covered with newly grown bone on up to 90% of their surface within 4 weeks (Fig. 13.10) (Ono *et al.*, 1990). Glass-ceramic A-W in a porous form was partially resolved and fully integrated with newly grown bone in a rabbit's tibia within 12 weeks (Fig. 13.11).

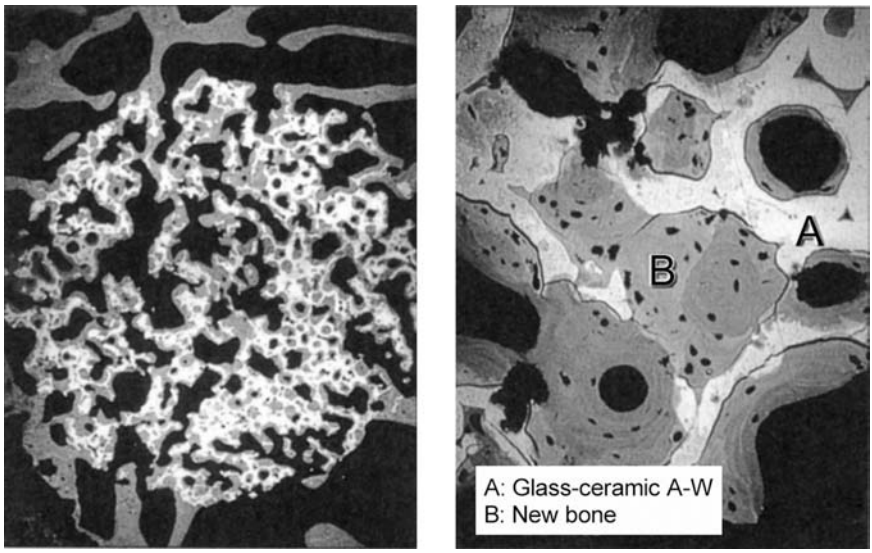

13.11 Bone ingrowth into pores of glass-ceramic A-W.

13.5 Bone-bonding mechanism of glass-ceramic A-W

A calcium phosphate layer was observed at the interface between glass-ceramic A-W and a rabbit's tibia using a scanning electron micrograph and energy dispersive X-ray analysis (Kitsugi *et al*., 1986, 1987b).

Using micro-X-ray diffraction data of an interface between glass-ceramic A-W and the vertebra of a sheep (Kitsugi *et al*., 1990; Kokubo *et al*., 1990c), and electron diffraction data of an interface between glass-ceramic A-W and a rat's tibia (Neo *et al*., 1992a,b), the calcium phosphate layer was identified as a layer of crystalline apatite having nanometre size. Glass-ceramic A-W connects to living bone through an apatite layer (Fig. 13.12).

This calcium phosphate layer was not observed at the interface of glass-ceramic A-W (Al), which contained a small amount of Al_2O_3, and bone, and so did not bond to living bone (Kitsugi *et al*., 1989). This means that the apatite layer plays an essential role in the bonding of glass-ceramic A-W to bone. The apatite layer on glass-ceramic A-W can be reproduced on its surface in an SBF (Fig. 13.13) (Kokubo *et al*., 1990a,b; Ohtsuki *et al*., 1995). According to detailed analysis using thin-film X-ray diffraction and Fourier transform infrared reflection spectroscopy of the surface layer, this consists of apatite composed of small crystallites and a small amount of carbonate ions (Kokubo *et al*., 1990a). These characteristics are common to bone

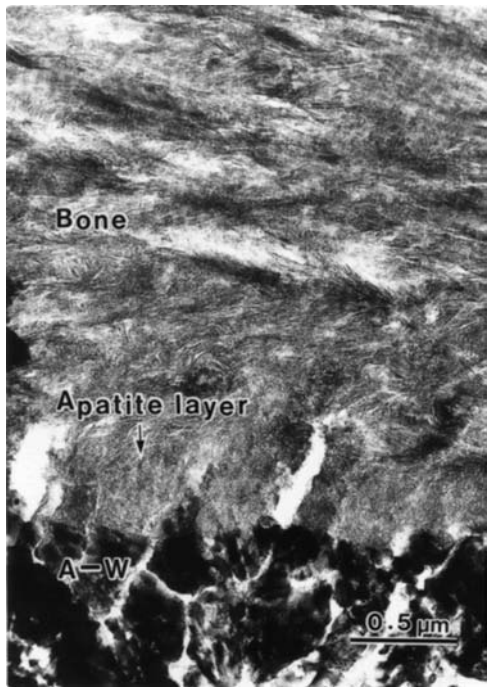

13.12 Transmission electron micrograph of an interface between glass-ceramic A-W and rat tibia (Neo *et al.*, 1992b).

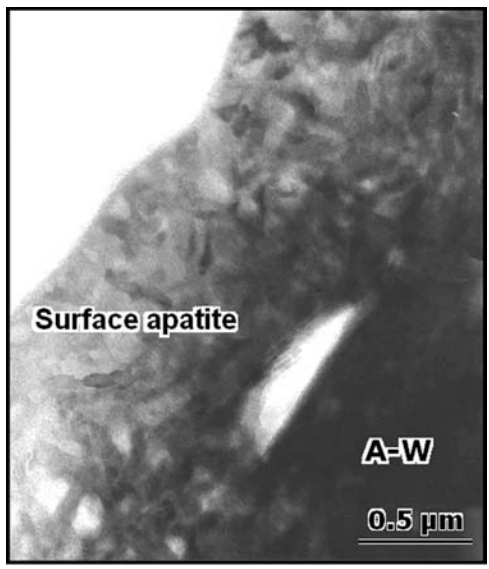

13.13 Cross-section of apatite layer formed on glass-ceramic A-W in SBF (Ohtsuki *et al.*, 1995).

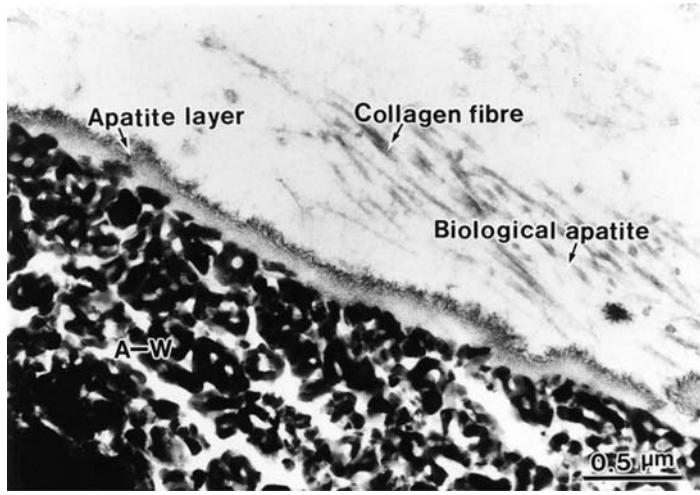

13.14 Transmission electron micrograph of cross-section of glass-ceramic A-W implanted into rat tibia at early stage after implantation (Neo *et al.*, 1993).

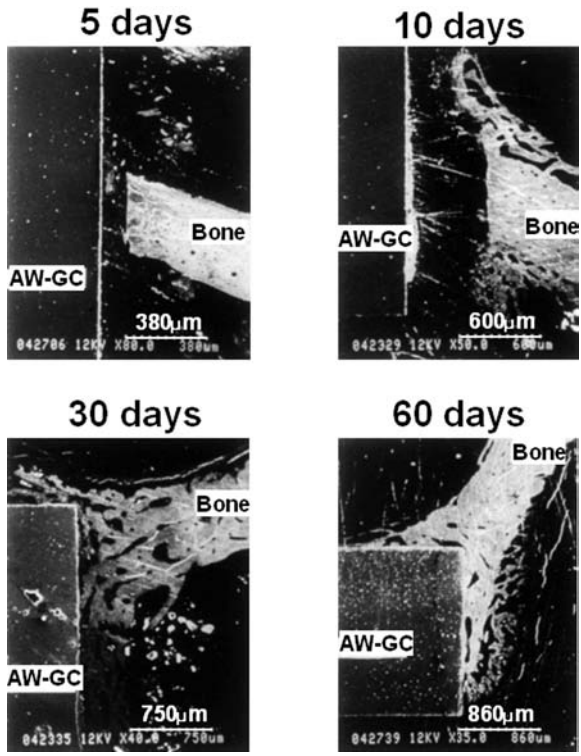

13.15 Optical micrograph of cross-section of an interface of glass-ceramic A-W and the surrounding bone as a function of time after implantation (Kitsugi *et al.*, 1987b).

minerals. The bonelike apatite on glass-ceramic A-W is easily resolved using osteoclasts, similar to bone (Yamada *et al*., 1994a,b).

It is expected that osteogenic cells can preferentially proliferate and differentiate on a bonelike apatite layer to produce collagen and apatite. In practice, it is observed under a transmission electron microscope that collagen and apatite are actively produced on the apatite layer formed on glass-ceramic A-W at an early stage after implantation into a rat's tibia (Fig. 13.14) (Neo *et al*., 1993). In a cell culture, it was observed that osteoblasts actively form bone tissue on the bonelike apatite layer formed on glass-ceramic A-W in an SBF (Loty *et al*., 2000). As a result, new bone grows from the surrounding bone, and soon reaches the surface of the glass-ceramic A-W (Fig. 13.15) (Kitsugi *et al*., 1987b). When this occurs, a tight chemical bond is formed between the surface apatite and the apatite in the bone to reduce the interface energy between them. The high bonding ability of the bonelike apatite formed on glass-ceramic A-W to another type of apatite in a body environment was confirmed *in vivo* as well as in an SBF (Kitsugi *et al*., 1987c; Kokubo *et al*., 1987b). This bonding mechanism of glass-ceramic A-W to living bone is shown schematically in Fig. 13.16.

13.6 Apatite-forming mechanism of glass-ceramic A-W

Glass-ceramic A-W dissolves a larger amount of calcium and silicate ions into an SBF than does glass-ceramic A-W (Al) (Kokubo *et al*., 1992). Glass-ceramic A-W (Al) does not form bonelike apatite on its surface in an SBF, but does form such a layer in an SBF with added calcium and silicate ions (Kokubo *et al*., 1993). This indicates that the calcium and silicate ions play an important role in forming the bonelike apatite layer on glass-ceramic A-W in an SBF as well as *in vivo*. The calcium and silicate ions may be dissolved from the glassy matrix as well as the wollastonite of the glass-ceramic A-W (Fig. 13.17). The phosphate ions are not dissolved from glass-ceramic A-W, as all the phosphate ions are incorporated into the apatite (Kokubo *et al*., 1992), and the SBF is already supersaturated with respect to the apatite.

The calcium ions may increase the ionic activity product of the apatite in the surrounding body fluid, which is already supersaturated with respect to the apatite (Neuman and Neuman, 1985), whereas the silicate ion may provide favourable sites for apatite nucleation on the surface of the glass-ceramic A-W. This has been shown by examining the formation of apatite on glasses in the $CaO–P_2O_5–SiO_2$ system (Ohtsuki *et al*., 1992). $CaO–SiO_2$ glasses dissolve a large amount of calcium ions into an SBF, whereas $CaO–P_2O_5$ glasses dissolve a large amount of phosphate ions into an SBF. Both

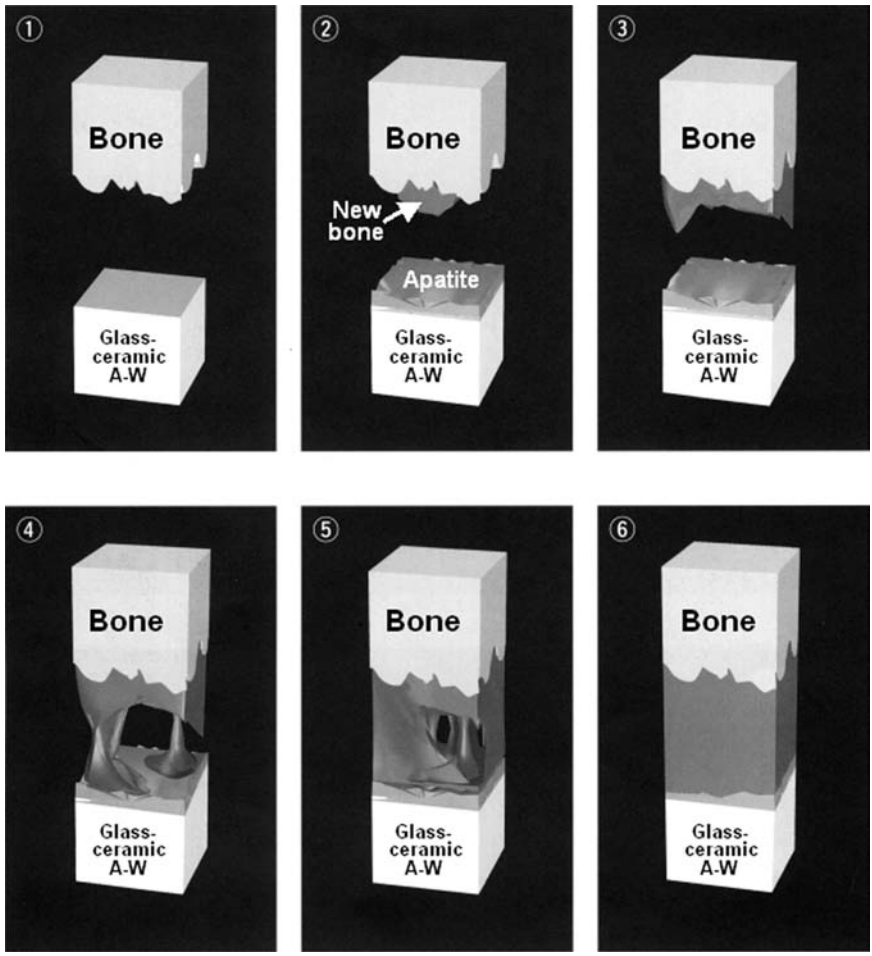

13.16 Mechanism of bonding of glass-ceramic A-W to bone: 1, just after implantation; 2, formation of bonelike apatite; 3, growth of new bone; 4, bonding of new bone with apatite layer; 5, 6, increase in density of new bone.

these dissolved ions increase the ionic activity product of the apatite in SBF almost equally (Fig. 13.18). Despite this, only $CaO–SiO_2$ glasses form bonelike apatite on their surface in an SBF, whereas $CaO–P_2O_5$ glasses do not form bonelike apatite on their surface (Fig. 13.19). This indicates that hydrated silica on the surface of the former glass provides favourable sites for the nucleation of apatite. The catalytic effect of Si–OH groups for the nucleation of apatite is shown by the observation that even pure silica gel forms apatite on its surface in an SBF (Li *et al*., 1992), as discussed in Chapter 7.

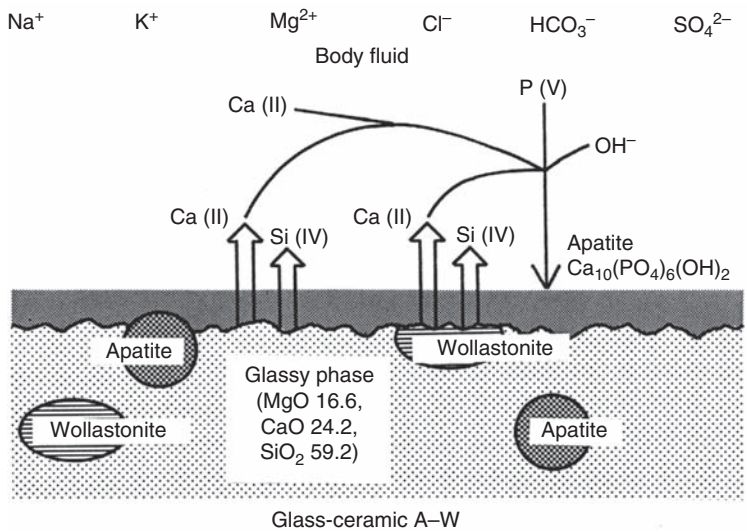

13.17 Release of ions from glass-ceramic A-W into body fluid and apatite formation on glass-ceramic A-W (Kokubo *et al.,* 1992).

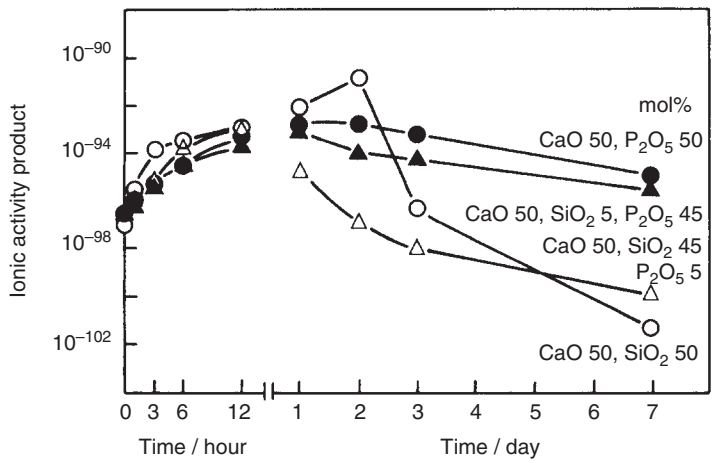

13.18 Variation of ionic activity product of apatite in SBF with soaking of $CaO \cdot SiO_2$ and $CaO \cdot P_2O_5$ based glasses as a function of soaking time (Ohtsuki *et al.,* 1992).

This mechanism of apatite formation on glass-ceramic A-W is essentially the same as that on Bioglass in the Na_2O–CaO–SiO_2–P_2O_5 system. However, it is interesting to note that glass-ceramic A-W forms an apatite layer on its surface without forming a silica gel layer on its surface (Ohtsuki *et al.*, 1995), whereas Bioglass forms an apatite layer on a silica gel layer (Hench

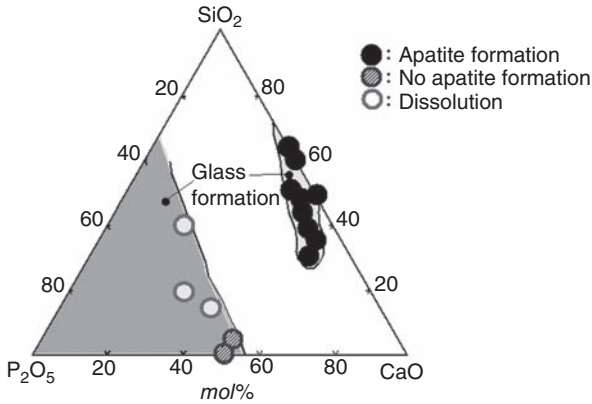

13.19 Glass formation in the system $CaO–SiO_2–P_2O_5$ and apatite formation on glasses in SBF (Ohtsuki *et al.,* 1992).

and Clarke, 1978). The high bonding strength of glass-ceramic A-W to bone (Nakamura *et al*., 1985) is attributed to the lack of a mechanically weak silica gel layer.

13.7 Summary

A glass powder compact in the $MgO–CaO–SiO_2–P_2O_5$ system gives a dense and homogeneous glass-ceramic, where nano-sized oxyfluoroapatite and β-wollastonite are uniformly dispersed in a glassy matrix after heat treatment. The resultant product exhibits a higher bending strength than that of human cortical bone. This glass-ceramic forms a bonelike apatite layer on its surface in the living body, and tightly bonds to living bone through this apatite layer. This formation of apatite is nucleated by Si–OH groups on the surface, and is accelerated by calcium ions dissolved from the glass-ceramic.

The processing and properties of this glass-ceramic was reviewed using literature references (Kokubo, 1990, 1991a,b and 1993a,b). The results of long-term clinical applications are described in Chapter 26.

13.8 References

Berger G, Sauer R, Steinborn G, Wihsmann F G, Thieme V, Kolhler St and Dressel H, (1989), 'Clinical application of surface reactive apatite/wollastonite containing glass-ceramics, in O. V. Mazurin *Proc. of XV International Congress on Glass*, 3A, Leningrad, Nauka, 120–26

Brömer H, Pfeil E and Käs H H, (1973) *German Patent* 2,326,100

Hench L L, Splinter R J, Allen W C and Greenlee T K Jr. (1972), 'Bonding mechanism at the interface of ceramic prosthetic materials', *J. Biomed. Mat. Res.* **2 1**, 117–41

Hench L L and Clark D E, (1978) 'Physical chemistry of glass surfaces', *J. Non-Cryst. Solids*, **28**, 83

Höland W, Vogel W, Naumann K and Gummel J, (1985), 'Interface reactions between machinable bioactive glass-ceramics and bone', *J. Biomed. Mater. Res.* **19**, 303–12.

Kitsugi T, Yamamuro T, Nakamura T, Higashi S, Kakutani Y, Hyakana K, Ito S, Kokubo T, Takagi M and Shibuya T, (1986) 'Bone bonding behavior of three kinds of apatite containing glass ceramics', *J. Biomed. Mater. Res.* **20**, 1295–307

Kitsugi T, Yamamuro T, Nakamura T, Kakutani Y, Hayashi T, Ito S, Kokubo T, Takagi M and Shibuya T, (1987a) 'Aging test and dynamic fatigue test of apatite-wollastonite-containing glass ceramics and dense hydroxyapatite', *J. Biomed. Mater. Res.* **21**, 467–84

Kitsugi T, Nakamura T, Yamamuro T, Kokubo T, Shibuya T and Takagi M, (1987b) 'SEM-EPMA observation of three types of apatite-containing glass-ceramics implanted in bone: the variance of a Ca-P-rich layer', *J. Biomed. Mater. Res.* **21**, 1255–71

Kitsugi T, Yamamuro T, Nakamura T, Kokubo T, Takagi M, Shibuya T, Takeuchi H and Ono M, (1987c) 'Bonding behavior between two bioactive ceramics *in vivo*', *J. Biomed. Mater. Res.* **21**, 1109–23

Kitsugi T, Yamamuro T, Nakamura T and Kokubo T, (1989) 'The bonding of glass ceramics to bone', *Int. Orthopaed.* **13**, 199–206

Kitsugi T, Yamamuro T and Kokubo T, (1990) 'Analysis of A-W glass-ceramic surface by micro-beam X-ray diffraction', *J. Biomed. Mater. Res.* **24**, 259–273

Kokubo T, (1990) 'Surface chemistry of bioactive glass-ceramics' *J. Non-Cryst. Solids* **120**, 138–151

Kokubo T, (1991a) 'Bioactive glass-ceramics: properties and applications', *Biomaterials* **12**, 155–63

Kokubo T, (1991b) 'Recent progress in glass-based materials for biomedical applications', *J. Ceram. Soc. Japan* **99**, 965–73

Kokubo T, (1993a) 'Bioactivity of glasses and glass-ceramics' in Ducheyne P, Kokubo T, and Van Blitterswijk CA, *Bone-bonding Materials*, Leiderdorp, Reed Health Care Comm. 31–46

Kokubo T, (1993b) 'A/W glass ceramics: processing and properties' in Hench LL and Wilson J, *Introduction to Bioceramics*, Singapore, World Scientific, 75–88

Kokubo T, Shigematsu M, Nagashima Y, Tashiro M, Yamamuro T and Higashi S, (1982) 'Apatite and wollastonite-containing glass-ceramics for prosthetic application', *Bull. Inst. Chem. Res., Kyoto Univ.*, **60**, 260–68.

Kokubo T, Ito S, Shigematsu M, Sakka S and Yamamuro T, (1985) 'Mechanical properties of a new type of apatite-containing glass-ceramic for prosthetic application', *J. Mater. Sci.* **20**, 2001–4

Kokubo T, Ito S, Sakka S and Yamamuro T, (1986), 'Formation of a high-strength bioactive glass-ceramic in the system $MgO–CaO–SiO_2–P_2O_5$', *J. Mater. Sci.* **21**, 536–40

Kokubo T, Ito S, Shigematsu M, Sakka S and Yamamuro T, (1987a) 'Fatigue and life-time of bioactive glass-ceramic A-W containing apatite and wollastonite', *J. Mater. Sci.* **22**, 4067–70

Kokubo T, Hayashi T, Sakka S, Kitsugi T and Yamamuro T, (1987b) 'Bonding between bioactive glasses, glass-ceramics or ceramics in a simulated body fluid', *Yogyo-Kyokai-Shi*, **95**,785–91

Kokubo T, Ito S, Huang Z T, Hayashi T, Sakka S, Kitsugi T and Yamamuro T, (1990a) 'Ca, P-rich layer formed on high-strength bioactive glass-ceramic A-W', *J. Biomed. Mater. Res.* **24**, 331–43

Kokubo T, Kushitani H, Sakka S, Kitsugi T and Yamamuro T, (1990b) 'Solutions able to reproduce *in vivo* surface–structure changes in bioactive glass-ceramic A-W', *J. Biomed. Mater. Res.* **24**, 721–34

Kokubo T, Ohtsuki C, Kotani S, Kitsugi T and Yamamuro T, (1990c) 'Surface structure of bioactive glass-ceramic A-W implanted into sheep and human vertebra' in Heimke, *Bioceramics*, Vol. 2. Cologne, German Ceramic Society, 105–12

Kokubo T, Kushitani H, Ohtsuki C, Sakka S and Yamamuro T, (1992) 'Chemical reaction of bioactive glass and glass-ceramics with a simulated body fluid', *J. Mater. Sci.: Mater. Med.* **3**, 79–83

Kokubo T, Kushitani H, Ohtsuki C, Sakka S and Yamamuro T, (1993) 'Effects of ions dissolved from bioactive glass-ceramic on surface apatite formation', *J. Mater. Sci.: Mater. Med.* **4**, 1–4

Li P, Ohtsuki C, Kokubo T, Nakanishi K, Soga N, Nakamura T and Yamamuro T, (1992) 'Apatite formation induced by silica gel in a simulated body fluid', *J. Am. Ceram. Soc.* **75**, 2094–7

Loty C, Sautier J-M, Boulekache H, Kokubo T, Kim H-M and Forest N, (2000) '*In vitro* bone formation on a bone-like apatite layer prepared by a biomimetic process on a bioactive glass-ceramic', *J. Biomed. Mater. Res.* **49**, 423–34

Miller C A, Kokubo T, Reaney I M, Hatton P V and James P F, (2002) 'Formation of apatite layers on modified canasite glass-ceramics in simulated body fluid', *J. Biomed. Mater. Res.* **59**, 473–80

Nakamura T, Yamamuro T, Higashi S, Kokubo T and Ito S, (1985) 'A new glass-ceramic for bone replacement: evaluation of its bonding to bone tissue', *J. Biomed. Mater. Res.* **19**, 685–98

Neo M, Kotani S, Fujita Y, Nakamura T, Yamamuro T, Bando Y, Ohtsuki C and Kokubo T, (1992a) 'Difference in ceramic–bone interface between surface-active ceramics and resorbable ceramics: a study by scanning and transmission electron microscopy', *J. Biomed. Mater. Res.* **26**, 255–67

Neo M, Kotani S, Nakamura T, Yamamuro T, Ohtsuki C, Kokubo T and Bando Y, (1992b) 'A comparative study of ultrastructures of the interfaces between four kinds of surface-active ceramic and bone', *J. Biomed. Mater. Res.* **26**, 1419–32

Neo M, Nakamura T, Yamamuro T, Ohtsuki C and Kokubo T, (1993) 'Apatite formation on three kinds of bioactive materials at an early stage *in vivo*: a comparative study by transmission electron microscopy', *J. Biomed. Mater. Res.* **27**, 999–1006

Neuman W and Neuman M, (1985) *The Chemical Dynamics of Bone Mineral*, University of Chicago, USA.

Ohtsuki C, Kokubo T and Yamamuro T, (1992) 'Mechanism of apatite formation on $CaO–SiO_2–P_2O_5$ glasses in a simulated body fluid', *J. Non-Cryst. Solids* **143**, 84–92

Ohtsuki C, Aoki Y, Kokubo T, Bando Y, Neo M and Nakamura T, (1995) 'Transmission electron microscopic observation of a glass-ceramic A-W and apatite layer formed on its surface in a simulated body fluid', *J. Ceram. Soc. Japan* **103**, 449–54

Ono K, Yamamuro T, Nakamura T and Kokubo T, (1990) 'Quantitative study on osteoconduction of apatite-wollastonite containing glass ceramic granules, hydroxyapatite granules, and alumina granules' , *Biomaterials*, **11**, 265–71

Yamada S, Nakamura T, Kokubo T, Oka M and Yamamuro T, (1994a) 'Osteoclassic resorption of apatite formed on apatite and wollastonite-containing glass-ceramic by a simulated body fluid', *J. Biomed. Mater. Res*. **28**, 1357–63

Yamada S, Nakamura T, Kokubo T, Oka M and Yamamuro T, (1994b) 'Degradation of the apatite layer formed on bioactive ceramics and of the underlying ceramic surface by osteoclasts in a culture system', *Cell Mater*. **4**, 347–56

14

Calcium sulfate

J L RICCI and M J WEINER,
New York University College of Dentistry, USA and
S MAMIDWAR and H ALEXANDER,
Orthogen Corporation, USA

14.1 Introduction

Calcium sulfate hemihydrate (CS), known as plaster of Paris, is made from gypsum, and has been used for thousands of years as a building material. It has also been used for over a hundred years in a variety of pharmaceutical, dental, and orthopedic applications, having been used as one of the first successful alloplastic bone repair materials (Dreesman, 1892). We have used and studied this material extensively as a bone repair material (Ricci *et al.*, 2000), as a binder for hydroxyapatite ceramic particles as part of a partially resorbable composite cement for filling bone defects (Parsons *et al.*, 1988), as a growth factor release agent *in vivo* and *in vitro* (Rosenblum *et al.*, 1993; Frenkel *et al.*, 2002), and as a timed release composite material (Mamidwar *et al.*, 2006a,b).

Bone grafting procedures are commonly performed in orthopedics and dentistry. In dentistry, many types of bone grafting materials and bone graft substitutes are used to fill small defects such as molar extractions, sinus defects, buccal wall defects, periapical lesions, and other applications. Autograft is still considered the gold standard of bone grafting, but its use involves a second surgery site and additional morbidity (Tay *et al.*, 1999). Many forms of processed allograft are commonly used, but these can be expensive and carry at least a perceived risk of disease transmission. These can undergo very slow degradation and are sometimes unreliable in performance (Hallman *et al.*, 2001). Formation of poor quality and quantity of bone has also been reported when demineralized freeze-dried bone allograft (DFDBA) was used as a bone graft material in maxillary sinuses (Whittaker *et al.*, 1989; Moy *et al.*, 1993; Pecora *et al.*, 1998). Additionally, many calcium phosphate materials have been used for this purpose because of their similarity to the mineral phase of bone, biocompatibility, osteoconductivity, and absence of antigenicity (LeGeros, 2002). Most of these materials undergo slow degradation but some newer materials undergo relatively faster degradation. Bioglass-based materials have been used in these applications

(Schepers and Ducheyne, 1997), but they also undergo prolonged degradation and some cases have shown more fibroconnective proliferation than true bone formation (Peltola *et al.*, 2001). CS has also been used extensively as an alloplastic bone repair material. It has some unique properties relative to other bone repair materials; it is the most rapidly dissolving of all available bone repair materials. And it has properties that we are just beginning to understand. In order to achieve this we must begin by understanding the physical properties of CS.

14.2 Fabrication, microstructure, physical properties, and mechanical properties

14.2.1 Gypsum and its derivatives

CS cements begin as gypsum, or calcium sulfate dihydrate ($CaSO_4 \cdot 2H_2O$), which is either mined from the earth or produced through more controlled chemical processes (Randolph, 1971). Gypsum and its products differ in purity and form, but the major feature of this material is the fact that its water of hydration can be driven off with controlled heating. It then becomes a material with interesting and useful properties. In certain forms, it can be mixed with water or aqueous solutions, and it will set to form a cement.

Gypsum is mined in many countries and in the United States alone it has been or is mined in at least 22 states. It is found in various forms, referred to as rock gypsum, alabaster, selenite, satin spar, and gypsite. A dense crystalline anhydrous rock form, referred to as the anhydrite, is also found. The gypsum (hydrated) forms of these materials are then processed and heated under controlled conditions to form plaster of Paris, or calcium sulfate hemihydrate (CS, $CaSO_4 \cdot 1/2H_2O$). Addition of water to this material, in proper quantities, causes setting of the plaster of Paris to form calcium sulfate dihydrate ($CaSO_4 \cdot 2H_2O$).

Plaster of Paris is one of the oldest and sturdiest building materials on earth. It has a rich history – it has been in use for at least 5000 years – and was used by the ancient Egyptians to decorate the burial tombs of the Pharaohs. Some of Leonardo da Vinci's most enduring masterpieces were painted on this material, and Benjamin Franklin introduced its use in the United States as a soil improver, after observing its use in Paris while he was the American ambassador to France in 1776. Currently it is used for many diverse applications. It is used as filler for paints, in the production of paper, baking powders, textiles, sulfuric acid, beer, and lime, and as a soil treatment. It is used most extensively in Portland cement, stucco and as preformed wallboard used in housing construction. Until recently its best known medical applications have been for dental plasters used in the

formation of models, and as orthopedic plaster casting used for external stabilization of fractures.

While this material has a long history of use, it has been used medically only relatively recently, and the chemistry of its setting has only been properly examined in the past 50 years. An examination of its properties includes processing, purity concerns, setting characteristics (including setting accelerators and inhibitors), mechanical properties, dissolution characteristics, and setting characteristics in the *in vivo* environment.

14.2.2 Processing of CS cements

CS materials are processed for setting using heating to drive off the water of hydration. This is referred to as calcination and occurs as shown below (Clifton, 1973):

$$CaSO_4 \cdot 2H_2O \leftrightarrow CaSO_4 \cdot \tfrac{1}{2}H_2O + 1\tfrac{1}{2}\,H_2O \text{ (hemihydrate)}$$

$$CaSO_4 \cdot \tfrac{1}{2}H_2O \leftrightarrow CaSO_4 + \tfrac{1}{2}H_2O \text{ (anhydrite)}$$

The reverse reaction (setting) will not occur at temperatures above 100 °C, and the hemihydrate and anhydrite forms of this material can reportedly be produced while in contact with water. These materials are industrially processed using kettle methods, which process the material in batches, and rotary kiln methods, which are continuous processing methods. When heated to about 160 °C gypsum is converted to its hemihydrate form, the form used in plaster of Paris. When heated to 220–300 °C the material becomes the soluble anhydrite form. This material has similar solubility to the hemihydrate, but does not set like the hemihydrate. It has an extreme affinity for water (is extremely hygroscopic) and is used extensively as drying agent. If heated above 532 °C the material becomes insoluble anhydrite (or 'dead burned' gypsum), a non-reactive form of the material.

14.2.3 Forms of hemihydrate

Calcium sulfate hemihydrate exists in two forms designated the α and β forms of the material. The most common form is the β form, which is used in most commercial grade materials. It uses large amounts of water (approximately 0.6 g/g of hemihydrate) in setting and sets to form a less dense material than the α form, which is used as a dental material referred to as dental stone. The α form material uses less water (approximately 0.3 g/g of hemihydrate) and sets to form an extremely dense dihydrate. This material is processed differently from the parameters listed above.

The α form material is also produced by heating gypsum, but this material is heated to 123 °C under approximately 1.2 kg/cm^2 (17 psi) of pressure, in

steam for 5 to 7 hours in an autoclave. Processing gypsum in this way produces more dense crystals with little porosity, and these crystals require less water for setting and produce the dense dihydrate. The α form material, because of its density, dissolves slower than the β form material. Thus the α form hemihydrate has been the material of choice for bone-filling applications because of its stability, although no conclusive studies have compared the two forms. The differences between them may explain some of the variability seen in results of bone repair studies. In past studies, both forms of material, and many variations on each form, have been used. This has led to widely variable results. Scanning electron microscopy of the α form hemihydrate material shows the distinctive particle shape and density of this material, as well as the particle size range of the material (Fig. 14.1a). This α hemihydrate is a highly pure, chromatography grade material.

14.2.4 Purity concerns

Purity of CS materials varies because of its many natural sources. This is a concern regarding medical grade materials (Wright Medical Technologies Monograph, 1997). Impurities found in CS comprise a list of naturally occurring carbonates and other minerals, and trace metals and elements shown in Table 14.1. Chemically purified CS is more consistent in composition than the mined materials. Food and medical grade materials must be assayed for these contaminants. Specifications for the food grade material are shown in Table 14.2.

Table 14.1 Impurities found in CS materials

$CaCO_3 \cdot MgCO_3$	$CaCO_3$
Silicates	Strontium
Fluoride	Arsenic
Selenium	

Table 14.2 Specifications of food grade CS

Calcium sulfate (%)	98–100
Arsenic (ppm maximum)	3
Fluoride (ppm maximum)	30
Heavy metals (as lead, ppm max)	10
Selenium (ppm maximum)	30

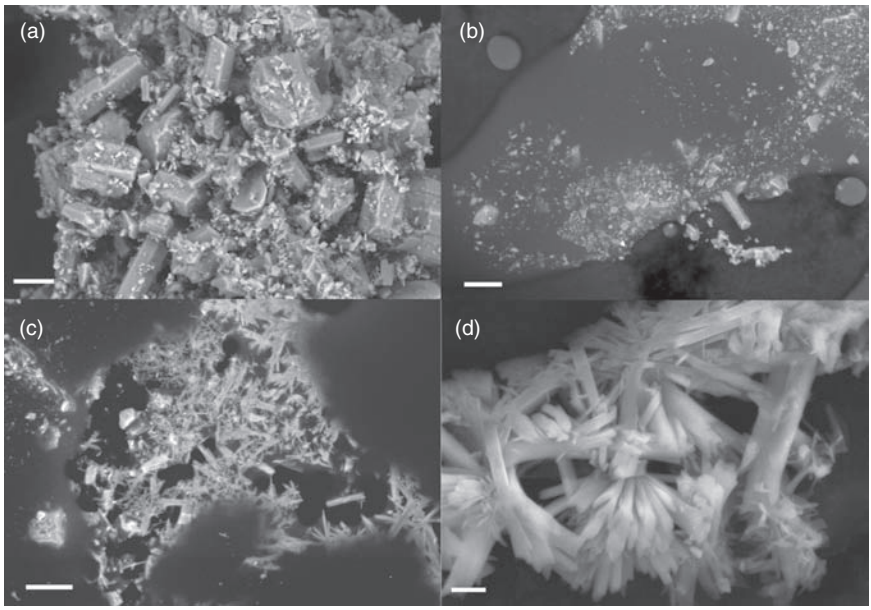

14.1 Composite scanning electron photomicrograph showing the four stages in the setting of CS, taken in an environmental microscope under wet conditions and variable atmospheric pressure. All pictures were taken either with a four quadrant backscattered electron detector or a variable pressure secondary electron detector. No gold or carbon coatings were used. (**a**) CS α hemihydrate in the dry state. Bar = 20 μm. (**b**) A condensed droplet of moisture that has enveloped some of the CS hemihydrate. Some of the undissolved material is visible through the surface of the liquid. Bar = 20 μm. (**c**) Droplets of water where the concentration of calcium and sulfate ion have reached saturation and crystals of the dihydrate are forming at the edges of the meniscus of each droplet. Bar = 20 μm. (**d**) Higher magnification view of fully set dihydrate crystals. They have obviously grown outward from nucleation sites. In a large volume of set CS these crystals interlock giving the material its strength. Bar = 4 μm.

14.2.5 Setting of CS cements

Setting and hardening of CS cements occur as the calcined hemihydrate form reacts with water to form the dihydrate:

$$CaSO_4 \cdot \tfrac{1}{2}H_2O + 1\tfrac{1}{2}H_2O \leftrightarrow CaSO_4 \cdot 2H_2O$$

This reaction is mildly exothermic and results in the growth of interlocking rod-like dihydrate crystals to form the set cement. In a series of scanning electron micrographs taken in a Zeiss EVO 50 environmental scanning electron microscope (ESEM) with a Peltier cooling stage, moisture introduction

system, variable pressure secondary electron (VPSE) detector, backscattered electron imaging (BEI) system, and variable vacuum system, we were able to image the α hemihydrate material (Fig. 14.1a), wet the material in the ESEM by condensing water droplets on the Peltier stage (Fig. 14.1b), remove some of the moisture so that dihydrate crystals formed at the meniscus of the water droplets (Fig. 14.1c), and form a fully set dihydrate mass by removing all of the water (Fig. 14.1d). While this was done under controlled conditions in the ESEM, setting under normal conditions is a different process with different variables. The time of setting depends on temperature, hemihydrate form and crystal size, and setting agent. The setting reaction has been attributed to both colloidal and crystallization mechanisms, with the crystallization theory being most consistent with experimental results. As this theory explains, the hemihydrate, when mixed with water, dissolves to form a solution highly supersaturated with respect to calcium sulfate dihydrate. This supersatured solution then crystallizes to produce the interlocking rod-like crystals observed in the set material. In the colloidal theory, intermediate colloidal products are produced which form the dihydrate crystals. We did not observe the colloidal products in the ESEM experiment.

Hydration studies have shown that setting occurs in two phases (Clifton, 1973). The first phase, or induction phase, is observed as the hemihydrate is dissolved, and nucleation of the dihydrate crystals occurs from the supersaturated solution. We observed nucleation sites in the ESEM experiment (Fig. 14.1c). In studies of the β form material using distilled water as a setting agent, the induction period can take up to 40 minutes, during which there is only a slight rise in temperature. The second phase, or rapid hydration phase, can take an additional 30–40 minutes, and corresponds to rapid crystal growth. This phase is much more exothermic and can result in a 30 °C increase in temperature in a 100 g sample of CS cement in an insulated reaction chamber. This is a much larger amount than that routinely used for repair of bone defects, and the correspondingly smaller amounts of heat generated during setting have not been observed to cause problems in clinical use. Final set of the material is observed after this phase and corresponds to cessation of both crystal growth and the observed exothermic reaction.

14.2.6 Setting agents and conditions

Regular tap water is routinely used to set CS cements used for construction purposes. However, water purity is of great concern when addressing setting properties, because ions contained in tap water can greatly influence setting properties.

Amounts of water used in setting are also important. Sufficient water must be used to allow a complete setting reaction to occur. However, excess water can prevent setting of material with optimal mechanical properties.

For use of the α form material in bone filling applications, approximately 0.3 g of water should be used for 1.0 g of the hemihydrate. In environments where significant bleeding is observed, slightly less water should be used.

Many setting agents have been used industrially and medically in attempts to control the setting characteristics of CS cements. A number of biocompatible salts have been shown to greatly accelerate setting. NaCl, Na_2SO_4, KCl, and K_2SO_4 have all been shown to decrease the setting times of CS cements when used in relatively low concentrations. Setting times can be reduced to 15 minutes or less, depending on concentration, using potassium salts. In general, the cation is most responsible for the acceleration, with K^+ and Na^+ being the most effective biologically acceptable alternatives. NH_4^+ is also effective but not an alternative for biologic use, and Ca^{2+}, Cu^{2+}, and Al^{3+} were not as effective. It should be noted that use of accelerants causes the reaction to become more exothermic. However, in the relatively small amounts used in bone-filling sites, this has not been observed to cause local temperature increase or tissue damage.

The mechanism behind this reduction in setting time is thought to be an effect of the density of seed crystals formed during the induction phase, with K^+ and Na^+ significantly increasing the density of these seed crystals, and significantly shortening induction time. Temperature was also found to influence setting by decreasing the induction period, with fastest setting occurring (in distilled water) at about 45 °C. Setting at 37 °C was nearly optimal. For biologic applications, a 4% K_2SO_4 solution has been shown to be optimal for causing almost immediate setting (less than 2 minutes), even in environments where small amounts of blood were present. This agent seems to reduce the seed crystal formation (induction time) time to almost zero, and greatly speed crystal formation.

Significant retardation of setting is observed when organic agents are present such as succinic acid, gelatin, or other proteins. This is significant for use in a biological environment where blood proteins are present. Small concentrations of these agents can cause final setting times to increase to over 200 minutes. They can also adversely alter the mechanical and dissolution properties of these materials. It is thought that these agents can either prevent full hydration of the hemihydrate and inhibit seed crystal formation (increasing induction time), or form complexes with the seed crystals to prevent crystal growth (increasing the rapid hydration time). In some cases the presence of proteins has been observed to prevent full setting, probably by poisoning crystal growth completely.

14.2.7 Setting in bone-filling sites

Bone defect sites usually show significant bleeding. In these situations, blood proteins can interfere with setting. There is also evidence that CS

cements set in the presence of blood dissolve more quickly. Thus, whenever possible, preset CS cement implants should be used since these will always dissolve more slowly and consistently than those set in the presence of blood. Also, it is always advantageous to work in as dry a bone site as possible in order to achieve proper setting. Working with a slightly 'dry' cement (using slightly less water or setting agent than needed) works well in these environments because some moisture is usually absorbed from the environment to complete setting. Better setting in these situations is also produced through the use of accelerants such as NaCl or K_2SO_4, which cause the material to set before significant blood proteins can infiltrate the cement. One method of clinical use that will be described in more detail later (Pecora *et al.*, 1998; De Leonardis and Pecora, 1999, 2000) suggests (1) packing of the site with CS hemihydrate powder with gauze to produce hemostasis, (2) removal of the gauze, (3) formation of a slightly dry cement using NaCl, (4) packing the operative site as densely as possible with this cement using a layered approach (referred to as the stratification method), (5) overfilling the site if possible (if soft tissue coverage allows), and (6) applying 4% K_2SO_4 to the surface to almost immediately set the surface of the defect and stabilize the CS filler.

14.2.8 Physical properties of CS cement

Set CS cement is a white, hard, ceramic with a specific gravity of 2.32–2.33 and a Mohs hardness of 1.5–2.0 (Lautenschlager, 1972). It is practically insoluble in most organic solvents, and is slightly soluble in water, having a maximum solubility of 2.1 g/liter at about 40 °C. It dissolves to form calcium and sulfate ions in solution:

$$CaSO_4 \cdot 2H_2O \xrightarrow{\text{aqueous solution}} Ca^{2+}, SO_4^{2-}, CaSO_4$$

Electrolytes in solution and in the CS material can affect its solubility. The setting agents mentioned previously, which become incorporated into the set cement, should increase the solubility of the cement, although no data are available concerning rates of solubility of these materials. Low pH also increases the solubility of CS.

Mechanically, the set CS cement has relatively high compressive strength and low tensile strength. It is relatively brittle and can be reinforced to produce material with better tensile properties. Some forms of CS cement that are used as building materials are reinforced with components such as wood fiber, silicates, and other fillers, to provide better mechanical properties and produce a lighter material. The mechanical properties of CS cement are summarized in Table 14.3 in comparison with cancellous

Table 14.3 Comparative mechanical properties of CS cement and bone

Typical mechanical properties	Wet calcium sulfate	Dry calcium sulfate	Cancellous bone	Cortical bone
Compressive strength (MPa)	10–15	20–30	5–10	162.2
Tensile strength (MPa)	2–4	4–6	10–15	151.8

and cortical bone. The observed properties of CS cement limit the material to space-filling applications and prevent its use in load-bearing applications.

14.2.9 CS use in biological environments as a bone filler

In past studies CS cements have been observed to act as fillers in bone sites to prevent soft tissue growth until bone has regenerated. However, some studies have reported that this material has been observed to resorb too quickly – before bone can regenerate. It is very likely that failed attempts to use this material as a bone filler have resulted from improper use of this material, and/or use of inconsistent and uncharacterized material. It is imperative that a medical practitioner, using CS cement as a bone filler material, have complete knowledge of its properties, and use a pure, well-characterized material.

The properties of this material suggest that certain rules should be followed when it is used as a bone filler. These are listed below.

Choice of material

- Only the dense α form of the material should be used as a bone filler.
- This material must be completely tested for impurities, and should consist of a consistent range of particle size to control setting properties.

Choice of implant site

- As noted above, the mechanical properties of CS cement suggest that its use as a bone filler is appropriate as long as it is not used in load-bearing applications.
- When possible it should be used in enclosed bony sites where it can be adequately packed and properly set.

Form of CS cement used and setting agent

- Whenever possible, pre-set material should be used as implants since CS cement set in contact with blood can exhibit variable setting properties and dissolve more quickly than preset material.
- When setting the cement in a bleeding bone site, every care should be taken to suppress bleeding since this can interfere with setting.
- When setting the cement in a bleeding bone site, accelerants should be used to speed setting and prevent blood infiltration of the unset cement.

14.3 Biological properties of CS as a bone repair material

14.3.1 Clinical use: early history

Calcium sulfate (CS) was first used in 1892 in Trendelenburg's clinic in Bonn, Germany. Dreesman (1892) used CS to fill bone defects in eight patients. Six of these patients presented with tuberculous cavities. Three of these six patients showed extensive bone formation and two of them showed no signs of healing. One patient had two cavities, of which one healed very well while the other one did not. Out of the remaining two patients, one patient had an enchondroma of the fifth metacarpal and the other one had a bone cavity due to osteomyelitis. In the case of the patient with the enchondroma, the tumor was excised and the resulting cavity was filled with CS pellets. This cavity showed significant bone growth. The osteomyelitis cavity also healed well. Overall, CS worked very well as a bone graft material. Although sporadic reports of CS use in bone repair appeared in the literature, the material was not widely used. Ljubovic and Nikulin (1956) published a detailed report about how CS works *in vivo* in rabbits. The following are their conclusions:

- Normal bone grew in areas implanted with CS.
- CS implantation in subperiosteal bone resections produced the same reaction as is normally present in an uninfected fracture.
- Bone regenerated earlier in areas of subperiosteal resection than when autogenous graft was implanted.
- CS implantation did not stimulate osteogenesis in absence of bone or periosteum.
- CS implantation did not produce any adverse effects in adjacent tissues or in distant organs.
- Slight elevation of serum calcium and alkaline phosphatase levels accompanied degradation of CS implanted in rabbit bones.

These studies demonstrated, for the first time, certain important aspects of CS use as a bone grafting material. Peltier (1959) conducted additional studies on dogs to examine the use of CS for bone grafting purposes. Based on his studies, he concluded:

- CS can be used safely and conveniently in a wide variety of bony defects.
- CS degradation and subsequent bone regeneration occurred rapidly over a period of weeks or months.
- CS presence in bone defect did not inhibit the normal healing of bone.
- CS implantation in infected cavities did not create additional complications.

He also concluded that CS acted mainly as a space filler and its most important property was its rate of degradation in the body. He also concluded that its rate of degradation coincided with the rate at which natural bone can grow into a defect. Since this publication CS has been considered by most to serve only as a space filler to prevent fibrous tissue formation in bone repair sites.

14.3.2 Clinical use: recent work

Extensive research has been conducted during the past decade that suggests additional properties and uses of CS. This work suggests that CS:

- has barrier membrane and hemostatic properties;
- has angiogenic properties;
- can be used as a drug/growth factor delivery vehicle;
- can be used successfully in combination with other bone graft materials;
- has osteoconductive properties and stimulates bone formation even when used without other types of bone graft materials.

CS as a barrier membrane and hemostatic agent

Guided tissue regeneration barrier membranes play an important role in healing of the bone defects by maintaining space for osteogenesis. Several studies have shown that calcium sulfate works as an effective barrier. Payne *et al.* (1996) studied *in vitro* the barrier properties of three different commonly used materials, i.e. polytetrafluoroethylene (PTFE), polylactic acid (PLA), and calcium sulfate. Human gingival fibroblasts were cultured on these barrier materials and on control surface (a polystyrene culture plate). A cell migration assay showed that there was significantly greater migration of fibroblasts on control surfaces compared with any of these barrier mem-

branes ($P < 0.05$). More interesting was the finding that mean migration distance of fibroblasts over calcium sulfate was greater than that on PLA. SEM studies showed that there was more cell migration and spreading on calcium sulfate compared with ePTFE or PLA. Calcium sulfate was also more conducive to cell survival. Based on these findings, it was concluded that calcium sulfate has excellent potential for use as a guided tissue regeneration barrier membrane compared to ePTFE or PLA. Pecora and others conducted animal studies on the use of CS as a barrier material and concluded that it worked as a barrier membrane in the defect area and allowed bone regeneration during healing (Pecora *et al.*, 1997a,b). Kim and his coworkers (1998a) also studied the use of CS as a barrier in a randomized controlled human clinical study. Twenty-six patients with periodontal infrabony defects were treated, half of whom were implanted with allogenic, demineralized freeze-dried bone matrix (DBM)/calcium sulfate composite with a CS barrier. The remaining half received gingival flap surgery alone and served as a control. Significantly better bone regeneration was observed in patients treated with DBM+CS combination than in the control patients. It is clear from the results of all these studies that CS is effective as a resorbable barrier material. ePTFE is one of the most commonly used barrier membranes, but is a nonresorbable and must be removed at the end of 4–6 weeks. Additionally, infection rates are higher with nonresorbable barriers. Thus CS offers significiant advantages over routinely used barrier membranes. In a paper on endodontic surgical technique, Kim and Rethnam (1997) noted that CS also has hemostatic properties. This is not surprising considering that calcium ion is a known coagulant. This was also noted by Pecora and his co-authors in papers listed below regarding sinus augmentation.

CS and angiogenesis

Recent studies showed evidence of increased angiogenesis in defects filled with CS compared with those filled with autograft. Strocci *et al.* (2002) studied the growth of blood vessels in the defects filled with CS and covered with a ePTFE barrier (group 1), CS alone (group 2), and autograft alone (group 3). Microvessel density in all these defects was evaluated at the end of 4 weeks. Mean comparative numbers of microvessels in group 1 were 9.88 ± 4.613; in group 2 microvessel density was 7.92 ± 1.998, and in group 3 the values were 5.56 ± 1.895. Mean differences between groups 1 and 2, groups 1 and 3, and groups 2 and 3 were statistically significant. These findings showed that CS is highly angiogenic, even when compared with autograft. Although the reason behind this phenomenon has been definitively demonstrated, this is an important finding and partly explains the efficacy of CS for bone grafting purposes. It is well known that blood vessels are

necessary for bone healing, and among others, Schmid *et al.* (1997) have shown the close correlation between the development of new blood vessels and bone formation.

CS as a delivery vehicle

CS also works as an effective vehicle for delivery of growth factors and drugs. Several studies have shown that CS can be effectively used as a drug delivery vehicle. Antibiotics such as tobramycin have been delivered locally using calcium sulfate. Beardmore *et al.* (2005) have shown that tobramycin impregnated calcium sulfate was useful in preventing development of infection in bone defects. In an infection-prone bone defect model in goats no infection was observed in defects filled with tobramycin impregnated calcium sulfate or defects filled with a combination of demineralized freeze-dried bone matrix and tobramycin impregnated calcium sulfate. However, infection developed in seven of the eight goats where the defects were filled with demineralized freeze-dried bone matrix alone, and six of the seven goats where the defects were left empty. This proved the effectiveness of calcium sulfate as an antibiotic delivery vehicle. Rosenblum *et al.* (1993) showed that fibroblast growth factor (FGF) was released at controlled rates from set CS cement disks, and that the FGF release was directly related to the dissolution rate of the CS cement. In a recent publication, Intini *et al.* (2007) showed that a combination of CS and platelet-rich plasma was not only an effective bone repair material, but that it had osseoinductive properties similar to bone morphogenetic proteins. Most bioactive molecules, in particular those that can be dissolved into water or salt-containing solutions, can be incorporated into set CS materials. These results suggest that CS can act as a simple and effective delivery vehicle for release of bioactive molecules into bone defect sites.

14.3.3 Current clinical uses of CS

As noted above, CS has been used successfully for periodontal bone defect repair. There are several additional papers supporting its use in a variety of periodontal applications (Mesimeris *et al.*, 1995; Anson, 1996, 1998; Kim *et al.*, 1998a,b; Bier and Sinensky, 1999). CS has also been used successfully for the repair of endodontic defects (Conner, 1996; Kim and Rethnam, 1997) such as apicoectomies, where the infected apex of a tooth root is removed surgically leaving an often large, non-sterile bony defect. These defects heal well when filled with CS, even though other bone repair material can become infected in this application. It is not clear why CS does not often become infected in this type of application, but it is clearly one of the reasons that CS is often used in craniofacial defects, where sterility

is often compromised. This pseudo-antiseptic property of CS may have to do with the pH changes described below, or it may be related to the rapid release of sulfate ion. It may simply be because the material dissolves too rapidly to become infected. Pecora and others have authored several papers on the use of CS for sinus augmentation surgery prior to dental implant placement (De Leonardis and Pecora, 1999, 2000; Pecora *et al.*, 1998). He describes a technique referred to as the 'stratification technique', whereby he fills this relatively large type of bony defect by first using CS as a hemostatic lining, and then using successive layers of densely packed CS, firmly set using the potassium sulfate 'fast set' agent described above, to fill the entire defect. This technique ensures that hemostasis does not allow blood to interfere with CS setting, and that the densely packed CS is placed in the most efficacious manner to prevent rapid dissolution. This is apparently a successful clinical technique, and the general rules of this procedure should be utilized wherever CS cements are used to fill bony defects. Sottosanti (1997) and Sottosanti and Anson (2003) have also used CS as a barrier or as a composite with demineralized freeze-dried bone with good success for periodontal repair. In this application the CS is used to hold the particles of processed bone graft in place and prevent particle migration, but their work suggests that CS also enhances the activity of the particulate graft material.

There are also several papers describing the generally successful use of CS, mostly in preset granular form, for repair of orthopedic defects (Hadjipavlou *et al.*, 2000; Gitelis *et al.*, 2001; Kelly *et al.*, 2001; Mirzayan *et al.*, 2001; Kelly and Wilkins, 2004), although CS is never used as a weight-bearing material in orthopedics, and these large defects do not always show the same level of success as the smaller bone defects treated in the dental arena. While it is beyond the scope of this chapter to conduct a detailed review of the many surgical applications, techniques, and results that have utilized CS for bone repair, it is important to note that there is an extensive body of literature that supports the use of this material for bone repair. This work also strongly suggests that CS is not a simple space-filling material, and that it has bioactive properties. These properties are at least partially described below.

14.3.4 CS stimulation of bone formation: possible mechanisms

Calcium phosphate precipitation

After over 115 year of use as a bone repair material we are beginning to understand that CS has properties that were not appreciated or understood until the last 15 years. Work conducted in our labs and others (Ricci *et al.*,

2000; Orsini *et al.*, 2001; Frenkel *et al.*, 2002) has indicated that CS is not only a space filler that allows bone to heal passively, but is also a soluble material that has bioactive properties and stimulates bone formation. We have found that, in two studies utilizing an implantable chamber model in a critical-sized defect, CS showed significant stimulation of bone formation compared with empty control defects that always show some degree of healing (Ricci *et al.*, 2000; Frenkel *et al.*, 2002). In one study we observed a 38% increase in bone formation compared with controls (Ricci *et al.*, 2000).

In these studies, as well as a rabbit tibial defect model (Orsini *et al.*, 2001), we have observed a phenomenon that suggests a bioactive mechanism that may explain the observed osteoconductive activity of CS. In the implantable chamber studies we observed the formation of calcium phosphate deposits at the edges of bone defects filled with CS at time periods as early as 2–4 weeks (Fig. 14.2) (Ricci *et al.*, 2000). These deposits were X-ray and electron dense and were observed in both microradiographs and in scanning electron micrographs in backscattered electron imaging (BEI) mode (Fig. 14.3). They were observed to form intermittently and were left behind in the tissue as the CS dissolved. They were then observed to become incorporated into ingrowing bone, and were osteoconductive. Osteoconductivity was indicated by the observation that trabecular bone attached to these

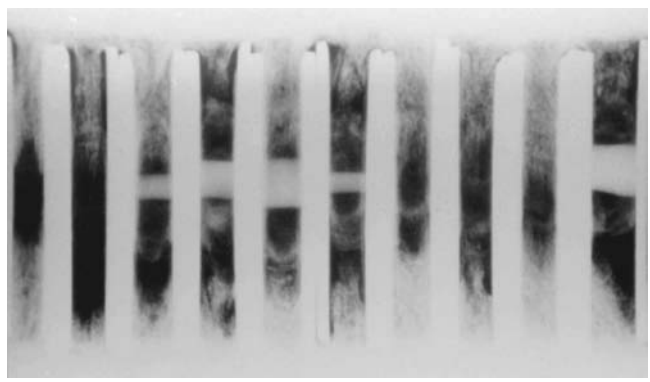

14.2 Microradiograph of an implantable chamber, 4 weeks after implantation, from Ricci *et al.*, 2000, reprinted with permission. Each of the vertical slots represent ingrowth channels between plates of either HA coated or roughened titanium alloy. Each channel was filled to the outer edge of the plates with set CS at the initiation of the experiment. After 4 weeks, most of the CS has dissolved except for small amounts in the centers of a few channels, bone has begun to grow into each channel from both top and bottom, and concentric bands of radiodense mineral are observed between the bone and the remaining CS, if present. Each channel is 1 mm in width.

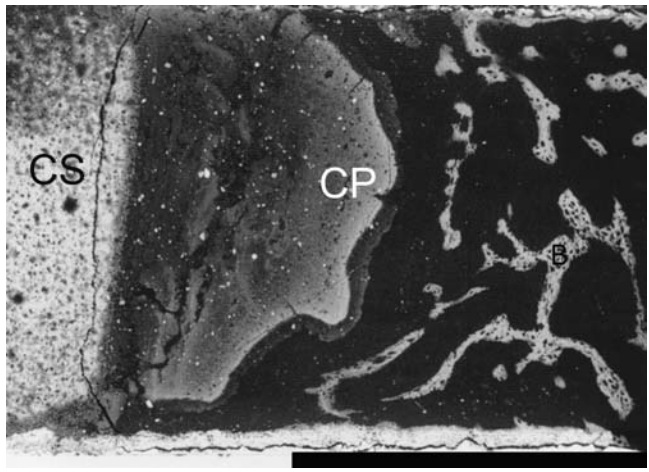

14.3 Scanning electron photomicrograph, in backscattered electron image (BEI) mode, showing the surface of a cross-section through one of the channels of a 4-week chamber like the one shown in Fig. 14.2. The upper and lower surfaces are hydroxyapatite-coated titanium. The solid mass (CS) at the left side is remaining calcium sulfate dihydrate. Ingrowing, immature trabecular bone (B) is observed growing into the chamber from the right. In between the CS and the bone is a mineral deposit band consisting of calcium phosphate (CP). This has precipitated as the CS dissolved as was left behind as further CS dissolution occurred. The composition of the band was confirmed by X-ray microprobe analysis, and *in vitro* experiments suggest that this mineral is carbonate apatite. Bar = 1 mm.

deposits and grew along their surfaces. These deposits were remodeled as the new woven bone remodeled to more mature bone, and in most cases were not observed at time periods of 12 weeks or longer in the dog model. In the rabbit tibial defect model we observed similar deposits at 15 and 30 days, with the CS being almost completely dissolved at 30 days. These deposits were evaluated using X-ray microanalysis (XRM) in the scanning electron microscope, and were discovered not to be residual CS, but consisted of calcium phosphate with a Ca/P ratio similar to that of bone mineral. We also found that incubation of disks of set CS in cell culture medium or simulated body fluid at 37 °C resulted in the precipitation, after as little as a few hours, of a surface layer of this calcium phosphate mineral. After a few days this layer would thicken and fall from the surface as the CS underneath continued to dissolve. Analysis of this material indicated that it was carbonate-substituted hydroxyapatite similar to the mineral phase in bone or dentin (Fig. 14.4) (Chan *et al.*, 2004). The precipitation of this material was observed consistently at early time periods around CS-filled sites, was observed to directly attach to and conduct new bone formation, and then

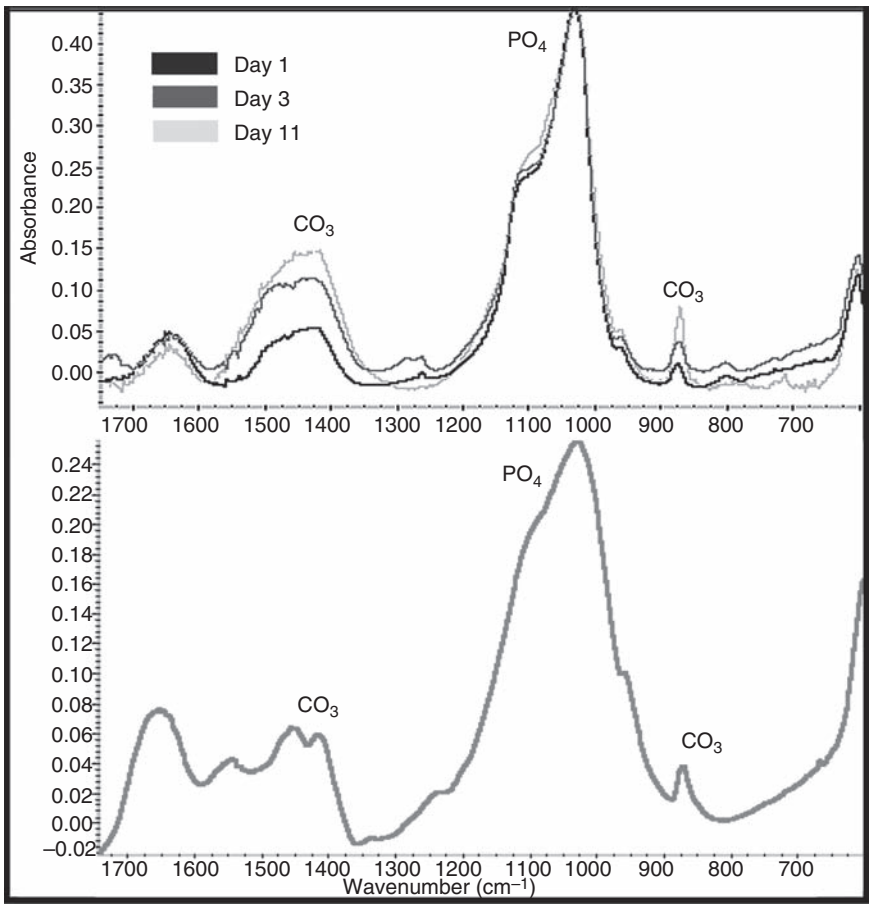

14.4 Graphs of Fourier-transformed infrared analysis (FTIR) of three calcium phosphate deposits removed from the surfaces of CS disks, in *in vitro* simulated body fluid experiments, after 1, 3, and 11 days (upper graph). They indicate that the deposits are carbonate apatite, and that the amounts of carbonate increase over time. The lower graph is an FTIR analysis of dentin mineral, for comparison.

be remodeled during bone maturation. This formation of a carbonate apatite 'trellis' for bone formation is apparently one of the mechanisms by which CS stimulates bone formation.

CS, when implanted in a bone defect and exposed to body fluids, undergoes dissolution to calcium and sulfate ions. The calcium ions combine with phosphorus ions from the body fluid to precipitate calcium phosphate, which forms at the CS surface and then is deposited in the bone defect. This material is a self-forming biologic apatite. Apparently, CS, which is slowly soluble in body fluids, causes precipitation of carbonate apatite, which is

stable under the same conditions and is left behind, becoming a bioactive component that stimulates bone formation. This often results in a concentric ring pattern of bone formation, as the precipitate bands are left behind as concentric rings, as the CS dissolves from the outer edge inward over time (Ricci *et al.*, 2000).

pH change and calcium ion release

There are other important aspects to be considered as CS dissolves in the body. *In vitro*, as the CS dissolves the local pH decreases. This is probably caused by a combination of sulfuric acid release and the precipitation of carbonate apatite. It may also explain why the observed precipitate forms in intermittent bands *in vivo* instead of forming a more consistent mass. *In vivo*, the local pH drop would be expected to interrupt apatite precipitation until local body fluids are buffered to a pH that again allows precipitation to again proceed, probably resulting in cyclic pH changes. This local drop in pH may lead to a chain of events that may also contribute towards development of bone in the defect. Walsh *et al.* (2003) reported important observations regarding this process. They implanted calcium sulfate pellets, calcium sulfate pellets plus autograft, and autograft alone in the distal femoral condyles of 12 skeletally mature adult sheep. One group of defects was left empty as negative controls. They studied immunostaining for BMP-2, BMP-7, TGF-β, and PDGF-BB in these defects. Results showed that CS augmented the effects of autograft, and that CS alone showed high levels of bioactivity. These observations indicated that there was increased expression of BMP-2, BMP-7, TGF-β, and PDGF-BB in the defects when calcium sulfate was implanted. They also observed, in this same study, local and abundant thick new trabecular bone formation around the sites of calcium sulfate pellet implantation. Walsh and his co-authors suggested that the increased expression of growth factors in bone surrounding the CS was caused by the local pH drop accompanying the CS dissolution. The authors suggested that the local pH decrease caused surface demineralization of surrounding bone, exposing the growth factors existing in the bone extracellular matrix and thereby causing their activation by exposing them to nearby cells. This mechanism might also explain the angiogenesis noted earlier, since the growth factors assayed in their study are known to be angiogenic.

A recent study by Lazary *et al.* (2007) suggests that calcium ion plays a significant role in stimulation of bone formation. They cultured MC3T3-E1 mouse preosteoblast cells on CS disks as well as control surfaces such as culture plates and polymethylmethacrylate (PMMA) surface. They compared cell proliferation, cell viability, alkaline phosphatase expression, and expression of genes important for bone repair. They found that the CS

substrate caused marked increase in proliferation, alkaline phosphatase expression, and expression of genes that are significant for bone repair. They were also able to mimic this response, to some degree, by adjusting the calcium levels of the cell culture medium to those levels observed in the CS cultures. This suggested that cell response to the CS surface, which was probably not CS but a surface layer of carbonate apatite, as well as calcium ion release, both play roles in stimulating bone repair.

Summary of mechanisms involved with CS and bone repair

A simple way to view these possible mechanisms is as a parallel series of interrelated physical chemical and molecular mechanisms triggered by dissolution of CS in the biologic environment of a bone defect (Fig. 14.5). Two actions result from this dissolution. The first action, release of calcium and sulfate ion, results in carbonate apatite formation and calcium ion stimulation of cellular activity. This is probably based on the calcium ion only, as body fluid levels of sulfate ion are low, and the effect of increase in sulfate ion concentration is unclear. The second action, decrease in pH, results in surface demineralization of existing bone and exposure of growth factors. Both actions stimulate bone healing.

In summary CS has been shown to stimulate bone growth in controlled defect studies. Its unique biologic properties are probably based on its *in vivo* dissolution. There are at least four proposed mechanisms by which CS could stimulate bone regeneration:

1 Space-filling/prevention of fibrous tissue ingrowth – At its most basic level, CS fills space in a bone defect, preventing the ingrowth of soft

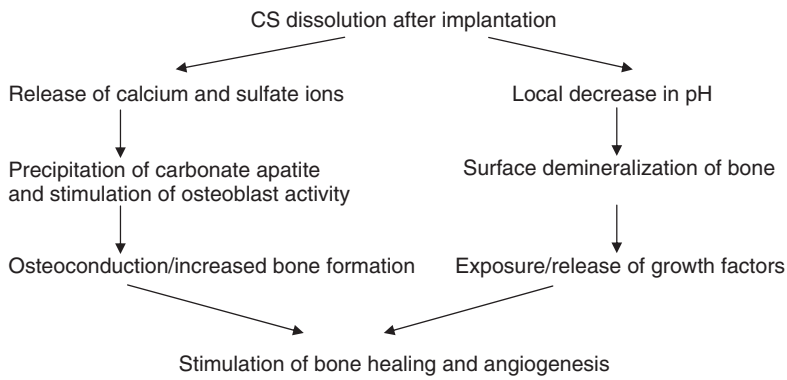

14.5 Schematic diagram summary of the process of CS dissolution and the two proposed pathways, calcium and sulfate ion release (left) and pH decrease (right), that stimulate bone formation using different mechanisms.

tissue, and retaining the space for bone regeneration. *In vivo*, in a bone defect filled with solid CS, the CS dissolves at about 1 mm per week from the outside inward. This can significantly outpace the formation of new bone, but nonetheless acts to reserve space for new bone.

2 Calcium release – Calcium ion release by the CS causes high local calcium ion concentrations in surrounding bone tissues. High calcium ion concentrations cause significant cellular changes including increased alkaline phosphatase activity and gene expression favorable to bone formation.

3 Carbonate apatite precipitation – One of the observed effects of CS dissolution is the local precipitation of carbonate-substituted apatite. This precipitate forms at the surface of the CS material as it dissolves, is left behind in the tissue as the CS dissolves away beneath it, and acts as a trellis for osseoconductive ingrowth of new bone.

4 pH changes – As the CS dissolves it causes a small local drop in pH. This happens because of CS dissolution, which releases sulfuric acid, and because of apatite precipitation, which also causes pH drop. It has been suggested that this causes local surface demineralization of existing bone, and exposure of bioactive molecules in the bone extracellular matrix, stimulating local bone formation.

14.4 Recent developments: timed release CS

The most significant criticism of CS as a bone graft material, and one that limits its effective use to small craniofacial defects, is its rapid dissolution. In most applications it degrades completely by 4–7 weeks, and its degradation often outpaces the rate of bone growth into the defect. To overcome this problem, we have developed a timed-release calcium sulfate bone graft material. This material is a granular composite of calcium sulfate and small amounts of poly-L-lactic acid (PLLA). We have tested this material as either a nanocomposite of the CS and the PLLA, or as CS granules coated with a thin layer of PLLA. CS granules (400–800 μm size) without PLLA had a half-life of about 9 days in simulated body fluid at 37 °C. A timed-release composite pellet, of the same size range, comprising 4% PLLA and 96% CS had a half-life of 68 days under the same conditions. While we have tested several formulations that degrade at very different rates (Mamidwar *et al.*, 2006b) we have extensively tested the above noted nanocomposite form and found it to have a half-life of about 2 months and a full degradation time of about 4 months *in vivo* (Mamidwar *et al.*, 2006a). We feel that this formulation may be appropriate for craniofacial defects where dental implants are to be placed, such as extraction sockets and sinus augmentation sites. This material has been shown to cause robust bone growth in a rabbit tibial defect model, between 2 and 4 months, when degradation of

the graft material occurs (Mamidwar *et al.*, 2006a). This is an unusual finding since rabbit bone healing generally takes place by 4–6 weeks. It suggests that this material may work well in humans because human bone healing is significantly slower than healing in rabbits, and occurs generally in a 1–3 month time period. This is a safe, novel, and unique bone graft material. We can adjust its dissolution time for different applications, and various antibiotics, drugs, and growth factors can be incorporated into the CS prior to nanocomposite formation. This will allow controlled release of these agents. This material is currently undergoing final formulation testing prior to human clinical trials.

14.5 Conclusion

Calcium sulfate is a fascinating material with unique physical and chemical properties. Although it has been used as a bone graft material for more than a century, we are just beginning to understand its biologic properties, and are thus just beginning to understand its potential. This material exists in many forms and variations, and materials intended for biomedical use must be well characterized and carefully produced. Thorough knowledge of the physical properties of this material, and its biological mechanisms, must be utilized in order to achieve optimum results when using it as a bone graft material. Recent studies indicate that it is fully soluble *in vivo* and causes significant bioactivity through calcium release, pH change, and local carbonate apatite precipitation. It can be used as a cement, or in preset granular form, and it also has significant potential as an antibiotic/drug release material. Newer forms of CS, such as timed-release CS composites, have excellent potential as fully soluble bone repair biomaterials.

14.6 References

Anson, D. (1996) Calcium sulfate: a 4-year observation of its use as a resorbable barrier in guided tissue regeneration of periodontal defects. *Compend Contin Educ Dent,* **17**, 895–9.

Anson, D. (1998) Saving periodontally 'hopeless teeth' using calcium sulfate and demineralized freeze-dried bone allograft. *Compend Contin Educ Dent,* **19**, 284–6.

Beardmore, A. A., Brooks, D. E., Wenke, J. C. & Thomas, D. B. (2005) Effectiveness of local antibiotic delivery with an osteoinductive and osteoconductive bone-graft substitute. *J Bone Joint Surg Am,* **87**, 107–12.

Bier, S. J. & Sinensky, M. C. (1999) The versatility of calcium sulfate: resolving periodontal challenges. *Compend Contin Educ Dent,* **20**, 655–61.

Chan, H., Mijares, D. & Ricci, J. L. (2004) *In vitro* dissolution of calcium sulfate: evidence of bioactivity. *Proceedings 7th World Congress on Biomaterials, Sydney, Australia*, 627.

Clifton, J. R. (1973) *Some Aspects of the Setting and Hardening of Gypsum Plaster.* Technical Note. US Dept. OF. Commerce, *National Bureau of Standards.*

Conner, H. D. (1996) Bone grafting with a calcium sulfate barrier after root amputation. *Compend Contin Educ Dent*, **17**, 42, 44, 46; quiz 48.

De Leonardis, D. & Pecora, G. E. (1999) Augmentation of the maxillary sinus with calcium sulfate: one-year clinical report from a prospective longitudinal study. *Int J Oral Maxillofac Implants*, **14**, 869–78.

De Leonardis, D. & Pecora, G. E. (2000) Prospective study on the augmentation of the maxillary sinus with calcium sulfate: histological results. *J Periodontol*, **71**, 940–7.

Dreesman, H. (1892) Ueber Knochenplombierung. *Beitr Klin Chir*, **9**, 804.

Frenkel, S. R., Simon, J., Alexander, H., Dennis, M. & Ricci, J. L. (2002) Osseointegration on metallic implant surfaces: effects of microgeometry and growth factor treatment. *J. Biomed Mater Res (Appl Biomater)*, **63**, 706–13.

Gitelis, S., Piasecki, P., Turner, T., Haggard, W., Charters, J. & Urban, R. (2001) Use of a calcium sulfate-based bone graft substitute for benign bone lesions. *Orthopedics*, **24**, 162–6.

Hadjipavlou, A. G., Simmons, J. W., Yang, J., Nicodemus, C. L., Esch, O. & Simmons, D. J. (2000) Plaster of Paris as an osteoconductive material for interbody vertebral fusion in mature sheep. *Spine*, **25**, 10–15; discussion 16.

Hallman, M., Lundgren, S. & Sennerby, L. (2001) Histologic analysis of clinical biopsies taken 6 months and 3 years after maxillary sinus floor augmentation with 80% bovine hydroxyapatite and 20% autogenous bone mixed with fibrin glue. *Clin Implant Dent Relat Res*, **3**, 87–96.

Intini, G., Andreana, S., Intini, F. E., Buhite, R. J. & Bobek, L. A. (2007) Calcium sulfate and platelet-rich plasma make a novel osteoinductive biomaterial for bone regeneration. *J Translational Med*, **5**, 13.

Kelly, C. M. & Wilkins, R. M. (2004) Treatment of benign bone lesions with an injectable calcium sulfate-based bone graft substitute. *Orthopedics*, **27**, s131–5.

Kelly, C. M., Wilkins, R. M., Gitelis, S., Hartjen, C., Watson, J. T. & Kim, P. T. (2001) The use of a surgical grade calcium sulfate as a bone graft substitute: results of a multicenter trial. *Clin Orthop Relat Res*, 42–50.

Kim, C. K., Chai, J. K., Cho, K. S., Moon, I. S., Choi, S. H., Sottosanti, J. S. & Wikesjo, U. M. (1998a) Periodontal repair in intrabony defects treated with a calcium sulfate implant and calcium sulfate barrier. *J Periodontol*, **69**, 1317–24.

Kim, C. K., Kim, H. Y., Chai, J. K., Cho, K. S., Moon, I. S., Choi, S. H., Sottosanti, J. S. & Wikesjo, U. M. (1998b) Effect of a calcium sulfate implant with calcium sulfate barrier on periodontal healing in 3-wall intrabony defects in dogs. *J Periodontol*, **69**, 982–8.

Kim, S. & Rethnam, S. (1997) Hemostasis in endodontic microsurgery. *Dent Clin North Am*, **41**, 499–511.

Lautenschlager, E. P. (1972) Ceramics in dentistry. In Greener, E. H., Harcourt, J. K. & Lautenschlager, E. P. (Eds.) *Materials Science in Dentistry.* Baltimore, MD USA, The Williams and Wilkins Co.

Lazary, A., Balla, B., Kosa, J. P., Bacsi, K., Nagy, Z., Takacs, I., Varga, P. P., Speer, G. & Lakatos, P. (2007) Effect of gypsum on proliferation and differentiation of MC3T3-E1 mouse osteoblastic cells. *Biomaterials*, **28**, 393–9.

LeGeros, R. Z. (2002) Properties of osteoconductive biomaterials: calcium phosphates. *Clin Orthop*, 81–98.

Ljubovic, E. & Nikulin, A. (1956) [Plastic plombage in experimental bone regeneration.] *Acta Med Iugosl*, **10**, 1–36.

Mamidwar, S., Alexander, H. & Ricci, J. L. (2006a) Bone repair with calcium sulfate-based bone grafts. *Inside Dentistry*, **2**, Special Edition 2, September.

Mamidwar, S. S., Arena, C., Kelly, S., Alexander, H. & Ricci, J. (2006b) *In vitro* characterization of a calcium sulfate/PLLA composite for use as a bone graft material. *J Biomed Mater Res (B) Appl Biomaters*, 2, special issue 2, 1–18.

Mesimeris, V., Sade, E. & Baer, P. N. (1995) Calcium sulfate as a biodegradable barrier membrane – a preliminary report on the 'Surgiplast' Technique. *Periodontal Clin Investig*, **17**, 13–16.

Mirzayan, R., Panossian, V., Avedian, R., Forrester, D. M. & Menendez, L. R. (2001) The use of calcium sulfate in the treatment of benign bone lesions. A preliminary report. *J Bone Joint Surg Am*, **83-A**, 355–8.

Moy, P. K., Lundgren, S. & Holmes, R. E. (1993) Maxillary sinus augmentation: histomorphometric analysis of graft materials for maxillary sinus floor augmentation. *J Oral Maxillofac Surg*, **51**, 857–62.

Orsini, M., Orsini, G., Benlloch, D., Aranda, J. J., Lazaro, P., Sanz, M., de Luca, M. & Piattelli, A. (2001) Comparison of calcium sulfate and autogenous bone graft to bioabsorbable membranes plus autogenous bone graft in the treatment of intrabony periodontal defects: a split-mouth study. *J Periodontol*, **72**, 296–302.

Parsons, J. R., Ricci, J. L., Alexander, H. & Bajpai, P. K. (1988) Osteoconductive composite grouts for orthopedic use. *Ann N Y Acad Sci*, **523**, 190–207.

Payne, J. M., Cobb, C. M., Rapley, J. W., Killoy, W. J. & Spencer, P. (1996) Migration of human gingival fibroblasts over guided tissue regeneration barrier materials. *J Periodontol*, **67**, 236–44.

Pecora, G., Andreana, S., Margarone, J. E., 3rd, Covani, U. & Sottosanti, J. S. (1997a) Bone regeneration with a calcium sulfate barrier. *Oral Surg Oral Med Oral Pathol Oral Radiol Endod*, **84**, 424–9.

Pecora, G., Baek, S. H., Rethnam, S. & Kim, S. (1997b) Barrier membrane techniques in endodontic microsurgery. *Dent Clin North Am*, **41**, 585–602.

Pecora, G. E., de Leonardis, D., Della Rocca, C., Cornelini, R. & Cortesini, C. (1998) Short-term healing following the use of calcium sulfate as a grafting material for sinus augmentation: a clinical report. *Int J Oral Maxillofac Implants*, **13**, 866–73.

Peltier, L. F. (1959) The use of plaster of Paris to fill large defects in bone: a preliminary report. *Clin Orthop Relat Res*, **2001,** 3–5.

Peltola, M. J., Suonpaa, J. T., Maattanen, H. S., Varpula, M. J., Aitasalo, K. M., Yli-Urpo, A. & Laippala, P. J. (2001) Clinical follow-up method for frontal sinus obliteration with bioactive glass S53P4. *J Biomed Mater Res*, **58**, 54–60.

Randolph, D. A. (1971) Gypsum and gypsum products. *Encyclopedia of Industrial Chemical Analysis, Vol. 14*, John Wiley and Sons, Inc. New York.

Ricci, J. L., Alexander, H., Nadkarni, P., Hawkins, M., Turner, J., Rosenblum, S., Brezenoff, L., Deleonardis, D. & Pecora, G. (2000) Biological mechanisms of calcium sulfate replacement by bone. In Davies, J. E. (Ed.) *Bone Engineering.* Toronto, Ont., Canada, em squared Inc.

Rosenblum, S. F., Frenkel, S., Ricci, J. L. & Alexander, H. (1993) Diffusion of fibroblast growth factor from a plaster of Paris carrier. *J Appl Biomater*, **4**, 67–72.

Schepers, E. J. & Ducheyne, P. (1997) Bioactive glass particles of narrow size range for the treatment of oral bone defects: a 1–24 month experiment with several materials and particle sizes and size ranges. *J Oral Rehabil*, **24**, 171–81.

Schmid, J. W. B., Hammerle, C. H. F., Gogolewski, S. & Lang, N. P. (1997) The significance of angiogenesis in guided bone regeneration: a case report of a rabbit experiment. *Clin Oral Impl Res*, **8**, 244–8.

Sottosanti, J. & Anson, D. (2003) Using calcium sulfate as a graft enhancer and membrane barrier. [Interview]. *Dent Implantol Update*, **14**, 1–8.

Sottosanti, J. S. (1997) Calcium sulfate: a valuable addition to the implant/bone regeneration complex. *Dent Implantol Update*, **8**, 25–9.

Strocchi, R., Orsini, G., Iezzi, G., Scarano, A., Rubini, C., Pecora, G. & Piattelli, A. (2002) Bone regeneration with calcium sulfate: evidence for increased angiogenesis in rabbits. *J Oral Implantol*, **28**, 273–8.

Tay, B. K., Patel, V. V. & Bradford, D. S. (1999) Calcium sulfate- and calcium phosphate-based bone substitutes. Mimicry of the mineral phase of bone. *Orthop Clin North Am*, **30**, 615–23.

Walsh, W. R., Morberg, P., Yu, Y., Yang, J. L., Haggard, W., Sheath, P. C., Svehla, M. & Bruce, W. J. (2003) Response of a calcium sulfate bone graft substitute in a confined cancellous defect. *Clin Orthop Relat Res*, 228–36.

Whittaker, J. M., James, R. A., Lozada, J., Cordova, C. & Garey, D. J. (1989) Histological response and clinical evaluation of heterograft and allograft materials in the elevation of the maxillary sinus for the preparation of endosteal dental implant sites. Simultaneous sinus elevation and root form implantation: an eight-month autopsy report. *J Oral Implantol*, **15**, 141–4.

Wright Medical Technologies Monograph (1997) *Medical Grade Calcium Sulfate. Bone Grafts and Bone Graft Substitutes.* Memphis, TN, USA, Wright Medical Technologies Inc.

15

Tricalcium phosphate-based ceramics

C REY, C COMBES and C DROUET, CIRIMAT, France and
S SOMRANI, IPEIT, Tunisia

15.1 Introduction

Tricalcium phosphates (TCP) are among the most commonly-used calcium phosphate compounds in implant materials. They are found in ceramic bone substitutes, metallic prosthesis coatings, cements and composite materials. Magnesium whitlockite, a tricalcium phosphate derivative, occurs in ectopic pathological calcifications (joint crystals, kidney stones, salivary and urinary calculi). There is some confusion surrounding the meaning of the term 'tricalcium phosphate'. It has been used to designate different compounds containing the orthophosphate ion PO_4^{3-} with a Ca/P atomic ratio close to 1.5, which corresponds approximately to the chemical formula: $Ca_3(PO_4)_2$. Some calcium-deficient phosphates with an apatite structure were thus commercialised as 'tricalcium phosphate' even though they did not exhibit the expected crystalline structure of tricalcium phosphate. From a strict chemical point of view, 'tricalcium phosphate' refers to a composition, even though, in the minds of many users, this term is used to describe a structure, generally that of β-tricalcium phosphate (β-TCP). Several types of tricalcium phosphates are in fact used as biomaterials: in addition to the high-temperature forms α- and β-TCP, amorphous tricalcium phosphate and apatitic tricalcium phosphate play an important role in metallic prosthesis coatings and in calcium phosphate cements. In the following pages, we will specify the structure of tricalcium phosphates by adding a prefix to the generic name TCP:

- am-TCP will hereby designate amorphous tricalcium phosphate;
- ap-TCP: apatitic tricalcium phosphate;
- β-TCP: the most widely used member of the TCP family having a β-TCP crystalline structure;
- α-TCP: the metastable high-temperature crystalline structure.

In this review we will not discuss α-TCP, an unstable, very high-temperature variety of TCP not used in biomaterials. Whitlockite will designate a pre-

cipitated, generally magnesium-substituted structure analogous to that of β-TCP showing, however, an altered composition and different biological properties.

An overview of TCPs will be presented first, followed by a review of the preparation methods of TCP-containing materials: their different structures and microstructures, their related physicochemical properties, the mechanical properties of TCP-based materials, their biological properties, and their different uses as biomaterials. Lastly, possible outcome and future evolution of these materials will be discussed.

15.2 Overview of tricalcium phosphates

Tricalcium phosphates $Ca_3(PO_4)_2$, exist in four different forms, all of which are used as biomaterials (Table 15.1). Amorphous tricalcium phosphate (am-TCP) and apatitic tricalcium phosphate (ap-TCP) are low-temperature, unstable phases generally obtained by precipitation, whereas α- and β-tricalcium phosphates (α- and β-TCP) are high-temperature

Table 15.1 Tricalcium phosphates as biomaterials

Type of material	Type of TCP involved	Application	Main TCP-related effects
Ceramics	α- and β-TCP	Bone substitutes Small bone replacement Tissue engineering	Biodegradable Dissolution and hydrolysis (for α-TCP)
Ca-P ionic Cements	α-TCP, am-TCP *ap-TCP* (*end-product*)	Bone substitutes Dental applications	Active hardening agents Bioresorbable, surface reactivity
	β-TCP (brushite cements)		Provider of Ca^{2+} and PO_4^{3-} ions
Coatings	am- and ap-TCP, α- and β-TCP	Coating of metallic prostheses	Biodegradable, reactive coating
Mineral-organic composites	am-TCP, α- and β-TCP	Bone replacement and bone substitutes Tissue engineering Dental restorative materials	Mechanical properties, Ca and P release in relation with biological activity

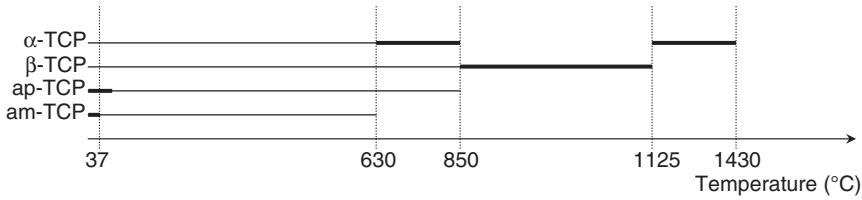

15.1 Formation domains of the different TCP phases (bold lines) and domains of existence (thin lines).

crystalline phases. The existence and formation domains of the different TCP phases are schematised in Fig. 15.1. Although formed at high temperature, β-TCP is stable over a large temperature domain: from room temperature to its transition temperature to the α-TCP phase (1125 °C). α-TCP is considered as a metastable phase at room temperature. It is obtained by quenching from its thermal stability domain; however, it also appears as a transient phase during the thermal conversion of pure am-TCP into crystalline TCP within a narrow temperature range (630–850 °C). The thermal decomposition of ap-TCP yields the stable β-TCP phase without any transient phases. The stability domains of TCPs determine their use as biomaterials (Table 15.1): sintered ceramics may only be obtained from α- and β-TCP; am-TCP and ap-TCP may only be processed at low and moderate temperatures and thereby enter into the composition of powders for calcium phosphate cements, in composite materials (polymer-mineral), or in low-temperature coating of medical devices.

Am-TCP and ap-TCP may vary from stoichiometric composition depending on their preparation and heating conditions, whereas non-stoichiometry has not generally been reported for high-temperature phases. Although several ionic substitutions are possible in all TCP phases, in this review we will consider only those that may have biological interest.

All TCPs are considered as more soluble than stoichiometric hydroxyapatite (HA); however, a specific solubility product has not yet been determined in the case of am- and ap-TCPs. They are all bioresorbable, in accordance with the general concept that calcium phosphates' biological resorbability is determined by their solubility (Legero *et al.*, 1995).

Whitlockite deserves special attention as it may form under physiological conditions, and crystallises, *in vivo*, in different disease states. The crystal structure of whitlockite is analogous to that of β-TCP; however, the crystal composition appears more complex and generally includes Mg^{2+} and HPO_4^{2-} species in biological systems. Although it has not been precisely determined, the solubility of whitlockite seems to be very low and possibly inferior to that of stoichiometric hydroxyapatite (Elliott, 1994), suggesting that it could be a non-bioresorbable phase.

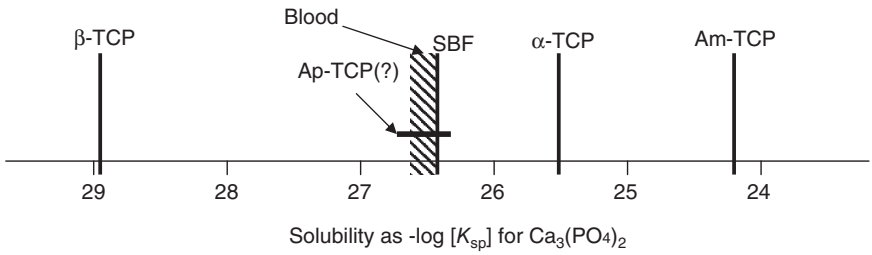

15.2 Comparison of solubility products of different TCP phases and the corresponding ionic products of biological fluids at 25 °C. The domain for ap-TCP is probably covering that of blood.

In addition to their bioresorbability, some TCP compounds, especially am-TCP and α-TCP, exhibit very high reactivity in aqueous media and they can readily transform into apatite. These fast hydrolysis reactions are used in self-setting cements and, when they occur *in vivo*, they result in the formation of neo-formed carbonate apatite crystals analogous to bone mineral crystals responsible for the biological activity of different materials. The expected behaviour of TCP *in vivo* is summarised in Fig. 15.2. Am-TCP and α-TCP are not stable in physiological conditions: they spontaneously dissolve and/or hydrolyse into poorly crystalline apatite analogous to bone mineral. Ap-TCP is probably within the range of bone solubility and should behave similarly to bone mineral. β-TCP cannot theoretically dissolve spontaneously *in vivo* nor hydrolyse into apatite in the absence of cell activity.

These few facts determine the behaviour of pure TCPs; however, some alteration may be observed depending on their chemical composition, structural and microstructural characteristics.

15.3 Synthesis, structure and physicochemical properties of the different TCP phases

The production of tricalcium phosphate-based ceramics generally involves TCP powder preparation and, in a successive stage, powder processing in order to obtain cohesive biomaterials in the form of dense or macroporous ceramics, coatings, cements or composites for bone filling, substitution and/or reconstruction applications. In several cases, however, TCP phases form during processing, as, for example, in the case of hydroxyapatite (HA) plasma spraying. In this section, we will focus on the elaboration of the different TCP phases (amorphous, apatitic, α- and β- polymorphic forms), their structure, and main physicochemical properties. The processing of such phases will be developed in the next section.

15.3.1 Preparation and structure of the different TCPs

Owing to their different domains of formation, two distinct synthesis routes can be distinguished for the preparation of powder TCPs. The first method is a solution-mediated route involving the precipitation of tricalcium phosphate under controlled experimental conditions (pH, temperature, ion concentrations, etc.). It relates to the preparation of the low-temperature phases: am- and ap-TCP as well as whitlockite. The second route involves dry, high-temperature methods that are specifically, but not exclusively, used for the synthesis of the two high-temperature crystalline forms of TCP: α- and β-TCP.

Amorphous tricalcium phosphate (am-TCP)

A growing interest in amorphous calcium phosphate (am-TCP) arose in the 1970s from this compound's supposed involvement in bone composition. The question of its occurrence during bone-mineral development, prior to final crystallisation of a hydroxyapatite-like phase, has indeed led to some discussion and controversy. Based on X-ray radial distribution function analysis carried out on various bone samples including embryonic ones, Grynpas *et al.* (1981) concluded, however, that the chemical and structural changes observed could not be accounted for by the presence of am-TCP. This hypothesis was thus progressively abandoned, and it is now admitted that bone mineral is mainly formed of a calcium-deficient poorly crystalline apatite.

Nevertheless, the initial attention focused on am-TCP did lead several researchers to intensify their investigations. am-TCP can be prepared by various solution-mediated routes. One of the most convenient preparation methods is double decomposition between a calcium salt solution and a hydrogen phosphate salt solution in aqueous media at ambient temperature and at a pH close to 10 (Heughebaert, 1977; Somrani *et al.*, 2005). It can also be obtained in hydroalcoholic solution (Lebugle *et al.*, 1986; Rodrigues and Lebugle, 1998). Rodrigues and Lebugle (1998) showed that the presence of ethanol in the precipitation medium influences the composition of the amorphous phase and especially its HPO_4^{2-} content and Ca/P ratio.

The main difficulties in the preparation of am-TCP are related to its instability and reactivity. Generally, am-TCP cannot be obtained at neutral or slightly acidic pH. However, it can be stabilised by various mineral ions or organic molecules which can be added to the precipitating and/or washing solutions. For example, am-TCP can be prepared under more acidic conditions (around pH 6) and in the presence of magnesium or citrate ions, known as crystal growth inhibitors of apatite phase (Holt *et al.*, 1989). Owing to its reactivity and rather high water content, precipitated am-TCP is generally freeze-dried and stored at –18°C to prevent any further

evolution. Dry, heated am-TCP can, however, be stored at room temperature in dry atmosphere.

In contrast with synthesis methods in solution, am-TCP can also be obtained via a dry, high-temperature route through rapid quenching of melted calcium phosphate. In the absence of ions other than Ca^{2+} and PO_4^{3-}, the amorphous phase which forms is analogous to anhydrous precipitated am-TCP (Ranz, 1996). However, in practice, other anions such as O^{2-} are also observed in the high-temperature amorphous phase, increasing its Ca/P atomic ratio (>1.5), especially in HA plasma-sprayed coatings.

Observed by transmission electron microscopy (TEM), am-TCP morphology is mostly spherical, although these particles generally tend to agglomerate into larger, irregularly shaped, branched clusters (Eanes, 2001). The size of the spheroid particles varies in a large range (20–200 nm) (Eanes, 1998). Lazic and Vukovic (1988) reported that spheroidal particles of 25 nm in size were the dominant and most stable morphology of am-TCP.

Independently of the preparation conditions, am-TCP has been shown to exhibit a short-distance atomic order. This local order was studied in detail by Posner and his collaborators in several works (Betts and Posner, 1974a, b; Posner and Beebe, 1975). In particular, the rapid decay of the radial distribution function led to a model based on the agglomeration of ion cluster units with individual diameters close to 9.5 Å corresponding to the chemical composition: $Ca_9(PO_4)_6$. The stability of Posner's clusters has been confirmed by theoretical calculations (Treboux *et al.*, 2000). They consist of a central column of three stacked Ca^{2+} ions, each of which is surrounded by six oxygen atoms arising from six phosphate groups and stabilised with six additional Ca^{2+} ions distributed at the periphery of the cluster (Fig. 15.3).

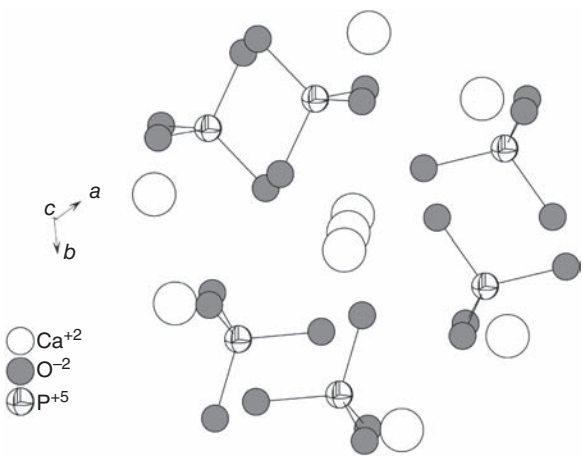

15.3 Representation of a 'Posner's cluster' associated with the structure of amorphous tricalcium phosphate. These clusters may also be found in hydroxyapatite and other calcium phosphate phases.

Similar ion clusters have been identified in apatite, OCP and crystalline TCPs, and seem to constitute a basic building unit of several calcium phosphates. Eanes also investigated am-TCP through thermochemical experiments and concluded that such amorphous calcium phosphate corresponded to a hydrated tricalcium phosphate phase (Eanes, 1970), suggesting a $Ca_3(PO_4)_2.n(H_2O)$ chemical formula. The presence of water is an intrinsic feature of am-TCP. Even freeze-dried, amorphous calcium phosphate still contains around 15–20 wt. % of water. Sedlack and Beebe (1974) concluded from temperature-programmed dehydration of am-TCP that two types of bound water exist in this compound: loosely held water, and tightly bound water held inside the amorphous particles (Kojima, 1994).

Am-TCP can also easily incorporate 'foreign' ions through ionic substitutions. Interestingly, am-TCP can trap carbonate ions from the preparation solutions (Greenfield and Eanes, 1972), and the carbonate content tends to increase with the solution pH. Other substitutions have also been reported, including Mg^{2+} and pyrophosphate ions. More generally, am-TCP can trap several mineral ions exhibiting biological activity (Sr, Zn, Mg, Mn, Cu, etc.). The incorporation of silver was recently shown to bring antimicrobial performances to am-TCP (Aimanova *et al.*, 2005).

Apatitic tricalcium phosphate (ap-TCP)

Apatitic tricalcium phosphate (ap-TCP) is the low-temperature crystallised form of am-TCP. It exhibits an apatite structure with a Ca/P ratio close to 1.5. This compound is derived from crystallisation in aqueous environment of am-TCP. Heughebaert showed that crystallisation is associated with an internal hydrolysis reaction of phosphate groups PO_4^{3-} (Heughebaert, 1977; Heughebaert and Montel, 1982):

$$PO_4^{3-} + H_2O \rightarrow HPO_4^{2-} + OH^-$$

leading to a crystalline apatite with equal amounts of HPO_4^{2-} and OH^-, represented by the chemical formula $Ca_9(PO_4)_{6-x}(HPO_4)_x(OH)_x$, which is one aspect of non-stoichiometric hydroxyapatite (Rey *et al.*, 2007).

Ap-TCP can be prepared by the methods already described above for the preparation of am-TCP powder, except for the drying stage which has to be carried out in an oven at 80 °C in order to allow internal hydrolysis and crystallisation to occur (Heughebaert, 1977; Lebugle *et al.*, 1986). The X-ray diffraction (XRD) pattern of ap-TCP is characteristic of calcium-deficient apatite: all the Fourier transform infrared (FTIR) bands of an apatitic structure are observed along with an additional band at around 875 cm^{-1} due to HPO_4^{2-} ions. Several ionic substitutions can occur in ap-TCP, as in other apatite compounds.

α- and β-tricalcium phosphates (α- and β-TCP)

Unlike amorphous and apatitic tricalcium phosphates, α-TCP and β-TCP powders cannot be directly precipitated in aqueous systems. These two anhydrous crystalline forms of tricalcium phosphate can, however, be obtained by an appropriate high-temperature treatment of am-TCP and/or ap-TCP or, more generally, any mixture of Ca-P salts with the appropriate Ca/P ratio.

Thermal treatment in air of the low-temperature phases am-TCP and ap-TCP at 900 °C for several hours does indeed lead to the formation of β-TCP, and this is a way to prepare this phase with high purity. When TCP's Ca/P atomic ratio is not exactly 1.5, impurities appear. The main impurities, hydroxyapatite (corresponding to a Ca/P atomic ratio above 1.5) and β-calcium pyrophosphate (corresponding to a Ca/P atomic ratio under 1.5), can be detected, respectively, by XRD and FTIR spectroscopy.

α-TCP is generally obtained by heating β-TCP above 1125 °C (the transition temperature for β→α), followed by rapid quenching. It is interesting to note that α-TCP can also be obtained transitorily by heating am-TCP at temperatures lower than 1125 °C (between 630 and 850 °C), but this method generally leads to a product containing traces of β-TCP (Eanes, 1970; Somrani *et al.*, 2003).

Both α- and β-TCP can also be prepared from other starting powders and, more conveniently, from mixtures of Ca-P phases with the adequate global Ca/P ratio of 1.5. For example, they can be obtained by heating an intimate mixture of $CaHPO_4$ (DCPA) and $CaCO_3$ in the molar ratio 2/1 at 1150–1200 °C for at least one day. α-TCP is then obtained by quenching in liquid nitrogen whereas prolonged heating at about 900 °C (until complete disappearance of α-TCP) leads to the production of β-TCP. Several authors also reported the synthesis of pure β-TCP by heating a $CaHPO_4.2H_2O$ (DCPD) : $CaCO_3$ mixture (2 : 1 molar) at 930 °C for 2 hours (Yang and Wang, 1998) or at 900 °C for 14 hours (Vallet-Regi *et al.*, 1997).

From a structural point of view, β-TCP is a stable anhydrous tricalcium phosphate phase. It crystallises in the rhombohedral system (space group R3c) with 21 formula units $Ca_3(PO_4)_2$ per hexagonal unit cell (Dickens *et al.*, 1974) (Table 15.2). A thorough structural description of this phase is given in the literature based mainly on a comparison with the phase $Ba_3(VO_4)_2$ and it will therefore not be reported here (Elliott, 1994). An interesting structural feature of β-TCP is, however, the presence of columns of ions (anions and cations) which can be distinguished parallel to the *c*-axis.

It is worthwhile noting that a great amount of calcium ions (generally reported up to 15%) in β-TCP can be substituted by Mg^{2+} ions without essentially altering the structure, thus leading to a Mg-β-TCP phase (Rowles,

Table 15.2 Crystallographic characteristics of pure α- and β-TCP

	α-TCP	β-TCP
Lattice	Monoclinic	Trigonal
Space group	$P2_1/a$	R3c
Unit cell parameters	$a = 1.2887$ nm $b = 2.7280$ nm $c = 1.5219$ nm $\beta = 126.20°$	(hexagonal setting) $a = b = 1.0439$ nm $c = 3.7375$ nm
Reference	Mathew *et al.* (1977)	Dickens *et al.* (1974)

1968; Terpstra *et al.*, 1983; Clement *et al.*, 1989). Magnesium has been shown to be preferentially located on specific cationic sites of the structure.

Other bivalent cations can substitute to calcium in β-TCP. Among the most interesting ones are Zn^{2+} and Sr^{2+} (Bigi *et al.*, 1997; Ito *et al.*, 2000). Zn^{2+} can substitute to calcium ions up to 20% and Sr^{2+} up to 80%. Zn^{2+} induces a non-linear variation of the lattice constants and an increase in the degeneracy of the phosphate IR absorption bands. Sr^{2+} causes a linear enlargement of the unit cell and a shift of the phosphate IR bands towards lower frequencies. Recently, β-TCP incorporating a small portion of Na^+ ions (up to 2.11%), corresponding to the chemical formula $Ca_{10}Na(PO_4)_7$, was obtained for biological use (Obadia, 2004).

β-TCP should not be mistaken for magnesium whitlockite, $Ca_9Mg(HPO_4)(PO_4)_6$, although they both crystallise in the same rhombohedral structure. Whitlockite can be prepared in aqueous media containing Mg^{2+} and HPO_4^{2-} ions. It can be obtained by double decomposition between a calcium and magnesium solution, and a phosphate solution, at various temperatures. An initial Mg/P molar ratio of 0.05, a temperature equal to 100 °C, and acidic pH (between 5 and 6) are experimental conditions that favour the precipitation of well-crystallised whitlockite. However, apatite and amorphous side-products can be formed during whitlockite preparation.

α-TCP is a metastable anhydrous tricalcium phosphate phase crystallising in the $P2_1/a$ monoclinic space group (Table 15.2). The unit cell comprises 24 formula units $Ca_3(PO_4)_2$ (Mackay, 1953). As for β-TCP, a noticeable feature of the structure of α-TCP is the presence of columns of ions (Ca^{2+} and PO_4^{3-}) parallel to the *c*-axis (Mathew *et al.*, 1977). A structural relationship with apatite can be obtained by the replacement of cation columns with anion columns (OH^- ions of hydroxyapatite), as described by Elliott (1994).

Ionic substitutions in α-TCP have been less investigated than in β-TCP. Zn^{2+} has been reported to substitute for Ca^{2+} (Ito *et al.*, 2002a), and silicate for phosphate (Sayer *et al.*, 2003; Reid *et al.*, 2006).

According to the structures of α- and β-TCP, each formula unit, $Ca_3(PO_4)_2$, occupies 180 Å^3 in α-TCP, compared with 168 Å^3 in β-TCP. The α form therefore exhibits less cohesion than β-TCP and has a higher internal energy. These points are consistent with the fact that the α form is the high-temperature phase and shows a greater reactivity in water than β-TCP.

15.3.2 Physicochemical properties of TCP phases

Solubility

The solubility behaviour of α- and β-TCP has been fully investigated and reported in the literature (Gregory *et al.*, 1974; Fowler and Kuroda, 1986). As a general trend, the solubility of these phases was found to decrease in the order α-TCP > β-TCP > Ca-deficient apatites > HA (Ducheyne *et al.*, 1993). The solubility products of these phases, at 25 °C, are presented in Table 15.3.

To our knowledge, the solubility product of apatitic tricalcium phosphate (Ca/P equal to 1.5) has not been determined accurately heretofore and probably depends on the hydrolysis ratio and the stoichiometry. According to its poorly crystalline structure, it may exhibit metastable solubility equilibrium, as recorded by Baig *et al.* (1999) in the case of bone mineral and non-stoichiometric apatites.

The solubility behaviour of amorphous tricalcium phosphate has also been investigated by several authors. However, the dispersion of the data seems very large and some of the reported values – rather unrealistic – could have been altered due to the hydrolysis reaction of this very unstable phase. The most probable value reported in Table 15.3 is related to the work of Somrani *et al.* (2005). As expected, this phase is much more soluble than the crystalline TCP phases.

Table 15.3 Solubility products of TCP phases in water at 25 °C

Phase	Chemical formula	pK_{sp} (25 °C)	References
α-TCP	α-$Ca_3(PO_4)_2$	25.5	Fowler and Kuroda (1986)
β-TCP	β-$Ca_3(PO_4)_2$	28.9	Gregory *et al.* (1974)
Ca-deficient apatite	$Ca_{10-x}(PO_4)_{6-x}(HPO_4)_x(OH)_{2-x}$	~85.1	Ratner *et al.* (1996)
Amorphous TCP	$Ca_3(PO_4)_2 \cdot n(H_2O)$	24.2	Somrani *et al.* (2005)
HA	$Ca_{10}(PO_4)_6(OH)_2$	117.2	Ratner *et al.* (1996)

Substituted β-TCPs containing Zn and Mg have been shown to exhibit a lower solubility than non-substituted ones, depending on the substitution ratio (Ito *et al.*, 2002b, 2005). Furthermore, the kinetics of dissolution of β-TCP seems very sensitive to the presence of foreign ions in the solution, especially Mg^{2+} and Zn^{2+}, and concentrations of Zn^{2+} as low as 2×10^{-6} mol.l^{-1} have been shown to completely inhibit dissolution (Tang *et al.*, 2001)

Thermal stability of TCP phases

No variation of the Ca/P ratio of TCP phases can occur on heating. Among the tricalcium phosphate phases, α-TCP is known as the high-temperature stable form. Its stability region ranges from 1125 °C to 1430 °C (Welch and Gutt, 1961). Under 1125 °C, β-TCP is the stable tricalcium phosphate phase. Rapid quenching from temperatures higher than 1125 °C, however, permits the preservation of the α-TCP phase at room temperature. The transition temperature between the β- and α-TCP phases may vary depending on ion impurities such as Mg, Zn and Fe which stabilise β-TCP. Apatitic TCP can be considered the low-temperature crystalline form of am-TCP (e.g. upon drying at 80 °C). On heating at temperatures higher than 800 °C, this phase transforms into β-TCP (Destainville *et al.*, 2003). Pure am-TCP remains amorphous when heated up to ca. 630 °C (Eanes, 1970). Above this temperature, it crystallises first into the metastable α-TCP generally associated with small fractions of β-TCP and, around 850 °C, into pure β-TCP. However, am-TCP containing Mg ions (or containing other elements stabilising the β-TCP phase such as Fe and Zn) transforms directly into the β-TCP phase without the intermediary formation of α-TCP. It has been suggested, based on thermodynamic and nuclear magnetic resonance (NMR) studies (Belgrand, 1993; Somrani *et al.*, 2003), that α-TCP formed by thermal crystallisation of am-TCP could be more stable and contain fewer defects than the α-TCP phase obtained by quenching from temperatures above the β- to α-TCP transition.

Aqueous evolution of TCP phases

In aqueous medium, it is worthwhile reminding that the first precipitates obtained under given conditions (pH, temperature and ion concentrations) from calcium phosphate solutions do not necessarily correspond to the thermodynamically most stable phase. For example, phases such as am-TCP or octacalcium phosphate (OCP) may form transiently in solution, somewhat analogous to precursor phases prior to their progressive hydrolysis into apatite (Tung, 1998). In particular, am-TCP is generally the first solid phase that spontaneously precipitates upon mixing alkaline calcium and phosphate solutions (Eanes, 2001).

When immersed in solution, the most soluble TCP phases, α-TCP and am-TCP, show a strong tendency to evolve towards a more stable phase through a hydrolysis process. In this case, solution parameters such as pH, ion concentrations and temperature are known to play a major role.

At alkaline and neutral pH, am-TCP progressively transforms into non-stoichiometric hydroxylated apatites (Eanes and Meyer, 1977). According to Heughebaert, in this process am-TCP is generally found to remain amorphous up to half hydrolysis corresponding to the composition: $Ca_9(PO_4)_5(HPO_4)(OH)$ and apatite structure crystallisation (Heughebaert, 1977). The apatite obtained by hydrolytic conversion of am-TCP may, however, evolve differently in the solution depending on pH, temperature, maturation time and ion content. Generally, an increase in the Ca/P ratio of the solid is noticed, associated with a decrease in HPO_4^{2-} content and an increase in OH^- content (Somrani *et al.*, 2005). It was found that an increase in the Ca/P ratio in the starting solutions led to faster crystallisation into hydroxyapatite (Kim *et al.*, 2004). Interestingly, the addition of some ionic species such as Mg^{2+}, CO_3^{2-}, and $P_2O_7^{4-}$ which inhibit apatite crystal growth was shown to delay this hydrolysis process (Boskey and Posner, 1974; LeGeros *et al.*, 2005). Considering heated am-TCP, the conversion rate into apatite has been shown to be related to the residual water content and rehydration of the powder appears as a determining stage (Somrani *et al.*, 2005). Two mechanisms have been discussed for the hydrolytic conversion of am-TCP into apatite: a restructuring of Posner's clusters and a dissolution–reprecipitation process which occurs in all cases. It has been suggested that the relative importance of these conversion mechanisms depends on the conditions of the hydrolysis reaction, especially pH, temperature and solid/solution ratio (Somrani *et al.*, 2005). The hydrolytic conversion rate depends strongly on the temperature (Heughebaert, 1977) and this property is used to regulate the setting reaction of am-TCP-based cements (Knaack *et al.*, 1998).

α-TCP also hydrolyses rapidly in aqueous solution (Monma, 1980; Monma *et al.*, 1981). The hydrolysis products are generally OCP and non-stoichiometric apatite, although dicalcium phosphate anhydrous (DCPA or monetite) and dicalcium phosphate dihydrate (DCPD or brushite) can also form. The transformation mechanism is generally identified with dissolution–reprecipitation reactions. Although less investigated than the hydrolysis of am-TCP, the hydrolysis of α-TCP is believed to depend on the same physicochemical factors (temperature, pH, hydrolysis time, solution composition and presence of ionic impurities).

In contrast, β-TCP does not show a tendency to hydrolyse rapidly in solution at physiological temperatures. However, pure β-TCP has been shown to hydrolyse completely into relatively well-crystallised non-stoichiometric apatitic phases in boiling aqueous suspensions within 24

hours (Rey, 1984). Faster hydrolysis of β-TCP into apatite also occurs under hydrothermal conditions (e.g. 120 °C in the presence of water vapour). These reactions have been found to depend strongly on the purity of β-TCP as they are strongly inhibited in the presence of traces of Mg ions.

Surface properties

Although the understanding of surface interactions between biomaterials and body fluids is of utmost importance for following biointegration and bioactivity, few data are available to date on the surface properties of TCP phases, despite their high involvement in the biomaterials field.

Among the indications reported in the literature concerning the surface properties or reactivity of tricalcium phosphates, most deal either with adsorption or ion exchange processes; however, the elucidation of the corresponding mechanisms and the relationship with intrinsic surface properties of the TCP phases involved are only rarely addressed.

Adsorption of recombinant human transforming growth factor β1 (rhTGF-β1) on tricalcium phosphate-coated titanium-based implants has been investigated in dogs (Lind *et al.*, 2001). In this work, the authors pointed out a clear increase in the bone volume formed around the implant coated with TCP with adsorbed rhTGF-β1 (0.3 μg), thus showing the potential importance of adsorption phenomena on TCP phases. Adsorption of various proteins on β-TCP and other calcium phosphates has been investigated by Ohta *et al.* (2001). Two kinds of adsorption sites were distinguished: positively charged sites (Ca sites) capable of adsorbing acidic proteins (e.g. bovine serum albumin, BSA) and negatively charged sites (P sites) which adsorb alkaline proteins. Also, the total number of calcium sites on β-TCP was then found to be significantly lower than on the other calcium phosphates tested, including hydroxyapatite.

Using a radioactive tracer technique, Govaerts (1954) followed the exchange of phosphate and calcium ions in the case of tricalcium phosphate subjected to solutions containing, respectively, Na_2HPO_4 and $CaCl_2$. This author came to the conclusion that such exchanges appeared to proceed in three kinetically separable stages, with a rapid step related to ion exchange involving the crystal surface and slower stages involving ions lying deeper in the crystal bulk.

15.4 Applications and uses of TCP-based bioceramics

Since the first trials of TCP-compound implantations as a suspension in animals (Albee and Morrison, 1920), β-TCP has become one of the first calcium phosphates to be used in bioceramics for bone substitution and repair thanks to its stability at high temperature and ease of processing as

ceramics (Nery *et al.*, 1975; Jarcho *et al.*, 1979; Metsger *et al.*, 1982). β-TCP-based ceramics have been commercialised for a long time and they are one of the major bioresorbable synthetic bone substitutes in use today by orthopaedic surgeons and dentists in their quotidian practice. These materials are in the form of porous ceramic pieces and granules. They are used in the reconstruction of all kinds of bone defects, from augmentation of alveolar ridge defects after a tooth extraction and before implant positioning, to sinus reconstruction (Szabo *et al.*, 2005; Horch *et al.*, 2006), correction of various deformities (Le Huec *et al.*, 1997; Nakagawa *et al.*, 2006), and bone reconstruction following injury or disease (Ogose *et al.*, 2005). More recently, α-TCP has also been put forward as ceramic materials for similar applications (Almirall *et al.*, 2004).

β-TCP-based ceramics were shown to be bioabsorbable and replaced by bone, whereas HA-based ceramics constituted non- or poorly biodegradable materials. Biphasic calcium phosphate (BCP) ceramics, which associate these two high-temperature crystalline calcium phosphates, allow the resorption rate of bioceramics to be controlled and they have been reported to offer superior biological properties (Daculsi *et al.*, 2003). They are progressively replacing β-TCP ceramics in Europe. The applications and uses of such BCP ceramics are developed in Chapter 17 of this book. Recently, a new biodegradable biphasic tricalcium phosphate associating α-TCP and β-TCP was proposed. This mixture of TCP phases was obtained by heating an am-TCP precursor at 800 °C (Li *et al.*, 2007).

A new technological step was made in the bioceramics field with the development of calcium phosphate cements (Brown and Chow, 1987); currently the second most important use of TCP compounds is in ionic self-setting cements. These materials are able to set and harden in a living body and most of them can be injected. Despite their poor mechanical properties, they offer a number of advantages and are increasingly used in clinical practice. Tricalcium phosphate in its various forms (am-, α- or β-TCP) is involved in many calcium phosphate cement compositions; many of them are commercialised (Table 15.4). am- and α-TCP are used especially in several cement compositions thanks to their fast hydrolysis reactions leading to poorly crystallised apatite crystal formation and entanglement responsible for cement hardening. In most α-TCP and am-TCP-based cements, a few hours after application, the main constituent considered to behave like bone mineral crystals is ap-TCP.

β-TCP is the main constituent of DCPD cements and it is sometimes used as an inert additive in other types of Ca-P cements. The uses of injectable cements have progressed over the past few years mainly in dentistry and for the filling of bone defects. However, one of their main drawbacks compared with ceramics is the preparation of the paste and, generally, the absence of macropores preventing cell invasion and rehabitation, whereas

Table 15.4 Compositions and compressive strength (σ_{comp}) of calcium phosphate cements containing TCP phases in the initial powder (Banu, 2005; Bohner *et al.*, 2005)

Main components (initial composition)	Final Ca-P phase (cement name, company name)	σ_{comp} (MPa)	References
Acid–base cements			
α-TCP, $CaCO_3$, MCPM	Carbonated apatite (Norian SRS® and Norian CRS®, Synthes-Norian)	30–50	Constantz *et al.* (1995)
α-TCP, TTCP, $Ca(OH)_2$, H_3PO_4	PCA (Cementek®, Teknimed SA)	20	Hatim *et al.* (1998)
α-TCP, TTCP, citric acid	PCA (Mimix™, Biomet Inc.)	–	Dornhoffer and Simmons (2003)
α-TCP, $CaCO_3$, DCP, HA	Carbonated apatite (Calcibon®, Merck GmbH)	50	Khairoun *et al.* (1997)
α-TCP, TTCP, DCPD	PCA (Biopax®, Mitsubishi Materials)	82	Kurashina *et al.* (1997)
α-TCP, $Mg_3(PO_4)_2$	PCA (KyphOs™, Kyphon)	–	
Monocomponent cements			
am-TCP, DCPD	PCA (α-BSM®, ETEX Corp. and Biobone®, Merck GmbH)	10–15	Lee *et al.* (2000)
α-TCP	PCA		Ginebra *et al.* (1997)
Hydrolysable phase-based cements			
β-TCP, MCPM, $CaSO_4$	DCPD (VitalOs®, CalciphOs)		Mirtchi *et al.* (1989)
β-TCP, $Na_4P_2O_7$, H_3PO_4	DCPD (Eurobone®, Kasios SA)		Frayssinet *et al.* (2000)
β-TCP, MCPM, $MgHPO_4$, $3H_2O$	DCPD (chronOS Inject, ™, Mathys Medical and Stratec Medical)	3	Bohner *et al.* (2003)

DCPD: dicalcium phosphate dihydrate (brushite), DCP: dicalcium phosphate (monetite), MCPM: monocalcium phosphate monohydrate, PCA: poorly crystalline apatite, TTCP: tetracalcium phosphate.

the main advantage of their use is their ability to fill any kind of bone defect and their injectability, allowing light surgical procedures.

TCP compounds (mainly α-, β-TCP and am-TCP) are also used as mineral ion-releasing substances in polymer materials although such composites have had few commercial applications. Many types of polymeric materials have been proposed. These are mainly degradable natural or synthetic polyesters (polylactic, polyglycolic acids, poly-ε-caprolactones, etc.) and natural proteins (collagen and chitosan) (Zhang and Zhang, 2001; Kikuchi *et al.*, 2004; Aunoble *et al.*, 2006; Matsuno *et al.*, 2006; Van Den Vreken *et al.*, 2006). The advantages of these associations have not always been demonstrated (Ekholm *et al.*, 2006) and the reasons for success or failure have not yet been clearly identified.

Although formed in several coating processes, especially in HA plasma-sprayed coatings, TCP compounds have not yet been commercialised as thermal coatings. A low-temperature coating involving am- and ap-TCP-like compounds (Barrere *et al.*, 2004) has been proposed.

15.5 Processing and mechanical properties of TCP-based biomaterials

One may distinguish high-temperature processing techniques of well-crystallised TCP phases (α- and β-TCP) and low-temperature techniques which, in comparison, preserve the characteristics of am- and ap-TCP.

15.5.1 Sintering, processing and mechanical properties of TCP ceramics

The main difficulty in sintering β-TCP ceramics is the transition temperature to α-TCP. For pure TCP, this transition occurs at 1125 °C; however, it can move to higher temperatures in the presence of trace element impurities such as Mg, Fe, Mn and Zn, thus facilitating the sintering process at higher temperatures. In spite of the role of these trace elements, especially Mg and Fe, the most common pollutants of calcium salts, they are seldom analysed in TCP. Practically all β-TCP powders are sintered between 1100 and 1250 °C, depending on the characteristics of the initial powder and the expected final density of the ceramic. Grain growth and reversible conversion into α-TCP are enhanced above 1250 °C, thus compromising the densification and mechanical properties of the ceramic. The composition of the initial powder is also a determinant parameter. An excess of calcium (Ca/P > 1.52) facilitates the transformation into α-TCP and a lower Ca/P ratio (Ca/P < 1.42) leads to the formation of calcium pyrophosphate (β-$Ca_2P_2O_7$) inclusions which slow down the sintering process.

Translucent fully dense pure β-TCP ceramics were obtained by hot pressing at 1150 °C and σ = 30 MPa for 1 hour (Tampieri *et al.*, 1997). The addition of calcium pyrophosphate $Ca_2P_2O_7$ in the range 0.5–3 wt% enables sintering of β-TCP at a higher temperature (1200 °C) without transformation into α-TCP. The ceramic thus obtained has a relative density of 95% (Ryu *et al.*, 2002). Commercialised β-TCP ceramics (Biosorb®) are processed by high pressure and sintering above 1000 °C.

Sintering conditions were shown to have an impact on the mechanical behaviour of β-TCP ceramics (Wang *et al.*, 2004). Under 1300 °C, hardness and Young's modulus were found to increase with the sintering temperature, but above this value, a drop in Young's modulus was observed. Around 1400 °C, part of the β-TCP in the ceramic was also found to transform into α-TCP, which contributed to a decrease in Young's modulus above this temperature. Raynaud *et al.* (1999) pointed out the importance of precise determination of the Ca/P ratio in order to control the ceramic fracture strength. Varma and Sureshbabu (2001) observed an oriented growth of β-TCP crystals at the surface of the sintered body and important differences in grain sizes between the surface and the bulk.

Non-conventional sintering techniques, such as spark plasma sintering (SPS), have been proposed to sinter am-TCP and β-TCP (Drouet *et al.*, 2006).

Biphasic calcium phosphate (BCP) ceramics with different HA/β-TCP ratios can be prepared by mechanical mixing and co-sintering of HA and β-TCP powders in desired quantities or by chemical methods producing calcium-deficient apatites (CDA: $Ca_{10-x}(HPO_4)_x(PO_4)_{6-x}(OH)_{2-x}$). These processes are reported in Chapter 17. α- and β-TCP biphasic ceramics with a controlled α to β ratio can be prepared by reactive sintering of hydroxyapatite and dicalcium phosphate mixtures impregnated either with Mg-acetate or Mg-nitrate solution stabilising the β-TCP phase (Famery *et al.*, 1994).

Several methods to prepare macroporous TCP-based bioceramics with interconnected pores ranging between 150 and 400 μm in diameter allowing cell seeding and/or migration, vascularisation and bone ingrowth throughout the ceramic and also control of bone substitute resorption, have been developed. Three main processes are used: (a) replicas of porous structure (polymeric sponge or coral exoskeleton), (b) introduction of porogenous substances which leave macropores by heating at a temperature below 200 °C (naphthalene or organic polymer) and (c) production of gas bubbles (hydrogen peroxide and carbon dioxide). Bohner reported the preparation of macroporous β-TCP blocks using α-TCP-oil emulsions incubated for 24 h, then washed with ether, dried and finally sintered at 1250 °C (Bohner, 2001). Macropore size can be modified by the emulsifier concentration without modifying the total pore volume and the microporosity of the ceramics; however, this method had to be optimised to improve the inter-

connectivity of the macropores. Porous α-TCP ceramics can be prepared using a replica of porous structure and conventional sintering of β-TCP above 1100 °C. β-TCP powder was mixed with an equivalent mass of potato starch and water was added to obtain a viscous slurry. A polyurethane sponge with a continuous 1000 µm diameter pore structure was then dipped into this slurry and dried at 60 °C for 1 h. Finally, several thermal treatments at 1000 °C for 3 h, and 1400 °C for 12 h, were then followed by cooling to room temperature at the natural cooling rate of the furnace (Kitamura *et al.*, 2004).

Macroporous TCP bioceramics generally exhibit low resistance to compression. This is roughly related to their porosity. Their weak compressive strength does not allow their direct use in load-bearing applications. The pore volume rarely exceeds 50% (Sous *et al.*, 1998), but can occasionally reach 80%; in addition to the mechanical behaviour, it determines the rate of resorption and cellular rehabitation. β-TCP ceramics are fabricated and commercialised in several countries under different names (Biosorb®, Calciresorb®, etc.).

Metsger *et al.* (1999) reported a comparative study on the mechanical properties of porous tricalcium phosphate and HA porous ceramics (10–50% of total volume porosity). Even if the type of TCP, a commercial tricalcium phosphate, is not specified in this study (probably β-TCP), the overall mechanical properties of porous TCP ceramics are better than those of HA ceramics: for total volume of porosity of 50%, the compressive strength is 13 MPa, Young's modulus 1.6 GPa and toughness 0.077 J/cm^3 for TCP ceramics; extrapolation to full density gives values of 315 MPa, 21 GPa and 2.3 J/cm^3 respectively (Metsger *et al.*, 1999).

15.5.2 Tricalcium phosphate-based cements

Several cement formulations contain TCP phases. One may distinguish active phases whose hydrolysis determines the setting reaction (α-TCP and am-TCP) and passive phases used for their nucleating ability (ap-TCP) or as providers of Ca and P ions (β-TCP, especially in brushite cements). Generally, the cement paste is obtained by mixing one or several calcium phosphate powders (solid phase) with an appropriate amount of aqueous solution (liquid phase). The wet paste is then usually placed at 37 °C for setting and hardening involving dissolution and precipitation of less soluble Ca-P phase(s). Moreover, the maturation of cement *in vitro* in an atmosphere saturated with water is an important parameter to study cements in conditions close to those occurring *in vivo*, i.e. in contact with biological tissues/fluids.

Different types of cements including TCP phases may be distinguished depending on the kind of setting reaction involved (see Table 15.4) (Bohner

et al., 2005). Owing to their rapid conversion into apatite, once placed in an aqueous medium, α-TCP and am-TCP are involved as powder components in several cement compositions. Most of the commercialised cements are microporous with a porosity around 50% and pore size less than a few μm. Thus, they cannot allow cell rehabitation.

The highest mechanical properties of cements are obtained after a hardening period that is usually distinct from the setting period. However, the compressive strength is generally low. It depends on the preparation conditions (liquid/solid ratio, etc.) and probably on cement uses. In this sense, the mechanical properties determined in strictly controlled conditions by the manufacturers might differ from those really observed in a clinical situation. The compressive strength of various commercialised TCP-based cements is reported in Table 15.4.

Most cements rely on an acid–base reaction between calcium phosphate phases. The acidic phase can be either a soluble Ca-P salt such as monocalcium phosphate monohydrate (MCPM: $Ca_2(H_2PO_4)_2$, H_2O) or even phosphoric acid (H_3PO_4), or an insoluble Ca–P salt at physiological pH such as DCPD. The alkaline phase is generally tetracalcium phosphate (TTCP: $Ca_4(PO_4)_2O$), but other phases such as calcium carbonate or even calcium oxide have also been proposed.

The setting reaction in these cements is often complex and difficult to control as each of the constituents can hydrolyse separately, in aqueous media, into apatite. The pH of the paste can undergo strong variations, from acidic to alkaline, during the setting time. The particle size is a critical parameter which determines the setting characteristics of the cement. Generally, the setting reaction involves several intermediates such as DCPD and/or OCP (Hatim, 1998). A multitude of formulations may be proposed for these cements and they offer a wide range of possibilities and characteristics. From a thermodynamic point of view, the acid–base reaction is always exothermic, although the release of heat is generally much less than that of the well-known polymethylmethacrylate (PMMA) biomedical cements (Baroud *et al.*, 2006).

Monocomponent Ca-P cements are based on the fast hydrolysis of one calcium phosphate salt into apatite: am-TCP and α-TCP have been proposed (Ginebra *et al.*, 1997; Lee *et al.*, 2000). In order to achieve the short setting times needed for orthopaedic applications, the hydrolysis reactions have to be fast and the constituent Ca-P phases should be rather unstable. Generally, the rate of the hydrolysis reaction is determined by the temperature. For amorphous calcium phosphate, for example, an increase of temperature causes an increase in the rate of conversion into apatite nanocrystals. Thus, at 20 °C the paste does not harden and it is only at body temperature that fast hardening is achieved. Monocomponent cements induce less pH variation during setting and there is a direct conversion into an apatitic

phase. These cements can easily be injected (Knaack *et al.*, 1998; Tofighi *et al.*, 2001).

A third class of Ca–P cements has been developed. It involves the formation of unstable phases at physiological pH that transform into apatite after implantation. The most frequently encountered examples are cements leading to the formation of DCPD based on an acid–base setting reaction involving an initial mixture of β-TCP and monocalcium phosphate monohydrate (MCPM) (Mirtchi *et al.*, 1989). DCPD is an unstable Ca-P phase at neutral pH and transforms into apatite at physiological pH.

Recently, Grover and coworkers (2005) showed that the replacement of the MCPM component (acid orthophosphate) in a β-TCP–MCPM cement composition (DCPD cement) by pyrophosphoric acid retarded the cement setting and improved its mechanical properties (compressive strength around 9 MPa for cement stored at 37 °C). The presence of pyrophosphate ions also has an effect on cement microstructure: more densely packed irregularly shaped particles were observed compared to blade-like crystals of 10–20 μm in length usually formed in classical DCPD cements.

Nillson *et al.* (2002) reported the preparation of biphasic calcium phosphate cements associating apatite and calcium sulphate dihydrate (resorbable phase) with adaptable strength depending on the composition of the initial solid phase consisting of α-TCP and calcium sulphate hemihydrate. Other examples of biphasic cement compositions including TCP compounds have been reported (Mirtchi *et al.*, 1990; Ohura *et al.*, 1996). Bohner (2004) suggested a synergistic effect of the amount of calcium sulphate dihydrate powder in the solid phase and phosphate concentration in the liquid phase to control the setting time of α-TCP–water paste. Several studies have shown that the association of TCP-based cements with a natural macromolecule such as chitosan or gelatin modified the setting time and the mechanical properties of the cement (Bigi *et al.*, 2004).

The cement route is an interesting way to prepare bioresorbable scaffolds for bone tissue engineering at low temperature and appears as an alternative to traditional sintered porous hydroxyapatite ceramics. A two-step process involving foaming and subsequent hydrolysis of a α-TCP paste leading to a calcium-deficient hydroxyapatite porous scaffold has been reported (Almirall *et al.*, 2004). α-TCP powder with controlled particle size is mixed with 2% (w/w) hydroxyapatite powder which serves as a seed in the solid phase to enhance the nucleation of calcium-deficient hydroxyapatite during the setting reaction. This solid phase is then mixed with a hydrogen peroxide (foaming agent) aqueous solution and heated at 60 °C for 2 hours to allow the decomposition of H_2O_2 and thus the foaming of the paste. The as-prepared calcium-deficient hydroxyapatite scaffold combines interconnected macroporosity with high microporosity.

15.5.3 Composites

Several composites for bone substitution or repair, or bone tissue engineering involving TCP associated with synthetic or natural polymers/proteins have been studied, yet very few of them have been commercialised. Example include Duosorb®, a composite consisting of 60% β-TCP and 40% polylactic acid DL (PLDL), and MBCP gel®, an injectable composite consisting of BCP granules and a hydrosoluble silanised-HPMC (hydroxypropyl methylcellulose) polymer carrier (Daculsi *et al.*, 2003).

In most of the composites designed and studied, α- or β-TCP is involved as a filler to reinforce and/or confer bioactivity properties to natural or synthetic polymer materials. Most of the methods used to prepare such composites are based on liquid/solid or solid/solid mixing of organic and TCP components (Zhang and Zhang, 2001; Kikuchi *et al.*, 2004; Aunoble *et al.*, 2006; Matsuno *et al.*, 2006; Van Den Vreken *et al.*, 2006). Sanginario *et al.* (2006) reported the preparation of biodegradable benzyl ester of hyaluronic acid (HYAFF11)/α-TCP composite hydrogels by mixing HYAFF11 polymer in dimethylsulphoxide (DMSO) solution with α-TCP powder to obtain a homogeneous paste which is then placed in a mould for setting and finally immersed in ethanol for DMSO extraction. Varying the composition of (HYAFF11)/α-TCP composite hydrogels can lead to composites with a range of mechanical properties (Sanginario *et al.*, 2006). These mechanical properties vary strongly with time up to 96 h due to a setting and hardening reaction (hydrolysis of α-TCP). An increase of α-TCP filler proportion leads to more brittle behaviour of the composite (higher Young's modulus and lower maximum deformation and compressive strength).

Other α-TCP and degradable polyester (PLA– or PGA–ε-caprolactone copolymers) composites with 40 or 80% w/w of α-TCP filler have been studied and the α-TCP content rather than the type of polyester has been shown to influence the conversion rate of α-TCP and the crystallinity of the apatite formed (Van Den Vreken *et al.*, 2006). Higher α-TCP content resulted in slower conversion rates and higher crystallinity. Similar bioresorbable composites were prepared with β-TCP and PLGA-ε-caprolactone copolymer using a heat-kneading method (Kikuchi *et al.*, 2004). Aunoble *et al.* (2006) reported the preparation of a β-TCP/PLLA composite (β-TCP %w < 60) from a mixture of β-TCP particles and PLLA heated at 60 °C for 24 h and then processed by injection moulding to the desired shape and size.

A new composite cement comprising β-TCP as the main powder component (79.5% w/w) and three kinds of methacrylate monomer (methylmethacrylate (MMA), urethane dimethacrylate (UDMA) and tetrahydrofurfuryl methacrylate (THFMA) monomers) as the liquid component has been evaluated in rat tibiae. The presence of UDMA and THFMA, both of which

have hydrophilic and hydrophobic parts, should create a bridging effect between hydrophobic PMMA and hydrophilic β-TCP and thus allow higher loading of the cement containing β-TCP (50% w/w β-TCP) (Goto *et al.*, 2006). This study has shown that this new composite is a biocompatible and osteoconductive biomaterial with good mechanical properties (higher compressive strength: 125 MPa and bending modulus: 6 MPa, but lower bending strength: 50 MPa compared with that of PMMA bone cements).

β-TCP/collagen sponge composites have been prepared by mixing β-TCP granules with a telocollagen hydrochloride solution (0.2 g/mL) (Matsuno *et al.*, 2006). β-TCP/chitosan macroporous composite has also been studied (Zhang and Zhang, 2001). The Calciresorb®-collagen resorbable composite prepared with β-TCP granules (96% w/w of the composite) and collagen fibres (types I and III) from the skin of young bovines has been commercialised for several years now.

Owing to the difference in chemical behaviour of the polymer and the mineral parts of the composite once in contact with biological-like fluids, a faster degradation of the former can be observed, thus leading to a roughened surface exposing part of the mineral granules initially located underneath the surface of the composite. A modification of porosity also occurs during the composite degradation. The presence of the TCP phase was also found to reduce the acidity produced by the degradation of the polymer.

15.5.4 Coatings

TCP-based coatings can be processed by very different techniques ranging from high-energy processing (plasma-sprayed, pulsed laser deposition, etc.), mainly for high-temperature crystalline TCP-phase deposition (α- and/or β-TCP), to solution-mediated processing, mainly for deposition of low-temperature unstable TCP phases (am-TCP and/or ap-TCP).

High-energy processing

Currently, HA plasma spraying is the most common industrial process for enhancing the bioactivity of metallic implants (orthopaedic and dental implants) and for improving early bone–implant bonding. Tricalcium phosphates are present as secondary phases in plasma-sprayed HA coating mainly as α-TCP and β-TCP and amorphous calcium phosphate due to partial decomposition and melting of HA particles at very high temperatures which modify the chemical, mechanical and biological behaviour of the coating (Kweh *et al.*, 2002; Carayon and Lacout, 2003).

A comparative study between HA and TCP plasma-sprayed coatings on TA6V implanted in dog trabecular humerus bone revealed higher fixation, bone ingrowth and stability for HA coatings than for TCP coatings (Lind

et al., 1999). Biphasic HA-β-TCP coatings (around 70–30% respectively) with thickness ranging between 50 and 125 μm obtained by plasma spraying have been shown to enhance osseointegration (osteoconductivity, tight bond at the bone–coating interface and bone ingrowth) of titanium implants in the long run as well as after a short period of implantation (Daculsi, 1998; Thanner *et al.*, 1999; Tetsuya *et al.*, 2002; Stewart *et al.*, 2004). These results could be related to a synergistic effect of HA and β-TCP not yet fully understood. Bilayered calcium phosphate coatings (first layer of HA and second layer of BCP) deposited by plasma spraying have also been shown to enhance bone apposition at the early stages (Goyenvalle *et al.*, 2006).

Amorphous calcium phosphate or α- and β-TCP coatings of about 2 μm can be obtained by pulsed laser deposition on TA6V alloy at 25 °C for amorphous calcium phosphate coating and at 560 °C for α-TCP + β-TCP coating. The target is a pellet of HA powder (Clèries *et al.*, 1998, 2000). HA and α-TCP biphasic coating with different proportions of α-TCP uniformly distributed can also be obtained using this technique (Clèries *et al.*, 1998), which allows partial control of coating dissolution and degradation.

Electrostatic spray deposition (ESD) has been used for various TCP coatings of 0.5–2 μm thickness. This technique involved a calcium salt and phosphoric acid in organic solvent, a substrate heated at 300 °C, and an electrical potential between the spraying nozzle and the substrate ranging from 5.5 to 8 kV (Leeuwenburgh *et al.*, 2004). The Ca and P precursor concentration and the acidity of the precursor solution are parameters that control the type of Ca-P phase deposited.

Solution-mediated processing

Amorphous-like coatings seem to play an important role in the nucleation and adhesion of biomimetic coatings on titanium implants (Barrere *et al.*, 2004). Although the composition of such layers is not accurately known, they could be close to am-TCP and ap-TCP. Several deposition processes of poorly crystalline apatites using SBF (simulated body fluid) or more supersaturated solutions have been proposed (Li, 2003a; Jalota *et al.*, 2007). The formation of apatitic coatings with a composition close to ap-TCP has been reported. These coatings exhibit different biological performances depending on their morphology (Chou *et al.*, 2005). Recently, Hosaka *et al.* (2005) showed that *β*-TCP coating prepared by generating an electrical discharge in a modified SBF (m-SBF) solution enhanced adsorption and crosslinking of collagen from subsequent cathodic polarization. This *β*-TCP-collagen coating on a titanium implant is claimed to exhibit better *in vitro* behaviour than hydroxyapatite-collagen coating. To avoid the use of super-

saturated solutions in industrial processing, other methods involving the slow hydrolysis of apatite precursors, such as am-TCP, first deposited on the metallic surface, have been developed (Cazalbou *et al.*, 2002).

15.6 Biological properties of TCP

15.6.1 SBF testing

Tests in SBF (Kokubo and Takodama, 2006) have become a prerequisite to the prediction of *in vivo* behaviour of orthopaedic biomaterials. In the case of TCPs, however, SBF testing might lead to very different results depending on the variety of TCP and the testing conditions. SBF at 37 °C is supersaturated with regard to β-TCP, and probably ap-TCP; however, it is undersaturated with respect to α-TCP and am-TCP. Concerning β-TCP and ap-TCP, they have been shown to favour the formation of a carbonate-apatite crystal layer in SBF. Although this ability is generally found to be rather poor (Ioku *et al.*, 2000; Xin *et al.*, 2005) in the case of β-TCP, it appears more prominent in ap-TCP than in stoichiometric hydroxyapatite (Yasuda *et al.*, 2006). These observations can probably be related to the nucleation abilities of these two TCPs: ap-TCP especially exhibits a large specific surface area most probably with many surface sites able to nucleate apatite and thus may induce epitaxial growth of carbonate-apatite from SBF. This is not the case for β-TCP which has been shown to be a poor nucleator for apatite (Nancollas and Wefel, 1976). Furthermore, the supersaturation of SBF with regard to β-TCP and ap-TCP is much lower than that relative to stoichiometric hydroxyapatite. Thus, the amount of Ca-P deposits which can form on TCPs in closed systems should be lower than that formed on stoichiometric hydroxyapatite. On the contrary, α-TCP and am-TCP should dissolve in SBF, and as unstable phases, they might undergo a hydrolysis reaction, transforming into apatite, or even into metastable phases more soluble than apatite but with a faster crystal growth rate, like OCP (Xin *et al.*, 2005).

For these TCPs, the formation of carbonated apatite (or even OCP in a few cases) often observed in SBF does not seem related to a nucleation ability but results essentially from the aqueous conversion of these unstable phases into a more stable phase, mainly apatite and occasionally OCP. In the presence of these unstable TCPs and a nucleating surface such as hydroxyapatite, the formation of apatite is even stronger as growing crystal nuclei are constantly fed by the dissolution of the most soluble TCPs (Hirakata *et al.*, 2003). Such combinations can be used in self-setting Ca–P cements (Lee *et al.*, 2000).

Considering the prediction of biological activity from SBF testing, the role of these various formation processes, which probably produce

neo-formed carbonated apatite phases with different characteristics, probably needs to be taken into consideration.

15.6.2 Cell cultures on TCPs

Many cell culture studies on TCP ceramics have been published involving osteoblasts, osteoclasts and bone cell precursors. These studies have often been conducted on poorly characterised samples (grain size, impurities, microstructure and surface roughness were considered). They dealt with different cell lines and different methods. Therefore, it is not possible to correlate the rather large data sets and to link the observations with the material physicochemical parameters. In addition, alterations of TCP surface ceramics in cell culture media have been reported that are capable of modifying cell behaviour during the course of the experiments. A follow-up of the mineral composition of the cell culture medium and an analysis of the ceramic surface after cell culture could probably help clarify some contradictory results.

Osteoblasts and osteoblast-like cell culture

It has been generally observed that TCP ceramics are not cytotoxic on contact with extract fluids. In the presence of TCP powders, which could be released from cement powders or from resorbing ceramics, osteoblast behaviour depends strongly on the amount of particles and particle size. Massive amounts of small particles impair cell growth (Sun *et al*., 1997; Pioletti *et al*., 2000) and may cause cell death, whereas small amounts of α-TCP powders have been shown to favour osteoblast proliferation and expression possibly related to the release of mineral ions, especially calcium and phosphate ions acting directly on cells (Ehara, 2003). A few reports indicate cell death on contact with *β*-TCP ceramics (Rice *et al*., 2003; John *et al*., 2003) which has been related to the formation of intramitochondrial Ca–P crystals, causing mitochondria lysis and subsequent cell death (Rice *et al*., 2003). However, the occurrences of these events have been rarely reported and could possibly be due to surface erosion of the ceramics. Osteoblast cell cultures on composite samples (biphasic calcium phosphates, TCP and collagen or polymers) generally give better results than on raw materials. Ion-substituted TCPs (Zn–*β*-TCP, Mg–*β*-TCP and Si–α-TCP cements) have also been claimed to improve osteoblast attachment and proliferation (Camire *et al*., 2006) sometimes related to an optimal ion substitution ratio (Ito *et al*., 2000) compared with pure TCP.

Considering ap-TCP coatings, osteoblast behaviour has been shown to be related to the coating morphology. According to Chou *et al*. (2005), early coatings formed of microspheres (Ca/P = 1.27) may induce cell death,

whereas mature coatings formed of large platelet crystals (Ca/P = 1.48) favour the expression of osteogenic markers. It thus appears that subtle changes in the apatite microenvironment may induce very different cell responses and could explain discrepancies between reported data.

Osteoclasts and osteoclast-like cell cultures

Only very few data have been published on osteoclast behaviour. Some authors failed to observe any activity on the surface of α- and β-TCP despite alterations in the calcium and phosphate concentration in cell culture medium (Doi *et al*., 1999). Specifically, possible reasons for this failure could be ion release and the probable existence of an alkaline surface reaction related to the surface hydrolysis, inhibiting osteoclast activity. In other cases, however, osteoclast attachment and resorption activity have been described, evidencing a much stronger degradation of β-TCP than HA (De Bruijn *et al*., 1994; Monchau *et al*., 2002), related to the rate of dissolution of these calcium phosphates. Such data seem to agree with *in vivo* studies. Recently, a study of chemokine expression involving osteoclast cells cultured on different substrates evidenced a specific interaction on Ca-P substrates compared to plastic (Grassi *et al*., 2003).

Bone cell progenitors

The possible use of α-, β- and Zn-containing β-TCP as scaffolds for bone tissue engineering has been investigated using bone marrow cells (Dong *et al*., 2002; Ikeuchi *et al*., 2003; Niemeyer *et al*., 2004). All of them have been shown to exhibit good biological properties in favouring cell adhesion, multiplication and differentiation. Implants seeded with precursor cells have shown the ability to generate bone tissue in non-osseous sites (Kasten *et al*., 2005) and the rate of bone healing has been shown to be higher using cell-seeded ceramics.

15.6.3 *In vivo* implantations

The numerous *in vivo* studies which have been performed agree generally on several points.

TCP degradation rates were roughly related to TCP dissolution rates, including structural and microstructural parameters such as crystal size, particle size and porosity of the ceramics. Thus, α-TCP has been shown to be more easily resorbed *in vivo* than β-TCP (Yamada *et al*., 2007). Similarly, Zn- and Mg-substituted β-TCP generally exhibit a lower resorption rate *in vivo* related to the effects of the substitutions on solubility (Ito *et al*., 2002b). However, it should be noted that the correlation between dissolution rates

and resorption rates *in vivo* is not always verified and in some cases similar degradation rates have been found for α- and β-TCP (Merten *et al*., 2001; Wiltfang *et al*., 2002). Parameters other than the crystal structure are involved in bioresorption of TCP ceramics (grain size, porosity and grain boundaries), and they are not always taken into consideration. The grain size, especially, may vary between the surface and the bulk (Varma and Sureshbabu, 2001) and thereby alter the rate of resorption. In addition, hydrolysis into less soluble compounds may occur rapidly *in vivo*, especially for am- and α-TCP, thus affecting their biodegradation.

Several authors (Wu *et al*., 1992; Basle *et al*., 1993) have suggested two resorption mechanisms of TCP ceramics: (i) classical degradation involving osteoclast-like cells (TRAP positive) attached to the ceramic surface, which dig resorption pits in the ceramic, and (ii) debris disaggregation and phagocytosis by multinucleated giant cells (TRAP negative). This observation suggests a dependence of ceramic degradation on its nature and sintering conditions (or porosity): samples with high solubility rates and presenting sintering defects (residual porosity and poor grain boundaries) could more easily release particles and favour multinucleated giant-cell types of resorption, whereas well-sintered samples with lower solubility rates would mainly be resorbed by osteoclast-like cells, in a similar manner to bone during natural remodelling. These degradation processes related to sintering quality could explain some discrepancies among reported data.

The relationship between TCP ceramics and the formation of bone tissue seems more complex. The analysis of implant interfaces has revealed that there was not a clear formation of an apatite intermediate layer on the surface of β-TCP (Kotani *et al*., 1991, Fujita *et al*., 2003). Generally, bone formation is observed on degraded β-TCP and α-TCP implant surfaces on contact with the materials (Kihara *et al*., 2006) and sometimes at a distance from the ceramic surface (Neo *et al*., 1998). This behaviour may be related to the resorbability of TCP implants which could be uncoupled to bone formation, unlike what is observed during bone remodelling, possibly because of the involvement of two resorption processes and the inability of TCP to promote the nucleation of apatite.

It should be noted that α-TCP and am-TCP may transform and hydrolyse *in vitro* in physiological-like conditions (pH, calcium and phosphate concentrations). However, for β-TCP and ap-TCP this is not possible. Thus, a local decrease of pH (and/or less likely of calcium and phosphate concentrations), possibly related to post-operative trauma, might explain the observed surface degradation.

In some cases, osteoinductive behaviour of raw β-TCP has been suggested (Yuan *et al*., 2001). However, other authors have reached opposite conclusions. Adjunction of growth factors such as BMP (bone morphoge-

netic protein) to TCP ceramics determines osteoinductive behaviour (Wu *et al*., 1992).

Specific aspects of biological behaviour related to implant nature

As for many other biomaterials, TCP behaviour depends on the nature of the implants.

Considering bulk materials, ceramics based on α- and *β*-TCP behave differently from cements (Frayssinet *et al*., 1998). In the case of ceramics, bone formation occurs preferentially on, or close to, the implant surface adjacent to the bone tissue. The implant is then progressively degraded and replaced by the growing bone, more or less regularly from the surface to the interior (this process is sometimes called 'centrifugal integration'). In the case of cements, however, bone trabeculae are often seen growing in the material, leading to an irregular surface ('centripetal integration'). When implantation of coarse, loose TCP ceramic particles in blood clot is performed, for bone augmentation for example, bone integration also generally appears 'centripetal'. These processes are probably related to loose particle binding and cement porosity compared with well-sintered ceramics and the frequent involvement of macrophages and multinucleated giant cells in the case of loose particles. The ceramic bone-integration process depends strongly on ceramic sintering quality, but occasionally centripetal integration may also be observed (Merten *et al*., 2001) in the case of association with disaggregation and debris formation.

Especially for α-TCP and am-TCP, the main difficulty is their evolution capabilities *in vivo*. Although these capabilities are rarely investigated, they probably have a strong impact on their biological behaviour. In addition to histological investigations, physicochemical characterisation of retrieved implants should be performed. Similar observations should also be noted in the case of cements. Although hardening reactions are generally correctly described *in vitro*, the alterations of these reactions *in vivo* are not well known, especially following contact of the cement paste with body fluids, and diffusion of mineral ions and/or organic additives from the cement to adjacent tissues.

15.7 Recent developments

The most recent developments are aimed at improving the biological properties of TCP compounds. As in the case of other Ca–P materials, three main areas of development have been investigated: ion substituted-TCPs, associations of TCPs with active molecules, and associations of TCPs with cells for tissue engineering applications.

Several types of ion-substituted TCPs have been synthesised and tested *in vitro* and *in vivo*: Mg-, Sr- and Zn-containing β-TCP, and Si-containing α-TCP. Some of these compounds have shown interesting properties and it is probable that they will undergo industrial development within the next few years. Some of the main advantages of these compounds are their low cost, their stability during the sterilisation procedure, and their excellent storage properties. Ag-containing TCPs have also been proposed for their antibacterial properties.

Several associations of TCP ceramics or cements with growth factors or active molecules have been proposed (Urist *et al*., 1984; Wu *et al*., 1992; Laffargue *et al*., 1999; Niedhart *et al*., 2003; Li *et al*., 2003; Jung *et al*., 2006). Associations were made directly with ceramics or granules and implied different growth factors. The increased potential of BMP activity when associated with β-TCP has been suggested by Urist *et al*. (1984), but has not been confirmed since then. TGF-β associated with β-TCP has also been reported to favour ossification (Okuda *et al*., 1995; Lind *et al*., 2001), although negative results have been reported using TGF-β3 in sheep and baboons (Steffen *et al*., 2001). Degradation of growth factors (rh-bFGF, rh-VEGF and rxBMP-4) on α-TCP ceramics has been reported (Ziegler *et al*., 2002). In addition to direct association with ceramic components, growth factors and active molecules have been delivered from composite compounds containing TCP, seemingly without any determinant advantage. Some associations involving BMP are in a pre-development stage and they are used in clinical programs. Despite a high cost and uncertainties on stability, they will probably appear on the market very soon, especially in the case of aged patients for whom bone repair potential is notably impaired. A difficulty associated with BMP-containing TCP compounds is the need for high concentration of growth factors, much higher than physiological doses, and the lack of efficiency of the actual associations. There is probably room for progress in the optimisation of growth factor release and control and also probably in considering the associations of several active molecules with complementary and/or synergistic activities.

Because of their resorbability, porous TCP ceramics have been successfully used in bone tissue engineering. Despite the high cost of these techniques, they are already available for the repair of critical-size defects in bone tissue, but only on an experimental basis.

15.8 Conclusion

The main characteristic of all TCP family members is their biological resorbability.

β-TCP is one of the oldest industrial synthetic bone substitute materials. However, it has been involved in several recent developments aimed at

improving its biological efficiency and, to a lesser extent, its mechanical properties. Ion-substituted β-TCP especially offers interesting low-cost possibilities and might compete in the future with pure β-TCP. Other TCP family members have undergone industrial development, especially in the formulation of self-setting cement pastes mainly involving α-TCP and am-TCP. These materials may probably still be improved and could be of special interest in association with biologically active molecules such as growth factors. The use of high-temperature crystalline TCPs in metallic prosthesis coating seems more limited owing to their lack of surface reactivity and their degradability; however, TCPs could be used as intermediate phases in 'reactive' coating involving a transformation of the coating material at the time of (or prior to) implantation. The association of TCPs with polymers in composite materials modifies mechanical properties and provides a source for calcium and phosphate ions which could determine bioactivity and remineralisation processes. Therefore, they will probably continue to develop in the future.

15.9 Acknowledgement

The authors would like to thank Transtyler founder Dr Andrew Kovacs for proofreading in English.

15.10 References

Aimanova O J, Legeros R Z, Sinyayev V A (2005), 'Antimicrobiologic properties of hydrated amorphous calcium phosphates containing silver', *Key Eng Mater*, **284–286**, 439–442.

Albee F H, Morrison H F (1920), 'Studies in bone growth, triple calcium phosphate as a stimulus to osteogenesis', *Ann Surg*, **71**, 32–36.

Almirall A, Larrecq G, Delgado J A, Martinez S, Planell J A, Ginebra M P (2004), 'Fabrication of low temperature macroporous hydroxyapatite scaffolds by foaming and hydrolysis of an α-TCP paste', *Biomaterials*, **25**, 3671–3680.

Aunoble S, Clément D, Frayssinet P, Harmand M F, Le Huec J C (2006), 'Biological performance of a new β-TCP/PLLA composite material for applications in spine surgery: *in vitro* and *in vivo* studies', *J Biomed Mater Res*, **78**, 416–422.

Baig A A, Fox J L, Wang Z, Higuchi W I, Miller S C, Barry A M, Otsuka M (1999), 'Metastable equilibrium solubility behavior of bone mineral', *Calcif Tissue Int*, **64**, 329–339.

Banu M (2005), 'Mise en forme d'apatites nanocristallines: céramiques et ciments', *PhD thesis n°2228*, Institut National Polytechnique, Toulouse, France.

Baroud G, Swanson T, Steffen T (2006), 'Setting properties of four acrylic and two calcium phosphate cements used in vertebroplasty', *J Long Term Eff Med Implants*, **16**, 51–59.

Barrere F, Snel M M E, van Blitterswijk C A, de Groot K, Layrolle P (2004), 'Nanoscale study of the nucleation and growth of calcium phosphate coating on titanium implants', *Biomaterials,* **25**, 2901–2910.

Basle M F, Rebel A, Grizon F, Daculsi G, Passuti N, Filmon R (1993), 'Cellular response to calcium phosphate ceramics implanted in rabbit bone', *J Mater Sci Mater Med,* **4**, 273–280.

Belgrand P (1993), 'Apport de la RMN; de l'état solide à l'étude de biocéramiques de phosphate tricalcique et de pathologies osseuses', *Thesis*, Université Paris VI, France.

Betts F, Posner A F (1974a), 'Structural model for amorphous calcium phosphate', *Trans Am Crystal Assoc*, **10**, 73–84.

Betts F, Posner A F (1974b), 'X-ray radial distribution study of amorphous calcium phosphate', *Mater Res Bull*, **9**(3), 353–360.

Bigi A, Foresti E, Gandolfi M, Gazzano M, Roveri N (1997), 'Isomorphous substitution in β-tricalcium phosphate: the different effects of zinc and strontium' *J Inorg Biochem*, **66**, 259–265.

Bigi A, Bracci B, Panzavolta S (2004), 'Influence of gelatine on the setting properties of α-tricalcium phosphate cement', *Key Eng Mater*, **254–256**, 229–232.

Bohner M (2001), 'Calcium phosphate emulsions: possible applications', *Key Eng Mater*, **192–195**, 765–768.

Bohner M (2004), 'New hydraulic cements based on α-tricalcium phosphate–calcium sulfate dihydrate mixtures', *Biomaterials*, **25**, 741–749.

Bohner M, Theiss F, Apelt D, Hirsiger W, Houriet R, Rizzoli G, Gnos E, Frei C, Auer J A, von Rechenberg B (2003), 'Compositional changes of a dicalcium phosphate dihydrate cement after implantation in sheep', *Biomaterials*, **24**, 3463–3474.

Bohner M, Gbureck U, Barralet J E (2005), 'Technological issues for the development of more efficient calcium phosphate bone cements: a critical assessment', *Biomaterials*, **26**, 6423–6429.

Boskey A L, Posner A S (1974),'Magnesium stabilization of calcium amorphous phosphate: a kinetic study', *Mat Res Bull*, **9**, 907–916.

Brown W E, Chow L C (1987), 'A new calcium phosphate water-setting cement', *In: Cement Research Progress,* Brown P (editor), Westerville OH: American Ceramic Society, 351–379.

Camire C L, Saint-Jean S J, Mochales C, Nevsten P, Wang J-S, Lidgren L, McCarty I, Ginebra M-P (2006), 'Material characterization and in vivo behavior of silicon substituted α-tricalcium phosphate cement', *J Biomed Mater Res B*, **76B**, 424–431.

Carayon M T, Lacout J L (2003), 'Study of the Ca/P atomic ratio of the amorphous phase in plasma-sprayed hydroxyapatite coatings', *J Solid State Chem*, **172**(2), 339–350.

Cazalbou S, Combes C, Rey C (2002), 'Procédé permettant de recouvrir à basse température des surfaces par des phosphates apatitiques nanocristallins à partir d'une suspension aqueuse de phosphate amorphe', *Patent no. FR0209514.*

Chou Y-F, Huang W, Dunn J C Y, Miller T A, Wu B M (2005), 'The effect of biomimetic apatite structure on osteoblast viability, proliferation, and gene expression', *Biomaterials*, **26**, 285–295.

Clement D, Tristan J M, Hamad M, Roux P, Heughebaert J C (1989), 'Etude de la substitution Mg^{2+}/Ca^{2+} dans l'orthophosphate tricalcique β', *J Solid State Chem*, **78**, 271–280.

Clèries L, Fernandez-Pradas J M, Sardin G, Morenza J L (1998), 'Dissolution behaviour of calcium phosphate coatings obtained by laser ablation', *Biomaterials*, **19**, 1483–1487.

Clèries L, Martinez E, Fernandez-Pradas J M, Sardin G, Esteve J, Morenza J L (2000), 'Mechanical properties of calcium phosphate coatings deposited by laser ablation', *Biomaterials*, **21**, 967–971.

Constantz B R, Ison I C, Fulmer M T, Poser R D, Smith S T, VanWagoner M, Ross J, Goldstein S A, Jupiter J B, Rosenthal D I (1995), 'Skeletal repair by *in situ* formation of the mineral phase of bone', *Science*, **267**, 1796–1798.

Daculsi G (1998), 'Biphasic calcium phosphate concept applied to artificial bone, implant coating and injectable bone substitute', *Biomaterials*, **19**, 1473–1478.

Daculsi G, Laboux O, Malard O, Weiss P (2003), 'Current state of the art of biphasic calcium phosphate bioceramics', *J Mater Sci Mater Med*, **14**, 195–200.

De Bruijn J D, Bovell Y P, Van Blitterswijk C A (1994), 'Osteoblast and osteoclast responses to calcium phosphates', *Bioceramics 7*, Pergamon/Elsevier, Oxford, UK, 293–298.

Destainville A, Champion E, Bernache-Assollant D, Laborde E (2003), 'Synthesis, characterization and thermal behavior of apatitic tricalcium phosphate', *Mater Chem Phys*, **80**, 269–277.

Dickens B, Schroeder L W, Brown W E (1974), 'Crystallographic studies of the role of Mg as a stabilizing impurity in β-$Ca_3(PO_4)_2$. I. The crystal structure of pure β-$Ca_3(PO_4)_2$', *J Solid State Chem*, **10**, 232–248.

Doi Y, Iwanaga H, Shibutani T, Moriwaki Y, Iwayama Y (1999), 'Osteoclastic response to various calcium phosphates in cell culture', *J Biomed Mater Res*, **47**, 424–433.

Dong J, Uemura T, Shirasaki Y, Tateishi T (2002), 'Promotion of bone formation using highly pure porous beta-TCP combined with bone marrow-derived osteoprogenitor cells', *Biomaterials,* **23**, 4493–4502.

Dornhoffer J, Simmons O (2003), 'Canal wall reconstruction with Mimix hydroxyapatite cement: results in an animal model case study', *Laryngoscope*, **113**, 2123–2128.

Drouet C, Largeot C, Raimbeaux G, Estournès C, Dechambre G, Combes C, Rey C (2006), 'Bioceramics: spark plasma sintering (SPS) of calcium phosphates', *Adv Sci Tech*, **49**, 45–50.

Ducheyne P, Radin S, King L (1993), 'The effect of calcium phosphate ceramic composition and structure on *in vitro* behavior. I. Dissolution', *J Biomed Mater Res*, **27**, 25–34.

Eanes E D (1970), 'Thermochemical studies on amorphous calcium phosphate', *Calcif Tissue Res*, **5**(2), 133–145.

Eanes E D (1998), 'Amorphous calcium phosphate: thermodynamic and kinetic consideration', In: *Calcium Phosphates in Biological and Industrial Systems*, Amjad Z (editor), Boston: Kluwer Academic Publishers, 21–39.

Eanes E D (2001), 'Amorphous calcium phosphate', In: *Octacalcium phosphate*, Chow L C and Eanes E D (editors); Monogr Oral Sci, Whitford G M (Ed.), Karger, Basel, **18**, 130–147.

Eanes E D, Meyer J L (1977), 'The maturation of crystalline calcium phosphates in aqueous suspensions at physiological pH', *Calcif Tissue Res*, **23**, 259–269.

Ehara A, Ogata K, Imazato S, Ebisu S, Nakano T, Umakoshi Y (2003), 'Effects of α-TCP and TetCP on MC3T3-E1 proliferation, differentiation and mineralization', *Biomaterials,* **24**, 831–836.

Ekholm M, Hietanen J, Tulamo R M, Muhonen J, Lindqvist C, Kellomaki M, Suuronen R (2006), 'The copolymer of epsilon-caprolactone-lactide and tricalcium phosphate does not enhance bone growth in mandibular defect of sheep', *J Mater Sci Mater Med*, **17**, 139–145.

Elliott J C (1994), *Structure and Chemistry of the Apatites and Other Calcium Orthophosphates*, Studies in Inorganic Chemistry, Amsterdam: Elsevier Science BV, 18.

Famery R, Richard N, Boch P (1994), 'Preparation of α- and β-tricalcium phosphate ceramics, with and without magnesium addition', *Ceramics Int*, **20**(5), 327–336.

Fowler B O, Kuroda S (1986), 'Changes in heated and laser-irradiated human tooth enamel and their probable effects on solubility', *Calcif Tissue Int*, **38**, 197–208.

Frayssinet P, Gineste L, Rouquet N (1998), 'Osseointegration of two different types of calcium phosphate materials: ceramics and ionic cements', *Morphologie*, **82**, 3–7.

Frayssinet P, Roudier M, Lerch A, Ceolin J L, Deprès E, Rouquet N (2000), 'Tissue reaction against a self-setting calcium phosphate cement set in bone or outside the organism', *J Mater Sci Mater Med*, **11**, 811–815.

Fujita R, Yokoyama A, Nodasaka Y, Kohgo T, Kawasaki T (2003), 'Ultrastucture of ceramic–bone interface using hydroxyapatite and beta-tricalcium phosphate ceramics and replacement mechanism of beta-tricalcium phosphate in bone', *Tissue Cell*, **35**, 427–440.

Ginebra M P, Fernandez E, De Maeyer E A, Verbeeck R M, Boltong M G, Ginebra J, Driessens F C, Planell J A (1997), 'Setting reaction and hardening of an apatitic calcium phosphate cement', *J Dent Res*, **76**, 905–912.

Goto K, Shinzato S, Fujibayashi S, Tamura J, Kawanabe K, Hasegawa S, Kowalski R (2006), *J Biomed Mater Res,* **78**, 629–637.

Govaerts J (1954), 'Isotopic exchange and the structure of tricalcium phosphate', *Anales Real Soc Espan Fis y Quim*, **50B**, 259–274.

Goyenvalle E, Aguado E, Nguyen J M, Passuti N, Le Guehennec L, Layrolle P, Daculsi G (2006), 'Osteintegration of femoral stem prostheses with a bilayered calcium phosphate coating', *Biomaterials*, **27**, 1119–1128.

Grassi F, Piacentini A, Cristino S, Toneguzzi S, Cavallo C, Facchini A, Lisignoli G (2003), 'Human osteoclast express different CXC chemokines depending on cell culture substrate: molecular and immunocytochemical evidence of high levels of CXCL 10 and CXCL 12', *Histochem Cell Biol*, **120**, 391–400.

Greenfield D J, Eanes E D (1972), 'Formation chemistry of amorphous calcium phosphates prepared from carbonate containing solutions', *Calcif Tissue Res*, **9**, 152–162.

Gregory T M, Moreno E C, Patel J M, Brown W E (1974), 'Solubility of β-$Ca_3(PO_4)_2$ in the system $Ca(OH)_2$-H_3PO_4-H_2O at 5, 15, 25, and 37 °C', *J Res Natl Bur Stand, 78A*, 667–674.

Grover L M, Gbureck U, Young A M, Wright A J, Barralet J E (2005), 'Temperature dependent setting kinetics and mechanical properties of β-TCP-pyrophosphoric acid cement', *J Mater Chem*, **15**, 4955–4962.

Grynpas M D, Bonar L C, Glimcher M J (1981), 'On the question of amorphous tricalcium phosphate in bone mineral', *Developments Biochem*, **22**, 279–283.

Hatim Z, Frèche M, Kheribech A, Lacout J L (1998), 'The setting mechanism of a phosphocalcium biological cement', *Ann Chim Sci Mat*, **23**, 65–68.

Heughebaert J C (1977), 'Contribution à l'étude de l'évolution des orthophosphates de calcium précipités amorphes en orthophosphates apatitiques', *Thesis*, Institut National Polytechnique, Toulouse, France.

Heughebaert J C, Montel G (1982), 'Conversion of amorphous tricalcium phosphate into apatitic tricalcium phosphate', *Calcif Tissue Int*, **34**, S103-S108.

Hirakata L M, Kon M, Asaoka K (2003), 'Evaluation of apatite ceramics containing alpha-tricalcium phosphate by immersion in simulated body fluid', *Biomed Mater Eng*, **13**, 247–259.

Holt C, Van Kemenade M J J M, Nelson L S, Hukins D W L, Bailey R T, Harries J E, Hasnain S S, De Bruyn P L (1989), 'Amorphous calcium phosphates prepared at pH 6.5 and 6.0', *Mater Res Bull*, **24**(1), 55–62.

Horch H H, Sader R, Pautke C, Neff A, Deppe H, Kolk A (2006), 'Synthetic pure-phase beta-tricalcium phosphate ceramic granules (Cerasorb®) for bone regeneration in the reconstructive surgery of the jaws', *Int J Oral Maxillofac Surg*, **35**, 708–713.

Hosaka M, Shibata Y, Miyasaki T (2005), 'Preliminary β-tricalcium phosphate coating prepared by discharging in a modified body fluid enhances collagen immobillization onto titanium', *J Biomed Mater Res B Appl Biomater*, **78**, 237–242.

Ikeuchi M, Ito A, Dohi Y, Ohgushi H, Shimaoka H, Yonemasu K, Tateishi T (2003), 'Osteogenic differentiation of cultured rat and human bone marrow cells on the surface of zinc-releasing calcium phosphate ceramics', *J Biomed Mater Res*, **67A**, 1115–1122.

Ioku K, Toya H, Fujimori H, Goto S (2000), '*In vitro* reaction for calcium phosphate bioceramics', *Korean J Ceram*, **6**, 214–218.

Ito A, Ojima K, Naito H, Ichinose N, Tateishi T (2000), 'Preparation, solubility and cytocompatibility of zinc-releasing calcium phosphates ceramics', *J Biomed Mater Res*, **50**, 178–183.

Ito A, Kamo M, Ichinose N, Sogo Y, Sakurai T (2002a) 'Fabrication and *in vitro* biocompability of zinc-containing α-tricalcium phosphate', *Key Eng Mater*, **218–220**, 183–186.

Ito A, Kawamura H, Miyakawa S, Layrolle P, Kanzaki N, Treboux G, Onuma K, Tsutsumi S (2002b), 'Resorbability and solubility of zinc-containing tricalcium phosphate', *J Biomed Mater Res*, **60**, 224–231.

Ito A, Otsuka M, Kawamura H, Ikeuchi M, Ohgushi H, Sogo Y, Ichinose N, (2005), 'Zinc-containing tricalcium phosphate and related materials for promoting bone formation', *Curr Appl Phys*, **5**, 402–406.

Jalota S, Bhaduri S B, Tas C A (2007), 'Osteoblast proliferation on neat and apatite-like calcium phosphate-coated titanium foam scaffolds', *Mater Sci Eng C*, **27**, 432–440.

Jarcho M, Salsbury R L, Thomas M B, Doremus R H (1979), 'Synthesis and fabrication of β-tricalcium phosphate ceramics for potential prosthetic applications', *J Mater Sci*, **14**, 142–150.

John A, Varma H K, Kumari T V (2003), 'Surface reactivity of calcium phosphate based ceramics in cell culture systems', *J Biomater Appl*, **18**, 63–68.

Jung U W, Choi S Y, Panq E K, Kim C S, Choi S H, Cho K S (2006), 'The effect of varying the particle size of beta tricalcium phosphate carrier of recombinant human bone morphogenetic protein-4 on bone formation in rat calvarial defects', *J Periodont*, **77**, 765–772.

Kasten P, Vogel J, Luginbuhl R, Niemeyer P, Tonak M, Lorenz H, Helbig L, Weiss S, Fellenberg J, Leo A, Simank H G, Richter W (2005), 'Ectopic bone formation associated with mesenchymal stem cells in a resorbable calcium deficient hydroxyapatite carrier', *Biomaterials*, **26**, 5879–5889.

Khairoun I, Boltong M G, Driessens F C M, Planell J A (1997), 'Effect of calcium carbonate on the compliance of an apatitic calcium phosphate bone cement', *Biomaterials*, **18**, 1535–1539.

Kihara H, Shiota M, Yamashita Y, Kasugai S (2006), 'Biodegradation of alpha TCP particles and new bone formation in a rabbit cranial defect model', *J Biomed Mater Res B*, **79**, 284–291.

Kikuchi M, Koyama Y, Yamada T, Imamura Y, Okada T, Shirahama N, Akita K, Takakuda K, Tanaka J (2004), 'Development of guided bone regeneration membrane composed of α-tricalcium phosphate and poly(L-lactide-co-glycolide-co-β-caprolactone) composites', *Biomaterials*, **25**, 5979–5986.

Kim S, Ryu H S, Jung H S, Hong K S (2004), 'Influence of Ca/P ratios of starting solutions on the crystallisation of amorphous calcium phosphate to hydroxyapatite', *Metals Mater Intl*, **10**(2), 171–175.

Kitamura M, Ohtsuki C, Iwasaki H, Ogata S I, Tanihara M (2004), 'The controlled resorption of porous α-tricalcium phosphate using a hydroxypropylcellulose coating', *J Mater Sci Mater Med*, **15**, 1153–1158.

Knaack D, Goad M E P, Ailova M, Rey C, Tofighi A, Chakravarthy P, Lee D (1998), 'Resorbable calcium phosphate bone substitute', *J Biomed Mater Res*, **43**, 399–409.

Kojima Y, Sakama K, Toyama T, Yasue T, Arai Y (1994), 'Dehydration of water molecule in amorphous calcium phosphate', *Phosphorus Res Bull*, **4**, 47–52.

Kokubo T, Takadama H (2006), 'How useful is SBF in predicting *in vivo* bone bioactivity', *Biomaterials*, **27**, 2907–2915.

Kotani S, Fujita Y, Kitsugi T, Nakamura T, Yamamuro T, Ohtsuki C, Kokubo T (1991), 'Bone bonding mechanism of beta-tricalcium phosphate', *J Biomed Mater Res*, **25**, 1303–1315.

Kurashina K, Kurita H, Kotani H, Takeuchi H, Hirano M (1997), '*In vivo* study of a calcium phosphate cement consisting of α-tricalcium phosphate/dicalcium phosphate dibasic/tetracalcium phosphate monoxide', *Biomaterials*, **18**, 147–151.

Kweh S W, Khor K A, Cheang P (2002), 'High temperature *in-situ* XRD of plasma sprayed Ha coatings', *Biomaterials*, **23**, 381–387.

Laffargue P, Hildebrand H F, Rtaimate M, Frayssinet P, Amoureux J P, Marchandise X (1999), 'Evaluation of bone morphogenetic protein-2-loaded tricalcium phosphate implants in rabbits bone defects', *Bone,* **25**, 55S-58S.

Lazic S, Vukovic Z (1988), 'Morphological properties of amorphous calcium phosphate', *J Serb Chem Soc*, **53**(1), 51–55.

Lebugle A, Zahidi E, Bonel G (1986), 'Effect of structure and composition on the thermal decomposition of calcium phosphates (Ca/P = 1.33)', *Reactivity of Solids*, **2**, 151–161.

Lee D, Rey C, Aiolova M, Tofighi A (2000), 'Methods and products related to the physical conversion of reactive amorphous calcium phosphate', *US patent no. 6117456*.

Leeuwenburgh S C G, Wolke J G C, Schoonman J, Jansen J A (2004), 'Influence of precursor solution parameters on chemical properties of calcium phosphate coatings prepared using electrostatic spray deposition (ESD)', *Biomaterials*, **25**, 641–649.

LeGeros R Z, LeGeros J P, Daculsi G, Kijkowska R (1995), 'Calcium phosphate biomaterials: preparation, properties and biodegradation', In: *Encyclopedic Handbook of Biomaterials and Bioengineering,* DB Wise *et al*. (editors), New York: Marcel Dekker, 1429–1463.

LeGeros R Z, Mijares D, Park J, Chang X F, Khairoun I, Kijkowska R, Dias R, Legeros J P (2005), 'Amorphous calcium phosphates (ACP): formation and stability', *Key Eng Mater*, **284–286**, 7–10.

Le Huec J C, Lesprit E, Delavigne C, Clement D, Chauveaux D, Le Rebeller A (1997), 'Tri-calcium phosphate ceramics and allografts as bone substitutes for spinal fusion in idiopathic scoliosis: comparative clinical results at four years', *Acta Orthop Belg*, **63**, 202–211.

Li P (2003), 'Biomimetic nano-apatite coating capable of promoting bone in growth', *J Biomed Mater Res*, **66A**, 79–85.

Li R H, Bouxsein M L, Blake C A, D'Augusta D, Kim H, Wozney J M, Seeherman H J (2003), 'rhBMP-2 injected in a calcium phosphate paste (alpha-BSM) accelerated healing in the rabbit ulnar osteotomy model', *J Orthop Res*, **21**, 997–1004.

Li Y, Weng W, Tam K C (2007), 'Novel highly biodegradable biphasic tricalcium phosphates composed by α-tricalcium phosphate and β-tricalcium phosphate', *Acta Biomater*, **3**, 251–254.

Lind M, Overgaard S, Bünger C, Soballe K (1999), 'Improved bone anchorage of hydroxyapatite coated implants compared with tricalcium-phosphate coated implants in trabecular bone in dogs', *Biomaterials*, **20**, 803–808.

Lind M, Overgaard S, Glerup H, Soballe K, Bunger C (2001), 'Transforming growth factor-β1 adsorbed to tricalcium phosphate coated implants increases peri-implant bone remodelling', *Biomaterials*, **22**, 189–193.

Mackay A L (1953), 'A preliminary examination of the structure of α-$Ca_3(PO_4)_2$', *Acta Cryst*, **6**, 743–744.

Mathew M, Schroeder L W, Dickens B, Brown W E (1977), 'The crystal structure of α-$Ca_3(PO_4)_2$', *Acta Cryst*, **B33**, 1325–1333.

Matsuno T, Nakamura T, Kuremoto K, Notazawa S, Nakahara T, Hashimoto Y, Satoh T, Shimizu Y (2006), 'Development of beta-tricalcium phosphate/collagen sponge composite for bone regeneration', *J Dent Res*, **25**, 138–144.

Merten H A, Wiltfang J, Grohmann U, Hoenig J F (2001), 'Intraindividual comparative animal study of alpha and beta-tricalcium phosphate degradation in conjunction with simultaneous insertion of dental implants', *J Craniofac Surg,* **12**, 59–68.

Metsger D S, Driskell T D, Paulsrud J R (1982), 'Tricalcium phosphate ceramic – a resorbable bone implant: review and current status', *J Am Dent Assoc,* **105**, 1035–1038.

Metsger D S, Rieger M R, Foreman D W (1999), 'Mechanical properties of sintered hydroxyapatite and tricalcium phosphate ceramic', *J Mater Sci Mater Med*, **10**, 9–17.

Mirtchi A A, Lemaitre J, Terao N (1989), 'Calcium phosphate cements: study of the beta-tricalcium phosphate-monocalcium phosphate system', *Biomaterials*, **10**, 475–480.

Mirtchi A A, Lemaître J, Munting E (1990), 'Calcium phosphate cements: study of the β-tricalcium phosphate-dicalcium phosphate-calcite cements' *Biomaterials,* **11**, 83–88.

Monchau F, Lefèvre A, Descamp M, Blequin-Myrdycz A, Laffargue P, Hildebrand H F (2002), '*In vitro* studies of human and rat osteoclast activity on hydroxyapatite, β-tricalcium phosphate, calcium carbonate', *Biomol Eng*, **19**, 143–52.

Monma H (1980), 'Preparation of octacalcium phosphate by the hydrolysis of α-tricalcium phosphate', *J Mater Sci*, **15**, 2428–2434.

Monma H, Ueno S, Kanazawa T (1981), 'Properties of hydroxyapatite prepared by the hydrolysis of tricalcium phosphate', *J Chem Tech Biotechnol*, **31**, 15–24.

Nakagawa N, Saegusa Y, Abe S, Miura Y, Yoshiya S (2006), 'The effectiveness of RA wrist fusion using beta-TCP without autogenous iliac bone grafting: a report of four cases', *Hand Surg*, **11**, 71–75.

Nancollas G H, Wefel J S (1976), 'Seeded growth of calcium phosphates: effect of different calcium phosphate seed material', *J Dent Res*, **55**, 617–624.

Neo M, Herbst H, Voigt C F, Gross U M (1998), 'Temporal and spacial patterns of osteoblast activation following implantation of beta-TCP particles into bone', *J Biomed Mater Res*, **39**, 71–76.

Nery E B, Lynch K L, Hirthe W M, Mueller K H (1975), 'Bioceramic implants in surgically produced infrabony defects', *J Periodontol*, **46**, 328–347.

Niedhart C, Maus U, Redmann E, Schmidt-Rohlfing B, Niethard F U, Siebert C H (2003), 'Stimulation of bone formation with an *in situ* setting tricalcium phosphate/rhBMP-2 composite in rats', *J Biomed Mater Res*, **65**, 17–23.

Niemeyer P, Krause U, Fellenberg J, Kasten P, Seckinger A, Ho A D, Simank H G (2004), 'Evaluation of mineralized collagen and alpha-tricalcium phosphate as scaffolds for tissue engineering of bone using human mesenchymal stem cells', *Cells Tissues Organs*, **177**, 68–78.

Nillson M, Fernandez E, Sarda S, Lidgren L, Planell J A (2002), 'Characterization of a novel calcium phosphate/sulphate bone cement', *J Biomed Mater Res*, **61**, 600–607.

Obadia L (2004), 'Synthèse et caractérisation de phosphates de calcium d'intérêt biologique: – structure et propriétés de phosphates tricalciques β dopés au sodium,–formation d'apatites non-stoechiométriques par hydrolyse de phosphate dicalcique dihydraté', *PhD Thesis*, University of Nantes, France.

Ogose A, Hotta T, Kawashima H, Kondo N, Gu W, Kamura T, Endo N (2005), 'Comparison of hydroxyapatite and beta tricalcium phosphate as bone substitutes after excision of bone tumors', *J Biomed Mater Res B Appl Biomat*, **72**, 94–101.

Ohta K, Monma H, Tkahashi S (2001), 'Adsorption characteristics of proteins on calcium phosphates using liquid chromatography', *J Biomed Mater Res*, **55**(3), 409–414.

Ohura K, Bohner M, Hardouin P, Lemaître J, Pasquier G, Flautre B (1996), 'Resorption of, and bone formation from, new β-tricalcium phosphate–monocalcium phosphate cements: an *in vivo* study', *J Biomed Mater Res*, **30**, 193–200.

Okuda K, Nakajima Y, Irie K, Sugimoto M, Kabasawa Y, Yoshie H, Hara K, Ozawa H (1995), 'Transforming growth factor-beta 1 coated beta-tricalcium phosphate pellets stimulate healing of experimental bone defects of rat calvaria', *Oral Dis*, **1**, 92–97.

Pioletti D P, Takei H, Lin T, Van Landuyt P, Ma Q J, Kwon S Y, Sung K-l P (2000), 'The effect of calcium phosphate cement particles on osteoblast functions', *Biomaterials*, **21**, 1103–1114.

Posner A S, Beebe R A (1975), 'Surface chemistry of bone mineral and related calcium phosphates', *Seminars in Arthritis and Rheumatism*, **4**(3), 267–291.

Ranz X (1996), 'Développement et caractérisation de dépôts d'apatite obtenus par projection plasma sur prothèses orthopédiques', *PhD Thesis no. 1162*, INPT, Toulouse, France.

Ratner B D, Hoffman A S, Schoen F J, Lemons J E (1996), *Biomaterials Science: An Introduction to Materials in Medicine*, Academic Press, San Diego.

Raynaud S, Champion E, Bernache-Assollant D (1999), 'Characterisation of hydroxyapatite–tricalcium phosphate bioceramics issued from Ca-deficient hydroxyapatite powders: influence of Ca/P ratio', *Phosphorus Res Bull*, **10**, 214–219.

Reid J W, Tuck L, Sayer M, Fargo K, Hendry J A (2006), 'Synthesis and characterization of single-phase silicon-substituted α-tricalcium phosphate', *Biomaterials*, **27**, 2916–2925.

Rey C (1984), 'Etude des relations entre apatites et composés moléculaires', *Thèse d'Etat,* INPT, Toulouse, France.

Rey C, Combes C, Drouet C, Sfihi H, Barroug A (2007), 'Physico-chemical properties of nanocrystalline apatites: implications for biominerals and biomaterials', *Mat Sci Eng C*, **27**, 198–205.

Rice J M, Hunt J A, Gallagher J A (2003), 'Quantitative evaluation of the biocompatible and osteogenic properties of a range of biphasic calcium phosphate granules using primary cultures of human osteoblasts and monocytes', *Calcif Tissue Int,* **72**, 726–736.

Rodrigues A, Lebugle A (1998), 'Influence of ethanol in the precipitation medium on the composition, structure and reactivity of tricalcium phosphate'**,** *Colloid Surf A*, **145**, 191–204.

Rowles S L (1968), 'The precipitation of whitlockite from aqueous solutions', *Bull Soc Chim Fr*, 1797–1802.

Ryu H S, Youn H J, Hong K S, Chang B S, Lee C K, Chung S S (2002), 'An improvement in sintering property of beta-tricalcium phosphate by addition of calcium pyrophosphate', *Biomaterials*, **23**, 909–914.

Sayer M, Statilatov A D, Reid J, Calderin L, Stott M, Yin X, MacKenzie M, Smith T J N, Hendry J A, Langstaff S D (2003), 'Structure and composition of silicon-stabilized tricalcium phosphate', *Biomaterials*, **24**, 369–382.

Sanginario V, Ginebra M P, Tanner K E (2006), 'Biodegradable and semi-degradable composite hydrogels as bone substitutes: morphology and mechanical characterization', *J Mater Sci Mater Med*, **17**, 447–454.

Sedlak J M, Beebe R A (1974), 'Temperature programmed dehydration of amorphous calcium phosphate', *J Coll Inter Sci*, **47**(2), 483–489.

Somrani S, Rey C, Jemal M (2003), 'Thermal evolution of amorphous tricalcium phosphate', *J Mater Chem,* **13**, 888–892.

Somrani S, Banu M, Rey C, Jemal M (2005), 'Physico-chemical and thermochemical studies of the hydrolytic conversion of amorphous tricalcium phosphate into apatite'. *J Solid State Chem*, **178**(5), 1337–1348.

Sous M, Bareille R, Rouais F, Clément D, Amédée J, Dupuy B, Baquey C (1998), 'Cellular biocompatibility and resistance to compression of macroporous β-tricalcium phosphate ceramics', *Biomaterials*, **19**, 2147–2153.

Steffen T, Stoll T, Arvinte T, Schenk R K (2001), 'Porous tricalcium phosphate and transforming growth factor used for anterior spine surgery', *Eur Spine J*, **10**(suppl 2), S132–140.

Stewart M, Welter J F, Goldberg V M (2004), 'Effect of hydroxyapatite/tricalcium phosphate coating on osseointegration of plasma-sprayed titanium alloy implant', *J Biomed Mater Res,* **69**, 1–10.

Sun J-S, Tsuang Y-H, Liao C-J, Liu H-C, Hang Y-S, Lin F-H (1997), 'The effects of calcium phosphate particles on the growth of osteoblasts', *J Biomed Mater Res,* **37,** 324–334.

Szabo G, Huys L, Coulthard P, Maiorana C, Garagiola U, Barabas J, Nemeth Z, Hrabak K, Suba Z (2005), 'A prospective multicenter randomized clinical trial of autogenous bone versus beta-tricalcium phosphate graft alone for bilateral sinus elevation: histologic and histomorphometric evaluation', *Int J Oral Maxillifac Implants,* **20**, 371–381.

Tampieri A, Celotti G, Szontagh F, Landi E (1997), 'Sintering and characterization of HA and TCP bioceramics with control of their strength and phase purity', *J Mater Sci Mater Med*, **8**, 29–32.

Tang R, Wu W, Haas M, Nancollas G (2001), 'Kinetics of dissolution of β-tricalcium phosphate', *Langmuir*, **17**, 3480–3485.

Terpstra R A, Driessens F C M, Schaeken H G, Verbeeck R M H (1983), 'The whitlockite phase in the system CaO-P_2O_5-MgO at 1000 °C', *Z Anorg Allg Chem*, **507**, 206–212.

Tetsuya J, Dwight T D, Goldberg V M (2002), 'Comparison of hydroxyapatite and hydroxyapatite-tricalcium-phosphate coatings', *J Arthroplasty*, **17**(7), 902–909.

Thanner J, Karrholm J, Herbets P, Malchau H (1999), 'Porous cups with and without hydroxylapatite-tricalcium phosphate coating: 23 matched pairs evaluated with radiostereometry', *J Arthroplasty*, **14**, 266–271.

Tofighi A, Mounic S, Chakravarthy P, Rey C, Lee D (2001), 'Setting reactions involved in injectable cements based on amorphous calcium phosphate', *Key Eng Mater*, **192–195**, 769–772.

Treboux G, Layrolle P, Kanzaki N, Onuma K, Ito A (2000), 'Existence of Posner's cluster in vacuum', *J Phys Chem A*, **104**, 5111–5114.

Tung M S (1998), 'Calcium phosphate: structure, composition, solubility, and stability', In: *Calcium Phosphates in Biological and Industrial Systems*, Amjad Z (editor), Boston: Kluwer Academic Publishers, 3–19.

Urist M R, Lietze A, Dawson E (1984), 'Beta-tricalcim phosphate delivery system for bone morphogenetic protein', *Clin Orthop Relat Res,* **187**, 277–280.

Vallet-Regi M, Gordo M, Ragel C V, Cabanas M V, San Roman J (1997), 'Synthesis of ceramic–polymer–drug biocomposites at room temperature', *Solid State Ionics*, **101–103**, 887–892.

Van Den Vreken N M, Pieters I Y, De Maeyer E A, Jackers G J, Schacht E H, Verbeeck R M (2006), 'Apatite formation in composites of alpha-TCP and degradable polyesters', *J Biomater Sci Polym Ed*, **17**(9), 953–967.

Varma H K, Sureshbabu S (2001), 'Oriented growth of surface grains in sintered b tricalcium phosphate bioceramics', *Mater Lett,* **49**, 83–85.

Wang C X, Zhou X, Wang M (2004), 'Influence of sintering temperatures on hardness and Young's modulus of tricalcium phosphate bioceramics by nanoindentation technique', *Materials Characterization*, **52**(4/5), 301–307.

Welch J H, Gutt W (1961), 'High-temperature studies of the system calcium oxide-phosphorus pentoxide', *J Chem Soc*, 4442–4444.

Wiltfang J, Merten H A, Schlegel K A, Schultze-Mosgau S, Kloss F R, Rupprecht S, Kessler P (2002), 'Degradation characteristics of alpha and beta tricalcium phosphate (TCP) in minipigs', *J Biomed Mater Res*, **63**, 115–121.

Wu C H, Hara K, Ozawa H (1992), 'Enhanced osteoinduction by intramuscular grafting of BMP-beta-TCP compounds pellets into murine models', *Arch Histol Cytol*, **55,** 97–112.

Xin R, Leng Y, Chen J, Zhang Q (2005), 'A comparative study of calcium phosphate formation on bioceramics *in vitro* and *in vivo*', *Biomaterials,* **26**, 6477–6486.

Yamada M, Shiota M, Yamashita Y, Kasugai S (2007), 'Histological and histomorphometrical comparative study of the degradation and osteoconductive characteristics of α- and β-tricalcium phosphate in block grafts', *J Biomed Mater Res B*, **82B**, 139–148.

Yang X, Wang Z (1998), 'Synthesis of biphasic ceramics of hydroxyapatite and b-tricalcium phosphate with controlled phase content and porosity', *J Mater Chem*, **8**, 2233–2237.

Yasuda H, Fujita Y, Fujitani W, Umakoshi Y, Sakka Y, Tang F, Takaoka A, Matsuura N (2006), 'Bone-like layer growth and adhesion of osteoblast-like cells on calcium deficient hydroxyapatite synthesized at different pH', *Mater Trans*, **45**, 1782–1787.

Yuan H, de Bruijn J D, Li Y, Yang Z, de Groot K, Zhang X (2001), 'Bone formation induced by calcium phosphate ceramics in soft tissue of dogs: a comparative study between porous alpha-TCP and beta-TCP', *J Mater Sci Mater Med*, **12**, 7–13.

Zhang Y, Zhang M (2001), 'Synthesis and characterization of macroporous chitosan/calcium phosphate composite scaffolds for tissue engineering', *J Biomed Mater Res*, **55**, 304–312.

Ziegler J, Mayr-Wohlfart U, Kessler S, Breitig D, Gunther K P (2002), 'Adsorption and release properties of growth factors from biodegradable implants', *J Biomed Mater Res* **59**, 422–428.

16

Hydroxyapatite

R Z LEGEROS and J P LEGEROS,
New York University College of Dentistry, USA

16.1 Introduction

The term 'apatite' describes a family of compounds having similar structures but not the same composition. Calcium hydroxyapatite, commonly referred to as HA, has a specific composition, $Ca_{10}(PO_4)_6(OH)_2$, with Ca/P stoichiometric ratio of 1.67; and has a specific crystallographic structure: hexagonal system, space group, $P6_3/m$ [1–3] Substitutions in the apatite structure (e.g. Sr for Ca, Mg for Ca, F for OH, Cl for OH, CO_3 for PO_4 or CO_3 for OH) and affect its properties such as lattice parameters, spectral properties, crystal size and morphology, which in turn, affect its chemical stability (solubility) and thermal stability [3–23]; the degree of the effect depending on the size and amount of the substituting ion.

Biologic apatites constitute the inorganic or mineral phases of normal calcified tissues (teeth and bones) and are also found in some pathologic calcifications (dental calculus, heart calcifications, urinary stones, soft-tissue calcifications, etc.) [12,14,24]. Biological apatites, unlike pure HA, contain important minor substitutents (e.g. CO_3^{2-}, Na^+, Mg^{2+}) and are more accurately described as carbonated apatite or carbonate apatite, CHA, approximated by the formula, $(Ca,Mg,Na)_{10}(PO_4,HPO_4,CO_3(OH)_2$ [12,14,24]. Other biologic apatite such as shark and other fish enameloids contain both fluoride (F^-) and carbonate (CO_3^{2-}) [16].

HA of synthetic or biologic origin (animal bones) have diverse non-medical applications including: protein chromatography [25], water defluoridation [26], components of dental products (as abrasive or mineralizing agent) and as abrasives for orthopedic and dental implants [27–29].

Biologic HA (e.g. from coral, bovine bone or marine algae) or synthetic HA are currently used for bone repair and bone regeneration in the form of granules, blocks and scaffolds, by itself or as composite with polymers or other ceramics or as coatings on orthopedic or dental implants. The rationale for its development as a bone substitute material is its similarity in composition to the bone mineral.

In this chapter, HA will refer to calcium hydroxyapatite with the composition $Ca_{10}(PO_4)_6(OH)_2$; HAP will refer to apatite preparations (by precipitation or hydrolysis) that are not sintered. Porous HA has often been used in the literature to refer both to HA derived from coral (coralline HA) and to HA or HAP that were especially prepared to introduce macroporosity. In this chapter, the term 'porous HA' or 'porous HAP' will refer to the physical structure and not to specific HA (e.g. coralline HA).

This chapter is an update of previous reviews on apatites [14,15,30,31] and focuses on its preparation, properties, cell and tissue response, and applications in medicine and dentistry.

16.1.1 Natural (mineral) and biologic apatites

Mineral apatites (e.g. hydroxyapatite, HA; fluorapatite, FA; chlorapatite, ClA; carbonate hydroxyapatite, CHA; fluorcarbonateapatite, CFA) occur in nature with different colors. *Ap atite* (Greek, 'to deceive') was the name given by Werner in 1788 to describe a group of mineral crystals appearing in different colors that were often mistaken for the more precious gems such as aquamarine, amethyst and topaz [32]. Based on the similarity in the X-ray diffraction (XRD) patterns of sintered bone to those of mineral apatites and on chemical analyses showing mainly calcium and phosphate ions, it was concluded that the inorganic phases of bones and teeth are basically a calcium hydroxyapatite, HA [33] or similar to fluoride substituted apatite, FA [1]. Based on mineral apatites containing carbonate (dahllite, staffellite), McConnell [34] speculated that apatites of dental enamel and bone are carbonate apatites similar to carbonate apatite minerals.

XRD profiles (Fig. 16.1A) and Fourier transform infrared (FT-IR) spectra of enamel, dentine and bone apatites show similarities and differences [12,14]. The well-defined XRD peaks in the XRD profile of enamel (Fig. 16.1Aa) indicate larger crystals than those of dentin (Fig. 16.1Ab) or bone (Fig. 16.1Ac). For many years, the mineral phases of calcified tissues have been idealized as hydroxyapatite or HA, $Ca_{10}(PO_4)_6(OH)_2$ [35]. However, based on studies on synthetic carbonate apatite and biologic apatites, and using a combination of analytical methods (XRD, IR spectroscopy, transmission electron microscopy (TEM), chemical analyses), LeGeros demonstrated for the first time that biologic apatite is not pure HA but is a carbonate apatite similar to synthetic apatite with the CO_3 substituting for the PO_4 groups [10,12], providing experimental evidence to McConnell's speculation of the similarity of biologic apatite to mineral carbonate apatite [34].

16.1.2 Synthetic apatites

Early studies on synthetic HA were spurred by the need to understand biologic apatites (especially bone apatite and enamel apatite) and the need

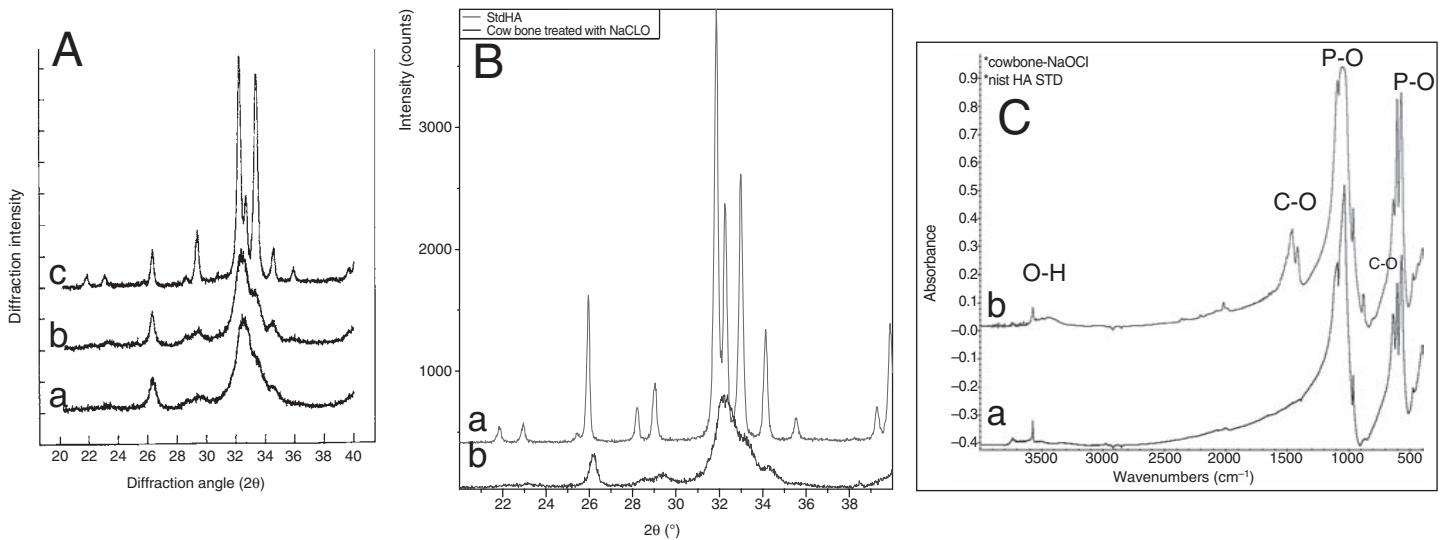

16.1 X-ray diffraction profiles: (A) enamel (a), dentine (b) and bone (c) mineral (carbonate apatites); (B) ceramic HA (a), bone (b). FT-IR spectra of (a) ceramic HA and (b) bone mineral.

to understand the role of fluoride in the demineralization and remineralization processes associated with dental caries [36].

Subsequent studies on synthetic HA and other calcium phosphates (e.g. beta-tricalcium phosphate, β-TCP, HA of biologic origin) that started in the late 1970s were motivated by the need to develop synthetic biomaterials for bone repair, substitution and augmentation that will replace autografts (bone from the same subject obtained from another anatomical location) and allografts (bone obtained from cadavers). Autografts (bone obtained from the same subject from another site), the gold standard, and allografts (bone obtained from cadavers) have definite advantages but also have serious disadvantages: limited supply, expensive, additional surgery, trauma, morbidity and additional expense, in the case of autografts; limited supply, expensive, and potential disease transmission (in the case of allografts). Synthetic HA for bone repair, augmentation or regeneration was developed to provide less expensive and safer alternatives to autografts and allografts. The rationale for developing HA biomaterials is the similarity in composition with bone mineral or bone apatite [37–43]. XRD profile (Fig. 16.1Ba) and FT-IR (Fig. 16.1Ca) spectrum of synthetic HA compared with bone shows similarities and differences in crystallinity (Fig. 16.1Bb) and composition, e.g. presence of carbonate in bone apatite (Fig. 16.1Cb).

16.1.3 HA and substituted HA for clinical applications

The first successful clinical application of calcium phosphate (described as 'triple calcium phosphate compound') for bony defect was reported by Albee in 1920 [44]. Fifty years later, some authors [45] described a method of preparing ceramic apatite and suggested its use in medicine and dentistry. The independent studies of Aoki [41], deGroot [37] and Jarcho [38,39] led to the commercialization of synthetic HA and were followed by HA derived from coral and non-sintered apatite or synthetic calcium-deficient apatites, CDA or HAP.

At the present time, numerous commercial products described as HA are available, in various physical forms (e.g. granules, specially designed blocks for specific applications) as listed in Table 16.1. HA/polymer composite (HA/polyethyelene, HAPEX^{TM}) is also commercially available as ear implants [45]. HA is also now commonly used in abrasives [27–29] and as a plasma-sprayed coating for orthopedic and dental implants [46–48].

Experimental substituted apatites include: apatites containing fluoride (FA), carbonate (CHA or CA), carbonate and fluoride (CFA), silicon, magnesium, strontium [8,14,49–56]. Experimental HA/polymer composites include: HA or CHA with natural polymers (collagen, chitosan) or synthetic polymers (e.g, polylactic polyglycolic acid, PLGA) [56,57].

Table 16.1 Commercial HA and HAP

Coral derived (complete conversion of $CaCO_3$ to coralline HA)
Interpore® 200, ProOsteon®200, ProOsteon® 500 (Interpore Int., California)
Coral derived (partial conversion of CaCO3 to coralline HA)
Prosteon™ 200R, ProOsteon™ 500R (Interpore Int, California)
Bovine bone apatite (unsintered)
BioOss® (EdGeitslich, Switzerland)
Bovine bone apatite (sintered)
Endobon® (Merck, Germany)
Osteograf®-N (Ceramed, Colorado)
Trubone® (Japan)
Synthetic HA
Calcitite® (Calcitek, California)
Osteograf® (Ceramed, Colorado)
Bioroc® (DePuy-Bioland, France)
Apaceram™ (Pentax Corporation, Tokyo)
Synthetic HAP (unsintered)
Osteogen® (Impladent, New York)
Ostim® (Germany)
HA/polymer composite
HA/polyethylene composite
HAPEX® (Gyrus, Tennessee)
CHA/collagen
Healos™ (Orquest Inc., California)
HA/mineral composite
HA/$CaSO_4$
Hapset® (Lifecore, Minnesota)

16.2 Fabrication

16.2.1 Bone graft materials

HA from biologic origin

Commercial HA products of biologic origin are those derived from coral, from bovine bone or from marine algae. Coralline HA is obtained by the hydrothermal conversion of coral, *Porites* (consisting of calcium carbonate in aragonite form), in the presence of ammonium phosphate [59]. The process is carried out at about 275 °C and 1200 psi. Coralline HA (e.g. Interpore®, ProOsteon®, Interpore International, Irivine, CA) differs from synthetic HA and from bone in physicochemical properties (crystal size, composition, dissolution properties) as shown in Tables 16.2, 16.3.

Bovine-derived products are of two types: (a) bovine bone apatite resulting from the deproteination (removal of organic phase) of bovine bone (e.g. BioOss®) or (b) bovine bone processed at high temperature, about 1000 °C (e.g. Osteograft® N, Ceramed, USA: Endobon®, Merck, Germany).

Table 16.2 Comparative properties of ceramic HA and coralline HA

Properties	Ceramic HA	Coralline HA
Composition		
XRD analysis	HA	HA + β-TCMP*
FTIR analysis	OH, PO_4	OH, PO4, CO_3
Chemical analysis	Ca, P	Ca, P, Mg, Sr, Mg
Porosity (SEM)	Dense	Macroporous
Crystallinity (XRD)		
$B_{1/2}$ (002)	0.12	0.25° 2θ
Crystal size (TEM)	0.25 × 1.0 μm	0.02 × 0.2 μm
Lattice parameters (XRD)		
a-axis (±0.003 Å)	9.419	9.453
c-axis (±0.003 Å)	6.881	6.893

*β-TCMP = Mg-substituted β-TCP, $(Ca,Mg)_3(PO_4)_2$. Ceramic HA, Calcitite®; coralline HA, Interpore®.

Table 16.3 Mechanical properties of bone compared with coralline HA and porous ceramic HA

Strength (MPa)	Cancellous bone	Cortical bone	Coralline HA	Porous ceramic HA
Compressive	5.5	162	9.3	60
Tensile	3	151	2.8	2.5

Sintering of biologic apatite results in loss of carbonate and an increase in crystal size [14].

Fluoridated hydroxyapatite is manufactured by hydrothermal transformation of marine algae, *Corallina officinalis*, into $Ca_{10}(PO_4)_6(OH,F)_2$ marketed as FRIOS® Algipore®, (Friadent, Mannheim, Germany) [60,61].

The hydrothermal conversion of coral to coralline HA (Interpore®, ProOsteon®, both from Interpore International, California) and of marine algae to fluoridated hydroxyapatite (FRIOS® Algipore®, (Friadent, Mannand) and special processing of bovine bone (Endobon®, Merck, Darmstadt, Germany) conserve the original macroporosity of the original biologic materials [59–64] as shown in Fig. 16.2.

Synthetic HA or HAP and substituted apatites

HA can be obtained by the following methods: (a) solid-state reaction; (b) hydrothermal reactions; (c) compacting and sintering HAP powder prepared by precipitation or hydrolysis reactions; (d) sol–gel.

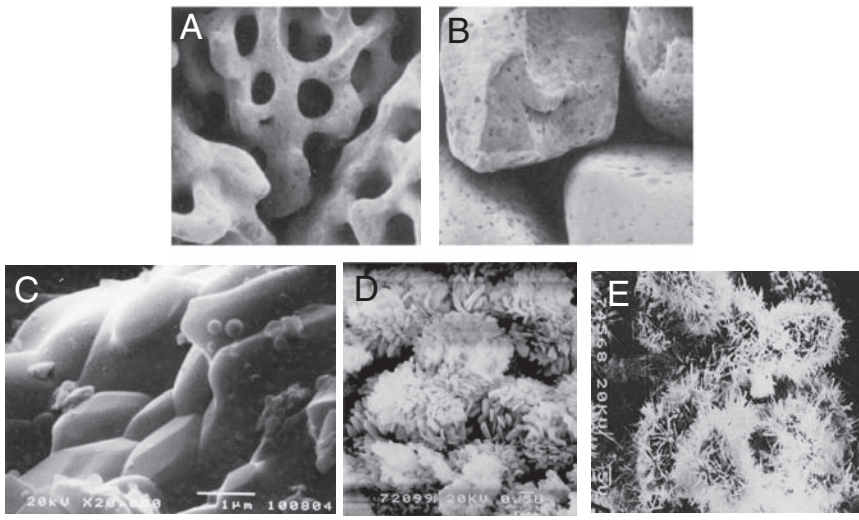

16.2 SEM micrographs of (A) coralline HA, (B) dense HA; (C) HA crystals; (D) coralline HA crystals; (E) precipitated (90 °C) calcium-deficient apatite, CDA.

The extent and type of substitution in the apatite is influenced by preparation method [11,14]. For example, full substitution of Cl for OH, $Ca_{10}(PO_4)_6Cl_2$, is achieved by solid-state reaction [21] while only partial substitution, $Ca_{10}(PO_4)_6(Cl,OH)_2$, is obtained in aqueous systems (precipitation or hydrolysis method) [14,22]. In the case of carbonate incorporation in the apatite, the mode of incorporation is affected by the preparation method: Type A (CO_3 for OH) is obtained at high temperatures, 1000 °C [4–6] and Type B (CO_3 for PO_4), prepared by precipitation or hydrolysis method at low temperatures (25–95 °C) [10,12,14,18,20,23].

Solid-state reactions

The calcium compounds are mixed thoroughly, compressed and sintered above 950 °C. For example, reaction of dicalcium phosphate anhydrous (DCPA) and calcium hydroxide (reaction 16.1), beta-tricalcium phosphate (β-TCP) and calcium hydroxide (reaction 16.2) or calcium carbonate ($CaCO_3$, calcite form) and DCPA (reaction 16.3).

$$\underset{\text{DCPA}}{6CaHPO_4} + 4Ca(OH)_2 \rightarrow \underset{\text{HA}}{Ca_{10}(PO_4)_6(OH)_2} + 6H_2O \qquad 16.1$$

$$\underset{\beta\text{-TCP}}{3Ca_3(PO_4)_2} + Ca(OH)_2 \rightarrow \underset{\text{HA}}{Ca_{10}(PO_4)_6(OH)_2} \qquad 16.2$$

$$6CaHPO_4 + 4CaCO_3 \rightarrow Ca_{10}(PO_4)_6(OH)_2 + 4CO_2 + 2H_2O \quad 16.3$$
DCPA calcite HA

Substituted apatites can be obtained by adding appropriate compounds to replace calcium phosphate or calcium hydroxide, $Ca(OH)_2$. For example, FA can be prepared by replacing $Ca(OH)_2$ with calcium fluoride, CaF_2 (reaction 16.4) and carbonate apatite, CA (Type A) obtained by passing carbon dioxide gas, CO_2, on HA at 1000 °C (reaction 16.5):

$$6CaHPO_4 + 3CaCO_3 + CaF_2 \rightarrow Ca_{10}(PO_4)_6F_2 + 3CO_2 + 3H_2O \quad 16.4$$
DCPA calcite FA

$$Ca_{10}(PO_4)_6(OH)_2 + CO_2 \rightarrow Ca_{10}(PO_4)_6CO_3 + H_2O \quad 16.5$$
HA CA

Hydrothermal reactions

HA and substituted apatites can also be prepared by hydrothermal reactions [9,10,65–67]. The reactants used for solid-state reaction (reactions 16.1, 16.2, 16.3 and 16.4) can also be used for hydrothermal reaction at 275 °C, under steam pressure of 12 000 psi. In addition to monetite or DCPA, and β-TCP, α-TCP, tetracalcium phosphate (TTCP), $Ca_4P_2O_9$ can also be used. For example, $CaCO_3$ (in calcite or aragonite form) in the presence of appropriate amounts of monetite or ammonium phosphate, $(NH_4)_2HPO_4$, can be hydrothermally converted to HA:

$$4CaCO_3 + 6CaHPO_4 \rightarrow Ca_{10}(PO_4)_6(OH)_2 + 2H_2O + 4CO_2 \quad 16.6$$
Calcite DCPA HA

$$10CaCO_3 + 6(NH_4)_2HPO_4 \rightarrow Ca_{10}(PO_4)_6(OH)_2 + H_2O + CO_2 \quad 16.7$$

The products from the above reaction may contain a small amount of carbonate (CO_3^{2-}) incorporated in the apatite. Hydrothermal transformation of coral ($CaCO_3$ in aragonite form) to corraline HA is achieved using reaction 16.6 [59]. However, because the original coral also contained small amounts of magnesium, the resulting product is not pure HA but HA (with a small amount of CO_3^{2-} incorporated) and a small amount of Mg-substituted beta-tricalcium phosphate, β-TCMP, or Mg-TCP [31,64].

Carbonate apatite single crystals have been prepared by the hydrothermal method [9]. Hydrothermal conversion of alpha-tricalcium phosphate, α-TCP, calcite or gypsum ($CaSO_4 \cdot 2H_2O$), to carbonate apatite has been reported by Ishikawa's group [65,66].

Preparation of HAP powder

HAP powder obtained either by precipitation or hydrolysis method is compacted and sintered to obtain dense or macroporous HA.

Precipitation method: Commercial HA is often prepared by compacting and sintering apatite powder prepared by precipitation reaction between calcium nitrate and ammonium phosphate solution [38–41]. Our method uses calcium acetate instead of calcium nitrate or calcium chloride solution to avoid potential incorporation of NO_3^{2-} or Cl^- ions in the apatite [10,12,19]. Ammonium phosphate or ammonium hydroxide are used as reagents to avoid potential incorporation of sodium (Na) or potassium (K) ions in the apatite.

$$10Ca(OH)_2 + 3H_3(PO_4)_2 \rightarrow \text{HAP precipitate} \quad 16.8$$

$$10Ca(NO_3)_2 + 6(NH_4)_2HPO_4 + 2NH_4OH \rightarrow \text{HAP precipitate} \quad 16.9$$

$$10Ca(CH_3COO)_2 + 6(NH_4)_2HPO_4 + 2NH_4OH \rightarrow \text{HAP precipitate} \quad 16.10$$

The precipitation reactions are sensitive to the concentrations of each of the reactant and the reaction pH to ensure that the HAP powder converts to HA upon sintering. Precipitation temperature ranges from 25 to 95 °C. The reaction temperature affects the crystallinity (crystal size) of the HAP powder [11,12].

Hydrolysis method. Apatites can be prepared by hydrolysis of non-apatitic calcium phosphates, for example: amorphous calcium phosphate, ACP; dicalcium phosphate dihydrate, DCPD, $CaHPO_4 \cdot 2H_2O$; DCPA, $CaHPO_4$; octacalcium phosphate, OCP, $Ca_8H_2(PO_4)_6 \cdot 5H_2O$, α-TCP, β-TCP, $Ca_3(PO_4)_2$) in ammonium, potassium or sodium hydroxide, carbonate, fluoride, or chloride solutions, depending on the desired composition of the apatite [10–12,14,18,68]. Other calcium compounds (calcium carbonate, calcium sulfate, calcium fluoride) can also be hydrolyzed to apatite [14].

For example, hydrolysis of DCPD, or OCP to apatite is achieved when using hydroxide solutions, NaOH, KOH, NH_4OH [10,11]; to CO_3 or F or (CO_3 + F)-substituted apatites (CHA, FA, CFA) when using solutions containing carbonate or fluoride or both ions. [10,12,14,18,69].

$$\underset{\text{OCP}}{Ca_8H_2(PO_4)_6 \cdot 5H_2O} + NH_4OH \rightarrow HAP + H_2O \quad 16.11$$

The growth of the apatite microcrystals followed the shape of the original much larger original OCP crystals [70] as shown in Fig. 16.3.

Preparation of substituted apatites

The incorporation of other ions is achieved by partial replacement of the calcium solution with the desired substituent (e.g. strontium, magnesium, manganese ions) or partial replacement of the phosphate solution (e.g. with carbonate) or addition of the desired amount of fluoride or chloride ions

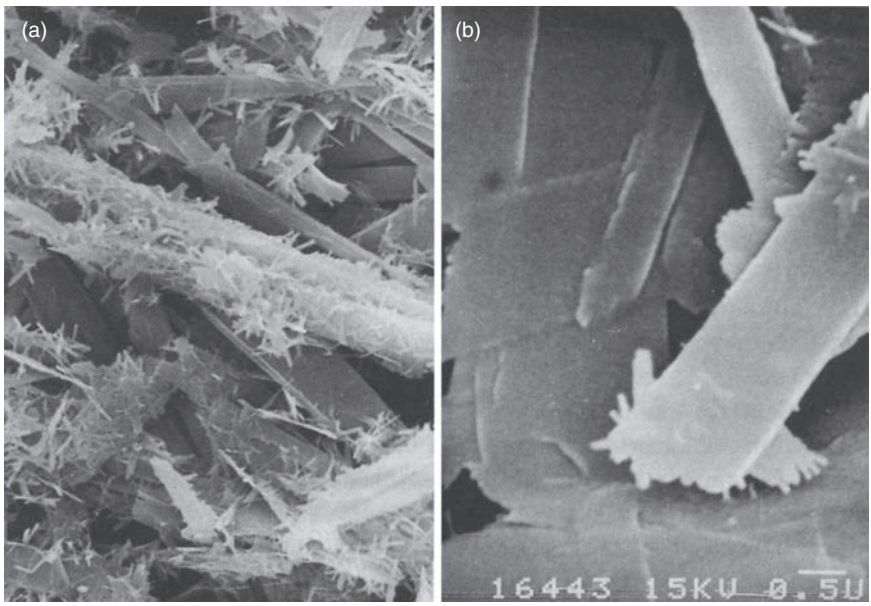

16.3 SEM of OCP converted to apatite by hydrolysis in NaOH solution. The much smaller apatite crystals grew following the outline of the original OCP crystals.

[11,12,14,19,22]. When a mixture of sodium phosphate and sodium bicarbonate is used in the preparation of carbonate-substituted apatite, CHA, a coupled substitution Na for Ca and CO_3 for PO_4 is obtained [10,14,18].

Carbonate-substituted apatites The first preparation and characterization of synthetic carbonate-containing apatite obtained at high temperature (1000 °C) and dry conditions was reported by Elliott [6] and Bonel and Montel [4,5]. The first preparation of carbonate containing apatite obtained from aqueous systems (by precipitation or hydrolysis methods) at low temperatures (25 to 95 °C) was reported by LeGeros [10,18,20,23]. These two carbonate apatites differed in the mode of substitution described by Bonel and Montel [4,5] as Type A (CO_3 for OH) or Type B (CO_3 for PO_4). The different mode of substitution is reflected in the effect in their lattice parameters: Type A (CO_3-for-OH) causes an increase in the *a*-axis and decrease in the *c*-axis dimension because the CO_3 group is larger than the OH group [4–6]; Type B (CO_3 for PO_4) causes a decrease in the *a*-axis and an increase in the c-axis dimension because the CO_3 group is smaller than the PO_4 group [10–12,14,18,20,23]. The characteristics of the infrared spectra are different for the two types of substitution. The spectral characteristics of biologic apatite is more similar to that of the synthetic carbonate apatite with Type B than Type A substitution.

Fluoride-substituted apatites (*FA*) Partially or fully substituted F-apatite can be prepared by precipitation, hydrolysis, hydrothermal or solid-state reactions.

Strontium-substituted apatites (Sr for Ca) These are prepared either by precipitation (or hydrolysis methods [12,14]). Sr-HA are prepared by sintering the precipitated Sr-containing apatite at 1250 °C [56].

Silicon-substituted apatites (SiO_4 for PO_4) These are prepared by precipitation and sintering [49,60].

Other methods of preparing HAP or FAP are from gel systems [70] or HAP by the sol–gel method [71].

16.3 Microstructure

16.3.1 Dense vs. macroporous structure

Synthetic HA can be made either dense or macroporous [71–74]. Dense HA is described as having a maximum microporosity of 5% by volume [40,41] and consisting of crystals with size exceeding 2000 Å. The HA or HAP powder is compressed or compacted into a mold at a pressure of 60–80 MPa. The powder may be mixed with a binder [41,73] before compacting. The compressed body can be sintered in air (conventional method) at the desired temperature, usually 950 to 1300 °C, heating rate of about 2–20 °C per minute and holding at the maximum temperature for several hours before cooling at the same rate as the heating rate. Another method of compressing is by hot isostatic pressing (HIP) where materials are compressed by gaseous pressures at high temperatures. This process results in dense HA of greater density and higher compressive strength than the conventional method (uniaxial pressing) of compacting.

Interconnecting macroporosity such as that observed in bone promotes vascularization and tissue ingrowth [75]. For this reason, more and more commercial and experimental synthetic HA and other calcium phosphate bone graft materials are provided with a macroporous structure. Several techniques are used to fabricate HA scaffolds with interconnecting porosity and pore size approximating those of bone. These techniques include: incorporation of porogens (e.g. naphthalene, H_2O_2, sugar, polymer beads, starch) [76,77], foam method [65,66], gel casting method or combination of gel casting and foam method [78,79], and rapid prototyping [80]. The hydrothermal conversion of coral to coralline HA [61], and the special processing of bovine bone [62] and of marine algae [60,61] preserve the interconnecting macroporosities originally present in these biologic materials (Fig. 16.2).

Porosity (pore size pore volume, degree of interconnectivity) influence tissue response to the biomaterials [81–87]. An appropriate geometry (a

combination of macro- and microporosity) appears to provide the environment that makes osteoconductive calcium phosphate biomaterials also osteoinductive [88–90].

16.3.2 Crystal properties affecting dissolution and bioactivity

Morphology (size and shape) of apatite crystals depend on reaction temperature, substitutions in the apatite structure, sintering temperature and preparation method (sintered or hydrothermal conversion). Apatites precipitated at 37 °C are nano-sized crystals with similar crystal size and morphology as bone apatite (Fig. 16.4). As stated in the previous section, substitution in the HAP causes changes in crystal size and morphology. Carbonate substitution in the apatite causes a reduction in crystal size and changes in morphology: from acicular to rodlike to equi-axed crystals, depending on the amount of CO_3 incorporated in the structure [10,12,14,18] while fluoride incorporation increases crystal thickness [12,14].

Ceramic HA vs. coralline HA

Ceramic HA and coralline HA differ in crystal morphology and crystal size (Fig. 16.3, Table 16.3) reflecting their origin (synthetic vs. biologic) and preparation method (precipitation and sintering at about 1000 °C vs. hydrothermal conversion at 275 °C, 12 000 psi). Ceramic HA has larger crystals than coralline HA (Fig. 16.2).

Crystal defects (dislocations, grain boundary regions, etc.) may affect *in vitro* and *in vivo* cellular reactions at the surfaces of the biomaterial or at the biomaterial/bone interfaces [91,92]. It was reported that three-dimensional defects were present in HAP sintered at 900 °C but were not observed in HA sintered at 1230 °C and more mineralized collagen

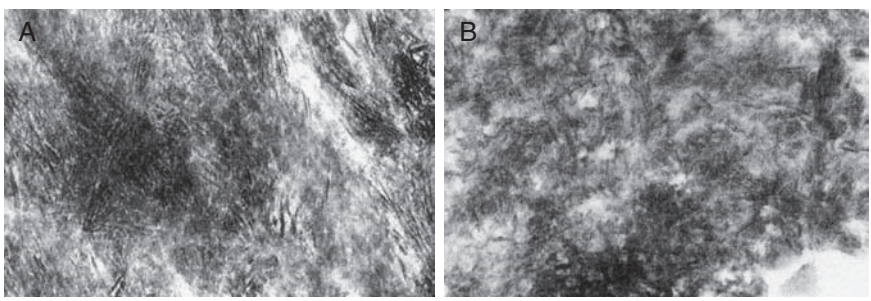

16.4 Tranmission electron micrographs of (A) bone apatite and (B) apatite precipitated at 37 °C.

was observed associated with HAP-900 compared with HAP-1230 [92]. It is also observed that dissolution pattern is different for biologic apatite (human enamel) compared with ceramic HA. [91]. Dissolution of biologic apatite preferentially starts at the crystal core while dissolution of ceramic HA does not have any preferential direction.

16.4 Chemical, physical and mechanical properties

16.4.1 Chemical composition

Pure HA, $Ca_{10}(PO_4)_6(OH)_2$, has a Ca/P molar ratio of 1.67, and consists principally of Ca^{2+} (40 wt%) and PO_4^{3-} (18.5 wt% as P); shows only the O–H (for OH group) and P–O (for PO_4 groups) absorption bands in the FT-IR β spectra. Coralline HA (derived from coral by hydrothermal conversion) consists of other ions besides Ca^{2+} and P^{-}, such as CO_3^{2-}, Mg^{2+} [63]. Sintered bovine bone (e.g. Osteograf-N, Ceramed) contains minor amounts of Mg^{2+}, Na^{-} and much less carbonate (CO_3^{2-}) than unsintered deproteinated bovine bone (e.g. BioOss®, Switzerland).

HAP (unsintered preparations by precipitation or hydrolysis methods) do not have the stoichiometric Ca/P molar ratio of 1.67. HAPs with Ca/P molar ratios less than 1.67 described as calcium-deficient, CDA. Heating CDA at 900 °C and higher results in the formation of biphasic calcium phosphates, BCP, consisting of an intimate mixture of HA and β-TCP of varying HA/β-TCP ratios [14,93].

16.4.2 Mechanical properties

The properties of the apatite powder, the compression and sintering conditions, macroporosity and microporosity influence the mechanical properties of the dense HA. Several mechanical properties (e.g. compressive strength) decrease with increasing amount of microporosity [73]. Increasing sintering temperature causes an increase in density, grain size, compressive, flexural, torsional strength and moduli of elasticity in compression [37,39,41]. The fracture toughness for HA ceramic increased for HA sintered from 1100 to 1150 °C, made no significant difference from 1150 to 1250 °C and decreased at sintering temperature above 1250 °C [41]. The difference in values of mechanical properties was also attributed to differences in the preparation of the apatite powder [74]. The difference in preparation methods causes difference in grain size (small grain size tends to give greater fracture toughness) and in composition. Flexural strength and fracture toughness of dense HA was reported to be less in dry than in wet conditions [73]. The modulus of elasticity of HA is 40–117 GPa compared with that of cortical bone of 12–18 GPa [41]. Table 16.3 shows the comparative compressive and tensile

strengths of cancellous bone, cortical bone, coralline HA and porous ceramic HA.

16.4.3 Chemical stability: dissolution properties

Chemical stability of apatites is influenced by the apatite composition and preparation method which also affects crystal size and composition. Substitution in the apatite structure affects apatite solubility [14]. For example, compared with unsubstituted apatites prepared by precipitation or hydrolysis method, strontium, magnesium or carbonate substitution causes an increase in solubility [12,14,17] while fluoride substitution causes a decrease in solubility [12,14,36]. Sintered bone apatite (e.g. Osteograf-N, Ceramed) is less soluble than unsintered bone apatite (BioOss®, EdGeitslich, Switzerland); sintered apatite (Calcitite®, Calcitek, USA) than unsintered precipitated apatite (Osteogen®, Impladent) or hydrothermally converted coral, coralline HA (Interpore®, Interpore) as shown in Fig. 16.5.

In vitro dissolution of HA depends on the properties of the solution (type and concentration of the buffered or unbuffered solutions, pH, degree of saturation), HA/solution ratio, and properties of the apatite (particle size, porosity, composition, crystallinity (reflecting crystal size or crystal perfection or strain) HA [14,17,36,94,95]. Powdered commercial HA of similar particle size showed decreasing extent of dissolution [94] as shown below:

BioOss® << Osteogen® << Osteograf-N® << Interpore® > Calcitite®

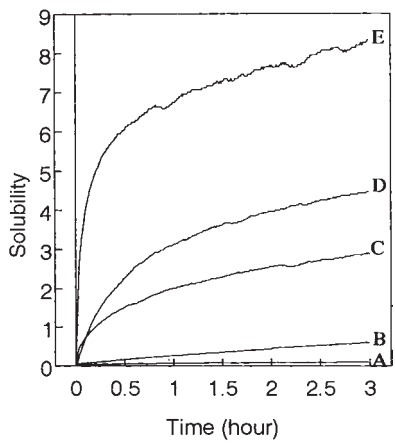

16.5 Comparative dissolution of different apatite-based bone-graft materials: ceramic HA, Calcitite® (A), coralline HA, Interpore® (B), ceramic HA, Bioroc® (C), calcium-deficient apatite, Osteogen® (D), bovine bone mineral, BioOss®.

16.5 Biological properties

16.5.1 *In vitro* cell response

In vitro cell culture studies are used to demonstrate cell response (proliferation, differentiation, phenotypic expression of bone markers) to various materials. Responses of osteoblast (bone-forming), osteoclast (bone-resorbing), odontoblast (dentin-forming) and periodontal (associated periodontal ligament attachment) cells to HA or HAP have been reported [8,96–98]. Substituted HA or HAP showed the following cell response: (a) carbonate-substituted apatite stimulate greater activity of osteoclasts compared with carbonate-free HAP or FAP [97] or F-treated dentin [99]; (b) stimulation of proliferation and phenotypic expression of F-containing HAP [8] or F-treated bovine bone [98]; (c) difference in response between odontoblasts and osteoblasts [8]. SEM of cell attachment, phagocytosis and partial dissolution of HA *in vivo* is shown in Fig. 16.6.

16.5.2 Tissue response

Tissue response to biomaterials depend on the following properties: bioactivity, osteoconductivity and osteoinductivity [90]. Tissue response in terms of bony ingrowth also depends on the porosity (pore size, pore structure, degree of pore interconnectivity, pore volume as cited above.

Bioactivity

Bioactivity is the ability of the material to directly 'bond' to bone through chemical interaction and not physical or mechanical attachment [100,101]. Bioactivity has been characterized *in vitro* and *in vivo* as the ability of the

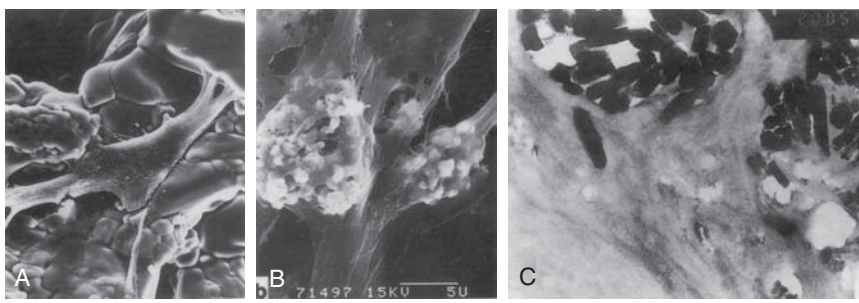

16.6 In vivo cell response to HA: (A) SEM image showing attachment of osteoblast-like cell to ceramic HA; (B) SEM image showing HA crystals phagocytized by cells; (C) TEM of partially dissolving HA crystals inside a cell.

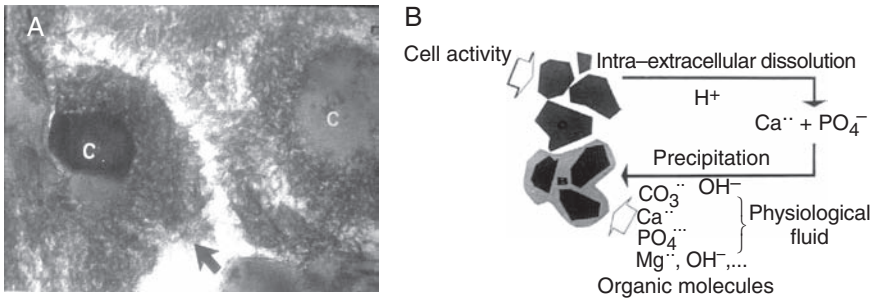

16.7 (A) Nano-apatite crystals (arrow) on surfaces of partially dissolving HA crystals (c). (B) Schematic representation of the dissolution–precipitation processes involved after implantation of HA: HA ceramic crystals are partially dissolved by the acid environment of the ostecolasts releasing calcium and phosphate ions on to the microenvironment, causing supersaturation and precipitation of nano-apatite crystals incorporating other ions (CO_3^{2-}, Mg^{2+}, Na^+, etc.) and associating with organic moieties.

material to form carbonate apatite (similar to bone apatite) on its surface [102–106].

TE micrographs showed formation of apatite nano-crystals similar to bone apatite on the surfaces of coralline HA crystals, but no significant crystal formation was observed associated with ceramic HA for the same amount of time of suspension in bovine serum [64]. *In vivo* nano carbonate apatite crystals were observed on surfaces of HA implanted in non-bony and bony sites [103–105] as shown in Fig. 16.7. The formation of CHA on calcium phosphate, CaP (HA, HAP, β-TCP) surfaces can be explained as cell-mediated dissolution and precipitation processes [103–106]: (a) partial dissolution of the CaP due to the acidic condition produced by osteoclasts, release calcium and phosphate ions in the microenvironment, (b) supersaturation of the microenvironment promotes precipitation of nano-apatite crystals incorporating other ions (e.g. carbonate, magnesium ions) present in the biologic fluid and associating with organic moieties; (c) the nano-crystals become part of the mineralizing collagen and developing new bone at the material/bone interface.

Osteoconductive property

Bioactive materials (calcium phosphates and bioactive glasses) also have osteoconductive properties – an ability to serve as a scaffold or template to guide the newly forming bone along its surfaces. Osteoconductive materials allow bone cell attachment, proliferation, migration and phenotypic expression, leading to formation of new bone in direct apposition to the biomaterial, thus creating a uniquely strong interface.

Osteoinductive property

Osteoinductive material (e.g. demineralized bone matrix, bone growth factors) support tissue ingrowth, allows *de novo* formation of bone even in non-bone-forming sites [107,108]. Calcium phosphate materials are bioactive and osteoconductive but usually not osteoinductive [90]. However, osteoinductive properties of some porous HA has been reported [88,89]. This osteoinductive property was believed to be associated with specific geometry and optimal pore size of the biomaterial.

16.6 Applications

16.6.1 HA as abrasive

A rougher Ti or Ti alloy implant surface was shown to promote greater osteointegration reflected by stronger bone–implant interface (higher pull-out value) [109]. Implant surface roughening is accomplished by grit-blasting with abrasives, usually silica or alumina. More recently, HA or apatitic abrasive (biphasic calcium phosphate) has gained popularity as the abrasive of choice for orthopedic and dental implant. Implant surface grit-blasted with HA or apatitic abrasive was shown to be cleaner (free of inclusions) compared with alumina [31] and appear to promote higher bone contact [30] as shown in Fig. 16.8.

16.6.2 Bone graft materials and scaffolds

Dental applications of HA materials include: implants as immediate tooth root replacement [72,73,110], alveolar ridge augmentation [111], pulp capping [112,113], periodontal defects [114], bone regeneration with guided tissue regeneration membrane [115]; alveolar distraction osteogenesis [116], peri-implantitis defects [115], reconstruction of severely atrophic human maxillae [116] and sinus lifts [117].

Medical applications include: repair of bone defects, chin augmentation, ear implant by itself, or as a composite with high molecular weight polyethylene, spine cage, tibial osteotomy in patients with osteoarthritis, and as a percutanous device [41,118–123]. HA or HAP is also used as component of calcium phosphate cement, CPC [124].

16.6.3 Implant coatings

In spite of the many good qualities of HA and related calcium phosphates (e.g. β-TCP) such as bioactivity and osteoconductivity, they cannot be used in load-bearing areas because of their low fracture strength. On the other hand, metal implants, primarily titanium (Ti) or Ti alloy, are not bioactive and therefore do not bond directly to bone. Plasma-sprayed HA coating was

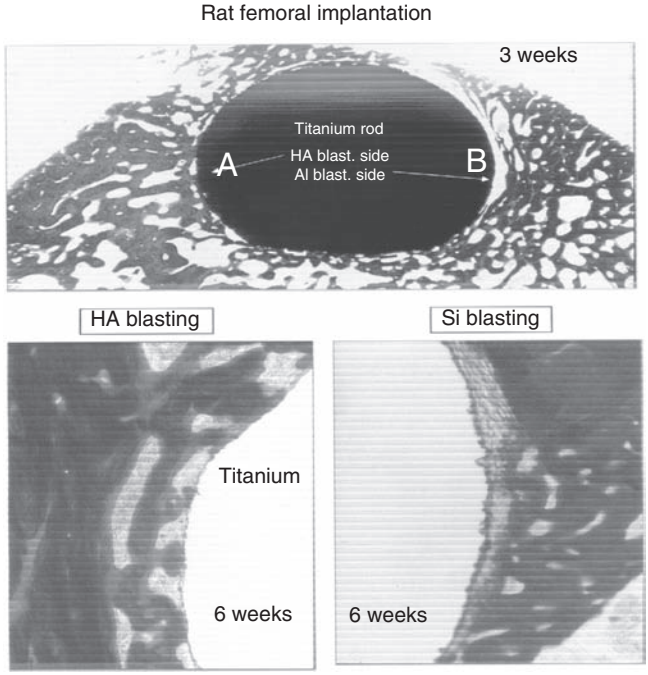

16.8 Bone growth and attachment on Ti alloy surfaces grit-blasted on one side with apatitic abrasive, on the other, with alumina abrasive. The side (A) grit-blasted with apatitite abrasive showed direct bone attachment; the other side (B) grit-blasted with alumina showed indirect bone attachment through non-mineralized fibrous encapsulation.

developed to combine the strength of the metal and the bioactivity of the HA. However, the plasma-spray methods involve very high temperatures causing the partial transformation of the HA to amorphous calcium phosphate (ACP) and HA (untransformed) according to the reaction below:

$$\underset{\text{HA}}{Ca_{10}(PO_4)_6(OH)_2} \rightarrow \underset{\text{ACP}}{Ca_x(PO_4)_y} + \underset{\text{HA}}{Ca_{10}(PO_4)_6(OH)_2} + \underset{\alpha\text{-TCP},\beta\text{-TCP}}{Ca_3(PO_4)_2}$$

XRD analyses of some commercial orthopedic and dental implants coated with plasma-sprayed HA showed that the coatings consists of a mixture of ACP and HA and small amounts of α-TCP and/or β-TCP and that the ACP/HA ranged from 30/70 to 70/30 depending on the manufacturer and sometimes even varying from the same manufacturer but different batch numbers [14,125–128]. Furthermore, the coating composition is not homogeneous: the ACP/HA ratio is higher in the coating layer closest to the metal substrate compared with that in the surface layer. Because ACP is much more soluble than HA [14,90], the dissolution properties and *in*

vivo degradation of the coatings will also vary [125,126]. It is conceivable that a coating with high ACP/HA could biodegrade prematurely and delaminate before the bone had the opportunity to attach to the implant, thereby causing loosening and eventual implant failure. In addition, because the plasma-spray method is a line of sight method, implants with complex geometry or porosity cannot have a homogeneous coating. Coating delamination has been reported [129].

An alternative method of depositing bioactive coating on metal implants is by the electrochemical deposition or precipitation method. The pulse-modulated electrochemical deposition method allows uniform deposition of coating of the desired composition, e.g. calcium-deficient apatite, carbonate apatite, F-apatite or OCP (Fig. 16.9) by appropriate manipulation of pH (6 to 8) and temperature (25–60 °C) [130]. The low temperature involved in this process allows the incorporation of bioactive molecules (e.g.

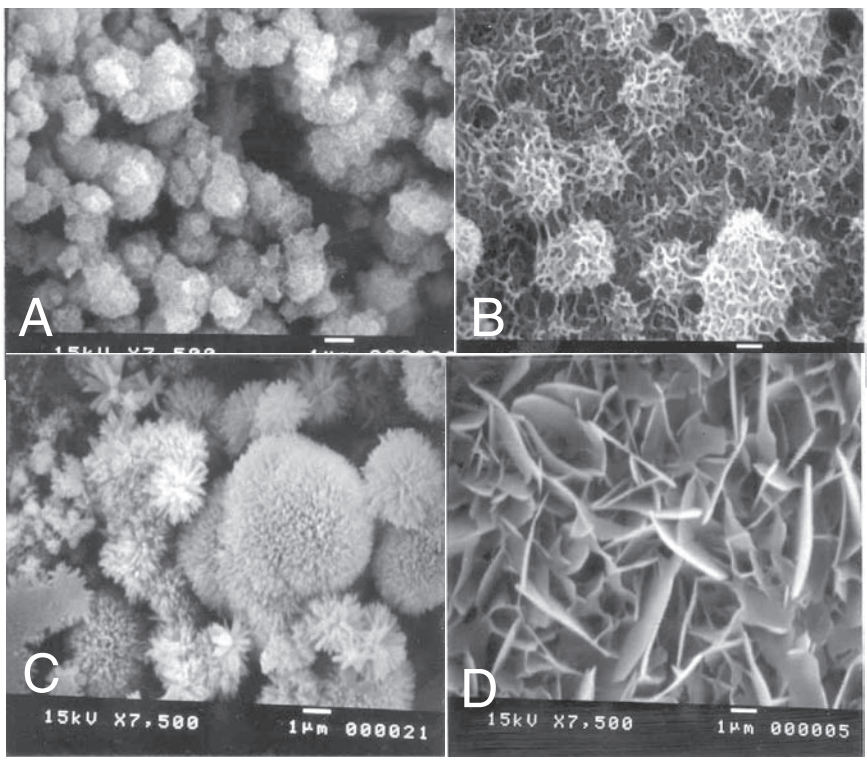

16.9 SEM of calcium phosphates grown by pulse-modulated electrochemical deposition on Ti alloy surfaces, depending on solution pH, temperature and composition: (A) calcium-deficient apatite, CDA; (B) carbonate hydroxyapatite, CHA; (C) F-substituted apatite, FAP; (D) octacalcium phosphate, OCP.

growth factors) if required. An alternative method is by precipitation [131]. Some orthopedic companies are already using precipitated apatite as a coating (Periapatite™, Styker Orthopedics).

16.6.4 Drug delivery and other applications

HA ceramic is used as gene carrier or transfection agents [132], for drug delivery such as delivery of anticancer drugs [133] or bisphosphonate [134], or as scaffolds for bone regeneration by tissue engineering [135].

16.7 Recent developments

Recent developments include: (a) improving mechanical properties of HA by reinforcing HA with zirconia [136] or TiO_2 [137]; (b) potential use of substituted apatites (e.g. Sr-, Si-, CO_3-, F-, Y-substituted apatites as bone-graft materials [8,49–56]; (c) optimizing porosity (macro- and microporosities) to bone-graft materials and scaffolds to introduce osteoinductive properties, and (d) alternative methods to plasma-spray method for depositing bioactive unsubstituted or substituted HA or HAP coatings on orthopedic and dental implants [130–131].

16.8 Summary

Hydroxyapatite (HA or HAP) of biologic (coral-, bovine- or marine algae-derived) or synthetic origin are commercially available for use in bone repair, substitution and augmentation and as scaffolds in tissue engineering for bone regeneration. HA is also used as abrasives to roughen metal implant surfaces and as source material for depositing bioactive coatings on orthopedic and dental implants. These materials can also be used as transfection agents, drug carriers and percutaneous devices. HA- or HAP-based biomaterials with improved properties included substituted apatites.

16.9 Acknowledgments

For our work cited in this chapter, we gratefully acknowledge the collaboration of the following colleagues: Drs G. Daculsi (Universite de Nantes), R. Kijkowska (Technical University of Krakow), R. Rohanizadeh (University of Sydney), S. Lin and D. Mijares (New York University). We thank Ms F. Yao for helping prepare some of the figures used in this chapter. Most of our work cited here was supported by research grants from the National Institutes of Health (NIH), USA.

16.10 References

1. Beevers CA, McIntyre DB (1956). The atomic structure of fluorapatite and its relation to that of tooth and bone mineral. *Miner Mat* **27**:254–259.
2. Kay M, Young RA, Posner AS (1964). The crystal structure of hydroxyapatite. *Nature* **204**:1050–1052.
3. Young RA, Elliott JC (1966). Atomic scale bases for several properties of apatites. *Arch Oral Biol* **11**:699–707.
4. Bonel G (1972). Conribution a l'etude de la carbonation des apatities. *Ann Chim* **7**:65–88.
5. Bonel G, Montel G (1974). Sur une nouvelle apatite carbonate synthetique. *CR Seance Acad Sci Paris* **258**:923–926.
6. Elliott JC (1964). *The crystallographic structure of dental enamel and related apatites.* PhD Thesis, University of London.
7. Fowler BO (1974). Infrared studies of apatites. II. Preparation of normal and isotopically substituted calcium, strontium and barium hydroxyapatites and spectra–structure–composition correlations. *Inorg Chem* **13**:207–214.
8. Inoue M, LeGeros RZ, Inoue M, Tsujigiwa H, Nagatsuka H, Yamamoto T, Nagai N (2004). *In vitro* response of osteoblast-like and odontoblast-like cells to unsubstituted and substituted apatites. *J Biomed Mater Res* **70**A:585–593.
9. Ito A, Nakamura S, Aoki H, Akao M, Traoka K, Tsutsumi S, Onuma K, Tateishi T (1996). Hydrothermal growth of carbonate-containing hydroxyapatite single crystals. *J Crystal Growth* **163**:311–317.
10. LeGeros RZ (1967). *Crystallographic studies of the carbonate substitution in the apatite structure*. PhD Thesis, New York University.
11. LeGeros RZ (1974). Unit cell dimensions of human enamel apatite: effect of chloride incorporation. *Arch Oral Biol* **20**:63–71.
12. LeGeros RZ (1981). Apatites in biological systems. *Prog Crystal Growth Charact* **4**:1–45.
13. LeGeros RZ (1984). Incorporation of magnesium in synthetic and in biological apatites. In: *Tooth Enamel IV*. Fearnhead RW, Suga S (Eds). Elsevier Science Publishers, Amsterdam, pp. 169–174.
14. LeGeros RZ (1991). *Calcium Phosphates in Oral Biology and Medicine*. Monographs in Oral Sciences, Vol 15. Myers H (Ed). Karger: Basel.
15. LeGeros RZ, LeGeros JP (1993). Dense hydroxyapatite. In: *An Introduction to Bioceramics.* Hench LL, Wilson J (Eds). World Scientific: Singapore, pp. 139–180.
16. LeGeros RZ, Suga S (1980). Crystallographic nature of fluoride in the enameloids of fish. *Calcif Tiss Int* **32**:169–174.
17. LeGeros RZ, Tung MS (1983). Chemical stability of carbonate- and fluoride-containing apatites. *Caries Res* **17**:419–429.
18. LeGeros RZ, LeGeros JP, Trautz OR, Shirra WP (1971). Conversion of monetite, $CaHPO_4$, to apatites: effect of carbonate on the crystallinity and morphology of apatite crystallites. *Adv X-ray Anal* **14**:57–66.
19. LeGeros RZ, Sakae T, Bautista C, Retino M, LeGeros JP (1996). Magnesium and carbonate in enamel and synthetic apatites. *Adv Dent Res* **19**:225–231.
20. LeGeros RZ, Trautz OR, LeGeros JP (1967). Apatite crystallites: effect of carbonate on morphology. *Science* **155**:1409–1411.

21. Prener JS (1967). The growth and crystallographic properties of calcium fluor- and chlorapatite crystals. *J Electrochem Soc* **114**:77–83.
22. Rokbani R, LeGeros RZ, Ariguib NK, Ayeti T, LeGeros JP (1998). Formation of apatites in the system: KCl–$CaCl_2$–$Ca_3(PO_4)_2$–K_3PO_4–H_2O at 25 °C. *Bioceramics* **11**:747–750.
23. Zapanta-LeGeros R (1965). Effect of carbonate on the lattice parameters of apatite. *Nature* **206**:403–405.
24. Rey C, Renugoplakrishan V, Collins B (1991). Fourier transform infrared spectroscopic study of the carbonate ions in bone mineral during aging. *Calcif Tissue Int* **49**:251–258.
25. Kawasaki T (1991). Hydroxyapatite as a liquid chromatographic packing. *J Chromatography* **544**:147–184.
26. Phantumvanit P, LeGeros RZ (1997). Characteristics of bone char related to efficacy of fluoride removal from highly-fluoridated water. *Fluoride* **30**:207–218.
27. Ishikawa K, Miyamoto Y, Nagayama M, Asaoka K (1997). Blast coating method: new method of coating titanium surface with hydroxyapatite at room temperature. *J Biomed Mater Res (Appl Biomater)* **38**:129–134.
28. LeGeros JP, Daculsi G, LeGeros RZ (1998). Tissue response to grit-blasted Ti alloy. *Proc. 25th Annual International Soc of Biomaterials* (abstract).
29. Salgado T, LeGeros JP, Wang J (1998). Effect of alumina and apatitic abrasives on Ti alloy substances. *Bioceramics* **11**:683–686.
30. Ben-Nissam B, LeGeros RZ (2007). Biologic and synthetic apatite. In: *Encyclopedia of Biomaterials and Biomedical Engineering*. Informa Healthcare: London.
31. LeGeros RZ (1988). Calcium phosphate materials in restorative dentistry: a review. *Adv Dent Res* **2**:164–183.
32. Deer WA, Howie Ra, Zussman J (1985). *An Introduction to Rock-forming Minerals.* Longman: Hong Kong, pp. 504–509.
33. DeJong WF (1926). La substance minerale dans les os. *Res Trav Chim* **45**:445–448.
34. McConnell D (1952). The crystal chemistry of carbonate apatites and their relationship to the composition of calcified tissue. *J Dent Res* **31**:53–63.
35. Kay M, Young RA, Posner AS (1964). The crystal structure of hydroxyapatite. *Nature* **204**:1050–1052.
36. Moreno EC, Kresak M, Zahradnik RT (1997). Physicochemical aspects of fluoride-apatite systems relevant to the study of dental caries. *Caires Res* (suppl 1) **11**:142–177.
37. deGroot K (1983). Ceramics of calcium phosphates: preparation and properties. In: *Bioceramics of Calcium Phosphate.* deGroot K (Ed). CRC Press: Boca Raton, pp. 100–114.
38. Jarcho M (1976). Hydroxylapatite synthesis and characterization in dense polycrystalline forms. *J Mater Sci* **11**:2027–2035.
39. Jarcho M (1981). Calcium phosphate ceramics as hard tissue prosthetics. *Clin Orthopaed* **157**:259–78.
40. Aoki H, Kato K, Ogiso M, Tabata T (1977). Sintered hydroxyapatite as as a new dental implant material. *J Dent Outlook* **49**:567–575.
41. Aoki H (1994). *Medical Applications of Hydroxyapatite*. Ishiyaku EuroAmerica, Inc.: Tokyo.

42. Holmes RE (1979). Bone regeneration within a coralline hydroxyapatite implant. *Plast Reconstr Surg* **63**:626–633.
43. Holmes RE, Hagler HK (1987). Porous hydroxylapatite as a bone graft substitute in mandibular contour augmentation. *J Oral Maxillofac Surg* **45**:421–426.
44. Albee FH (1920). Studies in bone growth: triple calcium phosphate as a stimulus to osteogenesis. *Ann Surg* **71**:32–36.
45. Monroe ZA, Votawa W, Bass DB, McMullen J (1971). New calcium phosphate ceramic material for bone and tooth implants. *J Dent Res* **50**: 860–862.
46. Bonfield W, Grynpas MD, Tully AE, Bowman J, Abram J (1981). Hydroxyapatite reinforced polyethylene – a mechanically compatible implant material for bone replacement. *Biomaterials* **2**:186–186. Prosthesis comprising composite materials UK Patent GB2085461B, The Patent Office, London, 1984.
47. Geesink RGT, Manley MT (eds) (1993). *Hydroxylapatite Coatings in Orthopaedic Surgery*. Raven Press: New York.
48. Golec TS, Krauser JT (1992). Long-term retrospective studies on hydroxyapatite-coated endosteal and subperiosteal implants. *Dental Clinics of North America* **36**:39–65.
49. LeGeros RZ, LeGeros JP, Kim Y, Kijkowska R, Zheng R, Bautista C, Wang JL (1995). Calcium phosphates in plasma-sprayed HA coatings. *Ceramic Trans* **48**:173–189.
50. Botelho CM, Brooks RA, Best SM, Lopez MA, Santos JD, Rushton N, Bonfield W (2006). Human osteoblast response to silicon-substituted hydroxyapatite. *J Biomed Mater Res* 79A:723–730.
51. Gibson IR, Best SM, Bonfield W (1999). Chemical characterization of silicon-substituted hydroxyapatite. *J Biomed Mater Res* **44**:422–428.
52. Gineste L, Gineste M, Ranz X, Ellefterio A, Guilhem A, Rouquet N, Frayssinet P (1999). Degradation of hydroxyapatite, fluorapatite and fluorhydroxyapatite coatings of dental implants in dogs. *J Biomed Mater Res (Appl Biomater)* **48**:224–234.
53. Hasegawa M, Ohashi T, Tani T, Doi Y (2001). Osteoconduction and bioresorption of sintered carbonate apatite. *Key Eng Mater* 192–**195**:453–456.
54. Sakae T, Ookubo A, LeGeros RZ, Shimogoryou R, Sato Y, Yamamoto H, Kozawa Y (2003). Bone formation induced by several carbonate- and fluoride-containing apatites implanted in dog mandible. *Key Engineer Mater* **240–242**:395–398.
55. Takeuchi A, Maruta M, Matsuya S, Nakagawa M, Ishikawa K (2006). Preparation of carbonate apatite block from gypsum by hydrothermal treatment. *Arch BioCeram Res* **6**:99–102.
56. Webster TJ, Ergun C, Deoremus R, Bizios R (2002). Hydroxylapatite with substituted magnesium, zinc, cadmium and yttrium. II. Mechanisms of osteoblast adhesion. *J Biomed Mater Res* **59**:312–317.
57. Xue W, Moore JL, Hosick HL, Bose S, Bandyopadhyay A, Lu WW, Cheung MC, Luk KDK (2006). Osteoprecursor cell response to strontium-containing hydroxyapatite ceramics. *J Biomed Mater Res* **79**A:804–814.
58. Lickorish D, Ramshaw JAM, Werkmeister JA, Glattauer V, Howlett CR (2004). Collagen-hydroxyapatite composite prepared by biomimetic process. *J Biomed Mater Res* **68**A:19–27.

59. Yunoki S, Ikoma T, Tsuchiya A, Monkawa A, Ohta K, Sotome S, Shinomiya K, Tanaka J (2007). Fabrication and mechanical and tissue ingrowth properties of unidirectionally porous hydroxyapatite/collagen composite. *J Biomed Mater Res* 80B:166–173.
60. Roy DM, Linnehan SA (1974). Hydroxyapatite formed from coral skeleton carbonate by hydrothermic exchange. *Nature* **247**:220–227.
61. Gunham O, Bal E, Alsum B, Sengum O, Finci RA (1994). Comparative histological study of non-porous and microporous (algae-derived) hydroxyapatite ceramics. *Aust Dent J* **39**:25–27.
62. Schopper C, Moser D, Sabbas A, Lagogiannis G, Spassova E, Konig F, Donath K, Ewers R (2003). The fluorohydroxyapatite (FHA) FRIOS® Algipore is a suitable biomaterial for the reconstruction of severely atrophic human maxillae. *Clin Oral Impl Res* **14**:741–749.
63. Dard M, Bauer A, Liebendorgen A, Wahlig H. Dingeldein E (1994). Preparation physicochemical and biological evaluation of a hydroxyapatite ceramic from bovine spongiosa. *Acta Odont Stom* **185**:61–69.
64. LeGeros RZ, Orly I, Gregoire M, Kazimiroff J (1991). Comparative properties and in vitro reactions of HA ceramic and coralline HA. *Apatite* **1**:229–233.
65. Hattori T, Iwadata Y (1990). Hydrothermal preparation of calcium hydroxyapatite powders. *J Am Ceram Soc* **73**:1803–1805.
66. Takeuchi A, Maruta M, Matsuya S, Nakagawa M, Ishikawa K (2006). Preparation of carbonate apatite block from gypsum by hydrothermal treatment. *Arch BioCeram Res* **6**:99–102.
67. Wakae H, Takeuchi A. Matsuya S, Munar M, LeGeros R, Nakagawa M, Udoh K, Ishikawa K (in press). Preparation of carbonatea apatite foam by hydrothermal treatment of α-TCP foam in carbonate salt solutions. *J Biomed Mater Res*.
68. LeGeros RZ, Daculsi G, Orly I, Abergas T, Torres W (1989). Solution-mediated transformation of octacalcium phosphate (OCP) to apatite. *Scann Microsc* **3**:129–138.
69. Obadia L, Rouillon T, Buhjoli B, Daculsi G, Bouler JM (2007). Calcium deficient apatite synthesized by ammonia hydrolysis of dicalcium phosphate dihydrate: Influence of temperature, time and pressure. *J Biomed Mater Res* **80**B:32–42.
70. LeGeros RZ, Morales P (1973). Renal stone crystals grown in gel systems. *Invest Urol* **11**:12–20.
71. Deptula A, Lada W, Olczak T, Borillo A, Alvani C, DiBartolomeo A (1992). Preparation of spherical powders of hydroxyapatite by sol–gel process. *J Non-cryst Solids* **147–148**:537–541.
72. Denissen H, deGroot K (1979). Immediate dental root implants from synthetic dense calcium hydroxyapatite. *J Prost Dent* **42**:551.
73. Denissen H, Mangano C, Venini G (1985). *Hydroxylapatite Implants.* Piccin Nuova Libraria, SPA: Padua.
74. Li SH, de Wijn JR, Layrolle P, deGroot K (2002). Synthesis of macroporous hydroxyapatite scaffolds for bone tissue engineering. *J Biomed Mater Res* **61**:109–120.

75. Klawitter JJJ, Bagwell JG, Weinstein AM, Sauer BW, Pruitt JR (1976). An evaluation of bone growth into porous high density polyethylene. *J Biomed Mater Res* **10**:311–323.
76. Hubbard W (1974). Physiological CaP as orthopedic implant material. PhD Thesis, Milwaukee, Marquette University.
77. Rodriguez-Lorenzo LM, Vallet-Regi M, Ferreira JMF (2002). Fabrication of porous hydroxyapatite apatite bodies by a new direct consolidation method: starch consolidation. *J Biomed Mater Res* **60**:232–240.
78. Ramay HR, Zhang M (2003). Preparation of porous hydroxyapatite scaffolds by combination of gel-casting and polymer sponge methods. *Biomaterials* **24**:3293–3302.
79. Sepulveda P, Ortega PS, Innocentini MDM, Pandolfelli VC (2000). Properties of highly porous hydroxyapatite obtained by the gelcasting of foams. *J Ceram Am Soc* **83**:3021–3024.
80. Wilson CE, deBruijn JD, van Blitterswijk CA, Verbout AJ, Dhert WJ (2004). Design and fabrication of standardized hydroxyapatite scaffolds with a defined macro-architecture by rapid prototyping for bone-tissue-engineering research. *J Biomed Mater Res* **68**:123–132.
81. Chang BS, Lee CK, Hong KS, Youn HJ, Ryu HS, Chung SS, Park KW (2000). Osteoconduction at porous hydroxyapatite with various pore configurations. *Biomaterials* **21**:1291–1298.
82. Gauthier O, Bouler J-M, Aguado E, Pilet P, Daculsi G (2006). Macroporous biphasic calcium phosphate ceramics: influence of macropore diameter and macroporosity percentage on bone ingrowth. *Biomaterials* **19**:133–139.
83. Hing KA, Best SM, Tanner KE, Bonfield W, Revell PA (2004). Mediation of bone ingrowth in porous hydroxyapatite bone graft substitutes. *J Biomed Mater Res* **68**A:187–200.
84. Liu JX, Flautre B, Anselme K (1999). Role of interconnections in porous bioceramics on bone recolonization *in vitro* and *in vivo*. *J Mater Sci Mater Med* **10**:111–120.
85. Lu WW, Zhao F, Luk KD, Yin YJ, Cheung KM, Cheng GX, Yao KD, Leong JC (2003). Controllable porosity hydroxyapatite ceramics as spine cage: fabrication and properties evaluation. *J Mater Sci Mater Med* **114**:1039–1046.
86. Mastrogiacomo M, Scaglione S, Martinette R, Dolcini L, Beltrame F, Canceda R, Quarto R (2006). Role of scaffold internal structure on *in vivo* bone formation in macroporous calcium phosphate ceramics. *Biomaterials* **27**:3230–3237.
87. Tamai N. Myoui A, Tomita T, Nakase T, Tanaka J, Ochi T, Yoshikawa H (2002). Novel hydroxyapatite ceramics with an interconnective porous structure exhibits superior osteoconduction *in vivo*. *J Biomed Mater Res* **59**:110–117.
88. Kuboki Y, Takita H, Kobayashi D (1998). BMP-induced osteogenesis on the surface of hydroxyapatite with geometrically feasible and nonfeasible structures. Topology of osteogenesis. *J Biomed Mater Res* **39**:190–199.
89. Ripamonti U, MaS, Reddi AH (1992). The critical role of geometry of porous hydroxyapatite delivery system induction of bone by osteogenin, a bone morphogenetic protein. *Matrix* **12**:202–212.
90. LeGeros RZ (2002). Properties of osteoconductive biomaterials: calcium phosphates. *Clin Orthopaed Rel Res* **395**:81–98.

91. Daculsi G, LeGeros JP (1996). Three-dimensional defects in hydroxyapatite of biological interest. *J Biomed Mater Res* **31**:495–501.
92. Daculsi G, LeGeros RZ, Mitre D (1989). Crystal dissolution of biological and ceramic apatites. *Calcif Tiss Int* **45**:95–103.
93. LeGeros RZ, Lin S, Rohanizadeh R, Mijares D, LeGeros JP (2003). Biphasic calcium phosphate bioceramics: preparation, properties and applications. *J Mater Sci Mater in Med* **13**:201–210.
94. LeGeros RZ, Bautista C, LeGeros JP, Vijaraghavan TV, Retino M (1995). Comparative properties of bioactive bone graft materials. In: *Bioceramics 8*. Hench L, Wilson J (Eds). Pergamon Press: London, pp. 1–7.
95. LeGeros, RZ (1993). Biodegradation and bioresorption of calcium phosphate ceramics. *Clin Mater* **14**:65–88.
96. Craig RC, LeGeros RZ (1999). Early events associated with periodontal connective tissue attachment formation on titanium and hydroxyapatite surfaces. *J Biomed Mater Res* **47**:585–594.
97. Fujimori Y, Mishima H, Sugaya K, Sakae T, LeGeros RZ, Kozawa Y, Nagura H (1998). In vitro interactions of osteoclast-like cells and hydroxyapatite ceramics. *Bioceramics* **11**:335–338.
98. Frondoza C, LeGeros RZ, Hungerford DS (1998). Effect of bovine bone-derived materials on human osteoblast-like cells *in vitro*. *Bioceramics* **11**:289–291.
99. Winters J, Kleckner A, LeGeros RZ (1989). Fluoride inhibits osteoclastic bone resorption *in vitro*. *J Dent Res* **68**:353.
100. Hench LL. Bioceramics (1994). From concept to clinic. *J Am Ceram Soc* **74**:1487–1510.
101. Osborn JF, Newesely H (1980). The material science of calcium phosphate ceramic. *Biomaterials* **1**:108–111.
102. Kokubo T (1996). Formation of biologically active bone-like apatite on metals and polymers by a biomimetic process. *Thermochim Acta* **280**:479–490.
103. Heughebaert M, LeGeros RZ, Gineste M, Guilhem A, Bonel G (1988). Physico-chemical characterization of deposits associated with HA ceramics implanted in non-osseous sites. *J Biomed Mater Res* **22**:254–268.
104. LeGeros RZ, Daculsi G (1990). *In vivo* transformation of biphasic calcium phosphate ceramics: histological ultrastructural and physico-chemical characterization. In: *Handbook in Bioactive Ceramics.* Vol 2. Yamamuro T, Hench L, Wison-Hench J (Eds). CRC Press: Boca Raton pp. 17–28.
105. LeGeros RZ, Orly I, Gregoire M, Daculsi G (1991). Substrate surface dissolution and interfacial biological mineralization. In: *The Bone–Biomaterial Interface*. Davies JE (Ed). Univ of Toronto Press, pp. 76–86.
106. Boyde A, Corsi A, Quarto R (1999). Osteoconduction on large macroporous hydroxyapatite ceramic implants: evidence for a complementary integration and disintegration mechanism. *Bone* **24**:579–589.
107. Reddi AH (2000). Morphogenesis and tissue engineering of bone and cartilage: Inductive signals, stem cells and biomimetic biomaterials. *Tissue Eng* **6**:351–359.
108. Urist MR (1965). Bone formation by autoinduction. *Science* **150**:893–898.

109. Buser B, Schenk RK, Steinman S, Fiorellini JP, Fox CH, Stich H (1991) Influence of surface characteristics on bone integration of titanium implants. A histomorphometric study in miniature pigs. *J Biomed Mater Res* **25**:889–902.
110. Ogiso M, Tabata T, Borgese D (1993). Clinical evaluation of two-piece apatite dental implants in 189 cases. *J Long-Term Effects Med Implants* **3**:57–68.
111. ElDeeb M, Tompach PC, Morstad AT, Know P (1991). Long-term follow-up of the use of nonporous hydroxyapatite for augmentation of the alveolar ridge. *J Oral Maxillofac Sur* **49**:257–261.
112. Frank RM, Widermann P, Hemmerle J, Freymann M (1991). Pulp capping with synthetic hydroxyapatite in human premolars. *J Appl Biomat* **2**:243–250.
113. Jean A, Kerebel B, Kerebel LM, LeGeros RZ, Hamel H (1988). Effects of various calcium phosphate biomaterials on reparative dentine bridge formation. *J Endo* **14**:83–87.
114. Knychalska-Karwan Z, Kaczmarczyk-Stachowska A, Slosarczyk A, Stobierska E, Paszkiewicz Z (1997). Long term results of hydroxyapatite application in the treatment of periodontal osseous defects. *Front Med Biol Eng* **8**:239–252.
115. Schwarz F, Bieling K, Latz T, Nuesry E, Becker J (2006). Healing of intrabony per-implantitis defects folowing appication of a nanocrystalline hydroxyapatite (Ostim) or a bovine-derived xenograft (BioOss) in combination with a collagen membrane (Bio-Gide). *J Clin Periodontol* **7**:491–499.
116. Aragon CE, Bohay RN (2005). The application of alveolar distraction osteogenesis following non-resorbable HA grafting in the anterior maxilla: a clinical report. *J Prosthet Dent* **93**:518–521.
117. Peltola MJ, Aitasalo KMJ, Sounpaa JTK, Yii-Urpo A, Laippala PJ (2001). *In vivo* model for frontal sinus and calvarial bone defect obliteration with bioactive glass S53P4 and hydroxyapatite. *J Biomed Mater Res Appl Biomat* **58**:261–269.
118. Heise U, Osborn JF, Duwe F (1990). Hydroxyapatite ceramic as a bone substitute. *Int Orthop* **14**:329–338.
119. Uchida A, Araki N, Shinto Y, Yoshikawa H, Kurisaki E, Ono K (1990). The use of calcium hydroxyapatite ceramic in bone tumour surgery. *J Bone Joint Surg* **72**B:298–302.
120. Andrade JC, Camilli JA, Kawachi EY, Betran CA (2002). Behavior of dense and porous hydroxyapatite implants and their response in rat femoral defects. *J Biomed Mater Res* **62**:30–36.
121. Kobayashi T, Shingaki S, Nakajima T, Hanada K (1993). Chin augmentation with porous hydroxyapatite blocks. *J Long-Term Effects Med Impl* **3**:283–294.
122. Jahn AF (1992). Experimental applications of porous (coralline) hydroxyapatite in middle ear and mastoid reconstruction. *Laryngoscope* **102**:289–299.
123. Koshino T, Murase T, Tagagi T, Saito T (2001). New bone formation around porous hydroxyapatite wedge implanted in opening wedge high tibial osteotomy in patients with osteoarthritis. *Biomaterials* **22**:1579–1582.
124. Niwa S, LeGeros RZ (2002). Injectable calcium phosphate cements for repair of bone defects. In: *Tissue Engineering and Biodegradable Equivalents: Scientific and Clinical Applications.* Lewandrowski K-U, Wise DL, Trantolo DJ, Gresser JD (Eds). Marcel Dekker Inc: New York, pp. 385–500.

125. LeGeros JP, LeGeros RZ, Burgess A, Edwards B, Zitelli J (1994). X-ray diffraction method for the quantitative characterization of calcium phosphate coatings. In: *Characterization and Performance of Calcium Phosphate Coatings for Implants*. Horowitz E, Parr Je (Eds). ASTM STP 1196, pp. 33–42.
126. LeGeros RZ, Kim YE, Kijikowska R, Zurita V, Bleiwas C, Huang PY, Edwards B, Dimaano F, LeGeros JP (1998). HA/ACP ratios in calcium phosphate coatings on dental and orthopedic implants: effect on properties. *Bioceramics* **11**:181–184.
127. Tufekci E, Brantley WA, Mitchell JC, Foreman DW, Georgette FS (1999). Crystallographic characteristics of plasma-sprayed calcium phosphate coatings on Ti-6-Al-4V. *J Oral Maxillofac Implants* **14**:661–672.
128. LeGeros RZ, LeGeros JP (2006). *In situ* characterization of degradation behavior of plasma-sprayed coatings on orthopedic and dental implants. *Adv Sci Tech* **49**:203–211.
129. Bloebaum RD, Cupont JA (1938). Osteolysis from a press-fit hydroxyapatite-coated implant. A case study. *J Arthop* **8**:195–202.
130. LeGeros JP, Lin S, Mijares D, Dimaano F, LeGeros RZ (2005). Electrochemically deposited calcium phosphate coating on titanium alloy substrates. *Key Engineer Mat* **284–286**:247–250.
131. Rohanizadeh R, LeGeros RZ, Harson M, Ben-David A (2004). Adherent apatite coating on titanium substrate using chemical deposition. *J Biomed Mater Res* **72**A:428–438.
132. Frayssinet P, Rouquet N, Mathon D (2006). Bone cell transfection in tissue culture using hydroxyapatite microparticles. *J Biomed Mater Res* **79**A:225–228.
133. Uchida A, Shinto Y, Araki N, Ono K (1992). Slow release of anticancer drugs from porous calcium hydroxyapatite ceramic. *J Orthop Res* **10**:440–445.
134. McLeod K, Anderson GI, Dutta NK, Smart RSC, Voelcker NH, Sekel R, Kumar S (2006). Adsorption of bisphosphonate onto hydroxyapatite using a novel co-precipitation technique for bone growth enhancement. *J Biomed Mater Res* **79**A:271–281.
135. Ohgushi H, Caplan AL (1999). Stem cell technology and bioceramics: from cell to gene engineering. *J Biomed Mater Res Appl Biomater* **48**:913–927.
136. Kong Y-M, Kin S, Kim H-E, Lee IS (1999). Reinforcement of hydroxyapatite ceramic by addition of ZrO_2 coated with Al_2O_3. *J Am Ceram Soc* **82**:2963–2968.
137. Chu C, Xue X, Zhu J, Yin Z (2006). Fabrication and characterization of titanium-matrix composite with 20 vol% hydroxyapatite for use as heavy load-bearing hard tissue replacement. *J Mater Sci Mater Med* **17**:245–251.

17

Tricalcium phosphate/hydroxyapatite biphasic ceramics

G DACULSI, INSERM, Nantes University and Bordeaux Hospital, France and R LEGEROS, New York University, College of Dentistry, USA

17.1 Introduction

Albee, in 1920, reported the first successful application of a calcium phosphate reagent for the repair of bone defect in human [1]. More than 50 years later, clinical use of a 'tricalcium phosphate' preparation in surgically created periodontal defects in animals was reported by Nery *et al.* [2] and use of dense hydroxyapatite (HA) as immediate tooth root replacements was reported by Denissen [3]. Largely through the separate efforts of Jarcho, de Groot and Aoki in the early 1980s [4–8], synthetic HA and β-tricalcium phosphate (β-TCP) became commercially available as bone substitute materials for dental and medical applications [5].

The term biphasic calcium phosphate (BCP) was first used by Ellinger *et al.* [9] to describe the bioceramic previously described as 'tricalcium phosphate' [2] but was shown by LeGeros in 1986 using X-ray diffraction (XRD) to consist of a mixture of 80% HA and 20% β-TCP [8]. The first basic studies on BCP with varying HA/β-TCP was reported by LeGeros and Daculsi and coworkers [10–12], demonstrating that the bioactivity of these ceramics may be controlled by manipulating the HA/β-TCP ratios. Subsequently, focused studies on BCP by Daculsi and coworkers [13–17] led to the significant increase in the manufacture and use of commercial BCP bioceramics as bone substitute materials for dental and orthopedic applications [16,18–25].

The development of BCP ceramics and other related biomaterials for bone graft involves control of the processes of biomaterials resorption and bone formation at the expense of the biomaterial. Synthetic bone graft materials are available as alternatives to autogeneous bone for repair, substitution or augmentation.

The BCP concept is based on an optimum balance between the more stable phase (HA) and the more soluble phase (β-TCP). BCP bioceramics are soluble and gradually dissolve *in vivo*, seeding new bone formation as MBCP releases calcium and phosphate ions into the biological medium.

Commercial BCP bioceramics consist of a mixture of HA, ($Ca_{10}(PO_4)_6(OH)_2$) and β-TCP ($Ca_3(PO_4)_2$) of varying HA/β-TCP ratios (Table 17.1).

The main attractive feature of bioactive bone graft materials such as BCP ceramic is their ability to form a strong direct bond with the host bone, resulting in a strong interface compared with bioinert or bio-tolerant materials which form a fibrous interface [5, 26–31]. The formation of the dynamic interface between bioactive materials and host bone is believed to result from a sequence of events involving interaction with cells; formation of carbonate hydroxyapatite (CHA; similar to bone mineral) by dissolution–precipitation processes [11,29–33].

At the present time, commercial BCPs are sold in Europe, the US, Brazil, Japan, Korea, Taiwan, China as bone-graft or bone substitute materials for orthopedic and dental applications under various trademarks (Table 17.1). Currently, BCP bioceramics are recommended for use as an alternative or additive to autogeneous bone for orthopedic and dental applications. These commercial BCPs are available in blocks, particulates (granules) and custom-designed shapes such as wedges for tibial opening osteotomy, cones for spine and knee, and inserts for vertebral cage fusion.

Exploratory studies demonstrated the potential uses of BCP ceramics as scaffold for tissue engineering for bone regeneration, gene therapy and drug delivery. More recently the BCP granules concept has been applied in the development of a new generation of injectible, moldable bone substitutes [34,35]. BCP granules are combined with various polymers, natural (e.g. fibrin sealent) or synthetic (e.g. hydrosoluble polymer) for the development of injectible bone substitute, IBS [36], or calcium phosphate cement

Table 17.1 Commercial BCP and BCP composites

HA/β-TCP ratio	
60/40; 20/80	MBCP® (Biomatlante, France)
20/80	Tribone 80® (Strycker Europe)
60/40	Osteosynt® (Einco Ltd, Brazil)
60/40	Triosite® (Zimmer, IND)
60/40	4Bone® (MIS Israel)
60/40	OptiMX® (Exactech USA)
55/45	Eurocer 400® (Depuy-Bioland, France)
65/35	Eurocer 200® (Depuy-Bioland, France)
Composites	
BCP/collagen	Allograft (Zimmer, IN)
BCP/HPMC	MBCP Gel ® (Biomatlante France)
BCP/fibrin	Tricos® (Baxter BioSciences BioSurgery)
BCP/silicon	FlexHA (Xomed, FL)
Calcium phosphate cement	MCPC™ (Biomatlante France)

to improve macroporosity and greater osteoconduction. New products recently developed include: MBCP Gel™ (an injectable, non-self-hardening biomaterial consisting of BCP granules combined with a hydrosoluble polymer); Tricos™ (combination of BCP and fibrin sealant as bone substitute biomaterials); and MCPC™ (a micro- and macroporous calcium phosphate cement containing BCP granules that produces a cement with interconnecting macroporosity).

17.2 Fabrication and properties

Biphasic calcium phosphate (BCP), or intimate mixtures of HA and β-TCP, is obtained when synthetic calcium-deficient apatites (CDAs) are sintered above 900 °C [11,26,29] according to the following reaction:

$$\underset{\text{(CDA)}}{Ca_{10-x}M_x(PO_4)_{6-y}(HPO_4)_y(OH)_2} \rightarrow \underset{\text{(HA)}}{Ca_{10}(PO_4)_6(OH)_2} + \underset{\text{(β-TCP)}}{Ca_3(PO_4)_2}$$

The apatite is considered calcium deficient when the Ca/P ratio is lower than the stoichiometric value of 1.67 for pure calcium hydroxyapatite, $\mathbf{Ca_{10}(PO_4)_6(OH)_2}$. CDAs may be represented by the formula $\mathbf{Ca_{10-x}M_x(PO_4)_{6-y}(HPO_4)_y(OH)_2}$ where M represents other ions (e.g. sodium, magnesium) that can substitute for calcium (Ca) ions. Calcium deficiency of the apatites depends on the synthesis conditions (precipitation or hydrolysis methods), reaction pH and/or temperature [26,29,34,37]. CDA may be obtained by the precipitation method under different conditions of pH and temperature; the lower the pH, the higher the temperature required for the precipitation of apatite [26,29]. For example, CDA is obtained by precipitation at 80–100 °C even at low pH (pH 4 to 6). At lower temperatures and low pH, non-apatitic calcium phosphates e.g. dicalcium phosphate dihydrate (DCPD), $CaHPO_4{\cdot}2H_2O$ or octacalcium phosphate (OCP), $Ca_8H_2(PO_4)_6{\cdot}5H_2O$, is obtained [29].

Another method of CDA preparation is by hydrolysis of non-apatitic calcium phosphates, including amorphous calcium phosphate (ACP), $Ca_x(PO_4, HPO_4)_y$; DCPD; dicalcium phosphate anhydrous (DCPA), $CaHPO_4$; OCP; or β-TCP, $Ca_3(PO_4)_2$ [26,29,36–38]. In the hydrolysis of DCPD in NaOH solutions, the calcium deficiency of the unsintered apatite and, subsequently, the HA/β-TCP ratio of the BCP obtained after sintering, can be controlled by two variables: the concentration of the NaOH solution and the ratio of the weight of the DCPD to the volume of the NaOH solution [37].

The BCP composition (HA/β-TCP ratio) obtained after sintering depends on the calcium deficiency of synthetic apatite and on the sintering temperature [26,29,38]. BCP ceramic may also be prepared by mechanically mixing two types of synthetic apatites or commercial calcium phosphate reagents:

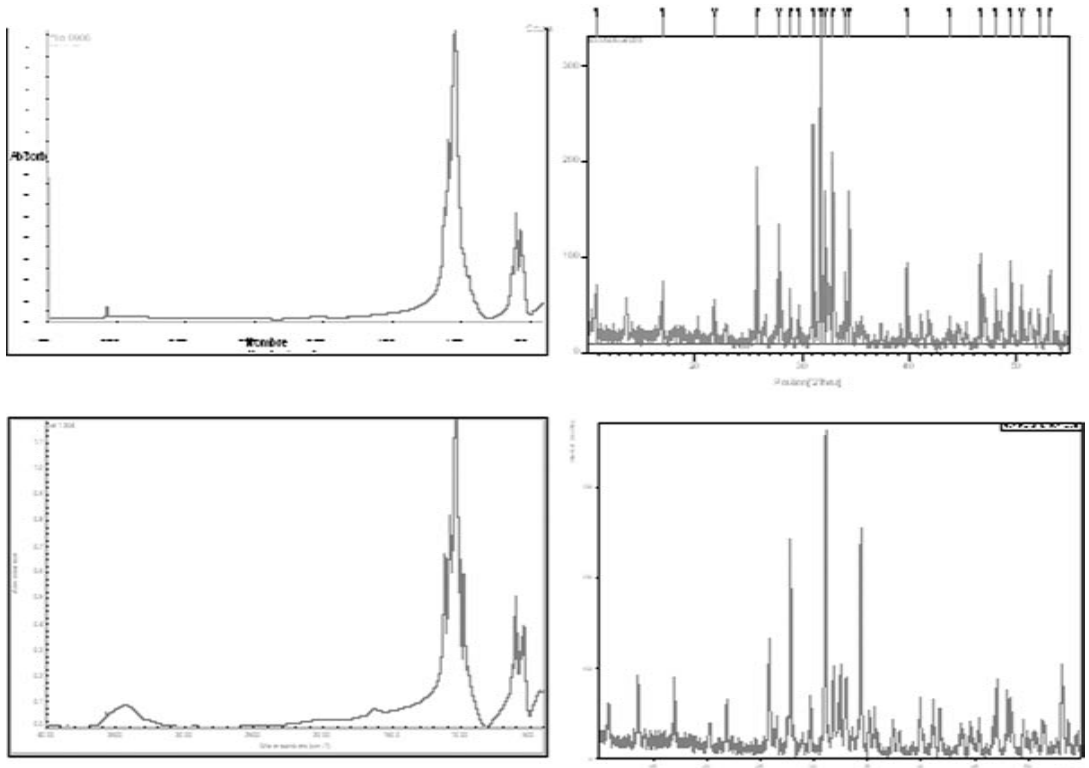

17.1 XRD profiles and FT-IR spectra of BCP with 60/40 and 20/80 HA/β-TCP ratio.

one preparation being that, when sintered above 900 °C, results in the formation of only HA, and the other preparation being, only β-TCP [26,39]. However, this process (mechanical mixing of two types of synthetic apatites) is not recommended for the production of BCP with reproducible HA/β-TCP ratio and homogeneous crystal distribution. XRD profiles and Fourier transform infrared (FT-IR) spectra of BCP with two different HA/β-TCP ratios are shown in Fig. 17.1.

17.2.1 Introduction of macroporosity and microporosity

Two physical properties of bioceramics are believed to be very important for optimum biological performance, including bioceramic–cell interaction, bioceramic resorption, bioceramic–tissue interface and new bone formation. These fundamental physical properties are interconnecting macroporosity and appropriate microporosity [40,41].

Macroporosity in the BCP ceramic is introduced by incorporating volatile materials (e.g. naphthalene, hydrogen peroxide or other porogens), heating at temperature below 200 °C and subsequent sintering at higher temperatures [26,39,40,42,43]. Macroporosity is formed resulting from the release of the volatile materials (Fig. 17.2a). Microporosity (Fig. 17.2b) is a consequence of the temperature and duration of sintering [26]: the higher the temperature, the lower the microporosity content and the lower the specific surface area (Fig. 17.3a and b).

Presently, commercial BCP products of different or similar HA/β-TCP ratios are manufactured in many parts of the world and their successful use in medicine and dentistry has been reported [14,16,18,21–24,44]. The total porosity (macroporosity plus microporosity) of these products is reported to be about 70% of the bioceramic volume. The current BCP commercial products with HA/β-TCP ratios ranging from 60/40 to 75/25 (Table 17.1), present similar percentage macroporosity (50–60%), but the percentage microporosities are very different (varying from 3–25%). Low-percentage microporosity and low surface area can result in lower bioactivity and lower dissolution property. A microporosity of at least 20% with specific surface area higher than 2 m^2/g is suggested for optimal BCP efficacy.

The ideal pore size for a bioceramic material should approximate that of bone. It has been demonstrated that microporosity (diameter < 10 μm) allows body fluid circulation whereas macroporosity (diameter > 100 μm) provides a scaffold for bone-cell colonization. It was reported that BCP ceramic with an average pore size diameter of 565 μm (compared with those with average pore size diameter of 300 μm) and 40% macroporosity (compared with 50% macroporosity) had greater bone ingrowth [17].

A significant improvement of the method for introducing macroporosity/microporosity was recently developed in the production

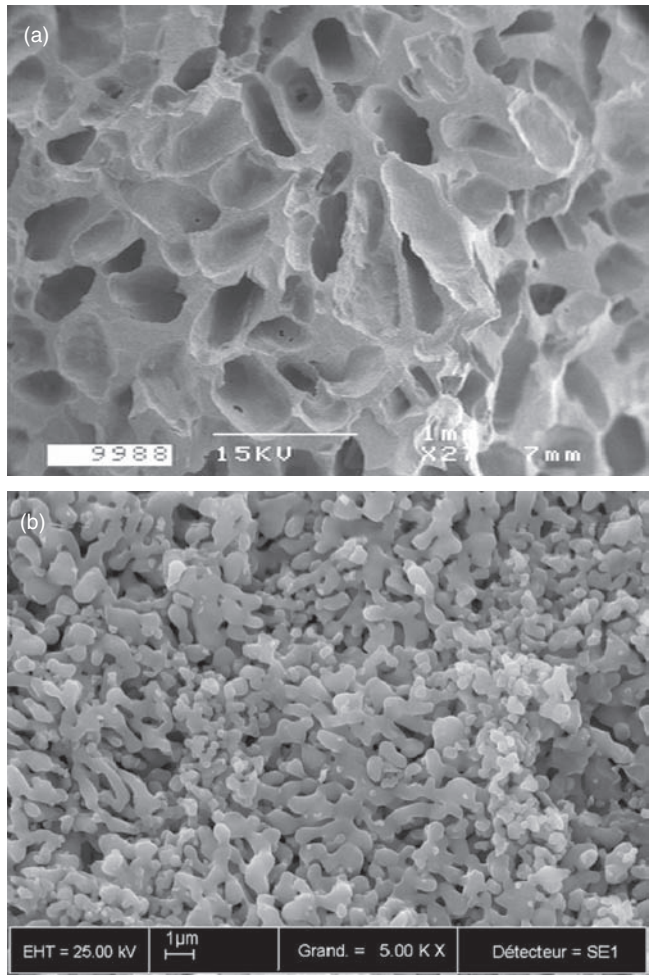

17.2 **(a)** SEM of micro–macroporous biphasic calcium phosphate showing macropores' distribution and porous interconnection; **(b)** SEM of micro–macroporous biphasic calcium phosphate (MBCP™, Biomatlante, France) showing micropores.

of micro–macroporous BCP (MBCP2000™, Biomatlante, France) [45]. In this method, CDA is mixed with a mixture of selected particles of naphthalene and sugar. After isostatic compaction, the CDA block is subjected to a specific process of sublimation/calcination. The BCP obtained using the classical naphthalene porogen (MBCP) compared with that using a mixture of porogens, naphthalene and sugar (MBCP2000) gave the following differences in properties: density, 0.75 g/cc (MBCP2000), 0.83 g/cc (MBCP); crystal size (µm), 0.5 (MBCP2000), 1.5 (MBCP); specific surface area (m^2/g), 1.6 (MBCP2000), 1.7 (MBCP); compression strength 4 MPa (MBCP2000),

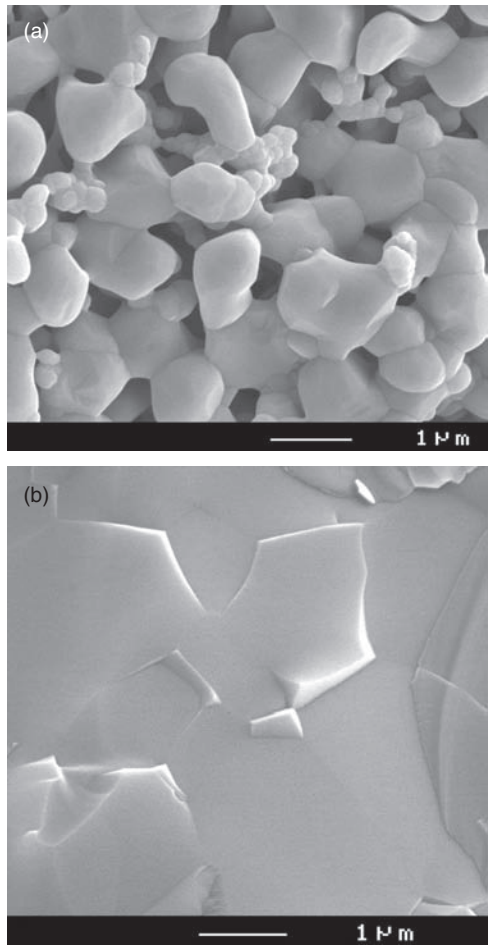

17.3 BCP with 60HA/40β-TCP sintered at 1050 °C (a) and 1200 °C (b).

6 MPa (MBCP); total porosity, 73% (MBCP2000), 69% (MBCP); permeability after incubation in bovine serum of MBCP2000 was two times higher than that of MBCP, and MBCP2000 showed a 30% increase in absorption compared with MBCP. The considerably higher permeability of MBCP2000 compared with MBCP cannot be explained by any difference in total porosity but may be attributed to the difference in the distribution of pore size, particularly, mesopores.

17.2.2 Physicochemical properties

Since β-TCP has a higher solubility than HA [46], the extent of dissolution of BCP ceramic of comparable macroporosity and particle size will depend

on the HA/β-TCP ratio: the higher the ratio, the lower the extent of dissolution [10,26,46,47]. The dissolution properties are also affected by the methods of obtaining BCP: whether from a single calcium-deficient apatite phase (BCP1) or from a mechanical mixture of two unsintered calcium phosphate preparations (BCP2): BCP2 exhibited higher extent of dissolution than BCP1 [39]. In some cases, BCP ceramic with similar HA/β-TCP ratios could present different dissolution rates [26]. This phenomenon may be caused by processing variables (sintering time and temperature) that could affect the total macroporosity and microporosity: the greater the macroporosity and microporosity, the greater the extent of dissolution. *In vivo*, dissolution of BCP ceramics is manifested by a decrease in crystal size and increase in macroporosity and microporosity [10,12,15].

17.2.3 Mechanical properties

It is expected that the pore size and percentage macroporosity of the BCP ceramic will affect the mechanical properties [17,39]. The preparation method was also found to have a significant influence on the compressive strength. BCP ceramic prepared from a single calcium-deficient apatite phase was reported to exhibit higher compressive strength (2–12 MPa) compared with BCP ceramic prepared by mixing two unsintered calcium phosphate preparations (2 MPa): one that after sintering at 1200 °C resulted in only HA and the other that resulted in only β-TCP [48]. The initial mechanical property is not the best criterion for efficacy of bone ingrowth. For example, BCP with high mechanical property due to low microporosity (resulting from high sintering temperature) may exhibit reduced bioresorption and bioactivity. On the contrary, it was demonstrated that the initial mechanical property of BCP increased two or three times (2–6 MPa) in a few weeks after implantation due to physicochemical events of dissolution and biological precipitation into the micropores [17].

17.2.4 Bioactivity and osteogenic properties

Bioactivity is described as the property of a material to form carbonate hydroxyapatite (CHA) on its surface *in vitro* [28,46] or *in vivo* [10,49–51]. Osteoinductivity or osteogenic property is the ability of the material to induce bone formation *de novo* or ectopically (in non-bone-forming sites). Bioceramics (calcium phosphates, bioactive glass) do not usually have osteoinductive property [40]. However, several reports indicated osteoinductive properties of some calcium phosphate bioceramics such as those reported for coralline HA (derived from coral) or observed in some studies using BCP [52–54]. Reddi [55] explains this apparent osteoinductive property as the ability of particular ceramics to concentrate bone growth factors

that are circulating in the biologic fluids, and that these growth factors induce bone formation. Ripamonti [52] and Kuboki *et al.* [53] independently postulated that the geometry of material is a critical parameter in bone induction. Others speculated that a low oxygen tension in the central region of implants might provoke a dedifferentiation of pericytes from blood microvessels into osteoblasts [56]. It has been also postulated that the nanostructured rough surface or the surface charge of implants might cause the asymmetrical division of stem cells into osteoblasts [57].

Surface microstructure appears to be a common property of materials inducing ectopic bone formation. Recent studies have indicated the critical role of micropores on the ceramic-induced osteogenesis. For example, it was reported that bone formation occurred in muscles of dogs inside porous calcium phosphate ceramics with surface microporosity but bone was not observed inside the dense surface of macroporous ceramics [58]. It was also reported that metal implants coated with a microporous layer of OCP could induce ectopic bone in muscles of goats while a smooth layer of carbonated apatite on these porous metal implants was not able to induce bone formation [59]. In all of the previous experiments, ectopic bone formation occurred inside macroporous ceramic blocks.

It has been demonstrated that sintering temperature drastically affects the microporosity of calcium phosphate ceramics: the higher the sintering temperature, the denser the ceramic surface [60]. Therefore, ceramic properties such as composition, geometry, porosity, size and microstructure should be considered critical parameters for bone induction. These properties play more important role in bone induction than mechanical stability [60].

Our explanation for such osteogenic/osteoinductive properties of BCP ceramics is the formation of microcrystals with Ca/P ratios similar to those of bone apatite crystals observed after implantation of the MBCP. The abundance of these crystals was directly related to the initial β-TCP/HA ratio in the BCP: the higher the ratio, the greater the abundance of the microcrystals associated with the BCP crystals [10,11]. Using high-resolution transmission electron microscopy (TEM), we demonstrated that the formation of these bone apatite-like microcrystals (Fig. 17.4) after implantation of calcium phosphates (HA, BCP) were non-specific, i.e. not related to implantation site (osseous or non-osseous sites), subjects of implantation and types of CaP ceramics [10–12,32–34].

The coalescing interfacial zone of biological apatite and residual BCP ceramic crystals (mostly HA) provide a scaffold for further bone–cell adhesion and stem cell differentiation in osteogenic lines, and further bone ingrowth. The bone repair or bone regeneration process involves dissolution of calcium phosphate crystals and then a precipitation of CHA needle-like crystallites in micropores close to the dissolving crystals. The coalescing

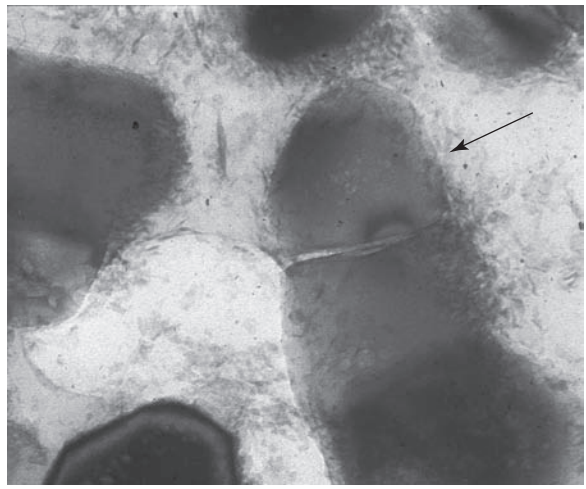

17.4 Biological apatite precipitation (*arrow*) on residual calcium phosphate crystals after implantation of BCP (high-resolution transmission microscopy).

zone constitutes the new biomaterial/bone interface, which includes the participation of proteins and CHA crystals originating from the BCP ceramic crystals. This has been described as a coalescing zone and dynamic interface [61].

17.3 Clinical applications

BCP bioceramics of various sizes and shapes are used in maxillofacial surgery, dentistry, ear, nose and throat (ENT) surgeries, and orthopedics. Examples of clinical applications of BCP are described below.

17.3.1 Applications in dentistry

Dental applications of BCP include prevention of bone loss after tooth extraction, repair of periodontal defects and sinus lift augmentation.

Prevention of bone resorption

Bone loss occurs after tooth extraction, causing reduction of alveolar ridge height and width, and resulting in difficulty in fitting dentures or placing dental implants. BCP granules with HA/TCP of 60/40 or 20/80 (MBCP™ and Tribone 80™, respectively) were placed in the alveolar cavity immediately after tooth extraction and followed up radiographically from 0 to 5 years. Biopsies were taken at different time periods from 6 months to 5

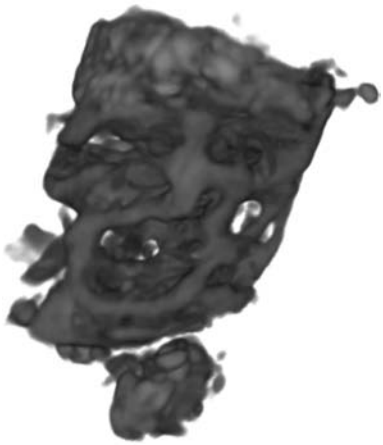

17.5 Micro CT of human biopsies after periodontal bone filling, showing bone trabeculae and few residual grains of unresorbed MBCP™ granules.

years. Radiographs revealed newly formed bone with higher density and residual BCP granules. After 6 months, fewer BCP granules with 20HA/80TCP compared with 50HA/40TCP were observed. In addition, during drilling, clinicians reported higher bone density without interference with residual granules. Organized and well-mineralized bone ingrowth was observed using micro-computer tomography (μ-CT) (Fig. 17.5), scanning electron microscopy (SEM) (Fig. 17.6) and light microscopy. In all cases, radio-opacity of the implantation sites decreased with time, indicating that resorption and bone ingrowth proceeded at the expense of the BCP granules but no statistical significant difference in resorption kinetics was observed regardless of the HA/TCP ratios of the BCPs. Observation after 1 year and 5 years showed that the alveolar ridge height was maintained, compared with the control (no BCP), which showed a decrease in alveolar ridge height of 2 to 5 mm. Five years after implantation, the resorption of the BCP was 78% for 60/40 and 87% for 20/80 and bone ingrowths were 38% and 32%, respectively. Resorption and bone ingrowth for were not significantly different for the BCP of different HA/TCP ratios.

Sinus lift augmentation

The increasing number of partially or completely edentulous patients is in close relationship with the rising aging population. Therefore, more comfortable and durable prosthetic rehabilitations are a great challenge for the scientific community. Esthetic and functional requirements from the patients

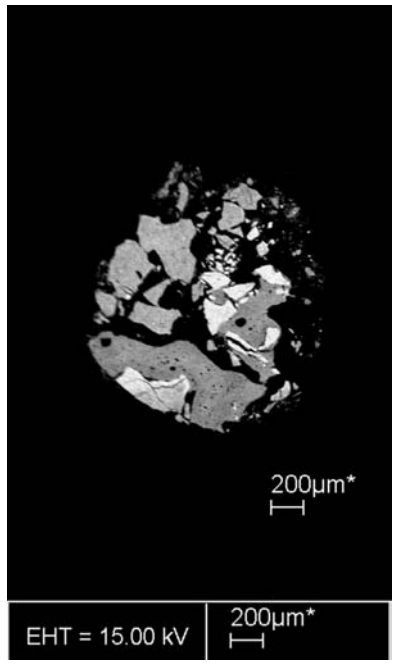

17.6 Backscattered electron image of human sample from periodontal pocket filling showing bone ingrowth at the expense of the granules of BCP (HA/TCP).

are more and more important and cannot be fulfilled without sufficient bone volume [64].

In many cases, bone in the maxilla needs to be built up (using the sinus lift procedure) prior to placement of dental implants. The use of autograft from the mandibular bone involves severe esthetic bone loss. Other bone substitute materials, including BCP, are being used. A case using BCP (MBCP™) for sinus lift grafting showed bone ingrowth and changes in radiodensity of unresorbed BCP granules (Fig. 17.7). More than 30% granule resorption was observed after 6 months and organized and well-mineralized bone ingrowth was observed.

The difficulty in delivering the MBCP granules into the tooth sockets discouraged many dental surgeons. A recently developed product consisting of MBCP granules in a polymer carrier provides a ready-to-use injectible bone substitute (MBCP Gel™, Biomatlante, France) [65–72]. The osteoconductive potential of this innovative biomaterial was previously demonstrated for clinical application in an animal model with the quantification of each component, BCP, bone and soft tissue [71,72]. Macroporous BCP in a polymer carrier was shown to be effective in filling dental sockets after

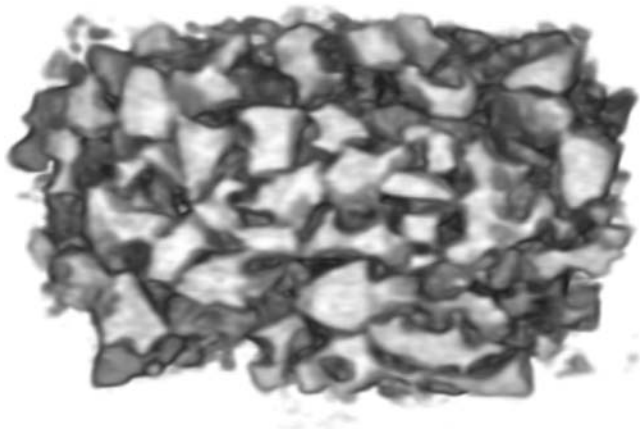

17.7 Micro-CT image of sinus lift grafting in human after 6 months showing bone ingrowth at the expense of the MBCP™ and architecture of newly formed bone.

tooth extraction because it maintained alveolar bone crest, supported bone healing and was gradually substituted by bone tissue.

In vivo resorption, just like *in vitro* dissolution, depends on the chemical composition and particle size [46]. MBCP Gel™ with 40–80 μm BCP granules was used for bone regeneration around dental implants placed in fresh extraction sockets in a dog model [73]. Three months after implantations, the BCP granules were no longer visible using SEM. In the same animal model and after the same time of implantation, most of the BCP granules (200–500 μm granules) was still present [71]. In the case of nano-particles (BCP particle size smaller than 10 μm), complete and fast resorption of the BCP granules was observed but significant inflammation was also observed [74]. Thus, the particle size of the BCP (or any resorbable biomaterials) should be adapted to the clinical situation. For pre-prosthetic surgery large granule size compatible with injection should be used preferably and for pre-implantation surgery, small granule size compatible with acceptable level of inflammation is recommended.

17.3.2 Applications in orthopedics

BCP has been used in orthopedic applications for the last 20 years. Micro–macroporous biphasic calcium phosphate bioceramics are largely used in orthopedics and efficacy has been demonstrated in numerous preclinical and clinical studies [15,17–20,75–78]. Below are brief descriptions of selected clinical situations using specific shaped blocks (custom-designed) for spine arthrodesis (cage insert) and wedges for tibial valgization osteotomy of valgization.

Cervical spine arthrodesis

Several studies have been published using bioceramic inserts for filling cage fusion [79–82] (Fig. 17.8). Pascal-Mousselard [83] recently reported a clinical study of a prospective, comparative, multicenter and randomized study comparing iliac graft and a macroporous BCP (MBCP™, Biomatlante, France) for anterior cervical fusion with Poly Ethyl Ether Ketone (PEEK) cage. PEEK cervical radiolucent fusion cages provide an immediate mechanical support after anterior cervical discectomy. The objective of this study was to compare the clinical efficiency and quality of the fusion after reconstruction with an anatomically shaped PEEK cage associated with a iliac crest autograft or with MBCP in the treatment of cervical disk. The addition of iliac autograft allows a great rate of fusion but is associated with increased morbidity and persistent pain at the donor site. Clinical reports by Scareo comparing the two techniques brought evidence of the clinical advantage of using MBCP and avoiding bone graft harvesting. Fifty-eight patients were selected in a multicenter, comparative and prospective study with a 24 month follow-up. The patients undergoing anterior cervical decompression and fusion were randomized for autologous graft or MBCP. The 58 patients presenting radiculopathy or cervical myelopathy from purely degenerative disk disease or degenerative osteophytes origin were implanted with a PEEK cage (SAMARYS, Scient'X France) filled with iliac crest autograft or with MBCP. One level fusion was performed in 51 cases and seven patients underwent two-level fusion. Pain and functionality as well as patient satisfaction were assessed. After 24 months, cervical X-rays demonstrated 87% complete fusion, 13% uncertain fusion and 0% real pseudo-arthrosis in the autograft group versus 86%, 10% and 4%, respectively, in the MBCP group. Those differences were not statistically significant. Pain and Neck Disability Index (NDI) improved in both group as early as 3 months follow-up and until 24 months post-operatively ($p < 0.01$).

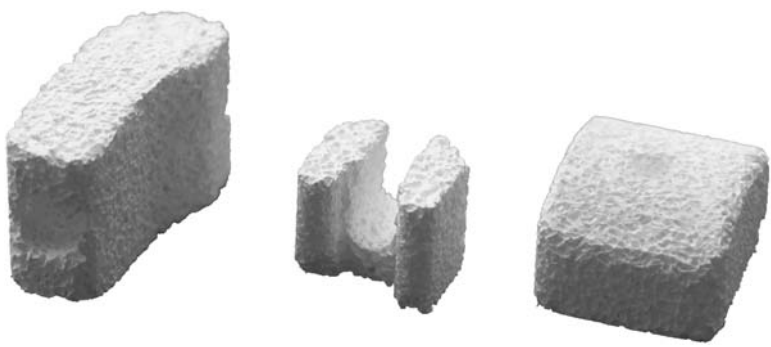

17.8 Typical size and shape of MBCP inserts used for cage fusion.

A greater improvement in global pain was observed in the MBCP group. The patient satisfaction rates were 82% in the bone group versus 96% in the MBCP group (ddl = 2; $\chi^2 = 0.2$; $\pi > 97\% > \alpha$). Pain at the donor site was significantly more important in the autograft group at 3 weeks, 3 months and 1 year follow-up. One pseudo-arthrosis revision and one subsidence greater than 2 mm occurred in the MBCP group. No implant failures were recorded. These results suggest that the use of MBCP™ insert associated with an anterior cage allows for a better recovery for the patients while achieving a corresponding fusion rate to ACDF with tricortical graft, and is free from associated complications. The use of MBCP insert is safe and avoids potential graft site morbidity and pain in comparison with an autologous graft procedure.

High tibial valgization osteotomy (HTVO)

Many surgical procedures are described for high tibial valgization osteotomy (HTVO) as a treatment for medial femorotibial arthritis with genu varum deformity, all with documented positive clinical results, evolution, and specifications [84–90]. Many authors seem to prefer osteotomy by medial open wedge resection procedure [91–93]; however, filling the cavity created by the opening has remained a problem, although various osteosynthetic solutions have been proposed. Bone substitutes have been used in a number of different cases [94–97].

A single center prospective study realized by Rouvillain [97] from December 1999 to December 2002 was completed involving 42 patients (13 females and 29 males, averaging 46 years of age) who underwent HTVO with medial addition for various deformity using custom-designed wedges constituted of micro–macroporous biphasic calcium phosphate bioceramic bone substitute (MBCP™) and orientable locking screw plate (Numelock II®, Stryker). Consolidation of the bone filling of the lateral triangular metaphyseal space was evaluated for appearance of peripheral cortical bridges and osseointegration between host bone and bone substitute, without the presence of a radiolucent line. The evolution of post-operative correction was evaluated by measurement of the medial tibial angle, calculated by measurement of the anatomical tibial axis and the angle of the 90° tangent to the tibial plateau (beta-angle) at different post-operative delays. After one year, correction was unchanged in 99.5% of cases. Histological analysis showed MBCP resorption and bone ingrowth into the pores at the expense of the bioceramic. Residual MBCP fragments showed ingrowth of trabecular and/or dense lamellar bone both on the surface and in the macropores. X-ray radiography and μ-CT revealed a well-organized and mineralized structure of newly formed bone [97].

In spite of some fractures of MBCP wedges during implantation or proximal screws fractured without compromising the stability or post-operative

correction angles, high bone ingrowth were reported. This study indicated that MBCP wedges in combination with orientable locking screws and plate provide a simple, safe and fast surgical technique for HTVO [97].

17.4 Recent developments

17.4.1 BCP scaffolds for bone tissue engineering

Tissue engineering for bone regeneration involves the seeding of osteogenic cells (e.g. mesenchymal stem cells, MSCs) on appropriate scaffolds and subsequent implantation of the seeded scaffolds in the bone defect. Bone marrow-derived MSCs are multipotential cells that are capable of differentiating into, at a minimum, osteoblasts, chondrocytes, adipocytes, tenocytes and myoblasts [98–100]. From a small volume of bone marrow, MSCs can be isolated and culture expanded into large numbers due to their proliferative capacity, and maintain their functionality after culture expansion and cryopreservation [101]. Thus, MSCs are thought to be a readily available and abundant source of cells for tissue engineering applications. Several reports have shown the efficiency of BCP scaffolds of different HA/β-TCP ratios [101–104].

17.4.2 BCP scaffolds with mesenchymal stem cells (MSCs)

Livingstone Arinzeh *et al.* [103] reported a comparative study of BCP with different HA/β-TCP ratios as scaffolds for human MSCs (hMSC) to induce bone formation. This was designed to determine the optimum HA/β-TCP ratio in BCP in combination with MSCs that would promote rapid and uniform bone formation *in vivo*. Their study demonstrated that the BCP scaffold with lower HA/β-TCP ratio (20/80) loaded with hMSCs promoted the greatest amount of bone and the new bone formed was uniformly distributed throughout the porous structure of the BCP scaffold. Scaffolds made from 100% HA, higher HA/β-TCP ratios and 100% TCP stimulated lessser amounts of bone formation at 6 weeks post-implantation. In their *in vitro* study of hMSC differentiation on 60/40 HA/β-TCP versus 20/80 HA/β-TCP, hMSCs expressed osteocalcin, a bone specific marker, when grown on 20/80 HA/TCP without the presence of the osteoinductive media by 4 weeks. The enhanced amount of bone formation for hMSC-loaded 20/80 HA/TCP *in vivo* and apparent differentiation into the bone cell phenotype, as characterized by the expression of osteocalcin *in vitro* under normal culture conditions, may be due in part to the rate of degradation, the degradation products and surface chemistry of 20/80 HA/β-TCP relative to the other BCP compositions. The concentration of degradation products and the hMSC interaction with the surface of varying chemistries

may be responsible for optimal bone formation exhibited by the 20/80 formulation.

The rate of degradation or resorption of HA/β-TCP ceramics *in vivo* can be accelerated by increasing the amount of the more soluble phase, TCP [10,11]. In order to design a scaffold that supports bone formation while gradually being replaced by bone, an optimum balance between the more stable HA phase and the more soluble β-TCP phase must be achieved.

Recent studies [45] compared the biologic performance of the new micro–macroporous biphasic calcium phosphate (MCPC™2000) with the classical MBCP™ implanted in femoral epiphysis of New Zealand rabbits After 6 and 12 weeks of implantation, bone ingrowth is observed in the two types of bioceramic, and newly formed bone progressively replaced the bioactive material, followed by haversian bone remodelling. Faster bone ingrowth into the macropores was observed at 6 weeks for MBCP2000. After 12 weeks of implantation, no statistical difference was noticed between the two implant types. The rate of resorption however is higher for MBCP 2000: 17% versus 12% at 6weeks, and 19% versus 17% after 12weeks, (no significant difference).

The *in vivo* experiment indicated that higher cell colonization of MBCP™2000 by osteogenic cells is due to this interconnected and microporous structure, resulting in higher solubility. However, owing to bone ingrowth at the expense of the implant, this phenomenon is less evident after long-term implantation. MBCP™2000 is a more suitable matrix for tissue engineering. The HA/βTCP ratio of 20/80 is also more efficient for combination with stem cell cultivation and expansion then implanted in a non-bony site compared with classical MBCP (60HA/40βTCP).

The kinetics of bone ingrowth by the osteogenic cell colonization needs to develop inside the macropores. Without macropores and mesopores the bioactive processes are unable to develop in the depth of the implanted bioceramic. The association of dissolution at the crystal levels, the diffusion of the biological fluid into the micropores, and the resorption of the bioceramic by the macrophages and osteoclastic cells at the surface and inside the macropores, involve a progressive bone substitution of the materials by true bone. The processes of resorption/bone substitution is common to MBCP ceramics. The higher efficacy of the MBCP2000 bioceramics makes them good candidates for scaffolds for bone tissue engineering.

17.4.3 BCP scaffolds for growth plate chondrocyte maturation

Recently, Teixera *et al.* [104] reported the efficiency of MBCP scaffold for cartilage regeneration. The purpose of the study was to create an *in vitro* cartilage template as the transient model for *in vivo* endochondral bone

formation. This study reported successful growth and maturation of chondrocytes (isolated from chick embryonic tibia on macroporous BCP. The thickness of the chondrocyte and extracellular matrix layer increased in the presence of retinoic acid. Alkaline phosphatase activity and expression, proteoglycans synthesis, cbfa1 and type I collagen mRNA levels also increased in the presence of retinoic acid. This study demonstrated for the first time the proliferation and maturation of chondrocytes, and the matrix deposition on MBCP, suggesting the potential for such scaffold in tissue engineering via the endochondral bone formation mechanism.

17.4.4 BCP composites

The need for a material for minimal invasive surgery (MIS) motivated the development of a BCP granules combined with a polymer or calcium phosphate cement for injectable/moldable bone substitutes. Four types of injectable/moldable bone substitutes have been developed by INSERM Nantes University.

17.4.5 BCP/polymer

MBCP Gel™ is an injectable non-self-hardening biomaterial. Which consists of BCP granules associated with a hydrosoluble polymer. Such materials have been shown to be perfectly biocompatible and potentially resorbable and, thanks to their initial plasticity, they assume the shape of the bone defects very easily, eliminating the need to shape the material to adjust to the implantation site. MBCP gel does not have mechanical properties like the hydraulic bone cements. However, bone cells are able to invade the spaces created by the disappearance of the polymer carrier. Bone ingrowth takes place all around the granules at the expense of the resorption of the BCP granules. In time, the mechanical property is increased owing to the presence of the newly formed bone [66,70–72].

17.4.6 BCP/fibrin glue

A fibrin/BCP composite was obtained by mixing fibrinogen, thrombin components fibrin sealant (Tisseel®Baxter BioSciences BioSurgery, Baxter) and BCP granules (TricOs®, Baxter). TricOs® is a BCP with a 60HA/40β-TCP ratio. Granules of 1–2 mm in diameter presenting both macroporosity (50–55%) and microporosity (30–35%) were used. To enhance the working time, a low thrombin concentration (4 U) was used. The ratio Tisseel/TricOs volume was 1/2. Numerous preclinical studies have been performed in rabbits and goats, both for biocompatibility and biofunctionality in sinus lift augmentation and bone filling in long bone [105,106].

17.4.7 BCP-based macroporous cements

Currently, several calcium phosphate bone cements are commercially available and more are being investigated since the concept was first introduced by LeGeros *et al.* in 1982 [107] and the first patent obtained by Brown and Chow [108] in 1986. All the current CPCs are reported to have good mechanical properties and reasonable setting times. However, after setting, these materials remain dense and do not provide rapid bone substitution because of the lack of macroporosity. Numerous studies have reported on the applications of currently available commercial calcium phosphate cements, CPC [109,110].

A new BCP-based calcium phosphate cement, MCPC, was recently developed [111]. The powder component of the MCPC comprises of a settable and resorbable matrix (which includes β-TCP, stabilized amorphous calcium phosphate (s-ACP) and monocalcium phosphate monohydrate, MCPM). A sieved fraction of macroporous biphasic calcium phosphate (BCP) granules ranging between 80 and 200 μm were incorporated into the matrix. The cement liquid is an aqueous solution of Na_2HPO_4. The mechanical properties in compression of such materials have been reported [8]. Briefly, after setting of MCPC in distilled water at 20 °C, the mechanical strengths obtained were 10 Mpa ± 2 at 24 hours and 15 MPa ± 2 after 48 hours. The cohesion time for injectability was reached after 20 mn. *In vivo,* the components of the cement resorb at different rates, allowing the formation of interconnecting macroporosity when the cement sets, and facilitating bone ingrowth and substitution of the cement with the newly forming bone [36]. *In vivo*, resorption of the ACP component of the MCPC produced macroporosity and facilitated bone ingrowth between and at the surface of BCP granules extending to the core of the implanted site. Light microscopy revealed bone ingrowth at the expense of MCPC matrix extending from the surface of the implant until the core of the defect. MBCP granules act as scaffold for bone osteoconduction (Fig. 17.9). The presence of macroporosity was evident even 24 hours after setting *in vitro*. The MCPC matrix dissolved as was expected, forming an open structure and interconnecting porosity. SEM analyses showed that organized bone trabeculae were well differentiated from the residual granules. After 12 weeks, few granules were fully integrated in the new cortical bone and deeper into the core, spongious bone was formed. Bone remodeling was in evidence. X-ray μ-CT demonstrated bone ingrowth at the expense of the cement and surrounding the residual BCP granules. Bone trabeculae were observed coming from the spongious bone to the implant site.

A study comparing the *in vivo* performance of MCPC and another cement, α-BSM™ (ETEX, Boston) showed that bone remodeling was observed with MCPC. In the case of the non-macroporous cement

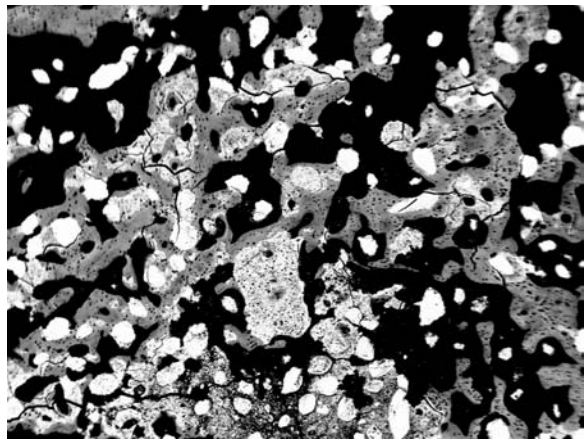

17.9 SEM of surgically created defect in rabbit epiphysis filled with MCPC, showing bone ingrowth at the expense of the cement and osteoconduction in all the defects at the surface of the BCP granules.

(α-BSM), unreproducible results were obtained: some implants were not resorbed, others partially and one fully resorbed. The same observation was obtained for the bone ingrowth, not necessarily associated with the cement resorption. On the other hand, animal studies using the new macroporous calcium phosphate cement MCPC showed that it develops a macroporous structure only after implantation, owing to the resorption of the matrix. The remaining BCP granules serve as a scaffold for bone cell osteoconduction and bone tissue ingrowth that extended from the surface to the core of the implanted cement. Replacement of the cement by new bone increases the mechanical strength. The *in vivo* performance of the MCPC was in contrast with that of α-BSM cement which was shown to have bone ingrowth limited to its surface in spite of its resorbable properties [36].

The efficiency of the new MCPC in promoting new bone formation and increasing the mechanical strength with time is attributed to the formation of macrostructure due to the resorption of the matrix and the presence of osteoconductive scaffolds (BCP granules).

Granules for drug delivery

Calcium phosphate bioceramics have often been proposed for adsorption of bioactive factors and for drug delivery system. However, recently Smucker *et al.* [112] reported for the first time a study demonstrating enhanced posterolateral spinal fusion rates in rabbit using different concentrations of a synthetic peptide (B2A2-K-NS) coated on micro-porous BCP granules

60HA/40βTCP ratio. The peptide is a synthetic receptor-target that appears to amplify the biological response to *rh*BMP-2. This study indicates more evidence of mature/immature bone ingrowth across the inter-transverse process spaces than did the controls. Micro–macroporous BCP bioceramic granules for peptide adsorption and local delivery will combine the osteoconductive/osteogenic properties of the BCP bioceramics and the osteoinductive properties of the peptide and growth factors.

17.5 Summary

The biphasic calcium phosphate (BCP) concept based on the intimate mixture of HA and β-TCP is founded on: (1) partial dissolution of the CaP ceramic macrocrystals (principally, β-TCP) causing an increase in the calcium and phosphate concentrations in the local microenvironment; (2) formation of carbonate hydroxyapatite, CHA (either by direct precipitation or by transformation of one calcium phosphate phase to another or by seeded growth) incorporating ions (principally carbonate) from the biological fluid during its formation; (3) association of the CHA crystals with an organic matrix; and (4) incorporation of these microcrystals with the collageneous matrix in the newly formed bone (in osseous sites). BCPs have the advantage of controlled bioactivity by controlling the HA/β-TCP ratio. BCP, like other bioactive bone substitute materials, is osteoconductive and has the possibility of acquiring osteoinductive properties through appropriate critical geometry of macroporosity and microporosity. Besides the medical and dental applications, BCP has a potential for other applications such as delivery system for drugs, antibiotics, hormones; carriers for growth factors; scaffolds for tissue engineering.

17.6 Acknowledgments

The collaboration of the following clinicians are gratefully acknowledged: Prof. Jean Louis Rouvillain (CHU Fort de France Martinique), Dr Hugues Mousselard (CHU Pitié Salpétrière Paris France), Dr Nicolas Mailhac (Tours France), Dr Clemencia Rodriguez (Bogota University, Colombia).

The authors also gratefully acknowledge collaborators from Nantes University and INSERM EMI 99 03, Nantes Hospital, Nantes Microscopy SC3M department, the Calcium Phosphate Research Lab at the New York University College of Dentistry (part of this review was reprinted with permission from reference 27), and the support of Bordeaux Hospital Clinical Research Department.

The technical assistance of Françoise Moreau and Paul Pilet, Monica Gotlieb and for manuscript correction are acknowledged.

17.7 References

1. Albee FH (1920). Studies in bone growth: triple calcium phosphate as a stimulus to osteogenesis. *Ann Surg* **71**: 32–36.
2. Nery EB, Lynch KL, Hirthe WM, Mueller KH (1975). Bioceramic implants in surgically produced infraboney defects. *J Periodontol* **63**: 729–735.
3. Denissen HW (1979). PhD Thesis, Amsterdam, Vrije Universiteit.
4. Jarcho M (1981). Calcium phosphate ceramics as hard tissue prosthetics. *Clin Orthop* **157**: 259–278.
5. De Groot K (1983). Ceramics of calcium phosphate: preparation and properties, In: *Bioceramics of Calcium Phosphates*. CRC Press, Boca Raton, 100–114.
6. Metsger SD, Driskell TD, Paulsrud JR (1982). Tricalcium phosphate ceramic: a resorbable bone implant: review and current uses. *J Am Dent Assoc* **105**: 1035–1048.
7. Aoki M, Aoki H, Kato K, Kato A (1982). β-Tricalcium phosphate for prosthetic application. *J Mater Sci*. **17**: 343–346.
8. LeGeros RZ (1988). Calcium phosphate materials in restorative dentistry. *Adv Dent Res* **2**: 164–183.
9. Ellinger RF, Nery EB, Lynch KL (1986). Histological assessment of periodontal osseous defects following implantation of hydroxyapatite and biphasic calcium phosphate ceramics: a case report. *J Periodont Restor Dent* **3**: 223.
10. LeGeros RZ, Nery E, Daculsi G, Lynch K, Kerebel B (1988). *In vivo* transformation of biphasic calcium phosphate of varying b-TCP/HA ratios: ultrastructural characterization. *Third World Biomaterials Congress*, Kyoto, Japan (abstract no. 35).
11. LeGeros RZ, Daculsi G (1990). *In vivo* transformation of biphasic calcium phosphate ceramics: ultrastructural and physicochemical characterization. In: Yamamuro N, Hench L, Wilson J (Eds). *Handbook of Bioactive Ceramics*, Vol. 2. Boca Raton CRC Press p. 1728.
12. Daculsi G, LeGeros RZ, Nery E, Lynch K, Kerebel B (1989). Transformation of biphasic calcium phosphate ceramics: ultrastructural and physico-chemical characterization. *J Biomed Mat Res* **23**: 883–894.
13. Nery EB, LeGeros RZ, Lynch KL, Kalbfleisch J (1992). Tissue response to biphasic calcium phosphate ceramic with different ratios of HA/β-TCP in periodontal osseous defects. *J Periodontol* **63**: 729–735.
14. Daculsi G, Passuti N (1990). Effect of macroporosity for osseous substitution of calcium phosphate ceramic. *Biomaterials* **11**: 86–87.
15. Daculsi G, Passuti N, Martin S, Deudon C, LeGeros, RZ (1990). Macroporous calcium phosphate ceramic for long bone surgery in human and dogs. *J Biomed Mater Res* **24**: 379–396.
16. Daculsi G, Bagot D'arc M, Corlieu P, Gersdorff M (1992). Macroporous biphasic calcium phosphate efficiency in mastoid cavity obliteration. *Ann Orol Rhinol Laryngol* **101**: 669–674.
17. Trecant M, Delecrin J, Royer J, Goyenvalle E, Daculsi G (1994). Mechanical changes in macroporous calcium phosphate ceramics after implantation in bone. *Clin Mater* **15**: 233–240.

18. Gouin F, Delecrin J, Passuti N, Touchais S, Poirier P, Bainvel JV (1995). Comblement osseux par céramique phosphocalcique biphasée macroporeuse: a propos de 23 cas. *Rev Chir Orthop* **81**: 59–65.
19. Ransford AO, Morley T, Edgar MA, Webb P, Passuti N, Chopin D, Morin C, Michel F, Garin C, Pries D (1998). Synthetic porous ceramic compared with autograft in scoliosis surgery. A prospective, randomized study of 341 patients. *J Bone Joint Surg Br* **80**(1): 13–18.
20. Cavagna R, Daculsi G, Bouler, J-M (1999). Macroporous biphasic calcium phosphate: a prospective study of 106 cases in lumbar spine fusion. *Long-term Effects Med Impl* **9**: 403–412.
21. Soares EJC, Franca VP, Wykrota L, Stumpf S (1998). Clinical evaluation of a new bioaceramic opthalmic implant. In: LeGeros RZ, LeGeros JP (Eds) *Bioceramics 11*, Singapore, World Scientific, pp. 633–636.
22. Wykrota LL, Garrido CA, Wykrota FHI (1998). Clinical evaluation of biphasic calcium phosphate ceramic use in orthopaedic lesions. In LeGeros RZ, LeGeros JP (Eds) *Bioceramics 11*, Singapore, World Scientific, pp. 641–644.
23. Malard O, Guicheux J, Bouler JM, Gauthier O, Beauvillain de Montreuil C, Aguado E, Pilet P, LeGeros R, Daculsi G (2005). Calcium phosphate scaffold and bone marrow for bone reconstruction in irradiated area: a dog study. *Bone* **36**: 323–330.
24. Daculsi G (1998). Biphasic calcium phosphate concept applied to artificial bone, implant coating and injectable bone substitute. *Biomaterials* **19**: 1473–1478.
25. Daculsi G, Laboux O, Malard O, Weiss P (2003). Current state of the art of biphasic calcium phosphate bioceramics. *J Mater Sci Mater Med* **14**(3): 195–200.
26. LeGeros RZ, Lin S, Rohanizadeh R, Mijares D, LeGeros JP (2003). Biphasic calcium phosphates: preparation and properties. *J Mater Sci: Mat Med* **14**: 201–210.
27. Hench LL, Splinter RJ, Allen WC, Greelee TK (1978). Bonding mechanisms at the interface of ceramic prosthetic materials. *J Biomed Mater Res* **2**: 117–141.
28. Hench LL (1994). Bioceramics: from concept to clinic. *J Am Ceram Soc* **74**: 1487–1510.
29. LeGeros RZ (1991). *Calcium Phosphates in Oral Biology and Medicine.* Monographs in Oral Sciences, Vol. 15, H. Myers, ed., S. Karger, Basel.
30. LeGeros RZ, Daculsi G, Orly I, LeGeros JP (1991). Substrate surface dissolution and interfacial biological mineralization. In: Davies JED (Ed). *The Bone Biomaterial Interface*, University of Toronto Press, Toronto, pp. 76–88.
31. Osborne J, Newesely H (1980). The material science of calcium phosphate ceramic. *Biomaterials* **1**: 108–111.
32. Heughebaert M, LeGeros RZ, Gineste M, Guilhem A (1988). Hydroxyapatite (HA) ceramics implanated in non-bone forming sites: physico-chemical characterization. *J Biomed Mat Res* **22**: 257–268.
33. Daculsi G, LeGeros RZ, Heugheaert M, Barbieux I (1990). Formation of carbonate apatite apatite crystals after implantation of calcium phosphate ceramics. *Calcif Tissue Int* **46**: 20–27.

34. Daculsi G (2006). *Biphasic Calcium Phosphate Granules Concept for Injectable and Mouldable Bone Substitute*. Advances in Science and Technology Volume 49, Trans Tech Publications, Switzerland, pp. 9–13.
35. Daculsi G, Weiss P, Bouler JM, Gauthier O, Aguado E (1999). Bcp/hpmc composite: a new concept for bone and dental substitution biomaterials. *Bone* **25**: 59–61.
36. Daculsi G, Khairoun I, LeGeros RZ, Moreau F, Pilet P, Bourges X, Weiss P, Gauthier O (2007). Bone ingrowth at the expense of a novel macroporous calcium phosphate cement. *Key Engineering Materials* **330–332**: 811–814.
37. Bouler JM, LeGeros, RZ Daculsi G (2000). Biphasic calcium phosphates: influence of three synthesis parameters on the HA/β-TCP ratio. *J Biomed Mater Res* **51**: 680–684.
38. LeGeros RZ, Zheng R, Kijkowska R, Fan D, LeGeros JP (1994). Variations in composition and crystallinity of 'hydroxyapatite (HA)' preparations. In: Horowitz E, Parr JE (Eds). *Characterization and Performance of Calcium Phosphate Coatings for Implants*, Philadelphia, American Society for Testing Materials STP 1198, pp. 43–53.
39. Bouler JM, Trécant M, Delécrin J, Royer J, Passuti N, Daculsi G (1996). Macroporous biphasic calcium phosphate ceramics: influence of five synthesis parameters on compressive strength. *J Biomed Mater Res* **32**: 603–609.
40. LeGeros RZ (2002). Properties of osteoconductive biomaterials: calcium phosphates. *Clin Orthopaed Rel Res* **395**: 81–98.
41. Bohne W, Pouezat JA, Peru L, Daculsi G (1993). Heating of calcium phosphate crystals: morphological consequences and biological implications. *Cells and Materials* **3**: 377–382.
42. Hubbard WG (1974). PhD Thesis, Milwaukee, Marquette University.
43. Schmitt M (2000). PhD Thesis, Nantes, University of Nantes.
44. Bagot d'Arc M, Daculsi G, Emam N (2004). Biphasic ceramics and fibrin sealant for bone reconstruction in ear surgery. *Ann Otol Rhinol Laryngol* **113**(9): 711–720.
45. Daculsi G (2006). High performance of new interconnected micromacroporous biphasic calcium phosphate matrices MBCP2000 for bone tissue engineering. *Proceedings 20^{rh} European Conference on Biomaterials*, Nantes, France.
46. LeGeros RZ (1993). Biodegradation and bioresoprtion of calcium phosphate ceramics. *Clin Mater* **14**: 65–88.
47. Gauthier O, Bouler Jm, Aguado E, Legeros Rz, Pilet P, Daculsi G (1999). Elaboration conditions influence physicochemical properties and *in vivo* bioactivity of macroporous biphasic calcium phosphate ceramics. *J Mater Sci: Mat Med* **10**: 199–204.
48. Rohanizadeh R, Padrines M, Bouler, J-M, Couchourel G, Fortun Y, Daculsi G (1998). Apatite precipitation after incubation of biphasic calcium-phosphate ceramic in various solutions: influence of seed species and proteins. *J Biomed Mater Res* **42**(4): 530–539.
49. Basle MF, Chappard D, Grizon F, Filmon R, Delecrin J, Daculsi G, Rebel A (1993). Osteoclastic resorption of CaP biomaterials implanted in rabbit bone. *Calcif Tiss Int* **53**: 348–356.
50. Gauthier O, Bouler J-M, Aguado E, Pilet P, Daculsi G (1998). Macroporous biphasic calcium phosphate ceramics: influence of macropore diameter

and macroporosity percentage on bone ingrowth. *Biomaterials* **19**(1–3): 133–139.
51. Kokubo T, Takadama H (2006). How useful is SBF in predicting *in vivo* bone bioactivity? *Biomaterials* **27**(15): 2907–2915.
52. Ripamonti U (1991). The morphogenesis of bone in replicas of porous hydroxyapatite obtained by conversion of calcium carbonate exoskeletons of coral. *J Bone Joint Surg Am* **73**: 692–703.
53. Kuboki Y, Takita H, Kobayashi D (1998). BMP-induced osteogenesis on the surface of hydroxyapatite with geometrically feasible and nonfeasible structures: topology of osteogenesis. *J Biomed Mater Res* **39**: 190–199.
54. Le Nihouannen D, Daculsi G, Saffarzadeh A, Gauthier O, Delplace S, Pilet P, Layrolle P (2005). Ectopic bone formation by microporous calcium phosphate ceramic particles in sheep muscles. *Bone* **36**(6): 1086–1093.
55. Reddi AH (2000). Morphogenesis and tissue engineering of bone and cartilage: inductive signals, stem cells and biomimetic biomaterials. *Tissue Eng* **6**: 351–359.
56. Diaz-Flores L, Gutierrez R, Lopez-Alonso A, Gonzalez R, and Varela H (1992). Pericytes as a supplementary source of osteoblasts in periosteal osteogenesis. *Clin Orthop Relat Res* **275**: 280–286.
57. Habibovic P, Yuan H, van der Valk CM, Meijer G, van Blitterswijk CA, De Groot K (2005). Microenvironment as essential element for osteoinduction by biomaterials. *Biomaterials* **26**: 3565–3575.
58. Yuan H, Kurashina K, Joost de Bruijn D, Li Y, de Groot K, Zhang X (1999). A preliminary study of osteoinduction of two kinds of calcium phosphate bioceramics. *Biomaterials* **20**: 1799–1806.
59. Barrere F, van der Valk CM, Dalmeijer RA, Meijer G, van Blitterswijk CA, de Groot K, Layrolle P (2003). Osteogenicity of octacalcium phosphate coatings applied on porous titanium. *J Biomed Mater Res* **66A**: 779.
60. Daculsi G, Legeros R, Grimandi G, Soueidan A, Aguado E, Goyenvalle E, Legeros J (2008). Effect of Sintering Process on Microporosity, and bone growth on Biphasic Calcium Phosphate Ceramics. *Key Engineering Materials,* vols 361–363, pp. 1139–1142, Trans Tech Publication, Switzerland.
61. Daculsi G, Dard M (1994). Bone–calcium-phosphate ceramic interface. *Osteosynthese Int* **2**: 153–156.
62. Clemencia Rodríguez M, Jean A, Kimakhe S, Sylvia Mitja S, Daculsi G (2007). Five years clinical follow up bone regeneration with CaP bioceramics. *Proceedings IADR 2007*, New Orleans.
63. Clemencia Rodríguez M, Jean A, Kimakhe S, Sylvia Mitja S, Daculsi G (2008). Five years clinical follow up bone regeneration with CaP bioceramics. *Key Engineering Materials*, vols 361–363, Trans Tech Publication, Switzerland.
64. Maillac N, Moreau F, Daculsi G (2008). Bone ingrowth for sinus lift augmentation with micro macroporous biphasic calcium human cases evaluation using microCT and histomorphometry. *Key Engineering Materials,* vols 361–363, 1347–1350. Trans Tech Publication, Switzerland.
65. Daculsi G, Weiss P, Delecrin J, Grimandi G, Passuti N, Guerin F (1994). Patent n°. 94-01-414 1994235, WO 95/21634 Composition pour biomatériaux – procédés de préparation.

66. Daculsi G, Weiss P, Bouler JM, Gauthier O, Aguado E (1999). Biphasic calcium phosphate hydrosoluble polymer composites: a new concept for bone and dental substitution biomaterials. *Bone* **25**: 59–61.
67. Millot F, Grimandi G, Weiss P, Daculsi G (1999). Preliminary *in vivo* studies of a new injectable bone substitute. *Cells Mat* **9**: 21–30.
68. Dupraz A, Nguyen TP, Richard M, Daculsi G, Passuti N (1999). Influence of a cellulosic ether carrier on the structure of biphasic calcium phosphate ceramic particles in an injectable composite material. *Biomaterial* **20**: 663–673.
69. Gauthier O, Boix D, Grimandi G, Aguado E, Bouler JM, Weiss P, Daculsi G (1999). A new injectable calcium phosphate for immediate bone filling of extraction sockets: a preliminary study in dogs. *J Periodontol* **70**: 375–383.
70. Gauthier O, Bouler JM, Aguado E, Legeros Rz, Pilet P, Daculsi G (1999). Elaboration conditions influence physicochemical properties and *in vivo* bioactivity of macroporous biphasic calcium phosphate ceramics. *J Mater Sci: Mat Med* **10**: 199–204.
71. Gauthier O, Bouler JM, Weiss P, Bosco J, Daculsi G, Aguado E (1999). Kinetic study of bone ingrowth and ceramic resorption associated with the implantation of different injectable calcium-phosphate bone substitutes. *J Biomed Mater Res* **47**(1): 28–35.
72. Gauthier O, Bouler JM, Weiss P, Bosco J, Aguado E, Daculsi G (1999). Short-term effects of mineral particle sizes on cellular degradation activity after implantation of injectable calcium phosphate biomaterials and consequences for bone substitution. *Bone* **25**: 71–74.
73. Boix D, Weiss P, Gauthier O, Guicheux J, Bouler JM, Pilet P, Daculsi G, Grimandi GJ (2006). Injectable bone substitute to preserve alveolar ridge resorption after tooth extraction: a study in dog. *J Mater Sci Mater Med* **17**(11): 1145–1152.
74. Malard O, Bouler JM, Guicheux J, Heymann D, Pilet P, Coquard C, Daculsi G (1999). Influence of biphasic calcium phosphate granulometry on bone ingrowth, ceramic resorption, and inflammatory reactions: preliminary *in vitro* and *in vivo* study. *J Biomed Mater Res* **46**: 103–111.
75. Daculsi G, Passuti N, Martin S, Deudon C, LeGeros RZ (1990). Macroporous calcium phosphate ceramic for long bone surgery in human dogs. Clinical and histological study. *J Biomed Mater Res* **24**: 379–396.
76. Passuti N, Delecrin J, Daculsi G (1992). Bone substitution for spine fusion. In: Williams DF, Christel P (Eds). *Implants in Orthopaedic Surgery*, Kent England, Edward Arnold, Ch 12A.
77. Daculsi G, Passuti N, Martin S, Le Nihouannen JC, Brulliard V, Delecrin J, Kerebel B (1989). Etude comparative de céramiques bioactives en phosphate de calcium après implantation en site osseux spongieux chez le chien. *Rev Chir Orthop* **75**: 65–71.
78. Delecrin J, Takahashi S, Gouin F, Passuti N (2000). A synthetic porous ceramic as a bone graft substitute in the surgical management of scoliosis: a prospective, randomized study. *Spine* **25**: 563–569.
79. Shima T, Keller JT, Alvira MM, Mayfield FH, Dunker SB (1979). Anterior cervical discectomy and interbody fusion. An experimental study using a synthetic tricalcium phosphate. *J. Neurosurg* **51**: 533–538.

80. Toth JM, An HS, Lim TH, Ran Y, Weiss NG, Lundberg WR, Xu RM, Lynch KL (1995). Evaluation of porous biphasic calcium phosphate ceramics for anterior cervical interbody fusion in a caprine model. *Spine* **20**(20): 2203–2210.
81. Zdeblick TA, Cooke ME, Wilson D, Kunz DN, McCabe R (1993). Anterior cervical discectomy, fusion and plating. A comparative animal study. *Spine* **18**(14): 1974–1983.
82. Zdeblick TA, Ghanayem AJ, Rapoff AJ, Swain C, Basset T, Cooke ME, Markel M (1998). Cervical interbody fusion. An animal model with and without bone morphogenetic protein. *Spine* **23**: 758–765.
83. Pascal-Moussellard H, Catonné Y, Robert R, Daculsi G (2007). Anterior cervical fusion with PEEK cages: clinical results of a prospective, comparative, multicenter and randomized study comparing iliac graft and a macroporous biphasic calcium phosphate. *Proceedings ESB 20*, Nantes, France.
84. Coventry MB (1985). Current concepts review: upper tibial osteotomy for osteoarthritis. *J Bone Joint Surg [Am.]* **67–A, 7**: 1136–1140.
85. Debeyre J, Artigou JM (1972). Résultats à distance de 260 ostéotomies tibiales pour déviations frontales du genou. *Rev Chir Orthop* **58**: 335–339.
86. Vainionpaa S, Läike E, Kirves P, Tiusanen (1981). Tibial osteotomy for osteoarthritis of the knee: a five to ten-year follow-up study. *J Bone Joint Surg [Am.]* **63-A**: 938–946.
87. Insall JN, Joseph DM, Msika C (1984). High tibial osteotomy for varus gonarthrosis: a long term follow-up study. *J Bone Joint Surg [Am.]* **66-A, 5**: 1040–1148.
88. Lootvoet L, Massinon A, Rossillon R, Himmer O, Lamber K, Ghosez JP (1993). Ostéotomie tibiale haute de valgisation externe pour gonarthrose sur genu varum (193 cas après 6 à 10 ans). *Rev Chir Orthop* **79**: 375–384.
89. Hernigou P (1996). Recul à plus de 20 ans de la gonarthrose fémoro-tibiale interne après ostéotomie tibiale de valgisation: ostéotomie unique versus ostéotomies ittératives. *Rev Chir Orthop* **82**: 241–250.
90. Jenny JY, Tavan A, Jenny G, Kehr P (1998). Taux de survie à long terme des ostéotomies tibiales de valgisation pour gonarthrose. *Rev Chir Orthop* **84**: 350–357.
91. Cauchoix J, Duparc J, Lemoine A, Deburge A (1968). L'ostéotomie dans les gonarthroses avec déviation angulaire dans le plan frontal. Résultats et indications thérapeutiques. *Rev Chir Orthop* **54**: 343–360.
92. Goutallier D, Hernigou P, Medevielle D, Debeyre J (1986). Devenir à plus de 10 ans de 93 ostéotomies tibiales. *Rev Chir Orthop* **72**: 101–114.
93. Hernigou PH, Medevielle D, Debeyre J, Goutallier D (1987). Proximal tibial osteotomy for osteoarthritis with varus deformity. A ten to thirteen-year follow-up study. *J Bone Joint Surg [Am.]* **69-A, 3**: 332–354.
94. Lascart T, Favard L, Burdin P, Traoré O (1998). Utilisation du phosphate tricalcique dans les ostéotomies tibiales de valgisation par addition interne. *Ann Orthop Ouest* **30**: 137–141.
95. Bonnevialle P, Abid A, Mansat P, Verhaeghe L, Clement D, Mansat M (2002). Ostéotomie tibiale de valgisation par addition médiale d'un coin de phosphate tricalcique. *Rev Chir Orthop* **88**: 486–492.

96. Koshino T, Murase T, Saito T (2003). Medial opening-wedge high tibial osteotomy with use of porous hydroxyapatite to treat medial compartment osteoarthritis of the knee. *J Bone Joint Surg [Am.]* **85-A**: 78–85.
97. Rouvillain JL (2007). MBCP™ wedges performance during open medial tibial osteotomy. *Proceedings ESB 20*, Nantes, France.
98. Pittenger MF, Mackay AM, Beck SC, Jaiswal RK, Douglas R, Mosca JD, Moorman MA, Simonetti DW, Craig S, Marshak DR (1999). Multilineage potential of adult human mesenchymal stem cells. *Science* **284**: 143–147.
99. Caplan AI, Fink DJ, Goto T, Linton AE, Young RG, Wakitani S, Goldberg V, Haynesworth SE (1993). In: Wetal JD (Ed). *The Anterior Cruciate Ligament: Current and Future Concepts*, Raven Press, New York, 405–417.
100. Jaiswal N, Haynesworth SE, Caplan AI, Bruder SP(1997). Osteogenic differentiation of purified culture-expanded human mesenchymal stem cells *in vitro*. *J Cell Biochem* **64**: 295–312.
101. Bruder SP, Jaiswal N, Haynesworth SE (1997). Growth kinetics, self-renewal, and the osteogenic potential of purified human mesenchymal stem cells during extensive subcultivation and following cryopreservation. *J Cell Biochem* **64**: 278–294.
102. Kadiyala S, Jaiswal N, Bruder SP (1997). Culture-expanded, bone marrow-derived mesenchymal stem cells can regenerate a critical-sized segmental bone defect. *Tissue Engi* **3**: 173–185.
103. Livingston Arinzeh T, Peter S, Archambault M, Van Den Bos C, Gordon S, Kraus K, Smith A, Kadiyala S (2003). Allogeneic mesenchymal stem cells regenerate bone in a critical-sized canine segmental defect. *J Bone Joint Surgery American* **85-A**: 1927–1935.
104. Teixeira CC, Nemelivsky Y, Karkia C, LeGeros RZ (2006). Biphasic calcium phosphate: a scaffold for growth plate chondrocytes. *Tissue Engi* **12**: 2283–2289.
105. LeNihouannen DL, Saffarzadeh A, Aguado E, Goyenvalle E, Gauthier O, Moreau F, Pilet P, Spaethe R, Daculsi G, Layrolle PJ (2007). Osteogenic properties of calcium phosphate ceramics and fibrin glue based composites. *J Mater Sci Mater Med* **18**(2): 225–235.
106. Le Guehennec L, Layrolle P, Daculsi G (2004). A review of bioceramics and fibrin sealant. *Eur Cell Mater* **8**: 1–11.
107. LeGeros RZ, Chohayeb A, Shulman A (1982). Apatitic calcium phosphates: possible restorative materials. *J Dent Res* **61** (Spec issue): 343.
108. Brown WE, Chow LC (1987). A new calcium phosphate water-setting cement. In: Brown PW (Ed). *Cement Research Progress 1986.* American Ceramic Society, Westerville, OH, pp. 352–379.
109. Niwa S, LeGeros RZ (2002). Injectable calcium phosphate cements for repair of bone defects. In: Lewandrowski K-U, Wise DL, Trantolo DJ, Gresser JD. *Tissue Engineering and Biodegradable Equivalents. Scientific and Clinical Applications*, Marcel Dekker, New York, pp. 385–400.
110. Constanz BR, Ison IC, Fulmer MT, Poser RD, Smith ST. Van Wagoner M, Ross J, Goldstein SA (1995). Skeletal repair by *in situ* formation of the mineral phase of bone, *Science* **267**: 1796–1799.

111. Khairoun I, LeGeros RZ, Daculsi G, Bouler JM, Guicheux J, Gauthier O (2004). Macroporous, resorbable and injectable calcium phosphate-based cements (MCPC) for bone repair, augmentation, regeneration and osteoporosis treatment. Provisional patent no. 11/054, 623.
112. Smucker JD, Aggarwal D, Zamora PO, Atkinson BL, Bobst JA, Nepola JV, Fredericks DC (2007). Assessment of B2A2-K-NS peptide coated on an osteoconductive granule in a rabbit posterolateral fusion model, *Proceedings AAOS 2007*, 12–14 February, San Diego, USA.

18

Si-substituted hydroxyapatite

E S THIAN and S M BEST, University of Cambridge, UK

18.1 Introduction

The idea of developing silicon-substituted hydroxyapatite (SiHA) is largely based on the role of silicon (Si) ions in bone and the excellent bioactivity of silica-based glasses and glass ceramics. Carlisle (1972, 1973, 1980) demonstrated that chicks fed on a diet with a low level of Si showed reduced growth, diminished feather development, abnormally shaped skulls and reduced thickness of their long bones. A similar study using a rat model by Schwarz and Milne (1972) also reported that Si deficiency led to retarded growth, and caused disturbances in the development of bone structures such as skull size and bone architecture.

Newly formed apatite layers are observed on the surface of bioglasses and glass ceramics within a few hours in acellular simulated body fluids (Hench *et al.* 1971; Phtsuki *et al.* 1992). The formation of surface silanol groups due to the release of Si ions from these bioactive materials has been proposed to act as a catalyst for apatite nucleation (Hench 1982; Hench and Andersson 1993; Yamamuro 1993; Arcos *et al.* 2002). Significant up-regulation of osteoblast proliferation and gene expression were also noted when exposed to low levels of released Si ions from bioactive glasses (Xynos *et al.* 2000, 2001; Gough *et al.* 2004). All of these studies suggested that Si incorporation into the hydroxyapatite (HA) structure would certainly lead to an enhancement of bioactive performance of HA.

This chapter will thus discuss the production and processing of SiHA, and then provide a review of the physical, mechanical and biological properties of SiHA, together with its clinical applications.

18.2 Fabrication

Several routes for the synthesis of silicon-substituted hydroxyapatite (SiHA) have been described, and can be classified into three categories, namely solid-state reaction, hydrothermal reaction and aqueous precipitation

reaction. It is generally accepted that silicon (Si) is incorporated into the HA lattice in the form of silicate groups which replace phosphate groups. However, the level of substitution is often referred to in terms of Si content. The amount of Si that can be incorporated into the lattice as a single substitution, while retaining phase purity seems to be limited, to levels up to 3 wt% (Gibson *et al.* 1999a; Kim *et al.* 2002, 2003; Arcos *et al.* 2004a).

18.2.1 Solid-state reaction

In solid-state reactions, SiHA is produced via the mixing of reactants in stoichiometric ratios at elevated temperatures. This method is susceptible to the formation of inhomogeneous end-products. Furthermore, it can induce the formation of intermediate phases of low reactivity due to the large number of initial reactants in the mixture.

Leshkivich and Monroe (1993) and Boyer *et al.* (1997) attempted to synthesise SiHA by the solid-state method, but in both cases, the addition of a secondary ion such as lanthanum or sulphate group is required, in addition to Si. Nevertheless, Arcos *et al.* (2004b) obtained phase-pure SiHA by mixing calcium pyrophosphate, calcium carbonate and silicon dioxide together before subjecting the mixture to heat treatment at 1100 °C for 72 h in an air atmosphere. This material contained 0.9 wt% Si.

18.2.2 Hydrothermal reaction

As the name implies, this route employs the use of temperature, pressure and a controlled atmosphere to convert a substance into another via an exchange reaction. This process has the disadvantage that it can be extremely time consuming.

Tanizawa and Suzuki (1994) reported that they obtained silicate-doped apatite by hydrothermal reaction at 145 °C, with approximately 3.5 wt% Si and 2.2 wt% carbonate. Another study by Sugiyama *et al.* (1995) reported the formation of silicate-containing hydroxyapatite using similar synthesis route, but of Ca/(P + Si) ratio higher than that of the stoichiometric ratio of 1.67.

18.2.3 Aqueous precipitation reaction

The precipitation reaction is by far the most established method to synthesise SiHA due to the simplicity of the equipment required and the potential to obtain a material with controlled chemical composition and morphology. The process involves reacting a calcium-containing solution with a phosphate-containing solution in the presence of a silicon-containing compound under conditions of controlled pH, temperature and atmosphere.

Gibson *et al.* (1999a, 2002) have synthesised a range of SiHAs by the aqueous precipitation method using calcium hydroxide, orthophosphoric acid and silicon acetate solutions. Si levels up to 1.6 wt% have been incorporated in a controlled manner, without the formation of secondary phases such as tricalcium phosphate (TCP), tetracalcium phosphate or calcium oxide. Marques *et al.* (2001) adopted the same approach to produce phase-pure SiHA with 0.15 wt% Si, but using different chemical reagents: calcium nitrate, ammounium hydrogen phosphate and silicon acetate solutions.

Kim *et al.* (2002, 2003) produced single-phase SiHA with a higher Si content of about 3 wt% via an aqueous precipitation route, using tetraethyl orthosilicate (TEOS) as a silicon source. A similar approach carried out by Ruys (1993) resulted in a final product that contained calcium silicophosphate and TCP besides HA, depending on the level of Si doping.

Arcos *et al.* (2004a) obtained a series of SiHA of varying Si contents from 0.6 to 2.6 wt% by a wet precipitation reaction, involving calcium nitrate, ammonium hydrogen phosphate and TEOS solutions. Material with a Si content of 0.6 wt% remained as phase-pure while higher Si contents led to decomposition of HA into TCP. Balas *et al.* (2003) conducted the same experiment but using silicon acetate as the silicon source. SiHAs up to 1.6 wt% were obtained and existed as a single apatite phase.

18.3 Microstructure

The morphology of SiHA is largely dependent on the fabrication route and processing conditions used. SiHA prepared via high-temperature synthesis (for example in solid-state reactions) often results in well-crystallised apatites with sizes of several tens of micrometres. On the other hand, nanocrystallites of SiHA, with a needle-like morphology, are usually obtained by low-temperature synthesis (for example in aqueous precipitation reactions) (Gibson *et al.* 2002; Kim *et al.* 2003).

There has been some discussion in the literature on the effect of silicon (Si) substitution on the morphology of SiHA. Gibson *et al.* (2002) noted that increasing the Si content of the substituted HA did not seem to have a significant effect on the crystallite size. Arcos *et al.* (2004a) on the other hand, reported that the mean crystal size of SiHA decreased with increasing Si incorporation. They indicated that the growth perpendicular to the *c*-axis of the crystal is shortened, thereby resulting in a more needle-like crystallite (Fig. 18.1). Porter *et al.* (2004a) observed, using transmission electron microscopy, that the density of triple junctions increased with Si content, and was significantly greater in a 1.5 wt% SiHA as compared with phase-pure HA (Table 18.1). This effect could potentially influence the solubility of substituted HA and subsequently, the rate of bone apposition (see Section 18.6 for more details).

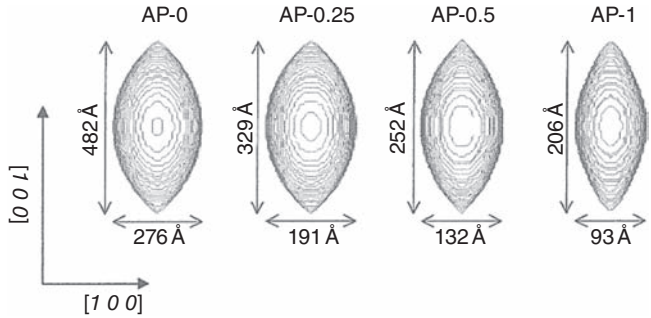

18.1 Crystallite shape of $Ca_{10}(PO_4)_{6-x}(SiO_4)_x(OH)_{2-x}$ for $x = 0, 0.25, 0.5, 1$ (Arcos *et al.* 2004a)

Table 18.1 Defect densities in phase-pure HA and SiHA (Porter *et al.* 2004a)

Material	Number of triple junctions / unit area (μm^2)
HA	0.21 ± 0.08
0.4 wt% SiHA	0.37 ± 0.14
0.8 wt% SiHA	0.59 ± 0.24
1.5 wt% SiHA	1.77 ± 0.50

Substitution of Si ions has also been shown to alter the final microstructure of SiHA upon sintering (Fig. 18.2). At 1200 °C, the grain size of HA was significantly larger than that observed for SiHAs and the grain size appeared to decrease with Si content (Gibson *et al.* 2002; Patel *et al.* 2003). Gibson and coworkers (2002) also reported a reduction in the sintered density of samples containing increased Si content as compared with pure HA processed under similar conditions (Fig. 18.3). This effect is particularly noticeable at low sintering temperatures (1000–1150 °C) (Gibson *et al.* 2002; Patel *et al.* 2003). However, this trend did not continue when the sintering temperature was 1200 °C. A comparable relative density of 94–96% was obtained. These findings appear to confirm that Si incorporation inhibits densification and grain growth.

18.4 Physical properties

Physical/chemical characterisation of SiHA is crucial in determining the underlying mechanisms of the bioactivity of this ceramic. A slight variation in the composition will have a profound effect on the biological response to the apatite ceramic.

The incorporation of silicate (SiO_4^{4-}) ions into the HA structure in the phosphate (PO_4^{3-}) ion positions has been reviewed by several authors

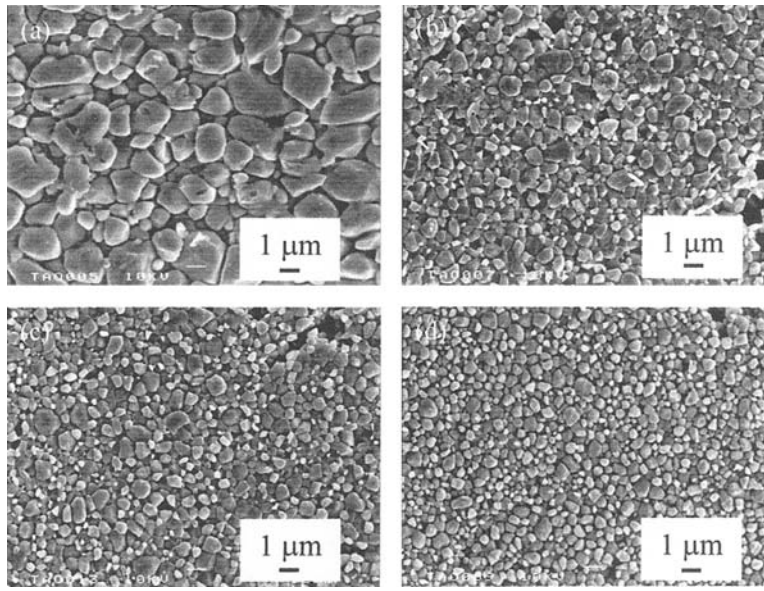

18.2 Scanning electron images of microstructure of sintered ceramics at 1200 °C: (a) HA, (b) 0.4 wt% SiHA, (c) 0.8 wt% SiHA, (d) 1.6 wt% SiHA (Gibson *et al.* 2002)

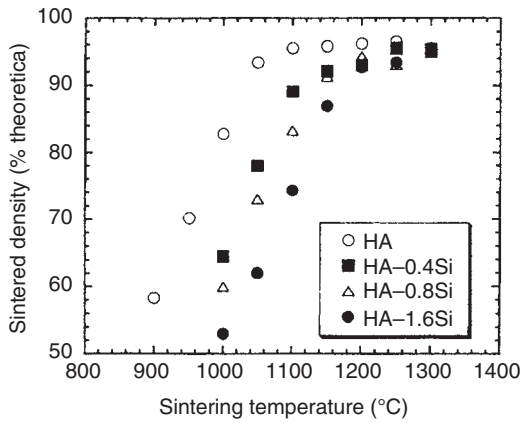

18.3 Variation of sintered density of HA with temperatures and silicon substitution (Gibson *et al.* 2002)

(Gibson *et al.* 1999a, 2002; Balas *et al.* 2003; Porter *et al.* 2004a). X-ray diffraction (XRD) patterns for HA and SiHA appeared to be similar and contained no secondary phases and all the diffraction peaks matched the JCPDS standard for HA (PDF card number 9-432). Although Gibson *et al.* (2002) and Porter *et al.* (2004a) reported that silicon addition has no direct

impact on the phase composition of HA, Balas and co-workers (2003) observed that the diffraction peaks were generally broader with increasing Si content.

A decrease in the *a*-axis and an increase in the *c*-axis of the unit cell of HA, together with an expansion in the unit cell volume, were observed with increasing Si substitution, as determined by Rietveld refinement of the XRD data (Porter *et al.* 2004a). Balas *et al.* (2003) reported an increase in both the unit cell of HA. Nevertheless, both studies clearly illustrate the changes in crystal structure of HA with Si addition.

The analysis of HA and SiHA by infrared (IR) spectroscopy reveals the effect of substitution on particular bond vibrations. Although the characteristic phosphate bands (ν_3 and ν_1 bands at around 1089, 1032 and 962 cm^{-1}; ν_4 band at around 631, 606 and 559 cm^{-1}) were identified in both HA and SiHA, the intensities of these peaks, especially for peaks at 960 and 692 cm^{-1}, were lower for SiHA. In some studies, additional peaks at 945, 890 and 840 cm^{-1} were observed in the spectrum for SiHA, and some of these peaks can be assigned to silicate (Gibson *et al.* 1999a; Botelho *et al.* 2002; Leventouri *et al.* 2003).

Botelho *et al.* (2002) conducted X-ray photoelectron spectroscopy analysis, and demonstrated that Si was fully incorporated as SiO_4^{4-} anions by replacing the PO_4^{3-} anions. On another occasion, Balas *et al.* (2003) obtained similar results, but reported that polymerisation of the silicate species tends to occur for an Si content of more than 1.6 wt%.

A reduction in the peak heights in the IR spectrum at 3570 and 630 cm^{-1} corresponding to hydroxyl groups, was also noted with Si incorporation (Kim *et al.* 2003). This effect was further confirmed by high-resolution neutron powder diffraction measurement, demonstrating a 13% reduction of the hydroxyl site occupancy when 0.4 wt% Si was added into the HA crystal structure. Such a reduction is necessary to compensate for the extra negative charge of the SiO_4^{4-} group by introducing vacancies on the hydroxyl site as Si is being substituted, thereby maintaining charge balance, given in equation (18.1) (Gibson *et al.* 1999a):

$$PO_4^{3-} + OH^- \rightarrow SiO_4^{4-} + \square \qquad 18.1$$

In this way, a mechanism used to synthesise SiHA can be described in equation (18.2) (Gibson *et al.* 1999a):

$$10Ca^{2+} + (6 - x)PO_4^{3-} + xSiO_4^{4-} + (2 - x)OH^- \rightarrow Ca_{10}(PO_4)_{6-x}(SiO_4)_x(OH)_{2-x} \qquad 18.2$$

At physiological pH of 7.4, the surface charge of SiHA is significantly lower as compared with a phase-pure HA, as determined by zeta potential measurement (Botelho *et al.* 2002). This effect could possibly enhance the bioactivity of SiHA (see Section 18.6 for more details).

18.5 Mechanical properties

There have been a limited number of studies on the effect of silicon substitution on the mechanical properties, such as Vickers hardness and Young's modulus of HA. As would be expected, both stoichiometric HA and SiHA compositions exhibit a gradual increase in hardness with increasing sintering temperature (Fig. 18.4) (Gibson *et al.* 2002). This effect is related to an increase in sintered density as the sintering temperature increases (van Landuyt *et al.* 1995). However, the hardness values of all SiHAs (~90 H_v) are relatively low as compared with that of HA (~240 H_v) at low sintering temperatures (<1000 °C) due to the low densities obtained for SiHA sintered at these temperatures. At 1100 °C and above, it was observed that the corresponding hardness values of all SiHAs were greater than HA, and the values increase with increasing Si addition (Gibson *et al.* 2002). At 1300 °C, SiHA containing 1.6 wt% Si had the highest value of ~600 H_v whilst HA had only a value of ~350 H_v. The improved hardness for SiHA at high sintering temperature was attributed to the smaller grain sizes obtained for SiHA as compared with phase-pure HA.

Patel *et al.* (2003) conducted a series of mechanical tests on HA and various SiHA compositions. The authors found that the hardness and modulus values were higher for HA at low sintering temperature, compared with SiHA. In contrast, the mechanical values of all samples at high sintering temperatures were comparable.

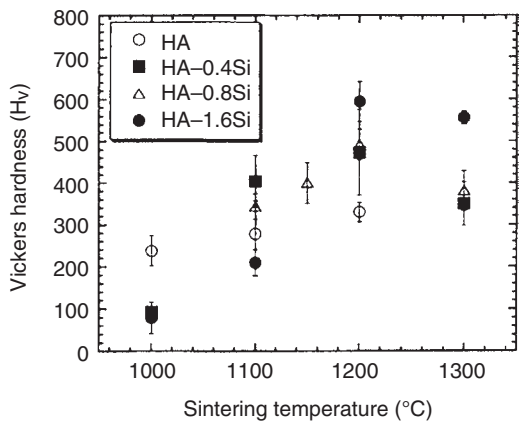

18.4 Variation of Vickers hardness of HA with sintering temperatures and silicon substitution (Gibson *et al.* 2002)

18.6 Biological properties

The characterisation of the bioactivity of SiHA has involved both *in vitro* and *in vivo* testing. These tests provide valuable fundamental information about the cellular and molecular interactions with SiHA.

18.6.1 *In vitro* acellular testing

Simulated body fluid (SBF) is a relatively cheap and easy technique to assess the bioactivity of different materials under physiological conditions. SBF study has been shown to be useful for predicting *in vivo* bioactivity of a material (Kokubo *et al.* 2006). SBF-K9 developed by Kokubo *et al.* (1990) is the most widely used solution for this purpose since it has ionic composition that closely resembles to human blood plasma.

Gibson and coworkers (1999b) demonstrated that the time required to form a newly-precipitated carbonate apatite layer on SiHA containing 0.8 wt% Si (17 days) decreased compared with pure HA (24 days) when subjected to SBF immersion. This effect was enhanced with increasing Si level, to 11 days for SiHA containing 1.6 wt% Si. Similarly, Balas *et al.* (2003) indicated that after 6 weeks of immersion in SBF, the surface of SiHA appeared to be covered by calcium phosphate material, but this was not the case for HA. Recently, high-resolution transmission electron microscopy (HR-TEM) technique was employed to study the dissolution of HA and SiHA in SBF. Porter *et al.* (2004a) found that extensive dissolution occurred on 0.8 wt% SiHA and 1.5 wt% SiHA, with numerous nodular apatites appearing to nucleate on the surfaces of SiHAs, at 24 and 6 h, respectively. On the other hand, this effect was only observed on phase-pure HA at 72 h.

18.6.2 *In vitro* cellular testing

In vitro models using cell cultures are crucial for the study of host tissue-implanted biomaterial interactions since they provide useful information regarding material biocompatibility and matrix synthesis. Gibson *et al.* (1999b) have shown that SiHA was non-cytotoxic to human osteosarcoma (HOS) cells *in vitro*. In addition, the metabolic activity of HOS cells on SiHA was higher than for HA at all time points. This study was later confirmed by Vallet-Regi and Acros (2005) who indicated a positive stimulatory effect of Si substitution on the proliferation of HOS cells. With a higher Si content, the cell proliferation increased with culturing time.

Botelho and coworkers (2006) reported an increase in the number of human osteoblast (HOB) cells growing on SiHA, along with significantly

higher level of osteoblast expression markers such as alkaline phosphatase, collagen type I and osteocalcin, compared with pure HA.

18.6.3 *In vivo* testing

Studies using animal models are a necessary step in the process of the development of clinical treatments of diseases in humans. As such, they act as a bridge between *in vitro* studies and clinical trials (Giardino *et al.* 1998).

Patel *et al.* (2002) reported that bone ingrowth was observed between both HA and SiHA granules when implanted into the femoral condyle of rabbits for 23 days. However, they found that the percentage of bone ingrowth (38% versus 22%) and bone/implant coverage (60% versus 47%) for 0.8 wt% SiHA were significantly higher than that for HA. Similarly, these authors again demonstrated enhanced bone ingrowth and coverage in femoral condyle of sheep for SiHA granule as compared with pure HA at weeks 6 and 12, which reaffirmed the previous findings (Patel *et al.* 2005).

HR-TEM studies indicated that organized collagen fibrils were observed at the bone/SiHA interface after 6 weeks of implantation in sheep while this phenomenon was observed only at the bone/HA interface at week 12 (Porter *et al.* 2004a). These findings implied that bone apposing SiHA was at a more developed stage of remodelling. The authors also reported that a greater depth of dissolution was seen at the surface of SiHA as compared with HA *in vivo*, as evidenced by the observation of larger needle-like apatite crystallites emanating from the deeper regions of SiHA (Porter *et al.* 2003).

All these studies demonstrated that substitution of Si into HA enhanced the rate and quality of bone repair. This fact arose from the enhanced dissolution rate of SiHA with increasing Si content. A possible explanation could be related to the increased number of triple-point junctions and grain boundaries in SiHA, which act as an initiation site for dissolution (Porter *et al.* 2004a). Si has also been shown to inhibit densification and crystal growth at high sintering temperatures, and, as such, a decrease in crystal size will inevitably increase the solubility of the material, releasing more calcium, phosphorus and silicon ions into the surrounding environment (Gibson *et al.* 2002). This effect will then facilitate the rapid development of a carbonate apatite layer, thereby providing favourable sites for bone cells to adhere, grow, express and mineralise bone matrix (Neo *et al.* 1993). Studies have also demonstrated that the surface of SiHA is more negatively charged than HA, which results in higher cellular adhesion and subsequently, higher cell proliferation on SiHA (Botelho *et al.* 2002). As such, the physicochemical properties of SiHA, namely surface property, have a positive effect on cellular response.

18.7 Applications

SiHA can be used in the human body to repair hard and soft tissue damage within the skeletal system, comprising bone, joint and tooth. Other clinical applications include maxillofacial reconstruction, cranial repair, ossicular reconstruction, ocular prosthetic and intervertebral disc substitute. The selection of an appropriate implant material is crucial in supporting bone ingrowth and osseointegration when used in orthopaedic, dental and maxillofacial applications. As such, SiHA is well suited for older patients where bone cells are less proliferative or even in younger, active patients where rapid bone healing process is desirable.

18.8 Recent developments

Current studies focused on developing SiHA as coatings on metallic implants, so as to improve the interaction of the implant material with the host tissue (Hijon *et al.* 2006; Thian *et al.* 2006a). SiHA thin films demonstrated enhanced bioactivity *in vitro* and, thus, are likely to be a good alternative to HA thin films (Thian *et al.* 2005, 2006b,c).

Recent research efforts have also been devoted to nanostructure processing of SiHA (Huang *et al.* 2005; Xu and Khor 2007). Literature reports that the unique properties of nanobiomaterials are likely to modulate protein interactions and, subsequently, control cellular functions (Huang *et al.* 2005). As such, nano-SiHA has extensive potential in improving the biological applications pertinent to orthopaedics.

Lately, considerable interest had been targeted towards the development of porous SiHA, so as to allow both cellular ingress and vascularisation, and at the same time, enhanced bioactivity and bioresorbability (Kim *et al.* 2005; Porter *et al.* 2006). Actifuse™, a phase-pure SiHA with a porosity level of 80%, manufactured by ApaTech Ltd is now commercially available, and is used clinically in impaction grafting and spinal fusion.

Significant progress has also been made towards the field of drug delivery systems during the last few decades. Local delivery of pharmaceuticals at targeted sites certainly has clear advantages, which in some cases may lead to bacterial resistance. Recent findings indicate that HA microspheres are being considered for drug delivery applications due to its excellent biocompatibility and high binding affinity to a variety of molecules (proteins, enzymes and nuclei acids) (Morris and Bajpai 1989; Pham *et al.* 2002; Ribeiro *et al.* 2004). This offers the potential for using SiHA to deliver a large variety of drugs in many clinical applications.

Advances in bone replacements have been focused on the production of biocomposites in an attempt to achieve a biomaterial as closely as possible to the biological apatites (Thomson *et al.* 1998; Di Silvio *et al.* 2002).

Thus, SiHA could potentially be used as particulates within a polymer matrix.

18.9 Summary

This chapter provides the reader a general overview of the scientific research conducted so far, concerning the fabrication, physical, chemical, mechanical and biological properties of silicon-substituted hydroxyapatite (SiHA). A few key points are discussed and summarised. Nevertheless, more in-depth studies are necessary to understand the mechanism that makes SiHA a better choice of biomaterial, especially at the genomic and proteomic levels.

- SiHA is usually synthesised via an aqueous precipitation reaction. However, due to its thermal instability and consequently, decomposition at high temperatures, reproducible production of phase-pure SiHA requires careful process control.
- The incorporation of Si into the HA lattice affects the crystallinity, microstructure, solubility, mechanical and biological properties of HA.
- *In vitro* and *in vivo* studies have indicated that Si substitution significantly enhanced the bioactivity of HA.

18.10 References and further reading

Arcos D, Greenspan D C and Vallet-Regi M (2002), 'Influence of the stabilization temperature on textural and structural features and ion release in SiO_2–CaO–P_2O_5 sol–gel glasses', *Chem Mater*, **14**, 1515–22.

Arcos D, Rodriguez-Carvajal J and Vallet-Regi M (2004a), 'Silicon incorporation in hydroxylapatite obtained by controlled crystallisation', *Chem Mater*, **16**, 2300–308.

Arcos D, Rodriguez-Carvajal J and Vallet-Regi M (2004b), 'The effect of the silicon incorporation on the hydroxylapatite structure. A neutron diffraction study', *Solid State Sci*, **6**, 987–94.

Balas F, Perez-Pariente J and Vallet-Regi M (2003), '*In vitro* bioactivity of silicon-substituted hydroxyapatites', *J Biomed Mater Res*, **66A**, 364–75.

Botelho C M, Lopes M A, Gibson I R, Best S M and Santos J D (2002), 'Structural analysis of Si-substituted hydroxyapatite: zeta potential and X-ray photoelectron spectroscopy', *J Mater Sci Mater Med*, **13**, 1123–7.

Botelho C M, Brooks R A, Best S M, Lopes M A, Santos J D, Rushton N and Bonfield W (2006), 'Human osteoblast response to silicon-substituted hydroxyapatite', *J Biomed Mater Res*, **79A**, 723–30.

Boyer L, Carpena J and Lacout J L (1997), 'Synthesis of phosphate-silicate apatites at atmospheric pressure', *Solid State Ionics*, **95**, 121–9.

Carlisle E M (1972), 'Silicon: an essential element for the chick', *Science*, **178**, 619–21.

Carlisle E M (1973), 'A skeletal alteration associated with silicon deficiency', *Fed Proc*, **32**, 930.

Carlisle E M (1980), 'Biochemical and morphological changes associated with long bone abnormalities in silicon deficiency', *J Nutr*, **110**, 1046–55.

Di Silvio L, Dalby M J and Bonfield W (2002), 'Osteoblast behaviour on HA/PE composite surfaces with different HA volumes', *Biomaterials*, **23**, 101–7.

Giardino R, Fini M and Giavaresi G (1998), 'Experimental surgery in the research of artificial organs', *Int J Artif Organs*, **21**, 506–8.

Gibson I R, Best S M and Bonfield W (1999a), 'Chemical characterisation of silicon-substituted hydroxyapatite', *J Biomed Mater Res*, **44**, 422–8.

Gibson I R, Huang J, Best S M and Bonfield W (1999b), 'Enhanced *in vitro* cell activity and surface apatite layer formation on novel silicon-substituted hydroxyapatites', in Ohgushi H, Hasting G W and Yoshikawa T, *Bioceramics 12*, Nara, Japan, 191–4.

Gibson I R, Best S M and Bonfield W (2002), 'Effect of silicon substitution on the sintering and microstructure of hydroxyapatite', *J Am Ceram Soc*, **85**, 2771–7.

Gough J E, Jones J R and Hench L L (2004), 'Nodule formation and mineralisation of human primary osteoblasts cultured on a porous bioactive glass scaffold', *Biomaterials*, **25**, 2039–46.

Hench L L (1982), 'Glass surfaces', *J Phys*, **43**, 625–36.

Hench L L and Andersson O (1993), 'Bioactive glass', in Hench L L and Wilson J, *An Introduction to Bioceramics*, Singapore, World Scientific Publishing Co. Pte. Ltd, 41–62.

Hench L L, Splinter R J, Allen W C and Greenlee T K (1971), 'Bonding mechanisms at the interface of ceramic prosthetic materials', *J Biomed Mater Res*, **5**, 117–41.

Hijon N, Cabanas M V, Pena J and Vallet-Regi M (2006), 'Dip-coated silicon-substituted hydroxyapatite films', *Acta Biomater*, **2**, 567–74.

Huang J, Jayasinghe S N, Best S M, Edirisinghe M J, Brooks R A, Rushton N and Bonfield W (2005), 'Novel deposition of nano-sized silicon-substituted hydroxyapatite by electrostatic spraying', *J Mater Sci Mater Med*, **16**, 1137–42.

Kim S R, Riu D H, Lee Y J and Kim Y H (2002), 'Synthesis and characterisation of silicon substituted hydroxyapatite', *Key Eng Mater*, **218–220**, 85–8.

Kim S R, Lee J H, Kim Y T, Riu D H, Jung S J, Lee Y J, Chung S C and Kim Y H (2003), 'Synthesis of Si, Mg substituted hydroxyapatites and their sintering behaviors', *Biomaterials*, **24**, 1389–98.

Kim Y H, Song H, Riu D H, Kim S R, Kim H J and Moon J H (2005), 'Preparation of porous Si-incorporated hydroxyapatite', *Curr Appl Phys*, **5**, 538–41.

Kokubo T and Takadama H (2006), 'How useful is SBF in predicting *in vivo* bone bioactivity?', *Biomaterials*, **27**, 2907–15.

Kokubo T, Kushitani H, Sakka S, Kitsugi T and Yamamuro T (1990), 'Solution able to reproduce *in vivo* surface-structure changes in bioactive glass-ceramic A-W', *J Biomed Mater Res*, **24**, 721–34.

Leshkivich K S and Monroe E A (1993), 'Solubility characteristics of synthetic silicate sulphate apatites', *J Mater Sci*, **28**, 9–14.

Leventouri Th, Bunaciu C E and Perdikatsis V (2003), 'Neutron powder diffraction studies of silicon-substituted hydroxyapatite', *Biomaterials*, **24**, 4205–11.

Marques P A A P, Magalhaes M C F, Correria R N and Vallet-Regi M (2001), 'Synthesis and characterisation of silicon-substituted hydroxyapatite', *Key Eng Mater*, **192–195**, 247–50.

Morris L and Bajpai P K (1989), 'Development of a resorbable tricalcium phosphate (TCP) amine antibiotic composite', in Hanker J S and Giammara B L, *Biomedical Materials and Devices*, Pittsburgh, PA, 293–300.

Neo M, Nakamura T, Ohtsuki C, Kokubo T and Yamamuro T (1993), 'Apatite formation on three kinds of bioactive materials at early stage *in vivo*: a comparative study by transmission electron microscopy', *J Biomed Mater Res*, **27**, 999–1006.

PDF card number 9-432, ICDD, Newton Square, Pennsylvania, USA.

Patel N, Best S M, Bonfield W, Gibson I R, Hing K A, Damien E and Revell P A (2002), 'A comparative study on the *in vivo* behavior of hydroxyapatite and silicon substituted hydroxyapatite granules', *J Mater Sci Mater Med*, **13**, 1199–206.

Patel N, Follon E L, Gibson I R, Best S M and Bonfield W (2003), 'Comparison of sintering and mechanical properties of hydroxyapatite and silicon-substituted hydroxyapatite', *Key Eng Mater*, **240–242**, 919–22.

Patel N, Brooks R A, Clarke M T, Lee P M T, Rushton N, Gibson I R, Best S M and Bonfield W (2005), '*In vivo* assessment of hydroxyapatite and silicate-substituted hydroxyapatite granules using an ovine defect model', *J Mater Sci Mater Med*, **16**, 429–40.

Pham H H, Luo P, Genin F and Dash A K (2002), 'Synthesis and characterization of hydroxyapatite–ciprofloxacin delivery systems by precipitation and spray drying technique', *AAPS PharmSciTech*, **3**, 1–9.

Phtsuki C, Kokubo T and Yamamuro T (1992), 'Mechanism of apatite formation on $CaO–SiO_2–P_2O_5$ glasses in a simulated body fluid', *J Non-Cryst Solids*, **143**, 84–92.

Porter A E, Patel N, Skepper J N, Best S M and Bonfield W (2003), 'Comparison of *in vivo* dissolution processes in hydroxyapatite and silicon-substituted hydroxyapatite bioceramics', *Biomaterials*, **24**, 4609–20.

Porter A E, Best S M and Bonfield W (2004a), 'Ultrastructural comparison of hydroxyapatite and silicon-substituted hydroxyapatite for biomedical applications', *J Biomed Mater Res*, **68A**, 133–41.

Porter A E, Patel N, Skepper J N, Best S M and Bonfield W (2004b), 'Effect of sintered silicate-substituted hydroxyapatite on remodelling processes at the bone–implant interface', *Biomaterials*, **25**, 3303–14.

Porter A E, Buckland T, Hing K A, Best S M and Bonfield W (2006), 'The structure of the bond between bone and porous silicon-substituted hydroxyapatite bioceramic implants', *J Biomed Mater Res*, **78A**, 25–33.

Ribeiro C C, Barrias C C and Barbosa M A (2004), 'Calcium phosphate-alginate microspheres as enzymes delivery matrices', *Biomaterials*, **25**, 4363–73.

Ruys A J (1993), 'Silicon-doped hydroxyapatite', *J Aust Ceram Soc*, **29**, 71–80.

Schwarz K and Milne D B (1972), 'Growth-promoting effects of silicon in rats', *Nature*, **239**, 333–4.

Sugiyama K, Suzuki T and Satoh T (1995), 'Bactericidal activity of silicate-containing hydroxyapatite', *J Antibact Antifun Agents*, **23**, 67–71.

Tanizawa Y and Suzuki T (1994), 'X-ray photoelectron spectroscopy study of silicate-containing apatite', *Phos Res Bull*, **4**, 83–8.

Thian E S, Huang J, Best S M, Barber Z H and Bonfield W (2005), 'Magnetron co-sputtered silicon-containing hydroxyapatite thin films – an *in-vitro* study', *Biomaterials*, **26**, 2947–56.

Thian E S, Huang J, Vickers M E, Best S M, Barber Z H and Bonfield W (2006a), 'Silicon-substituted hydroxyapatite (SiHA): a novel calcium phosphate coating for biomedical applications', *J Mater Sci*, **41**, 709–17.

Thian E S, Huang J, Best S M, Barber Z H and Bonfield W (2006b), 'Novel silicon-doped hydroxyapatite (Si-HA) for biomedical coatings: an *in vitro* study using acellular simulated body fluid', *J Biomed Mater Res*, **76B**, 326–33.

Thian E S, Huang J, Best S M, Barber Z H, Brooks R A, Rushton N and Bonfield W (2006c), 'The response of osteoblasts to nanocrystalline silicon-substituted hydroxyapatite thin films', *Biomaterials*, **27**, 2692–8.

Thomson R C, Yaszemski M J, Powers J M and Mikos A G (1998), 'Hydroxyapatite fiber reinforced poly(α-hydroxy ester) foams for bone regeneration', *Biomaterials*, **19**, 1935–43.

Vallet-Regi M and Arcos D (2005), 'Silicon-substituted hydroxyapatites. A method to upgrade calcium phosphate based implants', *J Mater Chem*, **15**, 1509–16.

van Landuyt P, Li F, Keustermans J P, Streydio J M, Delannay F and Munting E (1995), 'The influence of high sintering temperatures on the mechanical properties of hydroxyapatite', *J Mater Sci Mater Med*, **6**, 8–13.

Xu J L and Khor K A (2007), 'Chemical analysis of silica doped hydroxyapatite biomaterials consolidated by a spark plasma sintering method', *J Inorg Biochem*, **101**, 187–95.

Xynos I D, Hukkanen M V, Batten J J, Buttery L D, Hench L L and Polak J M (2000), 'Bioglass 45S5® stimulates osteoblast turnover and enhances bone formation *in vitro*: implications and applications for bone tissue engineering', *Calcif Tissue Int*, **67**, 321–9.

Xynos I D, Edgar A J, Buttery L D, Hench L L and Polak J M (2001), 'Gene-expression profiling of human osteoblasts following treatment with the ionic products of Bioglass® 45S5 dissolution', *J Biomed Mater Res*, **55**, 151–7.

Yamamuro T (1993), 'A/W glass ceramic: clinical applications', in Hench L L and Wilson J, *An Introduction to Bioceramics*, Singapore, World Scientific Publishing Co. Pte. Ltd, 89–104.

19

Calcium phosphate cement

K ISHIKAWA, Kyushu University, Japan

19.1 Introduction

As the name suggests, calcium phosphate cements (CPC) consist of one or a mixture of plural calcium phosphate powder(s). When the powder phase of calcium phosphate is mixed with its liquid phase, it forms hydroxyapatite (HA: $Ca_{10}(PO_4)_6(OH)_2$) or brushite (dicalcium phosphate dihydrate; DCPD: $CaHPO_4 \cdot 2H_2O$) based on the hardening reaction. CPC that forms HA is called apatite cement, hydroxyapatite cement or apatite CPC, and CPC that forms brushite or DCPD is called brushite cement, DCPD cement or DCPD-CPC. The latter is also sometimes called β-tricalcium phosphate cement since the major component of the powder phase is β-tricalcium phosphate (β-TCP: β-$Ca_3(PO_4)_2$). In the following text, the terms apatite cement and brushite cement will be used for simplicity. As a result of calcium phosphate formation, the set mass shows excellent tissue response. In the case of apatite cement, it also shows good osteoconductivity. Of course, a key advantage of CPC is its hardening property. Bone defects can be reconstructed by filling with CPC. Some CPC can be injected using syringe or tube (Fig. 19.1). Therefore, a minimally invasive surgical operation can be expected using CPC. It should be noted that the selection of clinical case is important. In other words, CPC should be used so that its hardening reaction can be fully guaranteed: when it fails to harden, it induces an inflammatory response caused by the response of tissue to powder known as the crystalline inflammatory response. When CPC is injected using a syringe, there is a good chance that the paste will be exposed to body fluid. In such a case, the CPC could be washed out and thus could cause an inflammatory response.

CPC was initially reported by Prof. Monma and Kanazawa in 1976 (Monma and Kanazawa 1976). They reported that α-tricalcium phosphate (α-TCP; α-$Ca_3(PO_4)_2$) set to form calcium-deficient HA with Ca/P molar ratio of 1.5 when α-TCP was hydrated in water at 60–100 °C and pH between 8.1 and 11.4. Although this was the initial finding of the apatite cement, the

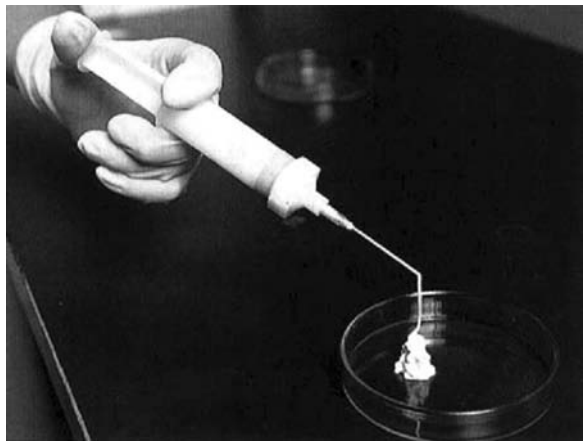

19.1 Injection of apatite cement (Biopex®) from syringe.

long setting time prevented its clinical use for a long period. In 1982, LeGeros *et al.* reported a CPC as a possible dental restorative materials (LeGeros *et al.* 1982). In 1986, Brown and Chow reported that a mixture of tetracalcium phosphate (TTCP: $Ca_4(PO_4)_2O$), and dicalcium phosphate anhydrous (DCPA: $CaHPO_4$) set within approximately 30–60 min at physiological temperature and forms apatitic product when mixed with aqueous solution (Brown and Chow 1986a; Chow *et al*. 1991b).

Brushite cement was invented after the invention of apatite cement by Lemaitre *et al*. (1987; Mirtchi *et al*. 1989) Basically, brushite cement consists of β-TCP and monocalcium phosphate monohydrate (MCPM: $Ca(H_2PO_4)_2 \cdot H_2O$) or phosphoric acid (H_3PO_4) and forms brushite based on the setting reaction.

Based on these initial findings, many types of calcium phosphate cements have been studied and developed up to date.

19.2 Fabrication of calcium phosphate cement

Obviously, CPCs consist of powder and liquid phases. Table 19.1 summarizes the calcium orthophosphate compounds and their solubility. In this table, the calcium orthophosphate compounds are listed in order of Ca/P value. In other words, calcium orthophosphates are listed from acidic to alkaline salts. Also, Fig. 19.2 summarizes the thermodynamic stability of calcium phosphate in an aqueous solution in terms of calcium concentration as a function of pH. As can be seen in Fig. 19.2, HAP, DCPD and MCPM are the most stable phases thermodynamically, depending on the pH. Basically, calcium phosphate powders are selected for their final product to be HAP or DCPD in composition.

Table 19.1 Calcium orthophosphates and their solubility product constants

Compound	Abbreviation	Chemical formula	Ca/P	log K_{sp}
Monocalcium phosphate monohydrate	MCPM	$Ca(H_2PO_4)_2{\cdot}H_2O$	0.5	Highly soluble
Monocalcium phosphate anhydrous	MCPA	$Ca(H_2PO_4)_2$	0.5	Highly soluble
Dicalcium phosphate dihydrate	DCPD	$CaHPO_4{\cdot}2H_2O$	1.0	6.59
Dicalcium phosphate anhydrous	DCPA	$CaHPO_4$	1.0	6.90
Octacalocium phosphate	OCP	$Ca_8H_2(PO_4)_6{\cdot}5H_2O$	1.33	96.6
α-Tricalcium phosphate	α-TCP	$Ca_3(PO_4)_2$	1.5	
β-Tricalcium phosphate	β-TCP	$Ca_3(PO_4)_2$	1.5	28.9
Hydroxyapatite	HAP	$Ca_{10}(PO_4)_6(OH)_2$	1.67	116.8
Fluoroapatite	FAP	$Ca_{10}(PO_4)_6F_2$	1.67	121
Tetracalcium phosphate	TTCP	$Ca_4(PO_4)_2O$	2.0	38–44

Composition of the commercially available apatite cements and brushite cements are listed in Tables 19.2 and 19.3, respectively. As can be seen in these tables, some salts that are not calcium phosphates are also used. CPC should be stable until use. However, calcium phosphate powders react partially with each other even without mixing liquid phases. As the result of an undesirable hardening reaction, the length of time the cement will be available will be shortened. To prevent this, a chemical that does not affect the hardening reaction or tissue response is added for stabilization. In the case of brushite cement additives play a more important role: brushite cement hardens too rapidly without additives. Therefore, additives known to prevent the formation of brushite are added to the brushite cement as retarders. Calcium pyrophosphate, calcium sulfate dihydrate and calcium sulfate hemihydrate increase the hardening time (Mirtchi *et al.* 1990).

After the determination of the calcium phosphate salt, its particle size regulation should be done properly. This is because the basic hardening reaction of CPC is based on so-called dissolution–reprecipitation reaction as stated below (Ishikawa and Asaoka 1995; Ishikawa *et al.* 2003). Therefore,

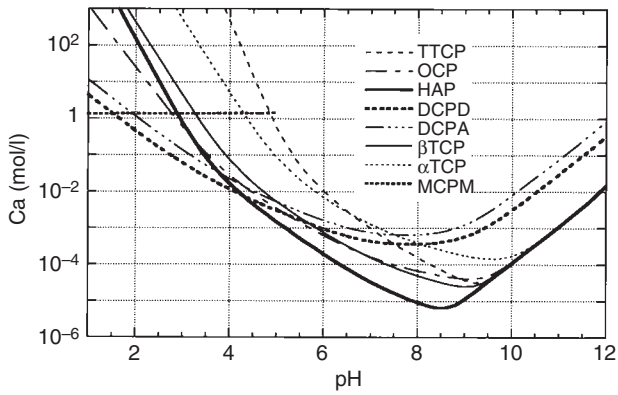

19.2 Solubility of Ca and P in various calcium phosphate compounds versus pH calculated from their solubility products given in Table 19.1.

both calcium and phosphate ions have to be supplied simultaneously for the precipitation of apatite or brushite. However, dissolution rate differs for different calcium phosphate salts even though the particle size may be the same. Powder size should be regulated to minimize dissolution rate difference. In other words, powder with large diameter, i.e. resulting smaller specific surface area, dissolves slowly whereas powder with small diameter, i.e. resulting large specific surface area, dissolves quickly. For example, large tetracalcium phosphate (TTCP: $Ca_4(PO_4)_2O$) powder and small dicalcium phosphate anhydrous (DCPA: $CaHPO_4$) powders must be mixed in the case of apatite cement consisting of an equimolar mixture of TTCP and DCPA since TTCP dissolves quickly whereas the dissolution rate of DCPA is slow.

Table 19.4 summarizes the example of the effect of particle size on the mechanical strength of hardened apatite cement consists of TTCP and DCPA. As shown in this table, apatite cement consisting of small TTCP and large DCPA does not set. On the other hand, the mechanical strength of apatite cement increases with the diameter ratio of TTCP/DCPA, and apatite cement with highest TTCP/DCPA diameter ratio or apatite cement consisting of large TTCP and small DCPA provides the best mechanical strength.

The liquid phase plays an important part in the initial hardening reaction, handling property, injectability as well as anti-washout property (Ishikawa *et al*. 1995a,b; Miyamoto *et al.* 1995a,b). The liquid phase of the apatite cement is made by simply dissolving required chemicals into distilled and sterilized water. The liquid phase sometimes contain stabilizers such as sodium hydrogen sulfite.

Table 19.2 Example of the commercially available apatite cement and its composition

Registered name	Powder	Liquid	Manufacture
Biopex®-R	α-TCP + TTCP + DCPD + HAP + $Mg_3(PO_4)_2$	Succinic acid, chondroitin sulfate and	Mitsubishi Materials
Primafix®	TTCP + DCPA	sodium hydrogen sulfite	NGK Spark Plug Co.
Cerapaste®	TTCP + DCPA	Sodium dextran sulfate sulfur 5	NGK Spark Plug Co.
BoneSource®	TTCP(73%) + DCPA (27%)	Sodium phosphate solution	Stryker
Norian SRS®	α-TCP(85%) + $CaCO_3$(12%) + MCPM(3%)	Disodium phosphate solution	Synthes
Norian CRS®	α-TCP(85%) + $CaCO_3$(12%) + MCPM(3%)	Disodium phosphate solution	Synthes
Norian SRS® Fast Set Putty	Not documented	Not documented	Synthes
Norian SRS® Fast Set Putty	Not documented	Not documented	Synthes
Calcibon®	α-TCP(61%) + DCPA(26%) + $CaCO_3$(10%) + HAP(3%)	Disodium phosphate solution	Biomet
Mimix™	TTCP + α-TCP + C_6H_5O-Na_3·$2H_2O$	Citric acid	Biomet
QuickSet Mimix™	Not documented	Not documented	Biomet
Cementek®	TTCP + α-TCP + $Ca(OH)_2$ + sodium glycerophosphate	Acidic Ca-PO_4	Teknimed
Cementek® LV	TTCP + α-TCP + $Ca(OH)_2$ + sodium glycerophosphate + dimethylssiloxane	Acidic Ca-PO_4	Teknimed
α-BSM®	ACP(50%) + DCPD(50%)	Saline	ETEX
Biobon®	ACP(50%) + DCPD(50%)	Saline	ETEX
Embare®	ACP(50%) + DCPD(50%)	Saline	ETEX
KyphO_S™	α-TCP(77%) + $Mg_3(PO_4)_2$(14%) + $MgHPO_4$(4.8%) + $SeCO_3$(3.6%)	3.5 mol/l diammonium hydrogen phosphate	Kyphon
Callos™	Not documented	Not documented	Skeletal Kinetics
Rebone	TTCP + DCPA	Water	Shanghai Rebone Biomaterials Co. Ltd

* Biobon® is the trade name of α-BSM in Europe.

Table 19.3 Example of the commercially available brushite cement and its composition

Registered name	Powder	Liquid	Manufacture
ChronOS™ Inject	β-TCP(73%) + MCPM(21%) + $MgHPO_4 \cdot 3H_2O$(5%) + $MgSO_4$(<1%) + $Na_2H_2P_2O_7$(<7%)	0.5% Sodium hyaluronate Sodium dextran sulfate sulfur 5	Norian
Eurobone®	β-TCP(98%) + $Na_4P_2O_7$(2%)	3 mol/l H_3PO_4 + 0.1 mol/l H_2SO_4	Kasios
VitalOs	Component 1: β-TCP(1.34 g) + $Na_2H_2P_2O_7$(0.025 g) Component 2: MCPM (0.78 g) + $CaSO_4 \cdot 2H_2O$ + 0.05 mol/l H_3PO_4	0.05 mol/l pH7.4 PBS	CalciOs

Table 19.4 Effects of particle size on the compressive strength of calcium phosphate cement consisting of tetracalcium phosphate and dicalcium phosphate anhydrous

Average particle diameter (μm)		Ratio of the average particle diameter of TTCP/DCPA	Compressive strength (MPa)
TTCP	DCPA		
1.6	11.9	0.13	0 (no setting)
12.4	11.9	1.04	7.1 ± 1.0
1.6	0.9	1.78	21.8 ± 4.4
12.4	0.9	13.78	51.0 ± 4.5

At the operation site, the powder and liquid phases are mixed to fabricate CPC paste. The manufacturers recommend a suitable liquid to powder mixing ratio. For the putty type, a lower liquid to powder mixing ratio is used whereas a larger liquid to powder mixing ratio is recommended for injection from a syringe or tube since more liquid results in a softer paste.

19.3 Hardening mechanisms

19.3.1 Basic hardening mechanism

The basic hardening mechanism of the CPC is the so-called dissolution–reprecipitation reaction based on different thermodynamic stabilities of

calcium phosphate salts (Ishikawa and Asaoka 1995; Ishikawa *et al.* 2003). As shown in Fig. 19.2, HA is the most stable phase thermodynamically when the pH of the solution is approximately 4.2 or higher. HA became unstable at lower pH and DCPD became the most stable phase when pH of the solution is lower than 4.2. When the pH was 1.5 or lower, DCPD was no longer the most stable phase, which was MCPM. Since the solubility of MCPM is high and its acidity is strong, no attempt has been made so far for the fabrication of MCPM cement.

The dissolution–reprecipitation reaction occurs when the powder phase of CPCs is mixed with their liquid phase. As stated above, HA is the most stable phase thermodynamically when the pH is 4.2 or higher whereas the DCPD is the most stable phase thermodynamically when the pH is between 1.5 and 4.2. Therefore, HA crystals are formed when appropriate calcium phosphate salts are mixed with the liquid phase to make the pH either neutral or alkaline, and DCPD crystals are formed when appropriate calcium phosphate salts are mixed with the liquid phase to make the pH acidic. The simplest CPC is the apatite cement consisting only of α-TCP; this cement was invented by Monma and Kanazawa (1976). The α-TCP is an unstable phase in water. In other words, α-TCP dissolves to supply calcium and phosphate ions as shown in eq (19.1). However, the solution is supersaturated with respect to the apatite at neutral and alkaline pH. Therefore, calcium and phosphate ions will be precipitated as calcium deficient apatite crystals as shown in eq (19.2).

$$3Ca_3(PO_4)_2 + H_2O \rightarrow 9Ca^{2+} + 6PO_4^{3-} + H_2O \qquad 19.1$$

$$9Ca^{2+} + 6PO_4^{3-} + H_2O \rightarrow Ca_9HPO_4(PO_4)_5(OH) \qquad 19.2$$

The precipitated calcium-deficient apatite crystals form a cluster, i.e. the precipitated crystals interlock, to form the hardened mass. This dissolution–reprecipitation reaction based on the difference of thermodynamical stability or the dissolution–reprecipitation reaction is also known as the hardening mechanism of gypsum. Figure 19.3 shows the solubility of calcium sulfate salts as a function of temperature (Sekiya 1964). The solubility of calcium sulfate hemihydrate at 20 °C is 0.82. Therefore, calcium and sulfate ions corresponding to 0.82 g $CaSO_4 \cdot 0.5H_2O$ are dissolved in water as shown in eq (19.3) if there is no other phase in equilibrium. However, such a solution is supersaturated with respect to calcium sulfate dihydrate ($CaSO_4 \cdot 2H_2O$) since its solubility is 0.20 at 20 °C. Therefore, calcium sulfate dihydrate crystals are precipitated, forming a cluster that sets.

$$CaSO_4 \cdot 0.5H_2O + 1.5H_2O \rightarrow Ca^{2+} + SO_4^{2-} + 2H_2O \qquad 19.3$$

$$Ca^{2+} + SO_4^{2-} + 2H_2O \rightarrow CaSO_4 \cdot 2H_2O \qquad 19.4$$

In the case of CPC consisting of many calcium phosphate salts, the hardening mechanism becomes more complex. For example, apatite cement

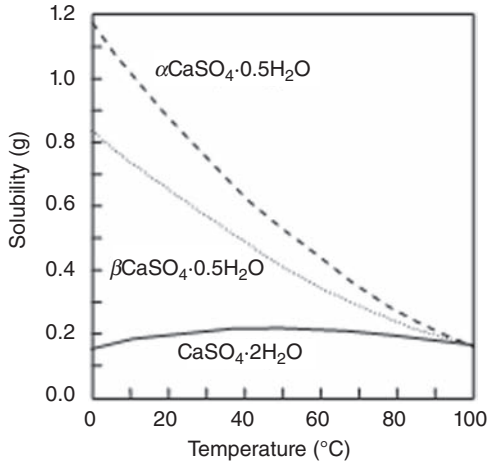

19.3 Solubility of calcium sulfate hemihydrate and dehydrate against temperature.

consisting of TTCP and DCPA supplies calcium and phosphate ions when the powder phase is mixed with its liquid phase as shown in eqs (19.5) and (19.6) since TTCP and DCPA are soluble calcium phosphates.

$$Ca_4(PO_4)_2O + H_2O \rightarrow 4Ca^{2+} + 2PO_4^{3-} + 2OH^- \qquad 19.5$$

$$CaHPO_4 \rightarrow Ca^{2+} + H^+ + PO_4^{3-} \qquad 19.6$$

$$2Ca_4(PO_4)_2O + 2CaHPO_4 \rightarrow 10Ca^{2+} + 6PO_4^{3-} + 2OH^- \rightarrow Ca_{10}(PO_4)_6(OH)_2 \qquad 19.7$$

However, the solution is supersaturated with respect to HA. Therefore, calcium and phosphate ions will be precipitated as HA crystals as shown in eq (19.7). The precipitated HA crystals form a cluster, i.e. the precipitated crystals interlock to form the hardened mass. Figure 19.4 shows a typical scanning electron microscope image of the hardened gypsum and apatite cement consisting of TTCP and DCPA. As shown in this figure, the microscopic morphology of the hardened mass is similar because of the same hardening mechanism.

19.3.2 Initial hardening mechanism of apatite cement

In contrast to the brushite cement which hardens very quickly, apatite cement takes time to set. The initial hardening time is longer than a day in the case of apatite cement consisting of only α-TCP, and 30–60 min in the case of apatite cement consisting of TTCP and DCPA when distilled water or saline is used as the liquid phase. Of course, these long hardening times

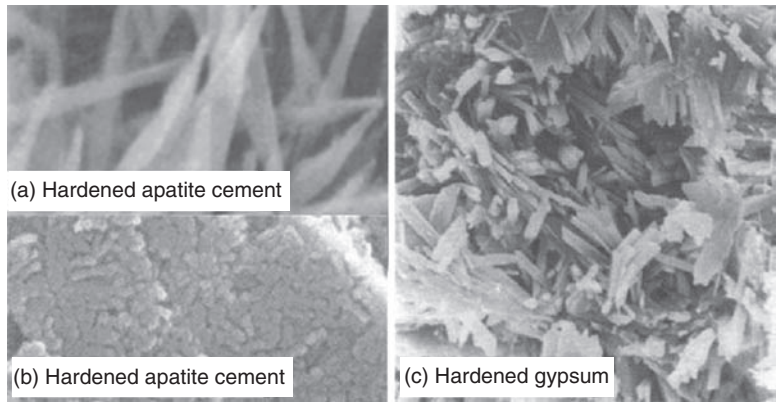

19.4 Typical scanning electron microscopic image of (a,b) apatite cement consisting of TTCP and DCPA, (c) gypsum. In both cases reprecipitated crystals interlock each other to form cluster-like structure.

Table 19.5 Effects of liquid phase on the setting time of calcium phosphate cement consisting of tetracalcium phosphate and dicalcium phosphate anhydrous

Liquid	Concentration (mol/L)	Setting time (min)
Distilled water	–	30–60
$Na_{1.8}H_{1.2}PO_4$*	0.2	5
$Na_{1.8}H_{1.2}PO_4$	0.6	5
$Na_{1.8}H_{1.2}PO_4$	1.0	5
$K_{1.8}H_{1.2}PO_4$	0.2	5
$K_{1.8}H_{1.2}PO_4$	0.6	5

*Solution was prepared by mixing 0.2 mol/L Na_2HPO_4 and 0.2 mol/L NaH_2PO_4 so that its pH became 7.4 The resulting solution has approximately $Na_{1.8}H_{1.2}PO_4$ as its chemical formula.

are not acceptable for clinical use. Therefore, basically two methods are used to shorten the initial hardening time of apatite cement.

One method accelerates the formation of apatite. In this method, sodium hydrogen phosphate aqueous solution is used as the liquid phase (Ishikawa *et al*. 1995a; Miyamoto *et al*. 1995a,b, 1997). Table 19.5 summarizes the effect of phosphate salts on setting time of CPC consisting of TTCP and DCPA. When distilled water is used as the liquid phase, its setting time is 30–60 min. Actually, this was the first commercially available apatite cement. In contrast, the setting time shortened significantly to 5 min when a phosphate salt solution is used as the liquid phase. Basically, no significant difference was

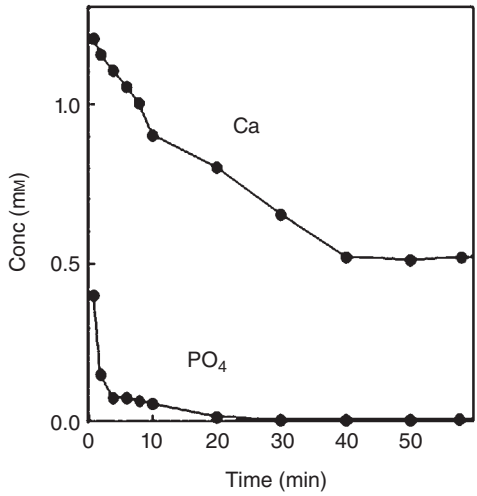

19.5 Example of the calcium and phosphate ions concentration in the suspension of apatite cement containing TTCP and DCPA. Calcium ion kept some concentration whereas phosphate concentration became less than the detection limit with time.

observed based on the kind of phosphate salt solution or the concentration of the phosphate salt solution. The mechanism of the acceleration of apatite formation or the hardening reaction with phosphate salt aqueous solution is explained by the supply of phosphate ion. In other words, the powder phase can supply only a limited amount of phosphate ion from DCPA. The cement employs larger TTCP – approximately 10 μm in average diameter – and smaller DCPA – approximately 1 μm in average diameter. Although this combination enhances the dissolution rate of DCPA as stated above, dissolution of DCPA is still the rate-determining step for the supply of calcium and phosphate ions needed for the formation of HAP. The Ca/P ratio of HAP is 1.0. On the other hand, the Ca/P ratio of TTCP is 2.0. Therefore, TTCP supplies more calcium than the amount of calcium and phosphate required for the formation of apatite. In contrast, the Ca/P ratio of DCPA is 1.0. Therefore, DCPA supplies more phosphate ions than the amount of calcium and phosphate ions required for the formation of apatite. Figure 19.5 summarizes the result of solution analysis when a mixture of TTCP and DCPA was suspended in the distilled water. As shown in this figure, the calcium ion concentration in the suspension was relatively high whereas the phosphate concentration in the suspension decreased with time to less than the detection limit. Of course, both calcium and phosphate ions were necessary for the solution to be supersaturated with respect to apatite and resulting apatite crystal precipitation. As a result of the smaller

dissolution rate of DCPA, phosphate supply became a rate-determining step for the formation of apatite. If the powder was mixed with phosphate salt solution, apatite was formed immediately, based on the dissolution of calcium phosphate powder since the calcium ion was easily supplied from TTCP. Precipitated apatite acted as the seed crystals and thus further apatite formation was also accelerated. Some of the commercially available apatite cement contains low-crystalline apatite from the beginning. Similarly, low-crystalline apatite acts as seed crystals for apatite formation. It should be noted that high-crystalline apatite shows a very limited seed effect. This may be due to the limited surface area in the case of high-crystalline apatite when the amounts were the same.

The other method to acquire the initial setting reaction is to employ dicarboxylic acids such as succinic acid or citric acids (Unezaki *et al*. 1993, 1996). In this method, initial setting is not related to the formation of apatite but is based on the formation of a chelate bonding between calcium compound and dicarboxylic acid. Unfortunately, the dicarboxylic acid is known to inhibit apatite formation. Therefore, component transformation from apatite cement to apatite is delayed even when compared with the apatite cement that employs distilled water. However, the amount of calcium phosphate is much higher than that of dicarboxylic acid. In the other words, dicarboxylic acid is required so that only the surface of the calcium phosphate salt reacts with dicarboxylic acid. Even after the chelate reaction, calcium phosphate salts under the surface of calcium phosphate salts continue to dissolve to supply calcium and phosphate. Since the dicarboxylic acid has already been used for the chelate reaction with the calcium phosphate salt surface, dissolved calcium and phosphate ions will be supplied to the reaction medium, resulting in the supersaturation with respect to apatite, and thus precipitated as apatite crystals. The crystals interlock to harden.

The initial setting and resulting appearance of mechanical strength is very important for the clinical result. It should be noted that the apatite cement shows good tissue response only when the cement hardened (Miyamoto *et al*. 1995a,b, 1999; Ueyama *et al*. 2001; Welkerling *et al*. 2003). The cement would disintegrate or calcium phosphate particles would be liberated when the mechanical strength is low owing to stress from skin. Also, the paste would be washed out as stated in the next section. In such cases, the inflammatory response will be observed due to the so-called crystalline inflammatory response.

19.4 Anti-washout property of the apatite cement

Anti-washout property is one of the key factors for good clinical results. Again, the apatite cements show good tissue response when they are hardened. In contrast, the apatite cement causes the inflammatory response

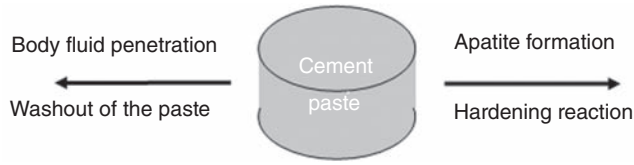

19.6 Illustration of the apatite cement paste when exposed to liquid phase. Two different reactions proceed competitively. Right hand side, hardening reaction of cement which is closely related to cement conversion to apatite. Left hand side, washout reaction induced by the penetration of liquid into cement paste.

when it failed to harden. Once apatite cement is hardened, it will not be washed out. However, it should be noted that apatite cement takes time to set and the paste will be washed out if it mixes with body fluid before its initial hardening reaction. In particular, washout of the paste will be a problem when the paste is transferred into a bone defect using a syringe or tube since a larger specific surface is exposed to the body fluid.

Once the apatite cement has been placed in the bone defect, two reactions take place competitively as shown in Fig. 19.6 (Ishikawa 1995c; Miyamoto *et al*. 1995a,b; Takechi *et al*. 1996; Ishikawa *et al*. 1999). One is the formation of apatite based on the dissolution–reprecipitation reaction. This reaction is of course desirable and the cause of the basic hardening reaction of apatite cement. On the other hand, penetration of the body fluid into the cement paste also takes place, and this induces washout of the cement paste. Since body fluid penetrates the paste where the paste is exposed to body fluid, more body fluid penetrates the injected paste and thus resulting washout occurs more easily due to the large specific surface.

The overall reaction is decided as a result of two competitive reactions. Therefore, one way to reduce the washout property of the apatite cement is to provide a fast-setting reaction. Originally, apatite cement consisting of TTCP and DCPA was commercialized without using phosphate salt liquid phase. Washout property is significantly improved by employing a phosphate salt liquid phase since that accelerates the setting reaction. However, too much acceleration results in too short a working time. Therefore, another reaction, penetration of body fluid into the paste, should be regulated simultaneously. One of the effective methods is to employ a gelling agent in the paste (Ishikawa *et al*. 1995b; Takechi *et al*. 1996; Cherng *et al*. 1997; Miyamoto *et al*. 1998). By adding a gelling agent to the liquid phase, body fluid penetration is significantly reduced. A gelling agent prevents the penetration of body fluid by filling the space between the calcium phosphate powders. Gelling agents that bind with calcium ions are more effective than other gelling agents since weak binding is formed between the calcium phosphate

powders. One example is sodium alginate. As little as 0.5 wt% of sodium alginate added to the liquid phase of the apatite cement completely suppresses washout. In fact, apatite cement containing more sodium alginate can be used for hemostatic purposes (Momota *et al.* 2002, 2004).

Addition of gelling agent also improves the handling property of the cement paste and injectability. These properties are important since a larger liquid to powder ratio, another method to improve handling property and injectability, reduces the mechanical strength of hardened apatite cement.

19.5 Injectability

Since CPC shows mobility before it hardens, the paste can be injected into a bone defect using a syringe or tube as shown in Fig. 19.7. This allows a minimally invasive surgical procedure. Figure 19.7 shows the clinical case in which apatite cement is injected through a syringe for the reconstruction of bone defect formed by a tumor. Injectability is governed by many factors

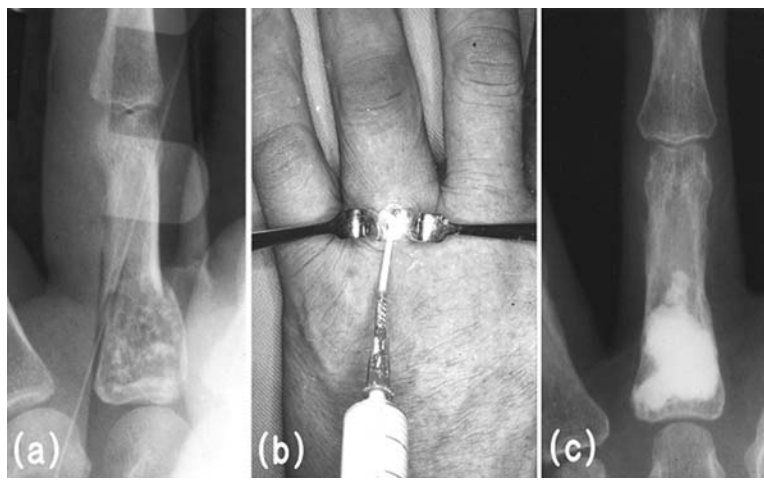

19.7 Case of filling into a bone defect which formed after bone tumor curettage. Chondroma in the proximal phalanx of the left ring finger, 71-year-old male: the pathologic fracture was treated conservatively by external fixation and the callus formation at the site of fracture was verified. Subsequently, BIOPEX® was injected. Bone adhesion at the site of pathologic fracture was observed at one month after surgery. Therefore, BIOPEX® did not impede bone adhesion in fracture. Six months after surgery, modification of bone cortex at the site of fracture was observed despite BIOPEX® remained. Neither pain nor restriction in the range of motion was observed (Department of Orthopedics, Kochi Medical School). Finding during surgery, Presurgery, One month after surgery, Six months after surgery.

including liquid to powder mixing ratio, liquid viscosity, particle size and morphology (Ishikawa *et al*. 2004; Bohner and Baroud 2005; Wang *et al*. 2006, 2007).

A higher liquid to powder mixing ratio allows a soft paste and results in higher injectability. Therefore, producers of apatite cements recommend a higher liquid to powder mixing ratio for injection use compared with putty-type use. However, it should be noted that there are significant drawbacks when a higher liquid to powder mixing ratio is used. One is the low anti-washout property. As stated above, CPC paste is washed out when it is exposed to plenty of body fluid before its setting reaction because of the penetration of body fluid into the paste. Obviously, a high liquid to powder mixing ratio is a similar situation when some of body fluid has already penetrated the paste. In addition, the mechanical strength of the hardened CPC is lower when a higher liquid to powder mixing ratio is employed. This is because interlocking of the apatite or brushite crystals is the cause of the setting reaction of the CPC. When a higher liquid to powder mixing ratio is used, fewer apatite or brushite crystals interlock and apatite or brushite mass with higher porosity is obtained. It should be noted that a higher porosity of the cement results in weak mechanical strength but faster replacement to bone since less apatite needs to be resorbed by osteoclasts.

Viscosity of the liquid phase is also a key factor for the paste injectability. When the paste is injected from syringe or tube, it is important that both liquid and powder be transferred to the bony defect. When a syringe with a small diameter needle is used, only the liquid phase is transferred to the bone defect similar to the filtration process. To prevent this phenomenon, viscous liquid is required. Even if a viscous liquid phase is used, separation of the powder phase from the liquid phase cannot be prevented completely if a syringe with a small diameter is used. In addition, a small diameter syringe results in thinner paste and thus paste with large specific surface area would not get through. This results in a higher chance of the CPC paste being washed out. Therefore, a relatively thicker syringe is recommended even though a thinner syringe is preferable for a minimally invasive surgical procedure.

Particle size and morphology are also factors that govern the injectability of the paste. Of course smaller particles allow more injectable paste. However, particle size is also one of the key factors that govern the hardening reaction and resulting mechanical strength of the hardened mass. Therefore, both injectability and mechanical properties have to be considered when determining the particle size. In addition to particle size, particle morphology also greatly affects paste injectability. A spherical-shaped powder is ideal for injectability. In the case of other cements, particles with roughened surfaces are preferable since they allow particles to interlock

with each other. However, in the case of CPC, the particles are dissolved and precipitated as apatite crystals. In other words, particles are used only as the source of calcium and phosphate ions. Therefore, spherical-shaped particles increase the injectability without sacrificing mechanical strength. Indeed, spherical-shaped particles could increase the mechanical strength of CPC since they allow a lower powder to liquid ratio without sacrificing handling property and injectability.

19.6 Tissue response and osteoconductivity of apatite cement

It has not been clarified why apatite shows excellent tissue response and good osteoconductivity. However, its use is established based on not only animal experiment but also many clinical cases over a long period. In the case of apatite cement, the composition of the hardened mass will be that of the apatite after the hardening reaction. As a result of apatite formation, hardened apatite cement shows excellent tissue response and good osteoconductivity. Figure 19.8 shows the histological picture of the TTCP-DCPA-based apatite cement when implanted at the bone defect made at the tibia. At 2 weeks, new bone began to cover the bone defect filled with apatite cement. No inflammatory response was found at this stage. The area covered with new bone increased with time and the whole surface was covered with new bone at 16 weeks.

It is also reported that apatite cement shows better osteoconductivity than sintered apatite, even though it has not been clarified why CPC shows better osteoconductivity. The differentiation process of the osteoblasts was

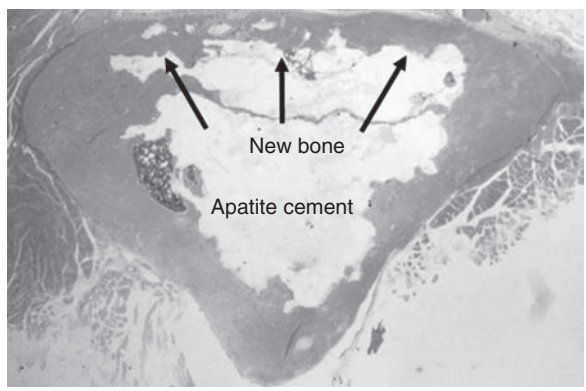

19.8 Histological pictures of bone defect made at the tibia of rat when reconstructed with TTCP-DCPA type apatite cement. After 16 weeks, bone defect was reconstructed with new bone.

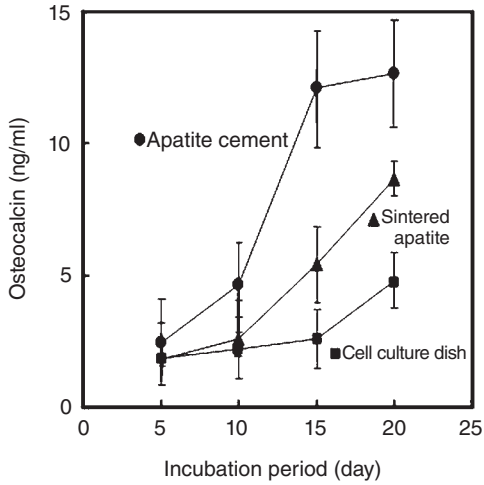

19.9 Osteocalcin when osteoblasts were incubated on the surface of TTCP-DCPA-type apatite cement, sintered apatite and cell culture plastic dish as a function of incubation time. Note that apatite cement elicits higher osteocalin than sintered apatite.

also higher in the case of apatite cement than sintered apatite as shown in Fig. 19.9. At present, four factors are thought to contribute to the improved osteoconductivity of apatite cement, one being the hardening property and resulting ideal filling of the bone defect as illustrated in Fig. 19.10. In other words, a bone defect can be filled with apatite cement without leaving a gap between the existing bone. In contrast, a gap is inherent between the existing bone and the sintered apatite block or granula. For the new bone formation, osteoblasts need to travel to the sintered apatite surface from existing bone. Any gap between the existing bone and sintered apatite prevents osteoblasts from moving. In addition, hardened apatite cement is stable and fixed. In contrast, granular apatite is not fixed and is thus unsteady. In other words, micromovement is undesirable.

The second factor is ion release from the hardened apatite cement. Although apatite cement sets to form apatite, the hardened mass contains some unreacted calcium phosphate, at least at the initial stage. The unreacted calcium phosphate dissolves to supply calcium and phosphate ions. Although these calcium and phosphate ions are used for further crystal growth of the apatite, some of them will be released from the hardened mass, and this elicits cell activity. This mechanism is similar to that of the higher osteoconducivity reported for biphasic calcium phosphate. In fact, hardened apatite cement should be treated as plural calcium phosphates.

The third factor is low crystallinity. The crystallinity of apatite formed by the hardening reaction of apatite cement is lower than that of sintered

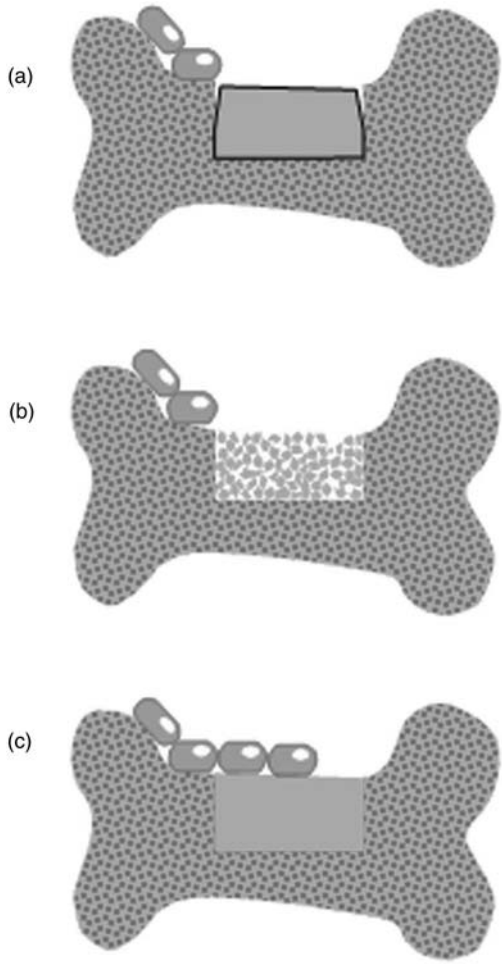

19.10 Illustration of bone defect filling with (a) block apatite (b) granular apatite and (c) apatite cement.

apatite. It is well known that apatite sintered at lower temperatures shows better osteoconductivity. Although a lower sintering temperature such as 900 °C is employed to maximize the osteoconductivity of the bone substitutes, it is still too high when compared with the temperature at which bone apatite is formed. In the case of apatite cement, apatite is formed at body temperature and thus low-crystalline apatite is formed. Although the degree of contribution to the higher osteoconductivity has not been established, low-crystalline apatite is thus thought to contribute to the higher osteoconductivity of the apatite cement.

The fourth factor is the formation of carbonate apatite. In the case of hardening reaction of apatite cement, carbonate apatite is formed on the surface of hardened apatite cement by taking carbonate ions from body fluid or air (detail will be stated in Section 19.8). In contrast to HA, carbonate apatite is resorbed by osteoclasts. Osteoclasts activated due to the resorption of carbonate apatite give a signal to osteoblasts based on cell–cell contact. As a result of activated osteoblasts, apatite cement shows higher osteoconductivity.

Again, it should be emphasized that excellent tissue response and good osteoconductivity are obtained only when apatite cements are hardened. Apatite cement causes an inflammatory response when it fails to harden owing to the release of calcium phosphate powder.

19.7 Tissue response to brushite cement

Initially, apatite cement attracted more attention than brushite cement since it is the inorganic component of the bone. Also, weaker mechanical strength and rapid physicochemical dissolution of brushite cement are thought to be important key factors that are inferior to apatite cement. Despite the fact that the acidic environment produced by the dissolution of brushite was thought to be a problem, *in vitro* and *in vivo* studies demonstrated that brushite cement was generally well tolerated by the bone and soft tissue environment (Constantz *et al*. 1998; Frayssinet *et al*. 1998). When a bone defect is reconstructed using brushite cement, brushite dissolves slightly since the body fluid is undersaturated with respect to brushite or DCPD. Dissolution of brushite, which is acidic calcium phosphate, reduces pH, and this results in the activation of macrophages. Then, phagocytic resorption of hardened brushite cement is made by mononuclear macrophage. After phagocytic resorption, carbonate apatite is formed at the bone defect. In contrast to the phagocytic response to brushite, osteoclastic resorption becomes dominant after brushite is converted to carbonate apatite (Constantz *et al*. 1998).

It should be noted that the reaction of brushite cement is different at the implant location. When brushite cement was used for the reconstruction of metaphysic defect, part of the brushite cement had been converted to carbonate apatite after 2 weeks. In contrast, brushite cement used for the reconstruction of diaphysis defect began to convert to another calcium phosphate phase only after 4 weeks. Although the mechanism of these differences has not yet been clarified, a decreased vascular supply to the diaphysis compared with cements implanted in the metaphysic may be one of the reasons. It is assumed that a more active metabolic state, greater blood flow and higher cement specific area may be favorable for the higher conversion rate from brushite to carbonate apatite.

19.8 Replacement of apatite cement with bone

In contrast to the sintered apatite, which remains in the bone tissue without being resorbed but keeping its original shape, apatite cement is reported to be replaced with bone similar to bone remodeling even though the process takes a long time and still there is controversy as to whether the apatite cement is replaced with bone.

Shindo *et al.* (1993) reported replacement of apatite cement by bone in facial skeletal augmentation in dogs. When apatite cement consisting of TTCP and DCPA was placed directly onto the bone of the supraorbital rim, about 45% progressive replacement implant by bone and osteoid was observed without loss of volume at 9 months. Constantino *et al.* (1992) made 2.5 cm diameter full-thickness parietal skull defects in cats and reconstructed them with apatite cement consisting of TTCP and DCPA. By 6 months, the apatite cement had been replaced by new bone and soft tissue 7.2 mm in depth from the cement surface. Of the replacement tissue, 77.3% was new bone and the remaining portion was soft tissue. In contrast, Friedman *et al.* (1991) found very little resorption or new bone deposition at 6 months when the frontal sinus in the cat was obliterated and reconstructed with apatite cement consisting of TTCP and DCPA. At 18 months, the content of the reconstructed frontal sinus was 63% new bone, 10% fibrous tissue and 27% residual cement. These differences are thought also to have arisen from the different circumstance of the hardened apatite cement including where the implant was used, and the age and sex of the patient or animal.

Replacement by bone is desirable since the function of the bone includes not only mechanical support of the body but also many biological functions such as hematopoietic function. Similar to the brushite cement, the reason why apatite cement is replaced with bone has not yet been fully clarified.

It is well known that two types of cell, osteoclasts and osteoblasts, play the dominant role in bone remodeling. Osteoclasts differentiated from hematopoietic stem cell resorb existing bone, and osteoblasts differentiated from mesenchymal stem cell form bone matrix (Fig. 19.11). Since both sintered apatite and hardened CPC shows osteoconduction, the formation of the bone matrix by osteoblasts is not a problem. In contrast, there is a clear difference on the osteoclastic resorption between sintered apatite and hardened CPC. Figure 19.12 shows scanning electron microscope (SEM) images when osteoclasts were incubated on the surface of (a) bone slice, (b) sintered apatite and (c) hardened apatite cement for 48 hours in an incubator. Osteoclastic resorption is clearly seen on the surface of bone. In contrast, no osteoclastic resorption was observed on the surface of sintered apatite. Of course, sintered apatite will not be dissolved in the human body physicochemically. Therefore, it is reasonable that sintered apatite would not be replaced with bone but would keep its original shape even after a

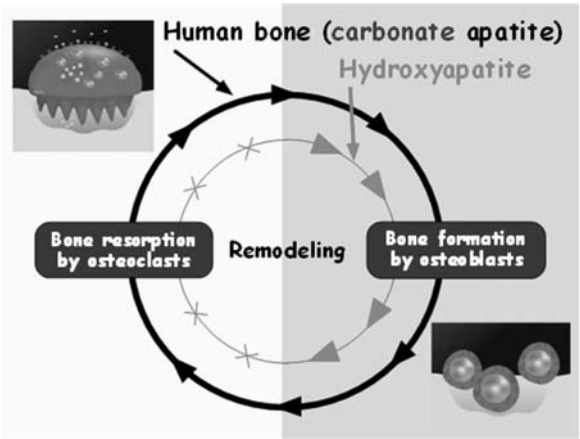

19.11 Illustration of bone remodeling process.

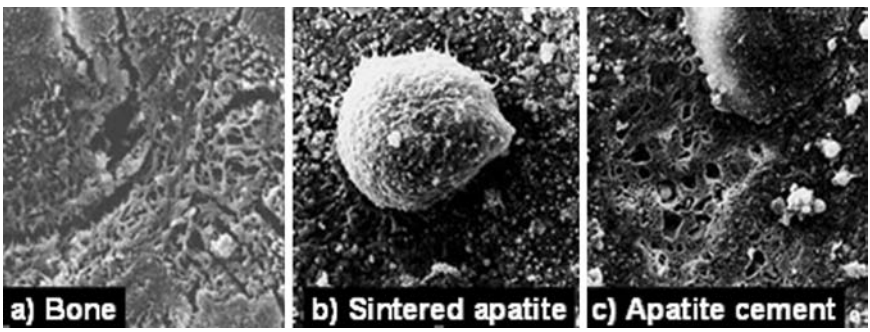

19.12 SEM image of the surface of (a) bone, (b)sintered apaite and (c) apatite cement onto which osteoclastic cells were incubated for 48 hours.

long period of implantation. In the case of apatite cement, however, osteoclastic resorption was observed similar to bone slice even though the amount of resorbed apatite cement was much smaller than that of bone slice. Yuasa *et al*. (2001) reported that the amount of resorption was only 2% in volume when compared with bone slice. Although the amount of osteoclastic resorption was limited, osteoclastic resorption is thought to be key for the replacement of CPC with bone.

Then, the next question is why apatite cement is resorbed by osteoclasts. Figure 19.13 illustrates the function of osteoclasts. As shown in this illustration, osteoclast dissolves collagen by lysosome enzymes such as cathepsin and β-glucuronidase and dissolves mineral by reducing the pH of Howship's lacuna based on H^+ and Cl^- supply. Sintered apatite and apatite cements

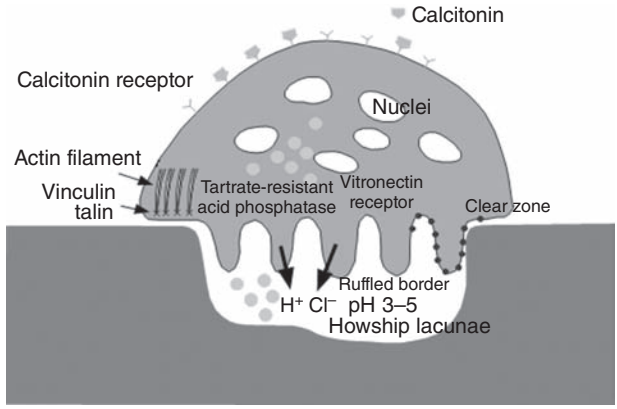

19.13 Illustration of the role of osteoclasts.

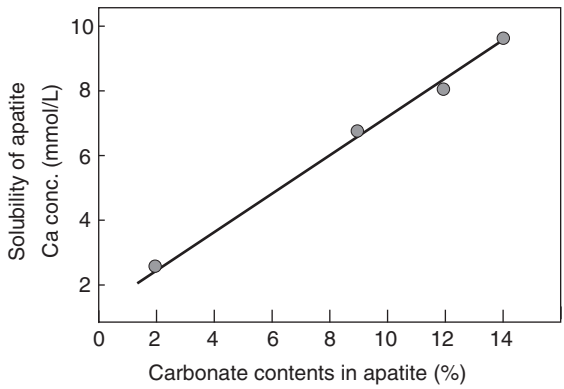

19.14 Effect of carbonate in apatite on solubility of apatite.

are free from collagen. Therefore, resorption is thought to be governed only by the dissolution of sintered apatite and apatite cement due to the acidic circumstance formed by osteoclasts. Basically, solubility of apatite is governed by two factors: crystallity and composition. High-crystalline apatite shows more limited solubility than low-crystalline apatite. As stated, apatite formed by the hardening reaction of calcium phosphate is low-crystalline apatite, compared with the sintered apatite which shows high crystallinity. However, the effect of crystalliity on the solubility is limited when compared with the effect of composition. In fact many elements are known to affect the solubility of apatite. For example, fluoroapatite, which contains fluorine is known to show very limited solubility and is thus used for tooth caries treatment. In contrast, carbonate is known to increase the solubility of apatite. Figure 19.14 shows the effect of carbonate ions on the solubility

Table 19.6 Hard tissue components of the human adult

	Enamel	Dentine	Bone
Ca^{2+}	36.5	35.1	34.8
PO_4 as P	17.7	16.9	15.2
Ca/P molar ratio	1.63	1.61	1.71
Na^{+}	0.5	0.6	0.9
Mg^{2+}	0.44	1.23	0.72
K^{+}	0.08	0.05	0.03
CO_3^{2-}	3.5	5.6	7.4
F^{-}	0.01	0.06	0.03
Cl^{-}	0.30	0.01	0.13
$P_2O_7^{4-}$	0.022	0.10	0.07
Total inorganic	97.0	70.0	65.0
Absorbed H_2O	1.5	10.0	10.0

of apatite. As shown in this figure, solubility of apatite increases with carbonate content. Osteoclasts cannot resorb sintered apatite since the solubility of sintered apatite in the weak acidic region is limited. In contrast osteoclasts resorb human bone since the solubility of bone is relatively high. It should be noted that the composition of the bone is not HA but carbonate apatite, which contains 7–8% carbonate as shown in Table 19.6. In the case of apatite cements, carbonate apatite is formed based on the hardening reaction if the component contains carbonate salts since carbonate apatite is more stable thermodynamically than HA. However, it should be noted that carbonate apatite is also formed for CPC containing no carbonate salt in its composition even though the amount is small. This is caused by the resorption of carbonate ion from the body fluid or the air. A larger amount of carbonate is introduced for apatite cement that contains an alkaline salt such as TTCP. Since carbonate ions will be introduced to apatite cement from the body fluid or the air, the carbonate content of the hardened CPC is higher at the surface of hardened apatite cement than in the interior. This may be one of the reasons why replacement of hardened calcium phosphate cement occurs relatively quickly at the initial stage or the surface of hardened CPC but complete replacement with bone is difficult to achieve.

19.9 Clinical results

Excellent results are reported for clinical use of apatite cements when their hardening reaction was guaranteed. When BoneSource® which consists of TTCP and DCPA was used for the repair of cranial defect, success rate was approximately 97% at follow-up period for a minimum of 24 months and maximum of 6 years (Friedman *et al.* 1998). The overall surgical site

infection rate was 5.8% and as small as 2.9% required implant removal, which compares quite favorably with the use of methylmethacrylate in cranial defects (Manson *et al*. 1989).

In the case of Norian SRS, significant differences were seen 6–8 weeks post-operatively, with better grip strength, wrist range of motion, digital motion, use of the hand, and social and emotional functions. This was less swelling in the patients treated with Norian SRS than in the control group, in which closed reduction of the fracture was followed by the application of a short arm cast or an external fixator, depending on the patients. The infection rate was significantly higher ($p < 0.001$) in the control group (16.7%) than in the group treated with Norian SRS (2.5%). At one year, no clinical differences had been detected (Cassidy *et al*. 2003). In this apatite cement (Norian SRS) as well, painful soft-tissue reaction was observed after curettage of enchondromas where a tourniquet could not be applied (Welkerling *et al*. 2003).

Few clinical results have been reported in the case of brushite cement owing to its relatively recent introduction to the market.

19.10 Summary

Calcium phosphate cement was a big invention in biomaterials and has altered the surgical procedure of bone reconstruction and regeneration. Current CPC has several shortcomings and thus further research and development is awaited. On the other hand, improvement of the clinical results could be expected if the clinicians better understood the properties of the CPC. Patients would like to be treated not by a clinician who knows about CPC but by a clinician who understands the calcium phosphate.

19.11 References

Bohner M, Baroud G (2005), 'Injectability of calcium phosphate pastes', *Biomaterials*, **26**(13), 1553–1563.

Brown W E, Chow L C (1986a), 'A new calcium phosphate, water-setting cement', in Brown P W, *Cement Research Progress*, Westerville, American Ceramic Society, 351–379.

Brown W E, Chow L C (1986b), 'Combination of sparingly soluble calcium phosphate cements in slurries and paste as mineralizers and cements', US Patent No. 4,612,059.

Cassidy C, Jupiter J B, Cohen M, Delli-Santi M, Fennell C, Leinberry C, Husband J, Ladd A, Seitz W R, Constantz B (2003), 'Norian SRS cement compared with conventional fixation in distal radial fractures', *J Bone Joint Surg*, **85**(11), 2127–2137.

Cherng A, Takagi S, Chow L C (1997), 'Effects of hydroxypropyl methylcellulose and other gelling agents on the handling properties of calcium phosphate cement', *J Biomed Mater Res*, **35**(3), 273–277.

Chow L C, Takagi S, Constantino P D, Friedman C D (1991), 'Self-setting calcium phosphate cement' in *Mat Res Soc Symp Proc* 179, Materials Research Society, 3–24.

Constantino P D, Friedman C C, Jones K, Chow L C, Sisson G A (1992), 'Experimental hydroxyapatite cement cranioplasty', *Plast Reconstr Surg*, **90**, 174–185.

Constantz B R, Barr B M, Ison I C, Fulmer M T, Baker J, McKinney L, Goodman S B, Gunasekaren S, Delaney D C, Ross J, Poser R D (1998), 'Histological, chemical, and crystallographic analysis of four calcium phosphate cements in different rabbit osseous sites', *J Biomed Mater Res*, **43**, 451–461.

Frayssinet P, Frayssinet P, Gineste L, Conte P, Fages J, Rouquet N (1998), 'Short-term implantation effects of a DCPD-based calcium phosphate cement', *Biomaterials,* **19**(11&12), 971–977.

Friedman C D, Constantino P D, Takagi S, Chow L C (1998), 'BoneSourceTM hydroxyapatite cement: a novel biomaterial for craniofacial skeletal tissue enginnering and regeneration', *J Biomed Mater Res: Appl Biomater*, **43**, 428–432.

Friedman C D, Constantino P D, Jones K, Chow L C, Pelzer H J, Sisson G A (1991), 'Hydroxyapatite cement. II: Obliteration and reconstruction of the cat frontal sinus', *Arch Otolaryngol Head Neck Surg*, **117**, 385–389.

Ishikawa K, Asaoka K (1995), 'Estimation of ideal mechanical strength and critical porosity of calcium phosphate cement' *J Biomed Mater Res*, **29**(12), 1537–1543.

Ishikawa K, Takagi S, Chow L C, Ishikawa Y (1995a), 'Properties and mechanisms of fast-setting calcium phosphate cements', *J Mater Sci: Mater Med*, **6**(9), 528–533.

Ishikawa K, Miyamoto Y, Kon M, Nagayama M, Asaoka K (1995b), 'Non-decay type fast-setting calcium phosphate cement: composite with sodium alginate', *Biomaterials*, **16**(7), 527–532.

Ishikawa K, Miyamoto Y, Takechi M, Ueyama Y, Suzuki K, Nagayama M, Matsumura T (1999), 'Effects of neutral sodium hydrogen phosphate on setting reaction and mechanical strength of hydroxyapatite putty,' *J Biomed Mater Res*, **44**(3), 322–329.

Ishikawa K, Matsuya S, Miyamoto Y, Kawate K (2003), Bioceramics. In I Milne, R O Ritchie, B Karihaloo eds *Comprehensive Structural Integrity*, Vol. 9, 169–214, Elsevier, USA.

Ishikawa K, Matsuya S, Nakagawa M, Udoh K, Suzuki K (2004), 'Basic properties of apatite cement containing spherical tetracalcium phosphate made with plasma melting method', *J Mater Sci Mater Med*, **15**(1), 13–17.

LeGeros R Z, Chohyeb A, Shulman A (1982), 'Apatitic calcium phosphates: possible dental restorative materials', *J Dent Res*, **61**, 343.

LeGeros R Z, Tung M S (1983), 'Chemical stability of carbonate and fluoride-containing apatites', *Caries Res*, **17**(5), 419–429.

Lemaitre J, Mirtchi A, Mortier A (1987), *Silicates Ind* 141.

Manson P N, Crawley W A, Hoopers J E (1989), 'Frontal cranioplasty: risk factors and choice of cranial vault reconstructive material', *Plast Reconstr Surg* **77**, 888.

Mirtchi A A, Lemaitre J, Terao N (1989), 'Calcium phosphate cements: action of setting regulators on the properties of the β-tricalcium phosphate–monocalcium phosphate cements', *Biomaterials*, **10**(7), 475–480.

Mirtchi A A, Lemaitre J, Munting E (1990), 'Calcium phosphate cements: study of the β-tricalcium phosphate–monocalcium phosphate system', *Biomaterials*, **11**(2), 83–88.

Miyamoto Y, Ishikawa K, Fukao H, Sawada M, Nagayama M, Kon M, Asaoka K (1995a), '*In vivo* setting behaviour of fast-setting calcium phosphate cement', *Biomaterials*, **16**(11), 855–860.

Miyamoto Y, Ishikawa K, Takechi M, Kon M, Yuasa M, Nagayama M, Asaoka K (1995b), 'Soft tissue response of calcium phosphate cements' *Bioceramics* **9**, 263–266.

Miyamoto Y, Ishikawa K, Takechi M, Toh T, Yoshida Y, Nagayama M, Kon M, Asaoka K (1997), 'Tissue response to fast-setting calcium phosphate cement in bone', *J Biomed Mater Res*, **37**(4), 457–464.

Miyamoto Y, Ishikawa K, Takechi M, Toh T, Yuasa T, Nagayama M, Suzuki K (1998), 'Basic properties of calcium phosphate cement containing atelocollagen in its liquid or powder phases', *Biomaterials*, **19**(7–9), 707–715.

Miyamoto Y, Ishikawa K, Takechi M, Toh T, Yuasa T, Nagayama M, Suzuki K (1999), 'Histological and compositional evaluations of three types of calcium phosphate cements when implanted in subcutaneous tissue immediately after mixing', *J Biomed Mater Res*, **48**(1), 36–42.

Momota Y, Miyamoto Y, Ishikawa K, Takechi M, Yuasa T, Tatehara S, Nagayama M, Suzuki K (2002), 'Evaluation of feasibility of hydroxyapatite putty as a local hemostatic agent for bone', *J Biomed Mater Res*, **63**(5), 542–547.

Momota Y, Miyamoto Y, Ishikawa K, Takechi M, Yuasa T, Tatehara S, Nagayama M (2004), 'Effects of neutral sodium hydrogen phosphate on the setting property and hemostatic ability of hydroxyapatite putty as a local hemostatic agent for bone', *J Biomed Mater Res*, **69**(1), 99–103.

Monma H, Kanazawa T (1976), 'The hydration of α-tricalcium phosphate', *Yogyo-Kyokai-Shi*, **84**, 209–213.

Sekiya M (1964), 'Gypsum' Gihodo, Tokyo, Japan.

Shindo M L, Constantino P D, Friedman C D, Chow L C (1993), 'Facial skeletal augmentation using hydroxyapatite cement', *Arch Otolaryngol Head Neck Surg*, **119**, 185–190.

Takechi M, Miyamoto Y, Ishikawa K, Yuasa M, Nagayama M, Kon M, Asaoka K (1996), 'Non-decay type fast-setting calcium phosphate cement using chitosan', *J Mater Sci: Mater Med*, **7**, 317–322.

Ueyama Y, Ishikawa K, Mano T, Koyama T, Nagatsuka H, Matsumura T, Suzuki K (2001), 'Initial tissue response to anti-washout apatite cement in the rat palatal region: comparison with conventional apatite cement, 1, *J Biomed Mater Res*, **55**(4), 652–660.

Unezaki Y, Eto T, Inoue H, Minamigawa K, Sugihara F (1993), 'A study of hardening material consisted of tetracalcium phosphate, dicalcium phosphate dehydrate and citric acid', *J Jpn Prosthodont Soc*, **37**, 61–66.

Unezaki Y, Ryumon H, Inoue H, Okuda H, Onishi H, Minamigawa K (1996), 'Histocompatibility of a bone graft cement, consisting of tetracalcium phosphate, dicalcium phosphate dehydrate and citric acid', *Bioceramics*, **9**, 251–253.

Wang X, Ye J, Wang H (2006), 'Effects of additives on the rheological properties and injectability of a calcium phosphate bone substitute material', *J Biomed Mater Res*, **78**(2), 259–264.

Wang X, Ye J, Wang Y, Chen L (2007), 'Self-setting properties of a beta-dicalcium silicate reinforced calcium phosphate cement', *J Biomed Mater Res*, **82**(1), 93–99.

Welkerling H, Raith J, Kastner N, Marschall C, Windhager R (2003), 'Painful soft-tissue reaction to injectable Norian SRS calcium phosphate cement after curettage of enchondromas', *J Bone Joint Surg Br*, **85**(2), 238–239.

Yuasa T, Miyamoto Y, Ishikawa K, Takechi M, Nagayama M, Suzuki K (2001), '*In vitro* resorption of three apatite cements with osteoclasts', *J Biomed Mater Res*, **54**(3), 344–350.

20

Calcium phosphate coatings

S C G LEEUWENBURGH, J G C WOLKE and J A JANSEN, Radboud University Nijmegen Medical Center, The Netherlands and K DE GROOT, University of Twente, The Netherlands

20.1 Introduction

Calcium phosphate (CaP) ceramics are widely studied for orthopaedic and dental applications due to their bioactive properties. Generally, bioactive materials interact with surrounding bone, resulting in the formation of a chemical bond to this tissue ('bone-bonding'). This phenomenon of bioactivity is determined mainly by chemical factors – such as the crystal phase and molecular structure of the material – as well as physical factors, such as surface roughness and porosity. CaP ceramics are too brittle for use as bulk material under loaded conditions, which means that CaP ceramics are frequently applied as coatings to the surface of metallic implant materials in order to combine the mechanical strength of metals with the excellent biological properties of CaP ceramics.

This chapter will present a general description of CaP coating characteristics in terms of mechanical, biological and clinical properties as well as an overview of various fabrication techniques for the deposition of CaP coatings.

20.2 Bioactive materials

20.2.1 Classification of biomaterials

During the second consensus conference on definitions in biomaterials (Williams *et al.*, 1992), biomaterials were defined as 'materials intended to interface with biological systems to evaluate, treat, augment, or replace any tissue, organ or function of the body'. These materials are capable of being in contact with body fluids and tissues for prolonged periods of time, while eliciting little if any adverse reactions. However, no foreign material placed within a living body can be completely compatible with the biological surroundings, with the notable exception of autogenous materials (autografts),

which are retrieved from the body itself. Any other foreign substance initiates a specific host-tissue response.

With respect to bone-substituting biomaterials, Osborn and Newesely (1980) classified three categories of biocompatibility based on the various reactions to surrounding bone tissue:

1 Biotolerant materials, such as stainless steel and Co–Cr alloys, are characterized by distant osteogenesis, which means that the implant surface is separated from adjacent bone by an intervening fibrous tissue layer.
2 Bioinert materials, such as titanium and aluminum oxide, do not provoke the formation of fibrous tissue and display contact osteogenesis, i.e. the creation of a direct contact to osseous tissue.
3 Bioactive materials, such as CaP ceramics and silica-based bioglasses, are truly bone-bonding materials, which are characterized by the formation of a very tight, chemical bond with bone (bonding osteogenesis). Bioactive materials enhance bone tissue forming reactions starting from the implant surface, and induce the formation of a continuous transition from tissue to implant surface, i.e. bonding.

20.2.2 The bone–implant interface

In order to clarify the above-mentioned concept of bone-bonding, first of all a brief outline will be given on the structure of bone tissue.

Bone

Bone is a mineralized tissue, which can be described as a natural composite material consisting of an organic matrix strengthened by an inorganic CaP phase. The extracellular organic matrix of bone consists of 90% collagenic proteins (type I collagen 97% and type V collagen 3%) and of 10% non-collagenic proteins (osteocalcin 20%, osteonectin 20%, bone sialoproteins 12%, proteoglycans 10%, osteopontin, fibronectin, growth factors, bone morphogenetic proteins, etc.). Regarding the inorganic phase, the most abundant mineral in human bone is apatite. The similarity between bone mineral and hydroxyapatite was first noticed by de Jong (1926). Investigations by LeGeros (1991) revealed that the crystal structure of bone mineral is more similar to the structure of carbonated apatites.

This calcified matrix embeds bone cells, which participate in the maintenance and organization of bone. Bone is a dynamic tissue subject to constant remodelling by osteoblasts and osteoclasts, i.e. bone-forming and bone-resorbing cells. Osteoblasts are responsible for the synthesis, deposition and mineralization of bone matrix. They are located at bone surfaces and form a continuous layer. Upon embedding in this matrix, osteoblasts

finally transform into quiescent osteocytes. Osteoclasts are large multinuclear cells that are involved in bone resorption. A main feature of this bone cell type is its ruffled border, which acts as a high surface area interface for excretion of proteins and (hydrochloric) acid. This acid decreases the local pH and dissolves CaP bone mineral. Generally, two types of bone tissue can be distinguished. Cortical (compact) bone is found at the external surfaces of bones, which is constructed of about 90% of dense bone. Trabecular (spongy) bone is found in the interior of bones, and is composed of a highly porous, spongeous network of so-called bone trabeculae. The intervening cavities are filled with blood vessels and bone marrow.

Bioactivity and bone-bonding

Until the early 1970s, basic clinical concepts for anchoring load-bearing implants within the skeletal system (such as impaction into bone, mechanical interlocking of the implants with bone through screws and other surface macrostructures, and polymerization of methylmethacrylate bone cement) had in common that a soft tissue layer was formed between the implant and bone at retrieval (Plenk, 1998). The lack of chemical inertness of the applied metallic and polymeric materials was suggested as responsible for this unfavourable tissue reaction. However, Hulbert *et al.* (1973) introduced a new concept of so-called biological fixation of skeletal implants by active bone growth onto the implant surface. These materials were oxidic ceramics and carbon materials, as well as metals which were covered with stable oxide layers.

At the same time, however, the principle of bioactive materials (mainly CaP ceramics and silicate-based glasses and glass-ceramics) was explored (Hench *et al.*, 1971; Greenspan and Hench, 1976; Gross *et al.*, 1981). As mentioned before, bioactivity refers to a material that interacts with the surrounding bone and forms a chemical bond to this tissue ('bone-bonding'). This occurs through a time-dependent kinetic modification of the surface, triggered by their implantation within the living bone (Hench, 1998; Saravanapavan *et al.*, 2003). An ion-exchange reaction between the bioactive implant and surrounding body fluids results in the formation of a carbonate apatite layer on the implant that is chemically and crystallographically equivalent to the mineral phase in bone. This correlation between bioactivity and the formation of a carbonate apatite layer is often inverted for preliminary *in vitro* testing of the potential bioactivity of biomaterials. The capacity to nucleate CaP formation under *in vitro* conditions is then interpreted as a first indication of possible bioactivity *in vivo*.

Cellular interactions with implant surfaces

A sequence of complex and strongly interrelated interactions takes place at the implant surface after installation of a prosthesis (Hench, 1998). First, ions and proteins adsorb onto the surface. This adsorption process is strongly dependent on the physicochemical characteristics of the implant surface, such as its topography (in terms of roughness, porosity, morphology, etc.), chemistry, energy and charge. As a result, both the amount and functionality of the adsorbed proteins are largely controlled by the biomaterial surface. This adsorbed biofilm subsequently determines cell adhesion, since proteins act as contact for the attachment of cells. This is accomplished by means of integrins, which are specific transmembrane receptors. These integrins bind to adhesive proteins on the biomaterial's surface and to components of the cytoskeleton through their extra- and intracellular domains, respectively. Although the biological side of the interface is more dynamic than the material side (Plenk, 1998), it should be stressed that the material's surface can also undergo significant alterations due to the physicochemical interaction between the surface and surrounding body fluids.

In general, the biocompatibility of bone-replacing biomaterials is closely related to osteoblast adhesion onto their surface (Keller *et al.*, 1997; Anselme *et al.*, 1999; Zinger *et al.*, 2004). Osteoblast attachment, adhesion and spreading will influence the capacity of these cells to proliferate and to differentiate upon contact with the implant. These latter processes are quintessential for the establishment of a mechanically solid interface with complete fusion between the implant surface and bone tissue without any intervening fibrous tissue layer.

20.3 Fabrication: calcium phosphate coating techniques

Bulk CaP products are currently marketed as bone fillers in dense or porous forms, which have been clinically applied in many areas of dentistry and orthopaedics (Nery *et al.*, 1978; Daculsi *et al.*, 1990), whereas injectable CaP bone graft substitutes represent another branch of bulk CaP ceramics (Chow, 2001; Ooms *et al.*, 2003). As bulk material, however, CaP ceramics are intrinsically brittle and relatively weak in comparison with other implant metals, such as titanium and its alloys, and high-strength ceramics, e.g. alumina and zirconia. Consequently, CaP ceramics are applied as coatings on mechanically strong implant materials in load-bearing implant applications in order to combine the mechanical strength of metals with the excellent biological properties of CaP ceramics.

20.3.1 Plasma-spraying

Plasma-spraying is a technique in which a DC (direct current) electric arc is struck between two electrodes, while a stream of (mixed) gasses passes through this arc. The arc turns these gases into an ionized mixture (a plasma) of high temperature and with a high speed of up to 400 m/s. The temperature of the plasma rapidly decreases as a function of distance. Within the arc, values of up to 20 000 K are reached, while 6 cm outside the electrodes, typical temperatures hover around 2000–3000 K. A metallic, ceramic or even polymeric powder, suspended in a carrier gas, can be fed into the plasma and impinged on a (partially) molten or plastic state towards a surface. Each substrate surface (from metallic, ceramic or even organic materials such as paper) that is placed in plasma can be coated with a layer of the same composition as the powder.

Plasma-spraying is usually considered to be a 'cold' process, although the temperature of the sprayed particles may be much higher. Appropriate cooling techniques keep the temperature of the surface to be coated below 100–150 °C. A partially molten ceramic powder particle has an outside temperature of at least 1000 °C, while a polymer particle still has a surface temperature of several hundred °C.

Owing to the very high temperatures of the plasma, the thermodynamic instability of CaP ceramics at such temperatures plays an important role in the final properties of the deposited coating. Ideally, only a thin outer layer of each powder particle gets into the molten plastic state which unavoidably undergoes phase transitions. This plastic state is necessary to ensure dense and adhesive coatings, but should constitute a negligible volume fraction of the CaP particle. By choosing an optimum relation between particle size (a molten layer of given thickness on a large particle occupies a smaller relative volume than on a smaller one), type of gas (the heat content of a plasma, and thus the ability to increase the temperature of a particle, depends strongly on the gas used), speed of the plasma (the longer a particle resides in a plasma, the higher its temperature), and cooling process of the coated surface, one obtains coatings with the desired CaP phase (mixture) and crystallinity (Cook *et al.*, 1988; Wolke *et al.*, 1992). Figure 20.1 shows a typical surface morphology of a plasma-sprayed CaP coating.

The plasma-spraying technique has been the most successful method to apply CaP coatings to implants to now because of its high deposition rate and the ability to coat large areas. Although the osteoconductive and bone-bonding behaviour of plasma-sprayed coatings is confirmed by numerous studies (Dhert, 1994; Lacefield, 1998; Geesink, 2002), still some serious concerns are related to the plasma-spraying technique (Lusquinos *et al.*, 2003):

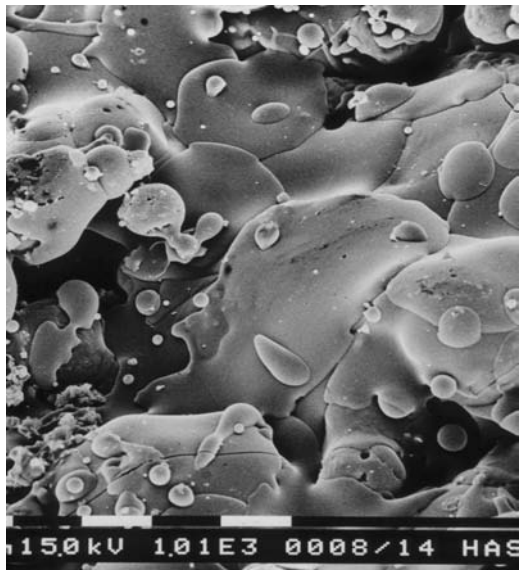

20.1 Typical surface morphology of an electrosprayed CaP coating. Bar size 10 μm.

- Plasma-sprayed coatings must be at least 50 μm thick to completely cover the implant. As a consequence, the adhesion of the thick plasma-sprayed coatings tends to be quite weak, which necessitates a pre-treatment of the substrates such as grit blasting to roughen the substrate and to increase the mechanical interlocking of the coating–substrate system.
- Phase changes in the CaP powder particles during the coating process are unpredictable owing to the high temperature differences in the plasma, leading to the formation of undesired phases such as tetraCaP, calcium oxide and α-triCaP. Moreover, particularly promising phases such as carbonate apatite (which is close to bone composition) and biological agents such as growth factors cannot be deposited using plasma-spraying.
- Particle release and delamination are specific drawbacks for the plasma-spraying technique. The crystallinity of plasma-sprayed coatings is not uniform, as the coatings consist of crystalline and amorphous regions. When CaP material is released from these heterogeneous coatings, the resultant particles may initiate inflammation in surrounding tissues.
- Poor control over thickness and surface morphology.

Therefore, researchers have been continuously inspired in the past two decades to explore alternative or complementary techniques for deposition

of CaP coatings onto implant surfaces. In order to overcome the above-mentioned drawbacks of plasma-sprayed coatings, various deposition methods have been proposed, which will be discussed in the following sections.

20.3.2 Vacuum plasma-spraying (VPS) or low-pressure plasma-spraying (LPPS)

Plasma-spraying performed under low pressure conditions opens up novel application fields for thermal spraying techniques. In particular, particle velocities can be increased, and any harmful gas-metal reactions can be avoided or reduced (Disam *et al.*, 1994; Steffens and Brune, 1995).

The low pressure in the working chamber (50–100 mbar) accounts for a considerable increase of the plasma-jet size. While atmospheric plasma-spraying gives a plasma jet length of 4–10 cm, a flame of 40–50 cm can be achieved by spraying in a low-pressure atmosphere. A disadvantage of low-pressure atmosphere is the increase of the substrate temperature. On the other hand, owing to the low pressure in the working chamber the plasma jet velocity can be increased up to three times the speed of sound, resulting into coatings with good adhesion.

20.3.3 High-velocity oxygen-fuel (HVOF) spraying

HVOF thermal spraying process is a combustion flame spray technique. A HVOF gun combines oxygen and fuel (hydrogen or propylene) to generate heat and extremely high particle velocities. Consequently, a high bond strength and coating density can be achieved (Oguchi *et al.*, 1992). The exhaust flow can attain velocities of about 1700 m/s, i.e. supersonic, with visible shock diamonds in the afflux. The velocity attained by injected particles is lower at about 100–800 m/s, whereas the flame temperature is limited to about 3000 °C, i.e. lower than a typical plasma.

As with any thermal spray process, the objective of the HVOF technology is to transfer energy (both kinetic and thermal) to the powder particles with a high degree of efficiency and balance. With the relatively low temperatures associated with the HVOF systems, the feedstock material is made highly plastic by convective heat transfer preventing superheating or vaporization of the individual particles. When the semi-molten particles collide with the substrate, their temperature peaks as the high kinetic energy is transformed into thermal energy. Upon impact, the thermal component is absorbed uniformly by the substrate, which results in a rapidly solidified coating with low residual stress. In general, HVOF coatings have a higher density and hardness than most thermal sprayed coatings as well as an improved bond strength.

20.3.4 Hot isostatic pressing

Using the hot isostatic pressing (HIP) technique, titanium cores are coated with hydroxyapatite powder and then heated to 500 °C to remove the organic binder from the coating. Subsequently, the coated rod is placed in a glass encapsulating tube and a vacuum is created to collapse the encapsulating material around the specimen. Finally, the specimens are heated for 2 h at 1000–1200 °C and 10 000–15 000 psi. Most of the hydroxyapatite coatings produced using this technique are contaminated with metal and SiO_2 particles due to the use of the glass encapsulating tube (Lacefield, 1988; Hero *et al.*, 1994).

20.3.5 Frit enamelling

A metal bar is dipped into a hydroxyapatite slurry, dried and sintered at 1100–1200 °C for a minimum of 3 h in a protective argon atmosphere. Coatings created in this way show a very low interfacial shear strength (shear strength of 0.22 MPa). The furnace atmosphere used for sintering is probably inadequate, which results in excessive substrate oxide layer thickness and a poor bonding (Lacefield, 1988).

20.3.6 Sputter deposition

Sputtering is the process whereby atoms or molecules of a material are ejected in a vacuum chamber by bombardment of high-energy ions. The dislodged particles deposit on a substrate, also placed into the vacuum chamber. There are several sputter techniques such as diode sputtering, radiofrequency (RF) or direct current (DC) sputtering, ion-beam sputtering and reactive sputtering (Barthell *et al.,* 1989; Ong *et al.*, 1992). However, a drawback inherent to all these techniques is the low deposition rate. By using a magnetically enhanced variant of diode sputtering, these problems can be solved. This magnetron sputtering is a high-rate vacuum coating technique for depositing a wide range of materials (including metals, alloys, ceramics).

RF magnetron sputtering was used as a method to deposit thin films of hydroxyapatite on titanium substrates, with a deposition rate of 1.0–1.5 μm/h and a film thickness of 0.5–10 μm. X-ray diffraction (XRD) demonstrated that the sputtered layer was amorphous or crystalline with a preferred (00l) crystallographic orientation with the *c*-axis perpendicular to the substrate surface. Scanning electron microscopy showed that the deposited films had a uniform and dense structure. The *in vitro* dissolution rate was determined by the degree of crystallinity of the coating (Cooley *et al.*, 1992; Jansen *et al.*, 1993; Wolke *et al.*, 1994).

20.3.7 Pulsed laser deposition

A pulsed laser deposition (PLD) process can also be used for forming thin 0.05–5 μm thick hydroxyapatite coatings on a polished substrate. The PLD process involves ablation of a hydroxyapatite target using a pulsed KrF excimer laser beam ($\lambda = 248$ nm) in a 0.3 torr/H_20 atmosphere and deposition of the ejected hydroxyapatite material onto a heated substrate (400–800 °C). The deposition rate of PLD is about 0.02–0.05 nm/laser shot. The sputtered layer is amorphous or crystalline with a preferred (00l) crystallographic orientation. The adhesion strength decreases for films produced at a high substrate temperature and appears to be related to the existence of an oxide at the interface between the film and the substrate (Cotell *et al.*, 1992).

20.3.8 Laser surface cladding

Laser surface cladding can be used to obtain CaP coatings onto titanium and its alloys that show near isotropic mechanical properties, good fusion bonding to the substrate, and which require minimum surface preparation methods (Lusquinos *et al.*, 2003). The method consists of blowing particles of the precursor material by mixing it with a carrier gas. This powder stream is injected into the area irradiated by the laser beam. The laser beam heats the precursor material and creates a molten pool on the metallic substrate where the particles impinge. To avoid oxidation in the interaction zone, a shielding inert gas is usually applied. Rapid quenching takes place when the molten pool leaves the laser-irradiated area. The relative movement between the laser and the substrate leads to the formation of a coating on the surface of the titanium alloy plate. Coatings produced by laser surface cladding have a composition that varies across its thickness from hydroxyapatite at the surface to calcium titanates and titanium phosphides at the coating–substrate interface, thereby ensuring the two main objectives of a bioactive coating: the inner part of the coating acts as a bonding agent to the implant, whereas the outer part of the coating bonds to the surrounding bone tissue. The biological performance was shown to be comparable *in vitro* to plasma-sprayed CaP coatings (De Carlos *et al.*, 2006).

20.3.9 Electrophoretic deposition

Electrophoretic deposition has been used to achieve uniform CaP coatings on metallic substrates. This approach is especially useful for porous metal structures such as orderly oriented wire meshes. To create the coatings, CaP powders are electrophoretically deposited onto titanium from a 3% suspension of powders in isopropanol or another suitable liquid. The coating

thicknesses can be varied by changing the electrical field strength and the time of deposition. The deposited powders are sintered in high vacuum (10^{-6}–10^{-7} torr) at 850–950 °C. The resulting coating consists of a mixture of CaP phases. Further, at the coating–substrate interface a Ti–P compound is formed due to P diffusion into the Ti substrate. Because of densification during sintering, shrinkage and cracking of the coating can occur. Also thermal stresses induced by the differences in thermal expansion coefficients between the metal and the ceramic film can lead to cracking during sintering and cooling (Ducheyne *et al.*, 1986, 1990).

20.3.10 Sol–gel deposition

The solution–sol–gel route is considered as a method that results in ceramic coatings with an exact chemical and microstructural composition. The approach can be considered as a wet chemistry approach in which reagents, consisting of the desired components for the coating, are mixed in solution as a colloidal suspension of inorganic particles, as metal alkoxides or as other organic precursors. The coatings are prepared at low reaction temperature and fired at temperatures in the range of 400–1000 °C. The resulting coatings can be extremely dense and adhere strongly to the underlying substrate (Ducheyne *et al.*, 1980).

20.3.11 Electrochemical deposition

Using electrochemical deposition, an aqueous electrolyte containing Ca and P ions is decomposed, which results into nucleation of calcium and phosphate crystals onto the titanium electrode. Subsequently, the obtained hydroxyapatite coating is heat-treated in steam at 125 °C for 4 h and then calcined in vacuum at 425 °C for 6 h to densify the film and to improve its bonding to the substrate. The thickness of such hydroxyapatite coatings is approximately 80 μm and the deposition rate is about 60 μm/h. HA coatings obtained by the electrochemical method have a uniform structure since the coating is formed gradually through a nucleation and growth process at a relatively low temperature. XRD indicates that the coating is mainly composed of small crystals. The crystallite dimension (D_{002}) is about 100 nm (Ban and Maruno, 1995; Rossler *et al.*, 2003).

20.3.12 Biomimetic deposition

Biomimetic deposition is a method whereby a biologically active bone-like apatite layer is formed on a substrate surface by immersion of the substrate in simulated body fluid (SBF) (Kokubo and Takadama, 2006) at 37 °C for several days. The main benefits of this deposition technique are the

possibility of including drugs and growth factors into the CaP coating, while complex implant geometries can be coated using this soaking procedure. Accelerated biomimetic strategies have been developed by employing metastable SBF solutions with a fivefold higher concentration of 5× SBF after supersaturation with carbon dioxide gas (Barrere *et al.*, 1999) or dissolution of sodium hydrogen carbonate salts (Li, 2003). In both cases, gradual release of CO_2 gas is accompanied by release of hydroxyl anions according to the reaction $HCO_3^- \rightarrow OH^- + CO_2$, thereby increasing the solution pH and triggering the accelerated deposition of biomimetic apatite crystals onto the substrate surface.

20.3.13 Electrostatic spray deposition (ESD)

The basic principle of ESD is the generation of an aerosol out of organic solvents containing inorganic precursors under the influence of a high voltage. An aerosol is defined as a dispersion of solid or liquid particles in a gas. This is accomplished by pumping the liquid through a nozzle. Usually a spherical droplet is then formed at the tip of the nozzle, but if a high voltage is applied between the nozzle and substrate, this droplet transforms into a conical shape and fans out to form a spray of highly charged droplets. The generated spray droplets are attracted by the grounded and heated substrate as a result of the applied potential difference. Consequently, the droplets impinge onto the heated substrate, where they lose their charge. After complete solvent evaporation, a thin layer is left on the substrate surface.

Using ESD, which is a simple and cheap deposition method for inorganic and organic coatings, it is possible to obtain thin CaP layers with an extremely wide range of chemical and morphological characteristics (Leeuwenburgh *et al.*, 2005, 2006a). Various CaP phases and phase mixtures can be deposited and a broad diversity of coating morphologies can be produced by varying deposition parameters related to the ESD apparatus and/or the precursor solutions. Typical ESD-derived, reticular coating morphologies consist of a porous network of variable pore size, as shown in Fig. 20.2. This specific coating morphology offers the possibility of varying the specific surface area of electrosprayed CaP coatings by chemical as well as physical coating parameters.

20.3.14 Molecular precursor method

Carbonate-containing hydroxyapatite was deposited on titanium using a molecular precursor method by adding dibutylammonium metaphosphate salt to an ethanol solution of Ca-ethylenediamine-*N*,*N*,*N*′,*N*′-tetraacetic acid/amine complex (Takahashi *et al.*, 2005). After firing the as-deposited

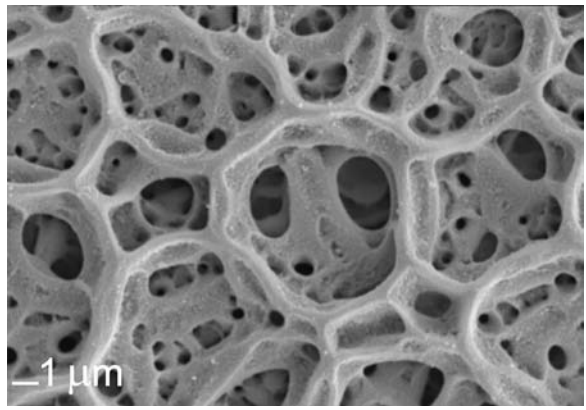

20.2 Typical surface morphology of a plasma-sprayed CaP coating. Bar size 1 μm.

films at temperatures higher than 500 °C for 2 h under atmospheric conditions, a crystalline carbonate-containing hydroxyapatite film was formed on the titanium substrate with a typical coating thickness of about 0.44 μm. The tensile bond strength measurement and scratch test showed an excellent adhesion of the coated film on the titanium after the PBS immersion.

20.4 Mechanical properties

The clinical success of orthopaedic and dental implants is strongly affected by their physicochemical surface characteristics, since the actual interaction between biomaterials and the biological surroundings takes place at the exposed surface of an implant (Ducheyne and Qiu, 1999). Consequently, research has focused on surface modification of biomaterials, thereby creating entirely new surfaces which are intended to improve the properties of a bulk implant.

Coatings must adhere satisfactorily to the underlying substrate irrespective of their intended function. Specifically, the mechanical stability of CaP coatings should be high enough to maintain their bioactive functionality after surgical installation. Generally, tensile adhesion testing according to standards such as ASTM C633 is the most common procedure to determine quantitative values for CaP coating adhesion to the underlying metallic substrates. However, this method can only be applied to coating thicknesses greater than 0.38 mm (Rohanizadeh *et al.*, 2005). This limitation was imposed because adhesive epoxy bonding agents are used in the test, which tend to penetrate into the pores of these porous coatings. Moreover, coatings do experience combined shear, bending, tensile and compressive stresses *in vivo*, which means that measurement of tensile adhesion strength can be

regarded as an oversimplification of the *in vivo* situation (Haman *et al.*, 1999). Therefore, other approaches are needed to evaluate the mechanical properties of CaP coatings under various stress conditions.

Fatigue and scratch testing are among the most valuable techniques to provide additional information on the mechanical behaviour of CaP coatings. Fatigue behaviour of CaP coatings is often investigated using a three-point bending test method in SBF under cyclic loading conditions in order to simulate the discontinuous forces that act on an implant, thereby revealing information on phenomena such as the bending flexibility, internal stresses, and crack formation tendency of CaP coatings as a result of cyclic loading (Wolke *et al.*, 1997; Clemens *et al.*, 1999). Scratch testing is usually performed to obtain insight into the CaP coating deformation mechanism under shear stress (Wu, 1991). Ductile coating failure modes are described by Bull (1991) as a failure mechanism characterized by small areas of uncovered substrate which are confined within the scratch track, whereas brittle failure is more extensive and often extends beyond the limits of the scratch track. Bull stated that there is a requirement for ductile failure for the best scratch adhesion, since critical loads L_c for ductile failure are much higher than those observed for brittle materials. Regarding scratch testing, however, it should be emphasized that caution should always be taken in determining critical load values L_c as a quantitative measurement for coating adhesion, since adhesion and mechanical strength (cohesion) of coatings are strictly separated phenomena. Without an unambiguous definition of a well-defined failure event (such as total coating delamination) by means of a scanning electron micrograph, which illustrates the particular failure mode, determination of L_c values is a rather arbitrary method of quantifying coating adhesion. Scratch testing is a good comparative test in order to obtain qualitative information on the major failure modes. Nevertheless, the scratch testing method is less suitable to acquire absolute values of critical loads (L_c) because of its dependence on numerous experimental parameters related to the testing system and specific coating-substrate system (Steinmann *et al.*, 1987; Wang *et al.*, 2004).

Generally, more than 350 different techniques for adhesion measurement of coatings have been documented, which illustrates the enormous complexity of adhesion testing (Mittal, 1993). Mittal stated that any of those techniques will rank coating-substrate samples in a series, but the best test for a practical adhesion measurement would be the one that simulates usage stress conditions as closely as possible (Mittal, 1993). From this point of view, a simple but valuable method was successfully introduced in a recent study to assess the adhesion and mechanical strength of biomedical CaP-coatings under conditions that mimic possible clinical situations as close as possible (Leeuwenburgh *et al.*, 2006b). In this investigation, the adhesion of porous, electrosprayed CaP coatings was evaluated directly by

means of implantation and immediate explantation of CaP-coated dental implant screws from the femoral condyle of goat cadavers. Characterization of CaP coating adhesion as well as cohesion by means of techniques such as scanning electron microscopy (SEM) and EDS provided a direct insight into the mechanical behaviour of CaP coatings upon surgical installion of dental implants into an osseous environment.

20.5 Biological properties

Plasma-sprayed hydroxyapatite coatings for orthopaedic and dental implants were introduced by de Groot *et al.* (1987) and Geesink *et al.* (1987). Since then numerous reports have been published about the osteoconductive properties of plasma-sprayed implants. Hydroxyapatite coatings are described to induce more bone contact to the implant (Dhert *et al.*, 1993; Jansen *et al.*, 1991; Thomas *et al.*, 1989), to improve the implant fixation (Søballe *et al.*, 1993), and to facilitate the bridging of small gaps between implant and surrounding bone (Stephenson *et al.*, 1991; Søballe *et al.*, 1991). As an example of the osteoconductive properties of CaP coatings, Fig. 20.3 shows a typical light micrograph of a histological section of an implant screw coated with a CaP-layer which causes direct bone apposition to the implant surface.

Besides the above-mentioned benefits, concerns have been raised regarding the viable use and clinical efficiency of plasma-spray coated implants. These concerns mainly deal with the large coating thickness of plasma-sprayed coatings of 50–200 μm, which give rise to problems related to the adhesion strength and fatigue behaviour. With increasing coating thickness, the general mechanical performance of CaP coatings gradually shifts from

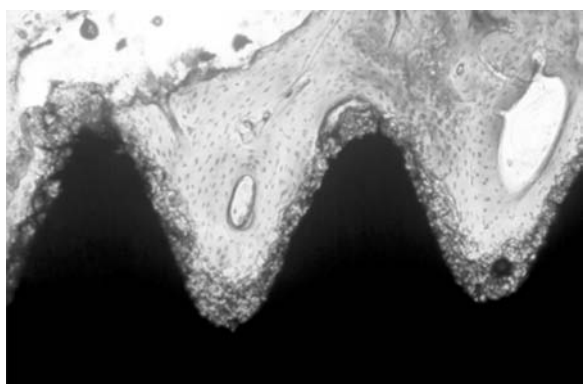

20.3 Bone apposition to a titanium implant screw coated with a plasma-sprayed apatitic layer.

thin-film behaviour with intrinsic small mismatch in mechanical properties between substrate and coating towards a bulk ceramic behaviour as characterized by a large mismatch in properties such as the elastic modulus and thermal expansion coefficient between coating and substrate. In other words, the CaP coatings lose their specific benefits as thin films on metallic substrates. Moreover, the typical heterogeneous crystallinity causes a heterogeneous dissolution profile of plasma-sprayed CaP coatings, which has been reported to cause third-body wear due to release of loosened, crystalline CaP particles around the implant and associated osteolysis (Gross *et al.* 2002).

Therefore, alternative CaP coating techniques have been tested *in vivo* since the early 1990s using various animal models. These results also strongly confirm the beneficial biological effects, i.e. the osteoconductive capacity of CaP coatings, with respect to, for example, sputtered (Yang *et al.*, 2005) and biomimetic CaP coatings (Barrere *et al.*, 2003), respectively. The osteoinductive potential of growth-factor (BMP-2) loaded biomimetic CaP coatings was proven in an ectopic site *in vivo* (Liu *et al.*, 2005).

20.6 Clinical applications

Clinically, the plasma-spraying technique is by far the most successful deposition method for ceramic coatings. Since the 1980s, several clinical studies have been undertaken using plasma-sprayed implants for orthopaedic and dental applications. Generally, reports on the clinical outcome of these experiments clearly indicate that uncemented, CaP-coated prostheses deserve a place in modern orthopaedic and dental practice, since the speed and effectiveness of bone-bonding of CaP-coated implants were clearly improved as compared to uncoated implants (Søballe and Overgaard, 1996; Shepperd and Apthorp, 2005).

The information concerning mandibular implants indicates that titanium devices coated with hydroxyapatite hold a slight advantage over uncoated versions, but concerns remain on the influence of the contaminated environment and reduced pH through bacterial colonalization in the mouth on CaP coating stability. In orthopaedics, the popularity of CaP-coated implants for total hip arthroplasty appears to be increasing, while the number of CaP-coated applications to achieve bone-bonding continues to expand to, for example, total knee replacement (Cross and Parish, 2005), ankle arthroplasty (Anderson *et al.*, 2004), shoulder resurfacing (Levy and Copeland, 2004), pins for external fixation of for instance wrist fractures (Magyar *et al.*, 1997) and coated pedicle screws for spinal fusion (Sanden *et al.*, 2002). Still, the vast majority of CaP-coated prostheses are applied in hip replacements. Fixation of the femoral stems was shown to be successful for a wide range of design concepts. Although the implant shape and coating properties differed

considerably, the clinical outcome was surprisingly consistent and as good as the best of published series of cemented hip stems (Shepperd and Apthorp, 2005). The acetabular cup has also shown advantages over comparable designs of uncemented implants, although adverse results have been published for the combination of hydroxyapatite-coated polyethylene liners.

Basically, the main advantage of bioactive CaP-coatings appears to be the rarity of reported adverse results. Generally, CaP-coated prostheses for orthopaedic surgery consistently perform as well as the very best of cemented or uncemented and uncoated systems, and substantially better than average. In essence, this forgives shortcomings in both design and surgical techniques to orthopaedic surgeons (Shepperd and Apthorp, 2005). This cannot be stated of cemented fixation procedures, for which a poor surgical technique is unforgiving although it remains a reliable – and most common – method of fixation in, for example, the United Kingdom.

Despite the proven efficacy of CaP-coatings for bone-bonding purposes, universal acceptance of CaP-coated systems has not been achieved. Several factors were suggested to be responsible for this phenomenon, such as commercially based pricing strategies which determine that cemented devices are currently cheaper. Generally, the effect of marketing efforts and national habit were suggested to be the main determinants (Shepperd and Apthorp, 2005). The large variability in quality of hydroxyapatite coatings from different companies and even between different batches has caused concerns about the long-term reliability of CaP-coated systems. Therefore, quality reports should be available for each batch in order to avoid the use of coatings of poor quality (Søballe and Overgaard, 1996).

20.7 Summary

This chapter has presented an overview of several deposition techniques that can be used to deposit CaP coatings onto implant surfaces (Section 20.3). Mechanical and biological properties of CaP-coatings were discussed in Sections 20.4 and 20.5, and the clinical performance of plasma-sprayed CaP-coatings was described in Section 20.6. In general, the main added value of the use of CaP-coated prostheses appears to be the rarity of reported adverse results as compared to conventional, cemented orthopaedic procedures. This fact provides the surgeon with a certain forgiveness for the shortcomings in implant design as well as surgical technique using CaP-coated implant systems.

20.8 References

Anderson T, Montgomery F, Carlsson A (2004), 'Uncemented STAR total ankle prostheses', *J Bone Joint Surg Am*, **86**, 103–111.

Anselme K, Noel B, Hardouin P (1999), 'Human osteoblast adhesion on titanium alloy, stainless steel, glass and plastic substrates with same surface topography', *J Mater Sci Mater Med*, **10**, 815–819.

Ban S, Maruno S (1995), 'Effect of temperature on electrochemical deposition of calcium phosphate coatings in a simulated body fluid', *Biomaterials*, **16**, 977–981.

Barrere F, Layrolle P, van Blitterswijk CA, de Groot K (1999), 'Biomimetic calcium phosphate coatings on Ti6Al4V: a crystal growth study of octacalcium phosphate and inhibition by Mg^{2+} and HCO^{3-}', *Bone*, **25**, 107S–111S.

Barrere F, van der Valk CM, Meijer G, Dalmeijer RA, de Groot K, Layrolle P (2003), 'Osteointegration of biomimetic apatite coating applied onto dense and porous metal implants in femurs of goats', *J Biomed Mater Res*, **67**, 655–665.

Barthell BL, Archuleta TA, Kossowsky R (1989), 'Ion beam deposition of calcium hydroxyapatite', *Mater Res Soc Symp Proc*, **110**, 709–714.

Bull SJ (1991), 'Failure modes in scratch adhesion testing', *Surf Coat Technol*, **50**, 25–32.

Chow LC (2001), 'CaP cements', *Monogr Oral Sci*, **18**, 148–163.

Clemens JAM, Wolke JGC, Klein CP, de Groot K (1999), 'Fatigue behavior of calcium phosphate coatings with different stability under dry and wet conditions', *J Biomed Mater Res*, **48**, 741–748.

Cook SD, Thomas KA, Kay JF, Jarcho M (1988), 'Hydroxylapatite coated titanium for orthopeadic implant applications', *Clin Orthop Rel Res*, **232**, 225–243.

Cooley DR, van Dellen AF, Burgess JO, Windeler S (1992), 'The advantages of coated titanium implants prepared by radiofrequency sputtering from hydroxyapatite', *J Prost Dent*, **67**, 93–100.

Cotell CM, Chrisey DB, Grabowski KS, Sprague JA, Grossett CR (1992), 'Pulsed laser deposition of hydroxylapatite thin films on Ti–6Al–4V', *J Appl Biomater*, **3**, 87–93.

Cross MJ, Parish EN (2005), 'A hydroxyapatite-coated total knee replacement: prospective analysis of 1000 patients', *J Bone Joint Surg Br*, **87**, 1073–1076.

Daculsi G, Passuti N, Martin S, Deudon C, LeGeros RZ, Raher S (1990), 'Macroporous CaP ceramic for long bone surgery in humans and dogs. Clinical and histological study', *J Biomed Mater Res*, **24**, 379–396.

De Carlos A, Lusquinos F, Pou J, Leon B, Perez-Amor M, Driessens FCM, Hing K, Best S, Bonfield W (2006), '*In vitro* testing of Nd:YAG laser processed calcium phosphate coatings', *J Mater Sci Mater Med*, **17**, 1153–1160.

Dhert WJA (1994), 'Retrieval studies on CaP-coated implants', *Med Prog Technol*, **20**, 143–154.

Dhert WJA, Klein CPAT, Jansen JA, van der Velde EA, Vriesde RC, Rozing PM, de Groot (1993), 'A histogical and histomorphometrical investigation of fluorapatite, magnesiumwhitlockite and hydroxylapatite plasma sprayed coatings in goats', *J Biomed Mater Res*, **27**, 127–138.

Disam J, Luebbers K, Neudert K, Sickinger A (1994), 'Effect of LPPS spray parameters on the structure of ceramic coating', *J Thermal Spray Technol*, **3**, 142–147.

Ducheyne P, Qiu Q (1999), 'Bioactive ceramics: the effect of surface reactivity on bone formation and bone cell function', *Biomaterials*, **20**, 2287–2303.

Ducheyne P, Hench LL, Kagan 2nd A, Martens M, Bursens A, Mulier JC (1980), 'Effect of hydroxyapatite impregnation on skeletal bonding of porous coated implant', *J Biomed Mater Res*, **14**, 225–237.

Ducheyne P, van Raemdonck W, Heughebaert JC, Heughebaert M (1986), 'Structural analysis of hydroxylapatite coatings on titanium', *Biomaterials*, **7**, 97–103.

Ducheyne P, Radin S, Heughebaert M, Heughebaert JC (1990), 'Calcium phosphate ceramic coatings on porous titanium: effect of structure and composition on electrophoretic deposition, vacuum sintering and *in vitro* dissolution', *Biomaterials*, **11**, 244–254.

Geesink RGT (2002), 'Osteoconductive coatings for total joint arthroplasty', *Clin Orthop Relat Res*, **395**, 53–65.

Geesink RGT, Klein CPAT, de Groot K (1987), 'Chemical implant fixation using hydroxylapatite coatings', *Clin Orthop*, **225**, 147–169.

Greenspan DC, Hench LL (1976), 'Chemical and mechanical behaviour of bioglass-coated alumina', *J Biomed Mater Res*, **10**, 503–509.

de Groot K, Geesink RGT, Klein CPAT, Serekian P (1987), 'Plasma-sprayed coatings of hydroxylapatite', *J Biomed Mater Res*, **21**, 1375–1381.

Gross U, Brandes J, Strunz V, Bab I, Sela J (1981), 'The ultrastructure of the interface between a glass ceramic and bone', *J Biomed Mater Res*, **15**, 291–305.

Gross KA, Ray N, Rokkum M (2002), 'The contribution of coating microstructure to degradation and particle release in hydroxyapatite coated prostheses', *J Biomed Mater Res* **63**, 106–114.

Haman JD, Chittur KK, Crawmer DE, Lucas LC (1999), 'Analytical and mechanical testing of high velocity oxy-fuel thermal sprayed and plasma sprayed calcium phosphate coatings', *J Biomed Mater Res*, **48**, 856–860.

Hench LL (1998), 'Bioceramics', *J Am Ceram Soc*, **81**, 1705–1728.

Hench LL, Splinter RJ, Allen WC (1971), 'Bonding mechanism at the interface if ceramic prosthetic materials', *J Biomed Mater Res Symp,* **2**, 117–141.

Hero H, Wie H, Jorgensen RB, Ruyter IE (1994), 'Hydroxyapatite coatings on Ti produced by hot isostatic pressing', *J Biomed Mater Res*, **28**, 343–348.

Hulbert SF, Cooke F, Klawitter JJ (1973), 'Attachment of prostheses to the musculoskeletal system by tissue ingrowth and mechanical interlocking', *J Biomed Mater Res Symp,* **4**, 1–23.

Jansen JA, van der Waerden JPCM, Wolke JGC, de Groot K (1991), 'Histologic evaluation of the osseous adaptation to titanium and hydroxylapatite-coated implants', *J Biomed Mater Res*, **25**, 973–989.

Jansen JA, Wolke JGC, Swann S, van der Waerden JPCM, de Groot K (1993), 'Application of magnetron sputtering for the producing ceramic coatings on implant materials', *Clin Oral Impl Res*, **4**, 28–34.

de Jong WF (1926), 'Le sustance mineral dans le os', *Rec Trav Chim*, **45**, 445–448.

Keller JC, Collins JG, Niederauer GG, McGee TD (1997), '*In vitro* attachment of osteoblast-like cells to osteoceramic materials', *Dent Mater*, **13**, 62–68.

Kokubo T, Takadama H (2006), 'How useful is SBF in predicting *in vivo* bone bioactivity?', *Biomaterials*, **27**, 2907–1915.

Lacefield WR (1988), 'Hydroxyapatite coatings', *Ann NY Acad Sci*, **523**, 72–80.

Lacefield WR (1998), 'Current status of ceramic coatings for dental implants', *Implant Dent*, **7**, 315–322.

Leeuwenburgh SCG, Wolke JGC, Schoonman J, Jansen JA (2005), 'Influence of deposition parameters on chemical properties of calcium phosphate coatings prepared by using electrostatic spray deposition', *J Biomed Mater Res*, **74**, 275–284.

Leeuwenburgh SCG, Heine M, Wolke JGC, Pratsinis S, Schoonman J, Jansen JA (2006a), 'Morphology of calcium phosphate coatings for biomedical applications deposited using electrostatic spray deposition', *Thin Solid Films*, **503**, 69–78.

Leeuwenburgh SCG, Wolke JGC, Lommen L, Pooters T, Schoonman J, Jansen JA (2006b), 'Mechanical properties of porous, electrosprayed calcium phosphate coatings', *J Biomed Mater Res*, **78**, 558–569.

LeGeros RZ (1991), *Calcium Phosphates in Oral Biology and Medicine*, Basel, Karger.

Levy O, Copeland SA (2004), 'Cementless surface replacement arthroplasty (Copeland (SRA)) for osteoarthritis of the shoulder', *J Shoulder Elbow Surg*, **13**, 266–271.

Li P (2003), 'Biomimetic nano-apatite coating capable of promoting bone ingrowth', *J Biomed Mater Res*, **66**, 79–85.

Liu Y, de Groot K, Hunziker EB (2005), 'BMP-2 liberated from biomimetic implant coatings induces and sustains direct ossification in an ectopic rat model', *Bone*, **36**, 745–757.

Lusquinos F, De Carlos A, Pou J, Arias JL, Boutinguiza M, Leon B, Perez-Amor M, Driessens FC, Hinh K, Gibson I, Best S, Bonfield W (2003), 'CaP coatings obtained by Nd : YAG laser cladding: physicochemical and biologic properties', *J Biomed Mater Res*, **64**, 630–637.

Magyar G, Toksvig-Larsen S, Moroni A (1997), 'Hydroxyapatite coating of threaded pins enhances fixation', *J Bone Joint Surg Br*, **79**, 487–489.

Mittal KL (1993), 'Adhesion measurement of films and coatings: a commentary', in Mittal KL, *Adhesion Measurement of Films and Coatings*, Utrecht, VSP BV, 1–13.

Nery EB, Kenneth LL, Rooney GE (1978), 'Alveolar ridge augmentation with triCaP ceramic', *J Prosth Dent*, **40**, 668–675.

Oguchi H, Ishikawa K, Ojima S, Hirayama Y, Seto K, Eguchi G (1992), 'Evaluation of a high-velocity flame-spraying technique for hydroxyapatite', *Biomaterials*, **13**, 471–477.

Ong JL, Lucas LC, Lacefield WR, Rigney ED (1992), 'Structure, solubility and bond-strength of thin calcium phosphate coating produced by ion beam sputter deposition', *Biomaterials*, **13**, 249–254.

Ooms EM, Wolke JG, van de Heuvel MT, Jeschke B, Jansen JA (2003), 'Histological evaluation of the bone response to CaP cement implanted in cortical bone', *Biomaterials*, **24**, 989–1000.

Osborn JF, Newesely H (1980), 'Dynamic aspects of implant/bone interface', in Heimke G, *Dental Implants*, Munich, Carl Hansen Verlag, 111–123.

Plenk H (1998), 'Prosthesis–bone interface' *J Biomed Mater Res (Appl Biomater)*, **43**, 350–355.

Rohanizadeh R, LeGeros RZ, Harsono M, Bendavid A (2005), 'Adherent apatite coating on titanium substrate using chemical deposition', *J Biomed Mater Res*, **72**, 428–438.

Rossler S, Sewing A, Stolzel M, Born R, Scharnweber D, Dard M, Worch H (2003), 'Electrochemically assisted deposition of thin calcium phosphate coatings at near-physiological pH and temperature', *J Biomed Mater Res*, **64**, 655–663.

Sanden B, Olerud C, Petren-Mallmin M, Larsson S (2002), 'Hydroxyapatite coating improves fixation of pedicle screws: a clinical study', *J Bone Joint Surg Br*, **84**, 387–391.

Saravanapavan P, Jones JR, Pryce RS, Hench LL (2003), 'Bioactivity of gel-glass powders in the $CaO–SiO_2$ system: a comparison with ternary ($CaO–P_2O_5–SiO_2$) and quaternary glasses ($SiO_2–CaO–P_2O_5–Na_2O$)', *J Biomed Mater Res*, **66**, 110–119.

Shepperd JAN, Apthorp H (2005), 'A contemporary snapshot of the use of hydroxyapatite coating in orthopaedic surgery', *J Bone Joint Surg Br*, **87**, 1046–1049.

Søballe K, Overgaard S (1996), 'The current status of hydroxyapatite coating of prostheses', *J Bone Joint Surg Br*, **78**, 689–691.

Søballe K, Hansen ES, Brockstedt-Rasmussen, Hjortdal VE, Juhl GI, Pedersen CM, Hvid I, Bünger C (1991), 'Gap healing enhanced by hydroxyapatite coatings in dogs', *Clin Orthop*, **272**, 300–307.

Søballe K, Hansen ES, Brockstedt-Rasmussen HB, Bünger C (1993), 'Hydroxyapatite coating converts fibrous tissue to bone around loaded implants', *J Bone Joint Surg*, **75**, 270–278.

Steffens HD, Brune M (1995), 'Vacuum-plasma-sprayed titanium-manganese electrode layers for MnO_2 deposition', *J Thermal Spray Technol*, **4**, 85–88.

Steinmann PA, Tardy Y, Hintermann HE (1987), 'Adhesion testing by the scratch method: the influence of intrinsic and extrinsic parameters on the critical load', *Thin Solid Films*, **154**, 333–349.

Stephenson PK, Freeman MAR, Revell PA, Germain J, Tuke M, Pirie CJ (1991), 'The effect of hydroxyapatite coating on ingrowth of bone into cavities in an implant', *J Arthopl*, **6**, 51–58.

Takahashi K, Hayakawa T, Yoshinari M, Hara H, Mochizuki C, Sato M, Nemoto K (2005), 'Molecular precursor method for thin calcium phosphate coating on titanium', *Thin Solid Films*, **484**, 1–9.

Thomas KA, Cook CD, Ray RJ, Jarcho M (1989), 'Biologic response to hydroxylapatite coated titanium hips', *J Arthropl*, **4**, 43–53.

Wang J, Layrolle P, Stigter M, de Groot K (2004), 'Biomimetic and electrolytic calcium phosphate coatings on titanium alloy: physicochemical characteristics and cell attachment', *Biomaterials*, **25**, 583–592.

Williams DF, Black J, Doherty PJ (1992), 'Second consensus conference on definitions in biomaterials', in Doherty PJ, Williams RF, Williams DF, Lee AJC, *Biomaterial-Tissue Interfaces. Advances in Biomaterials*, Amsterdam, Elsevier, 525–533.

Wolke JGC, de Blieck-Hogervorst JMA, Dhert WJA, Klein CPAT, de Groot K (1992), 'Studies on the thermal spraying of apatite bioceramics', *J Thermal Spray Technol*, **1**, 75–82.

Wolke JGC, van Dijk K, Schaeken HG, de Groot K, Jansen JA (1994), 'Study of the surface characteristics of magnetron-sputter calcium phosphate coatings', *J Biomed Mater Res*, **28**, 1477–1484.

Wolke JGC, van der Waerden JP, de Groot K, Jansen JA (1997), 'Stability of radiofrequency magnetron sputtered calcium phosphate coatings under cyclically loaded conditions', *Biomaterials*, **18**, 483–488.

Wu TW (1991), 'Microscratch and load relaxation tests for ultra-thin films', *J Mater Res*, **6**, 407–426.

Yang Y, Kim KH, Ong JL (2005), 'A review on calcium phosphate coatings produced using a sputtering process – an alternative to plasma spraying', *Biomaterials*, **26**, 327–337.

Zinger O, Anselme K, Denzer A, Habersetzer P, Wieland P, Wieland M, Jeanfils J, Hardouin P, Landolt D (2004), 'Time-dependent morphology and adhesion of osteoblastic cells on titanium model surfaces featuring scale-resolved topography', *Biomaterials*, **25**, 2695–2711.

21

Titania-based materials

T KOKUBO, H TAKADAMA and T MATSUSHITA,
Chubu University, Japan

21.1 Introduction

Various types of bioactive materials have been developed based on silicate and phosphate ceramics. In addition, it has been shown recently that some titanium oxide and titanate also bond to living bone. Titania-based materials are easily formed on titanium metal and its alloys by chemical and thermal treatments. As is well known, ceramics are brittle and not ductile, and they cannot be used under high load conditions. However, metals can be used under these conditions, because of their high fracture toughness, but they do not bond to living bone, and are usually fixed to the surrounding bone by a mechanical interlocking with the bone via a roughened surface, or by filling polymethylmethacrylate bone cement into a gap between a metallic implant and the bone. Fixation using these methods is not stable for long periods, and sometimes autogenous bone is transplanted around metallic implants for fixation. However, harvesting of the autogenous bone involves excessive invasion and sometimes leads to complications.

In view of these facts, it would be desirable for metallic implants to exhibit bone-bonding capability. To provide a bone-bonding capability to a metallic material, a coating of calcium phosphate on a metallic implant using a plasma-spray technique has been developed, and used clinically, as described in Chapter 20. However, in this method, calcium phosphate is only coated on the surfaces exposed to the plasma, and the coated layer is relatively thick; hence, a uniform bioactive layer cannot be formed on complex shapes. In contrast to this, thin, uniform titania-based coatings can be formed on all surfaces, even on complex shapes using solution and thermal treatments of the metal.

In this chapter, the formation of titania-based materials on metals, the properties of these titania-based materials, and the mechanism of apatite formation on these titania-based materials are described.

21.2 Formation of titania-based materials on metals

It has been shown that a titania gel prepared using a sol–gel method forms apatite on its surface in a simulated body fluid (SBF) with ion concentrations nearly equal to those of the human blood plasma, when it had been previously heat treated in the temperature range 500–800 °C to precipitate anatase or rutile (Uchida *et al.*, 2003). This indicates that some form of Ti-OH group on the gels is effective for apatite nucleation in a body environment. For example, it is expected that sodium titanate may form such Ti-OH groups on its surface when it is placed in body environment or soaked in an aqueous solution, since the Na^+ ions in it will exchange with H_3O^+ ions in the body environment or solution. Sodium titanate can form on the surface of titanium metal and its alloys when these metals are exposed to an NaOH solution. Then, it is expected that these metals with a sodium titanate layer on their surface can form bonelike apatite on their surface in the living body and bond to living bone through this apatite layer. Even metals with a titanium oxide layer formed by exposure to an NaOH solution and a subsequent water or acid treatment of their surface can show a high apatite-forming capability in a body environment and bond to living bone.

Based on these considerations, pure titanium metal was soaked in a 5M NaOH solution at 60 °C for a period of 24 h (Sample A) and subjected to heat treatment at 600 °C for a period of 1 h (Sample A-H) (Kokubo *et al.*, 1996; Kim *et al.*, 1996, 1997a,b). In another case, samples of the same pure titanium metal were soaked in a 0.5 mM HCl solution at 40 °C for a period of 24 h (Sample A-HC) after the NaOH treatment, and then subjected to the same heat treatment at 600 °C (Sample A-HC-H) (Uchida *et al.*, 2002).

Figure 21.1 shows scanning electron micrographs of the surfaces of titanium metal subjected to the four different treatments described above. All the samples showed a fine network structure. About 6 wt% of sodium was detected on surfaces of Samples A and A-H using energy dispersive X-ray (EDX) analysis. Figure 21.2 shows a depth profile of the Auger electron spectra (AES) of some elements from Samples A and A-H (Kim *et al.*, 1999). It can be seen from Fig. 21.2 that the sodium and oxygen ions penetrated the titanium metal after the NaOH treatment, and a sodium titanate layer with a graded structure is formed within a depth of 1 μm. The distribution of sodium was constant, whereas the distribution of the oxygen was extended to deeper regions after the heat treatment. Sodium was not detected on surface of Samples A-HC which was subjected to the HCl treatment after the NaOH treatment, using EDX analysis. Sample A-HC-H after the subsequent heat treatment also did not show sodium. This means that the sodium ions that had entered the titanium metal due to the NaOH treatment were leached by the HCl treatment.

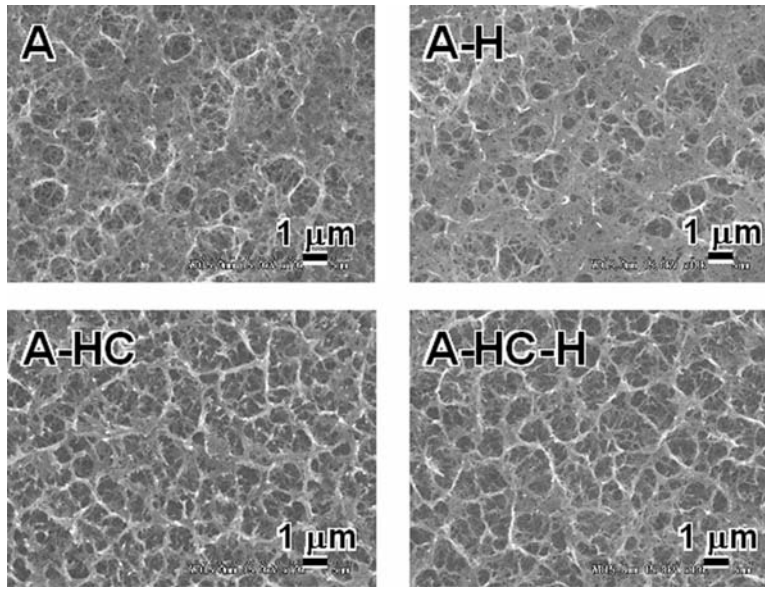

21.1 SEM pictures of surfaces of samples A, A-H, A-HC and A-HC-H.

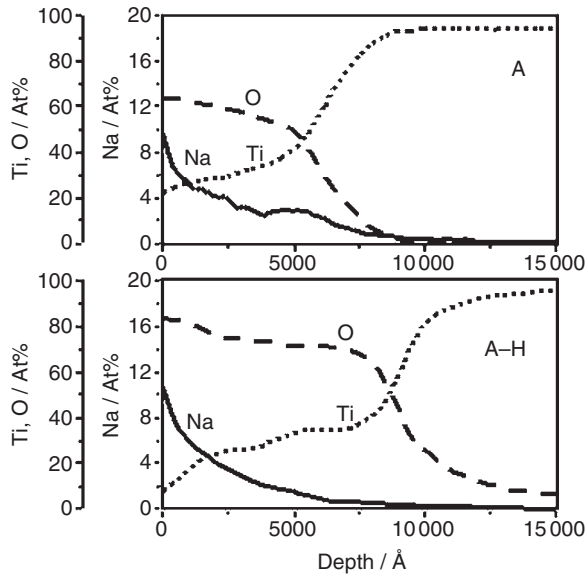

21.2 AES depth profiles of surfaces of samples A and A-H (Kim *et al.*, 1999).

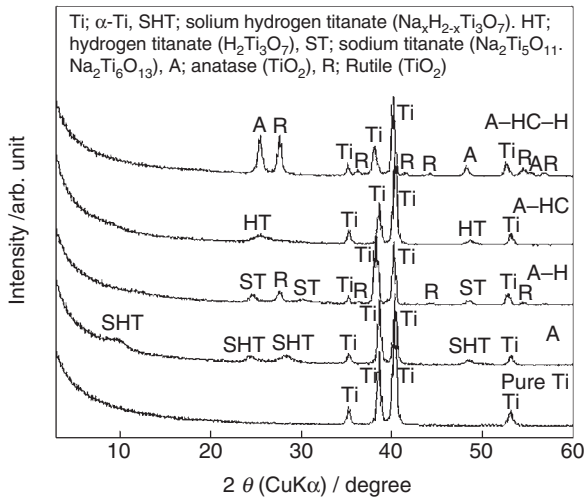

21.3 TF-XRD patterns of surfaces of samples A, A-H, A-HC and A-HC-H.

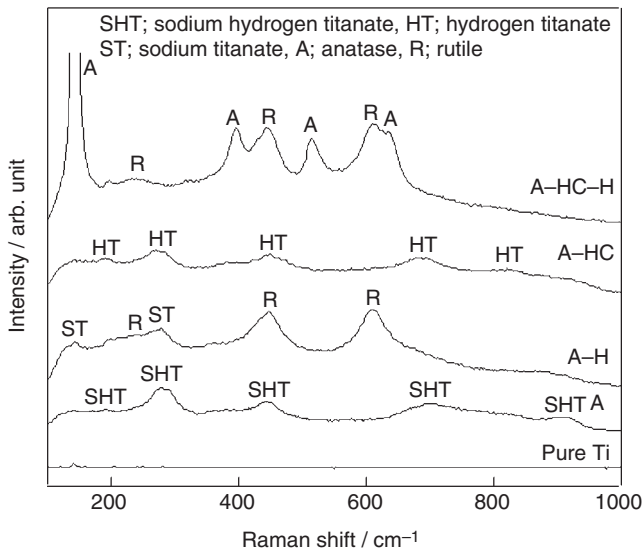

21.4 Raman spectra of surfaces of samples A, A-H, A-HC and A-HC-H.

Figures 21.3 and 21.4 show the thin-film X-ray diffraction (TF-XRD) patterns and Raman spectra, respectively, of the surfaces of titanium metal subjected to the four different treatments described above. The data in these figures indicate that a sodium hydrogen titanate phase ($Na_xH_{2-x}Ti_3O_7$) with small crystallites is formed on the surface of titanium metal by the

NaOH treatment, and that this transforms into sodium titanate ($Na_2Ti_5O_{11}$, $Na_2Ti_6O_{13}$ and/or $Na_2Ti_7O_{15}$) and rutile (TiO_2) owing to the subsequent heat treatment. The sodium hydrogen titanate is transformed into hydrogen titanate ($H_2Ti_3O_7$) isomorphously by the HCl treatment, and then into anatase (TiO_2) and rutile (TiO_2) by the subsequent heat treatment. Titanium-based alloys, such as Ti–6Al–4V, Ti–6Al–2Nb–Ta, and Ti–15Mo–5Zr–3Al also show similar structural changes on their surfaces after NaOH, HCl and heat treatments (Kim *et al.*, 1996, 2000a,b).

21.3 Physical and chemical properties of the titania-based layer on metals

The critical detaching load of the surface layer formed on titanium metals by the four different treatments described above were measured using an ultra-fine film scratch tester (Model CSR-2000, Rhesca, Japan). This was <10 mN for Samples A and A-HC before the heat treatment, whereas it was around 60 mN for both Samples A-H and A-HC-H after the heat treatment. This indicates that the surface layers formed by the chemical treatments are dehydrated and densified as layers of sodium titanate and titanium oxide, respectively, by the heat treatment. Figure 21.5 shows scanning

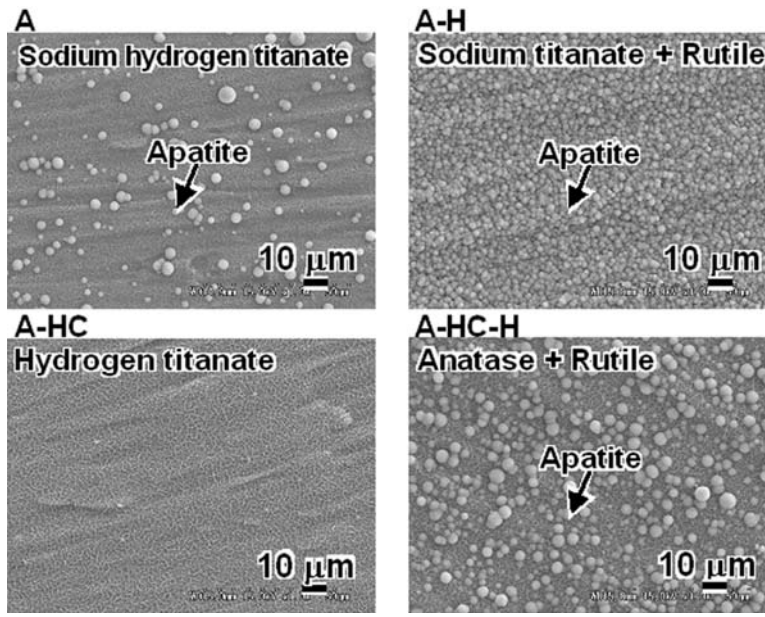

21.5 SEM pictures of surfaces of samples A, A-H, A-HC and A-HC-H after soaking in SBF for 1 day.

electron microscope (SEM) pictures of the surface of titanium metal subjected to the four different treatments described above, after soaking in the SBF for a period of 1 day at 36.5 °C. It can be seen from Fig. 21.5 that titanium metal as subjected to the NaOH treatment gives small apatite-forming ability in SBF, and the same metal subjected to the subsequent HCl treatment does not give apatite-forming ability. However, both these samples showed a high apatite-forming capability when they were subjected to the subsequent heat treatment to precipitate the sodium titanate and titanium oxide, respectively. This indicates that the dehydrated sodium titanate and titanium oxide are effective for apatite formation in body environment. Osaka and coworkers showed that a titanium oxide layer that could confer an apatite-forming capability in an SBF was also formed on titanium metal by an H_2O_2 and subsequent heat treatment (Wang *et al.*, 2002; Wu *et al.*, 2004).

21.4 Mechanism of apatite formation on titania-based materials

According to transmission electron microscopic observations and zeta-potential measurements, the mechanism of apatite formation on the surface of titanium metal formed with sodium titanate in an SBF is interpreted as shown in Fig. 21.6 (Takadama *et al.*, 2001a,b,c). The Na^+ ions are released from the surface via exchange with the H_3O^+ ions in the SBF to form a large number of Ti-OH groups on the surface. Thus, Ti-OH groups are negatively charged and react with the positively charged Ca^{2+} ions in the SBF, forming calcium titanate. As the calcium ions accumulate on the surface, the surface becomes positively charged and can react with the negatively charged phosphate ions, forming amorphous calcium phosphate.

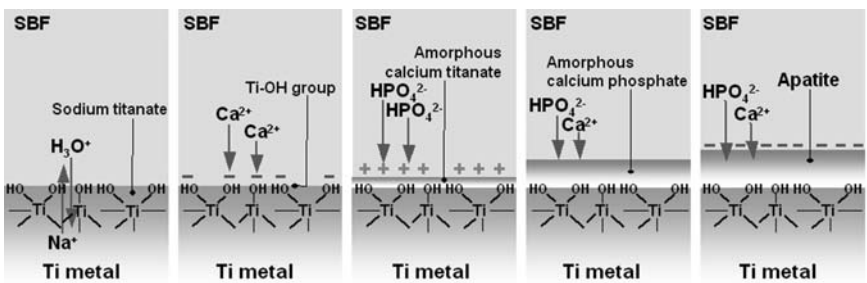

21.6 Schematic representation of mechanism of apatite formation on NaOH- and heat-treated titanium metal in SBF (Takadama *et al.*, 2001c).

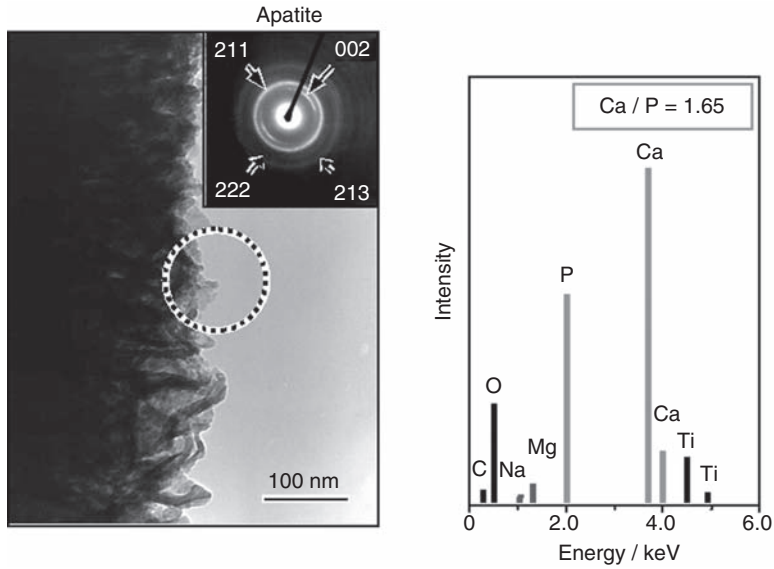

21.7 TEM picture and EDX spectrum of apatite formed on NaOH- and heat-treated titanium metal in SBF (Takadama *et al.,* 2001c).

Since this amorphous calcium phosphate is metastable, it eventually transforms into a stable crystalline apatite. Transmission electron micrograph (TEM) and energy dispersive X-ray (EDX) spectrum of the crystalline apatite formed are shown in Fig. 21.7, which shows that the apatite has a needle-like form, with a Ca/P ratio of Ca/P ≈ 1.65 and with a small amount of Na and Mg. These characteristics are very similar to those of bone mineral.

21.5 Biological properties of a titania-based layer on metals

A rectangular titanium metal sample with sodium titanate on its surface due to an NaOH and heat treatment was implanted into a rabbit's tibia, and was tightly bonded to living bone through the apatite layer formed on its surface in the living body, as shown in Fig. 21.8 (Yan *et al.*, 1997). When a tensile stress was applied to the interface, the detaching failure load increased with increasing period after implantation, as shown in Fig. 21.9 (Nishiguchi *et al.*, 1999a,b, 2001a; Nishio *et al.*, 2000). A rod of titanium metal that had received the same treatment was implanted into the intramedullary canal of a rabbit's femur. It formed an apatite layer on its surface, and

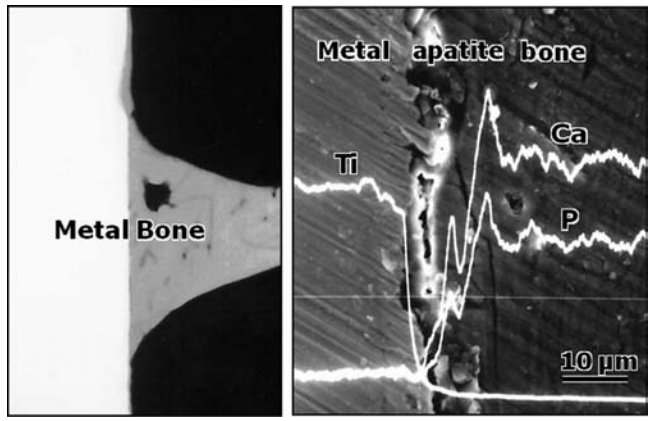

21.8 Contact microradiograph and SEM-EDX picture of a cross-section at an interface between rabbit tibia and NaOH- and heat-treated titanium metal (Yan *et al.,* 1997).

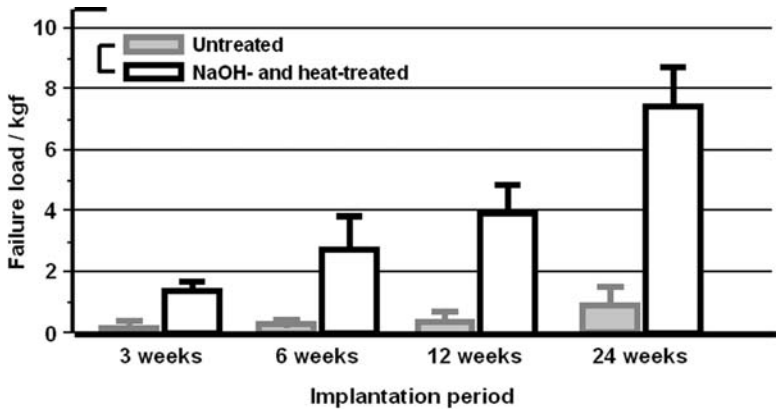

21.9 Detaching failure load of untreated and NaOH- and heat-treated titanium metals as a function of period after implantation into rabbit tibia.

was tightly bonded to the surrounding bone, as shown in Fig. 21.10 (Nishiguchi *et al.*, 2003). When the implant was pulled out, the failure load increased with increasing period after implantation, as shown in Fig. 21.11. The rod could not be pulled out without being accompanied by bone fragments, as shown in Fig. 21.12.

The NaOH and heat treatments were applied to a porous layer of titanium metal on a total hip joint made of Ti–6Al–2Nb–Ta alloy, as shown in Fig. 21.13 (Kim *et al.*, 2000c; Nishiguchi *et al.*, 2001b) and subjected to

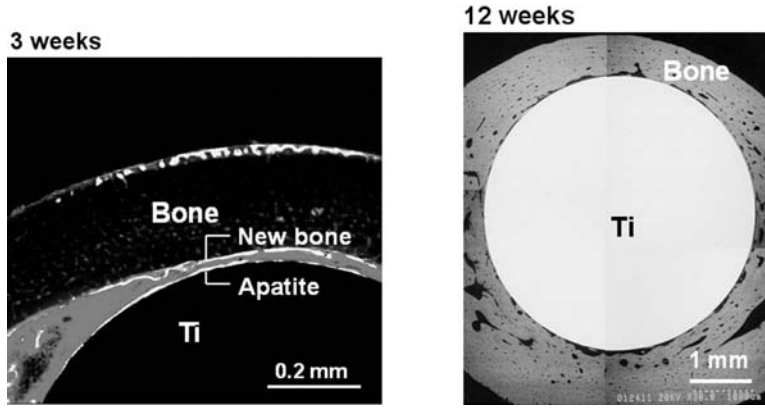

21.10 Confocal laser scanning micrograph (left) and SEM picture (right) of a cross-section of NaOH- and heat-treated titanium metal implanted into rabbit femur for 3 and 12 weeks, respectively (Nishiguchi *et al.,* 2003).

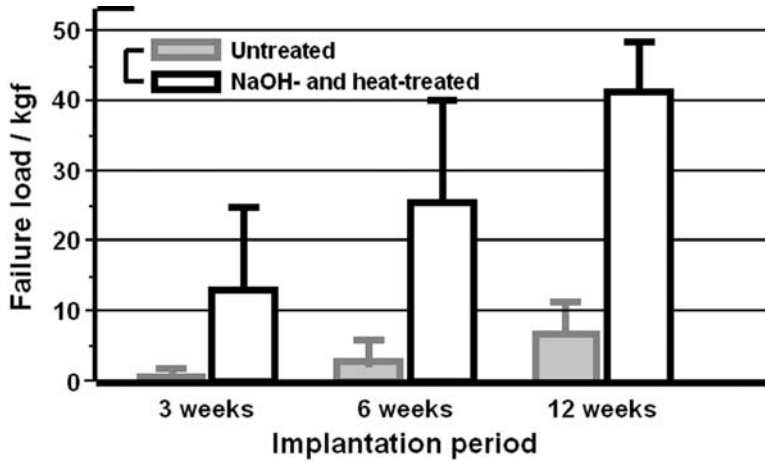

21.11 Pull-out failure load of untreated and NaOH- and heat-treated titanium metals as a function of period after implantation into rabbit femur (Nishiguchi *et al.*, 2003).

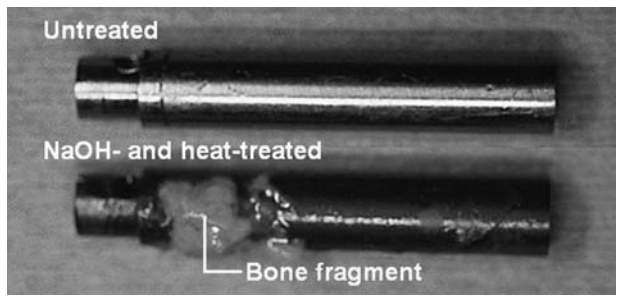

21.12 Untreated and NaOH- and heat-treated titanium rods pulled out from rabbit femur 12 weeks after implantation (Nishiguchi *et al.*, 2003).

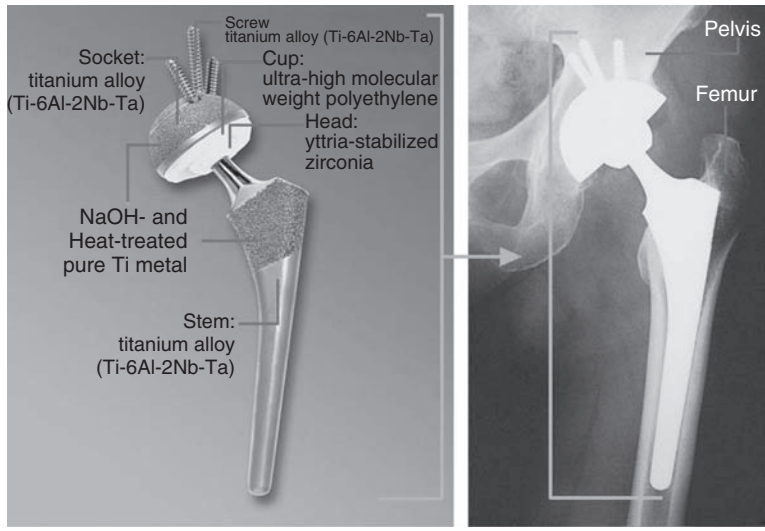

21.13 Total hip joint of Ti–6Al–2Nb–Ta alloy formed with NaOH- and heat-treated titanium metal porous layer.

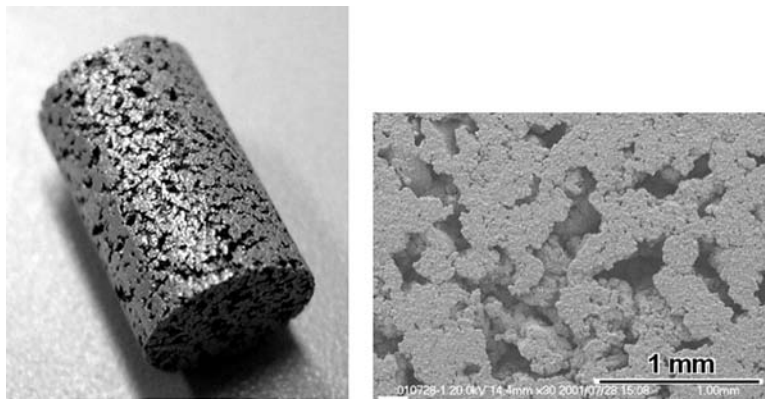

21.14 Porous titanium metal subjected to NaOH, HCl and heat treatments.

clinical trials for 70 patients. This artificial hip joint was approved for sales by the Japanese government in 2007.

The NaOH, HCl and heat treatments were applied to a porous body of titanium metal to form a uniform thin layer of titanium oxide on surfaces of the pore walls. The porous bodies were prepared using a plasma spray technique or by sintering of titanium metal powder, and contained

50–70 vol% of pores that were 200–500 μm in size. A cylindrical sample, given in Fig. 21.14, that was 6 mm in diameter and 15 mm long was implanted into a rabbit's femur. It was penetrated with newly grown bone from the outer surface and was tightly bonded to the bone, as shown in Fig. 21.15 (Fujibayashi *et al.*, 2001, 2003; Takemoto *et al.*, 2005; Otsuki *et al.*, 2006). In contrast, when the same sample was implanted into the muscle of a dog, it formed bone tissue from the interior within a period of 3 months, and this spread it to the periphery within a period of 12 months, as shown in Fig. 21.16 (Fujibayashi *et al.*, 2004; Takemoto *et al.*, 2006).

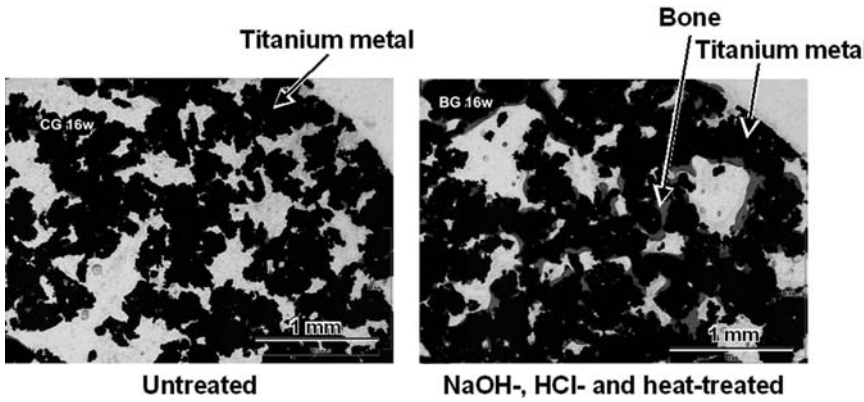

21.15 Bone ingrowth from the outer surface of untreated and NaOH, HCl and heat-treated porous titanium metals at 16 weeks after implanted into rabbit femur (Takemoto *et al.*, 2005).

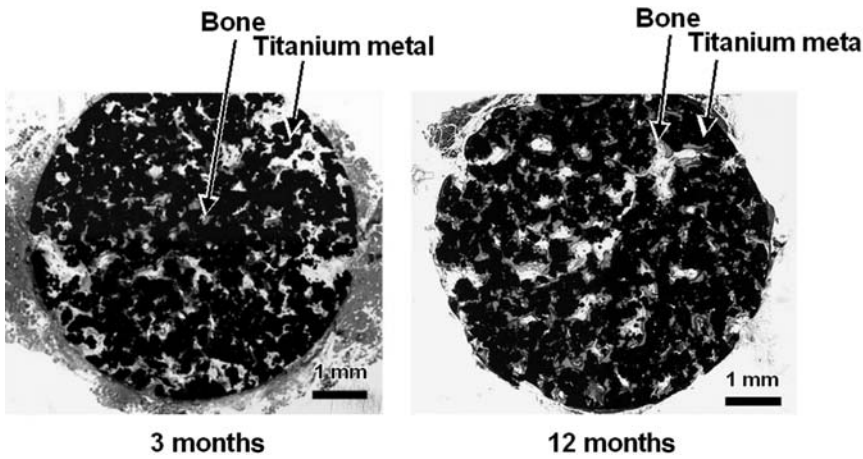

21.16 Bone induction from the interior of NaOH-, HCl- and heat-treated porous titanium metal in muscle of dog (Takemoto *et al.*, 2006).

This type of osteoinduction has also been observed in various types of porous calcium phosphate ceramics, as described in Chapter 9. However, these materials have a poor mechanical strength. Porous titanium metal can show mechanical properties that are compatible with those of the surrounding bone. Therefore, this type of osteoinductive and osteoconductive material with suitable mechanical properties is expected to be useful as implants for spinal interbody fusion and various types of bone substitute.

21.6 Some titania-based composites

A two-dimensional fabric of polyethylene terephthalate (PET) fibres was dipped into a titania sol solution prepared by mixing titanium isopropoxide, ethanol, water, and nitric acid in a 1.0:18.25:1.0:0.1 molar ratio, pulled up and soaked in a 0.1 M HCl solution at 80 °C for a period of 8 days to be covered with a thin layer of brookite. This modified PET fabric with titanium oxide on its surface formed uniform bonelike apatite on the surfaces of individual fibres constituting the fabric in the SBF, as shown in Fig. 21.17 (Kokubo *et al.*, 2007). This type of fabric is expected to be useful as a bioactive flexible bone substitute.

A titanium oxide powder with a mixed anatase-rutile phase, 2 μm in size, were mixed with 5 μm polymethylmethacrylate (PMMA) powder and a small amount of benzoyl peroxide. This powder mixture was mixed with a liquid mixture of methylmethacrylate and a small amount of *N*,*N*-dimethyl-*p*-toluidine. The mixed paste set within a period of 10 min, and had a mechanical strength comparable to that of commercial PMMA cement. When the mixed paste was injected into a bone defect in a rat's tibia, it tightly bonded to the surrounding bone without the intervention of fibrous tissue, as shown in Fig. 21.18 (Kokubo *et al.*, 2007). This type of cement is expected to be useful as a bioactive self-setting bone substitute.

21.7 Summary

Some kinds of titanium oxide and titanate form bonelike apatite on their surface in a body environment and bond to living bone through the apatite layer. This can be uniformly formed as a thin layer on titanium metal and its alloys using chemical and thermal treatments. When they are formed on the solid metal, osteoconductive materials with a high fracture toughness are obtained, and when they are formed on porous metals, osteoinductive

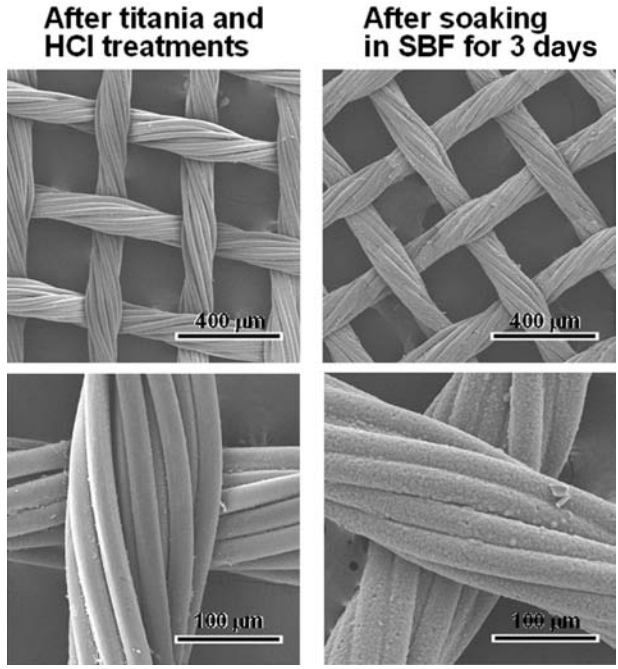

21.17 PET fabric coated with thin brookite-type titanium oxide layer and formation of bonelike apatite on its surface in SBF (Kokubo *et al.*, 2007).

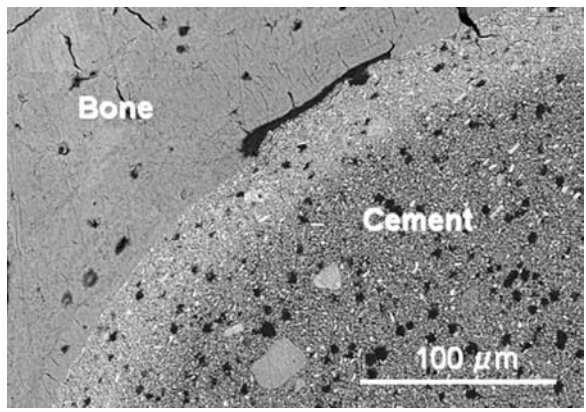

21.18 Back-scattering electron image of interface between TiO_2/PMMA cement and tibial bone of rat at 12 weeks after implantation (Kokubo *et al.*, 2007).

and osteoconductive materials with mechanical properties compatible with those of the surrounding bone are obtained. When they are formed on organic polymer fibres as a thin layer, bioactive flexible materials are then obtained. When these are mixed with PMMA cement in a fine powder, bioactive self-setting materials are obtained. These bioactive materials with different characteristics are expected to be useful as bone substitutes in various applications.

21.8 References

Fujibayashi S, Nakamura T, Nishiguchi S, Tamura J, Uchida M, Kim H-M and Kokubo T, (2001) 'Bioactive titanium: effect of sodium removal on the bone-bonding ability of bioactive titanium prepared by alkali and heat treatment', *J. Biomed. Mater. Res.*, **56**, 562–570

Fujibayashi S, Kim H-M, Neo M, Uchida M, Kokubo T and Nakamura T, (2003) 'Repair of segmental long bone defect in rabbit femur using bioactive titanium cylindrical mesh cage', *Biomaterials*, **24**, 3445–3451

Fujibayashi S, Neo M, Kim H-M, Kokubo T and Nakamura T, (2004) 'Osteoinduction of porous bioactive titanium metal', *Biomaterials*, **25**, 443–450

Kim H-M, Miyaji F, Kokubo T and Nakamura T, (1996) 'Preparation of bioactive Ti and its alloys via simple chemical surface treatment', *J. Biomed. Mater. Res.*, **32**, 409–417

Kim H-M, Miyaji F, Kokubo T and Nakamura T, (1997a) 'Apatite forming ability of alkali-treated Ti metal in body environment', *J. Ceram. Soc. Japan*, **105**, 111–116

Kim H-M, Miyaji F, Kokubo T and Nakamura T, (1997b) 'Effect of heat treatment on apatite forming ability of Ti metal induced by alkali treatment', *J. Mater. Sci.: Mater. Med.*, **8**, 341–347

Kim H-M, Miyaji F, Kokubo T, Nishiguchi S and Nakamura T, (1999) 'Graded surface structure of bioactive titanium metal prepared by chemical treatment', *J. Biomed. Mater. Res.*, **45**, 100–107

Kim H-M, Takadama H, Kokubo T, Nishiguchi S and Nakamura T, (2000a) 'Formation of a bioactive graded surface structure on Ti–15Mo–5Zr–3Al alloy by chemical treatments', *Biomaterials*, **21**, 353–358

Kim H-M, Takadama H, Miyaji F, Kokubo T, Nishiguchi S and Nakamura T, (2000b) 'Formation of bioactive functionally graded structure on Ti–6Al–4V alloy by chemical surface treatment', *J. Mater. Sci.: Mater. Med.*, **11**, 555–559

Kim H-M, Kokubo T, Fujibayashi S, Nishiguchi S and Nakamura T, (2000c) 'Bioactive macroporous titanium surface layer on titanium substrate', *J. Biomed. Mater. Res.*, **52**, 553–557

Kokubo T, Miyaji F, Kim H-M and Nakamura T, (1996) 'Spontaneous formation of bonelike apatite layer on chemically treated titanium metals', *J. Am. Ceram. Soc.*, **79**, 1127–1129

Kokubo T, Matsushita T and Takadama H, (2007) 'Titania-based bioactive materials', *J. Europ. Ceram. Soc.*, **27**, 1553–1558

Nishiguchi S, Nakamura T, Kobayashi M, Kim H-M, Miyaji F and Kokubo T, (1999a) 'The effect of heat treatment on bone-bonding ability of alkali-treated titanium', *Biomaterials*, **20**, 491–500

Nishiguchi S, Nakamura T, Kobayashi M, Kim H-M, Miyaji F and Kokubo T, (1999b) 'Enhancement of bone-bonding strength of titanium alloy implants by alkali and heat treatments', *J. Biomed. Mater. Res. (Appl. Biomater.)*, **48**, 689–696

Nishiguchi S, Kato H, Fujita H, Oka M, Kim H-M, Kokubo T and Nakamura T, (2001a) 'Titanium metals form direct bonding to bone after alkali and heat treatments', *Biomaterials*, **22**, 2525–2533

Nishiguchi S, Kato H, Neo M, Oka M, Kim H-M, Kokubo T and Nakamura T, (2001b) 'Alkali- and heat-treated porous titanium for orthopaedic implants', *J. Biomed. Mater. Res*., **54**, 198–208

Nishiguchi S, Fujibayashi S, Kim H-M, Kokubo T and Nakamura T, (2003) 'Biology of alkali-and heat-treated titanium implants', *J. Biomed. Mater. Res.*, **67A**, 26–35

Nishio K, Neo M, Akiyama H, Nishiguchi S, Kim H-M, Kokubo T and Nakamura T, (2000) 'The effect of alkali- and heat-treated titanium and apatite-formed titanium on osteoblastic differentiation of bone marrow cells', *J. Biomed. Mater. Res*., **52**, 652–661

Otsuki B, Takemoto M, Fujibayashi S, Neo M, Kokubo T and Nakamura T, (2006) 'Pore throat size and connectivity determine bone and tissue ingrowth into porous implants: three-dimensional micro-CT based structural analyses of porous bioactive titanium implants', *Biomaterials*, **27**, 5892–5900

Takadama H, Kim H-M, Kokubo T and Nakamura T, (2001a) 'An X-ray photoelectron spectroscopy study of process of apatite formation on bioactive titanium metal', *J. Biomed. Mater. Res*., **55**, 185–193

Takadama H, Kim H-M, Kokubo T and Nakamura T, (2001b) 'XPS study of the process of apatite formation on bioactive Ti–6Al–4V alloys in simulated body fluid', *Sci. Technol. Adv. Mater.*, **2,** 389–396

Takadama H, Kim H-M, Kokubo T and Nakamura T, (2001c) 'TEM-EDX Study of mechanism of bonelike apatite formation on bioactive titanium metal in simulated body fluid', *J. Biomed. Mater. Res.*, **57**, 441–448

Takemoto M, Fujibayashi S, Neo M, Suzuki J, Kokubo T and Nakamura T, (2005) 'Mechanical properties and osteoconductivity of porous bioactive titanium', *Biomaterials*, **26**, 6014–6023

Takemoto M, Fujibayashi S, Neo M, Swruki J, Matsusita T, Kokubo T and Nakamura T, (2006) 'Osteoinductive porous titanium implant: effect of sodium removal by dilute HCl treatment', *Biomaterials*, **27**, 2682–2691

Uchida M, Kim H-M, Kokubo T, Fujibayashi and Nakamura T, (2002) 'Effect of water treatment on the apatite-forming ability of NaOH-treated titanium metal', *J. Biomed. Mater. Res. (Appl. Biomater.)*, **63**, 522–530

Uchida M, Kim H-M, Kokubo T, Fujibayashi S and Nakamura T, (2003) 'Structual dependence of apatite formation on titania gels in a simulated body fluid', *J. Biomed. Mater. Res*., **64A**, 164–170

Wang X-X, Hayakawa S, Tsuru K and Osaka A, (2002) 'Bioactive titania gel layers formed by chemical treatment of Ti substrate with a H_2O_2/HCl solution', *Biomaterials*, **23**, 1353–1357

Wu J-M, Hayakawa S, Tsuru K and Osaka A, (2004) 'Low-temperature preparation of anatase and rutile layers on titanium substrates and their ability to induce *in vitro* apatite deposition', *J. Am. Ceram. Soc.*, **87**[9], 1635–1642

Yan W-Q, Nakamura T, Kobayashi M, Kim H-M, Miyaji F and Kokubo T, (1997) 'Bonding of chemically treated titanium implants to Bone', *J. Biomed. Mater. Res.*, **37**, 267–275

22

Ceramic–polymer composites

C OHTSUKI, Nagoya University, Japan

22.1 Introduction

Bone supports our body and enables us to do various kinds of motion. When a disease or an accident damages bone, quality of life (QOL) is decreased. Bone has a high ability to regenerate, so when the amount of the damaged bone tissue is relatively small, damaged tissues can spontaneously repair through the self-reconstructing ability of the tissues and the normal supply of nutrients. However, when the amount of damaged bone is too large to be repaired by self-reconstruction, the loss of bone may lead to the loss of function of related tissues. Autogenous or allogenic bone grafts are applied to repair large amounts of bone loss. In the case of autogenous bone grafts, a healthy part of the patient is damaged and the amount of bone available is limited. In the case of allogenic bone grafts, infections with viruses, bacteria and other agents may sometimes occur. Therefore, there are advantages in using artificial materials for bone repair, not only because they are free of viruses and bacteria, but also because there is less limitation on the amounts available when filling a defect. However, there are not sufficient materials that show both biological and mechanical affinity to natural bone. When artificial materials are implanted in bony defects they are generally encapsulated by a non-calcified fibrous tissue leading to them being isolated from the surrounding bone (Hulbert, 1993).

With so-called bioactive materials, contact with living bone is allowed producing strong bonds with surrounding tissues. The first discovery of the phenomena of direct bonding to living bone was reported by Hench and colleagues in the early 1970s. They reported that some glasses in the Na_2O–CaO–SiO_2–P_2O_5 system spontaneously bonded to living bone without fibrous tissue forming between the bone and the implanted materials (Hench, 1971). The ability of a material to bond to living bone is called bioactivity, and the glasses discovered by Hench *et al.* are known as Bioglass®. Since the discovery of Bioglass®, various types of ceramics, such as glass–ceramic Ceravital® containing crystalline apatite (Gross *et al.*, 1993);

sintered hydroxyapatite (HA, $Ca_{10}(PO_4)_6(OH)_2$) (Jarcho *et al.*, 1977); glass-ceramic A–W containing crystalline oxyapatite and wollastonite (Kokubo *et al.*, 1982); and glass-ceramic Bioverit® containing crystalline apatite and fluorophlogopite ($(Na, K)Mg_3(AlSi_3O_{10})F_2$) (Höland and Vogel, 1993) have been described. These ceramics are called bioactive ceramics and the phenomenon of new bone formation on the surface of the bioactive ceramics is defined as osteoconduction. Some of these ceramics are already used clinically as important bone substitutes, such as in artificial iliac crests, artificial vertebrae, artificial intervertebral discs, bone fillers, etc.

The bone-bonding behaviour of the bioactive ceramics results in tight fixation of the implanted materials against the surrounding bone, and hence reduces the risk of loosening. However, the use of these bioactive ceramics is limited due to their inferior mechanical properties, being more brittle and less formable than natural bone, and autografts and allografts are therefore still widely used. Furthermore, ceramic and metallic biomaterials generally have high elastic moduli, which increase the risk of stress-shielding phenomena resulting from irregular stresses on the surrounding bone. Figure 22.1 (Hench, 1998) summarizes the mechanical properties of bone and typical bioactive ceramics. The ceramics are essentially more brittle than bone. The bending strength of these bioactive ceramics is similar to that of bone, and their compressive strength is higher than that of bone. Although the higher mechanical strength is appropriate to the supporting function of bone in our body, higher mechanical strength allows a higher elastic modulus than that for bone. Therefore, the development of bioactive materials with low elastic modulus and high deformability is desired to give materials with appropriate mechanical performances for bone substitution.

Living bone is a composite that consists of 70 wt% of the inorganic component, hydroxyapatite (HA), and 30 wt% of the organic component, collagen (Park and Lakes, 1992), as shown in Fig. 22.2. Due to its unique

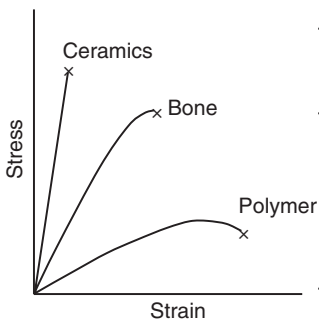

	Bending strength (MPa)	Compressive strength (MPa)	Young's modulus (GPa)
Bioglass®	42	–	35
Sintered hydroxyapatite	115–200	500–1000	80–110
Glass-ceramic A-W	215	1080	118
Cortical bone	50–150	100–230	7–30
Cancellous bone	10–20	2–12	0.05–0.5

–: not reported

22.1 Comparison of mechanical properties of bioactive ceramics and bones (data after Hench, 1998).

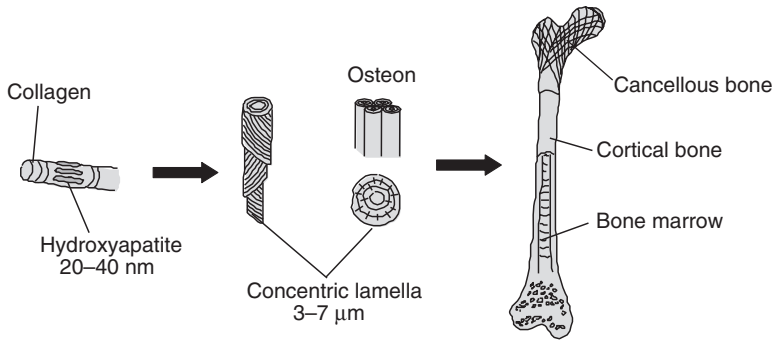

22.2 Schematic picture of structure of bone (Park and Lakes 1992).

composition and structure, natural bone shows not only high strength and high fracture toughness, but also deformability and a low elastic modulus. Therefore, one may expect that ideal bone substitute materials can be derived from organic–inorganic composites through the combination of bioactive ceramic materials and polymers with lower elastic modulus and deformability. In this chapter, bioactive composite materials that are used in clinical applications are reviewed, and then the progressive design of composite bone substitute materials is introduced.

22.2 Hydroxyapatite–polyethylene composites

22.2.1 Fabrication and microstructure

In order to obtain the artificial bone substitutes, in the 1980s Bonfield *et al.* (1981) developed a composite of HA particles with high-density polyethylene, aimed at achieving both biological and mechanical compatibility. Figure 22.3 shows an example of scanning election microscopy (SEM) images of a fractured surface of a certain type of composite consisting of HA particles in polyethylene matrix. HA particles of around 4 μm were dispersed in the polyethylene matrix. Polyethylene is typical material that shows high ductility and toughness, and has been used as the sockets of joint prostheses, but it does not show bioactivity, i.e. osteoconduction. Conversely, HA shows bioactivity, but does not show ductility. The polyethylene matrix and HA filler give ductility and bioactivity, respectively.

22.2.2 Mechanical properties

The effect of the volume fraction of HA on Young's modulus and the strain-to-failure of the polyethylene–hydroxyapatite composite has been reported (Bonfield, 1993). As HA shows higher Young's modulus than polyethylene,

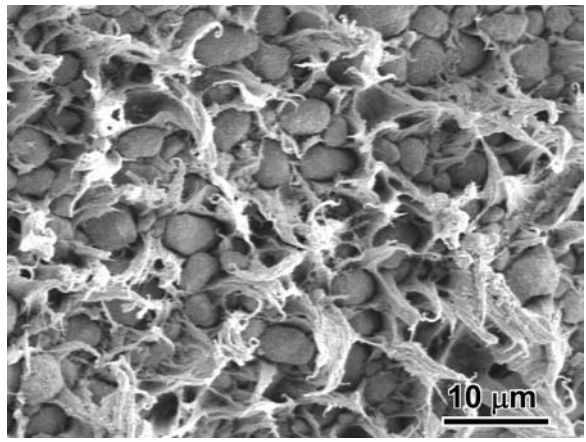

22.3 SEM images of a fractured surface of a certain type of composite consisting of HA–polyethylene.

the Young's modulus of the HA–polyethylene composites increases with increasing volume fraction of HA fillers, and approaches the value of cortical bone. The composites show ductility when they contain 40 vol% and less of HA fillers. However, the composites lose ductility and become brittle when the HA content exceeds 45 vol%. Wang *et al.* (1998a) also examined the effect of the HA particle size. The composites with smaller sized HA particles showed higher torsional moduli, tensile modulus and tensile strength, but lower strain-to-failure.

In addition to the ductility, ease in handling, in which the composite can be shaped by clinicians during the operation, is also an advantage of these materials.

22.2.3 Biological properties

HA shows bioactivity, while polyethylene does not. When polyethylene alone is implanted in the body, it is encapsulated by fibrous tissue and thus isolated from surrounding tissues. The addition of HA particles to polyethylene at amounts of greater than 20 vol% results in composites with bioactivity (Bonfield, 1993). Exposure of the HA particles on the surface of the composite is essential for the composite to show this bioactivity, since osteoconduction is established between the bioactive particles and the surrounding tissues.

22.2.4 Applications

HA–polyethylene composites with HA contents between 20 and 40 vol% show ductility and Young's moduli similar to bone, as well as bioactivity,

i.e. bone-bonding ability. The optimum composition is 40 vol% of HA particles because the fracture toughness of the composite remains significantly high with high bioactivity. The combination of HA and polyethylene gives a novel bone-repairing material matching the mechanical properties of bone. This composite material is used as a trimmable orbital implant for orbital floor fractures and for volume augmentation, and as trimmable shafts for middle ear implants.

22.2.5 Composites consisting of polyethylene and other bioactive ceramics

Composites of polyethylene and Bioglass® have also been developed (Wang *et al.*, 1998b). Bioglass® is a highly bioactive glass and can bond to both hard and soft tissues. Therefore, the composites obtained were expected to show the ability to bond not only to hard tissue, but also to soft tissue, such as soft connective tissue and cartilage. In this composite, the Young's modulus and microhardness increase with increasing Bioglass® content, although the tensile strength and fracture strain decrease. The composites form a bone-like apatite layer on their surface in the same way as bulk Bioglass® when placed in a simulated body fluid (SBF), with ion concentrations nearly equal to those of human blood plasma (Kokubo *et al.*, 1990, Kokubo and Takadama 2006). Materials that form bone-like apatite on their surfaces in SBF are expected to form a bone-like apatite layer and bond to living bone in the body. Therefore, the composite may have the potential to bond to living tissue in manner equivalent to bulk Bioglass®.

Glass-ceramic A-W (Kokubo *et al.*, 1982) is a bioactive glass-ceramic that shows high mechanical strength and high bioactivity, and hence is expected to be useful as filler in bioactive composites. Juhasz *et al.* (2003) reported a composite of polyethylene and glass-ceramic A-W. The Young's modulus, yield strength and bending strength increase and the strain-to-failure decreases with increasing glass-ceramics A-W content (Juhasz *et al.*, 2004). The composites show high apatite-forming ability in SBF and this ability increases with an increasing content of glass-ceramic A-W. By changing the types of fillers, we may tailor biological and mechanical properties of these composites.

22.3 Hydroxyapatite–poly-L-lactide (PLLA) composites

22.3.1 Fabrication and microstructure

Poly-L-lactide (PLLA) is a biodegradable polymer, and medical devices made of PLLA have been developed and are used clinically in orthopaedic, craniofacial and oral-maxillofacial surgeries. These devices still have some

problems, e.g. less rigidity than natural cortical bone, the low degradation rate of high-strength devices, and no osteoconductivity. To obtain both osteoconductivity, i.e. bioactivity, and high mechanical strength with this biodegradable polymer, combinations of PLLA with bioactive ceramic fillers have been developed. Several researchers have reported on composites in which calcium phosphate fibres or sintered HA particles are dispersed in the biodegradable organic polymers. However, these composites do not show complete resorption. Although several researchers have attempted to fabricate composites consisting of calcium phosphate and bioresorbable polymer, these composites did not satisfy the properties needed for bone fixation due to their low mechanical strength. Verheyen *et al.* (1992) tried to produce HA–PLLA composites with high mechanical strength by the as-polymerized method. However, the initial flexural strength of the composites was not adequate (about 70–90 MPa), with a short retention time (loss of 50% of flexural strength within three weeks).

Shikinami and Okuno (1999) reported the further development of HA–PLLA composites through a design processing starting from HA powders prepared without heat treatments such as calcination and sintering at high temperature. The unsintered HA powder (u-HA) was prepared using the reaction between calcium hydrogen phosphate anhydride ($CaHPO_4$) and calcium carbonate ($CaCO_3$). The starting compounds were reacted in aqueous solution at 90 °C. The chemical reaction is as follows.

$$6CaHPO_4 + 4CaCO_3 \rightarrow Ca_{10}(PO_4)_6(OH)_2 + 4CO_2 + 2H_2O$$

HA containing carbonate with a hexagonal prism shape was obtained through this process. The HA aggregates obtained were milled and sieved to obtain the particles with diameters within the range of 0.3–20 μm, with an average of about 3 μm. The resultant particles, without calcination or sintering, were denoted as u-HA. The u-HA particles were dispersed in PLLA polymer matrix, for the fabrication of the u-HA and PLLA composites. Small granules of uniformly distributed u-HA particles were first dispersed in PLLA matrix to form a mixture, which was then extruded to make a thick billet and subsequently forged into a thin billet for compression moulding. The devices were cut from the thin billet on the lathe. This processing results in high mechanical strength of the resultant composite. The measured densities of the resultant composites were similar to the theoretical value. Both the calculated and measured density values of the u-HA–PLLA composite with a u-HA fraction of 30 wt% were 1.508 g/cm^3. This implied that they contained few defects in their structure. The u-HA particles were homogeneously distributed in the matrix and were exposed on the surface by the lathe treatment to allow osteoconduction, i.e. bioactivity.

Table 22.1 Mechanical properties of u-HA–PLLA composite and PLLA (data after Shikinami and Okuno, 1999)

	Bending strength (MPa)	Bending modulus (GPa)
u-HA–PLLA	269.2	7.6
PLLA	258.5	6.5

22.3.2 Mechanical properties

The mechanical properties of u-HA–PLLA composites were reported with comparisons to those of u-HA-free PLLA bodies prepared through the same forging processing (Shikinami and Okuno, 1999). The bending strength increases with increasing u-HA powder content. It reaches approximately 270 MPa when the u-HA fraction is 30 wt%. This value is a little higher than that of the unfilled PLLA specimen, and is much higher than that of human cortical bone. The mechanical properties of the u-HA–PLLA with a u-HA fraction of 30 wt% are given in Table 22.1, in comparison with those of the u-HA-free PLLA body prepared through the same forging processing. This high strength can be achieved by the compactness of the almost complete filling through the forging process, which allows effective reinforcement of the u-HA particles in the polymer matrix. The bending modulus of the composite is a little higher than that of u-HA-free PLLA specimens, and is similar to that of human cortical bone. The Izod impact strength of the composite with a u-HA fraction of 30 wt% is much higher than that of u-HA-free PLLA or human cortical bone.

22.3.3 Biological properties

The biological properties of the u-HA–PLLA composites were examined *in vitro* and *in vivo*. The *in vitro* tests showed that the u-HA–PLLA composites formed bone-like apatite on the surface within three days after immersion in SBF (Shikinami and Okuno, 1999). This suggests that the composites have the potential to form a bone-like apatite layer on their surface and bond to living bone in the body, i.e. to show bioactivity, as bone-like apatite formation on materials in body environment is an essential condition to achieve osteoconduction after implantation in bony defects.

The *in vivo* testing using implantation in animals actually showed that u-HA–PLLA devices show higher affinity to bone than PLLA devices free from u-HA (Furukawa *et al.*, 2000a). Fibrous tissue was observed on the PLLA device, while direct contact with bone was observed for the u-HA–PLLA composite devices. This direct contact is caused by the formation of a bone-like apatite layer due to the exposure of the u-HA particles on the

surface after the machining treatment. Histological examination showed that new bone formation was also observed within 2 weeks of implantation, and that the bone gradually grew along the composite surface. No inflammatory or foreign body response was observed. These results support the finding that the u-HA–PLLA composite devices show osteoconduction, i.e. bioactivity. The bioactivity of the u-HA–PLLA composites brings early positional stability of the implant in bone. Gradual degradation of the u-HA–PLLA device implanted in the bony defect was observed to result in the replacement of the composite by bone tissue. When rods of the u-HA–PLLA composite were implanted in the subcutis, the bending strength of the rods maintained 85% of its initial value at 8 weeks and 80% at 25 weeks, although the molecular weight of the rods dropped to approximately 20% of their initial value at 25 weeks (Furukawa *et al.*, 2000b). The weight of the composite begins to decrease within 2 weeks and decreases at a significantly higher rate than the unfilled PLLA rods. In the unfilled PLLA rods, the weight begins to decrease at 4 weeks. The crystallinity of the PLLA in u-HA–PLLA composite rods gradually increased after implantation.

Generally, it takes more than 8–12 weeks for the union of a fractured human bone, although healing periods depend on many parameters, such as fracture site, stability and patient age. Fixation stability is regarded as a very important parameter during the healing period. Namely, the mechanical strength of the device should be maintained during the period to maintain stable fixation. Although the u-HA–PLLA composite showed faster degradation in bony defect than the PLLA alone made by the same method, the u-HA–PLLA composite rods can maintain their mechanical strength for the healing period of fractured bone. Therefore, this composite is useful in fixation devices for bone fractures.

The degradation tests *in vitro* showed similar degradation behaviour to that in the *in vivo* studies, suggesting that the composite degrades predominantly by hydrolysis in the body environment, as is the case for the device made from PLLA alone. Note that Shikinami and Okuno did not use sintered HA, but non-calcined non-sintered HA (u-HA) for fabrication of the composites. As these composites are used in bioresorbable devices, the complete composite body including the HA must be degraded during appropriate periods in the body. HA ceramic powder without calcination and sintering at high temperature is much more biodegradable than sintered HA. In fact, the u-HA in the near surface of the composite is lost soon after implantation, which suggests the biodegradability of u-HA. If HA particles remain because of low biodegradability, the HA particles may induce an adverse effect on the surrounding tissues, such as osteolysis. In this composite material, this adverse effect may be avoided, as the u-HA particles are biodegradable.

Shikinami *et al.* (2005) also reported the total degradation of bone-fixation devices following implantation of u-HA–PLLA rods into the femoral medullary cavities of rabbits. In the proximal medullary cavity, the rod was completely resorbed, and unbound u-HA particles were detected in and around the endosteum 5–6 years after implantation. In the distal femoral condyle, where direct contact with cancellous bone occurred, the PLLA matrix was completely resorbed after approximately 4.5–5.0 years, and holes created in the distal femoral condyle during the insertion procedure were almost filled with new bone. Almost of all of the u-HA particles were replaced with natural bone after 5.5 years, with no significant foreign body reaction. No inflammatory reaction was observed because the tissue reactions remained mild throughout the biodegradation and replacement process. On the other hand, the PLLA-only rods showed little bone conduction, and no inflammatory cells, such as neutrophils and macrophages, were seen in the subcutaneous tissue during the experimental period.

These results indicate that u-HA–PLLA composites can be replaced with bone in the distal femoral condyle, where they are in direct contact with the bone and new bone formation was anatomically necessary. In contrast, composite rods are resorbed without replacement in the proximal medullary cavity, where new bone growth is not needed.

22.3.4 Applications

The properties of u-HA–PLLA composites are quite useful for bioresorbable devices for the internal fixation of bone fractures (Fig. 22.4) (Shikinami and Okuno, 1999). This composite has many potential applications in

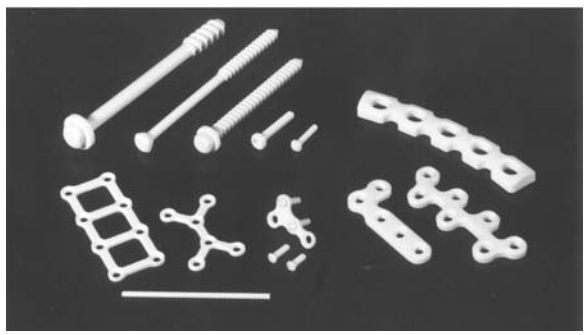

22.4 Photograph of devices made of u-HA–PLLA composite. (This photograph was taken with permission from *Biomaterials*, Vol. 20, Shikinami *et al.*, 'Bioresorbable devices made of forged composites of hydroxyapatite (HA) particles and poly-L-lactide (PLLA): Part I. Basic characteristics', pp. 859–877, Copyright Elsevier (1999).)

various clinical fields, including orthopaedic, plastic reconstructive, oral and maxillary/mandibular facial, cranial, thoracic, spinal and traumatic surgery. The major clinical application for bone substitutes is as a filler for bone defects caused by surgical removal of tumours, from trauma and so on. The required properties of bone substitutes are no toxicity, good osteoconductivity and biodegradability. Ideally, biodegradable bone substitutes should act as bone fillers that initially provide space filling with dimensional stability and then degrade at a predictable rate balanced with bone recovery. In response to these requirements, a porous composite consisting of u-HA and poly-DL-lactide (PDLLA) was fabricated. Hasegawa *et al.* (2005) examined the *in vivo* behaviour of a u-HA–PDLLA composite with an apparent density of 70% and a pore diameter of 40–480 μm (average 170 μm), with a frame consisting of 70 wt% u-HA and 30 wt% PDLLA. The compressive strength of the porous composite was 4.1 ± 0.4 MPa, which is equivalent to that of human cancellous bone. In addition, for handling in surgery, porous u-HA–PDLLA is not too hard or too brittle, and thus it can be cut using scissors or a scalpel to make shapes to fit any potential bone defect.

As well as the degradation of PDLLA, the biodegradability of the u-HA with lower initial crystallinity might contribute to the faster degradation of porous u-HA–PDLLA than porous sintered HA. Histological analysis indicated osteogenesis around and into the porous u-HA–PDLLA, with direct contact with the materials and no apparent adverse reactions. When the implant was resorbed completely, the amount of newly formed bone might reach a plateau of about 30%, which is equivalent to the percentage of cancellous bone in the intact condyle of the distal femur of the rabbit. Hence, porous u-HA–PDLLA is a desirable material for bone substitutes for reconstruction by implantation in cancellous bone in non-weight-bearing lesions. Porous u-HA–PDLLA may also be useful as a carrier for drug delivery systems and cells, as it shows not only high porosity, but also excellent biocompatibility, implying osteoconductivity and faster resorption than sintered HA.

22.4 Calcium phosphate–collagen composites

22.4.1 Collagraft®, a composite of collagen and biphasic calcium phosphate ceramic

Autograft is widely used in the orthopaedic field to fill bone defects and induce arthrodesis. The use of autogenous bone is the most popular procedure in spinal fusions. However, there are many problems, such as donor-site morbidity, pain, increased blood loss, increased use of blood products, increased surgical time, scars, possible nerve damage, wound problems and infection. The quantity of autogenous bone available is also the limiting

factor when large amounts of bone graft are needed. On the other hand, the use of allografts is limited because of their lower osteogenic potential, cost, and the risk of disease transmission. In order to solve these issues, artificial materials that are similar in structure to bone were developed through a combination of highly purified Type I collagen and biphasic calcium phosphate, that is 65% HA and 35% tricalcium phosphate ceramic. This composite is named Collagraft®. The composite was designed to give similarity to bone, as bone consists of collagen and HA. It is easy to imagine that a composite of collagen and calcium phosphate would be a useful material for bone reconstruction. The composite is approved as a substitute for autogenous bone grafts for treating acute long-bone fractures and traumatic defects when used with bone marrow and internal or internal fixation.

Chapman *et al.* (1997) reported the results of the clinical trial that was conducted to compare the safety and efficiency of the composite material consisting of purified bovine collagen, biphasic calcium phosphate ceramic and bone marrow, and autogenous bone graft obtained from the iliac crest for the treatment of fractures of long bones. They reported no significant differences between two treatment groups with respect to rates of union or functional measures. The prevalence of complications did not differ between the treatment groups, but the infection rate was higher in the patients who were managed with an autogenous graft. They concluded that the use of composite graft material was justified from the viewpoint of safety, efficiency, decreased operative time and the risk involved in obtaining an autogenous graft from the iliac crest. Walsh *et al.* (2000) also reported the effectiveness of a composite strip consisting of purified bovine collagen and biphasic calcium phosphate ceramic in an ovine lumbar fusion model. They used the composite as a bone graft substitute for spine fusion with and without the use of autologous bone marrow in an ovine lumbar spine model with pedicle screw fixation, and compared this with the autogenous corticocancellous bone grafts. The histological analysis showed that the composite was highly biocompatible and was well incorporated into the fusion mass. These results indicated that the composite acted effectively as a scaffold for new bone growth. The mineral densities in the two composite groups were significantly higher than in the autogenous bone graft group. They concluded that the composite strips, with and without bone marrow, performed as well as autogenous corticocancellous bone grafts in this ovine lumbar fusion model. These results well support the use of composites in spinal fusion with pedicle screw fixation.

As described above, the use of a composite of collagen and biphasic calcium phosphate ceramic is an effective use of substitutes for autogenous or allogenic corticocancellous or cancellous bone grafts to provide a matrix for the bone repair process.

22.4.2 Hydroxyapatite–collagen nanocomposite

An HA–collagen nanocomposite having a bone-like nanostructure was also reported by Kikuchi *et al.* (2001). This composite was synthesized through a simultaneous titration coprecipitation process started with $Ca(OH)_2$, H_3PO_4 and porcine atelocollagen. The HA–collagen composite obtained had a similar nanostructure to bone in which the *c*-axes of blade-shaped HA nanocrystals 50–100 nm in size were aligned along the collagen fibres due to chemical interaction between the HA and collagen. Thus, the composite was called an HA–collagen nanocomposite. The nanocomposite showed a bending strength of about 40 MPa and a Young's modulus of 2.5 GPa, which are similar to those measurements for autogenous bone and sufficient for bone substitutes. When the nanocomposite was implanted in beagle tibiae, the nanocomposite was incorporated into bone through remodelling processes; that is, the nanocomposite was resorbed by osteoclasts, and new bone was formed by osteoblasts after this resorption. This phenomenon looked similar to that after the implantation of autograft. These results promise the possibility that this nanocomposite consisting of HA and collagen is a useful bone substitute with high bioactivity and can replace autologous bone grafts.

22.5 Recent trends for development of bioactive composites

22.5.1 Sol–gel-derived bioactive materials

The sol–gel process is a popular process for the preparation of nanocomposites of organic and inorganic components because the process can be conducted at low temperature. It has been reported that organically modified silicates can be synthesized through hydrolysis and polycondensation of tetraethoxysilane and poly(dimethylsiloxane) (PDMS) (Mackenzie *et al.*, 1992). The resulting organic–inorganic nanocomposite has potential to show the properties of both organic and inorganic components. Based on the finding that a $CaO–SiO_2$ glass is effective in producing bioactivity (Ohtsuki *et al.*, 1992), Tsuru *et al.* (1997) synthesized PDMS–$CaO–SiO_2$ nanocomposites through a sol–gel process, and revealed that the nanocomposites obtained showed apatite-forming ability in SBF. This indicated that this type of organic–inorganic hybrid has high potential to produce novel materials with bioactivity and with flexibility from the organic substances.

Kokubo and coworkers then reported the synthesis of bioactive flexible organic–inorganic nanocomposites after a detailed examination of the synthetic conditions in the PDMS–$CaO–SiO_2–TiO_2$ system (Chen *et al.*, 2000).

As a result, bioactive nanocomposites with mechanical properties analogous to those of human cancellous bone were successfully prepared through sol–gel processing. The problems of organic modification of the $CaO–SiO_2$ components are thought to produce degradation of the hybrid materials, reducing mechanical strength (Kamitakahara *et al.*, 2004). One way to solve the issue is to reduce the components able to release reactive species after exposure to the body environment. Kokubo and coworkers synthesized the CaO-free organically modified TiO_2 nanocomposites, PDMS–TiO_2 (Kamitakahara *et al.*, 2003a) and poly(tetramethylene oxide) (PTMO)–TiO_2 (Kamitakahara *et al.*, 2003b), in order to obtain the bioactive nanocomposites that do not show degradation, and showed that these nanocomposites have apatite-forming ability in SBF if previously treated with hot water. The other method is to select biodegradable hybrids, and biodegradable nanocomposites with osteoconductivity were reported using the combination of a $CaO–SiO_2$ component with biodegradable polymer (Rhee *et al.*, 2002).

Modification of organic polymers with silanol groups, which induce heterogeneous nucleation of apatite, and calcium ions is also reported. Ohtsuki *et al.* (2002) synthesized organic–inorganic nanocomposites starting from methacryloxypropyl triethoxysilane and 2-hydroxyethylmethacrylate with the addition of a calcium salt. Ohtsuki *et al.* (2001; Miyazaki *et al.*, 2003a; Mori *et al.*, 2003) also applied organic modification with Si–OH and Ca^{2+} to a poly(methyl methacrylate) (PMMA) bone cement consisting of PMMA powder and methyl methacrylate liquid in order to induce bioactivity in the cement.

These sol–gel-derived nanocomposite materials have a potential to show flexibility and bone-bonding properties. As the biological and mechanical properties of nanocomposites can be tailored by selecting the combination of the organic and inorganic components, these nanocomposites may be useful in preparing flexible and bioactive nanocomposites.

22.5.2 Bone-like apatite/polymer composite using a biomimetic process

HA in bone is a carbonated HA with a small crystallite and low crystallinity. It has been reported that the formation of a layer consisting of bone-like apatite is an essential condition for bioactive materials to achieve direct bonding with living bone. This apatite formation can be reproduced in SBF. Body fluids and SBF are metastable solutions supersaturated with HA. A bone-like apatite layer can be formed on the surface of organic substrates in SBF or related solutions when functional groups that induce heterogeneous nucleation of apatite are introduced to the organic substrates. Coating of bone-like apatite layers through biomimetic processes has received much attention in the fabrication of novel composites with bone-bonding

properties, i.e. bioactivity, and mechanical properties analogous to those of living bone tissues. Kokubo and coworkers first proposed a biomimetic process in which a substrate is primarily soaked in SBF in contact with $CaO–SiO_2$-based glass particles and then soaked in another solution, such as SBF or a more saturated solution (Abe *et al.*, 1990). As SBF is supersaturated with respect to apatite even under normal conditions, apatite nuclei formed on the substrate surface in the primary step spontaneously grow to give an apatite layer, with consumption of the surrounding ions. Subsequently, many papers regarding the synthesis of composites of bone-like apatite and various polymers (Tanahashi *et al.*, 1994; Oyane *et al.*, 1999; Takeuchi *et al.*, 2003; Miyazaki *et al.*, 2003b; Kawai *et al.*, 2004; Kokubo *et al.*, 2004; Hosoya *et al.*, 2004) through this biomimetic process were published.

There have also been attempts to prepare apatite layers containing proteins with functionality. Recently, Uchida *et al.* (2004; Oyane *et al.*, 2005) reported a laminin–apatite composite coating on substrates to give cell-adhesive properties. In this method, a metastable calcium phosphate solution containing laminin was used. The coexistence of laminin in the formation of the apatite coating provides efficient incorporation of laminin into the apatite layer. We can prepare apatite layers containing proteins in this biomimetic process without loss of their activities, because the synthetic conditions are mild.

The biomimetic process may be a useful process with which to obtain materials with structure similar to bone.

22.6 Summary

This chapter overviewed ceramic–polymer composites, from commercially available materials to developing materials. Considering that bone mainly consists of an inorganic component, hydroxyapatite, and an organic component, collagen, the concept of the combination of inorganic and organic components is reasonable in the design of bone-repairing material. Although autografts and allografts are still widely used because of the disadvantages of the artificial materials, hydroxyapatite–polymer composites may provide attractive materials due to their similarity with the structure of bone. New types of composite biomaterials are now being investigated in the further development of bone-repairing materials.

22.7 References

Abe Y, Kokubo T and Yamamuro T (1990), 'Apatite coating on ceramics, metals and polymers utilizing a biological process', *J Mater Sci Mater Med*, **1**, 233–238.

Bonfield W (1993), 'Design of bioactive ceramic-polymer composites', in Hench L L and Wilson J, editors, *An Introduction to Bioceramics*, Singapore, World Scientific Publishing, 299–303.

Bonfield W, Grynpas M D, Tully A E, Bowman J and Abram J (1981), 'Hydroxyapatite reinforced polyethylene – a mechanically compatible implant', *Biomaterials*, **2**, 185–186.

Chapman M W, Bucholz R and Cornell C (1997), 'Treatment of acute fractures with a collagen-calcium phosphate graft material. A randomized clinical trial', *J Bone Joint Surgery (Amer)*, **79A**, 495–502.

Chen Q, Miyata N, Kokubo T and Nakamura T (2000), 'Bioactivity and mechanical properties of PDMS-modified $CaO–SiO_2–TiO_2$ hybrids prepared by sol–gel process', *J Biomed Mater Res*, **51**, 605–611.

Furukawa T, Matsusue Y, Yasunaga T, Nakagawa Y, Okada Y, Shikinami Y, Okuno M and Nakamura T (2000a), 'Histomorphometric study on high-strength hydroxyapatite/poly(L-lactide) composite rods for internal fixation of bone fractures', *J Biomed Mater Res*, **50**, 410–419.

Furukawa T, Matsusue Y, Yasunaga T, Shikinami Y, Okuno M and Nakamura T (2000b), 'Biodegradation behavior of ultra-high-strength hydroxyapatite/poly (L-lactide) composite rods for internal fixation of bone fractures', *Biomaterials*, **21**, 889–898.

Gross U M, Müller-Mai C and Voigt C (1993), 'Ceravital® bioactive ceramics', in Hench L L and Wilson J, editors, *An Introduction to Bioceramics*, Singapore, World Scientific Publishing, 105–124.

Hasegawa S, Tamura J, Neo M, Goto K, Shikinami Y, Saito M, Kita M and Nakamura T (2005), '*In vivo* evaluation of a porous hydroxyapatite/poly-DL-lactide composite for use as a bone substitute', *J Biomed Mater Res*, **75A**, 567–579.

Hench L L (1971), 'Bonding mechanism at the interface of ceramics prosthetic materials', *J Biomed Mater Res Symp*, **2**, 117–141.

Hench L L (1998), 'Bioceramics', *J Am Ceram Soc*, **81**, 1705–1728.

Höland W and Vogel W (1993), 'Machinable and phosphate glass-ceramics', in Hench L L and Wilson J, editors, *An Introduction to Bioceramics*, Singapore, World Scientific Publishing, 125–137.

Hosoya K, Ohtsuki C, Kawai T, Kamitakahara M, Ogata S, Miyazaki T and Tanihara M (2004), 'A novel covalently crosslinked gel of alginate and silane with the ability to form bone-like apatite', *J Biomed Mater Res*, **71A**, 596–601.

Hulbert S F (1993), 'The use of alumina and zirconia in surgical implants', in Hench L L and Wilson J, editors, *An Introduction to Bioceramics*, Singapore, World Scientific Publishing, 25–40.

Jarcho M, Kay J L, Gumaer R H and Drobeck H P (1977), 'Tissue, cellular and subcellular events at bone-ceramic hydroxyapatite interface', *J Bioeng*, **1**, 79–92.

Juhasz J A, Best S M, Bonfield W, Kawashita M, Miyata N, Kokubo T and Nakamura T (2003), 'Apatite-forming ability of glass-ceramic apatite-wollastonite–polyethylene composites: effect of filler content', *J Mater Sci Mater Med*, **14**, 489–95.

Juhasz J A, Best S M, Brooks R, Kawashita M, Miyata N, Kokubo T, Nakamura T and Bonfield W (2004), 'Mechanical properties of glass-ceramic A-W–polyethylene composites: effect of filler content and particle size', *Biomaterials*, **25**, 949–955.

Kamitakahara M, Kawashita M, Miyata N, Kokubo T and Nakamura T (2003a), 'Apatite formation on CaO-free polydimethylsiloxane(PDMS)–TiO_2 hybrids', *J Mater Sci Mater Med*, **14**, 1067–1072.

Kamitakahara M, Kawashita M, Miyata N, Kokubo T and Nakamura T (2003b), 'Apatite-forming ability and mechanical properties of CaO-free poly(tetramethylene oxide) (PTMO)–TiO_2 hybrids treated with hot water', *Biomaterials*, **24**, 1357–1363.

Kamitakahara M, Kawashita M, Miyata N, Kokubo T and Nakamura T (2004), 'Degradation of bioactive polydimethylsiloxane–CaO–SiO_2–TiO_2 and poly(tetramethylene oxide)–CaO–TiO_2 hybrids in a simulated body fluid', *J Am Ceram Soc*, **87**, 235–239.

Kawai T, Ohtsuki C, Kamitakahara M, Miyazaki T, Tanihara M, Sakaguchi Y and Konagaya S (2004), 'Coating of an apatite layer on polyamide films containing sulfonic groups by a biomimetic process', *Biomaterials*, **25**, 4529–4534.

Kikuchi M, Itoh S, Ichinose S, Shinomiya K and Tanaka J (2001), 'Self-organization mechanism in a bone-like hydroxyapatite/collagen nanocomposite synthesized *in vitro* and its biological reaction *in vivo*', *Biomaterials*, **22**, 1705–1711.

Kokubo T and Takadama H (2006), 'How useful is SBF in predicting *in vivo* bone bioactivity?', *Biomaterials*, **27**, 2907–2915.

Kokubo T, Shigematsu M, Nagashima Y, Tashiro M, Nakamura T, Yamamuro T and Higashi S (1982), 'Apatite- and wollastonite-containing glass-ceramics for prosthetic application', *Bull Inst Chem Res Kyoto Univ*, **60**, 260–268.

Kokubo T, Kushitani H, Sakka S, Kitsugi T and Yamamuro T (1990), 'Solutions able to reproduce *in vivo* surface-structure changes in bioactive glass-ceramic A-W', *J Biomed Mater Res*, **24**, 721–734.

Kokubo T, Hanakawa M, Kawashita M, Minoda M, Beppu T, Miyamoto T and Nakamura T (2004), 'Apatite-forming ability of alginate fibers treated with calcium hydroxide solution', *J Mater Sci Mater Med*, **15**, 1007–1012.

Mackenzie J D, Chung Y J and Hu Y (1992), 'Rubbery ormosils and their applications', *J Non-Cryst Solids*, **147/148**, 271–279.

Miyazaki T, Ohtsuki C, Kyomoto M, Tanihara M, Mori A and Kuramoto K (2003a), 'Bioactive PMMA bone cement prepared by modification with methacryloxy-propyltrimethoxysilane and calcium chloride', *J Biomed Mater Res*, **67A**, 1417–1423.

Miyazaki T, Ohtsuki C, Akioka Y, Tanihara M, Nakao J, Sakaguchi Y and Konagaya S (2003b), 'Apatite deposition on polyamide films containing carboxyl group in a biomimetic solution', *J Mater Sci Mater Med*, **14**, 569–574.

Mori A, Ohtsuki C, Sugino A, Kuramoto K, Miyazaki T, Tanihara M and Osaka A (2003), 'Bioactive PMMA-based bone cement modified with methacryloxypropyltrimethoxysilane and calcium salts – effects of calcium salts on apatite-forming ability', *J Ceram Soc Japan*, **111**, 738–742.

Ohtsuki C, Kokubo T and Yamamuro T (1992), 'Mechanism of apatite formation on CaO–SiO_2–P_2O_5 glasses in a simulated body fluid', *J Non-Cryst Solids*, **143**, 84–92.

Ohtsuki C, Miyazaki T, Kyomoto M, Tanihara M and Osaka A (2001), 'Development of bioactive PMMA-based cement by modification with alkoxysilane and calcium salt', *J Mater Sci Mater Med*, **12**, 895–899.

Ohtsuki C, Miyazaki T and Tanihara M (2002), 'Development of bioactive organic–inorganic hybrid for bone substitutes', *Mater Sci Eng C*, **22**, 27–34.

Oyane A, Minoda M, Miyamoto T, Takahashi R, Nakanishi K, Kim H M, Kokubo T and Nakamura T (1999), 'Apatite formation on ethylene-vinyl alcohol copolymer modified with silanol groups', *J Biomed Mater Res*, **47**, 367–373.

Oyane A, Uchida M and Ito A (2005), 'Laminin-apatite composite coating to enhance cell adhesion to ethylene–vinyl alcohol copolymer', *J Biomed Mater Res*, **72A**, 168–174.

Park J B and Lakes R S (1992), *Biomaterials*, *2nd Ed*., New York, Plenum Press, 185–222.

Rhee S H, Choi J Y and Kim H M (2002), 'Preparation of a bioactive and degradable poly(epsilon-caprolactone)/silica hybrid through a sol–gel method', *Biomaterials*, **23**, 4915–4921.

Shikinami Y and Okuno M (1999), 'Bioresorbable devices made of forged composites of hydroxyapatite (HA) particles and poly-L-lactide (PLLA): Part I. Basic characteristics', *Biomaterials*, **20**, 859–877.

Shikinami Y, Matsusue Y and Nakamura T (2005), 'The complete process of bioresorption and bone replacement using devices made of forged composites of raw hydroxyapatite particles/poly L-lactide (F-u-HA/PLLA)', *Biomaterials*, **26**, 5542–5551.

Takeuchi A, Ohtsuki C, Miyazaki T, Tanaka H, Yamazaki M and Tanihara M (2003), 'Deposition of bone-like apatite on silk fiber in a solution that mimics extracellular fluid', *J Biomed Mater Res*, **65A**, 283–289.

Tanahashi M, Yao T, Kokubo T, Minoda M, Miyamoto T, Nakamura T and Yamamuro T (1994), 'Apatite coating on organic polymers by a biomimetic process', *J Am Ceram Soc*, **77**, 2805–2808.

Tsuru K, Ohtsuki C, Osaka A, Iwamoto T and Mackenzie J D (1997), 'Bioactivity of sol–gel derived organically modified silicates, Part I: *In vitro* examination', *J Mater Sci Mater Med*, **8**, 157–161.

Uchida M, Oyane A, Kim H M, Kokubo T and Ito A (2004), 'Biomimetic coating of laminin–apatite composite on titanium metal and its excellent cell-adhesive properties', *Adv Mater*, **16**, 1071–1074.

Verheyen C C P M, de Wijn J R, van Blitterswijk C A and de Groot K (1992), 'Evaluation of hydroxyapatite/poly(L-lactide) composites: mechanical behavior', *J Biomed Mater Res*, **26**, 1277–1296.

Walsh W R, Harrison J, Loefler A, Martin T, Van Sickle D, Brown M K C and Sonnabend D H (2000), 'Mechanical and histologic evaluation of Collagraft (R) in an ovine lumbar fusion model', *Clinical Orthopaedics and Related Research*, **375**, 258–266.

Wang M, Joseph R and Bonfield W (1998a), 'Hydroxyapatite–polyethylene composites for bone substitution: effects of ceramic particle size and morphology', *Biomaterials*, **19**, 2357–2366.

Wang M, Hench L L, and Bonfield W (1998b), 'Bioglass®/high density polyethylene composite for soft tissue applications: preparation and evaluation', *J Biomed Mater Res*, **42**, 577–586.

23

Dental ceramics

V P THOMPSON and E D REKOW, New York University, USA

23.1 Introduction

Dental ceramics have evolved to include glasses (porcelains), glass-ceramics (covered in Chapter 24) and structural ceramics (aluminas and zirconia). These types of ceramics are utilized in a wide range of dental applications ranging from inlays and onlays, crowns and bridges, to metal implant fixture abutments and most recently to one piece all-ceramic implants.

Dental ceramics and in particular porcelains are principally utilized because of their esthetic qualities. However, highly esthetic porcelains are generally weak and must be combined with structural support, either metal or high-strength ceramics to function as posterior crowns or bridges. Glass-ceramics are an alternative approach to providing esthetics and strength for restorations in the anterior (front) of the mouth with studies of use in the posterior dentition being conducted. Structural ceramics suffer from a lack of translucency and must be of white color to be considered. Alumina and zirconia-based structural ceramics are utilized as crown cores and bridge frameworks but require application of an esthetic veneering ceramic for clinical use in replacement of tooth structure.

Dental ceramics and their composition and fabrication will be discussed below. The physical properties of these ceramics will be presented and how these relate to clinical findings will be overviewed. What is known about damage mode and damage accumulation in model structures of dental ceramic applications will be detailed as well as how these relate to clinical findings. Finally, future developments in dental ceramics will be proposed.

23.2 Types of dental ceramics

23.2.1 Dental porcelains

Dental porcelains are classified by manufacturers according to their firing temperatures with the following being a typical classification (Anusavice, 2003):

- High fusing – 1300 °C (2372 °F)
- Medium fusing – 1101–1300 °C (2013–2072 °F)
- Low fusing – 850–1100 °C (1562–2012 °F)
- Very low fusing – <850 °C (1562 °F)

High and medium fusing porcelains are primarily utilized for denture teeth. Low fusing porcelains have been used extensively for metal ceramic retainer (MCR) restorations (crowns and bridges) while very low fusing porcelains have been introduced to extend the range of metal alloys to which the porcelain can be fired, to lessen shrinkage stresses, and to try and reduce opposing tooth enamel wear (al-Hiyasat *et al.*, 1998; Clelland *et al.*, 2003; Imai *et al.*, 2000).

MCR veneering porcelains make use of extensive fritting and network modifiers to lower the fusion temperature. Very low fusing porcelains (Finesse, Dentsply Ceramco, Burlington, NJ, US; Optec OSP, Jeneric/Pentron, Wallington, CN, US) have been developed for application to lower melting alloys, reduction in shrinkage stresses and for making facial veneers for teeth with less interaction with refractory dies materials or for veneering of glass-ceramic crown core porcelains. The typical composition range for a low fusing porcelain is given in Table 23.1. Very low fusing porcelains often need to stabilize the leucite structure in tetragonal form and this is often accomplished by ion exchange (Denry, 1998 #335). The composition range for a fine grained leucite containing very low fusing porcelain is presented in Table 23.2.

Prior to the 1960s the dental use of ceramics was in the form of inlays or anterior crowns (usually central incisors) where feldspathic porcelain was utilized (Table 23.1) or for denture teeth. The feldspathic porcelain provided a translucency and coloration that closely approximated tooth structure in appearance. These restorations were constructed by layering and firing glass frits of varying translucency and color and depended upon the

Table 23.1 Typical composition of a leucite porcelain (US Patent # 5944884) for dental casting alloy veneering

Component	Amount (wt%)
SiO_2	57–66
Al_2O_3	7–15
K_2O	7–15
N_2O	7–12
Li_2O	0.5–3
CaO	0–3
MgO	0–7
F	0–4
CeO_2	0–1

Table 23.2 Compositional range for a rubidium stabilized tetragonal leucite containing very low fusing porcelain for veneering dental alloy and glass-ceramic cores (US Patent # 6120591)

Component	Amount (wt%)
SiO_2	57–65
Al_2O_3	6–12
K_2O	7–15
Na_2O	6–12
Li_2O	0.3–3
B_2O_3	0–5
BaO	0–2
CaO	0–3
MgO	0–4
Rb_2O	0.5–10
F	0–2
P_2O_5	0–3
CeO_2	0–1
Sb_2O_3	0–1
Acidic flux[a]	0.8–10
Alkaline flux[b]	6.3–15
Additives[c]	0–5

[a] $B_2O_3 + F + P_2O_5$.
[b] $Li_2O + Na_2O$.
[c] Pigments, opacifying agents, fluorescing agents.

skill of the dental technician to provide form and fit coupled with an aesthetic result. This technology dates to the work of Charles Lands in 1903 and is referred to as a porcelain jacket crown. The low flexural strength of the porcelain (<60 MPa), its low fracture toughness (<0.9) and slow crack growth led to increasing and unacceptably high failure rates with time for the anterior jacket crowns. Only non-adhesive cements (typically zinc phosphate) with high solubility where available and the majority of crown failures occurring on the lingual slope of the crowns in a typical horseshoe pattern which could be related to combination of cement solubility and slow crack growth in the porcelain. Today, porcelain veneers (described below) are fabricated in much the same way but because they are fused to an underlying structurally stronger core, failure rates are reduced by an order of magnitude. A typical porcelain-veneered crown configuration is shown in Fig. 23.1. The core can be metal, glass-ceramic or structural ceramic.

23.2.2 Porcelains for veneering metal

Since the 1960s the use of dental porcelains has increased rapidly with the development of MCRs for crowns and bridges where a thin metal crown

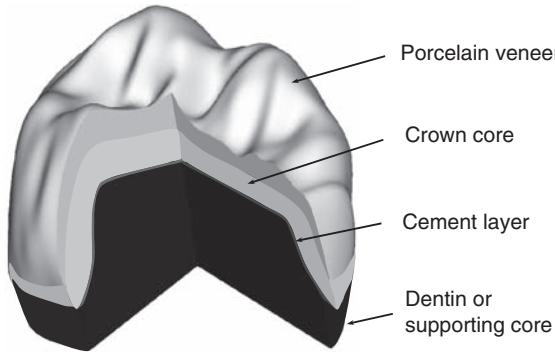

23.1 Schematic of maxillary first molar crown configuration. Note that the crown core can be made by casting an alloy, slip applied alumina or CAD/CAM alumina or Y-TZP while the veneer is porcelain (or hot-pressed glass ceramic) specifically CTE matched to the core.

core or bridge framework is veneered with porcelain. This requires application of thin opaque porcelain to mask the metal color followed by application of 'body' porcelain to simulate dentin and more translucent 'enamel' porcelain for final contours. More than 80% of all such restorations placed in the US are of this type. Weinstein *et al.* (1962a,b) pioneered the development of high casting temperature alloys with controlled surface oxides to which could be fired a high thermal coefficient of expansion (CTE) porcelain. Modifications to the casting alloys and to the porcelains were necessary; in particular, the inclusion of leucite into the feldspathic porcelain to control the CTE. Leucite is a potassium aluminum silicate mineral (K_2O–AI_2O_3–$4SiO_2$) with a high coefficient of thermal expansion and a polymorphic transformation accompanied by a large volume change. When combined, these characteristics produce a large contraction when the material is cooled from high temperatures, leaving the ceramic in compression (Mackert *et al.*, 1986, 2003). The large volume contraction of leucite has been used to advantage in dental MCR systems to raise the inherently low thermal expansion of feldspathic glasses to make them compatible with MCR alloys. Over the last 40 plus years both the alloys and the porcelains have been refined to make the MCR the standard for crown and bridge restorations (Rosenstiel *et al.*, 2006).

Recent research has been focused on hot-pressing of glass-ceramics directly to metal or metal with opaque porcelain applied which allows full contour wax patterns to be prepared, invested, burned out and the glass-ceramic pressed (Helvey, 2002; Schweitzer *et al.*, 2005; Stappert *et al.*, 2004). This avoids the hand building and firing of multiple layers of porcelain with necessary compensation for the very significant firing shrinkage (>20%)

which occurs. There are no clinical reports on the effectiveness of this hot-pressing to metal technique.

23.2.3 High-strength porcelains for dental restorations

Traditional dental porcelains are feldspathic glasses modified with kaolin and quartz, and differ from most domestic porcelains in the high translucency required to simulate tooth structure. Color frits to simulate tooth color (primarily in the yellow-orange range) are added. As noted above increases in the CTE are usually achieved by adding frits containing high amounts of leucite. Generally strength increases in dental porcelains has been achieved through addition of crystalline phase(s). The natural extension of MCR porcelains has been to increase the leucite content for application outside metal veneering where the high CTE would be less of a concern. Typically these have higher leucite content (in the range of 30–45 vol%) to achieve the increase properties. One such porcelain has 45% leucite (Optec HSP Jeneric/Pentron, Wallingford, CN, US) (Piche *et al.*, 1994). An alternative to leucite is to add sanidine ($KAlSi_3O_8$) which contributes both strength and some opacity to the porcelain (Vita Mark II, Vita Zahnfabrik, Bad Säckingen, DE) (Table 23.3). These higher-strength porcelains have been utilized for a dental office 'chairside' CAD/CAM system (CEREC, Sirona, Bensheim, DE) fabrication of inlay/only and anterior crown restorations. Both sol–gel and ion exchange firing techniques have been proposed to control composition.

23.3 Monolithic crown ceramics

Both the hot-pressing technique and CAD/CAM (computer-aided design/manufacturing) technology have spurred the development of higher strength and toughness porcelains. Pressable ceramics were introduced the mid-1980s with a glass-ceramic embodiment (Dicor, Dentsply International, York, PA, US) (Table 23.2) where a fluoroimica glass phase was matured with heat treatment after hot-pressing. Dicor appeared to have excellent physical properties and was designed to have material properties matching those of enamel. Unfortunately, when extended to posterior tooth crowns clinically unacceptable failure rates (>4% annually) occurred (Malament and Socransky, 1999; Malament *et al.*, 2003; Sjögren *et al.*, 1999b). An alternative material (IPS Empress, Ivoclar, Schann, Liechtenstein) with a high leucite content (~36%) (Guazzato *et al.*, 2004a), although of less strength, has enjoyed better success in the posterior dentition (El-Mowafy and Brochu, 2002; Fradeani and Redemagni, 2002; Sjögren *et al.*, 1999a). The reasons for this difference are not fully understood. Overall, clinicians are hesitant to employ monolithic hot-pressed glass-ceramic or CAD/CAM

Table 23.3 Dental ceramic material properties

Material	Class	Strength (Sd) (MPa)	*E* (GPa)	*H* (GPa)	*T* (K_{IC}) (MPa $m^{1/2}$)
Materials for monolithic crowns					
Dicor MGC	Glass-ceramic	70.3 (Tinschert *et al.*, 2000) 127 (Grossman, 1991)	50–70 (Quinn and Lloyd, 2001)		1.1–1.6 (Grossman, 1991; Wohlwend *et al.*, 1989)
IPS Empress	Porcelain	83.9 (Tinschert *et al.*, 2000) 160 (Lawn *et al.*, 2004b) 106 (17) 112 (Holand *et al.*, 2000)	67 (Lawn *et al.*, 2004a) 65 (Guazzato *et al.*, 2004a)	5.6 (Lawn *et al.*, 2004a) 6.5 (Guazzato *et al.*, 2004a)	1.4 (Lawn *et al.*, 2004a) 1.2 (Guazzato *et al.*, 2004a) 1.3 (Holand *et al.*, 2000)
Core materials					
Empress 2	Glass-ceramic	420 (Lawn *et al.*, 2004a) 306 (29) 400 (Holand *et al.*, 2000)	104 (Guazzato *et al.*, 2004a) (Lawn *et al.*, 2004a) 105	5.5 (Lawn *et al.*, 2004a) 5.3(0.2)	2.9 (Lawn *et al.*, 2004a) 2.9 (Guazzato *et al.*, 2004a) 3.3 (Holand *et al.*, 2000)
InCeram Al	Alumina (infiltrated)	429.3 (Guazzato *et al.*, 2002) 550 (Lawn *et al.*, 2004a) 520 (Guazzato *et al.*, 2004a) 600 (Guazzato *et al.*, 2002)	270 (Guazzato *et al.*, 2002) (Lawn *et al.*, 2004a) 257 (Guazzato *et al.*, 2004a) 267 (Guazzato *et al.*, 2002)	12.3 (Guazzato *et al.*, 2002) (Lawn *et al.*, 2004a) 11.5 (Guazzato *et al.*, 2002)	3.0 (Lawn *et al.*, 2004a) 3.2 (Guazzato *et al.*, 2004a) 3.2 IS (Guazzato *et al.*, 2002) 2.7 IF (Guazzato *et al.*, 2002)

Table 23.3 Continued

Material	Class	Strength (Sd) (MPa)	*E* (GPa)	*H* (GPa)	*T* (K_{IC}) (MPa $m^{1/2}$)
InCeram Al – dry pressed	Alumina (infiltrated)	440 (Guazzato *et al.*, 2004a)	265 (Guazzato *et al.*, 2004a)	11 (Guazzato *et al.*, 2004a)	3.6 (Guazzato *et al.*, 2004a)
InCeram Al – slip	Alumina (infiltrated)	594 (Guazzato *et al.*, 2004a)	265 (Guazzato *et al.*, 2004a)	11 (Guazzato *et al.*, 2004a)	4.4 (Guazzato *et al.*, 2004a)
Procera Al	Alumina (infiltrated)	687 (Wagner and Chu, 1996) 469 (Zeng *et al.*, 1998) 472 (Wen *et al.*, 1999) 450 (De Jager *et al.*, 2006)	400 (De Jager *et al.*, 2006)		4.48 (Wagner and Chu, 1996) 3.84 (Wen *et al.*, 1999)
InCeram Z	Zirconia (infiltrated)	440 (Lawn *et al.*, 2004a) 580 (Guazzato *et al.*, 2004b) 620 (Guazzato *et al.*, 2002)	245 (Lawn *et al.*, 2004a) 242 (Guazzato *et al.*, 2004b, Guazzato *et al.*, 2002) 242 (9.6)	13.1(Lawn *et al.*, 2004a) 10.0 (Guazzato *et al.*, 2002)	3.5 (Lawn *et al.*, 2004a) 3.2 4.0 IS (Guazzato *et al.*, 2002) 3.0 IF (Guazzato *et al.*, 2002) 4.0 (Guazzato *et al.*, 2004b)
Inceram Z – slip	Zirconia (infiltrated)	630 (Guazzato *et al.*, 2004b)	240 (Guazzato *et al.*, 2004b)	10.5 (Guazzato *et al.*, 2004b)	4.8 (Guazzato *et al.*, 2004b)
Procera Z	Zirconia	1400 (Lawn *et al.*, 2004a)	205 (Lawn *et al.*, 2004a)	12.0 (Lawn *et al.*, 2004a)	5.4 (Lawn *et al.*, 2004a)
Lava	Zirconia	786 (White *et al.*, 2005) 1100 (Kim *et al.*, 2007b)	224.4 (White *et al.*, 2005) 210 (Kim *et al.*, 2007b)	13.5 (Kim *et al.*, 2007b)	

DC-Zircon	Zirconia	1150 (Guazzato *et al.*, 2004c)	220 (Guazzato *et al.*, 2004c) 210 (De Jager *et al.*, 2006)		7.4 (De Jager *et al.*, 2006)
DCS Pecident	Zircionia	840 (Guazzato *et al.*, 2004b)	220 (Guazzato *et al.*, 2004b)	12 (Guazzato *et al.*, 2004b)	7.4 (Guazzato *et al.*, 2004b)
Prozyr	Zirconia (Y-TZP – hipped)	1400 (Lawn *et al.*, 2004a)	205 (Lawn *et al.*, 2004a)	12.0 (Lawn *et al.*, 2004a)	5.4 (Lawn *et al.*, 2004a)
Porcelains/veneers					
Cerec Mk 2	Porcelain	86.3 (Tinschert *et al.*, 2000) 130 (Lawn *et al.*, 2004a)	68 (Lawn *et al.*, 2004a)	6.4 (Lawn *et al.*, 2004a)	0.92 (Lawn *et al.*, 2004a)
Vita Mk II	Porcelain	130 (Lawn *et al.*, 2004a)	68 (Lawn *et al.*, 2004a)	6.4 (Lawn *et al.*, 2004a)	0.92 (Lawn *et al.*, 2004a)
Vita Mk 68	Porcelain	82.7 (Tinschert *et al.*, 2000)			
Vita Alpha Core	Porcelain	131.0 (Tinschert *et al.*, 2000)			
Vita Alpha Dentin	Porcelain	60.7 (Tinschert *et al.*, 2000)			
Vita Alpha	Porcelain	95 (Guazzato *et al.*, 2004c)	60 (Guazzato *et al.*, 2004c)		0.9 (Guazzato *et al.*, 2004c)
Vita D	Porcelain for zirconia	95 (Guazzato *et al.*, 2004c)	64 (Guazzato *et al.*, 2004d)		0.9 (Guazzato *et al.*, 2004d)

Note: IS = infiltrated slip, IF = infiltrated dry pressed.

porcelains for crowns in high-stress areas of the mouth such as for molar crowns based upon the above clinical findings.

23.4 Structural ceramic applications in dentistry

Strength requirements fostered by a growth in patient requests for more esthetic and metal-free restorations throughout the mouth have pushed dental ceramics manufacturers to bring to market a number of structural ceramics and a wide range of techniques for their fabrication for use in dental crown and bridge applications. Most recently developments in three dimensional scanning techniques and maturation in CAD/CAM technology has spurred the growth of structural ceramic applications in dentistry. What has evolved is a range of methods to fabricate structural ceramic cores to replace metal substructures for crown and bridge restorations. Below are some descriptions of the systems. Bear in mind that each system requires veneering porcelain to achieve an esthetic restoration with the requirement that each porcelain's CTE must be closely matched to the core.

23.4.1 Slip-cast structural ceramics for glass infiltration

Use of slip-cast ceramics in dental applications depended upon reliable techniques to provide an oversized die to which an aqueous slip of alumina could be applied. This concept was brought to market through research by Vita Zahnfabrik (Bad Säckingen, DE) in the 'In-Ceram' process. An alumina-based slip is applied to a gypsum refractory die designed to shrink during firing. The alumina content of the slip is more than 90%, with a particle size between 0.5 and 3.5 μm. After being fired for 4 hours at 1100 °C, the porous alumina crown core (coping) is shaped and infiltrated with a lanthanum-containing glass during a second firing at ~1150 °C for a number of hours. After removal of the excess glass, the restoration is veneered with matched CTE veneer porcelain (Probster and Diehl, 1992). This processing technique is unique in dentistry and leads to a high-strength material owing to the presence of densely packed alumina particles and the reduction of porosity. Two modified core compositions for the In-Ceram technique have been recently introduced. In-Ceram Spinel as its major crystalline phase contains a magnesium spinel ($MgAl_2O_4$) but retains traces of alpha-alumina. The spinel improves the translucency of the core and final restoration. In-Ceram Zirconia contains partially stabilized (12% CeO_2) tetragonal zirconia and alumina in nearly equal amounts (Guazzato *et al.*, 2004b). A variety of alumina-glass dental composites can be prepared by the glass-infiltration process. However, research has shown that the fracture toughness of the composites is relatively insensitive to the volume fraction of alumina in the range investigated (Wolf *et al.*, 1993).

23.4.2 Dry-pressed structural ceramic for glass infiltration

Utilizing binders with alumina particles is it becomes possible to manufacture blocks of alumina suitable for CAD/CAM milling (Vita Zahnfabrik). The CAD/CAM software mills and oversize crown core or bridge framework. The machined core is then sintered as above and glass infiltrated. In-Ceram Alumina and In-Ceram Zirconia are both available in dry pressed form and only differ slightly in composition from the slip-cast variety (Guazzato *et al.*, 2004b). The machined and sintered material is then lanthan glass infiltrated as above.

23.4.3 CAD/CAM milled structural ceramics

Two approaches have evolved for CAD/CAM of structural ceramics. Milling partially sintered blocks while allowing for ~25% shrinkage and then sintering to full density, the first of these being the Procera AllCeram system (Nobel Biocare, Stockholm, Sweden) (Ottl *et al.*, 2000) or, milling of full density hot isostatically pressed (HIP) 5 wt% Y_2O_3–TZP (DCS Precident System, Allschwil, CH). The majority of the systems on the market utilize the former approach for both Y-TZP (zirconia) (Cercon, Dentsply International, York, PA, US; LAVA, 3M/ESPE, St Paul, MN, US; Procera Zirconia, Nobel Biocare, Mahwah, NJ, US; Vita Zirconia, Bad Säckingen, DE; ZirCAD, Ivoclar, Schaan, Leichtenstein; and others) and alumina (Procera Alumina, Nobel Biocare).

The laboratory scanning and milling approach for partially sintered structural ceramics was developed by Nobel Biocare using alumina. This alumina has a grain size of 2–5 μm and after sintering at 1400 °C for 8 hours achieves 99% density (Wen *et al.*, 1999). Based upon higher than expected failure rates for alumina framework bridges (In-Ceram) the manufacturer moved to the Y-TZP for bridge frameworks as have the other manufacturers (Olsson *et al.*, 2003; Vult von Steyern *et al.*, 2001). Note that the fracture toughness for In-Ceram alumina is higher than for high density alumina while the flexural strength is lower (Wen *et al.*, 1999) which helped influence the decision to move to Y-TZP for bridge frameworks.

What have evolved are milling centers (almost all using various Y-TZPs) at selected sites in a given country or region. Dental laboratories use laser scanners to digitize dies or dental impressions. The information is sent via the Internet to the milling centers. The crown cores or bridge frameworks (up to 16 connected units are possible) are manufactured and then returned to the laboratory where dental veneering porcelain is applied to full contour and occlusion either by the usual hand stacking or now in small numbers by hot pressing. A recent excellent review of partially stabilized zirconia as

a structural ceramic for dental applications has recently been published (Kelly and Denry, 2007).

23.5 Mechanical properties and clinical performance of dental ceramic restorations

Strength, elastic modulus and fracture toughness values for a range of dental ceramics are presented in Table 23.3. The question remains as to whether these properties are sufficient, either alone or in combination, to reliably predict long-term clinical performance. Review of the performance of posterior all-ceramic crowns (Table 23.4) provides a sufficient clinical database with which to relate physical properties and what is know of failure modes that are operational *in vitro*. Posterior crowns, despite being fabricated from very strong core materials still fail at rates greater than material-related failures of MCR crowns. Y-TZP core crowns fail in different ways from alumina core crowns (Donovan, 2005; Rekow, 2006; Walter *et al.*, 2006). What factors are responsible for these differences?

23.5.1 Clinical performance of all-ceramic posterior crowns

Crown failures are frustrating for the clinician and patient alike. Failure rates determined in clinical studies of all-ceramic posterior crowns are summarized in Table 23.3. In general, across the spectrum of material classes, posterior crowns fail at a higher rate than anterior crowns (Kern, 2006). Problems with early monolithic ceramics used for posterior crowns motivated changes that led to a substantial improvement in clinical performance with layered, veneered core ceramics.

23.5.2 Fracture modes

Determining the cause of crown failure is exceedingly difficult. Patients may not be aware of a fracture when the crown remains intact; even when bulk fracture occurs, they may not present to the clinic immediately, which may complicate determination of the cause and initiation site and pieces of the fractured crown may be lost. Furthermore, the definition of failure is not always consistent throughout the literature. Is a chip in the veneering porcelain a fracture? Is it a clinical failure? Here, we will define fractures and failures as (1) pieces of the crown separating, including chips in the veneer, (2) cracks that penetrate the crown even though it may remain held in place by the adhesive cement and (3) bulk fracture.

Historically, it was believed that all crown fractures initiated at the cementation surface of the crown, propagated through the bulk of the material, leading to bulk fracture (Kelly *et al.*, 1989, 1990; Thompson *et al.*,

Table 23.4 Clinical studies and failure pecentage for all-ceramic molar crowns

Material	Total number of crowns	Number of molar crowns	Max time of study (month)	Failures on molar crowns (%)	Reference
Dicor	1444	339	177	26–52%[c]	Malament and Thompson (1999)
IPS Empress	78	37	59	10.8	Lehner *et al.* (1997); El-Mowafy and Brochu (2002)
	110	42	43	7	Sjögren *et al.* (1999a)
	125	32[a]	132	15.6[a]	Fradeani and Redemagni (2002)
Empress 2	27	Not reported	38	0	Zimmer 2004 from Kern (2006)
	155	Not reported	37	0	Edlehoff 2005 from Kern, (2006)
	20	3	24	0	Taskonak and Sertgoz (2006)
InCeram Al	95	68[a]	30	1.5[a]	Pröbster (1996)
	457	Not reported	72	5.0[b]	Rinke 1997 from Kern (2006)
	223	64	36	6.2	McLaren and White (2000)
	80	21	48	4.7	Haselton *et al.* (2000)
	546	192	70	0.8	Segal (2001)
In-Ceram Al and Sp	43	15	39	5.4	Bindl Mormann, (2002)
Procera Al	100	25	60	7.3	Odén *et al.* (1998)
	87	31	120	7[b]	Odman 2001
zirconia				Approx 7	(Anonymous, 2006)

[a] Molars and premolars reported together, unable to separate molars only from data presented.
[b] All crowns; failures on molar crowns was not reported separately.
[c] 52% on maxillary first molar, 51% on mandibular second molar, 33% on maxillary second molar, 26% on mandibular first molar.

1994). Examining failed crowns, fractographic analysis searches for classic mirror-mist-hackle patterns (Kelly *et al.*, 1989; Scherrer *et al.*, 2006) to ascertain the origin of failure from crack propagation patterns. Fractography has identified failure initiating cracks at the occlusal surface in Cerestore, Procera alumina, and In-ceram zirconia posterior crowns (Scherrer, 2003; Scherrer *et al.*, 2006). Real-time video capture of crack evolution in laboratory studies of model flat layer systems confirms these findings (Deng *et al.*, 2002).

Cracks predominately initiate in two areas: far-field cracks which develop at the cementation surface or near-field cracks which develop in close proximity to an applied load (e.g. the opposing tooth cusp) at or near the occlusal surface. In monolithic crowns (Fig. 23.2a), the far-field cracks (flexural radial cracks), initiate at the cementation surface and with continued loading, propagate through the crown, resulting in bulk fracture. In core–veneer crowns (Fig. 23.2b), the radial cracks can initiate either at the cementation surface of the core or in the veneer initiating from the veneer–core interface. In the core, the radial crack could propagate to the veneer and stop or it could continue to propagate through the veneer, resulting in bulk failure. In the veneer, the radial crack could propagate to the surface, creating a chip in the veneer. However, ceramic cores have a much greater modulus of elasticity and hardness than the veneering porcelains (described

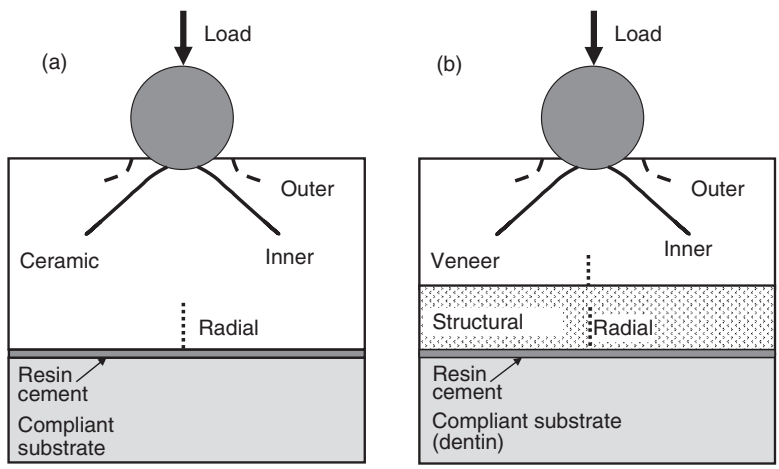

23.2 Schematic of fatigue contact failure modes operational in ceramic monolithic or bilayer structures supported by a compliant substrate such as tooth dentin and tested in water. When the ceramic layer is thick top surface cracks form with inner cone cracks predominating. If the monolithic ceramic is thin (>1 mm) then failure from far field radial cracks is likely. In the bilayer ceramic the higher modulus structural ceramic bears the load and radial fracture is possible, which can lead to radial failure in the veneer.

below) which minimizes the likelihood of radial cracks developing in the veneers. Radial fractures predominate in investigations of crowns or other test specimens subjected to an increasing load until fracture initiates and, propagates, and the specimen fails. The results of these investigations can be valuable in relative ranking of materials but they do not accurately represent the clinical conditions, particularly fatigue and contact fatigue, in which the crown is expected to perform, potentially yielding misleading expectations.

There are two fracture types that develop in the near-field (occlusal surface). The first is a classical cone crack which was described Hertz (1896; Lawn *et al.*, 1998). These cracks develop in flat specimens after only a few loading cycles or when one time heavy loads are applied. However, they do not always propagate. They can remain arrested, without leading to chipping or bulk fracture (see Fig. 23.3).

A second near-field fracture, inner cone cracks, has only recently begun to be appreciated. These cracks develop *only* with repeated loading and only in a fluid environment (Zhang *et al.*, 2005a,b). Inner cone cracks are the result of hydraulic pumping of water in the crack combined with slow crack growth. They develop beneath the indenter (opposing cusp) and have been observed during laboratory testing of both veneered alumina and Y-TZP specimens (Kim *et al.*, 2007b). In monolithic materials, these cracks propagate to the cementation surface and present as bulk fracture (Fig.

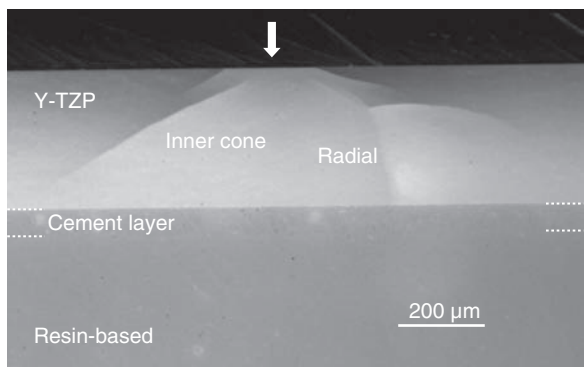

23.3 Cross-section though a mouth-motion Hertzian contact (r = 3.18 mm) fatigue of an unveneered Y-TZP plate after 110 000 cycles at 325 N load in water. This thin plate exhibits an early radial fracture perpendicular to the plane of the section that does not propagate to the surface but has interacted with the propagating inner cone crack. The inner cone crack on the opposite side shows normal evolution. Note the lack of propagation of the outer cone crack. These damage modes are common to all ceramics. Polarized light micrograph courtesy of Petra Guess.

23.3). In veneered crowns, this fracture mode manifests as chips in the veneer. With sliding contacts, these inner cones concentrate into one large crack, oriented perpendicular to the sliding direction and penetrating into the porcelain at several orders of magnitude fewer cycles than for uniaxial loading (Kim *et al.*, 2007a). Sliding contact fatigue damage for veneered alumina is shown in Fig. 23.4.

Part of the complication in understanding clinical fractures is that the first crack to appear does not necessarily lead to fracture. Outer cone cracks can develop and arrest, rarely leading to chipping of the veneer or bulk fracture. Cracks that develop later than outer cones (inner cones or radial fractures) ultimately cause the failures seen clinically. Which crack is ultimately the culprit, resulting in failure, depends on both the material and the loading history (Bhowmick *et al.*, 2005; Zhang, 2005a). In laboratory tests with cyclic loading in water, veneered alumina specimens subjected to typical occlusal loads, fail by either radial fracture from the cementation surface leading to bulk fracture of the specimen or by inner cone cracks which chip the veneer but do not fracture the core (Fig. 23.4). In veneered Y-TZP subjected to the same conditions, inner cone cracks are the most prominent failure mode as has been noted clinically (Raigrodski *et al.*, 2006; Sailer *et al.*, 2007a). Outer cone cracks develop in the veneer of specimens with either core, usually at very low numbers of loading cycles,

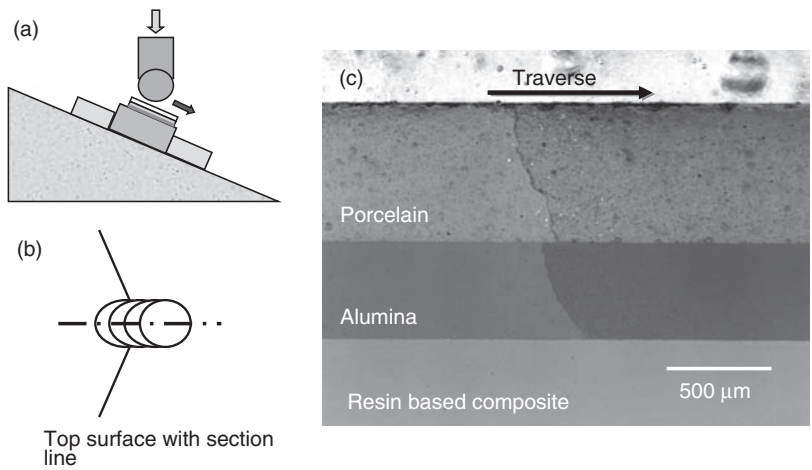

23.4 Sliding contact damage in a bilayer ceramic: (a) schematic of mouth-motion contact sliding configuration; (b) schematic of top view of sliding contact damage with dominate inner cone crack shown (dotted line is plane of cross-section); (c) cross-section showing combination of radial crack in alumina intersecting the inner cone extending from the sliding contact.

but these cracks do not propagate to cause the ultimate failure of the specimen.

While little has been reported on failure modes of Y-TZP core crowns, *in vitro* studies confirm differences between failure modes for alumina and Y-TZP cores (Kim *et al.*, 2007b). In laboratory tests of veneered cores supported on a compliant substrate simulating dentin (Z-100, 3M/ESPE), veneered Y-TZP specimens develop inner cone cracks whereas in veneered alumina specimens there is competition between inner cone cracks in the veneer and radial cracks in the core developing first (Kim *et al.*, 2007b). When supported by metal dies and loaded to failure in ambient air, veneered Y-TZP cores and bridge frameworks fractured in the veneers (outer cone cracks) (Sundh and Sjögren, 2004, 2006).

Fracture might originate from deformation of the crown as a unit and thus could be expected to originate from the junction (margin) of the stiff crown with the lower elastic modulus (15 GPa) tooth dentin (most dental crown preparations remove the entire higher modulus (80–90 GPa) enamel covering of the tooth). For glass hemispheres supported on a compliant base, loaded off-axis by a low modulus indenter (as might be the case with a monolithic crown on dentin with occlusal load applied through a bolus of food), fractures can propagate from margin defects, and propagate through the hemisphere in a pattern that emulates a semilunar fracture sometimes described in clinical failures (Qasim *et al.*, 2007).

23.5.3 Material properties and clinical function

Four principal material properties contribute to performance of ceramic crowns: strength, modulus of elasticity, hardness, and toughness. (Table 23.3 summarizes these values for many of the modern dental ceramics.) Intuitively, it would seem that strength should be a good predictor of clinical success. McLean (1983), based upon the history of MCR restoration and his personal experience with the high rate of failure of aluminous porcelain posterior crowns (>18% at 4 years), predicted that ceramic flexural strengths in the range of 450–600 MPa would be necessary for successful posterior restorations. As strength of materials for ceramic crowns increases, in general the failure rate drops. Much of the enthusiasm for Y-TZP crowns was based on the fact that its strength came close to that of core metals. The strength of Dicor, a glass ceramic intended to mimic enamel but no longer in use, was only approximately 70 MPa, slightly less than that of a microscope glass slide (Tinschert *et al.*, 2000). Aluminas, such as In-Ceram and Procera Alumina, are four to six times stronger (Table 23.2) than Dicor and their failure rates are substantially lower (Table 23.3), supporting the hypothesis that increasing strength yields improved performance. But the strength of Empress 1 is not substantially different from that of Dicor

(70.3 vs. 94–112 MPa) (Table 23.3) yet its failure rate is only half that of Dicor (Table 23.3). Similarly, the strength of Y-TZP are substantially greater than that for aluminas, yet their failure rates are similar (see Table 23.4). In addition strength is usually measured with flexural or biaxial testing of polished specimens. Structural ceramics, particularly with fine grain structures are sensitive to surface damage. Thus machining damage from CAD/CAM procedures, alumina particle abrasion to remove investment or during bonding procedures, or from 'fit adjustment' diamond bur cutting by a dentist can all reduce strength.

Using controlled Vickers indents on the far-field surface of layered structures subjected to Hertzian contact, Kim *et al.* (2001) demonstrated that Y-TZP (Prozyr, Table 23.3) was more vunerable to surface damage than alumina (In-Ceram) while dental porcelain (Vita Mk II) was little affected (Fig. 23.5). The strength of dental porcelain is controlled to a great extent by internal rather than surface flaws. The vertical lines in Fig. 23.5 are placed to indicate the range of flaws estimated to result from 50 μm alumina particle abrasion of these ceramics. In addition, when subjected to cyclic loading, like that of occlusal function, the strength of ceramics can drop, the result of slow crack growth. After the equivalent of approximately 10 years of function, the strength of both alumina and Y-TZP in layer structures

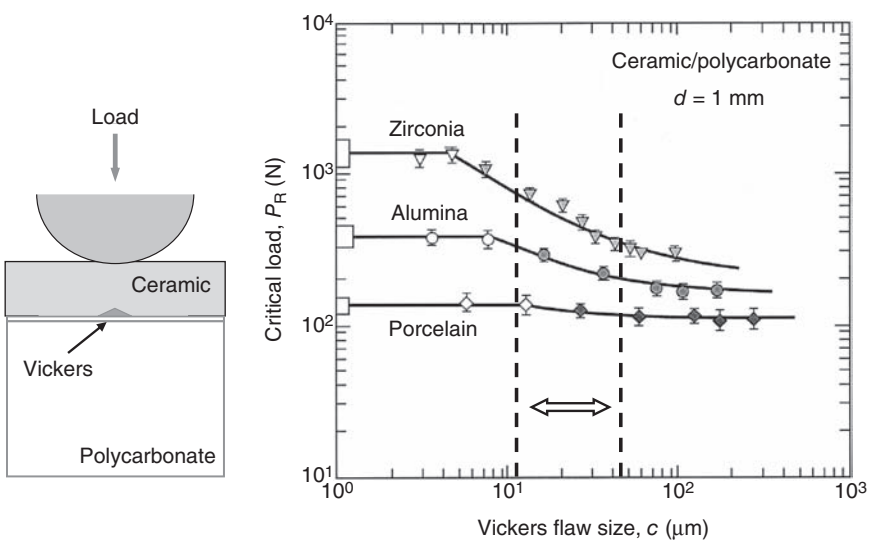

23.5 Hertzian contact load to failure results in monolithic ceramics with controlled flaws (Vickers indents) applied to cementation surface (see schematic) (Kim *et al.,* 2001). Dotted lines represent the range of damage sizes estimated for particle abrasion with 50 μm alumina particles at 0.5 MPa as commonly used by dentists and dental laboratories to prepare ceramic crown surfaces for bonding.

reduces to approximately 40% of its initial strength and this is accelerated by surface damage (Zhang and Lawn, 2005; Zhang *et al.*, 2004, 2006)! Thus, initial strength while important, does not completely account for failure rates.

Radial cracks initiate from the tensile surface of crowns and in general the higher the elastic modulus of the core ceramic the more load is carried by the core, increasing the tensile stress. An interesting situation is presented by comparing aluminas and Y-TZP (Table 23.3): E for Procera alumina is > 1.5× that of the currently used Y-TZP, yet their failure rates are nearly identical. This contradiction is discussed below and relates to the fact that while the failure rates of crowns from the two materials are nearly identical, predominate failure *modes* are different.

Since defects at the surface of a ceramic are often the site of crack initiation, the materials' resistance to plastic deformation should improve the clinical survivability of a crown. The hardness of aluminas and Y-TZP are similar, as are their failure rates (Table 23.4). On the other hand, the hardness of IPS Empress and glass-ceramic Empress 2 are also similar, yet their failure rates are quite different.

Fracture toughness of dental ceramics range from about 1 to 7 $MPa\,m^{1/2}$ (see Table 23.3) and cracks propagate easily (though a notable exception is outer cone cracks as discussed above). Fracture mechanics theory shows that there is a linear relationship between strength and toughness for brittle materials (Lawn *et al.*, 1993). However, it may not be true for every material class. In a study of the relationship between fracture toughness and strength of dental porcelains, Cesar *et al.* (2006) found that strength increased with toughness to a threshold but subsequent increases in toughness were accompanied by a *drop* in strength.

Taken alone, none of the primary material properties completely explains the wide difference in failure rates of posterior ceramic crowns. Lawn and coworker (Chai and Lawn, 2004; Deng *et al..,* 2002, 2003) have shown that crack initiation is a complex relationship of these parameters – and the relationship differs for various modes of fracture. For far-field radial fractures in dental ceramics (Fig. 23.2), those historically thought to be the most prevalent in posterior crowns, the load to initiate a crack, P_r, is described as:

$$P_r \approx \frac{\sigma_c d^2}{\log(E_c/E_s)} \qquad 23.1$$

where σ_c is the material strength, d is the ceramic thickness, E_c is the modulus of elasticity of the ceramic and E_s is the modulus of elasticity of the supporting substrate (cement and dentin for monolithic crowns on vital teeth).

Thickness is the most important factor relating to the load required to initiate radial fractures. As the thickness of the ceramic increases, the load

required to initiate fracture increases as the square of the thickness. This relationship holds over the entire spectrum of glasses, glass-ceramics and structural ceramics utilized in dentistry (Lawn *et al.*, 2001, 2002). Monolithic crowns from materials such as Dicor or IPS Empress are anticipated to fail by this mechanism if thin areas are subjected to cyclic loading above some threshold where damage can accumulate as will be discussed below. This theoretical relationship confirms clinical experience of improved performance with thicker crowns.

The modulus of the ceramic (E_c) plays a secondary role, particularly as it relates to the relative stiffness of the ceramic and the supporting tooth substrate (E_s). When the two moduli are similar, there is little contribution of this term to P_r; the stresses created by the load are distributed throughout the bulk of the ceramic and supporting structure. When there is a large mismatch, however, and the ceramic is much stiffer than the substrate, the substrate offers little support, and deflects easily in response to an increasing load, resulting in a higher tensile stress field on the ceramic cementation surface and lowering the load at which a crack can initiate. Conversely, if the substrate has a stiffness close to or higher than that of the ceramic (e.g. when a monolithic crown is supported by a metal or ceramic core or an implant), the substrate provides excellent support, minimizing the deflection at the cementation surface of the crown and thereby increasing the load required to initiate a crack. Clinical studies have confirmed increased crown survival on high modulus tooth core materials (Malament and Socransky, 2001).

Relationship [23.1] describes the theoretical relationship for monolithic materials. For core–veneer bilayers, the theoretical relationship is modified so the combined strength of the core and veneer replaces the term for the material strength; the thickness term reflects the combined core–veneer thickness; and the elastic modulus of the ceramic is modified to reflect the effective modulus of the core–veneer. Strengths of core–veneer combinations have been shown to be similar to monolithic core specimens over a range of ceramic classes (Bona *et al.*, 2003; Guazzato *et al.*, 2004c,d; Sundh and Sjögren, 2004; White *et al.*, 2005). The structural reliability of veneered core ceramics is controlled primarily by that of the core (Bona *et al.*, 2003). This experimental outcome was explained by the theory developed by Deng *et al.* (2002, 2003). For a fixed core–veneer thickness, there is little variation in load at which radial fractures initiate, P_r, despite substantial differences in the core thickness. This is comforting news relative to esthetic considerations that may demand thicker porcelain layers. Stresses leading to radial fracture in crowns are concentrated in the core and the higher the elastic modulus of the core the more is the load borne by the core. For the same core veneer thickness ratio the tensile stress at the core cementation interface is higher for alumina than for Y-TZP. A common failure mode

observed clinically for veneered alumina crowns is fracture through both the core and veneer (Fig. 23.6) which strongly suggests the alumina is bearing the load. The stresses in dental bridges can be distributed quite differently because of dissimilarities in the geometry of the two types of restorations. The types of failure modes expected for veneered core ceramic crowns based upon studies of layer structure is presented in Table 23.5 and shown in Fig. 23.7.

Crown surface (near-field) cracks comprise outer and inner cone cracks, initiating on the occlusal surface. During occlusally relevant multi-cycle loading in water, outer cone cracks initiate, propagate a short distance and then remain stable without further propagation. They probably are never detected clinically. Theoretical relationships, integrating the principal material properties, define the load to initiate the outer cone cracks, P_{oc}, by:

$$P_{oc} \approx (T^2/E_c)\, r \qquad 23.2$$

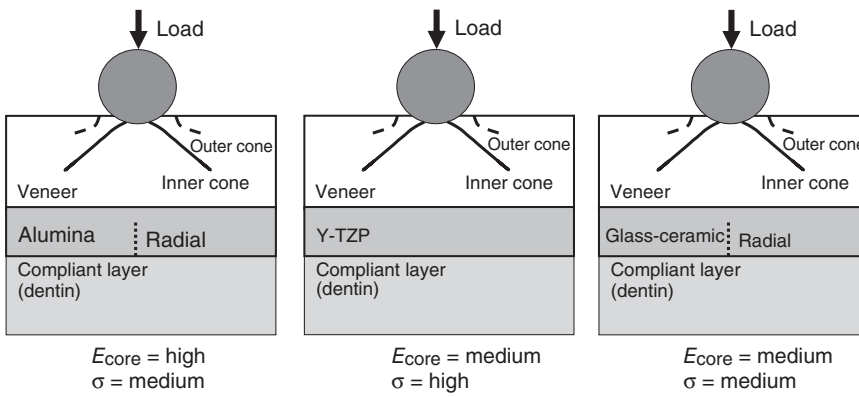

E_{core} = high
σ = medium

E_{core} = medium
σ = high

E_{core} = medium
σ = medium

23.6 Predicted fatigue failure modes of bilayer ceramic crown structures based upon the elastic modulus of the core, E_{core}, and strength of the core, σ. See also Table 23.5.

Table 23.5 Relative values of material properties of cores and fracture modes for three classes of core materials (see Fig 23.7)

Property	Alumina core	Y-TZP core	Glass ceramic core
Strength	Mid-range	High	Mid-range
Hardness	High	Low	Low
Modulus of elasticity	High	Mid-range	Low
Failure mode	Radial crack in core	Inner cone in veneer	Competition between radial in core and inner cone in veneer

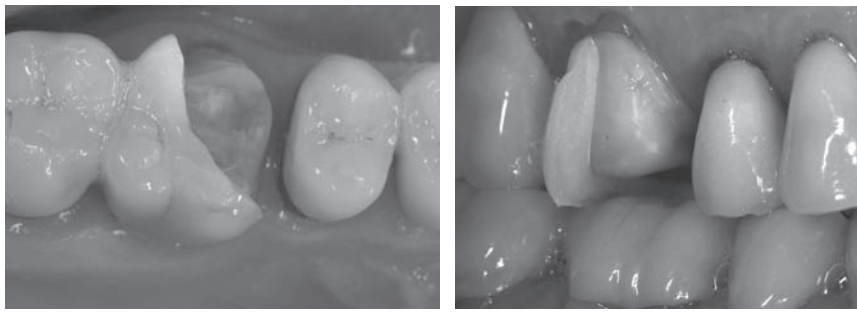

23.7 Occlusal and buccal views molar all-ceramic (veneered CAD/CAM alumina core) with a through core and veneer failure after 12 months in service. This clinical fatigue failure mode corresponds to predictions from fatigue studies on veneered alumina (see Fig. 23.6). Pictures courtesy of Irena Sailer.

where T is the material toughness, E_c is the modulus of elasticity of the ceramic and r is the radius of the opposing cusp tip. Note the resistance to outer cone cracks is primarily controlled by the damage resistance (toughness) of the material surface. Interestingly, loads to initiate these cracks are unrelated to the thickness of the crown (for crown thicknesses greater than 1 mm).

Relationship [23.2] is essentially the same for either monolithic or core–veneer crowns since it reflects a surface phenomenon. For core–veneer crowns, outer cone cracks initiate in the veneer. For very thin veneers, the value of the modulus (E_c) must be modified to reflect an effective modulus of the core–veneer combination.

Inner cone cracks are by far the least appreciated fracture type. In fact, they may be among the most common culprits for clinical failure, particularly when sliding contacts between opposing tooth cusps and the veneering porcelain are considered (Kim *et al.*, 2007a). As described above, they are only seen in response to cyclic loading – in a wet environment. Thus, they would not be expressed in most *in vitro* tests which are typically performed in ambient laboratory conditions (i.e. air). Inner cone cracks are likely the mode of failure of occlusal-initiated clinical fractures described in the literature (Scherrer, 2003; Scherrer *et al.*, 2006) and supported in a recent study (Scherrer *et al.*, 2007). Theoretical relationships integrating material properties are in process but have yet to be completed.

Damage maps of the competing near and far field crack evolution at various loads and fatigue cycles for glass have been elucidated for both uniaxial (Bhowmick *et al.*, 2005) and sliding contacts (Kim *et al.*, 2007a). These studies indicate that inner cone cracking propagating from the porcelain veneer surface interacting with residual stresses in the veneer is most

likely the cause of chipping/fracture of porcelain in both MCR and ceramic (especially Y-TZP) posterior bridges (Sailer *et al.*, 2007b). Stresses in the veneering porcelain with Y-TZP and alumina core crowns or bridge frame works may be related to the low thermal diffusivity of the core materials (with Y-TZP having 0.1× the diffusivity of alumina). Dental laboratory technicians have long maintained that control of the cooling rate of hand-stacked porcelains on metal frameworks was important for clinical success (Marrotta, 2006) as the residual stresses change with cooling rate. The cooling rate effects have been shown to be significant in studies in MCR systems (Anusavice and Hojiatie, 1991; Asaoka and Tesk, 1989, 1990; Dehoff and Anusavice, 1989). The slower cooling rate, particularly for Y-TZP, may contribute to changes in residual stress fostering veneer chipping.

23.6 Additional dental restorative applications of ceramics

Bonding of metal directly to tooth enamel permits replacement of a missing tooth without crown preparation referred to as the Maryland or Adhesion Bridge. This conservative approach was extended with the use of a glass-infiltrated alumina framework (In-Ceram) (Kern *et al.*, 1991). Clinical results indicated that for structural ceramic frameworks a cantilever design with one bonded abutment provided the best clinical results (Kern, 2005). This technique has now been expanded to include the use of cantilever Y-TZP framework adhesion bridges (Komine and Tomic, 2005) with good clinical results indicated at up to 5 years in function (Brodbeck, 2005).

Restoration of metal implant fixtures requires placement of a metal abutment that extends through the soft tissue upon which a crown can be placed. This metal can grey the tissue, which has led to the selective use of structural ceramics as implant abutments. Alumina has been used in this application for almost two decades and review of the results is available (Heydecke *et al.*, 2002). Y-TZP and zirconia-modified alumina implant abutments have low failure rates and are now replacing the alumina abutments because of strength considerations with good short-term (<5 years) clinical results (Andersson *et al.*, 2003; Ormianer and Schiroli, 2006).

The single piece (implant fixture and abutment combined) all-ceramic implant is the natural extension of the use of structural ceramics in dentistry (Fig. 23.8). This is based upon the excellent clinical response to titanium oxide on metal implants and aluminium oxide in the form of single crystal sapphire. Unfortunately the problems presented with single crystal sapphire ceramic implants introduced in 1972, particularly fracture, lead to serious concerns about use of all-ceramic implants. The single crystal sapphire performance results have recently been reviewed (Haubenreich *et al.*, 2005). The higher strengths of the newer structural ceramics has rekindled interest

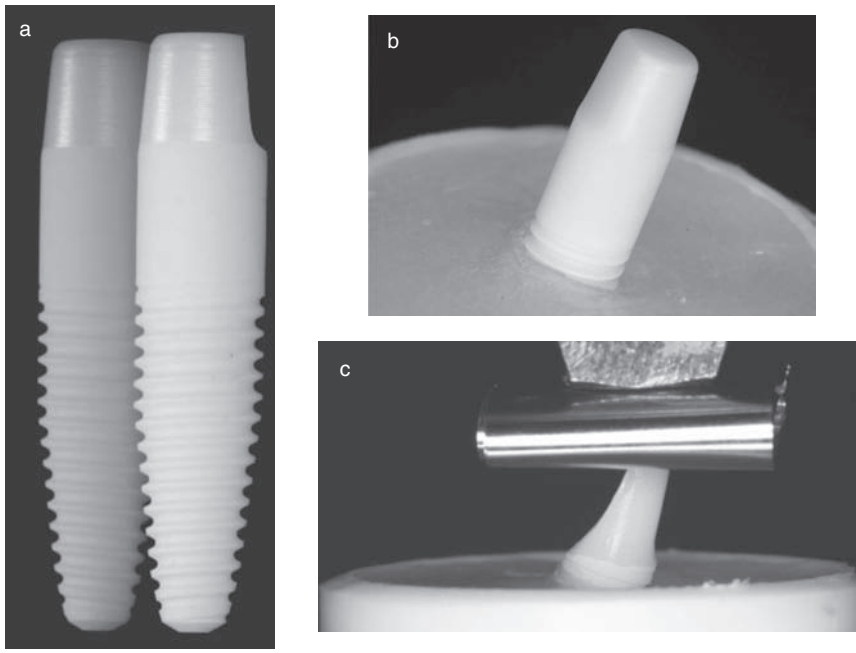

23.8 (a) Prototype one piece Y-TZP implant which combines the tooth root replacement fixture and crown abutment, (b) implant embedded in methyl methacylate at 30° for fatigue testing, and (c) crown abutment prepared implant undergoing fatigue testing.

in the one piece ceramic implant. A laboratory study suggests that Y-TZP is suitable for this application (Kohal *et al.*, 2006) with clinical trials continuing by several manufacturers.

23.7 Future trends

Advances in ceramic material science are exciting and hold promise for ever-improving clinical success of all-ceramic restorations. Particular interest resides in the development of colored and more translucent structural ceramics for improved esthetics and support of the veneering porcelain. In addition to basic improvements in structural ceramic physical properties, the areas currently under investigation include methods for CAD/CAM veneering porcelains and bonding porcelains with glass joins or high elastic modulus resin-based luting cements directly to the CAD/CAM structural ceramics core (Wang *et al.*, 2007). Appreciation of the roles of graded structures in biologic systems in reducing surface stresses has fostered interest in a graded interface for the inner (bonding) surface of crowns (Huang *et al.*, 2007) or for graded interface between the structural ceramic and the veneer.

23.8 Summary

Ceramics are playing an increasing role in the restoration of form and function in the mouth. MCR restorations are being slowly displaced by porcelain-veneered structural ceramics with a emphasis on Y-TZP as the current material of choice. Research on the damage and fatigue, particularly for layer structures in water, has shown the need for research into how materials properties and processing interacting with the geometry of the restoration result in damage accumulation. Until that time the rational design of all-ceramic crown and bridge restorations remains an exciting but empirical science.

23.9 References

Al-Hiyasat, A. S., Saunders, W. P., Sharkey, S. W., Smith, G. M. & Gilmour, W. H. (1998) Investigation of human enamel wear against four dental ceramics and gold. *J Dent*, **26**, 487–95.

Andersson, B., Glauser, R., Maglione, M. & Taylor, A. (2003) Ceramic implant abutments for short-span FPDs: a prospective 5-year multicenter study. *Int J Prosthodont*, **16**, 640–46.

Anusavice, K. J. (Ed.) (2003) *Phillips' Science of Dental Materials*, 11th edn. Rotterdam, Elsevier.

Anusavice, K. J. & Hojjatie, B. (1991) Effect of thermal tempering on strength and crack propagation behavior of feldspathic porcelains. *J Dent Res*, **70**, 1009–13.

Asaoka, K. & Tesk, J. A. (1989) Transient and residual stresses in dental porcelains as affected by cooling rates. *Dent Mater J*, **8**, 9–25.

Asaoka, K. & Tesk, J. A. (1990) Transient and residual stress in a porcelain–metal strip. *J Dent Res*, **69**, 463–9.

Bhowmick, S., Zhang, Y. & Lawn, B. R. (2005) Competing fracture modes in brittle materials subject to concentrated cyclic loading in liquid environments: bilayer structures. *J Mater Res*, **20**, 2792–800.

Bindl, A. & Mormann, W. H. (2002) An up to 5-year clinical evaluation of posterior in-ceram CAD/CAM core crowns. *Int J Prosthodont*, **15**, 451–6.

Bona, A. D., Anusavice, K. J. & Dehoff, P. H. (2003) Weibull analysis and flexural strength of hot-pressed core and veneered ceramic structures. *Dent Mater*, **19**, 662–9.

Brodbeck, U. (2005) *Clinical Results with All-ceramic Adhesion Bridges in A Private Practice*. Personal communication with Swiss Society of Reconstructive Dentistry.

Cesar, P. F., Yoshimura, H. N., Miranda, W. G., Jr., Miyazaki, C. L., Muta, L. M. & Rodrigues Filho, L. E. (2006) Relationship between fracture toughness and flexural strength in dental porcelains. *J Biomed Mater Res B Appl Biomater*, **78**, 265–73.

Chai, H. & Lawn, B. (2004) Fracture mode transitions in brittle coatings on compliant substrates as a function of thickness. *J Mater Res*, **19**, 1752–61.

Clelland, N. L., Agarwala, V., Knobloch, L. A. & Seghi, R. R. (2003) Relative wear of enamel opposing low-fusing dental porcelain. *J Prosthodont*, **12**, 168–75.

De Jager, N., De Kler, M. & Van Der Zel, J. M. (2006) The influence of different core material on the FEA-determined stress distribution in dental crowns. *Dent Mater*, **22**, 234–42.

Dehoff, P. H. & Anusavice, K. J. (1989) Tempering stresses in feldspathic porcelain. *J Dent Res*, **68**, 134–8.

Deng, Y., Lawn, B. R. & Lloyd, I. K. (2002) Characterization of damage modes in dental ceramic bilayer structures. *J Biomed Mater Res*, **63**, 137–45.

Deng, Y., Miranda, P., Pajares, A., Guiberteau, F. & Lawn, B. R. (2003) Fracture of ceramic/ceramic/polymer trilayers for biomechanical applications. *J Biomed Mater Res*, **67A**, 828–33.

Denry, I. L., Holloway, J. A. & Rosenstiel, S. F. (1998) Effect of ion exchange on the microstructure, strength, and thermal expansion behavior of a leucite-reinforced porcelain. *J Dent Res*, **77**(4): 583–8.

Donovan, T. E. (2005) Metal-free dentistry. *J Esthet Restor Dent*, **17**, 141–3.

El-Mowafy, O. & Brochu, J. F. (2002) Longevity and clinical performance of IPS-Empress ceramic restorations – a literature review. *J Can Dent Assoc*, **68**, 233–7.

Fradeani, M. & Redemagni, M. (2002) An 11-year clinical evaluation of leucite-reinforced glass-ceramic crowns: a retrospective study. *Quintessence Int*, **33**, 503–10.

Grossman, D. (1991) Structure and physical properties of Dicor/MGC glass-ceramic. In Moermann, W. (Ed.) *International Symposium on Computer Restorations.* Zurich, Switzerland, Quintessence.

Guazzato, M., Albakry, M., Swain, M. V. & Ironside, J. (2002) Mechanical properties of In-Ceram alumina and In-Ceram zirconia. *Int J Prosthodont*, **15**, 339–46.

Guazzato, M., Albakry, M., Ringer, S. P. & Swain, M. V. (2004a) Strength, fracture toughness and microstructure of a selection of all-ceramic materials. Part I. Pressable and alumina glass-infiltrated ceramics. *Dent Mater*, **20**, 441–8.

Guazzato, M., Albakry, M., Ringer, S. P. & Swain, M. V. (2004b) Strength, fracture toughness and microstructure of a selection of all-ceramic materials. Part II. Zirconia-based dental ceramics. *Dent Mater*, **20**, 449–56.

Guazzato, M., Proos, K., Quach, L. & Swain, M. V. (2004c) Strength, reliability and mode of fracture of bilayered porcelain/zirconia (Y-TZP) dental ceramics. *Biomaterials*, **25**, 5045–52.

Guazzato, M., Proos, K., Sara, G. & Swain, M. V. (2004d) Strength, reliability, and mode of fracture of bilayered porcelain/core ceramics. *Int J Prosthodont*, **17**, 142–9.

Haselton, D. R., Diaz-Arnold, A. M. & Hillis, S. L. (2000) Clinical assessment of high-strength all-ceramic crowns. *J Prosthet Dent*, **83**, 396–401.

Haubenreich, J. E., Robinson, F. G., West, K. P. & Frazer, R. Q. (2005) Did we push dental ceramics too far? A brief history of ceramic dental implants. *J Long Term Eff Med Implants*, **15**, 617–28.

Helvey, G. A. (2002) Fabrication of aesthetic, pressed, porcelain-fused-to-metal restorations. *Pract Proced Aesthet Dent*, **14**, 487–92.

Hertz, H. (1896) *Hertz's Miscellaneous Papers*, Chs. 5,6. London, Macmillan.

Heydecke, G., Sierraalta, M. & Razzoog, M. E. (2002) Evolution and use of aluminum oxide single-tooth implant abutments: a short review and presentation of two cases. *Int J Prosthodont*, **15**, 488–93.

Holand, W., Schweiger, M., Frank, M. & Rheinberger, V. (2000) A comparison of the microstructure and properties of the IPS Empress 2 and the IPS Empress glass-ceramics. *J Biomed Mater Res*, **53**, 297–303.

Huang, M., Wang, R., Thompson, V. P., Rekow, D. & Soboyejo, W. (2007) Bioinspired design of dental multilayers. *J Mat Sci, Mat Med*, **18**, 57–64.

Imai, Y., Suzuki, S. & Fukushima, S. (2000) Enamel wear of modified porcelains. *Am J Dent*, **13**, 315–23.

Kelly, J., Campbell, S. & Bowen, H. (1989) Fracture-surface analysis of dental ceramics. *J Prosthet Denti*, **62**, 536–41.

Kelly, J., Giodano, R., Pober, R. & Cima, M. (1990) Fracture surface analysis of dental ceramics: clinically failed restorations. *Int J Prosthodontics*, **3**, 430–40.

Kelly, J. R. & Denry, I. (2007) Stabilized zirconia as a structural ceramic: an overview. *Dent Mater*. (published on line).

Kern, M. (2005) Clinical long-term survival of two-retainer and single-retainer all-ceramic resin-bonded fixed partial dentures. *Quintessence Int*, **36**, 141–7.

Kern, M. (2006) Clinical performance of all-ceramic restorations. In Mörmann, W. (Ed.) *State of the Art of CAD/CAM Restorations: 20 Years of CEREC*. London, Quintessence 47–56.

Kern, M., Knode, H. & Strubb, J. R. (1991) The all-porcelain, resin-bonded bridge. *Quintessence Int*, **22**, 257–62.

Kim, H.-W., Deng, Y., Miranda, P., Pajares, A., Kim, D.-K., Kim, H.-E. & Lawn, B. (2001) Effect of flaw state on the strength of brittle coatings on soft substrates. *J Amer Ceramic Soc*, **84**, 2377–84.

Kim, J.-W., Kim, J.-H., Thompson, V. & Zhang, Y. (2007a) Sliding contact damage in layered ceramic structures. *J Dent Res*, **86**(11), 1046–50.

Kim, J. W., Bhowmick, S., Chai, H. & Lawn, B. R. (2007b) Role of substrate material in failure of crown-like layer structures. *J Biomed Mater Res B Appl Biomater*, **81**, 305–11.

Kohal, R. J., Klaus, G. & Strub, J. R. (2006) Zirconia-implant-supported all-ceramic crowns withstand long-term load: a pilot investigation. *Clin Oral Implants Res*, **17**, 565–71.

Komine, F. & Tomic, M. (2005) A single-retainer zirconium dioxide ceramic resin-bonded fixed partial denture for single tooth replacement: a clinical report. *J Oral Sci*, **47**, 139–42.

Lawn, B. R., Padture, N. P., Braun, L. M. & Bennison, S. J. (1993) Model for toughness-curves in two-phase ceramics: I. basic fracture mechanics. *J Amer Ceramic Soc*, **76**, 2235–40.

Lawn, B., Lee, S., Peterson, I. & Wuttiphan, S. (1998) A model of strength degradation from Hertzian contact damage in tough ceramics. *J Amer Ceramic Soc*, **81**, 1509–20.

Lawn, B., Deng, Y. & Thompson, V. (2001) Use of contact testing in the characterization and design of all-ceramic crownlike layer structures: a review. *J Prosthet Dent*, **86**, 495–510.

Lawn, B., Deng, Y., Lloyd, I., Janal, M., Rekow, E. & Thompson, V. (2002) Materials design of ceramic-based layer structures for crowns. *J Dental Res*, **81**, 433–8.

Lawn, B., Pajares, A., Zhang, Y., Deng, Y., Polack, M., Lloyd, I., Rekow, E. & Thompson, V. (2004a) Materials design in the performance of all-ceramic crowns. *Biomaterials*, **25**, 2885–92.

Lawn, B. R., Pajares, A., Zhang, Y., Deng, Y., Polack, M. A., Lloyd, I. K., Rekow, E. D. & Thompson, V. P. (2004b) Materials design in the performance of all-ceramic crowns. *Biomaterials*, **25**, 2885–92.

Lehner, C., Studer, S., Brodbeck, U. & Scharer, P. (1997) Short-term results of IPS-Empress full-porcelain crowns. *J Prosthodont*, **6**, 20–30.

Mackert, J. R., Jr., Butts, M. B. & Fairhurst, C. W. (1986) The effect of the leucite transformation on dental porcelain expansion. *Dent Mater*, **2**, 32–6.

Mackert, J. R., Jr., Sheen, G. W., Williams, A. L., Russell, C. M. & Ergle, J. W. (2003) Effects of local cooling rate and processing variables on leucite in dental porcelain. *Int J Prosthodont*, **16**, 647–52.

Malament, K. & Thompson, V. (1999) Weibull analysis of a clinical data base of molar ceramic crowns. In Rekow, E. & Thompson, V. (Eds) *International Symposium on Advanced Materials with Biomedical Applications*. US National Institute of Standards and Technology (NIST).

Malament, K. A. & Socransky, S. S. (1999) Survival of Dicor glass-ceramic dental restorations over 14 years: Part I. Survival of Dicor complete coverage restorations and effect of internal surface acid etching, tooth position, gender, and age. *J Prosthet Dent*, **81**, 23–32.

Malament, K. A. & Socransky, S. S. (2001) Survival of Dicor glass-ceramic dental restorations over 16 years. Part III: effect of luting agent and tooth or tooth-substitute core structure. *J Prosthet Dent*, **86**, 511–19.

Malament, K. A., Socransky, S. S., Thompson, V. & Rekow, D. (2003) Survival of glass-ceramic materials and involved clinical risk: variables affecting long-term survival. *Pract Proced Aesthet Dent*, Suppl, 5–11.

Marrotta, L. (2006) Personnal communication. Marrotta Dental Studio, Farmindale, NY, US.

McLaren, E. A. & White, S. N. (2000) Survival of In-Ceram crowns in a private practice: a prospective clinical trial. *J Prosthet Dent*, **83**, 216–22.

McLean, J. W. (1983) The future for dental porcelain. In McLean, J. W. (Ed.) *Proceedings of the First International Symposium on Ceramics*. Chicago, Quintessence Publishing Co.

Oden, A., Andersson, M., Krystek-Ondracek, I. & Magnusson, D. (1998) Five-year clinical evaluation of Procera AllCeram crowns. *J Prosthet Dent*, **80**, 450–6.

Odman, P. & Andersson, B. (2001) Procera AllCeram crowns followed for 5 to 10.5 years: a prospective clinical study. *Int J Prosthodont*, **14**(6): 504–9.

Olsson, K. G., Furst, B., Andersson, B. & Carlsson, G. E. (2003) A long-term retrospective and clinical follow-up study of In-Ceram Alumina FPDs. *Int J Prosthodont*, **16**, 150–56.

Ormianer, Z. & Schiroli, G. (2006) Maxillary single-tooth replacement utilizing a novel ceramic restorative system: results to 30 months. *J Oral Implantol*, **32**, 190–9.

Ottl, P., Piwowarczyk, A., Lauer, H. C. & Hegenbarth, E. A. (2000) The Procera AllCeram system. *Int J Periodontics Restorative Dent*, **20**, 151–61.

Piche, P. W., O'Brien, W. J., Groh, C. L. & Boenke, K. M. (1994) Leucite content of selected dental porcelains. *J Biomed Mater Res*, **28**, 603–9.

Pröbster, L. (1996) Four year clinical study of glass-infiltrated, sintered alumina crowns. *J Oral Rehabil*, **23**, 147–51.

Pröbster, L. & Diehl, J. (1992) Slip-casting alumina ceramics for crown and bridge restorations. *Quintessence Int*, **23**, 25–31.

Qasim, T., Ford, C., Bush, M. B., Hu, X., Malament, K. A. & Lawn, B. R. (2007) Margin failures in brittle dome structures: relevance to failure of dental crowns. *J Biomed Mater Res B Appl Biomater*, **80**, 78–85.

Quinn, J. B. & Lloyd, I. K. (2001) Flake and scratch size ratios in ceramics. In Varner, J. R., Quinn, G. D. & Frechette, V. D. (Eds) *Fratography of Glasses and Ceramics IV, Ceramics Transactions*. Westerville, Ohio, American Ceramic Society.

Raigrodski, A. J., Chiche, G. J., Potiket, N., Hochstedler, J. L., Mohamed, S. E., Billiot, S. & Mercante, D. E. (2006) The efficacy of posterior three-unit zirconium-oxide-based ceramic fixed partial dental prostheses: a prospective clinical pilot study. *J Prosthet Dent*, **96**, 237–44.

Rekow, E. D. (2006) Failure modes of veneered zirconia and alumina core crowns. Personal communication with Nobel Biocare and Vita Zahnfabrik.

Rosenstiel, S. F., Land, M. F. & Fujimoto, J. (2006) *Contemporary Fixed Prosthodontics*. New York, Mosby.

Sailer, I., Feher, A., Filser, F., Luthy, H. & Hammerle, C. H. (2007a) Five-year clinical results of zirconia frameworks for posterior fixed partial dentures. *Inter J Prosthodont*, **20**, 151–6.

Sailer, I., Pjetursson, B. E., Zwahlen, M. & Hammerle, C. H. (2007b) SSRD 2: a systematic review of the survival and complication rates of all-ceramic and metal-ceramic reconstructions after an observation period of a least three years. Part II: fixed dental prostheses *Clin Oral Impl Res*, **18**(suppl. 3), 86–96.

Scherrer, S. S. (2003) *Integration of Material Science in Failure Analysis of Dental Ceramics and Resin Composites. Facule de Medecine*, Geneva, University of Geneva.

Scherrer, S. S., Quinn, J. B., Quinn, G. D. & Kelly, J. R. (2006) Failure analysis of ceramic clinical cases using qualitative fractography. *Int J Prosthodont*, **19**, 185–92.

Scherrer, S. S., Quinn, G. D., Quinn, J. B. & Wiskott, H. W. A. (2007) Fractographic ceramic failure analysis using the replica technique. *Dent Mater* **23**(11): 1397–404.

Schweitzer, D. M., Goldstein, G. R., Ricci, J. L., Silva, N. R. & Hittelman, E. L. (2005) Comparison of bond strength of a pressed ceramic fused to metal versus feldspathic porcelain fused to metal. *J Prosthodont*, **14**, 239–47.

Segal, B. S. (2001) Retrospective assessment of 546 all-ceramic anterior and posterior crowns in a general practice. *J Prosthet Dent*, **85**, 544–50.

Sjögren, G., Lantto, R., Granberg, A., Sundstrom, B. O. & Tillberg, A. (1999a) Clinical examination of leucite-reinforced glass-ceramic crowns (Empress) in general practice: a retrospective study. *Int J Prosthodont*, **12**, 122–8.

Sjögren, G., Lantto, R. & Tillberg, A. (1999b) Clinical evaluation of all-ceramic crowns (Dicor) in general practice. *J Prosthet Dent*, **81**, 277–84.

Stappert, C. F., Dai, M., Chitmongkolsuk, S., Gerds, T. & Strub, J. R. (2004) Marginal adaptation of three-unit fixed partial dentures constructed from pressed ceramic systems. *Br Dent J*, **196**, 766–70; discussion 760, quiz 780.

Sundh, A. & Sjögren, G. (2004) A comparison of fracture strength of yttrium-oxide-partially-stabilized zirconia ceramic crowns with varying core thickness, shapes and veneer ceramics. *J Oral Rehabil*, **31**, 682–8.

Sundh, A. & Sjögren, G. (2006) Fracture resistance of all-ceramic zirconia bridges with differing phase stabilizers and quality of sintering. *Dent Mater*, **22**, 778–84.

Taskonak, B. & Sertgoz, A. (2006) Two-year clinical evaluation of lithia–disilicate-based all-ceramic crowns and fixed partial dentures. *Dent Mater*, **22**, 1008–13.

Thompson, J. Y., Anusavice, K. J., Naman, A. & Morris, H. F. (1994) Fracture surface characterization of clinically failed all-ceramic crowns. *J Dent Res*, **73**, 1824–32.

Tinschert, J., Zwez, D., Marx, R. & Anusavice, K. J. (2000) Structural reliability of alumina-, feldspar-, leucite-, mica- and zirconia-based ceramics. *J Dent*, **28**, 529–35.

Vult von Steyern, P., Jonsson, O. & Nilner, K. (2001) Five-year evaluation of posterior all-ceramic three-unit (In-Ceram) FPDs. *Int J Prosthodont*, **14**, 379–84.

Wagner, W. & Chu, T. (1996) Biaxial flexural strength and indentation fracture toughness of three dental core ceramics. *J Prosthet Dent*, **76**, 140–4.

Walter, M. H., Wolf, B. H., Wolf, A. E. & Boening, K. W. (2006) Six-year clinical performance of all-ceramic crowns with alumina cores. *Int J Prosthodont*, **19**, 162–3.

Wang, Y., Lee, J. J., Lloyd, I. K., Wilson, O. C., Jr., Rosenblum, M. & Thompson, V. (2007) High modulus nanopowder reinforced dimethacrylate matrix composites for dental cement applications. *J Biomed Mater Res A*, **82**(3): 651–7.

Weinstein, M., Katz, S. & Weinstein, A. B. (1962a) Fused porcelain-to-metal teeth. US patent: 3,052,982, Permadent Manufacturing Corporation.

Weinstein, M., Katz, S. & Weinstein, A. B. (1962b) Porcelain covered metal-reinforced teeth. US patent: 3,052,983, Permadent Manufacturing Corporation.

Wen, M. Y., Mueller, H. J., Chai, J. & Wozniak, W. T. (1999) Comparative mechanical property characterization of 3 all-ceramic core materials. *Int J Prosthodont*, **12**, 534–41.

White, S. N., Miklus, V. G., McLaren, E. A., Lang, L. A. & Caputo, A. A. (2005) Flexural strength of a layered zirconia and porcelain dental all-ceramic system. *J Prosthet Dent*, **94**, 125–31.

Wohlwend, A., Strub, J. R. & Scharer, P. (1989) Metal ceramic and all-porcelain restorations: current considerations. *Int J Prosthodont*, **2**, 13–26.

Wolf, W. D., Francis, L. F., Lin, C. P. & Douglas, W. H. (1993) Melt-infiltration processin and fracture toughtness of alumina-glass dental composites. *J Amer Ceramic Soc*, **76**, 2691–4.

Zeng, K., Oden, A. & Rowcliffe, D. (1998) Evaluation of mechanical properties of dental ceramic core materials in combination with porcelains. *Int J Prosthodont*, **11**, 183–9.

Zhang, Y. & Lawn, B. R. (2005) Fatigue sensitivity of Y-TZP to microscale sharp-contact flaws. *J Biomed Mater Res B Appl Biomater*, **72**, 388–92.

Zhang, Y., Pajares, A. & Lawn, B. R. (2004) Fatigue and damage tolerance of Y-TZP ceramics in layered biomechanical systems. *J Biomed Mater Res*, **71B**, 166–71.

Zhang, Y., Bhowmick, S. & Lawn, B. R. (2005a) Competing fracture modes in brittle materials subject to concentrated cyclic loading in liquid environments: monoliths. *J Mater Res*, **20**, 2021–9.

Zhang, Y., Song, J. K. & Lawn, B. R. (2005b) Deep-penetrating conical cracks in brittle layers from hydraulic cyclic contact. *J Biomed Mater Res B Appl Biomater*, **73**, 186–93.

Zhang, Y., Lawn, B. R., Malament, K. A., Van Thompson, P. & Rekow, E. D. (2006) Damage accumulation and fatigue life of particle-abraded ceramics. *Int J Prosthodont*, **19**, 442–8.

24

Dental glass-ceramics

W HÖLAND and V RHEINBERGER,
Ivoclar Vivadent AG, Liechtenstein

24.1 Introduction

The development of glass-ceramics has permitted a variety of different properties to be combined within one specific material. Based on a fundamental understanding of controlling the mechanisms of nucleation and crystallization in glasses, Höland and Beall (2002, 2006) reported on the chemical systems that allow glass-ceramics with special properties to be developed. Control over microstructure formation resulted in materials exhibiting the properties required for applications in a great variety of technical products ranging from the electrical, electronic and optical industries through to the construction sector.

Regarding the development of biomaterials for dental applications, special prerequisites must be met. The focus here is on dental restorative materials, that is, materials with which to restore the natural tooth structure. Typical products in this area of biomaterials are dental inlays, onlays, veneers and bridges. In contrast to bioactive materials, which bond to living bone, restorative material should possess high chemical durability, mechanical strength and toughness, and should exhibit optical properties that mimic the natural tooth microstructure so that the restorations are aesthetically pleasing. Glass-ceramics permit all these properties to be united within one material.

The general research method applied to develop a materials system based on fundamental chemical knowledge and to design a glass-ceramic in such a system is indicated by the path shown in Fig. 24.1.

Designing glass-ceramics in specific chemical systems is based on developing microstructures characterized by one or more crystal phases, or one or more glassy phases. Depending on the application, glass-ceramic systems have been developed either as sintered materials on metal frameworks, or materials for metal-free systems.

Typical glass-ceramics on metal frameworks are leucite and leucite–apatite-based materials. Leucite-reinforced glass-ceramics have also been

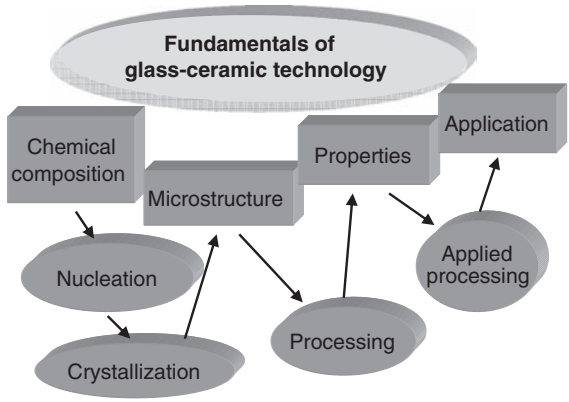

24.1 Glass-ceramics: from materials systems to application.

developed as metal-free biomaterials. Compared with leucite-type glass-ceramics, lithium disilicate glass-ceramics represented a notable improvement in the mechanical strength and fracture toughness of biomaterials. Glass-ceramics containing either ZrO_2 or apatite were developed to fuse to high-toughness sintered ZrO_2 ceramics and to lithium disilicate glass-ceramics, respectively.

24.2 Fabrication

24.2.1 Glass-ceramics fused to metal frameworks

The glass-ceramic of the type IPS d.SIGN® (Ivoclar Vivadent AG) represents a veneering material with optical properties highly matched to the natural tooth microstructure. This was achieved by precipitating two crystal phases within the glass-ceramic material. The dual mechanism governing this particular microstructural development is called two-fold nucleation and crystallization. One mechanism controls the formation and precipitation of the first phase and another one that of the second phase. Leucite, $KAlSi_2O_6$, represents the main crystal phase and fluoroapatite, $Ca_5(PO_4)_3F$, the secondary phase. The material is contained in the 49–58 wt% SiO_2, 11–21 Al_2O_3, 9–23 K_2O, 1–10 Na_2O, 2–12 CaO, 0.5–6 P_2O_5, 0.5–2 F composition range and obviously its chemistry is very complex.

Nucleation and crystallization were identified as critical mechanisms affecting the development of the microstructure by Höland and Beall (2002, 2006), and therefore each fabrication step to produce the material has to be controlled very precisely. Leucite is precipitated by surface nucleation and crystallization, and fluoroapatite by internal nucleation and crystallization in the bulk of the material. The driving force for the latter is an

amorphous-amorphous phase separation process (Höland and Beall, 2002, 2006). A particular morphological characteristic of fluoroapatite precipitation is the growth of the crystals with a needle-like habit. This gives the biomaterial its characteristically natural appearance.

Sintering technology is used to veneer the glass-ceramic to different types of metal alloys, including highly precious metals, in the dental laboratory.

24.2.2 Metal-free glass-ceramics

The first metal-free glass-ceramic was a mica-type glass-ceramic. The products based on this material were Dicor® and Dicor® MGC (Dentsply International). Mica is a layered silicate characterized by preferred cleavage along the 00l-plane of the crystal. Because of this preferred crystal cleavage, a glass-ceramic containing mica crystals is generally characterized by very good machinability (Beall, 1971; Grossman, 1991; Malament and Grossman, 1987). The inventors of this type of glass-ceramic showed that dental crowns and inlays with specific shapes could be fabricated from the material to suit a particular clinical situation. On the one hand the glassy matrix of the glass-ceramic permitted processing by centrifugal casting. This method was typical for Dicor®. On the other hand, the preferred cleavage of the crystals imparted good machinability. This characteristic was typically exploited when processing Dicor® MGC. The presence of crystals up to 2 μm in length in the material resulted in an improvement of the mechanical strength over other materials.

The SiO_2–Al_2O_3–K_2O system is very well known from the development of porcelains (Kingery *et al.*, 1975). The knowledge of the chemical nature of these materials gained from the work on chinaware products also formed the basis for developing biomaterials for dental restorations (McLean, 1972; O'Brian, 1978). Furthermore, the SiO_2–Al_2O_3–K_2O system is also the basis for glass-ceramics used in dental restorations. Glass-ceramics derived from this system contain leucite, $KAlSi_2O_6$, as the main crystal phase and a glassy silicate matrix phase. Leucite is an alumosilicate-framework crystal phase that is different from feldspar, the phase typically found in porcelains. The development and processing of this type of glass-ceramic require that the leucite crystal phase evolution be controlled in such a way that uniformly sized crystals are formed, which are randomly oriented in the glassy matrix. Accordingly, a controlled surface nucleation and crystallization mechanism was developed (Höland *et al.*, 1995). The preferred method for controlling the nucleation and crystal growth rates of leucite is tribochemical activation of the base glass.

Leucite-type glass-ceramics with chemical compositions in the 59–63 wt% SiO_2, 19–23.5 Al_2O_3, 10–14 K_2O, 3.5–6.5 Na_2O, 0–1 B_2O_3, 0–1 CeO_2, 0–3 CaO system are processed by surface nucleation and crystallization. Biomaterials

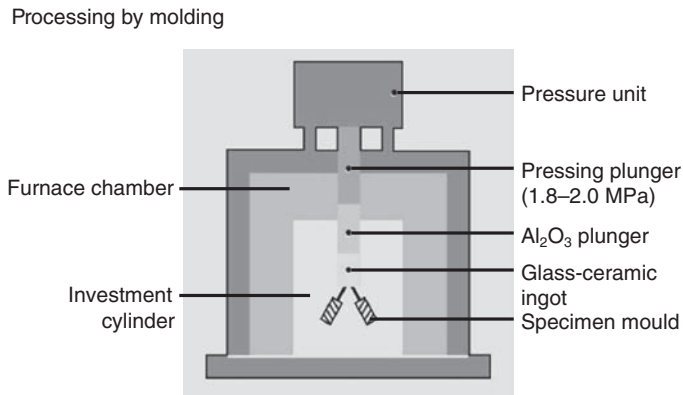

24.2 Moulding furnace for fabricating leucite-type dental restorations.

as metal-free products possess a high crystal content of approx. 35 vol%. This crystal content yields good mechanical properties and makes it possible to use this glass-ceramic as an individually shaped metal-free biomaterial. Shaping of individual restorations with high accuracy is made possible by the moulding process. Figure 24.2 shows a furnace used for moulding leucite-type glass-ceramics.

A typical metal-free glass-ceramic of the leucite-type is IPS Empress® (Ivoclar Vivadent AG). The dental technician has three processing options available when working with this glass-ceramic: moulding (with the so-called Empress technology,), sintering (IPS Empress layering materials) and machining (IPS ProCAD®, IPS Empress® CAD).

This moulding fabrication process differs from centrifugal casting and is characterized by high viscosity of the viscous flow process. Aluminosilicate glass-ceramics have a special 'long' viscosity–temperature characteristic, where so-called 'long' glasses exhibit a flat viscosity-temperature function. The first glass-ceramic processed with this technology was IPS Empress® (Ivoclar Vivadent AG) and enabled individual shaping of dental crowns, veneers and inlays. Leucite-type glass-ceramics can also be fabricated by sintering. The preferred area of application of this method is veneering the moulded dental IPS Empress® crown. These veneering glass-ceramics also possess special optical properties: translucency and shading can be controlled, and opalescence can be achieved.

The third option open to the dental technician or dentist for preparing leucite-type materials is machining with the aid of CAD/CAM technologies. The Cerec® apparatus (Sirona, Germany) and the D4D (USA) technology are the preferred methods to machine the glass-ceramics. Surprisingly, this moulding technology can also be applied for processing so-called 'short' glass-ceramics characterized by a steep viscosity–temperature function. A

typical glass-ceramic of this type is multi-component lithium disilicate, $Li_2Si_2O_5$, glass-ceramic. The crystal phase $Li_2Si_2O_5$ is a sheet silicate and it is possible to precipitate over 60 vol% of these crystals in the glassy matrix. A typical glass-ceramic with this characteristic is IPS Empress®2, which is derived from the 57–80 SiO_2, 11–19 Li_2O, 0.5–5 P_2O_5, 0.5–8 ZnO, 0.1–13 K_2O, 0.1–5 Al_2O_3 composition. The high crystalline content is made possible by a bulk nucleation and crystallization mechanism.

Lithium disilicate glass-ceramics are well known. The first glass-ceramic developed by Stookey (1959) was of this type. Beall (1971) developed various lithium silicate glass-ceramic products under the names Fotoform® and Fotoceram®. Based on the body of knowledge gained from developing the numerous lithium disilicate glass-ceramics and the research activities conducted to develop IPS Empress® 2, yet another different glass-ceramic containing lithium disilicate crystals could be developed in the 64–75 SiO_2, 13–17 Li_2O, 2–5 P_2O_5, 3–4.5 K_2O, 0.5–5 Al_2O_3 composition range. Analysis of the phase formation processes (Apel *et al.*, 2007; Höland *et al.*, 2006a) in this system revealed the nucleation mechanism to be based on nano-scale heterogeneous epitaxial nucleation. Nano-sized phosphate phases act as heterogeneous catalysts for the formation of both lithium metasilicate, Li_2SiO_3, and lithium disilicate crystals. Both of these crystal phases precipitate in parallel within the glassy matrix, but the rate of lithium metasilicate precipitation is higher than that of lithium disilicate.

On this basis a lithium metasilicate glass-ceramic can be fabricated as a blue-coloured intermediate glass-ceramic, which exhibits good machining properties. The dental technician or dentist is thus able to machine the material to prepare dental crowns. However, the colour of the material, the chemical durability and the mechanical strength of a lithium metasilicate glass-ceramic are not appropriate for dental applications. The desired properties for this role are developed by subjecting the lithium metasilicate to an additional heat treatment at 850 °C which transforms the material into a lithium disilicate glass-ceramic. A typical such machinable glass-ceramic with lithium disilicate glass-ceramic as the final dental product is IPS e.max® CAD (Ivoclar Vivadent AG) (Bürke, 2006; Rheinberger, 2005).

The dental technician also has a second option for fabricating dental products from the IPS e.max® press system, namely the moulding process. This glass-ceramic can be processed in the same way as the IPS Empress® 2 and IPS Empress® materials.

24.2.3 Glass-ceramics fused to high-strength sintered ceramics

The first glass-ceramic developed to be fused to high-strength ZrO_2 ceramic dental posts was a ZrO_2-containing glass-ceramic (Höland and Beall, 2002;

Schweiger *et al.*, 1996). This glass-ceramic derived from the SiO_2–ZrO_2–P_2O_5 system contains $Li_{12}ZrSi_6O_{15}$ crystals as the main crystal phase, but different types of ZrO_2 crystals are also precipitated in the glassy matrix. Because of their similar coefficients of thermal expansion (CTE) the glass-ceramic restoration can be fabricated by moulding the material to the sintered ZrO_2 dental post.

ZrO_2 has become a very interesting biomaterial not only in human medicine, but also in dental applications. High-strength and high-toughness dental posts, crowns and bridges can be prepared from this material. In order to adjust the properties of ZrO_2, especially its abrasion behaviour and optical properties, to the properties of the natural tooth, the bare ceramic has to be veneered. Glass-ceramics are good candidates with which to veneer ZrO_2-ceramics. The IPS e.max® ZirCAD materials system contains both lithium disilicate glass-ceramics and ZrO_2 sintered ceramics (Rothbrust, 2006) in addition to the relevant veneering glass-ceramics. An example of such a veneering material is an apatite-containing glass-ceramic whose main crystalline phase is nano-sized fluoroapatite embedded in a glassy matrix. The product names are IPS e.max® Ceram and IPS e.max® ZirPress (Schweiger, 2006). The chemical composition range of these types is 50–65 wt% SiO_2, 5–11 Na_2O, 4–8 K_2O, 1–4 CaO, 8–22 Al_2O_3, 0.1–2 P_2O_5, 0.2–2 F.

24.3 Microstructure

24.3.1 Glass-ceramics fused to metal frameworks

The IPS d.SIGN® glass-ceramic consists of leucite and fluoroapatite crystals and a glassy matrix. Microstructure formation in this glass-ceramic type is characterized by the growth of leucite, $KAlSi_2O_6$, from the surfaces of the individual glass grains into their bulk. The fluoroapatite phase grows in the bulk of the glass grains. The final glass-ceramic product exhibits needle-like fluoroapatite and leucite crystals embedded in a glassy matrix (Fig. 24.3).

Crystal coarsening in fluoroapatite has been shown to occur by an Ostwald ripening mechanism (Müller *et al.*, 1999). Heating the glass-ceramic to 1050 °C results in the growth of large crystals at the expense small crystals and a reduction in the total number of crystals present.

24.3.2 Metal-free glass-ceramics

IPS Empress® esthetic glass-ceramics contain leucite crystals as the main crystal phase. A surface crystallization mechanism initiates growth of the primary crystals, which grow out from an individual nucleation center like flower petals (Fig. 24.4). The final product, e.g. after moulding, shows

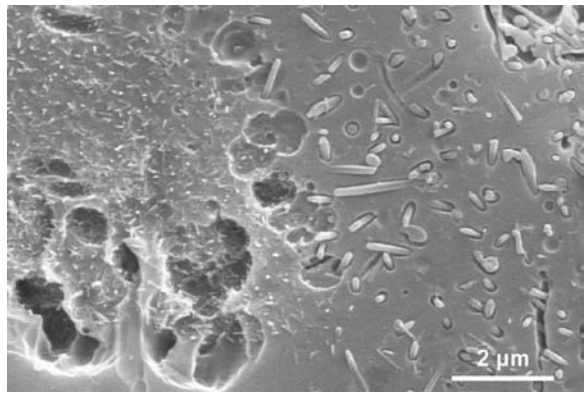

24.3 Microstructure of a leucite-apatite glass-ceramic (SEM, etched sample; Courtesy: reproduced from Höland, Beall (2002). Glass-ceramic technology. The American Ceramic Society, Westerville, Ohio, USA, www.ceramics.org., Copyright 2002. All rights reserved.

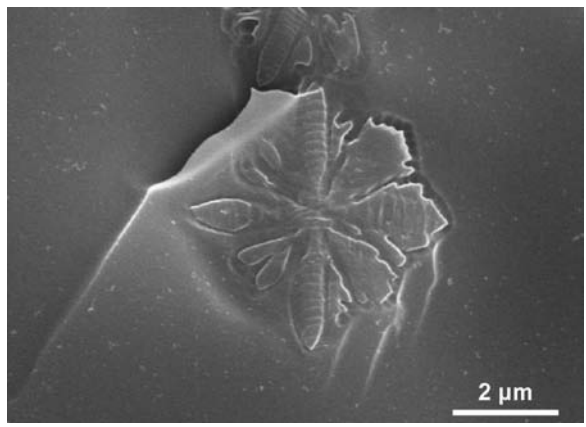

24.4 Microstructure formation in leucite-type glass-ceramics (SEM, etched samples). Beginning of crystal growth.

leucite crystals randomly distributed in the glassy matrix, and typically crystal twinning can be observed (Fig. 24.5).

The microstructure of IPS Empress® 2 shows lath-like lithium disilicate crystals embedded in a glassy matrix. After selective etching with HF to obtain a retentive microstructure suitable for adhesive cementation was obtained (Höland and Beall, 2002, 2006). The microstructure exhibits interlocking crystals and the total crystalline content is approx. 60 vol%.

The two-step technological process to fabricate the lithium disilicate glass-ceramics of IPS e.max® by machining involves lithium metasilicate

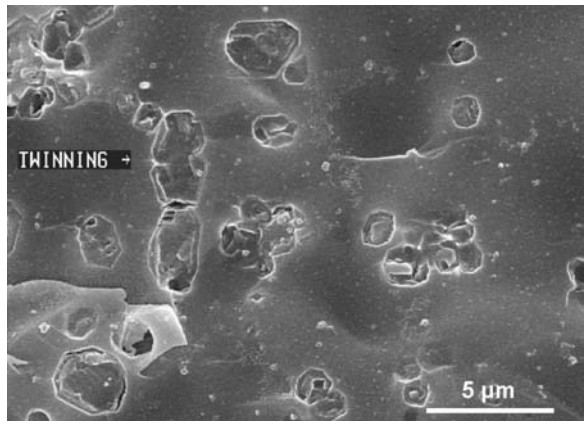

24.5 Microstructure formation in leucite-type glass-ceramics (SEM, etched samples). Final product. Courtesy: reproduced from Höland, Beall (2002). Glass-ceramic technology. The American Ceramic Society, Westerville, Ohio, USA, www.ceramics.org., Copyright 2002. All rights reserved.

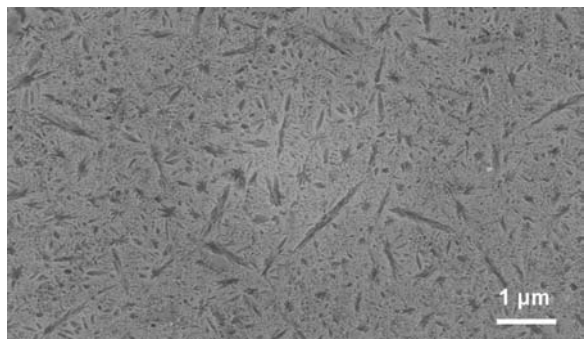

24.6 Microstructure of the lithium metasilicate glass-ceramic precursor blue material of IPS e.max® (SEM after etching). Courtesy: reproduced from: W. Höland, Glaskeramik, (2006), vdf / UTB, UTB-ISBN-13: 978 3 8252 2813 2.

glass-ceramic as the precursor material. Lithium metasilicate crystals grow dendritically in the glassy matrix. A typical microstructure of this blue-coloured glass-ceramic is shown in Fig. 24.6.

After machining, the lithium metasilicate glass-ceramic is transformed into a lithium disilicate glass-ceramic by heat treatment at 850 °C. The final glass-ceramic does not contain any lithium metasilicate crystals. The microstructure is characterized by a dense interlocking crystal morphology and the crystalline fraction can reach up to 70 vol%. Such a microstructure is shown in Fig. 24.7.

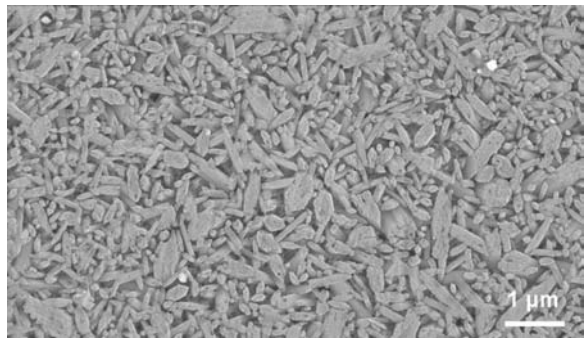

24.7 Interlocking microstructure of the lithium disilicate glass-ceramic in the IPS e.max® system. The glass-ceramic workpiece was shaped by machining and subsequently subjected to a heat treatment at 850 °C (SEM after etching). Courtesy: reproduced from: W. Höland, Glaskeramik, (2006), vdf / UTB, UTB-ISBN-13: 978 3 8252 2813 2.

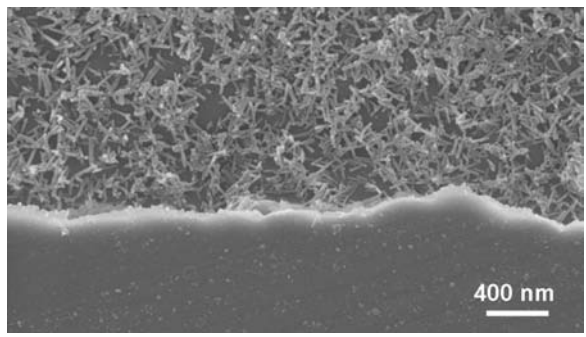

24.8 SEM micrograph of a fluoroapatite-containing glass-ceramic fused to a ZrO_2 dental crown. The nano-sized fluoroapatite crystals exhibit a needle-like habit.

24.3.3 Glass-ceramics fused to high-strength sintered ceramics

Glass-ceramics with high specific ZrO_2 contents were developed to fuse to sintered ZrO_2 ceramic posts. One type with high strength, but also high opacity, contained ZrO_2 crystals in its microstructure. A second type with translucent properties was obtained by precipitating $Li_{12}ZrSi_6O_{15}$ crystals in the glassy matrix (Höland and Beall, 2002, 2006).

Fluoroapatite-containing glass-ceramic is the preferred material to fuse to lithium disilicate glass-ceramics and to high-toughness sintered ZrO_2 ceramics. Needle-like nanometre-sized fluoroapatite crystals are precipitated in the glassy matrix in this glass-ceramic. The SEM micrograph in Fig. 24.8. Here the glass-ceramic was fused to a ZrO_2 ceramic of the IPS e.max®

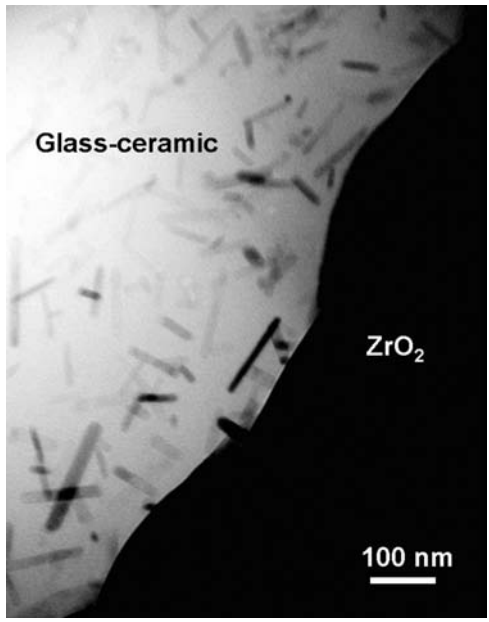

24.9 TEM image of the interface between the fluoroapatite glass-ceramic and the ZrO_2 ceramic showing very close contact between the two materials (Courtesy W. Siegler, Center for Transmission Electron Microscopy, MPI, Stuttgart, Germany).

system. Transmission electron microscopy (TEM) was applied to study the interface between the fluoroapatite-containing glass-ceramic and the ZrO_2. The analysis revealed a very close contact between the two materials and no gaps could be detected (Fig. 24.9).

24.4 Properties of the glass-ceramics

24.4.1 Glass-ceramics fused to metal frameworks

Sintered glass-ceramics such as IPS d. SIGN® must be divided into three groups of materials according to their areas of application: glass-ceramics that simulate the dentin of the natural tooth, glass-ceramics that simulate incisal and composites that contain glass-ceramics as opacifiers. The third group are inorganic–inorganic composites with glass-ceramic components, which are applied to metal frameworks, e.g. crowns or multi-unit bridges (four units or more) after casting and oxidizing. The layer is fixed to the framework by sintering and must have good contact with the underlying metal and must exhibit an opacifiying effect which enables the layer to hide the framework beneath it.

Table 24.1 Properties of IPS d.SIGN glass-ceramics

Properties	Leucite apatite glass-ceramic
Flexural strength	80 MPa
Translucency	10–90% absorption
CTE (25–500 °C)	11.5 to 13.1 $\times$ $10^{-6}K^{-1}$
Chemical durability	Less than 50 $\mu g/cm^2$

The mechanical properties of the dental restorations built on metal frameworks are largely imparted by the high-strength and high-toughness metal alloys used in their construction. Therefore, glass-ceramics used as dentin and incisal material must not exhibit particularly good mechanical properties. The physical and mechanical properties of IPS d.SIGN® are summarized in Table 24.1. These properties were determined according to dental standards (ISO 6872, 1998; ISO 9693, 1999; BS 5612, 1978).

A very important property with respect to the subsequent fusing of glass-ceramics to the opaquer on the metal framework is the CTE. The CTE of the material controls the surface stress condition, and accordingly a surface tension can be imparted, which increases the strength of the material. The chemical durability of the material was determined in 4% acetic acid according to the relevant dental standard. The weight loss of the material, determined after treatment at 80 °C for 16 h, was very low and completely fulfilled the requirements set by the standard (Kappert, 1999).

The optical properties, especially translucency and brightness, are controlled by the homogeneity of the crystalline leucite and apatite microstructure. This has permitted the development of different sub-types of materials within the IPS d.SIGN ® system showing varying degrees of light transmission. The following values indicate the absorption in percentage of several glass-ceramic materials (1 mm thick samples): Transpa material (10), incisal (20), dentin (40), margin (45), deep dentin (60), brilliant dentin (90).

The abrasion behaviour of the glass-ceramic materials in dental restorative applications is also very important. Ideally the glass-ceramic should show abrasion behaviour similar to that of the natural tooth so that the artificial biomaterial does not destroy the natural opposing teeth. Sorenson *et al.* (1999) demonstrated that the wear behaviour of IPS d.SIGN®-type glass-ceramics is compatible with that of natural teeth in *in vitro* experiments.

24.4.2 Metal-free glass-ceramics

Leucite-type glass-ceramics exhibit physical, chemical and mechanical properties which make them suitable biomaterials for use as dental inlays,

Table 24.2 Properties of leucite-type glass-ceramics (IPS Empress®) in comparison with lithium disilicate glass-ceramics (IPS Empress® 2)

Properties	Leucite glass-ceramic	Lithium disilicate glass-ceramic
Flexural strength	110–180 MPa	400 ± 40 MPa
K_{IC}	1.3 ± 0.1 MPa m$^{1/2}$	3.3 ± 0.3 MPa m$^{1/2}$
Translucency	Comparable to natural tooth	Comparable to natural tooth
CTE	15–16 × 10^{-6} K^{-1} (25–500 °C)	10.6 ± 0.25 × 10^{-6} K^{-1} (100–400 °C)
Chemical durability	Less than 100 μg/cm^2	50 μg/cm^2

onlays, veneers and crowns. Their main properties are summarized in Table 24.2, which shows how this type of material combines a number of very different specific properties. The flexural strength of more than 100 MPa (typically between 110 and 180 MPa) was determined by Dong *et al.* (1992). Ludwig (1994) showed that the load of 500 N held by a dental crown was more than double that required for this type of dental restoration.

A high CTE and good chemical durability are characteristic for leucite-type materials. The CTE of IPS Empress® materials measures 15–17 × 10^{-6} K^{-1} (100–500 °C). Leucite has a high CTE (Höland and Beall, 2002, 2006) and because a high volume fraction of this crystalline phase is present within the glass-ceramic, this material also shows a high CTE. The chemical durability of the leucite glass-ceramic meets the requirements of the relevant dental standards. Chemical durability with respect to the conditions in the human mouth is very important for a successful application. However, controlled etching with hydrogen fluoride gels is also required to permit the development of a retentive microstructure on the inner surface of the metal-free biomaterial. The reason for this is the preferred cementation situation on the natural tooth. The surface roughness of the etched glass-ceramic is of the order of several micrometres, thus yielding an optimally retentive situation for cementation.

It is very important that the finished metal-free biomaterial demonstrates optimal wear behaviour in its clinical application as a tooth restorative product. Heinzmann *et al.* (1990) and Krecji *et al.* (1992) simulated the mastication process and demonstrated abrasion behaviour of the material which compares favourably with that of natural tooth.

All the properties of leucite-type glass-ceramics manufactured by the moulding process are very similar to those of the machinable leucite-type glass-ceramics. Widely used CAD/CAM materials are IPS ProCAD® and

IPS Empress® CAD. A specific product in this range is called IPS Empress® CAD multi. The special characteristic of this CAD/CAM ingot material is that it exhibits a shade gradient similar to that found in natural teeth. The final machined dental product shows this shade gradient and suitable polishing or glazing makes additional shading unnecessary.

Lithium disilicate glass-ceramics possess much better mechanical properties than leucite-type glass-ceramics. The two mouldable materials IPS Empress® and IPS Empress® 2 are compared in Table 24.2. The flexural strength of the lithium disilicate Empress® 2 glass-ceramic is significantly higher at approx. 400 MPa (biaxial measurements by Sorenson *et al.*, 2000) and the fracture toughness in terms of the K_{IC}-value is improved by more than 3 MPa $m^{0.5}$.

The mouldable glass-ceramic IPS e.max® Press should exhibit even better mechanical properties. Albakry *et al.* (2003) determined the flexural strength and Weibull modulus of different materials in compliance with ASTM F 394-78. The strength of approx. 440 MPa measured for this material is clearly higher than that of IPS Empress®2. Furthermore, the Weibull modulus increased from approx. 8 to approx. 9. Because strength measurements in ceramic materials tend to yield a wide distribution of values, the Weibull strength $\sigma_{63.21\%}$ (the load at which 63.21% of all samples measured failed) was determined by Marx *et al.* (2001). This analysis yielded strengths of approx. 380 MPa for IPS e.max® Press and approx. 290 MPa for IPS Empress® 2.

After machining and heat treatment at 850 °C the machinable glass-ceramic IPS e.max® CAD shows a flexural strength of approx. 400 MPa. The other main properties are similar to those of IPS e.max® Press. The CTE, for example, is the same at $10.6 \times 10^{-6} K^{-1}$ and therefore the same veneering material can be used for both IPS e.max ® Press and IPS e.max® CAD.

Very high mechanical strengths were achieved in a special research programme studying lithium disilicate glass-ceramics derived from the ZnO-free SiO_2–Li_2O–K_2O–P_2O_5–Al_2O_3 system. Here a flexural strength of 740 MPa was measured (based on 60 glass-ceramic discs). Furthermore, a Weibull modulus of $m = 11$ was determined (Höland *et al.*, 2003, 2006b, 2007; Ritzberger *et al.*, 2006). These surprising results give an indication of how the mechanical strength of glass-ceramic biomaterials can be further improved in the future.

Sorenson *et al.* (1999) investigated the wear behaviour of lithium disilicate glass-ceramics. These examinations demonstrated wear characteristics similar to those of natural teeth. This surprising result, in addition to the good chemical durability of the material, confirms the suitability of this type of biomaterial for use in dental crowns and small three-unit bridges in the anterior area.

Table 24.3 Properties of IPS e.max® Zir Press, a fluoroapatite-containing glass-ceramic

Properties	Apatite containing glass-ceramic
Flexural strength	110 ± 10 MPa
Translucency	Comparable to natural tooth (incisal)
CTE (100–400 °C)	$9.75 \pm 0.25 \times 10^{-6} K^{-1}$
Chemical durability	Less than 30 μg/cm^2

24.4.3 Glass-ceramics fused to high-strength sintered ceramics

The most important property of the high ZrO_2-content glass-ceramics is the ability to fuse them to the dental post by applying moulding technology. The moulding procedure is conducted at 900 °C.

Apatite-containing glass-ceramics are used as veneering materials for both lithium disilicate glass-ceramics and ZrO_2 ceramics. The fluoroapatite crystals in the veneer match its optical properties to the controlled translucency and brightness of the glass-ceramic product underneath. IPS Empress® 2 glass-ceramics are veneered with IPS Eris for E2, and the glass-ceramics IPS e.max® Press, IPS e.max® CAD and the ceramic IPS e.max®Zir CAD are veneered with the fluoroapatite glass-ceramic IPS e.max®Ceram. The main properties of this last material are summarized in Table 24.3.

24.5 Application

24.5.1 Glass-ceramics fused to metal frameworks

The development of different shades of leucite-apatite glass-ceramic IPS d.SIGN® was carried out by H. Kerschbaumer, H.P. Foser (Liechtenstein), Cornell and Winter (2000). Clinical tests were successfully conducted by Winter and Cornell (USA) and by Reitemeier and Walter (Germany). Reitemeier cemented 59 crowns with the hybrid ionomer cement ProTecCEM in a 5 year clinical study. The metal framework was made of high-gold alloy Aquarius hpf (Williams). The glass-ceramic was concluded to be very good with regard to aesthetics and dental laboratory considerations. These glass-ceramics are generally used for dental crowns and dental bridges of more than three units, and since 1998, more than 60 million dental units have been successfully applied worldwide. One unit represents a single dental crown, an inlay or an veneer. Figure 24.10 shows a three-unit dental bridge on a metal framework.

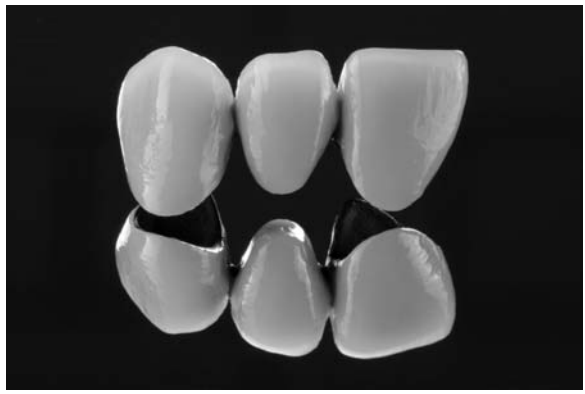

24.10 Application of leucite-apatite glass-ceramic on a metal framework. Product: IPS d.SIGN®. Courtesy: reproduced from W. Höland, *Glaskeramik*, (2006), vdf/UTB, UTB-ISBN:978-3-8252-2813-2.

24.5.2 Metal-free glass-ceramics

The leucite-type glass-ceramics with the IPS Empress® moulding system have been in use worldwide since 1990 and more than 26 million units have been successfully applied. Clinical studies have demonstrated the very high degree of survival of this particular biomaterial. Over a period of 11 years, Fradeani and Redemagni (2002) considered 54 patients with 125 crowns (93 anterior and 32 posterior) with recalls after 4–11 years. The quality was assessed according to CDA and Ryge criteria and the risk of fracture was determined by the Kaplan–Meier method. The combined estimated survival rate was 95.2% after 11 years, with the anterior crowns exhibiting 98.9% and the posterior crowns 88.4%. Only six crowns had to be replaced, and most of the crowns were characterized as excellent (in the nomenclature: alpha). Based on this clinical study, the clinical studies of

- Frankenberger and Petschelt (2000) – 6 year clinical study showing a survival rate of 92%;
- Studer *et al.* (1998) and Brodbeck (1996) – 7 year studies with inlays and onlays demonstrating a survival rate of 97.5%;
- Edelhoff *et al.* (2000) – investigation of conventionally and adhesively cemented crowns showing a survival rate of 97.9% for conventional and 98.1% for adhesively cemented crowns after 4 years

and an additional 13 clinical studies (the reports by Petschelt, Lutz, Richter, Pröbster, Sorensen, Roulet, Malament, Vreven, Van Dijken, Koch, Tidehag, Schmalz and Stachnis are available), showed that IPS Empress® crowns

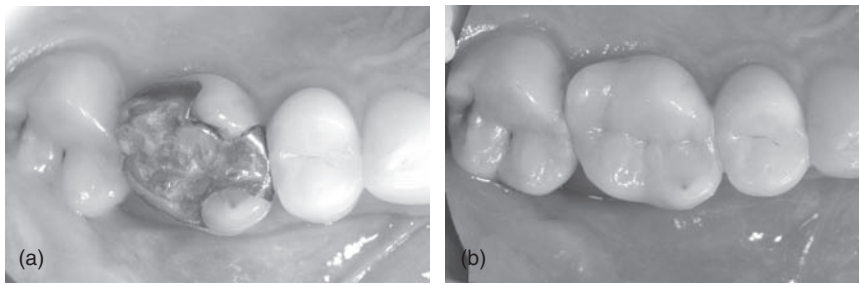

24.11 Aesthetics of an IPS Empress® dental onlay. (a) pre-clinical situation with amalgam filling, (b) final result with glass-ceramic. Courtesy: reproduced from W. Höland, *Glaskeramik*, (2006), vdf/UTB, UTB-ISBN:978-3-8252-2813-2.

attained a very good survival rate comparable to, or even better than, porcelain fused to metal restorations. Here it should be noted that the high survival rate is not only a function of the material, but that it is also based on correct adhesive cementation of the glass-ceramic to the natural tooth.

A glass-ceramic as a metal-free restoration shows much better aesthetics than materials applied to metal substrates. Figure 24.11 demonstrates the aesthetic appeal of a leucite glass-ceramic IPS Empress® dental only in a clinical situation. The glass-ceramic shows translucency similar to that of natural tooth and therefore blends in with the surrounding natural tooth.

Lithium disilicate glass-ceramics, e.g. IPS Empress® 2 veneered with IPS Eris for E2, demonstrate better mechanical properties than the leucite type glass-ceramics and are therefore suitable for indications of posterior crowns and small anterior bridges up to the second premolar. The clinical studies of Pospiech (see Kistler *et al.*, 2000), Edelhoff *et al.* (2002) and Sorenson and coworkers (Sorenson and Mito, 1998; Sorenson *et al.*, 1999, 2000) have demonstrated the clinical success of this material. However, a high clinical success rate will only be achieved if the technical specifications are carefully followed when preparing the restoration. The design of a dental bridge requires special attention: the connector area between the three units must measure 4 mm × 4 mm.

The clinical study by Edelhoff (2006) of the lithium disilicate glass-ceramic IPS e.max® Press considered 121 crowns and 18 bridges placed adhesively using glass ionomer cement. Not one framework fractured in the first 23 months. Anusavice (2005) determined a failure rate of approx. 10% in a 5 year clinical study, which also considered bite forces in detail. If the highest bite force and restorations with faulty connector design are excluded from this evaluation, the 5 year failure rate is reduced to 3.3%.

Clinical studies of the machinable lithium disilicate glass-ceramic IPS e.max® (e.g. Edelhoff, 2006; Kelly, 2006) showed dental crowns to be the preferred indication for this material. The glass-ceramic can be veneered

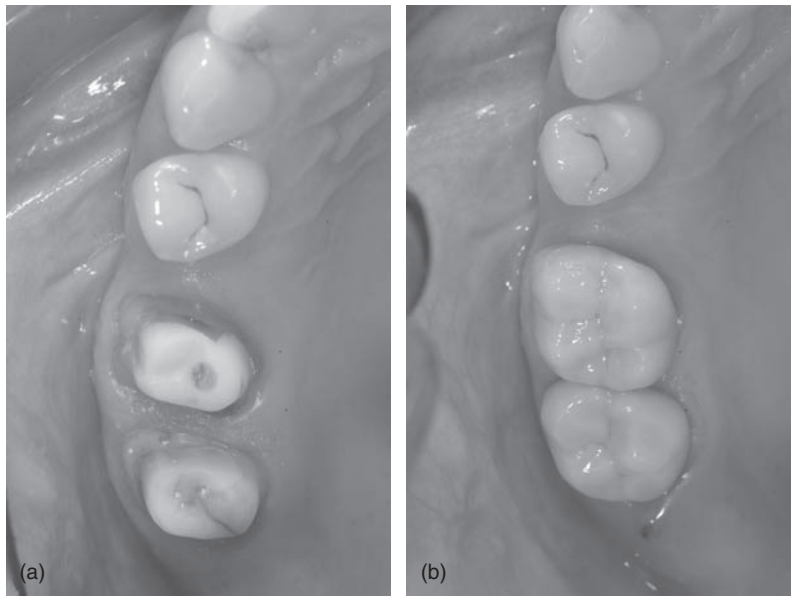

24.12 Dental crowns of IPS e.max® CAD type. (a) Preparation of tooth 16, 17. Reconstruction of the coronally compromised tooth 16 with fibre reinforced composite post and core (FRC Postec). (b) IPS e.max® CAD crowns on teeth 16, 17. Surface glaced. Courtesy: A. Stiefenhofer, F. Perkon.

with an apatite glass-ceramic. Figure 24.12 shows IPS e.max CAD glass-ceramic veneered with the apatite-containing glass-ceramic IPS e.max® Ceram.

24.5.3 Glass-ceramics fused to high-strength sintered ceramics

Clinical studies of the apatite-containing glass-ceramic IPS e.max® Ceram used as a veneering material for lithium disilicate glass-ceramics and ZrO_2 sintered ceramics were successfully conducted by Weigel, Nathanson, Kelly, Stanford, Sorenson, Fasbinder, Beuer, Rammelsberger, Strub and Tinschert. The 34 month study by Weigel (2005) resulted in a survival rate of 97.1%. All the experiments and clinical tests showed that the preparation of the surface of the framework must be carried out precisely according to the technical instructions and that careful temperature control during the sintering process is also very important. A highly aesthetic dental biomaterial results if the technical guidelines are carefully followed. The result of such careful work is shown in Fig. 24.13.

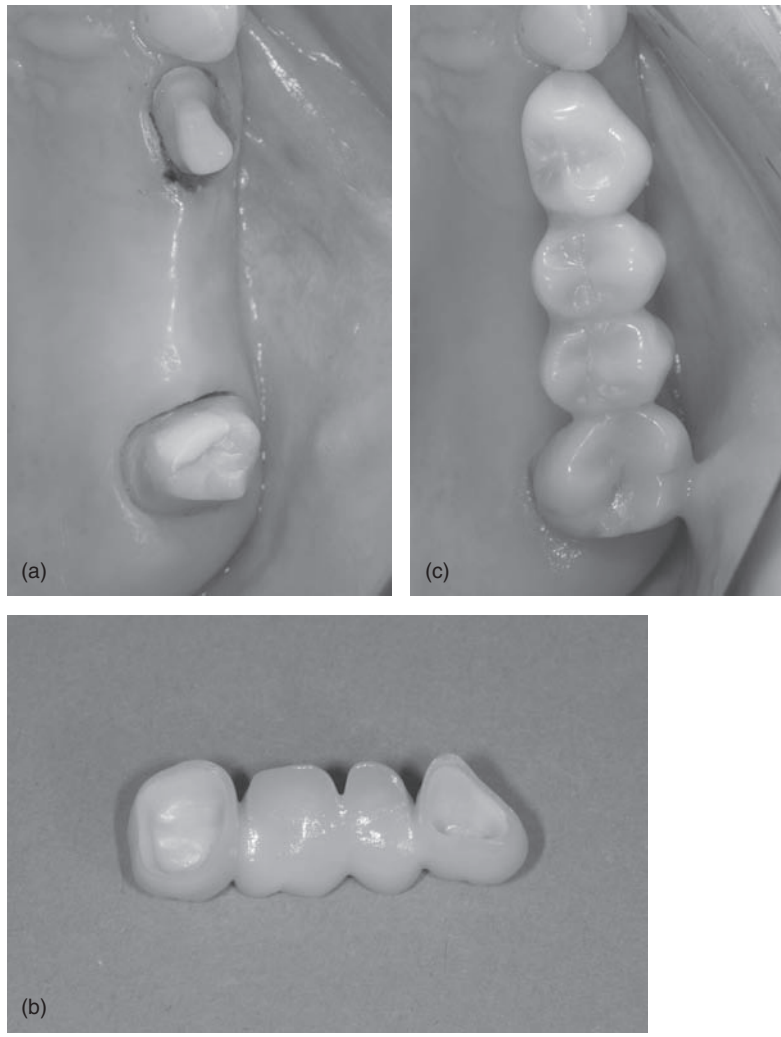

24.13 Four-unit dental bridge of a ZrO2 framework and veneered with apatite-containing glass-ceramic IPS e.max® ZirPress and IPS e.max® Ceram. (a) Preparation of tooth 24 and 27. (b) ZrO2 bridge of IPS e.max® ZirCAD framework and IPS e.max® ZirPress and IPS e.max® Ceram veneering. (c) All-ceramic bridge 24–27 in situ. Courtesy: A. Stiefenhofer, F. Perkon.

24.6 Summary

The mechanisms of controlled nucleation and crystallization of glasses have been applied to develop both glass-ceramics as veneering material for metal dental restorations and glass-ceramics as metal-free dental restorations. The

metal-free restorations were developed as leucite-type glass-ceramics by controlled surface nucleation and crystallization and lithium disilicate glass-ceramics applying the heterogeneous internal nucleation and crystallization mechanisms. Processing of both types of glass-ceramics is characterized by moulding or machining using CAD/CAM methods. The clinical successful application of leucite-type glass-ceramics is concentrated on dental inlays, crowns and veneers. The lithium disilicate glass-ceramics veneered with an apatite containing glass-ceramics are used as single unit biomaterials or small dental bridges. The apatite glass-ceramic is also applied as veneering material for ZrO_2 bridges.

24.7 References

Albakry M, Guazzato M, Swain MV (2003), 'Biaxial flexural strength, elastic moduli, and X-ray diffraction characterization of three pressable materials', *J Prothet Dent*, **89**, 374–380.

Anusavice KJ (2005), Ivoclar Vivadent Internal Report.

Apel E, van 't Hoen C, Rheinberger V, Höland W (2007), 'Influence of ZrO_2 on the crystallization and properties of lithium disilicate glass-ceramics derived from a multi-component system', *J Europ Ceram Soc*, **27**, 1571–1577.

Beall GH (1971), 'Structure, properties, and nucleation of glass-ceramics', in: *Advances in Nucleation and Crystallization in Glasses*, Spec Publ No 5, ed.: Hench LL, Freiman SW, The American Ceram Soc, Columbus, OH, 251–261.

Brodbeck U (1996), 'Six years of clinical experience with an all-ceramic system', *Signature Summer Edition*, 8–14.

Bürke H (2006), '*IPS e.max Press and IPS e.max CAD*', Report Ivoclar Vivadent, 6–16.

Cornell DF, Winter RR (2000), 'Eine neue Entwicklung: Glaskeramik zur Verwendung bei Metallen', *Dental Dialogue*, **1**, 58–71.

Dong JK, Lüthy H, Wohlwend A, Schärer P(1992), 'Heat-pressed ceramics–technology and strength', *Quintessenz*, **43**, 1373–1385.

Edelhoff D (2006), Presentation at Dental Congress Ivoclar Vivadent.

Edelhoff D, Hostkemper T, Richter EJ, Spiekermann H, Yildirim M (2000), 'Adhesiv und konventionell befestigte Empress- Kronen: Klinische Befunde nach vierjähriger Tragedauer', *Dt Zahnärztl Zeitschr*, **55** (5), 326–330.

Edelhoff D, Brauner J, Spiekermann H, Yilderim M (2002), 'Two-year clinical evaluation of crowns and bridges made of IPS Empress 2', *J Dent Res*, **81**, Spec Iss A, abstract 2584.

Fradeani M, Redemagni M (2002), 'An 11-year clinical evaluation of leucite-reinforced glass-ceramic crowns: a retrospective study', *Quintessence Int*, **33**, 503–510.

Frankenberger R, Petschelt A (2000), 'Leucite-reinforced glass-ceramic inlays and onlays after six years: clinical behavior', *Operative Dent*, **25**, 459–465.

Grossmann DG (1991), 'Structure and physical properties of Dicor/MGC glass-ceramic', *Int Symp on computer rest*, ed.: Mörmann WH, *Quintessence*, Chicago, IL, 103–115.

Heinzmann JL, Krejci I, Lutz F (1990), 'Wear and marginal adaptation of glass-ceramic inlays, amalgam and enamel', *J Dent Res*, **69**, 161.
Höland W, Beall GH (2002), '*Glass-ceramic Technology*', The American Ceramic Society, Westerville, OH.
Höland W, Beall GH (2006) *Glass-ceramic Technology*, Wiley, New York.
Höland W, Frank M, Rheinberger V (1995), 'Surface crystallization of leucite in glass', *J Non-Cryst Sol*, **180**, 292–307.
Höland W, Rheinberger V, Schweiger M (2003), 'Control of nucleation and crystallization in glass-ceramics', *Phil Trans R Soc London A*, **361**, 575–589.
Höland W, Rheinberger V, Apel E, van 't Hoen C, Höland M, Dommann A, Obrecht M, Mauth C, Graf-Hauser U (2006a), 'Clinical application of glass-ceramics in dentistry', *J Mat Sci: Mat in Med*, **17**, 1037–1042.
Höland W, Apel, E, van 't Hoen C, Rheinberger V (2006b), Studies of crystal phase formation in high-strength lithium disilicate glass-ceramics', *J Non-Cryst Sol*, **353**, 4041–4050.
Höland W, Rheinberger V, Apel E, van 't Hoen (2007), 'Principles and phenomena of bioengineering with glass-ceramics for dental restoration', *J Europ Ceram Soc*, **27**, 1521–1526.
Kappert HF (1999), Presentation at DGZPW, Germany.
Kelly R (2006), *Clinical Performance of IPS e.max Ceram*. Ivoclar Vivadent internal report.
Kingery WD, Bowen HK, Uhlmann DR (1975), *Introduction to Ceramics*, Wiley, New York.
Kistler S, Pospiech P, Frasch C, Gernet W (2000), 'Clinical performance of Empress 2 lithium disilicate glass-ceramic posterior crown: results up to two years', *J Dent Res*, **79**, abstract 230.
Krecji I, Krejci D, Lutz F (1992), 'Clinical evaluation of a new pressed glass-ceramic inlay material during 1.5 years', *Quintessence Int*, **23**, 181–186.
Ludwig K (1994), 'Untersuchungen zur Bruchfestigkeit von IPS Empress-Kronen in Abhängigkeit von den Zementierungsmodalitäten', *Quint Zahntech*, **20**, 247–256.
Mac Lean JW (1972), 'Dental porcelains', *Dental Material Research*, NBS Publications 354, ed. Dickson G, Cassel JM, Nat Bureau of Stand, Washington, DC, 77–83.
Marx R, Fischer H, Weber M, Jungwirth F (2001), 'Rissparameter und Weibullmodule: unterkritisches Risswachstum und Langzeitfestigkeit vollkeramischer Materialien', *Dt Zahnärtl Zeitschr*, **56**, 89–98.
Malament KA, Grossman D (1987), 'The cast glass-ceramic restoration', *J Prosthetic Dent*, **57**, 674–683.
Müller R, Abu-Hilal LA, Reinsch S, Höland W (1999), 'Coarsening of needle-shaped apatite crystals in the SiO_2-Al_2O_3-Na_2O-CaO-P_2O_5-F glass', *J Mat Sci*, **34**, 65–69.
O'Brian WJ (1978), '*Dental porcelains*', *An Outline of Dental Materials and their Selection*, ed. by O'Brian WJ, Ryge G, Saunders, Philadelphia, PA, 180–194.
Ritzberger C, Höland W, Rheinberger V (2006), 'Grundlagenforschung zur Phasenbildung von Apatitmischkristallen und Leuzit in Glaskeramiken', Presentation DGG conference, Nuremberg, Germany.
Rheinberger V (2005), '*Vom Experiment zur Erfolgsgeschichte-Materialforschung eröffnet heute breites Indikationsspektrum*', *Die Zahnarzt Woche, DZW*, **37**, 14–15.

Rothbrust F (2006), *IPS e.max ZirCAD*, Report Ivoclar Vivadent, 17–25.
Schweiger M, Frank M, Rheinberger V, Höland W (1996), 'New sintered glass-ceramic based on apatite and zirconia', *Proceedings Int Symp on Glass Problems*, Vol 2, 229–235.
Schweiger M (2006), *IPS e.max Ceram*, Report Ivoclar Vivadent, 25–36.
Sorensen JA, Mito WT (1998), 'Rational and clinical technique for esthetic restorations of endodontically treated teeth with the CosmoPost and IPS Empress Post system', *Qunit Dent Technol*, **21**, 81–90.
Sorensen JA, Cruz M, Mito WT, Merrideth H, Raffeiner O (1999), 'Empress 2 all-ceramic bridge clinical trails: status 1998', *J Dent Res*, 218.
Sorensen JA, Berge HX, Edelhoff D (2000), 'Effect of storage media and fatigue loading on ceramic strength', *J Dent Res*, **79**, 217.
Stookey DR (1959), 'Catalyzed crystallization of glass in theory and practice', *Ind Eng Chem*, **51**, 805–808.
Studer S, Lehner C, Schärer P (1998), 'Seven-year results of leucite-reinforced glass-ceramic inlays and onlays', *J Dent Res*, abstract 1375.
Weigel (2005), *Clinical Study*. Ivoclar Vivadent internal report.

Part III

Clinical applications of bioceramics

25

Clinical application of bioactive glasses

H O YLÄNEN, Åbo Akademi University and
University of Turku, Finland

25.1 Introduction

Bonding of glasses to bone has been demonstrated for a certain compositional range of bioactive glasses containing SiO_2, Na_2O, CaO and P_2O_5 in specific proportions (Hench and West, 1996). Three compositional changes differentiate bioactive glosses from soda lime–silica glasses: high Na_2O and CaO content, less than 60% SiO_2 and a high CaO/P_2O_5 ratio. These compositional features create highly reactive surfaces when exposed to an aqueous medium. However, in bioactive glasses, the amount of SiO_2, which is only about 45–60%, can easily cause problems in the form of phase separation and crystallization of the glassy material. Crystallization of the material will reduce the rate of bioactivity of the glass (Peitl Folho *et al.*, 1996), and partial crystallization leads to a glassy phase of incontrollable composition. Crystallization of a bioactive glass can be controlled by its chemical composition (Brink, 1997).

A new generation of bioactive glasses in the system Na_2O–K_2O–MgO–CaO–B_2O_3–P_2O_5–SiO_2 can be repeatedly heated without the risk of devitrification (Brink, 1997; Arstila *et al.*, 2004). Thus, for instance, microspheres can be manufactured and sintered into porous implants of different shapes and sizes (Ylänen *et al.*, 1999; Fröberg *et al.*, 2004). The porosity of a bioactive glass body does not only noticeably increase the total reacting surface of the glass, but also allows a three-dimensional formation of the healing bone tissue. The porosity and the mechanical strength of the bioactive glass implant can be controlled with different sintering temperatures and times (Fröberg *et al.*, 2004). For the best mechanical strength of the sintered implant, the glass must retain its amorphous structure during the heat treatment. The development of third-generation bioactive glasses at Åbo Akademi University, Turku, Finland has enabled spinning of high-quality thin (20–30 μm) bioactive glass fibres. From these fibres, a variety of bioactive glass fabrics can be made. Bioactive glass fibres can be woven together with, for example, biodegradable polymer fibres to form a fabric. The

polymer can be used as a carrier for biologically active molecules, etc. Moreover, an impulse laser beam can be used to melt a fine powder made from the new bioactive glass withstanding devitrification during the momentary heating exposure. As a result, a glass coating on a titanium implant can be relatively easily produced. This coating consists of very small glass droplets firmly attached to the titanium. The glass shows excellent bioactivity in spite of the repeated high-temperature procedures involved in the process (Moritz *et al.*, 2003; Vedel *et al.*, 2003).

When discussing the clinical application of bioactive glasses one must realize that these new bioactive glasses that show better and controllable technical and chemical properties will allow the development of a wide selection of bioactive glass and composite products in the near future.

25.2 Applications of bioactive glasses

25.2.1 Maxillofacial, ear, nose and throat applications

The composition of the first bioactive glass (Bioglass®, today available also as PerioGlas®, BioGran®) and the composition of S53P4 (BonAlive™ granules, plate) (Fig. 25.1), which have been widely used clinically, are presented in Table 25.1. Both bioactive glasses have been reported to have good bioactive properties. The glasses can be cast into shaped implants (BonAlive™ plate) for use as small medical devices in places subject to only minor mechanical loading. The glass is relatively soft and thus appropriate for microsurgical drilling techniques (Wilson *et al.*, 1993). Bioglass® has been used to replace small bones in the middle ear and as cone-shaped implants to fill defects in the mandible and maxilla. It also elicits a property of bonding to soft tissue, which has opened new possibilities for wider application, for example, in ear, nose and throat (ENT) surgery. In the treatment of profound deafness, various electronic components are used within

25.1 Bioactive glass granules and plates (BonAlive™) for bone cavity filling and reconstruction. Copyright Vivoxid Ltd.

Table 25.1 Compositions of some bioactive glasses with clinical applications (wt%)

Component	Bioglass® PerioGlas® BioGran®	BonAlive™
SiO_2	45	53
Na_2O	24.5	23
CaO	24.5	20
P_2O_5	6	4

appropriate devices. Electrodes attached to the electronic devices outside and inside the middle ear are coated with Bioglass® (Wilson *et al.*, 1993). The device is inserted so that a part is in contact with bone, resulting in a firm anchoring. The other part of the bioactive glass-coated anchor passes through the eardrum and bonds to the soft tissue, thus providing a seal between the inner and outer ear. Stanley *et al.* (1997) introduced the concept of filling a hole in the jawbone after extracting a tooth in order to prevent resorption of the bone. For this procedure, conical implants are made using injection molding. For the best possible fit of the conical implant, a mating drill bit is used to prepare the bone for the implant.

The management of orbital floor fractures continued to be debated until the early 1990s. By that time bioactive glasses were in the new group of materials developed for the repair of bone defects that were beyond any innate healing capacity due to their size. Kinnunen *et al.* (2000) compared the use of alloplastic implants (bioactive glass) with conventional autogenous grafts (cartilage plus or minus lyophilized dura) for the repair of orbital floor defects after trauma. In the study, 28 patients having orbital floor fractures with persistent diplopia, enophthalmos and/or infraorbital nerve paraesthesia were operated on from 1991 to 1995 at Turku University Central Hospital. Reconstruction was either with bioactive glass (S53P4) or autogenous cartilage implants. Post-operative tomograms in the 28 patients showed adequate maintenance of orbital and maxillary sinus volume without any evidence of resorption in either group. None of 14 patients in the study group had any evidence of dystopia or complications relating to implants at follow-up. One had infraorbital nerve paraesthesia and another had entropion post-operatively. Among the 14 control subjects there were three cases of persistent diplopia, two of infraorbital nerve paraesthesia and one of enophthalmos. Bioactive glass implants were well tolerated and provided a promising repair material for orbital floor fractures. Their use leads to less morbidity as no donor site operation is needed. Also it provides favourable healing as it is bioactive and biocompatible. Since then, solid-shaped

bioactive glass (S53P4) has been used in the treatment of facial injuries to replace the bone that supports the eye (BonAlive™ plate) (Fig. 25.2).

Several studies also show promising results of using crushed bioactive glass or paste as obliteration material in frontal sinusitis (BonAlive™ granules) (Fig. 25.3) and in special types of rhinitis (BonAlive™ plate) (Suonpää

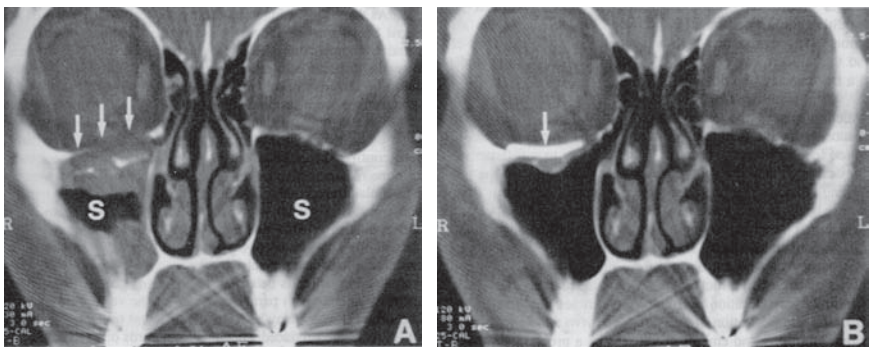

25.2 X-ray image showing a defect of orbital floor (A) and (B) where bioactive glass plate (BonAlive™ plate) has been used in orbital floor reconstruction. Copyright Vivoxid Ltd.

25.3 X-ray image showing sinus frontalis (circled) which has filled by bioactive glass granules (BonAlive™ granules) for sinus obliteration. Copyright Vivoxid Ltd.

et al., 1997; Peltola *et al.*, 1998; Stoor *et al.*, 1998; Aitasalo *et al.*, 2000). Many alloplastic materials have been used in clinical frontal sinus obliteration. It has been difficult to find reliable obliteration material without short- or long-term complications. The most common problem in frontal sinus obliteration is the resorption of occlusion material. An interesting report is given by a 9 year follow-up of using bioactive glass granules in frontal sinus obliteration (Aitasalo *et al.*, 2000). Bioactive glass (BAG) S53P4 (Bonalive™ granules) were used as obliteration material in a series of osteoplastic frontal sinus operations on 32 patients from 1990 to 1999 at the ENT Department of the Turku University Central Hospital. Five of consecutive patients of this material were accurately controlled by computed tomography (CT) scans at 1 week, 6, 12, 24, 36, 48 months and analysed with Region of Interest (ROI). Also in three cases at 12, 18 months and 8 years histopathologic samples were obtained. The average yearly decrease in Hounsfield Units (HU) was 7.1–18%. The decrease was similar on the surface and in the middle of the BAG mass. The histopathologic samples after 12 and 18 months showed dense fibrous tissue between the granules but no inflammatory changes. Eight years after obliteration the clinical status and CT scan were normal and in histopathologic examination there was a clear woven bone formation and no inflammatory or foreign body reactions. BAG is a good and well-tolerated bone substitute for osteoplastic frontal sinus operations. The results of the obliteration are maintained owing to the stability of the material and in a new bone formation capacity.

The findings of Stoor *et al.* (1998, 1999) and Munukka *et al.* (2007) suggest that the encouraging results of using bioactive glass crush in ENT surgery are partially because of the antibacterial effects of bioactive glass paste on oral micro-organisms. In an aqueous environment, ions are released from a BAG and the pH rises in its vicinity. This may influence both growth and colonization of microorganisms. Stoor *et al.* studied the effects of the BAG S53P4 on the atrophic rhinitis-associated microorganism *Klebsiella ozaenae*. The glass was used in the form of granules or discs. Growth inhibition was studied using an agar plate test. Adhesion was studied by incubating bacterial suspension with the glass. The effect of the presence of the bacteria on the formation of the Si-rich layer on the bioactive glass was also analysed. Furthermore, a follow-up study of 19–74 months with *ozaenae* patients surgically treated with the BAG S53P4 was performed. The bioactive glass showed no clear growth inhibition of *K. ozaenae* in the agar plate test. *K. ozaenae* showed low adherence to the BAG S53P4. No growth of the microbe was seen on the glass during the 8 hour incubations and the Si-rich layer was formed normally. The clinical follow-up study showed no infections of the implants and the symptoms of the patients were markedly reduced. Thus, the BAG S53P4 did not favour adhesion and colonization of

K. ozaenae, *in vitro*, which is supported by the *in vivo* findings showing no BAG-associated infections or reinfections.

Bioactive glass implants have also been used in some rare but difficult nasal problems associated with infections. When the medical therapy fails, trephination is the primary operation indicated in acute eroding sinusitis when drainage is necessary to avoid severe complications. In recent years endoscopic transnasal surgery has also been recommended for exenteration of the underlying disease in the ostiomeatal unit as well as for opening of the obstructed nasofrontal duct in acute phase of the disease. In Turku University Central Hospital endoscopic frontal sinus surgery is still reserved for cases with prolonged or delayed disease performed as a secondary operation after trephination and CT examination. Failures are common after these operations and both types of surgical treatment may be needed. Three per cent of the patients develop a persistent chronic infection inside the frontal sinus. In these cases external osteoplastic approach is recommended. In these operations the use of bioactive glass as obliteration material gives promising clinical results (Suonpää *et al.*, 1997).

Interpositional grafts between mucoperiosteal flaps are commonly used in the repair of septal perforations. The use of BAG S53P4 has been studied as an interpositional graft in patients suffering from septal perforations caused by microorganisms *Haemophilus influenzae* and *Streptococus pneumoniae* (Stoor *et al.*, 2001). The perforations were successfully closed in 10 of 11 patients. One patient had a near total septum perforation, which could not be closed. No BAG-associated infections were seen during the follow-up. The BAG S53P4 did not show any clear growth inhibition of the microorganism, which showed low adhesion to the material. Serum precoating increased the adsorption.

In sum, the area of indications for maxillofacial and ear, nose, and throat applications for BonAlive™ granules are:

- frontal sinus obliteration after severe chronic sinusitis;
- frontal sinus obliteration after fractures in the frontal bone area;
- reconstruction of bone defects in the frontal bone area;
- mastoid sinus obliteration and nasal cavity narrowing;
- skull bone defects including jaws.

BonAlive Plate™ can be used in orbital and cranial defects for:

- fractures;
- tumour surgery;
- reconstruction of bone defects.

Nasal applications are:

- nasal septum perforation reconstruction;
- nasal cavity narrowing.

25.2.2 Orthopaedic bone graft applications

The use of bioactive glass as granules is reported to enhance bonding because of the chemistry associated with the bioactivity, reactivity because of increased surface area, and the method of application. Bioactive glass granules have been reported to provide a promising option to be used alone as a filler material in bone defects or to fill the gap around the implants.

A prospective, randomized study compared BAG with autogenous bone (AB) as a filler in benign bone tumour surgery (Heikkilä *et al.*, 1995). Patient selection was made by the Turku University Bone Tumor Group. Pre-operative examinations and postoperative follow-up included plain films, CT, magnetic resonance imaging (MRI) and single photon emission computed tomography (SPECT). The mean follow-up period for the 12 patients was 15 months (range 4–24). No complications related to the filler materials were observed. All wounds healed well without signs of infection. The repair of the defects filled with BAG granules started from the periphery and advanced into the deeper parts of the defects during the follow-up. Plain films and CT revealed no resorptive changes at the BAG–bone interface. Bony sclerosis appeared both at the bone margins and outer part of the bone defect. Contrast-enhanced MRI indicated in-growth of fibrovascular tissue into the spaces between the granules. In radioisotope examinations using SPECT a centripetal activation of the defects was observed. One defect was explored 1 year post-operatively and the retrieved specimen analysed using histology, scanning electron microscopy and energy disperisng X-ray analysis. However, according to Virolainen *et al.* (1997), the bone-forming capacity of bioactive glass particulate seems to be lower compared with an autogenous bone graft. One of the indications for BonAlive™ Granules is bone cavity filling also in orthopedic bone defects.

25.2.3 Odontological applications

More than 10 years ago, a controlled study model was designed to study the healing and regeneration rate of periodontal bony defects with and without bioactive glass, S53P4 (Larmas *et al.*, 1995). Patients with two or three wall vertical bony defects of the same depth on both sides of the mandible or maxilla were recruited. A modified Widman flap was performed on both sides of the jaw on the same day by the same clinician. The bony defects on the experimental side were filled with bioactive glass granules (diameter 630–800 μm). Initial findings revealed a good clinical and radiographic response to the treatment. Evidence of osteogenesis and osteointegration of the glass granules could be seen in some radiographs. Since

25.4 Regeneration of periodontal bone defect by using bioactive glass granules (circled).

then, bioactive glass particles have been widely used to fill defects associated with periodontal disease (Fig. 25.4).

Various methods have been investigated in order to create sufficient amount of bone for placement of endosseous implants in the atrophic alveolar crest. Problems often exist in the posterior part of maxilla due to the proximity of the maxillary sinus and the insufficient quality and quantity of alveolar bone (Ulm *et al.*, 1995). Turunen *et al.* (2004) have shown that bioactive glass granules 800–1000 μm in diameter can be used as a bone adjunctive material in maxillary sinus floor augmentation when mixed with autologous bone chips. Before the clinical use of bioactive glass granules for this indication, the concept was studied using the following protocol: a bilateral sinus floor augmentation procedure was performed in 17 patients to study the effect of BAG granules mixed with AB chips on bone regeneration. The posterior part of 17 maxillary sinus was augmented with a 1:1 mixture of BAG granules (800–1000 μm) and AB chips harvested from the iliac crest (BAG–AB group). The anterior parts of the same sinus and the contralateral sinus, serving as a control (AB group), were filled with AB chips alone. Trephine biopsies for histological, scanning electron microscopy (SEM) and energy dispersive X-ray (EDX) analyses were taken from the posterior part of the sinus 21–34 weeks after the insertion of dental implants. Additionally, six biopsies were taken from the BAG–AB group and four biopsies were taken from the AB group in connection with abutment operation at 49–62 weeks.

Histological evaluation revealed lamellar bone growth in all the specimens. Although most of the BAG granules were without bone contact in the majority of the patients in the BAG–AB group, the bone lamellae were thicker than observed in the AB group. In the contact areas, bone was growing along the glass surface connecting the particles together.

Histomorphometrical analysis carried out from the SEM images at 21–34 weeks revealed 26% and 25% bone in the BAG–AB and the AB group, respectively. The corresponding figures for 49–62 weeks were 29% for the BAG–AB group and 25% for the AB group. Bone–BAG complex, i.e. the granules with intimate contact with bone, occupied 34% of the area measured at 21–34 weeks and 31% at 49–62 weeks. EDX analysis showed a tight contact and chemical bonding between the glass and bone. As a sign of dissolution, a few small Si-depleted areas were present in some BAG granules at 21–34 weeks, while more and larger Si-free areas were observed in the granules at 49–62 weeks. The results indicated that BAG granules (S53P4) can be used together with AB chips for sinus floor augmentation procedure, thus decreasing the amount of bone needed. Today, the procedure is successfully carried out using only bioactive glass granules.

Bioactive glass is also suitable for treating patients suffering from hypersensitive teeth. The recessing of gingival margins often leads to exposed dentin tubules. The tubules run to the pulp and according to the hydrodynamic theory liquid flow in tubules causes incising in the teeth. The most common reasons for gingival recessions are periodontal operations and poor tooth-brushing habits. The clinical influence of very fine bioactive glass powder (<45 μm) is depended on high amount of Si, Ca and P ions in treated areas. When a high concentration of Si, Ca and P ions is kept near dentin the precipitation of amorphous apatite takes place at and inside the tubules. The clinical applicability of the Novamin Technology, Inc., USA product series (SootheRX®, DenShield®, Oravive™, NuCare™, Nanosensitive hca®) has been tested with patients who report incising tooth surfaces after periodontal operation. One week after the periodontal operation, when the sutures had been removed, teeth in the operation area were tested with air blast and cold water. The incising teeth were covered with the bioactive glass powder material or control material and further with surgical baggage for 5 days. Patients were examined after 2 days, and 2, 5, 15 and 23 weeks after the application of active or control material. The estimation of the degree of incising was done verbally and visually with visual analog scale (VAS) method. The information was marked on a special formula. The sensation of pain decreased in the treated areas significantly already after a treatment of 1 week.

25.3 Future trends

At Åbo Akademi University in Turku, Finland, the development of new bioactive glasses has continued intensively. Today, it is possible to make tailor-made bioactive glasses for several purposes and to a number of products such an microspheres, fibres, sintered porous structures and woven fabrics. Also, composites are manufactured using biodegradable polymers

and bioactive glasses. In the future we will probably see products where the load-bearing structure is made by, for example, slowly biodegradable polymer reinforced by slowly reacting bioactive glass fibres and where the polymer also acts as a carrier for biologically active molecules. Bioactive glass in different forms can also be used for fixation of more stable and/or load-bearing devices.

25.4 Concluding remarks

As discussed in this chapter, the properties of bioactive glasses are strongly influenced by the synthesis methods employed, the chemistry and any other thermal processes used. All these factors contribute to their final structure and hence to their long-term performance as bioglasses. In the early 1970s, bioceramics were employed to perform biologically inert roles, such as providing parts for bone replacement. The realization that cells and tissues in the body perform many other vital regulatory and metabolic roles has highlighted the limitations of synthetic materials as tissue substitutes. The demands placed on bioceramics have changed from maintaining an essentially physical function without eliciting a host response to providing a more integrated interaction with the host, which has been accompanied by increasing demands on medical devices to improve the quality of life, as well as to extend its duration.

Bioactive glasses can be used as body interactive materials, helping the body to heal, or promoting regeneration of tissues, thus restoring physiological functions. This approach could be further explored in the development of next-generation bioglasses incorporating biogenic materials with a widened range of applications. Recently, the tissue-engineering field has been directed to take advantage of the combined use of living cells and tridimensional scaffolds to deliver vital cells to a patient's damaged site. Feasible and productive strategies have been aimed at combining a relatively traditional approach such as bioactive glass implants with the acquired knowledge applied to the field of cell growth and differentiation of osteogenic cells.

A common characteristic of bioactive glasses is a time-dependent kinetic modification of the surface that occurs after implantation. The surface forms a carbonate hydroxyapatite (hydroxycarbonate apatite) layer. Results of various studies show that bioactive glass affects the osteogenesis by increasing collagen synthesis and calcification of the extracellular matrix *in vitro* and promotes new bone formation in calvarial defects in Sprague–Dawley rats. Bonding of glass to bone has been observed to occur between 2 weeks and 2 months after implantation. Clinical studies are promising and their use in the orthopaedic field is increasing. Bioactive glasses are currently filling a gap in surgical orthopaedic and maxillofacial applications. However,

the challenge of providing safe and efficacious glass with the required properties and an acceptable biocompatibility level remains. As the field of biomaterials finds increasing applications in cellular and tissue engineering, it will continue to be used in new ways as part of the most innovative therapeutic strategies.

25.5 References

Aitasalo K, Peltola M, Suonpää J, Yli-Urpo A (2000), 'Bioactive glass S53P4 in frontal sinus obliteration'. A 9 years experience in *Bioceramics* vol. 13, Bologna, Trans Tech Publications, 877–880.

Arstila H E, Vedel E, Hupa L, Ylänen H, Hupa M (2004), 'Measuring the devitrification of bioactive glasses', *Key Engineer Mater*, **254–256**, 67–70.

Brink M (1997), 'Bioactive glasses with a large working range', *Ph.D. thesis*, Åbo Akademi University, Turku, Finland.

Fröberg L, Hupa L, Hupa M (2004), 'Porous bioactive glasses with controlled mechanical strength' *Key Engineer Mater*, **254–256**, 973–976.

Heikkilä J T, Mattila K T, Andersson Ö H, Knuuti J, Yli-Urpo A, Aho A J (1995), 'Behaviour of bioactive glass in human bone' in Wilson K, Hench L and Greenspan D, *Bioceramics* vol. 8, Singapore, World Scientific, 35–40.

Hench L L, West J K (1996), 'Biological applications of bioactive glasses', *Life Chem Rep* **13**, 187–241.

Kinnunen I, Aitasalo K, Pöllönen M, Varpula M (2000), 'Reconstruction of orbital floor fraction using bioactive glass', *J Cranio-Maxillofacial Surg*, **28**, 229–234.

Larmas E, Sewon L, Luostarinen T, Kangasniemi I, Yli-Urpo A (1995), 'Bioactive glass in periodontal bone defects. Initial clinical findings of soft tissue and osseus repair' in Wilson J, Hench L and Greenspan D, *Bioceramics* vol. 8, Singapore, World Scientific, 279–284.

Moritz N, Vedel E, Ylänen H, Jokinen M, Hupa M, Yli-Urpo A (2003), 'Creation of bioactive glass coating on titanium by local laser irradiation, Part I: Optimisation of the processing parameters', *Key Engineer Mater*, **240–242**, 221–224.

Munukka E, Leppäranta O, Korkeamäki M, Vaahtio M, Peltola T, Zhang D, Hupa L, Ylänen H, Salonen J I, Viljanen M K, Eerola E (2007), 'Bactericidical effects of bioactive glasses on clinically important aerobic bacteria', Epub ahead of print, *J Mater Sci: Mater Med.*

Peitl Filho O, LaTorre G P, Hench L L (1996), 'Effect of crystallization on apatite-layer formation of bioactive glass 45S5', *J Biomed Mater Res*, **30**(4), 509–514.

Peltola M, Suonpää J, Aitasalo K, Varpula M, Yli-Urpo A, Happonen R-P (1998), 'Obliteration of the frontal sinus cavity with bioactive glass', *Head Neck*, **20**(4), 315–318.

Stanley H R, Hall M B, Clark A E, King C J, III, Hench L L, Berte J J (1997), 'Using 45S5 bioglass cones as endosseous ridge maintenance implants to prevent alveolar ridge resorption: a 5-year evaluation', *Int J Oral Maxillofac Implants*, **12**(1), 95–105.

Stoor P, Söderling E, Salonen J I (1998), 'Antibacterial effects of a bioactive glass paste on oral micro organisms', *Acta Odontol Scand*, **56**(3), 161–165.

Stoor P, Söderling E, Grenman R (1999), 'Interactions between the bioactive glass S53P4 and the atropic rhinitis-associated micro organism *Klebsiella ozaenae*', *J Biomed Mater Res*, **48**(6), 869–874.

Stoor P, Söderling E, Grenman R (2001), 'Bioactive glass S53P4 in repair of septal perforations and its interactions with the respiratory infection-associated microorganisms haemophilus influenzae and streptococcus pneumoniae', *J Biomed Mater Res*, **58**, 113–120.

Suonpää J, Sipilä J, Aitasalo K, Antila J, Wide K (1997), 'Operative treatment of frontal sinusitis', *Acta Otolaryngol Suppl* (*Stockh*), **529**, 181–183.

Turunen T, Peltola J, Yli-Urpo A, Happonen R-P (2004), 'Bioactive glass granules as a bone adjunctive material in maxillary sinus floor augmentation', *Clin Oral Impl Res*, **15**, 135–141.

Ulm C W, Solar P, Gsellmann B, Matejka M, Watzek G (1995), 'The edentulous maxillary alveolar process in the region of the maxillary sinus – a study of physiological dimensions', *J Oral Maxillofac Surg*, **24**, 279–282.

Vedel E, Moritz N, Ylänen H, Jokinen M, Yli-Urpo A, Hupa M (2003), 'Creation of bioactive glass coating on titanium by local laser irradiation, Part II: Effect of the irradiation on the bioactivity of the glass', *Key Engineer Mater*, **240–242**, 225–228.

Wilson J, Yli-Urpo A, Happonen R-P (1993), 'Bioactive glasses: clinical applications' in Hench L L and Wilson J, *An Introduction to Bioceramics*, Singapore, World Scientific, 63–73.

Virolainen P, Heikkilä J, Yli-Urpo A, Vuorio E, Aro H T (1997), 'Histomorphometric and molecular biologic comparison of bioactive glass granules and autogenous bone grafts in augmentation of bone defect healing', *J Biomed Mater Res*, **35**(1), 9–17.

Ylänen H O, Helminen T, Helminen A, Rantakokko J, Mattila K, Karlsson K H, Aro H T (1999), 'Porous bioactive glass matrix in reconstruction of articular osteochondral defects', *Ann Chir Gyn*, **83**(3), 237–245.

26

Clinical application of bioactive glass-ceramics

T YAMAMURO, Kyoto University, Japan

26.1 Introduction

It is now widely known that bioactive ceramics such as Bioglass®, Ceravital®, synthetic hydroxyapatite (HA), apatite- and wollastonite-containing glass-ceramic (AW-GC) and β-tricalcium phosphate (β-TCP) have a character of osteoconduction and a capability of forming a direct bond to living bone tissue (Oonishi *et al.*, 1999, 2000). In other words, they are incorporated into living bone tissue in accordance with the pattern of bonding osteogenesis. In their clinical use, however, the mechanical property and the grade of bioactivity required to each material differ depending on the case, i.e., size, shape and location of the bone defect, and the purpose of application. For example, when they are to be used for replacing a vertebral body, high mechanical strength rather than high bioactivity is required, if both are not available at the same time. In contrast, when they are to be used as a coating material over the surface of joint prosthesis, high bioactivity rather than high mechanical strength is required. Generally in orthopaedic application of bioactive ceramics to substitute for a large bone defect, high mechanical strength is always required. For this reason, Bioglass® and Ceravital® which have much lower mechanical strength than human cortical bone have not been used in the field of orthopaedic surgery, although their bioactivity is higher than others. As β-TCP is a biodegradable ceramic, its mechanical property after implantation cannot be compared with those of others. The author's personal experience of their clinical use is, therefore, mostly limited to HA and AW-GC that were used in forms of either granular, porous or dense bone substitute in combination with autogenous bone, and also in forms of coating material for joint prosthesis or bioactive cement (Fig. 26.1).

26.2 Why glass-ceramic?

At Kyoto University Hospital, in 1981, probably for the first time in the world as far as is known from the literature and meetings, a large amount

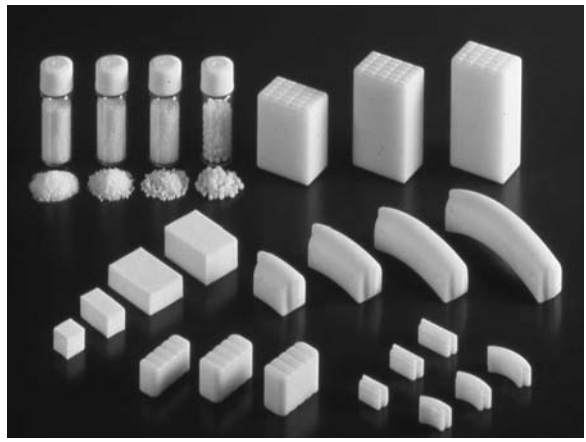

26.1 Bone substitutes of AW-GC in various shapes.

26.2 Large giant cell tumour developed in the right ilium of a 27-year-old female.

of synthetic HA granules was implanted into a human bone to replace a large giant cell tumour which developed in the right ilium of a 27-year-old female (Fig. 26.2). During the operation, the tumour was resected through a window made in the lateral wall of the ilium. The bone defect remained

in the pelvic bone after the resection since it was too large to be completely filled with autogenous bone chips, but bone allografts were not yet available in 1981. Then, a large amount of granular and porous HA was prepared, mixed with fibrin glue and autogenous bone chips, and the mixture compactly filled the bone defect. The clear line, which was demonstrated on the post-operative radiograph between the implanted mass and the pelvic bone, persisted for about 8 months after surgery suggesting that the implant had not yet united with the pelvic bone (Fig. 26.3). At 10 months after surgery, a biopsy of the implanted mass was performed and it was confirmed histologically that the implanted HA granules had directly united with the newly formed bone in places. The radiograph taken 1 year post-operatively showed no clear line between the implanted mass and the pelvic bone (Fig. 26.4). Then, the patient was allowed to bear the full body weight on the affected side. Thus, in this case, it took nearly a year after implantation to obtain complete gap filling and bone bonding with HA granules. The patient has been doing well for 25 years since surgery with neither recurrence of the tumour nor limitation of movements of the hip joint of the affected side.

What we learned from this case a quarter of century ago were; firstly, that synthetic HA really bonded to living bone tissue, but it took nearly a year after implantation for gap filling and bone bonding, indicating that HA has relatively low osteoconductivity, and, secondly, HA granules are mechanically too weak to be used under the situation where body weight should be loaded. Nevertheless, synthetic HA has widely been used since then in cases

26.3 Radiograph indicating a clear line between implanted HA and the pelvic bone (8 months after surgery).

26.4 Radiograph indicating direct bonding between implanted HA and the pelvic bone (12 months after surgery).

Table 26.1 Chemical composition (wt%) of AW-GC

MgO	4.6
CaO	44.9
SiO_2	34.2
P_2O_5	16.3
CaF_2	0.5

of bone tumours and hip revisions. In our surgical practice, however, often there is a need for a more bioactive and mechanically stronger bone substitute than synthetic HA, so that patients will be able to start weight bearing much earlier after surgery.

At Kyoto University, the research group led by Yamamuro and Kokubo attempted to synthesize a biomaterial that had a stronger bioactivity and a higher mechanical strength than synthetic HA, and finally reached the synthesis of a new glass-ceramic in 1982 which was named apatite- and wollastonite-containing glass-ceramic (AW-GC) (Kokubo *et al.*, 1982). Its chemical composition is shown in Table 26.1. It was found that dense AW-GC has a bending strength and compressive strength both significantly higher than those of the human cortical bone, while the bending strength of dense HA is considerably lower than that of the human cortical bone

Table 26.2 Mechanical properties of bone and ceramics

	Bending strength (MPa)	Compressive strength (MPa)	Elastic modules (GPa)
Natural bone	30–190	90–230	3.8–17
Synthesized hydroxyapatite	110–170	500–900	35–120
AW glass-ceramic	200–220	1000	120
Alumina polycrystal	300–400	2500–3000	350–380

Table 26.3 Apatite formation on the surface of bioactive ceramics soaked in simulated body fluid (SBF) (36.5 °C)

Ceramics	Apatite formation (days)
Bioglass	1
AW-GC	5–7
KGS (Ceravital)	7
TCP	(14)
HA	28

(Table 26.2). As for their bioactivity, when they were soaked in simulated body fluid (SBF) at body temperature, apatite formation was usually observed within 7 days over AW-GC, while it took 28 days for HA (Table 26.3). The fabrication process, microstructure, mechanical properties and biological properties of AW-GC are described in more detail by Kokubo in Chapter 13.

26.3 Application of AW-GC to the spine

26.3.1 Vertebral body prosthesis (Yamamuro *et al.*, 1990; Yamamuro, 1990a)

In February 1982, a vertebral body prosthesis made of AW-GC was first prepared to replace the lumbar vertebra of a sheep. The prosthesis was implanted into the spinal column of a sheep to replace the third and fourth vertebral bodies (Fig. 26.5). A contact microradiograph of the specimen harvested 6 months after implantation demonstrated that the prosthesis had already bonded to the bone trabeculae all the way around (Fig. 26.6). Animal experiments performed on a number of sheep suggested that the vertebral body prosthesis made of AW-GC would be clinically better

26.5 Vertebral prosthesis of AW-GC replacing the third and fourth vertebral bodies of sheep.

26.6 Contact micro-radiograph of the AW-GC vertebral prosthesis which bonded to the bone trabeculae of vertebral bodies of sheep (6 months after implantation).

applicable, owing to its stronger osteoconductivity as well as higher mechanical strength, than those made of HA. For these reasons, vertebral body prostheses made of AW-GC of different sizes were prepared for clinical application.

The case shown in Fig. 26.7 was a 50-year-old female who developed a breast cancer metastasis in the 10th thoracic vertebra with early sign of paraplegia. As the patient had multiple metastases in the bilateral ilia, it was difficult to harvest an autogenous bone graft. Therefore, in December 1982, the tumour in the spine was simply replaced with a vertebral body prosthesis made of AW-GC (Fig. 26.8), and the body weight-bearing was started 1 month after surgery. In spite of multiple metastases developing 5 years later in other organs, the patient survived 14 years after the first operation without paraplegia with the support of chemotherapy.

Figure 26.9 shows a radiograph of the spine of a 55-year-old male who developed a renal cancer metastasis in the fourth lumbar vertebra. The tumour was replaced with a vertebral body prosthesis made of AW-GC, and the patient had had no neurological problems until he died of lung metastasis 3 years after surgery. The radiograph of the operated spinal segment which was harvested by autopsy demonstrated that the 8 cm long prosthesis had firmly bonded to bone and no local recurrence of the tumour was

26.7 Breast cancer metastasis developed in the 10th thoracic vertebra of a 50-year-old female.

26.8 Post-operative radiograph of the case shown in Fig. 26.7.

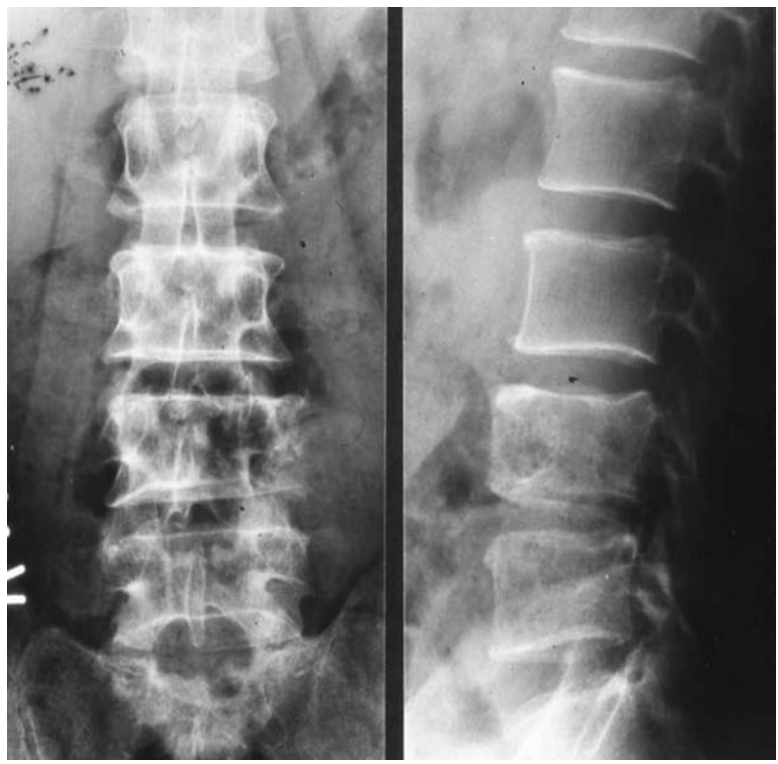

26.9 Renal cancer metastasis developed in the fourth lumbar vertebra of a 55-year-old male.

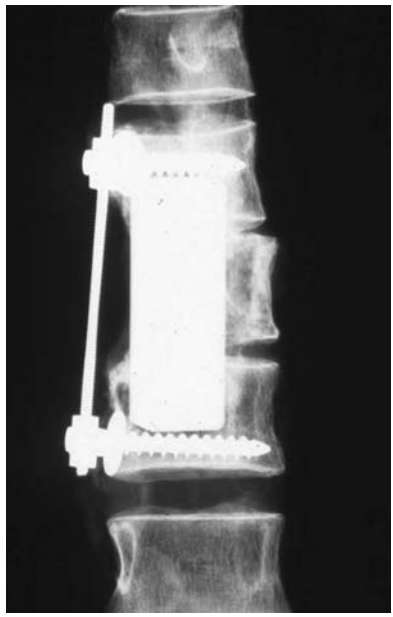

26.10 Postmortem radiograph of the case shown in Fig. 26.9 indicating bone bonding of the implanted AW-GC vertebral prosthesis and no local recurrence.

observed (Fig. 26.10). Figure 26.11 is a schematic illustration showing how to use the spinal instruments to fix the vertebral body prosthesis to the adjacent vertebrae. This surgical technique using a Kaneda device (Kaneda *et al.*, 1997) is now fully established and is also applied to treat burst fracture of vertebral bodies, which is often associated with cauda equina lesion.

Figure 26.12 demonstrates the time course of radiological changes around the AW-GC vertebral body prosthesis which was implanted to replace a metastasis of alveolar soft part sarcoma developed in the third lumbar vertebra of a 13-year-old female. No recurrence has been observed for 15 years, and bone trabeculae around the prosthesis became thicker as time passed after surgery.

During the period from 1983 to 1994, when the author retired from Kyoto University, the vertebral body prosthesis made of AW-GC had been used in 1070 cases in Japan to treat bone tumours, burst fractures, and fracture dislocations of the spine, and has now reached about 3000 cases according to the manufacturer's survey. As far as the author has been informed either personally or by publications, there have been no serious complications such as infection, loosening, collapse or breakage of prosthesis. The retarded bone bonding of the prosthesis in a few cases was virtually the only complication.

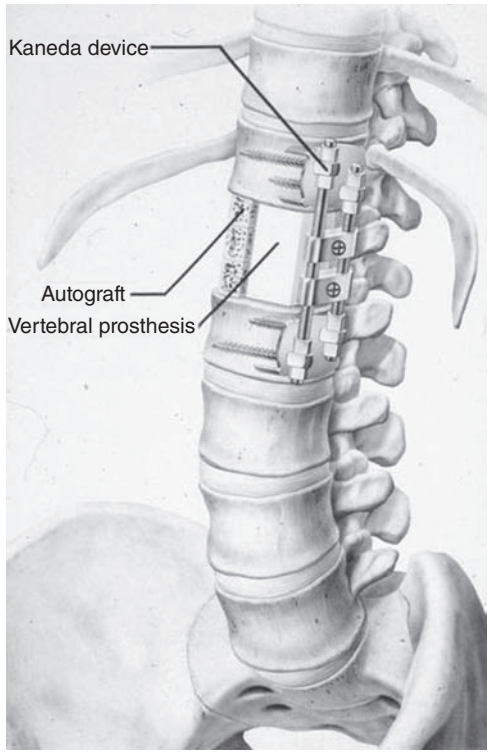

26.11 Schematic illustration of spinal instrumentation (Kaneda device) for fixing the vertebral prosthesis to the adjacent vertebrae.

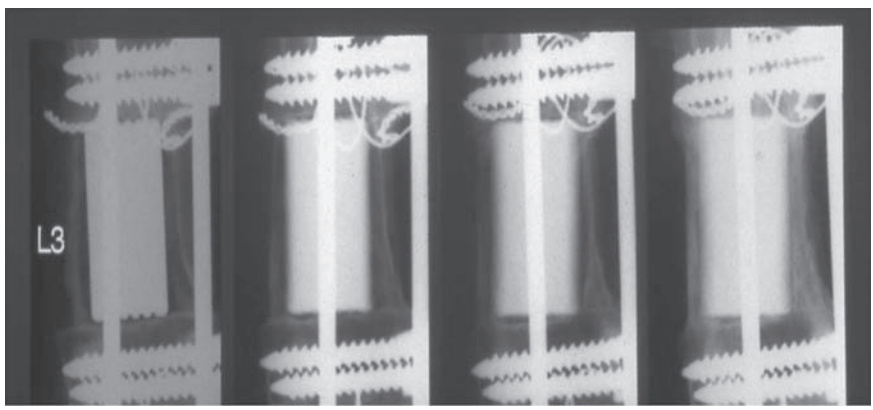

26.12 Radiographic changes around the AW-GC vertebral prosthesis which was used to replace a metastasis of alveolar soft part sarcoma developed in the third lumbar vertebra of a 13-year-old female.

26.3 Intervertebral spacer for the lumbar spine (Shimizu *et al.*, 1992; Yamamuro, 1993)

Intervertebral spacers were also made of AW-GC to be used for lumbar interbody fusion (Fig. 26.13). Usually, two spacers are implanted into one intervertebral space, and they are securely fixed to the adjacent vertebrae with Steffee's instruments.

Figure 26.14 shows a case of isthmic spondylolisthesis developed between the third and fourth lumbar vertebrae in a 40-year-old male, who complained of severe low back pain and neuralgia in both legs. At the operation,

26.13 Intervertebral spacer of AW-GC.

26.14 Isthmic spondylolisthesis developed between the third and fourth lumbar vertebra in a 40-year-old male.

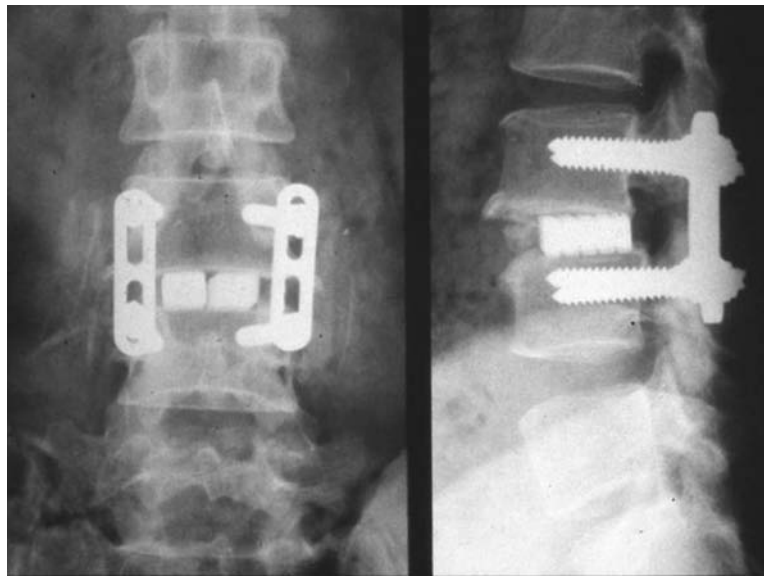

26.15 AW-GC spacers fixed to the adjacent vertebral bodies above and below by the use of the spinal instruments in the case of Fig. 26.14.

reduction of the slipping was attempted after a wide laminectomy of the affected vertebrae, and two AW-GC spacers were implanted together with some autogenous bone chips into the intervertebral space. The spacers were securely fixed to the adjacent vertebral bodies above and below by the use of the spinal instruments (Fig. 26.15).

Radiological follow-up studies of the patients who underwent implantation of the intervertebral spacers revealed that the spacer has an osteoconductive effect as demonstrated in Fig. 26.16. No case showed late narrowing of the intervertebral space that is often observed when bone autograft or allograft is used for the interbody fusion.

During the period from 1989 to 1994, the intervertebral spacer made of AW-GC was used in 1005 cases in Japan, and has now reached about 5000 cases. It is considered that the spacer is favourably indicated for lumbar interbody fusion in such conditions as lumbar spinal canal stenosis, degenerative spondylosis, degenerative spondylolisthesis and postdiscotomy syndrome.

26.3.3 Laminoplasty spacer for the cervical spine (Kamo *et al.*, 1992)

In 1987, laminoplasty spacers were manufactured of AW-GC to be used for the purpose of laminoplastic enlargement in cases of multiple spinal canal

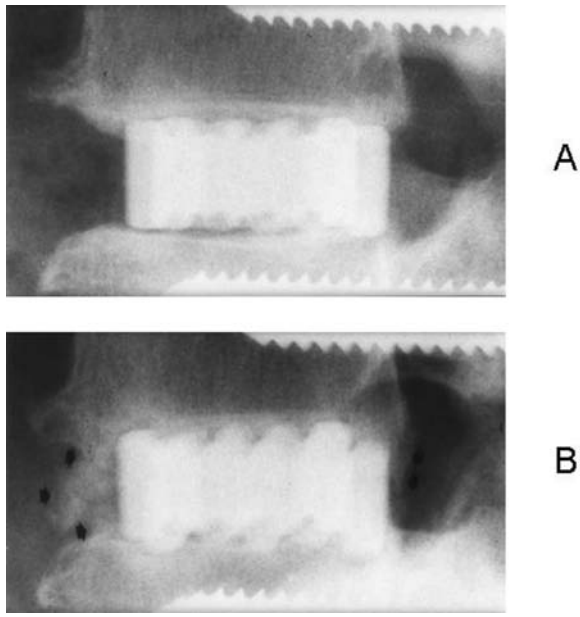

26.16 AW-GC spacer implanted into a 62-year-old male just after (A) and 39 months after implantation (B).

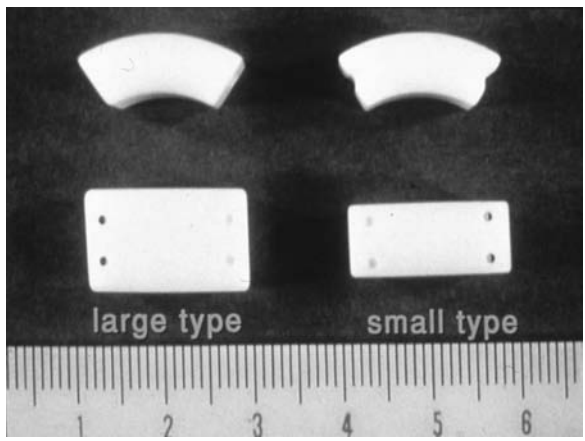

26.17 Laminoplasty spacers of AW-GC.

stenosis of the cervical spine (Fig. 26.17). At operation, multi-level laminae of the cervical spine are first exposed, then spinous processes are split vertically, and both split surfaces are opened with a spreader to enlarge the spinal canal. Usually, four to five laminae are enlarged, and bone defects remaining in each lamina are filled with the spacer, which is fixed to each spinous process with threads (Fig. 26.18).

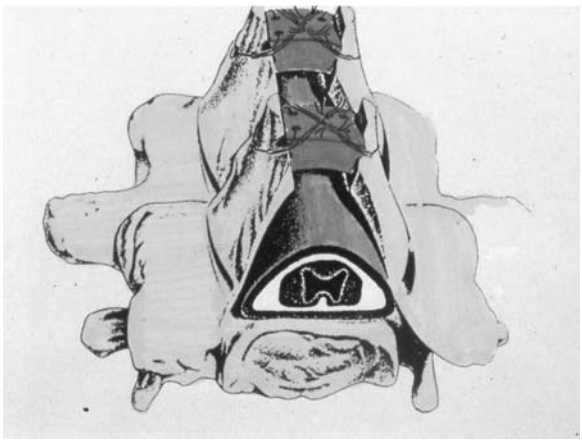

26.18 Schematic illustration of laminoplastic enlargement by the use of AW-GC spacers.

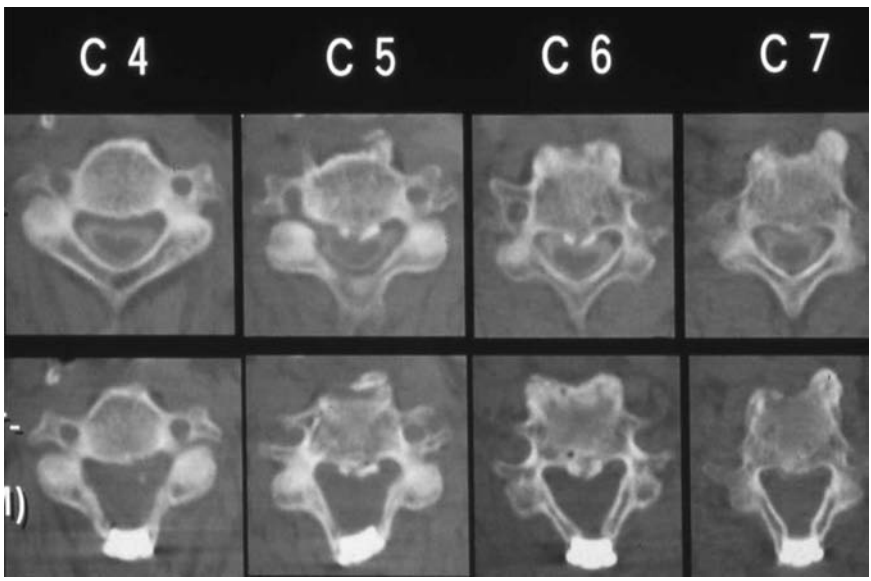

26.19 CT images of the fourth to seventh cervical spine of a 75-year-old male suffering from tetraplegia before (upper row) and 14 months after surgery (lower row).

The case shown in Fig. 26.19 was a 75-year-old male suffering from tetraplegia due to ossification of the posterior longitudinal ligament from the fourth to the seventh cervical vertebrae as demonstrated by the pre-operative computed tomography (CT) scanning images (upper row). In the

post-operative CT images (lower row), significant enlargement of the spinal canal is observed, and all spacers seem to have united to the adjacent laminae 14 months postoperatively. In most cases, bone bonding of the spacer was observed on CT images within 6 months after surgery, resulting in excellent stability of the spacer. The advantages of using the AW-GC spacer in laminoplastic enlargement are, firstly, no surgical intervention for harvesting bone graft is required, and secondly, late collapse of the implant never occurs because of its high mechanical strength.

During the period from 1988 to 1994, the laminoplasty spacer of AW-GC was used in 778 clinical cases in Japan, and has now reached about 12 000 cases. This operation is considered to be best indicated for myelopathy caused by multi-level spinal canal stenosis of the cervical spine.

26.4 The iliac crest prosthesis made of AW-GC (Yamamuro, 1990b)

A large bone defect remaining in the iliac crest after harvesting bone graft creates various cosmetic and neurological problems. They must be prevented, if possible. For this purpose, the iliac crest prosthesis made of AW-GC was manufactured in different sizes (Fig. 26.20). Figure 26.21 is a radiograph which shows the prosthesis in place, filling a large bone defect which remained in the iliac crest after a harvesting bone graft.

During the period from 1987 to 1994, the iliac crest prosthesis made of AW-GC was used in 4113 cases in Japan, and has now reached about 20 000 cases. It is reported that 97% of the patients are satisfied with the iliac crest prosthesis made of AW-GC (Ito *et al.*, 2005), while the similar prosthesis made of HA often breaks *in situ* after surgery by an accidental direct blow to the iliac crest. This is simply because the mechanical strength of HA is lower than that of AW-GC.

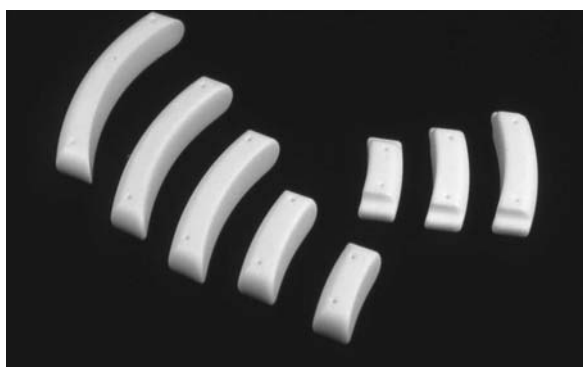

26.20 Iliac crest prosthesis of AW-GC.

26.21 AW-GC prosthesis filling a large bone defect remained in the iliac crest after harvesting bone graft.

26.22 Giant cell tumour developed in the proximal epi-metaphysis of the tibia of a 22-year-old male.

26.5 AW-GC to replace large bone tumours (Kasahara *et al.*, 1996)

The AW-GC spacers have been used to replace large bone tumours that have developed in the weight-bearing location of long bones. The case shown in Fig. 26.22 was a giant cell tumour in the proximal epi-metaphysis of the tibia of a 22-year-old male. The tumour was removed by the use of a high-speed bur and argon beam coagulator, and the spacer was implanted

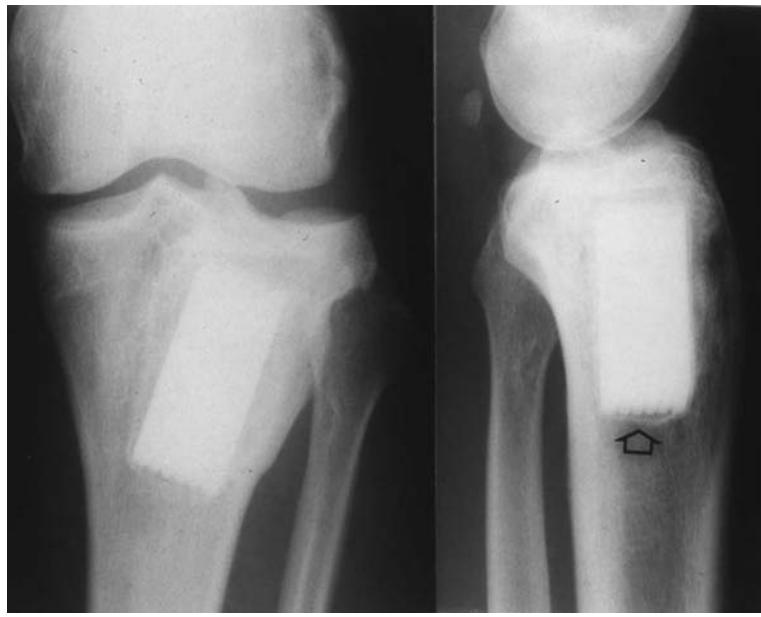

26.23 Radiograph taken 3 years after surgery demonstrating the AW-GC spacer which was implanted into the bone defect after resection of the tumour in the case of Fig. 26.22.

26.24 Giant cell tumour developed in the proximal tibia of a 15-year-old female.

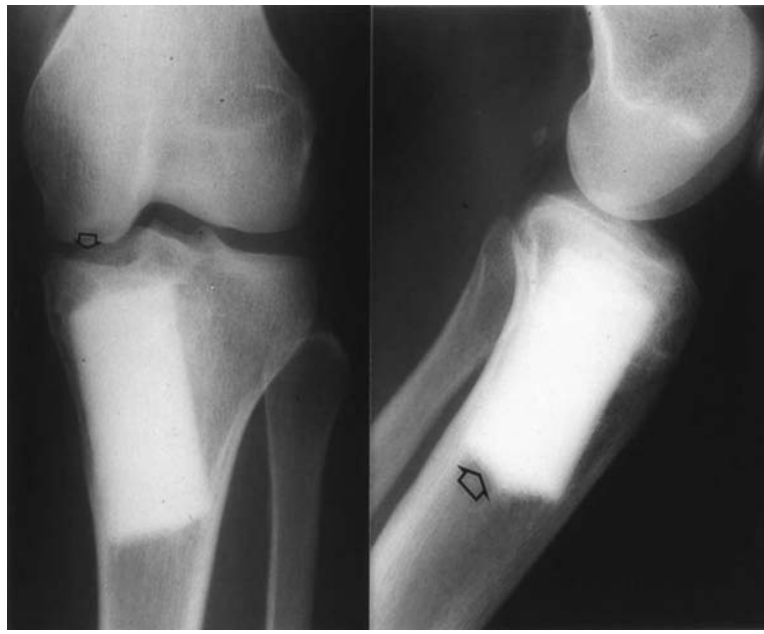

26.25 Radiograph taken 4 years after surgery demonstrating the AW-GC spacer bonding directly to the surrounding bone.

together with some autogenous bone into the remaining bone defect. Figure 26.23 is a radiograph taken 3 years post-operatively.

Figure 26.24 is a radiograph of another case of giant cell tumour that developed in the proximal tibia of a 15-year-old female. The same surgical procedure as above was performed. Figure 26.25 is a radiograph taken 4 years post-operatively. As some examples are demonstrated here, in many similar cases of large benign bone tumours developed in long bones, post-operative clinical and radiological results are quite satisfactory using the AW-GC spacer.

Thus, it was shown clinically that AW-GC can be used as a bone substitute in locations where HA cannot adequately be used.

26.6 AW-GC coating on hip prosthesis

It is now widely believed that an HA-coated hip prosthesis develops a stable fixation with the surrounding bone tissue due to the osteoconductive property of the HA-coated layer. However, at the foci of bone remodelling around the implant, osteoclast-mediated absorption of the HA-coated layer takes place constantly, as suggested by Bauer *et al.* (1991). *In vivo*, the osteoclastic bone absorption is usually followed by the new bone formation

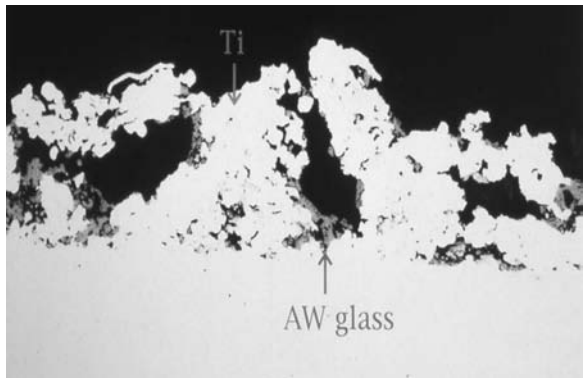

26.26 Contact micro-radiograph of a cross-section of AW-GC bottom coating over Ti plasma-sprayed porous surface.

by osteoblasts, but the newly formed bone which is generated over the prosthesis surface does not bond directly to the metal substrate. Therefore, in a hip prosthesis with a 50–100 μm thick HA-coated layer, it is anticipated that the major part of the prosthesis surface may become bare and biologically disconnected from the surrounding bone tissue in about 20–30 years. Based on the above assumption, the author designed a cementless hip prosthesis with two concepts that are (1) early bone ingrowth by AW-GC bottom coating and (2) persistent firm stability of the prosthesis by mechanical micro-anchoring with the ingrown bone. Figure 26.26 is a contact micro-radiograph demonstrating the AW-GC bottom coating over the Ti plasma sprayed porous surface. From our previous study (Yamamuro and Tagaki, 1991), it was confirmed that AW-GC bottom coating accelerates bone ingrowth as well as implant fixation better than HA-coating or AW-GC full coating. Figure 26.27 is a schematic illustration to show the difference between full coating and bottom coating.

In 1992, the author's research group together with Kobe Steel, Ltd (its biomaterials section, now Japan Medical Materials Co.) developed a cementless hip prosthesis that has the AW-GC bottom coating over the whole surface of the socket back and a small circumferential area at the proximal part of the stem. Its bearing mechanism consists of zirconia head and cross-linked polyethylene (Fig. 26.28).

This hip prosthesis has been used in about 10 000 cases in Japan. A follow-up study carried out 5–10 years after the hip replacement revealed an extremely low incidence of radiolucency at the porous coated area where the AW-GC bottom coating is applied (Table 26.4). Characteristic of this hip prosthesis is an early osseointegration at the AW-GC bottom-coated area (Fig. 26.29).

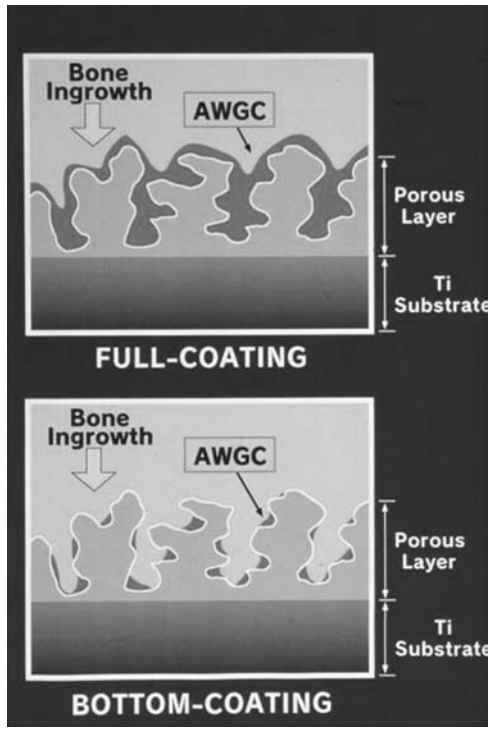

26.27 Schematic illustration of difference between full coating and bottom coating.

26.28 Cementless hip prosthesis which has AW-GC bottom coating over the whole surface of the socket back and small circumferential area at the proximal part of the stem.

Table 26.4 Radiological evaluation of total hip joints with AW-GC bottom coating, 5–10 years after operation (percentage)

Failure of prosthesis	0
Loosening of prosthesis	0
Partial radiolucency by the stem porous area	4
Other area	16
Partial radiolucency by the socket porous area	1
Other area	8
Heterotopic ossification	7

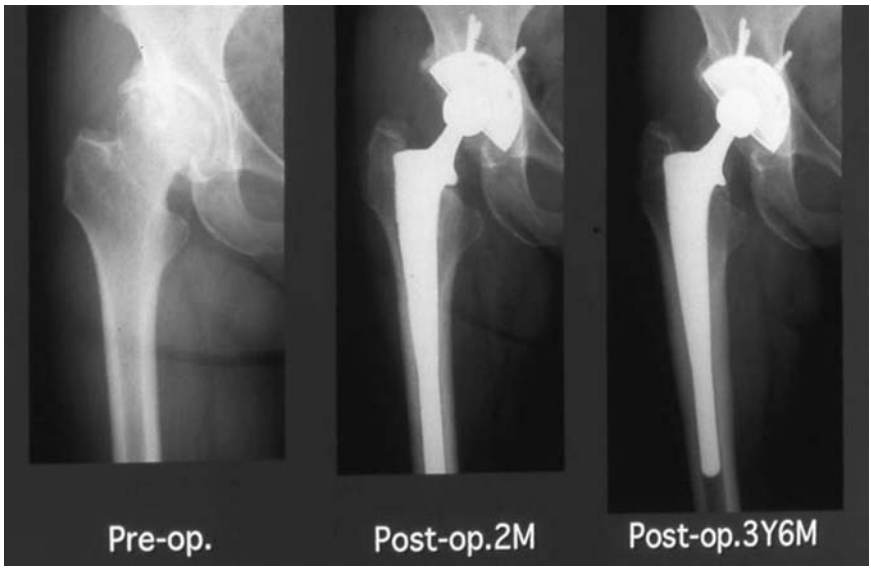

26.29 Radiographs of the hip joint of a 58-year-old female who underwent total hip replacement with an AW-GC bottom coated hip prosthesis.

26.7 Summary

Synthetic hydroxyapatite (HA) is now widely used as a bone substitute and as a coating material of joint prostheses, because it has a character of osteoconduction and an ability to form a direct bond to the living bone tissue. In the clinical practice, however, often there is a need for a material that has both stronger bioactivity and higher mechanical strength than HA in order to obtain earlier bone bonding with bone substitute and to let patients put their body weight earlier on the affected site, promoting their ambulatory life. Apatite- and wollastonite-containing glass-ceramic (AW-GC)

synthesized at Kyoto University in 1982 has stronger bioactivity as well as higher mechanical strength than HA, and therefore, AW-GC has been used to fabricate various types of prostheses and spacers to be used in the spinal surgery and tumour surgery. In particular, lumbar intervertebral spacers and cervical laminoplastic spacers have been used in thousands of clinical cases with excellent clinical, radiological and biomechanical results. AW-GC has also been used as a coating material of hip prostheses by the technique of bottom coating over the porous surface. A mid-term follow-up study of several thousands of clinical cases of hip replacement demonstrated the significantly earlier osseointegration at the AW-GC bottom-coated area compared with the HA-coated area. It is also anticipated, based on animal experiments, that the AW-GC bottom coating will ensure much longer stability of joint prostheses than the AW-GC full coating or HA full coating. Thus, it was shown clinically that the AW-GC is useful as a bone substitute as well as a coating material even in locations where HA cannot adequately be used.

26.8 References

Bauer TW, Geesink RGT, Zimmerman R, McMahon JT (1991), 'Hydroxyapatite-coated femoral stems: histologic analysis of components retrieved at autopsy', *J Bone Joint Surg*, **73-A**, 1439–1452.

Ito M, Abumi K, Moridaira H, Shono Y, Kotani Y, Minami A, Kaneda K (2005), 'Iliac crest reconstruction with a bioactive ceramic spacer', *Eur Spine J*, **14**, 99–102.

Kamo Y, Takemitsu Y, Hamada O, Yamaga S (1992), 'Cervical laminoplasty by splitting the spinous process using AW glass-ceramic lamina spacer' (in Japanese), *Clin Orthop Surg*, **27**, 1115–1122.

Kaneda K, Taneichi H, Abumi K, Hashimoto T, Satoh S, Fujiya M (1997), 'Anterior decompression and stabilization with the Kaneda Device for thoracolumbar burst fractures', *J Bone Joint Surg*, **79-A**, 69–83.

Kasahara K, Tuboyama N, Toguchida J, Nakamura T (1996), 'Joint preserving surgical technique for giant cell tumor of bone by the use of surgical adjuncts and AW glass-ceramic' (in Japanese), *Clin Orthop Surg*, **31**, 1321–1329.

Kokubo T, Shigematsu M, Nagashima Y, Tashiro M, Nakamura T, Yamamuro T, Higashi S (1982), 'Apatite- and wollastonite-containing glass-ceramic for prosthetic application', *Bull Inst Chem Res Kyoto Univ*, **60**, 260–268.

Oonishi H, Hench LL, Wilson J, Sugihara F, Tsuji E, Kushitani S, Iwaki H (1999), 'Comparative bone growth behavior in granules of bioceramic materials of various sizes', *J Biomed Mater Res*, **44**, 31–43.

Oonishi H, Hench LL, Wilson J, Sugihara F, Tsuji E, Matsuura M, Yamamoto T, Mizokawa S (2000), 'Quantitative comparison of bone growth behavior in granules of Bioglass® A-W glass-ceramic, and hydroxyapatite', *J Biomed Mater Res*, **48**, 37–46.

Shimizu K, Iwasaki R, Matsushita M, Yamamuro T (1992), 'Posterior lumbar interbody fusion using AW-GC vertebral spacer', in Yamamuro T, Kokubo T, Nakamura T, *Bioceramics* vol. 5, Kyoto, Kobunshi Kankoukai, 435–441.

Yamamuro T (1990a), 'Replacement of the spine with bioactive glass-ceramic prostheses', in Yamamuro T, Hench LL, Wilson J, *Handbook of Bioactive Ceramics*, Vol 1, Boca Raton, CRC Press, FL, 343–351.

Yamamuro T (1990b), 'Reconstruction of the iliac crest with bioactive glass-ceramic prostheses', in Yamamuro T, Hench LL, Wilson J, *Handbook of Bioactive Ceramics*, Vol 1, Boca Raton, CRC Press, FL, 335–342.

Yamamuro T (1993), 'A/W glass-ceramic: clinical applications', in Hench LL, Wilson J, *An Introduction to Bioceramics*, Singapore, World Scientific, 89–103.

Yamamuro T, Takagi H (1991), 'Bone bonding behavior of biomaterials with different surface characteristics under load-bearing conditions', in Davies JE, *The Bone-Biomaterial Interface*, Toronto, University of Toronto Press, 406–413.

Yamamuro T, Shikata J, Okumura H, Kitsugi T, Kakutani Y, Matsui T, Kokubo T (1990), 'Replacement of the lumbar vertebrae of sheep with ceramic prosthesis', *J Bone Joint Surg*, **72-B**, 889–893.

27

Clinical application of hydroxyapatite

H OONISHI, H OONISHI, JR, and S C KIM, Tominaga Hospital, Japan; L L HENCH and J WILSON, University of Florida, USA; E TSUJI, Osaka Prefectural Industrial Engineering Research Institute, Japan; H FUJITA, Kyoto Katsura Hospital, Japan; H OOHASHI, Osaka Nakatsu Saiseikai Hospital, Japan and K OOMAMIUDA, Olympus Terumo Biomaterials Corp, Japan

27.1 Introduction

Bioceramics have been widely used as bone replacement materials in orthopedic surgery. In particular, calcium phosphate ceramics such as hydroxyapatite (HA) have been applied as bioactive ceramics with bone-bonding capacities. In 1984 we used HA in the bony defect area at total hip and knee arthroplasty in some rheumatoid arthritic patients. Since 1986 we have used HA in bony deficiency as bony filler and bone cement as interface bioactive bone cement at total joint arthroplasty. As clinical use, generally HA has been used as a spacer, filler, and physicochemical bonding between bone and implant. Since porous HA block used as spacer is brittle and dense HA is difficult to make adhere to the bone, the use of HA spacer has decreased.

HA granules have been used as filler in a bony defect. The filler using bioactive ceramics has two aims: (1) filler will be absorbed and be replaced by physiological anatomical bone (resorbable ceramics) and (2) filler will not be absorbed and osteoconduction will be continued at the interface eternally (not-resorbable ceramics).

As physicochemical bonding between bone and implant, HA coating on the implant has been used for about 20 years. However, HA coating will be absorbed within 15 years after implantation, because amorphous HA is contained in HA coating. Long-term clinical results of HA coating and porous metal coating are not different. Most cases of prostheses with HA coating or metal porous coating will become loose in the bone about 15 year after surgery after onset of osteoporosis due to aging.

In order to curb the loosening of the prosthesis, osteoconduction has to be continued at the interface between bone and implant forever even after onset of osteoporosis and therefore not-resorbable crystalline HA has to be used. For this reason we have been using the interface bioactive bone

cement (IBBC) technique which involves interposing crystalline HA granules at the interface between bone and bone cement at cementing during surgery. As non-resorbable crystalline HA and other resorbable bioceramics are completely different materials, we have to understand their properties and characteristics accurately and they have to be applied in clinical cases. Consequently, different characteristics of HA and other bioceramics were compared and clinical application of HA was introduced.

27.2 Comparative bone growth behavior in granules of HA and other bioceramic materials

Bioceramics can be divided clinically into three categories: (a) bioinert ceramics, (b) surface-bioactive ceramics, and (c) resorbable bioactive ceramics. Bioinert ceramics are represented by alumina; surface-bioactive ceramics by sintered HA; and Bioglass® and A-W glass ceramics and resorbable bioactive ceramics by low-crystalline HA, α-tricalcium phosphate (α-TCP), β-TCP, tetracalcium phosphate (TeCP), and octacalcium phosphate.

When granules of these bioceramics are implanted into bone, bone growth behavior and reaction to the bone are expected to be different owing to the variation in materials and size of the granules. Biological responses such as bone bonding and resorption of bioactive ceramics are very important in clinical applications. Although they have been discussed for a long time, it is not yet certain whether all bioactive ceramics are persistent in long-term applications (Oonishi 1991a). Resorption is an important characteristic for biomaterials; it has a large influence on bone-bonding properties. Resorption characteristics must be considered from two viewpoints:

1 Solution-mediated dissolution processes.
2 Cell-mediated (phagocytic and/or resorbable) processes, which are particularly important for bone-replacing materials.

In this study, bone reaction to fine granules of several sizes of several kinds of bioceramics were compared in the same animal modes, a 6 mm hole in rabbit femur (Oonishi 1991a, 1992; Oonishi *et al.* 1991, 1992, 1997a).

27.2.1 Materials and methods

Materials used were alumina, HA sintered at 1200 °C (HA, $Ca_{10}(PO_4)_6(OH)_2$) and Bioglass™(45S5), 45 wt% SiO_2, 24.5 wt% CaO, 24.5 wt% Na_2O, 6 wt% P_2O_5 (supplied by US Biomaterials Corp. Alachua, FL).

Low-crystalline HA was used by hydrating α-TCP (10 μm in diameter) in phosphate-buffered solution (pH 8.0) for 24 h at room temperature. Also used were α-TCP, $Ca_3(PO_4)_2$, β-TCP, β-$Ca_3(PO_4)_2$, TeCP, $Ca_4O(PO_4)_2$, and

octacalcium phosphate (OCP) $[Ca_8H_2(PO_4)_6]\cdot 5H_2O$, by hydrating α-TCP (10 μm in diameter) in phosphate-buffered solution (pH 7.0) for 12 h at room temperature.

We also used a mixture of TeCP with dicalcium phosphate dehydrate (DCPD) ($CaHPO_4\cdot 2H_2O$) (called TeDCPD) and a mixture of TeCP with dicalcium phosphate anhydrate (DCPA) ($CaHPO_4$) (called TeDCPA). Only sintered HA was porous, and the porosity was near 65%. TeDCPD and TeDCPA were made by mixing TeCP (ca. 10 or 300 μm in diameter) with the same diameter DCPD or DCPA in equimolar proportions. The granules, except for sintered HA and Bioglass™, were made by granulating powders.

Holes 6 mm in diameter were drilled bilaterally in the femoral condyles of mature Japanese white rabbits (Oonishi *et al.* 1997a) and sufficient hemostasis was achieved by filling and compressing the holes with gauze for 5 min. Immediately after, the powders or granules of prepared bioceramics were placed in sufficient amounts to fill the holes. Three animals were used at each time period.

The animals were killed at appropriate intervals. The implant sites were embedded in polymethylmethacrylate, and sawn sections of approximately 30 μm were cut and stained with Toluidine blue. Sections for backscattered scanning electon microscopy (SEM) imaging were also cut from plastic-embedded material (Oonishi *et al.* 1997a). Demineralized material was embedded in paraffin, and sections of approximately 5 μm were cut and stained with hematoxylin and eosin. Unfilled drilled holes were used as controls.

27.2.2 Results: bioinert ceramics

Alumina (Al_2O_3) granules 100 μm in diameter

At 1 week, bone grew close to, but did not touch, the alumina granules. At 3–4 weeks, new bone grew into spaces between alumina granules to a depth of several layers, but it did not come into direct contact with the alumina granules (Fig. 27.1).

Al_2O_3 granules 10 μm in diameter

At 1 week, there were spaces of several to tens of micrometers between alumina granules and surrounding bone. A small amount of new bone was observed around some granules. At 3–4 weeks, the density of alumina granules remained unchanged, no new bone tissue was seen, and spaces remained between granules and surrounding bone (Fig. 27.2). At 6 weeks, new bone approached the granules; however, narrow spaces between granules and

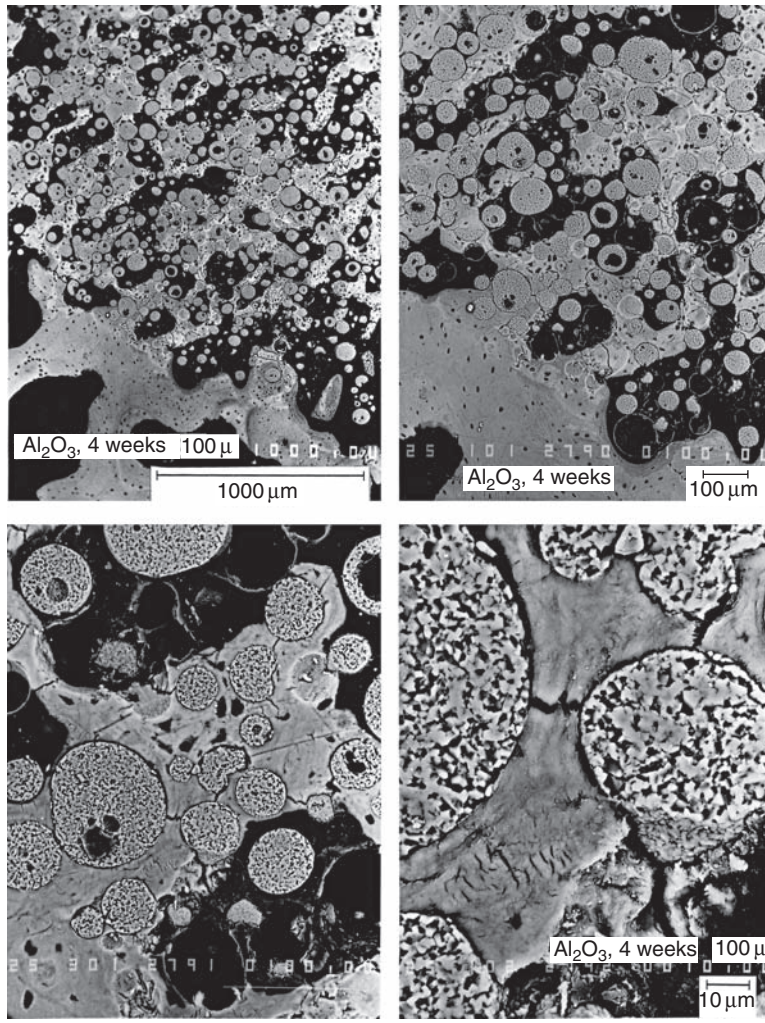

27.1 Bone growth around alumina (100 μm) at 4 weeks. Backscattered SEM.

surrounding bone remained. There was no inflammation or cell infiltration seen at any time period.

27.2.3 Results: surface-bioactive ceramics

Sintered HA [$Ca_{10}(PO_4)_6(OH)_2$] granules 100–300 μm in diameter

When sintered HA fine granules 100–300 μm in diameter were implanted, spaces of several tens to several hundreds of micrometers were left between

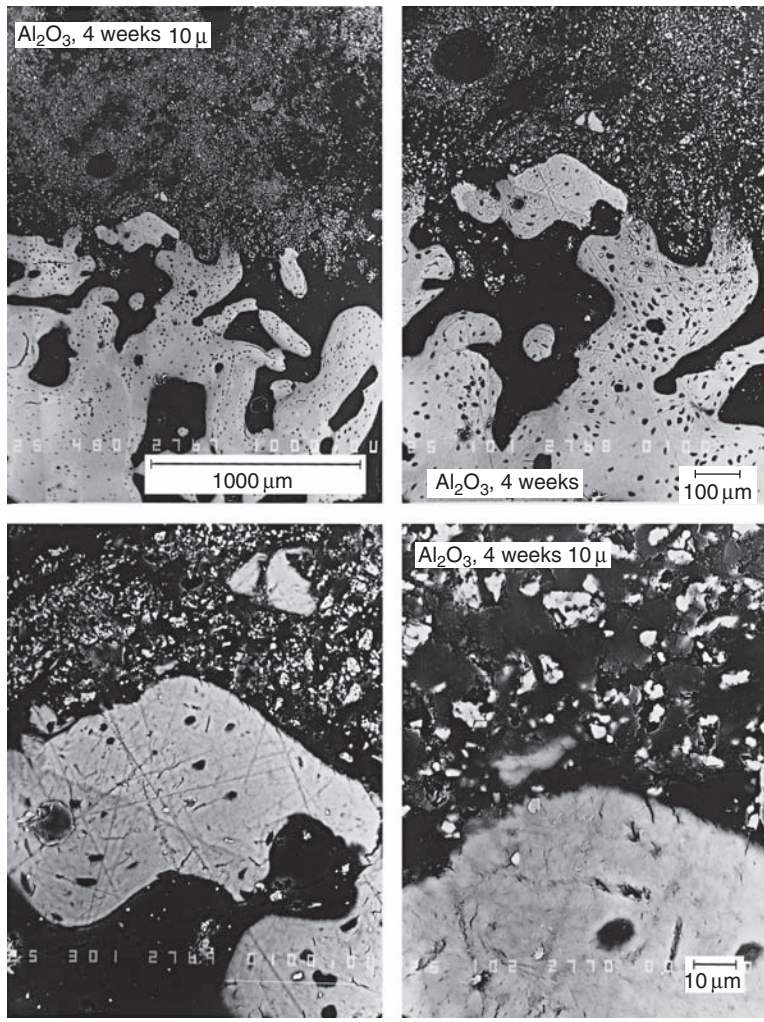

27.2 Bone growth around alumina (10 μm) at 4 weeks. Backscattered SEM.

most of the granules and surrounding bone immediately after implantation. However, at 1 week, new trabecular bone grew into spaces between HA granules by osteoconduction from the periphery, and reached the outermost layer of HA granules. Some new bone tissue was formed as a result of ingrowth binding with HA granules of the outer layer, almost enclosing them. In some areas, new bone grew into the second and third layers of HA granules (Oonishi *et al.* 1992, 1997a; Oonishi 1992). Most of these trabecular bone tissues ranged from 10 to several tens of micrometers in width.

At 2 weeks, new bone trabeculae originating from the surrounding bone and running into HA granules of the outermost layer increased in number and formed a network as a result of binding with each other. The resulting structure resembled cancellous bone. The circumference of HA granules of the outermost layer was almost completely enclosed by new bone. New bone tissue reached the third and fourth outer layers of HA granules.

At 3 weeks, bone formation seen in spaces between surrounding bone and HA granules was slightly denser and trabecular bone was slightly thicker than at 2 weeks. New bone tissue reached the sixth and seventh layers of HA granules, at the same time enclosing HA granules. New bone tissue was measured to a depth of 1000 μm. New trabecular bone was lower in density and smaller in amount as it reached deeper layers (Oonishi *et al.* 1997a). Some trabecular bone that had reached the second and third layers of HA granules was connected in spaces between HA granules. At these sites, spaces between granules were ~ <10 μm, new bone tissues ran close to one another, and their surfaces were sometimes completely bound to one another (Fig. 27.3).

At 6 weeks, new bone tissue seen in spaces between surrounding bone and HA granules of the outermost layer was much denser, and spaces that

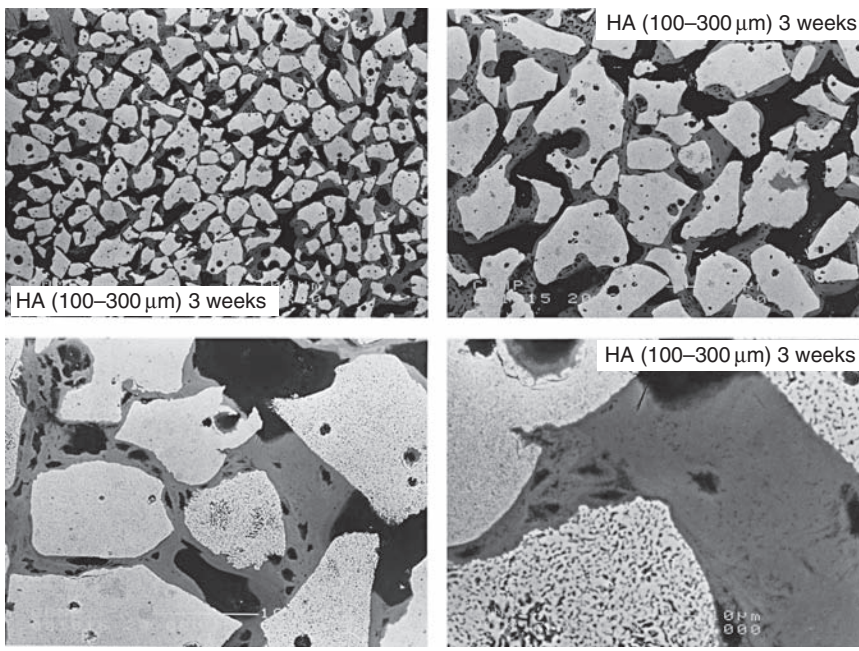

27.3 Bone growth on HA (100–300 μm) at 3 weeks. Backscattered SEM.

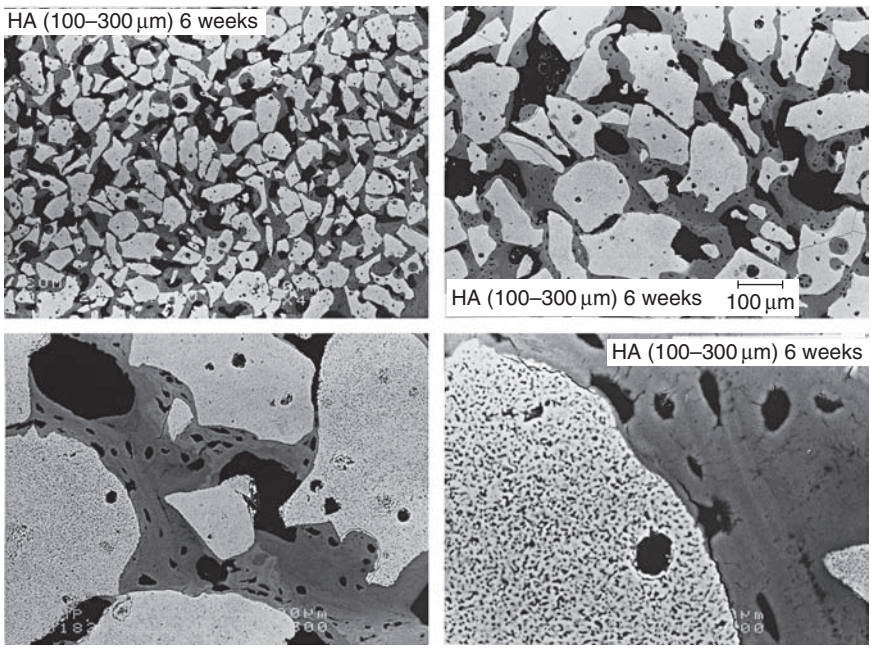

27.4 Bone growth on HA (100–300 μm) at 6 weeks. Spaces less than 20 μm are filled with new bone. Backscattered SEM.

initially were <20 μm were now almost completely filled with new bone. On the other hand, spaces >100 μm had no new bone growing from surrounding bone to HA granules, nor were they filled with new bone (Fig. 27.4). New bone reached the 15th and 16th layers from the circumference, reaching a depth of 2500 μm. In this area, all new bone tissue moving toward the center first enclosed by an HA granule, binding this with adjacent granules as if new trabecular bone had branched, and this branch then subsequently enclosed yet another HA granule. Where spaces were <10 μm (as at the third week), new tissue grew closely together and bound the surfaces. Generally, no new bone tissue was seen where HA granules were separated by >100 μm, although new bone tissue did enter large spaces when there was a bone bridge formed first. Spaces of about 20 μm were not filled with new bone tissue if nearby HA granules were not first enclosed by bone.

Sintered HA granules about 10 μm in diameter

At 1 week, new bone tissue from the surrounding bone grew close to parts of the HA periphery, reached a depth of one or two layers, surrounding

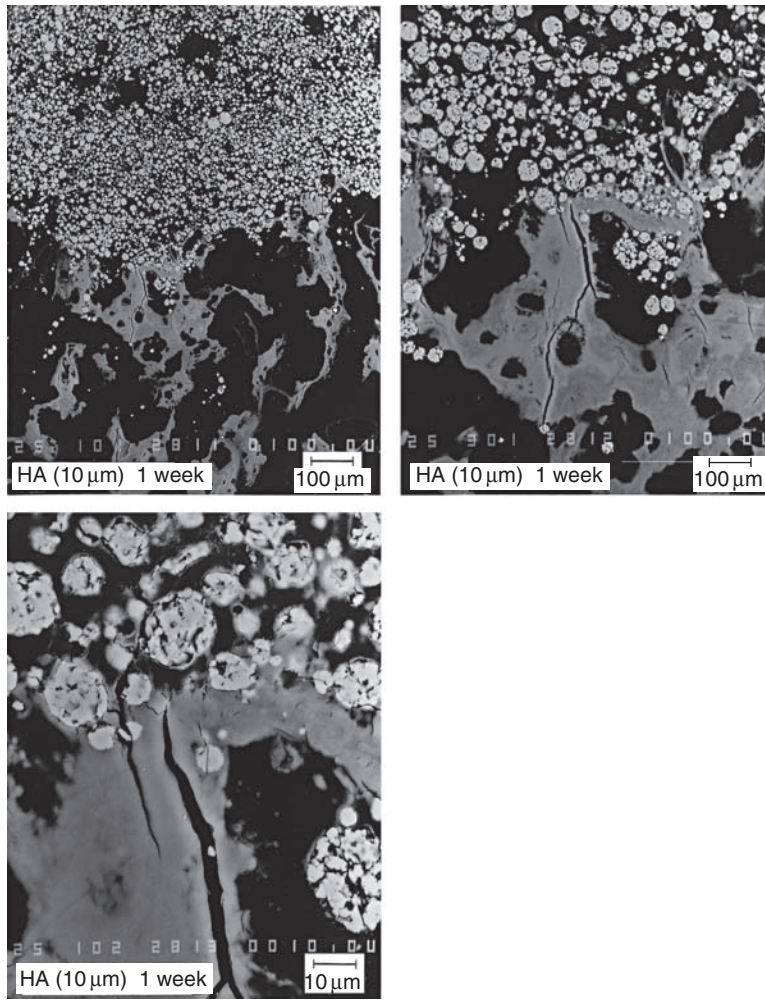

27.5 Bone growth on HA (10 μm) at 1 week. Backscattered SEM.

some HA granules and bonding to others. However, large spaces were often seen between the HA border and original bone (Fig. 27.5). At 3 weeks, new laminar bone tissue 50–150 μm wide had formed from the bone in which the hole had been drilled (Fig. 27.6). The new laminar trabecular bone tissue developed nearly to the center of the hole enclosing almost all of the HA granules. Consequently, the density of the cancellous bone in the HA-filled hole was much greater than in the control. Furthermore, individual HA granules remained at the center, and the quantity and density of HA granules had decreased. At 6 weeks, HA granules taken into

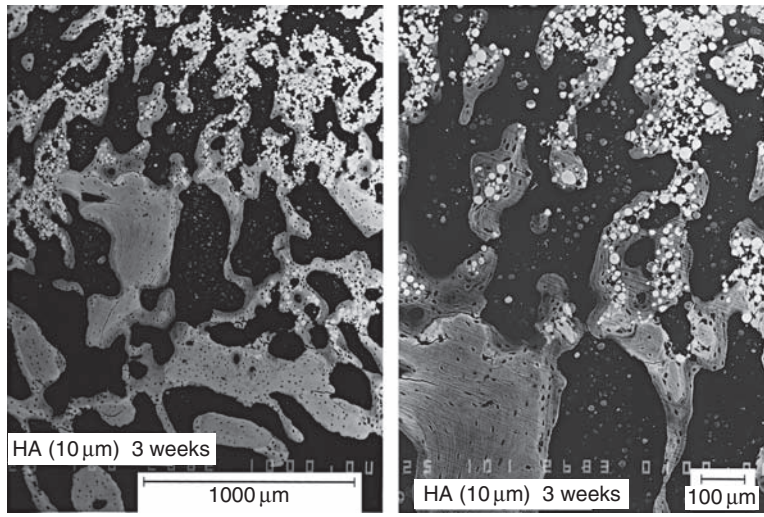

27.6 Bone growth on HA (10 μm) at 3 weeks. Backscattered SEM.

the trabecular bone remained, but some had disappeared from the trabecular bone (Fig. 27.7). Trabecular bone of about 100–200 μm width had formed.

At both 1 and 3 weeks, bone growth around 10 μm HA granules was effective. However, at 6 weeks, HA granules seen earlier within the trabecular bone had left the bone and were seen in the spaces. No inflammatory changes such as cell infiltration were seen at any time following implantation. At 12 weeks, HA granules had disappeared from the trabecular bone completely (Fig. 27.8).

HA powders 1–3 μm in diameter

Immediately after HA powders 1–3 μm in diameter were implanted, spaces of several hundred micrometers were observed between powder and surrounding bone. At 1 week, new bone tissue was observed in parts around the powder, while the spaces remained unchanged and the amount of bone tissue was small.

At 3 weeks, the density of HA powder distributed in the vicinity of bone was lower, and in places new bone grew through spaces in between HA powders. These shoots of new trabecular bone enclosed clusters of HA powders, forming them into small separated islands. The new bone tissues penetrated to a depth of about 300 μm. There was no new bone tissue in contact with HA, as spaces of 20–50 μm were left between growing new bone and the masses of HA powder. HA powders were taken into new

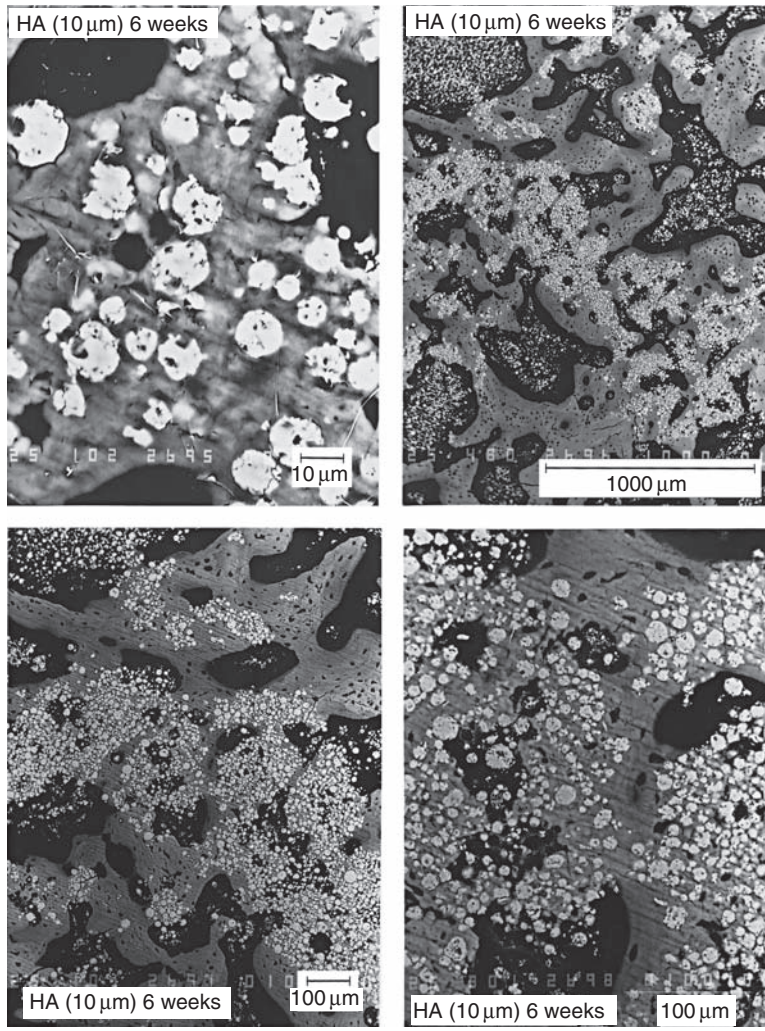

27.7 Bone growth on HA (10 μm) at 6 weeks. The traveculae contain large numbers of particles. Backscattered SEM.

trabecular bone, but only in very small quantities (Fig. 27.9). At 6 weeks, the depth of the new bone tissue had increased to 1000 μm. These new trabeculae were relatively wide and showed a morphology similar to that of an osteon. Spaces between new trabecular bone and HA powder masses were still visible, comparable with those seen in the third week. Hydroxyapatite powder decreased in quantity as more trabecular bone grew inward.

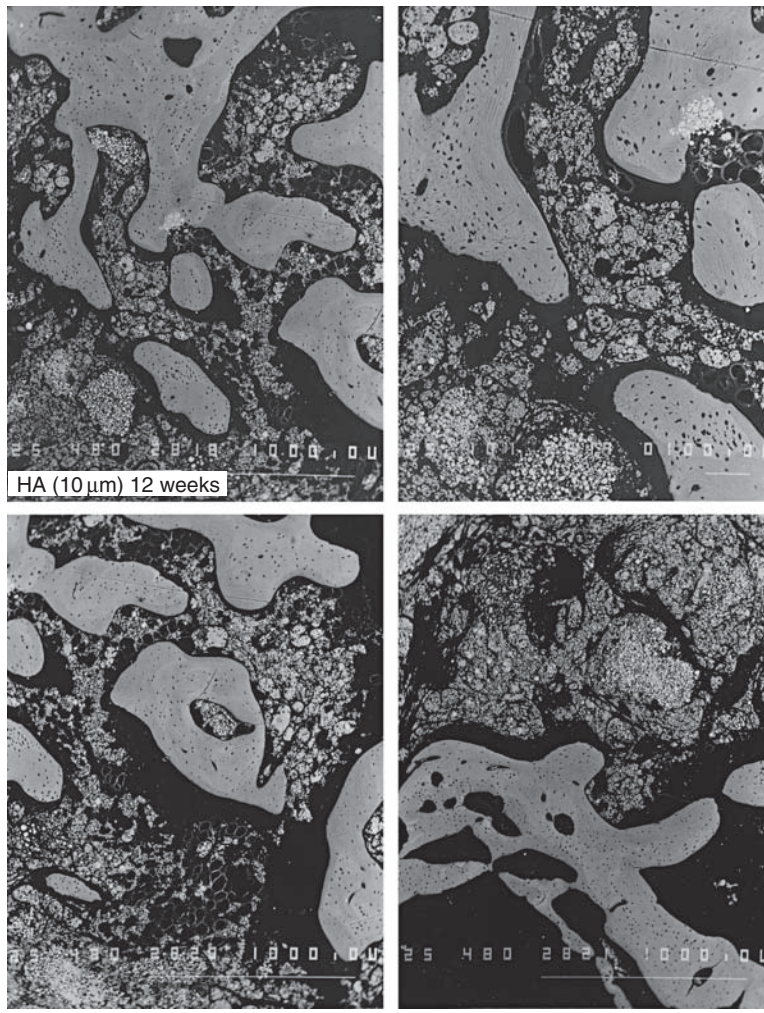

27.8 Bone growth on HA (10 μm) at 12 weeks. The trabeculae contain no particles. Backscattered SEM.

Comparison of particles of differing sizes

During implantation of HA granules 100–300 μm in diameter, no osteogenesis was seen when spaces of more than 100 μm were left between HA granules and surrounding bone. There was no binding of HA to bone. Conversely, in spaces <20 μm binding of HA to bone was almost certain. To achieve sound binding of HA and bone, the contact area should be extensive. Firm fixation is also important to establish secure contact between bone and HA. When implanting HA into the bone, it is important to pack HA granules firmly into the bone.

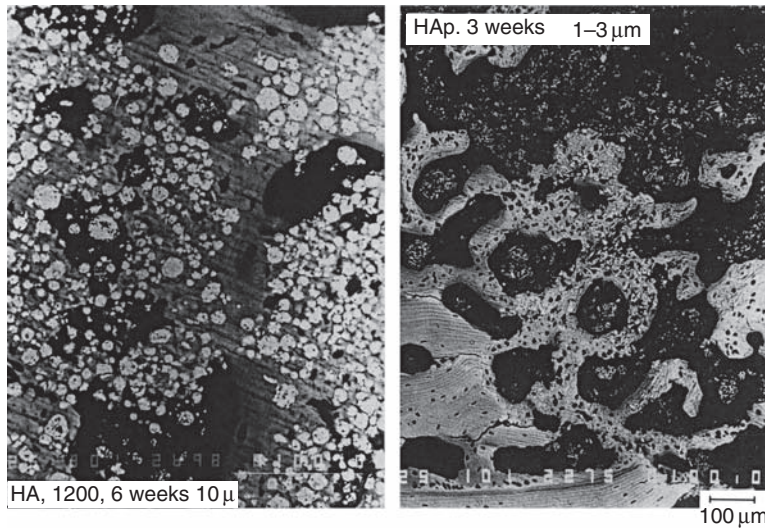

27.9 Bone growth on HA (1–3μm) at 3 weeks. The trabeculae contain small numbers of particles. Backscattered SEM.

New bone tissue could not enter spaces between HA granules which were separated by more than 100μm. Between 20 and 100μm, large portions were not filled by bone tissues, but spaces <20μm were almost always filled with new bone.

When HA granules 100–300μm in diameter were packed into bone, spaces of 50–200μm remained. The amount of bone entering the spaces between granules was relatively small; <30% of these spaces were occupied by new bone tissues. These results suggest that unless granules are firmly and densely packed, most of the spaces left between them will remain. Thus, because bone ingrowth into spaces is minimal, the site will remain permanently weak. When HA powders 1–3μm in diameter were packed into bone, the HA made no contact with the bone and the affinity of HA to bone was extremely poor. Spaces left after absorption of HA powders appeared to become occupied by new bone. This new bone grew in a similar manner to that of normal cancellous bone.

These results showed that a minimum HA particle size is required to make contact with bone. When HA granules of 10μm were packed into bone, they were incorporated by 3 weeks but were lost from the trabeculae by 6 weeks. Hence, particular care should be taken to avoid crushing the granules into fine powders whenever HA granules are packed or driven into bone for clinical use.

27.2.4 Results: 45S5 Bioglass™

Particles 100–300 μm in diameter

Two days after implantation of the 45S5 Bioglass™ particles (hereafter referred to as Bioglass™), the periphery of the particles in the outermost layer became rich in silica, calcium, and phosphate, as the reaction layer developed and foci of new bone had formed, which could be detected in backscattered electron images. By 5 days, new bone penetrated most of the first two layers of Bioglass™ which were bound directly to bone, consistent with earlier observations at 7 days (Oonishi 1992; Oonishi *et al.* 1997a). By 12 days after implantation, new bone surrounded most surfaces of Bioglass™ particles as far as the 8th to 10th outer layers (Oonishi *et al.* 1997a).

In Bioglass™ implantation sites at 3 weeks, new bone extended to spaces of the 10th layer of particles – that is, to the center of the hole – and surrounded most surfaces. At the center of the 6 mm defect, Bioglass™ particles were surrounded by thick new trabecular bone. Decalcified specimens showed active bone formation and many blood vessels. The new bone-filling spaces between Bioglass™ particles was more extensive and denser than that around HA (Fig. 27.10).

At 6 weeks, bone growth between Bioglass™ particles continued to increase in density, all particles were encased in thick new trabecular bone, and very few spaces remained unfilled (Fig. 27.11). The development of the reaction layers on the particles seen at 2 days continued at 3 and 6 weeks, eventually leading to complete resorption.

Comparison of Bioglass™ with HA granules

Bone growth between HA granules had reached only the fourth and fifth layers and surrounded surfaces of the first and second outer granule layers by 3 weeks. With HA, new bone took 6 weeks to reach the center and only surrounded small parts of the granules' surfaces. At 6 weeks, only the outer three layers of HA granules had been entirely encompassed. In deeper layers, new trabecular bone only partially surrounded HA granules, and very few of these spaces were filled with new bone. The speed of bone growth around Bioglass ™ particles was much faster and the new bone much denser than bone growth associated with HA at all time periods. Extensive new bone trabeculae had developed throughout the defect filled with Bioglass™ particles by 2 weeks; by 3 weeks, the defect was filled with mature trabecular bone that encased the glass particles.

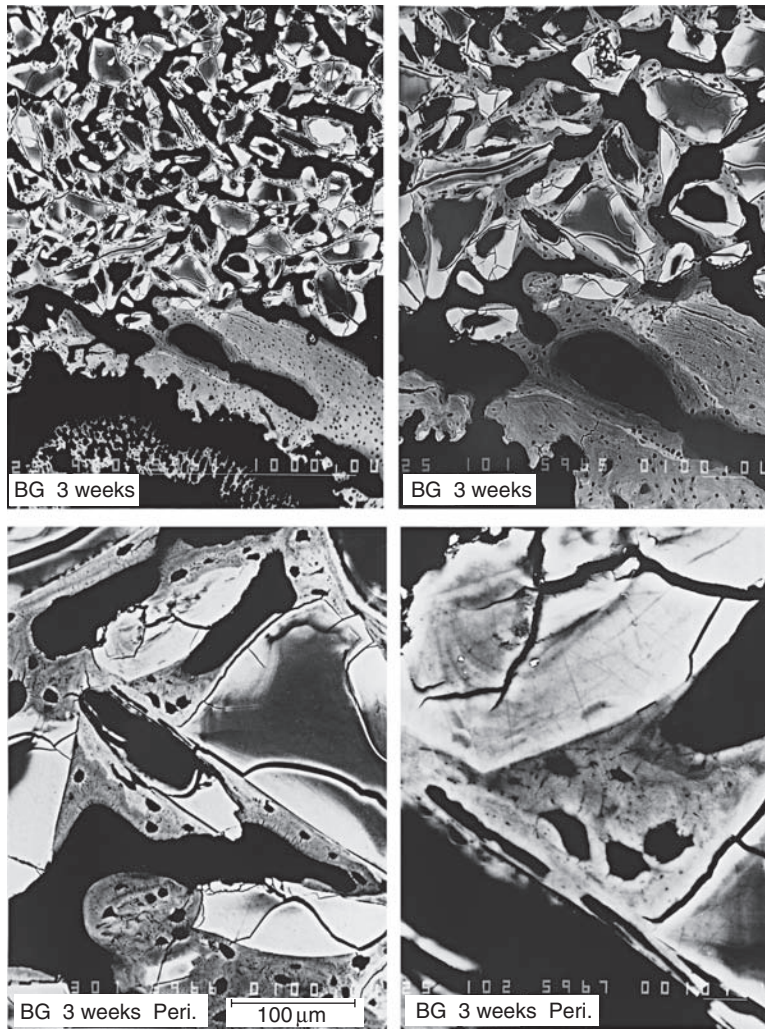

27.10 Bone growth on Bioglass® (100–300 μm) at 3 weeks. The pale area surrounding the particle is the reaction layer typical of this material. Backscattered SEM.

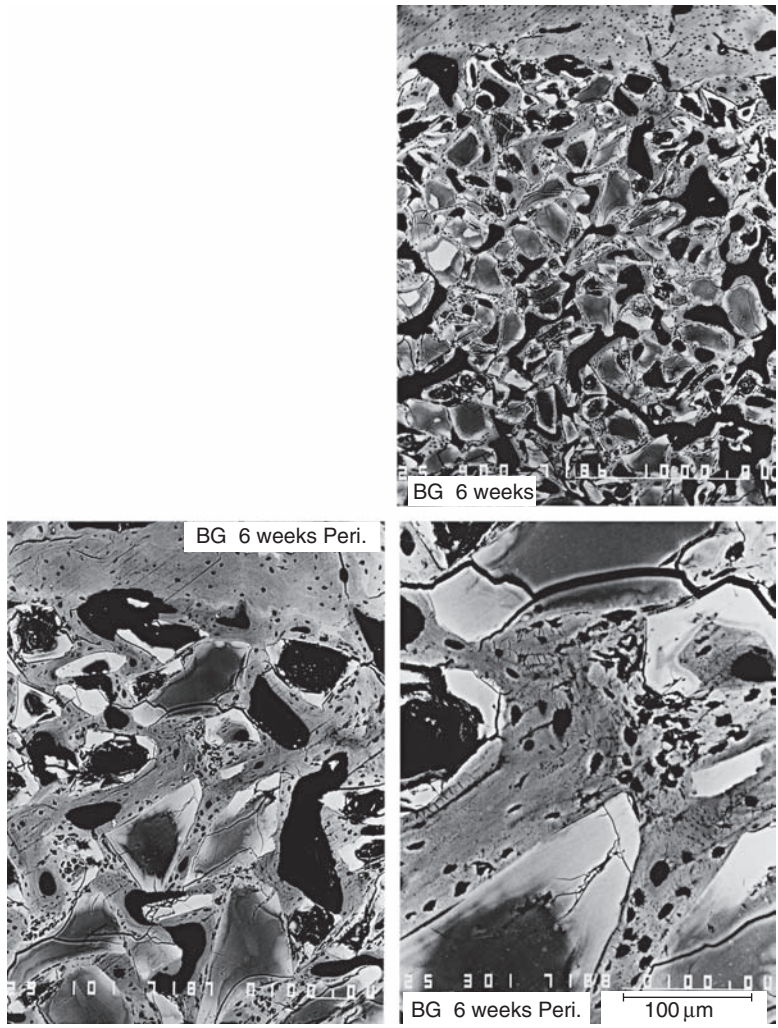

27.11 Bone growth on Bioglass® (100–300 μm) at 6 weeks. Travecular bone surrounds all the granules. Backscattered SEM.

27.2.5 Results: resobable bioactive ceramics

In this category, TeCP, α-TCP, β-TCP, OCP, TeDCPD, TeDCPA, and low-crystalline HA were used.

TeCP, TeDCPD and TeDCPA: granules 100–300 μm in diameter

One week after implantation, bone tissue was generated close to the TeCP, TeDCPD, and TeDCPA and replaced some of the granules, but only to a

very small extent. At 3 weeks, new laminar bone formed from the bone base. TeCP, TeDCPD, and TeDCPA in the vicinity of this new bone began to be slowly replaced by new bone from the periphery (Fig. 27.12); the calcium phosphates (CaPs) gradually diminished with time. At 12 weeks, most of the CaP granules were replaced by new trabecular bone.

Backscattered electron images at high magnification disclosed that these TeCP, TeDCPD, and TeDCPA crystals were being replaced by bone from their edges from 3 weeks after implantation onward. Close observation of these remaining crystals revealed that crystals gradually changed

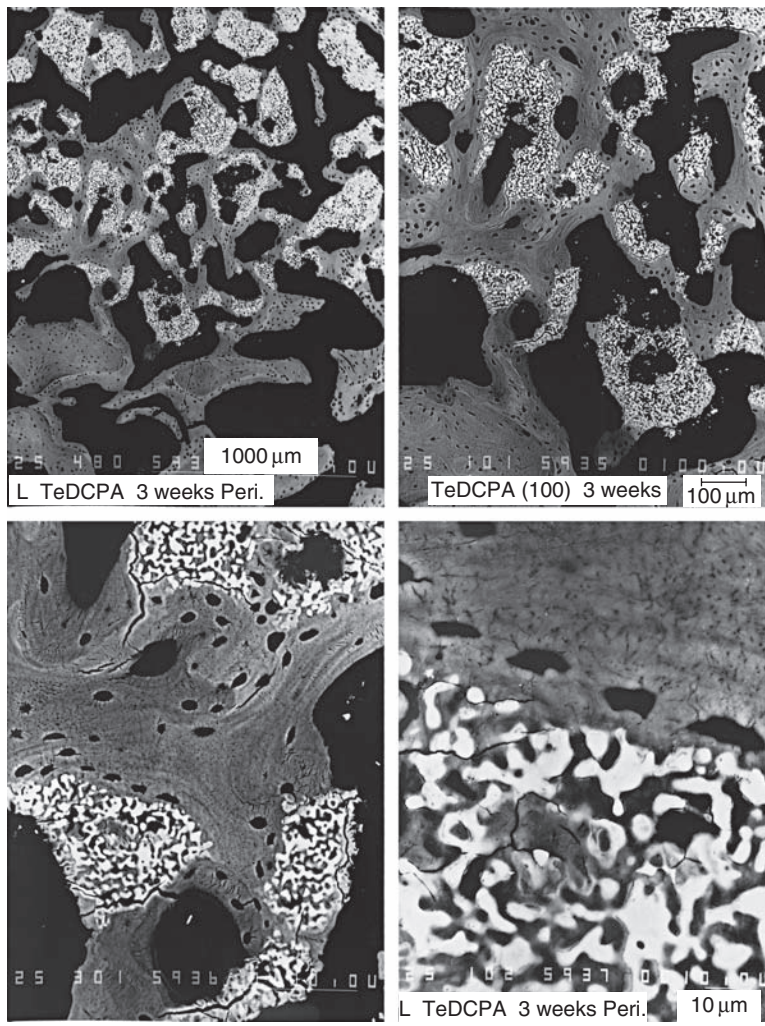

27.12 Bone growth on TeDCPA (100–300 μm) at 3 weeks. Backscattered SEM.

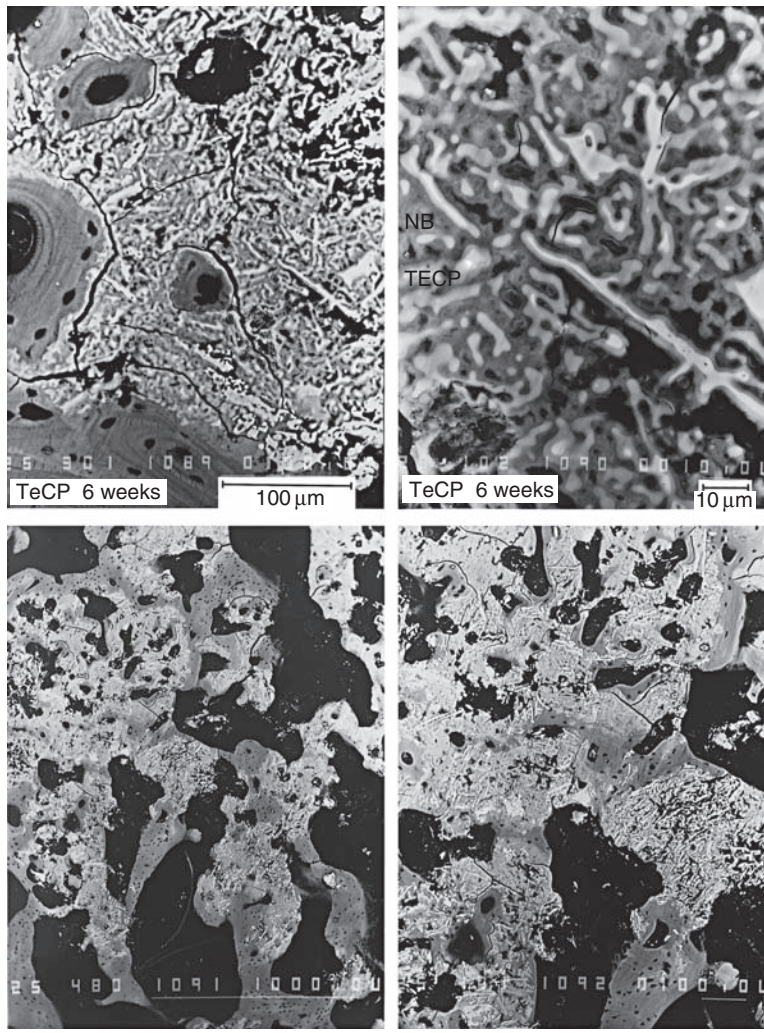

27.13 Bone growth on TeCP (100–300 μm) at 6 weeks. NB, new bone; TECP, residual calcium phosphate. Backscattered SEM.

backscattered electron images from white to black from their peripheries. Furthermore, the configuration of some crystals was unclear and the periphery of the crystal was hardly distinguishable from the new surrounding bone from 6 weeks onward (Fig. 27.13).

α-TCP and β-TCP: granules 100–300 μm in diameter

α-TCP and β-TCP showed almost the same reactions (and will be described together as α-/β-TCP). At 3 weeks, laminar new bone 100–200 μm wide

formed from the bone in which the hole had been drilled. The trabecular laminar new bone filled the hole that contained the α-/β-TCP granules. The density of the distribution of the trabecular bone was high (Fig. 27.14). No inflammatory reaction was observed. Bone growth behavior was very different from that of HA. With HA, new bone grew between HA granules; however, the laminar trabecular new bone tissue forming with α-/β-TCP granules showed results similar to those of TeCP granules. At 6 weeks, over half the mass of the α-/β-TCP granules was absorbed, and a density of the

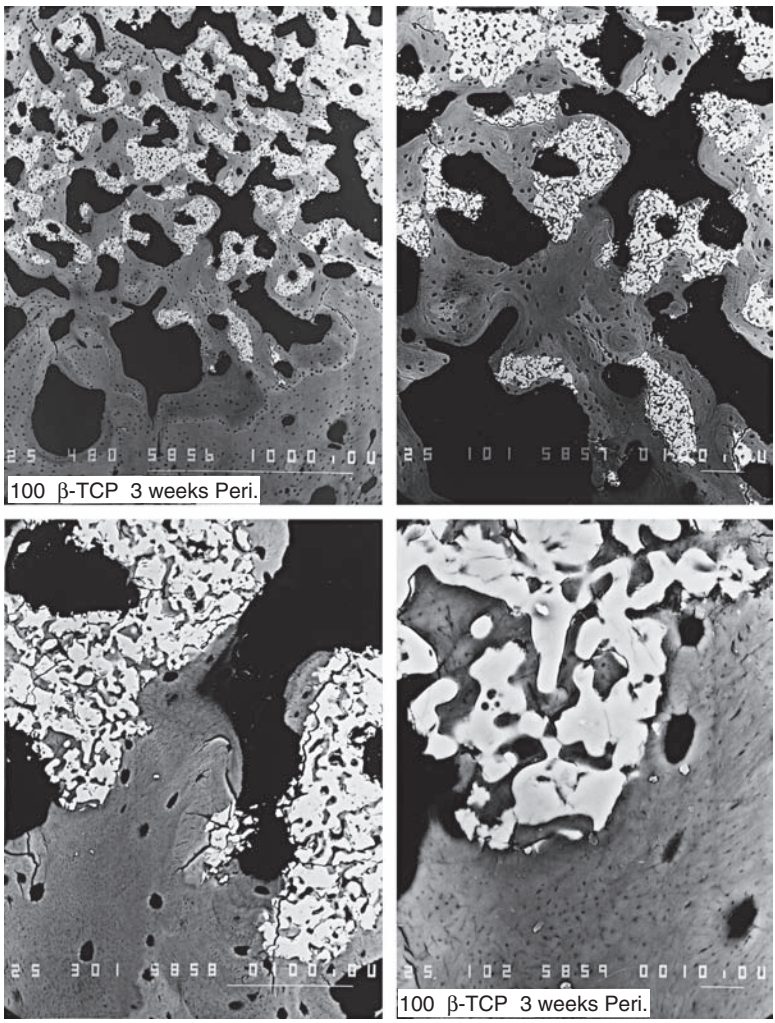

27.14 Bone growth on β-TCP (100–300 μm) at 3 weeks. Backscattered SEM.

distribution of the trabecular bone became lower. By 12 weeks, the size of the granules was smaller and only small amounts of α-/β-TCP granules remained. The trabecular bone remodeled and returned to its physiological structure. The interface between α-/β-TCP granules was distinct, which was different from the changes in TeCP, TeDCPD, and TeDCPA (Fig. 27.15). The amount of the powder of α-/β-TCP was less at 6 weeks and the size of the granules became smaller in proportion to the decrease of the amount of powder. However, in the case of TeCP, TeDCPD, and TeDCPA, as the

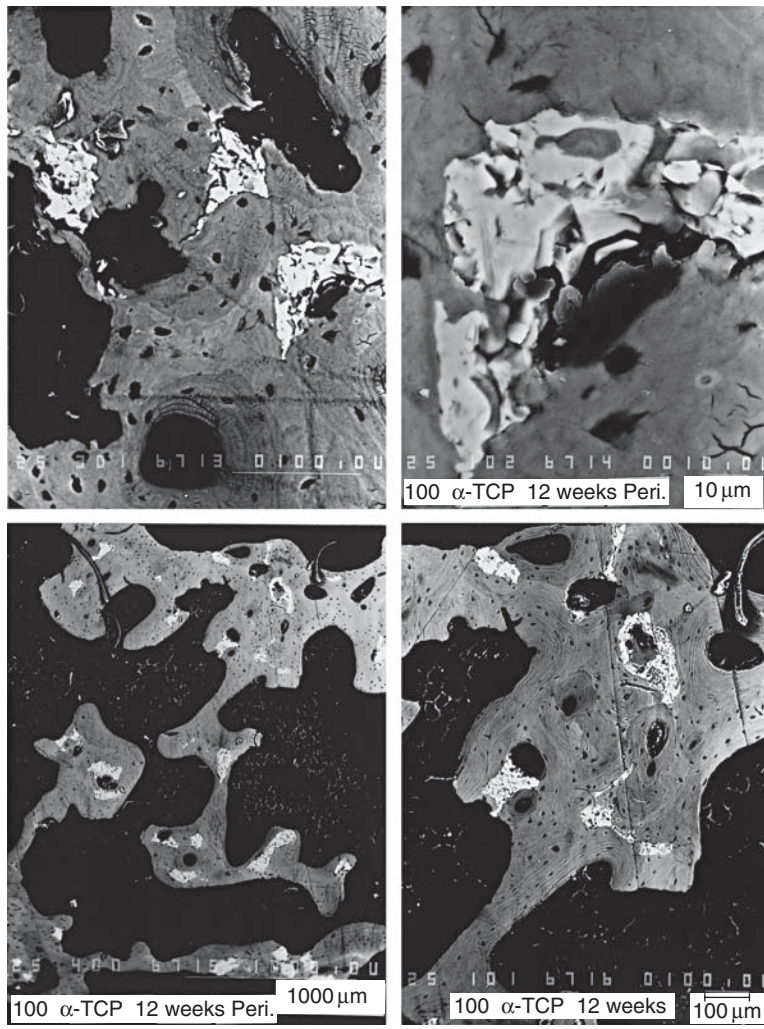

27.15 Bone growth on α-TCP (100–300 μm) at 12 weeks. Backscattered SEM.

powder was replaced by bone from the periphery and traces of the shape were left, the size of the granule was scarcely changed.

α-TCP, β-TCP, TeCP, TeDCPD, and TeDCPA: granules 10μm in diameter

At 3 weeks, little bone had grown into the spaces between granules of the α-TCP, β-TCP, TeCP, TeDCPD, and TeDCPA masses (Fig. 27.16). At 6 weeks, the bone growth was seen only around the granule mass; however, the amount of surrounding new bone increased. A slight inflammation with

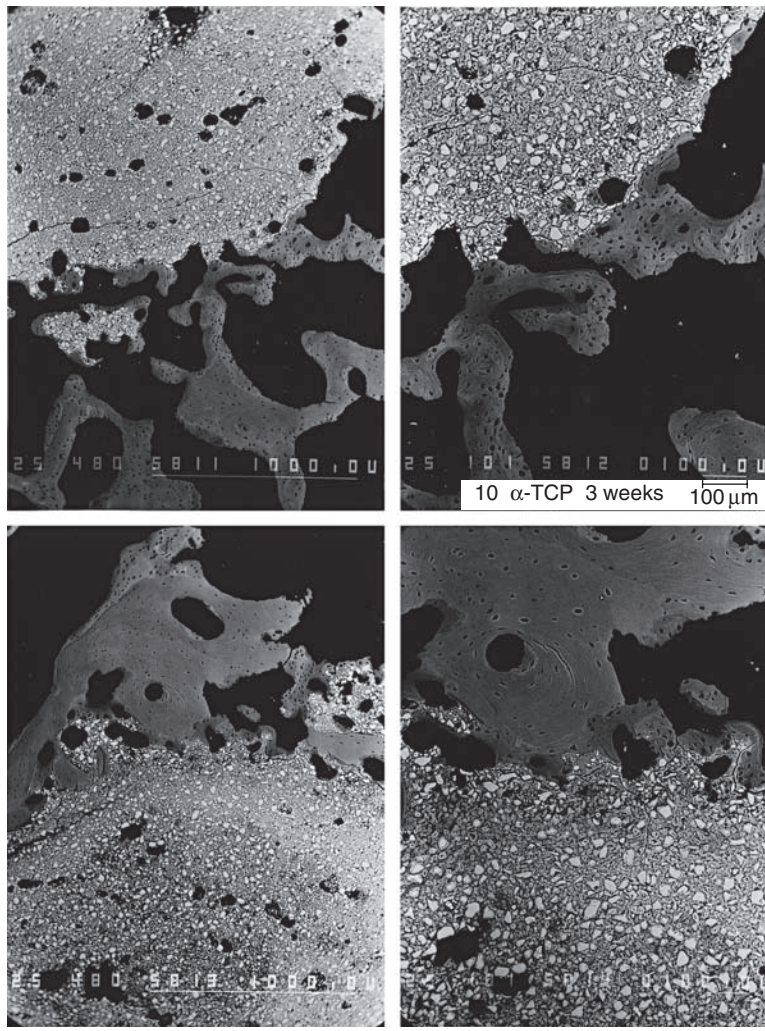

27.16 Bone growth on α-TCP (10μm) at 3 weeks. Bone is seen only on the partial outside of the mass. Backscattered SEM.

granulation, an increase of blood vessels, and congestion were observed around β-TCP. The inflammation was greater for β-TCP powder 10 μm in diameter than that for α-TCP powder of the same size. At 12 weeks, new bone surrounded almost all around TCP mass (Fig. 27.17).

By 6 weeks, the reaction to TeCP, TeDCPD, and TeDCPA was little different from that to α-TCP and β-TCP. The TeCP, TeDCPD, and TeDCPA powders 10 μm in diameter were being gradually incorporated into the trabecular bone which surrounded the mass of granules and then replaced by new trabecular bone. The behavior of 100–300 μm TeCP, TeDCPD, and

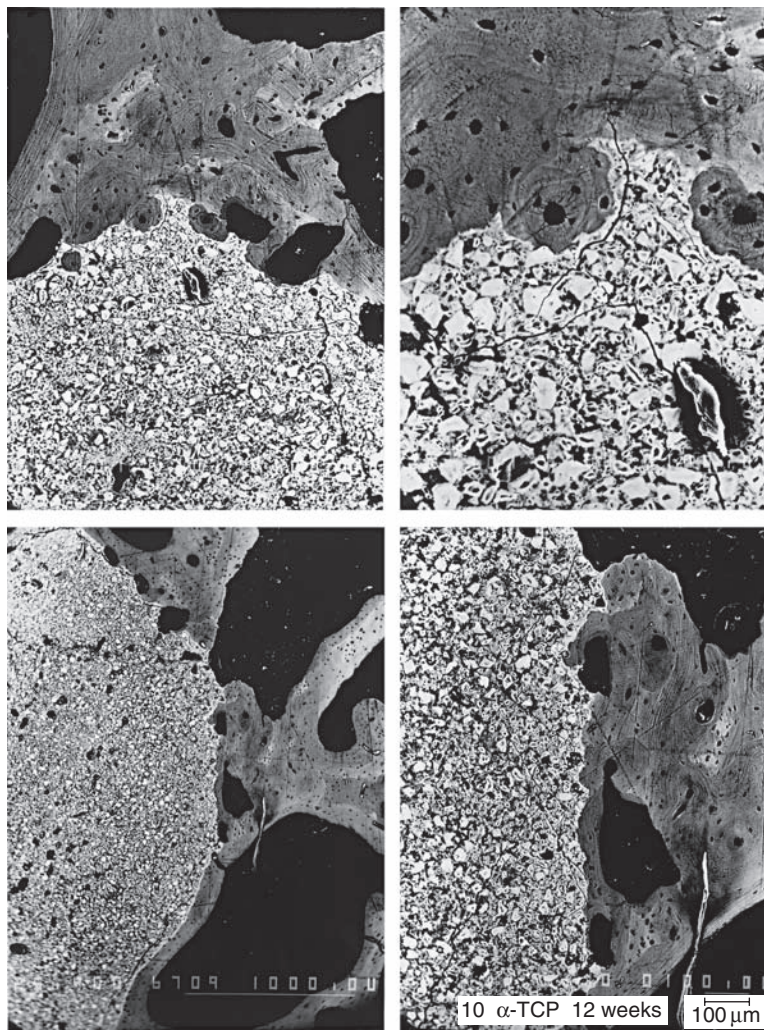

27.17 Bone growth on α-TCP (10 μm) at 12 weeks. New bone surrounds almost all the mass. Backscattered SEM.

TeDCPA granules was also different from that of α-TCP and β-TCP. From these observations, we conclude that TeCP, TeDCPD, and TeDCPA are more bioactive and more resorbable than α-TCP and β-TCP.

Low-crystalline HA and OCP; 10 μm granules

At 1 week, new bone entered a depth of one or two layers, surrounded some HA/OCP granules, and bonded to others. However, on the whole, large spaces were observed between the granule border and original bone (Fig. 27.18). At 3 weeks, laminar new bone 50–150 μm wide had begun to form.

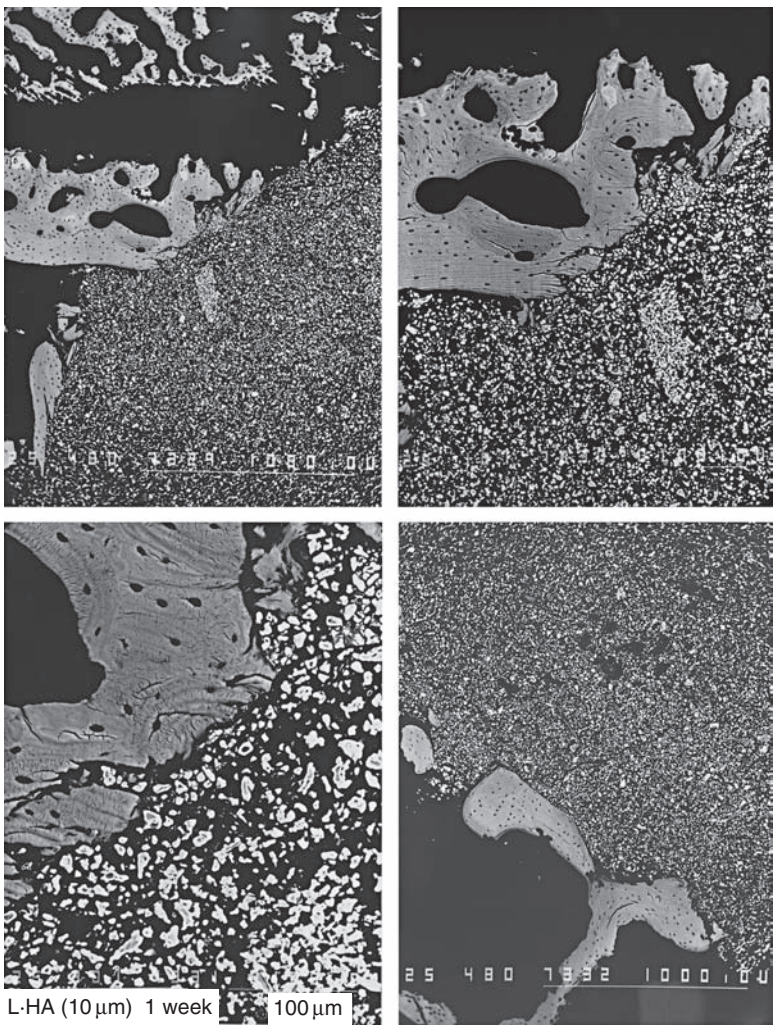

27.18 Bone growth on low-crystalline HA (10 μm) at 1 week. Backscattered SEM.

The trabecular new bone developed within the granules as was seen on 10μm HA granules (Fig. 27.19). AT 6 weeks, new bone had developed, intermingled with the granules at the center of the hole, with the HA/OCP granules being replaced by new bone from the granule periphery; and the number of granules diminished (Fig. 27.20). Low-crystalline HA and OCP granules 10μm in diameter showed very different behavior from sintered HA, which disappeared from the trabecular bone after earlier evidence of incorporation.

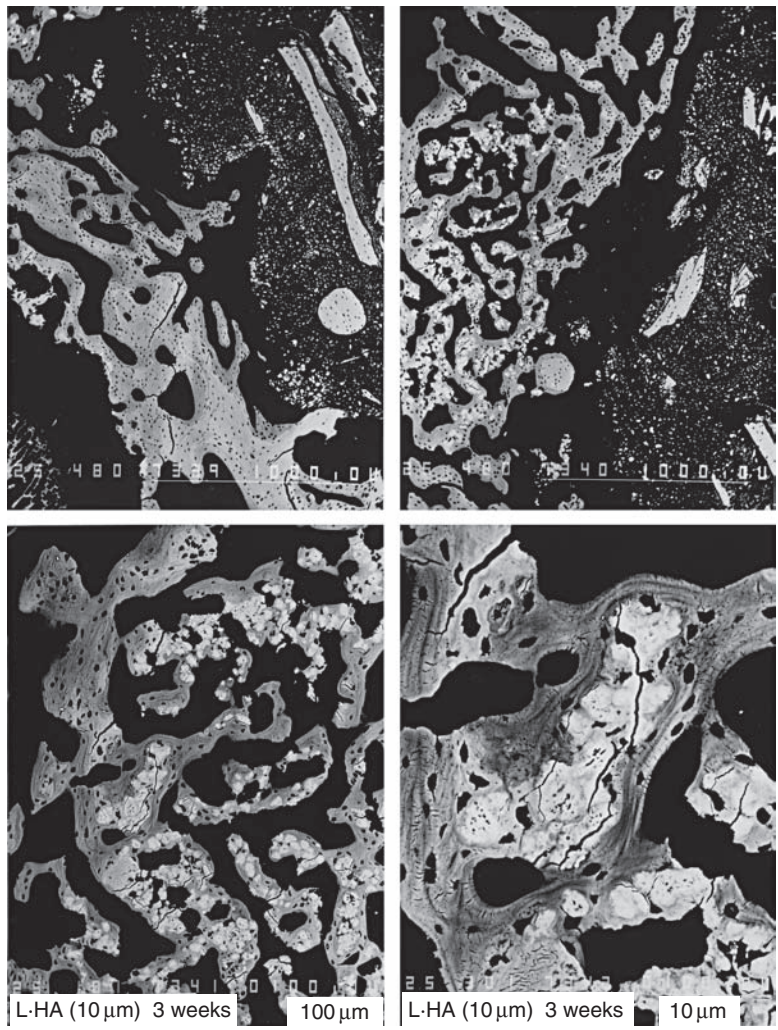

27.19 Bone growth on low-crystalline HA (10μm) at 3 weeks. Backscattered SEM.

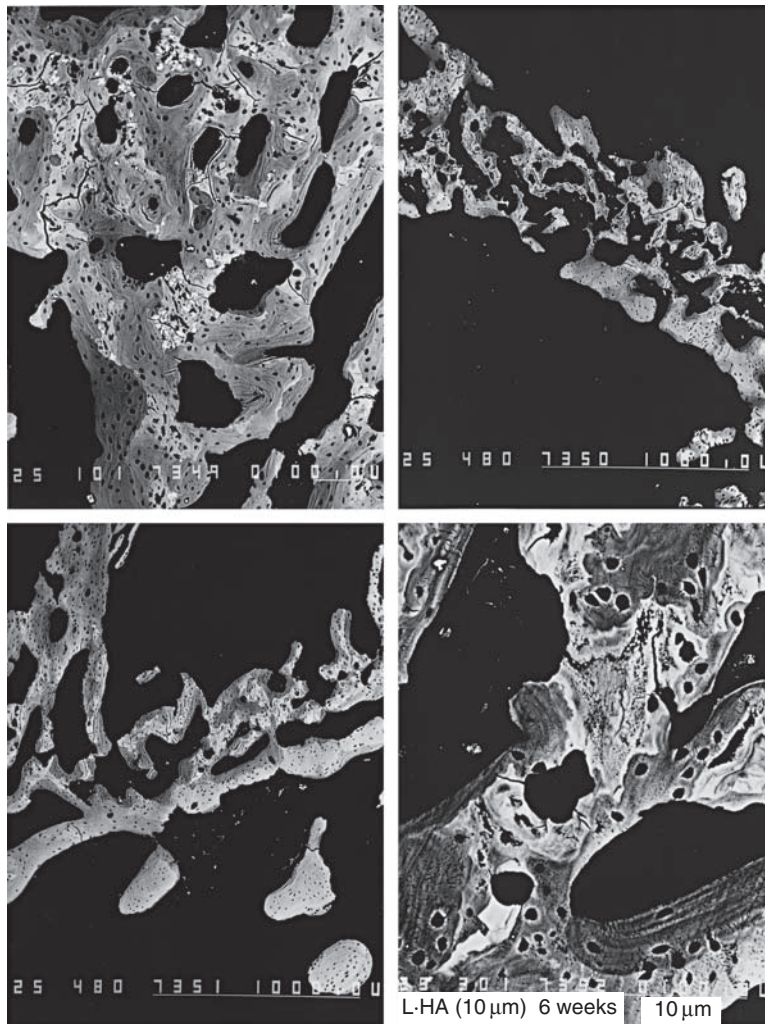

27.20 Bone growth on low-crystalline HA (10 μm) at 6 weeks. Backscattered SEM.

α-TCP, β-TCP, TeCP, TeDCPD, and TeDCPA also showed very different behaviors from low-crystalline HA and OCP. The former granules were surrounded *en masse* by new bone, and only a few granules from the periphery were taken into the trabeculae.

From these observations, we suppose that since sintered HA was surface-bioactive and insoluble, HA taken into the trabecular bone may have been removed by phagocytosis by 6 weeks. Low-crystalline HA and OCP with higher bioactivity and resobability did not leave the trabecular bone, but

were replaced by bone; thus, low-crystalline HA and OCP have a higher bioactivity and are more resorbable than α-TCP, β-TCP, TeCP, TeDCPD, and TeDCPA.

27.2.6 Controls and discussion

Control holes were drilled in the femoral condyles of mature rabbits and left unfilled. At 3 and 6 weeks, the density of bone formation in the unfilled hole was very low. At 12 weeks, cancellous bone formation in the cavity was back to normal. No changes were observable on surface cross-sections by the naked eye.

There was bone growth into the spaces between bioinert alumina 100 μm in diameter, from the surrounding bone where the spaces were less than several tens of micrometers between granules and the surrounding bone. However, there was no direct contact between bone and alumina, spaces less than several tens of micrometers were needed, and alumina never bonded directly to bone. On the other hand, there was bone growth into the spaces of surface-bioactive HA granules 100–300 μm in diameter, from the surrounding bone and the new bone bonded directly to the granules. However, spaces of <100 μm between the surrounding bone and the HA granules were essential for bone ingrowth (Fig. 27.21). HA powders of

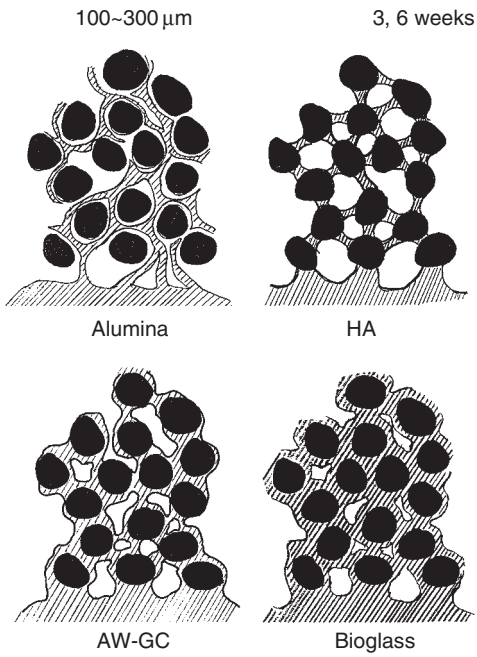

27.21 Bony tissue responses to a range of bioceramic test materials.

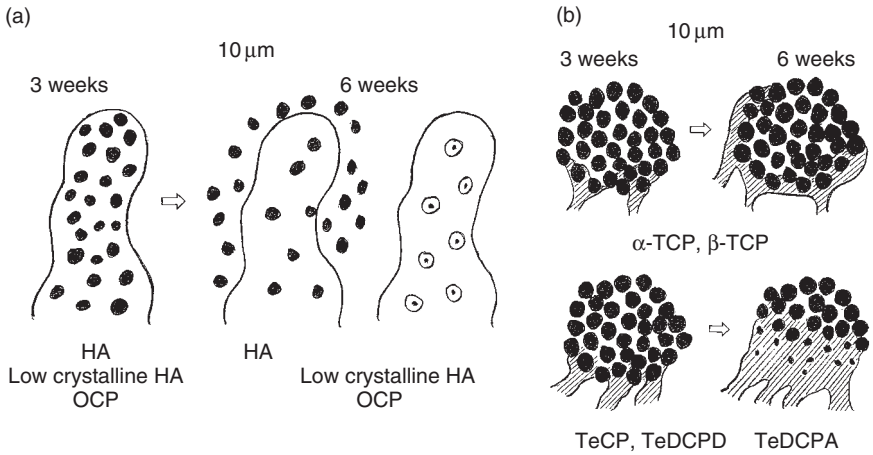

27.22 Bony tissue responses to a range of bioceramic test materials.

10 μm size were taken into the trabecular bone by 3 weeks but disappeared by 6 weeks (Fig. 27.22). New bone invaded 1–2 μm HA powders but left spaces between new bone and the HA powders. It appears the HA particles must be >10 μm for bone augmentation.

In the case of Bioglass™, the speed of bone growth into the 100–300 μm diameter granules was much faster and the new bone much denser than that associated with HA granules of the same size. Bone conduction and biocompatibility of Bioglass™ were much higher than those of HA (Fig. 27.21).

α-TCP and β-TCP of 100–300 μm size were taken into the trabecular bone and the size of the granules diminished with time; however, the shape was retained. TeCP, TeDCPD, and TeDCPA 100–300 μm in size were taken into the trabecular bone; the size of the trabecular bone and that of the granules became smaller with time, and they were slowly replaced by bone from the periphery. Their shape was not retained; it became indistinguishable from the surrounding bone. We observed that the granules had reduced in size but retained the form originally present in the fine powder from which they had been granulated (Fig. 27.23).

HA powders 10 μm in size were taken into the trabecular bone by 3 weeks but had disappeared by 6 weeks. Low-crystalline HA and OCP 10 μm in size were taken into the trabecular bone at 3 weeks, became smaller with time, and were slowly replaced by bone from the periphery. The original shapes were hardly distinguishable from the surrounding bone by 6 weeks (Fig. 27.22).

With α-TCP and β-TCP, TeCP, TeDCPD, and TeDCPA powders 10 μm in size, little bone grew into the spaces between these powders and around

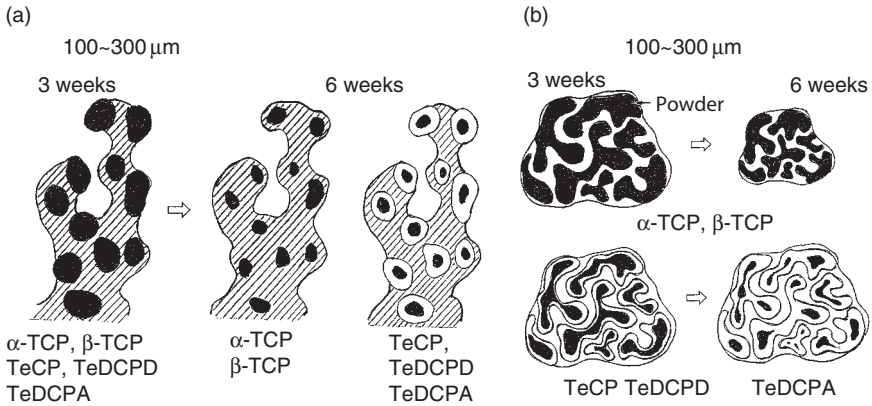

27.23 Bony tissue responses to a range of bioceramic test materials.

these masses at 3 weeks. At 6 weeks, in the case of α-TCP and β-TCP, bone growth into the spaces was seen only at the periphery of the masses. The quantity of new bone increased, and in the case of TeCP, TeDCPD, and TeDCPA, these powders were being gradually incorporated in the trabecular bone surrounding these masses and were replaced by new bone. TeCP, TeDCPD, and TeDCPA granules 100–300 μm in size also showed different behavior from α-TCP and β-TCP (Fig. 27.23). From these observations, we believe that TeCP, TeDCPD, and TeDCPA may have higher bioactivity or be more resorbable than α-TCP and β-TCP. Low-crystalline HA and OCP powders 10 μm in size were taken into the trabecular bone completely by 6 weeks. However, some TeCP, TeDCPD, and TeDCPA powders 10 μm in size were incorporated at 6 weeks by a different mechanism from low-crystalline HA and OCP. Thus, it appears that low-crystalline HA and OCP have higher biocompatibility or are more resorbable than TeCP, TeDCPD, and TeDCPA.

The degradation characteristics of CaPs, which can be divided into solution- and cell-mediated degradation, are governed by the chemical composition, crystal structure, crystal and grain size, microporosity, neck geometry, and neck dissolution rates of the materials. In our preliminary *in vitro* dissolution experiments for some CaPs, the order of dissolution rate in saline appeared to be as follows: TeCP > α-TCP > β-TCP > HA (sintered at 1200 °C). Ducheyne *et al.* (1993) showed that in a calcium and phosphate-free Trisbuffer solution at pH 7.3, the dissolution rate of CaPs increased in the following order: HA < calcium-deficient HA < β-TCP < α-TCP < TeCP.

Although the *in vivo* solution-mediated degradation may be the more important of the two processes, especially in the early stages after implantation, cell-mediated degradation could also take place with certain CaPs (de

Bruijn *et al.* 1994a). De Bruijn *et al.* (1994b) showed that more extensive dissolution/reprecipitation occurred on degrading and low-crystalline CaP surfaces, that bone tissue formed more rapidly on these dynamic material surfaces *in vivo*, and that osteoclasts appeared to have the ability to resorb the low-crystalline HA and β-TCP but not high-crystalline HA *in vitro*. These data suggest that more extensive dissolution/reprecipitation of CaPs caused more osteoconductive and cell-mediated degradation characteristics. For resorbable bioactive ceramics, therefore, these characteristics reflected the resorbable rates of CaPs.

From ultrastructural investigations of CaP materials suspended in cell culture and in serum *in vivo*, LeGeros *et al.* (1991) suggested that the following events occur on the surfaces and at the biomaterial–bone interface:

1 Partial dissolution of the CaP ceramic macrocrystals, which causes an increase in the calcium and phosphate ion concentrations in the local environment.
2 Formation of carbonate apatites (CO_3 apatites) intimately associated with an organic matrix.
3 Incorporation of the microcrystals and CaP macrocrystals with the collagenous matrix in the formation of new bone in osseous defects.

Especially in stage 2 of the process, microcrystals of CO_3 apatite may from directly by precipitation or indirectly by initial formation of any CaP phase, e.g. DCPD, OCP, TCP, and amorphous calcium phosphate (aCP) and subsequent transformation of any of these nonapatitic phases to apatite.

Thus, CO_3–apatite formation *in vitro* and *in vivo* is due to a process of dissolution of CaPs and precipitation of CO_3–apatite, incorporating CO_3 and Mg ions from the biological fluid. The dissolution rate of CaPs immersed in acid buffer solution is as follows: HA < β-TCP < α-TCP < TeCP < aCP (LeGeros and LeGeros 1996).

Upon analysis of the reactions of CaPs *in vitro* upon immersion in a simulated physiological solution (Radin and Ducheyne 1993), the minimum time for a measurable precipitate to form was found to increase in the order of: low-crystalline HA < well-crystallized, sintered HA < α-TCP < TeCP < β-TCP. Among these CaPs, only low-crystalline HA elicited immediate formation of CO_3–apatite. TeCP elicited the formation of CO_3–apatite with a large carbonate content after 1 day's immersion, α-TCP provoked aCP formation with a relatively low carbonate content, and β-TCP did not promote CO_3–apatite formation within 6 days.

These chemical reactions, especially the critical reprecipitation as CO_3–apatite or aCP on the surfaces of CaPs obtained from *in vitro* studies, support our *in vivo* data. We assume that β-TCP is a biodegradable or absorbable CaP without reprecipitation at least shortly after implantation,

but is not bioactive when in the form of 10 μm particles. In an *in vivo* study using *in situ* hybridization with procollagen α-1 (I) RNA probes, the β-TCP surface did not promote preosteoblast adhesion and differentiation (Neo *et al.* 1996a) and the labeled osteoblasts did not oridinate from the mesenchymal cells which existed in the clot, but from the precursor cells migrating from the bone-forming area. It is suggested that β-TCP is not bioactive but osteoconductive, and that bone was formed despite the presence of the β-TCP, whereas bone remodeling and regeneration of bone marrow occurred.

In the case of TeCP, characterized by dissolution followed by precipitation and extensive transformation to poorly crystallized CO_3–apatite after 2 days' immersion occurs without intermediate phase formation (Neo *et al.* 1996b). We have previously shown *in vivo* that TeCP was replaced by new bone. The gradual replacement of the TeCP microcrystals by bone minerals was demonstrated by SEM and backscattered electron imaging (Oonishi *et al.* 1991). TeCP is gradually transformed until replaced as shown in Fig. 27.8, and may be both bioactive and resorbable.

Te-DCPA and Te-DCPD, characterized as solid phase buffers, reacted in water to form a low-crystalline HA as follows:

$$2Ca_4(PO_4)_2O + 2CaHPO_4 = \text{(low-crystalline) } Ca_{10}(PO_4)_6(OH)_2$$
$$2Ca_4(PO_4)_2O + 2CaHPO_4 \cdot 2H_2O = \text{(low crystalline) } Ca_{10}(PO_4)_6(OH)_2 + 4H_2O$$

We believe that Te-DCPA and Te-DCPD are bioactive and bioresorbable, since they behave mainly as transformed low-crystalline HA or as TeCP after implantation in bone. Finally, OCP particles implanted in osseous tissue conducted massive amounts of bony tissue early and were then resorbed by osteoclast-like cells (Sugihara *et al.* 1995). OCP may also be considered bioactive and resorbable, since it also behaves like a low-crystalline HA after implantation (Fig. 27.19).

These findings strongly suggested that α-TCP, TeCP, TeDCPA, TeDCPD, OCP, and low-crystalline HA are bioactive CaPs forming carbonate-apatite or aCP including carbonate on the particle surfaces remodeled by osteoclasts or macrophages (Oonishi *et al.* 1999).

27.3 Quantitative comparison of bone growth behavior into HA granule mass with other surface-bioactive ceramics

Bioactive ceramics and glass, including synthetic hydroxyapatite, A-W glass-ceramic, and 45S5 Bioglass®, have been used clinically in various situations in which bone augmentation and restoration are required (Kitsugi *et al.*

1987; Hench 1991, 1994, 1998; Oonishi *et al.* 1997d, 1998a, 1999, 2000b). These are considered as surface bioactive ceramics.

In this study, bone reaction to granules of similar sizes of 45S5 Bioglass®, A-W glass-ceramic, and synthetic HA were compared quantitatively in the rabbit femur.

27.3.1 Materials and methods

These three kinds of materials were crushed into granules and sieved to produce particles 100–300 μm in diameter. Holes 6 mm in diameter were drilled bilaterally in the femoral condyles of mature rabbits, and sufficient hemostasis was achieved by filling and compressing the holes with gauze for 5 min. Immediately afterward, granules of Bioglass®, A-W glass-ceramic, and HA were placed in sufficient amounts to fill the holes in the femoral condyles. Five femoral condyles were used at each time period.

The animals were killed at 2, 3, and 5 days and 1, 2, 3, 6, 12, and 24 weeks. Nondecalcified specimens were observed by light microscopy and backscattered scanning electron microscopic imaging. The appearance of new bony tissue was identified from the light micrographs and backscattered scanning electron microscope images.

Bone ingrowth rates were measured by means of a high-performance image processor for analytical pathology (Sumika Technos Corp.). They were calculated by the measurements of new bony tissue areas in the implanted areas (Fig. 27.24).

27.3.2 Results

Morphological studies of bone ingrowth: up to 1 week after implantation

At 2 days, zones of 10–20 μm in width consisting of very fine granules appeared around the Bioglass® particles from the outmost layer to the third layer. These zones did not come into contact with the Bioglass®. At 5 days, the density of these very fine granules became higher and the width of these zones became greater (Fig. 27.25a). When these zones were observed by higher magnification on the backscattered electron images, they were found to be new bone (Fig. 27.25b). Aside from this new bone formation, new bone entered into the interparticle spaces from the periphery of the defect (Fig. 27.25a).

At 2 days, new bone formation could be detected around the Bioglass® particles in the first two to three layers. This new bone did not enter by osteoconduction from the periphery of the defect, but was formed directly around the Bioglass® particles. Consequently, the probable origin of the new bone was both from the periphery of the defect, where bone already

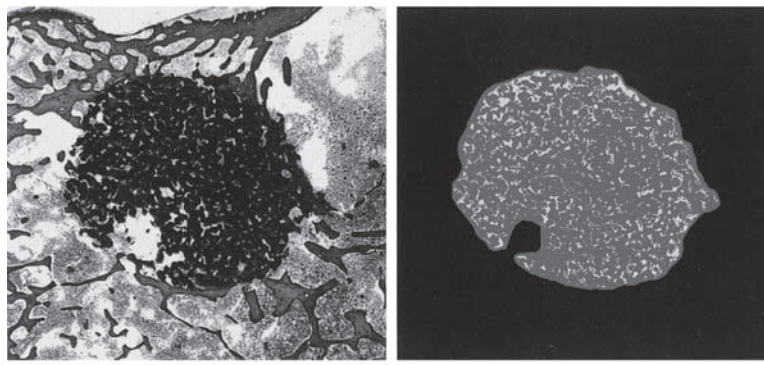

HA·100–300 μm 6 weeks (18.4%)

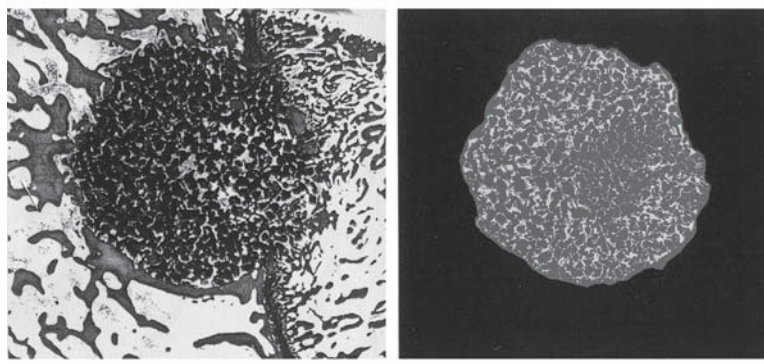

AW 100–300 μm 6 weeks (23.5%)

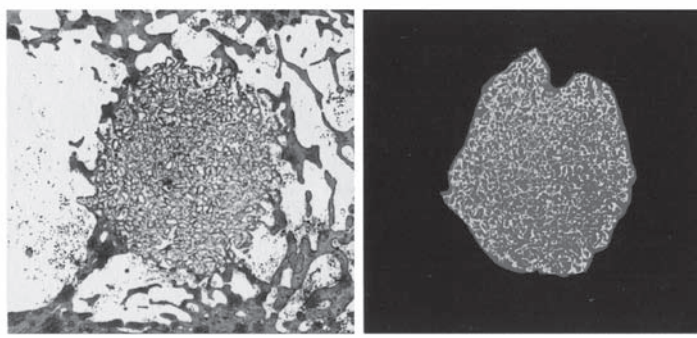

BG 100–300 μm 6 weeks (35.9%)

27.24 The bone ingrowth rate was calculated by the measurements of the area of new bony tissue in the implanted area. New bony tissue is shown as the White area on the figures on the right hand side.

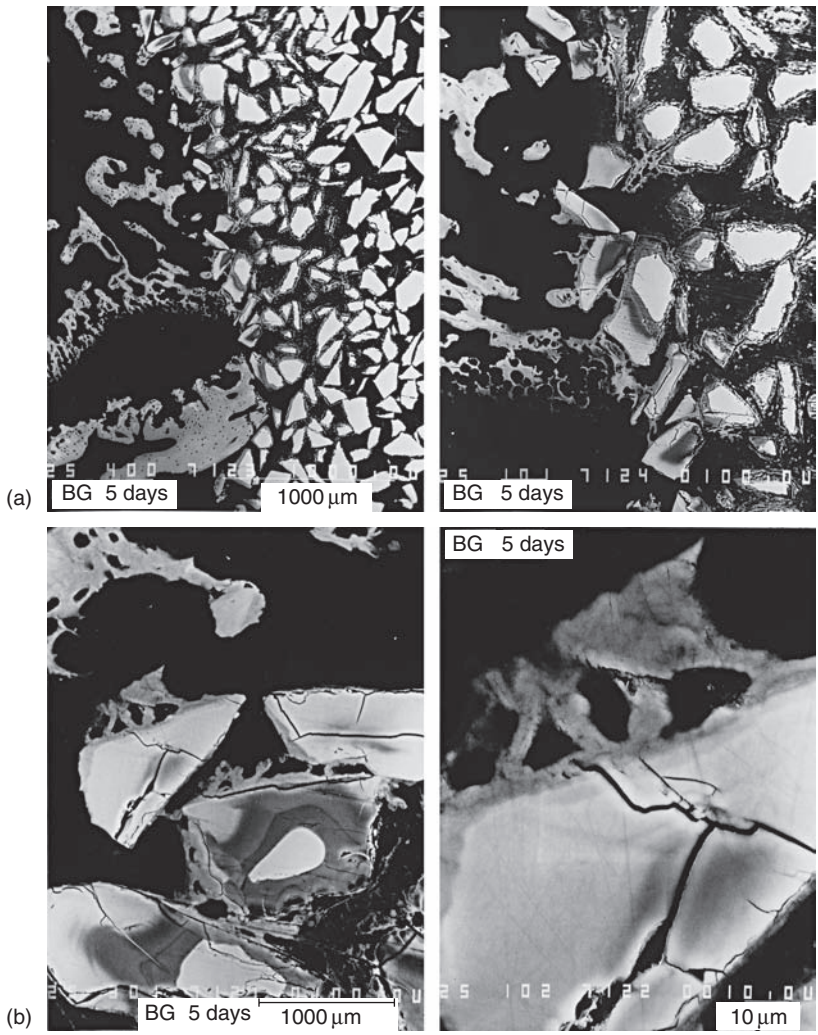

27.25 Osteoid formation at 45S5 Bioglass® interfaces at 5 days. Backscattered SEM.

existed (i.e. by osteoconduction), and directly on the particles (i.e. by osteoproduction).

At 3 days, a zone consisting of very fine granules, as seen on the Bioglass®, appeared around the A-W GC in some areas, which were indistinct. There was no osteoconduction from the periphery of the defect at this time. At 3 days, there was neither bone formation around the HA particles nor bony invasion from the periphery of the defect. At 5 days, new bone formation could be detected around HA particles in the first layer (Fig. 27.26; Tables 27.1 and 27.2).

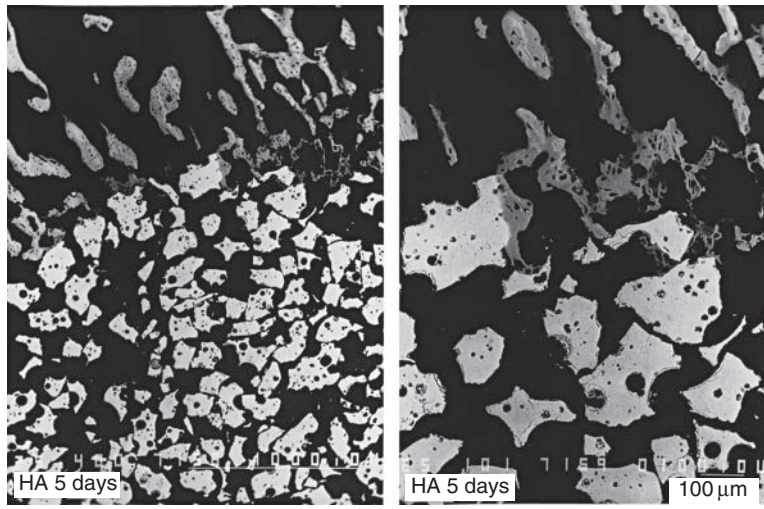

27.26 New bone formation around HA particles in the first layer at 5 days. Backscattered SEM.

Table 27.1 New bone formation around particle in defect at very early period

	Bioglass	A-W	HA
2 days	3 layers		
3 days		2 layers	
5 days	7 layers		
1 week	10 layers (center)		

Table 27.2 Depth (layers) of bone ingrowth from periphery

	Bioglass	A-W	HA
2 days			
3 days			
5 days	2 layers		1 layer
1 week	4–5 layers	3 layers	1–2 layers
2 weeks	10 layers (center)	7–8 layers	5–6 layers
3 weeks	10 layers (center)	10 layers (center)	10 layers (center)
6 weeks			

Morphological studies of bone ingrowth: 1 week after implantation

The zone of very fine granules around the Bioglass® particles appeared around every particle to the center of the defect, and new bone was found on the surface of the Bioglass® particles to the center of the defect (Fig. 27.27). Interparticle spaces were filled by new bone trabeculae to depth of at least four to five particle layers. The new bone was beginning to form a

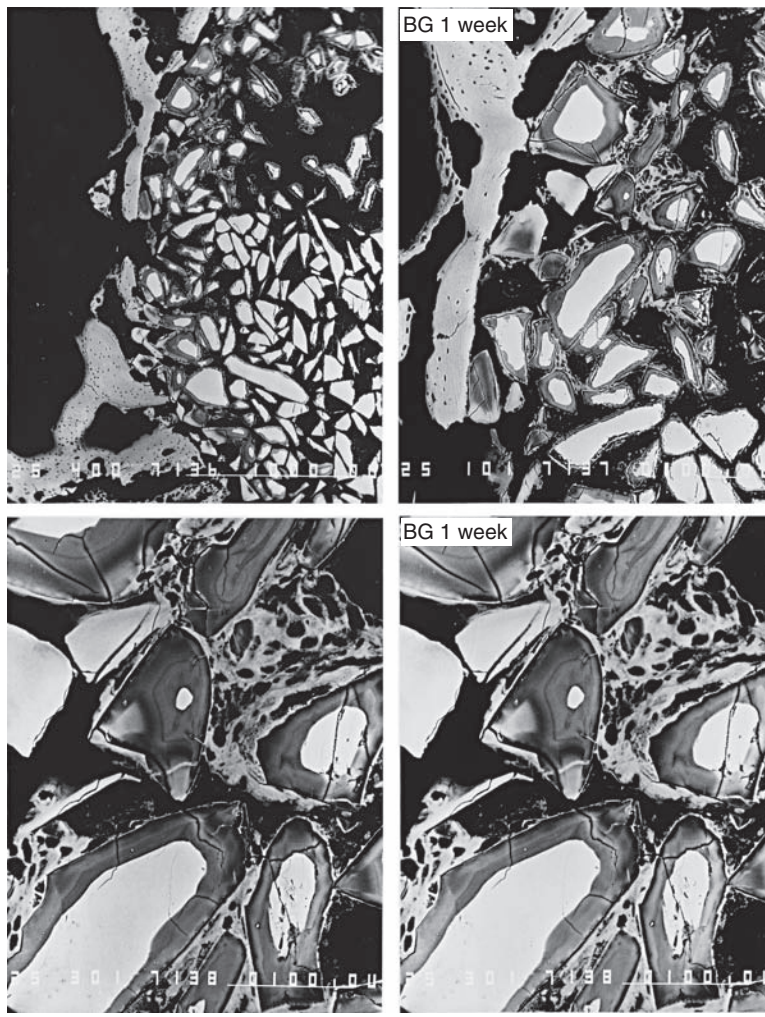

27.27 Extensive bone formation throughout the periphery of the bone defect at 1 week in the presence of Bioglass® particles.

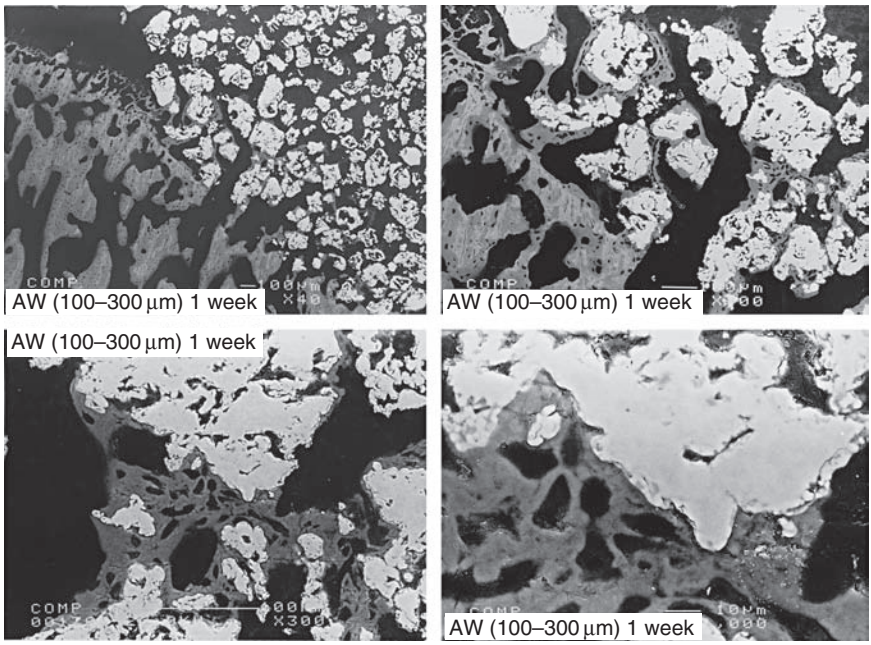

27.28 Bone formation to the third layer of AW-GC particles at 1 week.

trabecular architecture that incorporated the glass particles within the structure (Fig. 27.27).

In the case of A-W GC, new bone reached the third layer of A-W GC particles from the outer layer (Fig. 27.28). In the case of HA, new bone reached the first and second layers of the HA particles (Fig. 27.29). The amount of new bone around the Bioglass® and A-W GC particles was greater than that around the HA particles (Tables 27.1 and 27.2).

Morphological studies of bone ingrowth: 2 weeks after implantation

In Bioglass® samples, interparticle spaces were filled by new bone trabeculae to the 10th layer – that is, to the center of the defect. In A-W GC samples, interparticle spaces were filled by new bone trabeculae to the seventh and eighth layers. In the case of HA, bone had reached the fifth and sixth layers (Fig. 27.30) and in some areas bone had reached near the center (Fig. 27.31). The amount of new bone in the interparticle spaces of the Bioglass® and A-W GC particles was greater than that of the HA particles (Table 27.2).

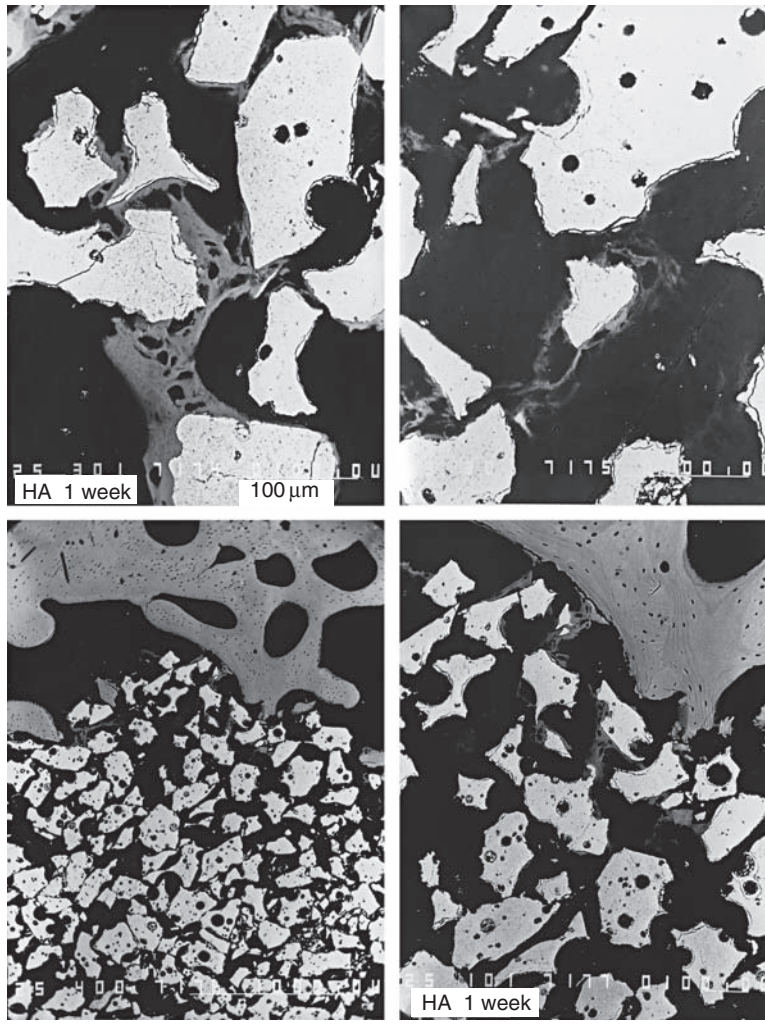

27.29 Onset of bone formation at outer layer of HA particles at 1 week.

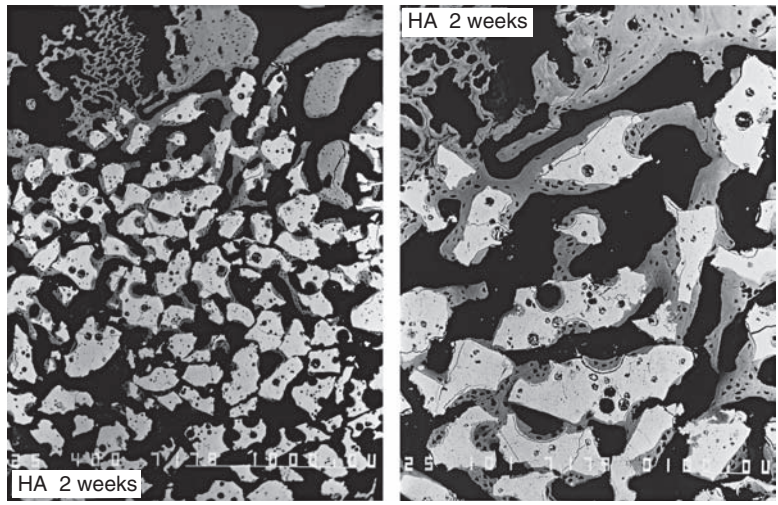

27.30 Bone formation around HA particles had reached the fifth and sixth layers.

Morphological studies of bone ingrowth: 3 weeks after implantation

Interparticle spaces of both A-W GC and HA were filled by new bone trabeculae to the center. The amount of new bone in the interparticle spaces of each type of particle increased (Table 27.2). The amount of the bone in the interparticles of HA on the peripheral layers was greater than that on the central layers (Figs 27.32 and 27.33).

Morphological studies of bone ingrowth: 6 weeks after implantation

New bone was complete around the particles of Bioglass® at 6 weeks and AW-GC between 6 and 12 weeks to the centers of the defects (Figs 27.34 and 27.35). For HA, new bone surrounded the particles in the outer second and third layers (Fig. 27.36). However, in the deeper layers new bone only partially covered the particles (Fig. 27.37 and Table 27.2).

Morphological studies of bone ingrowth: 12 weeks after implantation

The Si-rich layer in the center of the Bioglass® particles became smaller or disappeared and the size of the particles decreased to half or two-thirds their original size. Where the width between the particles became wider, in some areas the amount of bone around the particles decreased slightly, indicating remodeling of the trabecular architecture.

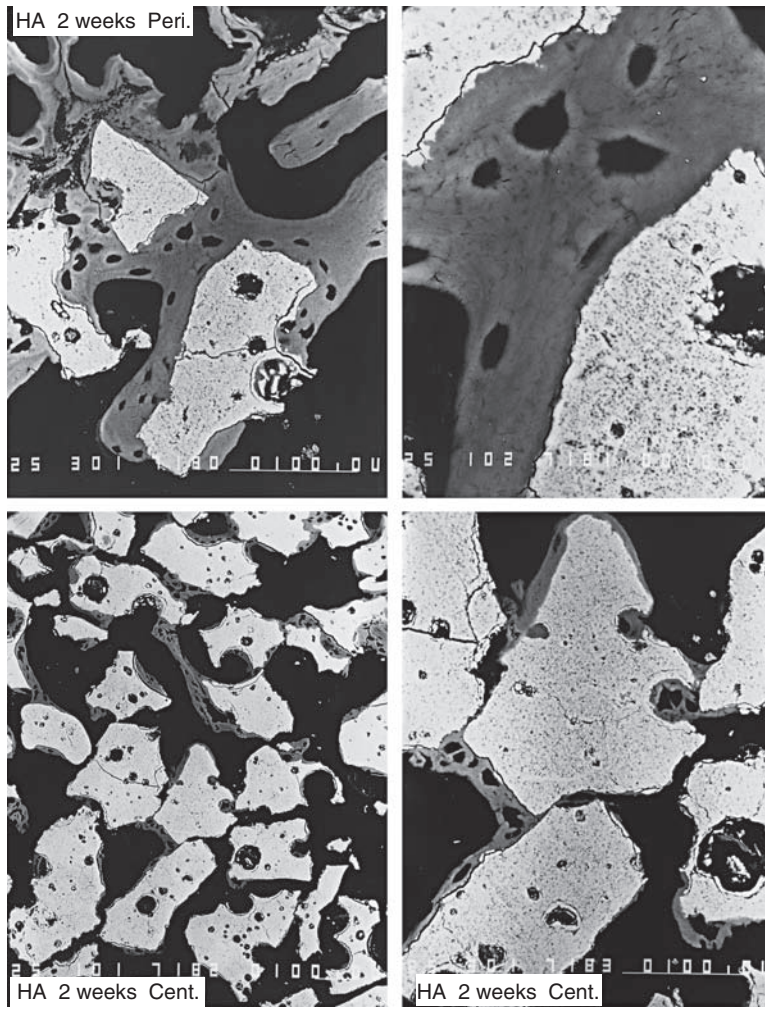

27.31 Bone formation around HA particles had almost reached the center in some areas.

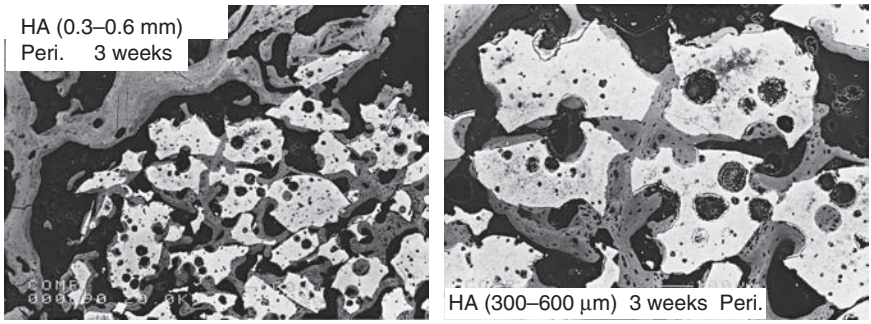

27.32 Bone bridges between HA particles in the peripheral layers at 3 weeks.

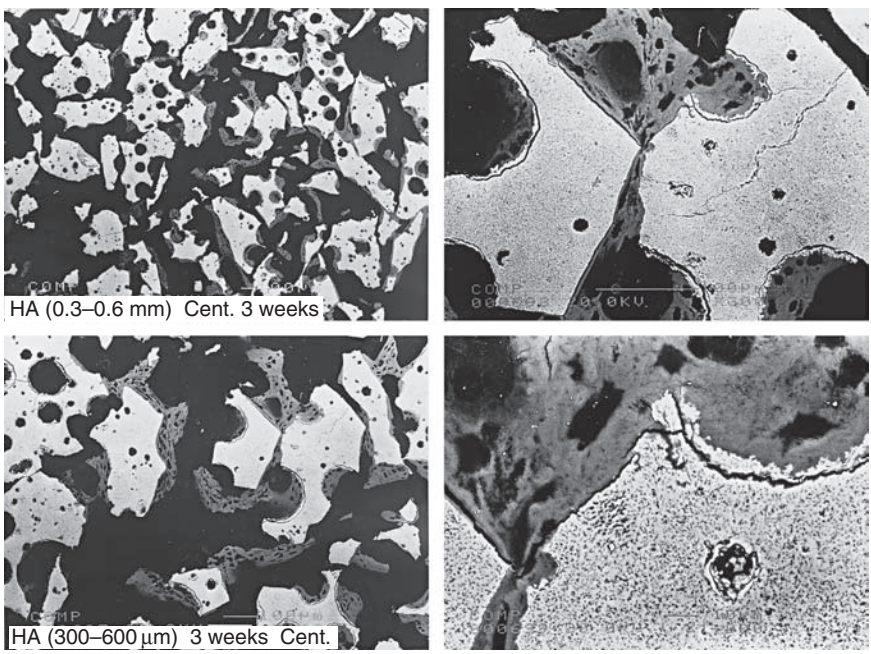

27.33 Bone bridges between HA particles in the central layers at 3 weeks.

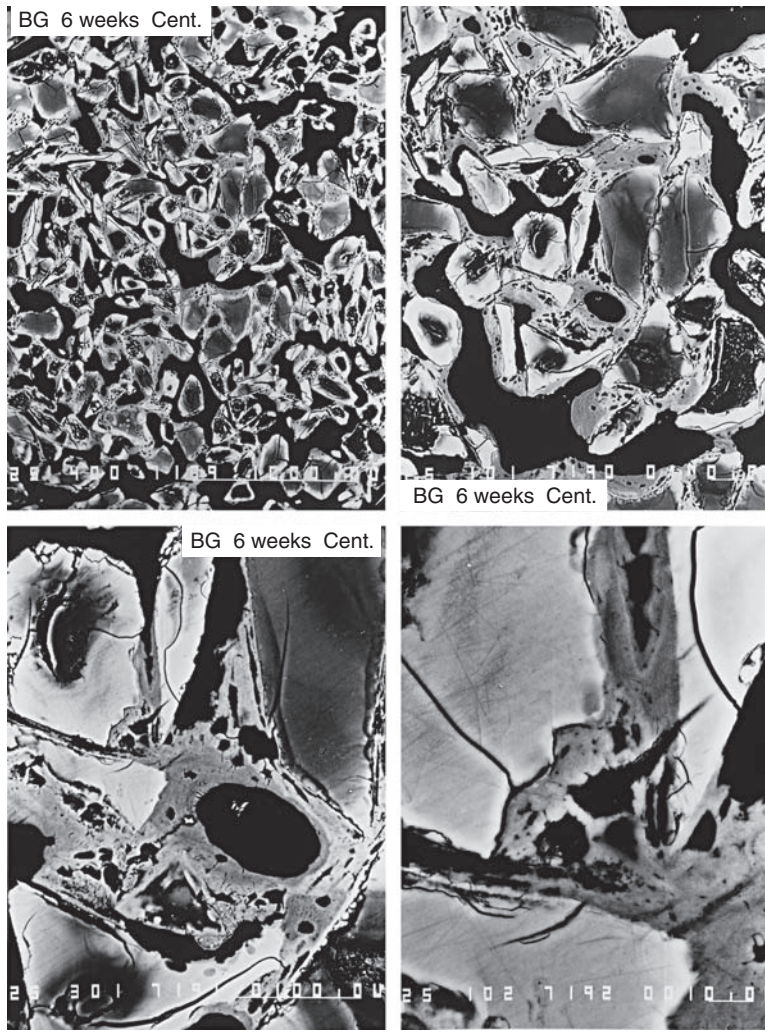

27.34 Bone formation in the bone defect with Bioglass® particles after 6 weeks.

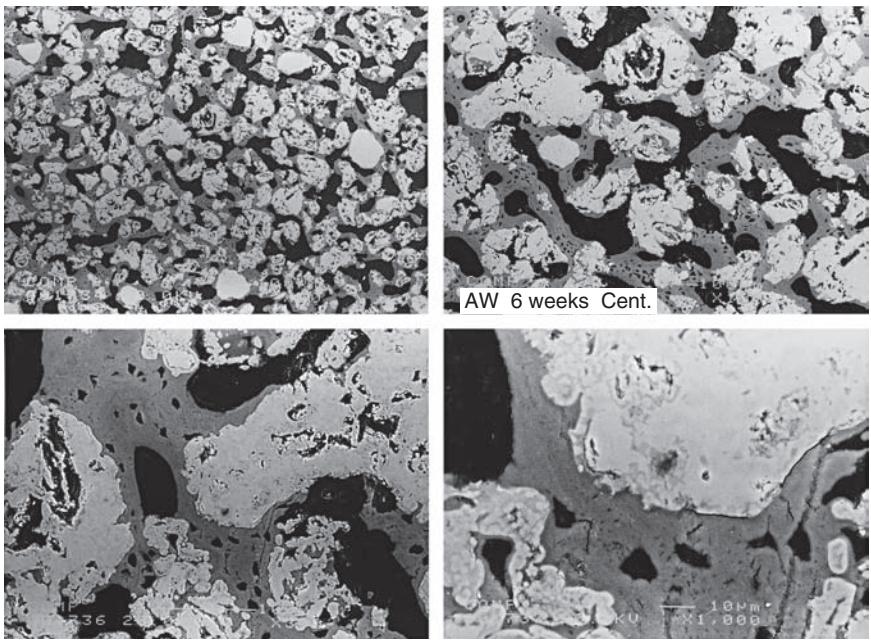

27.35 Bone formation in the bone defect with AW-GC particles after 6 weeks.

The size of A-W GC particles did not change. However, the periphery of the A-W GC particles became gray in the backscattered electron images. This change may indicate chemical changes in the A-W GC particles. New bone was formed all around the particles.

Bone formation in the interparticle spaces of HA was almost the same as after 6 weeks' implantation in the peripheral layer (Fig. 27.38). However, in the central layer the amount of new bone increased (Fig. 27.39). Absorption of Bioglass® particles began before 12 weeks' post-implantation, and evidence of absorption of AW-GC particles began around 12 weeks.

Morphological studies of bone ingrowth: 24 weeks after implantation

The size of Bioglass® decreased by 70–80%, and the number of particles decreased (Fig. 27.40). A-W GC particles decreased in size by 20% (Fig. 27.41). The particle size of HA did not change. Bone formation in the inter-particle spaces of HA was almost the same as after 12 weeks' implantation, and it was the same in the peripheral and central layers (Figs 27.42 and 27.43).

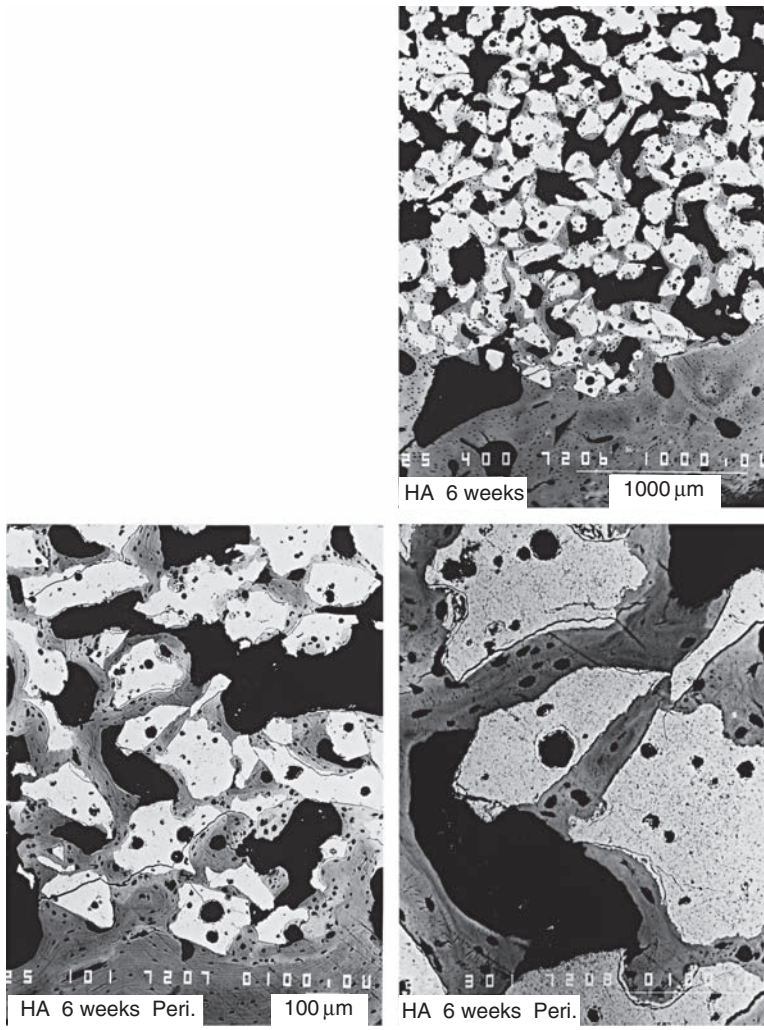

27.36 Bone formation in the bone defect with HA particles after 6 weeks: at the peripheral area.

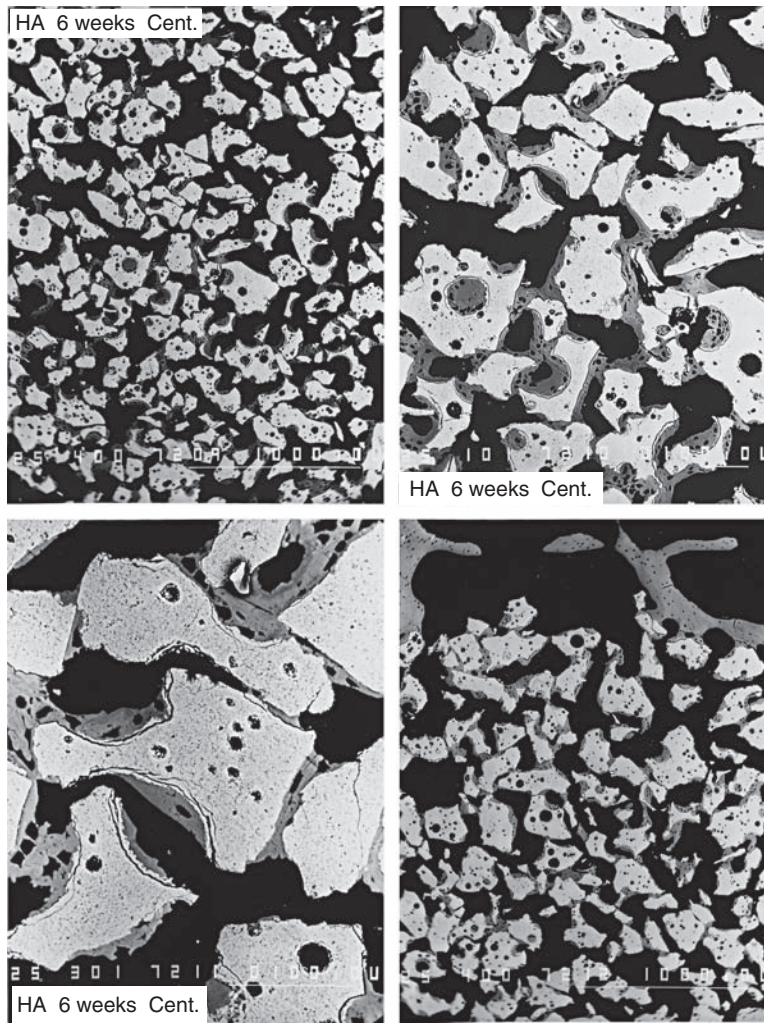

27.37 Bone formation in the bone defect with HA particles after 6 weeks: at the central area.

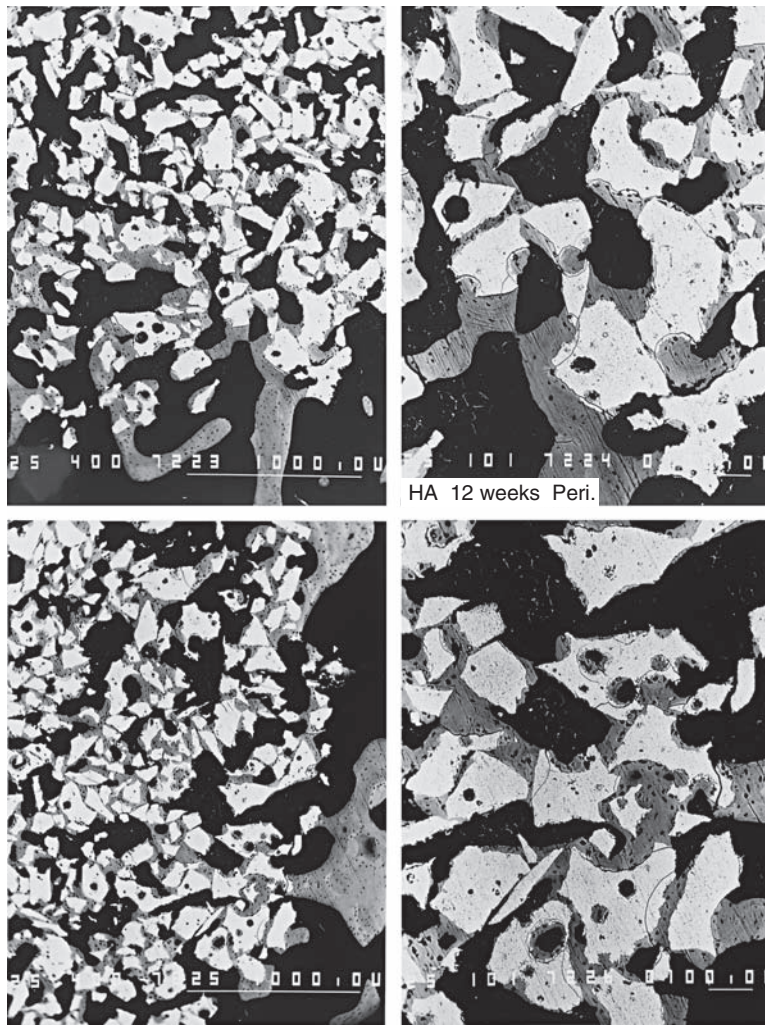

27.38 Bone formation in the interparticle spaces of HA at 12 weeks: at the peripheral area.

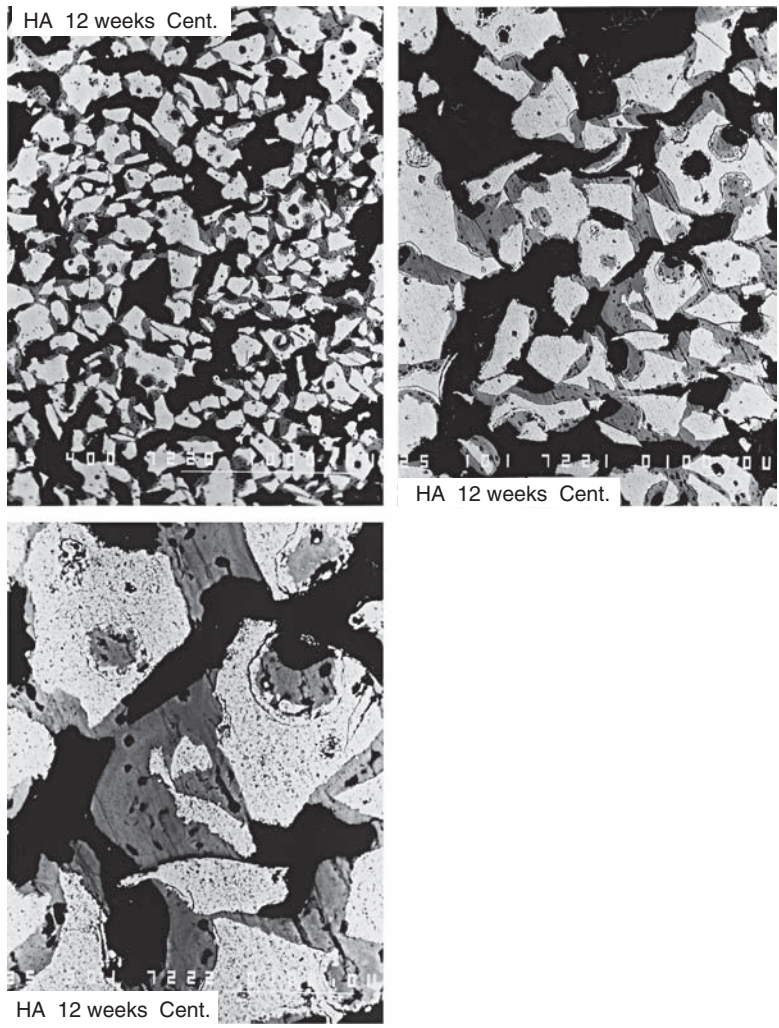

27.39 Bone formation in the interparticle spaces of HA at 12 weeks: at the central area.

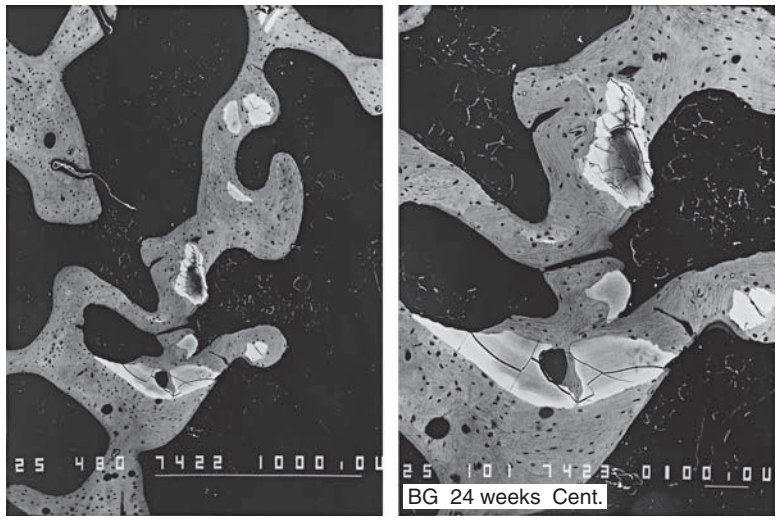

27.40 New bone around Bioglass® particles at 24 weeks.

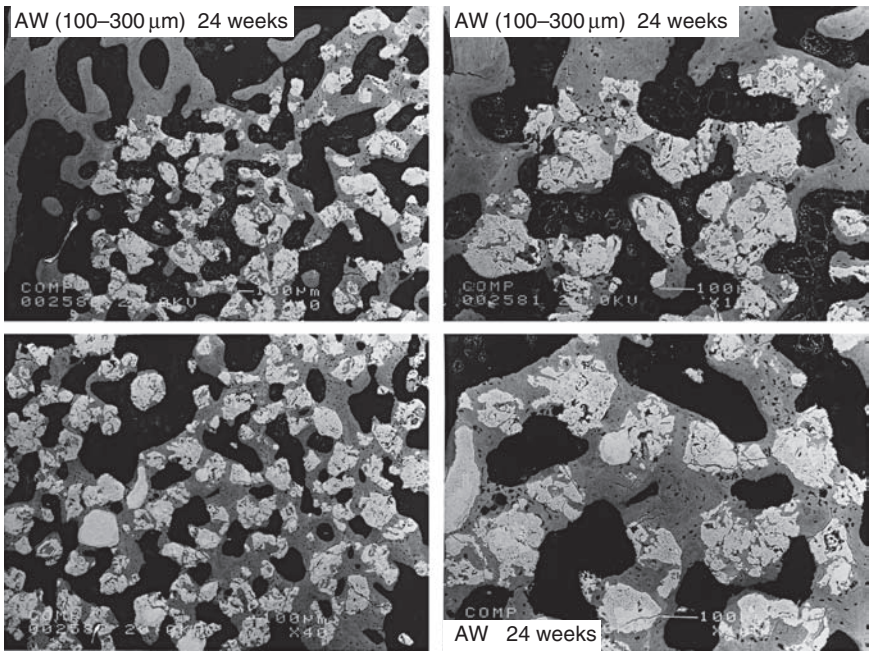

27.41 New bone around AW-GC particles at 24 weeks.

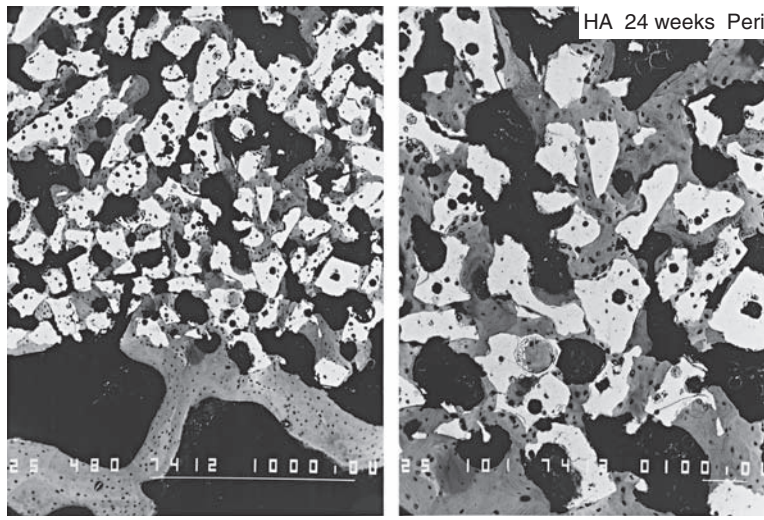

27.42 New bone around HA particles at 24 weeks. At the peripheral area.

Bone ingrowth rate

At 1, 2, 3, 6, 12, and 24 weeks after implantation of similar-size particles of Bioglass®, A-W glass ceramic, and hydroxyapatite, bone ingrowth rates (speed and quantity) into the spaces were compared. Comparing Bioglass® and HA, the bone ingrowth rate of Bioglass® particles was, at 1 week, 17 times, at 2 weeks, 3.3 times, at 3 weeks, 3.4 times (about 3 times after correction on the graph), at 6 weeks, 1.6 times (about 1.7 times after correction), and after 12 and 24 weeks, twice that of HA particles. Comparing A-W glass-ceramic and HA particles, the bone ingrowth rate of A-W glass-ceramic particles was 1.8, 2.0 1.6, 1.1, and 1.3 times that of HA particles at the same time periods (Fig. 27.44 and Table 27.3).

When the bone ingrowth rates of these three kinds of particles were compared overall, the speed and quantity of bone growth into Bioglass® particles, especially in the early period before 1 week, were eight times greater than A-W glass-ceramic and 17 times greater than HA, and increased continuously thereafter up to 12 weeks. The bone ingrowth rate into A-W glass ceramic particles was twice as fast as HA at 1–2 weeks and about 1.5 times at 3 weeks. At 6 weeks the rate of bone growth around A-W glass-ceramic particles was close to that around HA particles. Bone around A-W glass-ceramic particles continued to increase from 6 to 12 weeks, but around HA the amount of bone remained constant after 6 weeks. Consequently, by 12 weeks bone around A-W particles was 1.3 times that around hydroxyapatite particles (Fig. 27.44).

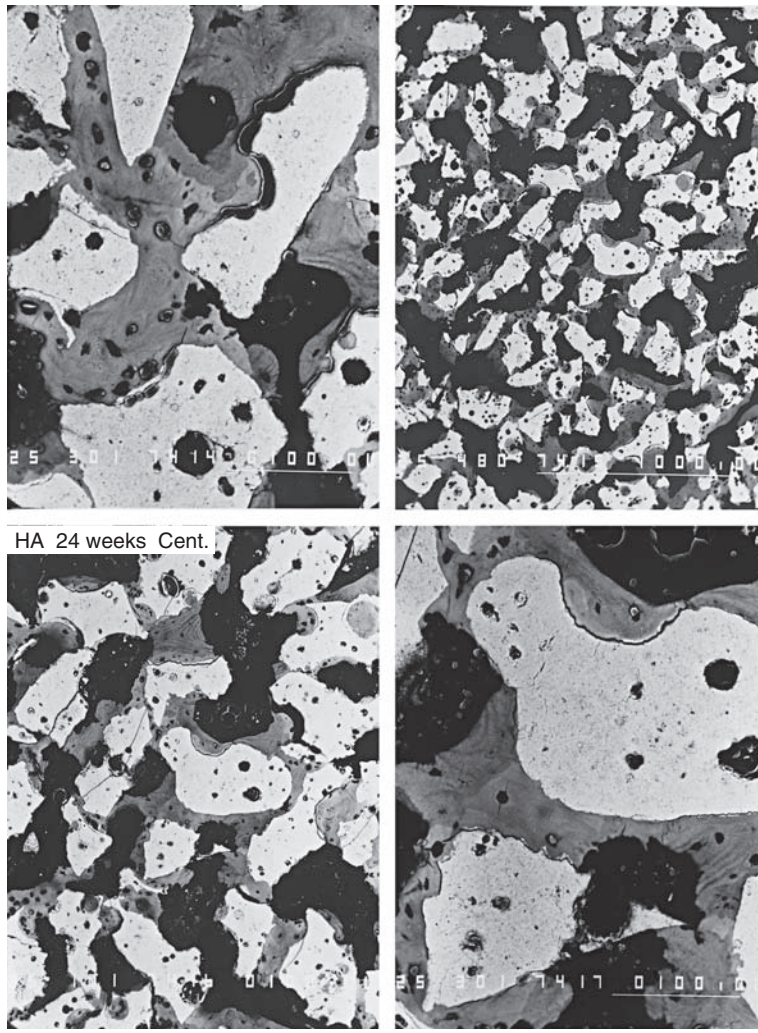

27.43 New bone around HA particles at 24 weeks: at the central area.

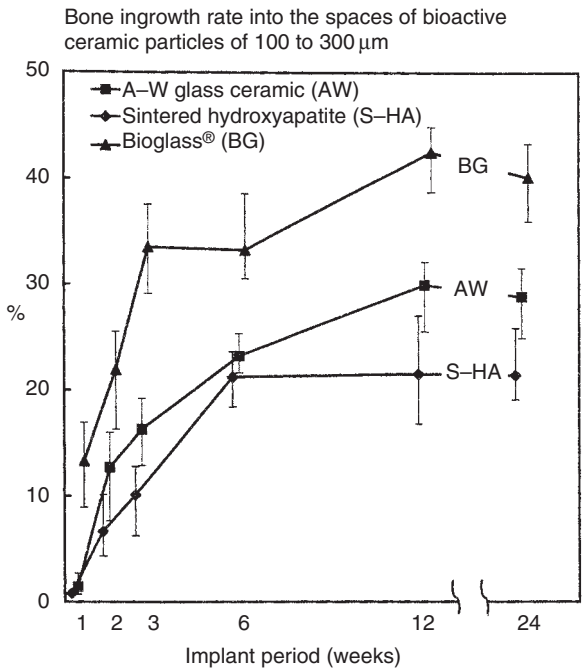

27.44 Quantitative comparison of the percentage of bone growth into the bone defect from 1 to 24 weeks due to 45S5 Bioglass®, AW-GC, and sintered HA particles of 100–300 μm.

Table 27.3 Bone in-growth rate into spaces of bioactive ceramic particles of 100–300 μm (%)

	1 week	2 weeks	3 weeks	6 weeks	12 weeks	24 weeks
Sintered	0.9	6.3	6.2	23.6	16.8	21.4
hydroxyapatite	0.7	10.1	12.2	20.3	18.5	25.8
	0.7	4.3	12.8	18.4	26.6	19.1
	1.1	8.4	10.0	22.7	24.1	21.8
	0.6	3.8	9.3	21.2	21.4	18.8
Average	0.8	6.6	10.1	21.2	21.5	21.4
A-W glass-	2.7	16.0	16.6	23.6	30.1	29.8
ceramic	0.7	17.4	14.4	21.6	25.5	30.5
	0.8	7.6	19.2	22.4	29.9	27.1
	1.1	9.7	18.4	25.3	31.8	31.5
	1.7	12.8	12.9	23.1	32.1	24.9
Average	1.4	12.7	16.3	23.2	29.9	28.8
Bioglass®	14.1	16.3	33.9	30.5	38.7	39.9
	8.9	19.8	35.8	35.4	44.2	40.8
	16.9	25.5	29.1	38.5	44.9	41.5
	10.8	24.6	37.5	32.7	42.0	35.9
	15.8	23.1	29.4	28.9	41.8	43.3
Average	13.3	21.9	33.1	33.2	42.3	40.3

Bone around Bioglass® and A-W glass ceramic particles continued to increase up to 12 weeks. In these experiments, changes between 12 and 24 weeks were not monitored, but by 24 weeks a slight decrease in bone was detected which appeared to be greater for Bioglass® than for A-W, but was not statistically significant.

27.3.3 Discussion

In these experiments it is shown that the rate of bone formation produced by a class A bioactive material, 45S5 Bioglass®, which was rapidly resorbed, is greater than that produced by two types of class B materials: A-W glass-ceramic, which was slowly resorbed, and synthetic HA, which was not. The rate of bone formation correlated with the dissolution of the particles and the provision of soluble silica to the osteoblasts in the growing bone.

These animal experiments were performed under unloaded condition. If they were to be performed under loaded condition, the quantity of the bone ingrowth would be greater and the speed of the bone ingrowth would be higher than under unloaded condition. The particle size of 100–300 μm had been used in the IBBC technique in total joint arthroplasty clinically, which will be described later in this chapter. If smaller particle size of these materials will be used, the reaction will be different.

27.4 Clinical applications: interface bioactive bone cement (IBBC)

Cemented total hip arthroplasty (THA) has been one of the most successful procedures in orthopedic surgery, since J. Charnley applied polymethylmethacrylate (PMMA) to fixing the components. Efforts to improve the mechanical bonding at the bone–bone cement interface have been made. Even with these contemporary techniques, cement fixation is often limited, especially in acetabular side. Furthermore, physicochemical bonding cannot be expected in addition to mechanical bonding, since the bone cement is not osteoconductive (Oh *et al.* 1978; Wroblewski 1986; Mulroy and Harris 1990; Sochart and Porter 1997; Callaghan *et al.* 1998).

To augment the bone–bone cement bonding, we applied a new cementing technique to achieve the enduring physicochemical bonding at the bone–bone cement interface by interposing osteoconductive crystalline HA granules. In this technique, bone cement is covered by HA granules at the interface, thus it seems that custom-made HA coated cemented implants. Since HA, which is used for cementless HA coated prosthesis, contains amorphous HA, this type of HA would be absorbed in the ten years following surgery. HA granules for our technique were pure crystal, thus they were scarcely absorbed and their osteoconductive activity can continue

indefinitely even after the onset of osteoporosis due to aging. We call this technique interface bioactive bone cement (IBBC) (Oonishi *et al.* 1989a, 1993a, 1998b, 2000a; Oonishi 1991a).

27.4.1 Materials and methods

This method involves placing less than two layers of porous HA granules 0.3–1.5 mm in diameter with a porosity of 35–48% (average 42%) between the bone and cement. Although HA granules of 0.3–0.5 mm in diameter were used initially, they were later reduced to 0.1–0.3 mm, as it was found those sizes adhere to bone more easily. HA must be used on the surface of completely hemostatic bone. On areas with slight bleeding, HA larger than 0.3 mm is more appropriate, as granules smaller than 0.3 mm will be covered by the blood. As a result, blood will be present between the HA and bone cement. Additionally, low-viscosity bone cements should not be used with HA granules, because the HA granules will sink in. We used CMW-Type I as the PMMA bone cement.

27.4.2 Experimental studies

Histological studies

Holes 6 mm in diameter and 10 mm in depth were made in both femoral condyles of mature rabbits, and HA granules of 300–500 μm in diameter were smeared in less than two layers over the bone surface of the hole, and the hole was filled with bone cement (Fig. 27.45). In groups of three, rabbits

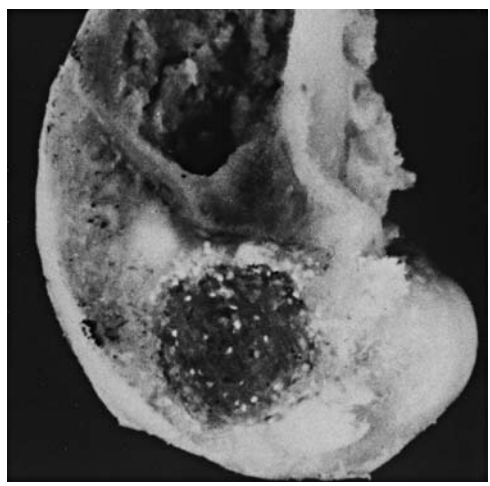

27.45 Cut surface of the femoral condyle 6 weeks after surgery.

were killed at 2, 3, 4, 6, 12, and 24 weeks, and at 3 years after implantation. Non-decalcified hard tissue specimens were prepared and examined by optical microscopy, scanning electron microscopy (SEM), and backscattered electron image.

One week after surgery, new bone began entering the first layer and adhering to the HA granules (Fig. 27.46). At 2–3 weeks after surgery, new bone had entered a majority of the spaces in the second layer (Fig. 27.47).

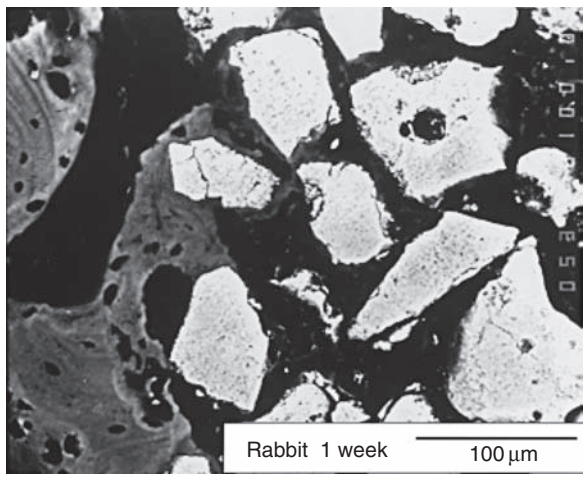

27.46 Backscattered SEM, 1 week after surgery. New bone ingrowth into the spaces of the first layer of HA granules began and the new bone surrounded the HA granules.

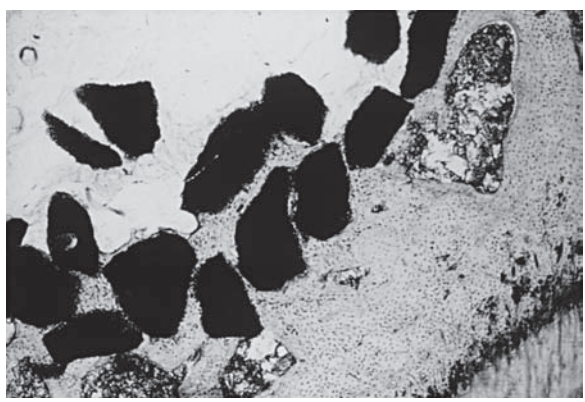

27.47 Stained hard tissue observed by optical microscopy; 2 weeks after surgery.

At 6 weeks, all spaces were filled with new bone, thus forming a unified body. Three years after surgery, bone ingrowth into the spaces of HA granules was the same as that seen at 6 weeks. The HA granules and bone cement bonded mechanically.

Bonding strength of the HA granules layer to bone

IBBC was tested on mature rabbits. Holes with a 6 mm diameter and a depth of 10 mm were made in both femoral condyles. The rabbits were killed in groups of three at 2, 4, 6, 12, and 24 weeks after implantation, and a push-out test was performed. HA coating applied to a smooth titanium surface was used as a control.

A relatively strong initial fixation was obtained immediately after implantation using the IBBC technique. Two weeks after implantation, the bonding strength of IBBC was higher than that of the HA coating, but at 6 weeks after implantation, the bonding strength of IBBC became similar to that of HA coating. The fractures resulting from the push-out test occurred in the HA granules layer from 2 to 6 weeks after implantation, and occurred in both the HA granules layer and the surrounding bone layer after 12 weeks. These results indicated that the strength of the HA granule layer gradually increased after surgery and reached almost the same level as the bone around the HA granule layer after 12 weeks. In these experiments, the bonding strength of bone cement to bone by interposing HA granules was found to be adequate.

In subsequent clinical cases, stress shielding was not found. When cement fixation using PMMA bone cement is performed, excellent initial fixation can be obtained. However, after a period of time, a connective tissue membrane may form between the bone and bone cement, particularly in the acetabulum. This may lead to component loosening.

When cementless fixation with a HA-coated component is performed, micromotion of the component may occur if the initial fixation is insufficient. Therefore, we are confident that IBBC combines the fixation advantages of both conventional PMMA bone cement and HA coating.

27.4.3 Clinical studies

Surgical technique

A cobalt–chromium alloy femoral component (KC, Kyocera Co. Ltd, Kyoto, Japan) with a 28 mm alumina head was used in combination with an all-polyethylene acetabular component. All operations were performed

by the senior author (H.O.) through anterolateral approach in supine position.

HA granules were manufactured by sintering at 1200 °C in Sumitomo-Osaka Cement Co. Ltd, Chiba, Japan. Porous HA granules 300–500 μm in diameter were used. For the acetabular side, several small anchor holes for initial fixation were made and intensive care was taken for sufficient hemostasis by means of hypotensive anesthesia (approximately 90 mmHg), temporal compression at the bleeding points with bone paste obtained by acetabular reaming, and rinsing with hydrogen peroxide followed by compressive gage packing. HA granules (2–3 g) were smeared on the bone surface just before cementing of acetabular component. CMW-I bone cement (C.M.W. Laboratories Ltd, Blackpool, UK) was used in all cases. Porous HA granules could easily adhere on the cancellous bone surface (Fig. 27.48a). For femoral side, hemostasis was achieved in the

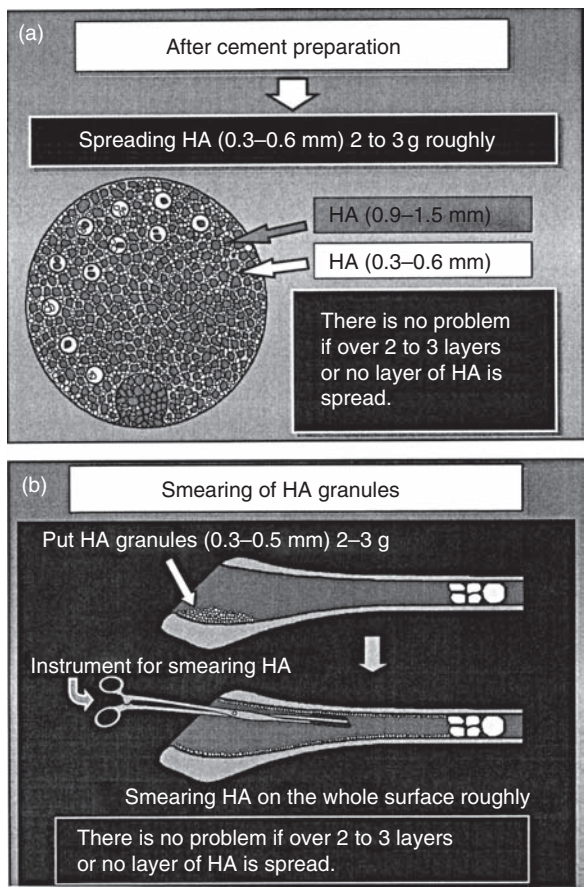

27.48 Surgical technique of IBBC: (a) acetabulum, (b) femur.

same manner and HA granules (2–3 g) were smeared on the inner surface of prepared femoral canal using a half-tube silicon (3–5 cm in length) clamped by a long-straight Kocher's hemostatic clamp (Fig. 27.48b). Femoral component was fixed with second-generation cementing technique using an intramedullary bone plug and cement gun. These procedures resulted in the presence of less than two to three layers of HA granules in most of the bone–bone cement interface, while bone cement directly contacted with bone without interposition in some part. The same cementing technique was applied for the conventional THA except for using HA granules.

We found in a rabbit model that the integrity of the bone–bone cement interface was significantly improved when HA granules were interposed at the interface. Based on the experimental results, this technique was applied in 55 hips from 1984 to 1986. After obtaining excellent radiological results, this technique has been used in all cases of THA and total knee arthroplasty (TKA) since 1986. It has been previously reported that the long-term clinical results in THA were excellent. This technique provides bioactivity on the surface of bone cement for prosthetic fixation.

The key points of surgical procedures were as follows:

- Hemostasis immediately before cementing is very important.
- Several small anchoring holes for initial fixation is necessary.
- HA impregnated by antibiotics as a drug delivery system is very effective for prevention of infection.

Change of IBBC technique

In the first generation, from 1986 to 1988, HA granules size of 0.3–0.5 mm in diameter were used, and several small anchoring holes of 3 mm in diameter were made. In the second generation, from 1989 to 1997, HA granules of 0.1–0.3 mm were used. Because, smaller size of HA adhered more easily. However, as a smaller size of HA was covered easily by blood in the bleeding area, the connection of the bone cement with HA was prevented. As the result, the space and sometimes the separation appeared between bone cement and HA.

Consequently, in the third generation, 1998 to 2001, HA granules of 0.3–0.5 mm were used again and several layer anchoring holes of 6 mm in diameter were made for stronger initial fixation. In the fourth generation, since 2001, HA granules of 0.3–0.5 mm and 1.0–1.5 mm were used and several layer anchoring holes more than 6 mm in diameter were made, to ensure safety even if IBBC was performed in the bleeding area.

Long-term clinical results for 15–20 years

The radiological findings in IBBC were completely different from the conventional cementing and cementless fixation (Figs 27.49 and 27.50). In conventional cementing and cementless fixation, the radiolucent line between bone and implant appeared several years after surgery and progressed, until finally the prosthesis loosened (Figs 27.51 and 27.52).

In IBBC, the space appeared between bone cement and HA several months after surgery, when IBBC was performed in the bleeding area, and the space did not progress. When the space appeared in the large part, sometimes the separation of the component with bone cement occurred from the HA. HA incorporated to the bone.

When wear particles of polyethylene increased, phagocytosis occurred and osteolysis appeared on the radiograph (Fig. 27.51). In follow-up term for 15–20 years, 562 joints were followed. In clinical results, the appearance rate of the radiolucent line, that is the spaces between bone cement and HA, was less than 2% and less than 6% at the restricted areas in both acetabulum and femur in the first and second generations, respectively. In the first generation the bigger size of HA granule was used.

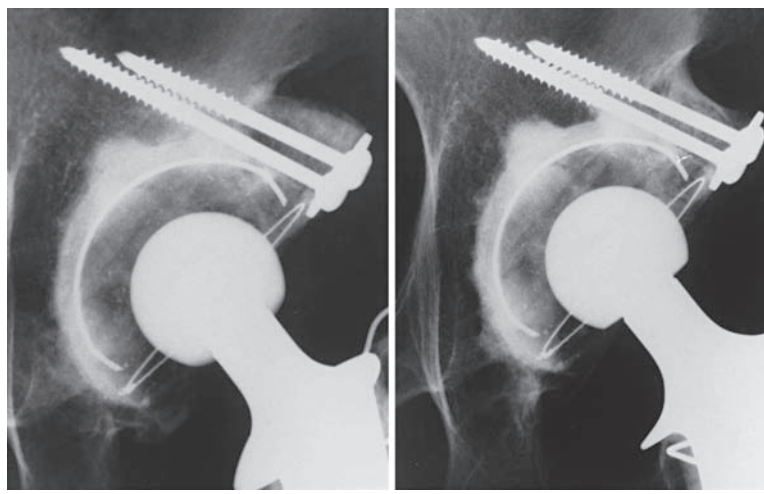

(a) (b)

27.49 IBBC technique was performed on the dysplasic acetabulum: (a) radiograph 3 months after surgery, (b) radiograph 19 years after surgery.

(a) (b)

27.50 IBBC technique was performed on the femur: (a) radiograph 3 months after surgery, (b) radiograph 19 years after surgery.

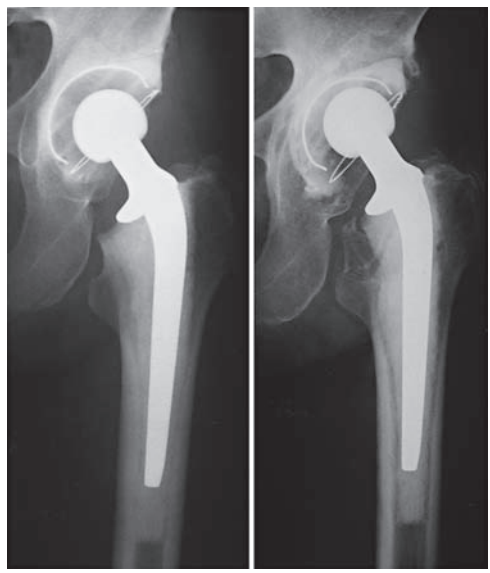

(a) (b)

27.51 Total hip arthroplasty was performed on the osteoarthritis of the hip joint using conventional bone cement technique (non-IBBC): (a) radiograph 3 months after surgery, (b) radiograph 19 years after surgery. Radiolucent line and a great amount of osteolysis were seen on both acetabulum and femur.

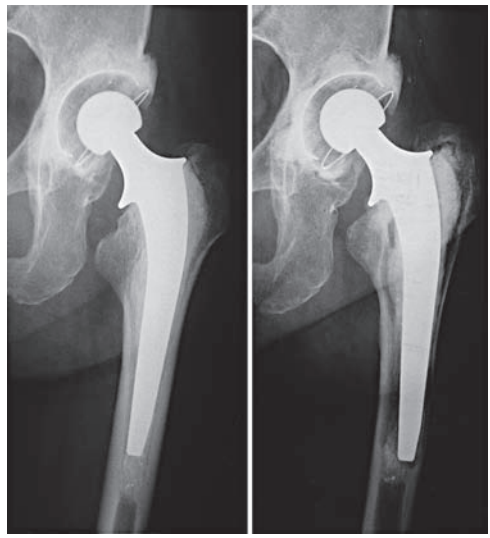

(a) (b)

27.52 Total hip arthroplasty was performed on the osteoarthritis of the hip joint using conventional bone cement technique (non-IBBC): (a) radiograph 3 months after surgery, (b) radiograph 19 years after surgery. Radiolucent line was seen on both acetabulum and femur, and loosening of the stem was seen on the femur.

The appearance rate of osteolysis was extremely low, that is less than 1.5%, at the restricted areas. Loosening, that is separation between bone cement and HA, occurred in the acetabulum in the second generation in two joints, that is 0.8%.

Since 2001, in order to prevent the occurrence of the spaces and the separation between bone cement and HA, several anchoring holes over 6 mm in diameter were made in the acetabulum and HA granules of 0.3–0.6 mm and 1.0–1.5 mm were smeared on the bone surface.

27.4.4 Comparative studies between THA with and without the IBBC technique in the same patients

Twenty-five women with bilateral coxalgia underwent THA with conventional cementing technique in one side between 1985 and 1986 and THA with IBBC technique in the other side in 1986. The interval between two operations ranged from 3 months to 1 year. Conventional THA preceded THA with IBBC technique in all cases.

The follow-up periods were 19.5–20.5 years in conventional THA and 19–19.5 years in THA with IBBC technique.

Revision and loosening

In THA with the IBBC technique, no revision THA and no loosening were experienced in both acetabular and femoral components. In conventional THA, three hips were revised due to loosening of acetabular components (one hip at 14 years post-operatively and two hips at 16 years post-operatively). Two acetabular components and two femoral components were radiologically defined as loose at 18 years post-operatively. The revision rate and the loosening rate in acetabular components were 17.4% and 26.0%, respectively. The loosening rate in femoral components was 8.7%.

Radiolucent lines and osteolysis in the acetabulum

In THA using the IBBC technique, the radiolucent line could be evaluated at the HA layer–bone cement interface or the bone cement–bone interface where HA granules were never interposed. As HA is osteoconductive, HA always bonds to bone except for one case. The radiolucent line at the HA layer–bone cement interface was identified in the acetabulum, although it was non-progressive after 3 months and did not influence the clinical outcome. Thus we focused on the radiolucent line at the bone cement–bone interface. In 16 hips without revision THA, a radiolucent line, less than 1 mm, was observed in one hip at zones 1 and 3 (Figs 27.53 and 27.54).

In conventional THA without revision a radiolucent line, less than 1 mm, was observed in nine hips at zone 1, in five hips at zone 2, and in seven hips at zone 3. A radiolucent line, more than 2 mm, was observed in four hips at zone 1, in two hips at zone 2, and in four hips at zone 3 (Figs 27.53 and 27.54). Osteolysis was observed in eight hips at zone 1, in three hips at zone 2, and in ten hips at zone 3 (Fig. 27.55).

Radiolucent lines and osteolysis in the femur

In THA using the IBBC technique, a radiolucent line, less than 1 mm, was observed in one hip at zones 3 and 7 (Fig. 27.54). Osteolysis was observed in one hip at zone 7 (Fig. 27.55). In conventional THA, the appearance of the radiolucent line is summarized in Fig. 27.54 and the appearance of osteolysis is summarized in Fig. 27.55.

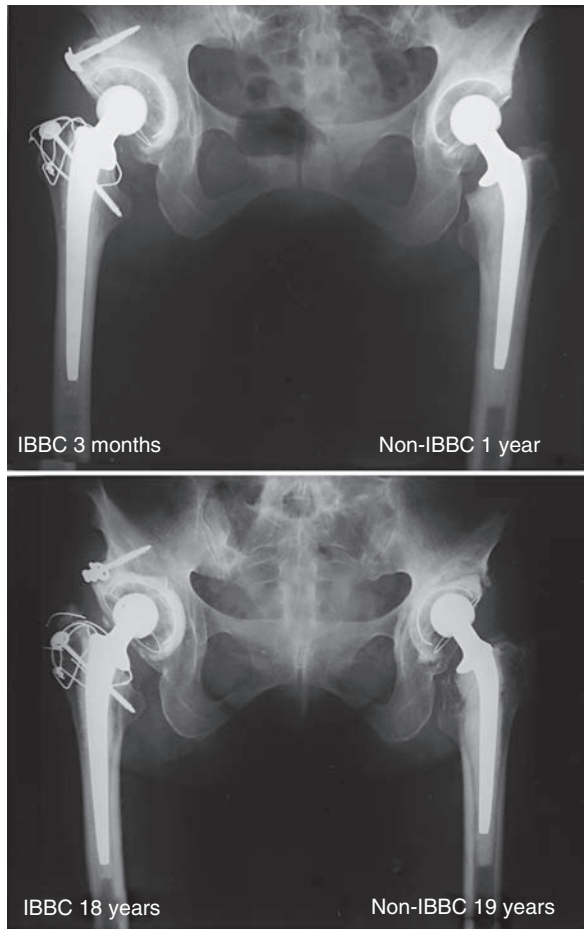

27.53 Comparative radiograph between total hip arthroplasty with IBBC technique and with conventional bone cement technique (non-IBBC) in the same patient. The IBBC technique was performed on the right hip and non-IBBC technique was performed on the left hip. (a) The right hip 3 months after surgery (IBBC) and the left hip 1 year after surgery (non-IBBC). (b) The right hip 18 years after surgery (IBBC). Neither radiolucent line nor osteolysis was seen. The left hip 19 years after surgery (non-IBBC). Radiolucent line and osteolysis were seen on both acetabulum and femur.

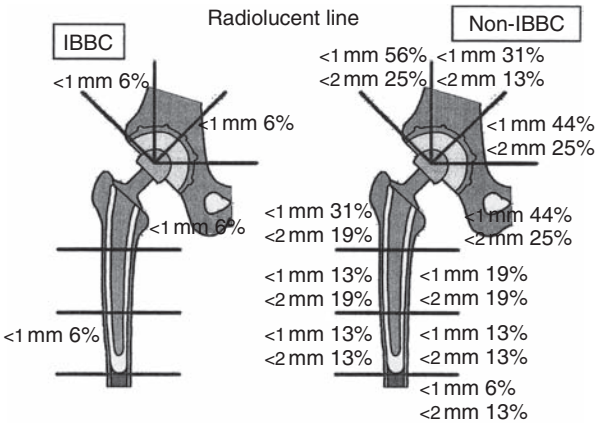

27.54 Comparative appearance rate of radiolucent line between total hip arthroplasty with IBBC and with conventional bone cement technique (non-IBBC) in the same patient.

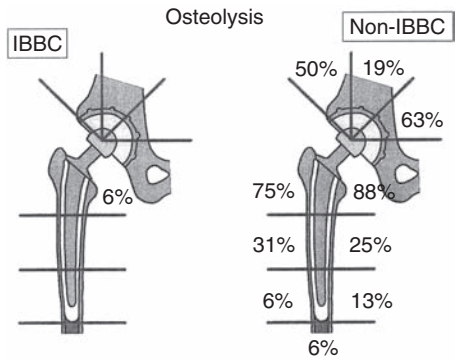

27.55 Comparative appearance rate of osteolysis between total hip arthroplasty with IBBC and non-IBBC in the same patient.

Stress shielding

The appearance of stress shielding was the same in both techniques.

27.4.5 Comparative histological studies on samples with and without HA granules in the same hip in IBBC technique

In early cases, from 1984 to 1988, HA granules were not always totally smeared on the bone surface of acetabulum and femur. These procedures resulted in the presence of less than two to three layers of HA granules in

most of the bone–bone cement interface, while, in some parts, bone cement was in directly contact with bone without the interposition of HA granules. Thus we could obtain specimens with and without HA granule layers from a hip.

Specimens were retrieved from two patients. In Case 1, revision THA was done 18 years after primary THA due to loosening of polyethylene cup from bone cement. The age at revision THA was 61 years. The specimens were taken from the superior-medial part of the acetabulum and from the inferior-medial part of the acetabulum. The former did not contain an HA granule layer and the latter contained an HA granule layer. In Case 2, revision THA was done 14 years after primary THA due to late infection. The age at revision THA was 60 years. The specimens were taken from the medial part of the acetabulum. One contained an HA granule layer and the other did not.

The specimens were obtained *en bloc* to keep the bone cement–HA granules–bone interface intact. They were fixed in 10% formalin. Nondecalcified specimens were cut perpendicular to the interface and were stained by Toluidine blue. They were investigated by an optical microscopy.

In the acetabulum, the amount of trabeculae of cancellous bone is variable from point to point. Generally, the trabeculae of cancellous bone are poor in the inferior-medial part of acetabulum (non-weight-bearing area) and are rich in superior-medial part (weight bearing area). These tendencies were observed in our retrieved specimens.

In Case 1, the specimen from the inferior-medial part contained multiple layers of HA granules (Fig. 27.56a). Bone ingrowth into the spaces of HA granules was obvious and thick bone layer with HA granules was in direct contact with the bone cement. The trabeculae in this part of the acetabulum were poor. In another specimen from the inferior-medial part, several layers of HA granules existed in some areas but HA granules scarcely existed in other areas. A thick and dense bone layer was observed where rich layers of HA granules existed, while bone formation was poor where HA granules were scattered. The specimen from medial-superior part did not contain HA granules (Fig. 27.56b). The trabeculae were rich in this part of the acetabulum, while the structure of trabeculae did not change at the bone–bone cement interface and dense bone layer was not observed.

In Case 2, bone ingrowth into the spaces of HA granules was observed as Case 1 (Fig. 27.57a). On the other hand, the trabeculae of cancellous bone were poor and the bone cement touched the bone in a very limited area in the specimens without HA granules (Fig. 27.57b). In both cases, the edge of HA granules was not smooth and we could not find any changes in shape and size of HA granules implanted in the human body for 14 and 18 years.

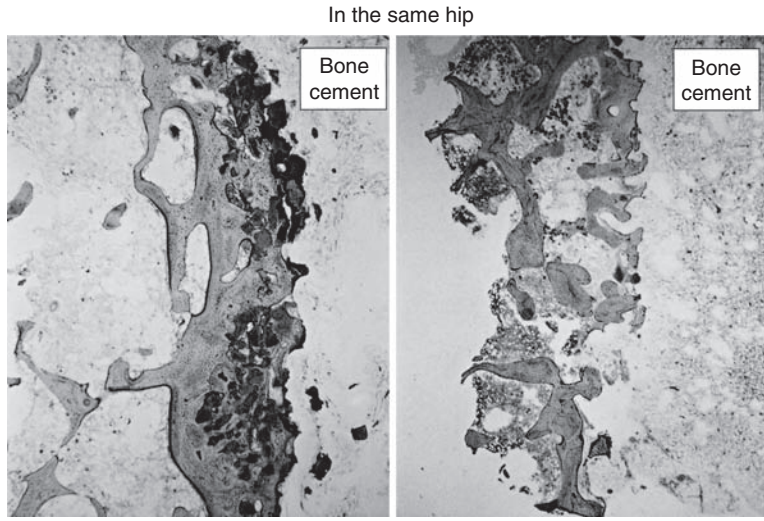

27.56 Comparative histology on samples with and without HA granules in the same hip in IBBC technique, 18 years after surgery: (a) area where HA granules were smeared (IBBC); (b) area where HA granules were not smeared (non-IBBC).

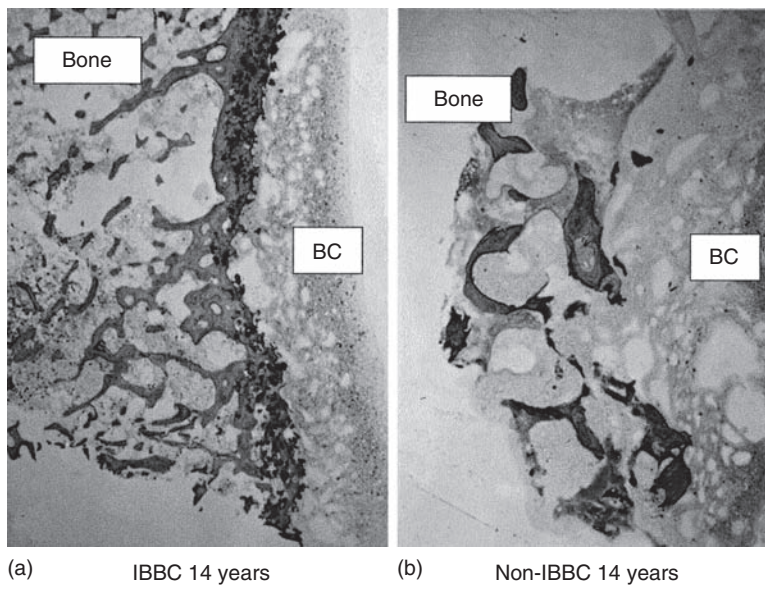

27.57 Comparative histology on samples with and without HA granules in the same hip in IBBC technique, 14 years after surgery: (a) area where HA granules were smeared (IBBC); (b) area where HA granules were not smeared (non-IBBC).

In this study, the differences of bone formation at the bone–bone cement interface with and without HA granules were investigated in the same hip after long-term follow-up. The structure of trabeculae in the acetabulum is variable from point to point; however, the difference between patients is considered much greater because the bony structures are influenced by patient age, gender, degree of osteoporosis, conditions of implants, and so on. Thus even if the retrieved points are different, it is possible to compare the bone reactions among specimens in this study.

27.4.6 Discussion

In the IBBC technique, HA granules exist on the surface of cement mantle. This seems to be an HA-coated prosthesis–bone cement composite. In cementless stems, it is reported that HA coating increased the amount of ingrowth and attachment of bone, achieved better bone fixation and enhanced the stability of the stem. The same effects can be expected for the cemented stem when the bone cement is coated with HA using IBBC technique. The clinical results using the IBBC technique was reported to be excellent. The characteristics of HA coated on a cementless prosthesis and HA granules for IBBC technique are different. As HA coated on a prosthesis contains amorphous HA, HA resorbs with time.

In contrast, HA granules in our technique were pure crystal, thus they were scarcely absorbed. We could not detect any sign of HA resorption in the retrieved specimens. It is expected that osteoconductive activity can continue indefinitely even after the onset of osteoporosis due to aging. Figure 27.58 shows our hypothetic time course of periprosthetic bone conditions; pre-osteoporotic bone smeared by HA granules at immediately after surgery and thick bone layer around HA granules surrounded by osteoporotic bone at 18 years after surgery.

A detailed biomechanical, histologic, and histomorphometric analysis of cemented THA reported that the biologic response to polyethylene wear debris had a more critical effect on destabilization of the cemented socket, while mechanical events tended to predominate the mode of destabilization of cemented femoral components. In IBBC, most HA granules were incorporated into bone, forming an integrated bone–bone cement interface. The reduced incidence of radiolucent lines was attributable to the continued bone formation and remodeling adjacent to the HA granules (Fig. 27.59a). In addition, this well-integrated bone–bone cement interface might prevent the migration of wear particles and subsequent osteolysis could be prevented or repaired by osteoconduction of HA (Fig. 27.59b). Clinical results showed low prevalence of osteolysis.

There were no untoward clinical complications attributable to the use of HA granules for 21 years. It was reported by us that HA granules less than

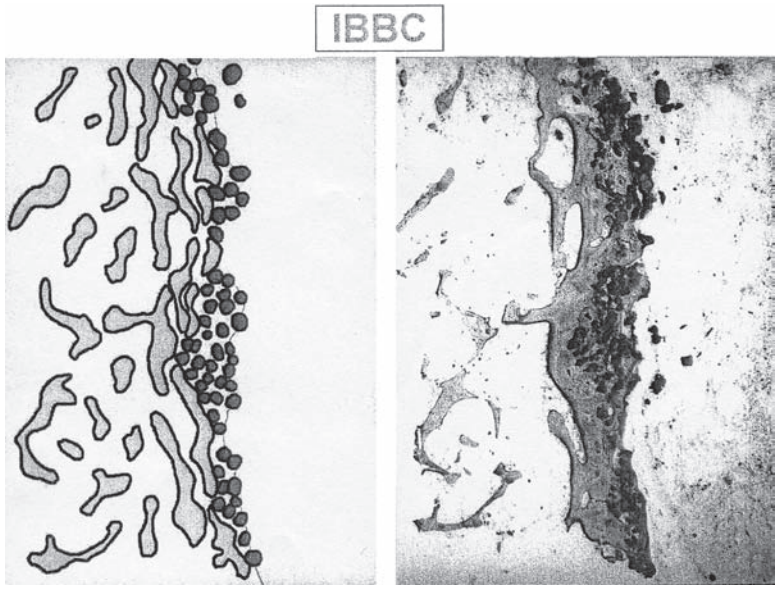

27.58 Hypothetical time course of periprosthetic bone condition: (a) immediately after surgery; (b) 18 years after surgery.

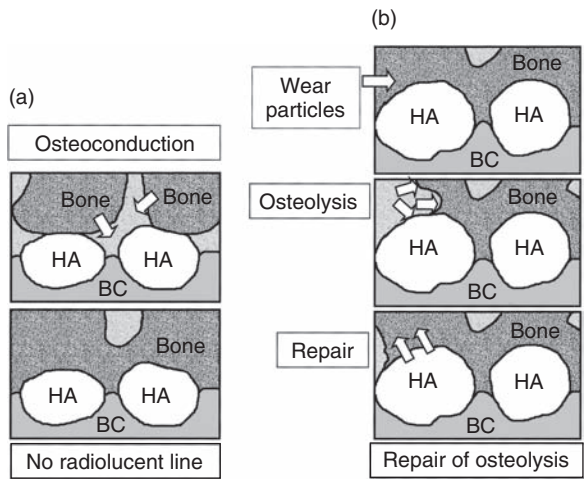

27.59 Scheme of effect of crystalline HA enduring osteoconduction in IBBC. (a) No radiolucent line appeared on radiograph due to the osteoconductive effect of HA. (b) If osteolysis occurred, it was repaired by the osteoconductive effect of HA. BC = bone cement.

10 μm could not be incorporated. From the histological examination, we confirmed negligible foreign body reactions in the retrieved specimens. The reasons were considered that the HA granules were larger than those that led to foreign body reactions, HA granules were scarcely absorbed, most of the HA granules were incorporated and HA granules strongly stuck to the wet tissue even if they were scattered on the soft tissue around the joint. The third-body wear was supposed to be another risk using HA granules. Radiological study reported the wear rate using an alumina head with IBBC technique in 111 hips. The linear wear rate depended on the thickness of polyethylene. The wear rate was reported as 0.14, 0.15, 0.12, 0.06, and 0.08 mm/year with 7, 8, 9, 10, and 11 mm of polyethylene thickness, respectively.

Consequently, the IBBC technique is expected to increase the longevity of THA even after the onset of osteoporosis due to aging and also after the increment of prosthetic wear (Fig. 27.60).

27.5 Reconstruction surgery of the acetabular huge bone deficiency by filling HA granules at revision total arthroplasty

Freeze-preserved, non-pathological allografts have been used in cases of massive bone deficiencies during revision THA for more than 20 years in Europe and in the USA, and excellent results have been reported (Denissen *et al.* 1980; Hoogendoorn *et al.* 1984; Borja and Mmaymneh 1985; Gross *et al.* 1985). Cases using allografts have also been reported in Japan (Itoman and Sunabe 1988), although in Japan materials other than femoral heads, partial femoral condyles, and partial tibial plateaus from patients undergoing arthroplasty are still very difficult to obtain. On the other hand, increasing interest in bioactive ceramics, particularly in HA over the past 20 years, has resulted in a significant increase in its clinical application during this period (McGann 1986; Jarcho *et al.* 1987; Oonishi 1988, 1991b, 1995; Oonishi *et al.* 1989b, 1993b, 1997b, 2002). Under these circumstances, we began to use sintered HA granules clinically. As a material, sintered HA is not resorbable, binds to the bone physicochemically, and is strong enough as a bone defect filler. We obtained good results in three revision cases by placing fine HA granules (300–500 μm) between the bone cement and the bone graft on the deficiencies of the femur in 1984 (Oonishi 1991a). In addition, since 1985 massive bone deficiencies have been filled with HA granules (Oonishi *et al.* 1989b, 1997b, 2002; Oonishi 1991b).

In the first generation (1986–1992), the entire surface of the exposed HA granules at the peripheral deficiencies after filling HA granules in the huge cavitary deficiency was covered with bone cement to reconstruct stabilized

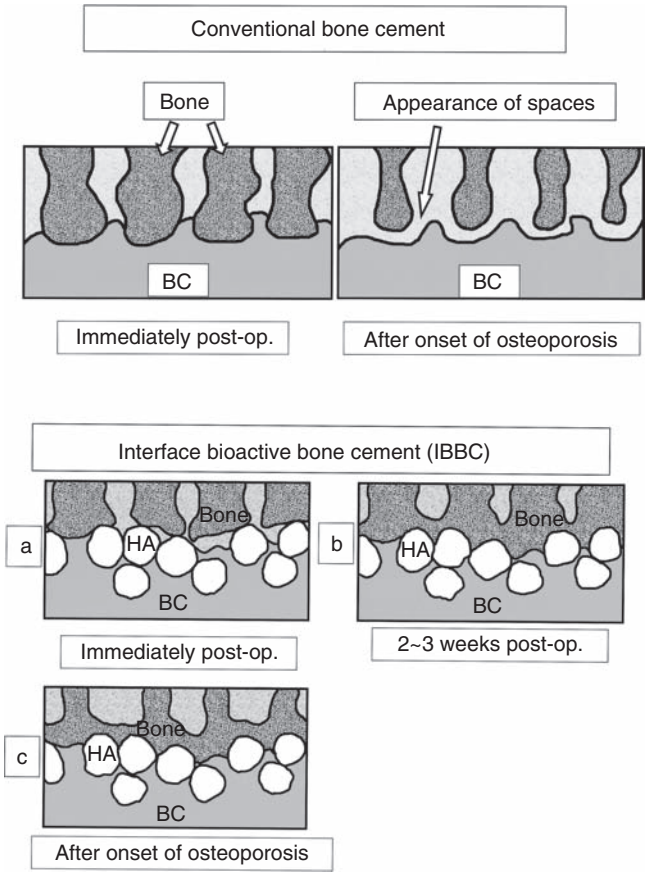

27.60 Comparative scheme immediately after surgery and after onset of osteoporosis due to aging on the conventional bone cement (non-IBBC) and IBBC. After onset of osteoporosis, bony density decreases and the space (radiolucent line) appears between bone and bone cement on the conventional bone cement (non-IBBC). However, on IBBC even if bony density decreases, bone cement binds to the bone by interposing HA granules and the space (radiolucent line) never appears.

complex. However, spaces appeared between HA granules in the nearby bone surface several months after surgery and the prostheses migrated in the case of a wall deficiency too enormous to allow stable filling with only HA granules (Oonishi 1988, 1991b, 1995; Oonishi *et al.* 1989b, 1993b, 1997b,c,d, 2000b,c, 2002). Consequently, in the second generation (since 1993), the peripheral segmental deficiency was covered with bulk allografts to gain stable filling of HA granules (Oonishi 1995, 2000; Oonishi *et al.*

1997c). When HA granule mass fills a huge deficiency, it is unstable and micromovement of HA granules continues; thus bone ingrowth into the spaces of HA granule mass will be disturbed.

27.5.1 The first generation (1986–1992)

Materials and methods: reconstruction procedures using HA for massive bone deficiencies in the acetabulum

HA granules were manufactured by sintering at 1200 °C with a porosity of 35–48% (average 42%), then sieved to obtain granules of several sizes (Bioceram P®. Sumitomo-Osaka Cement Co. Ltd, Tokyo, Japan). Granules of 0.3–0.6 mm (G-2), 0.9–1.2 mm (G-4), and 3.0–5.0 mm (G-6) are mixed at a ratio of 10 : 45 : 45. Physiological saline is added to the mixture to increase the mixing density and to facilitate the adhesion of granules with each other due to the porous characteristic of the powder. This results in firmer adhesion and more stable shape formation. The acetabulum is filled with the mixture. If the same size of HA granules are used, the mixing density decreases, a firmer and more stable filling cannot be obtained, and the shape easily breaks.

A hemispherical compresser 2 mm larger than the outer diameter of the socket is then inserted successively into the previously determined space for the socket installation and firmly struck into the acetabulum using a plastic hammer while continuously making adjustments to determine the best socket location (Fig. 27.61). In cases of small and moderate medial wall deficiencies, HA granules were sufficient for the filling.

When cementing the socket, a 2–3 mm thickness of cement of paste-like condition is placed on the entire surface of the acetabulum and compressed with a compressor 2 mm larger than the outer socket diameter until the cement hardened. When a bone defect extended over a large area on the superior periphery of the acetabulum and it was not possible to fill the defect sufficiently with HA granules, additional HA granules were placed in this region and fixed using a 1–2 mm thickness of cement.

Before the socket was cemented, the hardened cement surface was dried, and the socket fixed with cement in a sticky condition on the hardened cement. This procedure facilitates binding the cements together.

Clinical cases

Between 1986 and 1992, we carried out this procedure on 40 hips. The bone loss was assessed according to the AAOS classification of acetabular deficiencies (Kerboull 1985; D'Antonio *et al.* 1989). Whole peripheral segmental

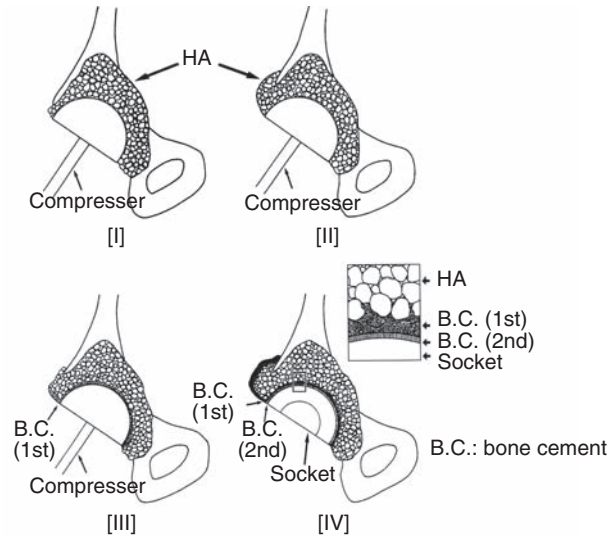

27.61 The first generation: reconstruction procedures using HA granules for massive bone deficiency in the acetabulum in the first generation.

and cavitary deficiencies with medial walls intact were found in 13 joints (33%), and peripheral cavitary deficiencies over the whole area with the medial wall absent were found in 18 joints (45%). They were very unstable cases after revision surgery. There were 2 men and 38 women, and their ages at operation ranged from 35 to 81 years. The follow-up period was from 15 to 21 years. Our original revision THR was performed because of osteoarthritis in 33 patients, rheumatoid arthritis in 5, avascular necrosis of the head of the femur in 1, and systemic lupus erythematosus in 1. In 36 joints, this was the first revision, in 3 it was the second, and in 1 it was the third.

Results: X-ray evaluation

When HA granules are firmly packed, a stable filling is attained, similar to a stone wall. Although narrow spaces were observed in areas at the interface between HA granules and bone immediately after surgery, these spaces gradually disappeared within 3 months following surgery. This was probably due to new bone formation into the space between the HA granules, and the subsequent binding with HA granules. Sclerotic bone surrounding loose components changed to cancellous bone over a period of 1–3 years following revision surgery.

Our radiographic evaluation showed neither morphological changes nor decreases in volume (Figs 27.62 and 27.63) except for some cases with very

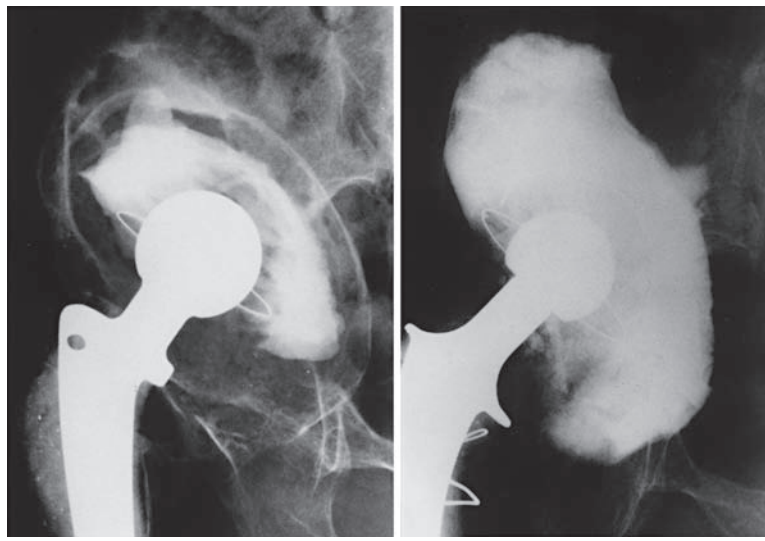

(a) (b)

27.62 The first case in which HA granules were filled in the acetabular massive bone defect at the revision total hip arthroplasty: (a) before revision total hip arthroplasty (65-year-old female); (b) 21 years after revision surgery (at age 86).

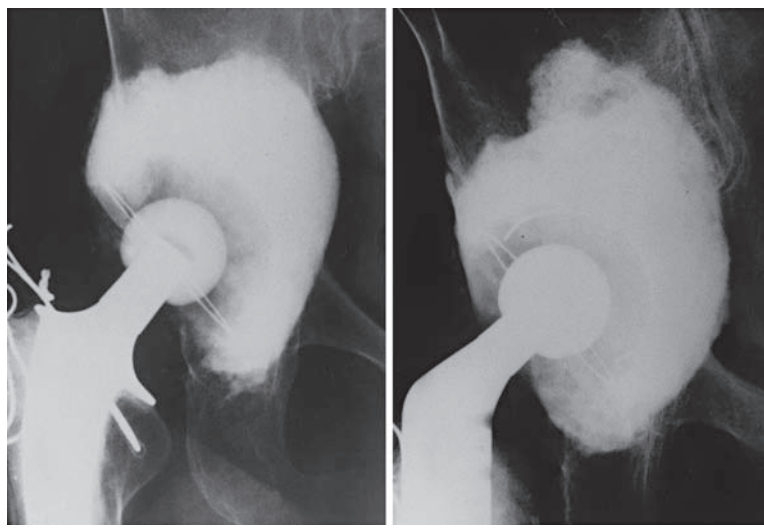

(a) (b)

27.63 (a) one month after revision total hip arthroplasty; (b) 21 years after revision total hip arthroplasty.

specific complications. In a case with a considerable cavitary and peripheral deficiency and a medial wall defect, HA granules were over-filled in the medial area of the acetabulum, and the socket settled laterally. Not only were there no detrimental effects radiographically or clinically, but the filled HA granules were also very stable following surgery.

In two cases, spaces were observed between HA granules near the bone at the latero-superior lesion. The width of the space increased very slowly, but stopped after 5–6 years; clinically, there were no problems. We theorized that rather wide spaces were left between the bony base and packed HA granules at surgery, and in the vicinity of the gaps, the bond between bone and HA granules was unstable after surgery. In addition, continuous micromotion most likely occurred right under the bone at these gaps before sufficient bone ingrowth into the spaces was obtained between HA granules, or sufficient bonding was obtained between bone and HA. In these cases, if the superior peripheral deficiencies had been covered with an allograft plate, such as a tibial plateau, HA granules could have been filled sufficiently in the superior peripheral region and, as a result, the appearance of the spaces could be avoided.

In two patients after the second revision and in one patient after the third revision, the large part of the medial wall was absent and the overall deficiency was too great to allow stable filling of the granules. The packed HA granules broke and the prostheses migrated. In the third revision case, bone formation was very poor because the patient's bony quality was very poor.

In three cases, peripheral bony wall deficiency should be covered by allograft bone to obtain stable HA granule filling (Oonishi and Fujita 2004).

27.5.2 The second generation (since 1992)

Materials and methods

In the second generation, since 1992, peripheral segmental deficiencies were covered with allograft bone from the femoral heads of patients undergoing arthroplasty to allow stable filling of HA granules. In some cases with a large cavitary deficiency combined with a large peripheral segmental deficiency, a large block of the femoral head was used. Since 1995, latero-superior large peripheral deficiencies were covered with an allograft plate from the tibial plateau (Fig. 27.64).

As a filler in the cavitary deficiency, mixtures of G-4 (0.9–1.2 mm) and G-6 (3.0–5.0 mm) HA granules were filled as in the first generation, and in some cases mixtures of HA granules of 0.9–1.2 mm (G-4) and small bone chips at a ratio of 30:70 or 50:50 were filled. From 1995 to 1997, the Kerboull metallic cross-plate was used. However, after the Kerboull cross-plate had broken at the hook in 30% of cases, it was discontinued.

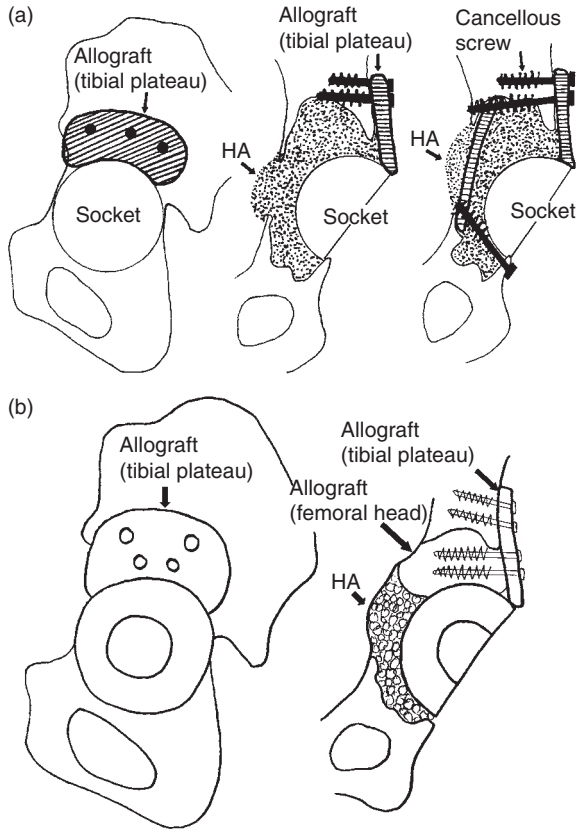

27.64 The second generation: latero-superior large peripheral deficiency was covered with an allograft of tibial plateau: (a) the whole cavital deficiency was filled with HA granules; (b) superior deficiency on the weight-bearing area was filled by bone block and other cavity was filled with HA granules.

Clinical cases

Between 1992 and 1997, 48 hips have been operated on using the procedure. The follow-up period was 10–15 years. Of the 48 hips, it was the first revision for 43, in 4 hips it was the second revision, and in 1 hip it was the third revision. They were very unstable cases, with great peripheral segmental and cavitary deficiencies, as in the first generation.

Results and complications

In general, when the whole peripheral segmental deficiency was covered with allografts, filled HA granules were very stable. In one case filled with mixture of HA granules and bone chips, a slight volume change was observed. However, there were no clinical symptoms, and the change did

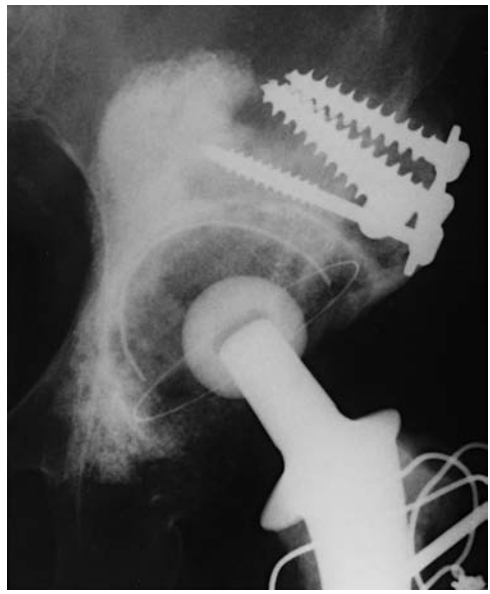

27.65 The whole peripheral segmental deficiency was covered with allograft and the cavitary deficiency was filled with HA granules, 13 years after revision total hip arthroplasty (Oonishi *et al.* 2004).

not increase. There was no difference radiographically between HA alone and a mixture of HA and bone chips as fillers when the peripheral segmental deficiency was covered with allografts (Fig. 27.65).

27.5.3 Comparative histological studies of retrieved specimens under a loaded condition and the specimens from animal experiment under an unloaded condition

Retrieved specimens under loaded condition

As Kerboull cross-plates as cup supporters broke in many cases, in two cases HA granule masses of approximately 2.0 and 2.5 cm in thickness were retrieved at 2 and 2.5 years after revision THA, respectively. They contained whole thickness of HA granules. Non-decalcified ground thin specimens stained by Toluidine blue were observed by optical microscopy and non-decalcified ground blocks were observed by backscattered electron image.

In clinical cases, in the weight-bearing condition, at the second revision THA, it was very difficult to drill into the HA granule mass and to cut the mass with a chisel. In histological studies, a large amount of dense bone ingrowth from the base of dense bone (Fig. 27.66) and a large amount of cancellous bone ingrowth from the base of cancellous bone (Fig. 27.67)

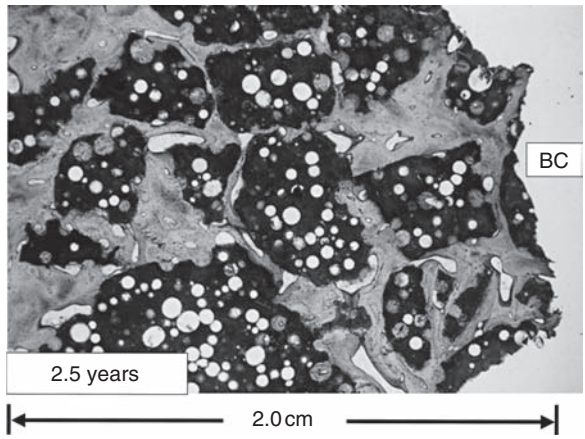

27.66 Non-decalcified hard tissue specimen stained by Methylene blue was observed by optical microscopy. In a retrieved case (2 years after surgery), from dense bone base, dense bone ingrowth was obtained in the spaces between HA granules to the entire depth of 2 cm. Left area in contact with acetabular bone base, and right area in contact with bone cement (BC).

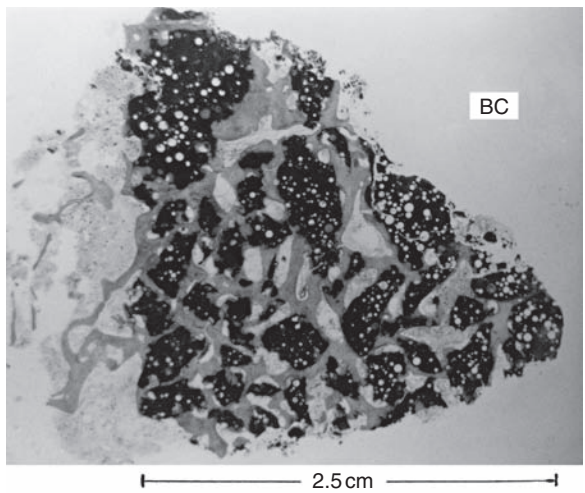

27.67 In a retrieved case (2 years and 6 months after surgery), from cancellous bone base, cancellous bone ingrowth was obtained in the spaces between HA granules to the entire depth of 2.5 cm. The left area contacted acetabular base, and the right area contacted bone cement (BC).

were found in the whole spaces between HA granules into the whole depth, respectively. New bone adhered to HA directly.

Specimens from animal experiment under unloaded condition

As a control in an animal experiment, mixtures of G-4 (0.9–1.2 mm) and G-6 (3.0–5.0 mm) HA granules as in clinical cases were filled into the cavity of 2 cm in diameter and 10 cm in length made at the proximal end of the tibia of a goat (Fig. 27.68). The proximal part of the tibia was cancellous bone and the distal part was cortical bone. Eighteen months after implantation, the animal was killed, and radiographs by X-ray of A-P view and lateral view (Fig. 27.69) and the section of several levels (Fig. 27.70) were taken. From these specimens non-decalcified hard sections were made. A small amount of the new bone had entered from the periphery and moved to the center. Where the surrounding bone was cortical bone, cortical bone entered (Fig. 27.71). When the surrounding bone was cancellous bone, cancellous bone entered (Fig. 27.72). As the quantity of bone ingrowth was small, some HA granules that filled the cavity dropped out while making non-decalcified hard tissue specimens, and some HA granules dislodged from the specimens.

In a clinical case, HA granules were filled in the weight-bearing area. However, in experimental studies HA granules were filled in the non-weight-bearing area. From these results, it can be assumed that, in the weight-bearing area, a great amount of new bone entered into the spaces of the HA granules and moved to the deep area. However, in the non-weight-bearing area, a large amount of bone ingrowth could be

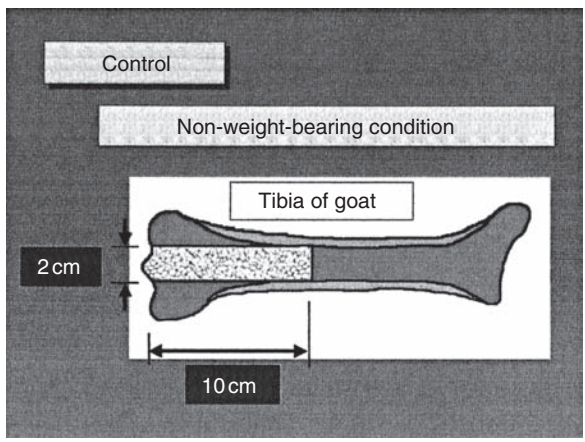

27.68 Scheme of animal experiment as a control under unloaded conditions.

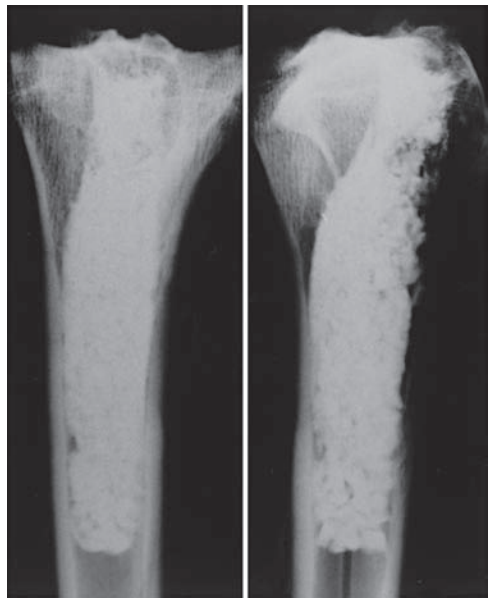

(a) (b)

27.69 Radiographs by X-ray 18 months after surgery: (a) A-P view; (b) lateral view.

expected only at the peripheral area of the cavity to approximately 5 mm in depth.

Discussion

The advantages of HA are follows: (1) HA is osteoconductive and is bound to bone physicochemically, (2) immunoreactions can be completely ignored, (3) post-operative morphological changes and volume decreases do not occur if a mixture of adequate granule sizes are packed densely and firmly during surgery, (4) post-operative HA absorption, if any, is small in amount and extremely slow, consequently, osteoconductivity can be continued, and (5) the occurrence of osteolysis by polyethylene wear particles at the interface of the bone is very small, because osteolysis can be recovered by osteoconduction of HA. We suggest that the reasons for the marked pain-relieving effect is that there were neither changes in the shape of packed HA granules, nor movement of the component, as HA granules were packed firmly and stably, bound to the bone physicochemically, and fixed with bone cement mechanically.

The spaces in part of the interface between HA granules and bone immediately after surgery gradually disappeared within 3 months because new

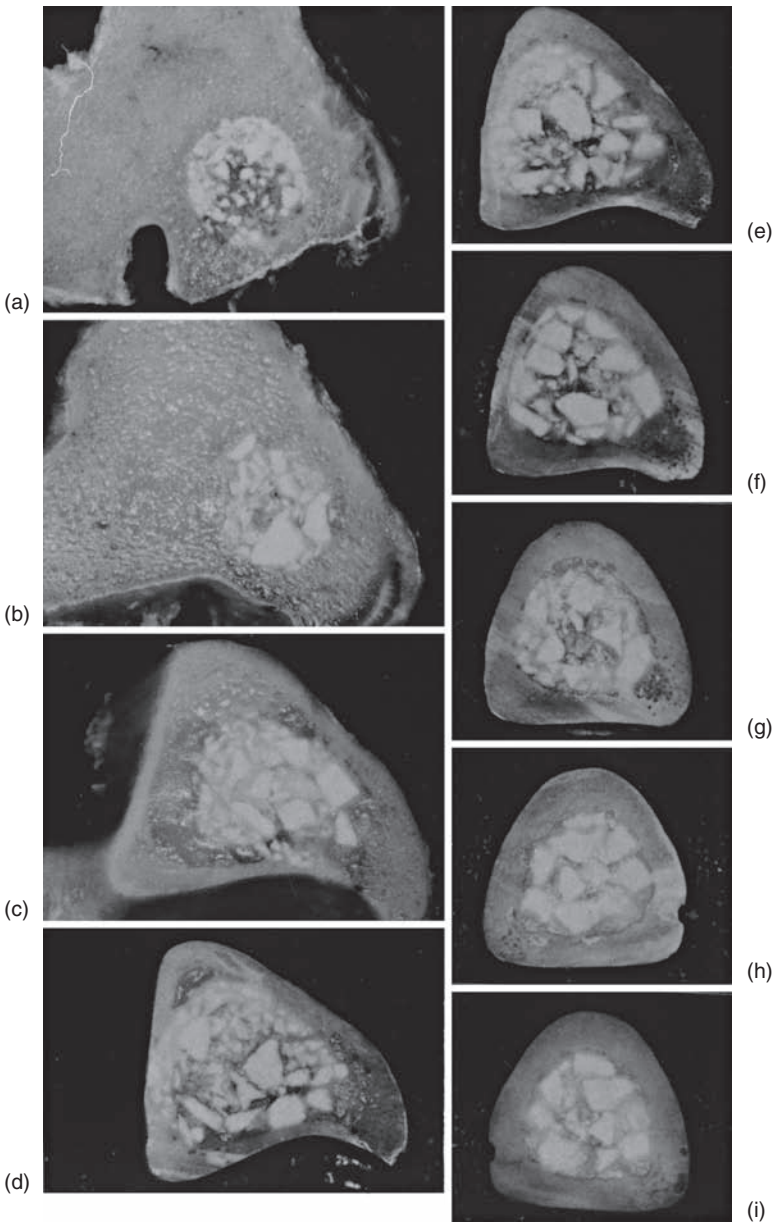

27.70 Sections were made from proximal part (a) to distal part (i). Radiographs by X-ray at the several levels were taken after section. Proximal parts were surrounded by cancellous bone and distal parts were surrounded by cortical bone.

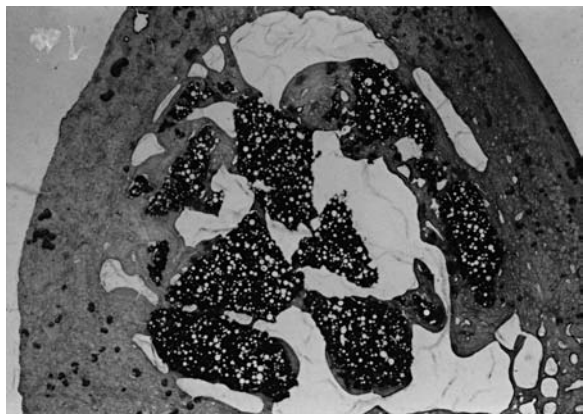

27.71 HA granules were impacted into cortical bone area.

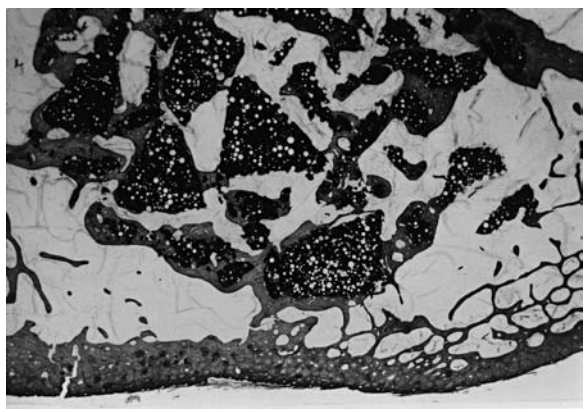

27.72 HA granules were impacted into cancellous bone area.

bone tissues entered into the space between the HA granules from the surface of the bony cavity. After filling HA granules into the cavitary deficiency, the sclerotic bone around the loosened socket changed to cancellous bone over a period of 1–3 years following revision surgery. This could be because the bone ingrowth into the spaces of HA granules from the surrounding sclerotic bone was obtained, and the HA granules may have physicochemically bound to the entire surface of the sclerotic bone wall. This phenomenon was very similar to bone union after non-union of fracture.

On the retrieved studies, HA granules had formed a homogeneous mass, which was difficult to make a drill hole in or to cut with a chisel, and it adhered to the bone very firmly. Histologically, bone ingrowth was obtained

2 years and 2.5 years after surgery in the majority of the spaces between HA granules to the entire depth of about 2 cm and 2.5 cm, respectively. Consequently, if HA granules were filled very firmly and stably, a very strong new acetabulum could be reconstructed.

In the retrieved case, HA granules were filled in the weight-bearing area. However, in an animal experiment using a tibia of a goat, HA granules were filled in the non-weight-bearing area, and much less bone ingrowth into the spaces of HA granules was obtained. Consequently, excellent results can be expected when a mixture of several grain sizes of HA are packed densely and firmly during surgery into the massive defect of the bone in the weight-bearing area (Oonishi *et al.* 1989b).

One of the complications we had was the appearance of spaces between HA granules at nearby bone at the latero-superior lesion (Zone I). In this case the filling of HA granules may not have been dense near the bone base at the latero-superior lesion (Zone I), because the superior peripheral deficiency was covered with bone cement after filling with HA granules. As a result, continuous micromotion probably caused occurrences of the gaps before sufficient bone growth could provide bonding. If the superior peripheral deficiency had been covered by an allograft plate, such as tibial plateau, or allograft block, such as femoral head, the HA granules would probably have filled the spaces more satisfactorily.

In the second generation, complications due to spaces between granules and the neighboring bony base at the latero-superior lesion of the acetabulum has not been observed, nor has socket migration, although breakage of the hook of Kerboull cross-plate was observed.

27.6 References

Borja FJ and Mmaymneh W (1985), 'Bone allografts in salvage of difficult hip arthroplasties', *Clin Orthop Rel Res*, **197**, 123–30.

de Bruijn JD, Bovell YP, Davies JE and van Blitterswijk CA (1994a), 'Osteoclastic resorption of calcium phosphates is potentiated in post osteogenic culture conditions', *J Biomed Mater Res*, **28**, 105–12.

de Bruijn JD, Bovell YP and van Blitterswijk CA (1994b), 'Osteoblast and osteoclast responses to calcium phosphates', in Andersson O, Happonen R-P and Yli-Urpo A, *Bioceramics Vol. 7*, Oxford, Butterworth-Heinemann, 293–8.

Callaghan JJ, Forest EE, Olejniczak JP *et al.* (1998), 'Charnley total hip arthroplasty in patients less than fifty years old. A twenty to twenty-five-year follow-up note', *J Bone Joint Surg [Am]*, **80**, 704–14.

D'Antonio JA, Capello WN and Borden LS (1989), 'Classification and management of acetabular abnormalities in total hip arthroplasty', *Clin Orthop*, **243**, 126–37.

Denissen HW, de Groot K, Makkes P.Ch, Van den Hooff A and Klopper PJ (1980), 'Tissue response to dense apatite implants in rats', *J Biomed Mater Res*, **14**, 713–21.

Ducheyne P, Radin S and King L (1993), 'The effect of calcium phosphate ceramic composition and structure on *in vivo* behavior. I Dissolution', *J Biomed Mater Res*, **27**, 25–34.

Gross AE, Lavoie MV, McDermott P and Marks P (1985), 'The use of allograft bone in revision of total hip arthroplasty', *Clin Orthop*, **197**, 115–22.

Hench LL (1991), 'Surface reaction kinetics and adsorption of biological moieties', in Davies JE, *The Bone–Biomaterial Interface*, Toronto, University of Toronto Press, 33–48.

Hench LL (1994), 'Bioactive ceramics: Theory and clinical applications', in Andersson O, Yli-Urpo A and Happonen R-P, *Bioceramics Vol. 7*, Oxford, Butterworth-Heinemann, 3–14.

Hench LL (1998), 'Bioactive glass: Present and future', in LeGeros RZ and LeGeros J, *Bioceramics Vol. 11*, Singapore, World Scientific Publishing, 31–6.

Hoogendoorn HA, Renooij W, Akkermans LMA, Visser W and Wittebol P (1984), 'Long-term study of large ceramic implants (porous hydroxyapatite) in dog femora', *Clin Orthop Rel Res*, **187**, 281–8.

Itoman M and Sunabe S (1988), 'Revision total hip replacement supplemented with allogenic bone grafting', *J Joint Surgery (Japan)*, **7**(3), 83–93.

Jarcho M, Kay JR, Gumaer KI, Doremus RH and Drobeck HP (1987), 'Tissue, cellular and subcellular events at a bone–ceramic hydroxyapatite interface', *J Bioengineering*, **1**, 79–92.

Kerboull M (1985), 'La reconstruction du cotyle', in Postel M *et al.*, *Arthroplastie total de hanche*, Heidelberg, Berlin, Springer-Verlag, 89–96.

Kitsugi T, Nakamura T, Yamamuro T, Kokubo T, Shibuya T and Takagi M (1987), 'SEM-EPMA observation of three types of apatite-containing glass ceramics implanted in bone: the variance of Ca-P rich layer', *J Biomed Mater Res*, **21**, 1255–71.

LeGeros RZ and LeGeros JP (1996), 'Calcium phosphate biomaterials in medical applications', in Kokubo T, Nakamura T and Miyaji F, *Bioceramics Vol. 9*, Pergamon Press, 7–10.

LeGeros RZ, Orly I, Gregoire M and Daculsi G (1991), 'Substrate surface dissolution and interfacial biological mineralization', in Davies JE, *The Bone–Biomaterial Interface*, Toronto, University of Toronto Press, 76–88.

McGann W (1986), 'Massive allografting for sever failed total hip replacement', *J Bone Joint Surg*, **68A**, 4–12.

Mulroy RD Jr and Harris WH (1990), 'The effect of improved cementing techniques on component loosening in total hip replacement. An 11-year radiographic review', *J Bone Joint Surg [Br]*, **72**, 757–60.

Neo M, Herbst H, Voigt CF and Gross UM (1996a), 'Osteoblast activation patterns after implantation of β-TCP particles into bone. *In situ* hybridization', in Kokubo T, Nakamura T and Miyaji F, *Bioceramics Vol. 9*, Pergamon Press, 57–60.

Neo M, Voigt CF, Herbst H and Gross UM (1996b), 'Analysis of osteoblast activity at biomaterial–bone interfaces by *in situ* hybridization', *J Biomed Mater Res*, **30**, 485–92.

Oh I, Carlson CE, Tomford WW and Harris WH (1978), 'Impproved fixation of the femoral component after total hip replacement using a methacrylate intramedullary plug', *J Bone Joint Surg [Am]*, **60**, 608–13.

Oonishi H (1988), 'Revision of THR for massive bone defects', *J Joint Surg (Japan)*, **7**(3), 49–60.

Oonishi H (1991a), 'Interfacial reactions to bioactive and non-bioactive bone cements', in Davies JE, *The Bone–Biomaterial Interface*, Toronto, University of Toronto Press, 321–33.

Oonishi H (1991b), 'Orthopaedic applications of hydroxyapatite', in Barbucci R, Oxford, *Biomaterials Vol. 12*, Butterworth-Heinemann Ltd, 171–8.

Oonishi H (1992), 'Interfacial reactions to bioactive and non-bioactive biomaterials', in Ducheyen P, New York, *Biomechanics in Orthopaedics*, Springer-Verlag, 307–21.

Oonishi H (1995), 'Long term clinical results after revision total hip arthroplasty by using HA', *J Joint Surgery (Japan)*, **14**(II), 51–64.

Oonishi H (2000), 'Reconstruction of the hip-revision surgery of acetabulum with massive bone defects; material', *OS Now Orthopaedic Surgery (Japan)*, **5**, 144–52.

Oonishi H and Fujita H (2004), 'Hydroxyapatite granules in acetabular reconstruction', in Epinette JA and Manley MT, *Fifteen Years of Clinical Experience with Hydroxyapatite Coating in Joint Arthroplastsy*, Paris and New York, Springer, 339–43.

Oonishi H, Kushitani S, Aono M, Madea E, Tsuji E and Ishimaru H (1989a), 'Interface bioactive bone cement by using PMMA and hydroxyapatite granules', in Oonishi H and Aoki H, *Bioceramics Vol. 1*, Tokyo, Ishiyaku-Euro America, 102–7.

Oonishi H, Kushitani S, Aono M, Ukon Y, Yamamoto M, Isimaru H and Tsuji E (1989b), 'The effect of HA coating on bone growth into porous titanium alloy implants', *J Bone Joint Surg*, **71-B**(2), 213–16.

Oonishi H, Tsuji E, Mizukoshi T, Kushitani S, Aono M, Minami K, Watanabe A, Ogino A and Fujisawa N (1991), 'The replacing behavior of tetra-calcium phosphate. Alteration to bone tissue *in-vivo*', in Bonfield W, Hastings G and Tanner S, *Bioceramics Vol. 4*, Oxford, Butterworth-Heinemann, 191–7.

Oonishi H, Tsuji E, Kushitani S, Aono M, Minami K and Hidaka T (1992), 'Bone ingrowth behavior differences into spaces between fine HAP and alumina granules', in Yamamuro T, Kokubo T and Nakamura T, *Bioceramics Vol. 5*, Japan, Kobunshi Kankokai, 149–53.

Oonishi H, Yamamoto M, Ishimaru H, Tsujie, Aono M and Ukon Y (1993a), 'The effect of hydroxyapatite coating on bone growth into porous titanium alloy implants', *J Bone Joint Surg*, **71B**, 213–16.

Oonishi H, Kushitani S, Murata N, Saito M, Maruoka A, Ysukawa E, Tsuji and Sugihara F (1993b), 'Long term bone growth behavior into the spaces of HAP granules packed into massive bone defect cavity', in Ducheyen P and Christiansen D, Oxford, *Bioceramics Vol. 6*, Butterworth-Heinemann, 157–61.

Oonishi H, Kushitani S, Yasukawa E, Iwaki H, Hench LL, Wilson J, Tsuji E and Sugihara T (1997a), 'Particulate Bioglass™ compared with hydroxyapatite as a bone graft substitute', *Clin Orthopaed Rel Res*, **334**, 316–25.

Oonishi H, Iwaki Y and Kin Y (1997b), 'Hydroxyapatite in revision of total hip replacements with massive acetabular defects', *J Bone Joint Surg Br*, **79**, 87–92.

Oonishi H, Iwaki Y and Kin N (1997c), 'Hydroxyapatite in revision of total hip replacements with massive acetabular defects', *J Bone Joint Surg [Br]*, **79-B**, 87–92.

Oonishi H, Kushitani S, Yasukawa E, Iwaki H, Hench LL, Wilson J, Tsuji E and Sugihara F (1997d), 'Particulate Bioglass® compared with hydroxyapatite as a bone graft substitute', *Clin Orthop Rel Res*, **334**, 316–25.

Oonishi H, Murata N, Saito M, Wakitani S, Imoto K, Kim N and Matsuura M (1998a), 'Comparison of bone growth behaviour into spaces of hydroxyapatite and AW glass ceramic particles', in LeGeros RZ and LeGeros J, *Bioceramics Vol. 11*, Singapore, World Scientific Publishing, 411–14.

Oonishi H, Kushitani S and Yasukawa E (1998b), 'Clinical results with interface bioactive bone cement. Hip surgery', in Sedel L and Cabannela M, London, *Material and Developments*, UK, Martin Dunitz, 65–74.

Oonishi H, Hench LL, Wilson J, Sugihara F, Tsuji E, Kushitani S and Iwaki H (1999), 'Comparative bone growth behavior in granules of bioceramic materials of various sizes', *J Biomed Mater Res*, **44**, 31–43.

Oonishi H, Kadoya Y, Iwaki H and Kim N (2000a), 'Hydroxyapatite granules interposed at bone-cement interface in total hip replacement. Histological study on retrieved specimens', *J Appli Biomat*, **53**, 174–80.

Oonishi H, Hench LL, Wilson J, Sugihara F, Tsuji E, Matsuoka M, Kin S, Yamamoto T and Mizokawa S (2000b), 'Quantitative comparison of bone growth behaviour in granules of Bioglass®, A-W glass-ceramics, and hydroxyapatite', *J Biomed Mater Res*, **51**, 37–46.

Oonishi H, Fujita H, Itoh S, Kin T and Oomamiuda K (2002), 'Histological studies on retrieved HA granules filled in acetabular massive bone defect in revision total hip arthroplasty', *Bioceramics* **14**, 423–6.

Oonishi H, Kim SC, Dohkawa H, Doiguchi Y, Takao Y and Oomamiuda K (2004), 'Excellent bone ingrowth into HA granules filled in acetabular massive bone defect under weight bearing condition', *Key Eng Mater*, **254**–**256**, 643–6.

Radin S and Ducheyne P (1993), 'The effect of calcium phosphate ceramic composition and structure on *in vivo* behavior. II Precipitation', *J Biomed Mater Res*, **27**, 35–45.

Sugihara F, Oonishi H, Kushitani S, Iwaki N, Mandai K, Minamigawa K, Tsuji E, Yoshikawa M and Toda T (1995), 'Bone tissue reaction of octacalcium phosphate', in Wilson J, Hench LL and Greenspan M, New York, *Bioceramics Vol. 8*, Pergamon Press, 89–91.

Sochart DH and Porter ML (1997), 'The long-term results of Charnley low-friction arthroplasty in young patients who have congenital dislocation, degenerative osteoarthrosis, or rheumatoid arthritis', *J Bone Joint Surg [Am]*, **79**, 1599–617.

Wroblewski BM (1986), 'Charnley low-friction arthroplasty: review of the past, present status, and prospects for the future', *Clin Orthop*, **210**, 37–42.

28

Clinical applications of ceramic-ceramic combinations in joint replacement

L SEDEL, University of Paris 7 and Hôpital Lariboisière (APHP), France

28.1 Introduction

The natural hip is a complex articulation joining the trunk to the lower limbs. It provides mobility and facilitates walking in a regular manner. When diseases of various origins, e.g. traumatic, avascular necrosis, osteoarthritis or others, destroy the hip's mechanism, the resulting disability is extreme. The patient experiences pain, stiffness, limping and inequality of leg length, and this disability is responsible for a marked limitation of daily activities. The natural hip is composed of different structures that enable it to function. In order to understand the function that artificial implants aim to reproduce, it is essential to understand how the natural joint operates. The supporting bone is a strong, elastic material, which, moreover, is adaptable because it is living material. Its structure and resistance are related to supporting stresses. Normal cortical bone adapts to the implantation of a wide range of biomaterials. This adaptation, known as the bone remodelling process, is the reason why implanted material is usually accepted without any major problem if it is well tolerated biologically. Articular cartilage, in association with synovial fluid, provides a very low coefficient of friction (0.001), hence without any resistance. Ligaments provide stability and muscles provide mobility. If one or more of these elements are destroyed or damaged by some illness affecting the hip, then the function is reduced, or even suppressed. Since scientists at the moment are not able to recreate normal joints, engineers and surgeons have developed artificial materials whose function mimics the natural joint. In the past, resection arthroplasty was performed. The other surgical option was hip fusion, which surgeons still recommend for very young people suffering from unilateral hip disease when they cannot offer total hip replacement, or do not trust its durability for this age group. Hip fusion provides a stable and pain-free hip, but with many problems related to stiffness, the consequences for knee and spine function and later deterioration. These problems lead these patients to seek hip reconstruction some years later. Total joint arthroplasty has gained

popularity because of its remarkable results and because of improvements in other disciplines such as anaesthesiology and rehabilitation.

28.2 History

The first clinical trial of arthroplasty started in the late 19th century when Ollier described resection arthroplasty, creating a pain-free, mobile joint without stability and shortening problems. At the beginning of the twentieth century, Gluck and others designed and implanted a real prosthesis made of metal to replace the femoral head. In 1947, the Judet brothers in France implanted the first femoral head made of acrylic material with a metal stem. This was not very successful and the material was replaced by a cobalt chromium alloy. In the United Kingdom, Mckee-Farrar invented the real total hip made of a cobalt chromium molybdenum alloy with a head sliding in a socket. It was very soon apparent that this material, which was simply implanted into the bone, was not totally safe. Many cases of loosening were reported that were attributed to the high friction coefficient produced by this metal-on-metal couple (Sedel, 1997).

In 1963, John Charnley popularised two major changes. He invented the low-friction concept based on a small metallic head sliding in a high molecular weight polyethylene socket, and the materials were cemented with methyl methacrylate, used at that time by dental surgeons. But this material was only released on the market 7 years later, after he had personally trained a significant number of surgeons. At this time, some researchers examined this polyethylene material and predicted that wear of the polyethylene would be a negative issue because of foreign body reactions. The German pathologist Willert described the mechanism of foreign body reaction related to the debris of polyethylene wear, and thus explained the failure of this sliding couple. Charnley was aware of these problems and described the rate of wear of his material as about 0.1 mm per year. He believed that if the patient did not walk too much and avoided sport or heavy work, this prosthesis would last long enough. He advocated that total hip replacement should not be used in young and active patients.

Other scientists, however, suspected that this material was insufficient for long-term total hip implantation. Other chemical studies presented the negative effects of polyethylene ageing and the possible long-term deterioration of this product. Since this early period, many papers have described the wear of the polyethylene material, resulting in stem or socket loosening. During the early period, many authors concluded that the cement was the cause of failure and they worked on a cementless design. However, it is now proven that the cement was not the weaker link: it was the polyethylene degradation (Catelas *et al.*, 1999). Other scientists decided to try a harder material, such as ceramics.

28.3 Background on ceramics

We will not describe here the material properties and advantages of alumina ceramic because this is the subject of other articles (Refior *et al.*, 1997; Clarke *et al.*, 2000). As surgeons, we were particularly interested in the sliding characteristics, especially the very limited amount of debris generated, the low friction system and the biological inertness of the product (Boutin *et al.*, 1988).

We were also concerned about the hardness and fragile mechanical behaviour of the product. With regard to hardness, we performed experimental work which showed that the hip system possessed a very sophisticated shock absorption mechanism (Christel *et al.*, 1976). Shock could be absorbed by different structures: by the whole leg including the foot, the knee and the iliopelvic joint. Local stresses might be limited in the long term by the bone remodelling process. In fact, our observations of the clinical series showed that this was exactly what occurred, except in the case of the very old age group with osteoporosis, where this material gave rise to more failures (Boutin *et al.*, 1988; Nizard *et al.*, 1992). We suspected that the hardness was the cause of these failures and did not select this group of patients for use of this ceramic material. Fracture risk was the second possible problem (Boutin *et al.*, 1981, 1988; Hannouche *et al.*, 2003, 2005), but after an initial phase, this problem became very limited. With improved material and improved design, we consider this fracture risk so small that it totally counteracts the other risks of hip prosthesis. At the moment the risk is considered negligible (Garino, 2000; Hannouche *et al.*, 2003). We have published many papers on the clinical results for this material (Sedel *et al.*, 1990, 1994; Hamadouche *et al.*, 1999; Hannouche *et al.*, 2003) and can demonstrate the remarkably low generation of debris, with very limited osteolytic lesions in regular cases, the very low fracture risk, and the excellent clinical results even in very young people (Sedel *et al.*, 1990; Bizot *et al.*, 2000a). Nevertheless, it was also clear that the main problem was the secure fixation of the ceramic into the bone for a long period of time. This was the reason for different socket designs in order to improve this matter.

Other experiments with all-alumina bearings were carried out in Germany (Mittelmeier and Heisel, 1992; Refior *et al.*, 1997), Italy (Toni *et al.*, 1995), Austria (Bohler *et al.*, 2000) and the United States (O'Leary *et al.*, 1988; Huo *et al.*, 1996). Except for some papers published in the United States, all the studies concluded that there was a lack of osteolysis and a good clinical outcome; the problems were mainly related to early ceramic fractures and to socket fixation problems. This material has been accepted by the Food and Drug Administration (FDA) since 2003 and is increasingly used in many developed countries in young and active patients (Garino, 2000; Capello *et al*., 2005).

28.4 Clinical data

Over the 36-year period since the first ceramic hip implantation by Pierre Boutin (1972; Boutin *et al.*, 1981), many attempts have been made to solve the problem of ceramic fixation. The first attempts used glue to secure the ceramic head to the neck trunion, leading to many head fractures (Fig. 28.1). Later, a screw-in device was used (Boutin *et al.*, 1988). The introduction of Morse cone technology to secure the ceramic head to the trunnion provided the final solution to the problem. The cone angle selected was 5°46′. At first, the size was 14/16, but in 1993 the angle was modified to 12/14 in order to comply with standards.

We started to use the modern design of the implant in 1977. This design (Figs 28.2 and 28.3) consisted of a bulky alumina socket cemented to a titanium alloy stem covered in a thin layer of titanium oxide. The stem was cemented using the first-generation cemented system. Its shape was slightly curved with a collar. The results for this stem were outstanding, with many papers (Sedel *et al.*, 1990; Nizard *et al.*, 1992; Sedel, 1997; LeMouel *et al.*, 1988; Hamadouche *et al.*, 2002; Hannouche *et al.*, 2005) demonstrating a 95–98% survivorship rate at 10 years. The initial results were good, but over time we observed many cases of acetabular loosening (Sedel, 1997). This occurred more frequently in elderly patients and was related to cement fracture. In younger patients, the results were better, perhaps because the bone support could adapt and prevent cement fracture (Bizot *et al.*, 2000a). Bulky alumina cementless implants have been used since 1983 in a limited number of very

28.1 Example of a glued ceramic head fracture in an early design.

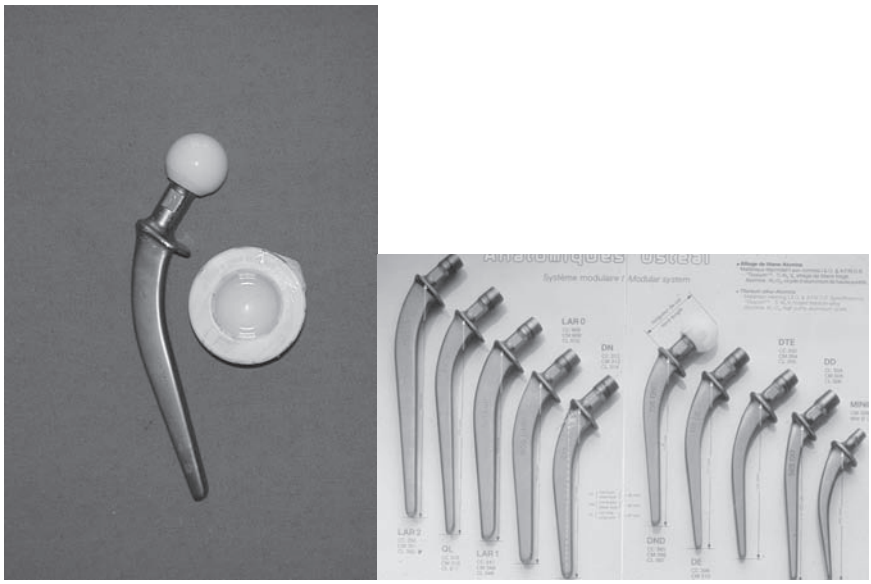

28.2 First-generation stem and socket.

28.3 Cemented prosthesis after 25 years' implantation in a very active, 25-year-old man. Clinical results are still excellent.

young and active patients, with quite acceptable results. Revisions were easy to perform and without major bone loss (Hamadouche *et al.*, 1999).

We were also able to trace patients operated on by Pierre Boutin in 1980 (Hamadouche *et al.*, 2002). The results at 20 years' follow-up showed a survivorship rate of 67%, but if we only looked at aseptic loosening in patients

implanted with a cementless socket, the figure was far better, with 87% survivors. In addition, the radiological results showed no evidence of osteolysis at 20 years' follow-up.

The most recent unpublished results are for young, active patients under the age of 50, operated on using a hybrid prosthesis with a socket of press-fit design, using a titanium shell covered with titanium mesh (Bizot *et al.*, 2000b). The results at 14 years' follow-up showed a 97% survival rate when determining the final failure event as aseptic loosening, and 93% when taking revision for any reason. We observed some radiolucent lines around the socket and two cases of osteolytic lesions in the femur. We assumed that the grid fixation on the shell was the cause of some of these appearances, and that was why we moved to a full cementless design in 1997 (Fig. 28.4), that is still currently in use.

During 2000 and 2001, we observed four cases of alumina liner fracture (Hannouche *et al.*, 2003), but these fractures only occurred in small samples (50 or 52 mm in diameter). We speculated that this failure was related to a change in the liner design and possibly in one case (Fig. 28.5) to ancillary material damage to the inner aspect of the shell. The manufacturer made a further modification to create a larger liner by reducing the thickness of the metal shell in order to increase the thickness of the ceramic and allow more material dedicated to alumina (Fig. 28.4c). Since these changes were made in 2001, we have not observed any fractures in more than 1000 hips implanted.

At the moment, an alumina-on-alumina couple for total hip replacement appears to be the best solution to the problems of wear and loosening, and allows us to treat very young patients. Patients can perform any activity, including strenuous activities or sport, with no adverse effects (Fig. 28.6). However, we must still be cautious about the material design and material implantation technique. Some problems are still encountered with the socket, but we consider that many of these are related to surgical technique and could be avoided by better placement and impaction of the components. Even these problems are limited in number and easy to solve. A simple operation to change the socket only is easy to perform with limited operating time, scarring or risks.

There are currently some concerns, especially in the United States and Australia, about noise generation and stripe wear (Garino, 2000; Capello *et al.*, 2005). In our experience, noise was very occasional and never resulted in revision. We suspect that some mechanical designs are the cause of this noise. It seems more frequent in some designs with very thin components, with some problems of component orientation or some special surgical techniques preserving the anterior soft tissue. It is possible that very low clearance between the components or some mobility of the liner when the angle is greater than 5°45′ could play a role. At the moment it is very

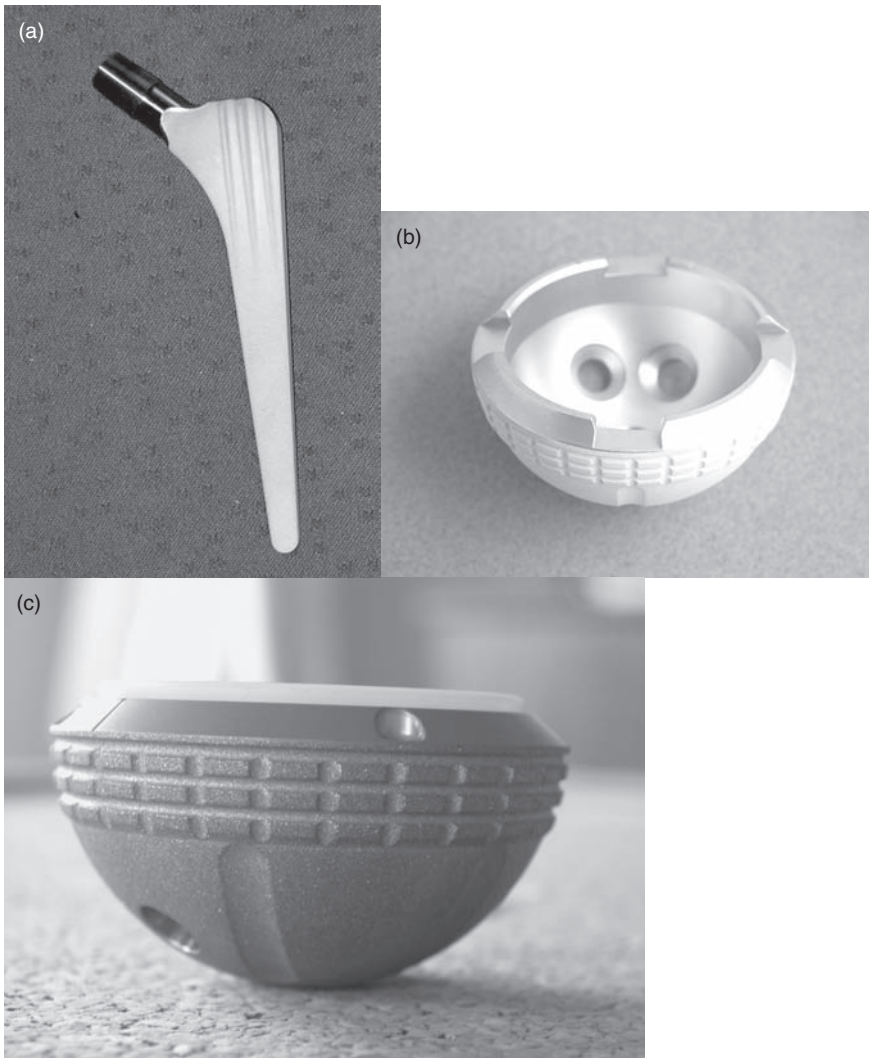

28.4 The current design implanted since 1998: (a) the stem; (b) socket design 1; (c) socket design 2.

difficult to draw conclusions. With regard to stripe wear, this was described by our team some 20 years ago (Boutin *et al.*, 1988; Dorlot, 1992) and John Fisher recognised that it was related to microseparation (Refior *et al.*, 1997; Nevelos *et al.*, 2000). At the moment, stripe wear does not appear to be a major concern for the long-term survival of the prosthesis; it seems to be more anecdotal than a cause for concern.

Many other surgeons and companies are now using and offering this ceramic couple. Some reports of success (Garino, 2000; Capello *et al.*, 2005)

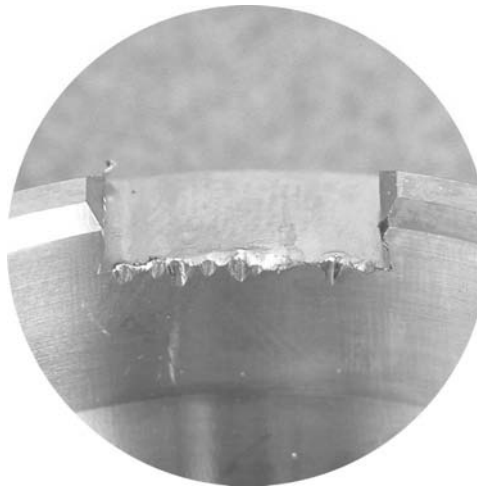

28.5 A case of liner fracture. Ancillary material was responsible for the inner scratch on the metal, resulting in a rise in stress and fracture.

28.6 X-ray photo after 71 months in a 45-year-old man who performs many sports, including running, golf and wind surfing.

are now coming from the United States, where this material has been available since 2003, confirming our initial results.

28.5 Discussion

Negative arguments with regard to these alumina-on-alumina bearings still relate to fracture. Some papers (Heck *et al.*, 1995) have presented other reasons for fractures in total hip replacement, and alumina head fractures were relatively unusual in a large series, compared with stem fractures, polyethylene socket or liner fractures, or other mechanical complications. Some materials are currently challenging this ceramic combination and metal-on-metal resurfacing is gaining in popularity. Comparing the recent figures for metal-on-metal resurfacing (Refior *et al.*, 1997) with our own results (Nevelos *et al.*, 2000) in two series of the same aetiology, i.e. osteonecrosis of the femoral head, at a mean follow-up of 6 years, metal-on-metal presented a survival rate of 93% at 6.1 years. This can easily be compared with our rate of 100% survival at 6 years and 88.5% at 10 years.

28.6 Conclusion

The selection of material for total hip reconstruction is still under debate. Some new materials are already on trial and highly cross-linked polyethylene could provide some solutions to the problem of wear. It has been used in implants in clinical practice for only 6 years, but preliminary results are good, even though some papers are already available showing some wear or foreign body reaction.

Metal-on-metal and hip resurfacing is gaining great popularity. The chromium cobalt alloy appears to produce a more aggressive reaction in the body than alumina debris. At the moment, there are some allergic problems and the increase of cobalt serum levels is of concern. We will have to wait in order to obtain really good information about these new products.

At the moment, alumina-on-alumina ceramic provides the best answer to the problems of wear and osteolysis. More than 30 years of results using this product demonstrate that it allows full activity without any specific problems.

28.7 References and further reading

Allain J, Le Mouel S, Goutallier D, Voisin MC: Poor eight-year survival of cemented zirconia–polyethylene total hip replacements. *J Bone Joint Surg* **81B**:835–842, 1999.

Bizot P, Banallec L, Sedel L, Nizard R: Alumina-on-alumina total hip prostheses in patients 40 years of age or younger. *Clin Orthop* **379**:68–76, 2000a.

Bizot P, Larrouy M, Witvoet J, Sedel L, Nizard R: Press-fit metal-backed alumina sockets. A minimum 5-year followup study. *Clin Orthop* **379**:134–142, 2000b.

Bohler M, Mochida Y, Bauer TW, Plenk Jr H, Salzer M: Wear debris from two different alumina-on-alumina total hip arthroplasties. *J Bone Joint Surg* **82B**:901–909, 2000.

Boutin P: Arthroplastie totale de la hanche par prothèse en alumine frittée. Etude expérimentale et premières applications cliniques. *Rev Chir Orthop Reparatrice Appar Mot* **58**:229–246, 1972.

Boutin P, Blanquaert D: Le frottement alumine-alumine en chirurgie de la hanche. 1205 arthroplasties totales. *Rev Chir Orthop Rep. Appar Mot* **67**:279–287, 1981.

Boutin P, Christel P, Dorlot JM, Meunier A, Witvoet J, Sedel L: The use of dense alumina-alumina ceramic combination in total hip replacement. *J Biomed Mater Res* **22**:1203–1232, 1988.

Capello WN, Dantonio JA, Feinberg JR, Manley MT: Alternative bearing surfaces: alumina ceramic bearings for total hip arthroplasty. *Instr Course Lect* **54**:171–176, 2005.

Catelas I, Petit A, Marchand R, *et al.*: Cytotoxicity and macrophage cytokine release induced by ceramic and polyethylene particles *in vitro*. *J Bone Joint Surg* **81B**:516–521, 1999.

Christel P, Derethe P, Sedel L: Mesure par simulation de l'amortissement d'une hanche normale et prothèsée, *Acta Orthopaedica Belgica* **42**, suppl.I, 183–193, 1976.

Clarke IC, Good V, Williams P, *et al.*: Ultra-low wear rates for rigid-on-rigid bearings in total hip replacements. *Proc Inst Mech Eng* **214**:331–347, 2000.

Dorlot JM: Long-term effects of alumina components in total hip prostheses. *Clin Orthop* **282**:47–52, 1992.

Garcia-Cimbrelo E, Martinez-Sayanes JM, Minuesa A, Munuera L: Mittelmeier ceramic–ceramic prosthesis after 10 years. *J Arthroplasty* **11**:773–781, 1996.

Garino JP: Modern ceramic-on-ceramic total hip systems in the United States: early results. *Clin Orthop* **379**:41–47, 2000.

Hamadouche M, Nizard RS, Meunier A, Bizot P, Sedel L: Cement-less bulk alumina socket: Preliminary results at 6 years. *J Arthroplasty* **14**:701–707, 1999.

Hamadouche M, Boutin P, Daussange J, Bolander M, Sedel L: Alumina-on-alumina total hip arthroplasty. A minimum 18.5-year follow-up study. *J Bone Joint Surg* **84A**:69–77, 2002.

Hannouche D, Nich C, Bizot P, Meunier A, Sedel L: Fractures of ceramic bearings: History and present status. *Clin Orthop* **417**:19–26, 2003.

Hannouche D, Hamadouche M, Nizard R, Bizot P, Meunier A, Sedel L: Ceramics in total hip replacement. *Clin Orthop* **430**:62–71, 2005.

Heck DA, Partridge CM, Reuben JD, *et al.*: Prosthetic component failures in hip arthroplasty surgery. *J Arthroplasty* **10**:575–580, 1995.

Huo MH, Martin RP, Zatorski LE, Keggi KJ: Total hip replacements using the ceramic Mittelmeier prosthesis. *Clin Orthop* **332**:143–150, 1996.

LeMouel S, Allain J, Goutallier D: 10-year actuarial analysis of a cohaort of 156 total hip prosthesis of a cemented polished alumina/polyethylene alloy. *Rev Chir orthop Reparatrice Appar Mot* **84**:338–345,1998.

Lerouge S, Huk O, Yahia L, Witvoet J, Sedel L: Ceramic–ceramic and metal–polyethylene total hip replacements: comparison of pseudomembranes after loosening. *J Bone Joint Surg* **79B**:135–139, 1997.

Mittelmeier H, Heisel J: Sixteen-years' experience with ceramic hip prostheses. *Clin Orthop* **282**:64–72, 1992.

Nevelos J, Ingham E, Doyle C, *et al.*: Microseparation of the centers of alumina-alumina artificial hip joints during simulator testing produces clinically relevant wear rates and patterns. *J Arthroplasty* **15**:793–795, 2000.

Nich C, El-Hadi SA, Hannouche D, Nizard R, Witvoet J, Sedel L, Bizot P: Long term results of alumina-on-alumina hip arthroplasty for osteonecrosis. *Clin Orthop* **417**:02–111, 2003.

Nizard RS, Sedel L, Christel P, Witvoet J, Sedel L: Ten-year survivorship of cemented ceramic-ceramic total hip prosthesis. *Clin Orthop* **282**:53–63, 1992.

O'Leary JF, Mallory TH, Kraus TJ, Lombardi AV Jr, Lye CL: Mittelmeier ceramic total hip arthroplasty. A retrospective study. *J Arthroplasty* **3**:87–96, 1988.

Prudhommeaux F, Hamadouche M, Nevelos J, *et al.*: Wear of alumina-on-alumina total hip arthroplasties at a mean 11-year followup. *Clin Orthop* **379**:113–122, 2000.

Refior HJ, Plitz W, Walter A: *Ex vivo* and *in vitro* analysis of the alumina/alumina bearing system for hip joint prostheses. In Sedel L, Rey C. *Bioceramics*. Vol 10. Oxford, UK, Elsevier Science 127–130, 1997.

Revell MP, McBryde CW, Bhatnagar S, Pynsent PB, Treacy RB: Metal on metal hip resurfacing in osteonevrosis of the femoral head. *J Bone Joint Surg* **88A**, supplement 3:98–103, 2006.

Sedel L: The tribology of hip replacement. In Kenwright J, Duparc J, Fulford P (eds). *European Instructional Course Lectures*. The British Editorial Society of Bone and Joint Surgery, London, Vol 3, 25–33, 1997.

Sedel L, Kerboull L, Christel P, Meunier A, Witvoet J: Alumina-on-alumina hip replacement. Results and survivorship in young patients. *J Bone Joint Surg* **72B**:331–332, 1990.

Sedel L, Nizard RS, Kerboull L, Witvoet J: Alumina–alumina hip replacement in patients younger than 50 years old. *Clin Orthop* **298**:175–183, 1994.

Sedel L, Simeon J, Meunier A, Villette JM, Launay SM: Prostaglandin E2 level in tissue surrounding aseptic failed total hips. Effects of materials. *Arch Orthop Trauma Surg* **111**:255–258, 1992.

Toni A, Terzi S, Sudanese A, *et al.*: The use of ceramic in prosthetic hip surgery. The state of the art. *Chir Organi Mov* **80**:125–137, 1995.

Witvoet J, Darman Z, Christel P, Fumery F: Arthroplastie totale de hanche avec anneau cotyloïdien en titane vissé. Devenir de 446 prothèses avec un recul moyen de 4 ans. *Rev Chir Orthop Reparatrice Appar Mot* **79**:542–552, 1993.

29

Clinical applications of ceramic-polyethylene combinations in joint replacement

H OONISHI, S C KIM, and H OONISHI JR.,
Tominaga Hospital, Japan and
S MASUDA, M KYOMOTO, and M UENO,
Japan Medical Materials Corporation, Japan

29.1 Introduction

Currently, total joint arthroplasty is widely used as a surgical treatment for serious joint diseases. The Charnley-type total hip prosthesis (THP), which consists of an ultra-high molecular weight polyethylene (UHMWPE) socket and a stainless steel (SUS) femoral component, has been used since the 1960s and has exhibited good clinical performance. However, THP used for arthroplasty has various problems, including deterioration of the components due to wear and the toxicity of wear debris. The production of wear debris from UHMWPE with subsequent osteolysis around the THP has been recognized as the major cause of long-term (longer than 10 years) failure in total joint arthroplasty. Increase in wear durability of THP is thus needed.

It is recognized that use of ceramics such as alumina to replace metallic material such as SUS for the femoral head decreases wear of UHMWPE sockets. The combination of ceramics and UHMWPE has been used not only for hip joints but also joints of the knee and ankle, and other joints. In this chapter, the clinical application of the artificial joints in combination of ceramics/UHMWPE is described.

29.2 Hip joint

A total joint prosthesis is an implant placed in the body as a substitute for a joint. When a joint becomes dysfunctional due to trauma or disease, it is surgically removed and replaced by a joint prosthesis. THPs, in particular, are placed in several hundred thousand patients annually in the world.

Underlying diseases that often necessitate joint replacements include rheumatoid arthritis and osteoarthritis, which are relatively frequently in the elderly. In the past, the patients with such diseases often became

bedridden due to severe joint pain. Total hip arthroplasty (THA) has now made it possible for these patients to walk, and has greatly contributed to improving their quality of life.

29.2.1 Charnley total hip prosthesis

The original model of the total hip prosthesis commonly in use today was established by John Charnley in the 1960s in the UK (Charnley, 1970, 1972; Charnley and Cupid, 1973; Charnley and Halley, 1975). It has since been improved by many physicians and engineers, and the type shown in Fig. 29.1 is currently in wide use. From the standpoint of engineering, THP is a ball-and-socket type joint, which generally uses UHMWPE for the acetabular (pelvic) side and metal (highly rigid cobalt chromium alloy) for the femoral head side for the functionally important sliding components.

Although Charnley initially used Teflon (polytetrafluoroethylene, PTFE) as a socket material (Charnley, 1970), it exhibited clinically unexpected

29.1 Total hip joint prosthesis.

wear within a few years, and the resulting wear debris caused severe inflammatory responses in adjacent tissue. Charnley then changed the socket material to UHMWPE, and made the diameter of the prosthetic femoral head smaller than that of the real femoral head and increased the thickness of the socket. This model has achieved excellent clinical results over the past decade.

UHMWPE is generally classified as a polyethylene, the average molecular weight of which exceeds one million. For total joint prostheses, UHMWPEs, which have molecular weights of 4–7 million, are used. When used in total joint prostheses, they have exhibited better wear resistance than Teflon; with metal prosthetic heads, the annual wear rate of the UHMWPE sockets is as little as about 0.1–0.2 mm/year (Charnley, 1970). This value was calculated from year-to-year radiographic study results after replacement surgery (i.e. measurement of positional relationship between the femoral head and the socket) and measurement of sockets after their removal from patients.

Efforts to improve various elements of total hip prostheses – designs and materials of the respective components, the method of fixation to bones, and surgical procedures and instruments – are ongoing. Today, the problems experienced in the early stage of development, such as the fracture of the prosthetic stem (i.e. femoral component), socket deformation and poor fixation of bone cement due to formation of bubbles in mixing of cement, have been solved, and remarkable clinical application results exceeding 10 years have been achieved in many cases. However, another problem due to wear has arisen, termed aseptic loosening, in which the THP becomes loose at its point of fixation with the bone and becomes unusable, without bacterial infection or other specifiable causes. The bone cement was initially suspected to be a cause of this problem, though the real cause was different (Amstutz *et al.*, 1992; Schmalzried *et al.*, 1998; Sochart, 1999; Oparaugo *et al.*, 2001).

Although UHMWPE is an excellent wear-resistant material, it is not completely free of wear, and some wear debris is produced. This accumulates over a long period of time and results in a series of biological reactions, which activate osteoclasts and cause osteolysis of the bones adjacent to the total joint prosthesis, leading to aseptic loosening. It is difficult to identify the cause of this, since reactions to wear debris differ among individuals and the socket wear rate depends on patient weight and activity. However, aseptic loosening is considered as a major determinant of the life of total hip prosthesis.

One possible solution to this problem is the use of ceramic heads to suppress wear of UHMWPE sockets. Based on this idea, the authors have since the 1970s been using THP consisting of a ceramic head and a UHMWPE socket (Oonishi *et al.*, 1989).

29.2.2 Alumina ceramics for total hip prostheses

The application of alumina ceramics to THP was first reported by Boutin (Boutin, 1971; Boutin *et al.*, 1988) in 1971, as the combination of a ceramic head and a ceramic socket. Semlitsch *et al.* (1977) subsequently reported a THP combining a ceramic head and a UHMWPE socket.

The authors began clinical use of total hip prostheses with an alumina ceramic head and a UHMWPE socket in 1977. The physical properties of the alumina ceramics used at that time were as follows: alumina purity 93%, density 3.99 g/ml, Young's modulus 380 GPa, hardness 1650 Hv, bending strength 450 MPa and average grain size 4.9 μm (Ueno *et al.*, 2000). In 1990, we began the use of new-grade alumina ceramics. The physical properties of the new grade material were as follows: alumina purity >99.5%, density 3.97 g/ml, Young's modulus 400 GPa, hardness 1900 Hv, bending strength 640 MPa and average grain size 1.4 μm. The principal feature of the new-grade material is its improvement of strength. Production of a smaller, approximately 22 mm diameter head – the size Charnley used for his metal head – became possible, though it had not been with the previous material due to its load capacity. In addition due to miniaturization of average grain size, it became possible to obtain a smoother finish of the bearing surface.

29.2.3 Clinical results of ceramic total hip prostheses

The usefulness of ceramics in total hip prosthesis has been reported by other authors (Heimke and Griss, 1981; Zichner and Willert, 1992; Bos *et al.*, 1993). The typical clinical case of THA is shown in Fig. 29.2. Little change was seen in surrounding bone and on the THP itself 18 years after surgery. The THP with ceramic femoral head has maintained the initial function over the long term clinically. We carried out THA of 847 cases between 1989 and 1996, 607 cases between 1997 and 2000, 1542 cases between 2001 and 2006, and have had only four cases of revision surgery.

We compared the inhibition of wear of ceramic heads and metal heads in UHMWPE sockets used in clinical total hip replacements (Oonishi *et al.*, 1989, 2000). We used Bioceram (Kyocera Co., Kyoto, Japan) for alumina ceramic heads and T-28 (Zimmer Inc., Indiana, USA) for metal heads. The diameter was approximately 28 mm for both heads. Wear of UHMWPE sockets was compared in 80 Bioceram THP of 956 patients at least 6 years after surgery performed between 1977 and 1988 and 15 T-28 total hip prostheses of 117 patients at least 6 years after surgery performed between 1975 and 1981 by measuring the thickness of UHMWPE sockets using clinical radiographs and analyses of them.

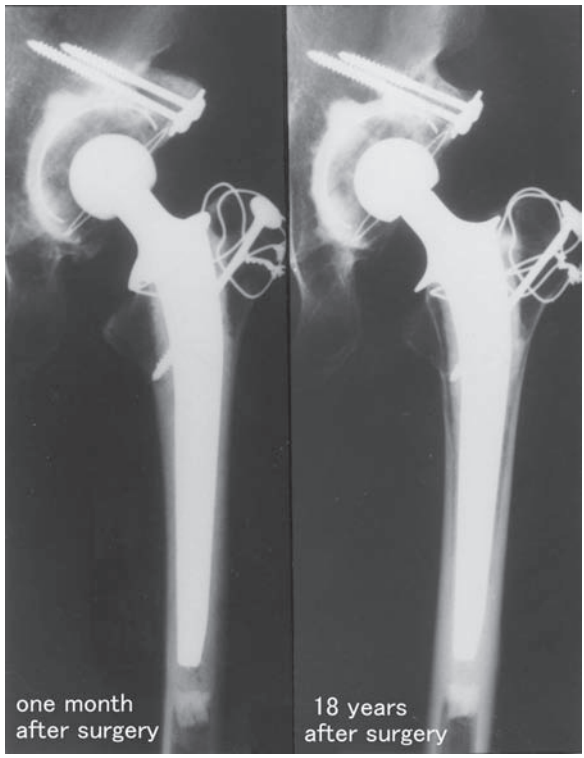

(a) (b)

29.2 Typical clinical radiographic images of THA, (a) 1 month after surgery, (b) 18 years after surgery.

The method of linear wear measurement by using of clinical radiographs is shown conceptually (see Fig. 29.3). Results showed that the wear rate of UHMWPE sockets implanted in combination with metal heads was 2.5 times that with ceramic heads (Table 29.1). In that study, wear rates tended to vary depending on the sizes of the UHMWPE sockets, even though the same ceramic heads were used. More specifically, the average wear rate was 0.14 mm/year for sockets with 42 mm outer diameter (thickness 7 mm), and 0.15, 0.12, 0.06, 0.08 mm/year for sockets thickness 8, 9, 10 and 11 mm, respectively. This showed that the thicker the socket, the less the wear. Since the outer diameter of sockets is limited due to anatomical requirements, ceramic heads of smaller diameter are desirable to increase the thickness of the sockets.

We confirmed these findings in a study of retrieved UHMWPE sockets (Oonishi *et al.*, 1998) (Table 29.2). The method of linear wear measurement by using retrieved sockets is shown conceptually (see Fig. 29.4). The relationship between linear wear, socket thickness and femoral head size is

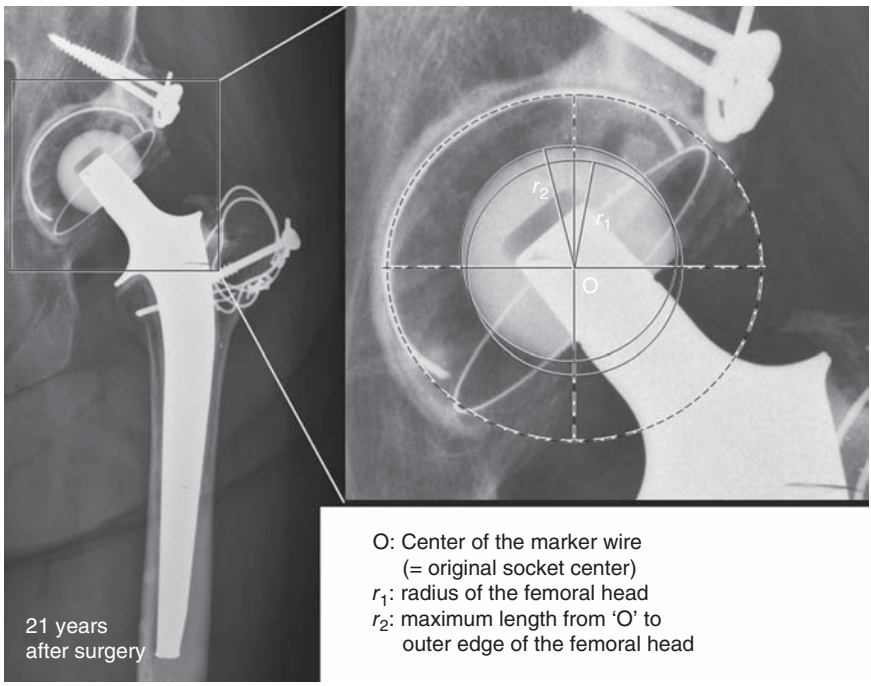

29.3 The method of linear wear measurement (linear wear) = $(r_2 - r_1) \times$ (magnification ratio of the picture).

Table 29.1 Linear wear rate of UHMWPE socket in THP (radiographic study)

Head materials	Socket thickness (mm)	Linear wear rate (mm/year)
Ceramics (alumina)	Average	0.10 ± 0.007
	7	0.14 ± 0.10
	8	0.15 ± 0.11
	9	0.12 ± 0.03
	10	0.06 ± 0.03
	11	0.08 ± 0.04
Metal (SUS)	Average	0.25 ± 0.02

Femoral head size: 28 mm.
From Oonishi *et al.* (2000).

demonstrated in Fig. 29.5. It was suggested that the socket thickness was a more important factor to the wear than the femoral head diameter. (Although the use of the highly cross-linked polyethylene was the most effective, this issue will be mentioned later.)

To produce a smaller head, the above new grade high-strength alumina ceramics were developed and smaller diameter ceramic heads became

Table 29.2 Linear wear rate of UHMWPE socket in THP (retrieved study)

Head materials	Socket thickness (mm)	Linear wear rate (mm/year)
Ceramics (alumina)	7	0.20 ± 0.03**
	8	0.19 ± 0.01**
	9	0.14± 0.08**
	11	0.10 ± 0.03**
Metal (COP*)	7	0.32 ± 0.04†
	8	0.29 ± 0.05†
	9	0.21 ± 0.07†

Femoral head size: 28 mm.
* COP = stainless steel containing 20% Co.
** From Oonishi *et al.* (2000).
† From Oonishi *et al.* (1998).

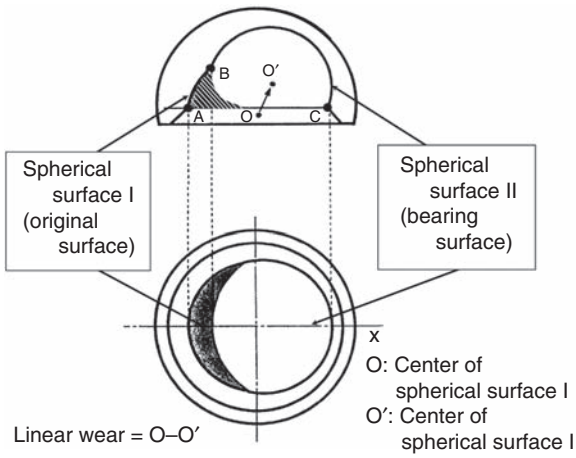

29.4 Schematic drawing of the retrieved socket.

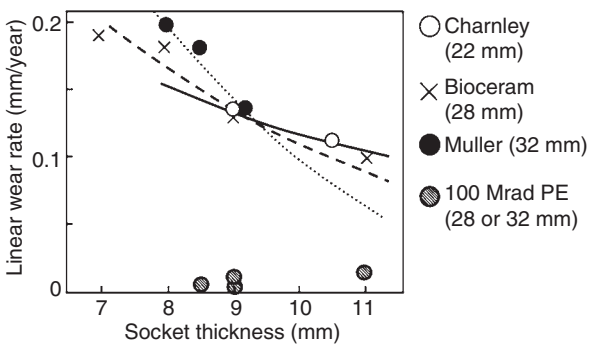

29.5 Relationship between linear wear, socket thickness and femoral head size. Charnley: SUS head of 22 mm of diameter, UHMWPE socket. Bioceram: alumina ceramic head of 28 mm of diameter, UHMWPE socket. Muller: CoCr alloy of 32 mm of diameter, UHMWPE socket. 100 Mrad PE: metal or ceramic head, highly cross-linked PE socket (dose = 100 Mrad).

available. In addition, a higher-strength ceramics, yttria-stabilized tetragonal zirconia ceramics (Y-TZP), was developed and began to be marketed in Japan in 1995. The physical properties of Y-TZP were as follows: purity of principal component >99%, density 6.05 g/ml, Young's modulus 210 GPa, hardness 1300 Hv, bending strength 1200 MPa and average grain size 0.3 μm (Ueno *et al.*, 2000).

29.2.4 Evaluation of wear by hip joint simulator

Clinical evaluation of wear requires a long period of time, and final results are not available until at least 10 years after the start of use. Therefore, testing using hip joint simulators, which evaluates the amount of wear in relatively short periods of time by sliding of total joint prosthesis components to simulate movement of the hip joint equivalent to few years of clinical use, has been used for wear testing of THPs.

To examine the effect of head ball material on UHMWPE socket wear, a hip joint simulator test was performed (Ueno *et al.*, 2000). For the head ball material, we used the alumina ceramics (new alumina) in use since 1990, Y-TZP (zirconia), which has been in use since 1995, and for comparison, a metal head (SUS; Ortron 90).

When conditions of the socket and head size were the same, the wear volumes of the UHMWPE socket were as follows: zirconia 13.4 (mm^3/million cycles) < new alumina 40.2 < Ortron 90 60.7, demonstrating the superiority of ceramic heads over the metal head. In addition the amounts of wear of heads of different sizes were compared with the same combination of materials. When 22, 26 and 28 mm head sizes were compared with the new alumina and UHMWPE socket combination with the same socket outer diameter, the amounts of wear were less with smaller heads. This result supported the above clinical findings noted above.

29.2.5 Advantages of ceramic femoral head in THP

Metal femoral heads are the mainstream even now. A risk of breakage of the ceramic femoral head prevents the spread of their use, though almost all orthopedists know that a ceramic head is superior to a metal head in the wear problem of UHMWPE socket. Recently, there was a worldwide problem about breakage of zirconia ceramic heads produced by a French manufacturer. We have surmised that the cause was the incomplete sintering of the ceramics due to defective process control. Ceramic, a brittle material, breaks catastrophically when it is loaded down

with exceeding stress. However, this is an issue in the design of the artificial joint.

In fact, our clinical results demonstrated that the probability of breakage after surgery of the ceramic head was under 0.01%. In other words, ceramic femoral heads are a safe material with correct design, good production process and proper usage.

29.2.6 Future trends

To address the problem of wear in THP, we have since 1970 worked towards improving the UHMWPE socket material, separately from the use of ceramic heads, and developed a highly cross-linked polyethylene socket prepared using high-dose gamma-irradiation, which was clinically used from 1971 to 1978 (Shikita *et al.*, 1977). Due to withdrawal of the manufacturer that co-developed the product, we were unable to continue clinical application of this material, but have confirmed its superb long-term clinical results and have reported them in symposia of scientific societies, etc. (Oonishi *et al.*, 1998, 2001a,b, 2004). Inspired in part by our reports, many manufacturers began to develop various new highly cross-linked polyethylenes. Currently, the majority of THP sockets are made of various types of highly cross-linked polyethylenes.

In fact, highly cross-linked polyethylene sockets, use of which became common around the year 2000, have greatly improved the wear resistance of THP (Oonishi *et al.*, 2006b). This effect outweighs the effect of replacement of head material from metal to ceramics. The problem of wear in THP thus appears to have been almost completely solved. Future development of ceramics for THP will therefore aim at improving clinical reliability, i.e. the development of ceramics with increased strength and toughness.

29.3 Knee joint

In humans, the knee joint is the largest joint in the body. The shapes of the knee joint components are more complex than those of the hip joint. Correspondingly, many knee joint prostheses of various designs have been developed. The original model of the total knee prosthesis (TKP) currently used is considered to be the Total Condylar knee prosthesis developed by Peter S. Walker and others in the 1970s. The sliding components are made of a combination of mirror-finished metal (femoral component) and UHMWPE (tibial component or tibial plate), which is similar to that

included in THP. The wear of UHMWPE components in long-term clinical use of TKP has also been a problem.

29.3.1 Total knee joint prosthesis with a ceramic femoral component

We started to use a combination of alumina ceramic and UHMWPE for TKP in the late 1970s based on our good clinical results with THP as well as the results of knee joint simulator tests (Oonishi and Hasegawa, 1981; Oonishi *et al.*, 1991, 2006a). Some refinements of the ceramic TKP designs have been made to improve the kinematic properties and the fixation of TKP with living bone (Fig. 29.6).

The first-generation TKP, used from 1981 to 1985, consisted of an alumina ceramic femoral component (F-comp), an alumina ceramic tibial component (T-comp) and an UHMWPE plate. The stem, of an alumina ceramic, was positioned at the center of the T-comp so that load would be transmitted from the stem to the cortical bone in the posterior portion of the tibia. On the area of the bone in contact with the F- and T- comp, small and shallow grooves were made. This TKP can be used with both cementless and cement fixation. In studies of the first-generation TKP, 137 joints have been followed up for 20–25 years after implantation. The rates of loosening, sinking and revision have been found to be very high in the cases of cementless fixation; but very low in those of cemented fixation (Oonishi *et al.*, 1992, 2002a,b).

Our second-generation TKP, used from 1990 to 1996, consisted of an alumina ceramic F-comp, a titanium alloy T-comp and an UHMWPE plate. The alumina ceramic T-comp was changed to a titanium alloy T-comp to improve mechanical strength and reliability. All of TKPs after the second-generation have been implanted with bone cement, given the relatively high incidences of sinking and occurrence of radiolucent lines observed with cementless fixation. The typical clinical cases of total knee arthroplasty (TKA) are shown in Fig 29.7. The upper pictures are the first-generation TKP 25 years after surgery, and the lower pictures are the second-generation TKP 19 years after surgery. In our third-generation TKP, used from 1993 to 1998, a porous coating of ceramic beads was made on the bone-contacting surface of the F-comp in order to improve fixation between the bone cement and the ceramic F-comp.

Recently, we have mainly used TKPs with zirconia ceramic F-comp. In Japan, zirconia ceramics has been used for TKA (KU type (Akagi *et al.*, 2000), Kyocera Corp., Kyoto, Japan) since 2001 principally because its strength is higher than that of alumina ceramics (Fig. 29.8). This type of ceramics is a Y-TZP polycrystal, which has the properties described in Section 29.2.3.

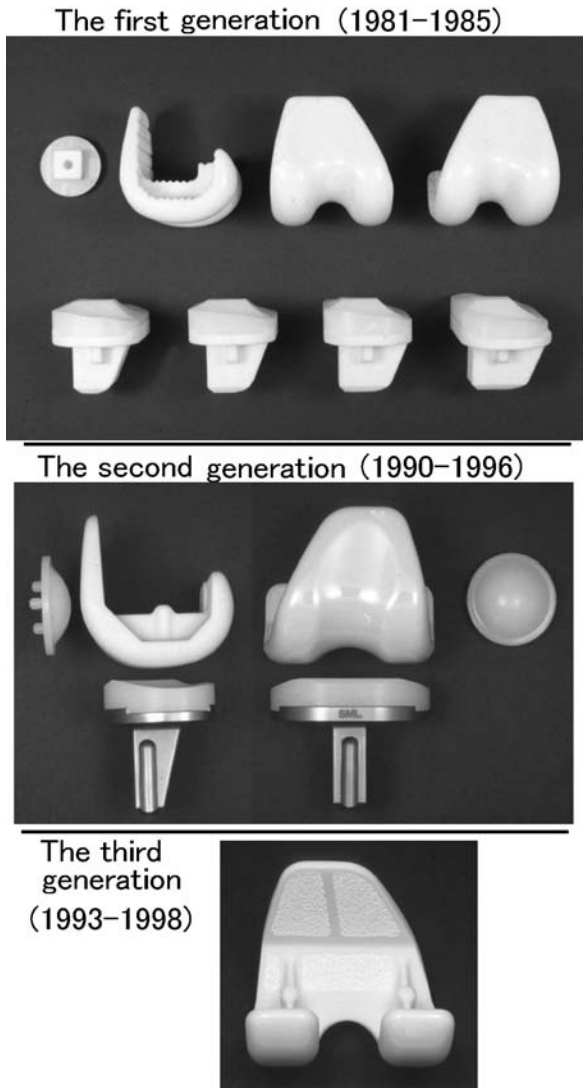

29.6 Development of ceramic TKP.

29.3.2 Clinical results with ceramic total knee prostheses

We examined the clinical results obtained with the second- and third-generation ceramic TKPs (total 534 joints, 1990–2005). All the components had been implanted with bone cement. In a total of 249 joints, over 8–16 years of follow-up, no case of loosening or sinking was observed. Radiolucent lines were observed at rates of 4.3% and 2.1% in the medial and lateral

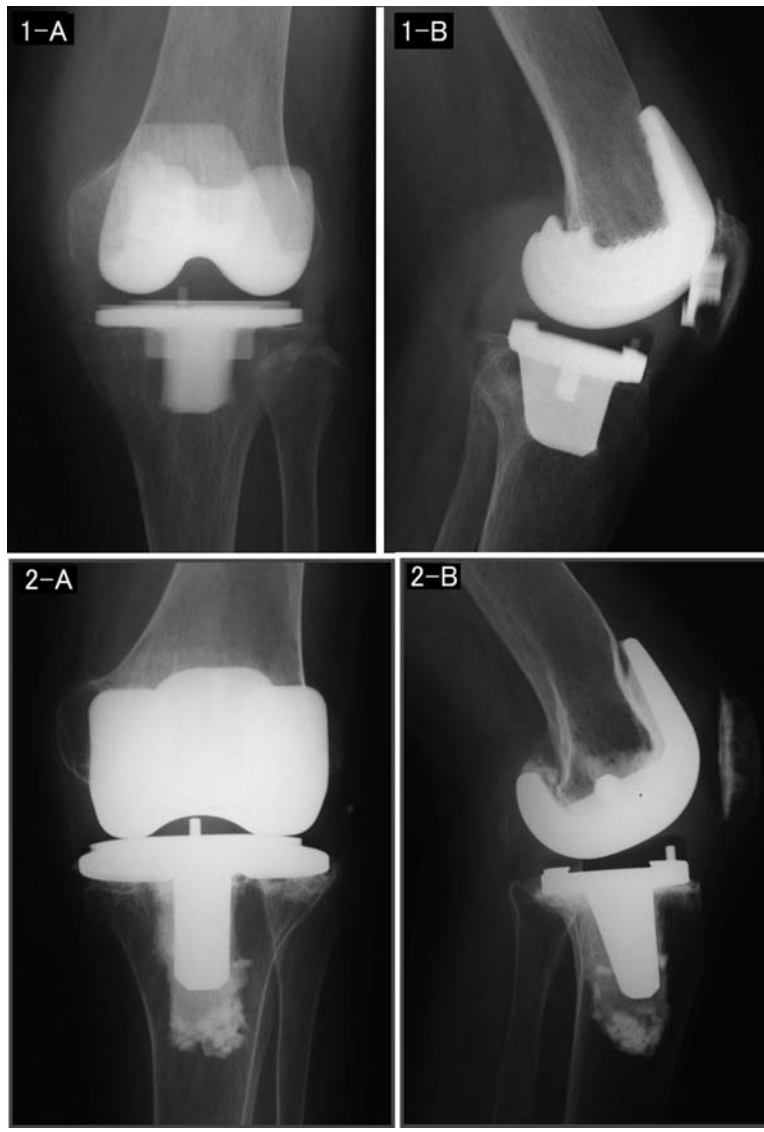

29.7 Typical clinical radiographic images of TKA: 25 years after surgery – (1-A) anteroposterior, (1-B) lateral; 19 years after surgery – (2-A) anteroposterior, (2-B) lateral.

areas of the tibia, respectively. No osteolysis was observed in any of the cases (Oonishi *et al.*, 2006a).

Because good clinical results have been obtained with the ceramic F-Comp and UHMWPE tibial plate, their basic structure has been retained

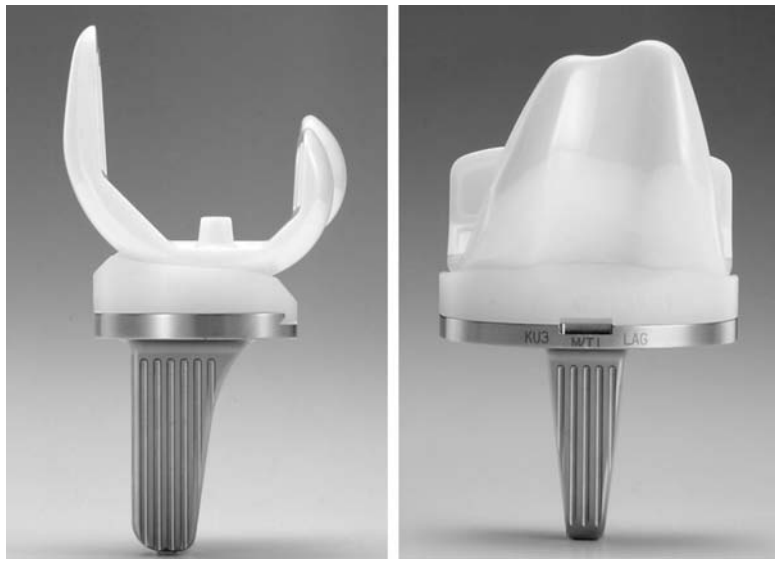

29.8 Zirconia ceramic TKP.

in our current TKP, which has the potential for extremely low clinical wear rates and, correspondingly, reduction of the risk of osteolysis.

29.3.3 Evaluation of wear by knee joint simulator

In our previous study (Oonishi *et al.*, 1991), comparative knee simulator wear tests were performed on two types of TKP: (1) an alumina ceramic F-comp with an UHMWPE plate, and (2) a Co-Cr alloy F-comp with an UHMWPE plate. After 1×10^6 cycles in the simulator test, the linear wear of the UHMWPE plate was approximately 0.2 mm in the case of combination with the metal F-comp, whereas almost no linear wear was observed in many portions of the UHMWPE with the alumina ceramic F-comp. The linear wear rate of the UHMWPE plate was in the latter less than one-tenth that in the former (see Fig. 29.9).

29.3.4 Study of retrieved ceramic and metal TKPs

We have reported the detailed wear pattern and wear volume of the retrieved ceramic TKP which had been used long term (23 years) (Oonishi *et al.*, 2005). The ceramic TKP implanted in 1979 and retrieved in 2002 was examined. The patient was a 60-year-old woman with osteoarthritis of the knee. The reason for the revision surgery was subsidence of the T-comp due

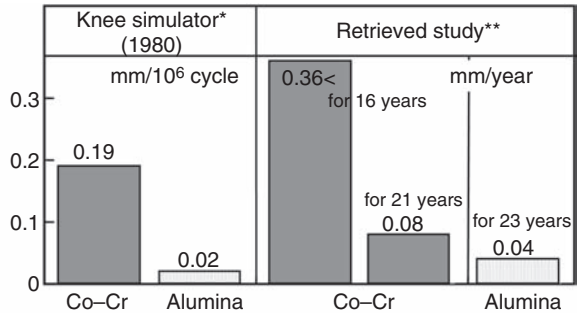

29.9 Wear of UHMWPE plate: simulator test and clinical results. * (Oonishi *et al.,* 1991) ** (Oonishi *et al.,* 2006a).

to osteoporosis. No osteolysis was observed on X-ray images in the course of the follow-up prior to sinking of the T-comp.

In another case, the metal TKP (case 1) was implanted in 1983, and retrieved in 2004 because of painless sinking of the T-comp. The original disease of the patient (female) was osteoarthritis of the knee. This TKP (made by Zimmer, Inc., Warsaw, IN) consisted of a Co-Cr alloy F-comp and an UHMWPE plate. In the other case (case 2), the retrieved metal TKP was implanted in 1987, and retrieved in 2004. The patient was female. This TKP (PCA type, made by Howmedica Corp., Rutherford, NJ) consisted of a Co-Cr alloy F-comp, a Co-Cr alloy T-comp and an UHMWPE plate.

The worn area of the F-comps and the UHMWPE plates surfaces were observed by scanning electron microscopy (SEM). The area of the load-bearing surface in the ceramic F-comp had maintained a nearly virgin surface (Fig. 29.10A), and relatively smooth surface was observed on the UHMWPE plate (Fig. 29.10C). In contrast, many wear scratches parallel to an anterior–posterior direction were clearly observed on the areas of load-bearing surface in metal F-comp (Fig. 29.10B). Many scratches were also observed on the surface of the UHMWPE plate (Fig. 29.10D).

The average and maximum surface roughnesses of the unworn and worn surfaces of retrieved F-comps were determined. For the ceramic F-comp, it was found that the surface roughness of the worn surface was not markedly different from that of the unworn surface. In contrast, the surface roughness of the metal F-comps was significantly higher on the worn surface than on the unworn surface (Fig. 29.11).

The linear wear and wear volume of the UHMWPE plates were determined using a three-dimensional form-measuring instrument (BHN-305, Mitsutoyo Co., Kanagawa, Japan) (see Fig. 29.9). The maximum distance of deformation from the original shape of the UHMWPE plate used with ceramic F-comp was 0.851 mm. The linear wear rate was estimated to be

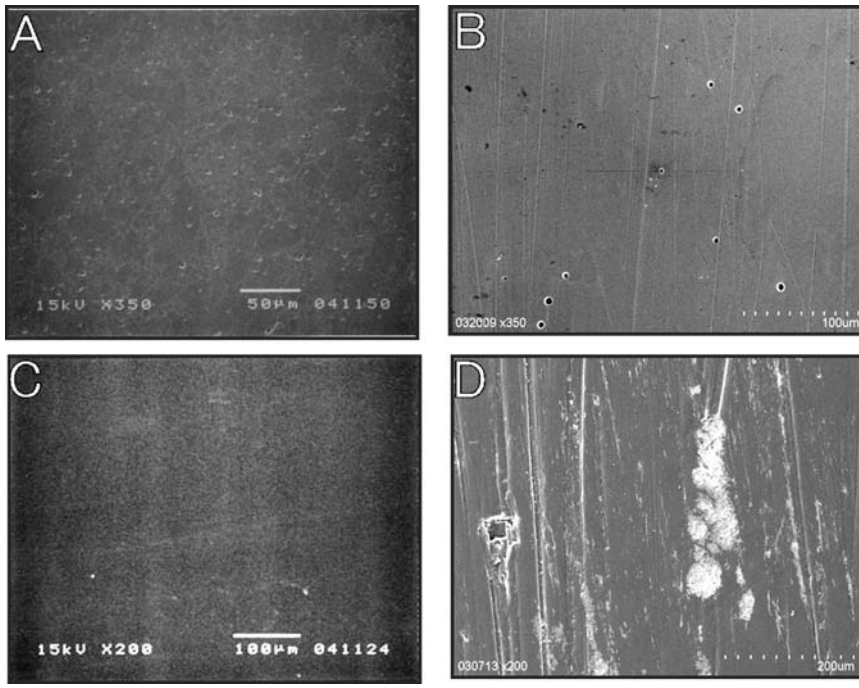

29.10 SEM images of bearing surface of retrieved TKPs:
(A) alumina ceramic F-comp; (B) metal F-comp (case 1);
(C) UHMWPE plate with alumina ceramic F-comp;
(D) UHMWPE plate with metal F-comp (case 1).

0.037 mm/year. On the other hand, the maximum distance of deformation of the UHMWPE plate used with the metal F-comp was 1.680 mm in case 1. The linear wear rate was calculated as 0.08 mm/year. In case 2, extreme damage of the medial area of the plate extended through the UHMWPE plate to the metallic T-comp. The linear wear was over 6 mm in this case. These findings demonstrated that the ceramic F-comp reduced the wear of the UHMWPE plate in TKP (Oonishi *et al.*, 2006a).

29.3.5 Advantages of ceramic TKP

Ceramic TKP is little used in the world except in Japan at present. The ceramic component has the advantage of decreasing the wear of the UHMWPE component in TKP as well as THP. Also in a severe wear condition such as the three-body wear condition, the worn area of ceramics will have a hollow profile, whereas that of metal will have a protruding profile. It is obvious which is preferable to reduce the wear of UHMWPE. Although ceramics is a brittle material, ceramic TKP is as safe

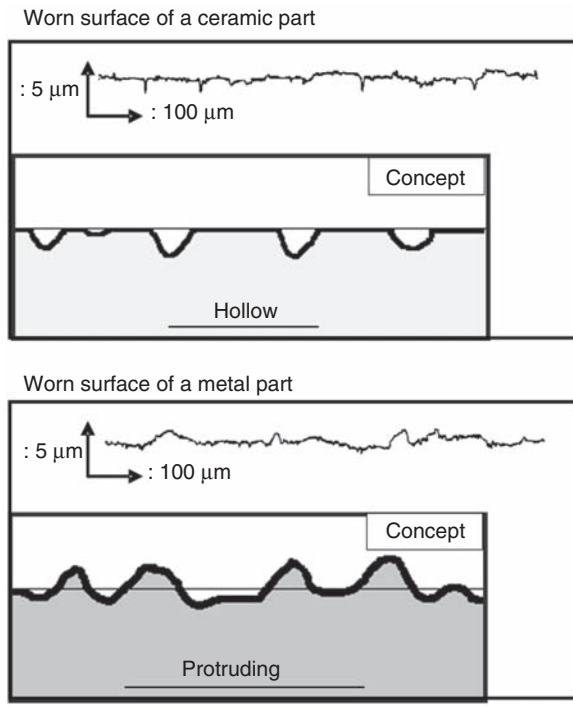

29.11 Surface profiles of a ceramic part and a metal part.

as ceramic THP, given correct design, good production process and proper usage.

29.3.6 Future trends

Highly cross-linked polyethylene for TKP have been developed by a couple of manufacturers recently. Although their clinical performance has not yet been published, results of wear tests using a knee joint simulator have revealed excellent durability on wear property (Muratoglu *et al.*, 2004; Akagi *et al.*, 2006). Highly cross-linked polyethylene will be a key material in solving the wear problem, if clinical results with it are good and it exhibits no problems.

A new femoral component made of zirconium alloy with a surface hardened by zirconium oxide is already on the market in Europe and the United States. However, a new zirconia–alumina composite ceramic has been developed for hip joint and knee joint prostheses (Nakanishi *et al.*, 2006). Future development of ceramics for total joint prostheses will aim to improve clinical reliability, i.e. the development of ceramics or ceramic–metal composite materials of increased strength and toughness.

29.4 Summary

One of the main problems with the total hip prostheses that originated from the Charnley-type prosthesis was wear of the UHMWPE socket. Our clinical and simulator studies clearly demonstrated that wear of UHMWPE sockets was reduced by changing the material of the femoral head of the THP to a ceramic from metal. For total condylar-type artificial knee joints as well, wear of UHMWPE was a principal problem. Use of ceramic femoral components was effective in decreasing wear of UHMWPE plates. It is our belief that the problem of wear in total hip joint prostheses has been almost completely solved with the use of highly cross-linked polyethylene. Although results for clinical performance of highly cross-linked polyethylene for knee joints are not yet available, results of wear tests using knee joint simulators have demonstrated excellent durability with little wear. Future development of ceramic materials for total joint prostheses will aim at improving clinical reliability, i.e. development of ceramics or ceramic-metal composite materials of increased strength and toughness.

29.5 References

Akagi M, Nakamura T, Matsusue Y, Ueo T, Nishijyo K, Ohnishi E (2000), 'The Bisurface total knee replacement: a unique design for flexion. Four-to-nine-year follow-up study', *J Bone Joint Surg Am* **82**: 1626–1633.

Akagi M, Asano T, Clarke IC, Niiyama N, Kyomoto M, Nakamura T, Hamanishi C (2006), 'Wear and toughness of crosslinked polyethylene for total knee replacements: a study using a simulator and small-punch testing', *J Orthop Res* **24**(10): 2021–2027.

Amstutz HC, Campbell P, Kossovsky N, Clarke IC (1992), 'Mechanism and clinical significance of wear debris-induced osteolysis', *Clin Orthop Relat Res* **276**: 7–18.

Bos I, Meeuwssen E, Henssge EJ, Lohrs U (1993), 'Differences in polyethylene wear between ceramic and metal on polyethylene hip prosthesis. A biopsy and postmortem study', *Z Orthop* **129**: 507.

Boutin P (1971), 'Alumina and its use in surgery of the hip', *Presse Med* **79**: 639–640.

Boutin P, Christel P, Dorlot JM, Meunier A, de Roquancourt A, Blanquaert D, Herman S, Sedel L, Witvoet J (1988), 'The use of dense alumina-alumina ceramic combination in total hip replacement', *J Biomed Mater Res* **22**: 1203–1232.

Charnley J (1970), 'Total hip replacement by low friction arthroplasty', *Clin Orthop Relat Res* **72**: 7–21.

Charnley J (1972), 'The long-term results of low-friction arthroplasty of the hip performed as a primary intervention', *J Bone J Surg Brit* **54B**: 61–77.

Charnley J, Cupid Z (1973), 'The nine and ten year results the low friction arthroplasty of the hip', *Clin Orthop Relat Res* **95**: 9–25.

Charnley J, Halley DK (1975), 'Rate of wear in total hip replacement', *Clin Orthop Relat Res* **112**: 170–179.

Heimke G, Griss P (1981), 'Five years experience with ceramic-metal-composites hip endoprostheses', *Arch Orthop Traumat Surg* **198**: 165.

Muratoglu OK, Bragdon CR, Jasty M, O'Connor DO, Von Knoch RS, Harris WH (2004), 'Knee-simulator testing of conventional and cross-linked polyethylene tibial inserts', *J Arthroplasty* **19**(7): 887–897.

Nakanishi T, Shikata K, Wang Y, Iwamoto M, Kondo M (2006), 'The characteristics of the new ceramic material for artificial joints', *Key Engineering Mater* **309–311**: 1235–1238.

Oonishi H, Hasegawa T (1981), 'Cementless alumina ceramic total knee prosthesis', *Orthopedic Ceramic Implants* **1**: 157–160.

Oonishi H, Igaki H, Takayama Y (1989), 'Comparisons of wear of UHMW polyethylene sliding against metal and alumina in total hip prostheses', in Oonishi H, Aoki H, Sawai K (eds). *Bioceramics* (*Proceedings of 1st International Bioceramic Symposium*), Tokyo Japan, Ishiyaku EuroAmerica, 272–277.

Oonishi H, Tsuji E, Mizukoshi T, *et al.* (1991), 'Wear of polyethylene and alumina in clinical cases of alumina total knee prostheses', *Bioceramics* **3**: 137–145.

Oonishi H, Aono M, Murata N, Kushitani S (1992), 'Alumina versus polyethylene in total knee arthroplasty', *Clin Orthop Relat Res* **282**: 95–104.

Oonishi H, Tsuji E, Kim YY (1998), 'Retrieved total hip prostheses. Part 1: The effect of cup thickness, head size and fusion defects on wear', *J Mater Sci: Mater Med* **9**: 393–401.

Oonishi H, Wakitani S, Murata N, Saito M, Imoto K, Kim S, Matsuura M (2000), 'Clinical experience with ceramics in total hip replacement', *Clin Orthop Relat Res* **379**: 77–84.

Oonishi H, Clarke IC, Masuda S, Amino H (2001a), 'Study of retrieved acetabular sockets made from high-dose, cross-linked polyethylene', *J Arthop* **16**(8); Suppl. 1: 129–133.

Oonishi H, Kadoya Y, Masuda S (2001b), 'Gamma-irradiated cross-linked polyethylene in total hip replacements – Analysis of retrieved sockets after long-term implantation', *J Biomed Mater Res (Appl Biomater)* **58**: 167–171.

Oonishi H, Fujita H, Itoh S, *et al.* (2002a), 'Development and improvement of ceramic TKA for 19 years and clinical results', *Key Eng Mater* **218–220**: 479–482.

Oonishi H, Fujita H, Itoh S, *et al.* (2002b), 'Surface analysis on retrieved ceramic total knee prosthesis', *Key Eng Mater* **218–220**: 499–502.

Oonishi H, Clarke IC, Yamamoto K, Masaoka T, Fujisawa A, Masuda S (2004), 'Assessment of wear in extensively irradiated UHMWPE cups in simulator studies', *J Biomed Mater Res* **68A**: 52–60.

Oonishi H, Kim SC, Kyomoto M, Masuda S, Asano T, Clarke IC (2005), 'Change in UHMWPE properties of retrieved ceramic total knee prosthesis in clinical use for 23 years', *J Biomed Mater Res Appl Biomater* **74B**: 754–759.

Oonishi H, Oonishi H, Kim SC, Kyomoto M, Iwamoto M, Masuda S, Ueno M (2006a), 'Ceramic total knee arthroplasty: advanced clinical experiences of 26 years', *Seminar in Arthroplasty* **17**: 134–140.

Oonishi H, Kim SC, Takao Y, Kyomoto M, Iwamoto M, Ueno M (2006b), 'Wear of highly cross-linked polyethylene acetabular cup in Japan', *J Arthrop* **21**(7): 944–949.

Oparaugo PC, Clarke IC, Malchau H, Herberts P (2001), 'Correlation of wear debris-induced osteolysis and revision with volumetric wear-rates of polyethylene. A survey of 8 reports in the literature', *Acta Orthop Scand* **72**: 22–28.

Schmalzried TP, Clarke IC, Mckellep H (1998), 'Bearing surface', in Callaghan JJ. and Rosenberg AG (eds). *The Adult Hip-us-*, USA, Lippincott Williams & Wilkins, 247–265.

Semlitsch M, Lehmann M, Weber H, Doerre E, Willert HG (1977), 'New prospects for a prolonged functional life-span of artificial hip joints by using the material combination polyethylene/aluminium oxide ceramin/metal', *J Biomed Mater Res* **11**(4): 537–552.

Shikita T, Oonishi H, Hashimoto Y, *et al.* (1977), 'Wear resistance of irradiated UHMW polyethylenes to Al_2O_3 ceramics in total hip prostheses', *Transactions of the 3rd Annual Meeting of the Society for Biomaterials* **3**: 118.

Sochart DH (1999), 'Relationship of acetabular wear to osteolysis and loosening in total hip arthroplasty', *Clin Orthop Relat Res* **363**: 135–150.

Ueno M, Okimatsu H, Amino H, Nishida M, Masuda S, Shimotoso T (2000), 'Experience on zirconia ceramic femoral heads in Japan', in *Zirconia Femoral Heads for Total Hip Protheses as a Proceedings of Sixth World Biomaterials Congress Workshops*, May 16, Hawaii, USA.

Zichner LP, Willert HG (1992), 'Comparison of alumina polyethylene and metal polyethylene in clinical trials', *Clinical Orthop Related Res* **292**: 86–94.

30

Tissue engineering using bioceramics

H OHGUSHI, National Institute of Advanced Industrial Science and Technology, Japan

30.1 Introduction: bioceramics as scaffolds for tissue engineering

When bioinert alumina (Al_2O_3) ceramics are implanted in the bone defects, fibrous tissue formation is seen between the host bone and ceramic surface and some areas show regenerated bone tissue in contact with the surface without other types of fibrous tissues intervening; however, the interface between the bone and the implants is not strong and the interface detaches easily upon shear and distraction loads. In contrast, when certain types of glass ceramics and calcium phosphate ceramics are implanted, chemical bonding is established between the regenerated bone tissue and the materials surface (Hench *et al.* 1971; Gross *et al.* 1988; Kokubo *et al.* 1986; Jarcho 1981; Kato *et al.* 1979). This bone/ceramics interface is very strong and stable, and breakage usually occurs inside the bone or ceramic but not at the interface upon loading. The ceramics are called bioactive ceramics (Hench *et al.* 1971).

Bone is formed by cells called osteoblasts which arise from progenitor cells in a multistep lineage cascade. At bone defect sites, the osteoblast progenitors are recruited from tissues of outside the bone and inside the bone (periosteum and bone marrow, respectively). That is, resected or injured bony sites induce the chemoattraction of multipotent mesenchymal progenitor cells, which originally reside in the marrow (Friedenstein *et al.* 1968; Owen 1985) or periosteum, and at the defect site, they become osteoblasts through a series of controlled differentiation steps. These progenitor cells are, herein, referred to as mesenchymal stem cells (MSCs) (Caplan 1991) and have capability to differentiate into various mesenchymal phenotypes, including osteogenic and chondrogenic cell types.

The MSCs can be expanded by tissue culture technique with small amount of human fresh bone marrow cells (Ohgushi and Okumura 1990; Haynesworth *et al.* 1992). The culture-expanded MSCs have capability to differentiate into active osteoblasts, which fabricate *in vitro* bone matrix

consisting of hydroxyapatite crystals (Maniatopoulos *et al.* 1988; de Bruijin *et al.* 1996; Ohgushi *et al.* 1996). We call the osteoblasts/bone matrix formation 'culture bone', which can show continuous new bone formation after *in vivo* implantation (Yoshikawa *et al.* 1996; Ohgushi and Caplan 1999). Importantly, the *in vitro* differentiation can be achieved by culturing on various materials including bioinert alumina ceramics (Kitamura *et al.* 2004). The present paper reviews the tissue engineered ceramics, which can show bone forming property resulting in direct bone contact without fibrous tissue intervening between thus formed bone and ceramic surface.

30.2 The experimental model for testing scaffold ceramics

As described, bioactive ceramics can show bone bonding property (Hench *et al.* 1971; Gross *et al.* 1988) and we hypothesized that the bonding can be achieved by the interaction between cells (osteoblasts) and surface of ceramics (Okumura *et al.* 1991a,b; Ohgushi and Caplan 1999; Ohgushi *et al.* 1992). The interaction can lead to tight bonding after fabrication of new bone by the osteoblasts onto the surface. To confirm the hypothesis, a unique experimental model was established. The model utilizes the heterotopic implantation of the marrow cells, which were impregnated into pore areas of the various ceramics (Fig. 30.1) (Ohgushi *et al.* 1989, 1990). The cells used were dispersed fresh marrow cells (not marrow tissue) as well as cultured MSCs (Ohgushi and Okumura 1990; Haynesworth *et al.* 1992). The ceramics used were bioactive and bioinert ceramics (Takaoka *et al.* 1996). The implantation sites were just under the skin; subcutaneous sites. As neither bone nor cartilage pre-exists at the sites, if we can detect the bone or cartilage, the tissue is *de novo* newly formed tissues. In fact, the marrow cells/porous hydroxyapatite (HA) ceramic composites can show obvious bone formation after 4 weeks' subcutaneous implantation.

30.3 Bioactive ceramics (composites of bioactive ceramics and marrow cells)

By analyzing rat marrow cells/porous HA composites implantation at heterotopic subcutaneous sites, consistent *de novo* bone formation has been observed (Ohgushi *et al.* 1989, 1990). Interestingly, the newly formed bone was usually found inside the internal pore regions and thus formed bone directly interfaced on the ceramic pore surface without fibrous tissue formation (Fig. 30.2). By analyzing the composite using scanning electron microscopy (SEM), the electrons prove microanalysis of (line analysis) at the bone/HA interface showed continuous high levels of calcium and phosphorus ions across the interface (Okumura *et al.* 1991a).

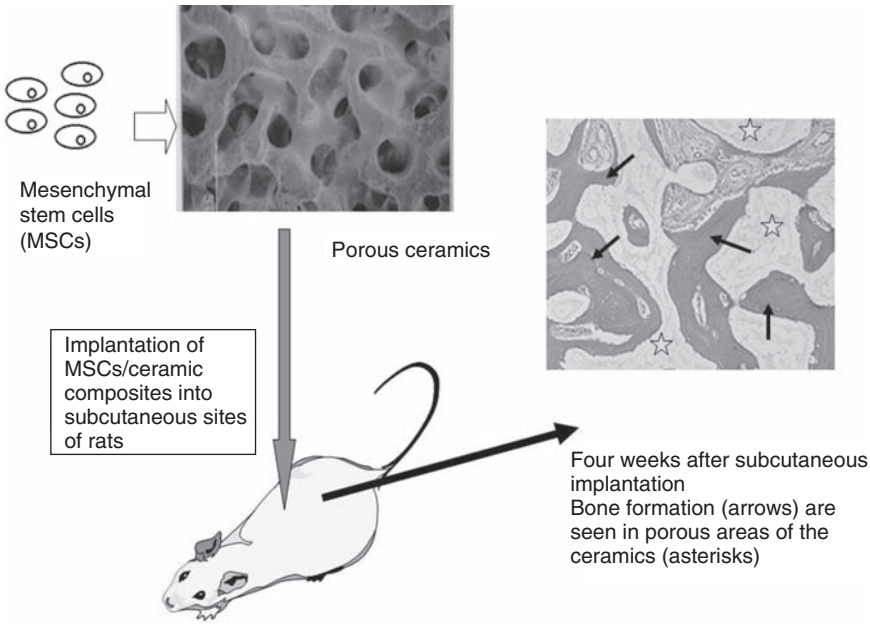

30.1 Schematic representation of marrow cells or MSCs /hydroxyapatite ceramic composite. About 4 weeks after the subcutaneous implantation, *de novo* bone formation (arrows in right figure) on ceramic (asterisks) pore areas can be observed.

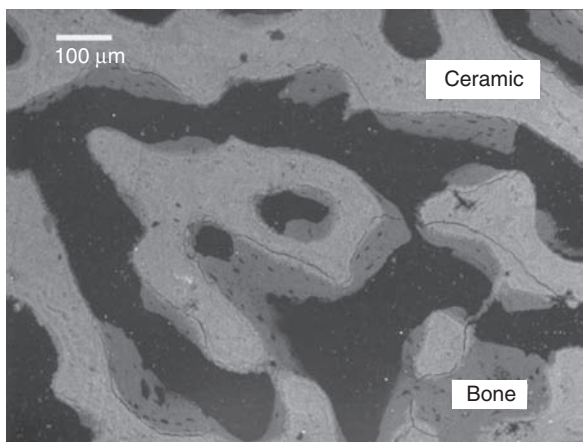

30.2 SEM of subcutaneous implantation of marrow/hydroxyapatite ceramic composite. Backscattered electron image which displays no intervening soft tissue (black area) between bone (gray area) and alumina ceramic (white area), indicating bone bonding to the ceramic surface. Reprinted from *Biomaterials* (1991), **12**, 411–416 'Bonding osteogenesis in coralline hydroxyapatite combined with bone marrow cells' by Okumura M., Ohgushi H. and Tamai S. with permission from Elsevier.

Undecalcified histological section of the composites showed that relatively small round cells attached on the surface of the ceramic and large round cells fabricated osteoid stream on the surface (Fig. 30.3). The SEM showed the matrix directly appositioned on the crystalline structure of HA surface; therefore there was no intervening soft tissue between HA and newly formed bone matrixes. These findings indicated that the round cells on the HA surface fabricated mineralized region initially on the surface. The cells can be recognized as osteoblasts because of their shape and capability to make mineralized region (osteoid). To prove the cells on the HA surface as osteoblasts, we performed immunohistochemical staining using antibody against osteocalcin and *in situ* hybridization to detect the mRNA of osteocalcin which is known to be the most reliable osteoblastic marker. The cluster of round (cuboidl) shaped cells on the HA surface were positive immunostaining against the antibody as well as mRNA, therefore the cells are recognized as osteoblasts (Okumura *et al.* 1997). Interestingly, relatively small shaped cells far upstream of the active osteoblasts lining on the HA

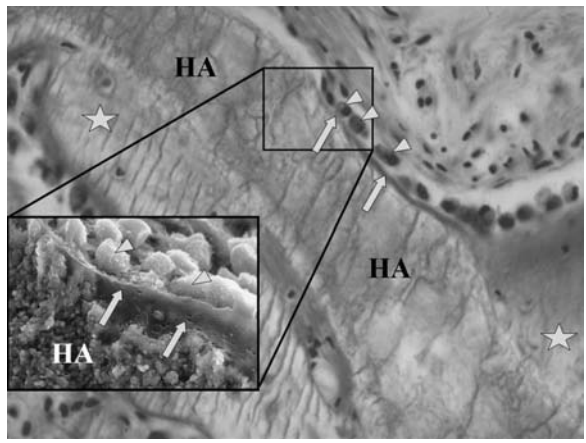

30.3 Unecalcified histological section of marrow/HA composite 3 weeks after subcutaneous implantation. The *de novo* bone (arrows) is directly appositioned on the surface of HA as partially mineralized bone and later become fully mineralized bone (asterisks). Cell lining of round shape osteoblasts (arrow heads) is clearly seen. Small round cell or rather fibroblastic cells (MSCs) are also seen on the surface of HA. The lower left figure demonstrates the fracture surface of the marrow/HA composites observed by SEM. Many large globular shaped cells (osteoblasts; arrow heads) are seen on the surface of HA. The osteoblasts make early partially mineralized bone (arrows) on the HA surface. Reprinted from *Biomaterials* (1991), **12**, 411–416 'Bonding osteogenesis in coralline hydroxyapatite combined with bone marrow cells' by Okumura M., Ohgushi H. and Tamai S. with permission from Elsevier.

surface were also stainable to osteocalcin antibody, though the stainability was relatively weak. The findings indicate that the small cells on the HA surface were probably preosteoblasts. We also used other types of bioactive ceramics such as AW-ceramics, tricalcium phosphate ceramics and calcium carbonate, all of which supported the osteoblast lining as well as tight bone bonding to the ceramic surface.

These sequential (temporal) analyses of the bone formation indicate that: (1) a few mesenchymal progenitor cells from whole dispersed marrow attach on the ceramic pore surface, (2) the attached cells proliferate on these ceramic surfaces, (3) the cells form a continuous cell layer on the surface of the pores, (4) cell differentiation of these progenitor cells results in the appearance of a continuous layer of osteoblasts on the pore surface, (5) the osteoblasts fabricate immature primary bone onto the surface and (6) the primary bone becomes mature and forms fully mineralized bone (Ohgushi *et al.* 1989, 1990; Okumura *et al.* 1997).

Before the attachment of these cells, the ceramics show the surface change including dissolution and precipitation phenomena which lead to carbonate containing hydroxyapatite precipitated layer on its surface (Kokubo *et al.* 1990; LeGeros *et al.* 1991; Ducheyne *et al.* 1992). It is well known that HA adsorbs many protein and other macromolecules, and thus during formation of the HA layer on the ceramics, other biological molecules also integrate into the layer. These surface changes favor cell attachment and subsequent cell differentiation. Though the nature of the biological molecules to evoke the attachment and differentiation is not certain, cell binding proteins having the RGD sequence probably have some role. In this regard, the appearance of osteopontin mRNA expression in the marrow/ceramic composite transplantation has been documented and exogenously added fibronectin or laminin promotes MSC attachment and osteoblastic differentiation of the composites (Dennis *et al.* 1992). Both osteopontin and fibronectin contain RGD peptide. Others also reported the importance of osteopontin and fibronectin molecules in bone/material interface. These molecules on the ceramics surface play a role in attracting MSCs and, thus, contribute to the osteoblastic differentiation process.

30.4 Bioinert ceramics (composites of alumina and marrow cells)

In contrast to the bone formation pattern in the implants of marrow cell/bioactive material composites, bone formation always starts away from the surface in the marrow cell/non-bioactive materials (Fig. 30.4). Usually an intervening fibrous layer covers and encapsulates the non-bioactive materials, and the *de novo* bone does not directly touch the material. However, in the composites of marrow cells and some non-bioactive materials, such as

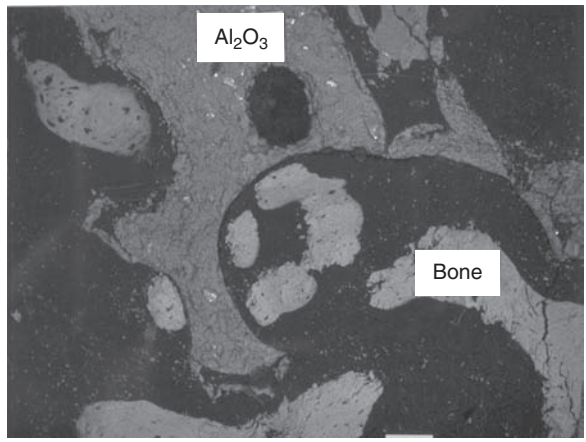

30.4 Subcutaneous implantation of marrow/alumina ceramic composite. Backscattered electron image which displays intervening soft tissue (black area) between bone (white area) and alumina ceramic (gray area).

alumina ceramics and titanium implants, some small areas showed bone apposition without intervening fibrous tissue (Takaoka *et al.* 1996). At these areas, newly formed bone formed towards the material surface and replaced the intervening fibrous tissue, thus bone bonding did not occur in this situation. It is also known that alumina does not show surface changes involved in apatite formation on its surface. Therefore, alumina is not classified as bioactive. Implanted marrow cell/titanium composites exhibit comparable results to marrow cell/alumina composites with some areas showing bone contact with the titanium, although bone formation started away from the titanium surface. However, titanium is somewhat different from alumina ceramics, because titanium is a reactive metal on which an oxide can spontaneously form; this oxide has been shown to react with mineral ions and fabricate a calcium/phosphate layer (Hanawa 1991; Kim *et al.* 1997). Therefore, there is the possibility that titanium can function as a bioactive material under some conditions. These observations of marrow/material composites showed that the implantation of composites is a useful tool to distinguish bioactive materials from non-bioactive materials.

30.5 Tissue engineering approach

30.5.1 *In vitro* bone matrix/osteoblasts formation on culture dish

MSCs were seeded at 100×10^3 cells/35 mm culture plate for culture in the presence of vitamin C, β-glycerophosphate and dexamethasone (DEX).

Phase contrast microscopy showed a cluster of many cuboidal cells surrounded by abundant extracellular matrices that appeared about 7 days post-culture. The central area of the cluster showed early mineralized area (nodule). The nodules were stained with alizarin red, indicating calcium deposition, and stained also with alkaline phosphatase (ALP). A northern blot analysis and *in situ* hybridization clearly showed the intensive signal of osteocalcin mRNA in DEX treated cells, whereas there was no signal of the mRNA in DEX untreated cells. These morphological findings support that the mineralized area found in the cultured cells by the treatment of DEX was not simple calcification produced by co-precipitation of calcium and phosphorus from the culture medium but bone mineral fabricated by differentiated active osteoblasts. Fourier transform infrared spectrometer (FTIR) spectra and X-ray analyses of the nodules indicated the poorly crystallized carbonated apatite formation, which is seen in natural bone crystals (Ohgushi *et al.* 1996).

Taken together, we propose the following overall process of mineralized nodule formation. Initially, a number of MSCs expand and cover the culture plate surface. They differentiate into osteoblasts and organize into an unmineralized matrix. Matrix mineralization (mineralization front) occurs at the surface of the culture plate and thus the osteoblasts are jacked up after this mineralization. Some osteoblasts remain in the mineralized matrix and further differentiate into osteocytes (upper figure in Fig. 30.5). This mineralization process of *in vitro* bone tissue is similar to that of *in vivo* natural bone regeneration such as appositional bone formation (lower figure in Fig. 30.5). Therefore, the *in vitro* mineralization is a counterpart of the *in vivo* bone formation and can be considered as 'cultured bone'. The results clearly show that the cultured bone is comparable to normal *in vivo* bone tissue.

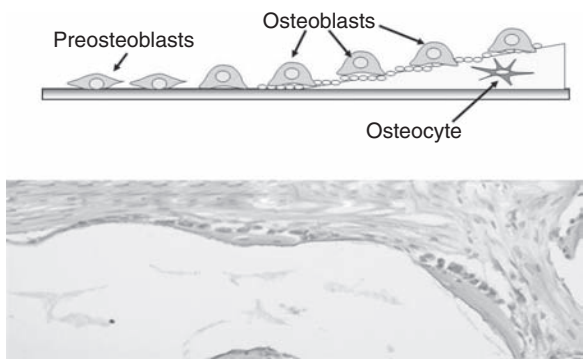

30.5 Schematic representation of *in vitro* bone formation (upper figure) and *in vivo* bone found in histological section (lower figure) of marrow/hydroxyapatite ceramic composite at subcutaneous sites.

This was confirmed by our novel approach using confocal laser scanning microscopy (CLSM), which depicts direct visualization of the 3D structure of the mineralized tissue such as osteoblast lining on bone matrix together with osteocytes in lacunae. Furthermore, this system of 3D visualization using CLSM enables continuous observation of the same sample during the culture period. This real-time monitoring system could be a useful tool for confirming the mechanism used by cells to organize into *in vitro* tissue (Kihara *et al.* 2004).

30.5.2 Characterization of human mesenchymal stem cells (MSCs)

The characterization of MSCs is of great interest or clinical applications. Nevertheless, definitive markers of MSCs have not been established. In much of the literature, the MSCs from bone marrow could easily adhere to the bottom of a culture dish *in vitro*. Their shapes are not round but rather fibroblast-like spindles, and thus the adherent cells from bone marrow with a fibroblastic profile are termed MSCs or mesenchymal progenitor cells. Hereafter, we use the term MSCs to mean the adherent fibroblastic cells derived from bone marrow. When we poured fresh bone marrow cells into tissue culture polystyrene (TCPS) dishes, the visible cells were mostly red blood cells with a scant amount of nucleated round cells. After two or three medium changes in the primary culture, adherent fibroblastic cells (MSCs) could be observed on the surface of the culture dishes after involuntary elimination of floating blood and hematopoietic stem cells, which also reside in fresh bone marrow preparation. After about 10 days, fibroblastic cells were observed throughout the TCPS dishes and there was little evidence of round or floating cells. These findings indicate that MSCs can be enriched without the contamination of hematopoietic cells (Kotobuki *et al.* 2004; Ohgushi *et al.* 2005).

We usually take 3 ml aspirated marrow cells from donor iliac bone and place them into two T-75 flasks. From this 3 ml of fresh bone marrow, we harvest about 10×10^6 adherent MSCs after about 10 days of the primary culture. For characterizations of the MSCs, we performed cell surface antigen analysis by flow cytometry. The analysis demonstrated that the fibroblastic cells were negative for hematopoietic markers (CD14 and CD34) but positive for antigens present in mesenchymal cells (CD29 and CD44). These results were similar to those of definitive MSCs, implying that the cultured cells derived from bone marrow were mesenchymal types (Fig. 30.6). Although the MSC number in marrow decreased with age, the number of MSCs can be expanded under *in vitro* culture conditions where MSCs retain their ability to differentiate into osteogenic lineage regardless of the original donor's age. Importantly, the culture-expanded MSCs from the

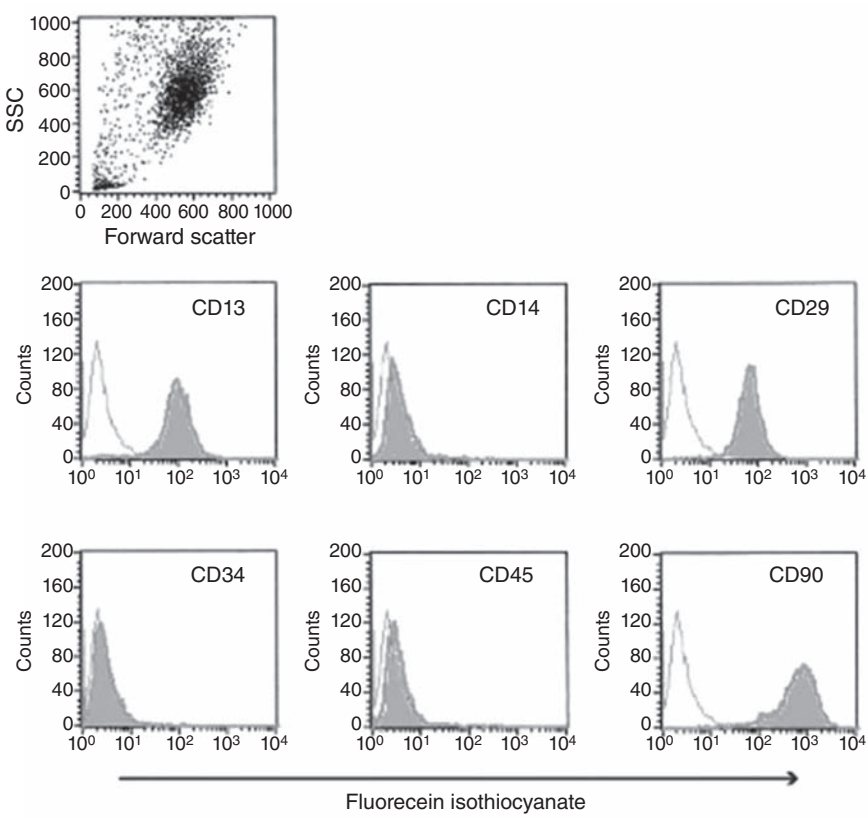

30.6 Cell surface antigen analysis of human adherent fibroblastic cell (MSCs) Human MSCs were cultured for 7 days up to 80% confluence. After trypsin treatment, cells were reacted with each CD antibody and then loaded into a flow cytometer. The open histograms show the fluorescence intensity of the cells with negative control IgG. The closed histograms show the fluorescence intensity of the cells with each CD antibody. Reprinted from *Biomaterials* (2005), **26**, 4654–4661 'Tissue engineered ceramic artificial joint' by Ohgushi H. *et al.* with permission from Elsevier.

marrow of very old patients can be expected to exhibit effective osteogenic differentiation. Thus, aged patients with skeletal defects can benefit from tissue engineering approaches to regenerate skeletal tissue. Our experience showed that fresh marrow from patients over 80 years old can be used for successful culture expansion of MSCs.

We also demonstrated the availability of cryopreserved MSCs. After storage for more than 3 years, cryopreserved cells had a surprisingly high degree of about 90% viability, indicating that long-term cryopreservation for several months is not a critical problem for cell viability (Kotobuki

et al. 2005). This durability may reflect the nature of the stem cells used in the preparation of our MSCs. Most of these living cells attached to culture-grade dishes in a manner similar to primary cultured cells. The attached cells proliferated well and showed a high degree of osteogenic activity comparable to that of primary cultured cells. Although several data indicated individual differences in cell viability and osteogenic activities, long-term cryopreservation did not seriously affect these aspects. The results clearly showed that cryopreserved human MSCs could be stored and maintain high degrees of viability and osteogenic potential. Furthermore, the cryopreserved cells were morphologically, phenotypically and functionally comparable with primary cultured MSCs. In future, cryopreserved MSCs could become a promising candidate of cell sources for the fabrication of culture bone tissues available for a wide range of solutions to bone/joint problems.

30.5.3 *In vitro* bone matrix/osteoblasts formation on bioinert alumina ceramic surface

To fabricate the bone matrix/osteoblasts (cultured bone) on bioinert alumina ceramics, we provided three types of culture substrate (Fig. 30.7).

Roughness average (Ra) and sessile contact angle (SCA)

	Ra (nm) ± SD	SCA (°) ± SD
P-alumina disk	5.4 ± 1.1	73.5 ± 3.2
S-alumina disk	5.0 ± 2.0	72.9 ± 3.7
TCPS dish	11.4 ± 4.0	67.1 ± 2.4

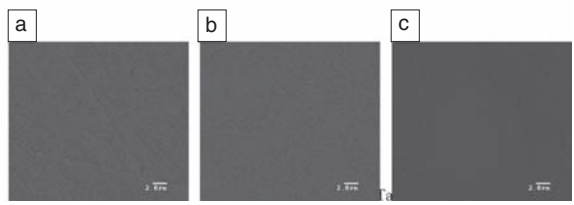

30.7 Surface roughness and SEM micrographs of P- and S-alumina disks and a TCPS dish. The surface structures of a polycrystalline–alumina (P-alumina) disk (a), single-crystal alumina (S-alumina) disk (b) and tissue culture polystyrene (TCPS) dish (c) all exhibit a very fine surface, with little grain structure being visible on the surface of the P-alumina disk (a). (Bar: 2μm.) Reprinted from *Artif Organs* (2004), **28**, 72–82 'Osteogenic differentiation of human bone marrow-derived mesenchymal cells cultured on alumina ceramics' by Kitamura S. *et al.* with permission from Blackwell Publishing.

Alumina ceramic disks (30 mm diameter, 1.5 mm thick, 99.5% pure polycrystalline–alumina: referred as P-alumina), transparent single-crystal alumina disk (referred as S-alumina) and gold standard for tissue culture; tissue culture polystyrene (TCPS) dishes. Human MSCs were cultured in the osteogenic media with DEX (Kitamura *et al.* 2004). During the 2 week culture period, the proliferation and differentiation of the MSCs on the transparent S-alumina disks, as well as the control TCPS dishes, were compared by phase contrast microscopy. Subsequently, the cells cultured on both substrates showed a similar proliferating pattern, and reached confluence at day 7. At day 14 of the culture, the DEX(+) cells cultured on both the S-alumina disks and TCPS dishes formed nodular aggregates indicating mineralization. Thus, cell attachment to the substrates, proliferation and the mineralization of MSCs occurred in much the same way on all the alumina surfaces as well on as the culture dish surface. ALP and Alizarin Red S staining of the cells cultured on the P- and S-alumina disks, as well as those on the control TCPS dishes, were performed. As shown in Fig. 30.8, the DEX-treated cells on each substrate were strongly stained with ALP, indicating osteoblastic differentiation of the MSCs.

Recently, we reported a novel quantitative method for detecting mineralization by cultured cells utilizing a calcium-binding fluorescent calcein dye. Calcein has been found to be specifically incorporated and deposited into extracellular bone matrix as evidenced by co-staining with Alizarin Red S (Uchimura *et al.* 2003). The advanced characteristics of the method included the monitoring of the mineralization of the same specimens of cultured cells in a time-dependent manner due to continuous cultivation without the fixation processes of the cell layers. To demonstrate the calcium deposition of the cultured MSCs over time period, we added calcein to the culture medium whenever the medium was renewed. The fluorescence of the calcein incorporated into the mineralized extracellular matrix of the S-alumina disks and control TCPS dishes was clearly visualized by using a fluorescence microscope. The calcein uptake of the cells cultured on the S-alumina disks appeared to be comparable to that of cells cultured on TCPS dishes (Fig. 30.9). At day 7 of the culture, many fluorescent spots could be seen in the cells cultured with DEX (Fig. 30.9, day 7+). Subsequently, the fluorescent areas enlarged with time such that, at day 14, fluorescent aggregates were observed in those locations where mineralization (dark/dim areas) were shown by phase contrast microscopy (Fig. 30.9, day 14+). In contrast, we could barely detect any fluorescence in those cells cultured without DEX (Fig. 30.9, day 14–).

These data indicate the osteogenic differentiation capability of human MSCs cultured on alumina disks as well as on TCPC dishes. Interestingly, the cells from elderly persons (62 and 75 years old), a middle-aged person (58 years old), and a young person (25 years old) showed similar high levels

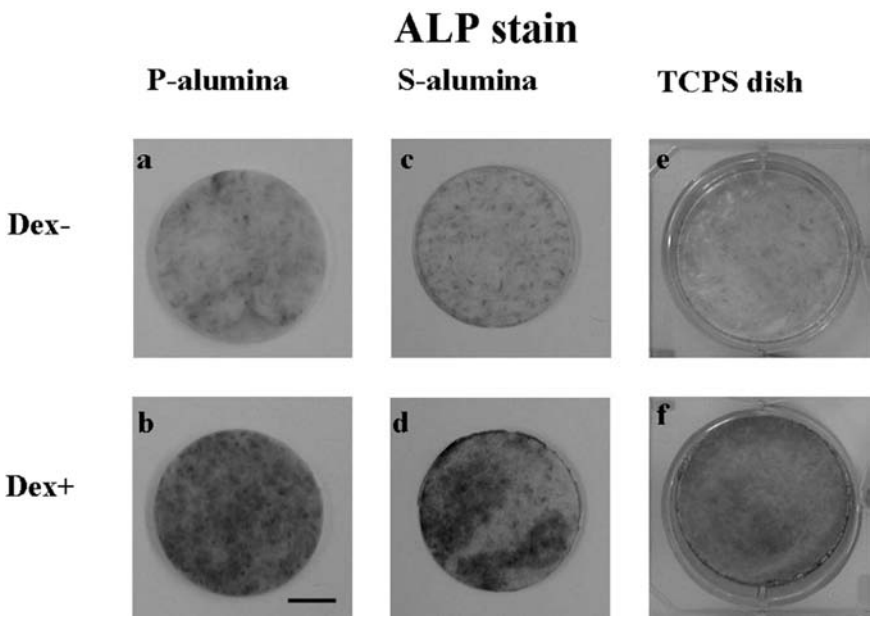

30.8 ALP stain of human MSCs cultured for 2 weeks on P- and S-alumina disks, and control TCPS dishes. The culture was done on P-alumina disks, S-alumina disks and TCPS dishes in the presence (DEX+) or absence (DEX–) of dexamethasone. After 2 weeks, ALP staining was performed. The cells cultured with DEX (b, d, f) were found to be more intensely stained with ALP than those cultured without DEX (a, c, e) on all culture substrates. (Bar: 10 mm.) Reprinted from *Artif Organs* (2004), **28**, 72–82 'Osteogenic differentiation of human bone marrow-derived mesenchymal cells cultured on alumina ceramics' by Kitamura S. *et al.* with permission from Blackwell Publishing.

of ALP activity, osteocalcin content and calcium content. These results proved that the human bone marrow obtained from an aged person could proliferate and differentiate into active osteoblasts that are concomitant with bone matrix formation on the alumina ceramic surface, i.e. fabrication of cultured bone (Kitamura *et al.* 2004).

30.6 Clinical application of tissue engineered ceramics

Total joint replacement means the bone surfaces within the joint are surgically removed and replaced with synthetic materials, usually prostheses made of durable, wear-resistant polyethylene and metal/ceramic. Following a successful procedure, most patients can resume an active, fulfilling lifestyle. However, countless papers report complications such as infection,

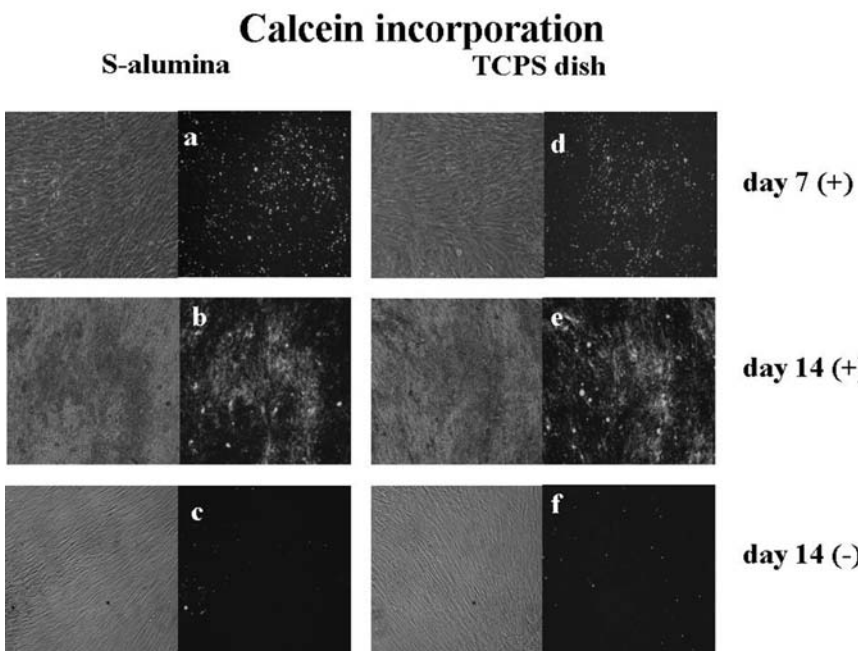

30.9 Fluorescent micrographs of the calcein incorporated into the human MSCs cultured on the S-alumina disks and control TCPS dishes. The MSCs were cultured on S-alumina disks and control TCPS dishes with (+) or without (–) dexamethasone (DEX). To demonstrate calcium deposition with time during the subsequent culture periods, calcein was added to the culture medium whenever the medium was renewed. The fluorescence of the calcein incorporated into the mineralized matrix of the MSCs cultured on the S-alumina disks and TCPS dishes was clearly visualized by fluorescent microscopy. Each micrograph (a to f) represents both the phase-contrast (left) and fluorescent (right) view, respectively. The calcein uptake of the cell layers on the S-alumina disks appeared to be comparable to those on the TCPS dishes. At day 7, many fluorescent spots were clearly observed in the cells cultured with DEX (a, d). After 14 days of culture, the location of the fluorescent uptake appeared to coincide with the dark areas seen in the phase contrast view (b, e). The dark areas in the phase contrast micrographs are the mineralized matrix of the cultured cells. Fluorescence (mineralization) was barely detected in those cells cultured without DEX (c, f) even after 14 days of culture. Reprinted from *Artif Organs* (2004), **28**, 72–82 'Osteogenic differentiation of human bone marrow-derived mesenchymal cells cultured on alumina ceramics' by Kitamura S. *et al.* with permission from Blackwell Publishing.

dislocation and loosening at the host bone–implant interface. Many patients with complications need to have revision surgery but the results of surgery are never as good as are obtained with initial procedures in general cases. Aseptic loosening around the joint prosthesis within the bone occurs in all kinds of prostheses and, thus, we tried the tissue engineering approach to establish a general method of solving the problem of joint loosening. The approach consists of three steps: (1) proliferation of mesenchymal cells from the patient's bone marrow by culture (Fig. 30.10A,B); (2) osteogenic differentiation of the culture expanded cells resulting in the appearance of bone-forming osteoblasts together with bone matrix formation (cultured bone formation) on the ceramic prosthesis (Fig. 30.10C,D) and (3) implantation of the prostheses in the same patient (total ankle joint replacement surgery: Fig. 30.11D,E).

To obtain the mesenchymal cells, we added the cells from 3 ml fresh marrow into two 75 cm^2 plastic culture flasks and cultured with the medium

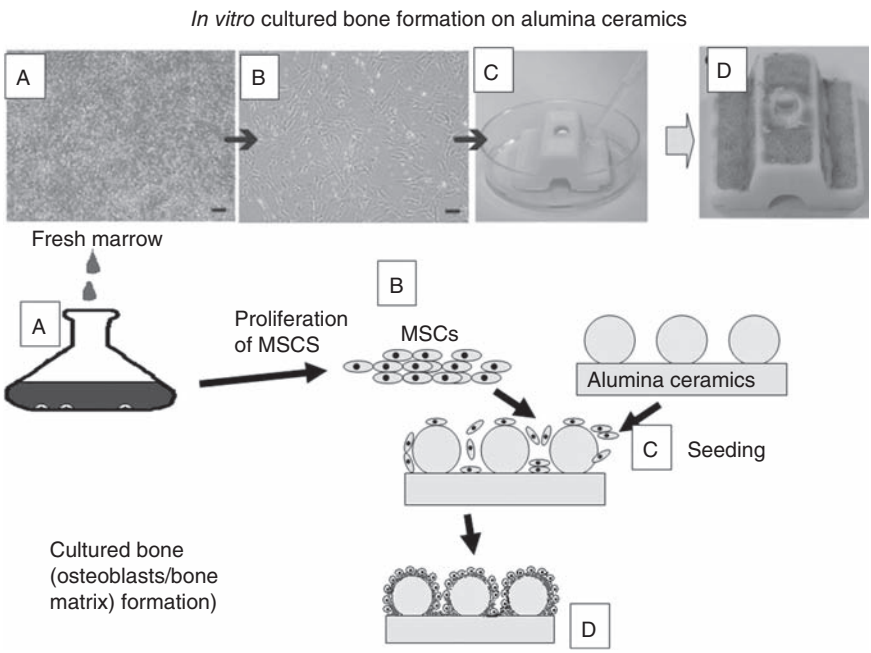

30.10 Schematic representation of fabrication of tissue engineered alumina ceramic implants. After expansion of MSCs from patients fresh marrow (A to B), the culture expanded MSCs were seeded on alumina ceramics (C). The seeded MSCs could undergo *in vitro* osteogenic differentiation, resulted in cultured bone formation (D). Upper figure is reprinted from *Biomaterials* (2005), **26**, 4654–4661 'Tissue engineered ceramic artificial joint' by Ohgushi H. *et al.* with permission from Elsevier.

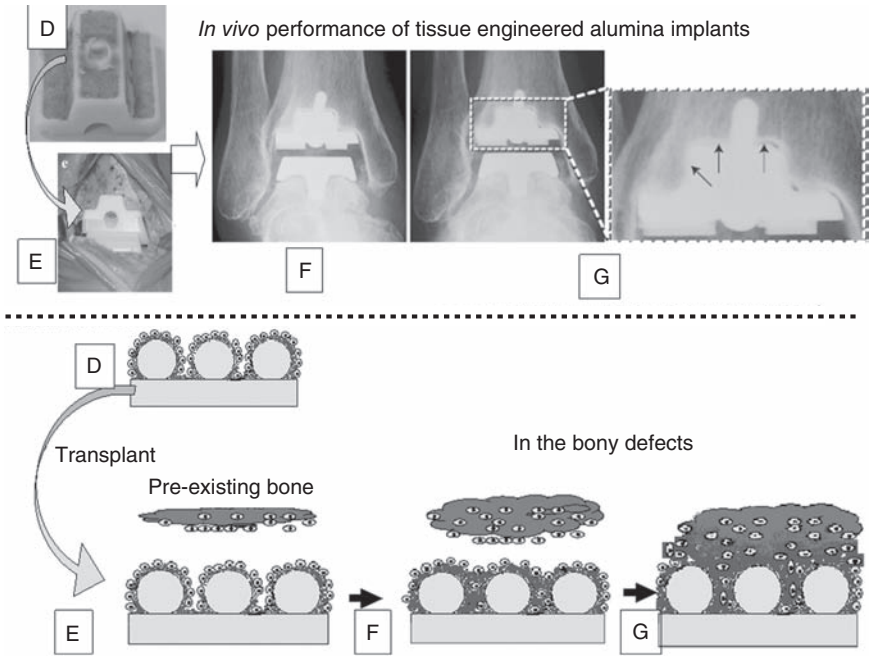

30.11 Schematic representation of *in vivo* performance of *in vitro* fabricated cultured bone after its implantation in bone defect. Tissue engineered alumina implants (D; implants having culture bone) can show new bone formation after implantation (F). The new bone well integrates with bone from host origin, resulting in firm bone union (G). Upper figure is reprinted from *Biomaterials* (2005), **26**, 4654–4661 'Tissue engineered ceramic artificial joint' by Ohgushi H. *et al.* with permission from Elsevier.

containing 15% patient's own serum. After 10–11 days, the number of adherent cells (MSCs) grew and reached more than several million. The MSCs were collected after trypsinization (first passage) and further cultured in other flasks. The adherent mesenchymal cells were trypsinized (second passage) and applied to the surface of ceramic ankle components (Fig. 30.10C) and cultured in the above medium supplemented with beta-glycerophosphate, vitamin C and DEX for 2 weeks (Fig. 30.10C,D). Calcium accumulation, ALP activity on ceramic were marked. The data indicated that the surface of the ceramic prosthesis was covered with the patient's derived cultured osteoblasts/bone matrix (cultured bone formation). Thus, we succeeded in fabricating tissue engineered total ankle prosthesis (Ohgushi *et al.* 2005).

Using the tissue engineered ankle prosthesis, we reported initial three cases of 61–70-year-old patients having osteoarthritic changes of ankle

joints. The follow-up period was 25–30 months. None of the patients exhibited any obvious inflammation or complications such as infection. Evaluation after the operation was undertaken using a clinical ankle score (maximum is 100 points). Before the operation, the average score was 26, while at 3, 6, 12 and 24 months after the operation the scores were 72, 86, 87 and 86 respectively. The X-ray findings showed that radiodense areas (indicating bone formation) began to appear around the cell-seeded areas on the prosthesis about 2–3 months after the operation, since the areas become clearly noticeable (Fig. 30.11F). The initial radiodense appearance together with a good clinical score proved the establishment of a stable host bone–prosthesis interface even a few months after the operation. The interface is quite durable even 2 years after the operation (Fig. 30.11G) and showed high clinical scores. Therefore, loosening of the total joints could be avoided with the tissue engineered approach using MSCs. The stable interface (radio dense areas) was localized at areas of the implants where the cultured cells were seeded (Fig. 30.11G, arrows). However, the unseeded areas of the implants did not show bone fixation at any time after the surgery. The findings confirmed the importance of cell seeding (tissue engineering approach) for early bone fixation.

Consequently, we can cover the alumina ankle prosthesis with bone matrix. The matrix was fabricated by osteoblasts derived from the patient's bone marrow and, significantly, the fabrication could be accomplished inside the pore areas of the ceramic. In addition to the matrix fabrication, active osteoblasts also existed in the pore regions. Therefore, we have succeeded in fabricating cultured bone on total ankle prosthesis, which can be expected to show successful bone-prosthesis fixation.

Fabrication of the tissue engineered prosthesis requires use of the patient's marrow cells containing mesenchymal cells. However, the amount of marrow cells required is very small (only 3 ml) and due to the minimum invasion (needle aspiration), none of the patients complained of severe pain or needed hospitalization until the actual joint surgery. Furthermore, use of an engineered prosthesis consisting of autologous cells avoided immunological reactions and did not cause inflammation around the implanted areas.

30.7 Summary

In conclusion, our current results confirm the *in vitro* osteogenic differentiation capability of human mesenchymal cells (MSCs) cultured on alumina ceramics. Importantly, the cells were derived from bone marrow cells obtained with minimum invasion using needle aspiration. The cultured bone could prevent the aseptic loosening of total joint prostheses having rough/porous alumina surfaces. Although, the clinical data describe a novel method using the patient's marrow cells for the treatment of total ankle

replacement, the method can be applied on any type of joint replacement including total hip and knee replacements. In addition, the mesenchymal cells can be cultured/differentiated into osteoblasts on many other biomaterials including metal and polymers. Therefore, this novel tissue engineering approach can be used for various clinical applications in the fields of orthopedic, craniomaxillofacial and plastic surgery.

30.8 Acknowledgments

I thank our colleagues at the National Institute of Advanced Industrial Science and Technology (AIST) and at Nara Medical University, Japan. Especially I thank Professor Y. Takakura at the Department of Orthopaedics, Nara Medical University, for his help concerning the clinical application of the tissue engineered ceramics. This work was supported by the Three-Dimensional Tissue Module Project of METI (a Millennium Project), grants from Scientific Research Japan and New Energy and Industrial Technology Development Organization of Japan.

30.9 References

de Bruijin J.D., vd Brink I. and Bovell Y.P. (1996). 'Development of human bone marrow culture to examine the interface between apatite and bone formed *in vitro*' in *Bioceramics* vol. 9, p. 45–48, T. Kokubo, T. Nakamura, F. Miyaji eds, Elsevier Science, Oxford, UK.

Caplan A.I. (1991). 'Mesenchymal stem cells.' *J. Ortho. Res.* **9**, 641–650

Dennis J.E., Haynesworth S.E., Young R.G. and Caplan A.I. (1992). 'Osteogenesis in marrow-derived mesenchymal cell porous ceramic composites transplanted subcutaneously: effect of fibronectin and laminin on cell retention and rate of osteogenic expression.' *Cell Transpl.* **1**, 23–32

Ducheyne P., Radin S. and Ishikawa K. (1992). 'The rate of calcium phosphate precipitation on metal and ceramics, and the relationship to bioactivity' in *Bone–bonding Biomaterials*, P. Ducheyne, T. Kokubo and van Blitterswijk C.A. (eds), Reed Healthcare Comm. Publ., Leiderdorp, The Netherlands, pp. 213–218.

Friedenstein A.J., Petrakova K.V., Kurolesova A.I. and Frolova G.D. (1968). 'Heterotopic transplants of bone marrow, analysis of precursor cells for osteogenic and haemopoietic tissues.' *Transplantation* **6**, 230–247

Gross U.M., Schmitz H.J. and Strunz V. (1988). 'Surface activities of bioactive glass, aluminum oxide and titanium in a living environment.' *Ann. NY Acad. Sci.* **523**, 211–226

Hanawa T. (1991). 'Titanium and its oxide film: a substrate for formation of apatite' in *The Bone–Biomaterial Interface*, J.E. Davies (ed.), University of Toronto Press, Toronto, pp. 49–61

Haynesworth S.E., Goshima J., Goldberg V.M. and Caplan A.I. (1992). 'Characterization of cells with osteogenic potential from human marrow.' *Bone* **13**, 81–88

Hench L.L., Spliner R.J., Allen W.C. and Greenlee T.K. (1971). 'Bonding mechansm at the interface of ceramic prosthetic materials.' *J. Biomed. Mater. Res. Symp.* **2**, 117–141

Jarcho M. (1981). 'Calcium phosphate ceramics as hard tissue prosthetics.' *Clin. Orthop.* **157**, 259–278

Kato H., Aoki H., Tabata T. and Ogiso M. (1979). 'Biocompatibility of apatite ceramics mandibles.' *Biomater. Med. Devices Artif. Organs.* **7**, 291–297

Kihara T., Oshima A., Hirose M. and Ohgushi H. (2004). 'Three-dimensional visualization analysis of *in vitro* cultured bone fabricated by rat marrow mesenchymal stem cells.' *Biochem. Biophys. Res. Commun.* **316**, 943–948

Kim H.M., Miyaji F., Kokubo T. and Nakamura T. (1997). 'Bonding strength of bonelike apatite layer to Ti metal substrate.' *J. Biomed. Mater. Res.* **38**, 121–127

Kitamura S., Ohgushi H., Hirose M., Funaoka H., Takakura Y. and Ito H. (2004). 'Osteogenic differentiation of human bone marrow-derived mesenchymal cells cultured on alumina ceramics.' *Artif. Organs.* **28**, 72–82

Kokubo T., Ito S., Sakka S. and Yamamuro T. (1986). 'Formation of a high-strength bioactive glass-ceramic in the system MgO–Ca–SiO_2–P_2O_5.' *J. Mater. Sci.* **21**, 536–540

Kokubo T., Kushitani H., Sakka S., Kitugi T. and Yamamuro T. (1990). 'Solutions able to reproduce *in vivo* surface-structure changes in bioactive glass-ceramic A-W.' *J. Biomed. Mater. Res.* **24**, 721–734

Kotobuki N., Hirose M., Takakura Y. and Ohgushi H. (2004). 'Cultured autologous human cells for hard tissue regeneration: preparation and characterization of mesenchymal stem cells from bone marrow.' *Artif. Organs.* **28**, 33–39

Kotobuki N., Hirose M., Machida H., Katou Y., Muraki K., Takakura Y. and Ohgushi H. (2005). 'Viability and osteogenic potential of cryopreserved human bone marrow-derived mesenchymal cells.' *Tissue Eng.* **11**, 663–673

LeGeros R.G., Orly I., Gregoire M. and Daculsi G. (1991). 'Substrate surface dissolution and interfacial biological mineralization' in *The Bone–Biomaterial Interface*, J.E. Davies (ed.), University of Toronto Press, Toronto, pp. 76–88

Maniatopoulos C., Sodek J. and Melcher A.H. (1988). 'Bone formation in vitro by stromal cells obtained from marrow of young adult rats.' *Cell Tissue Res.* **254**, 317–330

Ohgushi H. and Caplan A.I. (1999). 'Stem cell technology and bioceramics: from cell to gene engineering.' *J. Biomed. Mater. Res.* **48**, 913–927

Ohgushi H. and Okumura M. (1990). 'Osteogenic ability of rat and human marrow cells in porous ceramics.' *Acta Orthop. Scand.* **61**, 431–434

Ohgushi H., Goldberg V.M. and Caplan A.I. (1989). 'Heterotopic osteogenesis in porous ceramics induced by marrow cells.' *J. Orthop. Res.* **7**, 568–578

Ohgushi H., Okumura M., Tamai S., Shors E.C. and Caplan A.I. (1990). 'Marrow cell induced osteogenesis in porous hydroxyapatite and tricalcium phosphate.' *J. Biomed. Mat. Res.* **24**, 1563–1570

Ohgushi H., Okumura M., Yoshikawa T., Inoue K., Senpuke N. and Tamai S. (1992). 'Bone formation process in porous calcium carbonate and hydroxyapatite.' *J. Biomed. Mat. Res.* **26**, 885–895

Ohgushi H., Dohi Y., Katsuda T., Tamai S., Tabata S. and Suwa Y. (1996). '*In vitro* bone formation by rat marrow cell culture.' *J. Biomed. Mat. Res.* **32**, 333–340

Ohgushi H., Kotobuki N., Funaoka H., Machida H., Hirose M., Tanaka Y. and Takakura Y. (2005). 'Tissue engineered ceramic artificial joint – *ex vivo* osteogenic differentiation of patient mesenchymal cells on total ankle joints for treatment of osteoarthritis.' *Biomaterials* **26**, 465–466

Okumura M., Ohgushi H. and Tamai S. (1991a). 'Bonding osteogenesis in coralline hydroxyapatite combined with bone marrow cells.' *Biomaterials* **12**, 411–416

Okumura M., Ohgushi H., Tamai S. and Shors E.C. (1991b). 'Primary bone formation in porous hydroxyapatite ceramic: a light and scanning elecron microscopic study.' *Cells Mater* **1**, 29–34

Okumura M., Ohgushi, H. Dohi T., Katsuda T., Tamai S., Koerten H.K. and Tabata S. (1997). 'Osteoblastic phenotype expression on the surface of hydroxyapatite ceramics.' *J. Biomed. Mat. Res.* **37**, 122–129

Owen M. (1985). ' Lineage of osteogenic cells and their relationship to the stromal system' in *Bone and Mineral Research*, Vol. 3, W.A. Peck (ed.), Elsevier Science Publisher BV, The Netherlands, pp. 1–25

Takaoka T., Okumura M., Ohgushi H., Inoue K., Takakura Y. and Tamai S. (1996). 'Histological and biochemical evaluation of osteogenic response in porous hydroxyapatite coated alumina ceramics.' *Biomaterials* **17**, 1499–1505

Uchimura E., Machida H., Kotobuki N., Kihara T., Kitamura S., Ikeuchi M., Hirose M., Miyake J. and Ohgushi H. (2003). '*In-situ* visualization and quantification of mineralization of cultured osteogenetic cells.' *Calcif Tissue Int.* **73**, 575–583

Yoshikawa T., Ohgushi H. and Tamai S. (1996). 'Immediate bone forming capability of prefabricated osteogenic hydroxyapatite.' *J. Biomed. Mat. Res.* **32**, 481–492

Index